Technical Report

TR-08-05

Site description of Forsmark at completion of the site investigation phase

SDM-Site Forsmark

Svensk Kärnbränslehantering AB

December 2008

Svensk Kärnbränslehantering AB
Swedish Nuclear Fuel
and Waste Management Co

Box 250, SE-101 24 Stockholm
Phone +46 8 459 84 00

SKB

ISSN 1404-0344
SKB TR-08-05
ID 1199238
Updated 2013-08

Site description of Forsmark at completion of the site investigation phase

SDM-Site Forsmark

Svensk Kärnbränslehantering AB

December 2008

Update notice

The original report, dated December 2008, was found to contain both factual and editorial errors which have been corrected in this updated version. The corrected factual errors are presented below.

Updated 2013-08

Location	Original text	Corrected text
Page 266, Table 8-8, last column, last row	(–8.3, 1.0)	(–8.8, 1.0)
Page 359, paragraph 2, line 6	/Selnert et al. 2008/	/Widestrand et al. 2010/
Page 444, reference	Selnert et al. 2008	Reference removed
Page 448, reference		*New reference:* Widestrand et al. 2010
Page 470, paragraph Sampling and analyses of rock matrix porewater, row KFM02B	P-08-29	P-09-14
Page 493	P-08-29 Waber H N, Smellie J A T. Forsmark site investigation. Borehole KFM2B: Characterisation of pore water. Part 1: Diffusion experiments.	P-09-14 Waber H N, Smellie J A T. Forsmark site investigation. Borehole KFM02B. Characterisation of pore water. Part 1: Diffusion experiments and pore water data.

The updated table shows what was actually used in the groundwater flow modelling for SDM-Site Forsmark.

Preface

The Swedish Nuclear Fuel and Waste Management Company (SKB) is undertaking site characterisation at two different locations, the Forsmark and Laxemar-Simpevarp areas, with the objective of siting a deep geological repository for spent nuclear fuel. An integrated component in the characterisation work is the development of a site descriptive model (SDM) that constitutes a description of the site and its regional setting. The model addresses the current state of the geosphere and the biosphere as well as the ongoing natural processes that affect their long-term evolution.

The site descriptive model concluding the surface-based investigations at Forsmark, SDM-Site, is compiled in the present report. Prior to the SDM-Site report, three versions of a site descriptive model have been completed for the Forsmark area. Version 0 established the state of knowledge prior to the start of the site investigation programme. Version 1.1, which was essentially a training exercise, was completed during 2004 and version 1.2 in June 2005. Version 1.2 of the SDM, a preliminary site description, concluded the initial site investigation work.

Three analytical and modelling stages have been carried out during the complete site investigation work. An important component of each of these stages has been to address and continuously try to resolve uncertainties of importance for repository engineering and safety assessment. Stage 2.1 aimed to provide feedback from the modelling group to the site investigation team to enable completion of the site investigation work. Stages 2.2 and 2.3 have established the different discipline-specific models, which are combined into the framework of the integrated site descriptive model, SDM-Site. A synthesis of the SDM-Site report that focuses on model integration and the current understanding of the site is presented in chapter 11. In essence, this chapter serves as an executive summary.

The overall objective of the site descriptive modelling work at Forsmark is to develop and document an integrated description of the site, based on data from the complete site investigation work, as a basis for a site-adapted design of the final repository (Layout D2) and for assessment of the repository's long-term radiological safety (SR-Site).

The site descriptive modelling work performed within the Swedish site characterisation programme is conducted by multi-disciplinary project groups and associated discipline-specific working groups. All individuals and expert groups contributing to the projects are gratefully acknowledged, and especially the Forsmark multi-disciplinary project group, for making this report possible. Specifically, the following individuals and expert groups contributed to this final report:

- Kristina Skagius – project leader, editor and site synthesis.
- Lennart Ekman – site investigation data.
- Björn Söderbäck – site evolutionary aspects, abiotic and biotic properties of the surface system.
- Sten Berglund and other members of the SurfaceNet group – abiotic and biotic properties of the surface system.
- Michael Stephens – geology (deterministic modelling and integrated model), site synthesis and Appendix 4.
- Raymond Munier – geology (discrete fracture network modelling).
- Jan Sundberg and John Wrafter – thermal properties.
- Rune Glamheden – rock mechanics.
- Sven Follin – hydrogeology and site synthesis.
- Marcus Laaksoharju, John Smellie and Eva-Lena Tullborg – hydrogeochemistry.
- James Crawford – transport properties.
- Anders Lindblom – production of maps and figures.
- Assen Simeonov and Jakob Levén – Appendix 4.

The members of the multi-disciplinary project group completed Appendices 2 and 3.

Johan Andersson is specifically acknowledged for his ambitious and devoted efforts as a driving force for the confidence assessment work and as the editor of the report documenting the outcome (SKB R-08-82).

The report has been formally reviewed by the following members of SKB's international site investigation expert review group (Sierg): Per-Eric Ahlström (Chairman); Jordi Bruno (Amphos, Spain); John Hudson (Rock Engineering Consultants, UK); Ivars Neretnieks (Royal Institute of Technology, Sweden); Lars Söderberg (SKB); Michael C. Thorne (Mike Thorne and Associates Ltd, UK); Roland Pusch (GeoDevelopment AB); Thomas W Doe (Golder Associates Inc.); John Cosgrove (Imperial College, London); Alan Hooper (Alan Hooper Consulting Limited). The Sierg group provided many valuable comments and suggestions for this work. However, it is not to be held responsible for any remaining shortcomings of the report.

Anders Ström

Site Investigations – Analysis

Summary

The Swedish Nuclear Fuel and Waste Management Co., SKB, has undertaken site characterisation in two different areas, Forsmark and Laxemar-Simpevarp, in order to identify a suitable location for a geological repository of spent nuclear fuel according to the KBS-3 method. The site investigations have been conducted in campaigns, punctuated by data freezes. After each data freeze, the site data have been analysed and modelling has been carried out with the overall purpose to develop a site descriptive model (SDM). The site descriptive model is used by repository engineering to design the underground facility and to develop a repository layout adapted to the site. It is also essential for safety assessment, since the model is the only source for site-specific input. Another important use of the site descriptive model is in the environmental impact assessment.

An SDM is an integrated model for geology, thermal properties, rock mechanics, hydrogeology, hydrogeochemistry, bedrock transport properties and a description of the surface system. The site descriptive model compiled in the current report, SDM-Site, presents an integrated understanding of the Forsmark area at the completion of the surface-based investigations, which were conducted at Forsmark during the period 2002 to 2007. It also provides a summary of the abundant underlying data and the discipline-specific models that support the site understanding. The description relies heavily on background reports that address, in particular, details in data analyses and modelling in the different disciplines.

The Forsmark area is located in northern Uppland within the municipality of Östhammar, about 120 km north of Stockholm. The candidate area for site investigation is located along the shoreline of Öregrundsgrepen, within the north-western part of a major tectonic lens that formed between 1.87 and 1.85 billion years ago during the Svecokarelian orogeny. The candidate area is approximately 6 km long and 2 km wide. The north-western part of the candidate area lacks hydraulically conductive, gently dipping fracture zones at potential repository depth and was selected as the target area for the complete site investigation work, following the initial investigations at the site.

Prior to the presentation of the SDM-Site report, three versions of a site descriptive model have been completed for the Forsmark area and presented for peer review. The last version, referred to as version 1.2, was a preliminary site description that concluded the initial site investigation work and was presented in 2005. This preliminary site description formed the basis for a preliminary safety evaluation (PSE) of the Forsmark area, a preliminary repository layout (step D1), and the first evaluation of the long-term safety of this layout for KBS-3 repositories in the context of the SR-Can project.

The final site descriptive model, SDM-Site, builds on a coordinated geological model in 3D, into which other discipline-specific models have been integrated without any major conflicting interpretations. In particular, the thermal properties of the bedrock at the site have been coupled to identified rock domains in the geological model and an integrated model that links the current stress regime, the hydrogeology and the chemistry of the groundwater to fracture domains and fracture zones in the geological model has evolved. These mutually consistent results demonstrate that a fundamental understanding of the current state of conditions and the on-going processes in the Forsmark area, from the surface down to potential repository depth, has been achieved. In addition, the properties of the area can be explained in the context of an understanding of the past evolution, throughout a long period of geological history. This integrated understanding of the area is presented in chapter 11 of this report and this chapter serves as an executive summary.

A systematic assessment of the confidence in the model, including treatment of uncertainties and evaluation of alternative interpretations, has been carried out. This assessment has taken account of the feedback obtained from the work with the preliminary repository layout step D1 and from the safety assessment SR-Can, as well as the feedback obtained on earlier versions of the site description. The overall outcome of this assessment is that most properties of importance for both repository constructability and long-term safety are bounded sufficiently, and that data from underground now bears the prime potential to further reduce uncertainties in the target volume. However, complementary studies to reduce some of these uncertainties are also currently in progress. Uncertainties outside the target volume are larger, but are judged to be of less importance for the constructability and long-term safety of a repository.

Contents

1 Introduction 13
1.1 Background 13
1.2 Scope and role of the site description 14
1.3 Objectives and strategy 14
1.4 Feedback from reviews and assessments of previous model versions 16
1.5 Setting 16
1.6 Methodology and organisation of the work 20
1.6.1 Methodology 20
1.6.2 Interfaces between disciplines 22
1.6.3 Organisation of work 23
1.6.4 Quality assurance aspects 24
1.6.5 Nomenclature 24
1.7 This report and supporting documents 25

2 Investigations, available data and other prerequisites for modelling 29
2.1 Overview of investigations 29
2.1.1 Investigations and primary data acquired up to data freeze 1.2 29
2.1.2 Investigations and primary data aquired at data freezes 2.1, 2.2 and 2.3 30
2.2 Investigations of the surface system 30
2.2.1 Bedrock geology and ground geophysics 30
2.2.2 Quaternary geology and ground geophysics 32
2.2.3 Surface ecology 32
2.3 Borehole investigations 33
2.3.1 Drilling activities 41
2.3.2 Measurements completed in connection with drilling, geological mapping of drill cores and drill cuttings, and down-hole logging 41
2.3.3 Sampling and analysis of intact rock material for laboratory investigations 45
2.4 Monitoring 46
2.4.1 Background 46
2.4.2 Monitoring programme 46
2.5 Geographical data 47
2.6 Other data sources 48
2.7 Databases 48
2.8 Model versions prior to stages 2.2 and 2.3 49
2.9 Model volumes and model areas 50
2.9.1 Regional model area and volume 50
2.9.2 Local model area and volume 51

3 Evolutionary aspects of the Forsmark site 53
3.1 Bedrock evolution during the Proterozoic and Phanerozoic eons 53
3.1.1 Bedrock geological evolution in south-eastern Sweden 53
3.1.2 Bedrock geological evolution in the Forsmark area 56
3.2 Palaeoclimate and geological development during the Quaternary period 58
3.3 Seismicity during the Quaternary period 60
3.4 Groundwater evolution during the Quaternary period 62
3.5 Development of ecosystems during the late Quaternary period 63
3.6 Human population and land use 65

4 Surface system and surface-bedrock interactions 67
4.1 State of knowledge at the previous model version 67
4.2 Evaluation of primary data 67
4.2.1 Regolith and Quaternary geology 68
4.2.2 Hydrology and near-surface hydrogeology 72

4.2.3 Hydrochemistry 73
4.2.4 Ecosystems 74
4.2.5 Human population and land use 78
4.3 Modelling of the surface system 79
4.3.1 Hydrology and near-surface hydrogeology 79
4.3.2 Ecosystems 81
4.4 Implications for bedrock modelling 85
4.4.1 Hydrology and hydrogeology 86
4.4.2 Hydrochemistry 89
4.4.3 Solute transport 92
4.5 Summary description of the surface system at Forsmark 95
4.6 Evaluation of uncertainties 98

5 Bedrock geology 99
5.1 State of knowledge at the previous model version 99
5.2 Evaluation of primary data 100
5.2.1 Bedrock geological map at the surface 100
5.2.2 Rock units and possible deformation zones in the sub-surface realm 103
5.2.3 Rock types − properties, alteration, volumetric proportions and thickness of the subordinate rock amphibolite 107
5.2.4 Ductile deformation 110
5.2.5 Brittle deformation 114
5.2.6 Character and kinematics of deformation zones 122
5.2.7 Identification, character and geological significance of lineaments 124
5.2.8 Character and geological significance of seismic reflection data 128
5.2.9 Character and geological significance of seismic refraction data 131
5.3 Geological models in relation to data resolution 132
5.4 Deterministic model for rock domains 133
5.4.1 Data input 133
5.4.2 Conceptual model 133
5.4.3 Methodology, assumptions and feedback from other disciplines 134
5.4.4 Division into rock domains, geometries and property assignment 135
5.5 Deterministic model for deformation zones 139
5.5.1 Data input 139
5.5.2 Conceptual model 139
5.5.3 Methodology, assumptions and feedback from other disciplines 142
5.5.4 Geometric models and property assignment 144
5.6 Statistical model for fractures and minor deformation zones 153
5.6.1 Division into fracture domains 154
5.6.2 Modelling assumptions 158
5.6.3 Derivation of statistical fracture model 159
5.6.4 DFN models 165
5.7 Integrated geological model 166
5.8 Verification of the deterministic geological models 171
5.8.1 KFM08D 171
5.8.2 Gravity and petrophysical modelling 173
5.9 Remaining uncertainties 173
5.9.1 Deterministic model for rock domains 173
5.9.2 Deterministic model for deformation zones 174
5.9.3 Statistical model for fractures and minor deformation zones 175

6 Bedrock thermal properties 177
6.1 State of knowledge at the previous model version 177
6.2 Evaluation of primary data 177
6.2.1 Thermal conductivity determinations 178
6.2.2 Relationship between thermal conductivity and density 178
6.2.3 Measurement of anisotropy of thermal conductivity associated with foliation 180
6.2.4 Heat capacity 180

6.2.5 Thermal conductivity vs heat capacity 181
6.2.6 Temperature dependence of thermal properties 182
6.2.7 Pressure dependence in thermal conductivity 182
6.2.8 Coefficient of thermal expansion 182
6.2.9 ***In situ*** temperature 183
6.3 Strategy for thermal modelling 184
6.3.1 Conceptual model 184
6.3.2 Modelling approach 185
6.3.3 Modelling assumptions 186
6.3.4 Feedback from other disciplines 187
6.4 Geostatistical analyses and stochastic simulations 187
6.4.1 Thermal Rock Classes (TRC) – Definition, properties and proportions 187
6.4.2 Geological heterogeneity and division into thermal subdomains 188
6.4.3 Spatial statistical models of lithology 190
6.4.4 Stochastic simulations of lithology 191
6.4.5 Spatial statistical models of thermal conductivity 194
6.4.6 Stochastic simulations of thermal conductivity 196
6.5 Thermal domain model 198
6.5.1 Domain modelling results 198
6.5.2 Evaluation of domain modelling results 202
6.5.3 Summary of rock domain properties 202
6.6 Evaluation of uncertainties 204
6.6.1 Data uncertainty 204
6.6.2 Model uncertainty 204
6.6.3 Summing up 206

7 Rock mechanics 207
7.1 State of knowledge at the previous model version 207
7.2 Evaluation of primary data 208
7.2.1 Laboratory properties of intact rock 209
7.2.2 Laboratory properties of fractures 212
7.2.3 Characterisation of the rock mass quality 212
7.2.4 ***In situ*** state of stress 214
7.3 Rock mechanics model 217
7.3.1 Intact rock properties 217
7.3.2 Fracture properties 219
7.3.3 Rock mass properties 220
7.3.4 ***In situ*** state of stress 223
7.4 Evaluation of uncertainties 227
7.4.1 Uncertainty in mechanical properties 227
7.4.2 Uncertainty in the stress model 227

8 Bedrock hydrogeology 229
8.1 Context 229
8.1.1 Hydrogeological modelling in the SDM 229
8.1.2 Model development 230
8.1.3 Main characteristics of relevance to the model 231
8.2 State of knowledge at the previous model version 232
8.3 Evaluation of primary data 234
8.3.1 Deterministic versus stochastic features 234
8.3.2 Basic characteristics of the single-hole tests 236
8.3.3 Evaluation of single-hole hydraulic tests 237
8.3.4 Evaluation of hydraulic interference tests 242
8.4 Conceptual modelling 243
8.4.1 Deformation zones and associated hydraulic data 243
8.4.2 Fracture domains and associated hydraulic data 246
8.4.3 The bedrock bordering the target volume 252

8.4.4 The shallow bedrock aquifer 252
8.5 Parameterisation of deformation zones and fracture domains 259
8.5.1 Deformation zones 259
8.5.2 Fracture domains 260
8.6 Flow model calibration 271
8.6.1 Matching the 2006 interference test in HFM14 272
8.6.2 Matching natural groundwater levels 273
8.6.3 Matching hydrochemical profiles in cored boreholes 275
8.7 Bedrock hydrogeological model 280
8.7.1 Visualisations for interpretation of hydrochemistry 283
8.7.2 Visualisations for interpretation of flow and solute transport 287
8.8 Parameter sensitivity analysis 291
8.9 Confidence and remaining uncertainties 293
8.9.1 Groundwater levels in the shallow bedrock aquifer 293
8.9.2 Compartmentalised fracture networks at repository depth 295
8.9.3 Evaluation of PFL-f transmissivity data 295

9 Bedrock hydrogeochemistry 297
9.1 Introduction 297
9.2 State of knowledge at previous model version 298
9.3 Conceptual model 299
9.3.1 Major concepts and model input 299
9.3.2 Working hypothesis on the past groundwater evolution 305
9.4 Hydrogeochemical data 307
9.4.1 Borehole groundwater data 308
9.4.2 Representativity of the data 308
9.5 Explorative analysis and modelling 309
9.5.1 Initial data evaluation and visualisation 310
9.5.2 Mixing calculations 318
9.5.3 Redox modelling 319
9.5.4 Characterisation of microorganisms 322
9.5.5 Characterisation of colloids 324
9.5.6 Gases 325
9.5.7 Studies of fracture fillings 325
9.5.8 Porewater composition in bedrock 328
9.5.9 Groundwater residence time 333
9.5.10 Evaluation of uncertainties in field data and interpretation methods 336
9.6 Hydrogeochemical integrated site model 338
9.6.1 Hydrogeochemical visualisation 338
9.6.2 Consistency with the hydrogeological model 344
9.6.3 Confidence and uncertainty in the integrated hydrogeochemical model 345

10 Bedrock transport properties 349
10.1 State of knowledge at previous model version 349
10.2 Evaluation of primary data 349
10.2.1 Data and models from other disciplines 349
10.2.2 Transport data 350
10.3 Conceptual model 350
10.4 Transport properties of the bedrock 353
10.4.1 Overview of rock domains and fracture domains 353
10.4.2 Representative transport property data 356
10.4.3 Application of the retardation model 367
10.5 Flow-related transport properties 367
10.5.1 Conceptualisation of flow paths 367
10.5.2 F-factor estimation 369
10.5.3 Flow channelling 374

10.6 Transport of radionuclides 376
10.7 Field-scale confirmatory testing of transport properties 379
10.7.1 Multiple well tracer tests 379
10.7.2 Single well injection-withdrawal (SWIW) tests 380
10.7.3 Evaluation of tracer test data, interpretation and consequences for safety assessment 380
10.8 Evaluation of uncertainties 382

11 Current understanding of the site 385
11.1 Surface system 386
11.1.1 Evolution during the Quaternary period 386
11.1.2 Description of the surface system 388
11.1.3 Human population and land use 391
11.2 Rock domains and their associated thermal and rock mechanical properties 391
11.2.1 Rock crystallisation and cooling history 391
11.2.2 Rock composition and ductile deformation 392
11.2.3 Rock domain model 395
11.2.4 Mineral resources 396
11.2.5 Thermal properties 396
11.2.6 Strength and other mechanical properties of intact rock 398
11.3 Deformation zones, fracture domains and fractures 399
11.3.1 Formation and reactivation throughout geological time 399
11.3.2 Deterministic deformation zones 401
11.3.3 Fracture domains, fractures and DFN modelling 404
11.3.4 Fracture mineralogy 407
11.3.5 Mechanical properties of deformation zones and fractures 408
11.4 Rock stress 409
11.4.1 Stress evolution 409
11.4.2 Stress model 409
11.5 Bedrock hydraulic properties 411
11.5.1 Evolution 411
11.5.2 Hydraulic properties of deformation zones and fracture domains 411
11.6 Integrated fracture domain, hydrogeological DFN and rock stress models 415
11.7 Groundwater 416
11.7.1 Evolution during the Quaternary period 416
11.7.2 Groundwater composition 418
11.7.3 Groundwater flow and evolution of groundwater composition 421
11.8 Transport properties 423
11.8.1 Properties of the rock matrix 423
11.8.2 Flow-related properties 424
11.9 Overall confidence 427
11.9.1 Data usage 427
11.9.2 Key remaining issues and their treatment 427
11.9.3 Handling of alternatives 428
11.9.4 Consistency between disciplines 429
11.9.5 Confidence statement 429

12 Conclusions 431
12.1 Fulfilment of objectives 431
12.2 Key remaining issues 431
12.3 Implications for the underground construction phase 431

13 References 433

Appendix 1 Topography and place names in the Forsmark area 449

Appendix 2 Nomenclature 451

Appendix 3 Tables with references to primary data 455

Appendix 4 Properties of deformation zones modelled to intersect the target volume at –400 to –600 m elevation 497

1 Introduction

1.1 Background

Radioactive waste from nuclear power plants is managed by the Swedish Nuclear Fuel and Waste Management Co., SKB. The Swedish programme for geological disposal of spent nuclear fuel is approaching major milestones in the form of permit applications for an encapsulation plant and a final repository. For siting of the repository, SKB has undertaken site characterisation at two different locations, Forsmark and Laxemar-Simpevarp (Figure 1-1). The site investigations have been conducted in campaigns, punctuated by data freezes. After each data freeze, the site data have been analysed and modelling has been carried out with the overall purpose to develop a site descriptive model (SDM). An SDM is an integrated model for geology, thermal properties, rock mechanics, hydrogeology, hydrogeochemistry, bedrock transport properties and a description of the surface system.

The site descriptive model concluding the surface-based investigations at Forsmark, SDM-Site, is compiled in this site description. The report presents the integrated understanding of the Forsmark site at the completion of the surface-based investigations and provides a summary of the models and the underlying data supporting the site understanding. Prior to the SDM-Site, three versions of a site descriptive model had been completed for the Forsmark area. Version 0 /SKB 2002/ established the state of knowledge prior to the start of the site investigation phase. Version 1.1 /SKB 2004/ was essentially a training exercise and was completed during 2004. In June 2005, version 1.2 of the SDM /SKB 2005a/, a preliminary site description, concluded the initial site investigation work (ISI).

Three analytical and modelling stages have been carried out during the complete site investigation work (CSI). An important component of each of these stages has been to address and continuously try to resolve uncertainties of importance for repository engineering and safety assessment.

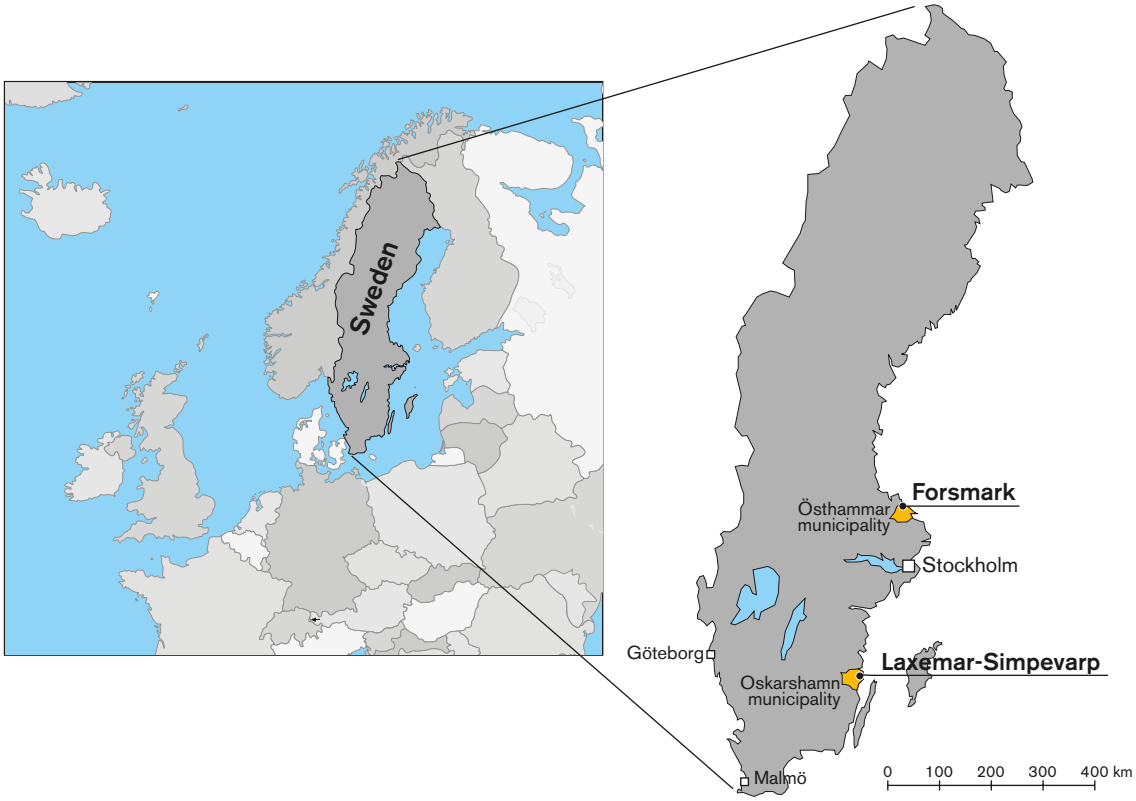

Figure 1-1. *Map of Sweden showing the location of the Forsmark and Laxemar-Simpevarp sites, located in the municipalities of Östhammar and Oskarshamn, respectively.*

Model stage 2.1 /SKB 2006a/ included an updated geological model for Forsmark and aimed to provide feedback from the modelling working group to the site investigation team to enable completion of the site investigation work. Model stages 2.2 and 2.3 have established the different discipline-specific models which are synthesised into the framework of the integrated site descriptive model SDM-Site presented in this report. This concludes the assessment of the surface-based site investigations at Forsmark.

1.2 Scope and role of the site description

Site characterisation should provide all data required for an integrated evaluation of the suitability of the investigated site for a deep geological repository and a fundamental component in the characterisation work is the development of a site descriptive model.

Quality-assured data from site investigations, stored in the SKB database Sicada and the SKB geographic information system (GIS), are the input to site descriptive modelling. The site descriptive model is used by repository engineering to design the underground facility and to develop a repository layout adapted to the site. It is also essential for safety assessment, since the model is the only source for site-specific input. Another important use of the site descriptive model is in the environmental impact assessment.

In order to ensure that all data and information needed for repository design and safety assessment are captured in the site characterisation work, there has been a continuous exchange of information between the various technical activities (Figure 1-2). Based on the preliminary site description (SDM version 1.2), compiled from data collected during the initial site investigation stage (ISI), a preliminary repository layout (step D1) /Brantberger et al. 2006/ was established and a preliminary safety evaluation (PSE) /SKB 2005b/ as well as a full safety assessment (SR-Can) /SKB 2006b/ were conducted (thin red arrows in Figure 1-2). In the course of the work with the design and the safety assessment, requests for new data and/or data with greater precision were raised. This feedback (blue arrows in Figure 1-2) was included in the final programme for the completion of the site investigation phase. In addition to this formal feedback via the site modelling report from stage 2.1 /SKB 2006a/, there has been another, less formalised feedback continuously ongoing from site modelling to the site investigation programme (dashed blue arrows in Figure 1-2). Repository engineering and safety assessment will now update their work based on the final site description, SDM-Site, which concludes the surface-based characterisation work (thick red arrows in Figure 1-2). The products within repository engineering that rely on an input from the site description are: the site engineering report, the layout report and the underground opening construction report. The corresponding reports in the safety assessment work are: the data report and the geosphere process report.

In the SKB programme, a site description is a description of the site covering the current state of the geosphere and the biosphere as well as descriptions of on-going natural processes that can affect their long-term evolution. However, it is not the task of the site description to present any predictions of the future evolution of site conditions. This is completed within safety assessment based on the understanding of the current conditions and of the past evolution as compiled in the site description. It is also not the task of the site descriptive modelling to evaluate the impact on current site conditions of the excavation or the operation of a repository at the site. This is carried out within the framework of repository engineering and as part of the environmental impact assessment, but again based on input from the site description.

1.3 Objectives and strategy

The overall objective of the current site descriptive modelling work (SDM-Site) at Forsmark is to develop and document an integrated description of the site, based on data from the complete site investigation work, as a basis for a site-adapted design of the final repository (Layout D2) and for assessment of the repository's long-term radiological safety (SR-Site). The description has to be based on, and demonstrate, a fundamental understanding of the rock and surface system, which is achieved by analysing the reliability and assessing the reasonableness of the assumptions made with

Figure 1-2. *Exchange of information between technical activities that provide data to site modelling or make use of the site description. Deliveries from (red arrows) and feedback to (blue arrows) site modelling are highlighted together with the final product from site modelling and the products of other technical activities that rely on this input.*

respect to the current state of the Forsmark site and naturally ongoing processes. Furthermore, the work is required to make use of all knowledge and understanding built into previous model versions and of the feedback obtained from the safety assessment SR-Can as well as of other feedback obtained on earlier versions of the site description.

The specific objectives of the work were to:

- analyse the primary data produced within the surface-based site investigation, i.e. including data available at data freezes 2.2 and 2.3,
- describe evolutionary aspects at the site from the time the bedrock formed to the current day,
- develop a complete three-dimensional integrated site descriptive model covering all disciplines,
- perform an overall confidence assessment including systematic treatment of uncertainties and evaluation of alternative interpretations, and
- perform modelling activities in close interaction with safety analysis and repository engineering.

The strategy applied for achieving the stated objectives was to base the site descriptive model on the quality assured, geoscientific and ecological field data from Forsmark that were available in the SKB databases Sicada and GIS at the date defined for data freeze 2.2, i.e. on September 30th 2006. This data freeze contained all data planned to be collected from the target volume, i.e. the rock volume that has been selected as potentially suitable for hosting a final repository (see further section 1.5). All new data that were available at the date defined for data freeze 2.3, i.e. on March 30th 2007, were used for complementary analyses and verification of the models. Since the site investigation has continued after data freeze 2.3, although to a very much smaller extent, additional data have also emerged after this data freeze. As far as possible, these "late" data have been assessed and commented upon in relation to the models established earlier.

The strategy outlined above implies that all discipline-specific modelling was completed on the basis of data available at data freeze 2.2. In order to achieve the specific objective of delivering documented models of geology, thermal properties, rock mechanical properties and hydrogeological

properties to repository engineering, it was decided to compile the results of the modelling based on data freeze 2.2 into modelling stage 2.2 reports for these disciplines, prior to conducting and reporting the complementary analyses and verification activities using new data in data freeze 2.3. For the remaining disciplines, the modelling based on data freeze 2.2 and the complementary and verification analyses are compiled into a single background report. The reports supporting the Forsmark SDM-Site are further described in section 1.7.

1.4 Feedback from reviews and assessments of previous model versions

Feedback on previous model versions has been received from downstream users of the models and from reviews of the previous model reports by SKB's own expert group Sierg, but also from expert groups set up by the authorities SKI (the Insite group) and SSI (the Oversite group). Specifically, the Insite and Oversite groups have continuously followed the progress of the work and the Insite group has regularly provided lists of issues of their concern to be addressed in the modelling work. The handling of the issues raised has been documented by SKB as formal responses to Insite and SKI.

All feedback issues related to the site descriptive modelling of the Forsmark site have been compiled and the remaining issues have been addressed in the modelling work. A main task of the model stage 2.1 work /SKB 2006a/ was to identify and compile remaining important issues/uncertainties and suggest how these should be handled in the forthcoming site investigation and modelling work. Uncertainties in the preliminary site description /SKB 2005a/, the results of analyses conducted during modelling stage 2.1, and experience from the work with repository layout D1 and the preliminary safety evaluation (PSE) for Forsmark formed the input to the compilation of issues. In the SR-Can safety assessment /SKB 2006b/, which was based on the preliminary site description /SKB 2005a/, remaining site characterisation issues of importance for assessing repository safety were identified and provided as feedback to the site investigation and modelling teams. These issues have been addressed in the final stages of site descriptive modelling together with issues of importance for repository design. The results were evaluated as part of the assessment of confidence and uncertainties in the site descriptive model at the conclusion of the surface-based site investigation work /SKB 2008/ and a summary is provided in section 11.9.

1.5 Setting

The Forsmark area is located in northern Uppland within the municipality of Östhammar, about 120 km north of Stockholm (Figure 1-1 and Figure 1-3). The candidate area for site investigation is located along the shoreline of Öregrundsgrepen. It extends from the Forsmark nuclear power plant and the access road to the SFR-facility, a repository for low- and intermediate level radioactive waste, in the north-west to Kallrigafjärden in the south-east (Figure 1-3 and map in Appendix 1). It is approximately 6 km long and 2 km wide. The north-western part of the candidate area was selected as the target area for the complete site investigation work /SKB 2005c/ (see Figure 1-4 and map in Appendix 1).

The Forsmark area consists of a crystalline bedrock that belongs to the Fennoscandian Shield, one of the ancient continental nuclei on the Earth. The bedrock at Forsmark in the south-western part of this shield formed between 1.89 and 1.85 billion years ago during the Svecokarelian orogeny /SKB 2005a/. It has been affected by both ductile and brittle deformation. The ductile deformation has resulted in large-scale, ductile high-strain belts and more discrete high-strain zones. Tectonic lenses, in which the bedrock is less affected by ductile deformation, are enclosed between the ductile high strain belts. The candidate area is located in the north-westernmost part of one of these tectonic lenses. This lens extends from north-west of the nuclear power plant south-eastwards to the area around Öregrund (Figure 1-5). The brittle deformation has given rise to reactivation of the ductile zones in the colder, brittle regime and the formation of new fracture zones with variable size.

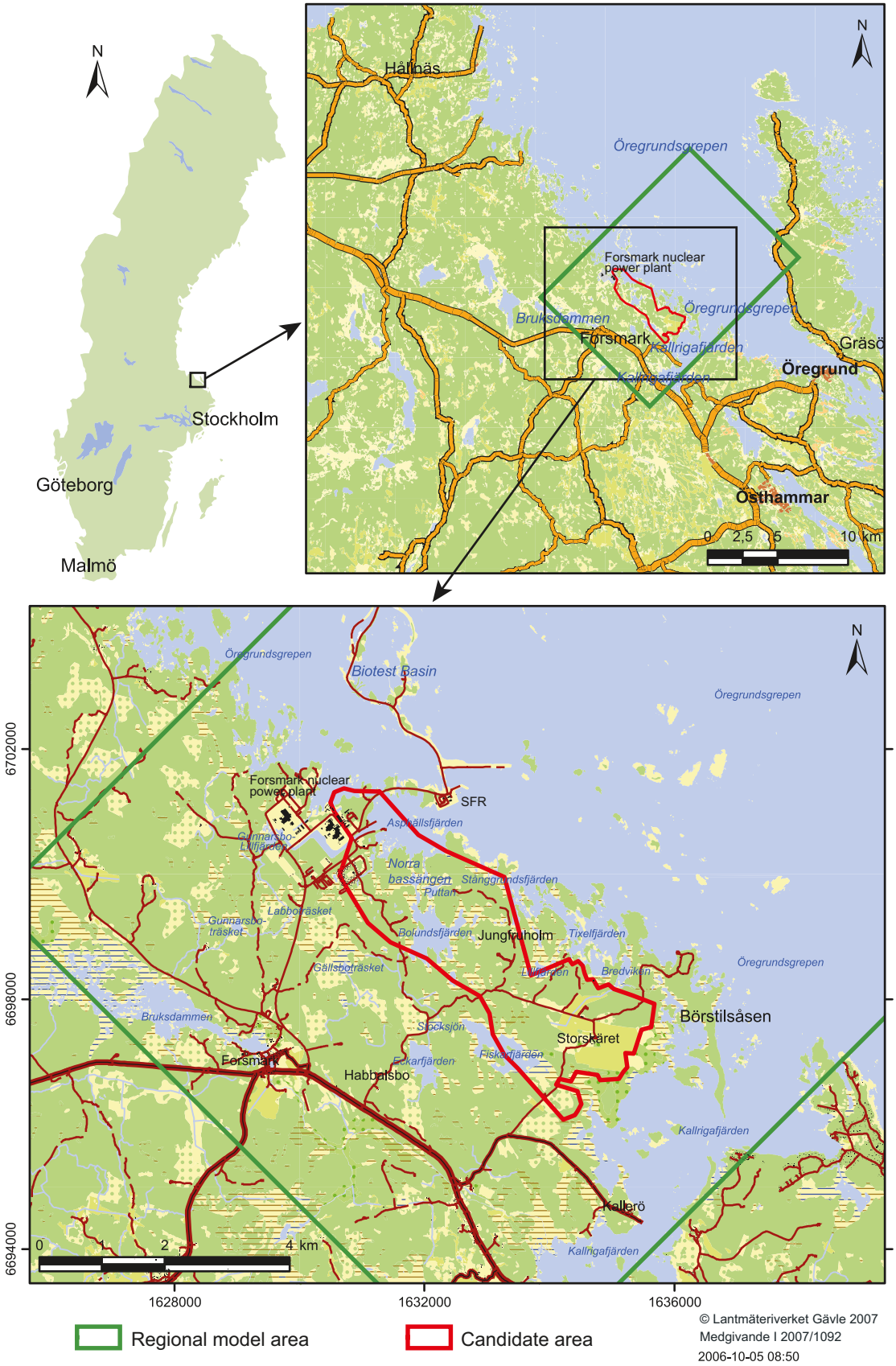

Figure 1-3. *Location of the Forsmark candidate area (red) for site investigation (see section 2.9 for definition of the regional model area).*

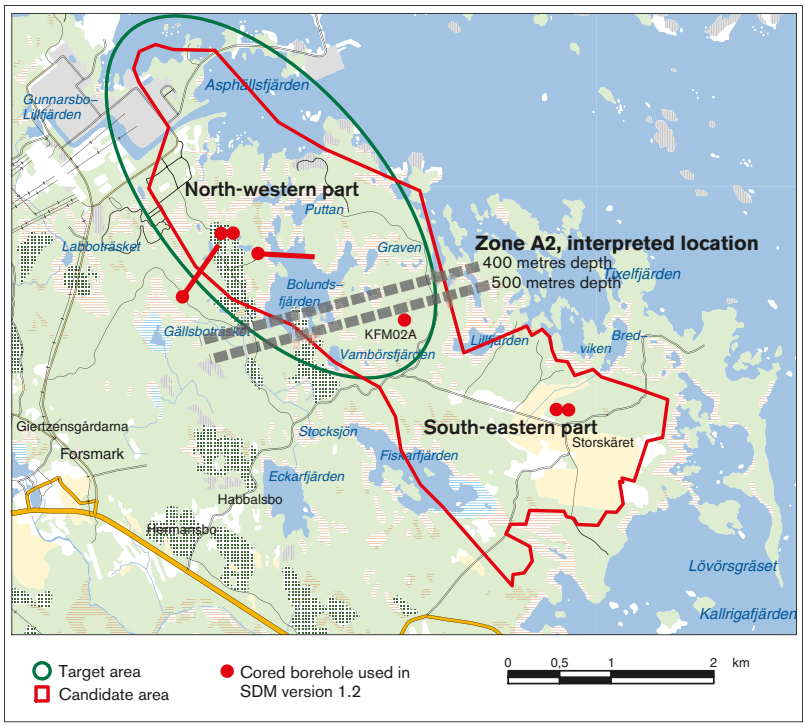

Figure 1-4. *The north-western part of the candidate area was selected as the target area for the complete site investigation work (modified after Figure 2-15 in /SKB 2005c/).*

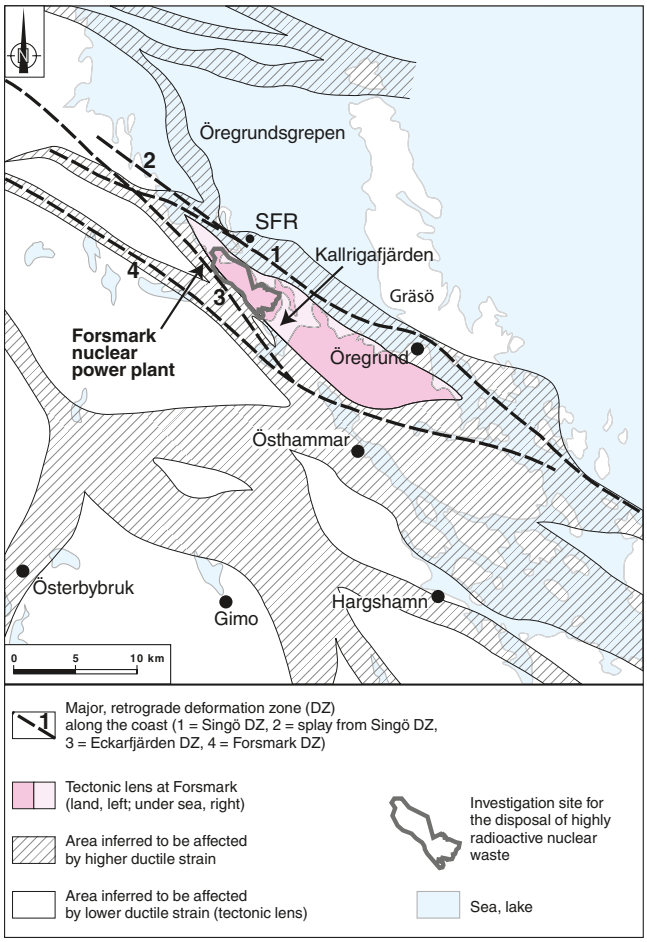

Figure 1-5. *Tectonic lens at Forsmark and areas affected by strong ductile deformation in the area close to Forsmark (Figure 4-1 in /Stephens et al. 2007/).*

The current ground surface in the Forsmark region forms a part of the sub-Cambrian peneplain in south-eastern Sweden. This peneplain represents a relatively flat topographic surface with a gentle dip towards the east that formed more than 540 million years ago. The candidate area at Forsmark is characterised by a small-scale topography at low altitude (Figure 1-6). The most elevated areas to the south-west of the candidate area are located at c. 25 m above current sea level. The whole area is located below the highest coastline associated with the last glaciation, and large parts of the candidate area emerged from the Baltic Sea only during the last 2,000 years. Both the flat topography and the still ongoing shoreline displacement of c. 6 mm per year strongly influence the current landscape (Figure 1-6). Sea bottoms are continuously transformed into new terrestrial areas or freshwater lakes, and lakes and wetlands are successively covered by peat.

Figure 1-6. *Photographs from Forsmark showing the flat topography and the low-gradient shoreline with recently isolated bays due to land uplift.*

1.6 Methodology and organisation of the work

1.6.1 Methodology

The project is multi-disciplinary, in that it covers all potential properties of the site that are of importance for its overall understanding, for the design of the deep repository, for safety assessment and for the environmental impact assessment. The overall strategy applied in the work (Figure 1-7) has been to develop discipline-specific models by interpretation and analyses of the quality-assured primary data that are stored in the SKB databases Sicada and GIS, and then to integrate these discipline-specific models into a unified site description. The quantitative, discipline-specific models are stored in the SKB model database Simon, from where quality-assured versions of the models can be accessed by the downstream users of the site description. Quality assurance aspects of the modelling procedure are further described in section 1.6.4.

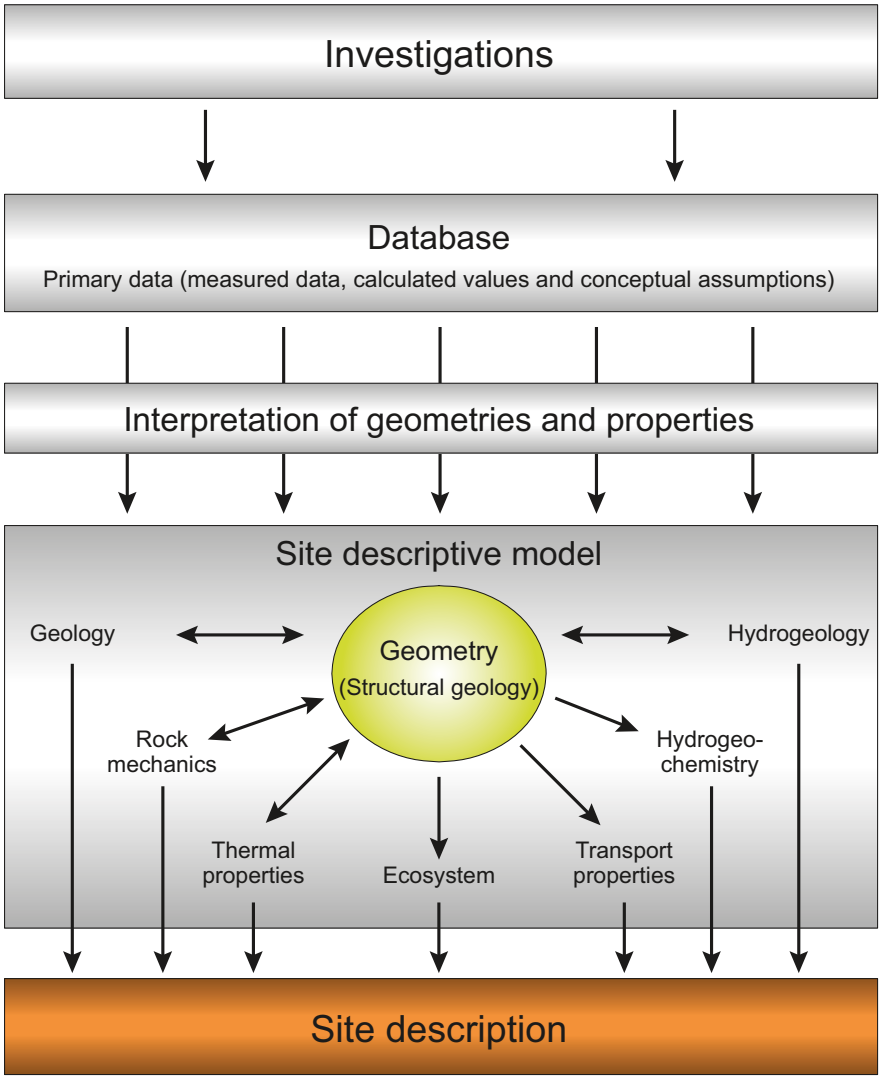

Figure 1-7. *From site investigations to site description. Quality-assured primary data from site investigations are collected in databases. Data are interpreted and presented in a site descriptive model, which consists of a description of the geometry of different features in the model and the corresponding properties of those features and of the site as a whole (modified after Figure 1-1 in /SKB 2002/).*

The site descriptive modelling comprises the iterative steps of evaluation of primary data, descriptive and quantitative modelling in 3D, and evaluation of the confidence in the resulting models. Data are first evaluated within each discipline and then the evaluations are cross-checked between the disciplines. Three-dimensional modelling, with the purpose of estimating the distribution of parameter values in space, as well as their uncertainties, follows. In this context, the geological models provide the geometrical framework for all discipline-specific modelling. The three-dimensional description presents the parameters with their spatial variability over a relevant and specified scale, with the uncertainty included in this description. If required, different alternative descriptions are provided.

Based on experience from earlier SKB projects, e.g. the Laxemar modelling project /Andersson et al. 2002a/, methodologies for generating site descriptive models were developed and documented in discipline-specific strategy reports. The work conducted during the development of the preliminary site description /SKB 2005a/ followed the guide-lines in these reports, which are:

- Geological site descriptive modelling /Munier et al. 2003/,
- Thermal site descriptive modelling /Sundberg 2003a/,
- Rock mechanics site descriptive modelling /Andersson et al. 2002b/,
- Hydrogeological site descriptive modelling /Rhén et al. 2003/,
- Hydrogeochemical site descriptive modelling /Smellie et al. 2002/,
- Transport properties site descriptive modelling /Berglund and Selroos 2004/,
- Ecosystem descriptive modelling /Löfgren and Lindborg 2003/.

In addition, a strategy for achieving sufficient integration between disciplines in producing site descriptive models is documented in a separate strategy report for integrated evaluation /Andersson 2003/.

New experience on methodology issues has been gained during the course of the iterative process of site descriptive modelling and also to some extent by following the progress of international projects, e.g. the AMIGO project /NEA 2004/. When appropriate, this has been built into the methodologies applied and also, in some cases, resulted in updates to, or amendments of, the strategy reports. The products expected from the geological discrete fracture network (DFN) modelling have been presented in detail and clarified in an updated version /Munier 2004/ of an appendix to the strategy document for geological site descriptive modelling /Munier et al. 2003/. The methodology applied for modelling of thermal properties has been considerably revised as compared with the methodology used previously. The updated strategy is based on stochastic simulations of lithologies and thermal conductivity as described in /Back and Sundberg 2007/. Finally, the strategy for hydrogeological modelling during the CSI stage has been updated to give more focus to assessing and demonstrating the understanding of the hydrogeology and on describing the hydrogeological properties of the potential repository volumes. A first test of the updated strategy was reported in /Follin et al. 2007a/.

According to the strategy report for integrated evaluation /Andersson 2003/, the overall confidence evaluation should be based on the results from the individual discipline modelling and involve the different modelling teams. The confidence is assessed by carrying out checks concerning, for example, the status and use of primary data, uncertainties in derived models, and various consistency checks, for example, between models and with previous model versions. Procedures for this assessment have been progressively refined during the course of the site descriptive modelling, and applied to all previous versions of the Forsmark site descriptive model. Since the surface-based site investigations are now concluded and the current site descriptive model (SDM-Site) is compiled with the purpose to support a license application to start construction of a spent nuclear fuel repository, the approach has been further developed in order to address more specifically the confidence in the site description.

1.6.2 Interfaces between disciplines

For several of the disciplines involved in the SDM work, e.g. geology, hydrogeology and hydrogeochemistry, a distinction is made between the surface system and the bedrock system. The reasons for this distinction are both practical (large amounts of data, different objectives and different users of results) and historical, as the SKB work traditionally has been focused on the bedrock system. The delimitation between the surface and bedrock systems is, of course, artificial and somewhat arbitrary.

Central to the description of the bedrock is the geological model which provides the geometrical context in terms of the characteristics of deformation zones and the rock mass between the zones (see section 1.6.5 for definitions). Using the geometric component in the bedrock geological models as a basis, descriptive models for other geoscientific disciplines (thermal properties, rock mechanics, hydrogeology, hydrogeochemistry and transport properties) have been developed for the bedrock. Development of these models has, in turn, highlighted issues of potential importance for the bedrock geological model. Another important interface is that between hydrogeology and hydrogeochemistry, which has been handled, for example, by regional palaeo-hydrogeological simulations of variable-density groundwater flow between 8000 BC and 2000 AD.

The interface between the surface and bedrock systems has been considered in the evaluation of shallow and deep groundwater movement, as well as in the groundwater chemistry description. The present conceptualisation of the hydraulic properties of the Quaternary deposits is implemented into the near-surface hydrogeological modelling in the bedrock and also into modelling and evaluation of the impact of infiltration on the present groundwater composition. The shallow groundwater system is modelled so as to include the uppermost part of the bedrock with flow conditions that are consistent with the bedrock hydrogeological model (see Figure 1-8).

The handling of the interfaces between disciplines is described in more detail in chapter 4 (surface system) and chapters 5 through 10 (bedrock system).

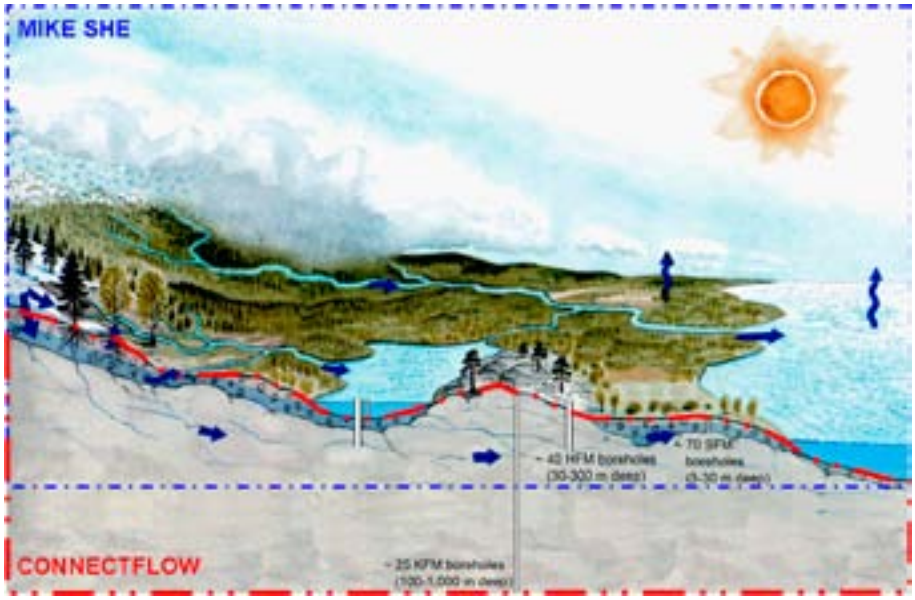

Figure 1-8. *Cartoon showing how the modelling of the hydrologic cycle is divided into a surface-based system and a bedrock-based system. The former is modelled with the MIKE SHE numerical modelling tool and the latter with the ConnectFlow numerical modelling tool. Reproduced from /Follin et al. 2007c/.*

1.6.3 Organisation of work

The work has been conducted by a project group with representatives of the disciplines geology, thermal properties, rock mechanics, hydrogeology, hydrogeochemistry, transport properties and surface systems. In addition, some group members have specific qualifications of importance in this type of project e.g. expertise in RVS (Rock Visualisation System) modelling, GIS-modelling and in statistical data analysis.

Each discipline representative in the project group was given the responsibility for the assessment and evaluation of primary data, and for the modelling work concerning his/her specific discipline. This task was then carried out either by the representatives themselves, or together with other experts or groups of experts outside the project group. In this context, discipline-specific networks, set up by SKB, play an important role. These networks are the same for both the Forsmark and Laxemar-Simpevarp site-modelling projects and they are essentially run by the discipline responsible, as assigned by SKB. The purpose of these networks is to carry out site modelling tasks and to provide technical links between the site organisations, the site modelling teams and the principal clients (repository engineering, safety assessment and environmental impact assessment). The discipline-specific, so-called Net-groups actively involved in the site modelling work are identified in Table 1-1.

In addition to traditional project work, the project group has had several workshops together with representatives of the Forsmark site investigation team addressing uncertainties and overall confidence in the data gathered and in the models produced. The objectives and scope of the uncertainty and confidence assessment have been modified during the course of the site descriptive modelling, reflecting the state of progress in the modelling work. During the initial site investigation stage, focus was on identifying important uncertainties in model versions 1.1 /SKB 2004/ and 1.2 /SKB 2005a/, and in data supporting these models, in order to guide further data collection and modelling activities. Similarly, the primary objective of the work conducted during modelling stage 2.1 /SKB 2006a/ was to provide feedback to the site investigations, in order to ensure that sufficient information was obtained during the remainder of the complete site investigation stage. The focus of the assessment of the final models included in SDM-Site has been on addressing confidence in the models and to provide arguments for the confidence statements.

Table 1-1. Discipline-specific networks involved in site descriptive modelling and their mandates/objectives.

Discipline	Net-group	Mandate
Geology	GeoNet	Provides a forum for the coordination of geological modelling tasks in both the Forsmark and Laxemar-Simpevarp site-modelling projects.
Rock mechanics and thermal properties	MekNet	Coordination of modelling tasks for rock mechanics and thermal properties. Resource for development and maintenance of method descriptions.
Hydrogeology	HydroNet	Execution of the hydrogeological modelling; constitutes a forum for all modellers within hydrogeology (needs of site modelling and safety assessment and repository engineering).
Hydrogeochemistry	ChemNet	Models the groundwater data from the sites and produces site descriptive hydrogeochemical models. Integrates the description with other disciplines and makes recommendations for further site investigations.
Bedrock transport properties	RetNet	Execution of the transport properties modelling; constitutes a forum for all transport-related modellers within site modelling and safety assessment.
Surface system	SurfaceNet	Models and describes the surface system by subdiscipline (biotic and abiotic), models the properties in a distributed way (maps and 3D), models the interdisciplinary processes (over space and time), describes the different ecosystems (conceptually and in site-specific terms), describes and models the flow of matter in the landscape, defines and connects the biosphere objects, and produces site descriptions to support environmental impact assessment (EIA).

1.6.4 Quality assurance aspects

In order to ensure that the site descriptive model builds on qualified data and that the model and sub-models derived from these qualified data are correct and are the models that are delivered to, and employed by, the downstream users, a number of quality assurance (QA) procedures and instructions in the SKB quality assurance system have been followed. The process to progress from collection of primary data to models available to the downstream users, as defined by the QA procedures and routines and applied in the site modelling, is summarised briefly below.

All primary data collected in the field and from laboratory measurements are stored in the SKB databases Sicada and GIS. Before delivery to the database operator, the data are reviewed and approved by the person responsible for the field activity providing the data (activity leader). The database operator transfers the data to the database and then makes an order of the same data from the database. The data export from the database is then checked by the database operator and the activity leader to ensure that no mistakes are made in the transfer of the data to the database. When everything is correct, the data are approved by the activity leader by signing the data. The execution of this process is specified in the SKB QA document SDK-508.

Primary data collected at the site and used in the site descriptive modelling are only extracted from the databases Sicada and GIS. Information regarding the procedures for data collection and circumstances of importance in the interpretation of data is given in the documentation (P-reports) of the data collection activity, but the hard data have to be ordered from the databases. Only data that are approved (signed) are allowed for delivery to users of the data. All orders and deliveries of data from the databases are registered, which means that it is possible to trace back all data deliveries. The execution of the process of order and delivery of data from the databases is specified in the SKB QA documents SD-112 (Sicada) and SD-113 (GIS).

Errors in data identified during the subsequent analytical and modelling work are reported by the modeller who discovers the error. The errors are compiled in a list that is published on SKB's internal web site. It is the responsibility of the users of the data to report all errors found and to be updated on the data errors reported. For all errors reported, the type of error is identified and corrective actions are taken. The actions taken are documented in the data error list and corrected data are transferred to the databases according to the procedure described above. The procedure for handling of errors in primary data is specified in the SKB QA document SDK-517.

The discipline-specific models developed within site modelling, using quality-assured data according to the procedures above, are stored in the SKB model database Simon. In this context, the term "models" refers to, for example, 3D models of the geometry of deformation zones, 2D models of surface objects, DFN model parameters. Before the models are officially released to downstream users, they are approved by the person who is responsible for a specific discipline at SKB. The only models that are allowed for further use by, for example, repository engineering and safety assessment are the approved versions downloaded from the model database. The model database is also used for internal deliveries within the site modelling project. All downloads of models in the database are registered, which means that it is possible to trace by whom, when and which model has been downloaded. Instructions for the use of the model database are compiled in the SKB QA document SDK-115.

The peer review of previous and the current model version conducted by SKB's own expert group Sierg and by the expert groups set up by the authorities (Insite and Oversite), as well as the list of issues of concern, continuously provided by the Insite group and responded to by SKB, are also important in a quality assurance context (see section 1.4).

1.6.5 Nomenclature

Some definitions are provided here for terms that are of basic importance for the modelling and description of the Forsmark site. Most of these are geological terms that are related to the geometrical framework of the modelling and are, as a consequence, common to all disciplines. The definitions of geological terms are based on section 2.4 in /Stephens et al. 2007/. Definitions of additional terms are provided in Appendix 2.

Candidate area/volume	The candidate area refers to the area at the ground surface that was recognised as suitable for a site investigation, following the feasibility study work /SKB 2000/. The extension at depth is referred to as the candidate volume.
Target area/volume	The target area/volume refers to the north-western part of the candidate area and the rock volume beneath that was selected during the site investigation process /SKB 2005c/ as potentially suitable for hosting a final repository for spent nuclear fuel.
Rock unit	A rock unit is defined on the basis of the composition, grain size and inferred relative age of the dominant rock type. Other geological features including the degree of bedrock homogeneity, the degree and style of ductile deformation, the occurrence of early-stage alteration (albitization) that affects the composition of the rock, and anomalous fracture frequency also help define and distinguish some rock units.
Rock domain	A rock domain refers to a rock volume in which rock units that show specifically similar composition, grain size, degree of bedrock homogeneity, and degree and style of ductile deformation have been combined and distinguished from each other. Different rock domains at Forsmark are referred to as RFMxxx.
Deformation zone	Deformation zone is a general term that refers to an essentially 2D structure along which there is a concentration of brittle, ductile or combined brittle and ductile deformation. Deformation zones at Forsmark are denoted ZFM followed by two to eight letters or digits. An indication of the orientation of the zone is included in the identification code.
Fracture zone	Fracture zone is a term used to denote a brittle deformation zone without any specification whether there has or has not been a shear sense of movement along the zone.
Fault zone	Fault zone is a term used for a fracture zone that shows a shear sense of movement along it.
Fracture domain	A fracture domain is a rock volume outside deformation zones in which rock units show similar fracture frequency characteristics. Fracture domains at Forsmark are denoted FFMxx.

1.7 This report and supporting documents

This report presents the integrated understanding of the Forsmark site at the completion of the surface-based investigations and provides a summary of the models and the underlying data supporting the site understanding. The report is intended to describe the properties and conditions at the site and to give the information essential for demonstrating this understanding, but relies heavily on background reports concerning details in data analyses and modelling. These background reports and their hierarchy in the SDM-Site reporting are illustrated in Figure 1-9 and further described below.

Chapter 2 in this description of the Forsmark site, SDM-Site, summarises available primary data and provides an overview of previous model versions and other prerequisites for the modelling. In chapter 3, the current understanding of the development of the geosphere and the surface system through time is described. Chapter 4 summarises the modelling of the surface system, with a focus on aspects of importance for the bedrock system. The integrated description of the surface system is provided in one of the background reports (see Figure 1-9 and text below). Chapters 5 to 10 provides summaries of the modelling of the bedrock geology, bedrock thermal properties, bedrock mechanics, hydrogeology, hydrogeochemistry and bedrock transport properties, respectively.

In chapter 11, the current understanding of the Forsmark site is summarised. It focuses on an integrated description that demonstrates consistency and, as such, it also functions as an executive summary for the SDM-Site. Chapter 12 provides the conclusions from the work in terms of fulfilment of objectives and a highlight of the most important issues judged to merit further study prior to and during the underground construction phase, in order to decrease the remaining uncertainties in the description of the target volume. Finally, it should be noted that a geographical map of the Forsmark area is provided in Appendix 1, where the location of different local geographical names that are referred to in the site description can be found.

The site descriptive modelling resulting in the final site description, SDM-Site, has involved two modelling stages. The first stage, denoted modelling stage 2.2, was based on data freeze 2.2 and resulted in the models that comprise the basis for the site description. The second stage, denoted modelling stage 2.3, utilised new data in data freeze 2.3 for verification and complementary analyses. The work conducted during modelling stages 2.2 and 2.3 is documented in discipline-specific background reports. The hierarchy of the reports is illustrated in Figure 1-9.

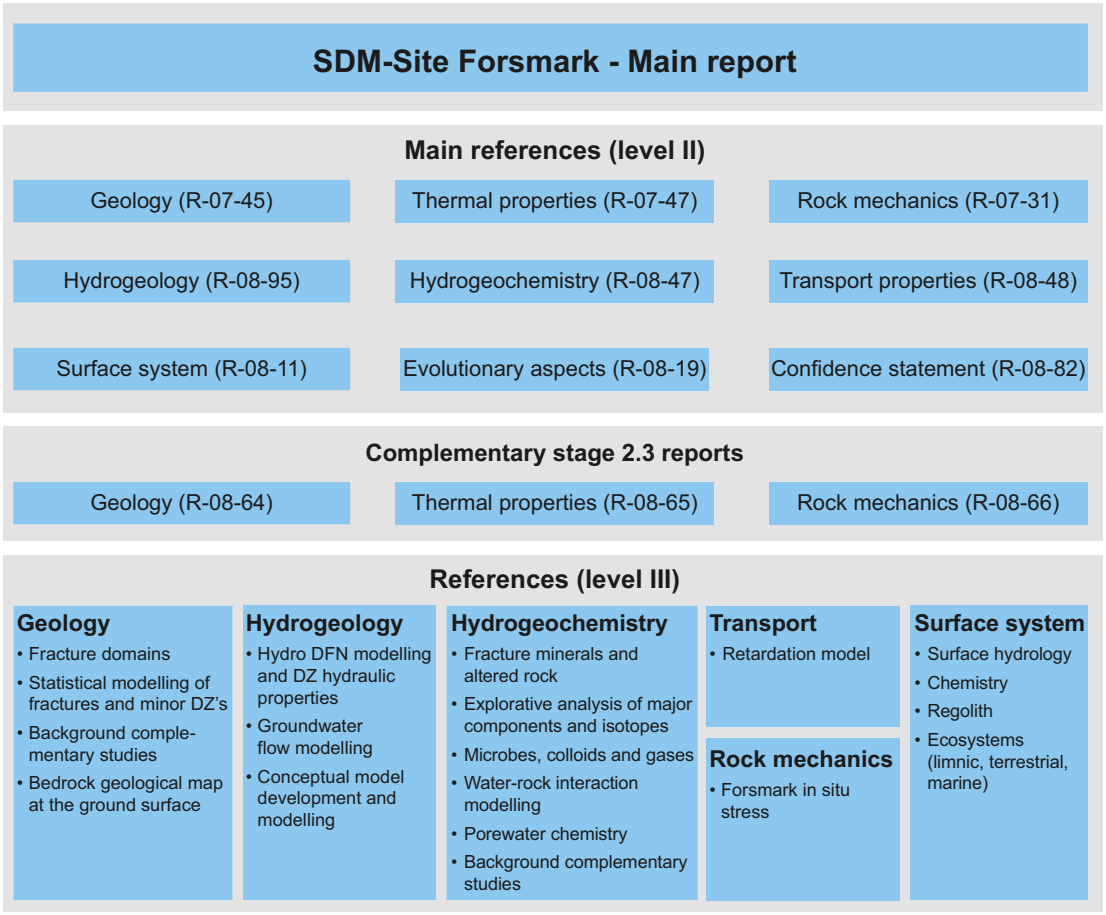

Figure 1-9. *SDM-Site main report and background reports on different levels produced during modelling stages 2.2 and 2.3.*

The primary downstream user of bedrock geology, bedrock thermal properties and bedrock mechanical properties, outside the site descriptive modelling team, is the repository engineering team who are responsible for the design of the underground repository. In order to be able to provide early input to repository engineering, the results of modelling stage 2.2 were reported prior to conducting the verification and complementary analysis in modelling stage 2.3. These reports comprise the main background reports for these disciplines as shown in Figure 1-9 (level II reports). The complementary analyses are documented in supporting stage 2.3 reports. The contents of these reports, which address the results of the verification and complementary analyses, are also important to the site description SDM-Site. For each of the remaining disciplines, the models derived based on data freeze 2.2 and the verification and complementary analyses during stage 2.3 are compiled in a single report that comprises the main background report for these disciplines (level II) to the SDM-Site report.

In addition to the discipline-specific background reports, there are two main background reports (level II) that provide important input to the site description. The procedure for, and results of, the confidence assessment of the site descriptive model are compiled in one of these reports. The other report, addressing evolutionary aspects, is compiled in common with the Laxemar-Simpevarp site modelling project and describes the long-term geological evolution, the palaeoclimate, and the post-glacial development of ecosystems and the human population at the two sites.

Bedrock hydrogeology, in terms of hydraulic properties of fractures and deformation zones, is also essential input to the design of the underground parts of a repository. For this reason, the results of analyses and modelling carried out during modelling stage 2.2 were reported in order to provide early input to repository engineering. The results are compiled in two background reports on level III (Figure 1-9), one documenting the hydraulic properties /Follin et al. 2007b/ and one the development of a conceptual flow model and the results of numerical implementation and calibration of the flow

model /Follin et al. 2007c/. Since the flow model with its calibrated hydraulic properties is also an essential input to the safety assessment, the stage 2.2 modelling as well as the verification and complementary modelling work carried out using new data in data freeze 2.3 are compiled in the main bedrock hydrogeology background report (level II).

As a complement to Figure 1-9, the background reports providing direct information to the site description SDM-Site are listed below.

- Geology Forsmark, Site descriptive modelling Forsmark stage 2.2 /Stephens et al. 2007/ (R-07-45).
- Thermal properties, Site descriptive modelling Forsmark stage 2.2 /Back et al. 2007/ (R-07-47).
- Rock mechanics Forsmark, Site descriptive modelling Forsmark stage 2.2 /Glamheden et al. 2007a/ (R-07-31).
- Bedrock hydrogeology Forsmark, Site descriptive modelling, SDM-Site Forsmark /Follin 2008/ (R-08-95).
- Bedrock hydrogeochemistry Forsmark, Site descriptive modelling, SDM-Site Forsmark /Laaksoharju et al. 2008a/ (R-08-47).
- Bedrock transport properties Forsmark, Site descriptive modelling, SDM-Site Forsmark /Crawford (ed) 2008/ (R-08-48).
- Surface systems Forsmark, Site descriptive modelling, SDM-Site Forsmark /Lindborg (ed) 2008/ (R-08-11).
- Geological evolution, palaeoclimate and historical development of the Forsmark and Laxemar-Simpevarp areas, Site descriptive modelling, SDM-Site /Söderbäck (ed) 2008/ (R-08-19).
- Confidence assessment Forsmark, Site descriptive modelling, SDM-Site Forsmark /SKB 2008/ (R-08-82).
- Bedrock geology Forsmark, modelling stage 2.3. Implications for and verification of the deterministic geological models based on complementary data /Stephens et al. 2008/ (R-08-64).
- Thermal properties Forsmark, modelling stage 2.3. Complementary analysis and verification of the thermal bedrock model /Sundberg et al. 2008/ (R-08-65).
- Rock mechanics Forsmark, modelling stage 2.3. Complementary analyses and verification of the rock mechanics model /Glamheden et al. 2008/ (R-08-66).

2 Investigations, available data and other prerequisites for modelling

Since the start of the site investigations in January 2002, successively more data have been added to the databases used in site descriptive modelling. The modelling has now reached the final integrated model version. This chapter provides a summary of the investigations behind the databases used for modelling.

A short overview of all investigations carried out at Forsmark is presented in section 2.1. More detailed comments on the different investigations in sections 2.2 to 2.4 are limited to the investigations performed after the first comprehensive modelling, which was undertaken during 2004−2005 and followed the investigation stage completed at data freeze 1.2, i.e. this chapter primarily addresses the investigations carried out during the period July 31st 2004 to March 30th 2007. Earlier investigations are described in more detail in /SKB 2005a/. Some investigations were planned or occurred at a late stage and could not be delivered in time for data freeze 2.3. As a consequence, special efforts were made to include all relevant and indispensable data in the final models or, if excluded, assess the implications for the final model version. This point is further commented on in sections 2.2 and 2.3. Geographical data and other data sources for the modelling work are presented in sections 2.5 and 2.6, respectively.

All reports belonging to the P-series[1] produced during the site investigation work are listed in Appendix 3. The P-reports display data or references to data in the SKB Sicada and GIS databases and also present descriptions of the execution of these investigations and other features. In this chapter, references are given to actual data sources (see section 2.7 and Appendix 3), but data *per se* are provided in only a few instances and the reader is referred to chapters 4 to 10 and /Söderbäck (ed) 2008/ for more details. Finally, a short summary of the model versions elaborated prior to stages 2.2 and 2.3 is presented in section 2.8 and the locations of the areas and volumes adopted in the modelling work are defined in section 2.9. Where it concerns minor nonconformities in relation to the programme for drilling and borehole investigations, the reader is referred to the respective P-reports listed in Appendix 3.

2.1 Overview of investigations

2.1.1 Investigations and primary data acquired up to data freeze 1.2

Besides "older" data already included in model version 0, the data used in model version 1.2 /SKB 2005a/ were acquired from the start of the site investigations at the beginning of 2002 until July 31st 2004, and include data from data freezes 1.1 and 1.2. The data acquisition comprised three main categories of investigations, and this investigation structure was also applied during the succeeding data freezes. The three investigation categories were:

1) Geoscientific and ecological investigations of the surface system. These included the compilation of bedrock and Quaternary cover geological maps.
2) Borehole investigations. They comprised:
   a. Drilling of long, so-called telescopic boreholes (the upper c. 100 metres are percussion drilled whereas the remainder is core drilled), conventionally drilled cored boreholes, percussion boreholes and shallow boreholes through Quaternary deposits.
   b. Measurements carried out during drilling, investigations of drill cores and drill cuttings during and after drilling, and down-hole logging. One example of these investigations is the geological mapping of boreholes using the Boremap system.
   c. Sampling of intact rock material for several types of laboratory investigations.

[1] The reports in the P-series present the results of the site investigations at Forsmark and Laxemar-Simpevarp. The P-reports are available at the SKB web site together with the reports in the R- and TR-series (www.skb.se).

3) Monitoring of geoscientific parameters and ecological objects. Monitoring has expanded successively during the entire site investigation period. The previous monitoring activities as well as the planned future monitoring after completion of the site investigations are presented in /SKB 2007/.

The extent and character of data acquisition up to data freeze 1.2 are described in detail in /SKB 2005a/ and in the associated P-reports.

2.1.2 Investigations and primary data aquired at data freezes 2.1, 2.2 and 2.3

The investigations associated with data collection during the period between data freezes 1.2 and 2.3 comprised the three main categories of investigations mentioned in the previous section. Summaries of these investigations are presented in sections 2.2 to 2.4. These summaries include data that became available after data freeze 2.3, here referred to as "late" data. In accordance with the earlier investigations, the data acquisition was logistically and administratively subdivided into three data freezes: data freeze 2.1 (July 29th 2005), 2.2 (September 30th 2006) and 2.3 (March 30th 2007). Following each of these data freezes, analytical and modelling work was completed. The major modelling activities were based on data from data freeze 2.2, whereas new data in data freeze 2.3 and also, if possible, "late" data have been used primarily for model verification purposes and complementary analysis work.

Several of the field investigations had rather long execution periods, sometimes overlapping the data freeze dates, and the time span for some field investigations, data evaluation and delivery of P-reports exceeded the data freeze time limit. For this reason, and since all data have been used in the final modelling work, no subdivision into data freezes is carried out in the presentation below, except regarding "late" data, i.e. data that were not available until after data freeze 2.3.

The major part of the site investigations after data freeze 1.2 has been performed in compliance with the programme report for completion of the site investigations /SKB 2005c/. However, this report only provides a general framework for the activities. The detailed strategy regarding, for example, localisation of new boreholes, selection of borehole sections for groundwater sampling, layout design for ground geophysical measurements etc was, to a large extent, established according to an iterative process, where previous results guided subsequent decisions concerning continued investigations. This process involved a close integration between the site investigation and site modelling working teams. Important decisions regarding investigation strategy have always been substantiated in so-called decision documents, which are registered in SKB's internal documentation database "SKBdoc" and as appendices in model reports.

2.2 Investigations of the surface system

The investigations of the surface system carried out between data freezes 1.2 and 2.3 involved the following disciplines:

1. Bedrock geology and ground geophysics,
2. Quaternary geology and ground geophysics,
3. Surface ecology.

In this section, the investigations that have generated the new data sets are presented. Geophysical data are treated together with bedrock or Quaternary geological data, due to their close interrelation with the geological information.

2.2.1 Bedrock geology and ground geophysics

Investigations performed between data freeze 1.2 and 2.3

After the mapping of rock units, ductile structures and fractures at the surface during the initial site investigation up to data freeze 1.2, the geological investigations in the Forsmark area have focused on adding new insight on brittle structures at depth using *reflection seismic measurements, refraction seismic measurements* and *lineament characterisation*. Other investigations, including

complementary *detailed mapping of fractures in the bedrock that is not transected by lineaments close to drill site 7* and *transient electromagnetic soundings*, have also been completed.

Stage 1 high-resolution measurements of *reflection seismics*, which were performed in 2002, were followed up by similar measurements during autumn 2004. In total, 25 km of profiles were measured during stage 2. The new profiles focused on areas outside the Forsmark tectonic lens and are situated north (up to the Biotest lake) and west (up to and beyond road 76) of the candidate area.

During the period May 2005 to March 2006, *a major refraction seismic survey* was completed, aiming at mapping the P-wave velocity in the bedrock material, as an aid in the identification of the presence of fracture zones and other possible low-velocity anomalies. Thirty-one profiles covered the area north-west of Lake Bolundsfjärden with a relatively dense net of measurement profiles, whereas the measurements within the areas surrounding Lake Bolundsfjärden to the east, west and south of this lake involved a less dense profile net. A couple of profiles were also studied across Lake Bolundsfjärden. The total profile length was 23.2 km.

Lineament characterisation, which is important for the identification of steeply dipping fracture zones, has been achieved by three main methods. Firstly, high-resolution ground magnetic measurements were carried out on an 11.1 km^2 area within the Forsmark investigation site. The main objective of the measurements was to provide a detailed ground magnetic representation of the bedrock. The second method was to excavate trenches across previously identified lineaments. Three trenches were machine-excavated and the bedrock surface uncovered. Two of the trenches were cut approximately perpendicular to each other close to the road between drill sites 2 and 6, and one trench was situated north-east of drill site 7 (Figure 2-1 and Figure 2-2 in section 2.3). The bedrock surface was carefully studied and the rock type and fracture distribution mapped. Ground geophysical measurements (detailed magnetometry, continuous vertical electric sounding and ground penetrating radar) were also performed on the exposed rock surface. The third strategy to characterise lineaments was to identify their inferred continuation as geological anomalies at depth by drilling.

An area was excavated south of drill site 7 (Figure 2-1 and Figure 2-2 in section 2.3) to carry out *complementary detailed mapping of fractures in the bedrock not transected by lineaments*. The same detailed geophysical measurements as those completed along the excavations across lineaments were performed at this site.

Seven *transient electromagnetic soundings* were conducted at locations inside and to the west and south of the candidate area. These measurements were carried out to provide estimates of the depth to saline groundwater.

All the investigations described above, together with the previously performed surface bedrock mapping and other investigations, have resulted in bedrock geological and geophysical data at the surface of high density and quality. The locations of excavations where fracture mapping has been carried out, areas where high-resolution ground magnetic data have been acquired, reflection seismic profiles and refraction seismic profiles are presented in sections 5.2.5, 5.2.7, 5.2.8 and 5.2.9, respectively, in connection with the evaluation of primary geological and geophysical data.

Data and/or P-reports available after data freeze 2.3

P- or R-reports from some of the surface *geological/geophysical investigations* and, in two cases also data did not become available until after data freeze 2.3. These activities are:

- Detailed ground magnetic survey and lineament interpretation carried out during the later part of 2006 and 2007 in the Forsmark area,
- Bedrock mapping and magnetic susceptibility measurements along trench AFM001265 for verification of lineament XFM0159A0 (only P-report),
- Detailed fracture mapping of excavated outcrop AFM001264 at drill site 7 (only P-report),
- Transient electromagnetic soundings at Forsmark and in the surrounding region.

An R-report that presented the results of an assessment of the validity of rock domain model version 1.2, based on the modelling of gravity and petrophysical data, was also completed after data freeze 2.3. However, no new data were generated in this study.

2.2.2 Quaternary geology and ground geophysics

Investigations performed between data freeze 1.2 and 2.3

Investigations of Quaternary deposits were initiated in 2002 and continued during 2003 and 2004. After data freeze 1.2, an effort has been directed towards the *completion of the Quaternary geological map in the shallow offshore area* and towards *stratigraphic studies*. The most important investigations are described briefly below.

The *mapping of Quaternary deposits* was completed with investigations of the bottom sediments in shallow bays offshore the coast at Forsmark. The results fill the gap between the previously produced map of Quaternary deposits on land and the marine geological map. The latter covers areas with a water depth exceeding 3 m. The mapping was performed by coring and probing from the sea ice and from a small boat. The resulting map includes 140 stratigraphic descriptions.

Stratigraphic investigations in the two machine-excavated trenches between drill sites 2 and 6 (see section 2.2.1) were carried out. Furthermore, samples from a total of 21 cores, most of them located inside the candidate area, were investigated in order to gain additional information on the Quaternary stratigraphy. Lithostratigraphic sampling, sample analysis and descriptions of Quaternary deposits were conducted on cores from three different types of wetlands and from some locally elevated sites within the Forsmark regional model area (see Figure 2-5).

Bio- and lithostratigraphic analyses were also made of a 6 m long sediment core collected offshore from Forsmark, relatively close to the island of Gräsö. The investigation provided data on, for example, sediment and organic carbon accumulation rates during different stages of Baltic Sea development, salinity distribution with time, sediment grain size composition and contents of carbonate.

Overall, a large number of observation points have provided data bearing on the depth and stratigraphy of Quaternary deposits at Forsmark.

Data and/or P-reports available after data freeze 2.3

As far as *Quaternary geology/geophysical investigations* are concerned, the following activity delivered data and a P-report after data freeze 2.3:

- Supplementary drilling for determination of regolith thickness in the area close to the sewage treatment plant at Forsmark (see map in Appendix 1).

2.2.3 Surface ecology

Investigations performed between data freeze 1.2 and 2.3

A variety of surface ecological investigations completed during the period from autumn 2004 to autumn 2007 are briefly described below.

Characterisation of the aquatic systems has been an essential part of the ecological investigations and has included, for example, inventories of the benthic macrofauna, the plant-associated macrofauna and the benthic vegetation in two shallow lakes. An investigation of the fish fauna in the Baltic Sea off the coast of Forsmark was also carried out. Furthermore, measurements of biomass and primary production, respiration and distribution of submerged vegetation in Lake Bolundsfjärden, as well as measurements of phytobenthic production and respiration in shallow bays and along shores in the Öregrundsgrepen area were performed.

Investigations of *ground layer respiration and primary production within the soil and ground layer* of seven terrestrial vegetation types have been completed. These studies were carried out within the Forsmark regional model area, partly inside the candidate area, and partly outside it, to the south-west and south-east.

Nineteen wetlands within the Forsmark regional model area were investigated and classified, from bogs to extremely rich fens, according to the composition of vascular plants. The majority of the investigated wetlands are situated within the candidate area.

Chemical analyses of 114 samples of deposits and biota were conducted. The samples from deposits consisted of sediment, peat and soil, whereas the biota samples were collected from both terrestrial

and limnic environments. Besides the contents of the macro-nutrients carbon, nitrogen and phosphate, all samples were analysed for 51 chemical elements. Furthermore, the biota samples were analysed for 10 additional elements (eight metals, P and Si), whereas the contents of the corresponding ten oxides (i.e. of the same eight metals, P and Si) were determined in the deposit samples except peat.

Determinations of *ground vegetation, surface organic layer and stoniness conditions* were made over two machine-cut trenches between drill sites 2 and 6 (Figure 2-1). Further studies involved rooting depth, soil-profile development, soil physical conditions of the regolith and chemical properties including soil acidity through pH measurements, as well as C, N and P contents and concentrations of alkaline earth cations.

The *distributions of live and dead fine roots and live/dead root ratios* were analysed for trees and field layer species at three forest stands representing different vegetation types at Forsmark. Samples were collected for analysis in the middle part of the candidate area, between Lake Bolundsfjärden and Storskäret (Figure 2-1). Data from the investigations are presented in /Persson and Stadenberg 2007/.

An investigation was made which provided *estimates of annual inputs of above-ground litter* from trees (dry mass and amounts of C and N), litter decomposition and changes in organic and inorganic components in litter during decomposition. The investigated areas are situated within the candidate area between Lake Bolundsfjärden and Storskäret.

The process of material displacement, so-called bioturbation, by earthworms and ants was investigated in areas situated within the candidate area between Lake Bolundsfjärden and Storskäret, as well as east and south-east of Storskäret and outside the candidate area to the south-west.

Seventeen environmental samples were collected within the Forsmark regional model area *and were analysed for several artificial and naturally occurring radioisotopes*. The samples included soil, sediment as well as plant and animal species from terrestrial, limnic and marine environments.

Finally, *a selection of terrestrial mammals was surveyed* with snow tracking along line transects, snow tracking along shorelines of lakes and water courses, aerial survey and faecal pellet counts within and close to the Forsmark regional model area and in the Hållnäs area north-west of Forsmark. The investigations provided density data for fourteen wild species, as well as for cats and dogs, within the investigated areas.

Data and/or P-reports available after data freeze 2.3

Surface ecological investigations that gathered data and/or P-reports after data freeze 2.3 were:

- Analyses of biogenic silica in sediment from Lake Eckarfjärden.
- A study of the distribution of fine roots in forest areas close to the Forsmark nuclear power plant.
- Input and turnover of forest tree litter in the Forsmark area.
- A survey of mammal populations in the areas adjacent to Forsmark.

2.3 Borehole investigations

The performance and technical design of different types of boreholes drilled during the site investigation at Forsmark, comprising telescopic boreholes, core-drilled boreholes of standard type, percussion-drilled boreholes in solid bedrock and shallow boreholes through Quaternary deposits (also designated soil boreholes) are fully described in SKB's method documents SKB MD 620.003, 610.003 and 630.003, as well as in, for example, /SKB 2005a/. Furthermore, detailed descriptions of each individual borehole are provided in the associated P-reports.

The locations of all telescopic, conventionally core-drilled and percussion-drilled boreholes produced during the site investigation, i.e. up to data freeze 2.3, are presented in Figure 2-1. Figure 2-2 provides a more detailed view of the twelve drill sites for deep boreholes, whereas all soil boreholes supplied with a groundwater stand-pipe are shown in Figure 2-3, where the drilling progress according to the data freeze sequence is also illustrated. Some geometrical borehole characteristics are displayed in Table 2-1 for telescopic and conventionally core-drilled boreholes and in Table 2-2 for percussion-drilled holes.

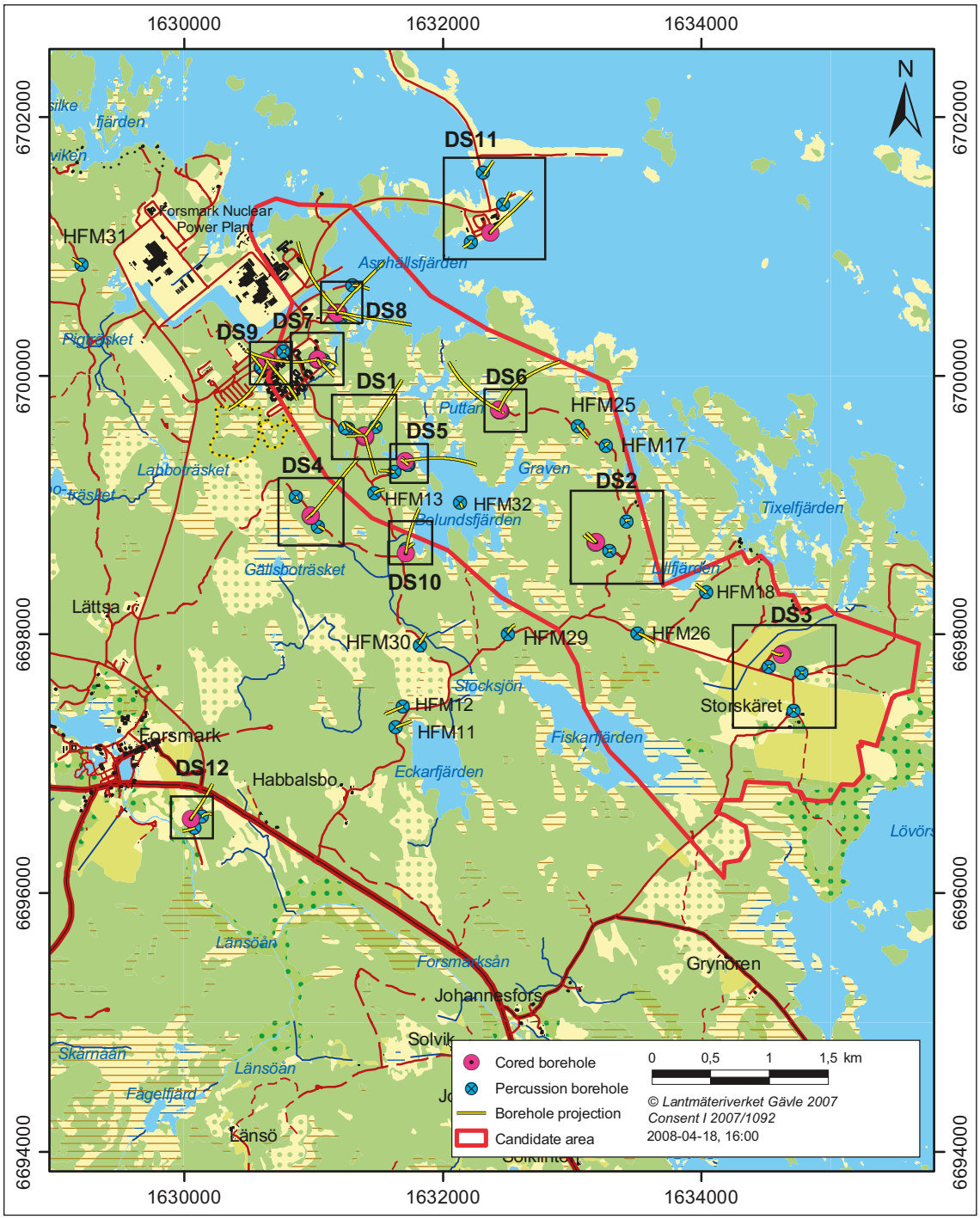

Figure 2-1. *All telescopic, conventionally core-drilled and percussion-drilled boreholes produced during the site investigation at Forsmark 2002–2007. The projection of the boreholes on the ground surface due to their inclination is also shown.*

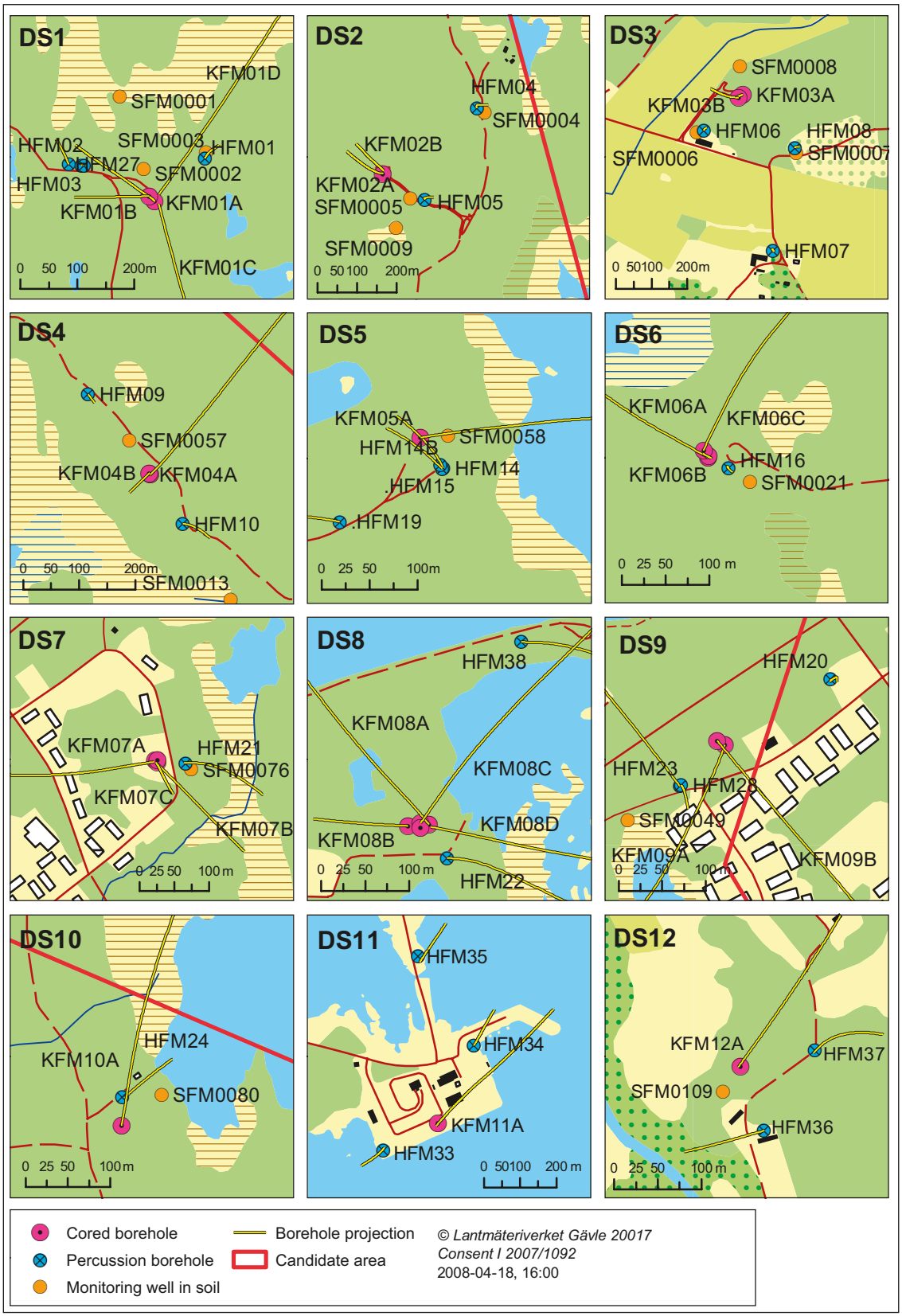

Figure 2-2. *Detailed maps of each drill site that show the location and projection of core- and percussion-drilled boreholes. Soil boreholes through the Quaternary deposits at or close to the drill sites are also included. The majority of the soil boreholes (see Figure 2-3) are supplied with groundwater stand pipes enabling groundwater level and hydrogeochemical monitoring.*

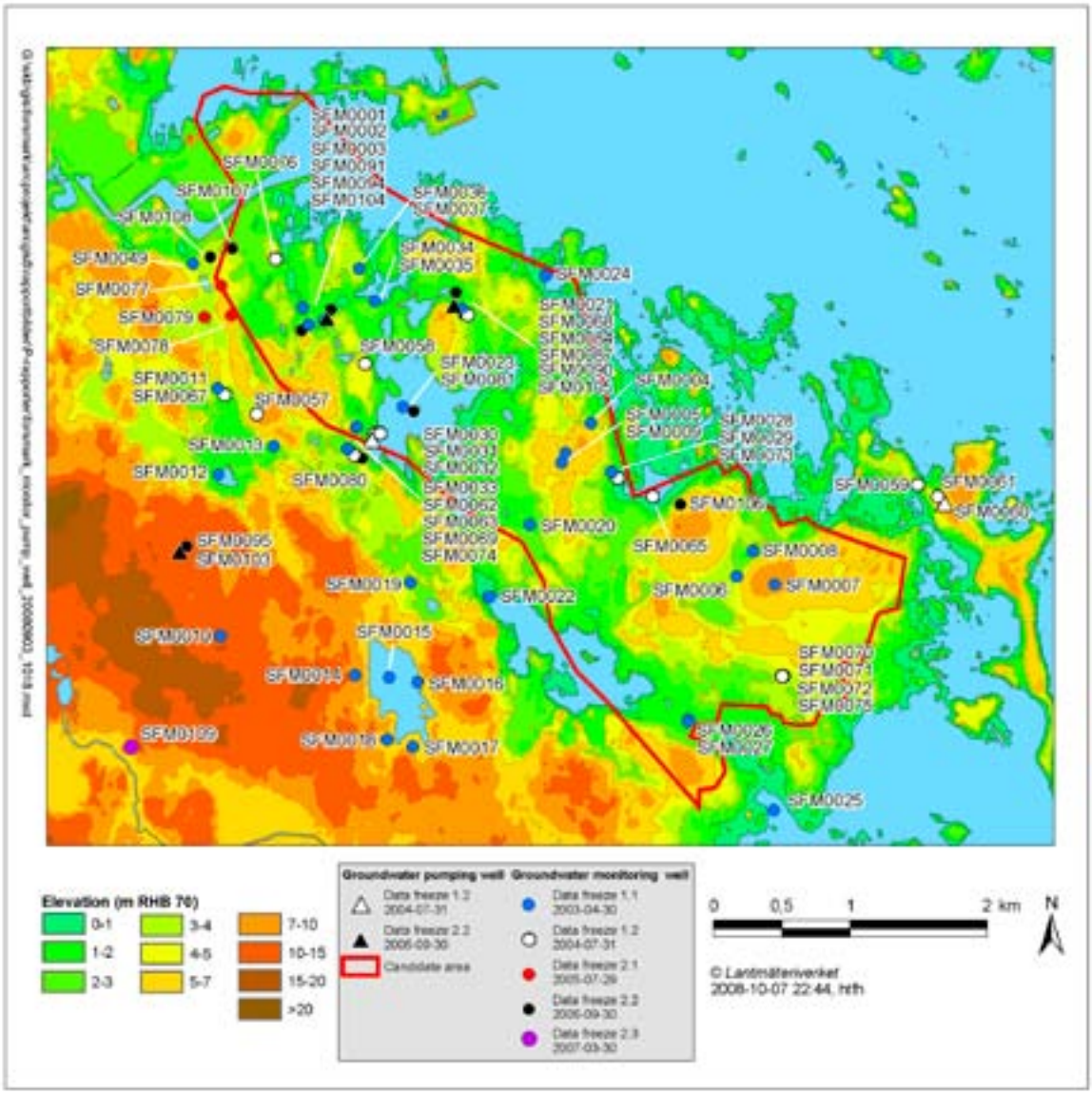

Figure 2-3. *Elevation map showing existing soil boreholes at Forsmark supplied with groundwater stand-pipes. Many of the soil boreholes penetrate the uppermost part of the bedrock. Fifty of the boreholes are included in the groundwater level monitoring programme and eighteen in the hydrogeochemical programme (see section 2.4.2).*

A major quality revision was undertaken between autumn 2006 and autumn 2007 that concerned the orientation of geological structures encountered in boreholes, for example fractures and rock contacts. These structures are identified during borehole logging with the so-called Borehole Imaging Processing System (BIPS), a down-hole video camera system which, together with inspection of the drill core or, for percussion boreholes, drill cuttings, is used to provide so-called Boremap mapping of cored and percussion-drilled boreholes. During processing of the images, the orientation of identified geological structures is calculated. The revision was initiated due to a technical problem identified in connection with performance of the BIPS logging procedure. This problem caused the uncertainty of the orientation determinations in some borehole sections to be unacceptably high. The quality revision comprised a re-check of all previously performed BIPS loggings and a correction of the errors identified /Döse et al. 2008/.

Due to physical/technical factors, all core-drilled and percussion-drilled boreholes deviate more or less from the initial inclination and direction at the top of the casing. For this reason, the borehole geometry cannot be described only by extrapolation of inclination and bearing at the borehole

collar, but down-hole deviation measurements have to be conducted. Precise borehole deviation measurements are crucial for allotting data from different surveys of borehole logging into correct positions in space. Furthermore, the accuracy of the orientation determinations of geological structures encountered in boreholes is dependent, not only on correct data from BIPS logging and processing, but also on the accurate measurement of borehole deviation. A high quality of borehole orientation data is essential for the modelling of, for example, rock domains and deformation zones (see chapter 5), i.e. the fundamental geometrical configuration of geological structures at the site (see Figure 1-7). For these reasons, a quality revision was conducted also for borehole deviation measurements /Nilsson and Nissen 2007/. Since full-scale calibration of the deviation logging equipment is seldom possible, the only available quality measure is reproducibility, i.e. comparison of several deviation loggings in the same borehole. A new strategy for processing deviation measurements was introduced which permits a combination of data from several deviation measurements. In connection with the revision work, improved deviation data replaced older, less reliable data.

In combination, these measures resulted in a significant quality upgrading, both regarding orientation data for geological structures and for borehole deviation data. Another important result of the revision was the introduction of uncertainty estimates for the parameters mentioned above /Munier and Stigsson 2007/. Two measures of the uncertainty of borehole geometry, elevation uncertainty and radial uncertainty, are shown in Table 2-1 and Table 2-2 for two or three levels in each borehole. Figure 2-4 illustrates the principles behind computing the borehole deviation, i.e. the borehole geometry, from several measurements, and also displays the concept of radial uncertainty. The results of the revision of borehole geometry and orientation of rock structures of primary importance for the modelling emerged during spring 2007, whereas the final results, including reporting, were not available until late in the site investigation, i.e. after data freeze 2.3.

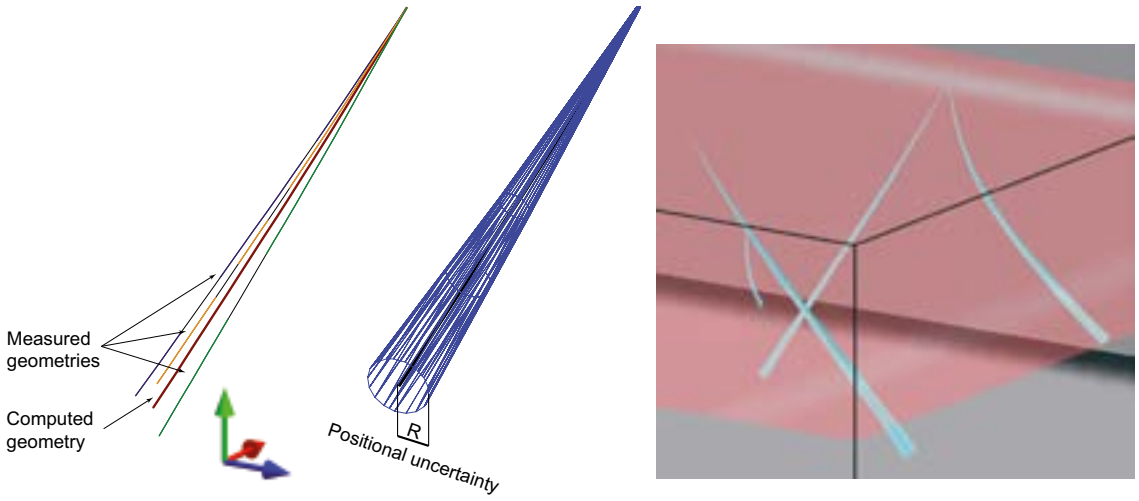

Figure 2-4. *The figure to the left is an illustration of the principles for calculating the borehole geometry from several deviation measurements. The two other figures illustrate one of the uncertainty measures introduced in connection with the SKB revision of borehole orientations. In the middle figure, "R" denotes "Radial uncertainty", representing a function, which monotonously increases with depth along the borehole axis, defining the shape of a cone surrounding the borehole axis and corresponding to the parameter in the column furthest to the right in Table 2-1 and Table 2-2. The figure to the right is a block diagram imaging four fictitious boreholes deviating in different ways and with radius uncertainty illustrated as blue cones (modified after Figures 4-1, 5-1 and 5-3 in /Munier and Stigsson 2007/).*

Table 2-1. Borehole length, elevation, inclination and bearing of all telescopic and conventionally core-drilled boreholes at Forsmark (except the short cored boreholes KFM90A–E). These borehole parameters are provided for TOC (Top Of Casing) and borehole bottom and also for repository depth (c. 400–500 m) for the boreholes that extend beyond this depth. Furthermore, both the elevation uncertainty and radial uncertainty (see illustration in Figure 2-4) are presented.

Borehole	Length (m)	Elevation (m RHB 70*)	Elevation uncertainty (m)	Inclinat. (degrees from horizon)	Bearing (degrees RT 90*)	Radial uncertainty (m)
KFM01A	0.00	3.13	0.00	–84.73	318.35	0.00
KFM01A	507.00	–499.82	1.99	–80.32	305.73	15.93
KFM01A	1,001.49	–982.27	5.37	–75.01	307.13	31.46
KFM01B	0.00	3.09	0.00	–79.04	267.59	0.00
KFM01B	500.52	–479.34	4.14	–71.46	271.34	15.72
KFM01C	0.00	2.91	0.00	–49.61	165.35	0.00
KFM01C	450.02	–332.70	0.71	–45.87	164.53	2.16
KFM01D	0.00	2.95	0.00	–54.90	35.03	0.00
KFM01D	510.00	–400.96	2.33	–48.55	32.47	4.10
KFM01D	800.24	–612.48	3.82	–45.09	31.17	6.72
KFM02A	0.00	7.35	0.00	–85.38	275.76	0.00
KFM02A	510.00	–500.94	0.25	–84.31	304.44	3.57
KFM02A	1,002.44	–988.85	0.65	–80.53	314.49	9.23
KFM02B	0.00	7.62	0.00	–80.27	313.06	0.00
KFM02B	414.00	–400.65	0.22	–80.09	316.85	1.99
KFM02B	573.87	–557.89	0.31	–79.17	314.60	2.83
KFM03A	0.00	8.29	0.00	–85.75	271.52	0.00
KFM03A	510.00	–500.02	1.30	–84.42	281.96	16.02
KFM03A	1,001.19	–988.17	3.01	–82.74	300.65	31.45
KFM03B	0.00	8.47	0.00	–85.30	264.49	0.00
KFM03B	101.54	–92.67	0.28	–84.57	268.74	3.19
KFM04A	0.00	8.77	0.00	–60.08	45.24	0.00
KFM04A	474.00	–399.09	1.55	–54.11	38.29	3.57
KFM04A	1,001.42	–796.41	3.79	–44.18	40.84	8.70
KFM05A	0.00	5.53	0.00	–59.81	80.93	0.00
KFM05A	600.00	–500.62	1.50	–54.80	94.32	9.58
KFM05A	1,002.71	–827.10	2.60	–53.10	108.22	16.60
KFM06A	0.00	4.10	0.00	–60.25	300.92	0.00
KFM06A	594.00	–500.77	3.22	–55.76	315.44	6.12
KFM06A	1,000.64	–827.47	5.71	–51.07	331.36	10.38
KFM06B	0.00	4.13	0.00	–83.52	296.96	0.00
KFM06B	100.33	–95.56	0.36	–83.60	298.44	3.15
KFM06C	0.00	4.09	0.00	–60.12	26.07	0.00
KFM06C	621.00	–500.25	4.06	–49.20	60.49	7.43
KFM06C	1,000.91	–781.42	6.94	–44.86	73.70	12.60
KFM07A	0.00	3.33	0.00	–59.29	261.47	0.00
KFM07A	594.00	–499.65	0.41	–54.98	279.13	3.30
KFM07A	1,002.10	–820.94	0.74	–46.53	297.29	5.92
KFM07B	0.00	3.36	0.00	–54.74	134.35	0.00
KFM07B	298.93	–237.91	5.31	–53.56	134.64	9.00
KFM07C	0.00	3.35	0.00	–85.33	142.71	0.00
KFM07C	500.34	–494.35	0.27	–84.22	146.55	3.01
KFM08A	0.00	2.49	0.00	–60.85	321.00	0.00
KFM08A	621.00	–500.88	5.10	–47.61	331.38	8.76
KFM08A	1,001.19	–759.40	9.03	–37.66	346.31	14.12
KFM08B	0.00	2.25	0.00	–58.85	270.45	0.00
KFM08B	200.54	–166.86	0.38	–56.10	275.99	3.27
KFM08C	0.00	2.47	0.00	–60.48	35.88	0.00
KFM08C	597.00	–498.90	0.25	–54.38	45.21	4.46

Borehole	Length (m)	Elevation (m RHB 70*)	Elevation uncertainty (m)	Inclinat. (degrees from horizon)	Bearing (degrees RT 90*)	Radial uncertainty (m)
KFM08C	951.08	–780.81	0.42	–51.16	42.18	7.42
KFM08D	0.00	2.61	0.00	–55.19	99.98	0.00
KFM08D	621.00	–499.43	0.19	–52.27	98.45	3.83
KFM08D	942.30	–748.28	0.30	–49.27	98.89	5.96
KFM09A	0.00	4.29	0.00	–59.46	200.08	0.00
KFM09A	624.00	–499.85	1.28	–47.00	229.83	11.29
KFM09A	799.67	–621.21	1.72	–40.79	238.70	15.20
KFM09B	0.00	4.30	0.00	–55.08	140.83	0.00
KFM09B	616.45	–472.00	8.91	–42.85	150.96	14.09
KFM10A	0.00	4.51	0.00	–50.13	10.42	0.00
KFM10A	500.16	–338.08	2.69	–34.87	24.77	4.28
KFM11A	0.00	2.95	0.00	–60.94	40.25	0.00
KFM11A	585.00	–501.05	5.40	–54.55	45.83	10.67
KFM11A	851.21	–713.24	8.33	–51.43	43.64	15.53
KFM12A	0.00	10.74	0.00	–60.56	36.20	0.00
KFM12A	480.00	–400.99	5.42	–56.67	28.51	10.55
KFM12A	601.40	–501.49	6.92	–55.11	25.82	13.22

* see section 2.5 for definitions of the coordinate system

Table 2-2. Borehole length, elevation, inclination and bearing of all percussion-drilled boreholes in solid rock at Forsmark. These borehole parameters are provided for TOC (Top Of Casing) and borehole bottom. Furthermore, both the elevation uncertainty and radial uncertainty (see illustration in Figure 2-4) are presented.

Borehole	Length (m)	Elevation (m RHB 70*)	Elevation uncertainty (m)	Inclinat. (degrees from horizon)	Bearing (degrees RT 90*)	Radial uncertainty (m)
HFM01	0.00	1.73	0.00	–77.51	34.06	0.00
HFM01	200.20	–195.35	1.09	–77.06	53.45	6.29
HFM02	0.00	3.05	0.00	–87.79	6.52	0.00
HFM02	100.00	96.86	0.13	–87.91	27.52	3.14
HFM03	0.00	3.15	0.00	–87.28	264.53	0.00
HFM03	26.00	–22.81	0.04	–86.56	267.87	0.82
HFM04	0.00	3.87	0.00	–84.53	336.87	0.00
HFM04	221.70	–214.15	1.11	–70.30	93.70	6.96
HFM05	0.00	7.67	0.00	–84.93	335.59	0.00
HFM05	200.10	–189.91	0.87	–72.20	94.90	6.29
HFM06	0.00	6.64	0.00	–84.80	2.44	0.00
HFM06	110.70	–103.30	0.40	–80.00	87.30	3.48
HFM07	0.00	5.78	0.00	–84.51	342.32	0.00
HFM07	122.50	–115.88	0.39	–77.25	139.00	3.85
HFM08	0.00	7.13	0.00	–84.67	348.69	0.00
HFM08	143.50	–135.30	0.49	–77.80	87.35	4.51
HFM09	0.00	5.15	0.00	–69.00	139.36	0.00
HFM09	50.25	–41.39	0.60	–66.70	141.50	1.64
HFM10	0.00	4.99	0.00	–68.95	92.93	0.00
HFM10	150.00	–134.11	1.76	–64.50	132.40	4.93
HFM11	0.00	7.56	0.00	–49.26	63.51	0.00
HFM11	182.35	–117.91	4.14	–35.60	68.90	11.27
HFM12	0.00	7.03	0.00	–49.33	245.16	0.00
HFM12	209.55	–136.71	4.77	–36.80	246.90	12.98
HFM13	0.00	5.69	0.00	–58.97	51.19	0.00
HFM13	175.60	–146.81	2.73	–58.30	85.60	7.44

Borehole	Length (m)	Elevation (m RHB 70*)	Elevation uncertainty (m)	Inclinat. (degrees from horizon)	Bearing (degrees RT 90*)	Radial uncertainty (m)
HFM14	0.00	3.91	0.00	–59.95	331.75	0.00
HFM14	150.50	–127.33	2.31	–58.90	307.10	6.29
HFM15	0.00	3.88	0.00	–44.25	314.31	0.00
HFM15	99.50	–65.51	2.24	–42.15	298.55	6.09
HFM16	0.00	3.21	0.00	–84.26	327.96	0.00
HFM16	132.50	–128.53	0.38	–77.50	126.20	4.16
HFM17	0.00	3.75	0.00	–84.44	318.58	0.00
HFM17	210.65	–203.90	1.05	–75.80	65.50	6.62
HFM18	0.00	5.04	0.00	–59.18	313.30	0.00
HFM18	180.65	–142.71	3.26	–49.90	303.82	8.87
HFM19	0.00	3.66	0.00	–58.30	280.91	0.00
HFM19	185.20	–143.94	3.51	–49.90	274.62	9.54
HFM20	0.00	2.97	0.00	–85.45	354.41	0.00
HFM20	301.00	–297.58	0.49	–86.20	229.02	9.45
HFM21	0.00	3.98	0.00	–58.48	88.81	0.00
HFM21	202.00	–153.37	3.95	–40.90	127.02	10.75
HFM22	0.00	1.54	0.00	–58.85	90.08	0.00
HFM22	222.00	–155.59	4.84	–34.00	115.82	13.17
HFM23	0.00	4.25	0.00	–58.94	324.35	0.00
HFM23	211.50	–72.78	0.82	9.35	319.53	1.03
HFM24	0.00	3.68	0.00	–59.56	47.29	0.00
HFM24	151.35	–129.28	2.26	–65.61	55.94	6.14
HFM25	0.00	3.86	0.00	–57.81	140.84	0.00
HFM25	187.50	–134.10	3.95	–38.42	137.65	10.74
HFM26	0.00	2.73	0.00	–53.75	112.42	0.00
HFM26	202.70	–144.06	4.38	–42.10	122.34	11.91
HFM27	0.00	2.44	0.00	–67.83	337.26	0.00
HFM27	127.50	–115.00	1.56	–67.13	327.89	4.24
HFM28	0.00	4.27	0.00	–84.76	146.78	0.00
HFM28	151.20	–143.77	0.92	–72.21	169.14	4.75
HFM29	0.00	4.47	0.00	–58.57	29.95	0.00
HFM29	199.70	–177.91	2.50	–71.51	70.45	7.04
HFM30	0.00	3.13	0.00	–55.59	28.81	0.00
HFM30	200.75	–170.57	3.14	–62.81	32.39	8.54
HFM31	0.00	6.07	0.00	–69.29	311.80	0.00
HFM31	200.75	–176.89	2.59	–62.05	299.83	7.05
HFM32	0.00	0.97	0.00	–86.06	116.15	0.00
HFM32	202.65	–198.45	1.08	–74.71	169.89	6.37
HFM33	0.00	2.62	0.00	–59.19	220.03	0.00
HFM33	140.20	–110.36	2.60	–49.59	238.18	7.08
HFM34	0.00	2.45	0.00	–58.59	30.50	0.00
HFM34	200.75	–161.28	3.63	–46.59	29.41	9.87
HFM35	0.00	1.90	0.00	–59.27	32.96	0.00
HFM35	200.75	–150.42	4.09	–44.14	32.42	11.12
HFM36	0.00	8.41	0.00	–59.01	256.61	0.00
HFM36	152.55	–110.29	3.00	–44.80	257.33	8.16
HFM37	0.00	11.39	0.00	–59.17	41.35	0.00
HFM37	191.75	–159.18	2.75	–60.45	101.63	7.47
HFM38	0.00	2.21	0.00	–54.56	93.62	0.00
HFM38	200.75	–140.68	4.40	–36.41	109.06	11.97

* see section 2.5 for definitions of the coordinate system

2.3.1 Drilling activities

Investigations performed between data freeze 1.2 and 2.3

A brief summary of all drilling activities carried out from data freeze 1.2 until data freeze 2.3 is presented for each type of borehole below.

The following boreholes were drilled.

1) Twelve telescopic boreholes within the length interval c. 500–1,000 m. They are, in chronological order: KFM06A, KFM07A, KFM08A, KFM06C, KFM01D, KFM08C, KFM010A, KFM07C, KFM08D, KFM02B, KFM12A and KFM11A.
2) Six cored boreholes of standard type with lengths between c. 100 and 800 m. These boreholes are, in chronological order: KFM08B, KFM06B, KFM07B, KFM09A, KFM09B and KFM01C.
3) Nineteen percussion-drilled boreholes ranging between c. 127 m and 301 m in length. They are, in chronological order: HFM20, HFM21, HFM23, HFM25, HFM22, HFM24, HFM28, HFM27, HFM26, HFM29, HFM32, HFM33, HFM30, HFM31, HFM34, HFM35, HFM38, HFM37, HFM36.

In addition to these long boreholes and boreholes with moderate length, the following shorter boreholes were drilled.

4) Five shallow (c. 20 m long) vertical cored boreholes, KFM90A–E, for the purpose of *in situ* thermal experiments.
5) Twenty-nine shallow boreholes through Quaternary deposits, 20 of which were later included in the groundwater level monitoring programme.

Data and/or P-reports available after data freeze 2.3

Although the following boreholes were drilled before data freeze 2.3, P-reports, and in several cases, data were not available until after this data freeze.

- Drilling of the telescopic and conventional cored boreholes KFM07B, 07C, 01C, 01D, 08C, 08D, 12A, 11A and 02B. Data from the first five of these boreholes were included in the major modelling activities based on data freeze 2.2. The drilling data were available prior to data freeze 2.2 but P-reports did not emerge until after data freeze 2.3. Data from the four remaining boreholes located at drill sites 2, 8, 11 and 12 (see Figure 2-1 and Figure 2-2) were, as planned, not included in stage 2.2 modelling activities. Of these boreholes, only KFM08D at drill site 8 is located inside the target volume. Borehole KFM02B was drilled inside the candidate area but outside the target volume. The remaining two cored boreholes are situated outside the candidate volume. Only data from KFM11A were available at data freeze 2.3, whereas data from the other boreholes became available soon after this deadline. The P-reports for all these four boreholes emerged after data freeze 2.3.
- Drilling of the percussion-drilled boreholes HFM33, 34, 35, 36, and 37. Data from these holes were also, as planned, not included in the data freeze 2.2 modelling. Drilling data from HFM33, 34 and 35 were available prior to data freeze 2.2 but P-reports did not emerge until after data freeze 2.3. By contrast, both the data and the P-reports from HFM36 and HFM37 became available after data freeze 2.3.
- Drilling of soil borehole SFM0109 at drill site 12. Both data and P-report emerged after data freeze 2.3.
- Supplementary drilling for determination of regolith thickness at 16 points in the area close to the sewage treatment plant at Forsmark (see map in Appendix 1).

2.3.2 Measurements completed in connection with drilling, geological mapping of drill cores and drill cuttings, and down-hole logging

Investigations performed between data freeze 1.2 and 2.3

During and after drilling, the different categories of boreholes produced were the subject of standardised investigation programmes by geological, geophysical, hydrogeological and hydrogeochemical methods. In addition to different SKB method documents, these programmes are described in detail in /SKB 2005a/, and the descriptions are not repeated here.

In the following text, a summary of the investigations performed after data freeze 1.2 and onwards is given. The investigations are presented and grouped according to geoscientific discipline and, within each discipline, roughly in chronological order, although investigations to some extent have been conducted simultaneously. Data and/or P-reports not available until after data freeze 2.3 are presented separately.

The results from *standard geological and geophysical borehole investigations and single-hole interpretations* became successively available from the new cored and percussion-drilled boreholes as they were completed, cf. the drilling succession in the previous section. However, the only investigations carried out in the shallow boreholes KFM90A–E were BIPS-logging, drill-core mapping and deviation measurements. More information on these standard investigations is presented in section 5.2.2.

Vertical seismic profiling measurements were undertaken in the two deep, almost vertical telescopic boreholes KFM01A and KFM02A in order to improve the resolution in the identification of seismic reflectors and to provide some constraints on the extension of geological structures. The surveys were conducted to a borehole length of 775 m in each borehole. Major seismic features were identified to depths exceeding 1.5 km and to a lateral distance of 2–3 km from the borehole collars.

Measurements of ground currents generated by the Fennoskan high-voltage cable were performed in boreholes KFM04A, 07A and 08A. Ground self-potential measurements were also conducted between drill sites 4 and 1.

An *in situ thermal experiment* was performed in the short cored boreholes KFM90A–E close to drill site 7. The main purpose was to explore the degree of anisotropy of thermal properties in the type of metamorphosed granite prevailing in rock domain RFM029. The results from this large-scale field experiment were compared with results from a small scale *in situ* experiment as well as with laboratory tests.

Overcoring rock stress measurements were conducted successively during drilling of boreholes KFM07B, 07C and 02B. Furthermore, *hydraulic fracturing (HF) and hydraulic tests on pre-existing fractures (HTPF)* were carried out in boreholes KFM07C, 08A, 09A and 09B.

A *pilot study of borehole breakouts* based on acoustic televiewer data from KFM01A and KFM01B was made, demonstrating that borehole breakouts and other fallout structures in the borehole wall, mainly micro-fallouts, exist in the deep boreholes at Forsmark. With these results in mind, this study was followed by an extended mapping (subdivided into two activities) in boreholes KFM01A, 01B, 02A, 03A, 03B, 04A, 05A, 06A, 07C, 08A, 08C, 09A, 09B and 90B. A re-logging with the acoustic televiewer was performed in KFM08A approximately two years after the first logging, in order to disclose if any time dependence could be observed regarding development of borehole breakouts and other fallout structures.

Single-hole hydraulic tests comprised both difference flow logging and double-packer injection tests in boreholes KFM06A, 07A, 08A, 08C and 11A. Furthermore, difference flow logging was carried out in KFM01D, 07C, 02B and 08D, whereas double-packer measurements were conducted in KFM04A, 05A, part of KFM02A (after hydraulic fracturing), KFM06B, 08B, 06C, 09A, 07B, 09B, 01C, 10A and 12A. All new percussion-drilled boreholes were flow logged with the HTHB-equipment (open hole pumping test). However, although attempts were made, flow logging was not possible in HFM25, 28, 29 and 31 due to very limited water yield.

A number of *multiple-hole interference tests* were performed with different purposes. Firstly, three short-term cross-hole tests between percussion-drilled and cored boreholes as well as between various percussion boreholes were carried out. The purpose of these tests was to investigate/verify hydraulic connections between boreholes at drill sites 1, 2, 3 and 4.

At a later stage, *two interference tests* were performed with percussion borehole HFM14 situated at drill site 5 used as the pumping hole. The main objective of the tests was to document how different fracture zones or fractured entities in the upper part of the bedrock are connected hydraulically, to quantify their hydraulic properties and to identify possible hydraulic boundaries in the area. In conjunction with the interference test, *groundwater flow measurements* were carried out along ten sections in boreholes with permanently installed equipment for flow measurements and groundwater sampling.

Groundwater flow was determined during both undisturbed and stressed conditions, the latter caused by pumping in HFM14. The aim was to further increase the understanding of the hydraulic conditions in the area and to assess the possibilities to later perform a large-scale, multiple-hole tracer test.

Hydrogeochemical logging and hydrogeochemical characterisation as well as microbial investigations were conducted in the telescopic boreholes KFM05A, 06A, 07A, 08A and 01D as well as in the conventional cored borehole KFM09A. Hydrogeochemical characterisation was also carried out in the telescopic boreholes KFM10A and KFM11A.

Results and a P-report from *a study of uranium oxidation states in groundwater* with high uranium concentrations were supplied immediately prior to data freeze 2.3.

In *percussion-drilled holes, chemical characterisation* is accomplished mainly by monitoring, i.e. recurrent sampling and analysis, in those boreholes which are supplied with monitoring equipment, see section 2.4. However, groundwater sampling in connection with other activities, mainly during HTHB-logging or interference tests, or sampling from boreholes serving as flushing water wells, has also contributed to the understanding of the hydrogeochemical conditions. Prior to data freeze 1.2, this kind of sampling/analysis was performed in percussion boreholes HFM03, 05, 06, 08, 09, 10, 11, 12, 14, 17 and 18. Between data freezes 1.2 and 2.3 boreholes HFM20, 22, 23, 24, 25, 26, 28, 29, 30, 33, 34, 35, 36, 37 and 38 were also included.

Interconnected porewater was successfully extracted by laboratory out-diffusion methods from about 20 drill core samples from KFM06A. The objective was to characterise these waters chemically and isotopically. In addition, the method of extraction, together with interfaced measurements of interconnected porosity, provides the opportunity to derive diffusion coefficient values. Subsequently, drill core samples from KFM01D, 02B, 08C and 09B were also collected for determination of rock matrix porewater composition.

In situ formation factor logging was performed in boreholes KFM03A, 04A, 01D and 08C and the results compared with formation factors obtained in the laboratory by electrical methods.

The results from the previously performed *in situ groundwater flow measurements with dilution technique and single-hole tracer tests* in KFM04A became available. Groundwater flow measurements were also conducted in KFM01A, 01D, 02A, 03A, 03B, 04A and 08A and single-hole tracer tests in KFM02A, 03A, 04A and 08A. The objectives of the activities were to achieve information about groundwater flow under *in situ* (i.e. undisturbed) hydraulic gradients and to determine transport properties of groundwater flow paths in fractures/fracture zones.

Data and/or P-reports available after data freeze 2.3

As far as *standard geological and geophysical investigations* are concerned, predominantly P-reports from the following boreholes were not available until after data freeze 2.3:

- KFM02B, 08D, 11A, 90B and 12A (geophysical logging).
- KFM07C, 02B, 08D, 11A and 12A as well as HFM36 and HFM37 (interpretation of geophysical borehole measurements).
- KFM02B, 08D and 12A (RAMAC and BIPS-logging).
- KFM02B, 12A and 08D as well as HFM33, 34, 35, 36 and 37 (Boremap mapping).

As far as *single-hole interpretations* are concerned, both data and P-reports from the following boreholes emerged after the data freeze 2.3:

- KFM11A, 08D, 02B and 12A as well as HFM33, 34, 35, 36 and 37.

The activities within the field of *thermal properties and rock mechanics* that were delayed are listed below.

- Evaluation of the *in situ* thermal experiment in the five short cored boreholes KFM90A–E, close to drill site 7. The results were not available until spring 2008.

- Data and P-reports from overcoring rock stress measurements in KFM07B, KFM07C and KFM02B. The major part of the field work was performed prior to data freeze 2.3, but became available during autumn 2007 and spring 2008.
- A draft report from the major campaign of hydraulic fracturing (HF) and hydraulic tests on pre-existing fractures (HTPF) comprising 13 tests in KFM07A, 15 tests in KFM07C, 23 tests in KFM08A, 16 tests in KFM09A and 18 tests in KFM09B was finished by late 2006, but the final P-report was delayed until the end of 2007, due to the major revision of borehole deviation measurements and fracture orientations performed by SKB.
- The pilot study of the existence of borehole breakouts and other types of fallouts from the borehole wall was completed early in 2005, but the report was not printed until after data freeze 2.3. However, the study did not generate data to Sicada.
- The mapping of borehole breakouts (and other fallout structures) from televiewer logging in boreholes KFM01A, 01B, 02A, 03A, 03B, 04A, 05A, 06A and 07C as well as from KFM08A, 08C, 09A, 09B and KFM90B provided data and two P-reports first after data freeze 2.3.
- A review was made of rock stress measurements conducted within the site investigation programme at Forsmark up to and including 2004. The study, which did not generate data to Sicada, was completed in April 2006, although the report was not printed until after data freeze 2.3. The stress data included in the analysis involved overcoring stress data from borehole KFM01B and the cored boreholes DBT-1 and DBT-3 situated at the Forsmark power plant III and drilled long before the Forsmark site investigations, as well as hydraulic stress data from boreholes KFM01A, KFM01B, KFM02A, and KFM04A.

The following *hydrogeological investigations (single-hole tests and multiple-hole interference tests)* were not fully completed until after data freeze 2.3.

- Difference flow logging in boreholes KFM02B, 08D and 11A. In KFM11A, flow logging was performed until an obstacle was encountered at 498 metres borehole length. Below this depth, double-packer injection tests were made instead.
- Two large-scale interference/tracer tests that used the percussion-drilled boreholes HFM14 at drill site 5 and HFM33 at drill site 11 as pumping boreholes were carried out during the summer and early autumn 2007, in order to verify previous assessments of the hydrogeological conditions in the north-western part of the Forsmark candidate area.

The following *hydrogeochemical investigations* were not fully completed until after data freeze 2.3.

- Hydrogeochemical characterisation in the telescopic boreholes KFM08D and KFM12A. In KFM12A, a simplified measurements approach was applied by employing SKB's double-packer injection test equipment. This equipment was also used in KFM11A for part of the hydrogeochemical sampling. Hydrogeochemical data and reports from these boreholes as well as from KFM10A, HFM36, HFM37 and HFM38 were not available until after data freeze 2.3. The investigations in KFM10A, 11A and 08D included the study of number, viability, and methabolic diversity of microrganisms, and in KFM11A also colloids.
- Results of the rock matrix porewater composition in drill core samples from KFM01D, 02B, 08C and 09B were not available until after data freeze 2.3. Part II of this project, chloride diffusion coefficient modelling, which needed to be evaluated on the basis of the tracer experiment performed in KFM02B, will not be reported until after the summer of 2008.

Some investigations regarding *transport properties* were also late.

- A tracer test between the nearby telescopic boreholes KFM02A and KFM02B was initiated prior to data freeze 2.3 and continued afterwards. Data and report were not available until spring 2008.
- *In situ* formation factor logging by electrical methods in KFM01D and KFM08C.
- *In situ* groundwater flow measurements and single-hole tracer tests in KFM01D.

2.3.3 Sampling and analysis of intact rock material for laboratory investigations

Drill core samples and geological specimens from the bedrock surface have been collected for different kinds of laboratory analyses throughout the entire site investigation. These analyses have included:

- Modal, geochemical and petrophysical analyses of rock types.
- Identification, relative age relationships and geochemistry of fracture minerals and wall-rock alteration.
- Geochronology of rocks and fracture minerals.
- Studies of the character and kinematics of deformation zones both along boreholes and at the surface.
- Establishment of thermal and rock mechanical properties.
- Establishment of transport properties.

The most important activities relating to sampling and analytical work performed between data freezes 1.2 and 2.3 are presented below. They have provided a large amount of data and several P-reports. Activities that resulted in data delivery to Sicada and/or P-reports after data freeze 2.3 are presented separately.

Investigations performed between data freeze 1.2 and 2.3

Complementary *modal, geochemical and petrophysical analyses of rock samples* from cored boreholes KFM04A, 05A, 06A and 09A were carried out with the aim to document the character of fresh rock. The mineralogical and geochemical changes that occur during the alteration referred to as albitization were also addressed in the study of samples from boreholes KFM04A, 05A and 06A.

The results from the *investigations of fracture minerals* in three sets of cored boreholes (KFM01B, 04A, 05A and 06A, KFM06B, 06C, 07A, 08A and 08B, and KFM01C, 01D, 02B, 06A, 06B, 07A, 08A, 08B, 08C, 08D, 09A, 09B, 010A and 11A) became available and a detailed study of the *alteration referred to as oxidation that occurs in the wall-rock to fractures* was carried out. Samples from ten boreholes (KFM01A, 01B, 02A, 03A, 04A, 05A, 07A, 08A, 08B and 09A) were analysed in the wall-rock alteration study which addressed the mineralogy, geochemistry, porosity and redox properties of the altered rock and a comparison with fresh rock.

Complementary, *geochronological analyses of rock samples* from both cored boreholes (KFM02A, 03A, 04A, 06A and 06B) and from the surface have been conducted, with the aim of using different isotopic systems ($^{40}Ar/^{39}Ar$ hornblende, $^{40}Ar/^{39}Ar$ muscovite, $^{40}Ar/^{39}Ar$ biotite, $^{40}Ar/^{39}Ar$ K-feldspar and (U-Th)/He apatite) to reconstruct the temperature-time history from shortly after crystallisation of the bedrock to the time the rocks were uplifted through the c. 70° C geotherm. Some constraints on *the timing of formation of some fracture minerals and fault breccias* have also been carried out in the cored boreholes KFM04A, 05A, 07A, 08A and 09A.

Following a pilot investigation, a major study of deformation zones was undertaken in three phases with the purpose of documenting the *detailed character and kinematics of the brittle deformational history of the area*. Structural data were obtained from all the 25 cored boreholes and from some outcrops, in particular along the Eckarfjärden deformation zone.

Sampling for *testing of thermal and rock mechanical properties* on drill core samples from boreholes KFM01A, 01B, 02A, 03A, 03B, 04A, 05A, 06A, 06B, 07A and 08A was completed. Furthermore, thermal properties were also determined on rock samples from boreholes KFM01C and 01D. Measurements of anisotropy in thermal properties were conducted on samples from the short cored borehole KFM90B. Thermal conductivity and thermal diffusivity were established using the transient plane source (TPS) method. Heat capacity was determined indirectly from the TPS method, and, in the case of samples from KFM01A, 01C, 01D, 04A, 05A, 06A, 07A and 08A, also by the calorimetric method. For boreholes KFM05A and KFM06A, extensometer measurements of the coefficient of the thermal expansion of rock were also carried out.

Sampling of the cored boreholes KFM01A, 01B, 02A, 03A, 03B, 04A, 05A, 06A, 06B, 07A, 08A, 08C, 09A and 10A for *investigations of transport properties* was accomplished.

Data and/or P-reports available after data freeze 2.3

P-reports and, in some cases data, which were not available until after data freeze 2.3, are listed below.

- Mineralogy and geochemistry of fractures in boreholes KFM01C, 01D, 02B, 04A, 06A, 06B, 07A, 08A, 08B, 08C, 08D, 09A, 09B, 10A and 11A.
- Investigations of $^{40}Ar/^{39}Ar$ and (U-Th)/He geochronology of rock samples, phase 2 (only P-report).
- Dating of fracture mineral and fault breccias in boreholes KFM04A, KFM08A and KFM09A.
- Data and the P-report from measurements of anisotropy in thermal properties on samples from borehole KFM90B were presented. The results were not available in Sicada until autumn 2007.
- Results from resistivity measurements on samples from KFM01A, 01B, 02A, 05A and 06A became available after data freeze 2.3. Later complementary resistivity measurements were made on samples from KFM01A, 02A, 06A, 08A, 06C and 09A.
- The determination of direct and indirect tensile strength estimates on cores from borehole KFM01D were presented.
- Uniaxial compression tests as well as indirect tensile strength tests were performed on cores from KFM08D. Uniaxial compression tests were also performed on core samples from KFM01C (post-failure tests) and KFM06A (the samples included sealed fractures).
- Results from rock matrix permeability measurements on core samples from borehole KFM01D became available.
- The microcrack volume was determined in hydrostatic triaxial compression tests performed on drill core samples from KFM01A and KFM02B.

2.4 Monitoring

2.4.1 Background

Monitoring of geoscientific parameters and ecological objects is an activity which has successively increased during the course of the site investigation work. Monitoring is defined as recurrent measurements of the same parameters/objects, so that time series are generated. The measured parameters and objects inventoried are characterised by a certain degree of time-dependent and site-specific variability. The objectives of the monitoring are 1) to establish “undisturbed” conditions, the so-called “baseline”, prior to a possible future siting of a deep repository, and 2) to enhance the knowledge about underlying, often complex processes that govern the time-dependent variations of the monitored parameters/objects.

The current monitoring programme is presented in this section. The programme will, with a few modifications, continue after completion of the site investigations. The full extent of the programme from July 2007 and onwards is described in detail elsewhere /SKB 2007/.

2.4.2 Monitoring programme

Monitoring of *rock movement at the ground surface* with the help of a high-resolution GPS technique was initiated during the autumn 2005 and has continued since that date.

Meteorological data have been acquired continuously from two weather stations within the candidate area from May 2003 to June 2007. Supplementary data were acquired from a number of stations in the vicinity and included in the national observation net of the Swedish Meteorological and Hydrogeological Institute (SMHI). From July 2007, monitoring at Forsmark has continued at just one of the two weather stations. Snow depth and the water content of snow, as well as ice coverage and ice break-up have also been monitored every winter since the start of the site investigations in 2002.

Since early in the site investigations, surface water levels have been monitored at two locations in the Baltic Sea and in six lakes within the *oceanographic/hydrological activities*. However, in November 2005, the station in the bay Kallrigafjärden was destroyed by ice pressure and, in December 2005,

the station in Lake Lillfjärden was likewise destroyed by ice. None of these stations have or will be repaired. However, monitoring at the remaining six stations has continued without major problems. Before data freeze 1.2, monitoring of surface water discharge, water electrical conductivity (EC) and water temperature was performed at one monitoring station. At the beginning of 2005, a further three monitoring stations for discharge, EC and water temperature were established as well as one station for monitoring of EC alone.

As regards *hydrogeological parameters*, the extent of monitoring of groundwater levels in boreholes has successively increased during the site investigation. At the end of 2007, groundwater levels were monitored in 25 telescopic and conventional core-drilled boreholes (i.e. all boreholes in these categories), 37 percussion-drilled boreholes (i.e. all boreholes except one in this category) and 50 groundwater observation wells in Quaternary deposits. Seven of these wells are supplied with a BAT-type filter tip for pore pressure measurements in low-transmissive soils.

Hydrogeochemical monitoring at Forsmark includes precipitation, surface water, near surface groundwater (i.e. groundwater in Quaternary deposits) and deep groundwater (groundwater in bedrock). Samples of precipitation have been collected and analysed since the autumn of 2002. From the start of the site investigation work, comprehensive chemical investigation campaigns for surface waters and near-surface waters (from soil pipes) were conducted for two years. This was followed by less extensive long-term monitoring programmes that started in July 2004 (surface water) and July 2005 (near surface water). The sampling objects in the reduced programmes comprise four lakes, three sea bays, four brooks, three private drinking water wells and 18 sampling points for near surface groundwater, i.e. soil boreholes with groundwater stand pipes, seven of which are supplied with BAT-type filter tips for groundwater sampling in low-transmissive, cohesive soils.

In the same manner as for groundwater level monitoring, the scope of hydrogeochemical monitoring in boreholes has been extended as new boreholes have been completed. At the end of 2007, hydrogeochemical monitoring was performed in 24 straddle-packer isolated borehole sections in 15 telescopic and conventional core-drilled boreholes, as well as in one section in each of 10 percussion-drilled holes.

There is also a programme for *groundwater flow monitoring* in packed off borehole sections. This programme is closely linked to the programme for groundwater sampling in core- and percussion-drilled boreholes. The two monitoring programmes include the same borehole sections, and partly the same equipment is used. Measurements within the current monitoring programme for groundwater flow, using the tracer dilution technique, have been performed since November 2005. A few borehole sections have also been measured in connection with hydraulic interference tests during the summers of 2005, 2006 and 2007.

Finally, within the discipline of *surface ecological investigations*, the bird life and the abundance and physiological status of the elk population have been monitored from the start of the site investigation programme, as an aid for the environmental impact assessment.

2.5 Geographical data

The geographical data available for the site descriptive model, version 1.2*,* described in /SKB 2005a/, are still valid for data freezes 2.1, 2.2 and 2.3. The coordinate system used is:

X/Y (N/E): the national 2.5 gon V 0:-15, RT 90 system (“RAK”),

Z (elevation): the national RHB 70 levelling system.

In order to represent terrain relief, a digital elevation model (DEM) is an efficient tool. Such a model is a digital representation of a continuous variable over a two-dimensional surface by a regular array of z-values referenced to a common datum. A DEM is required as input data for many types of surface models such as hydrological models, geomorphometrical models etc.

Two digital elevation models have been used in the Forsmark site investigations. Besides the model called 4,600 DEM, which is derived from aerial photographs taken at a height of 4,600 m and available for the whole of Sweden, a more detailed digital elevation model of the Forsmark area, called

2,300 DEM, has been developed. This model is based on aerial photographs at 2,300 m height. The DEM resolution is the size of the cells in the DEM. The DEM is constructed by interpolation from irregularly spaced elevation data. To construct both Forsmark models, the Kriging interpolation method was applied with the use of input data from many different sources. The reader is referred to /Lindborg (ed) 2005/ for more detailed descriptions of the data from which the DEMs have been derived.

The 2,300 DEM in its primary version served as the standard elevation database in the site investigations performed between data freezes 0 and 1.2, and further developed versions have been applied for special purposes /Brydsten 2004/ and /Brydsten and Strömgren 2004/. The most recent and elaborated version, in which bathymetric data from shallow and deep parts of the Baltic outside the candidate area are integrated /Lindborg (ed) 2005/, has been the model applied from data freeze 2.1 and onwards.

The height system and horizontal geodetic grid applied at the Forsmark site investigation were established already during early 2002. They were not documented previously in the form of a P-report, although data relating to grid corner points etc have been stored in Sicada. The data delivery was supported by a written PM. After data freeze 2.3, a P-report was written in Swedish /Brising 2008/, later complemented with a P-report in English /Brising and Nissen 2008/. These reports document the procedure of control point surveying, and provide height and coordinate data in written format according to the P-report template.

2.6 Other data sources

In addition to the data collected during the site investigation programme at Forsmark, older geological and geophysical data from the Forsmark nuclear power plant and SFR have been used in the *geological modelling work*. These data are only partly stored in the Sicada database, but they are not necessarily of the same quality as the data generated by the site investigation programme. Specific examples include seismic refraction data, borehole data from DBT-1 and DBT-2, borehole and tunnel data across the Singö deformation zone and photographs of sub-horizontal sheet joints along the channel that provides cooling water to the nuclear power plant. Furthermore, the structural models for SFR as presented in /Axelsson and Hansen 1997, Holmén and Stigsson 2001/ have been used in the deterministic modelling of deformation zones.

In the *rock mechanics evaluation*, stress data from Finnsjön, Björkö, Stockholm and Olkiluoto /Sjöberg et al. 2005/ have been used to estimate the regional state of stress in the Forsmark region.

In the *hydrogeological evaluation*, data from structural and hydrogeological characterisation conducted around the Forsmark nuclear power plant /Carlsson and Christiansson 2007/, SFR /Axelsson et al. 2002/ and at the Finnsjön study site /Andersson et al. 1991/ have been considered to various degrees in the conceptual and quantitative modelling. In addition, the yields of the percussion-drilled boreholes have been compared with data from the Swedish Geological Survey's archive of wells (see /Gentzschein et al. 2007/.

In the *hydrogeochemical evaluation*, data available in Sicada on groundwater conditions at near-by locations, such as SFR, and at other Swedish sites have been used as background information together with data from Finnish sites (e.g. /Pitkänen et al. 2004/).

2.7 Databases

The basis for the modelling work is quality-assured data acquired during the site investigations that are extracted from the two SKB databases Sicada and GIS. All available data are listed in tables in Appendix 3. The purpose of these tables is to give a specification of the data and a reference to the associated P-report where the data and the data acquisition procedure are described. Quality assurance aspects related to the handling of data in the modelling work are described in section 1.6.4. Evaluations of the different sets of data in the different modelling disciplines are presented in the respective chapters 4 to 10 in this report.

2.8 Model versions prior to stages 2.2 and 2.3

Prior to the site descriptive model, SDM-Site, three complete and integrated site descriptive models for Forsmark have been produced. Version 0 /SKB 2002/ was developed from the information available at the start of the surface-based site investigation programme. This information was mainly 2D in nature. It was also general and regional, rather than site-specific in character.

Two model versions, version 1.1 and version 1.2, were developed based on data from the initial site investigation stage (ISI). Version 1.1 /SKB 2004/, which was a training exercise, was built on a rather extensive set of data from the surface, whereas the data sets from boreholes were limited to one c. 1,000 m deep cored borehole (KFM01A) and eight c. 150–200 m deep percussion-drilled boreholes.

In general, the preliminary site descriptive model, version 1.2, confirmed the version 1.1 model. Considerably more sub-surface data implied only minor modifications in the description of rock units including the character of the ductile deformation in the bedrock (rock domain model). Enhanced confidence in rock strength and thermal properties was also achieved, since the analyses and modelling confirmed the ranges obtained in version 1.1. The main remaining uncertainties concerned the impact of subordinate rock types on thermal and strength properties of the rock in the target volume. Stress data and the rock stress modelling confirmed that rock stresses at Forsmark are relatively high compared with typical sites in the central part of Sweden, and that the maximum horizontal stress is aligned approximately NW-SE, i.e. parallel to the overall direction of the tectonic lens and the adjacent steeply dipping regional deformation zones.

The existence of deformation zones was confirmed by the analyses of new data for model version 1.2 and new zones were identified in the deformation zone model, in particular a number of gently dipping zones in the south-eastern part of the candidate area. The sensitivity of uncertainties in the geometry of deformation zones and in the hydrogeological properties of these zones were explored by the hydrogeological modelling work. These analyses suggested that the flow in the target volume is mainly local and that the heterogeneity in hydraulic properties within the candidate volume has a significant effect on the local flow distribution. However, these simulations did not consider the existence of highly-transmissive and sub-horizontal, well-connected structures in the uppermost part of the bedrock, as indicated by hydraulic data from the site. Division of the bedrock into hydraulic domains was carried out during model version 1.2 and this approach provided an important feedback to the geological modelling team.

The hydrogeochemical conditions at the site in terms of the origin of the groundwater and the processes that control the water composition were evaluated and described down to a depth of 1,000 m and the conceptual model of the development of post-glacial hydrogeochemistry was updated. Due to the limited set of site-specific data, the modelling of bedrock transport properties was restricted to parameterisation of rock mass porosity and diffusivity.

An integrated description of the surface system was provided for the first time in model version 1.2, including Quaternary cover thickness, shallow groundwater and surface water characteristics, as well as terrestrial, limnic and ecosystem models for the drainage area around Lake Bolundsfjärden.

No integrated site description was compiled as a result of modelling stage 2.1 /SKB 2006a/, but updated versions of the geological models for rock domains and deformation zones were developed, and, for the first time, at local scale with a higher resolution. The boundaries of the stage 2.1 local model volume have been maintained for the final site description, SDM-Site (Figure 2-5 in section 2.9). Compared with model version 1.2, two new, minor rock domains were added in the local model volume, whereas the regional rock domain model strongly resembled the previous versions. Furthermore, the regional model for deformation zones had several similarities to the earlier version, but there were significant changes in the length of especially the gently dipping zones. On the basis of particularly the observed three-dimensional spatial variability of open fractures and an inferred relationship between the occurrence of gently dipping fracture zones and the *in situ* stress magnitudes in the bedrock, a conceptual model for division of the rock in the target volume into fracture domains was developed.

2.9 Model volumes and model areas

The site descriptive modelling is performed using two different scales of model volume, the *regional* and the *local* model volume. Generally, the local model is required to cover the volume within which the repository is expected to be placed, including accesses and the immediate environs. Hence, the description of the local model volume should be detailed enough for the needs of repository engineering and safety assessment. In addition to the description on the local scale, a description is also devised for a much larger volume, the regional model volume, in order to place the local model in a larger context and to allow for sensitivity analyses of, mainly, hydrogeological boundary conditions. The difference between the regional and local model volumes is the resolution of the modelled objects, which has been chosen to balance modelling efforts against the needs of downstream users of the model. This is a consequence of ensuring a homogeneous resolution throughout all parts of the model volumes.

In selecting the model volumes for version 1.2 /SKB 2005a/, and also for the geological model in modelling stage 2.1 /SKB 2006a/, some rules of thumb, taken from the strategy document for integrated evaluation /Andersson 2003/ were applied. Since the model volumes have not changed, the arguments for the selected volumes still remain and are repeated below. It also needs to be understood that the distinct model sizes primarily concern the development of the geological model in the SKB rock visualisation system (RVS). This is also the reason why the model areas and volumes have rectangular shape.

It should be noted that the RT 90 and RHB 70 coordinate systems (see section 2.5) are always used in the site descriptive model presented in the following chapters, even if this point is not always stated in the text. In addition, depth is used in the text as a synonym for elevation, i.e. referring to depth below sea level if not otherwise stated. However, the difference between depth below sea level and depth below ground surface at Forsmark is only a few metres due to the low altitude and flat topography of the Forsmark area.

2.9.1 Regional model area and volume

The regional model area is shown in Figure 2-5. This model area and the corresponding volume are the same as the regional model area/volume in version 1.2 /SKB 2005a/ and the arguments for selecting this area/volume remain.

- It includes the candidate area and it is not prohibitively large as it has a surface area of 165 km^2.
- It captures relevant portions of the steeply dipping regional deformation zones, which strike in a north-westerly direction and surround the candidate area. Any expansions of the regional model area to the north-west or south-east would not provide any significant changes in the regional geological picture. With these considerations in mind, the size of the regional model area is sufficient for the needs of geological modelling. It should be noted that the geological evolution (chapter 3) is assessed in the context of a much larger area than the regional model area.
- It adequately covers the variations in rock type in the candidate area and its immediate surroundings.
- It captures the main hydrogeological features of the region, as the boundaries perpendicular to the shoreline are judged to be sufficiently far away from each other that they do not influence the groundwater flow in the candidate area. The boundary to the south-west lies on the south-western side of a local topographic divide, and the boundary to the north-east lies north-east of a major bathymetric break in Öregrundsgrepen. Sensitivity analyses undertaken in version 1.2 of the site descriptive modelling addressed the proper locations of the boundaries in the regional hydrogeological model and the results confirm that the selected regional volume is also appropriate from a hydrogeological point of view.
- A depth of 2,100 m below sea-level is considered to provide a reasonable vertical extent for description and is the maximum depth down to which any meaningful extrapolations of deformation zones could be made. To represent this depth in RVS, the size of the vertical dimension is set to 2,200 m since the upper boundary is set to +100 m above mean sea level.

The coordinates defining the regional model volume are (in metres):

RT 90 (RAK) system; (Easting, Northing): (1625400, 6699300), (1636007, 6709907), (1643785, 6702129), (1633178, 6691522).

RHB 70; +100, –2,100.

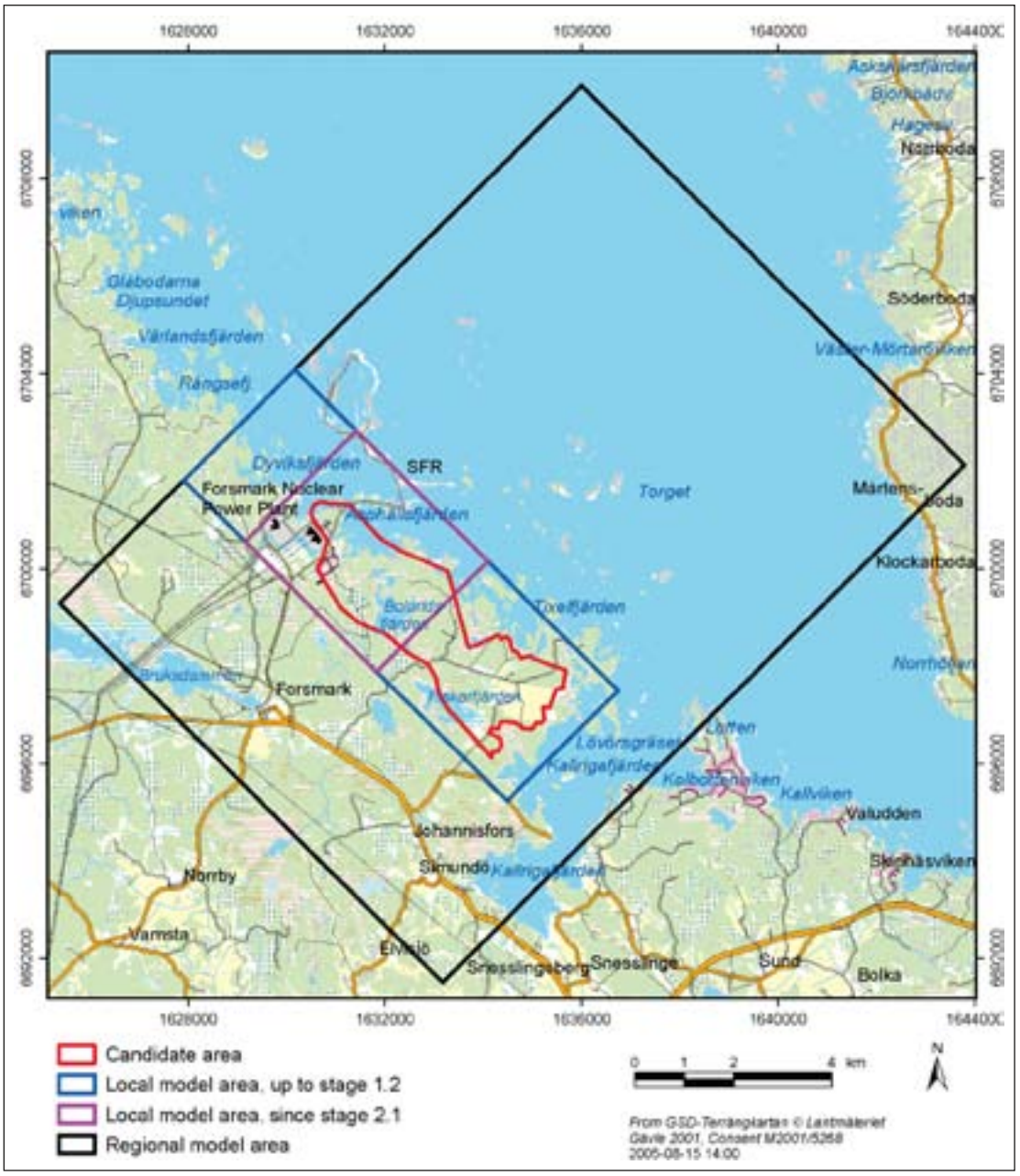

Figure 2-5. *Regional (black) and local (purple) model areas during and after model stage 2.1. The regional model area is the same as in model versions 0, 1.1 and 1.2. The local model area is smaller than in version 1.2 (blue line) and covers the north-western part of the candidate area selected as the target area for a potential repository.*

2.9.2 Local model area and volume

The local model area (and corresponding volume) is the same as that selected for the geological modelling in stage 2.1 /SKB 2006a/. It is smaller in size compared with the version 1.2 local model area, but is contained within the boundaries of the version 1.2 local model area, as shown in Figure 2-5. It includes the target area selected for a potential repository, where site investigations during the complete site investigation phase were largely focused. The arguments for selecting this local volume were given in /SKB 2006a/ and are repeated below.

- Both to the north-east and south-west, it includes the boundaries to more inhomogeneous and banded bedrock outside the candidate area.
- It includes key rock boundaries within and immediately adjacent to the candidate area which help to define the structural framework within the tectonic lens.

- The north-western and south-eastern model boundaries are located well outside the outer borders of the repository area according to the repository layout from step D1 /Brantberger et al. 2006/. Furthermore, the north-western boundary is positioned so that the parts of the tectonic lens below the current reactor site as well as potential access ramps from the SFR peninsula are included in the model.
- The surface area is c. 12 km^2, i.e. comparable with the size of 5 to 10 km^2 recommended in the general execution programme /SKB 2001/.
- A depth of 1,100 m beneath sea level permits inclusion of all information from the existing deep boreholes at the site. To represent this depth in RVS, the size of the vertical dimension is set to 1,200 m since the upper boundary is set to +100 m above mean sea level.

The coordinates defining the local model volume are (in metres):

RT 90 (RAK) system; (Easting, Northing): (1629171, 6700562), (1631434, 6702824), (1634099, 6700159), (1631841, 6697892).

RHB 70; elevation: +100, –1,100.

3 Evolutionary aspects of the Forsmark site

This chapter is a brief summary of the background report R-08-19 /Söderbäck (ed) 2008/, which provides a comprehensive account of the geological evolution, palaeoclimate and historical development of both the Forsmark and Laxemar-Simpevarp areas. A detailed reference list is given in the background report and here only a few, key references are included in the text.

3.1 Bedrock evolution during the Proterozoic and Phanerozoic eons

The Forsmark area is situated in the south-western part of one of the Earth's ancient continental nuclei, referred to as the Fennoscandian Shield /Koistinen et al. 2001/. This part of the shield belongs predominantly to the geological unit referred to as the Svecokarelian (or Svecofennian) orogen (Figure 3-1). The bedrock inside an orogen was affected by major tectonic activity at a particular time interval during the Earth's long geological evolution and the actual geological process is referred to as orogeny. Tectonic activity refers to regional deformation and metamorphism of the crust in combination with active volcanism and the intrusion of igneous rocks at depth, i.e. major igneous activity. In essence, the branch of geology referred to as "tectonics" addresses the broad architecture of the outer part of the Earth. The bedrock in the Svecokarelian orogen is dominated by Proterozoic igneous rocks that were affected by complex ductile strain and metamorphism at predominantly mid-crustal levels, prior to later exhumation to the current level of erosion.

In order to provide the necessary boundary conditions for an understanding of the bedrock geological evolution of both the Forsmark and Laxemar-Simpevarp areas /Söderbäck (ed) 2008/, these areas were viewed in a broader geological perspective. For this purpose, attention has been focused on an area in the southern and eastern part of Sweden, referred to as the geological reference area (Figure 3-1).

3.1.1 Bedrock geological evolution in south-eastern Sweden

The bedrock geology at the current level of erosion in the geological reference area in south-eastern Sweden (Figure 3-1) can be divided into several major tectonic domains. These domains trend WNW more or less parallel to an older, Archaean continental nucleus to the north-east (Figure 3-1). The predominantly igneous bedrock in all these domains had largely formed between 1.91 and 1.75 billion years ago (1.91–1.75 Ga). This bedrock was also affected by a variable degree of deformation in a hot, ductile regime and the various domains had amalgamated together, more or less into their current geometric configuration, during the same time interval. A remarkably thick continental crust throughout most of the Fennoscandian Shield (up to c. 60 km) is a heritage from the dramatic tectonic evolution predominantly during the later part of the Palaeoproterozoic era. The geological time scale that has been used for assessing the bedrock evolution is shown in Figure 3-2.

Although the bedrock in south-eastern Sweden had already started to stabilise after 1.75 Ga, tectonic activity that involved continued crustal growth and crustal reworking continued during the remainder of the Proterozoic to the west and south (Gothian, Hallandian and Sveconorwegian orogenies). By c. 900 Ma, the bedrock in the northern part of Europe had collided with other continental segments to form the supercontinent Rodinia. Break-up of Rodinia, drift of the newly-formed continent Baltica from cold latitudes in the southern hemisphere over the equator to northerly latitudes, and amalgamation of the new supercontinent Pangaea occurred between c. 600 and 300 Ma. Rifting of the continental crust, and opening and spreading of the North Atlantic Ocean dominated the subsequent geological evolution to the south and west of the geological reference area. This long period of extensional tectonic activity was interrupted during the Late Cretaceous and early Palaeogene by a more compressive tectonic regime, which can be related to the collision of Eurasia and Africa.

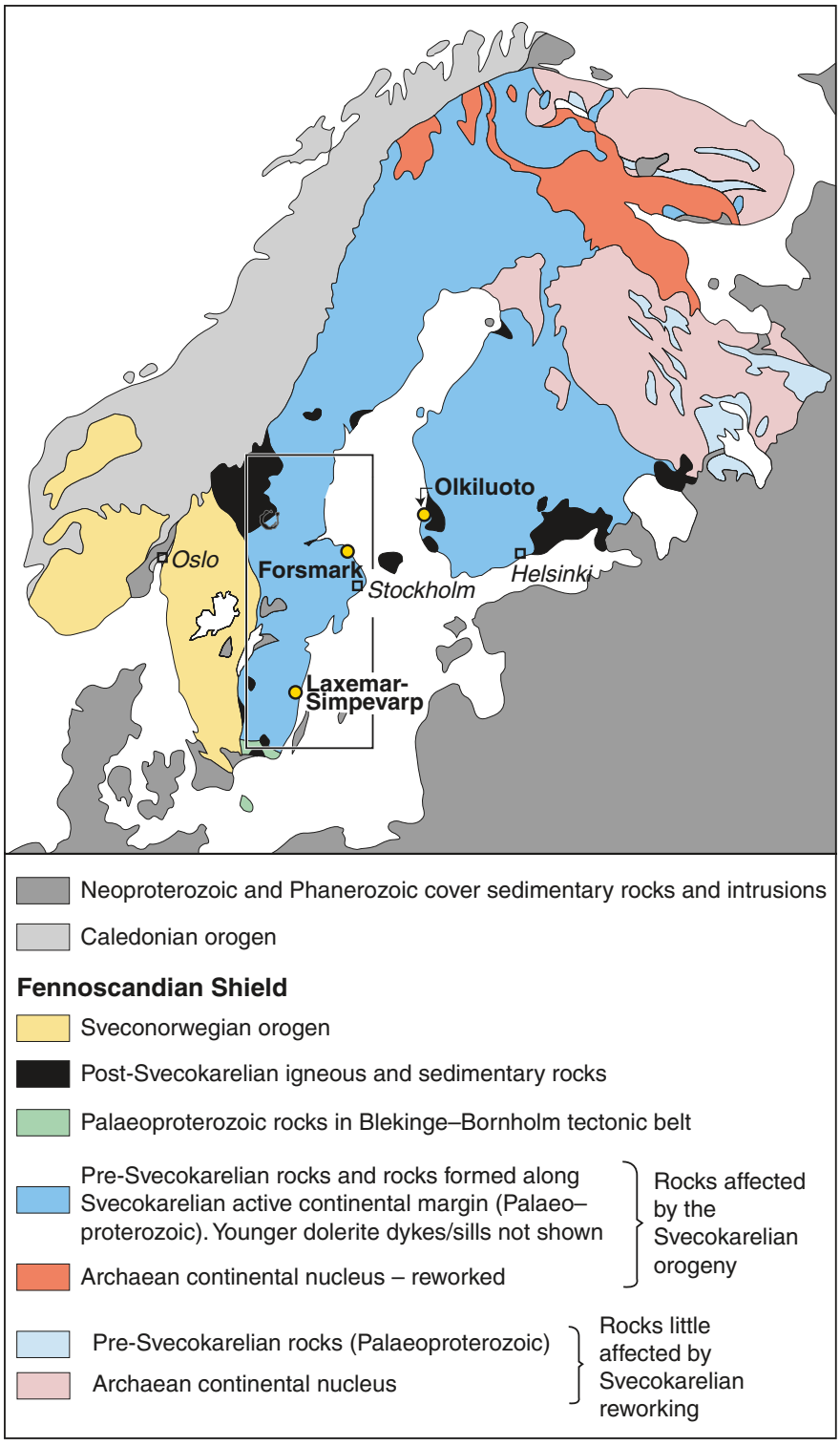

Figure 3-1. *Map showing the major tectonic units in the northern part of Europe at the current level of erosion (modified after /Koistinen et al. 2001/). The area referred to in section 3.1.1 and used to provide a regional geological perspective for both the Forsmark and Laxemar-Simpevarp areas is outlined by the rectangle. This area is referred to as the geological reference area /Söderbäck (ed) 2008/.*

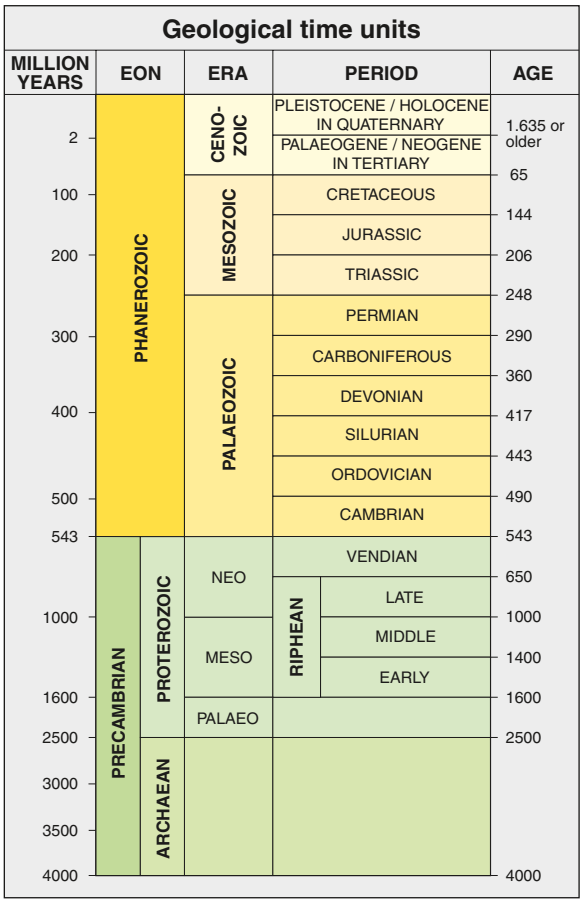

Figure 3-2. *Geological time scale based on the compilation used in /Koistinen et al. 2001/. Age is given in million years (Ma). 1 Ga = 1,000 Ma.*

An overview of the effects of these different, far-field tectonic events in the near-field realm represented in south-eastern Sweden is described in /Söderbäck (ed) 2008/. These effects gave rise to local igneous activity during the Proterozoic, burial and denudation of sedimentary cover rocks during the Proterozoic and Phanerozoic, and predominantly brittle deformation in the bedrock at different times throughout this long time interval. At least two episodes of pre-Quaternary exhumation of the ancient crystalline bedrock can be inferred, one prior to the Cambrian and the other after the Cretaceous, probably during the Neogene. The current ground surface corresponds to the sub-Cambrian unconformity that morphologically is referred to as the sub-Cambrian peneplain.

In conclusion, it appears that two fundamental types of geological process have made a profound impact on the geological evolution of the geological reference area in south-eastern Sweden (Figure 3-3):

- Igneous activity and crustal deformation along an active continental margin at different time intervals mostly during Proterozoic time.
- Loading and unloading cycles in connection with the burial and denudation, respectively, of sedimentary rocks, around and after c. 1.45 Ga.

As the effects of regional tectonic activity mostly waned in south-eastern Sweden and became prominent solely in the far-field realm, the effects of loading and unloading related to the burial and denudation of sedimentary rocks, respectively, increased in significance (Figure 3-3).

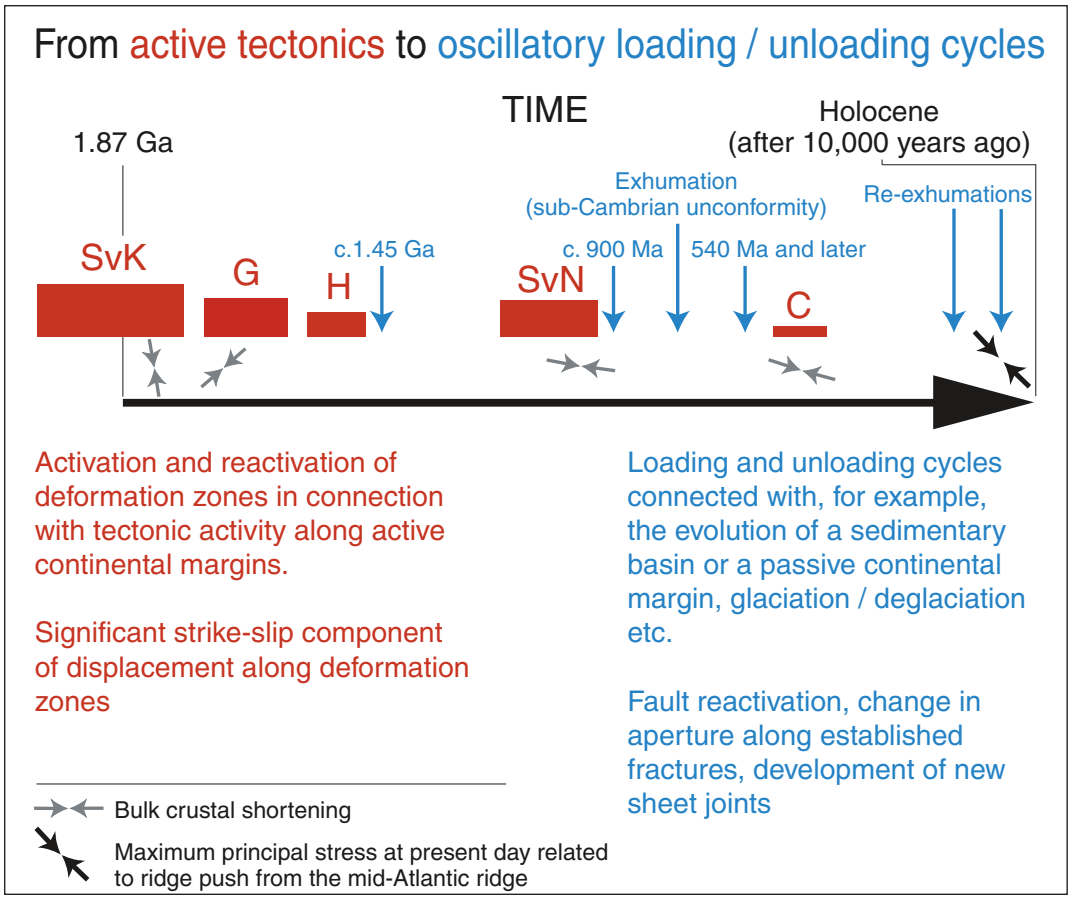

Figure 3-3. *Active tectonics (red) and oscillatory loading and unloading cycles (blue) during geological time in the geological reference area (modified after /Stephens et al. 2007/). The detailed evolution during the Quaternary period with several glaciations (loading) and deglaciations (unloading) is not shown. SvK = Svecokarelian orogeny, G = Gothian orogeny, H = Hallandian orogeny, SvN = Sveconorwegian orogeny, C = Caledonian orogeny.*

3.1.2 Bedrock geological evolution in the Forsmark area

The bedrock geological evolution in the Forsmark area has been evaluated with the help of surface and borehole observational data as well as geochronological data /Söderbäck (ed) 2008/. The geochronological data are summarised in Figure 3-4. In this area, an older suite of plutonic, calc-alkaline intrusive rocks formed between 1.89 and 1.87 Ga, and the metagranite inside the tectonic lens, where the target volume is situated (see chapter 5), is included within this suite. Amphibolites that intrude the metagranite and a younger suite of calc-alkaline rocks and granites formed between 1.87 Ga and 1.85 Ga. These two suites of intrusive rocks (Figure 3-4) have been included in separate Svecokarelian tectonic cycles at 1.91–1.86 Ga and 1.87–1.82 Ga, respectively, that have been recognised in south-eastern Sweden /Söderbäck (ed) 2008/.

Deformation in the Forsmark area initiated between 1.87 and 1.86 Ga (Figure 3-4) with the development of a penetrative grain-shape fabric, with planar and linear components, that formed under amphibolite-facies metamorphic conditions and at mid-crustal depths. The development of broad WNW-ESE to NW-SE belts with higher ductile strain that surround tectonic lenses with generally lower ductile strain also occurred around 1.86 Ga. The amphibolites and other intrusive rocks that belong to the younger suite intruded during the waning stages of and after the development of the penetrative, ductile strain in the area. Regional folding of the variably intense, planar grain-shape fabric also affected the amphibolites. Ductile deformation after 1.85 Ga occurred predominantly inside the high-strain WNW-ESE to NW-SE belts. It successively became more focused along ductile high-strain zones within these belts and cooling ages indicate that ductile strain along these zones probably occurred until at least 1.8 Ga. A combination of dextral strike-slip displacement along the

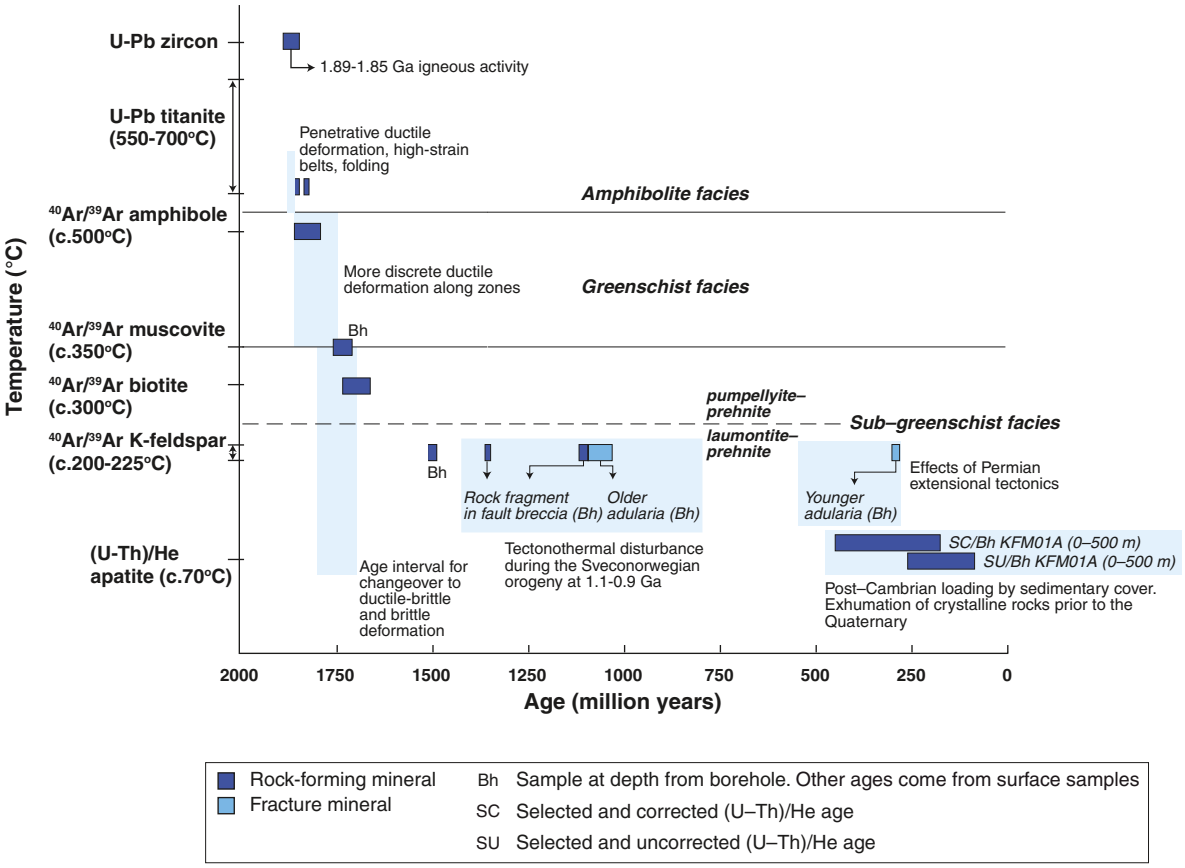

Figure 3-4. *Summary of the geochronological data that constrain the bedrock geological evolution in the Forsmark area from /Söderbäck (ed) 2008/. $^{40}Ar/^{39}Ar$ biotite data from depth in boreholes are not shown here. As expected, these data are somewhat younger than the equivalent surface data. Only a selection of (U-Th)/He data are shown. The procedure adopted concerning the interpretation of all the (U-Th)/He data, both corrected and uncorrected, is discussed in /Söderbäck (ed) 2008/. Important geological events that have been recognised in the Forsmark area are shown in pale blue rectangles with accompanying text on the figure.*

belts and shortening across them, so-called dextral transpressive deformation, has been inferred. This deformation is related to bulk crustal shortening in an approximately northward direction during oblique subduction of oceanic lithosphere. Subduction occurred beneath the ancient continental margin to the north-east (Figure 3-1).

The brittle deformational history at Forsmark, which initiated some time between 1.8 and 1.7 Ga (Figure 3-4), has been evaluated with the help of three lines of approach:

- The use of low-temperature geochronological data that shed light on the exhumation and cooling history (Figure 3-4).
- The relative time relationships between different fracture minerals and the absolute ages of the low-temperature variant of the mineral K-feldspar, referred to as adularia (Figure 3-4).
- A comparison of kinematic data from brittle structures along deformation zones (section 5.2.6) with the tectonic evolution in a regional perspective (section 3.1.1).

Different generations of fracture minerals have been recognised in the Forsmark area. An early period of precipitation of a high-temperature mineral assemblage, which includes epidote, was followed by a period of hydrothermal precipitation of different, lower temperature minerals, including adularia (older generation), hematite, prehnite, laumontite and calcite. The fractures that bear epidote formed prior to 1.1 Ga, i.e. are pre-Sveconorwegian in age. The effects of Sveconorwegian tectonothermal activity for the evolution of fracture mineral assemblages are evident (Figure 3-4). However, the close relationship between the stability field for the laumontite-prehnite mineral assemblage and the closure temperature at c. 200 to 225°C for the $^{40}Ar/^{39}Ar$ K-feldspar isotope system (Figure 3-4) illustrates the

sensitivity of this system for resetting during growth of, for example, laumontite. For this reason, it is not clear whether the older generation of adularia formed during or prior to the Sveconorwegian tectonothermal event. The integrated evaluation that makes use of the different lines of approach outlined above suggests that the different sets and sub-sets of deformation zones in the Forsmark area had formed and had already reactivated during Proterozoic time, in connection with the late Svecokarelian, Gothian and Sveconorwegian tectonic events (see also /Stephens et al. 2007/).

On the basis of the (U-Th)/He apatite data from boreholes, some constraints on when different segments of the bedrock at different crustal levels passed through the c. 70°C geotherm have been attained (Figure 3-4). These data indicate that a sedimentary cover was situated on top of the crystalline basement rocks throughout much of the Phanerozoic. At Forsmark, this cover was possibly c. 3 km thick during the Silurian. A generally slow exhumation rate in the order of 3 to 10 m/Ma occurred during the Late Palaeozoic and Mesozoic, and resulted in a reduction in thickness of the cover to c. 2 km by the Early Jurassic /Söderbäck (ed) 2008/. Some evidence for an increase in exhumation rate during the Permian is apparent.

Several lines of evidence indicate faulting after the establishment of the sub-Cambrian unconformity in the Forsmark area. Furthermore, precipitation of younger low-temperature minerals, including sulphides, clay minerals and calcite, occurred during and probably after Palaeozoic time. Both growth of adularia (younger generation) during the Permian (Figure 3-4) and migration of fluids downwards from the sedimentary cover into the crystalline bedrock have been established. Examples of downward fluid migration include the precipitation of oily asphaltite along fractures in the upper part of the bedrock. The asphaltite was derived from overlying Cambrian to Lower Ordovician oil shale that has now been eroded away. Furthermore, fluids that transported glacial sediment migrated downwards and filled new or reactivated fractures during the later part of the Quaternary period. The downward migration of different types of water during the Quaternary is addressed in more detail in section 3.4.

3.2 Palaeoclimate and geological development during the Quaternary period

The Quaternary climate is characterised by large and sometimes rapid changes in global temperature. The current period was preceded and will be followed by colder periods, during which ice sheets covered and will cover, respectively, larger areas than at present. The Forsmark area has been covered by glacier ice at least three times during the Quaternary period. However, the total number of glaciations that affected Forsmark is not known. The cold glacial periods were much longer than the warmer interglacial periods, which are characterised by a climate similar to the present. However, long ice-free periods have also occurred during the glacials. During these ice-free periods, the climate was colder than today and tundra conditions probably prevailed in large parts of Sweden. Consequently, it can be assumed that permafrost has prevailed in the Forsmark area for long periods. The latest glaciation (Weichselian) started c. 115,000 years ago, and there is geological evidence for at least two periods when a large part of Sweden was free of ice. However, the onset of the latest glacial coverage at Forsmark and the exact timing and duration of the ice-free periods at the site are unknown. By contrast, the timing of the latest deglaciation is rather well established along the coast of the Baltic Sea.

The present interglacial, the Holocene, started at the deglaciation of Mid-Sweden when the ice margin had not yet reached Forsmark. The climate during the deglaciation became successively warmer, although some periods with colder climate did occur. In southern Sweden, the warmer climate caused a gradual change from tundra vegetation to forest dominated by deciduous trees. The Mid-Holocene climate was characterised by temperatures a few degrees higher than today. The forests in southern Sweden have subsequently been dominated by coniferous forest. The areas covered by forest began to decrease c. 3000 BC due to the introduction of agriculture. However, the areas used as arable land are decreasing today and the forested areas are increasing.

The development of the Baltic Sea after the latest deglaciation has been characterised by ongoing shoreline displacement. The interaction between isostatic recovery related to the removal of ice and unloading, and eustatic sea level variations has caused variable depth in the straits connecting the Baltic Sea with the Atlantic Ocean in the west. In turn, this has caused variable salinity throughout the Holocene. The development of the Baltic Sea since the latest deglaciation has been divided into

four main stages (Figure 3-5). Three of these stages; Yoldia, Ancylus and Littorina, are named after molluscs, which reflect the salinity of the stages. The salinity variations in the open Bothnian Sea during the last c. 9,000 years is shown in Figure 3-6. During the period 4500–3000 BC, the salinity was almost twice as high as it is today.

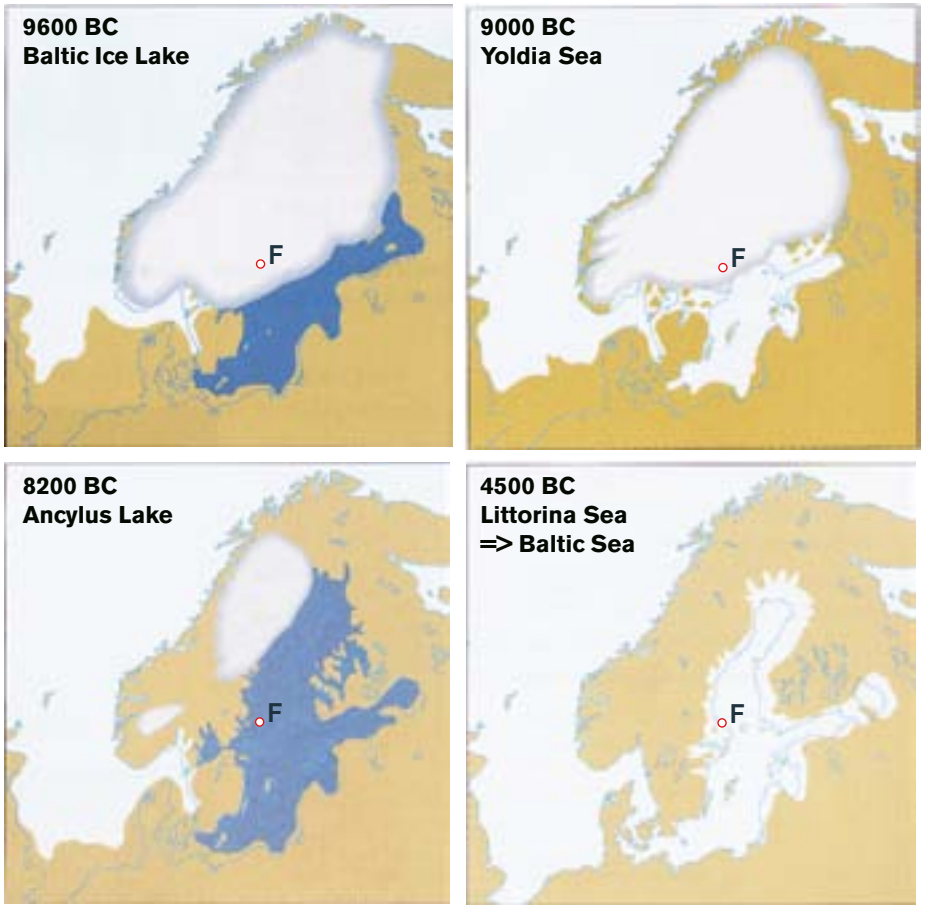

Figure 3-5. *Four main stages characterise the development of the Baltic Sea since the latest deglaciation: A) the Baltic Ice Lake (13,000–9500 BC), B) the Yoldia Sea (9500–8800 BC), C) the Ancylus Lake (8800–7500 BC) and D) the Littorina Sea (7500 BC-present). Fresh water is symbolised by dark blue and marine/brackish water by pale blue, modified after /Fredén (ed) 2002/. "F" indicates the location of Forsmark.*

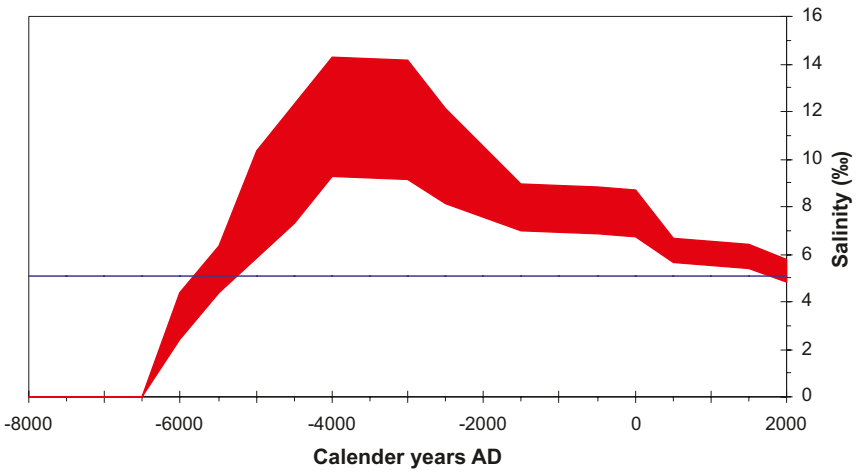

Figure 3-6. *Estimated range for the salinity of sea water in the open Bothnian Sea during the last c. 9,000 years. Maximum and minimum estimates are derived from /Westman et al. 1999/ and /Gustafsson 2004ab/. The present salinity in the area is shown as a horizontal reference line.*

The Forsmark regional model area is situated below the highest shoreline. During the deglaciation at c. 8800 BC, Forsmark was situated c. 150 m below the current sea level, and the first parts of the regional model area at Forsmark emerged from the sea around 500 years BC (Figure 3-7).

It is suggested that all known unconsolidated deposits at Forsmark were deposited during the last phase of the latest glaciation and after the following deglaciation (see chapter 4 in /Söderbäck (ed) 2008/). A till unit consisting of over-consolidated silty-clayey till was deposited during an earlier phase of the latest glaciation. However, the possibility of the occurrence of older deposits cannot be excluded and there are indications of older deposits in adjacent areas outside the regional model area.

Till and glaciofluvial material were deposited directly by the ice sheet and by glacial meltwater, respectively. During the deglaciation, glacial clay was deposited in the lowest topographical areas. The subsequent shoreline displacement had a major impact on the distribution and relocation of fine-grained Quaternary deposits. The most exposed areas were affected by wave washing and bottom currents. Sand and gravel were consequently eroded from older deposits, transported and deposited at more sheltered locations. Periods of erosion also occurred at sheltered locations, which caused erosion of fine-grained deposits such as glacial clay. Shoreline displacement is an ongoing process and new areas are currently exposed to erosion, whereas sheltered bays, with conditions favourable for deposition of clay gyttja, have formed elsewhere.

3.3 Seismicity during the Quaternary period

An earthquake is the result of a sudden release of energy through movement (faulting) along a deformation zone, resulting in the emission of seismic waves. This movement is normally the result of stresses that have accumulated over a certain time interval in a particular volume. Overviews of palaeoseismic activity in Sweden during the latest part of and after the Weichselian glaciation, with special focus on the Forsmark and Laxemar-Simpevarp areas, as well as of seismic activity in historical time from 1375 up to 2005 AD, over the northern part of Europe, are presented in /Söderbäck (ed) 2008/.

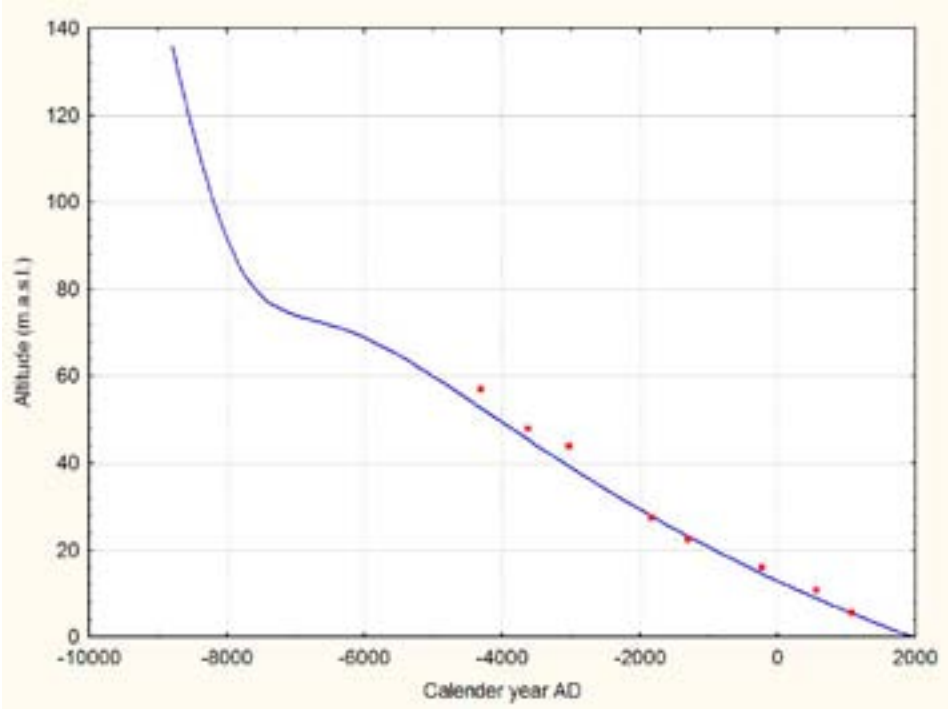

Figure 3-7. *Shoreline displacement curve for the Forsmark area after the latest deglaciation. The red symbols are from dating of the isolation events of lakes and mires /Hedenström and Risberg 2003/. The blue solid curve was calculated using a model from /Påsse 2001/.*

Palaeoseismic activity has been inferred directly by, for example, distinct displacement of the surface that separates the crystalline bedrock from the Quaternary cover or indirectly by seismically derived deformation of Quaternary sediment. The interpretation of aerial photographs provides a tool to identify morphologically conspicuous lineaments that are candidates for late- or post-glacial faults. A significant number of late- or post-glacial, reverse fault scarps have been identified in the northern part of Sweden and it has been inferred that the accompanying earthquakes reached magnitudes of up to M8 or even larger on the Richter magnitude scale. As yet, conclusive evidence for such fault movements is lacking in the southern part of Sweden.

With the help of a similar methodology that has been used in the northern part of the country, detailed investigations to evaluate the occurrence of palaeoseismic activity in and around the Forsmark area have been carried out in the context of the site investigation work. None of the morphological lineaments that have been recognised have been inferred to represent late- or post-glacial faults. Furthermore, no deformational features in Quaternary sediment have been unambiguously related to seismic activity. On the basis of these results, evidence in the geological record for major (magnitude > M7 on the Richter scale) earthquakes in the Forsmark area is lacking.

Compared with other parts of the world, especially close to plate boundaries, there is generally a low frequency of registered earthquakes throughout historical time in the northern part of Europe, and an absence of earthquakes with a magnitude ≥ M6 on the Richter scale (Figure 3-8). However, seismic activity in Sweden throughout historical time is not evenly distributed over the country (Figure 3-8). Areas of relatively high activity are conspicuous along linear alignments in the northern part of the country, in a broader region in south-western Sweden and, less conspicuously, in the southernmost part of the country (Skåne). By contrast, much of the geological reference area in south-eastern Sweden, including the Forsmark area, shows relatively little seismic activity (Figure 3-8).

The relatively high level of seismicity along the Baltic Sea coast is not an artefact of station distribution or some other factor. The linear alignments of earthquakes, at least in the northernmost part of the country and in adjacent areas in Finland and Norway, have been related to the late- or post-glacial faults that have been recognised with the help of palaeoseismic studies. The linear alignment along the Baltic Sea coast in Norrland occurs where both land uplift related to post-glacial isostatic rebound is greatest and where there is also a tendency for a decrease in crustal thickness. A correlation between an increased frequency of seismic events and crustal thinning is apparent in south-western and southernmost Sweden. The crustal thinning occurs in areas where Late Palaeozoic and younger extensional tectonics has taken place. The crust in Sweden below c. 35 km is seismically quiet and this changeover is most probably related to the more ductile character of the crust beneath this depth. If this interpretation is correct, an average geothermal gradient of approximately 8 to 12°C/km is inferred at the current time.

Although strike-slip movement is the dominant focal mechanism, irrespective of where in Sweden the seismic event occurred, reverse dip-slip or oblique-slip fault plane solutions are also present. Since seismic events predominantly occur along geologically ancient fractures or planes of weakness in the bedrock, the orientation of these structures has an influence on the focal mechanism. It is also important to keep in mind that the fault plane solutions discussed above pertain to crustal stress at depths affected by seismic activity. Considerable evidence points to a reverse sense of movement in the uppermost part of the crust (c. 1,000 m) in large parts of Sweden, with a vertical or sub-vertical minimum principal stress.

The maximum horizontal stress as inferred from the seismic data is oriented WNW-ESE. This direction is in accordance with that expected from plate tectonics with ridge push forces from the mid-Atlantic ridge. These considerations give support to the hypothesis that ongoing plate tectonic processes are important for an understanding of recent seismic activity. Palaeoseismic activity has been explained by the release of stress that accumulated earlier during glacial loading in association with long-term tectonic plate motions. An alternative mechanism that involves the release of high horizontal stresses induced by flexure during loading, in combination with the ambient plate tectonic stresses, has also been discussed. The release of stress and fault instability occurred during unloading and the rapid removal of the ice.

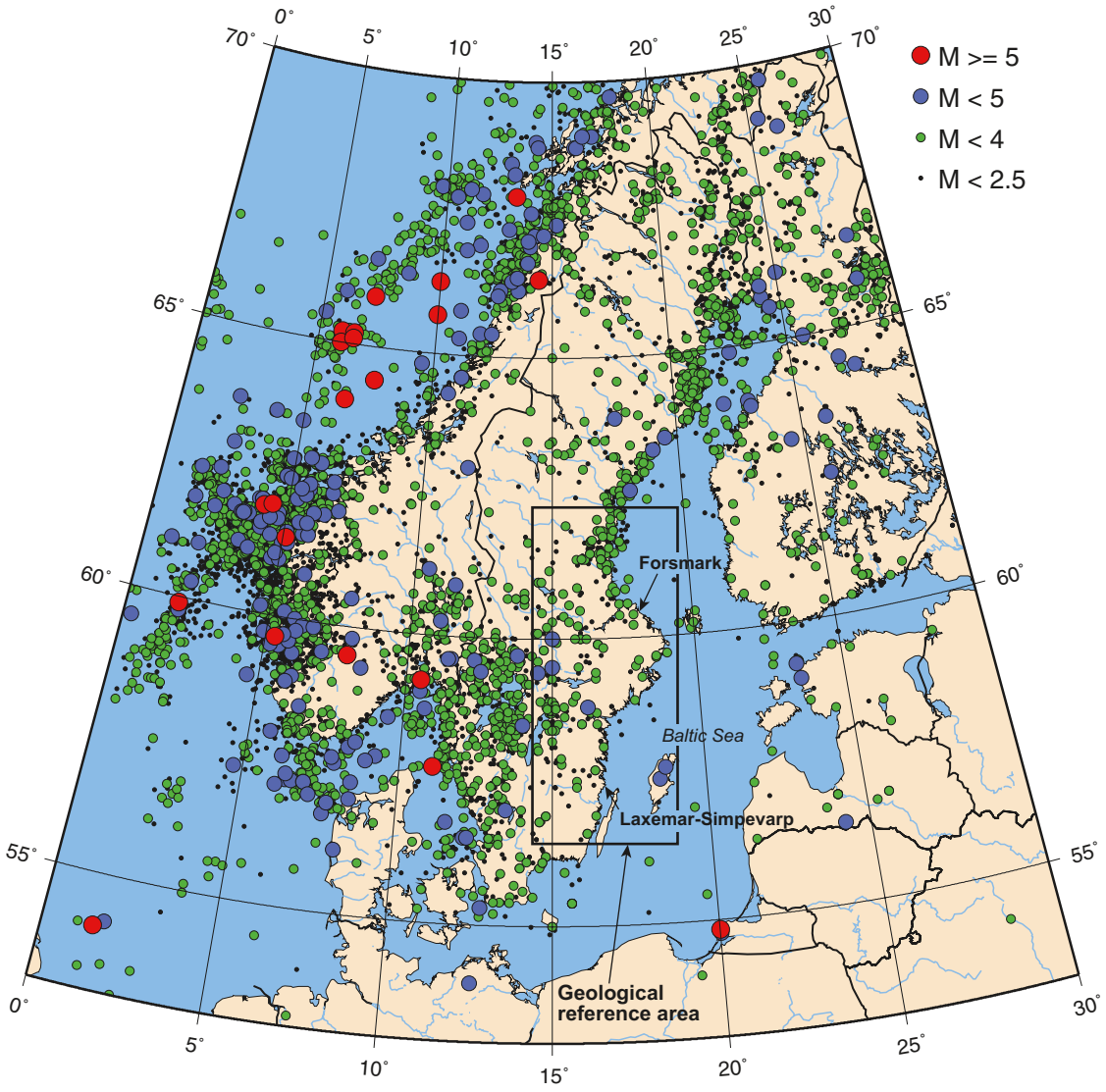

Figure 3-8. *Epicentre and magnitude of earthquakes on the Richter scale (M) in the northern part of Europe between 1375 and 2005 AD. There is no lower limit on the magnitude of the earthquakes shown in the figure. However, since the ability to detect smaller events has changed and gradually improved over time, no precise level of completeness for such data can be provided. Note that earthquake data for the neighbouring countries to the south of the Baltic Sea are also not complete. Modified after /Bödvarsson et al. 2006/.*

3.4 Groundwater evolution during the Quaternary period

The groundwater evolution in the Forsmark area has been strongly affected by climate changes in the past. Investigations have shown that the groundwaters observed today have different origins, including glacial meltwater, meteoric water and marine water, depending on the prevailing conditions. Shoreline displacement plays an important role in understanding the infiltration mechanism for these waters. It is particularly important for the intrusion of the saline Littorina Sea water into the bedrock, as well as for the subsequent flushing processes in the upper, more permeable bedrock horizons. It seems that the most recently recharged water tends to flush older water types, especially in the upper permeable part of the bedrock. However, hydraulic conditions vary over time, and remnants of earlier climatic fluctuations can be preserved in localised areas of low permeability. Thus, palaeohydrogeochemistry provides an important framework for understanding the bedrock hydrogeochemical evolution, which is crucial for the hydrogeochemical and hydrogeological understanding of the site. Changes in the hydrogeological development that have already taken place may be repeated during the lifespan of a repository (thousands to hundreds of thousands of years). As a result, water types such as brine, glacial water, marine and meteoric waters will intrude and be mixed in a complex manner at various levels in the bedrock.

The post-glacial development reveals that when the continental ice melted and retreated from the Forsmark area around 8800 BC, glacial meltwater was hydraulically forced under considerable head pressure into the bedrock. This took place before the development of the Ancylus Lake in the area. The exact penetration depth is unknown, but, according to hydrodynamic modelling (see, for example, /Jaquet and Siegel 2003, 2006/), depths exceeding several hundred metres are possible.

As described in section 3.2, the post-glacial development of the area close to the Baltic Sea can be divided into a number of non-saline and brackish lake/sea stages. Two stages with brackish water can be recognised; the Yoldia Sea (9500 to 8800 BC) and the Littorina Sea (7500 BC to the present). Since the deglaciation of the Forsmark region coincided with the end of the Yoldia Sea stage, there are no signs of water related to the Yoldia Sea in the bedrock. In contrast, the freshwater Ancylus Lake was developed after the deglaciation, followed by the Littorina Sea (see Figure 3-5). During the Littorina Sea stage, the salinity was considerably higher than at the present day, reaching a maximum of about 15‰ between 4500 and 3000 BC. Dense brackish seawater from the Littorina Sea was able to penetrate the bedrock, resulting in a density intrusion that affected the groundwater in the more conductive parts of the bedrock (see chapter 9). The density of the intruding seawater in relation to the density of the existing groundwater, together with the hydraulic properties of the bedrock, determined the final penetration depth. As the Littorina Sea stage provided the most saline groundwater, it is assumed to have had the deepest penetration depth, eventually mixing with the groundwater mixtures already present in the bedrock, e.g. deep saline water, old meteoric-glacial waters, and Holocene glacial melt water. During the last 2,000 years, the salinity has remained relatively constant (cf. Figure 3-6).

When the Forsmark regional model area subsequently emerged from the sea, starting around 500 BC, meteoric recharge water formed a layer on top of the saline water because of its low density. As a result of the flat topography of the Forsmark area and of the short period that has elapsed since the area emerged from the sea, the out-flushing of saline water has been limited. For this reason, a freshwater layer is restricted to shallow depth, from the surface down to 25–100 m depth, depending on hydraulic conditions.

As a result of the late- and post-glacial developments, five different water types can be identified. On the basis of the hydrogeochemical data, these water types are, in relative chronological order: Deep saline water (oldest) > Mix of old meteoric-glacial waters (hypothetical) > Glacial melt water from the last deglaciation > Littorina Sea water > Present-day meteoric water (most recent). The mix of old meteoric-glacial waters is not observed as a dominant component of the present-day groundwater, and the previous occurrence of this water type can only be hypothesised. A detailed description of the different water types is given in chapter 9 in this report.

In order to help understand the step-by-step evolution of groundwater in the Forsmark area during post-glacial time, i.e. during the Holocene, a conceptual model is presented in Figure 3-9. The palaeohydrological conditions in the area have changed rapidly over time and, as can be seen, the major driving mechanism behind the flow lines is the shoreline displacement due to land uplift. There remain some uncertainties with this conceptual model, and the uncertainties are greater further back in time. Hence, the largest uncertainties are associated with the stage showing the flushing of glacial meltwater.

3.5 Development of ecosystems during the late Quaternary period

Long-term ecosystem development in near-coastal areas of Fennoscandia is driven mainly by two different factors; climate change and shoreline displacement. In addition, human activities have also strongly influenced the development of both terrestrial and aquatic ecosystems, especially during the last millennia.

Shortly after the latest ice retreat, which started in southernmost Sweden c. 15,000 BC, the landscape was free of vegetation and can be characterised as polar desert. Relatively soon after the deglaciation, the ice-free areas were colonised and in southern Sweden the landscape was covered by a sparse Birch forest. Thereafter, the climate has oscillated between colder and warmer periods. During the cold period called the Younger Dryas (c. 11,000–9500 BC), large areas of the deglaciated parts of Sweden were again affected by permafrost and much of the previously established flora and fauna disappeared. From the onset of the Holocene (c. 9500 BC) and thereafter, southern Sweden has been more or less covered by forests, although the species composition has varied due to climatic changes. Most of the present

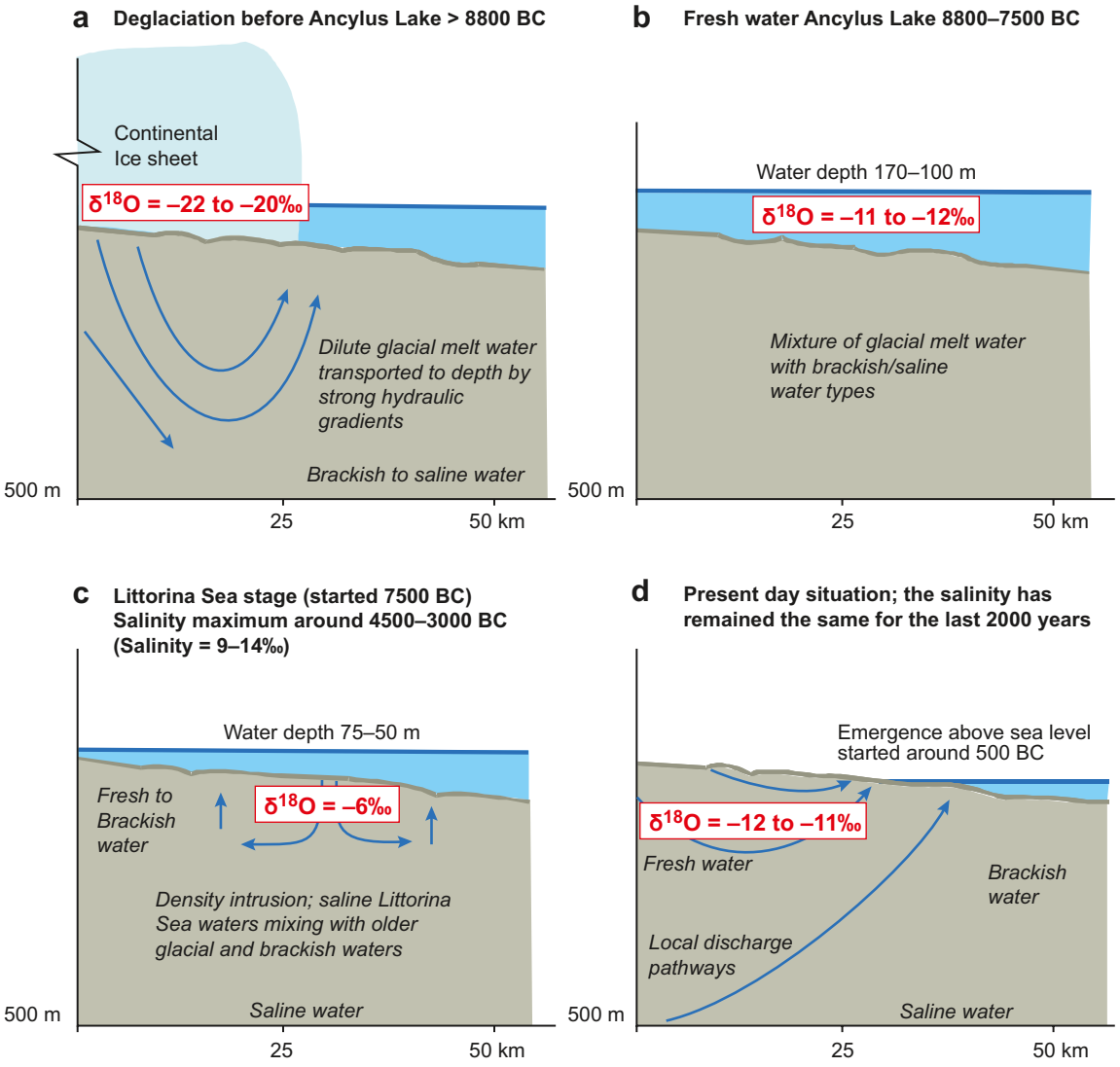

Figure 3-9. *Conceptual model for groundwater evolution in the Forsmark area during the post-glacial period a) the deglaciation before the Ancylus Lake (> 8800 BC), b) stagnant conditions during the freshwater Ancylus Lake stage between 8800 and 7500 BC, c) density driven intrusion of Littorina sea water between 7500 BC and 0 AD, and d) the present-day situation. Blue arrows indicate groundwater flow pattern.*

mammal fauna was established in southern Sweden during the early Holocene. During the last few thousand years, the composition of the vegetation has changed not only to due to climatic changes, but also due to human activities which have decreased the areas covered by forest. In southern Sweden, the introduction of agriculture and the subsequent opening of the landscape started c. 3000 BC.

In coastal areas like Forsmark, shoreline displacement has strongly affected ecosystem development and still causes a continuing change in the abiotic environment. As a result of an overall regressive shoreline displacement, the sea floor is uplifted and transformed into new terrestrial areas or to freshwater lakes. The initial conditions for ecosystem succession from the original near-shore sea floor are strongly dependent on the topographical conditions, where sheltered bays accumulate organic and fine-grained inorganic material, whereas the finer fractions are washed out from more wave-exposed shorelines with a large fetch. During the process of shoreline displacement, a sea bay may either be isolated from the sea at an early stage and thereafter gradually turn into a lake as the water becomes fresh, or it may remain as a bay until shoreline displacement turns it into a wetland.

After isolation from the sea, the lake ecosystem gradually matures in an ontogenetic process which includes subsequent sedimentation and deposition of substances originating from the surrounding catchment or produced within the lake. Hence, the long-term ultimate fate for all lakes is an inevitable fill-up and conversion to either a wetland or a more dry land area, the final result depending on local hydrological and climatic conditions. In Forsmark, all present-day lakes have developed into oligotrophic hardwater lakes that are characteristic of the area. These lakes show high pH (pH 7–8), low phosphorous concentration (tot-P often lower than 0.015 mg/L), high concentrations of major ions and high electrical conductivity. This is a combined effect of the calcium-rich Quaternary deposits, the recent emergence from the Baltic Sea and the shallow lake depths, resulting in high primary production at the light-illuminated sediment surface and very low production in the water mass. The high primary production at the sediment surface results in high benthic pH, which in turn causes benthic precipitation of $CaCO_3$ and co-precipitation of phosphorous. Much of the precipitated phosphorous is more or less permanently locked in the sediments by high pH and high O_2 concentration.

Mires are formed basically through three different processes; terrestrialisation, paludification and primary mire formation. Terrestrialisation is the filling-in of shallow lakes by sedimentation and establishment of vegetation. Paludification, which is the dominant process of mire formation in Sweden, is an ongoing water logging of more or less water-permeable soils, mainly by expanding mires. Primary mire formation is when peat is developed directly on fresh soils after emergence from water or ice. All three processes are likely to occur in the Forsmark area, but peatland filling in lakes (terrestrialisation) is probably the most common type of peatland development in the investigation area. The richer types of mires, which are typical of the Forsmark area, will undergo a natural long-term acidification when turning into more bog-like mires.

3.6 Human population and land use

The human prehistoric period in the Forsmark region, which is an investigation area around Forsmark including six parishes together covering c. 1,000 km^2 /Berg et al. 2006/, is relatively short, since Forsmark was covered with water until c. 500 years BC. Accordingly, the Forsmark region was not permanently settled until the end of the prehistoric period. In the register of prehistoric remains made by the National Heritage Board, there are about 30 places with one or several prehistoric or cultural remains registered in the investigated region. However, there are many prehistoric settlements further inland in the northern parts of Uppland. The oldest known remains in the Forsmark region are graves from the older Iron Age (300 BC–400 AD), today situated 10 to 15 m above sea level. When built, these graves were situated along the coastline.

The oldest information on settlements in the region is the tax register from 1312 AD, which includes three of the investigated parishes. This source indicates that the region was relatively densely populated in the early medieval period. Between 1312 and 1550 AD, there seems to have been a substantial decrease in the number of settlement units in the region, probably as an effect of the recurrent plague epidemics after 1349 AD /Berg et al. 2006/. During the medieval period, the Forsmark region was characterised by small villages, and new settlements were created in the peripheral areas of the older ones. At the end of the medieval period, the investigated parishes showed a dominance of freeholders and the proportion of farms that belonged to the nobility was small.

During the early modern period (i.e. 1550–1750 AD), the establishment of the iron industry in the Forsmark region dramatically affected the surrounding landscape. Production was geared towards the needs of the industry; charcoal production, mining and the production of fodder for animals used in the industry. The ownership structure also changed abruptly with the establishment of large estates. Similar to many other places in Sweden, there was a substantial population expansion. Many crofts were established in the forested areas around Forsmark, inhabited by people involved in the production of charcoal. The population doubled or increased at an even faster rate between the 1570s and the 1750s.

The large estates in the Forsmark region expanded during the 18th century and, accordingly, the number of freehold farms decreased. The population increased dramatically from the 1780s up to the late 19th century. At the turn of the century, the increase ceased and, during the latter part of the 20th century, the rural population decreased. The number of people involved in agriculture has decreased, and instead, the number of people employed in industry and crafts is greater than before.

The extent of arable land in the region increased continuously from the colonisation of the area until around 1950 AD. To increase the amount of hay that was fed to the farm animals, small farms and individual families carried out hay-making using the reeds and grasses on wetland areas. Since these areas were often distant and hard to reach, they were mainly used by poor families that needed to feed their animals. Until the middle of the 19th century, there were large wetland areas in the woodlands. From the beginning of the 18th century onwards, much of the new agricultural land was gained from ditching of wetlands. Some of these areas are still cultivated, whereas others are now deserted and, in some cases, have been turned into woodlands. From the early 1900s until the 1950s, most of the arable land in the Forsmark region did not change. However, following this time, a significant part of the former open land has been abandoned and the current land use is completely dominated by forestry. During the last decades, the establishment of the Forsmark nuclear power plant has resulted in substantial changes in land use, turning parts of the area from relatively pristine, rural conditions to an industrial park and a semi-urban society.

4 Surface system and surface-bedrock interactions

This chapter presents results from the work concerning the surface system, i.e. regolith and Quaternary geology, hydrology, chemistry, biota, as well as ecosystem models for the terrestrial-, limnic- and marine ecosystems. Furthermore, the surface-bedrock interactions are also addressed. An integrated description of the surface system at Forsmark, performed by the SurfaceNet project group, is given in /Lindborg (ed) 2008/.

The surface system starts where the upper part of the bedrock ends, except where the bedrock reaches the surface and outcrops thereby becomes a part of the surface system. This means that a number of different disciplines are represented in the description of patterns and processes at various spatial and temporal scales, and the present chapter constitutes a considerable condensation of a large number of background reports. Hence, this chapter functions partly as a pointer to the supporting background reports. The main references, developed to be used as input to the safety assessment, are listed in section 4.5.

The overall aim of the modelling is to produce a detailed description of the current conditions at the site. The site description is to be used in safety assessments as input data on properties, processes, overall system conceptualisation and understanding, but also as input to the EIA (Environmental Impact Assessment) and design of the repository. Even if the main focus is on the description of current conditions, it is almost equally important to know the history of the studied site, not only to understand the present patterns, but also to make projections of possible future conditions in the safety assessment.

The aim of the ecosystem modelling is to describe mass balances for different chemical elements in the terrestrial, limnic and marine environments. An important tool is the calculation of carbon budgets to estimate and predict flow and accumulation of organic matter and associated elements at a landscape scale in the safety assessment.

4.1 State of knowledge at the previous model version

Since the previous model version 1.2 /SKB 2005a/, the volume and variety of surface system data have increased considerably. This has refined the surface descriptions and the models of the site. Furthermore, the integration of the bedrock and the surface system has been analysed and an interface between the two systems has been characterised. This will facilitate the description and handling of potential flow paths and radionuclide retention processes between the bedrock- and surface systems in the radionuclide transport modelling.

The site description of the surface system has developed through the years to a general understanding of how the site functions in terms of properties in different volumes, the main functional units, processes and system descriptions from different scientific disciplines. The conceptual model that was developed at the beginning of the work in 2002 has been adjusted to site-specific features, and site data have been used to describe stocks, flows and accumulations of matter within and between different parts of the surface system at Forsmark.

4.2 Evaluation of primary data

The investigations performed in the Forsmark area are summarised in sections 2.1 and 2.2, and the data supporting the current model version are listed in Tables 7 and 8 in Appendix 3. The evaluation of these data is presented below.

4.2.1 Regolith and Quaternary geology

Thorough descriptions and evaluations of the input data and the methods used are presented in /Hedenström et al. 2008/. The description of the Quaternary deposits is focused on the spatial distribution of the different units, together with a description of their physical and chemical properties. The physical properties are used as input data for the hydrogeological modelling /Johansson 2008/, whereas the chemical properties contribute to the biological models of the upper geosphere and to the hydrogeochemical modelling /Tröjbom et al. 2007/.

Below follows a condensed description of the Quaternary geology and the distribution and properties of regolith in the Forsmark area. The description consists of a brief overview of the geological evolution of the area and the spatial distribution and properties of the different units. For a detailed description of the properties and distribution of the regolith at Forsmark, see /Hedenström and Sohlenius 2008/ and for the geological and historical development of the site, see chapter 3 as well as chapters 4 and 6 in /Söderbäck (ed) 2008/. A description of the semi-3D regolith depth model is found in /Hedenström et al. 2008/.

Distribution

Quaternary deposits cover c. 90% of the ground surface within the model domain (Figure 4-1). The average modelled regolith depth at Forsmark, including the bedrock outcrops, is 5.6 m

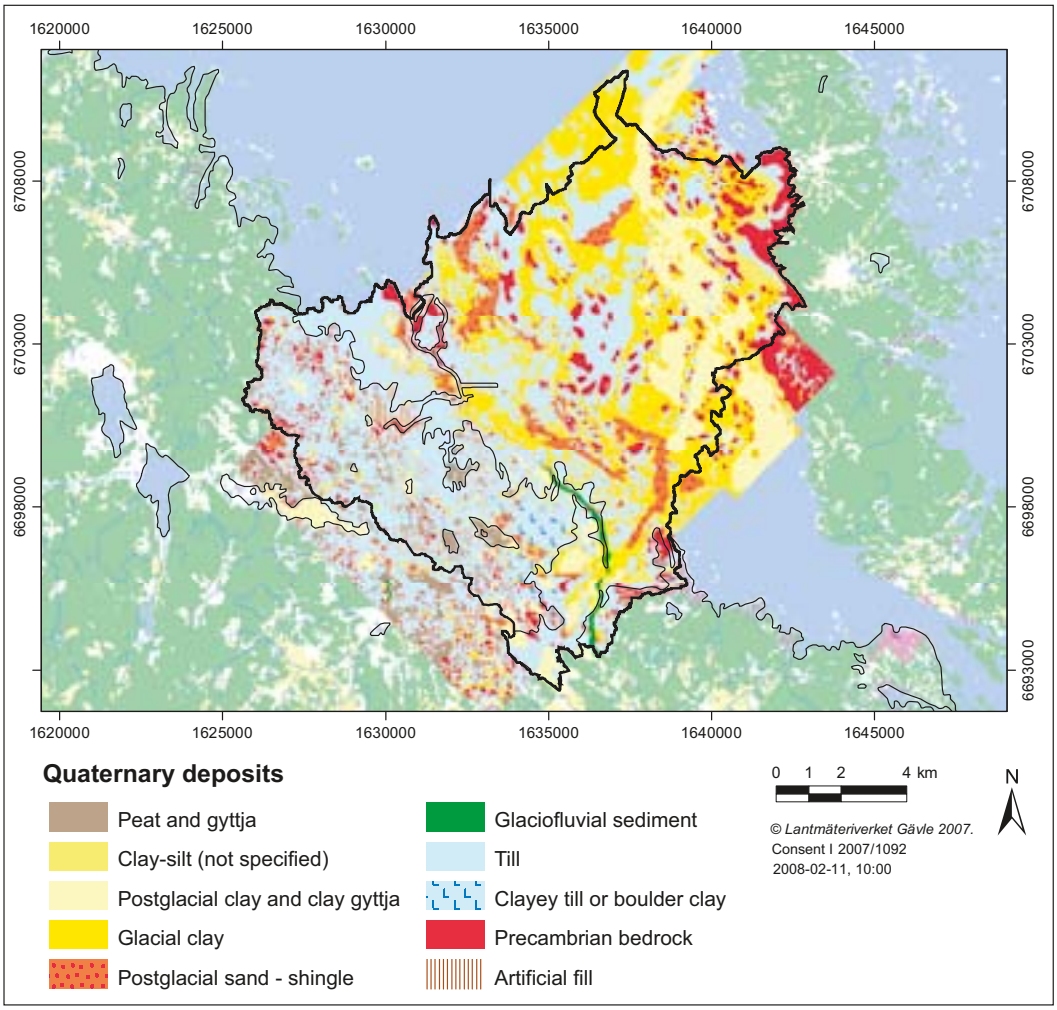

Figure 4-1. *Map showing the distribution of the Quaternary deposits in the Forsmark area (Figure 2-4 in /Hedenström et al. 2008/). The map is a compilation of six different geological maps, originally presented at different scales. It should be noted that the areas presently covered with water (under lakes, streams and in the sea) are presented without water. The black line shows the extension of the regolith depth model, see Figure 4-2.*

/Hedenström et al. 2008/. The spatial distribution of the regolith is highly dependent on the bedrock morphology. The more elevated areas in the south-western part are dominated by till and bedrock outcrops, whereas the fine-grained sediments are concentrated in the deeper areas offshore. Exposed bedrock or bedrock with only a thin regolith (< 0.5 m) occupies c. 9% of the area in the regional model area and only c. 5% of the central part (Table 4-1). Areas with low frequency of outcrops are e.g. the eastern part of Storskäret, west of Lake Bolundsfjärden, and the major part of the marine area. Areas with high frequency of bedrock outcrops are e.g. north of Bruksdammen, along the present shoreline and on several of the small islands. Many of the outcrops are abraded on the northern side, indicating active ice with a dominant flow direction from 350–360°, while an older ice-movement direction from the north-west is preserved on lee side positions.

All known regolith in the Forsmark regional model area has been deposited during, or after the Weichselian glaciation, i.e. during the last 115,000 years /Söderbäck (ed) 2008/. The oldest deposits are of glacial origin, i.e. deposited directly from the Weichselian ice sheet, or by water from the melting ice. The regolith in Forsmark, as in general in north-eastern Uppland, is characterised by a flat upper surface, young and un-weathered soils, high content of calcium carbonate in gravel and fine fractions, and the occurrence of till with high clay content. The calcium carbonate has its origin from Paleozoic limestone on the sea bottom north of Forsmark, incorporated into and deposited by the glaciers. The soils are typically poorly developed and dominated by Regosols, Gleysols and Histosols /Lundin et al. 2004/.

Till is the dominant Quaternary deposit at Forsmark (Figure 4-1 and Table 4-1). In the terrestrial area, the till has been divided into three areas, cf. /Sohlenius et al. 2004/. Till area I constitutes the major part of the Forsmark terrestrial area, especially in the western and southern parts of the model area. In this area, sandy till with a medium frequency of superficial boulders dominates. The average depth to bedrock within Till area I is 3.5 m (Figure 4-2). Till area II is dominated by clayey till and boulder clay, i.e. a clay content > 5% of the matrix. Clayey till dominates at Storskäret in the eastern part of the model area, and the major part of the arable land in Forsmark is located within this area. The average depth of the clayey till/boulder clay is 5.8 m /Hedenström et al. 2008/. Till area III is located in the eastern part of the investigated area, close to the Börstilåsen esker, and is characterised by a surface layer with a high frequency of large boulders.

The stratigraphical relation between the till units is more complex than the surface distribution. Sandy till has been observed on top of clayey or silty till in the western part whereas the reverse has been recorded in the east. At the transition between Till area I and II, the two till types have been nested into each other in a more or less random way /Hedenström and Sohlenius 2008/. A unit consisting of a hard clayey till has been observed under sandy till at several sites within Till area I.

Table 4-1. The proportions (%) of the area covered with different Quaternary deposits and bedrock exposures, overall and in subareas of the Forsmark area. The subareas are described in Figure 2-3 in /Hedenström et al. 2008/. Terrestrial refers to all areas excluding those covered by water. Detailed terrestrial refers to the central part of the model area /Sohlenius et al. 2004/.

	All areas	Terrestrial	Detailed terrestrial	Marine area
Bedrock exposures	9	13	5	6
Glacial clay	25	4	4	41
Postglacial clay (including gyttja clay and gyttja)	11	4	4	17
Postglacial sand and gravel	4	2	4	6
Till (sandy/clayey)	48.5 (46/2.5)	65 (58/7)	74 (63/11)	30
Glaciofluvial sediment	0.5	1	2	0
Peat	1	8	3	–
Artificial fill	1	3	4	–

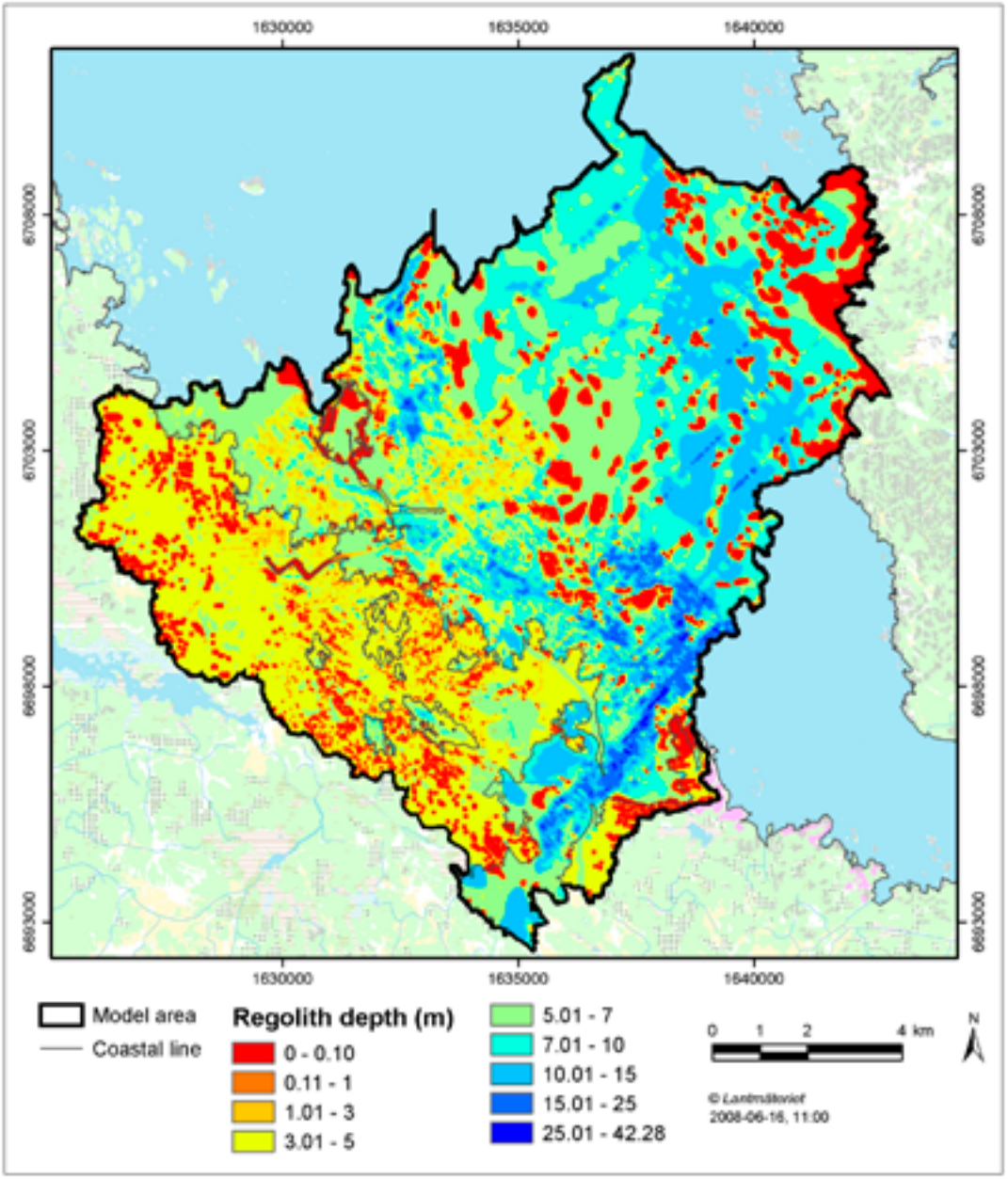

Figure 4-2. *The total modelled regolith depth from /Hedenström et al. 2008, Figure 4-1/. Generally, the regolith is deeper in the marine area (average c. 8 m) than in the terrestrial part (average c. 4 m). The average regolith depth within the whole model domain is c. 6 m.*

Glaciofluvial sediments in Forsmark are concentrated in one small esker, the Börstilåsen esker. Information from the site shows that c. 5–7 m glaciofluvial sand, gravel and stones are located directly on the bedrock. The finest particles, clay and silt, were deposited in deeper water, on top of till /Elhammer and Sandkvist 2005/. Hence, the major part of the glacial clay is found in the offshore area, especially in the areas with a water depth greater than 6 m. In the marine area, the average depth of glacial clay is c. 3 m /Elhammer and Sandkvist 2005/. In the terrestrial part, the areas covered with glacial clay are concentrated in local depressions such as the bottom of lakes and small ponds. Generally, glacial clay in terrestrial areas, especially those not associated with the larger lakes, is often only a few dm thick and is probably remnants after erosion on the bottom of the sea.

After the deglaciation c. 8800 BC, the water level in the Forsmark area was c. 150 m higher than at present /Påsse 2001/. Since the most elevated areas in Forsmark are only c. 25 m above sea level (m.a.s.l.), the Forsmark area has been situated below the Baltic Sea until the last few thousand years. Thus, the formation, erosion and relocation of postglacial deposits have mainly been taking place prior to the emergence from the Baltic Sea. Postglacial gravel and sand are frequently superimposed on glacial clay, interpreted to mainly represent deposition after erosion and transport by currents on the sea floor. Postglacial clay, including clay gyttja, is predominantly found in the deeper parts of valleys on the sea floor (Figure 4-1) and only minor occurrences are documented in the terrestrial area. In the marine area, the average depth of postglacial clay is 0.9 m /Elhammer and Sandkvist 2005/. The ongoing isostatic uplift transfers sedimentary basins to sheltered positions, favouring the accumulation of organic sediments. Clay gyttja is frequent in the surface of the wetlands located at low altitudes, e.g. along the shores of Lake Fiskarfjärden and Lake Gällsboträsket. Gyttja is formed in lakes and consist mainly of remnants from plants that had grown in the lake. In areas with calcareous soils, such as the Forsmark area, calcareous gyttja is formed when lime-saturated groundwater enters the lake and/or by biological precipitation by algae. Peatlands in the Forsmark area are generally young and nutrient rich. Bogs do occur but are few and still young, whereas rich fens are the dominating type of wetlands. Peat is found most frequently in the south-western part of the area, i.e. the most elevated parts that have been above the sea level long enough for infilling of basins and peat to form. Stenrösmossen and the mire at Rönningarna are two examples of mires, which, at least partly, are developed into bogs with an average depth of the peat layer of 1.4 m.

Properties

Table 4-2 presents a summary of grain-size distribution, sorting coefficient (D60/D10) and calcium carbonate ($CaCO_3$) content of the minerogenic deposits. The clay content in till samples is between 0.9% (sandy till) and 25.9% (boulder clay) and the $CaCO_3$ is between 1% (clayey till) and 34% (sandy till). The higher the sorting coefficient (D60/D10) is, the more poorly sorted are the minerogenic deposits.

Table 4-2. Summary of some physical parameters of the most common minerogenic deposits in Forsmark. The ratio D60/D10 (where D60 is the particle diameter corresponding to 60% finer on the grain-size curve, and D10 is the particle diameter corresponding to 10% finer on the grain-size curve) is also called coefficient of uniformity. The smaller the coefficient of uniformity, the more uniform the material. SD = standard deviation.

Deposit	Gravel % *(SD)*	Sand % *(SD)*	Silt % *(SD)*	Clay % *(SD)*	Porosity % *(SD)*	D60/D10 *(SD)*	$CaCO_3$ % *(SD)*
Sandy and sandy silty till (Till area I), n=66	22.1 *(7.8)*	50.8 *(10.1)*	23.5 *(8.9)*	3.6 *(1.1)*	9.47	46.4 *(29.5)*	19.1 *(5.7 (n=62))*
Clayey till and boulder clay (Till area II), n=103	15.8 *(8.1)*	41.2 *(6.8)*	32.3 *(7.2)*	10.8 *(4.4)*	8.5	104.0 *(155.4)*	23.4 *(6.6)*
Gravely till (Till area II), n=15	44.8 *(8.8)*	40.7 *(10.7)*	12.7 *(5.4)*	2.4 *(1.1)*		132.6 *(105.7)*	17.5 *(5.3)*
Gravel, n=5	53.1 *(6.7)*	44.2 *(6.1)*	1.5 *(1.2)*	1.2 *(1.1)*		16.8 *(4.1)*	
Sand, n=15	16.9 *(16.2)*	68.0 *(14.1)*	13.0 *(15.4)*	2.7 *(2.2)*		10.6 *(8.1)*	
Silt, n=4	0.2 *(0.5)*	15.9 *(13.7)*	68.9 *(12.6)*	15.0 *(6.8)*		9.9 *(not valid)*	
Clay, n=30	0.6 *(1.8)*	3.0 *(7.2)*	41.6 *(16.1)*	54.8 *(13.8)*			18.0 *(13.3 (n=29))*

The bulk density of the upper 60 cm of the regolith was investigated in a number of horizons in the soil type inventory /Lundin et al. 2004/. In the upper horizon (0–10 cm), bulk density is low; 0.4–1.5 g/cm^3. The density increases downward to 1.4–2.3 g/cm^3 (50–60 cm) /Lundin et al. 2004/. Bulk density measured in two trenches located in Till area I was 1.5–2 g/cm^3 in the top soil layers, whereas in the deeper layers it was 1.9 and 2.3 g/cm^3, respectively. Porosity is c. 30–40% in the surface and c. 10–20% at c. 2 m depth. The contents of carbon, nitrogen, sulphur and phosphorous in marine and lacustrine sediments and in peat are presented in Table 4-3. In general, the porosity is higher (37–90%) in the water-laid sediments than in the till, whereas the bulk density is generally lower in the organic sediments.

4.2.2 Hydrology and near-surface hydrogeology

Comprehensive hydrological and near-surface hydrogeological field investigations have been conducted within the site investigation, including monitoring of meteorological conditions, surface water levels and discharge, and groundwater levels in Quaternary deposits, as well as hydraulic characterisation of the Quaternary deposits (slug tests, pumping tests, permeameter tests on undisturbed core samples, analyses of water retention parameters). Thorough descriptions and evaluations of the input data and the methods used are presented in /Johansson 2008, Johansson and Öhman 2008, Bosson et al. 2008/.

The candidate area is characterised by a small-scale topography and is almost entirely located below 20 m.a.s.l. The mean annual precipitation and runoff are 560 and 150 mm, respectively. The largest lakes are Lake Fiskarfjärden (0.752 km^2), Lake Bolundsfjärden (0.609 km^2), Lake Eckarfjärden (0.282 km^2) and Lake Gällsboträsket (0.185 km^2). The lakes are shallow with mean and maximum depths ranging from approximately 0.1 to 1 m and 0.4 to 2 m, respectively. Seawater flows into the most low-lying lakes during events of very high seawater levels. Wetlands are frequent and cover as much as 25 to 35% in some of the sub-catchments.

No major water courses flow through the central part of the candidate area. The brooks downstream of Lake Gunnarsboträsket, Lake Eckarfjärden and Lake Gällsboträsket carry water most of the year, but can be dry for long periods during dry years such as 2003 and 2006. Many brooks in the area have been deepened for considerable distances for drainage purposes.

Based on measurements, the horizontal hydraulic conductivity and specific yield of the till are estimated to be $1.5 \cdot 10^{-5}$ m/s and 0.15, respectively, for the upper 0.6 m of the soil profile, and to be $1.5 \cdot 10^{-6}$ m/s and 0.05, and $1.5 \cdot 10^{-7}$ m/s and 0.03, below that depth for coarse and fine-grained till, respectively. The only vertical K-values for till are from laboratory permeameter tests with a geometric mean for till samples from depths larger than one metre of approximately $4.4 \cdot 10^{-8}$ m/s. Since the geometric mean of the horizontal K-value for till from the slug tests is $1.3 \cdot 10^{-6}$ m/s, this implies an anisotropy ratio (K_h/K_v) of about 30. However, this result should be used with caution since the test scale differs between the investigations. The vertical K-values for gyttja and peat/gyttja/clay obtained from leakage coefficients from the pumping tests are approximately $1 \cdot 10^{-8}$ m/s.

Table 4-3. General stratigraphical distribution and average contents of C, N, S and P as recorded in marine and lacustrine sediments and peat in Forsmark.

Environment	Lithology	Relative age	C %	N %	S %	P %	Water content %	Porosity %	Bulk density g/cm^3
Bog/Fen	Peat	Youngest	55	0.68	0.7	0.02	90	89.6	1.004
Freshwater lake	Gyttja	↑	18	1.4	1.9		93	90.1	1.031
Shallow Baltic basin	Clay gyttja	↑	6.2	0.6	1.6	0.09	86	79.2	1.085
Coast	Post-glacial sand and gravel						8.5	32	1.800 –2.300*
Postglacial Baltic basin	Post-glacial clay	↑	1.8						
Late-glacial Baltic basin	Glacial clay	Oldest	1.00	0.11	0.76		53	37.8	1.40

* = Generic data, /Talme and Almén 1975/.

Groundwater levels in the Quaternary deposits are very shallow; on average less than 0.7 m below ground surface during 50% of the year. Shallow groundwater levels imply a strong interaction between evapotranspiration, soil moisture and groundwater. Diurnal fluctuations of the groundwater levels, driven by evapotranspiration cycles, are evident in many groundwater wells. Furthermore, groundwater level measurements in the vicinity of the lakes show that the lakes may act as recharge sources to till aquifers in the riparian zone during summer.

There is a strong correlation between the topography and the groundwater levels in the Quaternary deposits. For groundwater levels in the upper bedrock there is no such strong coupling to the topography. This is most evident in the central part of the candidate area (i.e. within the target area), where the groundwater level gradients in the bedrock are very small, indicating a high transmissivity. Here, the groundwater levels in the till in general are considerably higher than in the bedrock. Hence, local, small-scale recharge (downward flow) and discharge (upward flow) areas, involving groundwater flow systems restricted to the Quaternary deposits, will overlie the larger-scale flow systems associated with groundwater flow in the bedrock. Also, in the middle of Lake Bolundsfjärden, located in the central part of the candidate area, the lake level and the groundwater level in the till below the lake are considerably higher than the levels in the bedrock down to 200 m depth, indicating a downward flow gradient from the lake and the Quaternary deposits to the bedrock.

The flow systems around and below the lakes seem to be quite complex. The lake water/groundwater level relationship, under natural as well as disturbed conditions, indicates that the lake sediments and the underlying till have low vertical hydraulic conductivities. The groundwaters below the lakes have relict marine chemical signatures, whereas groundwaters in the riparian zones are fresh.

4.2.3 Hydrochemistry

Evaluations of hydrochemical input data are presented in /Sonesten 2005, Tröjbom and Söderbäck 2006, Tröjbom et al. 2007/, whereas data on the chemical composition of the regolith are evaluated in /Tröjbom and Söderbäck 2006/.

The surface water and shallow groundwater at Forsmark is characterised by high pH-values and high contents of major constituents, especially calcium and bicarbonate /Sonesten 2005, Tröjbom and Söderbäck 2006/. The main reason for this is the glacial remnants, mostly in the form of a till layer, which were deposited during the Weichselian glaciation and deglaciation /Fredén (ed) 2002/. This till layer has a high content of calcite, originating from the sedimentary bedrock of Gävlebukten located about 100 km north of Forsmark. When the ice cover retreated about 11,000 years ago, these deposits were exposed on the sea floor. Due to the flat topography and isostatic land uplift, large parts of the candidate area have emerged from the sea during the last 2,000 years, and new land areas are continuously formed. The dissolution of calcite in terrestrial areas has a central role in determining the current hydrochemistry in surface systems, and is probably also of importance for the composition of the dilute, non-brackish, groundwater in the upper parts of the fractured bedrock. The rich supply of calcium and the high alkalinity affects the structure of the whole ecosystem, for example by forming the oligotrophic hardwater lakes which are characteristic of the area /Nordén et al. 2008/.

The flat topography of the Forsmark area and the recent withdrawal of the Baltic Sea are also important factors determining the surface and near-surface hydrochemistry, besides the exposure of calcite-rich glacial remnants. Marine remnants in the Quaternary deposits, as well as modern sea water intrusions, are strongly influencing the hydrochemistry, especially in areas at low altitude close to the coast. Some lakes are still in their final stages of separation from the Baltic Sea, which is evident by recurrent seawater intrusions (e.g. Lake Bolundsfjärden, cf. Figure 4-3). On the other hand, some of the coastal sampling sites, mainly in the bay Kallrigafjärden, are heavily affected by inflowing freshwater /Sonesten 2005/.

In groundwater samples from the upper parts of the bedrock extending down to depths of several hundred metres, as well as at some shallow groundwater sampling points in the Quaternary deposits, a brackish groundwater type with a clear relict marine signature prevails. Major ions in these groundwaters seem to originate mainly from a marine source but, at least to some extent, also from a deeper saline source /Tröjbom et al. 2007, section 3.2/. The isotope contens of the water

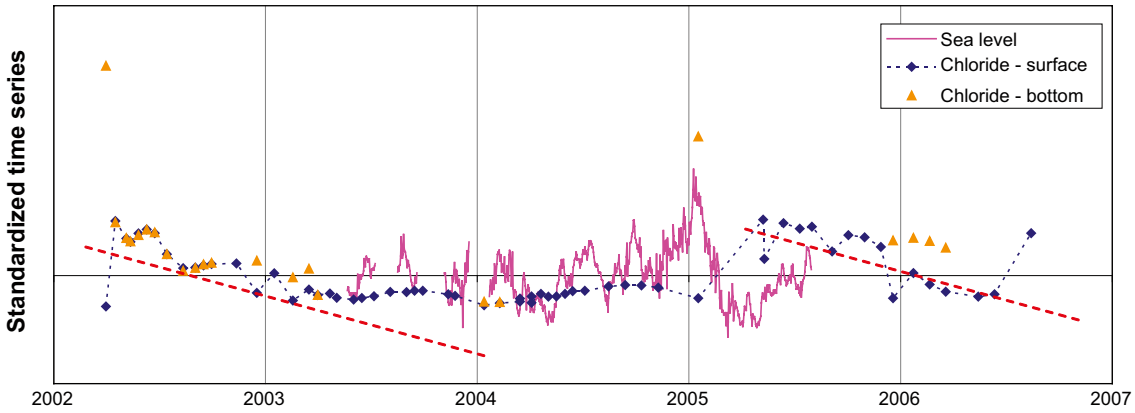

Figure 4-3. *Chloride concentrations in Lake Bolundsfjärden during the period 2002–2007, and measurements of the sea level in the Baltic Sea. Red dashed lines mark the gradual decrease in Cl concentration due to dilution by the supply of freshwater from the catchment (from /Tröjbom et al. 2007/).*

(i.e. ^{2}H, ^{18}O) also show a clear evaporation signature, which reflects the marine (Littorina) origin of the groundwater. However, the relict marine groundwater differs in isotopic composition from the present-day seawater in the Baltic, which may be interpreted as an influence of meteoric recharge during a previous period of cold climate.

The development of the hydrochemistry in the Forsmark area since the latest deglaciation 11,000 years ago is outlined in a conceptual model in chapter 8 in /Tröjbom et al. 2007/. This model describes a generalised hydrological picture, in combination with hydrochemical processes important for the interpretation of past and present hydrological patterns in the surface system and in groundwater in the upper parts of the bedrock. Large-scale marine gradients in the surface system are consistent with the conceptual model and the palaeo-hydrological history described above; areas recently emerged from the Baltic Sea show stronger marine influences compared with areas located at higher altitude. Discharge from Lake Eckarfjärden, located c. 5 m above sea level, contains low concentrations of marine ions, whereas discharge from Lake Gällsboträsket, which was separated from the Baltic more recently and is now located c. 2 m above sea level, still shows significantly elevated concentrations of e.g. Na and Cl due to the ongoing outwash.

An important issue is whether there are any indications of deep groundwater discharge in the surface system. According to observations in surface water and shallow groundwater, cf. section 5.1 in / Tröjbom et al. 2007/, and to the hydrological/hydrochemical conceptual model presented in /Tröjbom et al. 2007/, there is probably no or only limited ongoing deep discharge into the freshwater surface systems in the area. However, there are indications that relict marine remnants, which also may include deep saline signatures, prevail in the groundwater at relatively shallow depths in the Quaternary deposits in restricted areas. This hydrochemical pattern could be explained by influence from marine remnants formed under a previous hydrological regime, i.e. water may have entered the deposits from below when the area was covered by the Baltic Sea. These signatures may be preserved because of stagnant hydrological conditions in some areas, e.g. under and around Lake Bolundsfjärden, cf. section 4.3 in /Tröjbom et al. 2007/. The same seems to apply for Lake Gällsboträsket, but in addition to the indications on stagnant relict marine water under the lake sediments, there are also some indications of ongoing discharge of deep groundwater in the immediate surroundings of that lake (cf. section 4.4 below).

4.2.4 Ecosystems

The description of the terrestrial ecosystem contains both qualitative data such as descriptions of which species are dominant in the area and quantitative descriptions of a number of ecosystem properties. Information about the site-specific data from the terrestrial ecosystem, and the methods used for estimation/calculation, are presented in /Löfgren (ed) 2008/ and references therein. A number of investigations of the limnic ecosystem in the Forsmark area, mainly in the three largest lakes (Lake Bolundsfjärden, Lake Eckarfjärden and Lake Fiskarfjärden), and of the marine ecosystem have been

carried out. Thorough descriptions and evaluations of the input data (site-specific and generic) and of the methods used are presented in /Nordén et al. 2008/ for the limnic ecosystem and in /Wijnbladh et al. 2008/ for the marine ecosystem.

Terrestrial ecosystems

Vegetation

The terrestrial vegetation is strongly influenced by the characteristics of the Quaternary deposits and by human land use. The area is fairly young as an effect of the land uplift and the low topography /Söderbäck (ed) 2008/. The location at the sea coast makes the seashore a prominent feature in the east along with conifer forests, shallow lakes, mires and some agriculture land. Below follows a brief description of three major vegetation types within the regional model area, see /Löfgren (ed) 2008, chapter 4/ for more details.

Forests cover 73% of the land area at Forsmark and are dominated by Scots pine (*Sw. tall*) and Norway spruce (*Sw gran*) growing mainly on wave-washed till. The spruce becomes more abundant in areas with a deeper soil cover in combination with mesic-moist conditions. Outcrops are not prevalent in the Forsmark area, making pine forest on acid rocks quite scarce. The calcareous soil material provides nutrient-rich conditions, characterised by herbs and broad-leaved grasses, along with a number of orchid species, and predominant humus forms of mull and intermediate moder types /Lundin et al. 2004/. The deciduous tree species are dominated by silver birch *(Sw. våtbjörk),* common alder *(Sw. klibbal)* and rowan *(Sw. rönn)*, but also Norway maple *(Sw. skogslönn)* and ash *(Sw. ask)* are fairly common. The Forsmark area has a long history of forestry, currently revealed as a fairly high percentage of younger and older clear-cuts in different successional stages in the landscape. Silver birch is the dominate species in many of the earlier successional stages until it is replaced by young Norway spruce or Scots pine, depending on soil type and/or management.

Wetlands occur frequently and cover 10–20% of the area in the three major catchments, and up to 25–35% in some sub-catchments /Johansson et al. 2005/. A major part of the wetlands consists of coniferous forest swamps or open mires. The mires are characterised by a high calcareous influence, which makes the extremely to intermediately rich fen types common in this area /Göthberg and Wahlman 2006, Jonsell and Jonsell 1995/. Although not yet so numerous, bogs are also present in the inland areas, and are continuously created due to land uplift and mineral and nutrient leaching processes. Other important wetland types are the freshwater shores (wet meadows or marshes) and riparian deciduous forest swamps along streams. The latter are inundated by water at least once a year and affected by overbank sedimentation. The flat topography in the area promotes the occurrence of small floodplains that are flooded during high-flow periods /Carlsson et al. 2005/. Such areas may be of importance for the retention of different substances that otherwise would be transported by the water directly to the sea.

Agricultural land covers hardly 5% of the land area at Forsmark and is mainly located in the south-eastern part of the candidate area. The agricultural land consists of arable land and grasslands. It provides food for humans, either directly as crop production or as production of fodder for animals. Grasslands are used for browsing cattle (pastures) or for hay-making (meadows) and are mainly found close to settlements. Some arable land and to a large extent semi-natural grasslands (intensively used grassland with a long management tradition) in the area have been abandoned following the nation-wide general regression of agricultural activities during the past 60 years. The standard yield of the dominant grain species, barley, is 2,800 kg per ha (based on information from the year 2002).

Fauna

The fauna has been investigated in a number of different surveys, see section 4.2 in /Löfgren (ed) 2008/. The aims of the surveys were to 1) describe which species or functional groups are present in the area, 2) establish reliable density estimates of larger animals and birds, and quantify important pools/fluxes to be used for the ecosystem models, and 3) establish a baseline for the now ongoing monitoring programme that can be used to relate different kinds of disturbance to wildlife population changes. The fauna is more difficult to associate with specific habitats than vegetation, but for some species or functional groups an attempt has been made to distribute their consumption in the

landscape, either by using their habitat preferences or their feeding preferences, or both. Density and biomass estimates for all mammals, birds, amphibians and reptiles are presented in section 4.2 in /Löfgren (ed) 2008/, together with calculations of their production, consumption, egestion and respiration. The calculations are based on the field metabolic rate for each species.

Limnic ecosystems

The Forsmark area today contains 25 lakes. Most of them are small (lake areas range from 0.01–0.75 km^2). They are all very shallow (the "median lake" has an average depth of 0.3 m and a maximum depth of 1 m) and are classified as oligotrophic hard-water lakes, i.e. they contain high calcium levels, but low levels of nutrients, as phosphorus is precipitated together with the calcium. This kind of lake is common in the region, i.e. along the coast of northern Uppland, but is very uncommon in Sweden in general.

Due to the shallow depth, all lake bottoms are reached by sunlight, and vegetation occurs at all depths. The dominant vegetation is stoneworts (*Chara sp.*). At the top of the bottom sediment, algae and cyanobacteria are often found in thick layers. These two groups of primary producers dominate the biomass and primary production, making phytoplankton biomass and production less important. The lakes are surrounded by reed belts, which are extensive around smaller lakes.

The dense stands of *Chara* harbour various kinds of benthic fauna and also function as refuges for smaller fish. Common fish species are perch and roach, as well as tench and crucian carp. This last species survives low oxygen levels and is the only fish species present in the smaller lakes, where oxygen levels can be very low during winter.

The streams in the Forsmark area are very small and mostly resemble man-made ditches. In some stretches, the riverbanks are about two metres deep. Long stretches of the streams are dry during summer, but they may function as passages for migrating spawning fish during wetter conditions, especially in the more downstream areas.

An extensive compilation of all the data concerning limnic ecosystems in the Forsmark area is presented in /Nordén et al. 2008/. In that report, details about the ecosystem models and mass balance methodology, as well as results for lake ecosystems in the Forsmark area, are discussed.

The delimitations between different habitats in all lakes larger than 0.5 ha in the Forsmark area were determined in a study that also included identification of the watershed. An extensive amount of biological data, including biomass data on phytoplankton, bacterioplankton, zooplankton, benthic microphytes, benthic bacteria, benthic fauna, macrophytes and fish have been collected from Lake Eckarfjärden, one of the larger lakes in the area /Nordén et al. 2008, section 3.9.1/. Some of these functional groups have been sampled several times per year over two or three years. Moreover, also primary production of phytoplankton and benthic microphytes has been measured several times over two years.

Biological data from other large lakes in the area as well as from some of the smaller lakes (which often are in a later successional stage than the larger ones) are also available, although these data are not very extensive. Data on water chemistry are available for both large and small lakes as well as from streams in the area /Nordén et al. 2008, section 3.8/. Data on the chemical composition of biota are available for a limited number of functional groups from three different lakes /Nordén et al. 2008, section 3.10/.

Marine ecosystems

Forsmark is situated at the Bothnian Sea, a semi-closed part of the Baltic Sea with large net freshwater supply, separated by narrow connections from the Baltic Proper in the south. The freshwater influence and the separation from the Baltic Proper result in low salinity (c 5‰) in the Forsmark area. The low salinity strongly affects the marine environment, as few organisms are adapted to this brackish condition, but rather to either freshwater or saltwater. Therefore, a mix of few freshwater and marine species is found in the Forsmark area.

The marine area at Forsmark consists of a funnel-shaped bay (Öregrundsgrepen), separated from the open sea in the east by the Gräsö island. The area consists of a shallow (depth often less than 10 m) and sparse archipelago along the coast and a deeper trough in the eastern part, the Gräsö Trough, with a maximum depth of 58 m, Figure 4-4. Generally, the bottom in the area has a gentle slope.

Most investigations and studies of the marine ecosystem have been performed in the coastal area around the Forsmark power plant. The following description concerns this area, but also the open sea in the Öregrundsgrepen. Generally, physical characteristics, such as light and temperature, have been monitored continuously for several years at a few monitoring stations. Chemical characteristics have been monitored monthly or bi-weekly in three to five stations, whereas sediment conditions and biota have been surveyed once or twice, but with a higher spatial resolution.

The coastal water in the Forsmark area has an average light penetration depth of 5.5 m, which is low compared with the value recorded at the national monitoring station located further out in the Bothnian Sea (8.7 m). The light penetration varies, however, and the inner, less exposed, areas have Secchi depths (sea water transparency) of 2–3 m.

Due to the wide open boundary towards north, Öregrundsgrepen is strongly influenced by the large-scale circulation and dynamics of the Baltic Sea, especially by the southbound coastal current, with seasonal density fluctuations due to variations in the collective discharge to the Bothnian Sea from the major rivers in northern Sweden and Finland. The local freshwater discharge to Öregrundsgrepen is moderate with the streams Forsmarksån and Olandsån discharging about 3 and 6 m^3/s, respec-

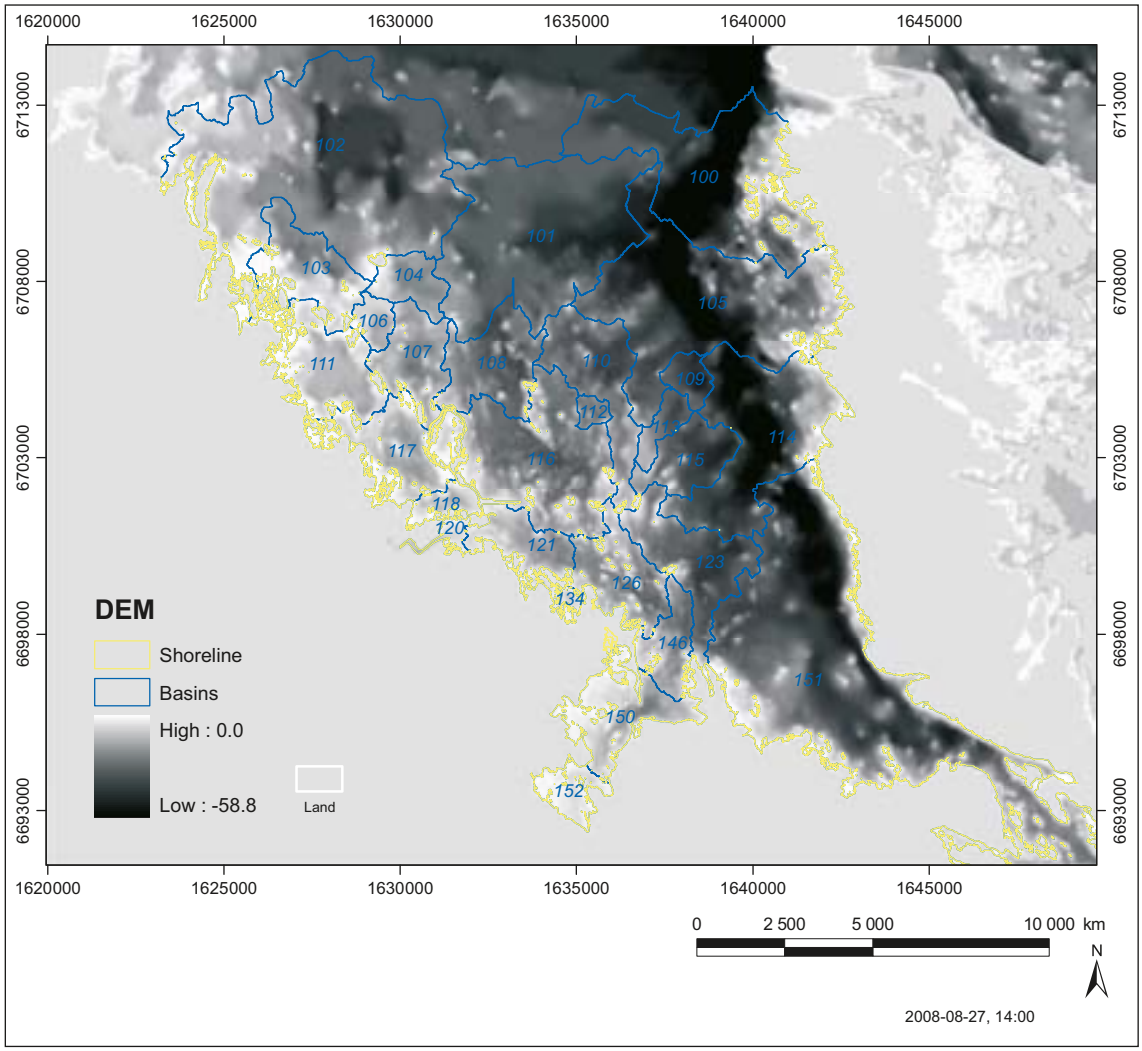

Figure 4-4. *The marine area at Forsmark and the sub-basins studied in Öregrundsgrepen. Increasing dark blue indicates increasing depth /Wijnbladh et al. 2008/.*

tively, as an annual average. Water exchange is estimated for modelling purposes for the 28 sub-basins in the area and presented as Average Age (AvA) of the water parcel. AvA values are small, less than one day, for all but two basins.

The dominance of shallow coastal areas enhances the importance of benthic communities and, hence, the marine biota in the area is dominated by benthic organisms. The benthic zone can be separated into soft and hard bottom communities and into photic and aphotic zones. Although the light penetration is rather low, most of the area is within the photic zone (receiving more than 1% of surface irradiance). However, the light intensity decreases rapidly and, therefore, most benthic organisms depending on light, i.e. macroalgae, vascular plants and benthic microalgae, are concentrated along the coast. On the soft bottom substrate area, rooted plants and the algae *Vaucheria* dominate, whereas bottoms with till or bedrock host brown, green and red algae. Detrivores, snails and mussels feeding on dead material dominate both hard and soft bottom substrates. The fish community is dominated by the marine species herring (*Sw. strömming*) in the pelagic area, whereas limnic species, especially eurasian perch (*Sw. aborre*), dominate in the coastal areas and in the secluded bays. In open sea, the zooplankton community is dominated by meso-zooplankton, especially copepods. Concentrations of chlorophyll in seawater indicate that the phytoplankton biomass in the Forsmark area is lower than that generally found in the national monitoring programme. The measured biomass varies between 30–180 µg/L and the plankton is dominated by ciliates, cryptophytes and diatoms.

An extensive compilation of all available data from the marine ecosystem in the Forsmark area is presented in chapter 3 in /Wijnbladh et al. 2008/. That report also presents details about the ecosystem models and mass balance calculations for marine ecosystem basins in the Forsmark area.

4.2.5 Human population and land use

Input data sources and calculated values for the parameters used to describe humans and land use in the Forsmark area and its surroundings are provided in detail in /Miliander et al. 2004/.

The short description below illustrates the situation in the parish of Forsmark, since many of the data were available at the parish level. The Forsmark parish is very similar in size to the regional model area and covers some 90% of its land area. The description of the human population and land use can be summarised as follows.

- The parish of Forsmark is sparsely populated.
- The main employment sector is within electricity supply. There is a clear net daily in-migration to the parish of Forsmark due to the dominant employer, the Forsmark nuclear power plant with more than 700 employees.
- The land use is dominated by commercial forestry; wood extraction is the only significant man-made outflow of biomass from the area.
- The dominant leisure activity, by far, is hunting. Besides this, the area is only occasionally used for leisure. This is probably a result of both the sparse population and the relative inaccessibility of the area and distance from major urban areas.
- The agriculture in the parish is limited in extent and the major crop is barley.
- The Forsmark power plant, situated partly within the Forsmark candidate area, constitutes a large industrial park in a landscape otherwise relatively unaffected by human activities.

The Forsmark area has no permanent inhabitants. Nevertheless, there are five holiday houses and three farm estates within the Forsmark area, which indicates that the area has a small holiday population. There is only one active agricultural enterprise within the Forsmark area today, and that one is situated at Storskäret. The agricultural area is only 4% of the total area, considerably lower than the average for the County of Uppsala, where it represents 25%. The forest area represents as much as 72.5% of the land area.

The carbon flow to humans from a selection of drainage areas has been calculated according to the methodology described in /Löfgren (ed) 2008, chapter 8/. The result is also presented in /Löfgren (ed) 2008, chapter 8/.

4.3 Modelling of the surface system

4.3.1 Hydrology and near-surface hydrogeology

Below is given a brief summary of the conceptual and quantitative modelling of the hydrology and near-surface hydrogeology. For detailed presentations the reader is referred to /Johansson 2008, Johansson and Öhman 2008, Bosson et al. 2008/.

Numerical modelling with the MIKE SHE tool has been performed as a part of the evaluation of the surface hydrology and near-surface hydrogeology at Forsmark. This modelling includes evapotranspiration processes, surface water flow and groundwater flow. However, in contrast to the hydrogeological modelling described in chapter 8, the modelling is performed for the present day conditions only. Furthermore, density driven flow is not modelled in MIKE SHE.

In Figure 4-5, the calculated distribution of recharge and discharge areas in the Quaternary deposits from the MIKE SHE modelling is shown /Bosson et al. 2008/. In this context, the mean groundwater head differences between the two uppermost calculation layers are used for the definition of recharge and discharge areas, i.e. areas where the head is higher in the top layer than in the layer below are defined as recharge areas and vice versa for discharge areas.

The difference between the levels in till and bedrock indicates limited hydraulic contact between Quaternary deposits and rock. A probable explanation for the low levels measured in the bedrock boreholes is that these intersect the highly conductive horizontal fractures/sheet joints shown to exist in the shallow bedrock (see section 8.4.4). The highly transmissive shallow bedrock acts as a drain for water coming from above as well as from below. The available data indicate that flow systems involving the bedrock do not have discharge areas on land in the northern part of the tectonic lens, but instead discharge into the sea.

The water balances for each layer in the saturated zone, as calculated in two simulation cases with the MIKE SHE model, is presented in Figure 4-6. The net annual area-averaged groundwater recharge from the unsaturated zone to the uppermost calculation layer containing the Quaternary

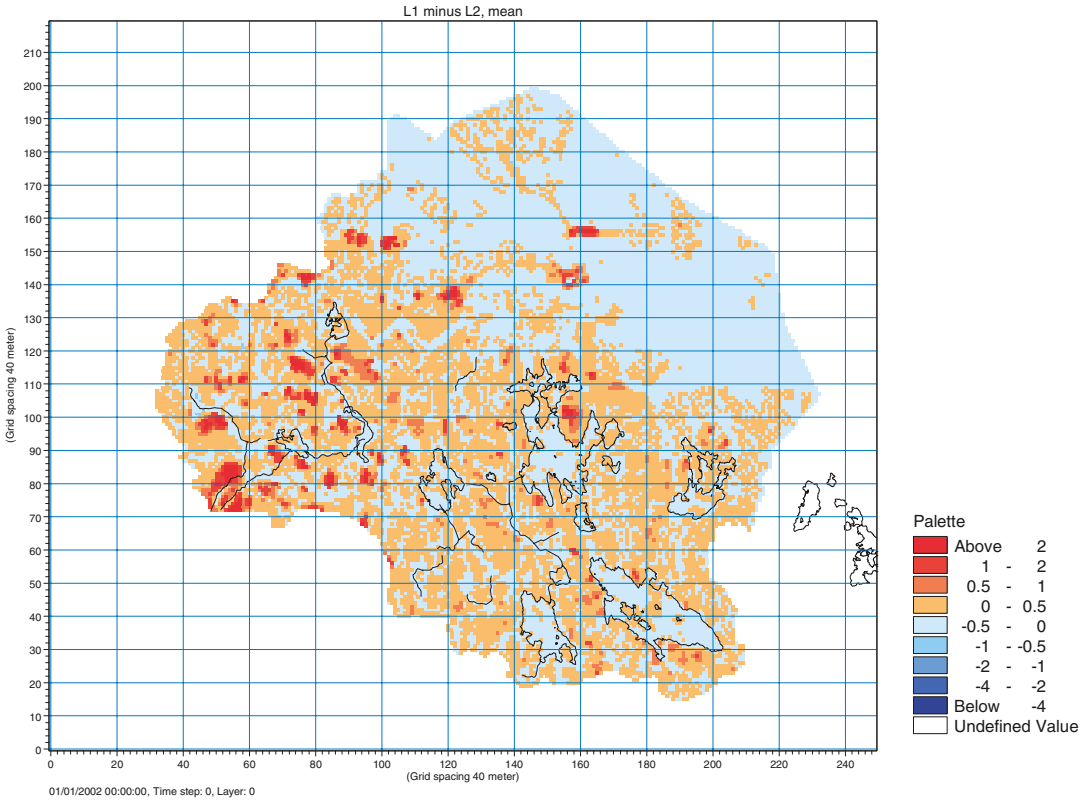

Figure 4-5. *The mean groundwater head difference between layer 1 and 2, i.e. recharge (red) and discharge (blue) areas in the Quaternary deposits /Bosson et al. 2008/.*

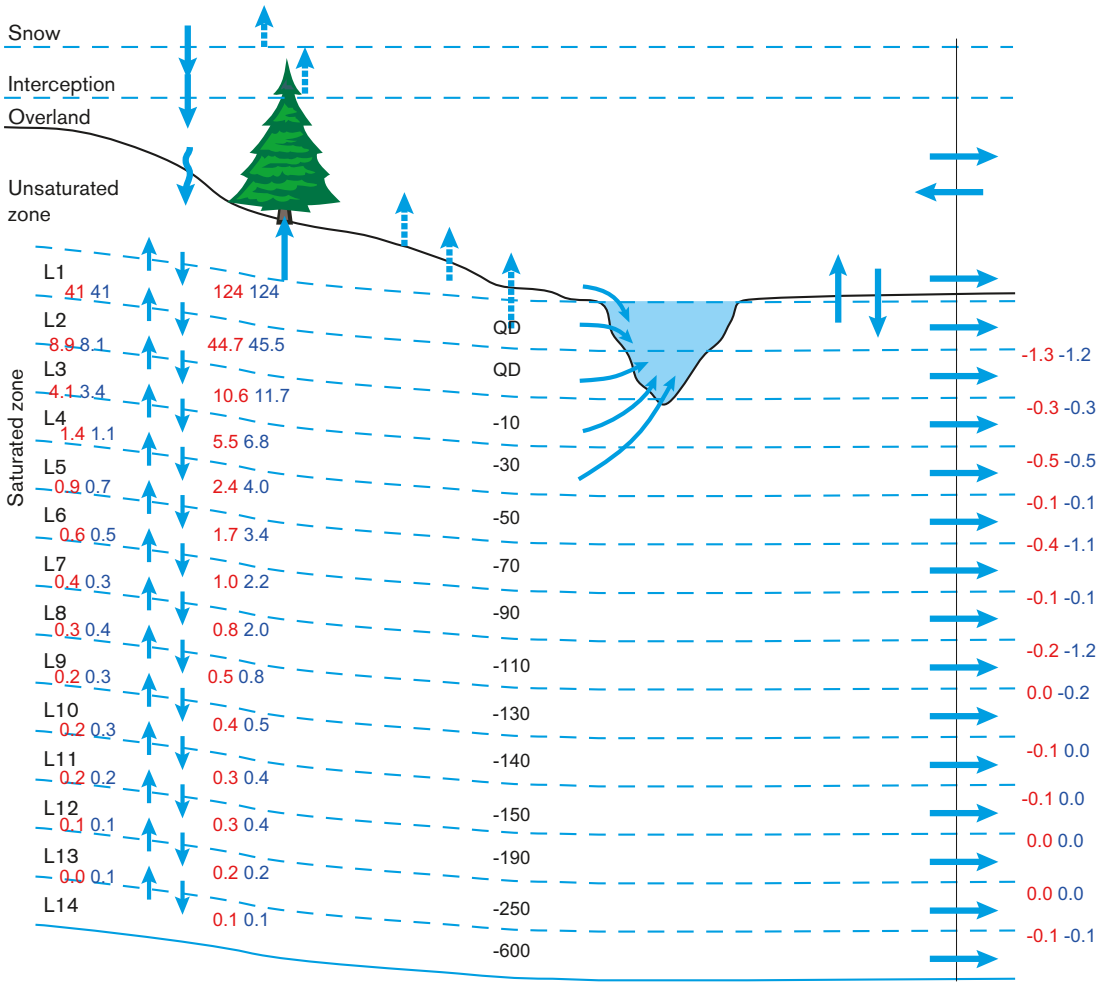

Figure 4-6. *Calculated water balance for each layer in the saturated zone in the Forsmark MIKE SHE model. The numbers beside the vertical arrows express annual vertical flows in mm (i.e. averaged over the MIKE SHE model area) in each calculation layer for two simulation cases. The mean lower boundary elevation (m RHB 70) for each layer is marked in the middle of the figure /Bosson et al. 2008/.*

deposits is 124 mm. There are many local recharge and discharge areas within the Quaternary deposits layers (L1 and L2). The upward and downward flows between the Quaternary deposits layers are both on the order of 45 mm. The recharge to the uppermost bedrock layer (layer L3 in the figure) is c. 11 mm. Since there is upward flow in parts of the model area, the net annual downward flow from Quaternary deposits to rock is much smaller, 2–3 mm (e.g. 10.6 minus 8.9 mm). The vertical groundwater flow at 150 m depth is 0.3–0.4 mm down and 0.2 mm up, i.e. a small downward net flow, see /Bosson et al. 2008/ for a detailed discussion.

Particle tracking simulations were performed based on the flow field of the calibrated MIKE SHE model. Several transport scenarios were simulated. In the simulations described here, particles were released at 150 m depth /Bosson et al. 2008/. Figure 4-7 shows results of a simulation where particles were released within the so-called target volume only. Specifically, one particle was released in each cell within an area corresponding to the horizontal extent of the area of the planned repository. In the simulation presented in Figure 4-7, particle tracking was modelled for a time period of 5,000 years.

In the simulation, only 10% of the particles had left the model volume after 300 years, and all these particles reached the surface system in the sea (Figure 4-7). The discharge points after 5,000 years are also shown in the figure. The transport times were generally long and after 5,000 years, 81% of the particles still remained in the model volume. All of these particles were found in the bedrock at

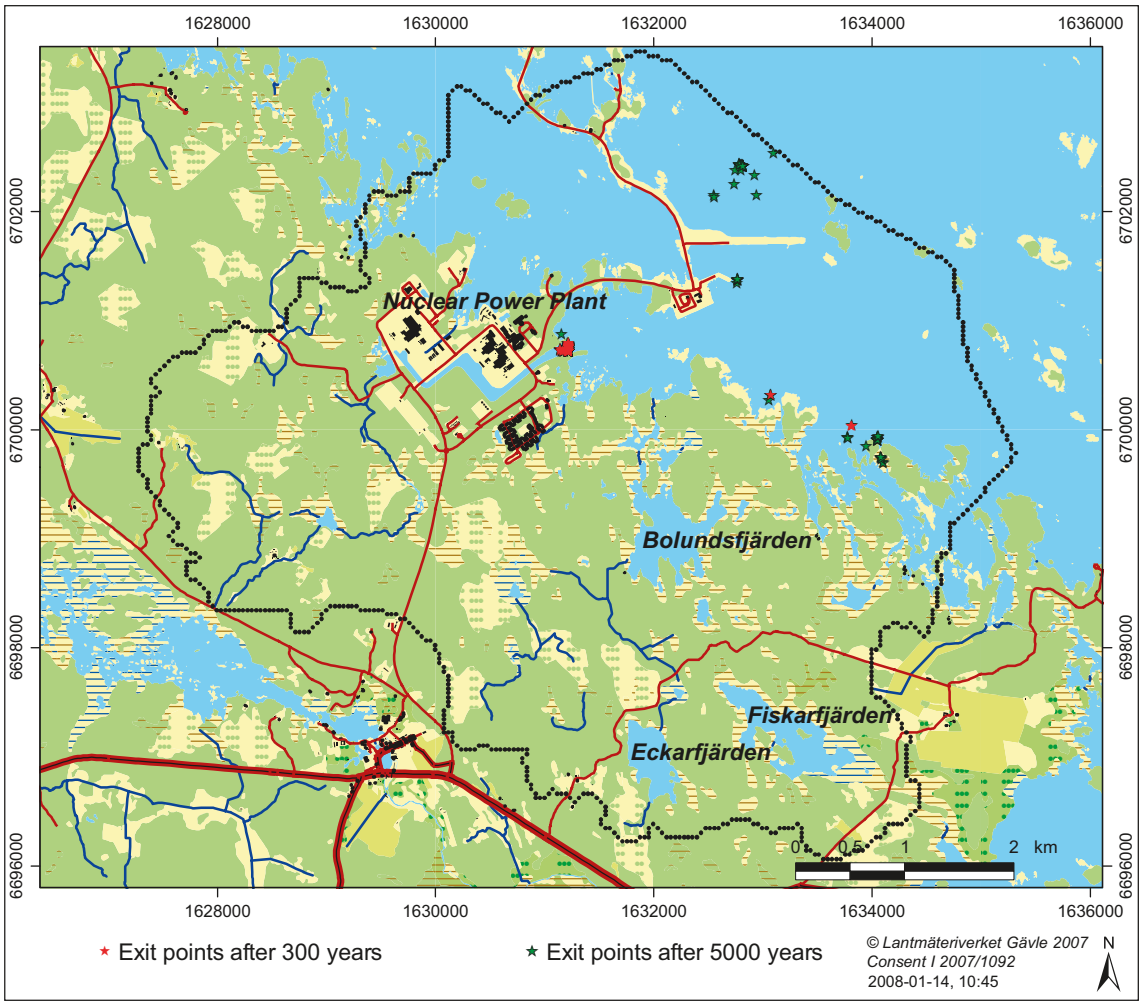

Figure 4-7. *Discharge points from a model case where particles were released at a depth of 150 m inside an area corresponding to the planned repository; the simulations are reported in /Bosson et al. 2008/.*

depths between 110 m and 600 m. No discharge points were found in the terrestrial part of the model area. These results support the conceptual model derived from observations at the site, which states that there is downward flow from the Quaternary deposits to the rock in terrestrial parts of the target area and that there is no or very limited discharge of bedrock groundwater there.

4.3.2 Ecosystems

In order to build up the knowledge about transport of elements within and between ecosystems, elemental transport models have been set up for the terrestrial, limnic and marine ecosystems in the Forsmark area. For this purpose, *ecosystem models* have been used to describe major pathways for flow of matter within the trophic web in each ecosystem and to reveal the major abiotic and biotic pools within the ecosystem.

In order to describe the flows of elements to and from ecosystems, as well as the permanent burial of elements in sediments and soils, the *mass balance* concept is used. The concept focuses on fluxes of matter, assuming that the difference between inflow and outflow represents the result of the biotic and abiotic processes occurring within the ecosystem. This is a more robust approach than ecosystem budgets as less data are needed, but it reveals much less detail. The *mass balance* identifies the major fluxes in and out of an ecosystem. Similarly to ecosystem budgets, the mass balance indicates, for example, whether a lake functions as a source or a sink for different elements. As a complement to the mass balance analysis, the amount of matter in "pools" within the ecosystem can be estimated.

The chemical behaviour of many bioavailable contaminants and radionuclides is similar to that of other bioavailable compounds or elements, such as macronutrients or trace elements /Whicker and Schultz 1982, Sterner and Elser 2002/ and these so called analogues can thus be utilised for modelling purposes. Similarly, there are elements that are subjected to passive uptake by plants and the transport of these elements may therefore be better described by water flow through the plant, e.g. transpiration /Greger 2004/. However, in general, a multitude of bioavailable radionuclides with various behaviours, assimilated into living tissue, will ultimately follow the fluxes of organic matter. Consequently, the production of organic material, the Net Primary Production (NPP), may define an upper limit to the incorporation of different elements in primary producers /Kumblad et al. 2006/. Fluxes to other trophic levels than the dominant vegetation, such as large herbivores, predators and humans, can be used to evaluate their potential exposure from food intake.

Models for element transport in the terrestrial ecosystem

Pools and fluxes of organic matter and water (Figure 4-8) were investigated and compiled for three localities, representing vegetation types that can be regarded as being important both in respect to area coverage and as potential sinks for organic matter, see Table 6-1 in /Löfgren (ed) 2008/. Two conifer forests, representing the dominant vegetation type, and one forested wetland were studied. All three investigated localities were net carbon sinks, where most of the carbon accumulated in the vegetation. The net primary production (NPP) was between 429 and 537 g C/(m^2·y). The forested wetland accumulated 74 g C/(m^2·y) in the soil organic carbon pool, whereas the two forests were close to zero with regard to soil carbon balance. This model described three ecosystems using site-specific field measurements of pools and fluxes, and served as a baseline for comparison with the results of dynamic modelling, see section 4.1.3 and chapter 7 in /Löfgren (ed) 2008/ and with more general literature data that may be used to describe pools and fluxes in long-term perspectives in the safety assessment.

The dynamic vegetation model LPJ-GUESS /Sitch et al. 2003/ was used to make a regional description of carbon balances for a number of different vegetation types dominating the investigation area. Some areas (sea shore, wetlands and forested wetlands) were not covered due to the extensive work required to adapt the model for these vegetation types. For these cases, ground-based measurements as well as literature data were presented, see chapter 7 in /Löfgren (ed) 2008/. The model results cover the vegetation types; young (25 y) and old (80 y) stands of Norway spruce, Scots pine, deciduous trees (Pedunculate oak (*Sw. ek*) and Silver birch (*Sw. våtbjörk*)), mixed forests, dry pine on acid rocks, meadows and arable land. The model results were validated against ground-based estimates, which confirmed that estimated carbon balances are realistic in relation to measurements. Estimates of carbon balances for 2005 for the different vegetation types were made using the model (Table 7-4 in /Löfgren (ed) 2008/). The modelled vegetation types were all net sinks except for the clear-cut that was a carbon source, mainly due to decomposition of the large litter pool originating from the residues after the clear-cut. NPP was between 461 and 664 g C/(m^2·y) for the forested vegetation types. A similar calculation of the net ecosystem production (NEP) as above showed that all vegetation types were accumulating carbon in the SOC pool or were close to zero, except for the dry pine forest and the previously mentioned clear-cut. The spatial variation of NPP was studied in the regional model area by combining remote sensing and dynamic vegetation modelling (Table 7-6 in /Löfgren (ed) 2008/). Finally, the temporal variation of a number of ecosystem properties was investigated by modelling 400 years of forest succession using a set of 100 y of site-specific climate data repeated four times.

The regional ecosystem description was combined with estimates of site-specific element concentrations for different pools and elemental fluxes in order to determine *mass balances* for a number of different elements using the discharge areas as the geographical extents over which the mass balances were determined, see chapter 8 in /Löfgren (ed) 2008/.

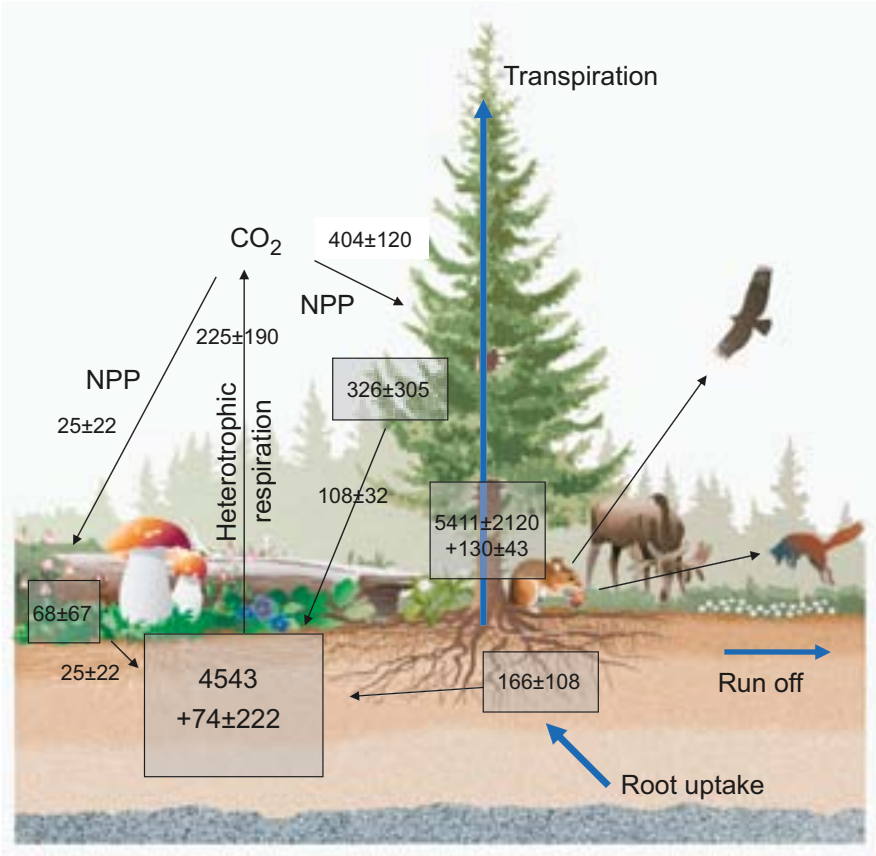

Figure 4-8. *The major pools and fluxes of carbon and water in an Alder-Norway spruce swamp forest. Figures within boxes describe pools, whereas figures outside are fluxes. A change in a pool is expressed with a figure preceded with a ± (decrease/increase). Pools are in g C/m² and fluxes are g C/(m²·y). The sizes of the water fluxes are illustrated by the length of the arrow (data from Table 6-10 in /Löfgren (ed) 2008/).*

Models for element transport in the limnic ecosystem

Ecosystem *carbon models* have been developed for both larger and smaller lakes in the area, see chapter 5 in /Nordén et al. 2008/. An example of an ecosystem carbon budget for one of the larger lakes, Lake Eckarfjärden, is presented in Figure 4-9. In both the larger and the smaller lakes, biomass is mainly associated with the benthic habitat, where more than 90% of total biomass in the lake is found. Also, the primary production is concentrated in the benthic habitat, which can be expected in shallow hard-water lakes. This makes the Forsmark lakes different from Swedish lakes in general, where phytoplankton is an important group of primary producers. The reason for the difference is, of course, the shallow water depth of the Forsmark lakes which, together with the clear water, makes all bottom areas available for primary producers.

The processing of organic matter in freshwater ecosystems has been found to significantly affect the overall carbon balance of freshwater-rich landscapes such as the Swedish boreal forest. Both the carbon budget and the carbon mass balance show that, contrary to typical Swedish lakes, production exceeds respiration in the larger Forsmark lakes, making them carbon sinks. In some of the smaller lakes, the respiration and primary production are of similar sizes. As many elements follow the carbon flow in ecosystems, the same flows can often be attributed to other elements that are incorporated into biota.

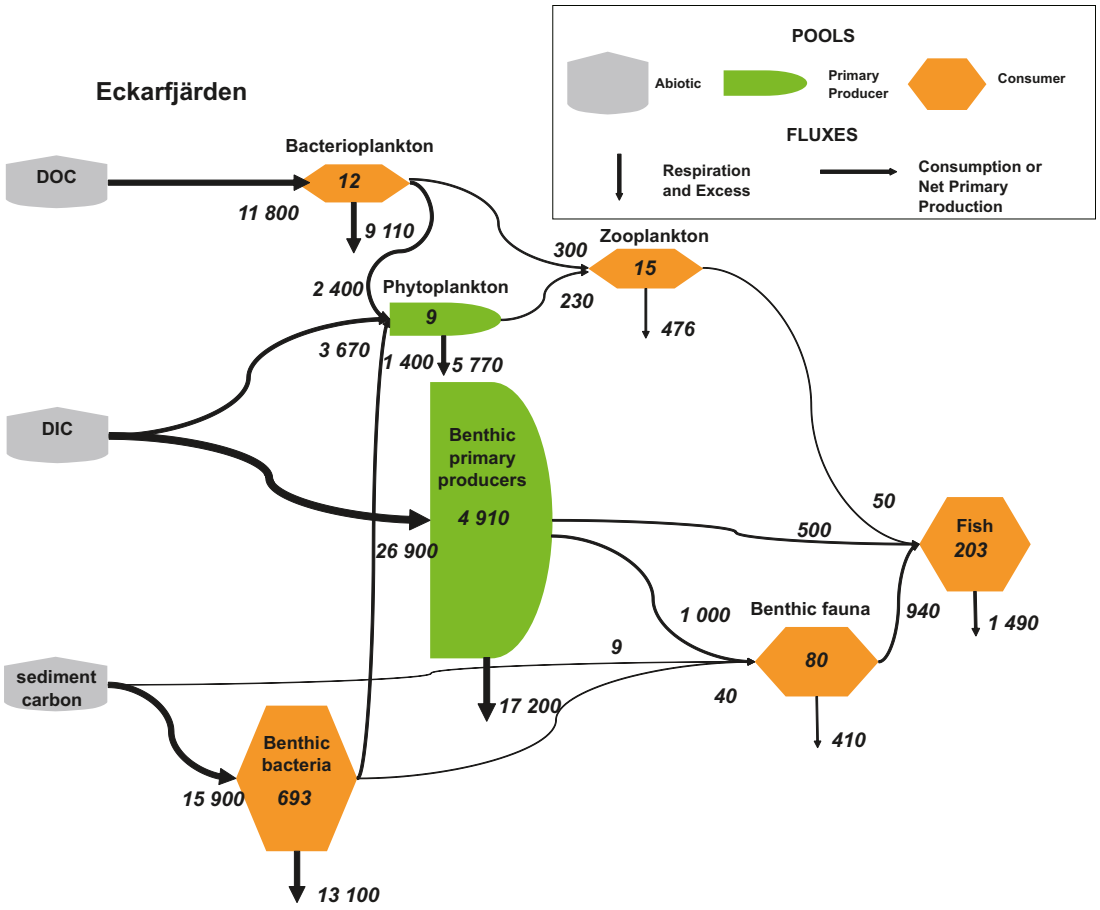

Figure 4-9. *Carbon flow (kg C/y) in the ecosystem model for Eckarfjärden /Nordén et al. 2008/. Sizes of boxes and arrows are relative to the sizes of pools and fluxes in the model. The consumption of phyto-, zoo- and bacterioplankton by benthic fauna is included in the consumption of sediment carbon in the figure. Note that consumption within the same functional group is not shown, e.g. the consumption of fish by carnivorous fish. DOC = Dissolved Organic Carbon, DIC = Dissolved Inorganic Carbon, POC = Particulate Organic Carbon.*

Element *mass balances* have been calculated for a number of other elements, together with an assessment of the major pools of each element, see chapters 5 and 7 in /Nordén et al. 2008/. As an example, the mass balance for phosphorus in Lake Bolundsfjärden is presented in Figure 4-10. The mass balance shows, for example, that the sediment is by far the largest phosphorus pool in the lake. Biota contains considerably more phosphorus than the water pools. Moreover, all fluxes (inflow, deposition, outflow, and sediment accumulation) are of the same order of magnitude. The phosphorus pools in the lake are larger than the annual inputs (inflow and deposition) and outflows (outflow and sediment accumulation), and thus the lake is probably more influenced by internal circulation of phosphorus than by phosphorus entering the lake from the catchment.

Models for element transport in the marine ecosystem

The marine ecosystem and its characteristics are conceptualised in an *ecosystem model*. The model was calculated on a spatial domain consisting of 1,500×1,500 grid-cells, each with a 20×20 m size. To enable the model calculations, a database including important ecosystem components with a 20 m resolution was created, using the site-specific data and various interpolation methods described in detail in chapter 4 in /Wijnbladh et al. 2008/. The area studied was divided into 28 sub-basins based on the bathymetry of today and future drainage areas (Figure 4-4). Model output was presented for the whole area and for the individual basins, both as values per square metre and per basin. The pools and fluxes of matter were summarised for each basin, using carbon as a proxy. Coarse-grained *mass balances*, identifying the major pools and fluxes, were calculated per basin for a large number of other elements.

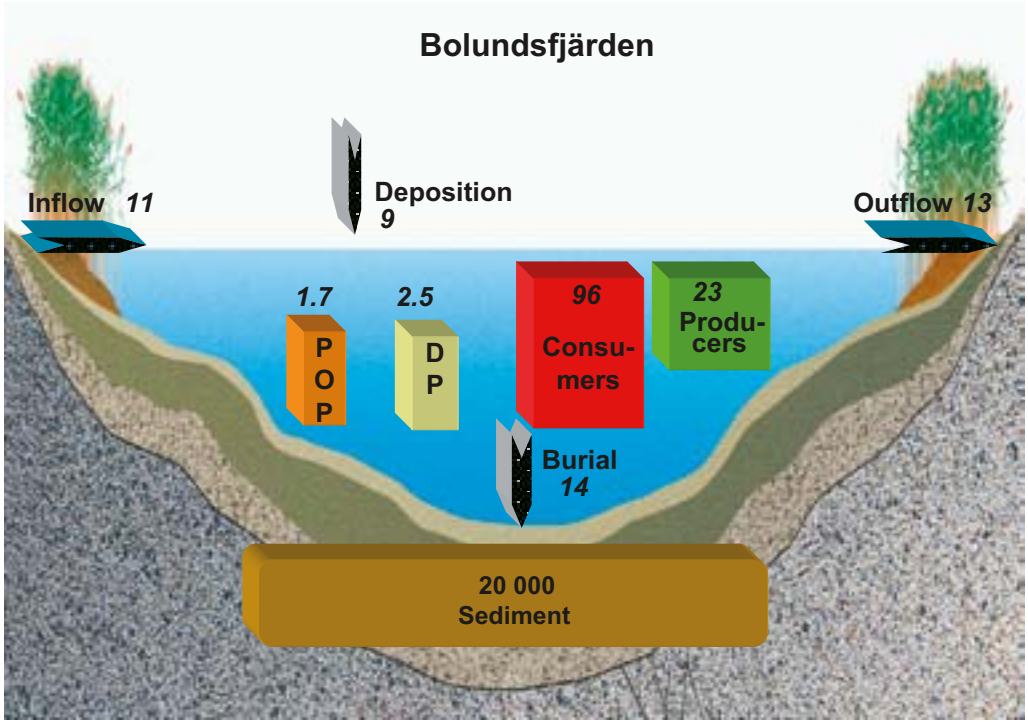

Figure 4-10. *Phosphorus mass balance for Lake Bolundsfjärden /Nordén et al. 2008/. Sizes of boxes and arrows are relative to the sizes of pools and fluxes in the model. Note that the sediment box is down-scaled to fit into the figure. Values in kg P or kg P/y. POP = Particulate Organic Phosphorus, DP = Dissolved Phosphorus.*

Five basins, localised in the immediate vicinity of the target area for the repository, were studied in more detail. The sediment pool in the studied basins, and indeed most of the Öregrundsgrepen, is the dominant pool for carbon (and for many other elements). Among biotic pools, macrophytes and benthic fauna, especially detrivores, are the largest. The dominant flux within the food-web model is uptake of carbon by these functional groups, including bacteria. The flux of elements from one trophic level to another is small. Instead, the major part follows other paths, such as respiration or excretion. In most basins, the flux to and from the basin through advective transport is many times larger than the fluxes within the system.

The results show that although most parts of the area are heterotrophic, the total mean of the whole area is autotrophic, i.e. more carbon is fixed in biomass by primary producers than is released from respiration by all organisms. The mean Net Ecosystem Production (NEP) in the model area is 14.8 g C/(m^2·y), but ranges between –55 to 228 g C/(m^2·y) in separate basins. The inner, shallow coastal areas tend to be autotrophic, whereas the outer are heterotrophic. A difference between inner and outer coastal areas can also be seen in biomass. This is mainly an effect of the benthic component, especially primary producers, being more abundant in shallow areas.

4.4 Implications for bedrock modelling

The integration and linking of the bedrock and surface systems is a multidisciplinary task. The aim of the integrated system descriptions is to describe the conceptual understanding and properties of the deep rock volumes and the upper parts of the rock, the transition between the rock and the regolith, and finally the regolith itself. However, it should be kept in mind that the ultimate goal of this integration is to provide a context for descriptions of solute transport in rock and regolith. Solute transport scenarios of interest include transport from the deep rock to the surface system, primarily radionuclide transport from the potential repository, but also from surface to rock (mainly of substances with potential influence on the conditions in the repository).

The focus of the present section is on the various aspects of the surface system that are of importance for the bedrock modelling. Specifically, these aspects include the following parameters, models and observations.

- Parameters describing the properties of the upper part of the integrated rock-regolith model domains. Integrated model domains are considered primarily within the hydrogeological (chapter 8) and hydrogeochemical (chapter 9) modelling.
- Models produced and presented within the surface system modelling that are used as direct inputs to hydrogeological and hydrogeochemical models. In particular, these inputs include geometric descriptions such as the topographic and shoreline displacement models.
- Other inputs used as a basis for setting (top) boundary conditions, i.e. groundwater pressure and flux data for use in hydrogeological models and chemical compositions of infiltrating groundwater in hydrogeochemical models.
- Measured and modelled data in surface system descriptions that are used for data interpretation and/or otherwise as supporting evidence in the development of bedrock models. For example, hydrogeological and chemical data providing information on discharge of deep groundwater are important for the bedrock modelling.

The digital elevation model (DEM) describing the topography and bathymetry in the Forsmark area constitutes a basic input to several modelling activities. A DEM with a horizontal resolution of 10 m was presented in /Brydsten and Strömgren 2004/. This DEM is classified due to national security reasons, which implies restrictions on its use. Recently, a non-classified DEM with a resolution of 20 m was presented /Strömgren and Brydsten 2008/. This non-classified DEM is used as a basis for all hydrological and hydrogeological modelling in SDM-Site Forsmark.

In the remainder of this chapter, hydrological-hydrogeological and chemical data and models relevant for the bedrock modelling are summarised, followed by a short discussion on the implications for solute transport in the rock-regolith system. Clearly, the aim is not to present a complete description of the items listed above, but rather to summarise some important aspects and provide references.

4.4.1 Hydrology and hydrogeology

The conceptualisation of the hydrological-hydrogeological system at Forsmark is summarised in chapter 8; more detailed descriptions are given in the background reports for surface hydrology and near-surface hydrogeology /Johansson 2008/ and bedrock hydrogeology /Follin 2008/. The present section summarises results from surface system modelling activities and joint interpretations considered important for the bedrock modelling. In particular, hydrogeological properties and time-series data on groundwater levels are discussed.

As described in some detail in e.g. /Follin et al. 2007c/, the uppermost rock is a key component in the overall groundwater flow system at Forsmark. The transmissivities measured in this part of the rock are, in many cases, exceptionally high, in particular in the north-western part of the candidate area (the target area). Therefore, it was suggested that there can be a “hydraulic cage phenomenon” caused by a lattice of high-transmissive structures consisting of extensive horizontal fractures/sheet joints. The shallow and anisotropic bedrock aquifer (see section 8.2), intercepts the recharge from above as well as the discharge from below. This implies that it has important implications for the groundwater exchange between the Quaternary deposits and the rock within the target area.

The geology of the regolith in the Forsmark area is described in /Hedenström and Sohlenius 2008/ and in section 4.2.1. Till is the dominant Quaternary deposit in the area, whereas fine-grained materials such as gyttja and glacial and post-glacial clay are found below lakes and wetlands. Based on a simplified conceptual model in which the regolith was subdivided into a limited number of layers, available data on surface distribution, total depth and stratigraphy were used to construct a three-dimensional geometric model of the distribution of Quaternary deposits /Hedenström et al. 2008/. This model, in turn, was used as a basis for the development of the hydrogeological model of the regolith. Specifically, the various layers in the geometric model were assigned hydrogeological parameters, see /Johansson 2008/ and /Bosson et al. 2008/ for details.

Regarding hydrogeological properties, the following should also be noted /Johansson 2008/.

- The hydraulic conductivity (K) values for till in the Quaternary deposits model /Johansson 2008/ are horizontal conductivities obtained from slug tests. The only vertical K-values from till are from the laboratory permeameter tests, which indicate a K_h/K_v ratio of about 30. Note that this result should be used with caution since the scales of the tests are not the same.
- The hydraulic conductivities are considerably higher in the uppermost c. one metre of the soil profile. The difference, due to impact of soil forming processes, is 2 to 3 orders of magnitude. In the model, this was considered by including a differentiation of the hydraulic properties between the upper 0.6 metre of the profile and the deeper part of the profile for some of the Quaternary deposits.
- A pumping test in till with observation wells near and below Lake Bolundsfjärden showed that there is a limited hydraulic contact, potentially determined by low-permeability lake sediments between Lake Bolundsfjärden and the pumped aquifer. The evaluation of the vertical leakage through the gyttja sediments indicates a vertical K of the gyttja of 10^{-8} to 10^{-9} m/s.

Groundwater levels in Quaternary deposits are of potential interest as a basis for setting the upper boundary conditions in hydrogeological models. Measured groundwater elevations in Quaternary deposits at Forsmark range from about –1 m to +13 m. However, the range in groundwater levels is only about 5.5 m when represented as depths below surface. The majority of wells form a tight cluster with reported groundwater levels in the range of approximately +0.25 to –1.5 m relative to the surface /Johansson 2008/. These wells typically show a strong uniformity in response to drier summer conditions in July and August. Similarly, these wells also display uniformity in response to recharge events following major precipitation and snow melting.

Figure 4-11 summarises the strong correlation that was observed between mean observed groundwater and ground surface elevations in the Quaternary deposits. With a few exceptions, it can be stated that the average position of groundwater in the Quaternary deposits appears to be largely determined by the local ground surface elevation. In other words, the shape of the groundwater surface in the Quaternary deposits generally follows that of the ground surface. The most pronounced outliers are located below the ridge of the glaciofluvial deposit Börstilåsen, or in typical recharge areas (see /Johansson 2008/ for a detailed discussion on the outliers).

Modelling of groundwater flow in the bedrock at Forsmark has also been performed using flux boundary conditions at the top boundary; in fact, this has been the most common option in the later stages of the site descriptive modelling. Water balances provide a basic input when assigning flux

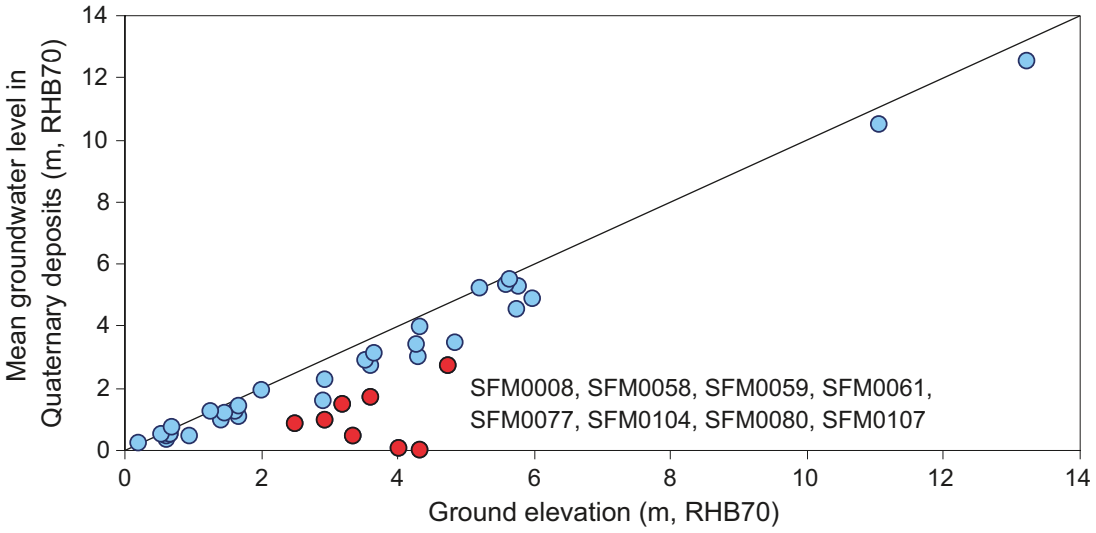

Figure 4-11. *Cross-plot of average groundwater level elevations in the Quaternary deposits versus ground elevations at the well locations. The red dots represent outliers; the ID numbers of these wells are listed in the figure.*

boundary conditions, and for Forsmark both measured and calculated water balances are available. In particular, the water balance of the saturated zone is needed, so that the groundwater recharge can be estimated. However, at Forsmark overland flow is small, implying that the groundwater recharge is approximately the same as total discharge.

According to /Johansson 2008/, the long-term average specific discharge in the Forsmark area is estimated to be 150–160 mm/y. However, it should be noted that this is a spatial average for the whole model area, including both (recharge) areas, where recharge actually takes place, and the discharge areas. In some cases, spatial distributions or values representing recharge areas only are more relevant. As indicated by Figure 4-5, this information can be obtained from the available modelling results.

/Johansson 2008/ used a systems approach to describe the hydrological and near-surface hydrogeological flow system of the central parts of the regional model area. The description is to a large extent based on a joint evaluation and interpretation of time-series data from Quaternary deposits and rock, see also /Johansson and Öhman 2008, Juston et al. 2007/. Some results of particular interest for the bedrock modelling and the interactions between Quaternary deposits and rock are summarised in the following.

- Correlations between seawater levels and groundwater levels in rock and in Quaternary deposits were investigated by several methods. The regression coefficients for the groundwater levels in Quaternary deposits with sea levels were very low with the exception of two wells located in glaciofluvial material within 100 m distance from the sea.
- The regression coefficients were also quite low for groundwater levels in the rock and sea levels, with the exception of boreholes located at the SFR-peninsula. The analysis indicated that seasonal precipitation and variations in evapotranspiration determined the main part of the variations in groundwater level.
- During events of very high seawater levels, seawater flows into several of the lakes. During these events, the sea obviously has an impact on both surface and groundwater flow systems in these lakes and their surroundings.
- Direct recharge from precipitation is the dominant source of groundwater recharge. However, the groundwater level measurements in the vicinity of Lake Bolundsfjärden and Lake Eckarfjärden show that the lakes may act as recharge sources to the till aquifers in this immediate vicinity during summer. Also, the Baltic Sea can potentially act as a source of groundwater recharge during periods of high seawater levels.
- The strong correlation between the mean groundwater elevations observed in the till and ground elevation data means that the average vertical hydraulic flux at some point below the surface is considerably less than the net infiltration into the saturated zone of the till. This could partly result from a contrast in vertical hydraulic conductivity between the till and the bedrock (with the uppermost bedrock having a lower K_v).
- The groundwater level in the till seems to be considerably higher than that in the rock within the tectonic lens. At drill site 1, for example, absolute groundwater levels in the Quaternary deposits are well above the point water heads in bedrock except during dry summer conditions.
- The groundwater levels in the bedrock boreholes are above the interface between Quaternary deposits and rock under undisturbed conditions, indicating that no unsaturated zone exists below this interface.
- In general, there is no discernable response in the groundwater levels in Quaternary deposits to disturbances in the groundwater levels in the bedrock. On the other hand, groundwater levels in both Quaternary deposits and bedrock are correlated to precipitation and evapotranspiration.
- Variations in groundwater levels in the till and in the bedrock are correlated. The natural groundwater level fluctuations are, however, smaller in the bedrock, but still to a great extent controlled by the annual precipitation and evapotranspiration cycles. The conditions prevailing within the northern part of the tectonic lens, with a lower groundwater level in the bedrock than in Quaternary deposits, mean that the groundwater flow has a downward component at the sites studied, implying an inflow from the till into the bedrock. The difference between the levels in till and in bedrock indicates a limited hydraulic contact between Quaternary deposits and rock.

- Outside the tectonic lens, for example at drill site 4 and in the area around Lake Eckarfjärden, the groundwater level in the bedrock may be well above the groundwater levels in Quaternary deposits in nearby low-lying areas, implying that flow systems involving the bedrock may have local discharge areas.
- The lake water level-groundwater level relationship indicates that the lake sediments and the underlying till have low vertical hydraulic conductivities. If the hydraulic contact had been good, the situation with groundwater level drawdown from evapotranspiration extending below the lakes, and the quick and extensive drawdowns from the pumping would not have appeared.

Figure 4-12 shows the groundwater levels in wells in Quaternary deposits and bedrock at drill site 1 located within the tectonic lens. The groundwater levels in the Quaternary deposits are above those in the rock except during the summers of 2003 and 2006. Figure 4-13 shows the groundwater levels in a monitoring well in till below the middle of Lake Bolundsfjärden (SFM0023) and in a nearby percussion-drilled borehole (HFM32) located on a small island in the lake. Water levels in the sea and in the lake are also shown in the figure. The lake level and the groundwater level in till are considerably higher than the levels in the four sections of HFM32. The heads are lowest in the two deepest sections. The results indicate a downward flow gradient from the lake and the Quaternary deposits to the bedrock.

4.4.2 Hydrochemistry

This section summarises a recent set of analyses in which hydrochemical data have been used for interpretation of flow systems. The emphasis is on the conditions within potential discharge areas for groundwater below the lakes, especially focusing on evidence for deep groundwater discharge. This analysis is based on and extends the description in /Tröjbom et al. 2007/ (see section 4.3.1), in terms of the integration between hydrology and hydrogeochemistry. The work summarised below is reported in /Johansson 2008/.

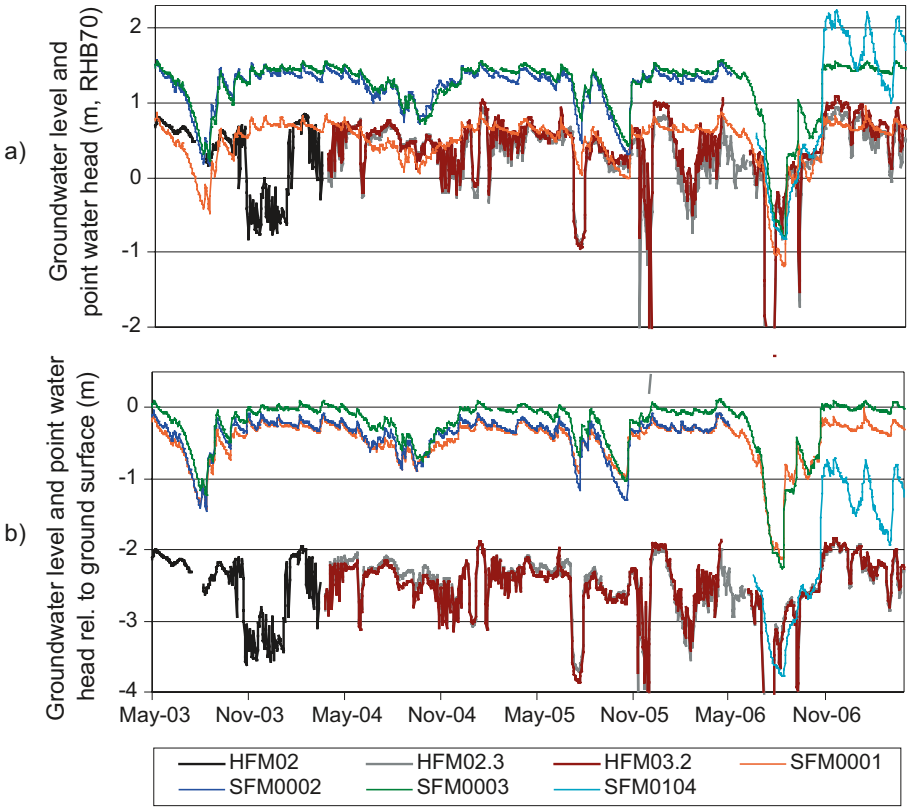

Figure 4-12. *Comparison of groundwater levels in wells in Quaternary deposits (SFM) and in bedrock (HFM) at drill site 1 in terms of a) metres above sea level and b) depth below ground surface. Data from the shallowest HFM-sections are shown.*

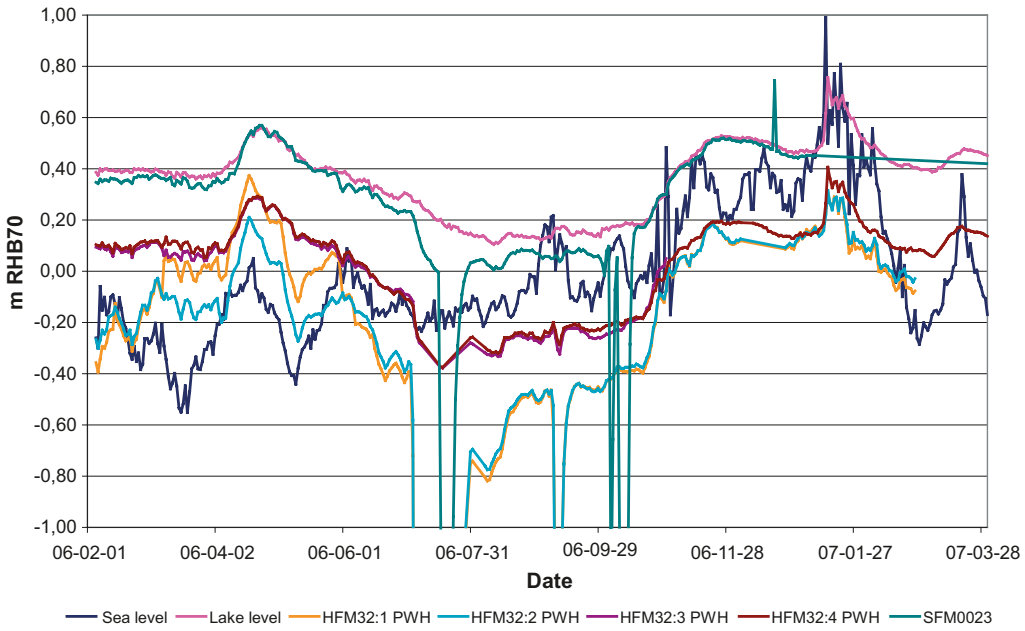

Figure 4-13. *Water level in the Baltic Sea and Lake Bolundsfjärden plotted together with groundwater levels in till below the lake (SFM0023) and in sections in the bedrock borehole HFM32 (Depth in m RHB 70: HFM32:1: –198.75 to –96.27; HFM32:2: –95.27 to –30.95; HFM32:3: –29.95 to –24.97; HFM32:4: –23.97 to +0.97).*

In /Tröjbom et al. 2007/, the method of principal component analysis (PCA) was applied to establish an ion-source model for the Forsmark data. In a first step, only data from percussion-drilled and core-drilled boreholes were used to optimise a model for separating the groundwater types found in the bedrock. This model was then applied to observations of surface water and groundwater in Quaternary deposits, revealing similarities in hydrochemical composition between these observations and the main patterns found in the groundwater in the bedrock.

In Figure 4-14, the ion-source model developed in /Tröjbom et al. 2007/ is shown for labelled monitoring wells in Quaternary deposits with different possible ion sources and possible groundwater types. Five major water types are identified:

- *Modern sea water*.
- Water with *influence of relict marine water* (Littorina).
- *Deep saline water* significantly influenced by shield brine (shield brine is a highly saline groundwater present at great depths in the granitic environment of the Scandinavian Shield).
- *Altered meteoric water* of meteoric origin, but significantly altered by processes in the Quaternary deposits.
- *Freshwaters* include both surface water and shallow groundwater, showing “immature” ion signatures from biogenetic CO_2 and calcite dissolution.

Most of the samples are classified as belonging to the *fresh water* and *altered meteoric groundwater* groups. The wells placed in till below lakes and the sea show quite different chemical compositions. In general, the waters from these wells have a high salinity, including high chloride content. The well below Lake Gällsboträsket (SFM0012) and the wells located in the Gällsboträsket depression (SFM0011 and SFM0013) are classified as belonging to the *influence from relict marine water* group and have chloride contents of approximately 2,000 mg/L.

Interestingly, SFM0057 located at the edge of the Gällsboträsket depression has a signature indicating an influence from deep saline water and shows similarities with the signatures of HFM11 and HFM12. These boreholes are located near Lake Eckarfjärden and in the major Eckarfjärden deformation zone (chapter 5), which also passes below Lake Gällsboträsket. The water in SFM0057 is, however, quite diluted with an average chloride content of c. 250 mg/L.

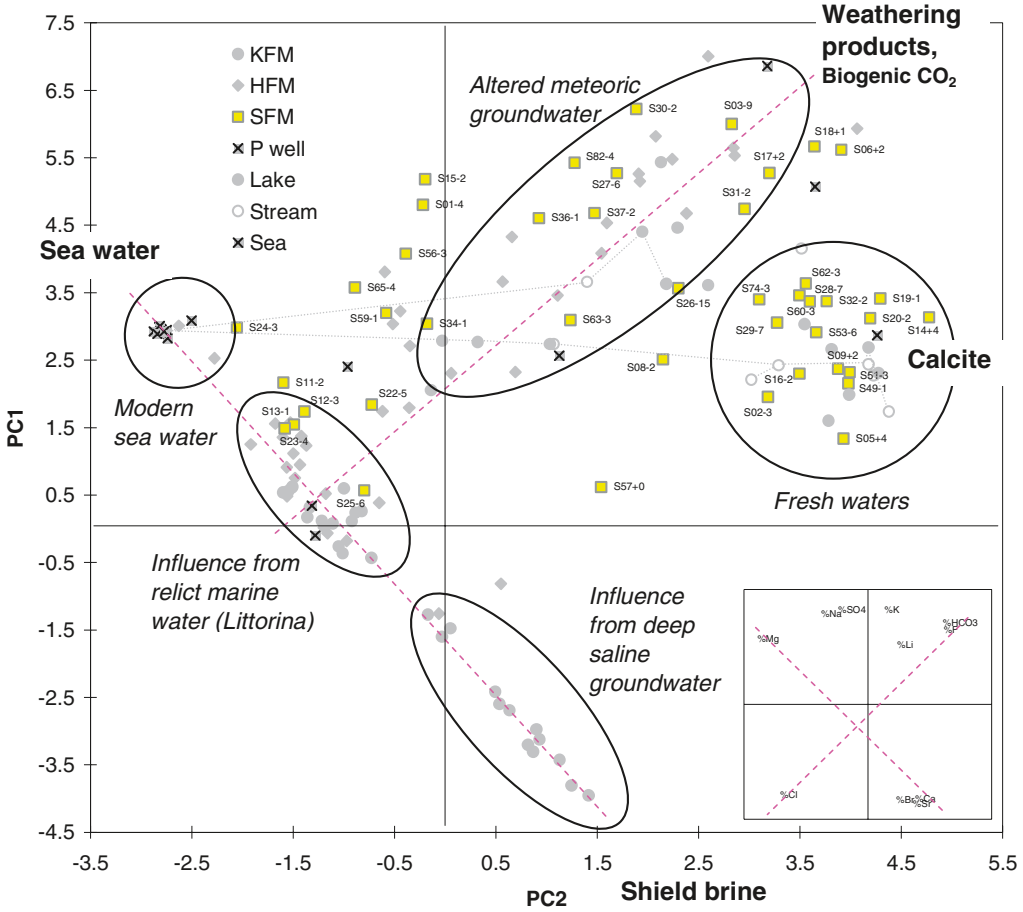

Figure 4-14. *The ion-source model showing labelled monitoring wells in Quaternary deposits with different possible ion sources and possible groundwater types (modified from /Tröjbom et al. 2007/, where a detailed description of the model is given). Note that FM and two zeros have been deleted from the well numbers, and that the last part of the well number is the mean elevation (m RHB 70) of the sampling interval (therefore, it is preceded by either "+" or "–").*

The well in the middle of Lake Bolundsfjärden (SFM0023) also belongs to the *influence from relict marine water* group and has a chloride concentration of c. 3,775 mg/L. The chloride concentration is approximately the same as in the nearby percussion-drilled borehole HFM32 down to a depth of c. 100 m. Also, the well SFM0022 below Lake Fiskarfjärden shows a chemical signature clearly influenced by relict marine water. The water from the well below Lake Eckarfjärden (SFM0015), however, shows a quite different chemical composition and is in the ion-source model closest to the group *altered meteoric water*. The chloride content in the SFM0022 well is c. 300 mg/L.

The occurrence of water belonging to the group *influenced by relict marine water (Littorina)* below Lake Bolundsfjärden, Lake Fiskarfjärden and Lake Gällsboträsket is a strong indication of very low flow rates in the flow systems involving these parts of the regional site investigation area. In the perspective of the total annual water balance of the area, the water can be considered as stagnant. At Lake Bolundsfjärden, no flow from below reaches the till at present according to the groundwater levels measured in the Quaternary deposits and the bedrock (see Figure 4-14). Furthermore, the water composition indicates that the leakage from the lake through the sediments must be very small. The hydrogeological and hydrochemical interpretations indicate that shallow groundwater flow systems involving only Quaternary deposits have discharge areas around the lake and in the near-shore parts of the lake, while deeper systems are drained by the highly transmissive shallow bedrock.

The chemistry of the water flowing out of Lake Eckarfjärden and Lake Gällsboträsket gives an opportunity to investigate to what extent relict marine water and deep saline groundwater are present in the flow systems generating surface discharge. Chloride is considered as a good tracer since it follows the water, and due to the big difference in concentrations between water containing chloride

from atmospheric deposition only and relict marine and deep saline water. In /Johansson 2008/, an evaluation of the transport of chloride from Lake Eckarfjärden and Lake Gällsboträsket is reported. The quantification of chloride transport is based on the hydrochemical analysis in /Tröjbom et al. 2007/ and the hydrological data presented in /Johansson and Öhman 2008/.

The average Cl concentration measured at the outlet of Lake Eckarfjärden is 5.1 mg/L. This chloride concentration corresponds to what can be assumed to originate from atmospheric deposition. The chloride concentration in the discharge from Lake Gällsboträsket, measured upstream of the conjunction with the brook from Lake Eckarfjärden, is considerably higher (the average is 29 mg/L) and it was concluded in /Johansson 2008/ that an additional source besides atmospheric deposition has to exist.

By using the continuous discharge and electrical conductivity (EC) measurements and the correlation between EC and the chloride concentration, daily values of the transport of chloride from Lake Gällsboträsket have been calculated. The average annual chloride transport for the period Dec. 8, 2004-March 31, 2007 was approximately 9,900 kg. The annual atmospheric deposition in the catchment area was 1,800 kg, leaving approximately 8,000 kg originating from another source. From the regolith depth and stratigraphy model, the volume of the Quaternary deposits in the Gällsboträsket depression below 2.5 m was calculated, and the total water volume in the Quaternary deposits was estimated from values of the total porosity.

Based on this volume and the mean chloride concentration of c. 2,000 mg/L in the three wells in Quaternary deposits in the depression, the storage of chloride in the Quaternary deposits was estimated at c. 500 tonnes. With the current transport rate, this storage will be depleted in approximately 60 years. Further analysis of the relationship between discharge and hydrochemical composition indicated influence of deep saline water. This, together with the current outflow rate compared with the estimated storage in the Quaternary deposits, raises the question of whether there is an additional source of chloride, i.e. upward flow of deep saline groundwater, in the Gällsboträsket area (see /Johansson 2008/ for a more detailed description of the analysis).

Concentrations of ^{3}H, $\delta^{18}O$ and ^{2}H, as well as the concentration of chloride, may contain information on the origin of the sampled groundwater that is not used in the ion-source model. These parameters are plotted on the ion-source model in Figure 4-15. Specifically, the three wells below the lakes Bolundsfjärden (SFM0023), Eckarfjärden (SFM15) and Gällsboträsket (SFM0012) are labelled. In general, the SFM0012 and SFM0023 wells show similarities for the presented parameters. SFM0015, below Lake Eckarfjärden, deviates significantly from SFM0012 and SFM0023, with slightly higher ^{18}O and lower ^{2}H excess values as well as a considerably lower chloride concentration. The combined picture is difficult to interpret, but may be a result of a mixed water with component(s) exposed to evaporation.

4.4.3 Solute transport

This section is based on /Lindborg (ed) 2008/ and summarises some implications of the near-surface and surface system modelling results for radionuclide transport. Thus, the focus is on transport of radionuclides from a hypothetical repository in the deep rock, whereas transport scenarios associated with, for example, the composition of the groundwater flowing downwards to the rock are not discussed here (see /Tröjbom et al. 2007/ for details on the chemistry of the surface system). Figure 4-16 and Figure 4-17 show two different types of conceptual models developed within the site descriptive modelling, i.e. a flowpath-based model showing alternative flow and transport paths in the uppermost part of the system and a compartment model based on the different types of systems considered in the ecosystems modelling /Lindborg (ed) 2008/.

Figure 4-16 and Figure 4-17 illustrates the key role of the horizontal structures, which, as explained in section 4.4.1 and chapter 8, may short-circuit flow paths from the deep rock and divert them towards the sea. The main implication of this would be that there are no discharge areas within the present land area for flow paths from the deep rock in the target area, and, consequently, that the terrestrial, mire and lake/brook compartments would be by-passed in a model for the present conditions.

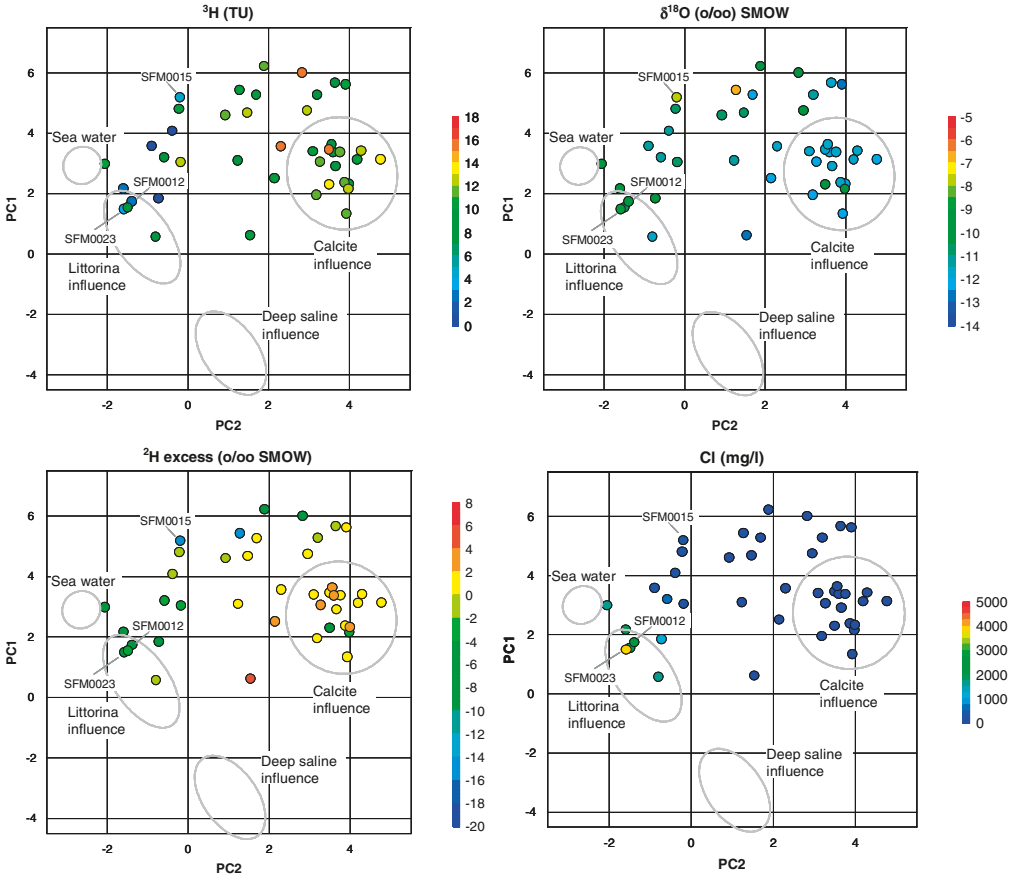

Figure 4-15. *The parameters ^{3}H, δ^{18}O and ^{2}H as well as the concentration of chloride in the wells in Quaternary deposits, plotted on the ion-source model, with the wells SFM0012, SFM0015 and SFM0023 labeled (modified from /Tröjbom et al. 2008/).*

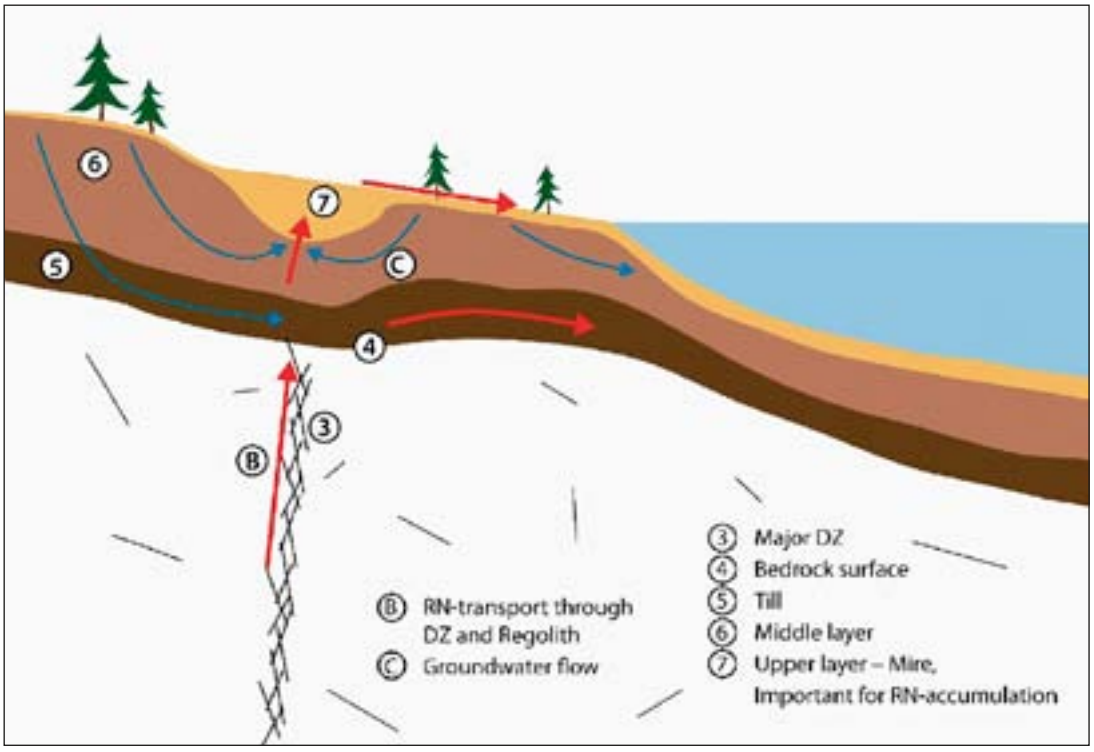

Figure 4-16. *Example illustration of possible solute transport paths to a recipient from a source in the subsurface.*

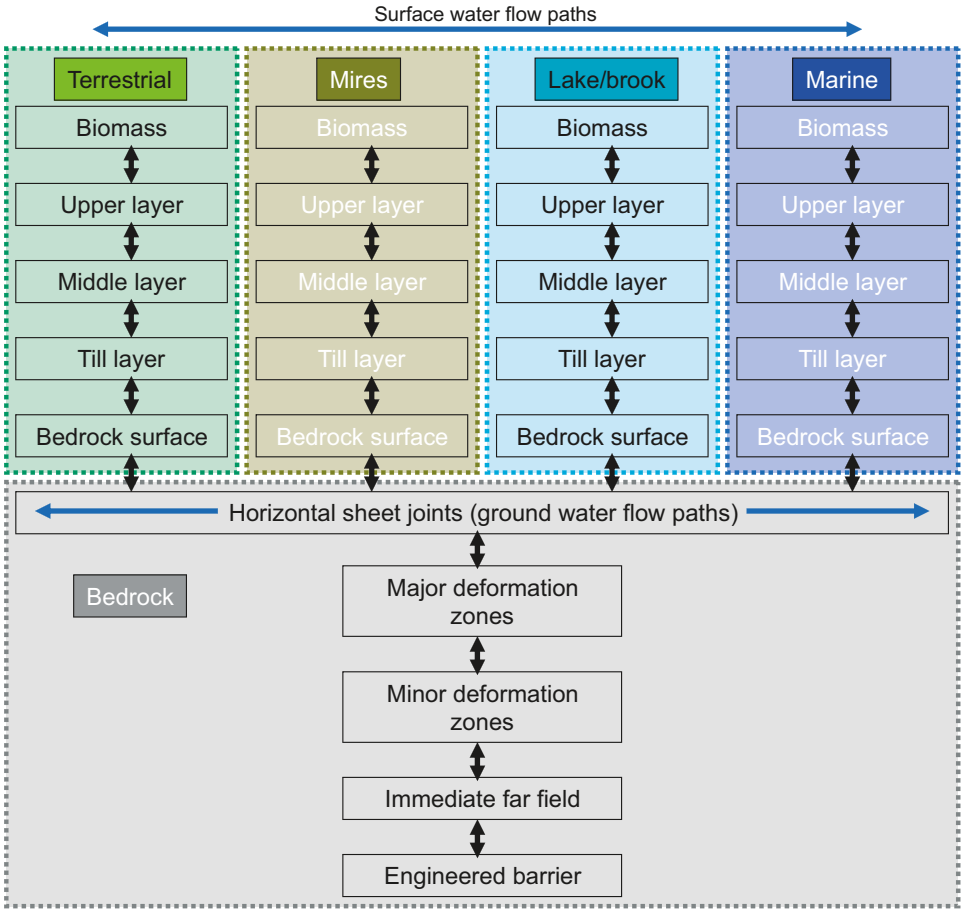

Figure 4-17. *Conceptual illustration of transport domains at the Forsmark site.*

In general, the particle-tracking simulations performed as part of the site descriptive modelling confirm that most flow paths discharge in the sea. However, some differences regarding the extent of deep groundwater discharge on land and horizontal transport distances below the sea can be observed when comparing results from different models /Follin et al. 2008a, Bosson et al. 2008/. This indicates that the modelling of the horizontal fractures/sheet joints and their interactions with the regolith are associated with uncertainties, which implies that different scenarios need to be considered in the forthcoming safety assessment.

Figure 4-16 illustrates another uncertainty related to the near-surface part of the flow paths, namely the role of the Quaternary deposits-bedrock interface. If upward, vertical transport through the upper bedrock takes place, the flow paths may continue along the Quaternary deposits-bedrock interface and/or vertically through the Quaternary deposits. As indicated in the figure, this implies that different flow paths in the Quaternary deposits (i.e. spreading associated with spatial and temporal variability in flow) and discharge points in different parts of the surface water system are possible.

Comparison of results from slug tests in till in groundwater monitoring wells installed across the Quaternary deposits-bedrock interface and in Quaternary deposits only shows that K-values are higher in the interface region. Furthermore, the hydrochemical evaluation summarised above indicates that the groundwater is more or less stagnant below some of the lakes in the Forsmark area, i.e. in areas that in absence of the horizontal fractures/sheet joints would be considered as typical discharge areas. These observations indicate that the Quaternary deposits-bedrock interface could be important for transport of radionuclides potentially reaching the near-surface system from below. However, this must be studied in more detail before more definite conclusions can be drawn.

In addition to its effects on advective transport (i.e. on flow paths, discharge points and dilution) the surface system may also provide a capacity for radionuclide retention by processes such as sorption and precipitation, additional to that offered by the rock. Parameters of interest for modelling

of retention properties, including mineralogy and geochemistry, are presented in /Hedenström and Sohlenius 2008/. Based on this information and on hydrochemical data available in the Forsmark data freeze 1.2, /Grandia et al. 2007/ evaluated potential retention processes for a set of selected radionuclides. The result of the process evaluation is shown in Table 4-4.

In /Grandia et al. 2007/, the conceptual retention process models for different radionuclides were also implemented in a numerical model. Results of test simulations of transport of uranium, strontium and caesium in till and clay systems are reported in /Grandia et al. 2007/. In short, these results demonstrate that the regolith may provide significant radionuclide retention, but also that predictions of its retention capacity can be highly sensitive to assumptions made in the development of the process models.

4.5 Summary description of the surface system at Forsmark

The Forsmark area is unique in many ways. The area does not represent a typical coastal Swedish site located at the shoreline of the Baltic Sea. The shoreline displacement in combination with the flat topography has resulted in a very young terrestrial system that contains a number of newborn shallow lakes and wetlands. The lakes themselves are also of a specific type that only can be found in northern Uppland. Shallow and with sediments rich in calcium, the lakes are unique to Sweden. Hydrologically, the area also differs from the regional pattern; high hydraulic conductivities in the upper part of the bedrock is the result of a complex network of gently dipping and sub-horizontal, open and partly open fractures.

The latest deglaciation in Forsmark took place during the Preboreal climatic stage, c. 8800 BC /Fredén (ed) 2002, Persson 1992, Strömberg 1989/. Forsmark is situated below the highest coastline, and at the deglaciation the area was covered by c. 150 m of water. The closest shore/land area at that time was situated c. 80 km to the west of Forsmark. Shoreline displacement has strongly affected the landscape development and still causes a continuous and relatively predictable change in the abiotic and biotic environment, e.g. in water and nutrient availability. The first parts of Forsmark emerged from the sea around year 500 BC. Thus, the post-glacial development is determined mainly by the development of the Baltic basin and by the shoreline displacement /Söderbäck (ed) 2008/.

Table 4-4. Evaluation of retention processes reported in /Grandia et al. 2007/. The mechanisms that are "able to retain" and are likely to occur under the conditions found in the Quaternary deposits at Forsmark are indicated by black cells. Processes judged "able to retain" but of questionable occurrence at Forsmark are grey-shadowed. Processes considered "unable to retain" and/or unlikely are indicated by colourless cells in the table. Many processes occurring at low redox potentials (e.g. precipitation of selenium in sulphides) are in grey since reducing conditions are not confirmed to occur in the Forsmark near-surface system.

Radionuclide / *Retention process*	*U*	*^{79}Se*	*^{129}I*	*^{135}Cs*	*Sr*
Precipitation as pure phases					
Sorption onto phyllosilicates					
Sorption on organic matter					
Sorption onto Fe-Mn-Al oxyhydroxydes					
Association with carbonates					
Association with phosphates					
Association with sulphides					

Favourable and possible

Favourable but perhaps unlikely

Unfavourable and/or unlikely

The candidate area is characterised by a low altitude and is almost entirely located below 20 m.a.s.l. Till is the dominant Quaternary deposit and granite is the dominant rock type. The annual precipitation and runoff are 560 and 150 mm, respectively. The main lakes are Fiskarfjärden, Bolundsfjärden, Eckarfjärden and Gällsboträsket. The lakes are shallow with a maximum depth ranging from 0.4 to 2 m. Seawater flows into the most low-lying lakes during events of very high seawater levels. Wetlands are frequent and cover between 25 and 35% of some of the delineated sub-catchments.

There are no major water courses in the candidate area. The brooks downstream of Lake Gunnarsboträsket, Lake Eckarfjärden and Lake Gällsboträsket carry water most of the year, but can be dry for long periods during dry years such as 2003 and 2006. Substantial parts of the brooks in the area have been artificially deepened for drainage purposes.

Measurements show that the horizontal hydraulic conductivity and specific yield of the till are typical of, or slightly higher than, those of the surrounding region. Groundwater levels in Quaternary deposits are very shallow; on average less than 0.7 m below ground surface for 50% of the time. Shallow groundwater levels imply a strong interaction between evapotranspiration, soil moisture and groundwater. Diurnal fluctuations of the groundwater levels, driven by evapotranspiration cycles, are evident in many groundwater wells. Furthermore, groundwater level measurements in the vicinity of the lakes show that the lakes may act as recharge sources to till aquifers in the riparian zone during summer.

There is a close correlation between the topography and the groundwater levels in the Quaternary deposits. For groundwater levels in the upper bedrock there is no such strong coupling to the topography. This is most evident in the central part of the candidate area, where the groundwater level gradients in the bedrock are very small, indicating a high transmissivity. Here, the groundwater levels in the till are often considerably higher than in the bedrock. This implies that local, small-scale recharge and discharge areas, involving groundwater flow systems restricted to Quaternary deposits, overlie the more large-scale flow systems associated with groundwater flow in the bedrock. In the middle of Lake Bolundsfjärden, located in the central part of the study area, the lake water level and the groundwater level in till are considerably higher than the levels in the bedrock down to 200 m depth. This indicates a downward flow gradient from the lake and Quaternary deposits to the bedrock.

The surface water and shallow groundwater at Forsmark is characterised by high pH-values and high contents of major constituents, especially calcium and bicarbonate /Sonesten 2005, Tröjbom and Söderbäck 2006/. The main reason for this is glacial remnants, mostly in the form of a till layer, which were deposited during the Weichselian glaciation and deglaciation /Fredén (ed) 2002/. This till layer, originating from the sedimentary bedrock of Gävlebukten about 100 km north of Forsmark, has a rich content of calcite.

The marine ecosystem in the Forsmark area is a relatively productive coastal area in a region of otherwise fairly low primary production. This is due to up-welling along the mainland /Eriksson et al. 1977/. The surface water has a nutrient concentration ranging from 330 to790 µg/L total nitrogen and 12 to 25 µg/L total phosphorous. The seabed consists mostly of erosion and transport bottoms with heterogeneous and mobile sediment, mainly sand and gravel with varying fractions of glacial clay. Some areas of the seabed close to the mainland have rocky bottoms, partly covered with coarse till. The results from modelling show that although most parts of the area are heterotrophic, the mean of the whole model area is autotrophic, i.e. more carbon is fixed in biomass by primary producers than is released by all organisms /Wijnbladh et al. 2008/.

The characteristics of the limnic ecosystem in the Forsmark regional model area are, to a major extent, determined by the small topographic gradients in combination with the ongoing shoreline displacement, the close proximity to the sea, and by the occurrence of calcium-rich deposits. The lakes are classified as oligotrophic hardwater lakes, i.e. they contain high calcium levels, but low levels of nutrients, as phosphorus is precipitated together with the calcium. This kind of lake is common along the coast of northern Uppland, but is not generally very common in Sweden /Nordén et al. 2008/.

The terrestrial vegetation is, among other things, affected by the bedrock, the Quaternary deposits and human land use. The Quaternary deposits are mainly wave-washed till, on which conifer forests are common. In depressions, a deeper regolith layer is found, with fairly high calcium content. The calcareous influence is typical for the north-eastern part of Uppland and is manifested in the flora. The Forsmark area has a long history of forestry, which is seen today as a fairly high percentage of younger and older clear-cuts in the landscape. Wetlands occur frequently and cover 10–20% of the area in the three major catchments and up to 25–35% in some sub-catchments /Johansson et al. 2005/. A major part of the wetlands are coniferous forest swamps and open mires. Arable land, pastures and clear cuts dominate the open land. Arable land and pastures are found close to settlements. Many pastures were earlier intensively used but are today a part of the abandoned farmland, following the nationwide general regression of agricultural activities /Löfgren (ed) 2008/.

In conclusion, the surface system site description has increased the general understanding of how the site functions in terms of properties in different volumes, main functional units, processes and system descriptions arising from different scientific disciplines. The initial conceptual model, developed at the beginning of the work in 2002, has been adjusted to site-specific features, and site data have been used to describe flows and accumulation of matter in and between different parts of the surface system at Forsmark.

The site description will be used in safety assessments to achieve input on properties and processes, and on overall system conceptualisation and understanding. The main supporting background reports developed to be used as input to the safety assessment are:

- Surface system Forsmark, Site descriptive modelling, SDM-Site Forsmark (R-08-11).
- Geological evolution, palaeoclimate and historical development of the Forsmark and Laxemar-Simpevarp areas, Site descriptive modelling, SDM-Site (R-08-19).
- The terrestrial ecosystems at Forsmark and Laxemar, Site descriptive modelling, SDM-Site (R-08-01).
- The limnic ecosystems at Forsmark and Laxemar, Site descriptive modelling, SDM-Site (R-08-02).
- The marine ecosystems at Forsmark and Laxemar, Site descriptive modelling, SDM-Site (R-08-03).
- Hydrochemistry of surface water and shallow groundwater, Site descriptive modelling, SDM-Site Forsmark (R-07-55).
- Description of surface hydrology and near-surface hydrogeology at Forsmark, Site descriptive modelling, SDM-Site Forsmark (R-08-08).
- Description of the regolith at Forsmark, Site descriptive modelling, SDM-Site Forsmark (R-08-04).

The present site description covers all information available on the surface system at Forsmark. The wealth of information, both in the form of data from the site investigations and of conceptual and numerical models, comprises a comprehensive foundation for the environmental impact assessment (EIA). Main SDM references for the EIA are the ecosystem reports covering the biotic and abiotic descriptions of the Forsmark surface system. The hydrology and the properties of the Quaternary deposits are also available, together with the chemical description of Forsmark waters, soils and biota. No description on nature values is made in the SDM, but all relevant information, e.g. the occurrence of threatened or vulnerable species, collected during site investigations is stored in the SKB databases.

A number of properties and models, beside the general description, are available to use as input to the design of the potential repository. Important information for planning the above-ground facilities is contained in the reports describing Quaternary deposits (regolith), surface hydrology, and the digital elevation model.

4.6 Evaluation of uncertainties

As described in the previous section, the site descriptive model for the surface system consists of a large number of sub-models, covering a wide range of disciplines. In many cases, sub-models are combined and used as input for new models. For example, in the modelling of surface hydrology the digital elevation model (DEM), the horizontal distribution and stratigraphy of the regolith, the hydraulic properties of till, and the distribution of different vegetation types, are used as important input data. Each sub-model contains its own uncertainties. These uncertainties are accumulated in the aggregated models, together with uncertainties associated with the assumptions and simplifications made in the development of the aggregated model.

The approach to evaluate uncertainties in the aggregated models is firstly to assess uncertainties in the underlying sub-models upon which the aggregated model is built, and secondly, to evaluate the assumptions made within the aggregated model. No quantification of uncertainties associated with the site descriptive model for the surface system is made here, since this is done separately in each of the discipline-specific background reports (see section 4.5). Instead, a brief summary of the confidence in some of the most important sub-models and aggregated models is given here.

Generally, the site descriptive model for the surface system is based on a wealth of site data. Uncertainties associated with the sub-models have been thoroughly evaluated, and descriptions and model results are in most cases consistent with regional/generic data and/or with the results from alternative models.

Some aspects of the site descriptive model for the surface system have low uncertainty and high confidence, whereas other aspects have higher degree of uncertainty and, accordingly, lower confidence (see Table 4-5). However, none of these are judged to be of critical importance for the long-term safety assessment or for engineering.

Table 4-5. Degree of uncertainty for some of the most important sub-models and input data in the site descriptive model.

Aspects	Degree of uncertainty
The past development of the site, including climate changes, description of shoreline displacement, and salinity changes in the Baltic basin.	Low
Geometries, e.g. the digital elevation model, delimitation of catchment areas, horizontal distribution and stratigraphy of the regolith, distribution of vegetation types.	Low
Overall water balance, surface- and groundwater levels, general groundwater flow pattern.	Low
Hydrochemistry of surface waters with regard to nutrients, macro elements, temporal variation and mass transport in drainage areas.	Low
Hydraulic properties of till.	Low
Chemistry in biota and Quaternary deposits – the data amounts are limited and spatial extrapolation of the available data is required.	Higher
In spite of the fact that the general groundwater flow pattern is considered to be well-known, the exact location of discharge areas of deep groundwater is difficult to establish due to the complex geometry and varying hydraulic properties of the horizontal fractures/sheet joints which determine groundwater flow in the near-surface bedrock.	Higher
Depth distribution of the regolith, especially outside the central area.	Higher
Process estimates (e.g. plant uptake and respiration) – there are generally few measurements and short time series.	Higher
Influence of chemical processes on the transport of elements.	Higher

5 Bedrock geology

The selection of a site for the disposal of highly radioactive nuclear waste requires a robust understanding of the bedrock geology prior to modelling work in other disciplines, the design of a potential repository, and the assessment of safety and environmental impact. Deterministic geological modelling work has addressed three aspects that serve the needs of different users; rock domains, deformation zones and fracture domains. The identification and description of fracture domains has also provided a basis for the statistical modelling of fractures and minor deformation zones, so-called discrete fracture network modelling (DFN). In order to differentiate between the DFN models described here, and the DFN model described in the hydrogeological modelling work, the former is, where necessary, referred to as the "geological DFN". In addition, the evaluation of primary data bearing on subordinate rock types has provided an input for the development of stochastic models for the spatial distribution of these rock types inside the rock domains that comprise the target volume. These stochastic models are presented in the context of the thermal modelling work (see chapter 6).

Following establishment of the state of knowledge prior to the site investigation work in model version 0 /SKB 2002/, deterministic modelling work in SDM versions 1.1 and 1.2 /SKB 2004, 2005a/ focused entirely on the development of geological models in the regional model volume (Figure 2-5). The geological DFN modelling in SDM version 1.2 /La Pointe et al. 2005/ addressed a local model volume that included the candidate volume (Figure 2-5). Following the decision to target further investigations in the north-western part of this volume /SKB 2005c/, focus shifted in the deterministic geological modelling work during model stages 2.1 /SKB 2006a/ and 2.2 /Stephens et al. 2007, Stephens and Skagius (ed) 2007/ to a local model volume that includes the target volume (Figure 2-5). The geological DFN modelling work in stage 2.2 /Fox et al. 2007/ addressed the fracture domains /Olofsson et al. 2007/ inside this target volume.

This chapter summarises the evaluation of primary geological data completed through the geological modelling work and presents the various geological models for the site, both individually and in an integrated manner. The deterministic models and the geological DFN models conform to those presented in model stage 2.2 /Stephens et al. 2007, Fox et al. 2007/ and these two reports form the principal background references. Data from model stage 2.3 have only been used as a means of verifying the deterministic geological models and the results from the stage 2.3 work /Stephens et al. 2008/ are also included in this chapter.

5.1 State of knowledge at the previous model version

A tectonic concept for the spatial distribution of major rock units and ductile structures at the Forsmark site was established in connection with SDM versions 1.1 and 1.2 /SKB 2004, 2005a/. This concept laid the foundation at an early stage for the rock domain modelling work. The conceptual thinking, with a tectonic lens encased in more highly strained bedrock, has been confirmed by the data from boreholes during model stages 2.1 /SKB 2006a/ and 2.2 /Stephens et al. 2007/ and only minor modifications to the rock domain model, at both regional and local scales, have taken place after SDM version 1.2.

The modelling of deformation zones achieved a major stride forward with the full use of the surface reflection seismic data and the modelling of gently dipping zones in the candidate volume in SDM version 1.2 /SKB 2005a/. However, considerable uncertainties remained concerning the geological significance of lineaments and the interpretation of steeply dipping structures. Major advances came during model stage 2.1 /SKB 2006a/, when the strategic decisions were made to address solely lineaments derived from magnetic data and to acquire high-resolution magnetic data on the ground. Furthermore, excavations and focused drilling across and through low magnetic lineaments confirmed the occurrence of strongly altered and fractured bedrock, i.e. brittle deformation zones, along most of the investigated lineaments.

Considerable uncertainty remained after SDM version 1.2 /SKB 2005a/ concerning the geometries, directions and spatial distributions of the fractures within the geological DFN modelling work. The recognition of spatial variability in the fracture pattern and feedback from the hydrogeological modelling team provoked the need for a subdivision into fracture domains, as envisaged generically in the strategic

planning for geological modelling work, e.g. /Munier et al. 2003, Munier 2004/. Early progress with the conceptual thinking for fracture domains at the site was achieved during model stage 2.1 /SKB 2006a/ and a mature concept and geometric model were presented during an early part of model stage 2.2 /Olofsson et al. 2007/. An integration of the fracture domain concept with hydrogeological, hydrogeochemical and rock mechanical data sets was also completed at this stage /Olofsson et al. 2007/.

5.2 Evaluation of primary data

The geological and geophysical investigations performed in the Forsmark area are summarised in sections 2.1, 2.2 and 2.3 and the data supporting the current model version are listed in Table 1 in Appendix 3. The evaluation of these data is presented below.

5.2.1 Bedrock geological map at the surface

Acquisition of field data, map compilation and map quality

A bedrock geological map over the mainland and archipelago at Forsmark, at the scale 1:10,000, has been compiled primarily on the basis of outcrop data assembled during the bedrock mapping programme (Figure 5-1). An interpretation of the magnetic anomaly map (inset in Figure 5-1), compiled predominantly from helicopter airborne data, has also been used. In the vicinity of the nuclear power plant and SFR, rock units were identified by an inspection of various reports and some older cored boreholes. Previous literature and geological maps have also been used to compile the geology, especially in the marginal parts of the regional model area. The frequency and quality of outcrop data, and the intrinsic complexity of the geology, as inferred from earlier investigations, are essential ingredients that determine the quality of the bedrock map. On the basis of these considerations, a judgement on the quality of this map in the regional model area, in the form of three categories (low, variable but generally low, generally high), has been made (Figure 5-1).

Different versions of the bedrock geological map have been produced at different stages in the modelling work /SKB 2004, 2005a, Stephens et al. 2007/. The geological map presented in connection with the initial site investigation /SKB 2005a/ has formed the keystone throughout the work at the site. This version was compiled after completion of the bedrock mapping work at the surface and the acquisition of helicopter airborne geophysical measurements. Nearly 2,150 observation points acquired in connection with the surface mapping during 2002 and 2003 /Stephens et al. 2003a, Bergman et al. 2004a/ formed the foundation of this compilation (Figure 5-1). Only minor adjustments to this map, in connection with the acquisition of high-resolution ground magnetic data in the target area (see section 5.2.7) as well as data close to the surface from boreholes (see section 5.2.2), have subsequently been carried out /Stephens et al. 2007/.

The bedrock geological map (Figure 5-2) presents a 2D model for the distribution of rock units at the ground surface. A description of the map, including the distribution of rock units and the ductile structures within them, was presented in /SKB 2005a/. The absolute ages of the different groups of rock, the relative time relationships between these groups and the deformation at the site, and the exhumation and cooling history have been published in several peer-reviewed articles /Hermansson et al. 2007, 2008, in press, Söderlund et al. in press/. These geochronological data have been evaluated and used in the establishment of the geological evolution of the site (/Söderbäck (ed) 2008/ and section 3.1). The character of the rock types and ductile structures are addressed in more detail in sections 5.2.3 and 5.2.4, respectively.

Rock units and tectonic lenses

The major groups of rocks in the Forsmark area (A to D) are distinguished solely on the basis of their relative age relationships (Table 5-1). One or more rock units, which are distinguished on the basis of the character of the dominant rock type, are included in each group. Rock types within each unit are distinguished on the basis of their composition, grain size and relative age. The bedrock map also distinguishes units where the rocks are banded and/or affected by a strong, ductile tectonic foliation (black dots in Figure 5-2) from units where the rocks are folded and more lineated in character (black dots absent in Figure 5-2). The former are inferred to be affected by higher ductile strain and anastomose around the more folded and lineated bedrock with lower ductile strain inside several tectonic lenses. The candidate area is situated inside one of these tectonic lenses and includes the target area in its north-western part, between Lake Bolundsfjärden and the nuclear power plant (Figure 5-2). This lens is referred to in the following text as the Forsmark tectonic lens (see Figure 5-1).

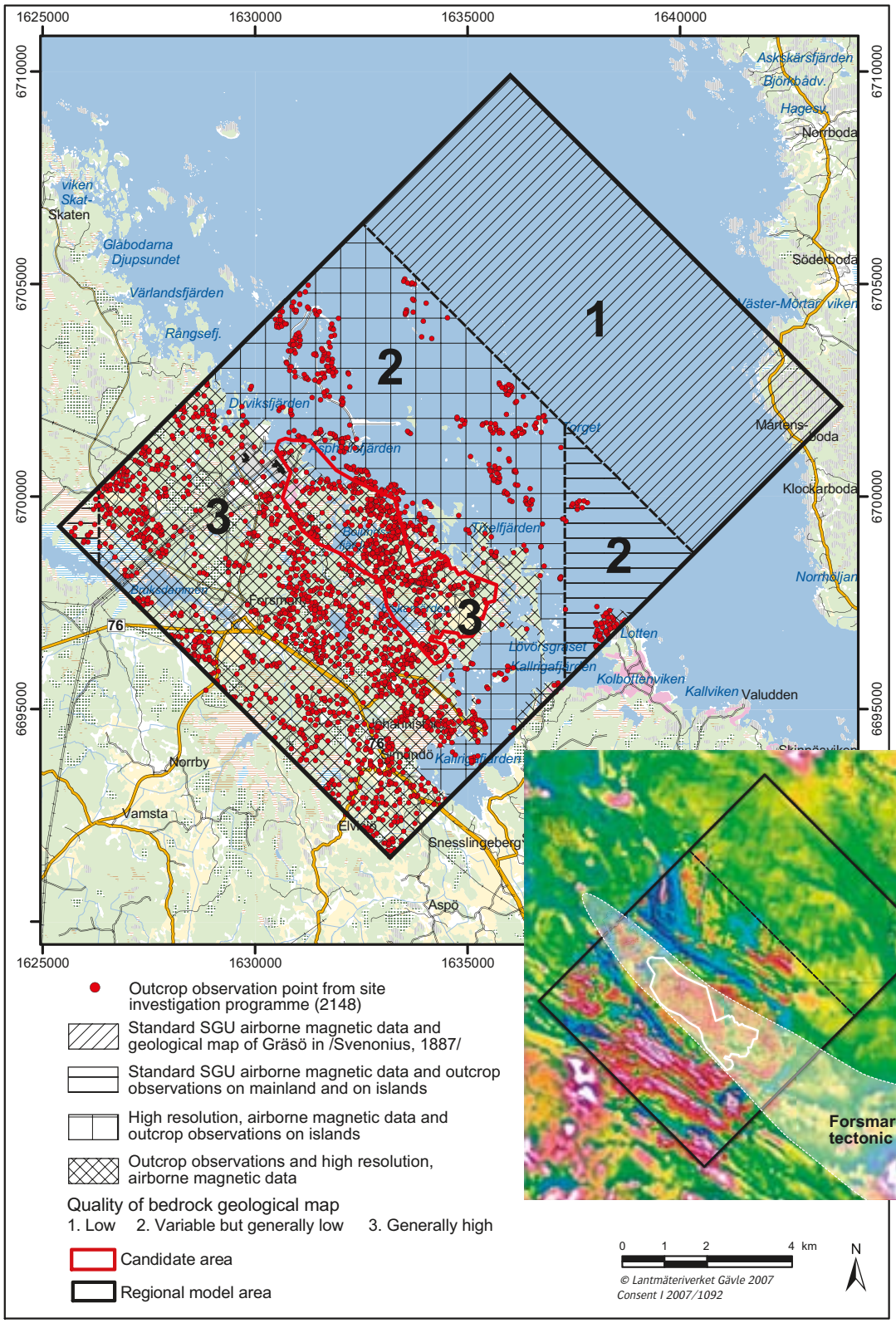

Figure 5-1. *Summary of the base data used in the compilation of the bedrock geology over the regional model area and a judgement of the quality of the bedrock geological map. A map of the magnetic total field over the regional model area that shows the tectonic lens at Forsmark is presented in the inset. The marked contrast in data resolution between the older fixed-wing airborne and the helicopter airborne (north-south flight direction) measurements is apparent in the inset map (see also section 5.2.7). The red-lilac end of the colour spectrum indicates more strongly magnetic bedrock and the blue end of the spectrum indicates more weakly magnetic bedrock.*

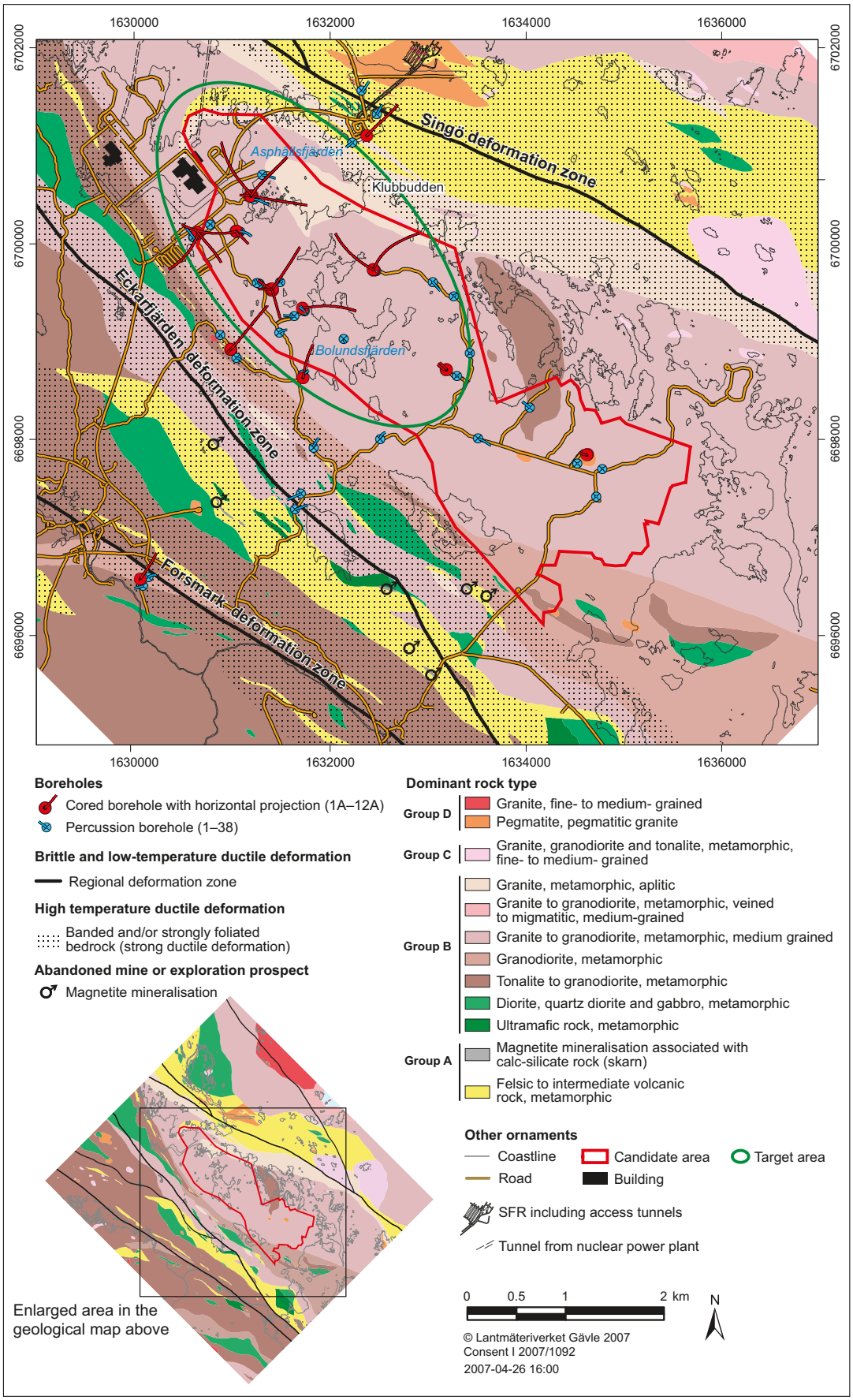

Figure 5-2. *Bedrock geological map of the candidate area and its surroundings at Forsmark. The regional deformation zones (trace length longer than 10 km) are also shown on the map. Coordinates are provided using the RT 90 (RAK) system. Drill sites and boreholes are named in Figure 2-1 and Figure 2-2.*

Table 5-1. Major groups of rocks and rock units at Forsmark based on /Stephens et al. 2005/. SKB rock codes that distinguish different rock types within a rock unit are shown in brackets. The alteration code 104 for albitization is also included.

Rock groups	Rock units on the bedrock geological map
All rocks are affected by brittle deformation. The fractures generally cut the boundaries between the different rock types. The boundaries are predominantly not fractured.	
Rocks in Group D are affected only partly by ductile deformation and metamorphism.	
Group D	• Fine- to medium-grained granite and aplite (111058). Pegmatitic granite and pegmatite (101061). Age partly 1.85 Ga. Variable age relationships with respect to Group C. Occur as dykes and minor bodies that are commonly discordant and, locally, strongly discordant to ductile deformation in older rocks.
Rocks in Group C are affected by penetrative ductile deformation under lower amphibolite-facies metamorphic conditions.	
Group C	• Fine- to medium-grained granodiorite, tonalite and subordinate granite (101051). Age 1.86 Ga. Occur as lenses and dykes in Groups A and B. Intruded after some ductile deformation in the rocks belonging to Groups A and B with weakly discordant contacts to ductile deformation in these older rocks.
Rocks in Groups A and B are affected by penetrative ductile deformation under amphibolite-facies metamorphic conditions.	
Group B	• Biotite-bearing granite (to granodiorite) (101057) and aplitic granite (101058), both with amphibolite (102017) as dykes and irregular inclusions. Local albitization (104) of granitic rocks. Age 1.87 to 1.86 Ga. • Tonalite to granodiorite (101054) with amphibolite (102017) enclaves. Granodiorite (101056). Age 1.88 Ga. • Ultramafic rock (101004). Gabbro, diorite and quartz diorite (101033). Age 1.89 Ga.
Group A	• Sulphide mineralisation, possibly epigenetic (109010). • Volcanic rock (103076), calc-silicate rock (108019) and iron oxide mineralisation (109014). Subordinate sedimentary rocks (106001). Age 1.89 Ga or older.

Metamorphosed, medium-grained granite (to granodiorite), dated to 1.87 Ga, is dominant inside the target area. It is suggested that the occasional granodioritic composition is caused by an incipient stage of the alteration referred to as albitization (see section 5.2.3) and that the rock was initially granitic in composition throughout the target area. In the north-eastern part of this area, close to Asphällsfjärden and Klubbudden (Figure 5-2), fine-grained granitic rocks that, in part, also show alteration referred to as albitization are conspicuous. Subordinate rock types throughout the target area are pegmatitic granite/pegmatite, amphibolite, metamorphosed fine- to medium-grained granitoid, and fine- to medium-grained granite that shows little effect of metamorphism. The subordinate rocks occur as dyke-like bodies and small irregular intrusions. They range in age from 1.87 to 1.85 Ga.

Exploration potential

An assessment of the potential of the Forsmark area for exploration after metallic and industrial mineral deposits has been presented in /Lindroos et al. 2004/. A potential for iron oxide mineralisation and possibly base metals was recognised to the south-west of the candidate area, predominantly in the felsic to intermediate metavolcanic rocks (Figure 5-2). However, the small iron mineralisations in the Forsmark area have no economic value and this judgement was also deemed to be valid in a long-term perspective /Lindroos et al. 2004/.

5.2.2 Rock units and possible deformation zones in the sub-surface realm

Geological, geophysical and radar logs

All the 25 cored boreholes and the 38 percussion boreholes have been mapped geologically using the Boremap methodology adopted by SKB. This involves an inspection of both the drill core and

the oriented images of the borehole provided by the Borehole Image Processing System (BIPS). The terminology and procedures used in the acquisition of fracture data are described in /SKB 2005a, p. 194/. Significant changes in the documentation of data relevant to fractures, including aperture size and the recognition of sealed fracture networks, occurred after the mapping of the earliest boreholes KFM01A, KFM02A, KFM03A and KFM03B /Olofsson et al. 2007, p. 14/. Since no routine was developed to measure linear structural features in a systematic manner in the boreholes, ductile linear fabric data from depth are lacking. Shear striae along fault planes in deformation zones (see section 5.2.6) were measured with the help of fracture orientation data from Boremap and a drill core holder, which allowed the drill core to be positioned in a correct manner in 3D space. The uncertainties in borehole orientation data, which involve uncertainties in both the orientation of boreholes and BIPS images, have been evaluated in /Munier and Stigsson 2007/. They are addressed briefly in section 2.3.

Standard geophysical and radar logs complement the oriented image logs generated along each borehole with the help of BIPS. A summary of the data that have been acquired in the geophysical logging work is presented in /SKB 2005a, p. 192–194/. A combination of some of the geophysical data (e.g. density, natural gamma radiation) with relevant petrophysical data (see section 5.2.3) provides support to the mapping of the bedrock in the boreholes, especially in the percussion boreholes, where drill core is absent. A special study that evaluated the geological interpretation of radar anomalies along possible deformation zones /Carlsten 2007/ showed that this geophysical tool is able to detect rock contacts more efficiently than it does broken fractures, crush rock or breccias. Furthermore, the method is not effective for the detection of unbroken fractures, sealed fracture networks, alteration and ductile structures. A careful assessment of the geological character under consideration needs to be made before any conclusions are drawn from these data that concern the orientation of a deformation zone.

The geological mapping of the boreholes and the geophysical and radar logging programmes generate primary sub-surface data that bear on the geological features; rock type, rock alteration, ductile deformation and brittle deformation. Ninety data reports have been produced (see chapter 2 and Table 1 in Appendix 3). These programmes have provided the input to the single-hole interpretations.

Single-hole interpretation – rock units and possible deformation zones

The single-hole interpretation of a borehole provides an integrated synthesis of the geological and geophysical information from the borehole. The results of this synthesis are presented in nineteen data reports, all produced by the same working team. A description of the procedures adopted during the various stages of the single-hole interpretation work is provided in section 3.3 in /Stephens et al. 2007/.

During the first stage of the single-hole interpretation, rock units and possible deformation zones in each borehole were identified and described. Furthermore, the interpretation of each geological feature was assigned a level of confidence. Key data, which are predominantly geological in character, and the results of the single-hole interpretation have been presented in the form of WellCad diagrams for each of the twenty-one cored boreholes addressed in stage 2.2 (Appendix 3 in /Stephens et al. 2007/) and for the remaining four cored boreholes in /Stephens et al. 2008/. One example is presented in Figure 5-3**.** The second stage of the single-hole interpretation work has involved a more detailed description of the characteristics of the possible deformation zones that were recognised with high confidence. Adjustments of boundaries to rock units and possible deformation zones during the modelling work, as well as the identification of possible minor zones in connection with a data reappraisal at a higher level of resolution are both documented in Table 3-2 in /Stephens et al. 2007/.

Rock units (RU) have been defined primarily on the basis of the composition, grain size and the inferred relative age of the dominant rock type, i.e. in the same manner as that used for the surface data. In some cases, rock units have been defined with the help of, for example, the frequency of open and partly open fractures outside possible deformation zones, the degree of ductile deformation or the occurrence of the alteration referred to as albitization (see section 5.2.3). Rock units extend over the total length in each borehole and, for this reason, include the borehole intervals where possible deformation zones have been recognised.

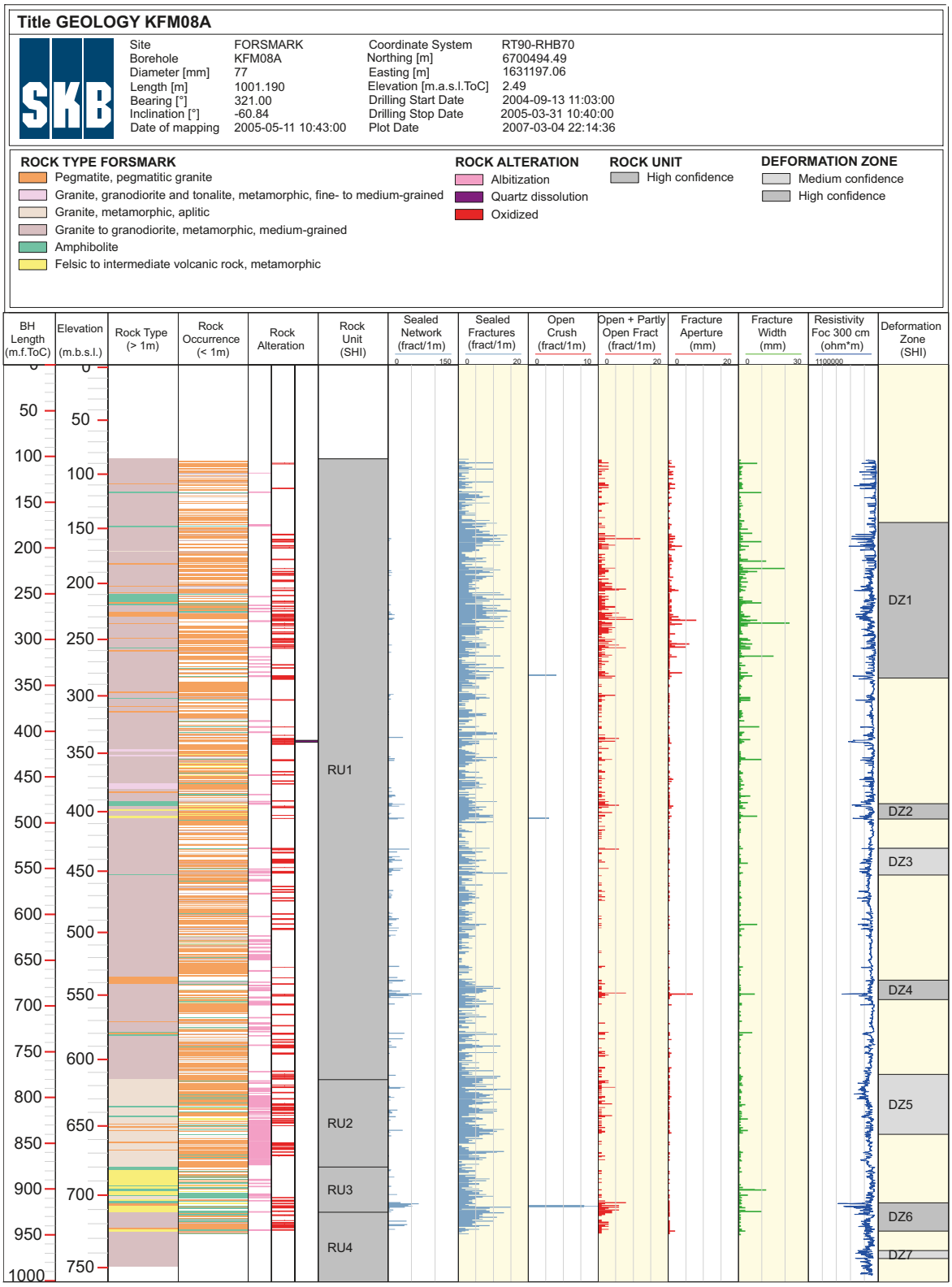

Figure 5-3. *WellCad diagram for the cored borehole KFM08A, showing a suite of key base geological and geophysical data that have been used to identify rock units and possible deformation zones in the single-hole interpretation of boreholes (see also /Stephens et al. 2007/).*

Fifteen cored boreholes intersect, along their entire length, the bedrock that is typical of that mapped inside the tectonic lens at the surface (Figure 5-2). Furthermore, the long boreholes KFM01A, KFM02A and KFM03A confirm that the rock unit dominated by medium-grained metagranite (101057) at the surface (Figure 5-2) continues to at least 1,000 m depth. Four boreholes (KFM06A, KFM06C, KFM08C and KFM08D) in the north-eastern part of the target volume (Figure 5-2) contain significant proportions of metagranite that is also affected by the alteration referred to as albitization (101057_104 or 101058_104). The upper part of several boreholes inside the target volume contains an increased frequency of fractures with conspicuous apertures (Figure 5-4a), even though these rock units are situated predominantly outside possible deformation zones.

Five cored boreholes (KFM04A, KFM06C, KFM07A, KFM08A and KFM09A) provide constraints on the continuation at depth of the rock units that are marginal to the metagranite inside the target volume (Figure 5-2). For example, the fine-grained metagranite and metavolcanic rocks that occur at the surface between the nuclear power plant and SFR are encountered at c. 615−710 m depth along borehole KFM08A (Figure 5-3). Two boreholes (KFM11A and KFM12A) also confirm how rock units that were recognised during the geological mapping outside the tectonic lens can be followed a considerable distance at depth as steeply dipping, geological entities.

The possible deformation zones (DZ) identified inside the target volume are solely brittle in character, i.e. they are possible fracture zones. These zones have been defined in the single-hole interpretation work primarily with the help of the geological and geophysical data sets fracture frequency, rock alteration and focused resistivity. Other features, which have assisted in their identification, include the occurrence of low radar amplitude anomalies in the borehole radar data, low magnetic susceptibility and the occurrence of caliper anomalies.

Sealed fractures and sealed fracture networks, the presence of well-defined steeply and gently dipping fracture sets, and an alteration that involved red-staining of fracture minerals or fracture walls dominate the possible fracture zones inside the target volume (see, for example, Figure 5-4b). Relative to the bedrock outside possible deformation zones, open and partly open fractures also increase in occurrence along these zones (see, for example, Figure 5-3). By contrast, possible deformation zones in the four cored boreholes KFM02A, KFM02B, KFM03A and KFM03B, to the south-east of the target volume (Figure 5-2), contain a conspicuous occurrence of open and partly open fractures that dip gently. Brittle deformation and fracture mineralogy along cored boreholes are addressed in more detail in section 5.2.5, and the character and kinematics of deformation zones are presented in section 5.2.6.

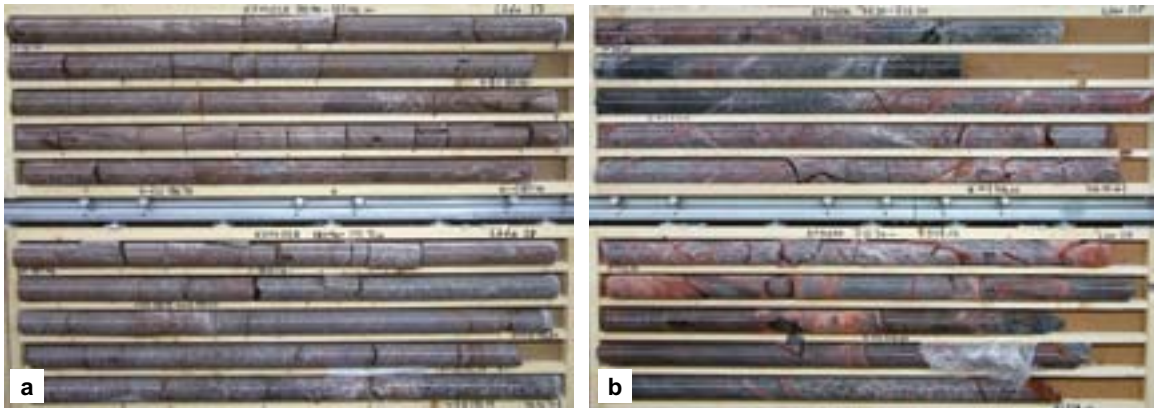

Figure 5-4. *a) High frequency of sub-horizontal to gently dipping fractures and some hematite staining in the borehole interval c. 182−193 m along RU1 in KFM01A. The fractures intersect this sub-vertical borehole at a high angle. Virtually all fractures are interpreted as open. This section lies outside a possible deformation zone. b) Metagranite (101057) and, in the lower drill core box, fine- to medium-grained metagranitoid (101051) affected by fracture networks sealed with laumontite and calcite in the borehole interval c. 711−721 m along part of DZ3 in KFM05A (modelled zone ENE0401A). Several fractures along this borehole interval actually opened up during the drilling but are interpreted as sealed structures.*

5.2.3 Rock types − properties, alteration, volumetric proportions and thickness of the subordinate rock amphibolite

Properties

Modal, whole-rock geochemical and petrophysical analyses of samples of different rock types, from both the surface and from boreholes, have been acquired. Parameters bearing on the petrophysical properties of each rock type include density (kg/m^3), porosity (%), magnetic susceptibility (SI units), electrical resistivity in fresh water (ohm m), as well as uranium content (ppm) and natural exposure rate (microR/h = microrad/hour where 1R = 0.01 Gray, i.e. 0.01 Gy), both of which are calculated from gamma ray spectrometry data. During the initial site investigation, these properties were established on the basis of the analysis of rocks in the regional model volume /SKB 2005a, p. 134−148/. In model stage 2.2, a revision of the mineral composition and petrophysical properties of the rock types in the local model volume was carried out /Stephens et al. 2007, p. 45−52/. This analysis not only made use of new data that had emerged after model version 1.2, but also focused attention on analytical data from the local model volume. Key results of this upgrading work for the local model volume are summarised below.

The classification of rock types based on an optical inspection during the mapping, both at the surface and along boreholes, is in good agreement with the compositions determined from the modal analyses and from the silicate density values (Table 5-2). An important implication of this observation is that silicate density measurements in the geophysical logs can provide a continuous assessment of at least the composition of the bedrock along boreholes.

Both surface and borehole samples of analysed intrusive rocks (Groups B, C and D, see Table 5-1) show the same distinctive gabbro−diorite−quartz diorite−granitoid igneous compositional trend (Figure 5-5). Quartz-poor, monzonitic and monzodioritic rocks are absent. This feature illustrates that the character of the rocks at the surface is a good guide to the character of the rocks in the sub-surface realm. The content of quartz in the metagranite (SKB code 101057), which strongly dominates inside the local model volume, ranges between 24.2 and 46.4%, with a mean value of 36.3% and a standard deviation of 5.8% (Table 5-2). The silicate density of this rock type, as estimated from samples inside the local model volume, ranges between 2,640 and 2,695 kg/m^3, with a mean value of 2,656 kg/m^3 and a standard deviation of 12 kg/m^3 (Table 5-2). The quartz-rich character of the bedrock has particularly important consequences for its thermal and mechanical properties (see chapters 6 and 7, respectively).

Table 5-2. Quartz content (%), silicate density (kg/m^3), uranium content (ppm) and natural exposure rate (microR/h) for the different rock types in the local model volume. The quartz content has been calculated from modal analyses, the density is based on laboratory measurements, and the uranium content and natural exposure rate are based on *in situ,* gamma-ray spectrometry measurements. Data from both surface and borehole samples are included. The code classification for each rock type is based on that assigned during the surface or borehole mapping. N = Number of analyses.

Code (SKB)	Age group, composition and grain size	Quartz content (%)		Silicate density (kg/m^3)		Uranium content (ppm)		Natural exposure rate (microR/h)	
		Range	Mean/StD	Range	Mean/StD	Range	Mean/StD	Range	Mean/StD
101057	Group B granite (to granodiorite), metamorphic, medium-grained	24.2−46.4 (N = 25)	36.3/5.8	2,640−2,695 (N = 31)	2,656/12	2.2−6.5 (N = 24)	4.7/1.2	10.0−15.0 (N = 24)	12.6/1.2
101058	Group B granite, metamorphic, aplitic	30.8−44.4 (N = 6)	37.4/4.9	2,620−2,649 (N = 6)	2,639/12	2.9−7.6 (N = 7)	5.4/1.6	10.8−18.9 (N = 7)	13.9/2.8
101057_ 101058_104	Group B granite, albitized, metamorphic	34.4−50.0 (N = 9)	40.2/6.4	2,633−2,722 (N = 13)	2,655/23	2.4−9.0 (N = 9)	5.2/2.4	6.3−12.2 (N = 9)	9.8/1.8
101061	Group D pegmatitic granite, pegmatite	29.2−38.1 (N = 5)	34.0/3.7	2,640−2,695 (N = 8)	2,656/12	1.1−61.7 (N = 29)	13.7/12.6	9.9−54.3 (N = 29)	20.9/8.8
102017	Group B amphibolite	0−6.4 (N = 3)	2.6/2.9	2,886−3,083 (N = 10)	2,963/75	0.2−2.4 (N = 6)	1.4/0.8	2.1−5.5 (N = 6)	3.5/1.2
101051	Group C granodiorite to tonalite, metamorphic, fine- to medium-grained	19.2−35.4 (N = 17)	28.4/4.1	2,642−2,713 (N = 9)	2,688/28	2.0−7.5 (N = 10)	4.6/1.8	6.0−22.8 (N = 10)	10.9/5.0
111058	Group D granite, fine- to medium-grained	25.4−42.8 (N = 5)	32.4/6.4	2,627−2,645 (N = 3)	2,634/10	3.4−14.9 (N = 6)	8.3/3.8	12.7−22.9 (N = 6)	19.0/3.6

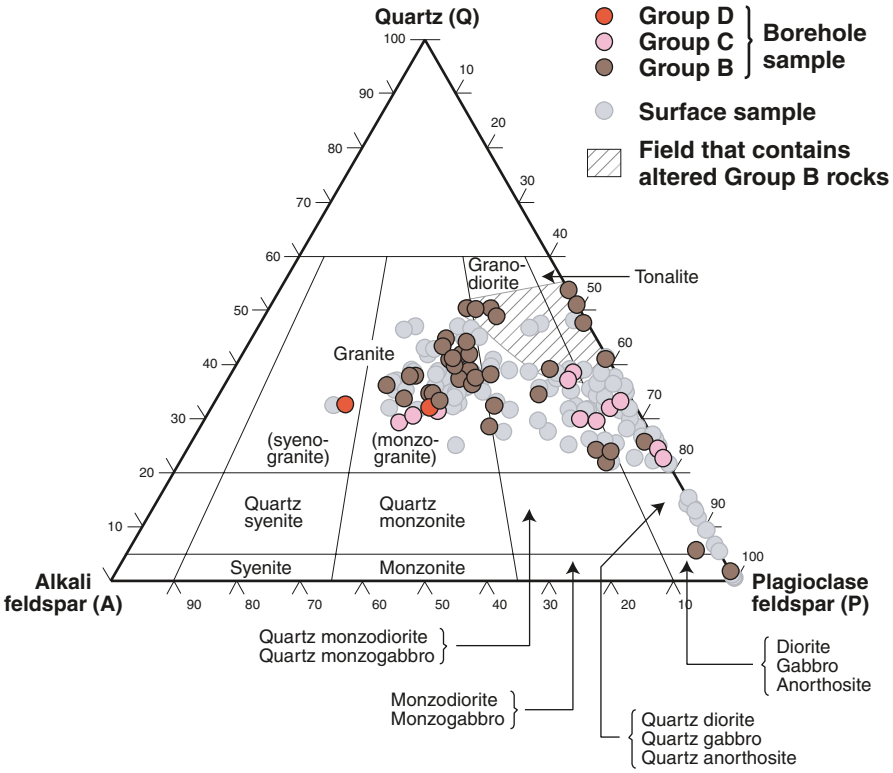

Figure 5-5. *QAP (F = 0) modal classification of all the analysed intrusive rock samples at the Forsmark site (Groups B, C and D). The classification is based on /Streckeisen 1976/. Groups B, C and D are defined in Table 5-1. Nearly 70% of the borehole samples shown on this diagram come from the local model volume. By contrast, there is no such focus for the surface samples; over 75% of these samples lie outside the local model volume. Notwithstanding this discrepancy, the trends are identical in both sample sets.*

Anomalously high uranium contents and natural exposure rates are restricted to the Group D rocks (Table 5-2), i.e. pegmatitic granite and pegmatite (101061) and fine- to medium granite (111058). This observation supports the correlation between these rock types and an increased natural gamma radiation that has been observed in the integrated single-hole interpretation work. These observations need to be considered when the source of anomalies in the uranium content of fracture coatings and groundwater are assessed. However, Cambrian to Lower Ordovician oil shale, which covered the Precambrian crystalline rocks at Forsmark during the earlier part of the Phanerozoic (see section 3.1), and which is known to be uranium-rich where preserved in fault-controlled outliers in southern Sweden /Andersson et al. 1985/, is also a potential ultimate source of uranium. It should be noted that the natural exposure rate in pegmatitic granite and pegmatite (101061) varies much less than the uranium content because of the contribution of potassium and thorium to the natural exposure rate.

Alteration

The type and degree of bedrock alteration, within and outside possible deformation zones, were presented on a borehole by borehole basis in Appendix 7 in /Stephens et al. 2007/. The red-staining of fracture minerals or the walls to fractures (Figure 5-6a) is by far the most abundant type of alteration at Forsmark, and is mapped and referred to as oxidation. The major mineralogical changes in such altered rock are a fine dissemination of hematite inside and along boundaries of plagioclase grains, an almost complete saussuritisation of plagioclase and a chloritisation of biotite /Sandström and Tullborg 2006/. However, the large-scale geochemical redistribution, including the degree of oxidation, is limited /Sandström and Tullborg 2006/. An analysis of its spatial occurrence along cored boreholes demonstrates that it is strongly associated with hydrothermal fluid movement along fracture zones and occurs independently of depth /Stephens et al. 2007/. It has been inferred that this type of alteration is an ancient geological feature and is not related to near-surface processes (see also section 5.2.5).

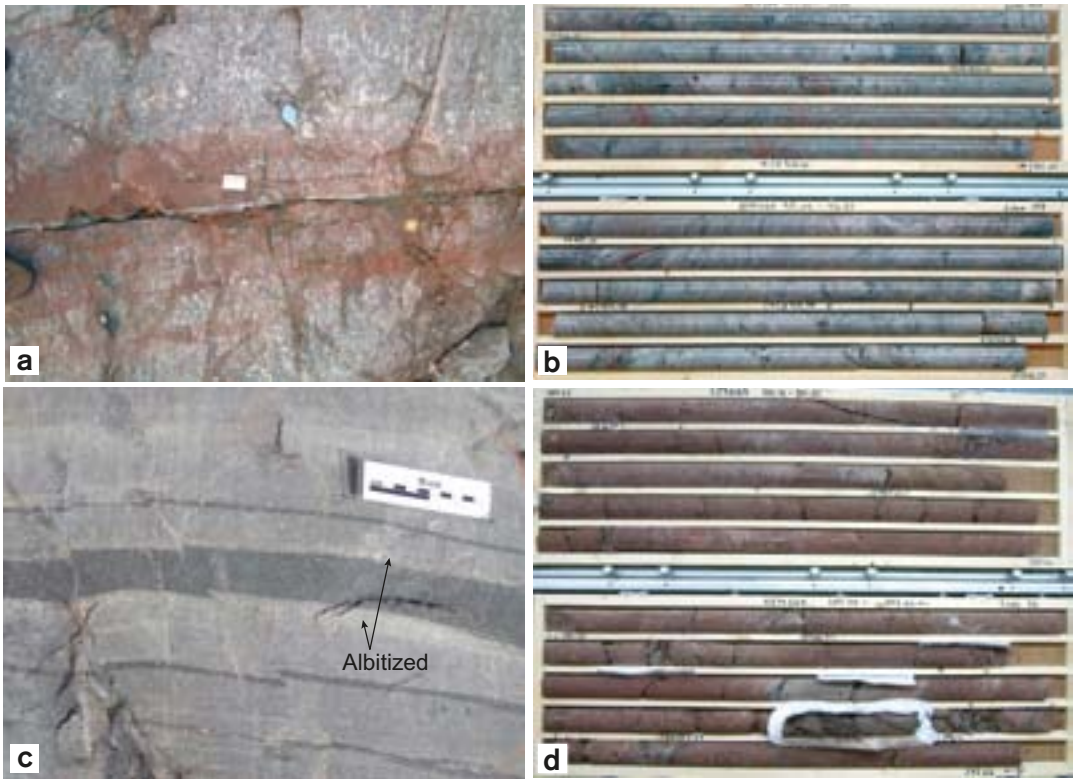

Figure 5-6. *Principal types of hydrothermal alteration at Forsmark. a) Fine dissemination of hematite and red staining in the altered wall rock adjacent to a fracture filled with quartz at surface excavation AFM001243. b) Albitized and metamorphosed granite in borehole KFM06A in the interval c. 906–917 m. c) Albitized and metamorphosed granite along the contact to an amphibolite dyke in a tectonically banded sequence at Klubbudden (see Figure 5-2). d) Strongly altered and vuggy metagranite in borehole KFM02A in the interval c. 282–293 m. The incoherent section (in plastic casing) is a strongly altered amphibolite that has been modified to a rock composed of chlorite, albite, hematite, Ti-oxide and quartz.*

In particularly the north-eastern part of the target volume, the Group B granitic rocks are affected by an alteration that has been mapped and referred to as albitization. On a mesoscopic scale, this alteration is recognised by a whitening of the feldspar in the granitic rocks (Figure 5-6b). Compared with the unaltered equivalents, it is characterised by a deficiency of K-feldspar relative to plagioclase and an increased content of quartz (Figure 5-5 and Table 5-2). Plagioclase is generally more albite-rich than in the unaltered equivalent, but is still not pure albite /Petersson et al. 2005/. The natural exposure rate is lower in these altered granitic rocks relative to that in the fresh equivalents (Table 5-2). This reduction is related to a reduced content of potassium, which is coupled to the removal of K-feldspar during alteration. Since the alteration shows no simple relationship to fracture zones, is absent in some of the younger rocks and occurs as contact rims adjacent to amphibolite (Figure 5-6c), it is inferred to be a syn-magmatic or syn-metamorphic feature, triggered by the heat supply provided by the younger amphibolites and even Group C metagranitoids /Stephens et al. 2007/.

Vuggy rock, which formed by the selective dissolution of quartz, corresponds to the alteration more generally referred to in the literature as episyenitisation /Möller et al. 2003/. In the alteration zones, the quartz dissolution, often combined with strong oxidation, affected all rock types indiscriminately (Figure 5-6d), but the texture of the host rock was maintained. Individual occurrences are typically a few metres in borehole length, although one occurrence along borehole KFM02A is approximately 50 m /Möller et al. 2003/. Virtually all occurrences occur inside or immediately adjacent to fracture zones /Stephens et al. 2007/. The conspicuous occurrence in KFM02A has been modelled /Stephens et al. 2007/ as a narrow, steeply inclined alteration pipe that links two gently dipping fracture zones (zones ZFMA2 and ZFMA3). It is inferred that this alteration took place after the rock mass had entered the brittle regime, i.e. after 1.8−1.7 Ga (see section 3.1), but under the influence of hot hydrothermal fluids at temperatures corresponding to greenschist facies conditions. It gave rise to significant changes in the physical properties of the host rock, including decreased density, porosity and resistivity.

Volumetric proportions

Quantitative estimates (volume %) of the proportions of different rock types from close to the surface down, in some cases, to c. 1,000 m depth have been calculated on a borehole by borehole basis and presented in the form of histograms and summary tables in successive model versions and stages /SKB 2005a, 2006a, Appendix 4 in Stephens et al. 2007/. Only the data from cored boreholes, which have a varied bearing and inclination, have been used. However, no consideration of the orientation of rock contacts and, thereby, the true thickness of rock intersections has been carried out in this analysis.

On the basis of the pre-conditions that the borehole is greater than 200 m in length and that it is situated entirely in both the local model volume and the Forsmark tectonic lens, estimates of the proportions of different rock types have been determined for the volume that has been selected as a potential repository. Metagranite (101057 or 101058) with a range between 68 and 83%, a mean value of 75% and a standard deviation of 5%, dominates inside this volume (Table 5-3). Along three of these cored boreholes (KFM06A, KFM08C and KFM08D) as well as borehole KFM06C, which are all in the north-eastern part of the target volume, these granitic rocks are affected, in part, by the type of alteration referred to as albitization (see above). The volumetric proportions of the subordinate rock types in this volume are also provided in Table 5-3.

Thickness of amphibolite

Although the subordinate rock amphibolite is clearly affected by ductile deformation and is, by definition, metamorphic in character, this rock is inferred to have intruded originally as dykes. Amphibolite occurs as narrow, dyke-like tabular bodies and irregular inclusions that are elongate in the direction of the mineral stretching lineation (see also section 5.2.4). Due to the low content or absence of quartz in this rock type, it requires special treatment in the thermal modelling work (see chapter 6).

On the basis of the borehole length and the orientation of the contacts of amphibolites in twenty-one cored boreholes, estimates of true thickness have been calculated (Appendix 5 in /Stephens et al. 2007/). Although some bodies are more than a few metres in thickness and, locally (e.g. KFM06C, KFM08D), are some tens of metres thick, most are inferred to be minor rock occurrences, i.e. thin geological entities. The thicker bodies in boreholes KFM06C and KFM08D occur in different parts of the fine-grained and partly albitized granitic rocks in the north-eastern part of the target volume. An amphibolite with similar thickness is also exposed at the ground surface in this area. Stochastic simulations of the subordinate rocks in the target volume, including amphibolite, are presented in chapter 6.

5.2.4 Ductile deformation

Character of ductile structures

The Forsmark site has been affected by penetrative ductile deformation, with a variable degree of intensity, that was followed by folding on different scales (see also section 3.1). This ductile strain developed at mid-crustal depths and under high-temperature (> 500–550°C), so-called amphibolite-

Table 5-3. Volumetric proportions of different rock types based on data from cored boreholes longer than 200 m in the volume selected as a location for a potential repository (boreholes KFM01A, KFM01B, KFM01C, KFM01D, KFM05A, KFM06A, KFM07B, KFM07C, KFM08C, KFM08D, KFM09B and KFM10A). Minor amounts (< 1%) of other rock types are also present.

Code (SKB)	Composition and grain size	Range (%)	Mean (%)	Standard deviation (%)
101057/ 101058	Granite (to granodiorite), metamorphic. Medium-grained or aplitic, in part albitized.	68–83	75	5
101061	Pegmatitic granite, pegmatite.	7–23	13	5
102017/ 101033	Amphibolite and other mafic rocks.	3–7	5	1
101051	Granodiorite to tonalite, metamorphic, fine- to medium-grained.	1–11	4	3
111058	Granite, fine- to medium-grained.	0–5	1	1

facies metamorphic conditions. Later ductile strain (section 3.1) occurred predominantly along more discrete deformation zones in the high-strain belts around the tectonic lenses.

Structures measured during the bedrock mapping work at the surface (Figure 5-1) include a planar grain-shape fabric (tectonic foliation), a tectonic banding, a linear grain-shape fabric, which is inferred to correspond to the direction of stretching (mineral stretching lineation), and minor fold axes. Breakdown and analysis of these data in the context of separate subareas were completed in model version 1.2 /SKB 2005a/. Laboratory measurements of the anisotropy of magnetic susceptibility (AMS) from surface samples were also evaluated in /SKB 2005a/. AMS data provide an independent assessment of the orientation of ductile structures in the bedrock. They also provide complementary information bearing on the degree and character of the ductile strain.

Only planar structures, including tectonic foliation and minor ductile and ductile-brittle shear zones, have been measured during the geological mapping of boreholes. The orientation data for these ductile structures as well as the contacts of mafic rock units (predominantly amphibolite) have been presented on a systematic, borehole by borehole basis in model stage 2.2 (Appendix 6 in /Stephens et al. 2007/).

Deformation inside the Forsmark tectonic lens

Folding inside the Forsmark tectonic lens is apparent at different scales. On a larger scale, the boundaries between the dominant metagranite and other rock units are folded (Figure 5-2) and it is inferred that the lens is affected by a major fold structure. These rock units include a metatonalite (Figure 5-7a) in the south-eastern part of the lens and a tectonically banded, heterogeneous unit with metagranite, felsic to intermediate metavolcanic rock and amphibolite, affected by high ductile strain (Figure 5-7b) and intruded by pegmatite, in the north-westernmost part, between the nuclear power plant and SFR.

Figure 5-7. *Character of the bedrock inside the Forsmark tectonic lens. a) Lineated and weakly foliated medium-grained metatonalite (101054), intruded by finer-grained metatonalite (101051), which, in turn, is intruded by pegmatite (101061). This rock unit forms a folded mega-xenolith inside the metagranite in the tectonic lens. b) Tectonically banded, foliated and lineated meta-igneous rocks, with intra-folial fold structures, in the coastal area between the nuclear power plant and SFR. The strongly deformed rocks in this outcrop are folded around the major synform inside the lens. c) Folded tectonic foliation with minor shear zone development in metagranite (101057) close to drill site 6. The tectonic foliation is discordant to a Group D granite dyke (111058). d) Folded tectonic foliation and rock contact between metagranite (101057) and amphibolite (102017) south-west of drill site 5, in the marginal part of the tectonic lens.*

On a smaller scale, folding of the penetrative tectonic foliation (Figure 5-7c) with an inferred fold axis that plunges moderately to the south-east is indicated from the outcrop data (Figure 5-8a). Furthermore, data from individual boreholes that intersect the bedrock inside the tectonic lens confirm the presence of large-scale folding (Figure 5-9a, b). The ductile structures along the fold hinge are also more steeply inclined in the north-western (Figure 5-9a, b) compared with the south-eastern (Figure 5-9a, c) part of the lens (see also /Stephens and Forssberg 2006/). Both the mineral stretching lineation and the measured fold axes (Figure 5-8a) plunge to the south-east. It is apparent that fold axes are sub-parallel to the stretching direction in the bedrock.

The smaller-scale features indicate that the major folding is synformal in character in the north-western part of the lens, where the target area is situated, and antiformal in character further to the south-east, i.e. the fold is tube-like in character (see also section 5.5). In general, the mineral stretching lineation is more prominent than the tectonic foliation (LS-tectonites). Outcrop observations indicate that the amphibolites that intrude the metagranite are folded (Figure 5-7d). This is also apparent from the borehole data, where the amphibolites show different orientation distribution patterns close to the hinge (Figure 5-9a, b), along the hinge (Figure 5-9a, c) and on the south-western limb (Figure 5-9a, d) of the major fold structure inside the tectonic lens. It is clear that the amphibolites consistently follow the orientation of the folded planar ductile structures in the bedrock /Stephens et al. 2007/.

The AMS data measured in the laboratory (Figure 5-8b) and the ductile structural data measured at outcrop (Figure 5-8a) are in excellent agreement with each other /SKB 2005a/. The AMS data confirm both the conclusions drawn concerning the orientation of the major folding inside the tectonic lens and its more constrictive ductile strain. They also indicate a generally lower degree of ductile strain inside the tectonic lens compared with that outside it to the south-west.

Deformation along the margin to and outside the Forsmark tectonic lens

As the margins of the Forsmark tectonic lens are approached, the tectonic foliation in the metagranite increases in intensity. Minor ductile shear zones along the tectonic foliation in the south-western limb of the major synform show dextral strike-slip deformation /Nordgulen and Saintot 2006/. Outside the tectonic lens, strongly deformed rocks are present, both to the south-west (Figure 5-10a) and to the north-east (Figure 5-10b–d) of the lens on both flanks of the major synform. The rocks are foliated, lineated and, in part, also heterogeneous and banded (SL- and BSL-tectonites). Even on the north-eastern limb of the major synform, a dextral strike-slip component of displacement along the high-strain fabric is present (Figure 5-10b). The intense tectonic banding is deformed by minor folds (Figure 5-10c) that are inferred to be parasitic and related to the major synform. Locally, eye-shaped, tubular folds are present (Figure 5-10d). The structural data from, for example, borehole KFM04A, which lies partly inside the highly strained rocks to the south-west of the tectonic lens and partly inside the marginal part of the lens, illustrate the consistent steep dips to the south-west at depth in this subarea (Figure 5-9a, d).

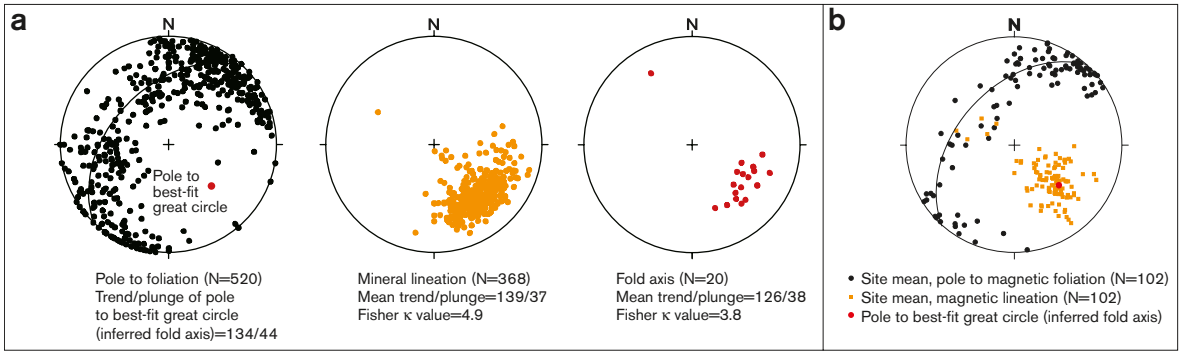

Figure 5-8. *a) Orientation of planar and linear ductile structures measured in the field inside the tectonic lens. b) Orientation of the mean values of magnetic foliation and magnetic lineation in field samples from Groups A and B. The majority of these AMS data come from the tectonic lens and the values are from laboratory measurements. All structures have been plotted on the lower hemisphere of an equal-area stereographic projection.*

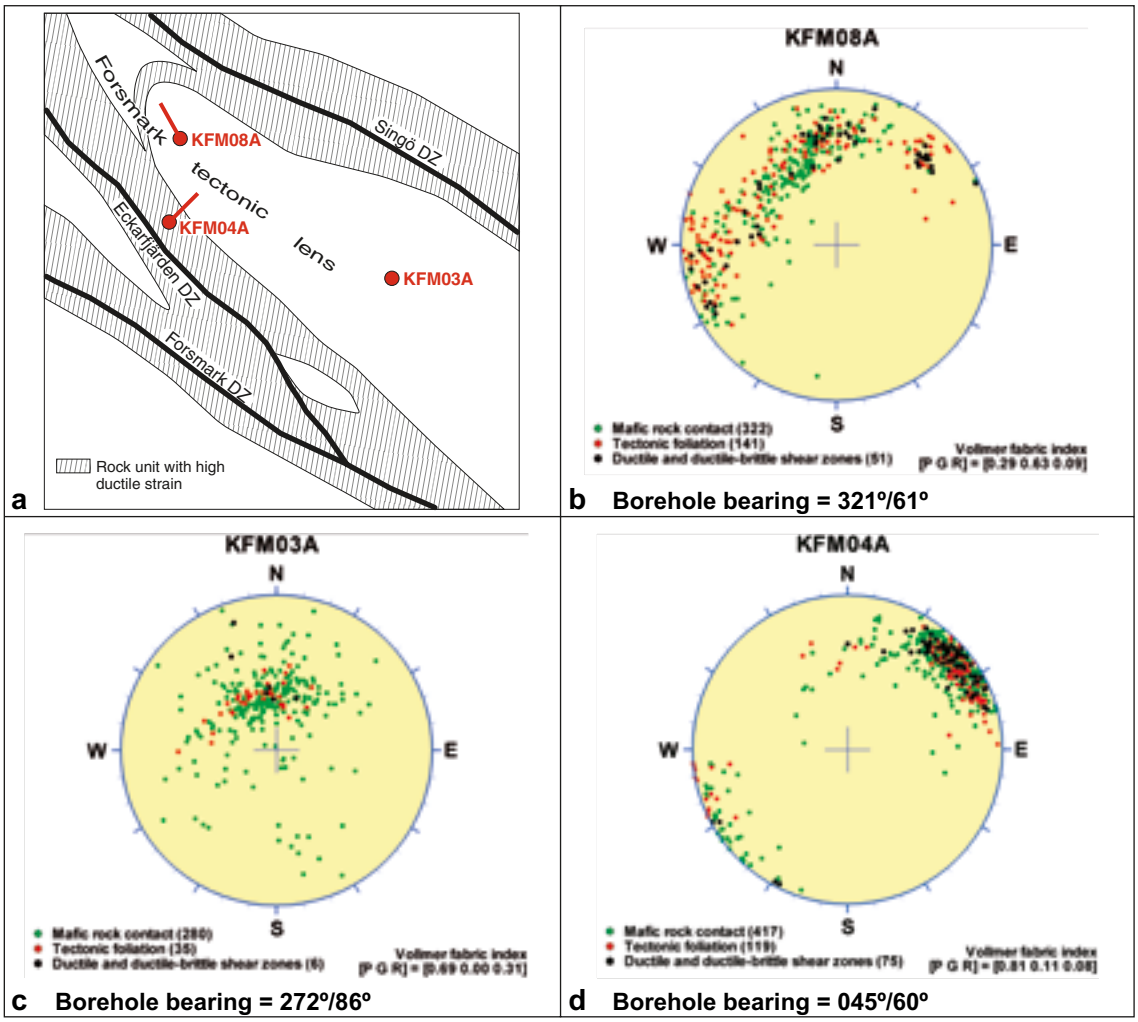

Figure 5-9. *Orientation of planar ductile structures and mafic rock contacts (mostly amphibolite) in selected cored boreholes. An estimation of the degree of point, girdle or random distribution pattern (Vollmer fabric index, PGR) in the raw data is provided for each borehole. The pole to each planar structure is plotted on the lower hemisphere of an equal-area stereographic projection. No Terzaghi correction has been applied. However, the orientation of each borehole is provided, in order to help judge the significance of this bias. (a) Location of boreholes in relation to the Forsmark tectonic lens. (b) Borehole KFM08A. (c) Borehole KFM03A. (d) Borehole KFM04A.*

Implications for modelling work

The evaluation of the ductile deformation has important implications for the modelling work. This concerns both the establishment of a conceptual model for rock domains (see section 5.4) as well as an understanding of the spatial distribution of different types of brittle structures. In particular, the ductile deformation has contributed to the development of a strong bedrock anisotropy that has steered the development of younger brittle deformation at the site (see section 5.5).

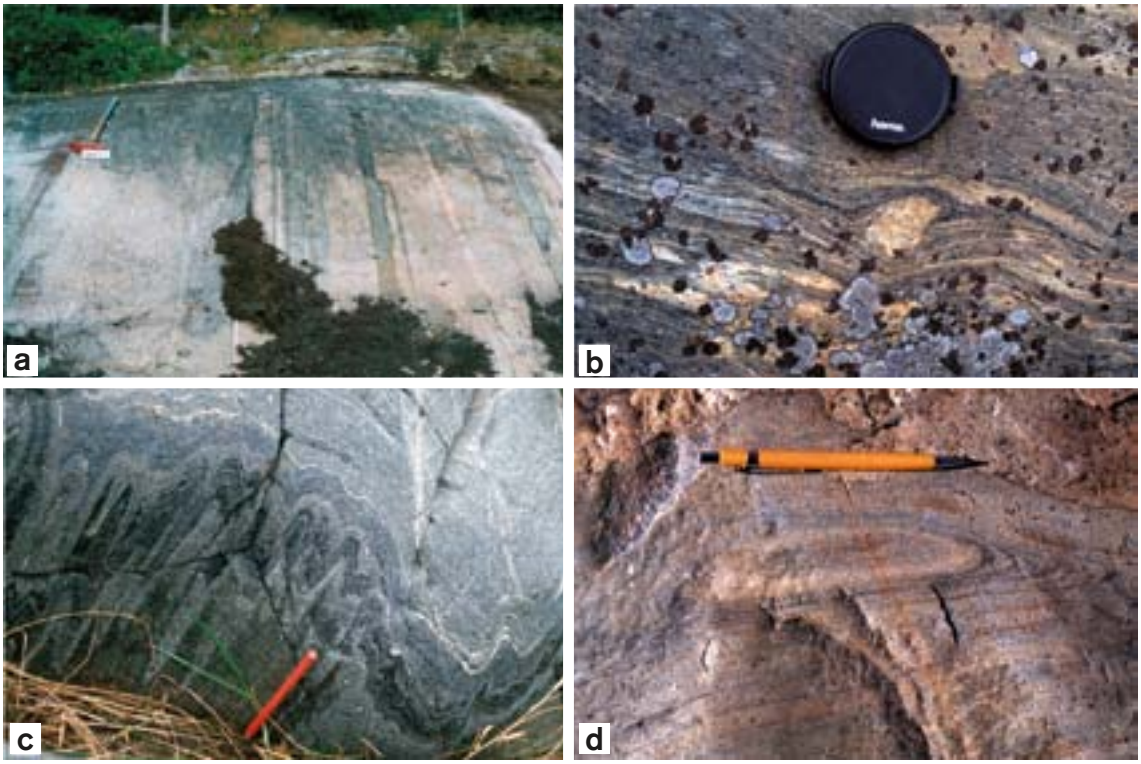

Figure 5-10. *Character of the bedrock outside the Forsmark tectonic lens. a) Tectonically banded, foliated and lineated meta-igneous rocks close to drill site 4, south-west of the major synform inside the lens. b) Winged porphyroclast (δ-type) in rocks affected by high ductile strain close to SFR, to the north-east of the major synform inside the lens. A component of dextral strike-slip displacement is inferred. The highly strained rocks at this locality (PFM001235) are also folded. c) Folding of the highly-strained rocks at PFM001235. Folds of this type in this outcrop are dominated by S-asymmetry and are parasitic to the major synform. d) Eye-shaped, tubular fold in outcrop close to SFR.*

5.2.5 Brittle deformation

Detailed mapping of fractures at the ground surface

The detailed mapping of fractures, in accordance with the SKB method description, has been completed at nine outcrops at the Forsmark site (Figure 5-11). The outcrops mapped include rock surfaces excavated for use as drill pads for boreholes (AFM000053, -000054, -001097 and -100201) or specifically for fracture mapping purposes (AFM001264), trenches excavated to investigate lineaments (AFM001243, -001244 and -001265) and one large natural exposure of the bedrock (AFM001098 at Klubbudden, see Figure 5-2). These outcrops are located both inside the candidate area (Forsmark tectonic lens) and along high-strain belts on both sides of the lens (Figure 5-11). Only fracture traces longer than 50 cm were recorded during the mapping work. Geological maps with fracture traces were presented in Appendix 8 in /Stephens et al. 2007/. The data have been used as primary input to the geological DFN orientation and size modelling work (/Fox et al. 2007/; see also section 5.6). Scan-line surveys were also completed on each outcrop, using two orthogonal scan lines along which fractures with trace lengths longer than 20 cm were measured. The data from these surveys were not used in the DFN work.

The detailed mapping of fractures described above was complemented during the bedrock mapping programme by orthogonal scan-line surveys along 44 smaller outcrops predominantly inside the tectonic lens (Figure 5-11) and across two lineaments in the north-eastern part of the lens (Figure 5-11). These surveys did not strictly follow the SKB method description for detailed fracture mapping. The complementary outcrop mapping involved an assessment of only the frequency, orientation and mineralogy of fractures longer than 100 cm in each outcrop. The lineament mapping only acquired data bearing on the frequency, orientation, width, aperture, mineralogy and sense of shear along fractures that are longer than 40 cm.

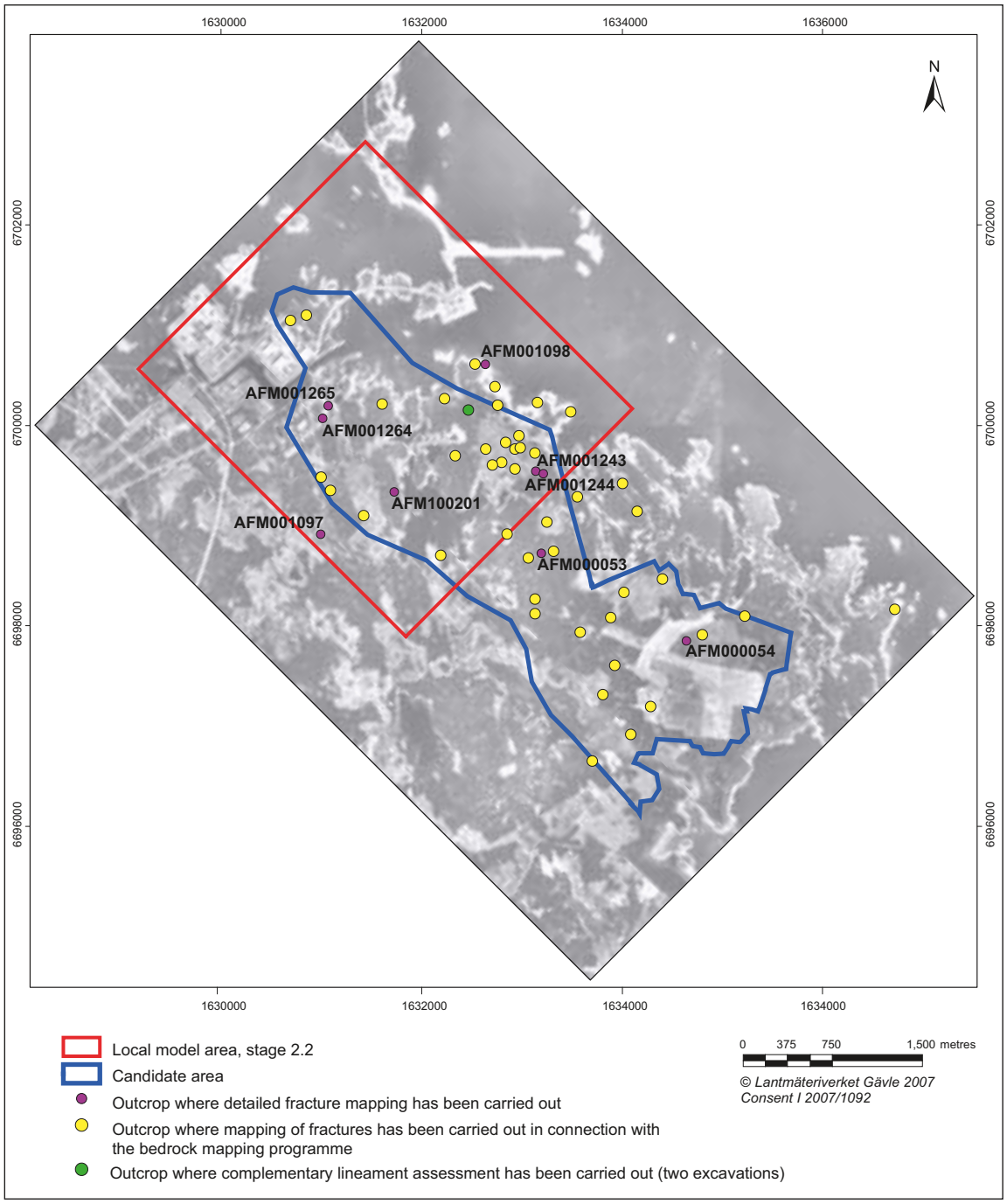

Figure 5-11. *Location of outcrops where detailed fracture mapping has been carried out. Data that have been acquired according to the SKB method description are presented in /Hermanson et al. 2003a, 2003b, 2004, Leijon (ed) 2005, Cronquist et al. 2005, Forssberg et al. 2007, Petersson et al. 2007a/. Complementary data from outcrops and across lineaments that do not strictly follow the SKB method description are presented and evaluated in /Stephens et al. 2003a, 2003b/ and /Petersson et al. 2007b/.*

The detailed mapping across lineaments /Cronquist et al. 2005, Petersson et al. 2007ab/ confirmed that magnetic minima at four of the five excavations correspond to fracture zones (/SKB 2006a, Petersson et al. 2007b/ and see also section 5.2.7). The lineament defined by magnetic minima at the fifth excavation (AFM001244) corresponds to a swarm of Group D granite and pegmatite dykes with low magnetic susceptibility /SKB 2006a/. Excavation work also revealed a minor fracture zone that dips steeply to the NW at drill site 4 (AFM001097). The data from the other outcrops are judged to be relevant for the characterisation of fractures at the ground surface in the parts of rock domains unaffected by deformation zones or swarms of Group D intrusions, i.e. the background fracturing.

Fracture orientation from cored borehole data

The orientations of fractures outside possible deformation zones, which were identified in the single-hole interpretation of boreholes during stage 2.2, have been compiled in /Stephens et al. 2007/. The modifications to the single-hole interpretations /Stephens et al. 2007, Table 3-2/ were taken into account in this work. Orientation data for sealed fractures, for open and partly open fractures, and for all fractures are shown for each borehole. No distinction was made in this analysis between fractures marked "visible in BIPS" and those marked "not visible in BIPS" (cf. geological DFN modelling work). Examples of orientation plots for four boreholes from the marginal and internal parts of the tectonic lens are shown in Figure 5-12. For purposes of simplicity in the text that follows, the strike of steeply dipping fracture sets is presented as a single direction (e.g. NE). The fractures in the different sets may dip in both directions (e.g. NW and SE) and can also be described as sub-vertical. Thus, the procedure does not strictly follow the right-hand-rule method (see also section 2.4 in /Stephens et al. 2007/).

The data outside possible deformation zones show similar patterns in the different boreholes. Two steeply dipping fracture sets that strike approximately NE and NW are visible in nearly all the boreholes (Figure 5-12). However, especially the strike of the fractures in these sets varies, not least in the NE set (see, for example, KFM05A and KFM06A in Figure 5-12). In addition to the dominant NE and NW sets, other potential fracture sets with variable intensities in different boreholes are visible. For example, a steeply dipping set with NNW strike is present in boreholes KFM06A and KFM07A (Figure 5-12). Furthermore, all boreholes intersect fractures that are gently dipping to sub-horizontal (Figure 5-12). The concentration of open and partly open fractures is significantly

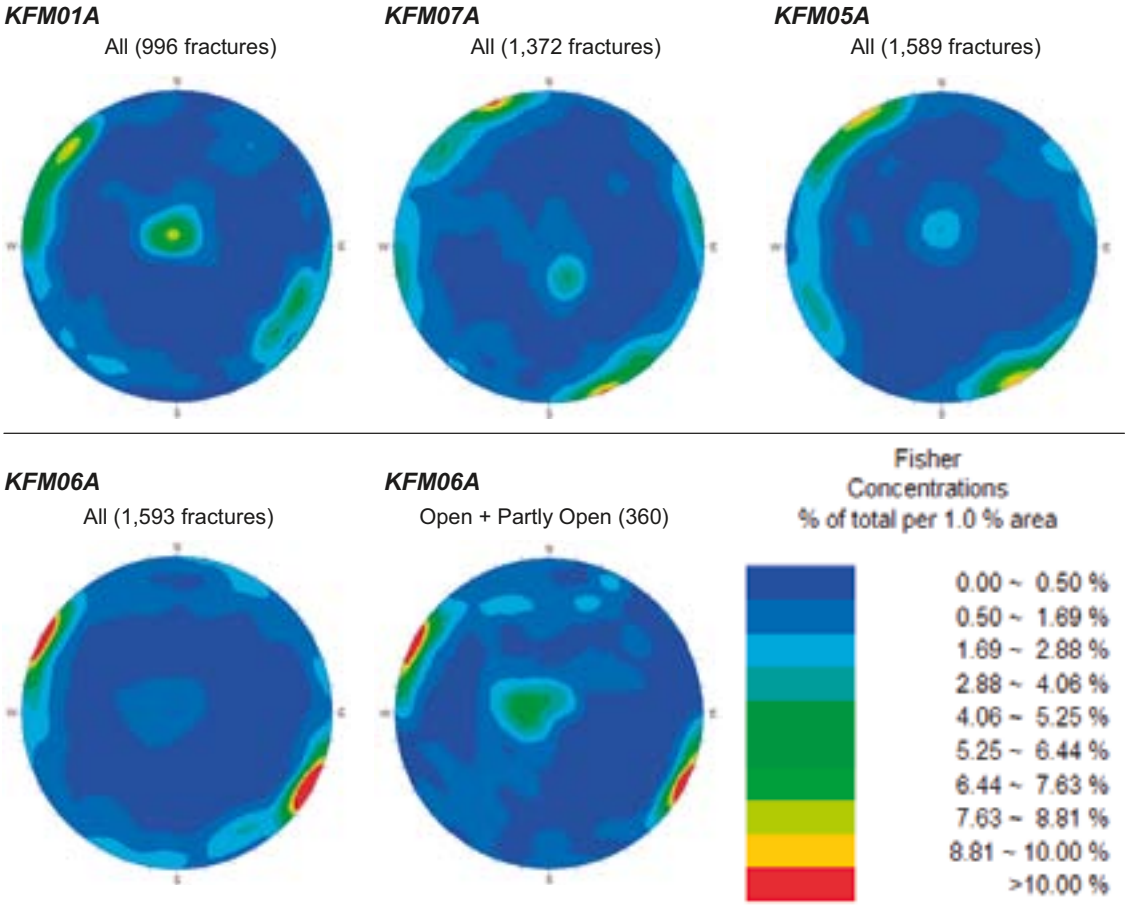

Figure 5-12. *Orientation of fractures in boreholes KFM01A, KFM07A, KFM05A, KFM06A (all fractures) and KFM06A (open/partly open fractures). The fractures have been plotted as poles to planes on the lower hemisphere of an equal-area stereographic projection. Fisher concentrations are shown as a percentage of the total number of poles per 1.0% of stereonet area. A Terzaghi correction has been applied to each stereonet.*

higher in this fracture set relative to that in the steeply dipping sets (see, for example, KFM06A in Figure 5-12). A compilation of the orientation of fractures inside different fracture domains as a prerequisite for the geological DFN modelling work is presented in section 5.6.1.

The orientations of fractures inside possible deformation zones have been presented in Appendix 9 in /Stephens et al. 2007/. Orientation data for sealed fractures, open fractures and partly open fractures are distinguished in each possible zone. All fractures that are not visible in BIPS were excluded from the analysis.

Steeply dipping fractures that strike WNW to NW, ENE to NNE and NNW as well as gently dipping to sub-horizontal fractures are conspicuous. Along some zones, there is also an indication that the steeply dipping fractures with ENE to NNE strike can be divided into two sub-sets /Stephens et al. 2007/. These features are strongly reminiscent of the orientation of fractures outside possible deformation zones (see above). A second characteristic feature is that more than one set of fractures occurs along many of the possible deformation zones. It is inferred that the different sets of fractures, in particular the steeply and gently dipping fractures, are genetically related and formed close in time during the geological history. Compilations of the orientations of fractures along the different sets of modelled deformation zones are presented in section 5.5.4.

Fracture frequency from cored borehole data

The fracture frequency statistics for each of the cored boreholes used in model stage 2.2, both for the whole length of a borehole and for the part that lies outside possible deformation zones, has been presented in /Stephens et al. 2007, Tables 3-11 and 3-12, respectively/. Apart from borehole KFM01C, the frequency of fractures per metre in the bedrock outside possible deformation zones ranges between 1.24 and 5.55. These values decrease somewhat, if borehole intervals that are situated between or very close to possible deformation zones and that are judged to have been affected by the brittle deformation along the zones /Olofsson et al. 2007/ are excluded. Borehole KFM01C, designed to investigate lineaments, is a notable anomaly and the entire length of this borehole has possibly been affected by the brittle deformation along the zones in this borehole. For this reason, the data from KFM01C were omitted from the geological DFN intensity modelling work /Fox et al. 2007/.

Moving average and cumulative frequency plots for each of the cored boreholes used in model stage 2.2, which show the mode of variation for different types of fractures with depth in each borehole, were presented in Appendix 10 in /Stephens et al. 2007/. This type of analysis is one of the tools that has been used in the single-hole interpretation work, as an aid in the identification of possible deformation zones (see section 5.2.2). Furthermore, it has had major implications for the identification of fracture domains at Forsmark (/Olofsson et al. 2007/ and section 5.6.1).

On the basis of analyses initially in /SKB 2005a/ and with the help of more borehole data in /Olofsson et al. 2007/, it has been inferred that the north-western and south-eastern parts of the candidate volume differ from each other, where it concerns the variation in the frequency of particularly open and partly open fractures down to approximately 1,000 m depth (Figure 5-13). Furthermore, inside the targeted, north-western part of the candidate volume, the boundary between bedrock with an anomalously high frequency of open and partly open fractures (upper part), and bedrock with a strong dominance of sealed fractures (lower part), does not occur at the same elevation in the boreholes. This boundary varies between c. 40 m (e.g. drill site 8) and c. 200 m (e.g. drill site 1) below sea level. Boreholes KFM01A and KFM03A provide type logs that distinguish the contrasting variations in fracture frequency with depth inside the candidate volume (Figure 5-13).

Fracture mineralogy from cored borehole data

Various aspects of the minerals that coat and fill fractures at Forsmark have been addressed in seven primary data reports and in two peer-reviewed publications /Sandström et al. 2006, Sandström and Tullborg 2007/. An overview report that integrates the results of this work has been presented in /Sandström et al. 2008/. Work that documents more quantitatively the amount of different minerals along fractures is in progress and will be presented in a separate, complementary document. The necessity of these data for the purposes of bedrock transport properties was recognised at a late stage during the site investigation programme.

KFM01A

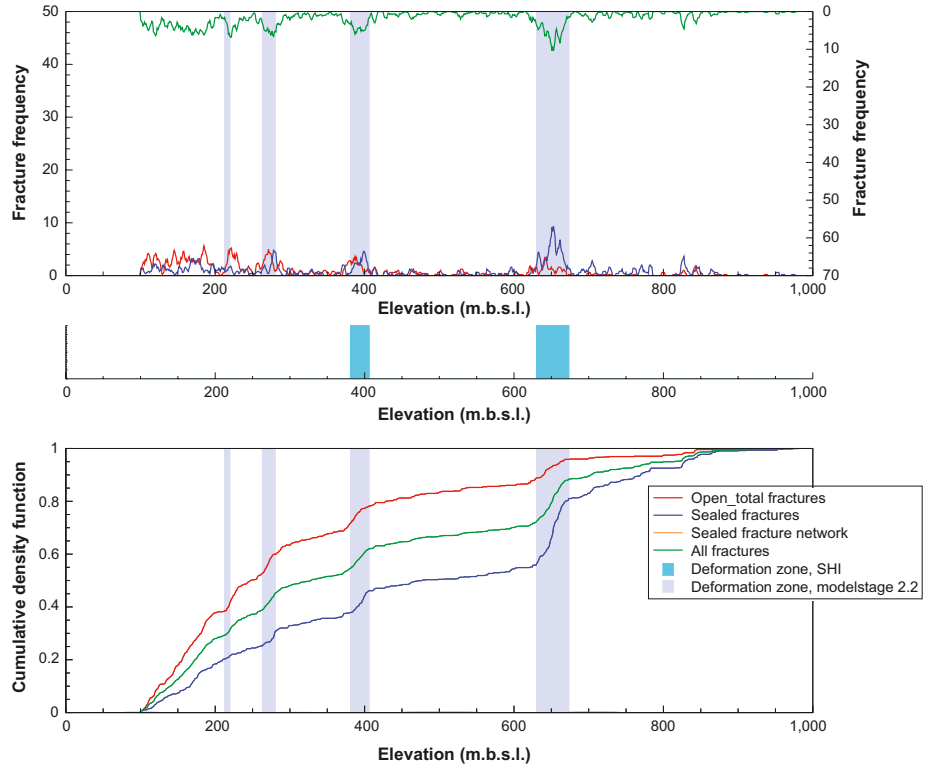

KFM03A

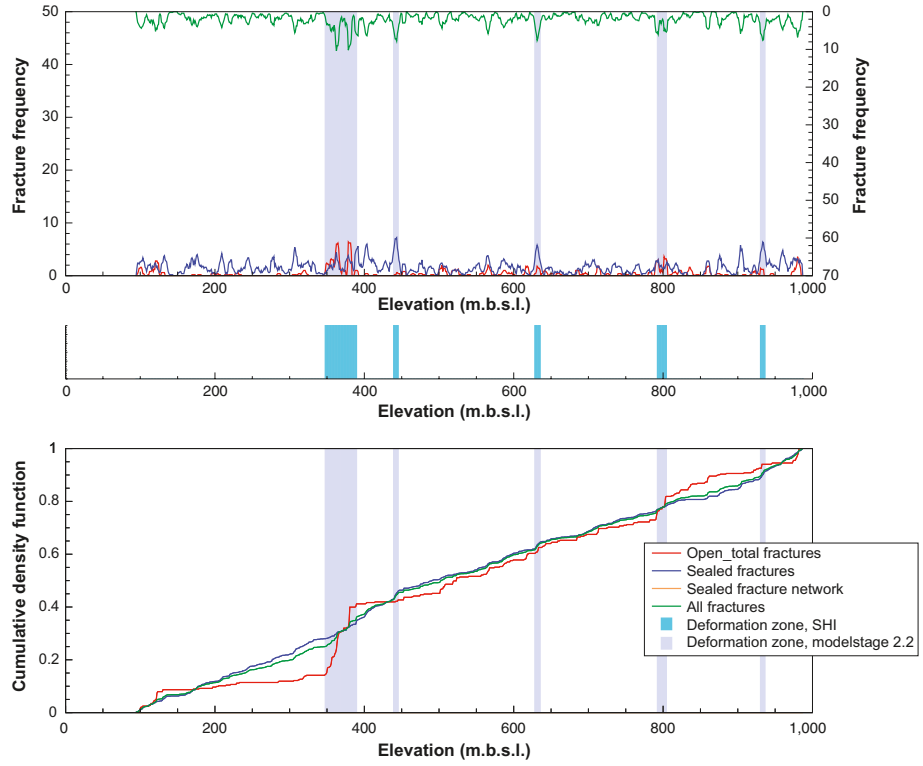

Figure 5-13. *Fracture frequency plots for the cored boreholes KFM01A and KFM03A. The upper diagram in each figure is a moving average plot with a 5 m window and 1 m steps, and the lower diagram is a cumulative frequency plot. The deformation zones included in model stage 2.2 are marked on both figures. Possible deformation zones, as defined in the single-hole interpretation (SHI), are presented, for comparison purposes, in the middle part of each figure. In KFM01A, approximately 40% of all the open and partly open fractures are concentrated in the upper 200 m, whereas, in KFM03A, less than 10% of all the open and partly open fractures occur above 200 m depth and approximately 60% above 600 m depth.*

Relative and absolute ages of fracture minerals

Different generations of fracture minerals have been recognised at Forsmark (Figure 5-14). The relative time relationships between these different generations as well as the data bearing on absolute age determinations have been evaluated and used in the establishment of the geological evolution of the site (/Söderbäck (ed) 2008/ and section 3.1).

An early period of precipitation of a high-temperature mineral assemblage, which includes epidote (Figure 5-14a), chlorite and quartz was followed by a period (or periods) of hydrothermal precipitation of different, lower temperature minerals, including adularia (older generation), hematite, prehnite, laumontite and calcite (Figure 5-14b, c). The fractures that bear epidote formed prior to the Sveconorwegian tectonothermal event, i.e. they formed prior to 1.1 Ga. The fractures that contain the older generation of adularia formed either during or prior to this event. A combination of these two possibilities is also viable.

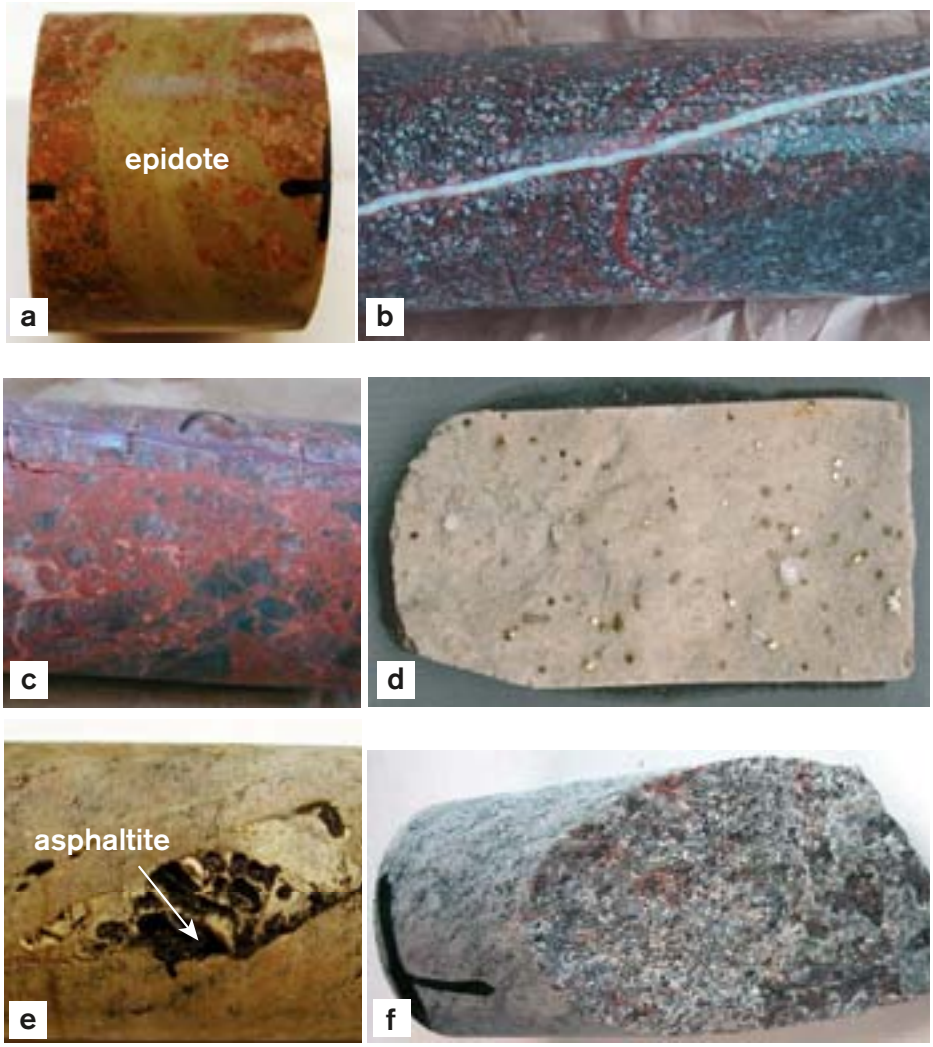

Figure 5-14. *Drill core photographs showing fracture minerals in the four different generations recognised at Forsmark. a) Generation 1. Epidote-bearing cataclasite (KFM06A, 268.77–268.82 m, /Sandström and Tullborg 2005/). b) Generation 2. Fracture filled by brick-red, hematite-stained adularia cut by a fracture filled with prehnite (KFM05A, 689.33–689.61 m, /Sandström and Tullborg 2005/). c) Generation 2. Laumontite-sealed breccia (KFM04A, 244.46–244.58 m, /Sandström and Tullborg 2005/. d) Generation 3. Calcite and pyrite crystals on top of a fracture surface coated with quartz (KFM01A, 267.0 m, /Sandström et al. 2004/). e) Generation 3. Asphaltite in voids in older, partly dissolved calcite along a steeply dipping fracture (KFM06A, 106.94–107.14 m, /Sandström and Tullborg 2005/). f) Generation 4. Open fracture with a thin coating of calcite. This generation of calcite often occurs together with clay minerals (KFM08B, 97.37–97.43 m, /Sandström and Tullborg 2006/).*

Precipitation of younger low-temperature minerals along fractures – including sulphides, oily asphaltite, clay minerals and calcite (Figure 5-14d, e, f) – occurred during Phanerozoic time. The asphaltite was derived from Cambrian to Lower Ordovician oil shale. Together with limestone and other clastic sedimentary rocks, this oil shale covered the crystalline bedrock at Forsmark during much of the Phanerozoic (/Söderbäck (ed) 2008/ and section 3.1). Furthermore, growth of adularia (younger generation) occurred during the Permian. The youngest generation of calcite occurs in hydraulically conductive fractures and zones. This mineral may have precipitated over a long period extending to the present. Fluids, which transported glacial sediment, also migrated downwards and filled new or reactivated fractures at Forsmark during the later part of the Quaternary /Carlsson 1979, Leijon (ed) 2005/.

Distribution of fracture minerals

The identification and significance of different fracture minerals along each possible zone in the single-hole interpretations have been addressed in /Stephens et al. 2007, section 3.6.5/. The number of occurrences of each mineral in each zone are shown in Appendix 11 in /Stephens et al. 2007/ and the orientation of fractures divided on the basis of fracture mineralogy are presented in Appendix 12 in /Stephens et al. 2007/. Identical analyses have also been completed for fracture minerals in fracture domains /Sandström et al. 2008/. The occurrences of fracture minerals along different sets of deformation zones have been addressed in /Stephens et al. 2007, sections 5.3.2 and 5.5/ and a summary is provided here in section 5.5.4. For comparison purposes, a summary of the occurrence and orientation of fracture minerals in fracture domains, based on /Sandström et al. 2008, section 6.1/, is presented in section 5.6.1.

The occurrence of similar minerals and wall-rock alteration along different fracture orientation sets within a single deformation zone provides support to the inference drawn earlier that the different sets are genetically related. Although, for example, laumontite is conspicuous along steeply dipping fractures that strike approximately NE (see also /SKB 2005a/), the older mineral epidote and the younger minerals pyrite and clay minerals are also present along fractures with this orientation. This observation suggests that fractures with this orientation have both an older history prior to the growth of laumontite and a younger history following the growth of this mineral. Thus, the analytical work provides strong evidence for the presence of different generations of minerals, which formed under different metamorphic conditions, along a single zone, i.e. zone reactivation occurred. It needs to be kept in mind that the temperature along the zones, with their hot hydrothermal fluids, can be higher than that in the surrounding bedrock.

The variation in the occurrence of different fracture minerals with depth was addressed in /Stephens et al. 2007, section 3.6.5/, while a more focused analysis of the variation of minerals along open fractures, in the upper 100 m of the bedrock, was presented in /Sandström et al. 2008, section 6.2/. In order to assess the variation of fracture minerals with depth, the frequency of occurrence of a particular mineral in a particular type of fracture, as well as the overall frequency of occurrence of this fracture type, has been documented for each 10 m vertical depth interval along a borehole /Stephens et al. 2007/. Nearly 900 mineral distribution plots have been generated in this analysis. A few examples are presented in Figure 5-15.

As for the wall-rock alteration referred to as oxidation (see section 5.2.3), the minerals in the older parageneses (epidote and adularia-prehnite-laumontite) show no relationship between frequency of occurrence and depth (Figure 5-15a). By contrast, apart from borehole KFM12A, which intersects the regionally important Forsmark deformation zone, the younger mineral asphaltite is restricted entirely to the uppermost part of the bedrock (Figure 5-15b). In some boreholes, other younger minerals, for example pyrite and clay minerals (Figure 5-15c), show a similar concentration in the upper part of the bedrock. It needs to be kept in mind that the current ground surface is more or less the same surface that existed prior to c. 540 million years ago (the sub-Cambrian unconformity or sub-Cambrian peneplain) and, for this reason, the correlation with depth may have been established several hundred million years ago.

Fractures without any minerals are predominantly, but not exclusively sub-horizontal or gently dipping /Sandström et al. 2008, section 4.4/. They show a variable depth relationship in the boreholes /Stephens et al. 2007, section 3.6.5/. In some boreholes (e.g. KFM01A and KFM05A), they are

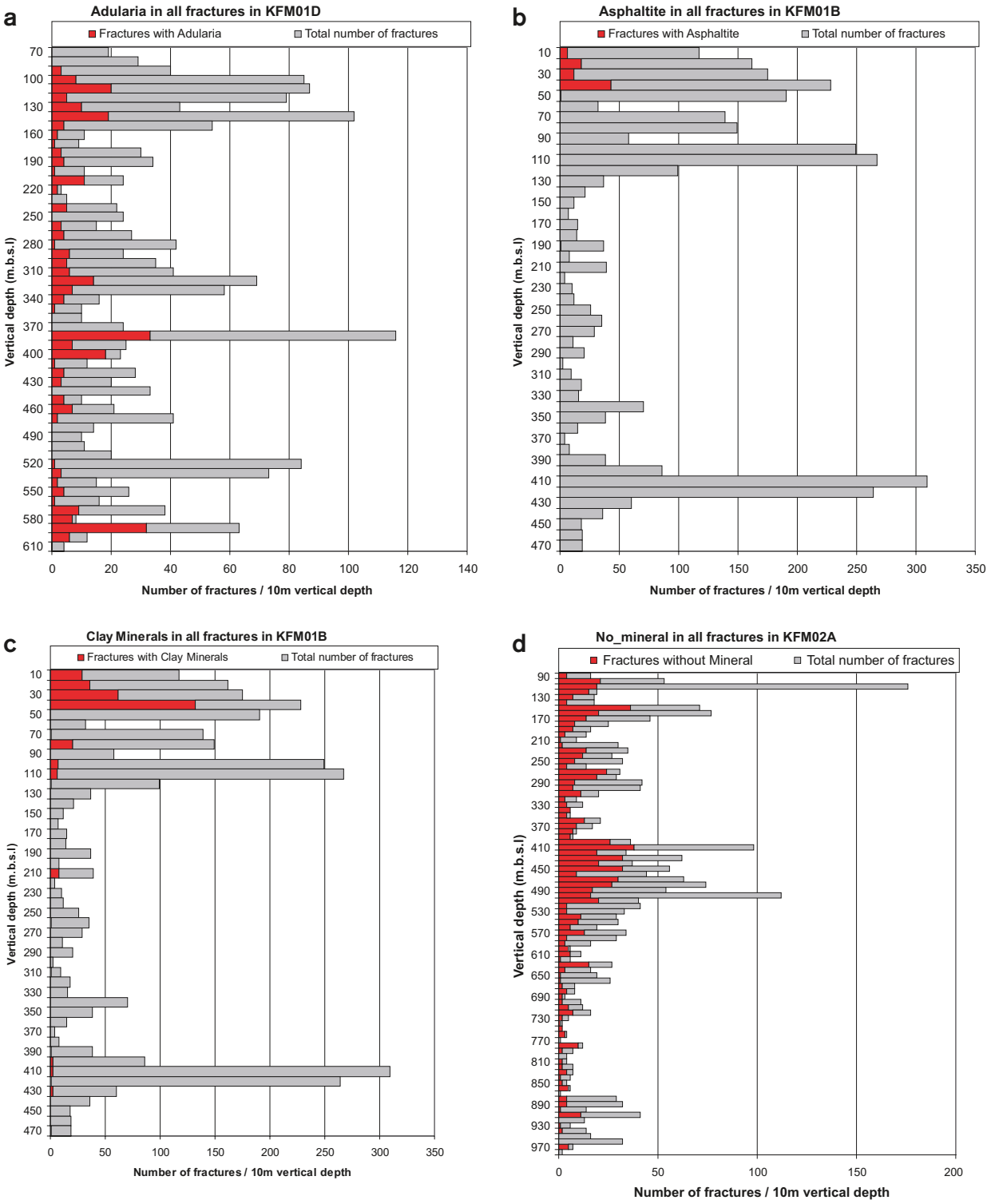

Figure 5-15. *Variation with depth of a) adularia (older generation) in KFM01D, b) asphaltite in KFM01B, c) clay minerals in KFM01B and d) fractures with no minerals in KFM02A. For each mineral, the analysis has addressed the occurrence in all fractures. The total number of fractures/10 m borehole interval is also shown.*

concentrated in the upper part of the borehole, at shallow depths, but they are also locally present at a depth of 400 to 500 m. This observation indicates some relationship to the establishment of the current ground surface, at least for these fractures. By contrast in boreholes KFM02A (Figure 5-15d) and KFM03A, there is no simple relationship with depth in the borehole, but there is a clear concentration along sections where possible deformation zones with gently dipping fractures have been inferred in the single-hole interpretations.

Several hypotheses were discussed in /Stephens et al. 2007, section 3.6.5/ that may account for the occurrence of these structures, and further work on the occurrence and origin of particularly open fractures, which neither contain a mineral coating nor any wall-rock alteration, was recommended /Stephens et al. 2007, p. 91/. This work has recently been initiated and the results of this study will be reported separately in a complementary document. At this stage, it is premature to make any firm conclusions concerning their significance or origin. However, errors in the mapping procedure, the occurence of drilling-induced fractures, particulary where problems with drilling were encountered, or the possibility that at least some of the fractures without mineral coating represent a relatively young geological feature, i.e. they formed after the establishment of the sub-Cambrian unconformity, merit particular attention.

5.2.6 Character and kinematics of deformation zones

Data acquisition

Data bearing on the character and kinematics of the possible deformation zones identified with high confidence in the single-hole interpretations have been acquired in three separate phases /Nordgulen and Saintot 2006, 2008, Saintot and Nordgulen 2007/. Bearing in mind the focused nature of the drilling activity, most of these data originate from zones that intersect the targeted, north-western part of the tectonic lens at Forsmark (Figure 5-2). Kinematic data have also been obtained from three deformation zones that are exposed at the ground surface, either in outcrop (Eckarfjärden deformation zone referred to as zone NW0003 and zone NW1200) or along an excavated trench (zone ENE0159A) /Nordgulen and Saintot 2006/. Furthermore, complementary outcrop observations bearing on the kinematics of the deformation along the Singö deformation zone and a steeply dipping minor zone with NE-SW strike at drill site 4 have also been provided by the bedrock mapping work.

Data from phase 1 /Nordgulen and Saintot 2006/ were available during model stage 2.2 and were compiled, evaluated and utilised in the modelling work at this stage /Stephens et al. 2007, section 3.7 and chapter 5/. The data acquired during phases 2 and 3 /Saintot and Nordgulen 2007, Nordgulen and Saintot 2008/, which became available in connection with model stage 2.3, have been compiled and evaluated in /Stephens et al. 2008/. It is apparent that the additional kinematic data obtained during stage 2.3 confirm the conclusions made during stage 2.2 based on the more limited phase 1 data /Stephens et al. 2007/. A brief summary of the results of these studies is provided below.

Occurrence and character of fault core

Fault core sections have been recognised in 55% of all the possible deformation zones at the site. They are narrow features, generally up to a few metres in borehole length (apparent thickness). Several deformation zones or the parts of zones not classified as fault core are classified as transition zones (see also section 5.5.2 for the terminology used in fault architecture).

Fault core sections along possible deformation zones in boreholes have been recognised on the basis of an anomalously high frequency of fractures, especially sealed fractures commonly in the form of complex networks, and the occurrence of cohesive breccia and cataclasite. Rock alteration (oxidation) is also conspicuous. Although incohesive crush rock is locally present, fault gouge has not been documented along any of these zones. /Stephens et al. 2007/ concluded that this feature appears to be an intrinsic property of the zones at the site, rather than the results of removal of non-cohesive gouge during drilling. The absence of such gouge possibly reflects the ancient character of the deformation zones and the lack of significant, incohesive rock granulation at the time when the bedrock had exhumed to high levels in the crust. However, it cannot be ruled out that some fractures filled with clay minerals have been misinterpreted and are indeed fault gouge.

Kinematics

Virtually all the possible deformation zones (85% of eighty-nine possible zones) contain one or more broken fractures, along which shear striae are present (shear fractures). Thus, evidence for shear displacement along minor faults within the possible deformation zones is apparent. However, since sealed fractures are common along the possible deformation zones and many of these fractures are unbroken, the identification of shear fractures along the boreholes is strongly restricted by the character of the fractures in the zones. Fault-slip data and evidence for shear deformation are absent along a higher proportion of the zones that have been modelled deterministically as gently dipping structures (30% of twenty-nine modelled zones). The fractures along such zones can be classified as joints.

The regional deformation zones, Eckarfjärden, Singö and Forsmark (Figure 5-2), which strike WNW-ESE or NW-SE and dip steeply, were all affected by low-temperature ductile deformation at an early stage in their history. Mylonites (Figure 5-16a) and shear bands in protomylonites that show a dextral strike-slip component of displacement (Figure 5-16b) are both present. This deformation was followed by polyphase reactivation under brittle conditions in different compressive tectonic

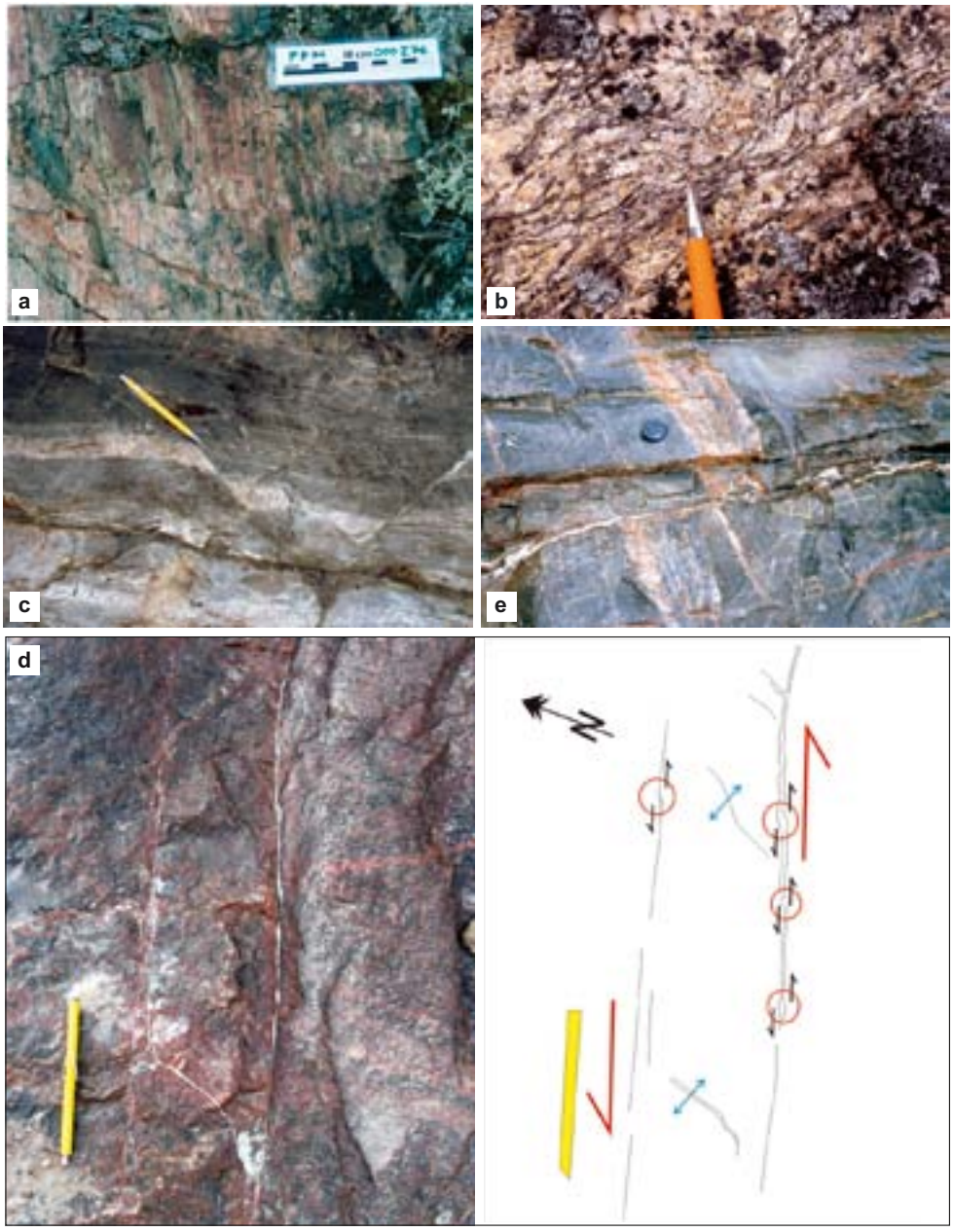

Figure 5-16. *a) Mylonite formed under low-temperature ductile conditions along the Eckarfjärden deformation zone. Note also the intense hematite- and epidote-rich alteration. b) Shear bands in pegmatite, affected by low-temperature ductile strain, indicate a dextral strike-slip component of displacement. This field observation point (PFM001637) occurs along the high-strain belt that hosts the Singö deformation zone and its splays to the north. NW-SE to N-S compression is inferred. c) Conjugate set of fractures at drill site 4, inferred to have formed in association with an approximate NE-SW compression. The main ductile fabric at this site strikes NW-SE (right-left in picture) and dips steeply to the SW. Top view on a sub-horizontal surface. d) En echelon distribution of quartz-filled tension gashes with NNE-SSW strike along the steeply dipping zone ENE0159A, inferred to represent sinistral strike-slip displacement along the zone. Sinistral steps along quartz veins (red circles) are also present (after /Nordgulen and Saintot 2006/). N-S to NE-SW compression is inferred. e) Apparent dextral strike-slip displacement along the minor fracture zone NE1188 at drill site 4. This zone strikes NE-SW and dips steeply to the NW. Approximately E-W compression is inferred.*

regimes. The complexity of the kinematic data is illustrated by the evidence for conspicuous sinistral strike-slip deformation in the brittle regime along zone NW1200 /Nordgulen and Saintot 2006/. Furthermore, both sinistral (Figure 5-16c, d) and dextral (Figure 5-16e) strike-slip deformation have occurred along steeply dipping structures with ENE-WSW strike.

Although the data from drill cores are far more abundant than those obtained from the surface, the quality of the kinematic determinations from boreholes varies considerably and is not always sufficient to constrain, in more detail, the strike-slip or dip-slip sense of movement (dextral/sinistral and normal/reverse, respectively). Nevertheless, the overall importance of compressive, strike-slip deformation along steeply dipping structures and a complexity that is inferred to be related to more than one phase of deformation are apparent. For example, sinistral strike-slip deformation is conspicuous along zone WNW0123 and both sinistral and dextral strike-slip deformation in the brittle regime have been observed along steeply dipping structures with ENE-WNW to NNE-SSW strike. Furthermore, reverse dip-slip and subordinate strike-slip senses of movement have occurred along gently dipping zones.

The magnitude of both strike-slip and dip-slip displacement along brittle deformation zones inside the target volume is poorly constrained. However, assessment of magnetic and reflection seismic data indicates only minor displacements /Stephens et al. 2007/.

5.2.7 Identification, character and geological significance of lineaments

Data acquisition, identification of lineaments and uncertainties

The use of lineaments in the modelling of steeply dipping deformation zones has developed successively during the site investigation work at Forsmark. Up to and including SDM version 1.2 /SKB 2005a/, lineaments were identified on the basis of anomalies in predominantly airborne magnetic data, high-resolution topographic data and bathymetric data /Isaksson et al. 2004, Isaksson and Keisu 2005/. Electromagnetic (EM and VLF) data were of limited, additional help. Both fixed-wing airborne geophysical data, which were generated predominantly by the Geological Survey of Sweden (SGU), and similar helicopter airborne data, with considerably higher resolution (Table 5-4), were used (Figure 5-17). Linear arrays of low velocity anomalies in the older refraction seismic data close to the nuclear power plant were also interpreted as lineaments along the surface that separates the crystalline bedrock from the Quaternary cover (see also section 5.2.9). Ground magnetic and EM (slingram) data in restricted areas inside the candidate area were also evaluated in /SKB 2005a/.

Short method-specific lineaments, identified on the basis of a single data set with specific attributes (e.g. low magnetic lineament with high confidence), short co-ordinated lineaments that represent a combination of different types of lineament, and longer linked lineaments that integrate the co-ordinated segments into a single inferred lineament were acquired /Isaksson and Keisu 2005/. The methodology, results and uncertainties in the technique used were addressed in /SKB 2005a/.

Table 5-4. Characteristics of geophysical surveys used for the detection of lineaments in the Forsmark area. The resolution of the data obtained from ground surveys in the north-western part of the candidate area is five times greater than that obtained from helicopter airborne measurements, which, in turn, is four times greater than that obtained by the Geological Survey of Sweden from fixed-wing airborne measurements in connection with their standard mapping activities.

Type of survey	Contractor	Line spacing	Station spacing	Survey direction	Survey elevation	Grid resolution
Airborne, fixed-wing (magnetic, VLF)	SGU	200 m	17 or 40 m	EW	60 m (30 m older data)	40×40 m
Airborne, helicopter (magnetic, EM, VLF)	NGU	50 m	3 m	NS and EW	45 m	10×10 m
Ground on land, sea and lake (magnetic)	GeoVista AB	10 m	5 m (2–3 m in the marine survey)	150°/330°	c. 1.5–2 m	4×4 m

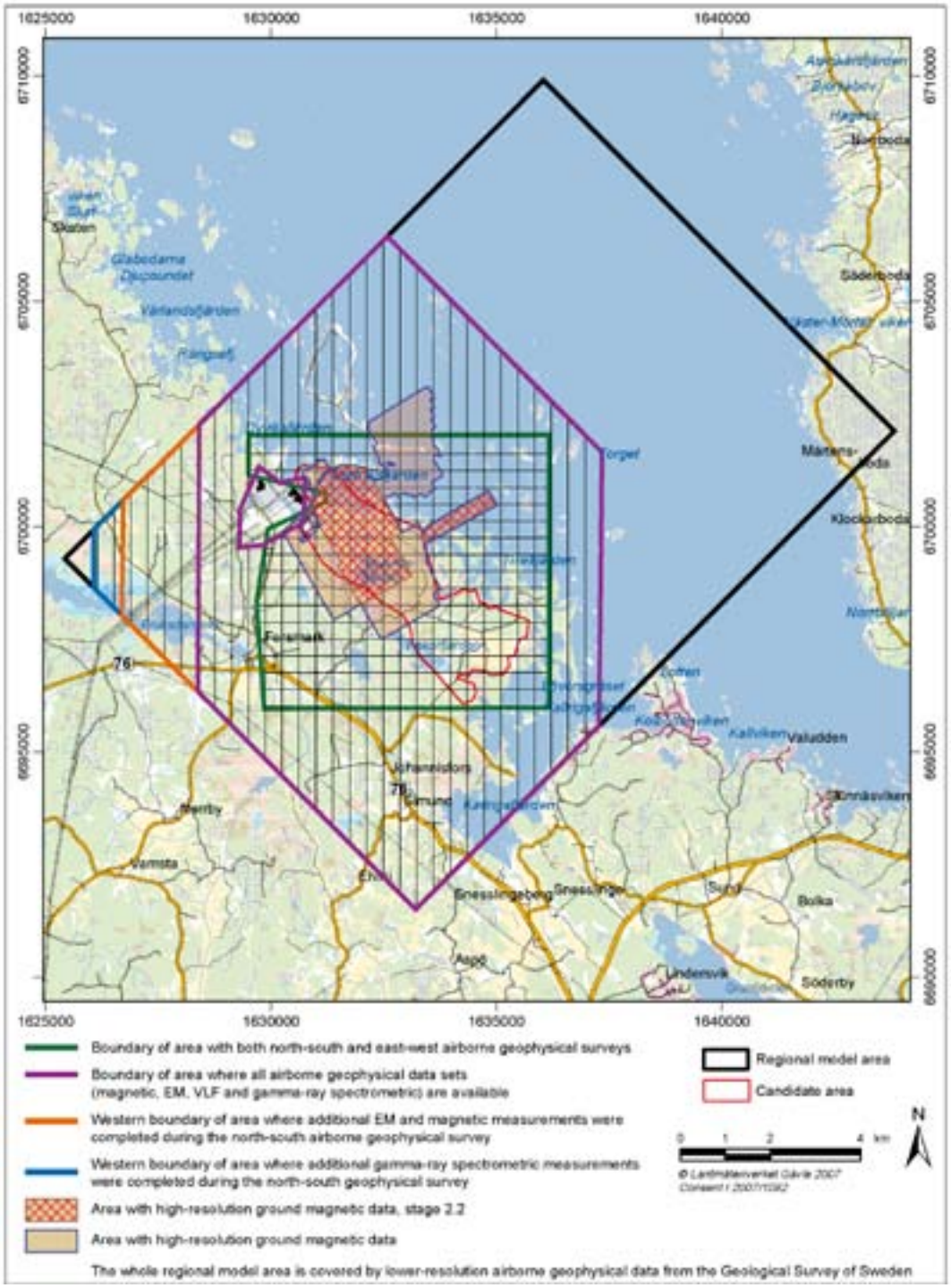

Figure 5-17. *Coverage of airborne and ground geophysical data used for the detection of lineaments in the Forsmark area. Only magnetic data have been used in the interpretation of lineaments during model stages 2.1, 2.2 and 2.3.*

The interpretation of lineaments is subjective in character and serious questions arise concerning the reproducibility of the results, not least the trace length of an individual structure. Furthermore, there are intrinsic problems that bear on the geological character of a lineament; a deformation zone or anisotropy related to rock type and/or pervasive ductile strain in the bedrock? The low topographic relief in the area also gives rise to serious difficulties in the interpretation of digital topographic data. Bearing in mind these uncertainties, an alternative interpretation of lineaments was carried out inside and immediately around the candidate area by an independent working group /Korhonen et al. 2004/.

A comparative study of the two lineament interpretations showed, in principle, good reproducibility /Johansson 2005, SKB 2005a/. However, some discrepancies in the two interpretations, especially for shorter lineaments and lineaments identified with a lower degree of confidence, were recognised. Naturally, these discrepancies are enhanced when different method-specific lineaments are combined into linked lineaments.

On the basis of reflection seismic data along c. 16 km of continuous seismic profiles (see section 5.2.8) in combination with refraction velocities calculated from refraction seismic data at three sites, /Bergman et al. 2004b/ estimated the thickness of the Quaternary cover sequence along the profiles. This study demonstrated the generally poor correlation between the topographies of the ground surface and the crystalline bedrock surface. The intrinsic difficulties with the interpretation of the topographic data motivated the use of solely low magnetic lineaments in subsequent (after version 1.2) geological modelling work. Use of a single type of lineament also reduced the uncertainty in the evaluation of the critical attribute trace length. In addition, ground magnetic data with a resolution five times greater than the helicopter airborne data (Table 5-4) were acquired during model stages 2.2 and 2.3 inside the target area and in some offshore areas (Figure 5-17). These data provided a radical improvement for the interpretation of lineaments in these areas. However, the complementary data acquired during stage 2.3 were not available for use in the stage 2.2 geological modelling work (see also section 5.5.3).

Integration of low magnetic lineaments derived from both the high-resolution ground magnetic data and the airborne helicopter data inside and immediately around the target area has dominated subsequent work during model stages 2.2 and 2.3 /Isaksson et al. 2006a, 2006b, 2007/. General estimates of the uncertainty in the spatial position of a point along a lineament interpreted from these two data sets are ±10 m and ±20 m, respectively, e.g. /Isaksson and Keisu 2005, Isaksson et al. 2006a/.

Low magnetic lineaments and their geological significance

Two types of low magnetic lineament are present inside the Forsmark tectonic lens in the north-western part of the candidate area (Figure 5-18):

- Magnetic minima that are discordant to the tectonic foliation, rock units and the banded magnetic anomaly pattern.
- Magnetic minima connections that are concordant with the same geological and geophysical features and are locally folded.

Excavations of lineaments classified as magnetic minima inside the Forsmark tectonic lens (see also section 5.2.5) show that they represent either steeply dipping fracture zones (4 out of 5 cases) or are related to a swarm of dykes of Group D granite and pegmatite with low magnetic susceptibility (1 out of 5 cases). The steeply dipping fracture zones are associated with wall rock hydrothermal alteration that consists of intense hematite dissemination in the bedrock and is optically visible as red staining (Figure 5-19). This is identical to the alteration observed along possible deformation zones in the boreholes (cf. sections 5.2.2 and 5.2.3). These findings provide strong support to the change in strategy that favoured the sole use of low magnetic lineaments in the identification of steeply dipping fracture zones. Magnetic minima with a span in trend of 25−70°, and a dominant trend of 50−65° are present inside the north-western part of the candidate area, i.e. the target area /Isaksson et al. 2007/.

Inside the Forsmark tectonic lens, lineaments classified as magnetic minima connections are inferred to be related primarily to lithological contrasts that are aligned parallel to the ductile tectonic foliation in the bedrock /Stephens et al. 2007/. However, the occurrence of minor fracture zones along the tectonic foliation cannot be excluded as a contributory factor. By contrast, in the ductile high-strain belts outside this lens, where all structures are concordant, it is generally impossible to distinguish magnetic minima connections that are simply related to lithological contrasts from those that are related to deformation zones.

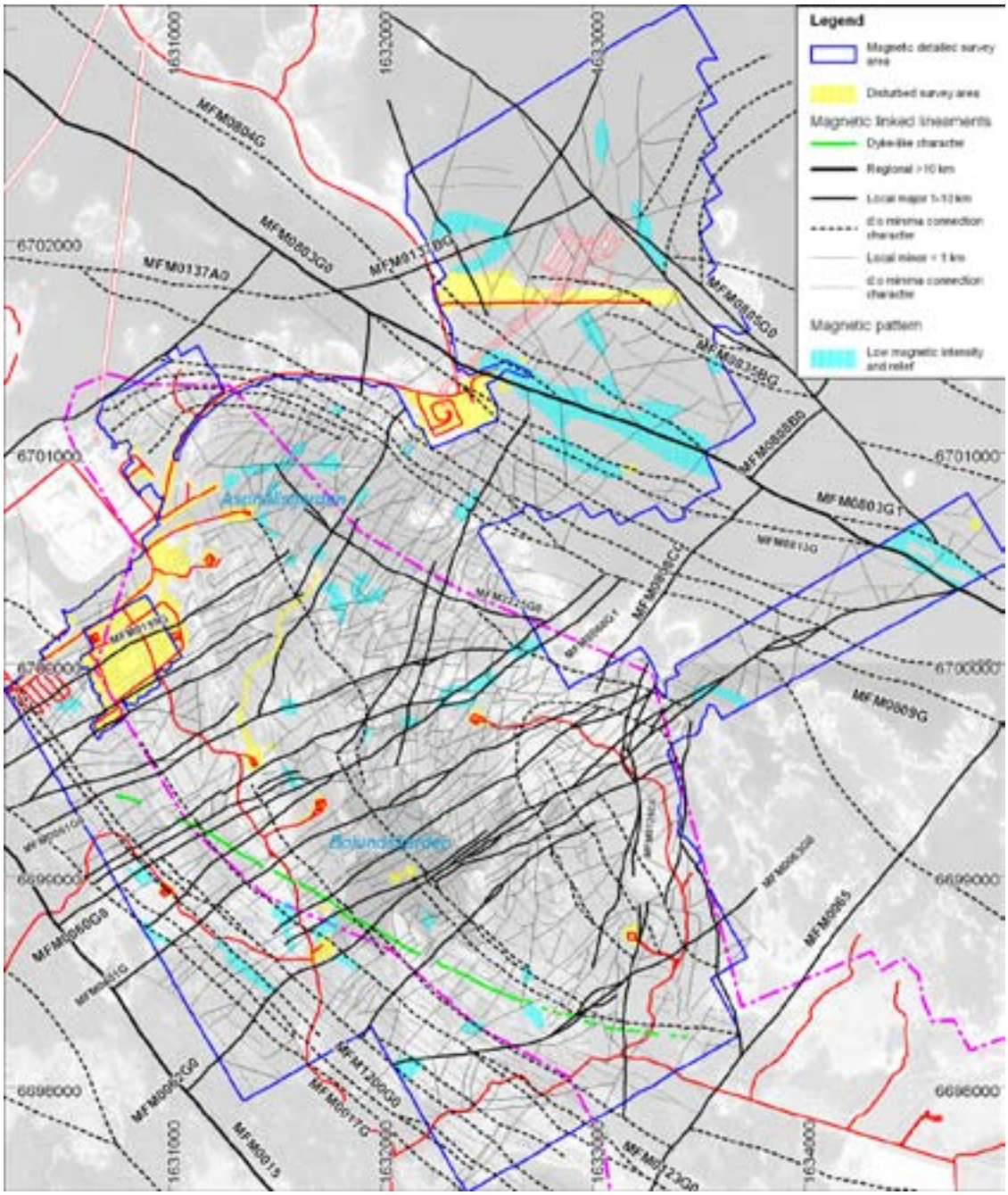

Figure 5-18. *Low magnetic lineaments inferred from the integration of high-resolution ground magnetic and airborne helicopter data. The SFR underground facilities and the cooling water tunnels from reactors 1-2 and 3 are shown with pink lines and white filling, the candidate area with a thick dot-dashed, magenta line, and roads and drill sites in red. © Lantmäteriverket Gävle 2007. Consent I 2007/1092. After /Isaksson et al. 2007/.*

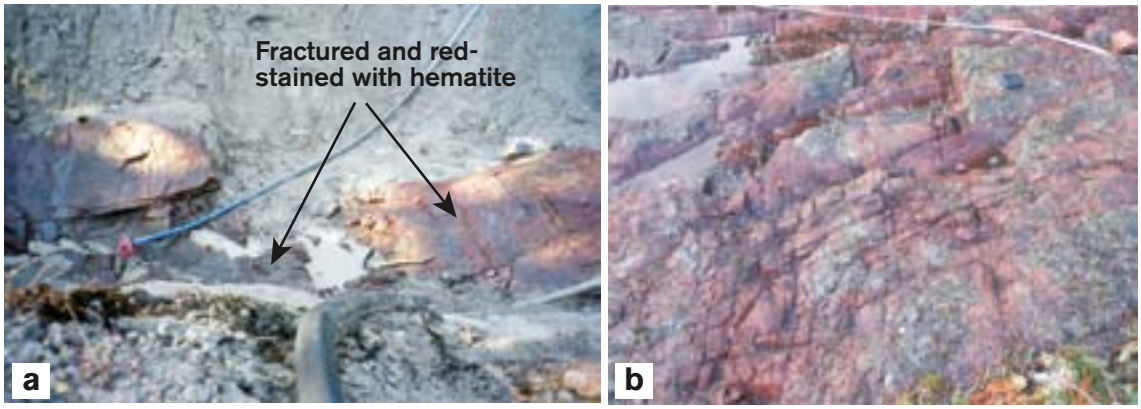

Figure 5-19. *Fracturing and wall rock alteration (red-staining referred to as oxidation) along exposed lineaments classified as magnetic minima inside the target area. a) Excavation site AFM001243 /Cronquist et al. 2005/ where lineament MFM0062G0 is exposed. This lineament has been modelled as fracture zone ENE0062A. b) Excavation site LFM001027 where lineament MFM2273G is exposed /Petersson et al. 2007b/. This lineament has been modelled as the minor fracture zone NNE2273.*

A faintly discordant anomaly of dyke-like character, which consists of combined magnetic minima and maxima, has been identified on the basis of the high-resolution, ground magnetic data in the south-westernmost part of the detailed survey area, close to Bolundsfjärden (Figure 5-18). Areas with low magnetic intensity and with low relief (Figure 5-18) are inferred to be related to intersections of magnetic minima. Areas with a diffuse magnetic pattern may indicate a deeper bedrock source and/or the presence of fractured and altered surface rock.

5.2.8 Character and geological significance of seismic reflection data

Data acquisition

Surface reflection seismic data were acquired and interpreted in connection with model versions 1.2 and 2.1 /Juhlin et al. 2002, Juhlin and Bergman 2004, Juhlin and Palm 2005/, in order to provide geometrical constraints on the occurrence of gently dipping fracture zones. Approximately 40 km of high-resolution (10 m shot and receiver spacing) data were generated along fifteen profile lines (Figure 5-20). In order to aid their use in the modelling work, the reflections were placed in 3D space with the help of the method described in /Cosma et al. 2003/ and the results of this exercise are presented in /Cosma et al. 2003, Balu and Cosma 2005, Cosma et al. 2006/. A general estimate of the uncertainty in the spatial position of a point in the central part of a reflector is ±15 m, e.g. /Cosma et al. 2003/.

Borehole seismic data (VSP), with a much higher data resolution, were subsequently acquired for boreholes KFM01A and KFM02A /Cosma et al. 2005/. Some reprocessing of the surface data that aimed to evaluate more closely the extension of some reflectors and a focused study designed to integrate the surface and borehole data were completed during stage 2.2 /Juhlin 2007/. In addition, an evaluation of the geological significance of the VSP data was also carried out /Enescu and Cosma 2007/.

Seismic reflectors and their geological significance

Inside the candidate area, reflectors that dip gently to the SSE and SE are prominent. Furthermore, there is a much stronger concentration of well-defined, gently dipping reflectors in the upper 2 km of bedrock in the south-eastern part of the candidate area (Figure 5-21a), relative to that observed in the north-western part, closer to the nuclear power plant (Figure 5-21b). The reflectors A2, A8, B7, F1–F2 and possibly B4 are conspicuous above c. 1 km depth and north-west of drill site 2 inside the target volume (Figure 5-21c).

Integration of the surface reflection seismic data in /Juhlin et al. 2002, Juhlin and Bergman 2004/, the VSP data from borehole KFM02A, and standard geological, geophysical and hydrogeological

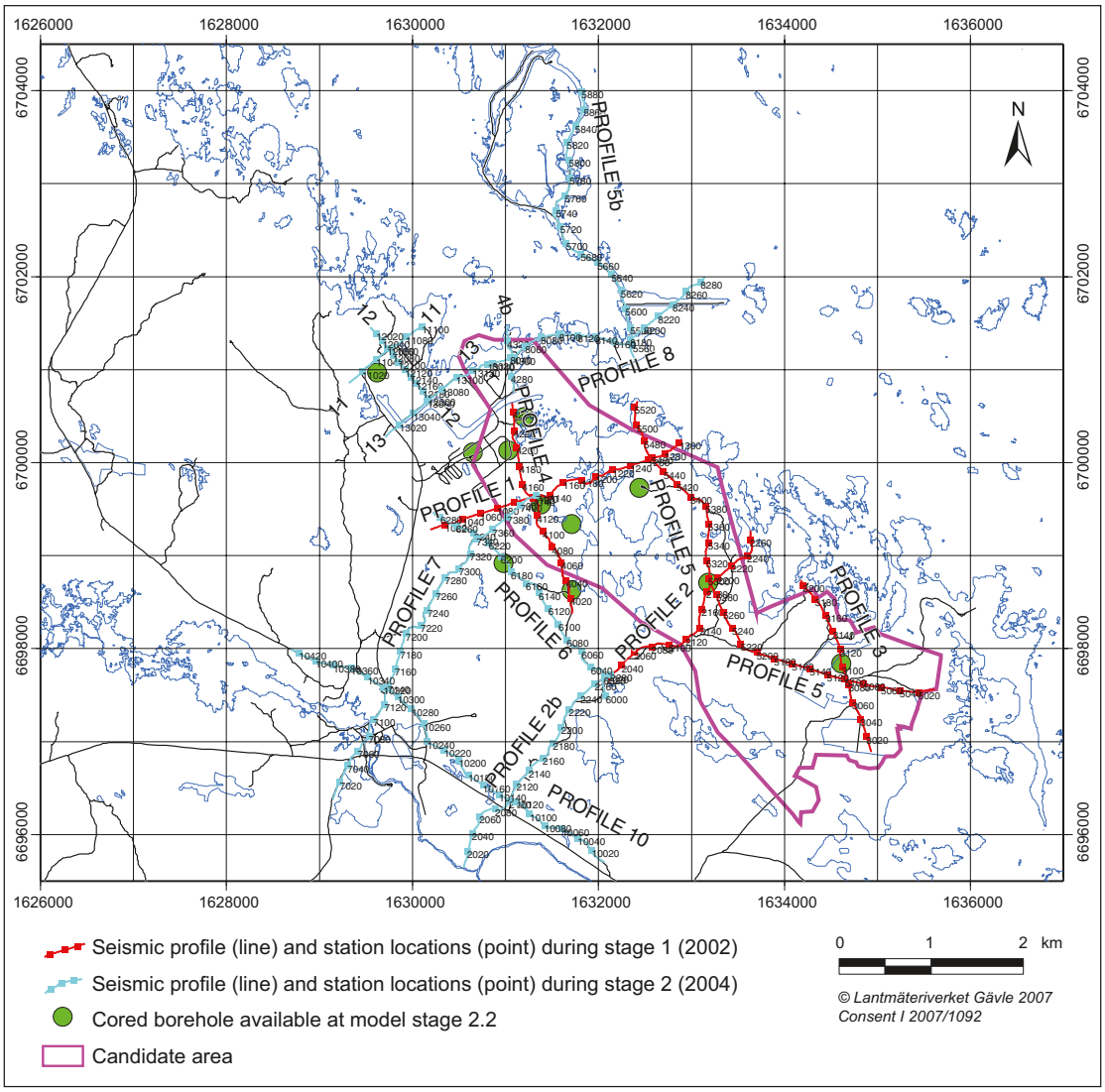

Figure 5-20. *Profiles along which surface reflection seismic data have been acquired. Coordinates are provided using the RT 90 (RAK) system.*

data from boreholes KFM02A, KFM03A and KFM03B have shown that the prominent, gently dipping reflectors in the south-eastern part of the candidate area (Figure 5-21a) represent hydraulically conductive fracture zones /SKB 2005a, Juhlin and Stephens 2006/. In particular, the prominent F1 and A2 reflectors correspond to the lower and upper parts, respectively, of the highly fractured and groundwater-bearing borehole interval along DZ6 in borehole KFM02A /Juhlin 2007/.

The single-hole interpretations of boreholes KFM02A, KFM03A and KFM03B, combined with an inspection of their density and sonic logs, indicate that several of the gently dipping zones occur along or close to the contact between metagranite and the subordinate rocks amphibolite or Group C, fine- to medium-grained metagranitoid /Juhlin and Stephens 2006, Stephens et al. 2007/. It has been suggested that these denser rocks actually enhance the reflectivity of the hydraulically conductive, gently dipping fracture zones. However, there is no consistent correlation between occurrence of zones, reflectors and rock contacts. Inspection of the high-resolution VSP data in boreholes KFM01A and KFM02A, for example, shows that many reflectors are simply related to rock contacts between metagranite and various subordinate rocks of different density, and are not fracture zones or other types of high-strain zones /Enescu and Cosma 2007/. This correlation may explain, for example, the occurrence of VSP reflectors that dip moderately to steeply to the south-west /Cosma et al. 2005/. Further discussion of the relationship between the orientation of amphibolite and the frequency of occurrence of gently dipping fracture zones is addressed in the context of the conceptual understanding of these zones in section 5.5.2.

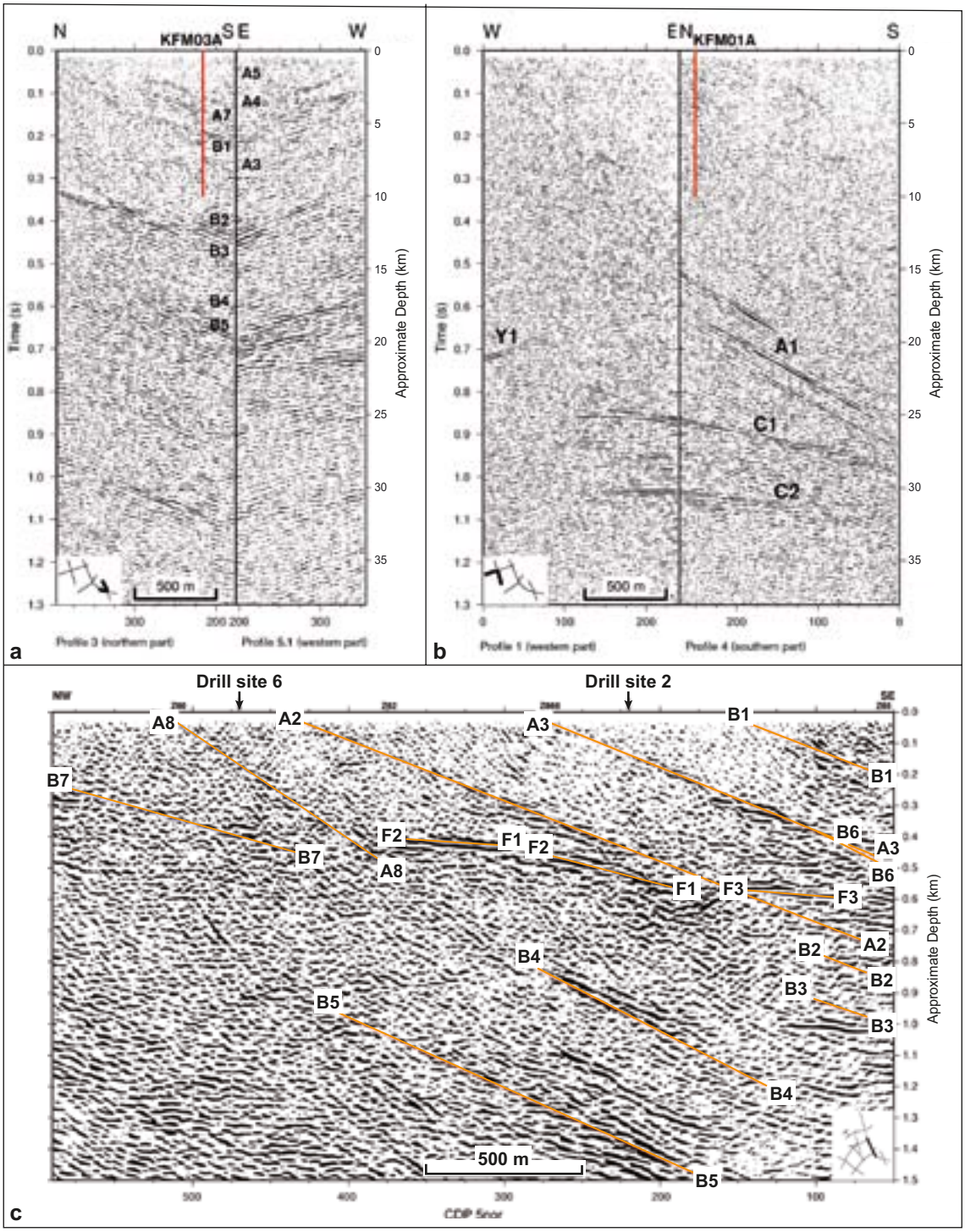

Figure 5-21. *a) Correlation of stacks along the intersection of profiles 3 and 5.1 in the south-eastern part of the candidate area. b) Correlation of stacks along the intersection of profiles 1 and 4 in the north-western part of the candidate area. c) Migrated section of the reprocessed northern part of profile 5 down to 0.5 seconds (c. 1.5 km depth). The majority of the reflectors have been identified (e.g. F1) and are shown by an orange line. Location of each section is shown in the lower part of each figure. The depth scale along the vertical axis is only approximate. The numbers along the horizontal axis refer to the CDP line along which the data have been projected for stacking and interpretation. The figures are modified slightly after /Juhlin et al. 2002, Juhlin and Bergman 2004, Juhlin 2007/.*

5.2.9 Character and geological significance of seismic refraction data

Data acquisition and P-wave velocity of the bedrock

Refraction seismic data in the Forsmark area were acquired during older investigations (1970–1982) in connection with the construction of the nuclear power plant and SFR, and more recently (2004–2006) inside and adjacent to the targeted area during the site investigation programme (Figure 5-22). The mode bedrock velocity (P-wave velocity), based on the data from within and immediately adjacent to the target area, is 5,400 m/s and, along more than 88% of the total measured profile length, the bedrock velocity exceeds 5,000 m/s /Nissen 2007/. The older data from the nuclear power plant and SFR show a similar velocity distribution and the

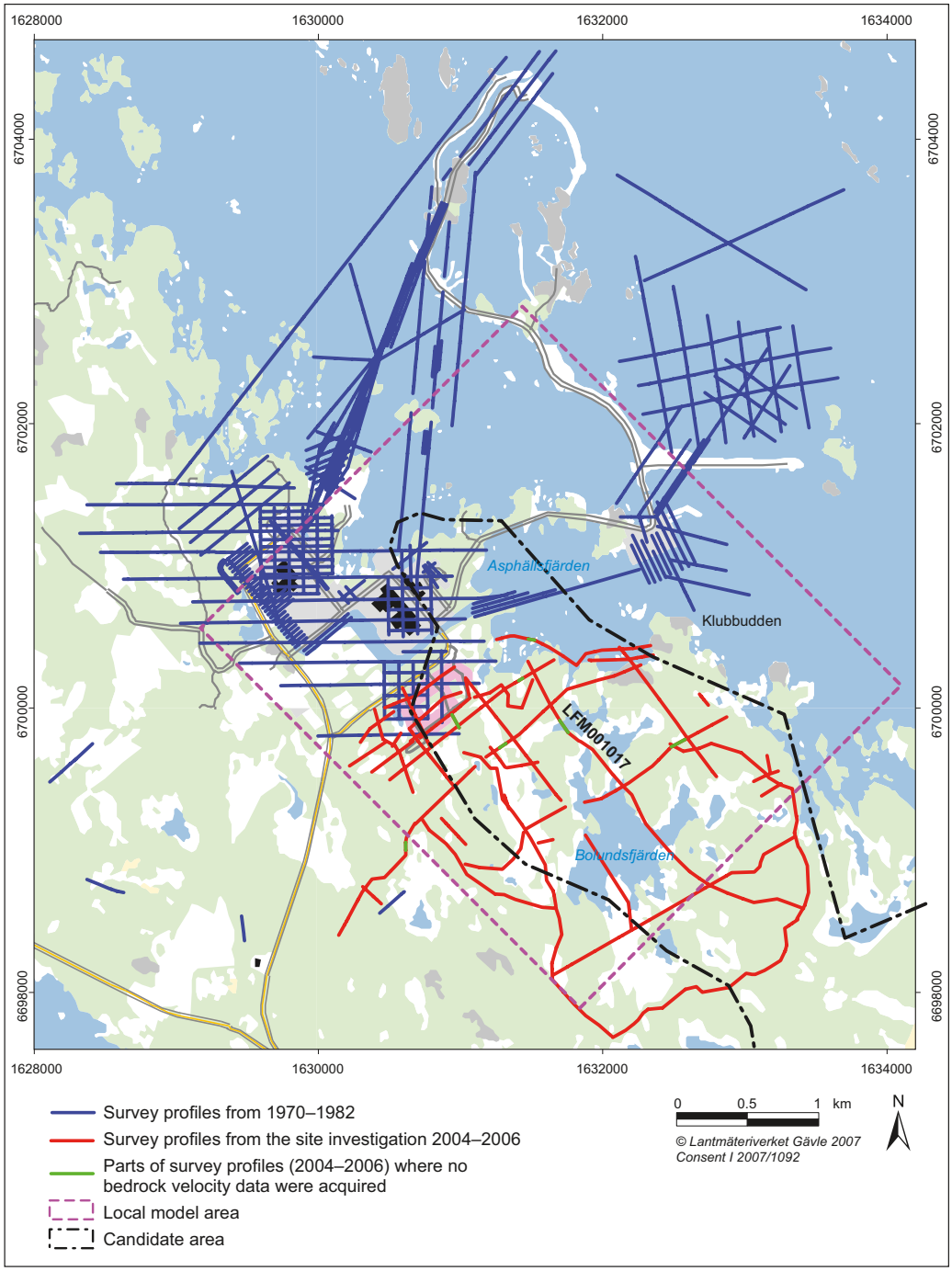

Figure 5-22. *Refraction seismic profiles in the Forsmark area. Figure based on /Isaksson 2007/.*

corresponding values are 5,500 m/s and 75%, respectively /Isaksson and Keisu 2005/. However, the frequency of low rock velocity sections (≤ 4,000 m/s) is somewhat higher in the older data and the frequency of medium velocity sections (4,000−5,000 m/s) is more than double that observed in the data from the target area /Nissen 2007/.

Geological significance of low velocity anomalies

Correlations between some connected low velocity anomalies in the bedrock and lineaments were identified using the older data set during model version 1.2 /SKB 2005a, p. 184–185/. A more systematic evaluation of the correlation between low velocity anomalies and lineaments defined by magnetic minima or modelled deformation zones was completed for both data sets during model stage 2.2 /Isaksson 2007/. In order to avoid the use of a single velocity threshold (≤ 4,000 m/s) in the identification of low velocity anomalies, an attempt was also made /Mattsson 2007/ to use wave path travel time tomography along one of the seismic profiles (LFM001017, see Figure 5-22).

/Isaksson 2007/ showed that there is only a moderate correlation between low velocity anomalies and lineaments defined by magnetic minima or modelled deformation zones. Bearing in mind that low velocity anomalies detect anomalous concentrations of open fractures or non-cohesive crush rock and that sealed fractures dominate inside the fracture zones at Forsmark, there is an intrinsic limitation to the use of this geophysical method to detect fracture zones at the site. Furthermore, since the fracture zones at the site are heterogeneous, where it concerns the frequency of open fractures, and since most of the refraction seismic surveys have been carried out with a geophone spacing of 5 m, it is probable that individual low velocity intervals narrower than 5 m have simply not been detected. The low velocity anomalies that do not match low magnetic lineaments and/or deformation zones may be related to local, narrow depressions in the bedrock surface that correlate with fractured near-surface bedrock (see section 5.2.2) or are simply filled with Quaternary cover material.

In summary, the geological conditions at the site, in combination with survey methodology, explain the absence of a strong correlation between low velocity anomalies and lineaments defined by magnetic minima or deformation zones. The survey methodology also contributed to the ambiguous results obtained with the help of the tomography inversion model technique /Mattsson 2007/.

5.3 Geological models in relation to data resolution

An important modelling prerequisite /Munier et al. 2003/ is that the resolution of the modelled objects should be the same throughout the model volume, at any particular modelling scale. For this reason, it is essential to define, for each model, the size of the smallest object to be modelled deterministically. The choice of this limit is guided by the intended use of the model, at a particular scale, and the data density within the model volume. These features are balanced against the efforts required to fill the volume homogeneously with modelled objects. The selection process has also taken account of the documentation of properties, quality assessment and comments by reviewers.

Inside the local model volume that has been used since stage 2.1 (Figure 2-5), the regional and local rock domain models differ only in the division of rock domain RFM029 in the regional model (RFM029R) into rock domains RFM029 and RFM045 in the local model. These two local domains show similar rock composition, but they differ on the basis of the degree of early stage alteration that is referred to as albitization (section 5.2.3). Since this alteration is related to the occurrence of amphibolite (section 5.2.3), this division was deemed necessary for especially the purposes of thermal and mechanical modelling work.

As far as the deterministic deformation zone and geological DFN models are concerned, it was judged practical to set the size limit at structures that have produced trace lengths at the ground surface of 1,000 m. Structures that are 1,000 m or longer are included in the deterministic, local deformation zone model and structures shorter than 1,000 m, corresponding to an equivalent radius of 564 m (see section 5.6.2), are addressed in the geological DFN model. The latter are described in statistical terms in this model and, using the various derived parameters, can be modelled stochastically in various applications. Some minor zones that are shorter than 1,000 m have been modelled deterministically and assigned properties, but were not included in the local block model for deformation zones.

Deformation zones that are 3,000 m or longer are included in the deterministic, regional model. Considerations of respect distance /Munier and Hökmark 2004/ has guided the selection of a size boundary for deformation zones included in the local and regional models. The length of gently dipping zones is difficult to estimate and varies considerably with depth. Furthermore, these structures are important from a hydrogeological viewpoint (see chapter 8). For these reasons, all the identified gently dipping zones have been included in the regional model.

5.4 Deterministic model for rock domains

5.4.1 Data input

The deterministic modelling of rock domains has primarily made use of the following data and interpretations:

- The distribution of rock units at the ground surface as presented in the bedrock geological map (section 5.2.1).
- The rock units identified in the single-hole interpretation of c. 15 km of bedrock extracted from twenty-one cored boreholes, complemented with the single-hole interpretation of thirty-three shallow percussion boreholes (section 5.2.2).
- The character of rock types in each rock unit as inferred in data both from the ground surface and from boreholes (section 5.2.3).
- The character and variation in the style of ductile deformation as inferred in data both from the ground surface and from boreholes (section 5.2.4).

5.4.2 Conceptual model

The bedrock inside the Forsmark tectonic lens is dominated by medium-grained granite. Between 1.87 and 1.86 Ga, both this granite and the surrounding rocks were affected by penetrative ductile deformation at mid-crustal depths and under high-temperature metamorphic conditions (/Söderbäck (ed) 2008/ and section 3.1). Amphibolite and fine- to medium-grained granitoid intruded syntectonically as dykes and minor bodies during this time interval and, locally, at least the amphibolites gave rise to conspicuous alteration (albitization) in the older granitic rocks. Ductile deformation with folding continued to affect the younger intrusive rocks, including amphibolite, under lower metamorphic conditions, prior to 1.85 Ga. Subsequently, until at least 1.8 Ga, the ductile strain continued to affect the bedrock, predominantly along the margins of the tectonic lens along discrete zones (/Söderbäck (ed) 2008/ and section 3.1). Borehole data indicate that the tectonic lens is a major geological structure that can be traced from the surface down to at least 1,000 m depth.

Folding of a ductile fabric and a generally lower degree of ductile strain are inferred to be present inside the lens, including the target volume in its north-western part. By contrast, the surrounding rocks are affected by a higher degree of ductile strain and a conspicuous WNW to NW structural trend. The ductile structures at the site are characteristic of regions where variable degrees of ductile strain, folding and stretching are intimately related during strong, progressive, non-coaxial deformation.

Compressive deformation in the Forsmark region was absorbed initially by dextral strike-slip shear along high-strain belts with WNW to NW trend, combined with shortening across these belts expressed by grain-shape fabric development. As the ductile strain progressed, these structures were folded at different scales. This transpressive deformation was accompanied by continuous extrusion of material in a south-easterly direction. Folding developed initially with a normal cylindrical shape, but, to variable extent, the folds were progressively drawn out in the stretching direction into tubular-shaped structures, i.e. sheath folds. A major sheath fold is inferred to be present inside the tectonic lens (Figure 5-23). This fold is synformal in character in the part of the lens occupied by the target volume (Figure 5-23).

The Group B metatonalite that is situated outside the local model volume in the south-eastern part of the Forsmark lens (Figure 5-2) is inferred to be a mega-xenolith inside the metagranite. The geochronological data (/Hermansson et al. 2008/ and section 3.1) support this concept. A younger

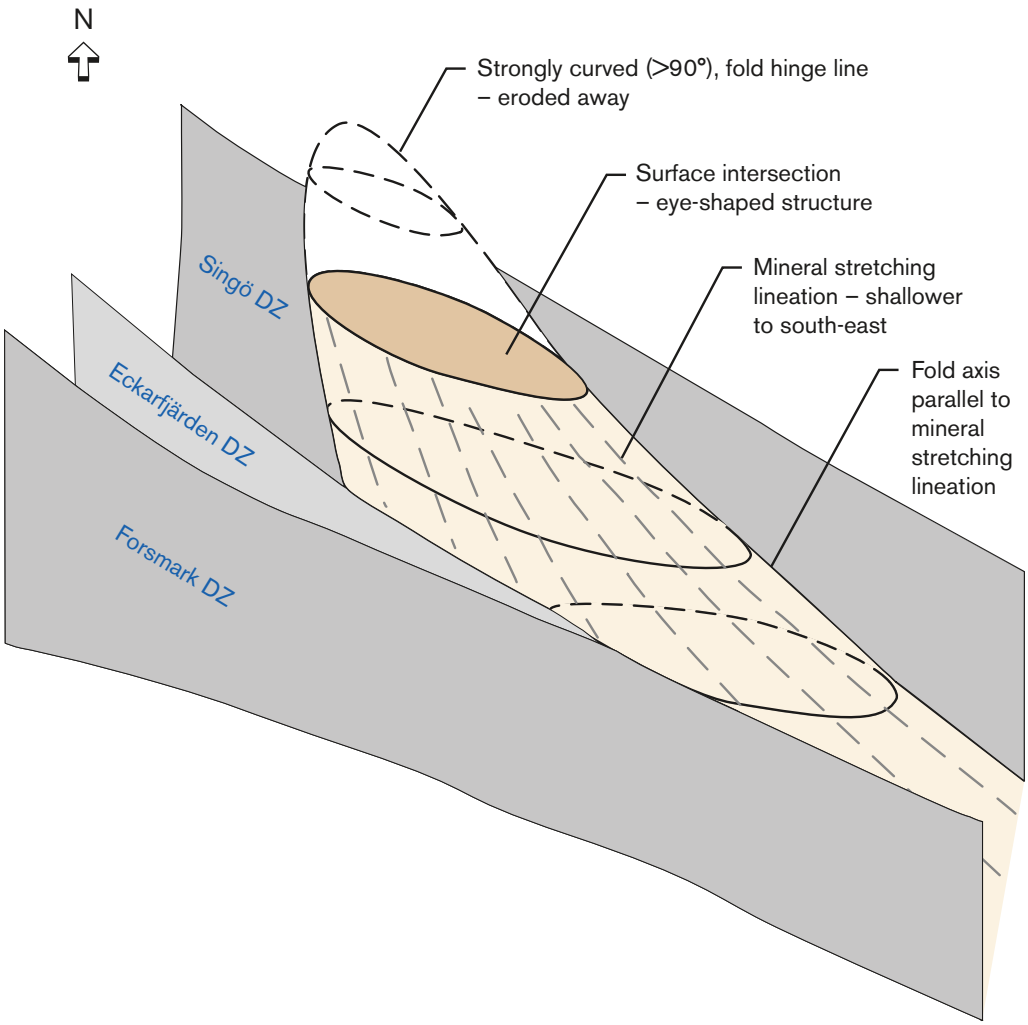

Figure 5-23. *Conceptual model for the development of sheath folding inside the tectonic lens at Forsmark, with fold axes sub-parallel to the mineral stretching lineation.*

Group D granite body, which is situated in the archipelago north of the candidate area and outside the local model volume (see inset map in Figure 5-2), has been treated conceptually as a laccolith. It shows a broad extension at the surface, but a rapidly decreasing extension at depth. This geological feature has not been drilled and remains as an unconfirmed concept.

The bedrock anisotropy at Forsmark, which was established at an early stage in the geological evolution in the high-temperature ductile regime, has important implications for an understanding of the spatial distribution of younger deformation zones at the site and for uncertainties in the modelling of such zones. These implications are discussed further in sections 5.5 and 5.9.

5.4.3 Methodology, assumptions and feedback from other disciplines

The conceptual model has provided the basis for the modelling of rock domains inside and around the target volume. Furthermore, geological data generated in connection with the surface mapping has formed the keystone in the modelling work.

The mean values of ductile structural data from both the surface and from boreholes (Table 2-3 in /Stephens and Forssberg 2006/), as well as critical fixed point intersections for rock domain boundaries in eleven boreholes (Table 4-4 in /Stephens et al. 2007/) were used to project rock domains at the surface down to the base of the regional and local model volumes. The local orientation of the contacts between rock units in boreholes that correspond to rock domain boundaries (see section 5.4.4) was not employed. Thus, the modelling methodology is not sensitive to uncertainties in the

orientation of geological objects in the boreholes, only to the actual orientation of the boreholes, i.e. to the borehole deviation measurements /Munier and Stigsson 2007/. The absence of linear grain-shape fabric data at depth is an intrinsic weakness in the modelling work.

The following assumptions are inherent in the modelling procedure:

- The mean values of the orientation of planar ductile structures (tectonic foliation and tectonic banding) in each rock domain are assumed to provide an estimate of the orientation of the contacts between the domains.
- Rock domains that form isolated bodies of metamorphosed intrusive rocks at the ground surface are assumed to plunge downwards in approximately the direction of the mineral stretching lineation as flattened rod-shaped entities – these formed in a setting dominated by constrictional strain.
- The major rock domains at the ground surface with steeply dipping contacts, which are included in the regional model volume, are assumed to extend downwards to, at least, the base of this volume (–2,100 m).
- The rock domain composed of partly albitized and metamorphosed granite close to Asphällsfjärden, which is restricted to the local model volume, is assumed to extend downwards to, at least, the base of this volume (–1,100 m).
- The rock domains outside the local model volume, which are conceptually handled as a mega-xenolith or laccolith, are modelled as gently dipping rock sheets and do not extend to the base of the regional model volume (Figure 4-15 in /Stephens et al. 2007/).

As in previous models, judgements concerning the confidence of existence of a rock domain both at the surface and at depth (–2,100 m in the regional model, –1,100 m in the local model) are provided for each domain. The assessment of confidence at the surface is coupled to the confidence in the geological map of the bedrock in the regional model area. The assessment of confidence at depth is coupled to the number and depth of intersections of a particular domain in the boreholes.

The documented properties of each rock domain include the character of the dominant and subordinate rock types, the degree of homogeneity, the character of alteration and metamorphism, and the character and orientation of the ductile structures. The properties of the dominant rock type in a domain include, for example, quartz content from modal analyses, density, and natural exposure rate from *in situ* gamma-ray spectrometry measurements. Quantitative estimates of the uncertainty in some of the properties, the source of the primary data used in the assignment of a particular property and the level of confidence in the assignment (high, medium or low) are all presented.

Integration with the modelling of thermal properties (see chapter 6) recognised the need for a better understanding of the thickness, the frequency of different thickness classes, and the orientation of subordinate rock types in the target volume, in particular the metamorphosed dykes and lenses that occur as amphibolite (/Stephens et al. 2007/ and section 5.2.3). This work has contributed to the stochastic simulations of the subordinate rock types in the target volume (see chapter 6). The defined rock domains were judged appropriate for the purposes of safety assessment and no feedback was obtained from SR-Can on this subject (see /SKB 2006b/).

5.4.4 Division into rock domains, geometries and property assignment

The identification of rock domains was initiated at the surface and made use of the division of the bedrock during the bedrock mapping work into two different types of rock units (see Table 4-3 in /Stephens et al. 2007/ and section 5.2.1). These are defined on the basis of:

- The composition and to, some extent, the grain size of the dominant rock type.
- The degree of bedrock homogeneity in combination with the style and degree of ductile deformation.

The inferred distributions of rock domains at the surface in both the regional and local model areas are shown in Figure 5-24. Rock domains have been identified on the basis of all the combinations in the two types of rock unit described above. For example, the composition of the rocks in domains

RFM012 and RFM044 are similar to those in domain RFM029, but the rocks in domains RFM012 and RFM044 are affected by a higher degree of ductile strain with the development of a conspicuous SL-fabric compared with domain RFM029.

Apart from the identification of some rock units on the basis of the character and frequency of fractures, the principles for the division of rock units in the boreholes during the single-hole interpretation followed those used during the surface mapping work. This permits a correlation with the rock domains as defined on the basis of the surface data (Table 4-4 in /Stephens et al. 2007/). Rock domains along all the twenty-one cored boreholes used in model stage 2.2 are presented in Appendix 13 in /Stephens et al. 2007/.

Fourteen rock domains have been recognised inside the local model volume. Most of these domains are situated outside the tectonic lens and target volume, on the south-western or north-eastern limbs of the synform that is part of the inferred major sheath fold (Figure 5-25). All the domains in these marginal volumes dip steeply towards the south-west. Key domains RFM029 and RFM045 occur inside the tectonic lens and target volume, in the hinge of the synform, which plunges moderately to steeply (55–60°) to the south-east (Figure 5-25). The properties of the rock domains have been presented in Appendix 14 in /Stephens et al. 2007/. A description of the key domains RFM029 and RFM045 follows below.

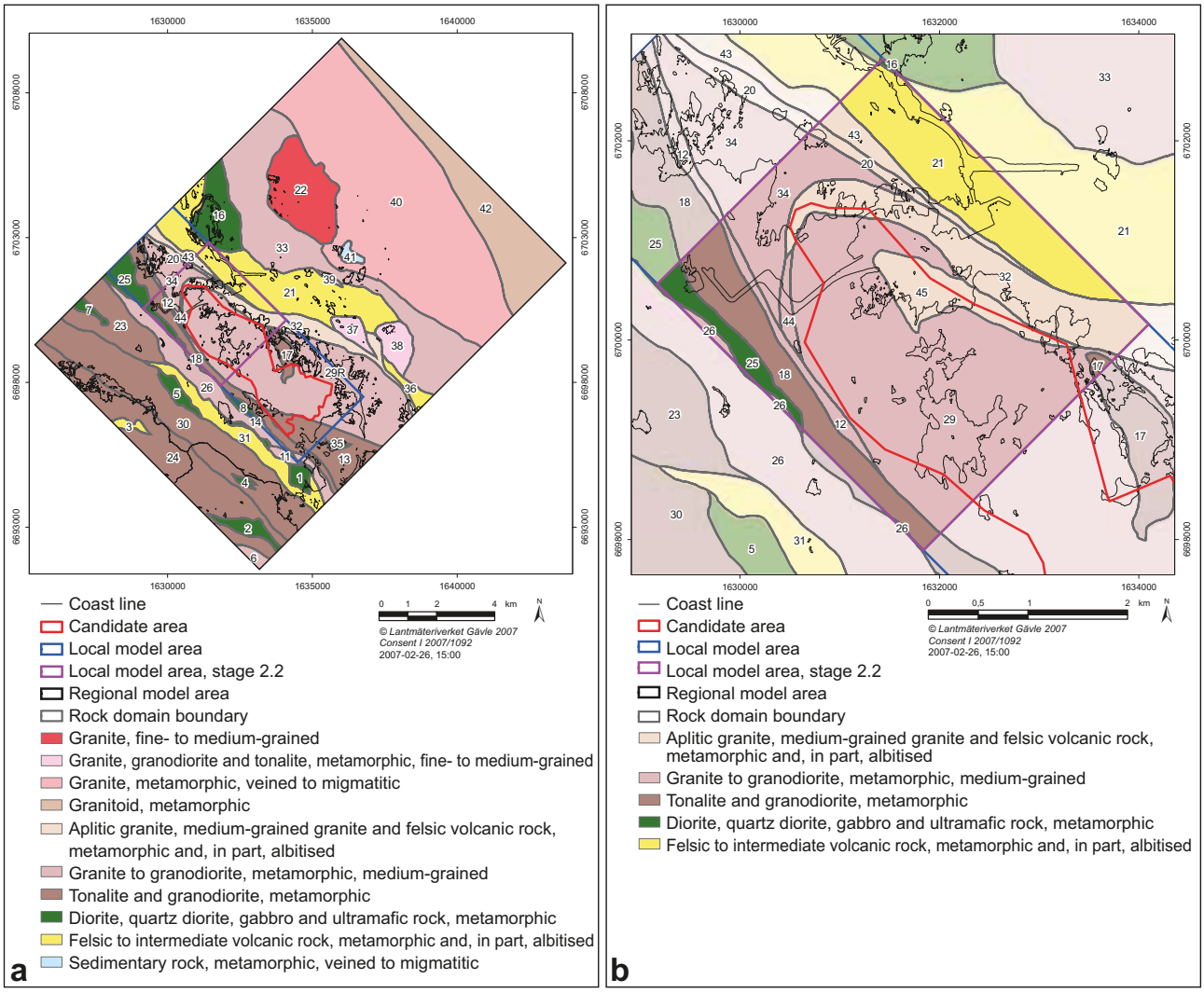

Figure 5-24. *Rock domains included in the two dimensional models at the ground surface, stage 2.2. a) Model inside the regional model area. b) Model inside the local model area (darker colours). The different colours represent the dominant rock type in each domain. As in previous models, the degree of homogeneity in combination with the style and degree of ductile deformation (not shown here) have also been used to distinguish domains. Coordinates are provided using the RT 90 (RAK) system.*

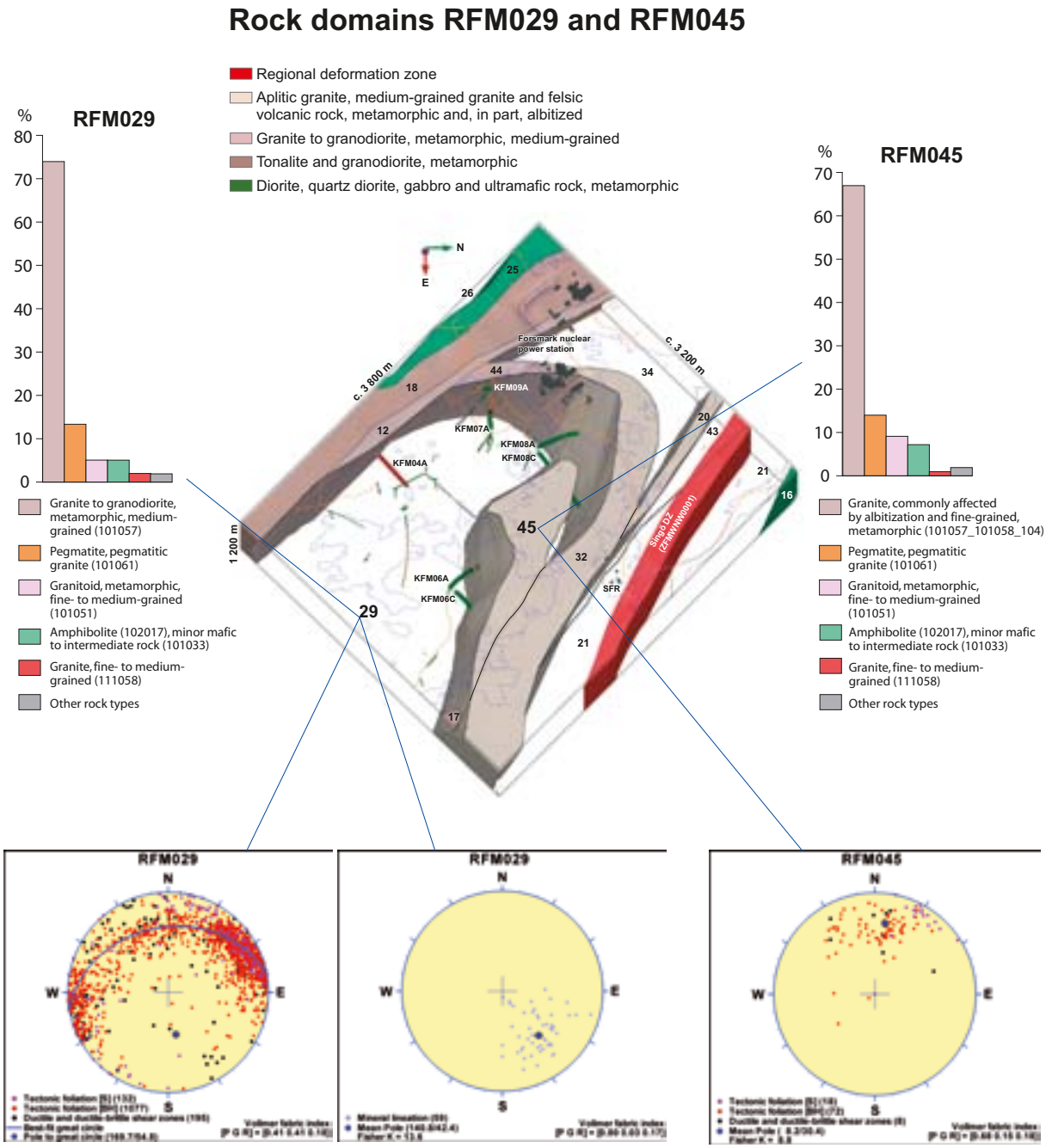

Figure 5-25. *Rock domains (numbered) included in the three dimensional local model, stage 2.2. The model is viewed to the west towards SFR and the nuclear power station from a position above the local model volume and approximately 2 km to the south-east of the SFR repository. The target volume consists of domains RFM029 and RFM045 in the hinge of the major synform. Boreholes marked by larger cylinders constrain the boundaries between different domains with the help of fixed-point intersections. Quantitative estimates of the proportions of different rock types in rock domains RFM029 and RFM045 are shown in the histograms and the orientation of ductile structures inside these two rock domains are shown in the stereographic projections (equal-area, lower hemisphere). Planar structures are plotted as poles to planes. An estimation of the degree of point, girdle or random distribution pattern (Vollmer fabric index, PGR) is provided. No Terzaghi correction has been applied. The data come from the surface and from several boreholes with different orientations.*

Rock domain RFM029

Rock domain RFM029 is the volumetrically most significant domain inside that part of the Forsmark tectonic lens that is situated inside the local model volume, i.e. the target volume for a potential repository (Figure 5-24b and Figure 5-25). It has been modelled by simply infilling the volume that is situated between the surrounding domains, the geometries of which are constrained by surface data and fixed point intersections along cored boreholes. It is estimated that medium-grained metagranite comprises 74% of this domain, pegmatite and pegmatitic granite 13%, Group C fine- to medium-grained metagranitoid 5%, and amphibolite and other minor mafic to intermediate rocks 5% (Figure 5-25 and /Stephens et al. 2007/). The subordinate rocks occur as hypabyssal intrusions in the form of isolated minor bodies and lenses or dyke-like sheets.

An analysis of the character and degree of alteration in rock domain RFM029 indicates that, excluding deformation zones, the rocks are essentially fresh /Stephens et al. 2007/. The tendency for a few modal analyses of medium-grained meta-igneous rock to show a granodioritic composition is possibly related to incipient albitization, similar to that observed more frequently in rock domain RFM045 (see below).

Ductile planar structures (i.e. the tectonic foliation and the ductile or ductile-brittle shear zones) define a girdle distribution pattern on the lower hemisphere of an equal-area stereographic projection (Figure 5-25). This pattern confirms large-scale folding of these ductile structures inside the domain with a fold axis that plunges 170°/55° (Figure 5-25). This is in good agreement with the orientation of the major synform inside the Forsmark tectonic lens as inferred from the geometric modelling work (55–60° to the south-east). The mean value of the mineral lineation data from the surface is similar in orientation to, but plunges more to the east and a little more gently than the major fold axis inferred inside the local model volume (Figure 5-25). A linear anisotropy, with both folding and stretching that plunge moderately to the SSE and SE, respectively, is apparent in domain RFM029.

Rock domain RFM045

Rock domain RFM045 forms a subordinate component inside the target volume (Figure 5-24b and Figure 5-25). The domain is distinguished primarily by the conspicuous occurrence of albitized and metamorphosed granitic rocks, and a generally finer grain size than rock domain RFM029. This domain has been modelled as a constricted rod, more or less parallel to the mineral stretching lineation in the north-western part of the tectonic lens. It lies in the hinge of the major synform and has been modelled to extend to the base of the local model volume.

Granitic rocks, with a variable content of biotite and a variable grain size, comprise 67% of this rock domain (Figure 5-25). These rocks are commonly but not pervasively affected by the alteration referred to as albitization. Modal analyses indicate that this alteration gave rise to an increased content of quartz and a marked decrease in the content of K-feldspar, relative to the equivalent unaltered rocks (see section 5.2.3). The latter is also expressed by lower values for the natural exposure rate that are calculated on the basis of *in situ* gamma-ray spectrometry measurements. Subordinate rock types include, in relative order of volumetric importance (Figure 5-25), pegmatite and pegmatitic granite (14%), Group C fine- to medium-grained metagranitoid (9%), and amphibolite and other minor mafic to intermediate rocks (7%). It is suggested that the increase in the younger intrusive rocks, amphibolite and even Group C fine- to medium-grained metagranitoid, relative to that observed in rock domain RFM029, accounts for the prominent, pre-metamorphic alteration in this domain (see also section 5.2.3).

Ductile planar structures (i.e. the tectonic foliation and the ductile or ductile-brittle shear zones) vary somewhat in orientation as can be seen on the lower hemisphere of the equal-area stereographic projection (Figure 5-25). The mean pole to these planar structures plunges moderately to steeply (60°) towards the SSW and the Fisher κ value for the pole data is low (< 10). There are too few measurements of mineral lineation at the surface to justify any comment on their broader implications.

5.5 Deterministic model for deformation zones

5.5.1 Data input

The deterministic modelling of deformation zones has primarily made use of the following data and interpretations:

- The geological evolution of the Forsmark area in a regional geological perspective (/Söderbäck (ed) 2008/ and summary in section 3.1).
- The geological framework established during the crystallisation and ductile deformational history of the site, which is expressed in both 2D and 3D geological models (sections 5.2.1 and 5.4, respectively).
- The identification and description of possible deformation zones in the single-hole interpretation of cored and percussion boreholes (section 5.2.2).
- The characterisation of brittle strain along deformation zones with the help of data both from the surface and from boreholes (sections 5.2.5 and 5.2.6).
- The character and evaluation of the geological significance of lineaments that have been inferred with the help of helicopter airborne magnetic data and, in the target area, high-resolution ground magnetic data (section 5.2.7).
- The character and evaluation of the geological significance of seismic reflection data (section 5.2.8).
- The evaluation of the complex interplay between lineaments and seismic refraction data (section 5.2.9).

5.5.2 Conceptual model

Influence of anisotropy in the ductile regime on deformation in the brittle regime

The ductile deformation between 1.87 and 1.85 Ga at Forsmark contributed to the development of strong bedrock anisotropy at the site. The subsequent, 1.85 Ga and younger tectonic evolution gave rise to sets (and sub-sets) of deformation zones with different orientations, properties and spatial distributions, guided by the older bedrock anisotropy /Stephens et al. 2007/.

Vertical and steeply dipping deformation zones that strike WNW-ESE and NW-SE are restricted to the margins of and to the high-strain belts outside the Forsmark tectonic lens. Several of these zones show both ductile and polyphase brittle strain. The zones with a dip less than 90° dip to the south or south-west. For purposes of simplicity in the text that follows, these zones are referred to as the steep (or steeply dipping) WNW and NW sub-sets, respectively, (see /Stephens et al. 2007, section 2.4/ for nomenclatural considerations).

By contrast, the target volume at 400 to 500 m depth inside the lens is intersected by vertical and steeply dipping brittle deformation zones (fracture zones) that strike ENE-WSW to NNE-SSW. The zones with a dip less than 90° dip in both directions but predominantly to the NNW to WNW. These zones are labelled steep (or steeply dipping) ENE (NE) and NNE sub-sets in the following text. Since there are relatively few zones in this group that strike strictly NE-SW, the direction NE has been enclosed in parentheses. Although some gently, south- and SE-dipping fracture zones occur in this volume above 500 m depth, such zones are more conspicuous in the south-eastern part of the tectonic lens, outside the target volume. In this part of the bedrock, the ductile deformational structures and rock contacts are also gently dipping. Finally, a few vertical and steeply dipping deformation zones with NNW-SSE strike are present both inside and outside the Forsmark tectonic lens. The zones with a dip less than 90° dip in both directions, mostly to the WSW but also to the ENE. Once again, for purposes of simplicity, these zones are referred to as the steep (or steeply dipping) NNW set.

Conceptually, it is proposed that the gently dipping zones in the south-eastern part of the Forsmark lens follow boudinaged layers of amphibolite /Juhlin and Stephens 2006, Stephens et al. 2007, p. 158–159/, a subordinate rock type that is oriented parallel to the ductile fabric in the bedrock (see section 5.2.4). This spatial relationship steers the increased frequency of such structures in the south-eastern compared with the targeted, north-western part of the tectonic lens. The termination of the gently dipping zones in the geological model is based on the concept that they formed after the steeply dipping WNW and NW zones, and more or less at the same time as the steeply dipping ENE to NNE zones and at least some of the steeply dipping NNW zones. Moderately to steeply dipping and folded contacts and ductile structures inside the targeted, north-western part of the lens mitigates against any simple correlation between the occurrence of fracture zones and the occurrence of subordinate rock types in this volume.

Geodynamic evolution

Two different types of geological process have provided a profound impact on the geodynamic evolution in south-eastern Sweden, including the Forsmark area (section 3.1 and Figure 3-3), and thereby influence the conceptual thinking. These types of process comprise the following.

- Igneous activity and crustal deformation along an active continental margin at different time intervals mostly during Proterozoic time.
- Loading and unloading cycles around and after c. 1.45 Ga that are related to the deposition and denudation, respectively, of sedimentary rocks or glacial material. The sedimentary rocks formed in response to far-field tectonic activity, and glaciations occurred due to radical change in climate. The loading and unloading cycles are coupled with the burial and exhumation, respectively, of the older crystalline bedrock.

As the effects of regional tectonic activity waned in south-eastern Sweden and shifted to a far-field realm, so the effects of loading with stress build-up and unloading with release of stress, increased in significance (see Figure 3-3 in chapter 3). Naturally, the variation in the build up of stress at any single place will depend on other factors. The inferred bulk crustal shortening during different regional tectonic events are shown in Figure 3-3 in chapter 3.

A conceptual model for the formation and reactivation of the different sets of deformation zones has successively grown in confidence as progressively more data have been acquired /SKB 2005a, 2006a, Juhlin and Stephens 2006, Stephens et al. 2007/. The current model for the site is shown in Figure 5-26. Bearing in mind the character of the zones, this model predominantly concerns the brittle deformational history. The model has emerged with the use of low-temperature geochronological data that has shed light on the exhumation and cooling history, the relative time relationships and absolute ages of fracture minerals, and a comparison of kinematic data from brittle structures along deformation zones with the tectonic evolution in a regional perspective. For a more detailed overview and evaluation of these data, the reader is referred to /Söderbäck (ed) 2008/ and section 5.2.6.

General character of a fracture zone at potential repository depth at Forsmark

The conceptual thinking also penetrates upwards in scale, to an individual, steeply dipping fracture zone at 400 to 500 m depth inside the north-western, targeted part of the tectonic lens at Forsmark (Figure 5-27). This is necessary as a prerequisite to the modelling work, since such zones are relevant in this volume and since data bearing on their character arise, in general, from a highly limited number of borehole intersections and even more limited surface data. The fracture zone concept makes use of the generally accepted division of zones into undeformed host rock, transition or damage zone, and fault core, e.g. /Caine et al. 1996, Gudmundsson et al. 2001, Munier et al. 2003/, as well as the site-specific characterisation in the single-hole interpretation work (section 5.2.6).

The host rock outside a steeply dipping fracture zone inside the lens shows a low frequency of fractures and little or no pervasive alteration. The transition or damage part of the zone, which can range in thickness from a few metres up to several tens of metres, contains a higher frequency of fractures and a more conspicuous hydrothermal alteration. The latter is defined by fine-grained

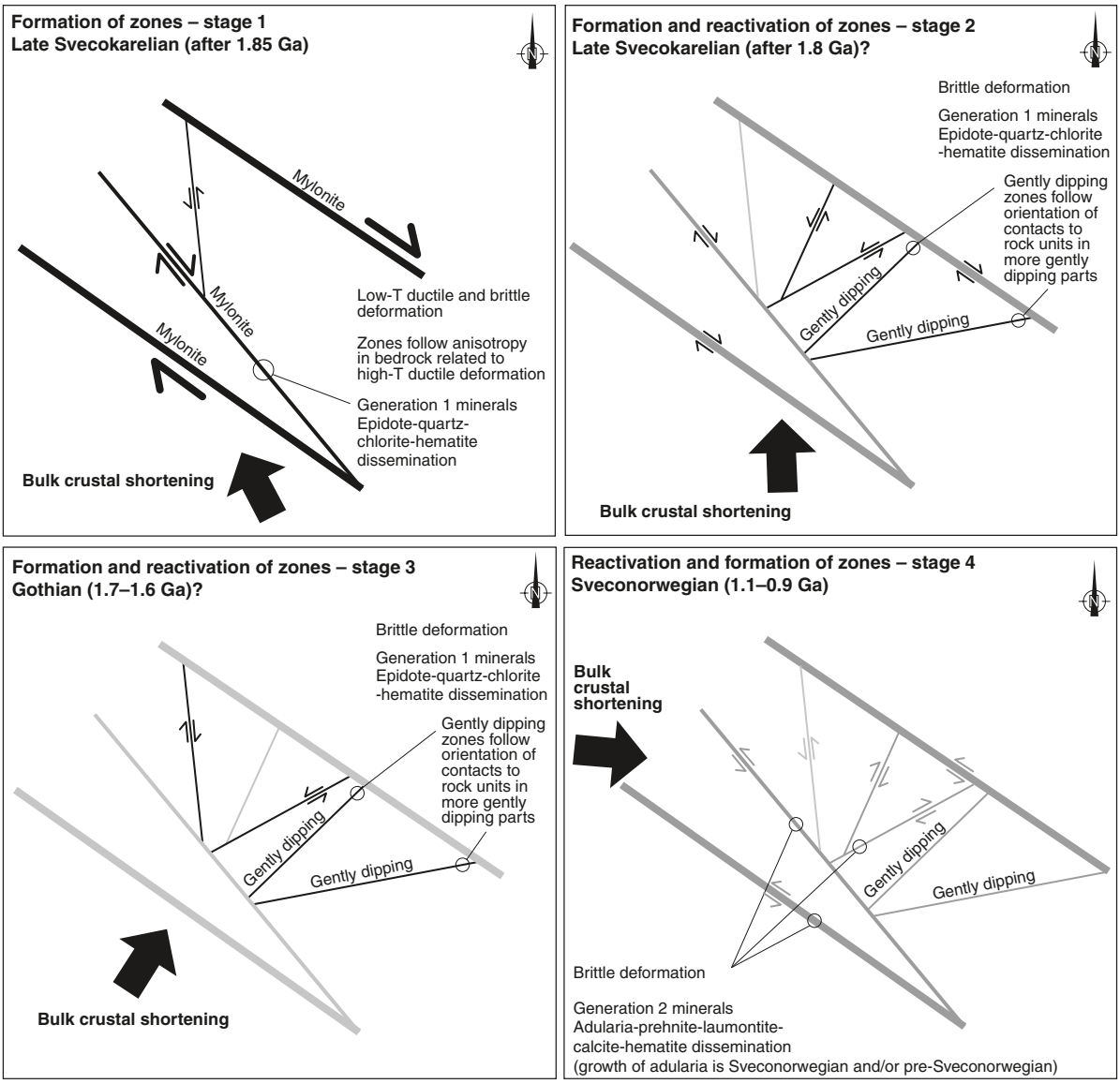

Figure 5-26. *Two-dimensional cartoons illustrating the regional scale geodynamics during the formation and reactivation of the different sets of deformation zones at the Forsmark site. This includes late Svecokarelian, low-T ductile and brittle deformation (stage 1), late Svecokarelian brittle deformation (stage 2), Gothian brittle deformation (stage 3), and a major phase of brittle reactivation during the Sveconorwegian orogeny (stage 4). Formation of fractures and fracture zones during stage 4 cannot be ruled out. The different colour shadings along the zones indicate an inferred variable degree of response (strongest is black, intermediate is grey, weakest is pale grey) in each tectonic regime (modified after /Stephens et al. 2007/).*

hematite dissemination (red staining) of the minerals along and the wall rock adjacent to fractures. Both sealed and open fractures usually increase in abundance inside the zones. However, the transition zone can also contain segments of bedrock that resemble the unaffected host rock outside the fracture zone (Figure 5-27).

In the cases where a fault core has been recognised along a zone (55% of the zones studied in boreholes), it is composed of a high frequency, especially of sealed fractures, commonly in the form of a complex sealed fracture network, in combination with rock alteration. Cohesive breccia or cataclasite are also conspicuous along some fault cores at Forsmark. The thickness of the fault core may vary from a few centimetres up to a few metres. Fault gouge has not been recognised along the fracture zones.

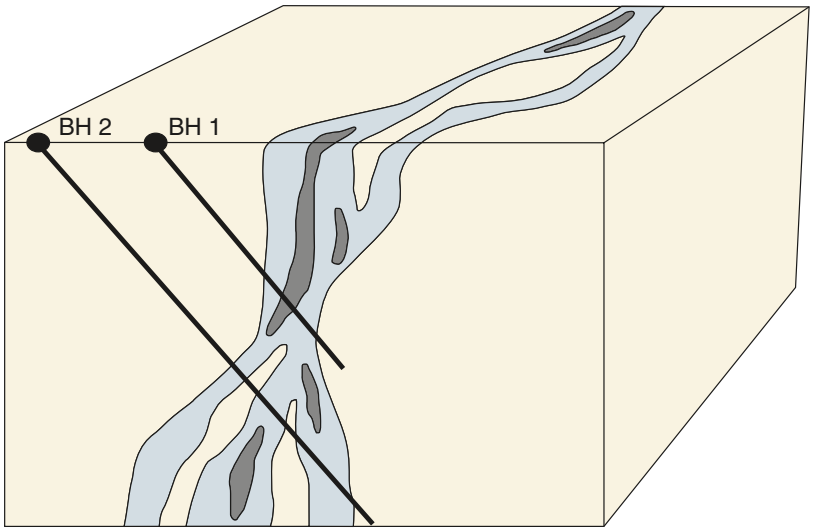

Fault core (e.g. sealed network, cohesive breccia, cataclasite, rock alteration)

Transition (damage) zone (fracture frequency and rock alteration anomalous relative to rock outside zone)

Rock outside brittle deformation zone

(redrawn after /Caine et al. 1996/)

Figure 5-27. *Schematic cartoon illustrating a conceptual geometric model for a fracture zone inside the north-western, targeted part of the tectonic lens at Forsmark (redrawn after /Caine et al. 1996/). Minor shear displacement has occurred along the zone at different times during the long geological history.*

5.5.3 Methodology, assumptions and feedback from other disciplines

Identification and geometric modelling of steeply dipping or vertical deformation zones

The structural model for the steeply dipping (> 70°) or vertical deformation zones in the vicinity of SFR and along tunnels 1-2 and 3 /Axelsson and Hansen 1997, Glamheden et al. 2007b/ has been incorporated, with only minor modification, into the stage 2.2 deterministic model for deformation zones at the Forsmark site /Stephens et al. 2007/. All other steeply dipping or vertical deformation zones have been identified by an integration of low magnetic lineaments with borehole and, to a less extent, tunnel data.

The matching of a low magnetic lineament to a possible deformation zone in the single-hole interpretation, or, in a few cases, along a tunnel, makes use of the overall character of the zone in the borehole or tunnel, in particular the analysis of the orientation of fractures and the character of the hydrothermal alteration along the zone. All fractures not visible in BIPS were removed from the orientation analysis. Apart from two minor zones that have been modelled deterministically, the orientation of a zone is not determined by the orientation of fractures inside the zone. The orientation of fractures along an inferred zone has only been used as a support for the correlation procedure. Thus, as for rock domains, the modelling methodology is only sensitive to the orientation of the boreholes, i.e. to the borehole deviation measurements /Munier and Stigsson 2007/.

In the cases where a deformation zone is inferred to correspond at the surface to a low magnetic lineament, the strike of the zone is assumed to be determined by the trend of the matching lineament. The decision to match a particular low magnetic lineament with a particular borehole determines the dip of the zone. The dip of medium confidence zones (see below) is estimated by comparison with the dip of high confidence zones in the same set or sub-set.

The along-strike termination of steeply dipping or vertical zones is determined by the truncation pattern of the corresponding lineaments, and follows the conceptual model for the site. In this manner, the surface length of such zones is determined by the length of the matching lineament. Termination

of zones at depth, which fail to intersect other zones, is carried out on the assumption that the zone extends to a depth that is approximately the same as its trace length at the surface.

Identification and geometric modelling of gently dipping deformation zones

The structural model for the gently dipping fracture zone H2 in the vicinity of SFR /Holmén and Stigsson 2001/ has been incorporated, with only minor modification, into the stage 2.2 deterministic model for deformation zones at the site /Stephens et al. 2007/. Other gently dipping zones have been identified on the basis of the occurrence of prominent reflectors in the seismic reflection data, with minor adjustments that take account of fixed point intersections with possible deformation zones in the single-hole interpretations. The orientation of the gently dipping zones is provided by the inferred orientation of the corresponding seismic reflector in the surface data. Once again, the orientation of fractures along an inferred zone has only been used as a support for the correlation procedure. It is emphasised again that the orientation of the modelled zone is not based on the orientation of the fractures inside the zone.

In accordance with the conceptual model for the site, the gently dipping zones are assumed to terminate against the spatially nearest, significant steeply dipping deformation zone, both along their strike and in the down-dip direction. Some gently dipping zones have also been terminated against other gently dipping zones and this has resulted in a splay-like relationship between these structures.

Confidence of existence

A high confidence of existence is applied to all zones that have been confirmed directly by geological data from a borehole or tunnel, or from the surface (see Appendix 13 in /Stephens et al. 2007/). In general, indirect data (e.g. low magnetic lineament, seismic reflector) are also present. By contrast, a medium confidence zone generally lacks direct confirmatory data and the zone has been identified solely by the occurrence of a low magnetic lineament or a seismic reflector. In a few cases, a zone has been classified as medium confidence on the basis of low fracture frequency and limited bedrock alteration along borehole intersections.

Assignment of properties

The properties assigned to each deformation zone include spatial position, orientation, thickness, trace length at the ground surface, style of deformation, character of alteration, fracture orientation, fracture frequency, fracture filling and sense of displacement. Mean poles and Fisher κ values in fracture orientation sets have been derived in the same manner as in the DFN work (see Appendix 15 in /Stephens et al. 2007/ and section 5.6.3). Numerical estimates of the uncertainty in some of these properties, the source of the primary data used in the assignment of a particular property, and the level of confidence in the assignment are all presented. These features are discussed in more detail in Appendix 15 in /Stephens et al. 2007/.

Where geological and geophysical data from borehole, tunnel or surface investigations are available, the properties of the zones are relatively well-constrained and, in many cases, a property is assigned a high level of confidence. However, properties are most commonly derived from a restricted number of borehole intersections and, only in a few cases, from tunnel investigations, surface outcrops or surface excavation. For this reason, the estimates of properties need to be treated with extreme care when extrapolating to the bedrock between, for example, borehole intersections. Where geological and geophysical data from borehole, tunnel or surface investigations are lacking, the assignment of properties is much more limited.

Feedback from other disciplines

The results of hydraulic interference tests (section 8.3.3), carried out with the aim of investigating the hydraulic connection between different boreholes along specific deformation zones, have provided important support for the geometric modelling of these zones. Interference tests have also demonstrated an excellent hydraulic connection in the upper part of the bedrock in the target volume (section 8.4.4). The integration of structural geological data, hydrogeological data and data bearing on the orientation and magnitude of the current principal stresses in the bedrock have resulted in a broader conceptual understanding of the site (/Juhlin and Stephens 2006, Follin et al. 2008b/, and

sections 5.5.2, 5.6.1 and 11.6). A critical feedback from the SR-Can project for the deterministic modelling of deformation zones concerns the necessity to identify and to assign properties to all zones with a trace length at the ground surface that exceeds 3,000 m /SKB 2006b/.

5.5.4 Geometric models and property assignment

Sixty deformation zones, the majority of which have been assigned a high confidence of existence, are included in the local model, stage 2.2 /Stephens et al. 2007/. Inspection of the orientation plot (Figure 5-28a) indicates that these zones are predominantly vertical or steeply dipping, with WNW, NW, ENE (NE) and NNE sub-sets, or gently dipping with dips to the south and SE. A few deformation zones that are vertical or steeply dipping and oriented NNW or E-W are also present (Figure 5-28a). The frequency of the vertical and steeply dipping zones increases as their surface length decreases and the size of these zones follows a power-law distribution with a slope of 1.08 (Figure 5-28b).

Both the orientation and size distribution of the vertical and steeply dipping zones, in the regional model, strongly resemble the equivalent parameters in the local model (Figure 5-28a, b and c). However, relative to the local model, the regional model is characterised by a higher proportion of vertical and steeply dipping zones in the WNW and NW sub-sets and an increased proportion of gently dipping zones /Stephens et al. 2007/. The modelling work inside the local model volume also identified several minor fracture zones with trace lengths at the ground surface shorter than 1,000 m /Stephens et al. 2007/. These zones are vertical or steeply dipping and belong predominantly to the ENE to NNE set (Figure 5-28d). A few minor zones that are oriented NNW, WNW and E-W are also present.

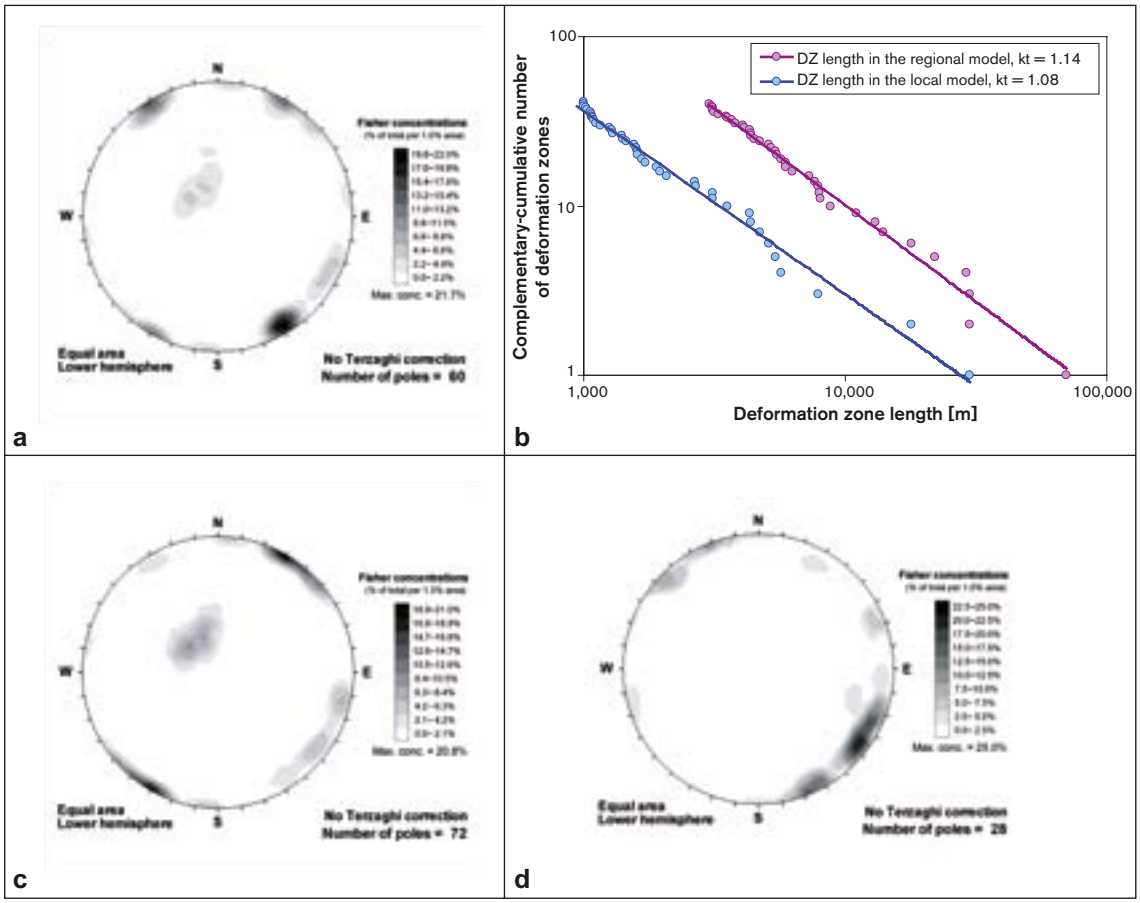

Figure 5-28. Orientation and trace length distribution of deformation zones at Forsmark. a) Orientation of deformation zones included in the local model (stage 2.2). b) Trace length distribution of the vertical and steeply dipping deformation zones included in the local and regional models (stage 2.2). c) Orientation of deformation zones included in the regional model (stage 2.2). d) Orientation of minor fracture zones that were modelled deterministically inside the local model volume during model stage 2.2. The orientations of zones in the stereographic projections (equal-area, lower hemisphere) are shown as poles to planes.

The vertical or steeply dipping deformation zones in the sub-sets referred to as WNW and NW, occur in the south-western and north-eastern peripheral parts of the local model volume, i.e. along or outside the margins of the Forsmark tectonic lens (Figure 5-29). Several of these zones have trace

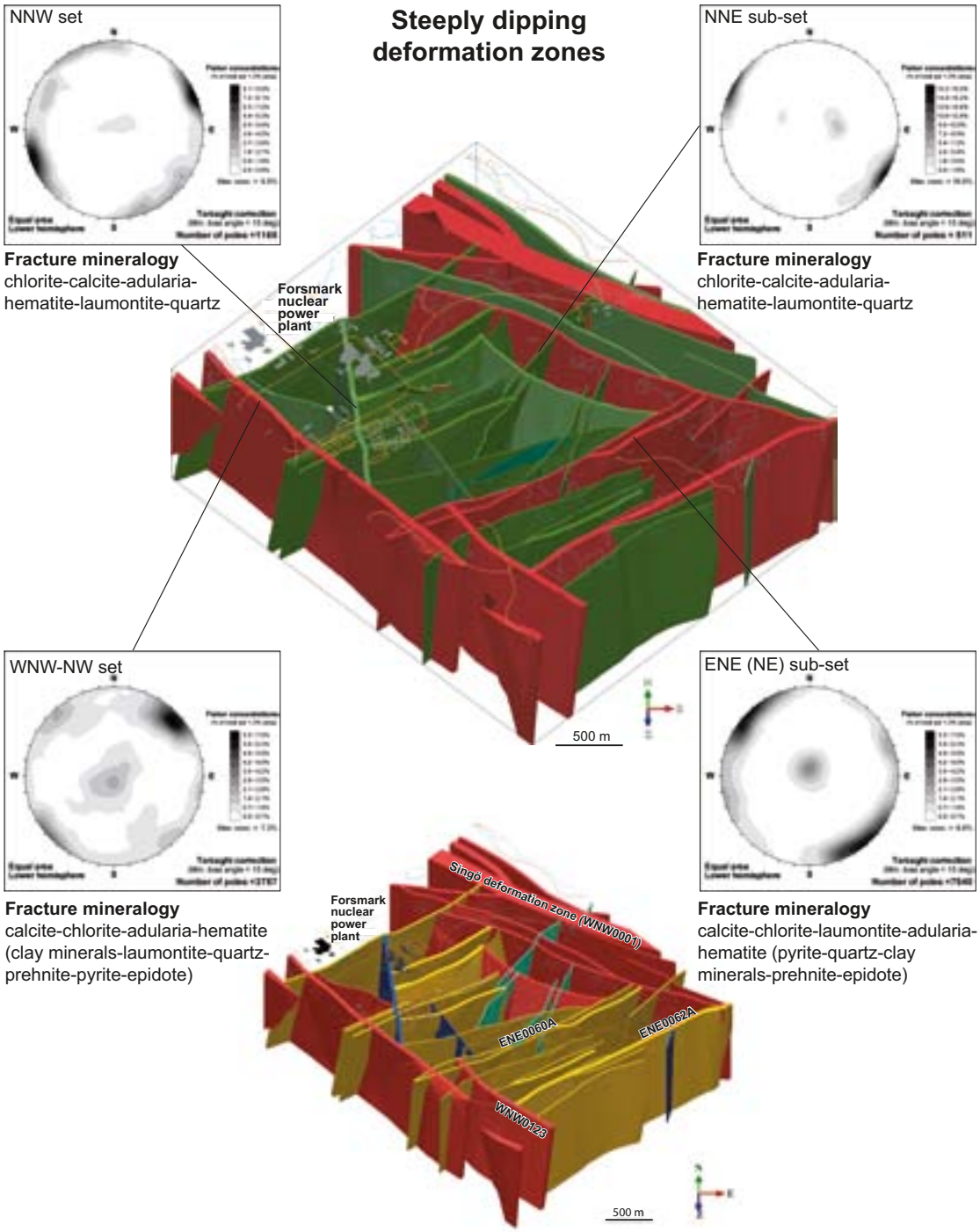

Figure 5-29. *Vertical or steeply dipping deformation zones included in the three dimensional local model, stage 2.2. In the upper model figure (viewed to the north), zones marked in red have a trace length at the ground surface longer than 3,000 m and zones marked in green are between 1,000 and 3,000 m in trace length. The orientation of fractures inside the different sets or sub-sets of vertical or steeply dipping deformation zones, which are included in the local model (stage 2.2), are plotted as poles to planes in stereographic projections (equal-area, lower hemisphere) and contoured. A Terzaghi correction has been applied in these plots. The fracture mineralogy along each set or sub-set is also shown and the order of mineral presentation reflects the order of abundance (based on Figure 5-18 and Appendix 17 in /Stephens et al. 2007/). The zones in each orientation set or sub-set are distinguished in the lower model figure (viewed to the north). In this figure, red = WNW to NW set, yellow = ENE (NE) sub-set, green = NNE sub-set and blue = NNW set.*

lengths at the ground surface longer than 3,000 m. These zones follow the general structural trend defined by rock contacts and the ductile planar grain-shape fabric. The subordinate set of vertical and steeply dipping fracture zones referred to as NNW also follows the ductile fabric in the bedrock.

By contrast, inside the local model volume and tectonic lens, where the ductile fabric is folded and more variable in orientation (see section 5.2.4), the bedrock is intersected, more or less exclusively, by vertical or steeply dipping zones that are included in the ENE (NE) and NNE sub-sets (Figure 5-29). The zones in these two sub-sets are distributed in clusters inside the local model volume. Most conspicuously, there is a concentration of ENE (NE) zones in the south-eastern part and NNE zones in the central part of the local model volume (see also /Stephens et al. 2007, p. 165/). The surface trace length of these zones is predominantly between 1,000 and 3,000 m (Figure 5-29).

Although the position and trace length of several lineaments were modified in connection with an evaluation of the complementary, high-resolution ground magnetic data acquired during stage 2.3, the overall implications for the stage 2.2 geological modelling work are limited in character /Stephens et al. 2008/. In particular, no new deformation zones with a trace length at the ground surface longer than 3,000 m have emerged. The data acquired along borehole KFM08D during stage 2.3, following the establishment of the deformation zone model /Stephens et al. 2007/, confirm the significance of ENE and NNE deformation zones with a trace length shorter than 3,000 m inside the target volume (/Stephens et al. 2008/ and section 5.8). Furthermore, the new data acquired along boreholes KFM11A and KFM12A constrain the properties of the regionally significant Singö and Forsmark zones /Stephens et al. 2008/.

The majority of gently dipping deformation zones are situated outside or in the south-eastern, peripheral part of the local model volume (Figure 5-30a). Only zones A2, A8, B7, F1, 1203 and possibly B4 merit closer attention in the repository design work. From north to south in the south-eastern part of and outside the local model volume, zones A8, A2, F1 and A3 appear to splay off each other in an integrated mesh (Figure 5-30b). In particular, zone A2 in this family defines the roof of the volume that has been identified as potentially suitable for the excavation of a repository /SKB 2005c/. The gently dipping zones A8, B7 and 1203 occupy restricted volumes at predominantly shallow crustal levels in this volume (Figure 5-30a). The data acquired along borehole KFM02B during stage 2.3 have confirmed the occurrence of the gently dipping zones 866, A3, A2 and F1 beneath drill site 2 /Stephens et al. 2008/.

The properties of deformation zones included in the deterministic models at different scales were presented in Appendix 15 in /Stephens et al. 2007/. Most of the data have been acquired from the local model volume. In addition, the properties of some minor deformation zones with surface trace lengths shorter than 1,000 m, which are located in the local model volume, were presented in Appendix 16 in /Stephens et al. 2007/. Compilations of fracture orientation, fracture mineralogy and the orientation of fractures separated on the basis of fracture mineralogy in each set (or sub-set) of deformation zones were presented in section 5.3.2 and Appendix 17 in /Stephens et al. 2007/. A generalised summary of the properties for each set (or sub-set), based on these detailed property tables, is presented below.

The geological and hydrogeological properties of the zones that are present at 400 to 600 m depth, inside the potential repository volume, are compiled in Appendix 4. This compilation makes use of an integration of stage 2.2 and stage 2.3 geological and hydrogeological data and stage 2.2 modelling results. The zones in this compilation belong, more or less exclusively, to the vertical or steeply dipping ENE to NNE set.

Vertical or steeply dipping zones in ENE to NNE set

The vertical or steeply dipping deformation zones in the ENE to NNE set have been studied along four excavations at the surface and along several intersections in virtually all the cored boreholes in the local model volume. Zones 3 (NNE0869 in the current nomenclature) and 9 (minor zone NE0870) at SFR are also included in this set.

The surface trace length of the zones included in the local model varies from c. 1,000 m (minor splays or attached branches excluded) to 3,500 m, and most are less than 2,000 m. Only two zones with a surface trace length longer than 3,000 m intersect the target volume (zones ENE0060A and ENE0062A with their attached branches, see Figure 5-29). The thickness of the zones in the ENE

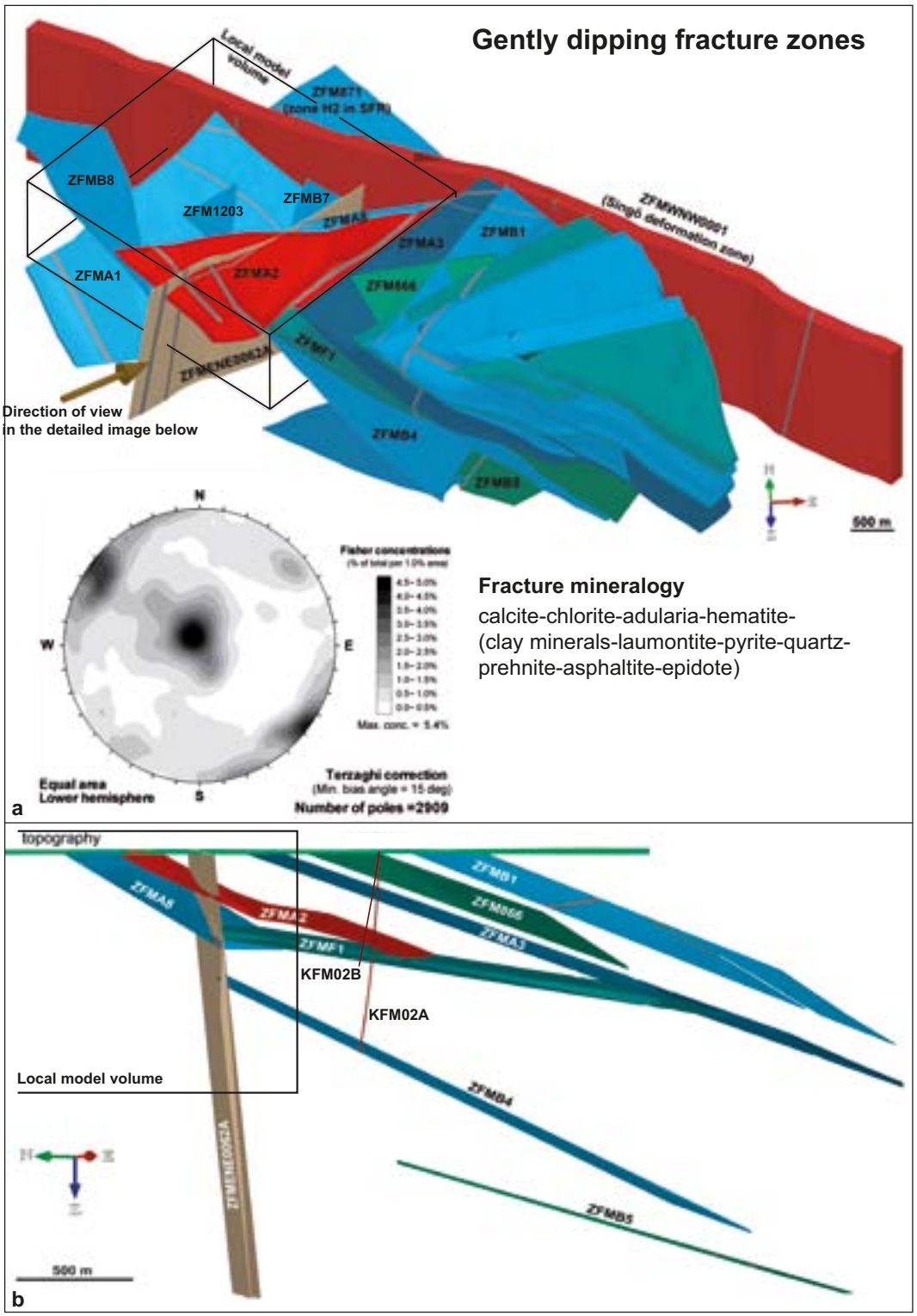

Figure 5-30. *a) Gently dipping deformation zones on both sides of the Singö zone (WNW0001) extracted from the three dimensional regional model for deformation zones. The orientation of fractures inside the gently dipping deformation zones, which are included in the local model (stage 2.2), are plotted as poles to planes in a stereographic projection (equal-area, lower hemisphere) and contoured. In order to limit the bias that is related to the orientation of boreholes, a Terzaghi correction has been applied in this plot. The fracture mineralogy in the gently dipping zones is also shown and the order of mineral presentation reflects the order of abundance (based on Figure 5-18 and Appendix 17 in /Stephens et al. 2007/). b) Apparent splay-like pattern between zones A2, A8, F1 and A3 in the south-eastern part of and outside the local model volume. Boreholes KFM02A and KFM02B and three of the boundaries to the local model volume are also shown. The boundary of the local model volume to the north lies outside the view of the figure.*

to NNE set (21 measurements) varies considerably, with a range between 2 and 45 m, a mean value of 18 m and a standard deviation of 13 m. The measured thickness includes the transition and, if present, the fault core parts of a zone (Figure 5-27). Twenty-three zones, which either show a trace length at the ground surface of 1,000 m or longer or form minor splays or attached branches to such zones, are present at 400 to 600 m depth inside the potential repository volume. A comparison of the properties of minor zones with their longer counterparts in the ENE to NNE set indicates that the properties of the two size classes in this set are very similar /Stephens et al. 2007, p. 181–186/.

The zones in the ENE to NNE set show only brittle deformation and are fracture zones. They have a distinct expression at the surface in the form of lineaments classified as magnetic minima (Figure 5-31a). They are characterised by a high frequency of especially sealed fractures (Figure 5-31b) and conspicuous alteration in the form of red staining (Figure 5-31c). The alteration is related to a fine-grained dissemination of hematite, in both the wall rock to the fractures in the zone as well as in certain minerals (e.g. laumontite, adularia) that fill or coat these fractures. Alteration referred to as quartz dissolution that gave rise to a vuggy rock is also locally present. Fault core intervals consist of a highly elevated fracture frequency, commonly with sealed fracture networks (Figure 5-31b). Locally, cohesive breccia and cataclasite are also present. Fault gouge has not been documented along any of these zones.

Two sets of vertical or steeply dipping fractures that strike ENE to NNE (dominant) and NNW (subordinate), as well as gently dipping to sub-horizontal fractures are conspicuous in the ENE (NE) sub-set of zones (Figure 5-29). Both vertical or steeply dipping fractures that strike NNE and gently dipping fractures are present in the NNE sub-set (Figure 5-29). Calcite and chlorite, together with the minerals laumontite, adularia and hematite, which formed in connection with and/or prior to the Sveconorwegian orogeny, are conspicuous along the fractures in the ENE (NE) sub-set (Figure 5-29). However, the older mineral epidote and younger minerals such as pyrite and clay minerals are also present. The fracture mineralogy is similar in the NNE sub-set. However, adularia and hematite dominate over laumontite.

The kinematic data indicate a dominance of strike-slip displacement and there is evidence for both sinistral and dextral movement along minor, steeply dipping faults that strike ENE to NE inside the zones. Sinistral displacement is more dominant along the NNE minor faults. Nevertheless, dip-slip movement along minor faults has also occurred, even along the same minor fault set inside a specific zone. A complex tectonic evolution under different stress regimes is inferred. Inspection of the magnetic anomaly map suggests that at least the amount of bulk strike-slip displacement along these zones is limited.

Gently dipping zones

The gently dipping deformation zones have been studied along intersections in several cored boreholes, but especially in KFM02A and KFM03A to the south-east of and outside the local model volume. Zone H2 (zone 871 in the current nomenclature) at SFR is also included in this set.

Zones B4 and F1 have been modelled to terminate to the north-west against the steeply dipping zone ENE0062A and only three gently dipping zones (A2, A8 and B7, see Figure 5-30a) enter the target volume between 400 and 600 m depth, north-west of zone ENE0062A. As indicated above, two of these zones, A2 and A8, belong to a family of gently dipping structures that occur along or close to the roof of the volume that has been identified as potentially suitable for the excavation of a waste repository. The thickness of the zones that are present inside the local model volume (10 measurements) varies considerably, with a range between 6 and 44 m, a mean value of 21 m and a standard deviation of 13 m.

The zones in the gently dipping set show only brittle deformation and are fracture zones. They have a distinct expression in the sub-surface realm in the form of seismic reflectors (Figure 5-32a). Relative to all the other sets, they contain a higher frequency of open fractures and non-cohesive crush rock (Figure 5-32b and c). In a similar manner to the steeply dipping or vertical sets, most of the gently dipping zones show bedrock alteration in the form of red staining related to hematite dissemination (Figure 5-32c). Altered vuggy rock with quartz dissolution is also present along some of them (e.g. zone A3). If present, fault core intervals consist of a highly elevated fracture frequency, occasionally with sealed fracture networks or non-cohesive crush rock (Figure 5-32b and c), cohesive breccia and cataclasite. Fault gouge has not been documented along these zones.

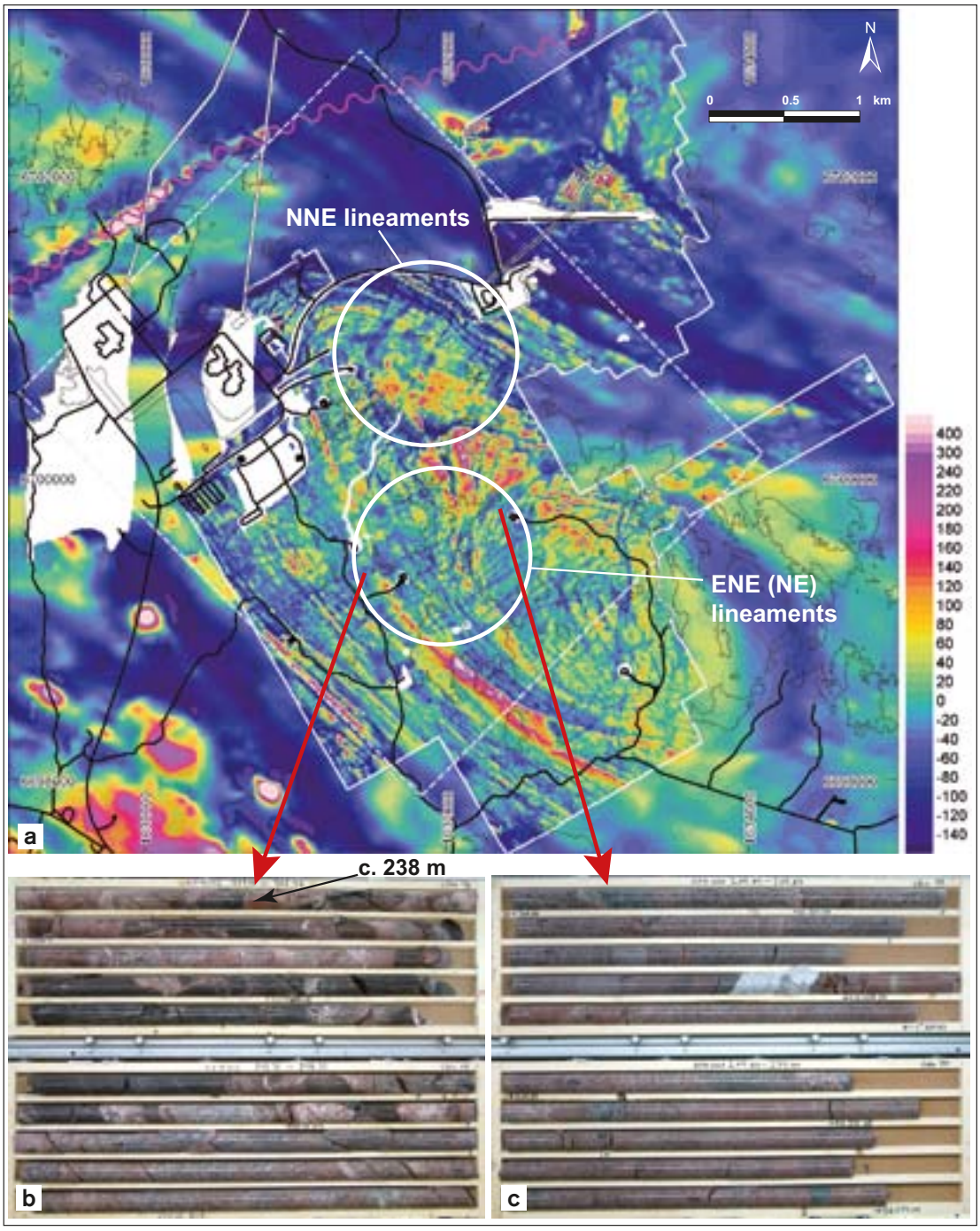

Figure 5-31. *Character of fracture zones in the vertical or steeply dipping, ENE to NNE set. a) Link to lineaments defined by magnetic minima. The map of the total magnetic field is composed of the NS-directed helicopter survey and the high-resolution ground magnetic survey. Units in nanoTesla [nT]. Base level (zero in legend) for the helicopter-borne survey is 51,230 nT and for the ground survey 51,407 nT. The local model area is outlined by a dashed white line and the ground survey areas by a solid white line. White areas represent areas with poor coverage or poor quality due to disturbances. The magenta wavy line represents the location of the Fenno-Scan HVDC (high voltage, direct current) cable. Buildings, roads and drill sites in black. Tunnels and under-ground facilities at SFR are outlined by black lines and white filling. © Lantmäteri-verket Gävle 2007. Consent I 2007/1092. b) Dominance of sealed fractures and sealed fracture networks. The view is from fracture zone ENE0060A in the borehole interval c. 237−248 m in KFM01C (DZ3). It shows metagranite and, in the middle part of the view, amphibolite affected by fractures and fracture networks that are predominantly sealed with laumontite and calcite. A fault core interval has been recognised at c. 238 m /Saintot and Nordgulen 2007/. c) Pervasive dissemination of hematite and red staining. The view is from fracture zone ENE0060B and shows altered metagranite in the borehole interval c. 265−274 m in KFM06A (DZ3).*

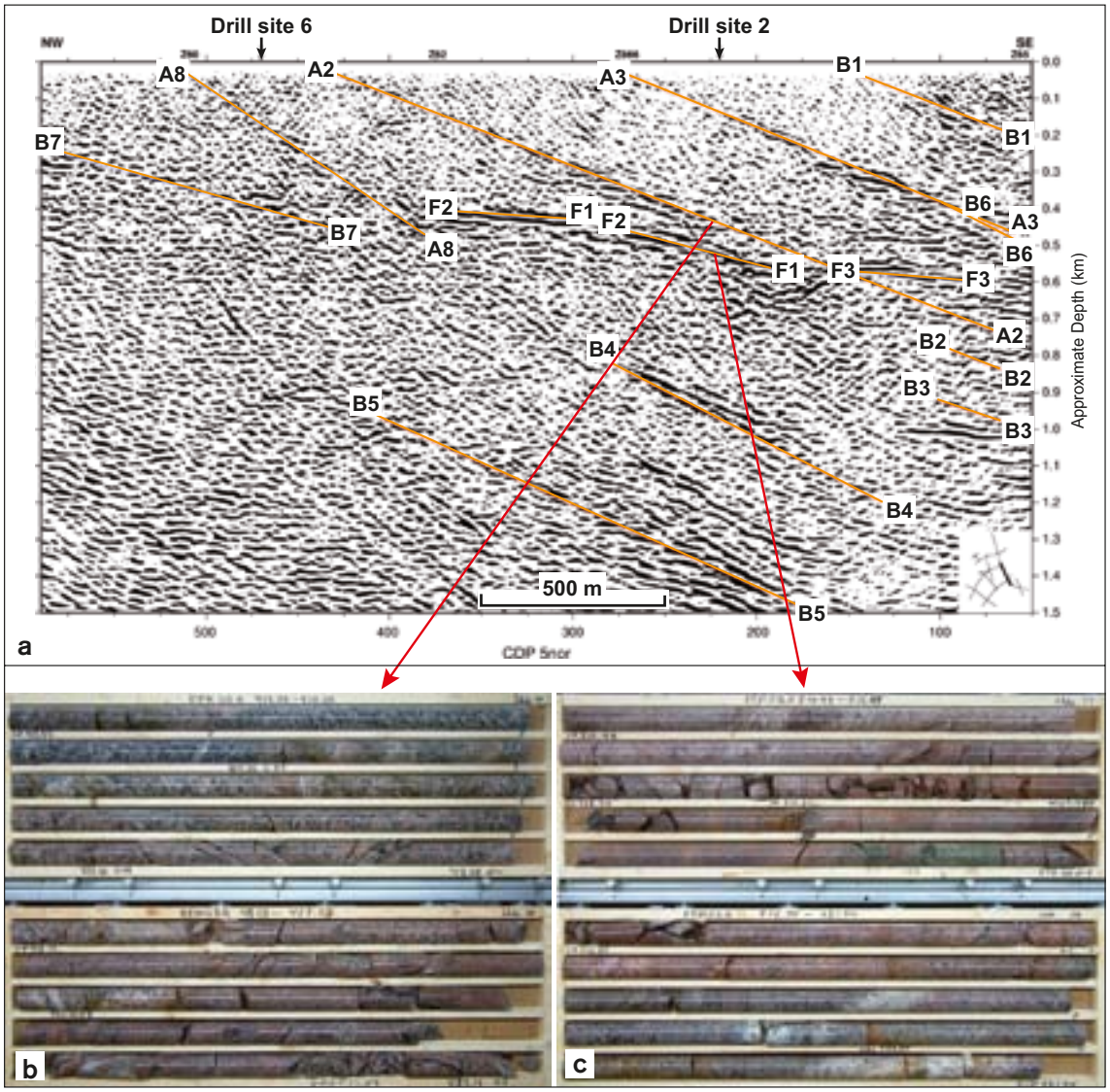

Figure 5-32. *Character of fracture zones in the gently dipping set. a) Link to seismic reflectors (see Figure 5-21). b) Borehole interval c. 413 to 423 m in KFM02A. This interval marks the transition from the bedrock above zone A2, predominantly in the upper drill core box, into the bedrock affected by zone A2 predominantly in the lower drill core box. Open and sealed fractures, crush zones and alteration defined by hematite dissemination and red staining are prominent along zone A2. c) Borehole interval c. 510 to 522 m in KFM02A. This view shows the transition from the bedrock inside zone F1, predominantly in the upper drill core box and approximately half of the lower drill core box, into the bedrock beneath zone F1, in the remainder of the lower drill core box. Similar features as in zone A2 are present inside zone F1. In the single-hole interpretation, both these zones were included in DZ6 along KFM02A.*

Gently dipping to sub-horizontal fractures dominate along the gently dipping zones. However, vertical or steeply dipping fractures that strike ENE to NNE (dominant) and steeply dipping fractures that dip to the south-west (subordinate) are also conspicuous (Figure 5-30a). Fracture mineralogy (Figure 5-30a) is variable. Most zones show a simple fracture mineralogy dominated by calcite and chlorite. Less frequently, adularia and hematite are present, even along the gently dipping fractures in a zone, and clay minerals occur most conspicuously along the gently dipping fractures. By contrast, some zones show a more complex mineralogy with one or more of the minerals that belong to different generations, including laumontite, pyrite, quartz, prehnite, asphaltite and epidote (Figure 5-30a). Furthermore, restricted wall-rock alteration and a high frequency of fractures with no mineral coating or filling are conspicuous along some zones.

It is inferred that fluid movement has occurred along the gently dipping zones at several times during geological time. The apparently simple fracture mineralogy in most zones is an artefact obscuring a long and complex hydrothermal history, i.e. repeated precipitation and dissolution of the older fracture minerals. The possibility that new fractures formed along these zones in connection with and/or after the development of the sub-Cambrian unconformity is suggested by the occurrence of fractures that lack both wall-rock alteration and mineral coating.

Both reverse dip-slip and subordinate strike-slip senses of movement are present along the gently dipping zones, suggesting movement in one or more compressive tectonic regimes /Juhlin and Stephens 2006/. However, fault-slip data are absent along some of them (e.g. zone B1) and these structures are possibly joint zones.

Vertical or steeply dipping zones in WNW to NW set

Only two zones in the WNW to NW set (WNW0123 and WNW2225), with a trace length at the ground surface greater than 1,000 m, are present inside the target volume between 400 and 600 m depth. Both these zones are present in the marginal parts of this volume and one of these zones (WNW0123), along the south-western margin, is longer than 5,000 m (Figure 5-29). The estimated thicknesses of these two zones are 52 m (WNW0123) and 25 m (WNW2225). By contrast, several zones in the WNW to NW set are present along the high-strain belts that surround the Forsmark tectonic lens. These include the regionally important Singö (with associated splays), Forsmark and Eckarfjärden deformation zones (Figure 5-2), all of which are situated a considerable distance (> 1 km) from the targeted part of the local model volume (zones WNW0001, WNW0004 and NW0003, respectively).

Considerable tunnel and borehole (e.g. KFM11A) data, which arise from different depths, are available from the Singö deformation zone. By contrast, only data from one cored borehole (KFM12A) and one percussion borehole (HFM37), and from some outcrops and two percussion boreholes (HFM11 and HFM12) are available from the Forsmark and Eckarfjärden zones, respectively. These three regional deformation zones extend for several tens of kilometres at the ground surface in the northern part of Uppland and range in thickness between c. 50 and 170 m. The summary of the properties of the WNW to NW set of zones below is based mainly on the data from these regional structures.

The zones in the WNW to NW set have a distinct expression at the surface in the form of lineaments that are predominantly concordant with the ductile structural grain in the bedrock, i.e. magnetic minima connections (Figure 5-33a). The zones are dominated by sealed fractures and sealed fracture networks. However, an increased frequency of open fractures and non-cohesive crush rock is also present at different intervals inside several of these zones. Both ductile and brittle fault rocks, including mylonites and protomylonites (Figure 5-16a and Figure 5-16b, respectively), cataclastic rocks and cohesive breccias, are present.

Several fault core intervals, which are up to several tens of metres thick, are present within the regionally important Singö and Forsmark zones (Figure 5-33b, c). In particular, strongly cataclastic rock, along a c. 25 m borehole interval, defines the most conspicuous fault core interval along the Forsmark zone (Figure 5-33c). Although non-cohesive crush rock and fractures filled with clay minerals have been recorded along fault core intervals in tunnels that intersect the Singö zone /Glamheden et al. 2007b/, no fault gouge has been documented along any of the zones. It is clear that the zones in the WNW to NW set initiated their development in the ductile regime but continued to be active in the brittle regime, i.e. they are composite structures.

Alteration in the form of red staining that is related to hematite dissemination is common and quartz dissolution with the development of vuggy rock is present along some of the zones (e.g. Forsmark zone, zone WNW0123). Other types of alteration, which gave rise to the development of muscovite- and talc-rich rocks, are present at depth inside the Singö zone.

The zones in the WNW to NW set contain vertical or steeply dipping sets of fractures that strike NW, NE and NNE, as well as gently dipping to sub-horizontal fractures (Figure 5-29). Epidote and chlorite are conspicuous along the fractures studied along the surface in the Eckarfjärden zone (NW0003), while calcite, chlorite and, less commonly, adularia and hematite are more conspicuous in the intersections of the WNW to NW set of zones along boreholes (Figure 5-29). Other minerals, including clay minerals, laumontite, quartz, prehnite, pyrite and epidote, are also present along

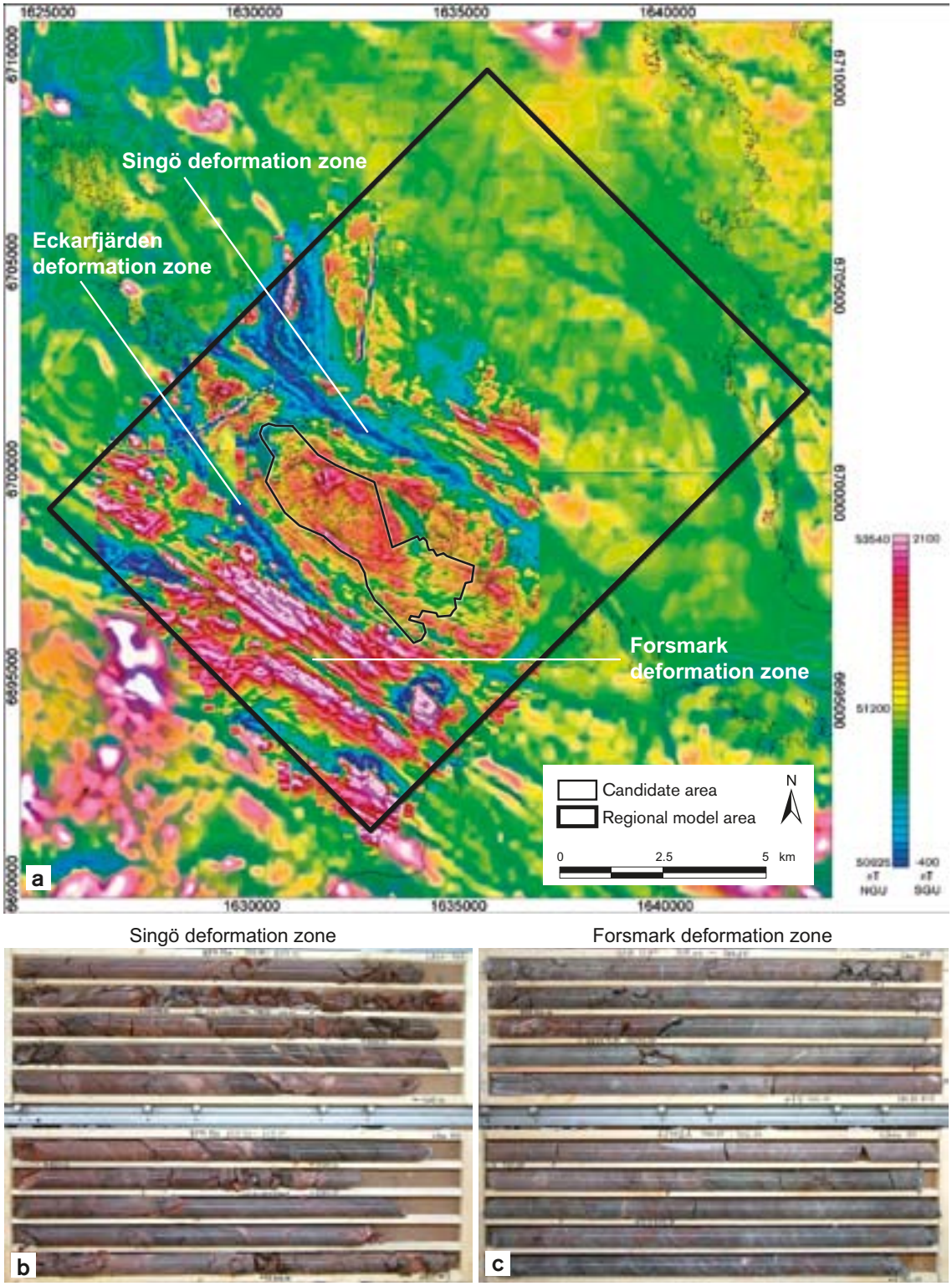

Figure 5-33. *Character of deformation zones in the vertical or steeply dipping, WNW to NW set. a) Link to lineaments defined predominantly by magnetic minima connections that are concordant with the ductile structural grain in the bedrock. b) Crush zones, laumontite-sealed cataclasites and networks, and wall-rock alteration defined by dissemination of hematite and red staining, along part of a fault core interval in the Singö deformation zone (WNW0001) in borehole KFM11A (borehole interval c. 597 to 608 m). c) Cataclasite and fault breccia cut by younger fractures and networks sealed with quartz, calcite and other fracture minerals, along part of a pronounced fault core interval in the Forsmark deformation zone (WNW0004) in borehole KFM12A (borehole interval c. 315 to 326 m).*

some of the zones intersected along boreholes (Figure 5-29). The complex character of the fracture mineralogy attests to multiple zone reactivation at different times during the geological evolution.

The kinematic data along the Singö, Forsmark and Eckarfjärden zones confirm that these zones have been affected by brittle deformation under different stress regimes. The Eckarfjärden zone, for example, was affected by approximately NW-SE and N-S compressive phases and a younger approximately NE-SW compressive phase /Stephens et al. 2007, section 3.7/. Epidote is a conspicuous coating along the fractures in all these phases. Displacement in accordance with an approximately WNW-ESE compressive phase is also apparent along zone WNW1200.

Vertical or steeply dipping zones in NNW set

The vertical or steeply dipping deformation zones in the NNW set have only been studied along a few intersections in five cored boreholes in the local model volume (Figure 5-29). Only one zone (NNW0404) with a trace length at the ground surface of c. 1,000 m is conspicuous at 400 to 600 m depth inside the targeted part of the local model volume. A second zone (NNW0101) occurs to the south-east of zone ENE0062A, against which it terminates. The surface trace length of the three zones included in the local model varies between c. 1,000 and 2,000 m. The measured thicknesses in boreholes vary between 10 and 41 m. Zone 6 at SFR (minor zone NNW1209), which lies outside the local model volume, is also included in this set.

All zones in this set show a concentration of brittle deformation and have been linked, at least partly, to magnetic lineaments. One of these zones (NNW0100) follows the ductile high-strain belt in rock domain RFM044. However, there remains some uncertainty concerning whether or not this ductile deformation is an integral part of the deformation along this zone. The dominance of sealed fractures, the character of wall-rock alteration, the character of the fault core (if present) and the fracture mineralogy (Figure 5-29) all resemble the corresponding features in the vertical or steeply dipping zones in the ENE to NNE set, especially the zones in the NNE sub-set.

Vertical or steeply dipping fractures that strike NNW dominate in the NNW zones (Figure 5-29). However, vertical or steeply dipping fractures that strike ENE to NNE and gently dipping to sub-horizontal fractures are also conspicuous. Apart from the relative importance of the different sets of steeply dipping fractures, the fracture orientation pattern is similar to that observed in the ENE to NNE set of zones. Sinistral strike-slip displacement dominates strongly, but dextral strike-slip and dip-slip movements have also taken place along this set.

5.6 Statistical model for fractures and minor deformation zones

This section presents the third component of the geological model at Forsmark, the geological discrete fracture network (DFN) model. The stage 2.2 geological DFN model for Forsmark aimed to provide an input for hydrogeological and mechanical modelling work, to provide fracture-related data for repository design and engineering planning, and to provide an input for safety assessment and licensing work. The model is presented as a mathematical description of the fracturing, not as a 3D object model or realisation. The goal of the geological DFN model is to provide downstream users with a means to estimate the fracture orientations, intensity, size, spatial patterns and fracture geology at a location within the target volume at Forsmark, along with the uncertainty in these estimates.

The results of the modelling work presented in /Fox et al. 2007/, with some modification, are summarised here. The division of the part of the Forsmark tectonic lens that lies inside the local model volume into fracture domains /Olofsson et al. 2007/, referred to as FFM01, FFM02, FFM03 and FFM06, is presented firstly in section 5.6.1. These domains represent the volumes within which various aspects of the DFN models are valid. In section 5.6.2, the geological DFN modelling assumptions are presented. Based on these assumptions, the procedure used to derive the models is outlined in section 5.6.3, where also the main alternative models (size-intensity) in /Fox et al. 2007/ are presented. An alternative concept was discussed within the framework of uncertainty assessment /Fox et al. 2007, section 5.1 and erratum December 2008/ and this concept has been adopted here to develop an additional alternative model. This model is also addressed in section 5.6.3. All the geologial DFN models for the fracture domain that includes the potential repository volume are summarised in section 5.6.4. The reader is referred to /Fox et al. 2007/ for the statistical main alternative models in other fracture domains. The limitations and remaining uncertainties are addressed later in section 5.9.

5.6.1 Division into fracture domains

Already during the single-hole interpretation work (see section 5.2.2), it was recognised that the upper part of the bedrock inside the tectonic lens at Forsmark contains an increased frequency of sub-horizontal and gently dipping, open and partly open fractures. A systematic assessment of the variation in the frequency of particularly open and partly open fractures with depth along each borehole (p. 30–32 and Appendix 3 in /Olofsson et al. 2007/ and section 5.2.5 in this report) contributed significantly to the division of the bedrock between deformation zones into fracture domains /Olofsson et al. 2007, p. 33–39/. The intervals along which each fracture domain is inferred to be present in each cored borehole were illustrated in borehole logs /Stephens et al. 2007, Appendix 13/.

The allocation of a borehole section to a particular fracture domain was carried out as a working hypothesis for the subsequent statistical modelling of fractures and minor deformation zones at the site. Furthermore, on the basis of these borehole data, a 3D geometric model for four of the six fracture domains (FFM01, FFM02, FFM03 and FFM06), inside the target volume, was constructed (/Olofsson et al. 2007, p. 40–43/ and Figure 5-34). Since few data are available outside this volume and the character of fracture domains FFM04 and FFM05 are poorly constrained, no model for these two fracture domains could be constructed /Olofsson et al. 2007/. Fracture domains FFM01, FFM02, FFM03 and FFM06 are addressed in the DFN modelling work /Fox et al. 2007/ and are described briefly in the following text.

Fracture domain FFM01

Fracture domain FFM01 (Figure 5-34) is situated within rock domain RFM029 inside the target volume. It lies north-west of the steeply dipping zone NE0065, beneath the gently dipping or sub-horizontal zones A2, A3 and F1, and beneath a depth that varies from c. 40 m (large distance from zone A2) to c. 200 m (close to zone A2).

Relative to the overlying fracture domain FFM02, the bedrock in this domain shows a lower frequency of open and partly open fractures. Furthermore, gently dipping or sub-horizontal fracture zones are also uncommon inside this part of rock domain RFM029. It is apparent that the character of this domain is favourable to a local accumulation of high *in situ* rock stresses (see chapter 7) at one or more times during geological history, in connection with, for example, sedimentary loading processes /SKB 2006a, Stephens et al. 2007, p. 155/.

Vertical or steeply dipping fractures that strike ENE to NNE and NNW, as well as gently dipping to sub-horizontal fractures are conspicuous in this domain (Figure 5-34). Fracture minerals are dominated by calcite, chlorite, laumontite, adularia, hematite and quartz (Figure 5-34). Both epidote (older generation) and laumontite are present along the different sets of fractures (Figure 5-35a) and reactivation of these fractures under different metamorphic conditions is apparent. However, laumontite is more conspicuous in the steeply dipping compared with the gently dipping to sub-horizontal fractures (Figure 5-35a). By contrast, clay minerals, which belong to a younger generation of minerals, are present most conspicuously along the gently dipping and sub-horizontal fractures (Figure 5-35a). All these features are similar to those observed in the ENE (NE) sub-set of fracture zones that is also prevalent in this part of the target volume (cf. Figure 5-29).

Fracture domain FFM02

Fracture domain FFM02 is situated close to the surface inside the target volume, directly above fracture domains FFM01 and FFM06 (Figure 5-34). It is characterised by a complex network of gently dipping and sub-horizontal, open and partly open fractures, which, conceptually, are considered to merge into minor fracture zones. The gently dipping and sub-horizontal fractures are oriented at a large angle to the present-day minimum principal stress in the bedrock (see chapter 7 and Figure 5-36). This relationship favours the reactivation of older, gently dipping fractures as extensional joints, the formation of new sub-horizontal sheet joints and the overall development of conspicuous apertures along gently dipping to sub-horizontal fractures in the current stress regime. These structural developments all contribute to a general release of the high *in situ* rock stress in this fracture domain.

Gently dipping to sub-horizontal fractures and vertical to steeply dipping fractures that strike ENE or NNW are most conspicuous in this domain (Figure 5-34). As in domain FFM01, calcite, chlorite, laumontite, adularia, hematite and quartz are present along the different sets of fractures

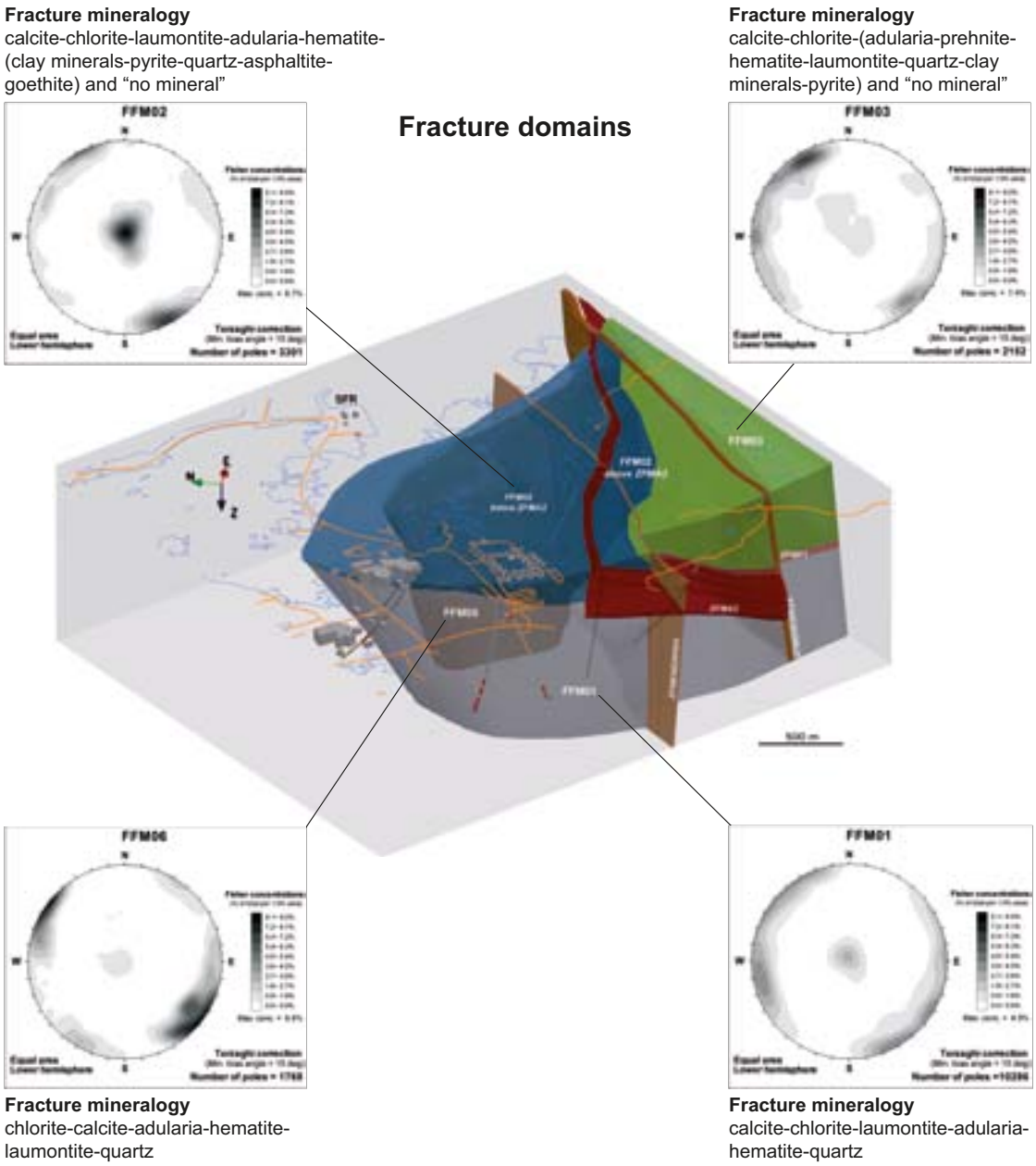

Figure 5-34. *Three-dimensional model for fracture domains FFM01, FFM02, FFM03 and FFM06 in the north-western part of the Forsmark tectonic lens, viewed towards the ENE. The local model block is shown in pale grey. The gently dipping and sub-horizontal zones A2 and F1 as well as the steeply dipping deformation zones ENE0060A and ENE0062A are also shown (after /Olofsson et al. 2007/). The orientation of fractures inside the different fracture domains are plotted as poles to planes in stereographic projections (equal-area, lower hemisphere) and contoured. In order to limit the bias that is related to the orientation of boreholes, a Terzaghi correction has been applied in these plots. The fracture mineralogy in each domain is also shown and the order of mineral presentation reflects the order of abundance (based on /Sandström et al. 2008, section 6.1/).*

(Figure 5-34). However, clay minerals, pyrite, asphaltite and goethite, which all belong to the younger generations of minerals, are more conspicuous in fracture domain FFM02 relative to all the other domains. Furthermore, fractures without any mineral coating or filling (“no mineral”) are also prominent in FFM02. However, there remain some uncertainties concerning the mapping of these fractures (see section 5.2.5 and /Stephens et al. 2007, p. 90/), and a complementary investigation has been initiated to shed more light on these structures. Once again, the older minerals epidote and laumontite, which formed at different times in the geological evolution, occur along the three different sets of fractures in FFM02 (Figure 5-35b), while clay minerals (Figure 5-35b), pyrite and goethite in the younger generations and “no mineral” are most conspicuous along the gently dipping to sub-horizontal fractures.

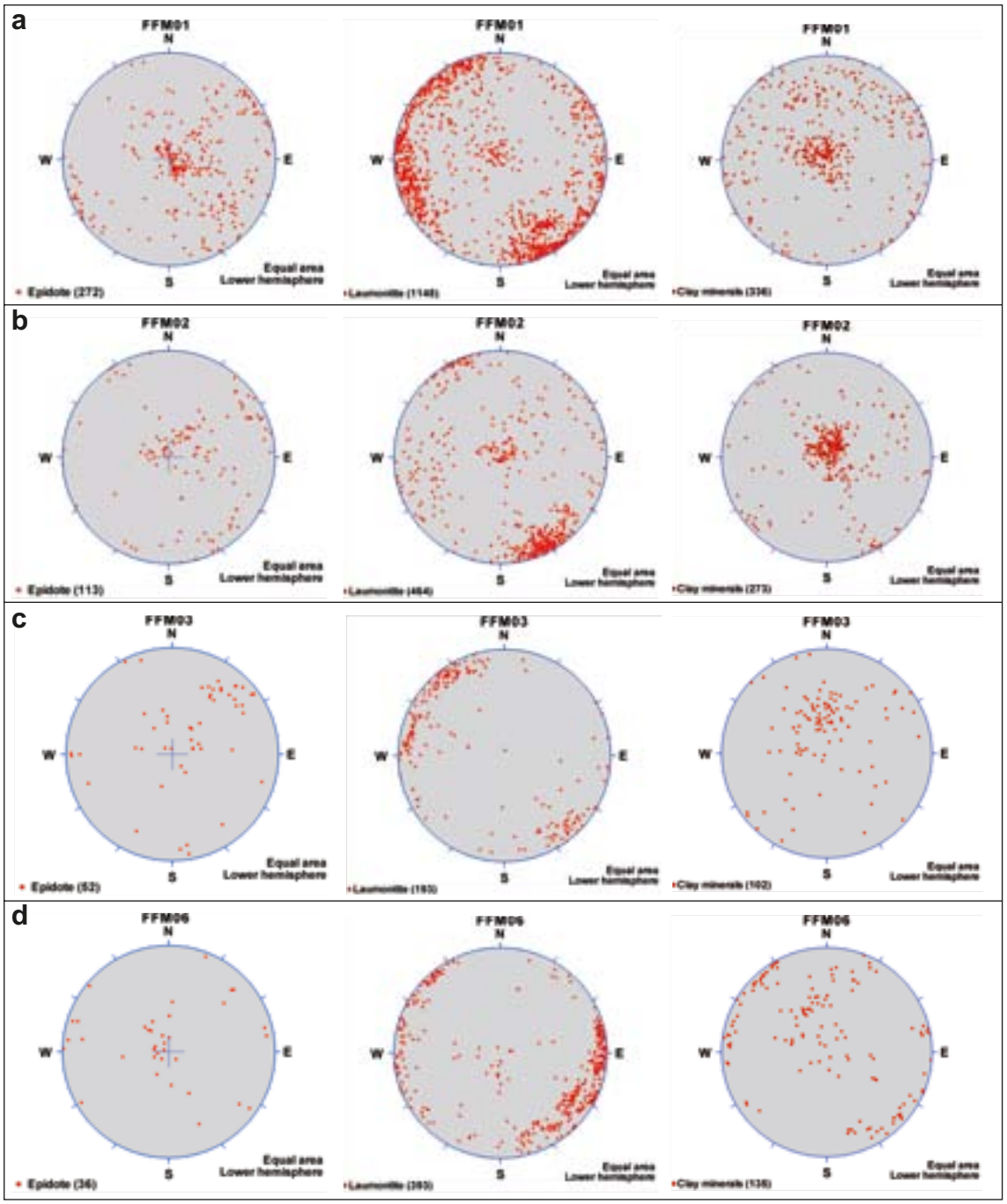

Figure 5-35. *Orientation of fractures with epidote, laumontite and clay minerals, i.e. from three different mineral generations, inside the fracture domains. a) FFM01. b) FFM02. c) FFM03. d) FFM06. The orientation of the fractures in each figure is shown as poles to planes in a stereographic projection (equal-area, lower hemisphere). In order to limit the bias that is related to the orientation of boreholes in the contoured plot, a Terzaghi correction has been applied in each of these plots.*

These observations provide support to the conceptual understanding of the evolution of the site in the brittle regime presented earlier (section 5.5.2). Whereas the effects of ancient tectonic processes are prevalent throughout the whole target volume, irrespective of depth, an additional process, which involved the release of high *in situ* rock stress, gave rise to a concentration of gently dipping or sub-horizontal fractures with younger or possibly no minerals in the upper part of the bedrock, i.e. close to the sub-Cambrian unconformity and current ground surface, inside the target volume.

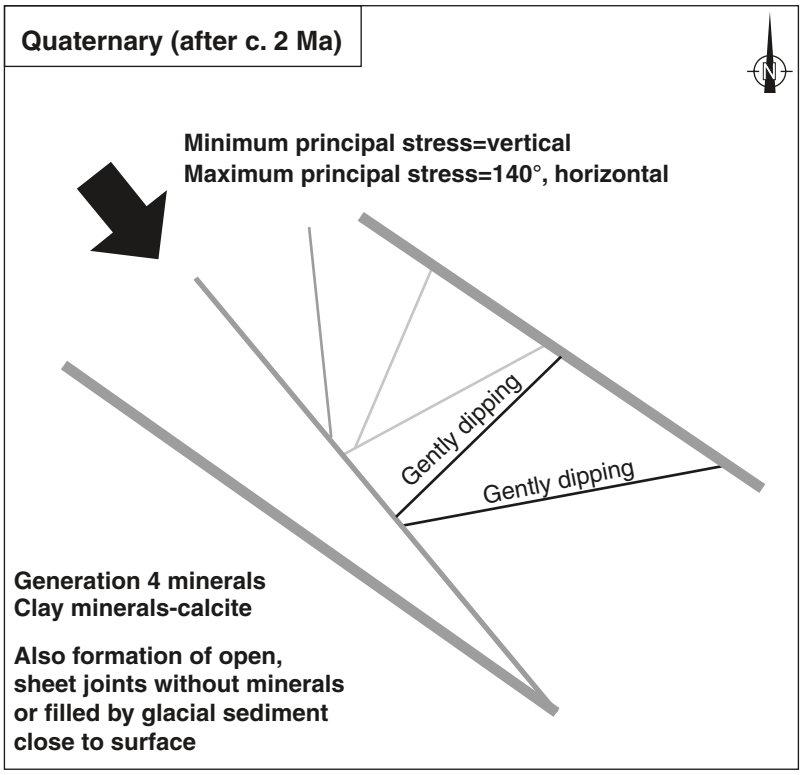

Figure 5-36. *Two-dimensional cartoon that illustrates the conceptual model for the possible reactivation of fractures with different orientations as extensional joints in the current stress regime (Quaternary). The orientations chosen correspond to the different sets of deformation zones (see section 5.7). The black line along the gently dipping structures indicates a considerable change in aperture; the dark grey line indicates a moderate change, and the pale grey line restricted change. These effects are most conspicuous close to the surface in fracture domain FFM02 and, particularly close to ancient gently dipping fracture zones. Sub-horizontal sheet joints may also have formed during the Quaternary, especially in this fracture domain.*

Fracture domain FFM03

Fracture domain FFM03 (Figure 5-34) is situated within rock domains RFM029 and RFM017, south-east of and outside the target volume. In particular, it is inferred to be present above zone A2 in borehole KFM02A and along the whole length of the boreholes KFM03A and KFM03B to the south-east of the local model volume. The rock domains in this volume are characterised by a high frequency of gently dipping fracture zones containing both open and sealed fractures. This structural feature inhibited the local build-up of rock stresses in connection with, for example, sedimentary loading processes /SKB 2006a, p. 121–126/. By corollary, the development of a significant stress-release fracture domain close to the surface, with the characteristics of domain FFM02, is also not favoured.

Vertical or steeply dipping fractures that strike ENE to N-S and NW, as well as gently dipping to sub-horizontal fractures are present in this domain (Figure 5-34). Calcite and chlorite dominate along the fractures; adularia, prehnite, hematite, laumontite, quartz, clay minerals and pyrite are also present (Figure 5-34). The subordinate mineral epidote occurs along the steeply dipping NW set of fractures and the gently dipping to sub-horizontal set, while laumontite is common along the steeply dipping ENE to N-S set of fractures (Figure 5-35c). It is inferred that at least these two generations of fracture minerals occur in different sets of fractures in this domain. Once again, clay minerals in the younger generation of minerals occur predominantly along gently dipping fractures (Figure 5-35c). Apart from some difference in the relative importance of steeply and gently dipping fractures, these features are strongly reminiscent of the orientation and mineralogy of the fractures in the contiguous, gently dipping fracture zones (cf. Figure 5-30a).

Fracture domain FFM06

Fracture domain FFM06 is situated within rock domain RFM045, inside the target volume. It resembles fracture domain FFM01 in the sense that it lies beneath both zone A2 and fracture domain FFM02 (Figure 5-34). It is distinguished from domain FFM01 by the widespread occurrence of fine-grained, altered (albitized) granitic rock, with slightly higher contents of quartz compared with unaltered granitic rock, i.e. on the basis of lithological characteristics.

Two sets of vertical or steeply dipping fractures that strike NE to N-S and NW to WNW, as well as gently dipping to sub-horizontal fractures are conspicuous in this domain (Figure 5-34). Fracture minerals are dominated by chlorite, calcite, adularia, hematite, laumontite and quartz (Figure 5-34). Epidote is relatively uncommon along the fractures in this domain (Figure 5-35d). The more common mineral laumontite is predominantly found along the steeply dipping NE to N-S fractures (Figure 5-35d). However, some occurrences are also present along the fractures with other orientations. Clay minerals, in the youngest generation of minerals, are present in both the steeply and gently dipping fractures (Figure 5-35d). These features are very similar to those observed in the NNE sub-set of fracture zones that is also prevalent in this part of the target volume (cf. Figure 5-29).

5.6.2 Modelling assumptions

The key assumptions required to generate the Forsmark geological DFN model are as follows.

- Fractures can be approximated as planar, circular discs with thickness described as a parameter (aperture), and with radii independent of position.
- The main alternative DFN models are valid for a size range scale of 0.5 m up to 564 m and the additional alternative model for a size range scale of 0.039 to 564 m, all expressed as the radius (r) of the area of an equivalent disc-shaped fracture (see also section 5.3).
- Only fractures marked “visible in BIPS” are used in the orientation analysis, due to the uncertainty in the orientations of fractures that are visible in the drill core but not in the BIPS imagery. In addition, orientation data from boreholes KFM02A and KFM09B have been excluded from the fracture set orientation modelling; these boreholes possess a total average uncertainty in orientation (Ω) greater than 10°. This exclusion follows the recommendations in /Munier and Stigsson 2007/.
- DFN model statistical properties are only valid within their target fracture domains. The spatial analysis results suggest that the current fracture domains, as defined in /Olofsson et al. 2007/, are appropriate boundaries for subdivision of the background fracture model. However, some model properties (specifically, fracture intensity and fracture location) may vary spatially or lithologically within a fracture domain and will require either additional subdivision or conditional simulation.
- Deformation zones and minor deformation zones identified in boreholes are complete, correct and constitute a population of fractures distinct from the background fractures in fracture domains. As such, the mathematical model for the background fractures is a distinct model from that describing the deformation zones.
- The fracture domains FFM01 and FFM06, which contain the potential repository volume, are not exposed at the surface. For this reason, it has been necessary to assume that the character of the fracture size distribution is the same as that in fracture domain FFM02 in the main alternative models in /Fox et al. 2007/. This assumption is avoided in the additional alternative model.
- An assumption that is implied for all the geological DFN models, but not expressly stated in /Fox et al. 2007/, is that the general lack of clustering demonstrated at outcrop scale is also present at the scale of the local model area. The low magnetic lineaments and the surface traces of deformation zones are treated as having a homogeneous density in space and the structural anisotropy of the Forsmark area (see section 5.5) is not taken into account. The rationale behind this assumption is that the division of traces by fracture domain requires clipping individual traces against domain boundaries. This would introduce severe truncation effects on the trace length distributions, potentially causing significant biases in the resulting size-intensity models. The major drawback of this assumption is that the resulting size-intensity models for each fracture domain include the size and intensity of large ($r > 28$ m) fractures and minor deformation zones (MDZ) over the local model volume rather than over the individual fracture domain. The consequences of this assumption for the size modelling procedure are discussed further below (section 5.6.3).

5.6.3 Derivation of statistical fracture model

The basic methodology behind the DFN model, e.g. /Munier 2004/, involves a division of the background fracturing in each fracture domain into distinct sets, based on their orientations and termination relationships. Once the orientation set model is completed, the additional properties necessary to describe the statistical fracture network are calculated. A division into distinct sets has also been recognised on a larger scale for lineaments and deformation zone traces (see section 5.5.2).

In its most compact form, the geological DFN model consists of the following components.

- Orientation. This is described by the mean orientation of each identified fracture set, expressed in terms of an orientation distribution with measurement(s) of spread.
- Size. For each identified fracture set, this is described in terms of a size distribution with its parameters.
- Intensity. For each identified fracture set, the amount of fracturing is expressed in terms of fracture intensity (P_{32}), i.e. the areal density per unit volume (m^2/m^3).

In addition, the scaling of intensities needs to be quantified. Commonly, a Euclidian (linear) scaling is applied. Euclidean scaling describes a model in which the number of fractures is linearly proportional to area, in the case of outcrops, or length, in the case of boreholes, and by inference, to volume in three dimensions. This means that an increase of the model volume is matched by an equal increase in the number of fractures (e.g. if the model volume is doubled, the number of fractures is also doubled). However, equally common in the literature is a non-linear, fractal scaling of fracture intensities. This means that an increase of the model volume by a certain factor is matched by an increase in the number of fractures by a different factor (e.g. doubling the model volume might render an increase in the number of fractures by a factor 1.8).

The scaling aspect is intimately, and intricately, related to the spatial arrangement (spatial correlation) of fractures. A Euclidian scaling assumes no correlation between fracture positions, i.e. the position of a fracture does not influence the position of its neighbouring fracture. However, this does not exclude the possibility of obtaining local clusters which sporadically may occur as an effect of the random process. By contrast, a fractal scaling assumes a (self-similar) correlation between fracture positions, quantified by the fractal exponent (dimension). A discussion of this issue can be found in /Bonnet et al. 2001/ and the reader is referred to /Fox et al. 2007/ for details on how this has been addressed in the current DFN modelling work.

The basic methodology behind the DFN model, e.g. /Munier 2004/, involves a division of the background fracturing in each fracture domain into distinct sets, based on their orientations and termination relationships. Once the orientation set model is completed, the additional properties necessary to describe the statistical fracture network are calculated.

DFN orientation model

The fracture set orientation model was developed primarily from the orientations, geological properties and geometric relationships recorded during the detailed mapping of nine outcrops within and immediately outside the candidate area at Forsmark (section 5.2.5 and Figure 5-11). The work-flow used to construct the DFN orientation model is as follows /Fox et al. 2007/.

1. Fracture orientation sets were identified on the basis of the outcrop mapping data. A fracture orientation set is a statistically homogeneous sub-population identified through consistent fracture pole orientations and termination relationships.
2. Once outcrop sets had been assigned, qualitative analysis of the stereoplots was performed to determine if any significant geological associations could be found and, if so, could they be used as predictors for reducing uncertainty in the spatial variability of set orientations.
3. Orientation sets were quantified by assigning a spherical probability distribution to them. The orientations of fractures in a fracture set are characterised by a mean pole vector (φ, θ) and a set of concentration parameters that describe how the fracture pole vectors cluster around the mean pole. Univariate Fisher, bivariate Fisher, bivariate Normal and bivariate Bingham spherical probability distributions were fitted to the sets identified on each outcrop, both for linked and unlinked fracture traces.

4. Identified outcrop sets were assigned names based on their general strike orientations. The sets were then listed in a matrix and classified into one of two categories:

   Global: A fracture orientation set visible in all or nearly all of the mapped outcrops. In the case of the EW and WNW sets, the two sets were combined into a single global set based on their mutual exclusion (any outcrop with the WNW set did not possess the EW set, and vice versa).

   Local: A fracture orientation set visible only in a small sub-set of the mapped outcrops. Local sets may represent variations in local stress conditions or tectonic history that are not applicable throughout the entire model volume. A key point is that, in terms of model parameterisation, local sets do not exist throughout the entire model volume.

5. The outcrop sets identified in step 1 were then used as guides to assign borehole fractures in each fracture domain into discrete sets. It should be noted that, in contrast to past geological DFN models, hard-sectored orientations were not used to divide the fractures into sets. Rather, the generic outcrop sets (NE, ENE, NW etc) were only used as initial starting points for the orientation modelling. Within each fracture domain, fracture sets were locally defined for each borehole, for multiple types of spherical probability distributions, using the software ISIS /Dershowitz et al. 1998/. All set assignments utilised Terzaghi-corrected data with a maximum correction value of 5. However, the fractures added to the data set by the Terzaghi correction were deleted after the set assignment was completed.
6. Fitted orientation distributions for each fracture set in each fracture domain for borehole and outcrop data were compiled into a single data set. Only the univariate Fisher distribution fits were included in this data set. The final orientation model for each fracture set consists of:
   a. A mean pole (φ,θ) of all the mean poles of the data points fitted for a single fracture domain. For example, the mean pole orientation for the NE fracture set in domain FFM02 was calculated by placing the fitted mean poles for the NE sets for both borehole and outcrop data set into FracSys/ISIS, and then by calculating the mean pole of the combined mean poles.
   b. A univariate Fisher concentration parameter that represents the potential variation in the mean pole location (κ_{mp}). This value was calculated when the orientation of the mean pole of all the fitted sets had been assigned. The κ_{mp} value should only be used if, for a given set (NE, NW etc), the modeller wishes to simulate a variable set mean pole (i.e. a set where the average orientation varies spatially according to a univariate Fisher distribution) instead of a single fixed mean pole value.
   c. An average value for the Fisher concentration parameter (κ). The average concentration parameter was calculated by computing the mean value of the individual κ values for all set fits. For example, for the NE set in fracture domain FFM02, each borehole and each outcrop has its own univariate Fisher distribution fit. The κ values from each of these individual fits were combined and the mean value calculated.
7. Parameter variability was quantified with the help of the specification of a statistical distribution for the Fisher concentration parameter κ (normal distribution), and the specification of probability distributions and 95% confidence cones for the distribution of fitted set mean poles.

Analyses conducted as part of the geological DFN parameterisation suggested that, for three of the fracture domains (FFM01, FFM03 and FFM06), four global orientation sets were consistently identified. These were the NE, NS, NW, and SH (sub-horizontal) sets. In domain FFM02, two additional sets with global scope were identified; the ENE and EW sets. These two sets exist in the other domains as local sets with limited spatial extents.

Figure 5-37 shows a stereonet in which all sets have been assigned the same amount of fractures. The use of such a stereograph is simply to visualise the spread from the mean direction, and to visually compare this spread for different fracture sets. Figure 5-37 confirms the orientation model (e.g. Table 5-5), in that the difference in spread from the mean pole is essentially the same for all sets, i.e. the Fisher κ values /Fisher et al. 1993, Mardia and Jupp 2000/ are essentially similar.

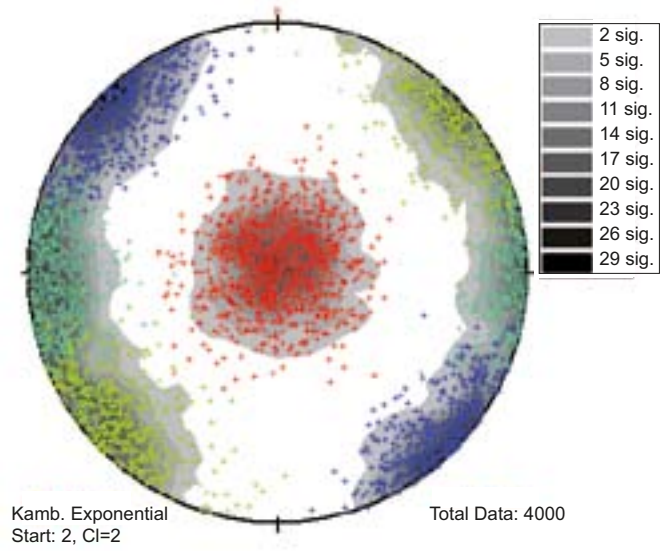

Figure 5-37. *Representation of the DFN orientation model. For comparative purposes, all sets have been assigned the same amount of fractures.*

DFN size model

The size model refers to a mathematical description of the area of the fractures. Previous analyses at Forsmark during SDM version 1.2 /La Pointe et al. 2005/ recognised that different fracture sets are likely to require different (and potentially unique) size models. Furthermore, since fracture domains have been identified that are distinguished from each other on the basis of different geological characteristics (see /Olofsson et al. 2007/ and section 5.6.1), it is reasonable to assume that the size model for the fractures differs in each fracture domain. With this reasoning in mind, size models were developed for individual fracture sets within each fracture domain.

Main alternative models

The methodology for quantifying a fracture size distribution for a fracture set in both fracture domains FFM02 and FFM03, in the main alternative models, involved fitting a scalar probability distribution based on r (the radius, in metres, of a disc-shaped equivalent-area fracture), to fracture trace length data observed in outcrop and to trace lengths derived from the interpretation of low magnetic lineaments (/Isaksson et al. 2006b/ and section 5.2.7), and the inferred intercepts of the mid-planes of deformation zones in the stage 2.2 deterministic model (/Stephens et al. 2007/ and section 5.5). The low magnetic lineaments and deformation zone traces function as a ‘pivot point’; the radius exponent (k_r) in an individual fracture domain is then determined by fitting the regional trace lengths together with outcrop data from the target domain.

As far as fracture domains FFM01 and FFM06 are concerned, the main alternative models are based on the assumption that the distributions of outcrop traces, mapped within FFM02 and FFM03, are representative also for these domains. This is a necessity, since domains FFM01 and FFM06 do not reach the ground surface. The size/intensity scaling for these models made use of the parameter r_0 to match intensities observed in boreholes within FFM01 and FFM06. Thus, the fracture radius scaling exponent (k_r) calculated from trace data for FFM02 is also used for domains FFM01 and FFM06.

The main alternative models at Forsmark /Fox et al. 2007/ contain two distinct size model alternatives, which these authors designed to encompass two end-members of a theoretical spectrum.

1. Tectonic continuum model (TCM and TCMF): This model assumes that the fracture population extends in size over a very large range in scale (Figure 5-38a). In this model, the fractures in outcrop with traces on the scale of metres are part of the same fracture population as lineaments or deformation zones with traces on the scale of kilometres. This model allows for the combination of data sets at multiple scales.

   It is important to note that the TCM is a coupled size-intensity model, i.e. it describes both the distribution of fracture sizes and their intensity (P_{32}). It is not possible to separate the two components without invalidating the model. The scaling exponent k_r has been calibrated against the distribution of trace lengths in outcrops within FFM02, while the minimum radius r_0 has been calibrated on the basis of both outcrops within FFM02 and borehole data from each domain (FFM01, FFM02, FFM03 and FFM06). /Fox et al. 2007/ proposed two variants of the TCM model; one assuming Euclidean size-intensity scaling (TCM), and one assuming fractal size-intensity scaling based on the fractal mass dimension. (TCMF)

2. Outcrop scale model (OSM) in combination with tectonic fault model (TFM): This model is a composite size model that does not assume a *single* coupled size-intensity relationship (Figure 5-38b). In this specific parameterisation, fractures have been hypothesised to belong to different populations (joints and faults) with different intensities at different scales. This model has the following two components.
   a. OSM – The outcrop scale model is a size model that is based solely on matching the sizes and intensities of fractures recorded as outcrop traces to the intensities in borehole data. Fundamentally, it treats fracture traces exposed in outcrop as joints.
   b. TFM – The tectonic fault model is a size model designed to be used in conjunction with the OSM. The TFM has been fitted solely to the lengths and intensities (P_{21}) of the deformation zone traces inside the regional and local model volumes, and to the high-resolution, ground magnetic lineaments inside the north-western part of the candidate area. The fundamental hypothesis is that these structures represent faults, rather than joints. The TFM uses an r_{min} value of 28 m, which is the radius of a fracture that will most likely produce a trace length of 50 m. This lower size limit is highly uncertain. As for the OSM, the TFM is valid up to a maximum size (r_{max}) of 564 m.

The TCM models imply that there are fewer overall fractures in FFM01 and FFM06, relative to FFM02, but that they are larger. The OSM + TFM model implies that there are more small fractures in FFM01 and FFM06 than FFM02, as well as fewer fractures overall. Together, the models cover a wide range of parameter space. Clearly, the size model parameterisation of the fracture sets in FFM01 and FFM06 are more uncertain than in FFM02 and FFM03, largely due to the lack of trace length or other size data from these domains.

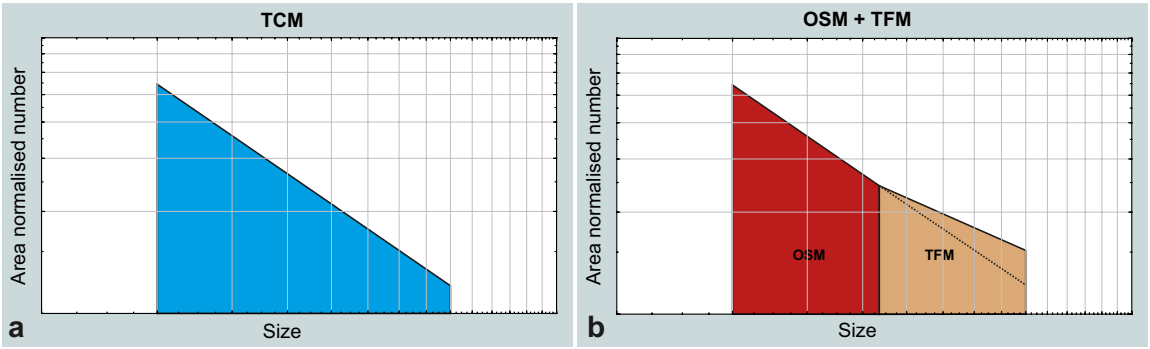

Figure 5-38. *Schematic cartoon illustrating the difference between the TCM (a) and composite OSM + TFM (b) models. This figure is simplified after /Fox et al. 2007/.*

Additional alternative model

Bearing in mind the geological understanding of the site (see sections 5.5.2 and 5.6.1), with the effects of different geological processes at depth compared with the surface and near-surface realm, it is possible that the fracture size distributions deduced from outcrops, especially in fracture domain FFM02, are different from those in fracture domains FFM01 and FFM06. For this reason, an alternative concept was discussed within the framework of uncertainty assessment in /Fox et al. 2007/.

In this alternative concept, rather than tuning r_0 to match the intensity in boreholes, r_0 was fixed to equal the borehole radius and, instead, the scaling parameter k_r of the power-law distribution was tuned to simultaneously match intensity in the boreholes and the intensity of lineaments and deformation zones (see /Fox et al. 2007, section 5.1.1, p. 213/ for details), i.e. the alternative approach utilises borehole fracture frequency data, whereas the main alternative models utilise surface fracture trace data in the determination of the fracture size distribution. This approach forms the foundation to the additional alternative model here referred to as the "r_0-fixed" model alternative.

The approach to keep r_0 fixed to equal the borehole radius has also been employed in the hydrogeological DFN modelling work (see section 8.5). However, the approach used in the hydrogeological DFN modelling to determine the intensity of larger-scale structures is different (see chapter 8).

Heterogeneity in the density of lineaments and deformation zones

Since the low magnetic lineaments and the surface traces of deformation zones were assumed to have an homogeneous density in space and these structures were not subdivided into fracture domains (see section 5.6.2), the same sets of trace lengths for these structures were used in the parameterisation of all fracture domains in all model alternatives in the geological DFN modelling.

This methodology is appropriate for a case where the lineament and deformation zone density is roughly isotropic across all domains. However, at Forsmark, there is a clear variation in the occurrence of lineaments and steeply dipping deformation zones with WNW-ESE to NW-SE strike in different volumes (see section 5.5.4); the intensity of these structures is much higher outside relative to that inside the tectonic lens where domains FFM01, FFM02, FFM03 and FFM06 are situated. Furthermore, gently dipping deformation zones are also less common in the target volume in the north-western part of the candidate volume, where domains FFM01, FFM02 and FFM06 are present. Thus, a consequence of this assumption is that the geological DFN model parameterisation for these domains shown in section 5.6.4 will tend to overestimate the intensity of NW-striking fractures in the MDZ size range 28 m to 564 m.

The issue of lineament and DZ heterogeneity also applies to the global sub-horizontal (SH) set in all model alternatives. It is not possible to identify lineaments from the high-resolution ground magnetic data set as sub-vertically or sub-horizontally dipping. Therefore, it is also not possible to assign lineaments to the SH set. As a consequence, the radius exponent (k_r) for the SH set for the TCM/TCMF and OSM/TFM models is based only on the trace data from outcrops and the surface traces of SH deformation zones in the regional model volume. There is no available information on the size of lineaments within the MDZ size range (< 564 m). In addition, the significant heterogeneity in the spatial distribution of SH-dipping deterministic deformation zones, with a concentration in the southern half of the local model area largely inside domain FFM03, is important. Therefore, it is also possible that the intensity of MDZ-size structures in the SH set is over- or under-predicted by the geological DFN modelling work; there is not sufficient data available to determine which (over- or under-prediction) is the case at Forsmark.

DFN intensity model

The stage 2.2 DFN model at Forsmark presents fracture intensity estimates in several forms.

1. As a single matching intensity value in the coupled size-intensity models. These models are based on the arithmetic mean P_{32} intensity in borehole data for a given fracture set within a given fracture domain.
2. As a set of descriptive statistics for each fracture set, by fracture domain. Statistics include the arithmetic mean, standard deviation, median, quartiles and percentiles. No assumption is made about the form of the distribution.
3. As a gamma distribution, where applicable (see /Fox et al. 2007/ for more details).
4. As a "lithology correction factor", based on the bedrock lithology.

Fracture set intensities depend significantly upon the linear fracture intensity data (P_{10}) collected in the cored borehole logs. P_{32} values were calculated for individual borehole sections at multiple intervals (6 m, 15 m and 30 m); the resulting values were then combined by set and domain. Outcrop fracture intensity (P_{21}) was used to bound the coupled size-intensity models, and as a validation tool for the final model parameterisation.

Multivariate statistical analyses suggest that fracture intensity varies in part due to local variations in lithology. The base rock for all DFN simulations (mean P_{32} described in the first bullet item) is assumed to be medium-grained, metamorphosed granite to granodiorite (SKB code 101057). A "lithology correction factor" can be applied to generate DFN models in other rock types.

Fracture intensities were computed for both sealed and open fractures; no distinction between these two types of fractures was carried out in the geological DFN model. However, global and local sets were treated differently in terms of model intensity parameterisation. Global sets were hypothesised to exist everywhere within the model volume. For this reason, intervals with no fractures were considered as a part of the spatial distribution of the global sets, and were included in the intensity statistics and gamma distribution calculations. By contrast, local sets were hypothesised to represent truly local phenomena and, for this reason, intervals without fractures in the local set were not considered as a part of the spatial distribution of the local fractures. Therefore, zero intervals in the local fracture set data were omitted before the intensity statistics and gamma distributions were calculated.

DFN spatial model

The spatial model describes how many fractures occur in a specific volume of rock at a specific location in the modelled fracture domain. As such, the model may depend upon depth, rock type, the influence of geological processes, the volume of interest and other factors. It may also differ by fracture set. The assessment of the spatial variation and the mathematical description of this variation were based on analysis of the scaling properties of the fractures, in combination with multivariate statistical analyses to identify any statistically significant relations between mappable geological parameters and fracture intensity variations.

The mass dimension, which models how fracture intensity changes as a function of scale, was computed for the traces in outcrop and for the fracture locations in boreholes. This analysis produced a set of data for each analysis consisting of the scale and the average fracture intensity at that scale, with intensity measured as P_{21} for outcrop traces and P_{10} for borehole data. The results were displayed on graphs with doubly logarithmic axes. This methodology makes it visually apparent as to whether the scaling behaviour is a power law, i.e. Euclidean, and, thus, consistent with the tectonic continuum hypothesis, or some other mathematical form, which might have other implications for the spatial model. The key parameter in these mass dimension plots is whether the data conform to a straight line in the doubly logarithmic display, which would support the tectonic continuum hypothesis, whether it is better modelled by two or more straight line segments, implying different characteristic intensities at different scales, or whether it fails to conform to a straight line over any portion of the data record. For portions of the data that do conform to straight line segments, the slope of the line that approximates the data describes the scaling model.

The analyses in /Fox et al. 2007, section 4.3.2/ show that, for the global fracture sets in the geological DFN model, fracture locations are best represented by a Euclidean scaling at model scales of 30 m and larger. Mild fractal clustering (mean fractal dimension of 1.9) was observed at scales less than 30 m. However, the 95% confidence interval surrounding D is ±0.23. This suggests that it may be difficult to distinguish between the natural variability inherent in a Poisson model following Euclidean scaling and a modestly fractally-clustered model. For this reason, /Fox et al. 2007, section 7.4/ recommended the use of Euclidean scaling (TCM) at all scales.

As far as the local fracture sets in the stage 2.2 geological DFN are concerned, no significant geological or morphological trends were noted. These sets were hypothesised to represent highly local variations in the past stress fields and rock properties. For this reason, /Fox et al. 2007, section 7.4/ recommended the use of either a bootstrap model based on local borehole conditioning of fracture intensity or a probabilistic approach based on the intersection probability calculated from the 6 m binned borehole data record.

5.6.4 DFN models

Main alternative models

Bearing in mind the considerations above, the geological DFN model for each fracture domain consists of three main alternatives /Fox et al. 2007/:

1. OSM + TFM, the combined joint-fault model,
2. TCM, the model assuming a single size model for all scales and,
3. TCMF, the variant of TCM assuming fractal intensity scaling.

All these models can be fine-tuned with respect to various factors such as rock type /Fox et al. 2007, section 4.4.4/, or depth /Fox et al. 2007, section 4.4.5/. The models for fracture domain FFM01 are reproduced from /Fox et al. 2007, chapter 7/ in Table 5-5 to Table 5-7. For purposes of comparison, all P_{32} values reproduced here were also recomputed for the size range 1 m to 564 m, using Equation 4-1 in /Fox et al. 2007, p. 193/. /Fox et al. 2007, section 7.2/ recommended the tectonic continuum model as the preferred model alternative, based on ease of use and applicability to a wide range of scales.

Additional alternative model

The DFN parameters for fracture domain FFM01, calculated with the help of the conceptually different r_0-fixed model alternative, are displayed in Table 5-8. The difference in k_r obtained, according to the procedures described above, results in a 30% to 60% (depending on fracture set) lower intensity within the size range r = 28–564 m relative to the intensities in the models presented in Table 5-5 to Table 5-7 for the same size range. Once again, for purposes of comparison, the intensities provided in /Fox et al. 2007, Table 5-3, p. 214/ were rescaled to the range 1 m to 564 m in Table 5-8, using Equation 4-1 in /Fox et al. 2007, p. 193/.

Table 5-5. DFN model for fracture domain FFM01. OSM + TFM model alternative.

Component	Set ID	Trend	Plunge	Kappa	r_0	k_r	P_{32} [r_0-∞]	P_{32} [1-564]
OSM	NE	314.9	1.3	20.94	0.0385	2.64	1.7350	1.9470
OSM	NS	270.1	5.3	21.34	0.0385	2.90	1.2931	1.3618
OSM	NW	230.1	4.6	15.70	0.0385	2.44	0.9506	1.1635
OSM	SH	0.8	87.3	17.42	0.0385	2.61	0.6263	0.7103
TFM	NE	314.9	1.3	20.94	28	3.00	2.8511E–02	
TFM	NS	270.1	5.3	21.34	28	2.20	3.3863E–04	
TFM	NW	230.1	4.6	15.70	28	2.06	2.5555E–04	
TFM	SH	0.8	87.3	17.42	28	2.83	2.8612E–02	
TFM	ENE	157.5	3.1	34.11	28	3.14	8.7065E–02	
TFM	EW	0.4	11.9	13.89	28	2.85	1.3832E–03	

Table 5-6. DFN model for fracture domain FFM01. TCM model alternative.

Set ID	Trend	Plunge	Kappa	r_0	k_r	P_{32} [r_0-∞]	P_{32} [1-564]
NE	314.9	1.3	20.94	0.6592	3.02	1.7350	1.1324
NS	270.1	5.3	21.34	0.0593	2.78	1.2931	0.1427
NW	230.1	4.6	15.70	0.5937	2.85	0.9506	0.6075
SH	0.8	87.3	17.42	0.8163	2.85	0.6263	0.5246

Table 5-7. DFN model for fracture domain FFM01. TCMF model alternative.

Set ID	Trend	Plunge	Kappa	r_0	k_r	P_{32} [r_0-∞]	P_{32} [1-564]
NE	314.9	1.3	20.94	0.7179	3.01	1.7350	1.2393
NS	270.1	5.3	21.34	0.0621	2.76	1.2931	0.1552
NW	230.1	4.6	15.70	0.6256	2.85	0.9506	0.6351
SH	0.8	87.3	17.42	0.7224	2.83	0.6263	0.4757

Table 5-8. DFN model for fracture domain FFM01. r_0-fixed model alternative.

Domain	Set ID	Trend	Plunge	Kappa	r_0	k_r	P_{32} [r_0-∞]*	P_{32} [1-564]*
FFM01	NE	314.9	1.3	20.94	0.039	2.72	1.74	0.17
	NS	270.1	5.3	21.34	0.039	2.75	1.29	0.11
	NW	230.1	4.6	15.70	0.039	2.61	0.95	0.13
	SH	0.8	87.3	17.42	0.039	2.58	0.63	0.09
FFM06	NE	314.9	1.3	20.94	0.039	2.79	3.30	0.26
	NS	270.1	5.6	21.34	0.039	2.78	2.15	0.17
	NW	230.1	4.6	15.70	0.039	2.66	1.61	0.18
	SH	0.8	87.3	17.42	0.039	2.58	0.64	0.09

* Match P_{32} represents the correlated size-intensity at which both the outcrop trace data and the borehole intensity data are matched, i.e. the size-intensity model will simultaneously fit the outcrop and the borehole data. The match P_{32} is valid from the minimum radius of the distribution (r_0) to infinity. Note that in all calculations for Forsmark stage 2.2, infinity is assumed to be equal to $1 \cdot 10^{31}$ m. Match P_{32} is equivalent to the arithmetic mean value of P_{32} for a given fracture domain, calculated from 6 m length intervals, outside all deformation zones, and excluding intervals marked as 'Affected By DZ'.

Concluding remarks

The interplay between the different DFN parameters in a particular model, as summarised in Table 5-5 to Table 5-8, can be fairly intricate and the overall nature of fracturing in the bedrock is difficult to address without some visualisation of the results of the model. For this reason, several realisations of different aspects of the markedly different, TCM and r_0-fixed alternative models for fracture domain FFM01 are shown in Figure 5-39 and Figure 5-40, respectively. In each of these figures, the realisation procedure has been carried out inside a 50 m^3 cubic volume in this domain.

The figures denoted "a" show the contoured stereonet of fractures in the size range 1 m to 10 m, whereas fractures with a size greater than 10 m are displayed in the figures denoted "b". The number of larger fractures was too small for contouring to be meaningful in these two figures. In the figures denoted "c", a horizontal section through this cube is shown. This exercise has generated a 50 m^2 trace map of fractures in the size range 1 m to 564 m for each alternative model.

The two models displayed in Figure 5-39 and Figure 5-40 are different in many aspects, which is perhaps not immediately apparent from Table 5-6 and Table 5-8. These differences are listed below.

- The intensity of the TCM model for the size range 1 m to 564 m is roughly 4.5 times higher than the r_0-fixed model.
- Relative to the other sets, the NE set is more intense in the TCM model than in the r_0-fixed model. This is due to the larger k_r value for the NE set in the TCM model, which thereby favours small fractures.
- The NS set, which is conspicuous in the r_0-fixed model, is suppressed by the NE set in the TCM model.

5.7 Integrated geological model

An attempt has been made in Figure 5-41 and Figure 5-42 to present rock domains, deformation zones and fracture domains, at the Forsmark site, in an integrated geological model. The upper part of Figure 5-41 shows the different rock domains in a regional perspective, and all the deformation zones with trace lengths at the ground surface longer than 10 km. The lower part of this figure shows two vertical profiles across the north-western part of the candidate volume, i.e. the target volume, and along the candidate volume. All these images have been extracted from the deterministic regional geological models for the site. The horizontal map sections in Figure 5-42 have been extracted from the deterministic local geological models. They provide information at a higher degree of resolution and at two different elevations, –150 m and –500 m (RHB 70), in the local model volume.

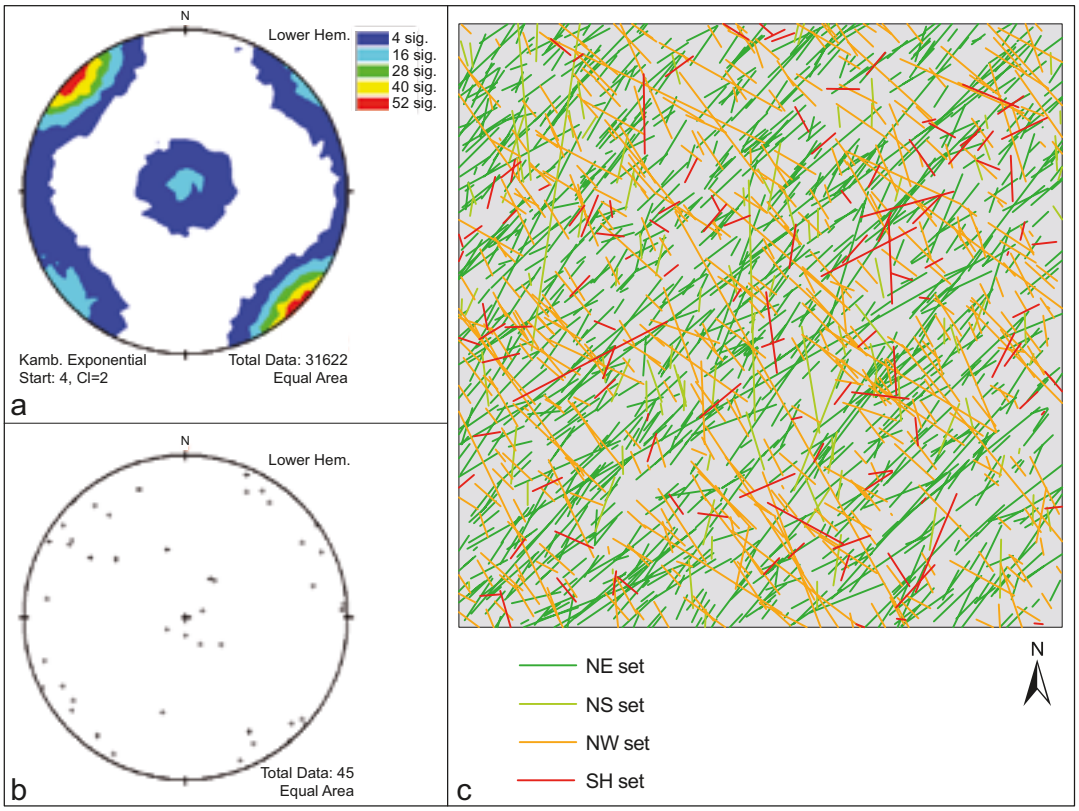

Figure 5-39. *Realisation of the TCM alternative model inside a 50 m³ cubic volume in fracture domain FFM01. See text for further description.*

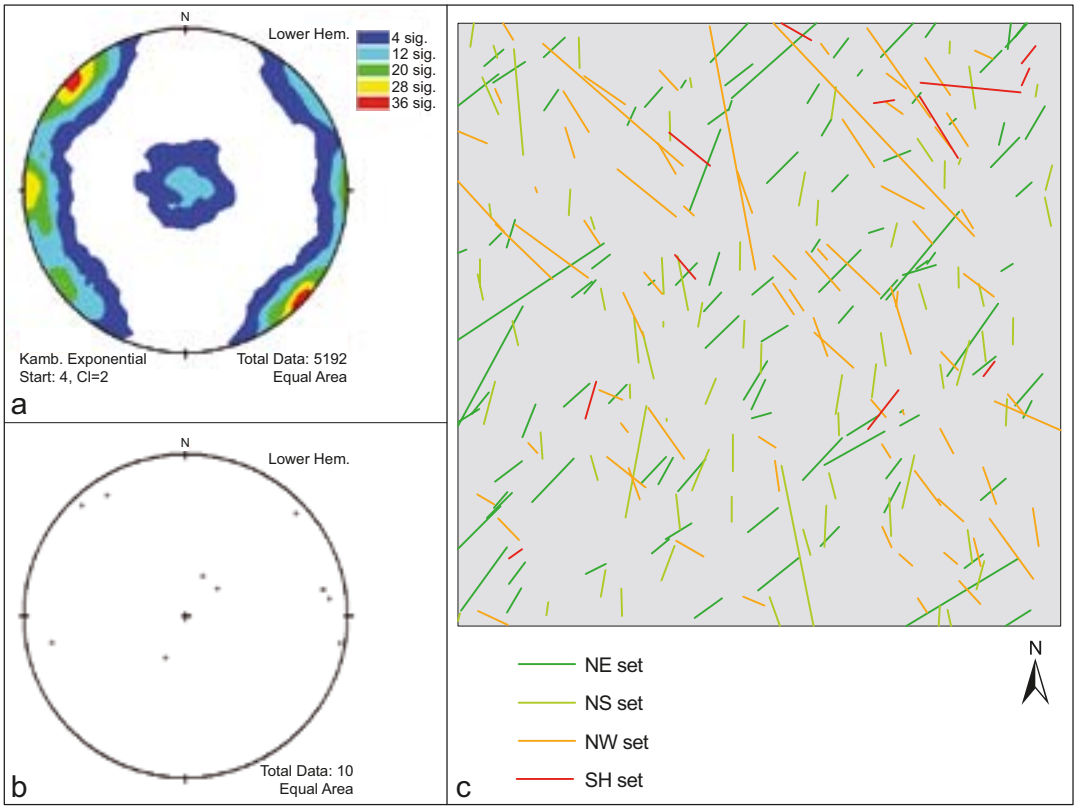

Figure 5-40. *Realisation of the r_0-fixed alternative model inside a 50 m³ cubic volume in fracture domain FFM01. See text for further description.*

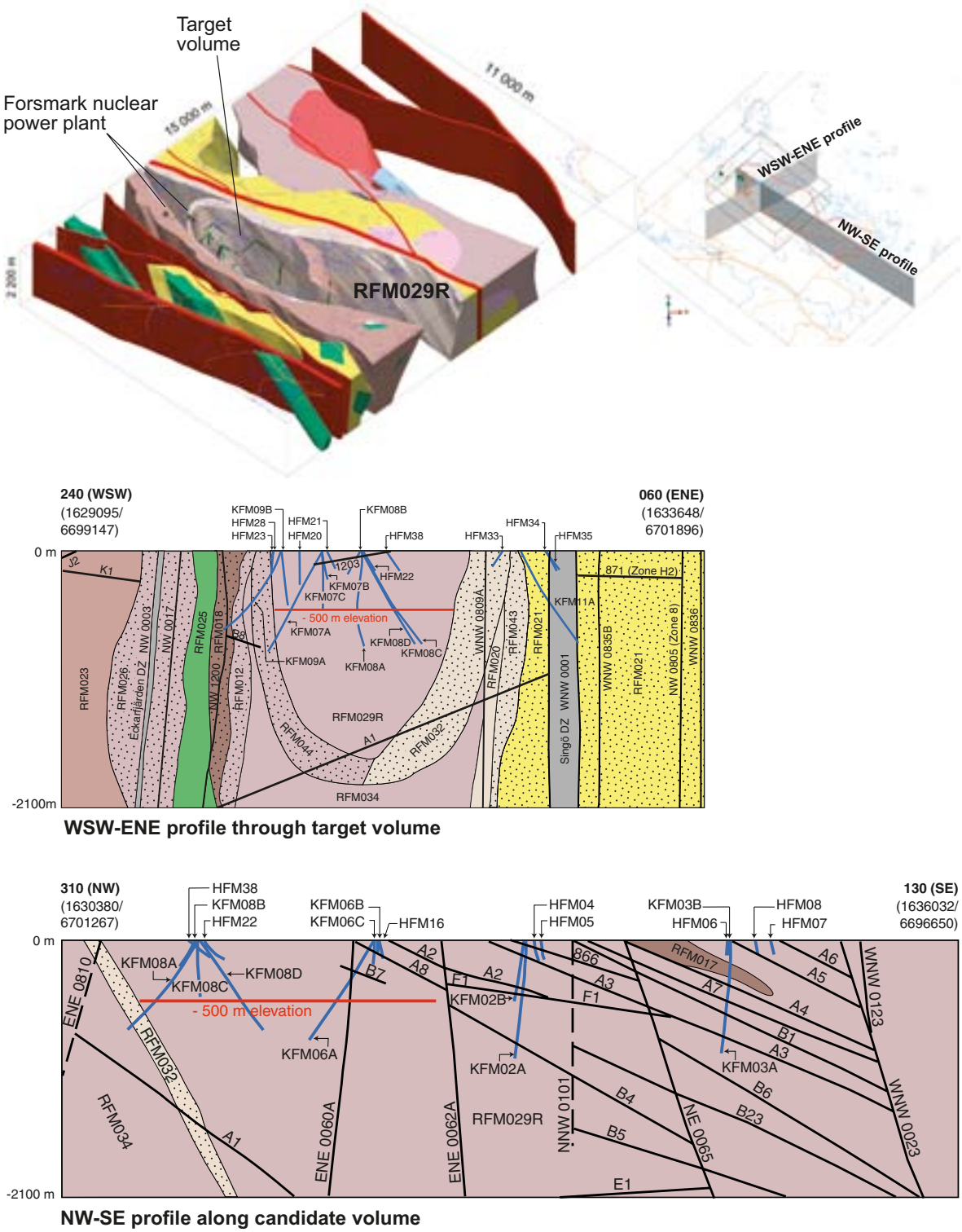

Figure 5-41. *Integrated geological model for rock domains and deformation zones at the Forsmark site in a regional model scale perspective. The reader is referred to the legend in Figure 5-24a for an explanation of the different colours in the 3D regional model in the upper part of the figure (view to north) and in the 2D profiles in the lower part of the figure. These colours represent the dominant rock type in each rock domain. Regional deformation zones are marked in dark red (3D image) or grey (profiles). Other deformation zones in the profiles are marked as black lines. Dotted ornament in the profiles indicates bedrock with high ductile strain. The profile planes are shown in the small inset.*

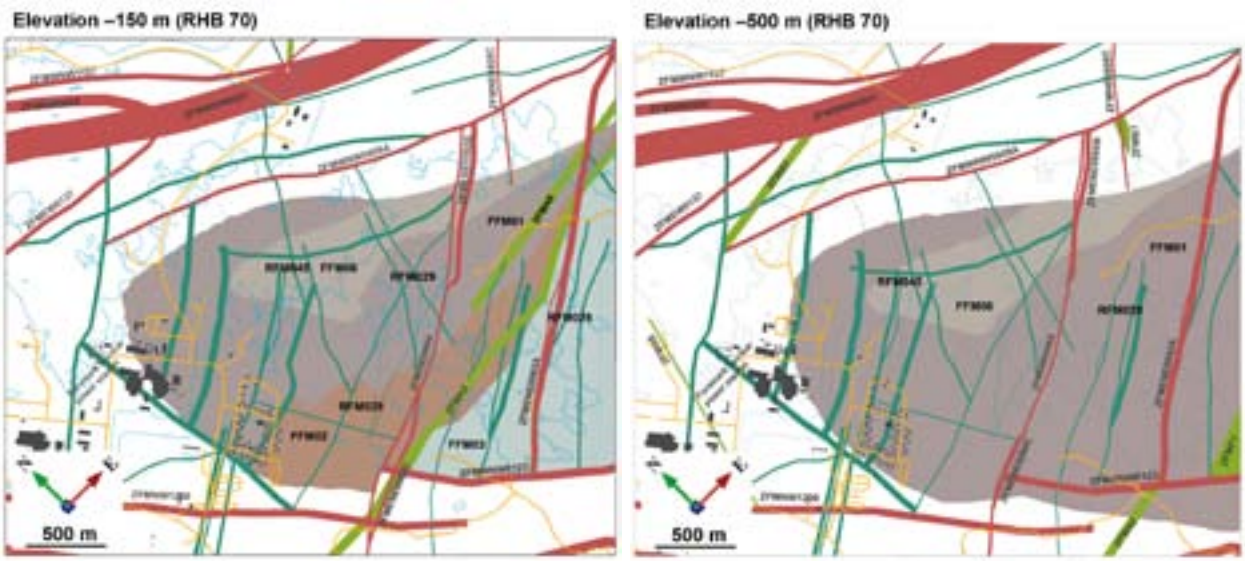

Figure 5-42. *Integrated geological model for rock domains, deformation zones and fracture domains at the Forsmark site in a local model scale perspective. The figure shows two dimensional horizontal surface models at different elevations, –150 m and –500 m (RHB 70), inside the local model volume. In each figure, zones marked in red are steeply dipping or vertical and have a trace length at the surface longer than 3,000 m. Zones marked in blue-green are steeply dipping or vertical and are less than 3,000 m in length. Zones marked in green are gently dipping. Other features are labelled directly on the figures.*

The rock domain marked as RFM029R in the regional model volume contains the potential repository for the disposal of highly radioactive nuclear waste. This domain occurs within a tectonic lens with lower ductile strain, and is surrounded by rocks that show a strong anisotropy in a WNW to NW direction (Figure 5-41). The higher ductile strain associated with this anisotropy has influenced the orientation of the different rock domains outside the tectonic lens. A moderately to steeply plunging synform is conspicuous in the target volume in the north-western part of the lens, and both the boundaries between rock domains and the penetrative ductile fabric in the lens dip more gently in the south-eastern part of the lens. These structural features are conspicuous in the two profiles (Figure 5-41).

The regional deformation zones are located entirely outside the tectonic lens in the bedrock which contains a strong anisotropy generated as a result of ductile deformation. Furthermore, the gently dipping zones are concentrated in the south-eastern part of the lens, where the ductile structures and rock contacts, in particular the contacts between amphibolite and metagranite, also dip more gently. These features are conspicuous in the 3D regional model and the NW-SE profile, respectively (Figure 5-41).

In the local model, domain RFM029R has been divided into domains RFM029 and RFM045, on the basis of the degree of alteration referred to as albitization. Only three steeply dipping fracture zones (ENE0060A and ENE0062A with their attached branches, and WNW0123), with a trace length longer than 3,000 m, intersect these domains in the targeted part of the local model volume (Figure 5-42). As indicated on the map at –500 m elevation (Figure 5-42) and in the NW-SE profile (Figure 5-41), no gently dipping zones intersect this depth in the volume north-west of zone ENE0062A. The division of the north-western part of the tectonic lens into fracture domains FFM01, FFM02 and FFM06 (Figure 5-42), and the spatial distribution of these domains (Figure 5-34), have been determined by three factors; proximity to the ground surface, the distance to the gently dipping zone A2 and lithology. Fracture domains FFM01 and FFM06 occur at the depth of a potential repository. The overlying fracture domain FFM02 extends to greater depths in the vicinity of zone A2, where it is also present above this zone. Fracture domain FFM03 is located solely above zone A2, i.e. in its hanging wall.

The following ten bullets provide a summary of the key geological aspects of the Forsmark site.

- The bedrock in rock domains RFM029 and RFM045 is dominated by a rock type with high quartz content (metagranite). Mean values of the quartz content in two different varieties of this rock type are 36 and 40%. The subordinate rock type referred to as amphibolite contains little or no quartz (range 0 to 6%). This rock type is a more conspicuous component in the more altered rock domain RFM045. Field relationships suggest that the increased degree of alteration in this domain is, at least partly, related to the increased frequency of occurrence of amphibolite. These features have important implications for the thermal and rock mechanical modelling work.
- The bedrock anisotropy, which was established in the high-temperature ductile regime at 1.87 to 1.85 Ga, has influenced the variable spatial distribution of the different sets of deformation zones at the site: Steep WNW-NW and NNW sets lie predominantly outside the tectonic lens in the high-strain belts; the steep ENE to NE set lies inside the tectonic lens, in particular in the targeted north-western part; gently dipping zones are predominantly present where the ductile structures and rock contacts are more gently dipping in the south-eastern part of the candidate area. Only the WNW-NW set shows clear evidence of a combined ductile and brittle deformational history. The other sets are solely brittle in character, i.e. they are fracture zones. Ductile deformation along the steep WNW-NW set of deformation zones occurred after 1.85 Ga. The bedrock at the site was first able to respond to deformation in a brittle manner some time between 1.8 and 1.7 Ga.
- The different sets of fractures inside the deformation zones are genetically related to the zones that were established prior to 1.1 Ga, probably during the Palaeoproterozoic between 1.8 and 1.6 Ga. However, the influence of different compressive tectonic regimes for the development of the deformation zones in the brittle regime is apparent from the kinematic data along shear fractures, i.e. minor faults. Strike-slip displacement, both dextral and sinistral, is conspicuous along minor faults in each steeply dipping set, while both reverse dip-slip and subordinate strike-slip senses of movement have occurred along the gently dipping structures. Both the kinematic data and the mineralogy along fractures suggest that all four sets of deformation zones were affected by reactivation under brittle conditions, not least around 1.1 to 0.9 Ga. New fractures may also have formed during progressively younger geological events. On the basis of these considerations, it is uncertain exactly how the different sets of fractures along a zone are related both to each other and to the zone.
- The different sets of fractures at the site responded differently to fluid flow at different times during the geological evolution. In particular, the apparently simple mineralogy along the gently dipping fracture zones is an artefact obscuring a long and complex hydrothermal history. In the current stress regime, it is apparent that changes in aperture can be expected most significantly along the gently dipping fractures and to a less extent along the steeply dipping fractures that strike WNW to NNW.
- The orientation and mineralogy of the fractures inside domains FFM01, FFM03 and FFM06 resemble the orientation and mineralogy of fractures in the contiguous fracture zones, i.e. the steep ENE (NE), gentle and steep NNE sets of fracture zones, respectively. However, this correlation breaks down in domain FFM02. In this domain, there is a significant occurrence of gently dipping to sub-horizontal fractures but relatively few gently dipping zones, and there is a relatively high level of occurrence of fracture minerals from the younger mineral generations as well as fractures without any mineral coating or filling.
- It is suggested that a long geological history of tectonic processes during Proterozoic time has influenced the fracture pattern at deeper crustal levels in fracture domains FFM01, FFM03 and FFM06. However, a combination of these tectonic processes and a second geological process, related to unloading and release of stress, has influenced the fracture pattern in the near-surface realm, close to the sub-Cambrian unconformity and current ground surface in fracture domain FFM02. It is envisaged that reactivation of ancient fractures and even formation of new fractures (sheet joints) in connection with exhumation of the sub-Cambrian unconformity during the later part of the Neoproterozoic, during the Cenozoic or, as indicated in Figure 5-36, during the Quaternary has occurred.
- The influence of different geological processes at depth and in the near-surface realm cause difficulties to apply coupled size-intensity geological DFN models, which are based on surface data, to the two fracture domains at repository depth that do not outcrop, FFM01 and FFM06.

There are also uncertainties in the continuity of tectonic processes at different size scales. These difficulties have been addressed using alternative geological DFN models. These are referred to as the TCM, TCMF, OSM+TFM and r_0-fixed models.

- The alternative geological DFN models differ in method (e.g. TCM and r_0-fixed) and even in concept (TCM, TCMF and r_0-fixed versus OSM+TFM). However, none of the models considered have taken into account the heterogeneity in the density of larger structures at the Forsmark site when the scaling exponent (shape parameter) k_r values have been calculated.
- The TCM, TCMF and r_0-fixed models are all based on the assumption of a *single* power law function (tectonic continuum) to encompass a size-intensity relationship for all fracture radii up to 564 m. However, they use different methodologies to derive size-intensity relationships in fracture domains FFM01 and FFM06 at depth. The TCM and TCMF models for these domains use *surface trace length data on all size scales*. Account is taken of differences in the influence of different geological processes close to the surface and at depth only in the accompanying spatial model. In contrast, the r_0-fixed model combines *fracture frequency data from boreholes with surface trace length data for lineaments and deformation zones.* It avoids the use of fracture size data from outcrop.
- The OSM+TFM model combines the size distributions derived from outcrop with the size distributions derived independently from lineaments and deformation zone traces, with a change in slope of the power law function at r = 50 m, i.e. two power-law functions. Although this model, to some degree, better honours data derived from both small and large scales simultaneously, there is, to our knowledge, little support for such a model in the literature. Furthermore, the model does not explain the similarity between the orientation and mineralogy of fractures inside domains FFM01, FFM06 and even FFM03 and the respective, contiguous zones.

5.8 Verification of the deterministic geological models

The stage 2.3 geological and geophysical data, which were not included in the stage 2.2 geological models, mostly provide information on the bedrock outside the target volume (ground magnetic data and the data from the boreholes KFM02B, KFM11A, KFM12A and HFM33 to HFM37) or simply complement older information of identical character, both inside and outside this volume (character and kinematics of deformation zones, fracture mineralogy). In general terms, it can be stated that these new data have only minor effects on the final deterministic geological models, stage 2.2 /Stephens et al. 2008/.

By contrast, the cored borehole KFM08D intersects the central part of the target volume (Figure 5-2 and Figure 2-2) and the data from this borehole were deemed suitable to test the validity of the stage 2.2 deterministic geological models inside this critical volume. The verification of these models has been carried out on a prediction−outcome basis, using the stage 2.2 local geological models /Stephens et al. 2007/ and the single-hole interpretation (SHI) of borehole KFM08D /Carlsten et al. 2007/, respectively. Since gravity measurements at the site /Aaro 2003/ have never been used in the development of the geological models, it was also decided that the modelling of gravity and petrophysical data could provide an independent test of the validity of the regional rock domain model for the site. The results of these verification tests have been presented in /Stephens et al. 2008/ and /Isaksson and Stephens 2007/, respectively. A summary of these results is provided below.

5.8.1 KFM08D

The boundary between rock domains RFM029 and RFM045 (as well as fracture domains FFM01 and FFM06) along KFM08D occurs only c. 30 m deeper than that predicted. The predicted continuation of RFM045 and FFM06 in the volume intersected by the remainder of this borehole has been confirmed by the drilling. There are some narrow, low resistivity anomalies in the bedrock above c. 145 m depth in this borehole, which are possibly related to single, open fractures. However, inclusion of the upper part of the borehole in fracture domain FFM01, as carried out in the fracture domain model stage 2.2, is considered to be acceptable, bearing in mind the results from the adjacent borehole KFM08B.

The fracture orientation, fracture mineralogy, alteration and style of deformation of the twelve possible deformation zones identified in the single-hole interpretation /Carlsten et al. 2007/ support the correlation of nine of these zones with deformation zones already modelled deterministically in stage 2.2 (Figure 5-43). The latter intersect the possible deformation zones along KFM08D directly, without any need for modification (three zones), or after a minor modification of the dip or strike between 1° and 10° (six zones). The required changes lie predominantly within the range of uncertainty provided in the property tables for the orientation of these zones (Appendices 15 and 16 in /Stephens et al. 2007/). These changes include a steepening of zone WNW2225 so that it does not intersect borehole KFM08D. Instead, zone NNE2300 is inferred to correspond to the inferred zone recognised at the base of this borehole. It should be kept in mind that several of these modelled zones were assigned a medium confidence of existence and their dip was judged to be highly uncertain (e.g. zone NNE2308 which corresponds to DZ8 in the SHI). The results from KFM08D confirm the existence of these zones, permit an upgrading to a high level of confidence in their existence, and constrain more tightly their dip. Three possible deformation zones identified in the SHI, with a low or medium confidence, cannot be linked to a deterministically modelled zone in stage 2.2 or to a low magnetic lineament at the ground surface. These geological features remain as possible deformation zones (Figure 5-43).

All the deformation zones along KFM08D are steeply dipping fracture zones that can be included in the ENE and NNE sub-sets /Stephens et al. 2007/. They are either local major zones with a trace length at the ground surface between 1,000 and 3,000 m or are minor zones with a trace length at the ground surface less than 1,000 m. Sealed fractures and sealed fracture networks dominate, in agreement with previous findings at Forsmark. It has been concluded that the results from the drilling of KFM08D verify in a highly satisfactory manner the parts of the stage 2.2 geological models that lie inside the target volume /Stephens et al. 2008/. In particular, no additional zones that have trace lengths longer than 3,000 m have been detected inside the target volume.

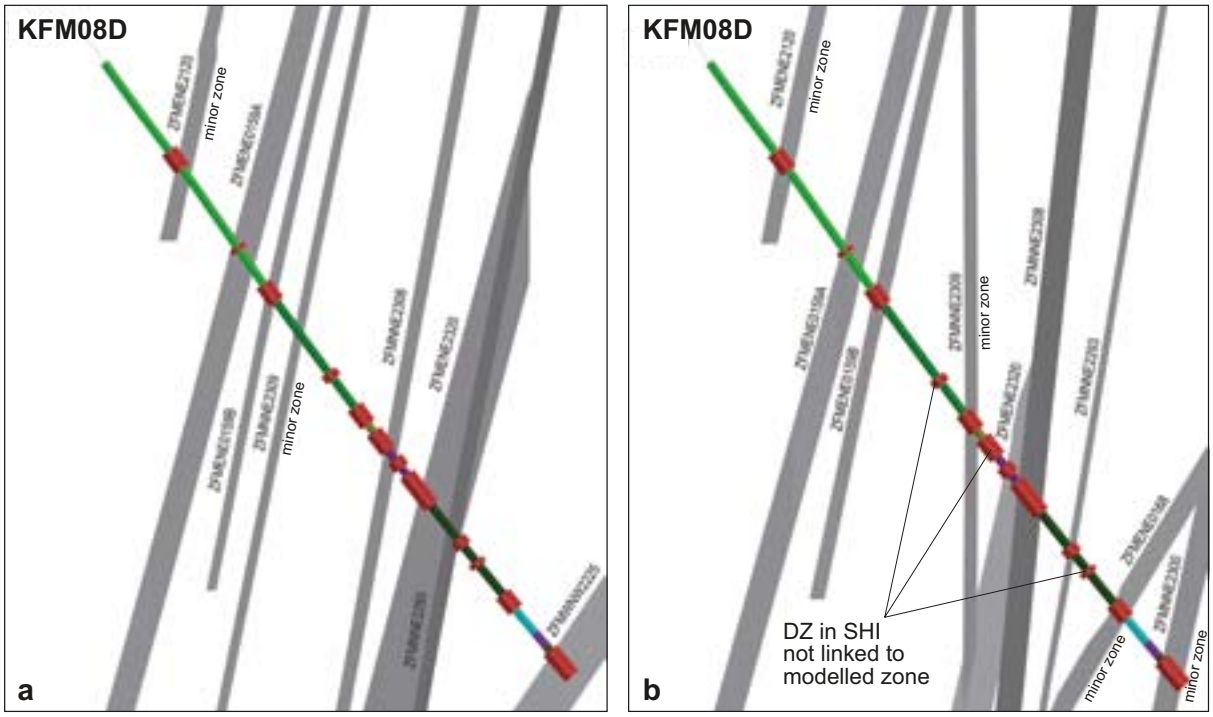

Figure 5-43. *Prediction−outcome verification test for deformation zones along borehole KFM08D. a) Modelled deformation zones stage 2.2 (ZFM), including minor zones, compared with the twelve possible deformation zones in the single-hole interpretation (red ornaments). b) Modification of zones necessary to satisfactorily match the single-hole interpretation. The length of borehole KFM08D is c. 942 m. See text for further description.*

5.8.2 Gravity and petrophysical modelling

The verification test that made use of the modelling of gravity and petrophysical data was initiated prior to the completion of model stage 2.2 and was carried out on the regional rock domain model, version 1.2 /SKB 2005a/. Since there are few differences between the different versions of this model /Stephens et al. 2007/, this test is also relevant for the stage 2.2 model.

The verification was carried out by comparing the calculated gravity response from the regional rock domain model, with a local gravity anomaly derived from the measured data. The model response from the rock domain model utilised the geometry in this model as well as silicate density petrophysical data for the different rock types in each domain /Isaksson and Stephens 2007/. The modelling work was strongly restricted by the paucity of quantitative data that bear on the volumetric proportions of subordinate rock types in each domain. This uncertainty was addressed by the development of alternative models that do not solely take account of the average density of the dominant rock type /Isaksson and Stephens 2007/. Gravity model responses were calculated in three stages that consisted of an initial model, a base model and a refined base model. The refined base model was preferred and used for comparison purposes.

The modelling work showed that there is, in general, a good agreement between the refined base model and the local gravity anomaly derived from the measured gravity data, not least where it concerns the geometry of the critical rock domain RFM029 (Figure 5-44 and /Isaksson and Stephens 2007/). The most significant discrepancy occurs in the area that extends from the SFR office to the underground SFR facility and further to the north-west, where there is conspicuous mass surplus (large blue dots on Figure 5-44). It is inferred that this discrepancy is caused by a combination of an overestimation of the volume of gabbro−diorite in rock domain RFM016 (Figure 5-44), which dips towards the south-east, and an underestimation of the volume of occurrence of lower density pegmatite, pegmatitic granite and metagranitoid that are known to be present and occur as larger bodies around the SFR facility, especially in rock domain RFM021 (cf. Figure 5-2 and Figure 5-24a). Other less significant discrepancies have been noted in rock domains RFM017, RFM022 and RFM023 (Figure 5-44). However, all rock domains with discrepancies are situated more or less completely outside the local model volume, stage 2.2 (Figure 5-44).

5.9 Remaining uncertainties

5.9.1 Deterministic model for rock domains

Despite the significant increase in borehole data in the local model volume after model stage 2.1, only very minor changes have taken place in the rock domain model in this volume compared with that in model stage 2.1. Furthermore, the predictions provided by model stage 2.2 for the intersection of rock domains RFM029 and RFM045 in borehole KFM08D have been verified satisfactorily during model stage 2.3. In addition, few changes in the regional rock domain model have occurred since SDM version 1.2. Bearing in mind these three observations, it is judged that the intrinsic uncertainties in the positions of the boundaries between rock units on the surface geological map and in the boreholes at depth /Munier and Stigsson 2007/ are of little significance for the modelling of rock domains, particularly in the local model volume. The uncertainties in the modelling work that concern the extension at depth of virtually all the rock domains outside the local model volume and the quantitative estimates of the proportions of different rock types in most of the rock domains remain. However, these uncertainties are not judged to be significant for the understanding of the geological relationships inside the target volume.

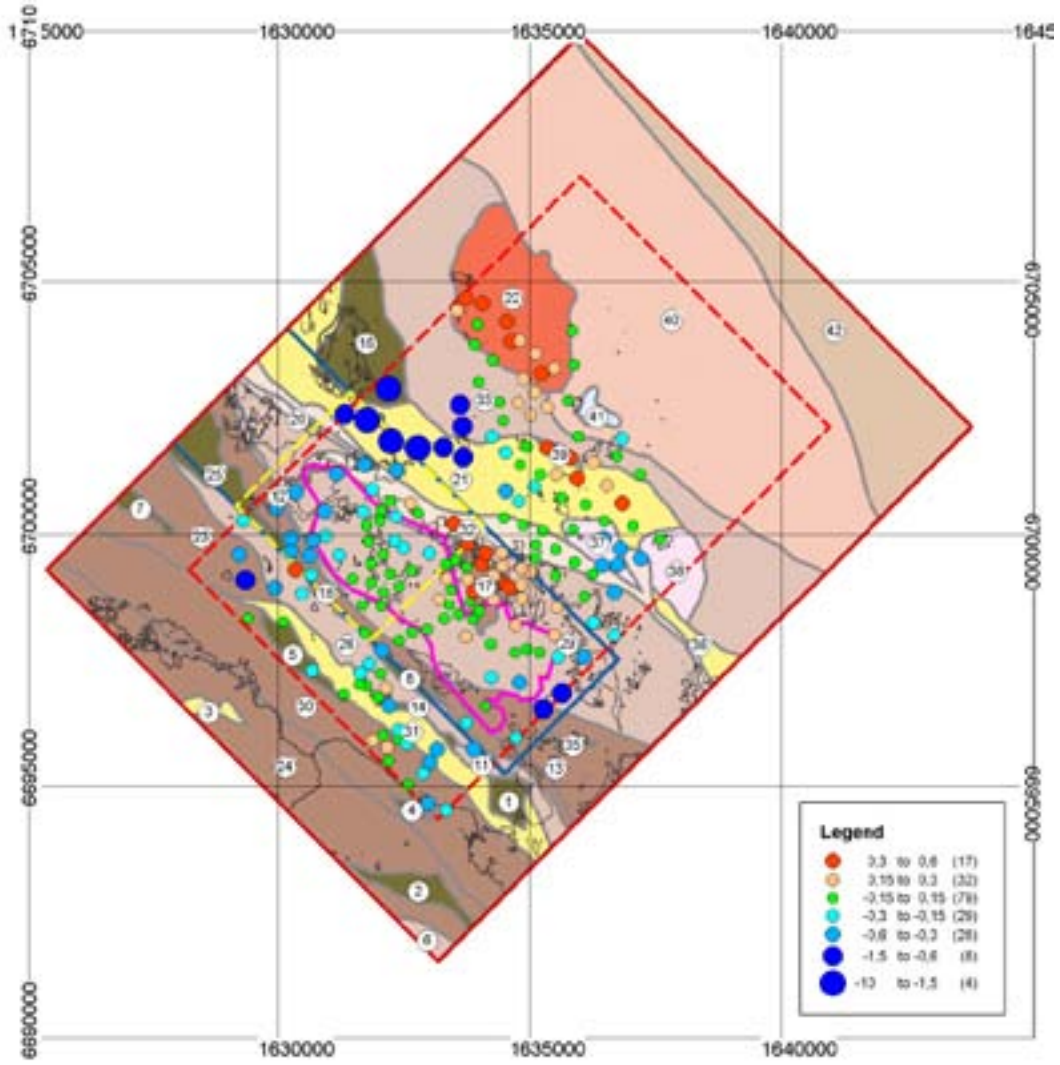

Figure 5-44. *Refined base model for modelling the gravity response from rock domains, version 1.2, inside the regional model area (solid red line). Rock domains are numbered (cf. Figure 5-24a). Responses are only shown within the boundary buffer area (dashed red line). The residual between the input gravity anomaly and the model anomaly [mgal] has been calculated for each survey station and is shown on the map. Blue colours indicate a mass surplus in the rock domain model and red colours indicate a mass deficiency. The candidate area is shown with a solid magenta line. The local model areas for version 1.2 and stage 2.2 are shown with a solid blue line and a dashed yellow line, respectively.*

5.9.2 Deterministic model for deformation zones

Deterministic modelling, not least of deformation zones, is strongly dependent on an accurate positioning of boreholes at depth. The uncertainty calculated for the spatial position of boreholes in all three dimensions generally increases somewhat with depth and is more significant in the horizontal plane than in the vertical dimension /Munier and Stigsson 2007/. The estimated uncertainty in the position of, for example, a possible deformation zone in a borehole does not exceed c. 30 m in the horizontal plane. In most cases, the uncertainty is less than 10 m in the horizontal plane and less than 6 m in the vertical dimension. These uncertainties are approximately of the same order of magnitude as the uncertainty in the position of low magnetic lineaments /Isaksson and Keisu 2005, Isaksson et al. 2006a/ and seismic reflectors /Cosma et al. 2003/, and are all relatively minor in significance.

Since the orientation of a deformation zone is not based on the orientation of fractures inside the zone, the implications of the uncertainty in the orientation of fractures for the deterministic modelling work is judged to be very low. Furthermore, only very minor changes have occurred in the

orientation of sets of fractures in some deformation zones, when data corrected after the completion of model stage 2.2 have been used /Stephens et al. 2008/. The zones selected for this analysis lie in the north-western part of the tectonic lens (zones ENE0060A, WNW0123, A2, A8 and F1).

The judgement in the modelling work to match a particular low magnetic lineament to a particular deformation zone in a single-hole interpretation, as well as the assumption concerning the down-dip extension of steeply dipping or vertical zones are intrinsic weaknesses in the modelling procedure. These features affect directly the estimate of the dip of the modelled zone, its thickness and its predicted intercept at 400−500 m depth. However, the predictions provided by local model stage 2.2 for the position and character of the intersections of deformation zones in the four cored boreholes not used in this model have been verified highly satisfactorily during model stage 2.3 /Stephens et al. 2008/. Furthermore, the additional ground magnetic data acquired during stage 2.3 only have a limited effect on the position and trace length of deformation zones at the ground surface in model stage 2.2 /Stephens et al. 2008/. As predicted in model stage 2.2 /Stephens et al. 2007/, no new deformation zones with a trace length longer than 3,000 m at the ground surface have emerged. Nevertheless, if Forsmark is selected as the site for the deep geological repository, then it will be necessary to complete minor modifications to the deterministic geological models prior to construction work.

All the observations summarised above provide a basis for confidence in the deterministic models for deformation zones, notwithstanding the intrinsic weaknesses noted above. It is suggested that the successful predictability of the occurrence and character of deformation zones is related to the significant bedrock anisotropy that was established over 1,850 million years ago, when the bedrock was situated at mid-crustal depths and was affected by penetrative, ductile deformation under high-temperature metamorphic conditions.

The following summarises the two remaining more significant uncertainties in the modelling of deformation zones.

- The size of gently dipping fracture zones. The significance of this uncertainty has been reduced somewhat through the selection of the target volume /SKB 2005c/. However, it remains for the gently dipping zones that are present above 500 m depth in this volume. It also needs to be kept in mind that the absence of gently dipping zones in approximately the north-eastern half of the regional model volume is coupled directly to an inherent data bias in the regional model, since reflection seismic data are not available for this area.
- The orientation and size of the possible deformation zones in the single-hole interpretations that have not been modelled deterministically. Since it has not been possible to link these geological features to a low magnetic lineament or seismic reflector and since they commonly occur along short borehole intervals, it is judged that they predominantly represent intersections with minor zones.

5.9.3 Statistical model for fractures and minor deformation zones

Limitations

The data available from surface outcrops lie entirely within fracture domains FFM02 and FFM03. Borehole data come from both these two domains as well as from domains FFM01 and FFM06. Since the coupled size/intensity models for the outcrop scale and the TCM models are based wholly or partly on outcrop data, the models have the least uncertainty when applied to fracture domains FFM02 and FFM03. Application to FFM01 is more uncertain, since there are no outcrop data to support the size model, although there are borehole data for quantifying relations between intensity, rock type and depth. The limited volume of data from domain FFM06 was *not* used in the uncertainty analysis. As a result, the application of the model to FFM01 has a much higher uncertainty than the application of the model to FFM02 or FFM03. Application to FFM06 is uncertain to a degree that could not be quantified with the data available.

The tectonic fault model (TFM), which is calibrated in part on the ground magnetic lineament data, has a higher degree of uncertainty than the other models. There is a mismatch, an over-prediction, between the number of larger fractures predicted by the model and the number obtained by measure-

ments. However, the detection reliability of the method has not been quantified. It is therefore possible, until the opposite can be demonstrated, that the ground magnetic measurements fail to detect the portion of the fracture array which shows weak magnetic signatures. Thus, the detection reliability of the magnetic lineament data and the TFM alternative model based on them should be carefully assessed by any user.

Key uncertainties

The key identified uncertainties are:

- Does the tectonic continuum exist, allowing for the development of a single model to encompass borehole, outcrop, ground magnetic lineament and deformation zone data?
- If the tectonic continuum does not exist, and there are distinct populations of joints and reactivated joints that differ from fault/deformation zone related fractures, then what is the upper size limit to the joints or the lower size limit to the deformation zone related fractures?
- What is the impact of fracture intensity variations by rock type? Can intensities for rock types be combined, and if so, what magnitude of uncertainty does this produce?
- Does the mean pole of a fracture set vary spatially within a fracture domain? If so, what uncertainty is likely to be induced if a constant mean orientation is used for each set within each fracture domain?

Complementary studies on fracture mineralogy

Two complementary studies are in progress at the current time, the results of which have not been assessed in this report. These studies were designed to reduce uncertainties in some aspects of the fracture mineralogy (see section 5.2.5). The first of these studies concerns a more quantitative evaluation of the amount of different minerals along fractures. The second aims to provide more detailed information bearing on the significance and origin of fractures that lack a mineral coating or filling and wall-rock alteration.

6 Bedrock thermal properties

The heat generated by the spent nuclear fuel will increase the temperature of all components of the KBS-3 repository: barriers, tunnels, seals and the host rock itself. To ensure the long-term sealing capacity and the mechanical function of the bentonite buffer surrounding each individual canister, a maximum bentonite temperature is prescribed in the design requirement. This important requirement, which relates to the safety assessment, means that the canisters cannot be deposited arbitrarily close to each other. Unnecessarily large distances between the canisters, on the other hand, will mean inefficient and costly use of the rock volume considered for the repository. In order to determine the minimum canister spacing required to meet the temperature criterion for all canister positions, including those in the least conductive parts of the different rock domains where near-field temperatures will be particularly high, it is necessary to establish an adequate description, of the site rock thermal properties and their spatial variation at the relevant canister scale. The thermal modelling performed for the Forsmark site to establish a thermal site description that is adequate for the layout issue as well as for thermo-mechanical simulations is outlined in this chapter.

The methodology employed for thermal modelling has been fundamentally revised compared with previous model versions, and has been documented in a separate strategy report /Back and Sundberg 2007/. The modelling involves stochastic simulation based on both the spatial statistical structure of rock types and the spatial distribution of thermal conductivities. By merging the realisations of the lithological and thermal simulations, a distribution of thermal properties is produced that takes into account the spatial variability both within and between different rock types. The realisations of thermal properties can be used for subsequent numerical temperature simulations for the thermal design of a repository, i.e. for determining the minimum canister and tunnel spacing required to meet the buffer temperature criterion and to perform any layout optimisations. The strategy for such thermal dimensioning is described in /Hökmark et al. 2009/.

The thermal site description in this SDM-Site report is based on separate reports from stage 2.2 /Back et al. 2007/ and 2.3 /Sundberg et al. 2008/. In these reports, the thermal modelling is more extensively described. In /Sundberg et al. 2008/, the thermal modelling of rock domain RFM045 has been totally revised. Thus, the earlier results presented in /Back et al. 2007/ are only applicable to domain RFM029. The geology of these two domains is described in section 5.4.4.

6.1 State of knowledge at the previous model version

The development of the thermal model for the Forsmark area has been made in different stages and versions. Model version 1.2 and model stage 2.1 are reported in /Sundberg et al. 2005a/ and /SKB 2006a/. Based on modelling performed in version 1.2 /Sundberg et al. 2005a/, thermal properties were reported for two rock domains, namely RFM029 and RFM012. In modelling stage 2.1, new data, in addition to limited modelling efforts, indicated that the statistics of thermal conductivity for domain RFM029 required revision /SKB 2006a/.

It is important to point out that previous model versions were based on an earlier version of the geological rock domain model. This is particularly relevant for domain RFM045. This domain had not been defined in version 1.2 of the geological model, and since little thermal modelling was performed during stage 2.1, there are no previous modelling results available for comparison.

6.2 Evaluation of primary data

The investigations of thermal properties performed in the Forsmark area are summarised in sections 2.1 and 2.3 and the data supporting the current model version are listed in Table 2 in Appendix 3. The evaluation of these data is presented below. A more complete treatment of the data is given in /Back et al. 2007/ and /Sundberg et al. 2008/.

6.2.1 Thermal conductivity determinations

Laboratory measurements of the thermal conductivity and thermal diffusivity of water saturated rock samples have been performed using the TPS (Transient Plane Source) method (see description in /Sundberg 2003a/). The measurements are made on small rock volumes (approximately 10 cm^3). Summary statistics of thermal conductivity for each rock type are presented in Table 6-1. The results of all thermal conductivity measurements are visualised in Figure 6-1. The dominant granitoid rocks in domains RFM029 and RFM045 have high thermal conductivity, whereas granite, granodiorite and tonalite (101051) and amphibolite (102017) have intermediate or low thermal conductivity. A comparison of data from different boreholes and different depths (Figure 6-1) indicates limited large-scale spatial variation in thermal conductivity for the dominant granite (101057) (for sample locations, see Table 3-2 in /Back et al. 2007/).

The difference in thermal conductivity between fresh and altered (albitized) samples of aplitic metagranite (101058) based on TPS measurements is statistically insignificant.

Thermal conductivities have also been determined with the SCA-method /Back et al. 2007/, based on mineral compositions (from modal analysis) and thermal conductivities of different minerals. Investigations of fresh and oxidised samples of granite to granodiorite (101057)- and granite, granodiorite and tonalite (101051) show that, for a given quartz content, the calculated thermal conductivity for oxidised samples is consistently higher than that for unaltered samples.

6.2.2 Relationship between thermal conductivity and density

A relationship between density and measured (TPS) thermal conductivity for Ävrö granite in Laxemar/Simpevarp is well established /Sundberg et al. 2005b, Wrafter et al. 2006, Sundberg et al. 2009/, and when applied to borehole density logging data, has been used for modelling of thermal conductivity along continuous sections of boreholes.

Establishing relationships between density and thermal conductivity is important since it provides support for the use of borehole density data for analysing the spatial correlation structure of thermal properties as described in section 6.4.5. The relationship between density and thermal conductivity for all investigated rock types is illustrated in Figure 6-2. For rock types other than fine- to medium-grained granite, granodiorite and tonalite (101051) and amphibolite (102017), no obvious relationships are apparent within individual rock types. However, the observed relationship between density and thermal conductivity for all rock types together is a function of the mineral constituents and is consistent with the results of theoretical calculations of density and thermal conductivity based on the mineralogy of different rock types presented in /Sundberg et al. 2009/. It provides support for the modelling assumption that the spatial correlation structure of density and thermal conductivity are similar within different rock types.

Table 6-1. Measured thermal conductivity (W/(m·K)) at room temperature (20–25°C) of different rock types using the TPS method.

Rock code	Rock name	Mean	St. dev.	Max	Min	Number of samples
101057	Granite to granodiorite, metamorphic, medium-grained	3.68	0.17	4.01	3.25	74[1]
101056	Granodiorite, metamorphic	3.04	0.09	3.20	2.98	5
101054	Tonalite to granodiorite, metamorphic	2.73	0.19	2.94	2.45	5
101051	Granite, granodiorite and tonalite, metamorphic, fine- to medium-grained	2.85	0.26	3.39	2.46	12
101058	Granite, metamorphic, aplitic	3.85	0.13	4.06	3.68	12[2]
101061	Pegmatite, pegmatitic granite	3.33	0.20	3.50	3.07	4
102017	Amphibolite	2.33	0.10	2.48	2.21	12
111058	Granite, fine- to medium-grained	3.47	0.17	3.62	3.22	5
103076	Felsic to intermediate volcanic rock, metamorphic	2.54		2.99	2.09	2
101033	Diorite, quartz diorite and gabbro, metamorphic	2.28				1

[1]Includes four oxidised samples. [2]Both altered and unaltered samples included.

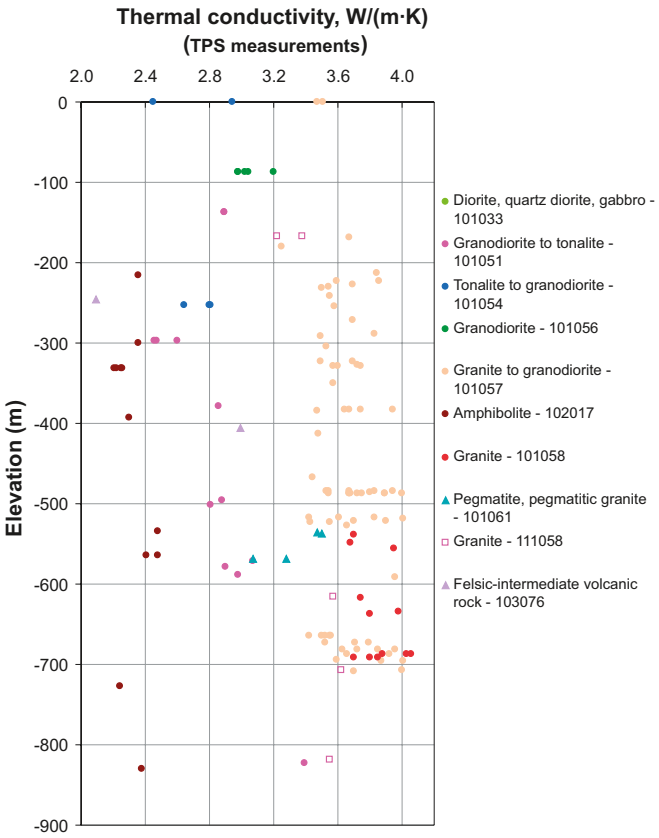

Figure 6-1. *Thermal conductivity versus elevation for different rock types. Samples measured using the TPS method.*

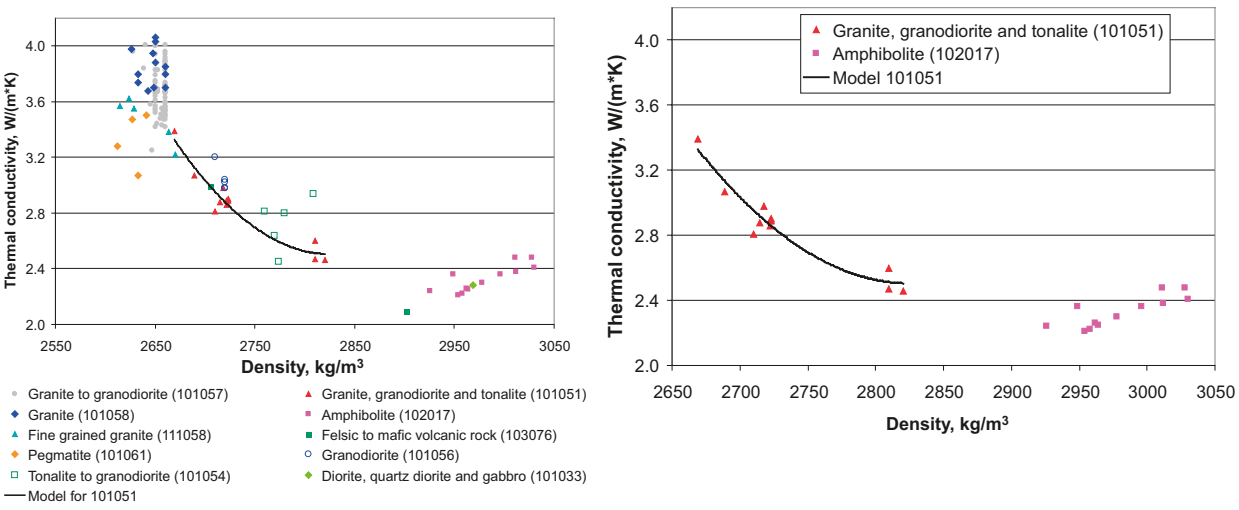

Figure 6-2. *Relationships between density and thermal conductivity for all rock types (left) and for granite, granodiorite and tonalite (101051) and amphibolite (102017) (right). Model refers to granite, granodiorite and tonalite (101051).*

Based on the relationship between density and thermal conductivity, thermal conductivity has been calculated for granite, granodiorite and tonalite (101051) from the density logging of boreholes. The results of these calculations are further described in section 3.4.3 in /Back et al. 2007/.

6.2.3 Measurement of anisotropy of thermal conductivity associated with foliation

All rock types in rock domains RFM029 and RFM045 have been subjected to some degree of ductile deformation, which has produced both a lineation and a foliation. The preferred alignment of mineral grains produced by this deformation may produce anisotropy in thermal transport properties. A higher thermal conductivity can be assumed parallel to the alignment of minerals compared to the perpendicular direction, in analogy with parallel and serial connection of resistors. Anisotropy of thermal properties in the rock mass may impact on the design of a deep repository. For this reason, the directional dependence of thermal properties caused by foliation within deformed granite at the Forsmark site has been investigated in a large-scale field experiment, combined with laboratory and field testing at a smaller scale /Sundberg et al. 2007/.

The investigations were carried out in the vicinity of drill site 7, situated in the north-western, marginal part of the Forsmark tectonic lens (see sections 5.2.1 and 5.2.4). The rock at this site is characterised by a relatively strong tectonic foliation that strikes NNW and dips steeply. Laboratory measurements at the centimetre scale, using a modified TPS method, indicate that thermal conductivity parallel with the foliation is, on average, a factor of 1.4 times greater than conductivity perpendicular to the foliation. Field measurements, including a large-scale experiment that measured larger volumes of rock, have yielded anisotropy factors of approximately 1.15, considerably lower than for the laboratory measurements. A distinct scale dependence on the anisotropy factor is indicated. The results of this investigation are summarised in Table 6-2 with regard to the scale dependence of anisotropy of thermal conductivity.

Given that most of the rock mass displays less intense deformation than that shown by the rock close to drill site 7, lower anisotropy factors would be expected for the greater part of the target volume. However, the anisotropy cannot be neglected.

6.2.4 Heat capacity

Heat capacity has been determined indirectly from thermal conductivity and diffusivity measurements using the TPS method, and directly using the calorimetric method. Results, for samples for which both direct and indirect methods have been used are shown in Table 6-3 and Figure 6-3.

Since the calorimetric measurements are considered to be more reliable, Figure 6-3 indicates that there probably is a bias in the heat capacity determined by the TPS method. The bias is probably caused by the anisotropy in the samples in combination with how thermal conductivity and diffusivity are measured by the TPS method. This is further discussed in section 6.6.1. Calorimetric measurements have been used in the modelling when available.

Table 6-2. Results of investigation of scale dependence on anisotropy of thermal conductivity in the dominant granite. Factor of anisotropy and the effective thermal conductivity (geometric mean of the two principal directions).

Scale	Thermal conductivity	
	Mean factor of anisotropy $\lambda_{pa}/\lambda_{pe}$	Geometric mean W/(m·K)
Centimetre scale	1.40	3.45
Decimetre to metre scale	1.15	3.42

$\lambda_{pa}/\lambda_{pe}$ = thermal conductivity parallel to the foliation divided by thermal conductivity perpendicular to the foliation.

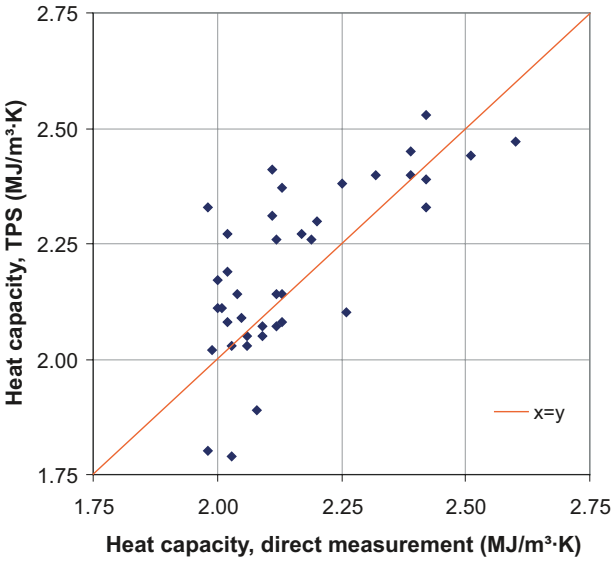

Figure 6-3. *Comparison between heat capacity determined by two different methods, TPS and direct measurement (calorimetric method). Correlation coefficient = 0.709.*

Table 6-3. Heat capacity, determined at room temperature by TPS and the calorimetric method (direct measurement) (MJ/m³·K) on the same samples.

Rock type	TPS		Calorimetric		Number of samples
	Mean	Std dev.	Mean	Std dev.	
Granite to granodiorite, 101057	2.09	0.17	2.06	0.06	14*
Granite, granodiorite and tonalite, 101051	2.23	0.13	2.15	0.05	8
Granite, metamorphic, aplitic, 101058	2.05	0.05	2.01	0.02	3
Amphibolite, 102017	2.43	0.05	2.41	0.11	8
Felsic to intermediate volcanic rock, 103076	2.33	–	2.42	–	1
Granite, fine- to medium-grained, 111058	2.14	0.10	2.06	0.05	5

* Includes three altered samples, see /Back et al. 2007/.

6.2.5 Thermal conductivity vs heat capacity

The relationship between thermal conductivity and density is discussed in section 6.2.2. It is reasonable to assume a corresponding relationship between density and heat capacity. Such a relationship has been found previously /Sundberg 2003b/, although weaker than that for thermal conductivity versus density. In Figure 6-4, heat capacity determined by both the TPS and the calorimetric methods are plotted against thermal conductivity. For the investigated rock types, the relationship between the more reliable heat capacity values from calorimetric measurements and the thermal conductivity measurements is described by a second-order regression equation. The relationship is described in Figure 3-11 in /Back et al. 2007/ and further developed in /Sundberg et al. 2008/.

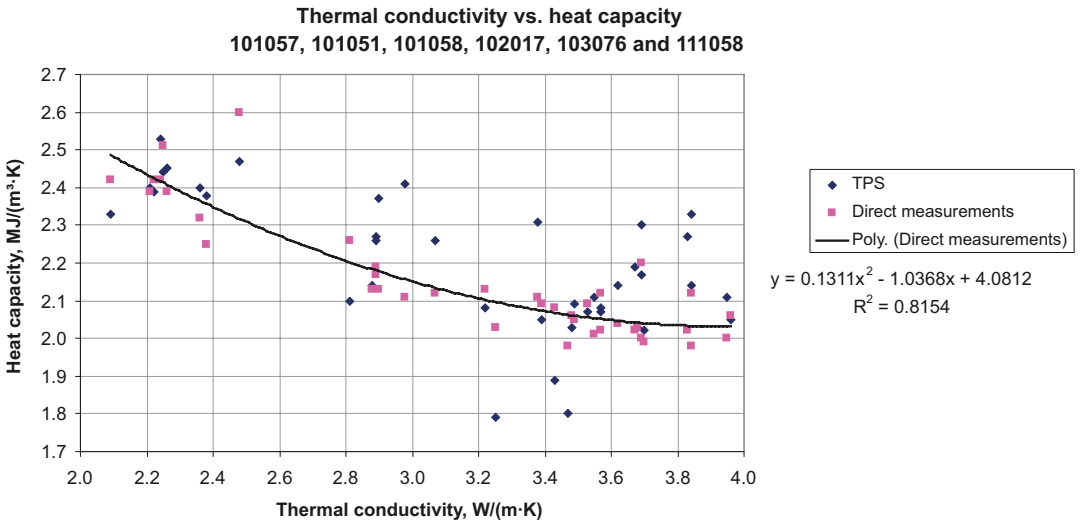

Figure 6-4. *Heat capacity vs. thermal conductivity (room temperature). The heat capacity is calculated from TPS determinations and from calorimetric (direct) measurements. The second-order relationship is based on calorimetric measurements only.*

6.2.6 Temperature dependence of thermal properties

The temperature dependence of the thermal properties has been investigated by TPS measurements on 18 samples of the dominant rock type, granite to granodiorite (101057), at three different temperatures (20, 50 and 80°C); see section 4.3.3 in /Sundberg et al. 2005a/. With increasing temperature, the mean value of the thermal conductivity decreases by 9.8%/100°C temperature increase. The decrease in thermal conductivity varies from 6.6% to 11.7% for the individual samples. With increasing temperature, the heat capacity increases by 28.9%/100°C temperature increase. The increase varies from 16.4% to 63.1% for the individual samples.

For rock types with a lower quartz content than granite to granodiorite (101057), the temperature dependence in thermal conductivity is expected to be less pronounced /Sundberg et al. 2008/.

6.2.7 Pressure dependence in thermal conductivity

The thermal conductivity is lower in stress-released samples compared with determinations at higher pressure (larger depths). The reason is assumed to be the closing of micro cracks at higher pressure. However, the pressure influence is low if the samples are water saturated /Walsh and Decker 1966/. All determinations of thermal conductivity in the site investigation programme have been made on water-saturated samples. The pressure dependence has therefore been neglected in the evaluation.

6.2.8 Coefficient of thermal expansion

The coefficient of thermal expansion has been measured on samples from five different rock types, see Table 6-4. The mean values of measured thermal expansion for the different rock types are rather similar. Samples of amphibolite (102017) have not been investigated.

Table 6-4. Measured thermal expansion (m/(m·K)) on samples with different rock types (interval of temperature: 20–80°C).

Rock code	Rock name	Arithmetic mean	St. dev.	Min	Max	No. of samples
101057	Granite to granodiorite	$7.7 \cdot 10^{-6}$	$2.2 \cdot 10^{-6}$	$2.1 \cdot 10^{-6}$	$1.5 \cdot 10^{-5}$	56
101056	Granodiorite	$8.1 \cdot 10^{-6}$	$3.4 \cdot 10^{-6}$	$5.2 \cdot 10^{-6}$	$1.4 \cdot 10^{-5}$	6
101054	Tonalite to granodiorite	$7.2 \cdot 10^{-6}$		$5.3 \cdot 10^{-6}$	$8.2 \cdot 10^{-6}$	3
101051	Granite, granodiorite and tonalite	$7.8 \cdot 10^{-6}$	$1.2 \cdot 10^{-6}$	$6.5 \cdot 10^{-6}$	$1.0 \cdot 10^{-5}$	6
101058	Granite, aplitic	$7.5 \cdot 10^{-6}$		$6.9 \cdot 10^{-6}$	$8.0 \cdot 10^{-6}$	3

6.2.9 *In situ* temperature

Fluid temperature has been measured in most cored boreholes at Forsmark. Large differences in logged temperature for the same depth in different boreholes were noted in earlier model stages. Uncertainties associated with the data were judged to be high. For this reason, the fluid temperature loggings for each borehole have been re-evaluated with the objective of assessing their reliability. The criteria considered were 1) errors associated with the logging probe, and 2) time between drilling and logging. The evaluation of temperature data on the basis of these criteria has resulted in a number of "approved" boreholes (see /Sundberg et al. 2008/).

The results from the temperature loggings, and the calculated gradients, for the "approved" boreholes are shown in Figure 6-5. In Table 6-5, the fluid temperature at depths 400 m, 500 m and 600 m in the boreholes are presented. The measured temperatures at 500 m depth fall within the interval 11.2–12.0°C for the boreholes KFM01A, KFM02A, KFM03A, KFM04A, KFM06C and KFM08C (see Figure 6-5). A trend of increasing gradient with depth can be observed, from about 10°C/km at 300 m to about 13°C/km at 700 m depth (see also /Sundberg et al. 2008/).

Mean annual air temperatures recorded at meteorological stations close to the Forsmark area are between 5°C and 5.5°C /Johansson et al. 2005/.

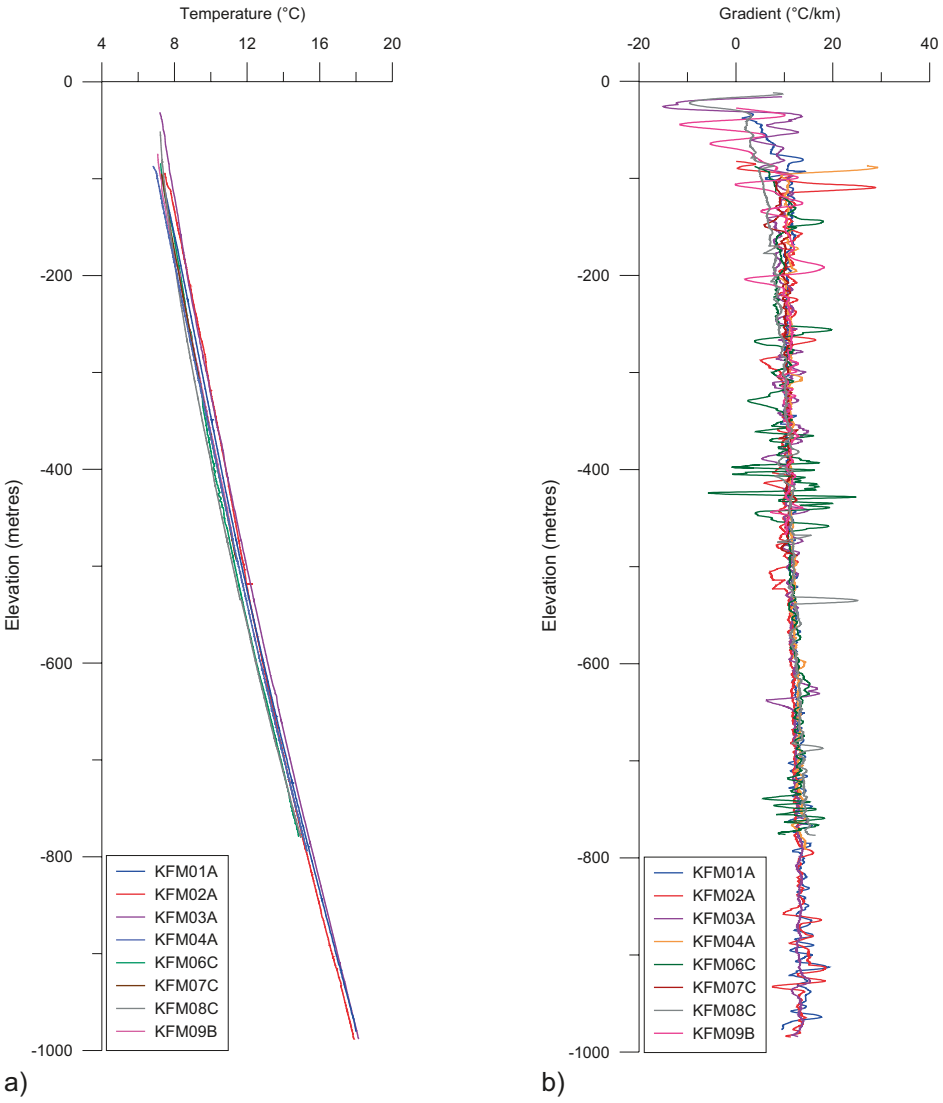

Figure 6-5. *Summary of fluid temperature (a) and vertical temperature gradient calculated for nine metres intervals (b) for eight boreholes at Forsmark. The results are from fluid temperature loggings.*

Table 6-5. Temperature (°C) at different levels for the "approved" boreholes at the Forsmark site. Borehole inclinations are also included, given as lowest and highest angle /Sundberg et al. 2008/.

Borehole	Temperature at depth 400 m	Temperature at depth 500 m	Temperature at depth 600 m	Inclination (°)
KFM01A	10.6	11.7	12.9	75–85
KFM01C*	–	–	–	46–50
KFM02A	10.8	11.8	12.9	80–86
KFM03A	10.8	12.0	13.1	83–86
KFM04A	10.4	11.5	12.7	44–63
KFM06C	10.2	11.3	12.5	45–60
KFM07C*	10.4	11.4**	–	84–85
KFM08C	10.1	11.2	12.5	59–60
KFM09B*	10.4	–	–	41–55
Arithmetic mean	10.5	11.6	12.8	

* Maximum vertical depth of KFM01C is about 340 m, KFM07C about 490 m, and KFM09B about 470 m.

** At 493 m (vertical depth).

6.3 Strategy for thermal modelling

6.3.1 Conceptual model

The methodology employed for thermal modelling has been fundamentally revised compared with previous model versions, and has been documented in a separate strategy report /Back and Sundberg 2007/ and implemented in the Forsmark site modelling stage 2.2 /Back et al. 2007/. The strategy for thermal modelling is based on a conceptual model which considers a range of properties, for example, lithology, rock alteration, thermal properties of rock types, spatial variability and correlation. The conceptual model explains the spatial variability of thermal conductivity in terms of lithological and mineralogical heterogeneity (variability), and also provides an explanation for anisotropy of thermal properties.

Thermal properties, especially thermal conductivity, vary significantly between different rock types but also within the rock types. The variability is essentially a result of variations in the mineral compositions of the original igneous rock types, but also post-magmatic metamorphism and alteration. "Within rock type" variability is also a function of the way rocks have been classified; for example, a particular rock type may include two or more subtypes.

Based on the considerations above, the total variability within a rock domain depends on the lithology and the thermal properties of each rock type. The lower tail of the thermal conductivity distribution at a certain scale is determined by the fraction and size distribution of the low-conducting rock types. This lower tail is important for the design of the repository.

The rock mass at Forsmark may display anisotropy in thermal properties. There are at least two main causes of thermal anisotropy to consider:

1. Anisotropy due to foliation/lineation.
2. Anisotropy due to orientation of subordinate rock bodies.

The first type is caused by penetrative ductile deformation within a rock type. The foliation and lineation imply a directional orientation of the minerals in the rock mass. The thermal conductivity is generally higher parallel to the mineral foliation and lower perpendicular to the foliation.

The second type of anisotropy is a result of the spatial orientation of rock bodies, primarily subordinate rocks. These bodies may have preferential directions in space, resulting in anisotropy of the thermal properties at larger spatial scales. Tabular bodies of amphibolite parallel to the foliation at Forsmark are typical examples of this anisotropy (section 5.2.4). At Forsmark, the orientation of the subordinate rock types and the foliation are generally parallel or sub-parallel to each other.

6.3.2 Modelling approach

Introduction

The strategy for the thermal site descriptive modelling involves producing spatial statistical models of both lithology and thermal properties, and generating stochastic simulations to give spatial 3D realisations of thermal properties that are representative of the modelled rock domain. These realisations are used to represent the rock domain statistically. The methodology is described in detail in /Back and Sundberg 2007, Back et al. 2007/.

There are different objectives for which the modelling approach can be used. In this report, the focus is on description. Of special interest for the description is to:

- determine the low percentiles of thermal conductivity,
- model how the thermal conductivity varies with scale, and
- produce realisations of the spatial distribution of thermal properties that can be used for subsequent modelling work, such as numerical temperature simulations for the thermal design of a repository (distances between canisters and tunnels).

For the description problem, no concern is given to specific locations in the rock mass; only the statistics of the rock domain of interest are addressed. The methodology for this type of problem is based on unconditional stochastic simulation (distributes simulated data spatially without honouring measurements at specific locations). Due to the large rock volumes and computer limitations, conditional stochastic simulation with high resolution can only be used for small parts of a rock domain.

The focus of the modelling approach is on thermal conductivity. In addition to thermal conductivity, the corresponding heat capacity distribution is determined based on the relationship between thermal conductivity and heat capacity for rock types in the Forsmark area (see section 6.2.5). The realisations of thermal conductivity are used as input to these calculations, and the result is a heat capacity distribution that represents the rock domain.

Outline of the methodology

The methodology, outlined in Figure 6-6, is applied separately for each rock domain. The simulation scale (1) is defined first. This scale determines how lithological data (2) should be prepared and if a change of support (5) is required for the thermal data (4) (change of support, or upscaling, refers to the change of the scale of data or simulated values). The lithological data acquired from boreholes and mapping of the rock surface need to be reclassified into thermal rock classes, TRCs (3). The main reason for this is that only a limited number of classes can be handled in the lithological simulations.

The lithological data are used to construct models of the transition between different TRCs, thus describing the spatial statistical structure of each TRC (7). The result is a set of transition probability models that are used in the simulation of TRCs (8). The intermediate result of this first stochastic simulation is a number of realisations of the spatial distribution of groups of rock types in each domain.

Based on the thermal data, a spatial statistical thermal conductivity model is constructed for each TRC (9). It consists of a statistical distribution and a variogram for each TRC. These are used in the stochastic simulation of thermal conductivity (10), which results in a number of equally probable realisations of thermal conductivity for the TRC.

In the next step, the realisations of TRCs (lithology) and thermal conductivity are merged (11), i.e. each realisation of lithology is filled with simulated thermal conductivity values. The result is a set of realisations of thermal conductivity for each rock domain that considers both the difference in thermal properties between different TRCs, and the variability within each TRC. If the result is desired at a scale different from the simulation scale, upscaling of the realisations can be performed (12) to a scale not larger than the size of the simulation domain. In practice, upscaling should be made to a much smaller scale, preferably the canister scale. The results (13) can be presented in a number of ways, for example as 3D illustrations, histograms and statistical parameters for the rock mass, probabilities of encountering low thermal conductivity values, *etc*.

The methodology can also be used for other types of rock properties, once the appropriate upscaling procedure is determined.

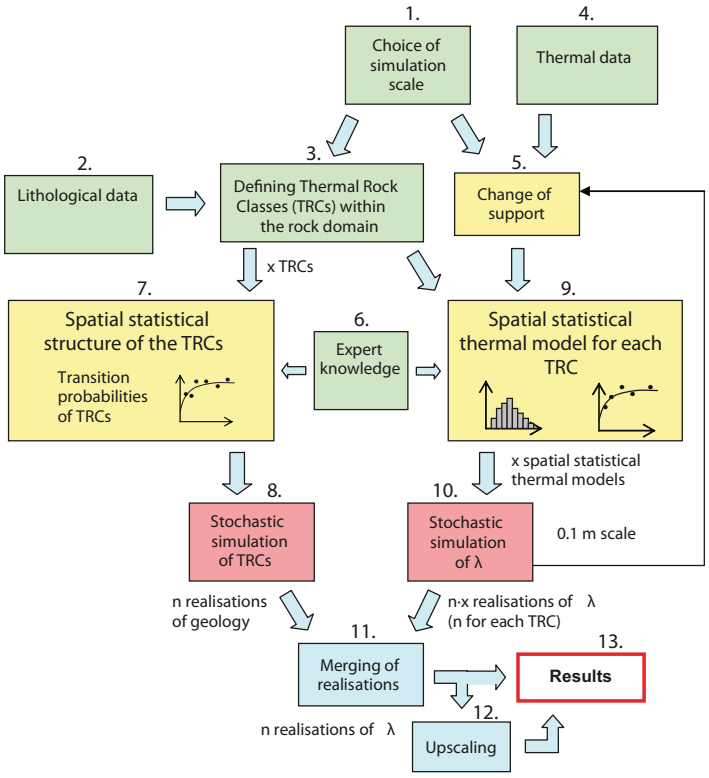

Figure 6-6. *Schematic description of the approach for thermal conductivity modelling of a rock domain (λ represents thermal conductivity).*

6.3.3 Modelling assumptions

The modelling approach requires a number of assumptions in various steps of the modelling process. The most important ones are listed below.

- It is assumed that thermal conductivity data (from TPS and SCA methods – section 6.2.1) represent the 0.1 m scale, which is the scale at which the initial simulations are performed (cells of cubic shape with 0.1 m sides).
- The 1 m scale is assumed to be sufficiently small to properly represent the subordinate rock types in the lithological simulations.
- The simulation volumes ($50\times50\times50$ m^3 for scale 1 m) are assumed to be sufficiently large for the objectives of the simulations, see 6.3.2.
- Borehole information from Boremap and core samples used for measurements are assumed to be representative of the rock domain.
- Water movements are not considered in the modelling. It is assumed that modelling such effects could lead to non-conservative estimates of thermal properties.
- The modelling is performed using effective values of thermal conductivity (isotropic assumption) – this also applies to the upscaling methodology, where effective values are calculated using the SCA approach (described in section 2.3.4 in /Back and Sundberg 2007/).
- Geological interpretations, based on expert opinion, have been used in the simulations.
- For the purpose of lithological simulations, a rock domain is divided into thermal subdomains, each of which is assumed to be statistically homogeneous.
- In the lithological simulations, the transition between TRCs are assumed to follow a Markov process.
- Various assumptions regarding the shapes of statistical distributions and variograms for the thermal conductivity of a TRC are required.
- It is assumed that the spatial statistical thermal model for a TRC (statistical distribution and variogram) is the same for all rock types that belong to that TRC.

- Spatial correlation in thermal conductivity between different parts of a rock type body is assumed not to be "broken" by the presence of a different type of rock separating these parts.
- The presence of rock stress components is assumed to have no effect on the thermal properties.

Detailed information regarding the assumptions made for the lithological and the spatial statistical thermal models for each TRC is provided in the following sections.

6.3.4 Feedback from other disciplines

The rock domain model presented in section 5.4 provides the geological framework for the description of thermal properties of the rock mass within the target volume at Forsmark. Two key rock domains have been identified inside the tectonic lens and target volume. These are the volumetrically more important domain RFM029, and the subordinate domain RFM045. The thermal properties of these two domains are evaluated here. A geological description of the two domains that addresses, for example, the dominant and subordinate rock types is provided in section 5.4.

Valuable cooperation with the geologists in the Forsmark modelling team has been established and maintained throughout the thermal modelling stages. Integration with geology was particularly close concerning the geological interpretations used as input in the stochastic simulations of lithologies.

6.4 Geostatistical analyses and stochastic simulations

6.4.1 Thermal Rock Classes (TRC) – Definition, properties and proportions

Geological borehole data form the basis for the stochastic simulation of lithologies, an important component of the thermal modelling procedure. To keep the lithological simulations at a manageable level of complexity, the number of lithological classes should not exceed five. For this reason, the rock types are grouped into classes, called thermal rock classes (TRC). Rock types with similar thermal and lithological properties were assigned to the same class. The classification of rock types into TRCs for domain RFM029 and domain RFM045 are presented in Table 6-6 and Table 6-7, respectively. Each domain consists of four TRCs, three of which are common to both domains. The fourth differs on the basis of the occurrence of alteration referred to as albitization. The code for a TRC is defined by using the two last digits of the rock code for the dominant rock type in that class.

Table 6-6. Division of rock types into TRCs for domain RFM029. Proportions of different rock types and geological characteristics are according to /Stephens et al. 2007/ and proportions of TRCs are from /Sundberg et al. 2008/.

TRC	Rock name/code	Mean thermal conductivity (TPS), (W/(m·K))	Composition, mode of occurrence, etc.	Proportions of rock types from geological model 2.2, (%)	Proportions of TRCs in boreholes used for lithological simulations (%), 95% confidence intervals in brackets
57	Granite to granodiorite, 101057	3.68	Felsic composition, group B rocks.	74	78.9 (76.4–82.4)
	Granite, aplitic, 101058	3.85		1	
51	Granite, granodiorite and tonalite, 101051	2.85	Felsic to more intermediate compositions, group A and C rocks.	5	3.8 (1.2–4.8)
	Felsic to intermediate volcanic rock, 103076	2.54		< 1	
61	Pegmatite, pegmatitic granite, 101061	3.33	Felsic composition, group D rocks. Late tectonic dykes, segregations, veins.	13	13.1 (9.6–16.7)
	Granite, 111058	3.47		2	
17	Amphibolite, 102017	2.33	Mafic composition, group B rocks. Dykes and minor bodies or lenses.	4	4.2 (2.5–5.6)
	Diorite, quartz diorite and gabbro, 101033	2.28		< 1	

Estimates of the confidence intervals, performed by the bootstrapping method, take into consideration borehole lengths, as well as expert judgements regarding the relative proportions of the two subdomains (marginal and internal).

Table 6-7. Division of rock types into TRCs for domain RFM045. Proportions of different rock types and geological characteristics are according to /Stephens et al. 2007/ and proportions of TRCs are from /Sundberg et al. 2008/.

TRC	Rock code	Mean thermal conductivity (TPS), (W/(m·K))	Composition, mode of occurrence, etc.	Proportions of rock types from geological model 2.2, (%)	Proportions of TRCs in boreholes used for lithological simulations (%), 95% confidence intervals in brackets
58	Granite, aplitic, 101058	3.85	Felsic composition, group B rocks commonly affected by albitization.	49	67.7 (62.8–77.6)
	Granite to granodiorite, 101057	3.68		18	
51	Granite, granodiorite and tonalite, 101051	2.85	Felsic to more intermediate compositions, group A and C rocks.	9	10.6 (6.0–13.1)
	Felsic to intermediate volcanic rock, 103076	2.54		1	
61	Pegmatite, pegmatitic granite, 101061	3.33	Felsic composition, group D rocks. Late tectonic dykes, segregations, veins.	14	14.6 (11.2–17.7)
	Granite, 111058	3.47		1	
17	Amphibolite, 102017	2.33	Mafic composition, group B rocks. Dykes and minor bodies or lenses.	6	7.0 (1.8–9.4)
	Diorite, quartz diorite and gabbro, 101033	2.28		< 1	

Estimates of the confidence intervals, performed by the bootstrapping method.

Proportions of TRCs in domains RFM029 and RFM045 are presented in Table 6-6 and Table 6-7. In addition, the 95% confidence intervals for these estimates are calculated for borehole scale /Sundberg et al. 2008/. Proportions based on boreholes selected to characterise each domain in the lithological simulations differ slightly from proportions estimated in the geological model, as documented in Figure 4-9 and Figure 4-12 in /Stephens et al. 2007/. The reason for the observed discrepancies is discussed in section 6.6. The uncertainties associated with the estimates of the mean TRC proportions in domain RFM045 are relatively large because of the small number of boreholes combined with the rather heterogeneous geology.

6.4.2 Geological heterogeneity and division into thermal subdomains

Stochastic simulations were used to simulate the spatial distribution of lithologies in domains RFM029 and RFM045. In order to capture the geological heterogeneity present within these rock domains, each domain was divided into thermal subdomains, each of which was assumed to be statistically homogeneous. Each subdomain was then simulated separately.

The investigated rock volume is situated within a tectonic lens formed in connection with penetrative ductile deformation as described in section 5.2.4. The internal part of this lens is dominated by rocks with a lower ductile strain, and with a deformation style that is more lineated than foliated. The margins of the lens are characterised by more intense foliation. In domain RFM029, the geometry and orientation of subordinate rocks, in particular amphibolite, are largely determined by these different deformation styles. Since the spatial orientation of subordinate rock bodies may result in anisotropy in the thermal properties, it was decided to divide domain RFM029 into two subdomains for the purposes of lithological simulation as follows; see Table 5-3 in /Back et al. 2007/:

1. margins of the tectonic lens dominated by foliation, and
2. internal part of the tectonic lens where lineation is more prominent than foliation.

Each of these subdomains is considered to be more homogenous with regard to the orientation and geometry of amphibolite bodies. Throughout the domain, the amphibolites consistently follow the orientation of the ductile structures (section 5.2.4). Thus, in the margins, they are assumed to be flattened parallel to the foliation, whereas in the internal part of the domain, they are, in addition to flattening, assumed to be elongated in the direction of the mineral stretching lineation.

The tectonic lens is affected by a major fold structure, which determines the orientations of the contacts between the dominant metagranite and the subordinate rocks types, including amphibolite (section 5.2.4 and Figure 5-25). Boreholes which show foliation and amphibolite contact orientations typical for the Forsmark tectonic lens, i.e. predominantly NW to NNW strike with moderate to steep dips to the W, are used in the analysis. Boreholes/borehole sections with anomalous foliation/amphibolite contact orientations were excluded. These include boreholes KFM01B and KFM08A. In terms of TRC proportions this does not bias the results significantly.

For domain RFM045, a similar analysis has been performed for the borehole sections assigned to this domain. Domain RFM045 is considered to possess a deformation style typical of the internal part of the tectonic lens at Forsmark /Stephens et al. 2007/, which means that, although a foliation is present, lineation is assumed to be the dominant result of the ductile deformation. In model stage 2.2 /Back et al. 2007/, the domain was not subdivided, i.e. the whole domain was considered to be statistically homogeneous in the modelling. However, a new analysis was performed in model stage 2.3 /Sundberg et al. 2008/ in order to better describe the lithological heterogeneity within domain RFM045, in particular with regard to amphibolite bodies. On the basis of data from four boreholes, two subdomains were defined, the characteristics of which are described in Table 6-8.

Borehole sections dominated by aplitic granite (101058) and granite to granodiorite (101057) with only minor occurrences of subordinate rocks (thermal subdomain A) can be distinguished from sections comprising larger bodies of amphibolite (102017) and granite, granodiorite and tonalite (101051) (thermal subdomain B). Borehole sections of subdomain A dominate the domain. Subdomain A required further subdivision (A1 and A2), due to the variable orientations of boreholes in relation to the axes of anisotropy. It should be noted that these subdomains are not geometrically bounded (see section 5.2.3).

The orientation and geometry of subordinate rock types are modelled in the lithological simulations of domains RFM029 and RFM045. Judgements of the typical orientations and geometries were elicited from the geological modelling team and from Appendix 6 in /Stephens et al. 2007/. Interpretations of orientation and geometry rely heavily on an understanding of the ductile deformation within the tectonic lens at Forsmark, as well as on impressions gained by geologists in the field.

Table 6-9 summarises assumptions made regarding the orientation and geometry of amphibolite bodies (TRC 17) in the boreholes selected to represent the different parts of domain RFM029. Boreholes with anomalous amphibolite orientations, occurring in the hinge of the large-scale synform within the tectonic lens, were excluded. TRC 51, essentially granite, granodiorite and tonalite (101051), is assumed to have similar orientation and geometry to amphibolite. TRC 61 (pegmatite, 101061) is modelled identically in both subdomains, i.e. as dyke-like bodies lying parallel to the foliation and having a diameter three times their thickness.

Table 6-10 summarises the assumptions regarding the orientation of subordinate rocks in boreholes assigned to domain RFM045. The boreholes representing this domain occur close to the hinge of the large-scale synform and therefore display more variable orientations of amphibolite bodies. The assumed geometries of subordinate rocks are similar to those selected for the internal part of domain RFM029 (Table 6-9), with the exception of TRC 61 (mainly pegmatite), which is modelled with a stronger degree of anisotropy (5:5:1).

Table 6-8. Description of subdomains in rock domain RFM045.

Thermal subdomain	Lithological character	True thickness of amphibolite bodies
A	Low proportions of both TRC 17 (mainly amphibolite: 2%) and TRC 51 (mainly granite, granodiorite and tonalite: 6%)	Thin, < 1 m
B	High proportions of both TRC 17 (18%) and TRC 51 (19%)	Thick (c. 5–30 m)

Table 6-9. Assumed orientation and geometry of amphibolite bodies in domain RFM029.

	Orientation of amphibolite contacts		Orientation of longest axis. Based on mineral stretching lineation		Ratio between longest, intermediate and shortest axes
	Strike	Dip	Trend	Plunge	
Domain 29, Margin	150°	80°W			3:3:1
Domain 29, Internal	150°	80°W	157°	38°	4:2:1

Table 6-10. Assumed orientation of amphibolite bodies in boreholes in domain RFM045.

Boreholes in domain RFM045	Orientation of amphibolite contacts		Orientation of longest axis. Based on mineral stretching lineation	
	Strike	Dip	Trend	Plunge
KFM06A	112.5°	60°S	145°	42°
KFM06C	112.5°	60°S	145°	42°
KFM08C	60°	60°S	145°	60°
KFM08D	125°	70°S	145°	42°

6.4.3 Spatial statistical models of lithology

To model the geometrical distribution of different lithologies (TRCs), Markov chain analysis was used to calculate transition probabilities. This method allows the incorporation of geological expert judgements /Carle and Fogg 1997/.

The spatial structure of lithologies was modelled from borehole data which were first processed, as further described in section 5.3.1 in /Back et al. 2007/, to match the 1 m simulation scale chosen. The typical lens length and juxtapositional tendencies of TRCs were calculated through the transition probability analysis of borehole data as described in detail in section 5.4.1 in /Back et al. 2007/ and in /Sundberg et al. 2008/. Anisotropy in the geometry of subordinate rock bodies was taken into account, based on the feedback from the geological modelling team. In the context of the lithological simulations, anisotropy refers to subordinate rock types having dimensions in a particular direction that are different from those in another direction.

In order to take anisotropy into account, the borehole data were transformed to a local coordinate system (x’’’, y’’’, z’’’) oriented in the principal direction of anisotropy defined by the mineral stretching lineation and foliation plane (see /Back et al. 2007/ for domain RFM029 and /Sundberg et al. 2008/ for domain RFM045). To minimise errors due to borehole deviations from anisotropy directions, only the boreholes with an orientation close to one of the axes x’’’, y’’’ or z’’’ were used. For description of the boreholes used in the geological modelling see /Back et al. 2007/ (RFM029) and /Sundberg et al. 2008/ (RFM045).

The results of the spatial analysis for each domain for 1 m data are given in /Sundberg et al. 2008/ (domain RFM045) and /Back et al. 2007/ (domain RFM029). In Table 6-11, these results are exemplified by those for the internal part of domain RFM029.

Table 6-11. Proportions, transition probabilities and typical lengths for domain RFM029 Internal, used in 1 m simulations. Transition probabilities are shown as embedded probabilities of going from one TRC to other TRCs. Diagonal terms (bold) show the typical lengths of TRCs based on all boreholes and without consideration of anisotropy. "Typical TRC lengths" show the typical anisotropic lengths for directions x''', y''' and z'''.

TRC	Proportion (%)	Isotropic transition probabilities to TRCs (embedded) and typical lengths (m). (Lengths shown in bold)				Typical TRC lengths (m)		
		TRC 17	TRC 51	TRC 57	TRC 61	X'''	Y'''	Z'''
TRC 17	3.8	**1.89**	0.03	0.89	0.08	4.10	2.05	1.03
TRC 51	4.5	0.07	**3.00**	0.67	0.26	6.52	3.26	1.63
TRC 57	78.7	0.16	0.08	**6.97**	0.76	b.g.	b.g.	b.g.
TRC 61	13.1	0.01	0.06	0.93	**1.42**	1.12	1.12	0.37

b.g. = background material in the realisations, not calculated for anisotropy directions.

6.4.4 Stochastic simulations of lithology

Results

For the purpose of lithological simulation of the rock domains, a simulation volume of 50×50×50 m^3, divided into grid cells (cubes) of size 1×1×1 m^3, was selected. Stochastic unconditional simulations were performed using the spatial properties derived from the analysis described in section 6.4.3. The simulations were made as follows:

- Domain RFM029, Internal: 667 realisations,
- Domain RFM029, Marginal: 333 realisations,
- Domain RFM045, A1: 105 realisations,
- Domain RFM045, A2: 229 realisations, and
- Domain RFM045, B: 166 realisations.

The number of realisations selected for each subdomain reflects their volumetric importance, which was based on judgements made in consultation with the geological modelling team. Results of the simulations are exemplified in Figure 6-7 and Figure 6-8.

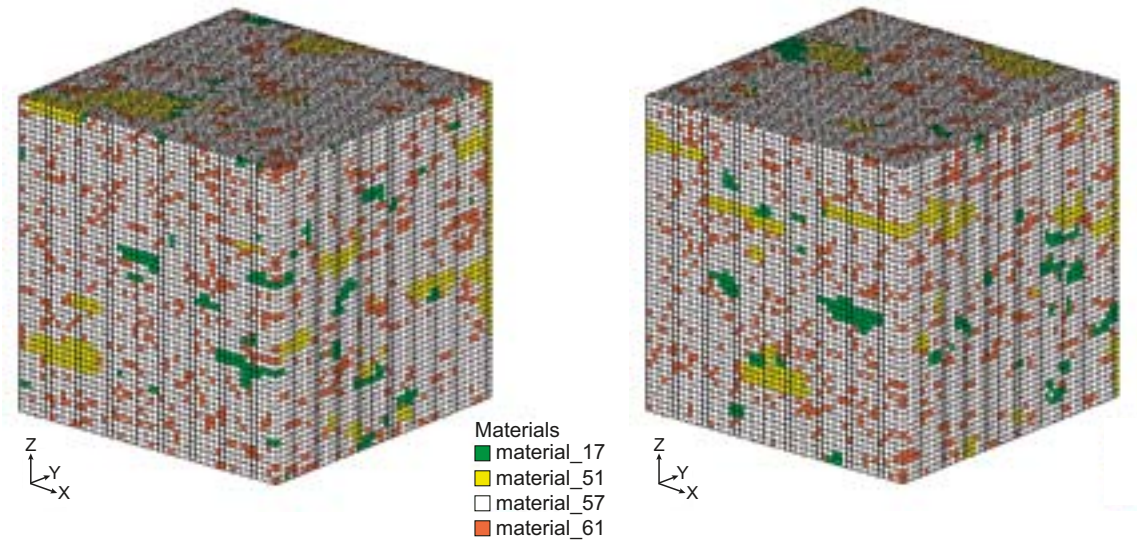

Figure 6-7. *Two 1 m realisations of domain RFM029 Internal. The simulated rock volume has dimensions 50×50×50 m. The simulated TRCs are TRC 57 (white), TRC 61 (orange), TRC 51 (yellow) and TRC 17 (green). For explanation of TRCs, see Table 6-6.*

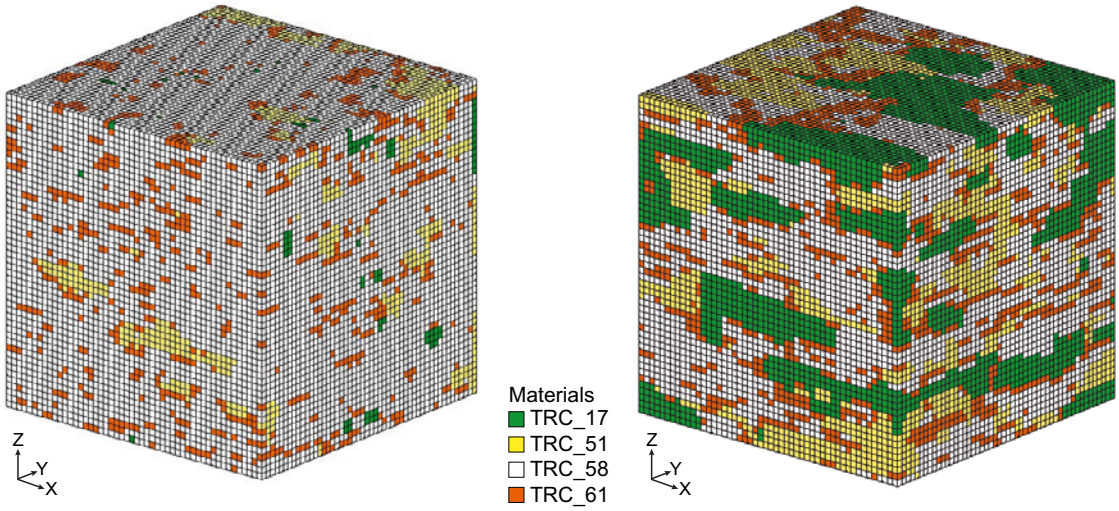

Figure 6-8. *Two 1 m realisations of thermal subdomains in domain RFM045; subdomain A1 (left) and subdomain B (right). For explanation, see Figure 6-7 and Table 6-7.*

Analysis and verification of results

The statistical properties, i.e. the proportions of categories (TRCs), the typical lengths of categories and the spatial properties of categories are assumed to be stationary for all realisations for a specific thermal subdomain. The relevance of the results of the simulations has been analysed and verified by means of statistical analysis with respect to the ability of reproducing the following characteristics.

- The proportions of the TRCs from input data.
- Typical (mean) lengths of TRCs calculated by transition probability analysis of borehole data. "Borings" through randomly selected realisations were used to estimate the typical simulated lengths of TRCs 17, 51 and 61. These can be compared with the typical lengths calculated from borehole data (see Table 6-12 for example). TRCs 57 and 58 constitute the "background" in the realisations and are therefore not relevant to the analysis.
- The distribution of TRC lengths observed in borehole data. Histograms of the lengths of the TRCs were made from "borings" along each direction (x, y and z) in randomly selected realisations and visually compared with histograms based on borehole data.

This analysis, described in detail in /Back et al. 2007/ (RFM029) and /Sundberg et al. 2008/ (RFM045), gave the following results.

- The simulations nearly exactly reproduced the proportions of the TRCs for all realisations.
- The typical lengths of the TRCs can be reproduced very well if the typical lengths are approximately 2.3 m or longer. For shorter lengths there seems to be an overestimation of the typical lengths. The reason for overestimation of shorter lengths is the discretisation in the model, where 1 metre is the shortest length that can be represented. This is exemplified for TRC 51 in domain RFM029 Internal in Table 6-12.
- The simulations are able to realistically reproduce the TRC lengths registered in the borehole data. A visual comparison was made of the histograms from the "borings" with lengths observed in the corresponding borehole data. An example is provided for TRC 17 (amphibolite) in Figure 6-9 and Figure 6-10. As can be seen in the figures, lengths of up to 13 m for TRC 17, which is similar to the maximum length observed in the borehole, could be simulated for the x-direction of the simulated rock volume. The x-direction is the major direction of anisotropy, as given from expert judgement.

Table 6-12. Typical lengths of TRC 51 in rock domain RFM029 Internal.

Typical length (m), from realisations	Typical length (m), from borehole analysis	Comment to simulated values
μ_x = 5.90 ±1.40	6.52	OK
μ_y = 3.58 ±0.78	3.26	OK
μ_z = 2.00 ±0.23	1.63	Somewhat high /Back et al. 2007/

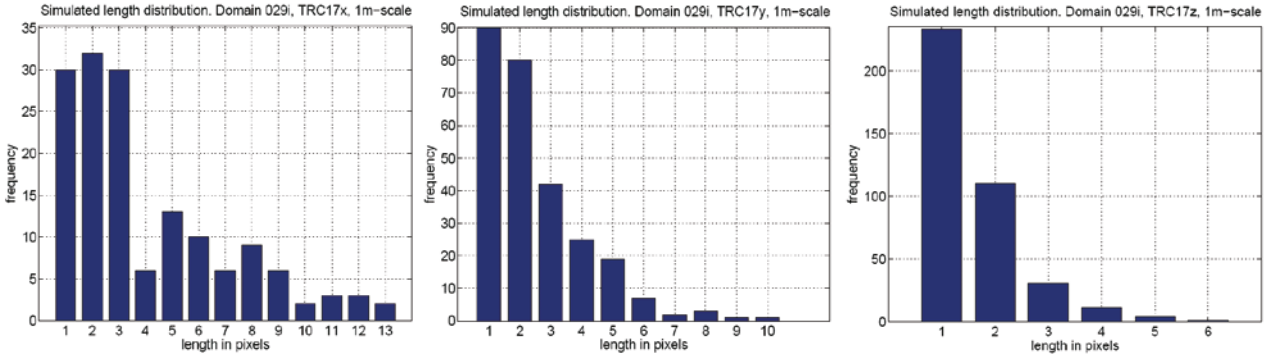

Figure 6-9. *Histograms from 10 randomly selected realisations of TRC 17 in the x, y and z directions (lengths on x axis, in metres) in rock domain RFM029 Internal.*

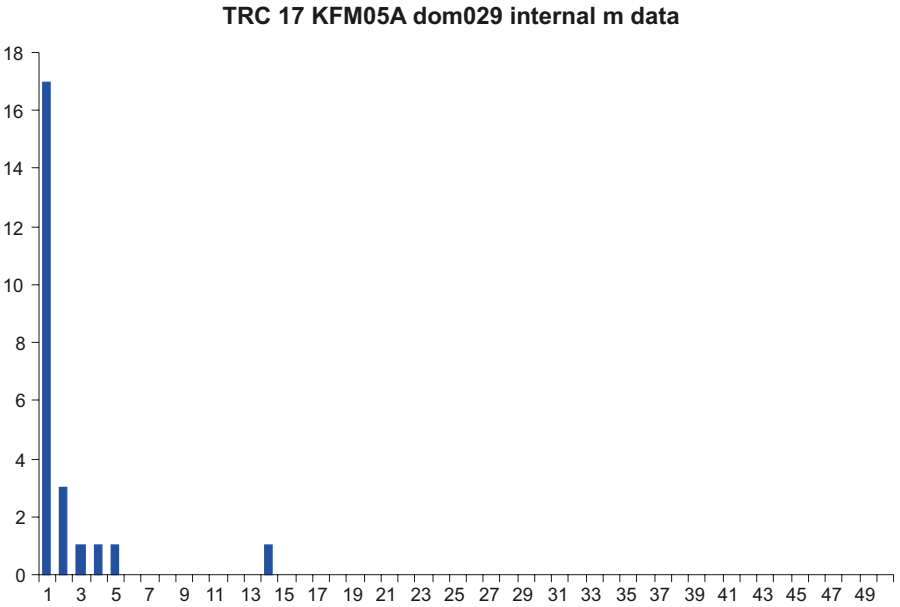

Figure 6-10. *Histogram of TRC lengths in borehole KFM05A in domain RFM029 Internal. The borehole is parallel to the x-direction in Figure 6-9.*

The analysis also showed that the simulations can reproduce the relative anisotropy between different directions reasonably well. An exception is TRC 17 in subdomain B. The long nominal length in the x-direction is underestimated in the simulations, whereas simulations reproduce typical lengths in the y and z directions. This means that anisotropy is not as pronounced in the simulations of subdomain B as predicted by the model parameters. This is tentatively suggested to be an effect of the limited simulation volume. A more complete presentation of the results of this analysis can be found in /Back et al. 2007/ and /Sundberg et al. 2008/.

6.4.5 Spatial statistical models of thermal conductivity

Approach

Spatial statistical thermal conductivity models at the 0.1 m scale are required for each TRC in order to perform simulations at the scale at which the measurement data are applicable. Upscaling of the simulated 0.1 m values is performed in order to define thermal models for the 1 m scale, which is the same scale as that used in the lithological simulations. The models for each TRC comprise two components: a statistical distribution model and a model describing spatial correlation, i.e. a variogram model.

Once the thermal models for the 0.1 m scale are defined, the thermal models for the 1 m scale are easily determined by an upscaling procedure, see section 4.2 in /Back et al. 2007/. Therefore, the focus of the presentation of the thermal models is on the 0.1 m scale. The models for the 1 m scale are presented in section 6.4.6 and the modelling approach is described in Figure 6-6.

Statistical distribution models – 0.1 m scale

Statistical distribution models of thermal conductivity for each TRC are produced from histograms. Histograms for individual rock types and the models for different TRCs are given in Appendix C in /Back et al. 2007/. A histogram describes the variability in thermal conductivity within a TRC, without consideration of spatial aspects and anisotropy.

The statistical distribution models for each TRC are based on data values from the rock types making up the TRC; for details see section 5.2.4 in /Back et al. 2007/. For example, TRC 57 combines data from the two rock types, granite to granodiorite (101057) and granite (101058). The data are weighted according to the relative proportions of each rock type, as well as the number of data values available for each rock type. For the TRCs common to both rock domains RFM029 and RFM045, the data are weighted according to the proportions of each rock type in domain RFM029, which are broadly similar to those in rock domain RFM045.

Thermal conductivity values determined from samples of oxidised rock were included in the data sets. For the common rock types, the relative amount of data derived from oxidised samples is roughly equivalent to the proportion of the rock mass outside the deformation zones which has been mapped as oxidised within the modelled domains; see Figure 4-10 and Figure 4-13 in /Stephens et al. 2007/.

The TRCs are not modelled by standard statistical distributions. Distribution models are instead based on smoothing of the sample histograms, performed using a smoothing algorithm in the geostatistical software GSLIB /Deutsch and Journel 1998/. Smoothing is desirable because of relatively small data sets. Theoretical lower and upper limits of thermal conductivity for each TRC were generally approximated from SCA calculations based on “extreme”, but possible, mineral compositions of each rock type (see section 5.4.2 in /Back et al. 2007/ for more details).

Histograms of the data for TRC 57 and TRC 58 (both dominated by granites) are shown in Figure 6-11, and histograms for TRC 61 (mainly pegmatite) and TRC 17 (amphibolite) are shown in Figure 6-12.

The histogram of all thermal data for TRC 51 is shown in Figure 6-13. Three sub-TRCs were defined in order to characterise the different populations represented by the thermal data. This subdivision reflects the wide range of compositions displayed by granite, granodiorite and tonalite (101051), the dominant rock type in this TRC /Stephens et al. 2007/. Since the thermal conductivity of fine- to medium-grained granite, granodiorite and tonalite (101051) show a correlation with density (section 6.2.2), borehole density logging data could be used to facilitate this subdivision. Details about the approach for TRC 51 are provided in section 5.4.2 in /Back et al. 2007/.

Table 6-13 summarises the thermal conductivity statistics for each TRC.

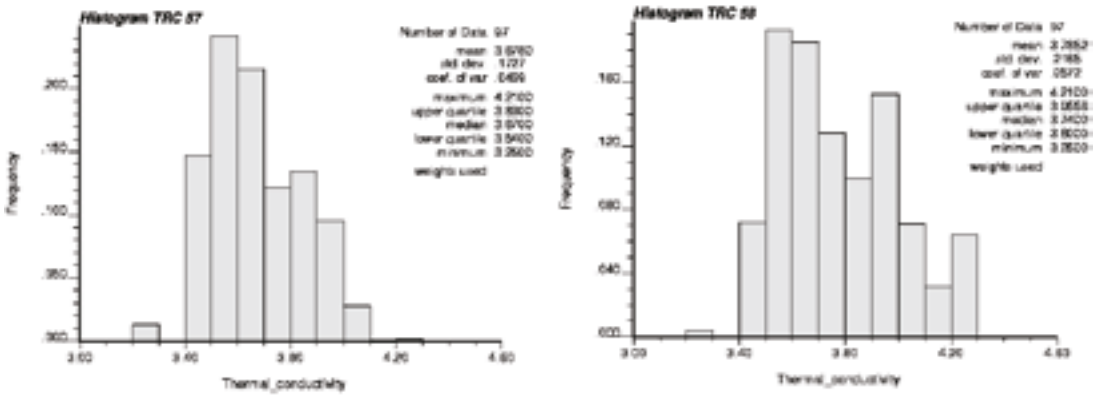

Figure 6-11. *Histograms of thermal conductivity derived for TRC 57 and TRC 58.*

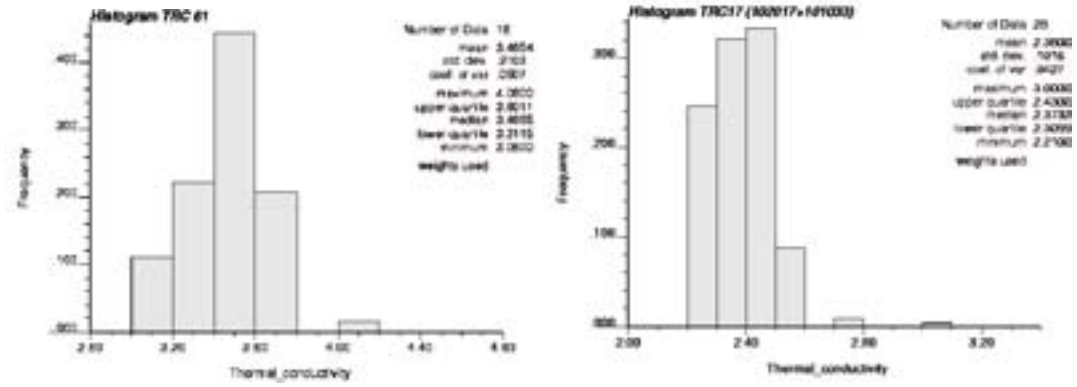

Figure 6-12. *Histograms of thermal conductivity derived for TRC 61 and TRC 17.*

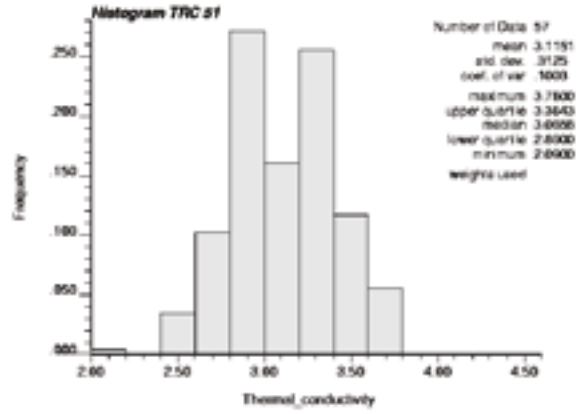

Figure 6-13. *Histogram of thermal conductivity derived for TRC 51.*

Table 6-13. Statistics for each TRC of the empirical thermal conductivity data on which distribution models used for simulation are based.

TRC	Mean (W/(m·K))	Standard deviation (W/(m·K))	Number of samples
TRC 57	3.68	0.17	97
TRC 58	3.79	0.22	97
TRC 61	3.47	0.21	18
TRC 17	2.38	0.10	28
TRC 51A	3.42	0.16	22
TRC 51B	2.97	0.10	24
TRC 51C	2.63	0.12	11

Variogram models – 0.1 m scale

The spatial correlation structure of thermal conductivity within each TRC is modelled by a variogram based on the dominant rock type in the TRC. The variogram models are primarily based on density loggings (approximately 0.1 m scale) in boreholes, supported by TPS data if a sufficient amount of data were available. A relationship between thermal conductivity and density has been established (see section 6.2.2). Therefore, it is reasonable to assume that any spatial dependence in density, as indicated by a variogram, also reflects spatial dependence in thermal conductivity /Sundberg et al. 2009/.

The procedure and principles followed in order to create variograms for each TRC are described in section 5.2.4 in /Back el al. 2007/. The primary purpose of calculating variograms based on density loggings is to estimate the range, i.e. the separation distance over which spatial dependence is apparent. In other words, locations separated by distances closer than the range are spatially correlated.

The nugget of the variogram models was based on TPS data when sufficient data were available (TRC 57 and 58). Otherwise, density variograms have been used to approximate not only the range but also the nugget. It is difficult to say whether the nugget estimated from density variograms underestimates or overestimates the nugget; there are phenomena working in both directions. This is further discussed in section 5.2.4 in /Back et al. 2007/.

Nuggets and ranges for all TRC are listed in Table 6-14 and example variograms for TRC 57 and TRC 17 are shown in Figure 6-14. Variograms for other TRCs are provided in section 5.2.4 in /Back et al. 2007/. A low nugget and a long range imply a greater degree of spatial continuity of thermal conductivity.

6.4.6 Stochastic simulations of thermal conductivity

Procedure

Stochastic simulation of thermal conductivity was performed for each TRC at two scales, 0.1 m and 1 m. The software used to perform the simulations is GSLIB. Each TRC was simulated using the spatial statistical thermal models defined below for the 1 m scale (see previous section for the 0.1 m scale). Verification of the simulations was performed by variogram and histogram reproduction (see Appendices E and F in /Back et al. 2007/).

Spatial statistical thermal models – 1 m scale

Simulations at scale 1 m require a spatial statistical thermal model (distribution model and variogram model) for each TRC determined for this particular scale. In order to obtain a histogram for the 1 m scale, simulations are performed at the 0.1 m scale (5×5×5 m cube) for each TRC and the simulation results are upscaled to 1 m. The histogram of the upscaled values (1 m scale) provides the basis for the statistical distribution model used for simulations at the 1 m scale.

Similarly, the variogram models for the 1 m scale are modified from the variograms determined for the 0.1 m scale. The principles for upscaling of the variogram models are presented in /Back and Sundberg 2007, Back et al. 2007/. The determined parameters for the variograms representing the 1 m scale are given in Table 6-15 for each TRC.

Table 6-14. Variogram models for TRCs at 0.1 m scale. Nuggets and sills are standardised to the variance of the empirical data. Data from dominant rock type in each TRC; see also /Back et al. 2007/.

TRC	Structure	Semivariance	Range, m
TRC 57	Nugget	0.6	
	Exponential	0.4	25
TRC 58	Nugget	0.4	
	Exponential	0.6	18
TRC 51A	Nugget	0.5	
	Spherical	0.5	5
TRC 51B	Nugget	0.5	
	Spherical	0.5	5
TRC 51C	Nugget	0.6	
	Spherical	0.4	5
TRC 61	Nugget	0.75	
	Spherical	0.25	15
TRC 17	Nugget	0.35	
	Spherical	0.65	25

Table 6-15. Variogram parameters for modelling at 1 m scale for each TRC. Nugget is set at zero due to upscaling.

TRC	Range	Model	Comment
TRC 57	25 m	exponential	
TRC 58	40 m	spherical	Range chosen to fit the large-scale structure.
TRC 61	15 m	spherical	
TRC 51A	6 m	spherical	
TRC 51B	6 m	spherical	
TRC 51B	6 m	spherical	
TRC 17	25 m	spherical	

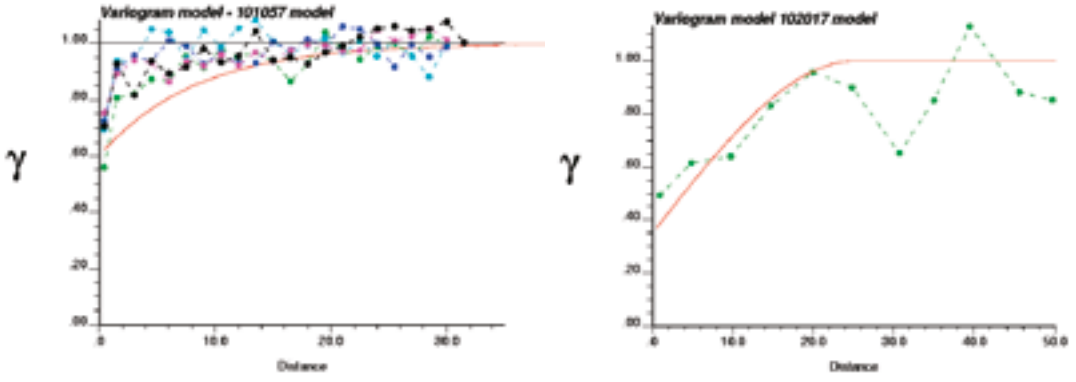

Figure 6-14. *Variogram models for TRC 57 (left) and TRC 17 (right). Lag distance (x axis) in metres. Variogram is standardised to the variance of the empirical data.*

Results of simulation of thermal conductivity

The results of the simulations at 1 m scale are presented in Table 5-28 and Appendix G in /Back et al. 2007/. For each TRC, a variety of plots and diagrams have been produced to illustrate the results and validate the method. An example is shown in Figure 6-15, illustrating the result of upscaling from 0.1 m to 1 m for TRC 57. For further analysis, the reader is referred to section 5.5.3 in /Back et al. 2007/.

The upscaling of simulation results produces a marked reduction in variance, in particular for TRCs that show a low degree of spatial correlation, e.g. TRC 57 and TRC 61. Results indicate that for the dominant TRC 57 in rock domain RFM029, approximately 70% of the variability present at the cm-dm scale is evened out at the 1 m scale. The variance reduction caused by the upscaling to the 1 m scale varied between 56% and 80% for the different TRCs.

6.5 Thermal domain model

6.5.1 Domain modelling results

Thermal conductivity

The final modelling steps involve merging the lithological simulations (section 6.4.4) with the thermal conductivity simulations (section 6.4.6), followed by scaling up of the results to 5 m scale. The results of these steps are presented below for the two rock domains, RFM029 and RFM045. Examples of 2D-slices of the 3D realisations for domains RFM029 and RFM045 are visualised in Figure 6-16 and Figure 6-17, respectively. The impact of larger bodies of low-conductive rock (mainly amphibolite) in the thermal subdomain B in domain RFM045 is conspicuous. Subdomain A in domain RFM045 is similar in character to domain RFM029.

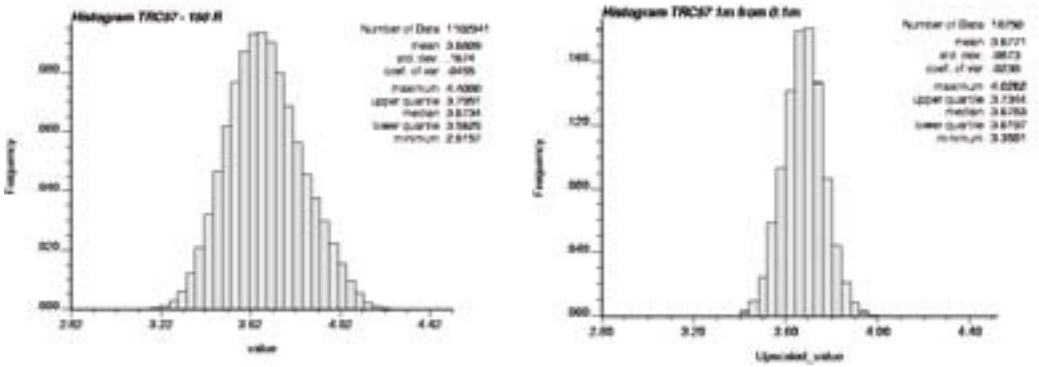

Figure 6-15. *Histogram of simulation results of TRC 57 at 0.1 m scale (left) and upscaled to 1 m (right).*

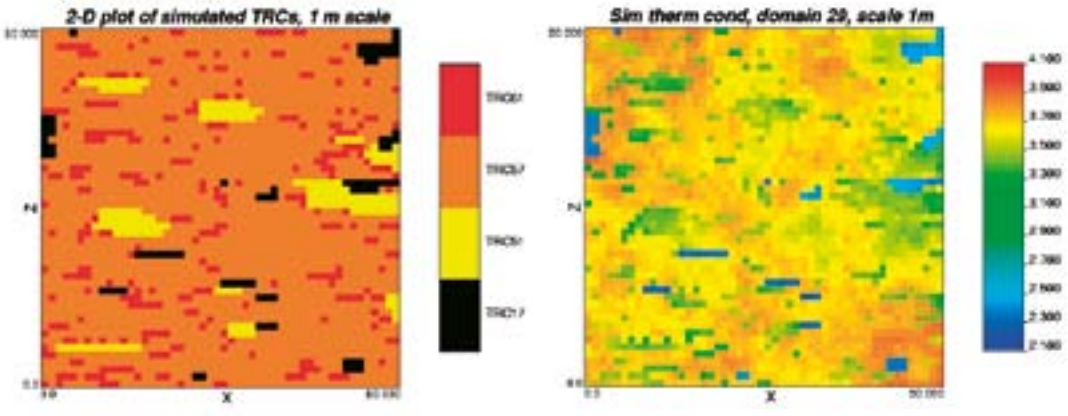

Figure 6-16. *Example 2D visualisations of the lithological simulations (left) and the corresponding realisation of thermal conductivity (right) for domain RFM029 (Internal) simulated at the 1 m scale. Slices in xz-plane.*

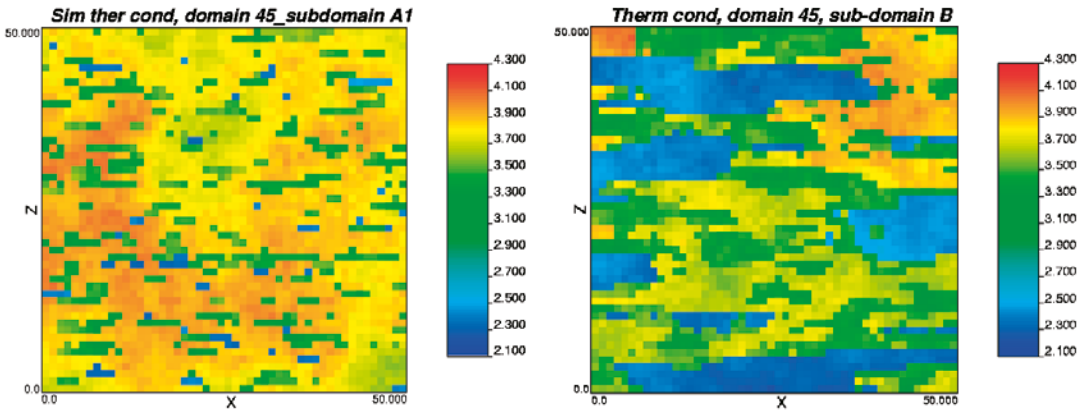

Figure 6-17. *Example 2D visualisations of the realisations of thermal conductivity (slices in xz-plane) for domain RFM045 simulated at the 1 m scale. Left: subdomain A1; Right: subdomain B.*

The distribution of simulated thermal conductivity values for rock domain RFM029 are illustrated in Figure 6-18 for the 1 m and 5 m scales. Upscaling of the realisations has the effect of smoothing the histogram. In the 5 m scale, the pronounced lower tail of the distribution has more or less disappeared.

The corresponding results for domain RFM045 at the 1 m and 5 m scales are illustrated in Figure 6-19. Again, upscaling of the realisations has a smoothing effect on the histogram. The pronounced lower tail and its strange shape is a result of low-conductive rock, mainly amphibolite (TRC17) and granite, granodiorite and tonalite (TRC51). Even at the 5 m scale, a pronounced lower tail of thermal conductivity values is conspicuous, which reflects the presence of large bodies of low-conductive rock in domain RFM045.

Simulation results have also been compiled for the individual thermal subdomains within rock domain RFM045. Histograms of thermal conductivity for the 333 realisations representing sub-domain A (A1 and A2) and for the 167 realisations of subdomain B are presented in Figure 6-20. Only results at the 5 m scale are shown. The lower tail is much more pronounced in subdomain B due to the presence of large amphibolite (TRC 17) bodies. A more detailed discussion of this is provided in /Sundberg et al. 2008/.

In the geological model /Stephens et al. 2007/, domain RFM045 has not been divided into two subdomains (see section 5.2.3). Thus, the statistics for the modelled subdomains do not apply to any specific volumes of rock, but provide one possible scenario regarding the make-up of rock domain RFM045, i.e. two-thirds of the domain is dominated by aplitic granite (101058) and granite to granodiorite (101057) with subordinate amounts of thin amphibolites, and one-third is characterised by greater lithological heterogeneity including the presence of large bodies of amphibolite.

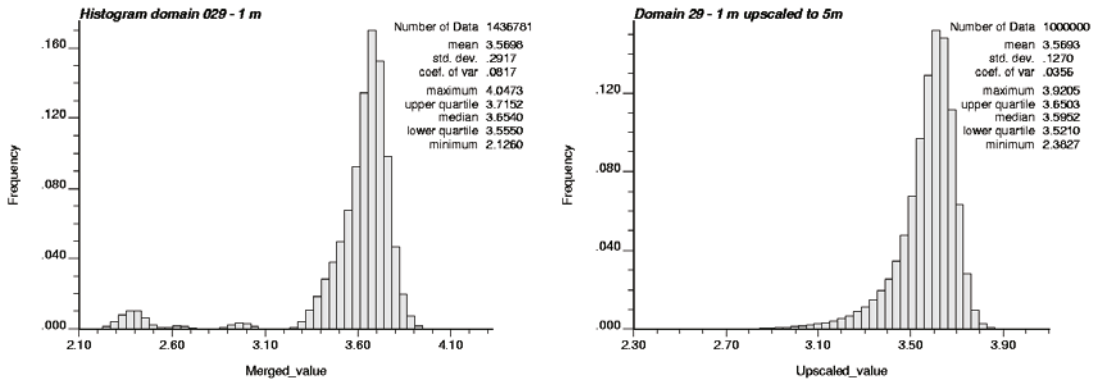

Figure 6-18. *Histogram of thermal conductivity for domain RFM029 simulated at the 1 m scale (left) and upscaled to 5 m (right) (1,000 realisations).*

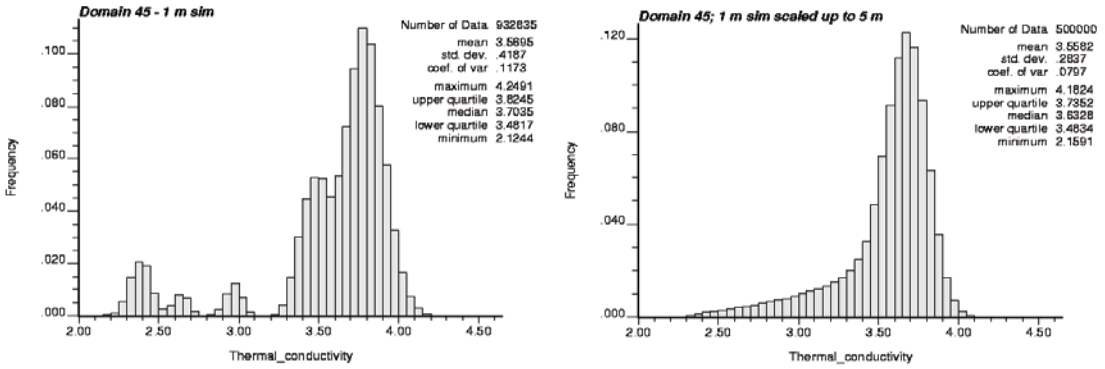

Figure 6-19. *Histogram of thermal conductivity for domain RFM045 simulated at the 1 m scale (left) and upscaled to 5 m (right) (500 realisations).*

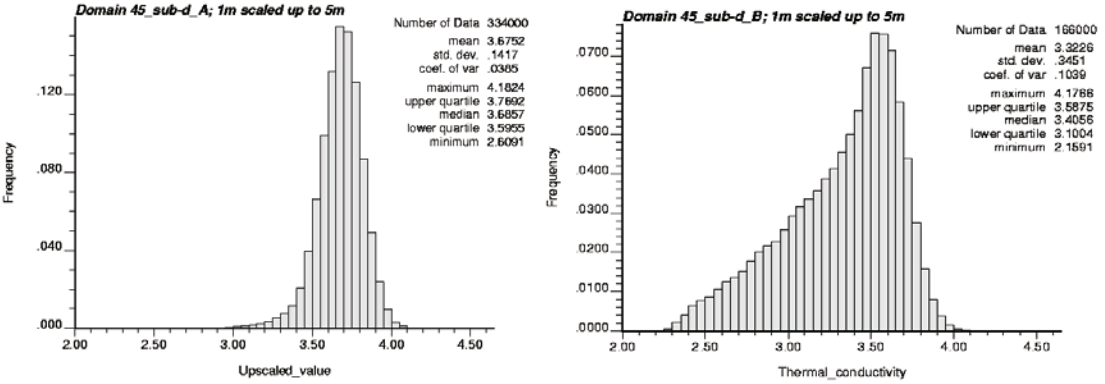

Figure 6-20. *Histogram of thermal conductivity for subdomain A (left) and B (right) in RFM045 at the 5 m scale.*

Heat capacity

A relationship, described by a second order regression equation, between heat capacity from direct measurements and thermal conductivity was established in the thermal modelling, stage 2.2. In stage 2.3, this relationship was used to calculate heat capacity, C, from thermal conductivity, λ /Sundberg et al. 2008/. Using this approach, together with the output from the simulations of thermal conductivity, heat capacity distributions at domain level can be determined. The results for the 1 m scale for rock domains RFM029 and RFM045 are presented in Figure 6-21.

Size distribution of TRCs

Based on the results of stochastic simulations of lithologies, it is possible to calculate the size distribution of subordinate rock types. However, a large number of simulations are required at several scales for this analysis. This work is on-going and will be reported in the near future.

To illustrate the information that can be obtained from a size-distribution analysis, the results of simulations at two scales, 0.1 m and 1 m, have been analysed for TRC 17 and TRC 61 in domain RFM029. In Figure 6-22 and Figure 6-23 the size distributions of TRC 17 (mainly amphibolite) and TRC 61 (mainly pegmatite) are shown. The figures for TRC 17 can usefully be compared with the true thickness distribution of amphibolite estimated from borehole data described in section 3.4.3 in /Stephens et al. 2007/ and in section 5.2.3. Both studies indicate a predominance of small bodies, e.g. in the case of borehole data true thickness less than 1 m.

Due to discretisation into 0.1 m and 1 m cells, respectively, the size distribution results for the lower part of the curve for each scale are not well resolved. Even the data for the largest bodies, i.e. “the upper end”, are uncertain, due to limited simulation volumes, as well as the removal of boundary bodies. In future work, determining the type of distribution, e.g. power-law, that describes these data will be central to the understanding of the size distribution.

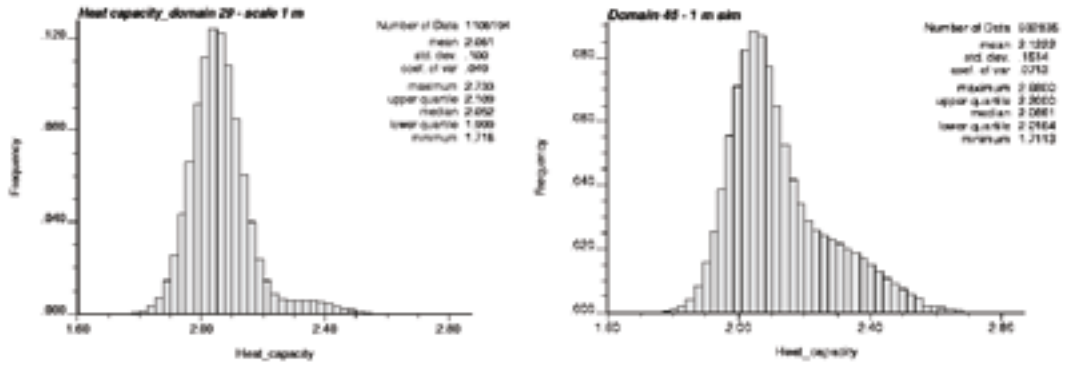

Figure 6-21. *Histogram of heat capacity for rock domains RFM029 (left) and RFM045 (right) based on realisations of thermal conductivity at the 1 m scale.*

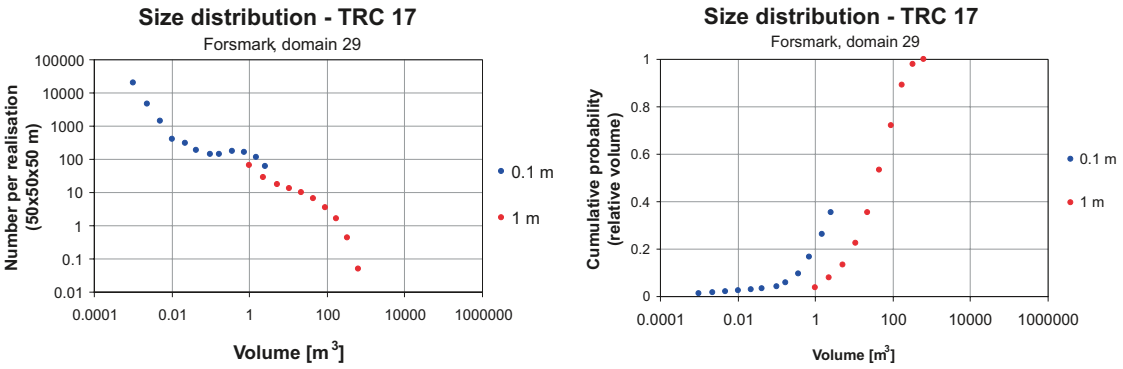

Figure 6-22. *Size distribution of rock bodies of TRC 17 in RFM029, based on stochastic simulation at 0.1 m and 1 m scales. A single realisation at 1 m scale represents a rock volume of 125,000 m³.*

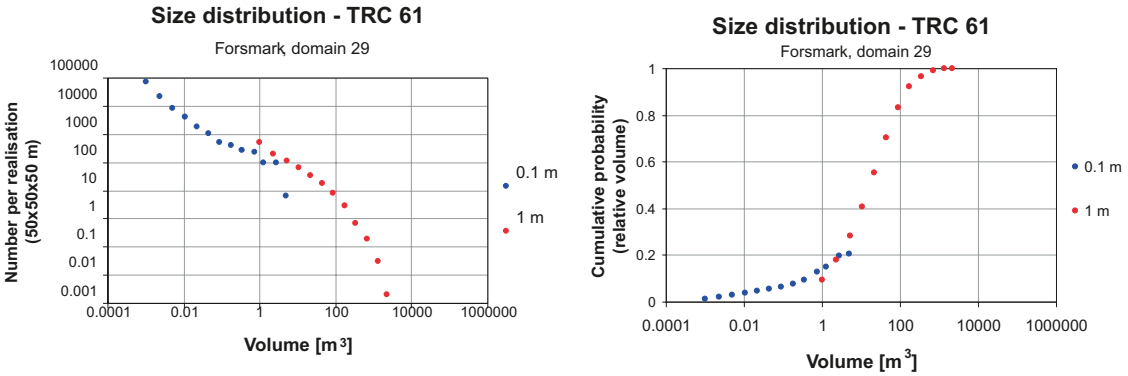

Figure 6-23. *Size distribution of rock bodies of TRC 61 in RFM029, based on stochastic simulation at 0.1 m and 1 m scales. A single realisation at 1 m scale represents a rock volume of 125,000 m³.*

6.5.2 Evaluation of domain modelling results

The lower tail of the thermal conductivity distribution is of great importance for the design of a repository. The modelling results were therefore analysed in detail in this respect. The results are presented in Figure 6-24 for both rock domain RFM029 and RFM045. The plots illustrate how the lower percentiles increase when the scale increases. This is a way of describing how the variance reduction affects the lower percentiles and how sensitive they are to the choice of scale. The variance reduction is much higher for domain RFM029 than for RFM045, mainly due to larger amphibolite bodies in the latter. The new lithological simulations of rock domain RFM045 made in stage 2.3 /Sundberg et al. 2008/ are compared with results from stage 2.2 in Figure 6-24 (right). Whereas the 1-percentile is almost identical for the 1 m scale, the same percentile is significantly higher for the 5 m scale in the model from stage 2.3. The results are described in more detail for rock domain RFM029 in chapter 6 in /Back et al. 2007/ and for domain RFM045 in chapter 5 in /Sundberg et al. 2008/.

6.5.3 Summary of rock domain properties

Thermal conductivity

The main result of the thermal modelling is a set of realisations of thermal properties for the two rock domains RFM029 and RFM045. These realisations can be used for further processing, most importantly for numerical temperature simulations for the thermal design of repository layout, the strategy for which is described in /Hökmark et al. 2009/.

The thermal conductivity at domain level for the 5 m scale are summarised in Table 6-16. The properties for rock domain RFM045 are strongly affected by how the spatial structure of TRC 17 (amphibolite) was modelled. The modelling was originally made in /Back et al. 2007/, but remodelling was performed in /Sundberg et al. 2008/. The reason for the remodelling was to introduce thermal subdomains in order to better describe the heterogeneity in the spatial structure of large amphibolite bodies.

The values in Table 6-16 are valid at 20°C. With increasing temperature the thermal conductivity of the dominant granitoid rock decreases by about 10% per 100°C temperature increase, calculated as a mean value. For the impact on other rock types, see /Sundberg et al. 2008/.

Table 6-16. Thermal conductivity (W/(m·K)) for domains RFM029 and RFM045 based on simulations at the 1 m scale and upscaled to 5 m /Back et al. 2007, Sundberg et al. 2008/.

Statistical parameter	RFM029 5 m scale	RFM045 5 m scale
Mean	3.57	3.56
Standard deviation	0.13	0.28
0.1-percentile	2.87	2.36
1-percentile	3.12	2.56
2.5-percentile	3.23	2.73

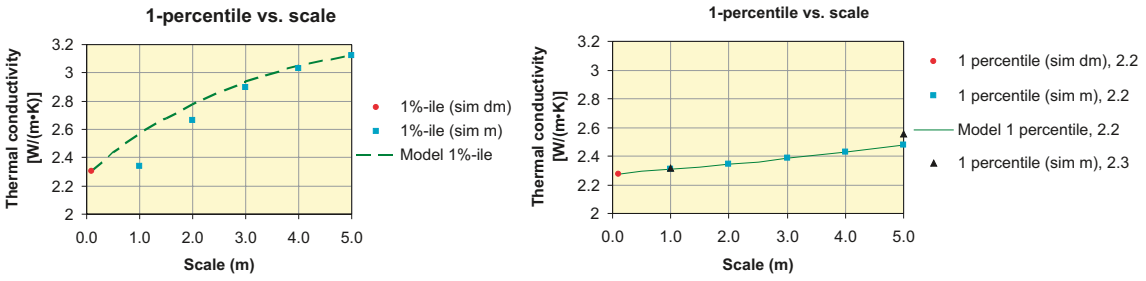

Figure 6-24. The 1-percentile (0.01 quantile) versus the scale for domain RFM029 (left) and RFM045 (right). Upscaling was performed on simulated values at the 0.1 m scale (red) and simulated values at the 1 m scale (blue). A model (green) was fitted to the most reliable values in model stage 2.2 /Back et al. 2007/. The black symbols represent model stage 2.3 /Sundberg et al. 2008/.

Thermal anisotropy

Anisotropy in thermal conductivity due to foliation/lineation in the dominant granite to granodiorite has been measured *in situ* at one site. Field measurements indicate that thermal conductivity parallel to the foliation plane is higher, by a factor of approximately 1.15, than conductivity perpendicular to the foliation.

Evaluation of anisotropy due to the occurrence of subordinate rock bodies, primarily amphibolite, indicates a slightly lower thermal conductivity at the 5 m scale in a direction perpendicular to the plane of maximum flattening of the amphibolites (the z'''-direction). The largest calculated relative difference from the z´´´-direction was found for the y'''-direction, for which the thermal conductivity at the 0.1 percentile was found to be more than 7% larger than that for the z'''-direction (anisotropy factor 1.07). The anisotropy factor decreases for higher percentiles. The reason that the anisotropy is strongest at the extreme end of the lower tail is because this part of the tail is dominated by amphibolite. A stronger anisotropic effect is assumed for scales less than 5 m. The methodology and results for the evaluation of anisotropy due to subordinate rock bodies are further described in section 6.2.3 in /Back et al. 2007/.

Heat capacity

Heat capacity distributions at rock domain level have been determined. The results for the 1 m scale for rock domains RFM029 and RFM045 are presented in Table 6-17. These values are valid at 20°C. With increasing temperature, the mean value of the heat capacity of the dominant granite to granodiorite (101057) increases by about 29% per 100°C temperature increase.

Thermal expansion coefficient

The mean thermal expansion coefficients for the main granitoid rock types within the target volume varies between $7.5 \cdot 10^{-6}$ and $7.8 \cdot 10^{-6}$ m/(m·K). For the dominant granite to granodiorite (101057), the mean thermal expansion coefficient is $7.7 \cdot 10^{-6}$ m/(m·K). Data for amphibolite (102017) are not available. Domain modelling has not been performed. The conclusion presented in model stage 1.2 /Sundberg et al. 2005a/, i.e. a mean coefficient of thermal expansion of $7–8 \cdot 10^{-6}$ m/(m·K) for the different rock domains, is still valid.

In situ temperature

The mean *in situ* temperature measured in 8 boreholes at 400 m, 500 m and 600 m depth is estimated at 10.5°C, 11.6°C, and 12.8°C respectively. The uncertainties reported in the Forsmark stage 2.1 report /SKB 2006a/ regarding the quality of *in situ* temperature measurements have now been identified /Sundberg et al. 2008/. The mean values reported here are based on borehole loggings that are considered to be reliable.

Table 6-17. Heat capacity (MJ/(m³·K)) for domains RFM029 and RFM045 based on the relationship between heat capacity and thermal conductivity, and simulations of thermal conductivity at the 1 m scale /Sundberg et al. 2008/.

Statistical parameter	RFM029 1 m scale	RFM045 1 m scale
Mean	2.06	2.12
Standard deviation	0.10	0.15

6.6 Evaluation of uncertainties

6.6.1 Data uncertainty

The main data uncertainties are described below. A more detailed description of uncertainties is given in /Back et al. 2007/ and /Sundberg et al. 2008/.

Boremap data

The uncertainties in the orientation of the boreholes and in the orientation of geological objects in the boreholes, documented by /Munier and Stigsson 2007/, are judged to have little or no effect on the results of thermal modelling. Other uncertainties in boremap data are discussed in 6.6.2.

Thermal conductivity and heat capacity

The TPS measurements on isotropic samples are considered to be quite reliable, especially the thermal conductivity. If the samples show anisotropic thermal behaviour, which to some degree is the normal case in the Forsmark area (foliated or lineated samples), the uncertainty is larger, especially in the determination of thermal diffusivity (see section 3.6 in /Back et al. 2007/) and consequently also regarding the determined heat capacity. However, the heat capacity has also been determined directly by a calorimetric method and these measurements are considered to be more reliable. The impact on the domain results are therefore considered to be small.

Uncertainties are also associated with the thermal anisotropic properties of the dominant granite (lineation/foliation), mainly due to few determinations. The mean values of the thermal anisotropic factor are thought to be quite reliable but the spatial variability has large uncertainties.

Thermal expansion coefficient

The representativeness of samples selected for thermal expansion measurements can be questioned. The samples are few and relate to limited parts of the rock volume.

Temperature

In the current model version, the reliability of temperature loggings due to calibration error and disturbance from drilling has been evaluated. As a result of this, only “approved” boreholes have been used in the description. The uncertainties are therefore much smaller than in earlier model versions.

6.6.2 Model uncertainty

Major model uncertainties

The thermal stochastic modelling primarily concerns thermal conductivity. There are several uncertainties associated with the different steps of this modelling, further described in /Back et al. 2007/ and /Sundberg et al. 2008/. Here, a summary is given of the five uncertainties that are believed to be most important for the results at rock domain level. These are associated with: the simulation scale, the simulation volume, the spatial statistical structure of TRCs (lithology), the spatial statistical thermal models, and the simulation technique.

Each of these uncertainties is discussed below. A more detailed discussion is provided in /Back et al. 2007/ and /Sundberg et al. 2008/.

The simulation scale

The effect of using a simulation scale of 1 m to represent subordinate rock types is not fully known. The evaluation indicates that the 1 m simulations give a too conservative estimate of the lower percentiles for rock domain RFM029 due to discretisation errors. However, it is reasonable to assume that this uncertainty is more or less eliminated at the 5 m scale. A discretisation error may also affect results for domain RFM045, but it is believed to be much smaller, due to the larger rock bodies of amphibolite present in this domain.

The results of the analysis of the size distribution of subordinate rock bodies are also influenced by the choice of simulation scale and simulation volume. In order to describe the size distribution of subordinate rock types in an accurate way it is necessary to perform simulations at a number of different scales.

The simulation volume

There are two situations when the limited simulation volumes could be a problem: (1) when the lithological simulation volume is so small that the statistics of the corresponding rock volume deviate from the true domain statistics, and (2) when the correlation lengths of thermal properties are similar to, or longer than, the length of the simulation volume. It can be concluded that although there are uncertainties associated with the simulation volume, neither of these is believed to have had any major impact on the thermal modelling results in canister scale.

The description of the size distribution of subordinate rock bodies is also influenced by the limited simulation volume, see "Simulation scale above". The same applies to the proportions of TRCs, see below.

The spatial statistical structure of TRCs (lithology)

The thermal models used for the lithological simulations are largely based on "best estimates" of uncertain parameters. There are several uncertainties associated with the developed models of the proportions and the spatial statistical structure of the TRCs. Most of these are coupled to the lack of knowledge concerning detailed geological information.

There are also uncertainties linked to the degree to which geological inhomogeneity has been reproduced in the lithological simulations. This is related to the variability in proportions of TRCs. In the simulation volume, the proportions of TRCs are held constant in each realisation ("best estimates" have been used). In reality, the proportions are variable at the scale of the simulation volume due to lithological heterogeneity. These uncertainties are largest for rock types with low proportions and heterogeneous rock domains. For rock domain RFM029, heterogeneity is mainly related to variability in orientation and geometries of subordinate rocks. For rock domain RFM045, lithological heterogeneity is more important. Geological heterogeneities were dealt with by dividing the domains into subdomains, according to the strategy outlined in chapter 3 in /Back and Sundberg 2007/. This is believed to have reduced the uncertainty significantly. The remaining uncertainty concerning the variability in proportions is believed to be small. Based on confidence intervals for TRC proportions at borehole scale (see section 6.4.1), this uncertainty has only a minor effect on the lower thermal conductivity tail (the 1-percentile may vary by about 1%).

The proportions of each TRC in the lithological simulations deviate somewhat from the proportions of different rock types estimated as part of the modelling carried out by the geological team /Stephens et al. 2007/. The main reasons for the observed discrepancies are: borehole occurrences shorter than 5 cm were excluded from borehole data used in the lithological simulations and the estimations are based on slightly different sets of boreholes. In addition, problems in the lithological simulations have resulted in small deviations in proportions. The effect of these discrepancies on the thermal model at the 5 m scale is considered to be small.

The complementary lithological simulations of rock domain RFM045 in stage 2.3, based on more data, honour the borehole data to a much higher degree, and therefore the lower tail percentiles of thermal conductivity are considered more reliable /Sundberg et al. 2008/. However, there is still uncertainty concerning the size distributions of subordinate rock types or TRCs in rock domain RFM045.

The spatial statistical thermal models

Limited data for some TRCs result in uncertain spatial statistical thermal models. When data are few and show large variability, the shape of a histogram cannot only be based on measurements. In addition, the lower limit of thermal conductivity of a TRC is usually not known and must be determined based on expert opinion. The variograms require even more data. It has been assumed that thermal

conductivity exhibits a similar correlation structure to density. This is a reasonable assumption that makes possible the creation of variograms, but the associated uncertainty is not known.

In spite of the uncertainties, the spatial statistical thermal conductivity models are believed to be more reliable than in previous versions of the thermal site descriptive modelling.

The simulation technique

The simulation technique is a source of uncertainty. This uncertainty is closely related to the simulation scale and the simulation volume. The principle is simple: The result of a simulation is compared against the input models. Deviations indicate that there is uncertainty. This type of verification was performed both for the lithological and the thermal simulations. The conclusion is that the output resembles the input relatively well. This uncertainty is believed to have only a minor influence on the results.

6.6.3 Summing up

The thermal models presented here are judged to represent the modelled rock domains and their variability in an appropriate way. The main reasons for this confidence is that the spatial statistical thermal models for most thermal rock classes are based on a satisfactory amount of data. Furthermore, the modelling approach allows upscaling to be performed in a theoretically robust way.

Small uncertainties in the lower tail of the thermal conductivity distributions will have a significant impact on canister spacing in the repository design. For this reason, the uncertainties in the thermal model focus on the lower tail of the thermal conductivity distribution. Confidence in the lower tails of the thermal conductivity distributions is higher for rock domain RFM029 than for rock domain RFM045. For the latter, this uncertainty is related to the spatial and size distribution of amphibolite.

As regards the overall distribution of thermal conductivities for each rock domain, the highest confidence is again placed in the results for domain RFM029, because of its higher degree of homogeneity in geology and thermal properties compared to domain RFM045. The rather large uncertainties associated with the output of the geological simulations for domain RFM045, in particular the proportions of rock types and proportions of thermal subdomains, imply that the overall distribution of thermal conductivity is somewhat uncertain for this domain.

Overall confidence in the thermal model is reinforced by the mutual consistency between understanding of the geology and the thermal properties description.

7 Rock mechanics

The two important components of the rock mechanics model for site description are:

1. the geometrical and mechanical characterisation model and
2. the model of the *in situ* stress state.

This chapter synthesises the mechanical characterisation of the intact rock, rock fractures and rock mass. It also presents the current model for the state of stress. The geometrical division into rock domains, fracture domains and deformation zones, which is the basis for the rock mechanics modelling, is provided in /Stephens et al. 2007/ and in chapter 5.

The development of the mechanical model required extensive laboratory (small scale) testing to establish the primary data on the intact rock and discrete fractures. These primary data were then used in combination with the geological model as input to two modelling approaches, one empirical and one theoretical, to estimate the mechanical properties of the rock mass (at the deposition drift and hole scale). The empirical approach estimates the rock mass properties based on classification indexes and empirical relationships routinely used in rock engineering, whereas the theoretical approach, which utilises numerical models, was developed specifically for the SDM /Olofsson and Fredriksson 2005/.

The *in situ* stress model was developed from direct and indirect measurements, and numerical modelling that respected the geometry and structure in the geological models. The numerical model provided the anticipated spatial distribution of stress magnitudes and orientations in the target volume. It also provided an independent assessment on the possible horizontal stress magnitudes that could be expected at repository depth.

The presentation here is concentrated on the modelling results in the target volume, principally, fracture domain FFM01 and FFM06. The modelling results for other fracture domains, as well as rock domains adjacent to the target volume, are provided in /Glamheden et al. 2007a/.

7.1 State of knowledge at the previous model version

The initial site investigation work (ISI), which was concluded in version 1.2 of the SDM, presented a rock mechanics model based on samples from four boreholes: KFM01A, KFM02A, KFM03A and KFM04A /SKB 2005a/. The available laboratory tests included those on samples of intact rock of the two dominant rock types and on several natural fractures. The state of stress in the rock mass was estimated based on measurements in boreholes KFM01A, KFM01B, KFM02A and KFM04A in combination with previous measurements in the Forsmark area. The main conclusions reported in model version 1.2 were that the rock mechanical properties in rock domain RFM029 were favourable for a potential repository, while the stress modelling carried out in 1.2 indicated that the magnitudes of *in situ* stresses at 500 m depth could range between 40–50 MPa. However, the uncertainties of the evaluated state of stress were considerable.

Modelling stage 2.1, the first stage of the complete site investigation (CSI), included new data from sampling of boreholes KFM05A and KFM06A /SKB 2006a/. Although the rock mechanics properties in the main rock types within the target volume were established, a need for additional characterisation of the subordinate rock types was identified. Further stress measurements and analyses of stress by indirect methods were suggested. A need for numerical stress modelling of the impact of gently dipping deformation zones was also identified.

Modelling stage 2.2 included additional laboratory test results from boreholes: KFM01C, KFM01D, KFM02B, KFM07A, KFM08A and KFM09A /Glamheden et al. 2007a/. The *in situ* stress state at Forsmark was re-evaluated based on additional stress measurements and indirect observations of the stress state in several boreholes. The work carried out during modelling stage 2.2 confirmed

the previous model and also increased the understanding of the Forsmark site. Furthermore, the confidence in the *in situ* state of stress was increased by means of the indirect observations of the stress field and additional stress modelling.

Modelling stage 2.3 completes the rock mechanics model. The purpose was to validate and reduce the uncertainty in the model. The results from model stage 2.3 are presented in a complementary report /Glamheden et al. 2008/.

7.2 Evaluation of primary data

The investigations of rock mechanics properties performed in the Forsmark area are summarised in sections 2.1 and 2.3 and the data supporting the current model version are listed in Table 3 in Appendix 3.

The primary data in the rock mechanics modelling consist of results from laboratory tests on intact rock and fractures, results from characterisation of the rock mass quality, as well as *in situ* stress observations. The primary data from laboratory tests are described below, whereas the primary data based on rock mass characterisation and *in situ* stress observations are described in sections 7.2.3 and 7.2.4.

The overall strategy in sample selection for rock mechanics testing has been based on:

- consultation with site geologists on the representativeness of potential test objects,
- collection of samples in batches at depth with a number of specimens as close to each other as practically achievable.

During the initial site investigations, the focus was to sample boreholes at roughly 300 m, 500 m and 700 m depth to obtain a preliminary indication of spatial variability in the target volume. During the complete site investigations, the sampling was focused at a depth of 400–500 m within fracture domains FFM01 and FFM06, see section 5.6.1. Additional details of the strategy in sample selection for rock mechanics testing are provided in /Glamheden et al. 2007a/.

The majority of the laboratory tests were performed at the Swedish National Testing and Research Institute (SP). Tests performed at other laboratories comprise direct tensile tests performed by Mining and Mineral Sciences Laboratories of Canada (CANMET) and P-wave velocity tests on core samples and tilt tests on fracture samples performed by the Norwegian Geotechnical Institute (NGI). A comparison study of the measurement consistency and repeatability between the different laboratories was also carried out /Glamheden et al. 2007a/.

The laboratory testing was carried out using the procedures and standards outlined in SKB method descriptions. The method descriptions related to rock mechanics testing are listed in /Glamheden et al. 2007a/.

The test programme on intact rock performed by SP included in total 122 uniaxial compressive tests, 94 triaxial compressive tests and 195 indirect tensile tests. The laboratory tests on discrete fractures included tilt tests on 163 fractures, direct shear tests on 57 open fractures and 4 tests on sealed fractures. The total length of cores examined for developing the rock mechanics model was 5,815 m in the target volume.

A three dimensional view of the sampling locations and the results of the uniaxial compressive tests in relation to fracture domains and deformation zones (see chapter 5) is presented in Figure 7-1. Additional plots showing the sampling locations for other laboratory tests as well as the primary data used for characterisation of the rock mass quality are provided in /Glamheden et al. 2007a/. The test results in relation to geological features are presented in WellCad plots included in /Olofsson et al. 2007/.

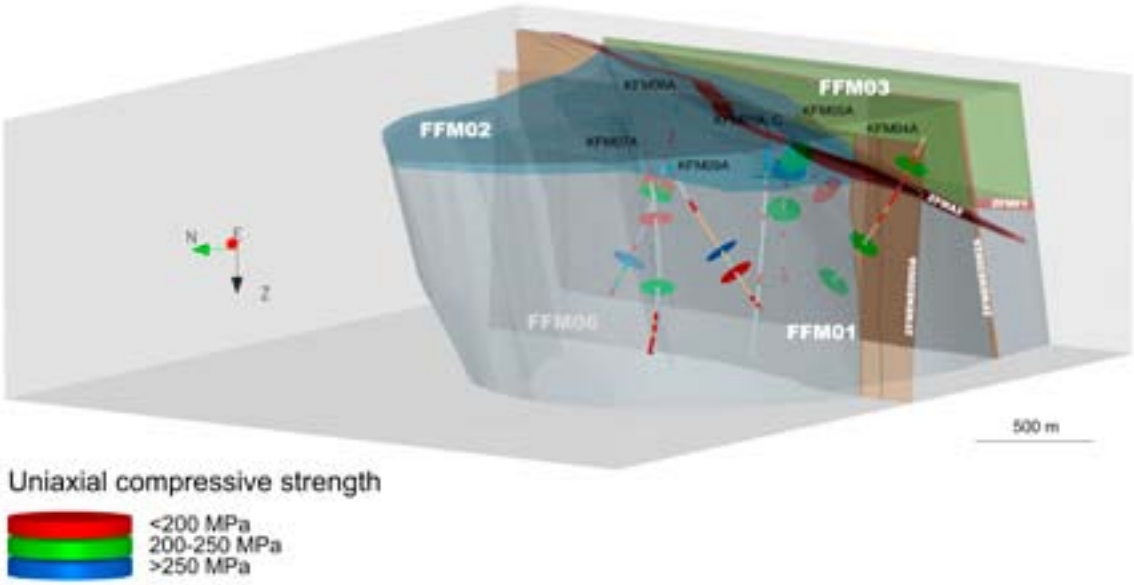

Figure 7-1. *Location and results of the uniaxial compressive tests. Since the samples are situated close to one another, some sample locations are hidden.*

7.2.1 Laboratory properties of intact rock

Deformation properties

The elastic properties Young's modulus and Poisson's ratio are used in the safety assessment to analyse thermo-mechanically induced changes in the repository near field /SKB 2006b/. The intact rock Young's modulus is based on the tangent modulus evaluated at 50% of the uniaxial compressive strength. The laboratory deformation properties presented here were determined from the uniaxial compression tests. A comparison of Young's modulus and Poisson's ratio determined from the laboratory uniaxial and triaxial compressive tests is given in /Glamheden et al. 2007a/. The frequency distributions of Young's modulus and Poisson's ratio from uniaxial tests on intact rock in fracture domains FFM01 and FFM06 are shown in Figure 7-2.

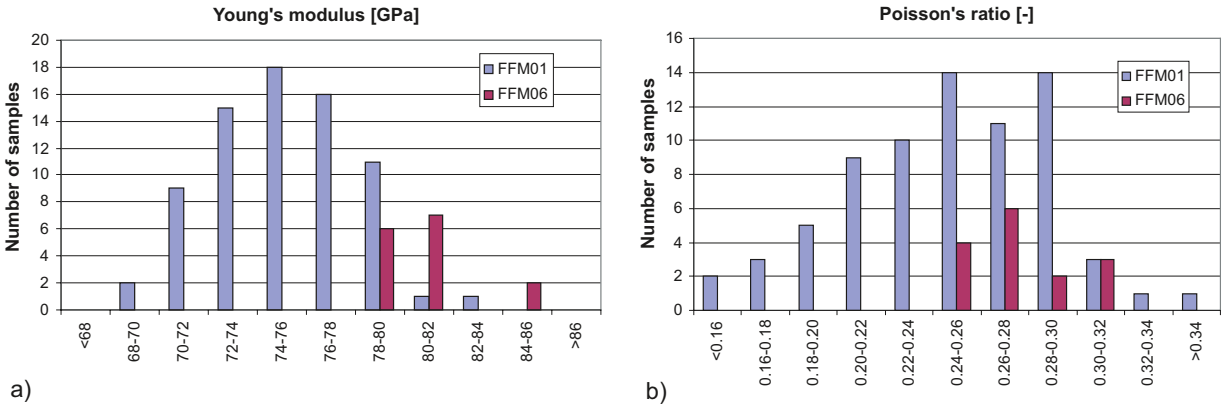

Figure 7-2. *Frequency distribution of Young's modulus (a) and Poisson's ratio (b) from uniaxial tests on intact rock in fracture domains FFM01 and FFM06. The analysed samples in FFM06 are albitized.*

Strength properties

The laboratory strength properties presented here include uniaxial compressive strength (UCS) and tensile strength of intact rock. The uniaxial compressive strength, as well as the crack initiation stress, are parameters that are used to evaluate the potential risk for excavation-induced and thermal-induced spalling in deposition holes /SKB 2006b/. The tensile strength is one of several rock mechanics parameters established for repository safety assessment /SKB 2006b/. Triaxial compression tests were also carried out and the results were combined with the results from the uniaxial compression and tension tests to establish Hoek-Brown's and Mohr-Coloumb's failure envelopes for intact rock (section 7.3.1).

The frequency distributions of the uniaxial compressive strength of intact rock in fracture domains FFM01 and FFM06 are shown in Figure 7-3 and the indirect tensile strength for the same fracture domains is given in Figure 7-4. The compressive strength values of the dominant rock type (medium-grained metagranite) in FFM01 would be classed as R5-very strong (mean 226 MPa), and the dominant rock type in FFM06 (albitized metagranite) would be classed as R6-extremely strong (mean 373 MPa), using the ISRM classification given in /Hoek et al. 1995/. The laboratory test results on intact samples taken from deformation zones are similar to those observed in fracture domain FFM01.

The tensile strength based on indirect tests of intact rock ranges from 8.4 to 20.9 MPa in fracture domain FFM01 and from 12.8 to 16.6 MPa in FFM06. Results from indirect tensile tests of samples taken parallel and perpendicular to the foliation, as well as results from direct tensile tests are described in /Glamheden et al. 2007a/. Results compiled by /Glamheden et al. 2007a/ show a ratio between the mean direct and mean indirect tensile strength of approximately 0.6.

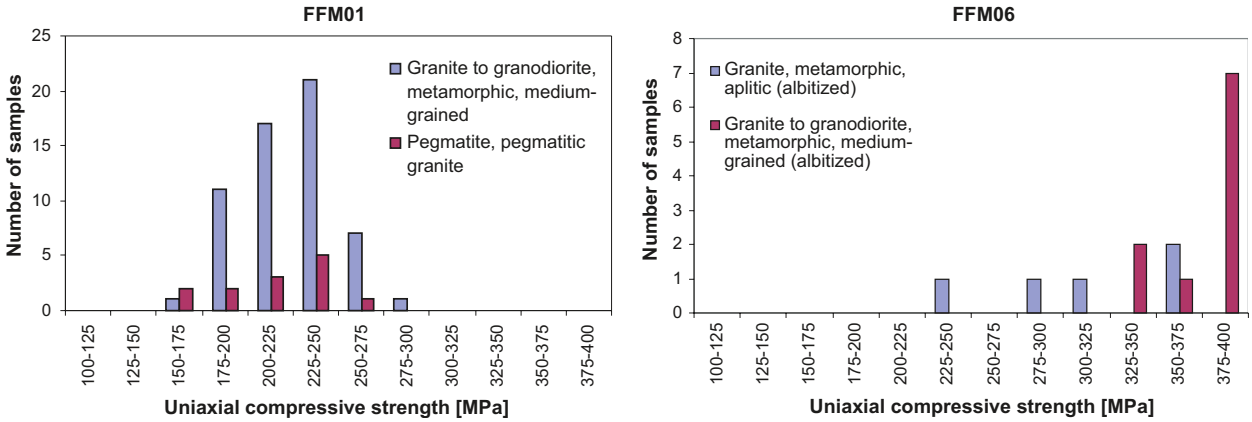

Figure 7-3. *The frequency distribution of uniaxial compressive strength of intact rock in fracture domains FFM01 and FFM06. The analysed samples from FFM06 are albitized.*

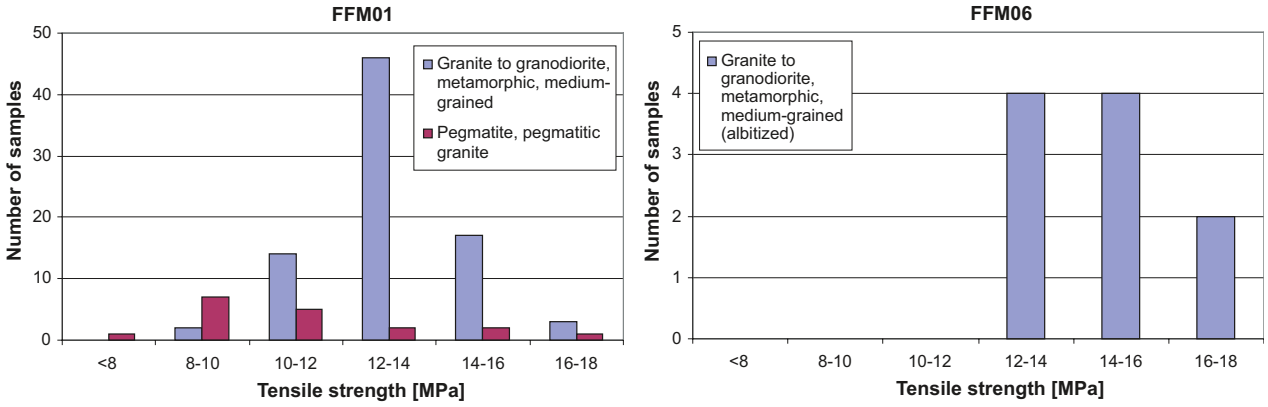

Figure 7-4. *The frequency distribution of indirect tensile strength of intact rock in fracture domains FFM01 and FFM06. The analysed samples from FFM06 are albitized.*

Microcrack volume measurements

Coring of granite at depth may induce microcracking /Martin and Stimpson 1994/. The microcracking originates from stress relaxation and mechanical/thermal effects from drilling. The drill core sample is under no confining stress in the laboratory, whereas the rock *in situ* is under a certain confining stress, depending on depth and location. Moderate microcracking influences the porosity of the intact sample, whereas significant microcracking affects the mechanical properties of laboratory samples. /Martin and Stimpson 1994/ showed that an increase in stress-induced microcracking provides a systematic bias in the laboratory test results that underestimates the strength and deformation properties of the intact rock *in situ*. The microcrack volume measurements can help indicate differences in stress state between boreholes or sites and differences in deformation behaviour between rock types. Furthermore, information on the microcrack volume is used by hydrogeochemistry in calculating the composition of the natural matrix porewater and in the determination of the transport properties of the intact rock (see chapters 9 and 10).

One method to estimate the amount of microcracking is to measure the degree of non-linear volumetric strain recorded in hydrostatic triaxial compression tests. Based on this method, two test series (total 15 samples) from boreholes KFM01A and KFM02B were performed in order to evaluate the microcrack volume in samples of medium-grained metagranite (101057) /Jacobsson 2007/. The results show a linear increase of crack volume with depth in the samples from borehole KFM01A, whereas depth dependency is indistinct in samples from borehole KFM02B, see Figure 7-5. The estimated microcrack volume for samples in KFM01A and KFM02B is in the range 0.04–0.12% and 0.02–0.04%, respectively. The results indicate a microcrack volume that, depending on the depth, corresponds to 5–30% of the measured mean natural porosity (0.4%) of the medium-grained metagranite.

The estimated crack volume in the samples from Forsmark is considerably less than the crack volumes recorded in samples investigated at URL in Canada /Martin and Stimpson 1994/. The slight increase in crack volume with depth suggests that the impact of microcracking on laboratory determinations of mechanical properties is relatively minor. More importantly, when comparing the data with the results from /Martin and Stimpson 1994/, the results suggest a gradual increase in stress magnitudes with depth.

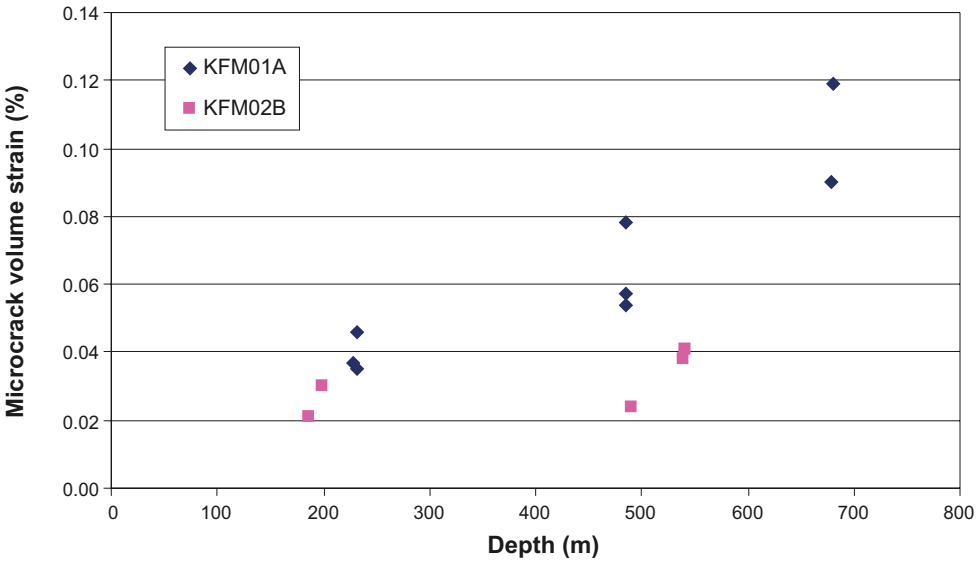

Figure 7-5. *Measured microcrack volume versus sampling level (elevation). Adapted from /Jacobsson 2007/.*

7.2.2 Laboratory properties of fractures

The laboratory mechanical properties of fractures were determined by tilt tests and by direct shear tests. The methodology used for the laboratory testing and the parameter evaluation is described in /Glamheden et al. 2007a/. The testing procedure for the direct shear tests involved three different test configurations. This resulted in modifications to the final testing procedures that improved the methodology for calculating the fracture stiffness. Previous results were corrected once the testing procedure was finalised /Glamheden et al. 2007a/.

The sizes of the samples used in the tilt tests and the direct shear tests were approximately 100 mm and 55 mm, respectively. For fracture domain FFM01, the tilt tests comprise 64 samples and the direct shear tests 29 samples. No samples were taken in FFM06 because of scheduling constraints. However, visual inspection of the fractures in FFM06 suggests similar properties to those obtained for the fractures in domain FFM01. Properties of fractures occurring within deformation zones were determined by 34 tilt tests distributed among twelve zones and 10 direct shear tests distributed among three zones. The zones that the samples were taken from are reported in /Olofsson et al. 2007/. Detailed information on the sampling strategy is provided in /Glamheden et al. 2007a/.

The normal stiffness was evaluated for a normal load up to 10 MPa and the shear strength was evaluated at normal stresses of 0.5, 5 and 20 MPa. The normal stiffness of fractures is based on the secant stiffness, and the shear stiffness is evaluated as tangent stiffness at 50% of the shear failure. The shear strength of the fractures from direct shear tests was determined using a linear Mohr-Coulomb criterion, whereas the shear strength from the tilt tests was determined using the non-linear Barton-Bandis criterion /Barton and Bandis 1990/.

Results from tilt tests, as well as the results from the direct shear tests of fractures in fracture domain FFM01 and in the deformation zones show insignificant differences in the evaluated properties between fractures in FFM01 and in deformation zones. Calculated results from tilt tests and results from direct shear tests on samples from other fracture domains are presented in /Glamheden et al. 2007a/.

The possible correlation of fracture orientation with the mechanical properties determined by tilt and shear tests was examined in modelling stage 2.1 /SKB 2006a/. The study concluded that the mechanical properties did not correlate with orientation. Thus, the subsequent modelling stage has instead focused on correlating mechanical properties to the fracture domains.

The direct shear tests also included tests on four sealed fractures from borehole KFM01D. Three specimens were prepared from each fracture and tested at three different normal stress levels. The initial test was followed by three shear cycles at the normal stress levels 0.5 MPa, 5 MPa and 20 MPa, on the open fracture that was created after breaking the sealed fracture. The results are shown in Figure 7-6. The friction angles for the sealed fractures are slightly lower than that of intact rock, 53° compared with 60° for intact rock, while the measured cohesion is considerably lower, 4 MPa compared with 28 MPa for intact rock. The results from the shear test after breaking the sealed fracture are similar to the results of the tests on open fractures.

7.2.3 Characterisation of the rock mass quality

The rock mechanics site descriptive model utilises two modelling approaches to estimate the rock mass properties, an empirical and a theoretical approach. This section summarises the primary data used in the empirical approach to estimate the rock mass mechanical properties. The resulting rock mass deformation and strength properties are presented in section 7.3.3.

The empirical characterisation of the rock mass was carried out on 5 m long borehole sections, using the Q and RMR classification systems and the methodology developed for the Äspö Test Case /Andersson et al. 2002b, Röshoff et al. 2002/. The total length of the drill cores examined in the target volume included 2,565 m from fracture domain FFM01, 525 m from fracture domain FFM06 and 1,355 m from deformation zones.

The results of the Q- and RMR rock mass characterisations within the target volume are summarised in Table 7-1. Estimated Q-values (mode) for each 5 m interval are shown in relation to the geological model for fracture domains and some deformation zones (section 5.6.1) in Figure 7-7. A more comprehensive compilation of the results from the rock mass characterisation is provided in /Glamheden et al. 2007a/. Results from rock mass characterisation of the major deformation zones Singö and Forsmark (see section 5.5.4) are provided in /Glamheden et al. 2008/.

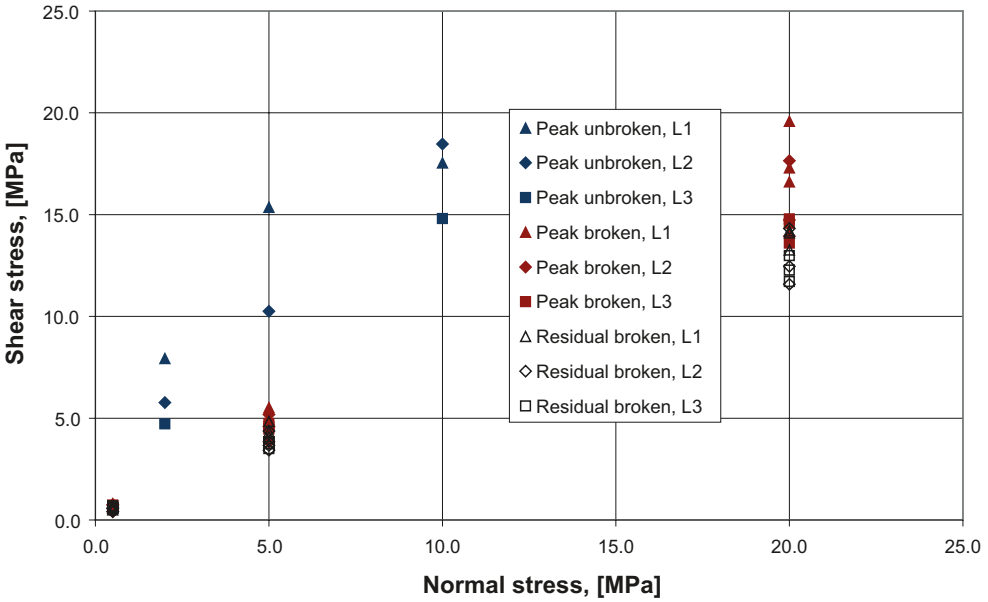

Figure 7-6. *Shear tests on sealed fractures from borehole KFM01D at three different elevations, L1: –380 m, L2: –459 m, and L3: –511 m.*

Table 7-1. Q and RMR values for fracture domains FFM01 and FFM06 and deformation zones in the target volume. The reported values correspond to borehole sections of 5 m.

	Borehole length (m)	Number of sections	Q-value Min	Mean [mode]	Max	RMR-value Min	Mean [mode]	Max
Fracture domain								
FFM01	2,565	513	6	477 [150]	2,133	74	89 [90]	98
FFM06	525	105	20	287 [150]	800	74	87 [88]	94
Deformation zones								
Major DZ	750	150	2	66 [29]	1,067	64	81 [80]	94
Minor DZ	350	70	4	55 [33]	400	70	82 [81]	94
Possible DZ	255	51	10	99 [60]	1,067	75	82 [81]	91

Note: The most frequent value (mode) is reported for Q since it varies over several orders of magnitude on a logarithmic scale.

The estimated mean Q values in fracture domains FFM01 and FFM06 are 477 and 287, respectively. These Q values class the rock mass as “Exceptionally Good (400–1,000)” and “Extremely Good (100–400)” /Barton 2002/. The estimated mean RMR values in fracture domains FFM01 and FFM06 are 89 and 87, respectively. These RMR values class the rock mass as “Very Good (81–100)” /Bienawski 1989/. The deformation zones within the target volume were divided into major, minor and possible following the terminology described in /Stephens et al. 2007/. These were also evaluated using Q and RMR. The corresponding mean Q values for the three categories of deformation zones within the target volume range from 55 to 99, and are classed as “Very Good (40–100)”. The corresponding mean RMR values for the three categories of deformation zones were all approximately 81 and are also classed as “Very Good (80–100)”.

A site-specific correlation between Q and RMR has been examined for the rock mass in rock domain RFM029 and RFM045, see Appendix A3.2 in /Glamheden et al. 2007a/.

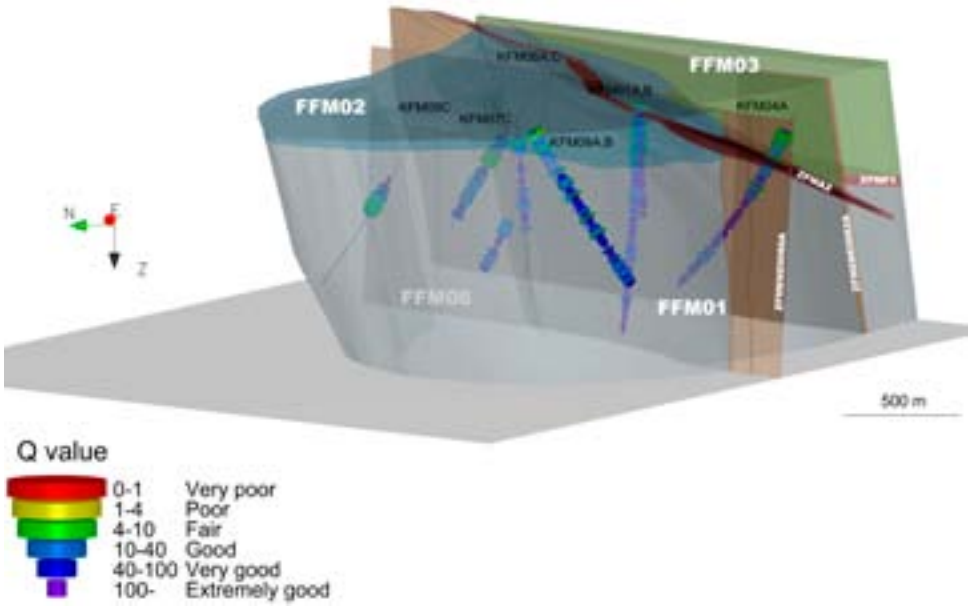

Figure 7-7. *Q value (mode) for each 5 m interval, viewed towards the east. In KFM06A, KFM06C and KFM08C, only sections in FFM06 were characterised.*

7.2.4 *In situ* state of stress

The observations of the *in situ* stress state at the Forsmark site include both direct measurements and indirect observations. Borehole methods used for direct measurements at the site were overcoring, hydraulic fracturing (HF) and hydraulic tests on pre-existing fractures (HTPF). Indirect observations included borehole breakout studies, core disking and microcrack porosity in laboratory samples. The primary data available in the SKB database, Sicada, are provided in a series of WellCad plots, one for each cored borehole, in /Glamheden et al. 2007a/. A comprehensive compilation and analysis of all observations from the site was reported in /Martin 2007/.

Borehole breakouts at Forsmark have been analysed based on the acoustic televiewer logging /Ask and Ask 2007, Ringgaard 2007ab/. In an initial study, the data provided from nine boreholes (KFM01A, KFM01B, KFM02A, KFM03A, KFM03B, KFM04A, KFM05A, KFM06A and KFM07C) were analysed and interpreted relative to the geology by /Martin 2007/. Four additional boreholes (KFM08A, KFM08C, KFM09A and KFM09B) were analysed and reported in /Glamheden et al. 2008/. The analyses show that the proportion of the total borehole length consisting of "classical" borehole breakouts (breakouts with large extent and depth) varies from 0.24% in KFM03B to 5.64% in KFM02A for all the boreholes examined at Forsmark. Furthermore, the data show no noticeable increase in the frequency of occurrence or extent of borehole breakouts with depth. This observation constrains the magnitude of the major principal stress to an upper stress limit.

The televiewer surveys in KFM08A were carried out in April 2005 and repeated in March 2007. The breakouts that were observed in KFM08A in 2005 showed no extension by 2007 suggesting the borehole wall remained stable over this period, despite the tool tripping and other testing carried out in this borehole during this two year period.

The locations of the rock stress measurements made by the overcoring method are presented in relation to fracture domains and deformation zones in Figure 7-8. A similar plot showing the location of the hydraulic fracturing data is provided in Figure 7-9. Overcoring data are available from three boreholes in FFM01 and FFM02 (KFM01B, KFM07B, KFM07C), one borehole in FFM03 (KFM02B) and two boreholes in FFM04 (KFK001, KFK003). Hydraulic fracturing data are available from nine boreholes in FFM01 and FFM02 (KFM01A, KFM01B, lower part of KFM02A, KFM04A, KFM07A, KFM07C, KFM08A, KFM09A, KFM09B), one borehole (upper part of KFM02A) provides data for fracture domain FFM03 and one borehole in FFM04 (KFK001). No stress measurements have been carried out in fracture domain FFM06.

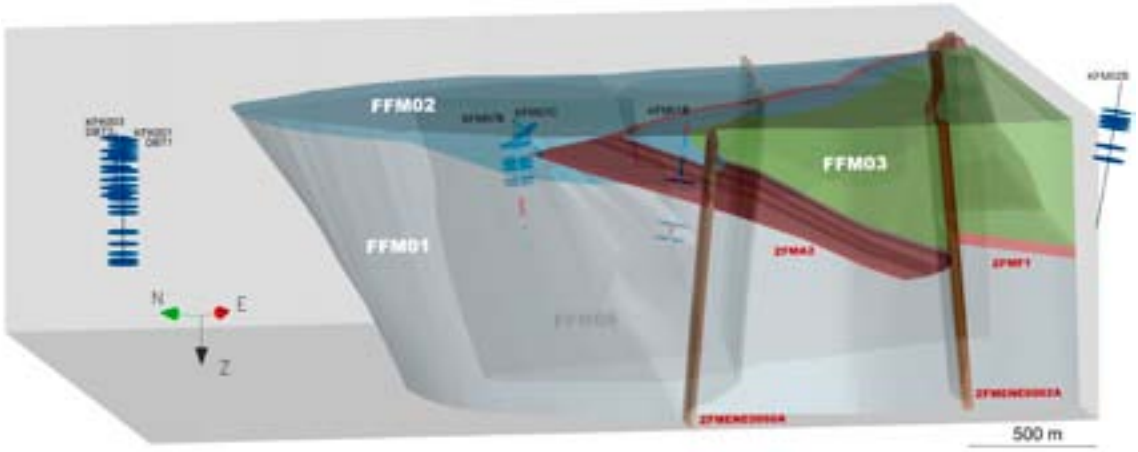

Figure 7-8. *Three-dimensional image showing the location of the in situ stress measurements by the overcoring method in boreholes KFK001 (DBT1) and KFK003 (DBT3), and in boreholes that transect fracture domain FFM01, FFM02 and FFM03.*

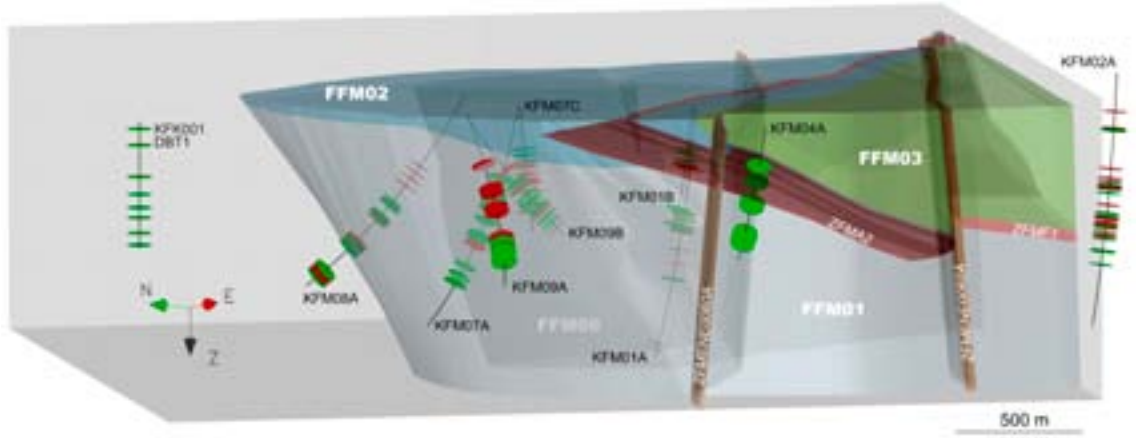

Figure 7-9. *Three-dimensional image showing the location of the in situ stress measurements by the hydraulic fracturing method in relation to fracture domains FFM01, FFM02 and FFM03 and deformation zones in the target volume. The green discs indicate successful attempts and the red ones failed attempts.*

Figure 7-10 shows the maximum horizontal, minimum horizontal and vertical *in situ* stresses from the overcoring measurements for individual boreholes at different depths. It should be noted that the deepest overcoring measurements from KFK001 (DBT1) are questionable. The reasons for this are described and discussed in detail in /Martin 2007/, where also established trends in the data sets are presented, expressed as, for example, the mean stress and the ratios between the principal stresses.

Direct measurements, both overcoring and hydraulic testing, as well as indirect observations all indicate a general orientation of the major principal stress in the range of N120° to 150° in the Forsmark area. This major principal stress orientation is also consistent with the orientation of regional compression derived from seismic studies as well as with the overall trend for NW Europe due to the mid Atlantic ridge push /Glamheden et al. 2007a/. Despite the consistent orientation in the trend of maximum compression, the *in situ* stress magnitudes show considerable scatter.

Two stress models were developed for Forsmark. The model by /Ask et al. 2007/ used the results from hydraulic fracturing and hydraulic testing of pre-existing fractures whereas the model by /Martin 2007/ relied on the overcoring data and indirect observations (Table 7-2). The results in Table 7-2 show large differences in the predicted stress magnitudes for the proposed repository depth and only the overcoring data have been used in the stress model presented in section 7.3.4.

The reason for excluding the hydraulic fracturing data is that it is suspected that the hydraulic measurements do not measure the correct minimum horizontal stress, but rather the vertical stress /Martin 2007/. Furthermore, the results from these methods do not indicate that a thrust regime is prevailing, and this does not agree with the evaluated state of stress in the Fennoscandian shield based on data in the Rock Stress Data base /Stephansson et al. 1991/.

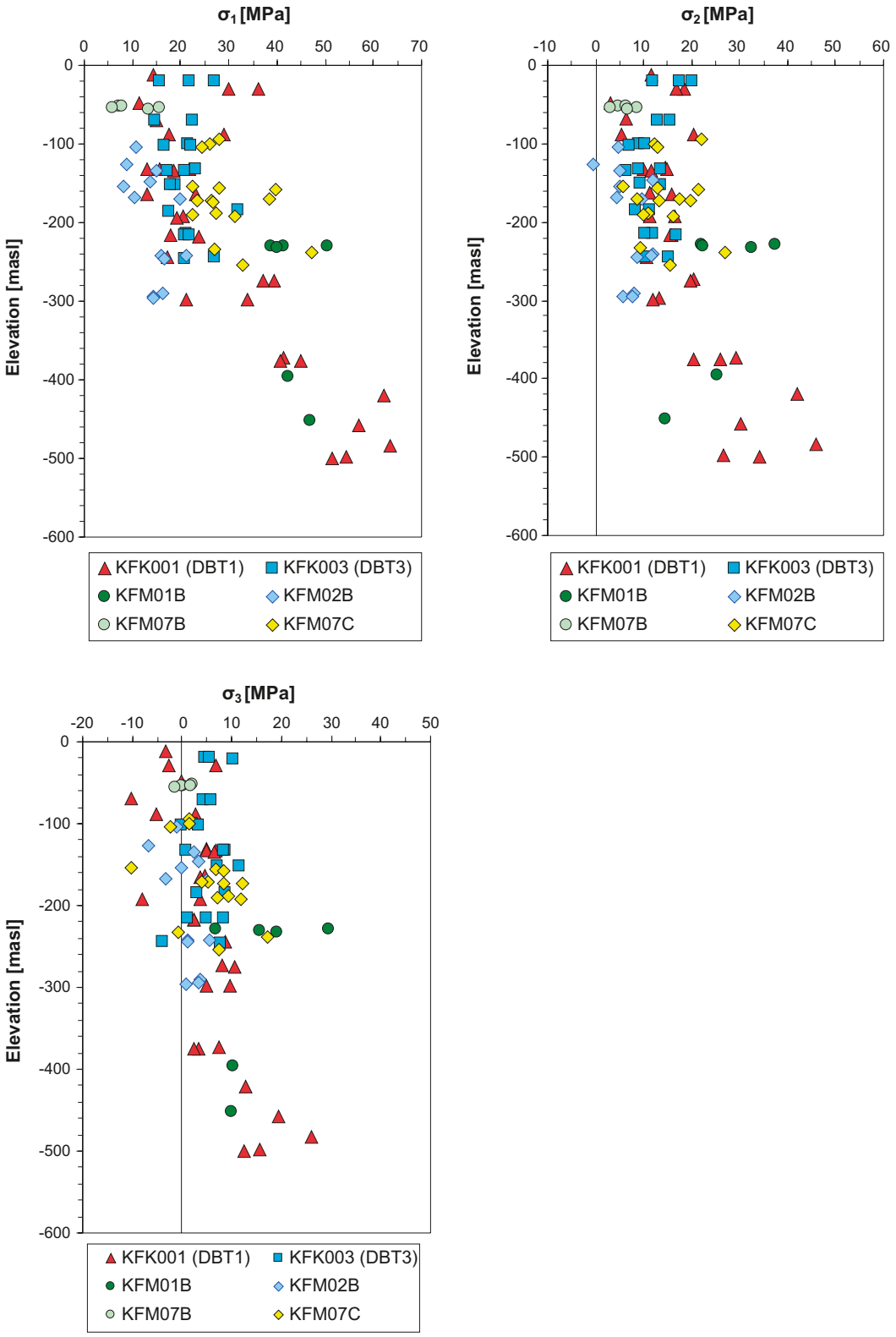

Figure 7-10. *Principal stresses (major σ_1, intermediate σ_2 and minor σ_3) based on overcoring measurement data from boreholes in fracture domains FFM01, FFM02, FFM03 and FFM04.*

Table 7-2. Comparison of the horizontal and vertical stress magnitudes at 400 and 500 m depth. The values by /Martin 2007/ are based primarily on overcoring data whereas the values by /Ask et al. 2007/ are based on hydraulic fracturing and hydraulic testing of pre-existing fractures.

Depth (m)	Maximum horizontal stress (MPa)	Trend (deg)	Minimum horizontal stress (MPa)	Trend (deg)	Vertical stress (MPa)
/Martin 2007/					
400	38.7 ±5.8	145 ±15	20.4 ±4.0	55	10.6 ±0.2
500	41.0 ±6.2	145 ±15	23.2 ±4.6	55	13.2 ±0.3
/Ask et al. 2007/					
400	19.2 ±0.7	124 ±6	9.3 ±1.1	34	10.4
500	22.7 ±1.1	124 ±6	10.2 ±1.6	34	13.0

7.3 Rock mechanics model

The basis for the rock mechanics modelling is the geometrical division of the geological models into rock domains, fracture domains and deformation zones /Stephens et al. 2007/ and chapter 5. As the available site-specific data only cover a small portion of the investigated site, the mechanical properties have been evaluated on the fundamental assumption that the rock volume within each geological domain has similar mechanical characteristics throughout.

For assessment of constructability and the long-term safety of a repository, it is necessary that the rock mechanics model describes the conditions in rock volumes that range from the size of a deposition hole up to the volume of a full repository /Andersson et al 2002b/. The deformation properties Young's modulus and Poisson's ratio are employed in the safety assessment to analyse thermo-mechanically induced changes in the repository near field /SKB 2006b/. This implies that the mechanical properties of the intact rock and discrete fractures as well as the properties of the fractured rock mass must be quantified. In the following sections, representative rock mechanics properties are summarised for each geological domain within the target volume.

7.3.1 Intact rock properties

Deformation and strength properties

The evaluated deformation and strength properties for intact rock in fracture domains FFM01 and FFM06 and for deformation zones are summarised in Table 7-3. Minimum and maximum truncation values are based on the observed min and max for the tested population. The uncertainty of the mean is quantified for a 95% confidence interval. The estimated uncertainties in the model are further discussed in section 7.4.1.

Young's modulus ranges from 69 to 83 GPa in fracture domain FFM01 and from 78 to 86 GPa in fracture domain FFM06, suggesting slightly stiffer intact rock in FFM06 than in FFM01. Corresponding values for Poisson's ratio are 0.14 to 0.35 in FFM01 and 0.25 to 0.31 in FFM06. The test results of intact samples from two steeply dipping deformation zones with different orientation are similar to those observed in fracture domain FFM01.

The results for the dominant rock type 101057 (granite to granodiorite, metamorphic, medium-grained) and the subordinate rock type 101061 (pegmatite, pegmatitic granite) within fracture domain FFM01, and the more altered (albitized) variants of rocks 101057 (granite to granodiorite, metamorphic, medium-grained) and 101058 (granite, metamorphic, aplitic) within FFM06 demonstrate that the intact rock is stiff and strong, and relatively homogeneous. Although fewer samples from FFM06 were tested, the results clearly show higher compressive strength than in FFM01. The consistently higher values for the rock types in domain FFM06 are attributed to the albitization of the rock, which increases the quartz content, (cf. section 5.2.3).

Young's modulus and Poisson's ratio in adjacent domains mainly correlate with the data from FFM01, while the evaluated strength is consistently somewhat lower /Glamheden et al. 2007a/. The results for samples inside or in the vicinity of deformation zones are in the same range as the results for

Table 7-3. Deformation and strength properties for intact rock in fracture domains FFM01 and FFM06 and for deformation zones composed mainly of sealed fractures.

Parameter	FFM01		FFM06		DZ[1]		PDZ[2]
	101057 Mean/stdev Min–Max Uncertainty	101061 Mean/stdev Min–Max Uncertainty	101057 Mean/stdev Min–Max Uncertainty	101058 Mean/stdev Min–Max Uncertainty	101056[3] Mean/stdev Min–Max Uncertainty	101057[4] Mean/stdev Min–Max Uncertainty	101057 Mean/stdev Min–Max Uncertainty
Number of tests	47	13	10	5	4	5	4
Young's modulus (GPa)	76/3 69–83 *±1%*	74/4 69–80 *±3%*	80/1 78–82 *±1%*	83/3 80–86 *±3%*	77/3 73–81 *±4%*	71/1 69–72 *±1%*	78/1 77–79 *±1%*
Poisson's ratio	0.23/0.04 0.14–0.30 ±4%	0.30/0.03 0.26–0.35 ±5%	0.29/0.02 0.26–0.31 ±4%	0.27/0.03 0.25–0.31 ±8%	0.23/0.03 0.19–0.25 ±11%	0.25/0.01 0.24–0.27 ±4%	0.22/0.02 0.20–0.24 ±8%
Uniaxial compressive strength (MPa)	226/29 157–289 ±4%	214/32.8 158–266 ±8%	373/20 338–391 ±3%	310/58 229–371 ±16%	236/12 222–249 ±5%	220/17 191–233 ±7%	205/33 166–242 ±16%
Crack initiation stress (MPa)	116/23 60–187 ±7%	114/18 85–140 ±15%	196/20 180–250 ±6%	169/29 125–200 ±15%	–	112/18 85–130 ±14%	105/22 85–134 ±20%
Cohesion M-C (MPa)	28	33	–	–	–	–	24
Friction angle M-C (MPa)	60	56	–	–	–	–	62
Constant m_i H-B	28	18	–	–	–	–	37
Number of tests	82	12	10	–	11	–	
Indirect tensile strength (MPa)	13/2 10–18 ±2%	12/3 8–16 ±9%	15/1 13–17 ±5%	–	18/1 17–20 ±3%	–	13/2 11–17 ±9%

Note: The uncertainty of the mean is quantified for a 95% confidence interval. Minimum and maximum truncation values are based on the observed min' and max' for the tested population. The cohesion and friction angle are determined for a confinement stress between 0 and 15 MPa.
101056 – Granodiorite, metamorphic.
101057 – Granite to granodiorite, metamorphic, medium grained (albitized in FFM06).
101058 – Granite, metamorphic, aplitic (albitized).
101061 – Pegmatite, pegmatitic granite.
1) DZ – Deformation zones modelled deterministically.
2) PDZ – Possible deformation zones.
3) Intact samples from ZFMNW1200.
4) Samples from ZFMENE0060A composed of sealed fracture network.

samples taken in the host rock outside deformation zones (Table 7-3). This finding is in accordance with the geological description of the steeply dipping deformation zones that are predominantly composed of sealed fractures (cf. section 5.5).

The values in Table 7-3 evaluated for the cohesion and the friction angle correspond to values for very strong rock, while the value for the constant m_i corresponds to normal values for granite /Hoek 2007/.

The values for tensile strength in Table 7-3 are based entirely on results from indirect tests (Brazilian tests). Tensile tests carried out perpendicular and parallel to the foliation gave values that are essentially independent of direction, suggesting an isotropic-strength rock mass within the target volume /Glamheden et al. 2007a/.

Young's modulus, the uniaxial compressive strength and the indirect tensile strength of the dominant rock type 101057 all display a slight decrease (Young's modulus 2–4%, compressive strength 5–10% and tensile strength 10–15%) in the values with depth /Glamheden et al. 2007a/. The decrease in these values with depth is likely related to an increasing volume of micro-cracks in the samples. Support for this proposed explanation is provided by the microcrack volume measurements (cf. section 7.2.1) and the P-wave measurements on laboratory samples /Glamheden et al. 2007a/.

The variability in results between modelling steps is small. The increasing number of test has not changed the evaluated mean values that seem to be representative for the studied main rock type. Thus, the number of tests of intact rock from the target volume seems to be sufficient.

Stochastic modelling according to the concept developed for the thermal modelling /Back et al. 2007/ has been conducted in order to describe the spatial variability of the rock compressive strength. The simulations focused on rock domains RFM029 and RFM045 in the target volume. The outcome of the modelling confirms the results of the analyses of laboratory tests on rock samples. Moreover, the modelling enlightens the spatial variability of the rock compressive strength in larger rock volumes. The overall modelling procedure and the results are described in /Glamheden et al. 2008/.

7.3.2 Fracture properties

A summary of the results from direct shear tests on open fractures in fracture domain FFM01 and three deformation zones intersecting the target volume (ZFMNW1200, ZFMENE1192, ZFMENE101061) is shown in Table 7-4. The estimated uncertainties in the model are discussed in section 7.4.1. These values are from the direct shear tests and are based on direct measurements with a normal stress magnitude comparable to that expected at the tentative repository depth in the Forsmark target volume. The values from tilt tests are not included in Table 7-4 because of the low normal stress used in the test procedure. However, such tests provide similar values.

Samples from the adjacent fracture domains (FFM02, FFM03, FFM04 and FFM05) on the whole show similar results to samples from FFM01. This is also the case for the samples examined from the deformation zones. The differences that exist chiefly concern the normal stiffness, which differs somewhat between the fracture domains. The stiffness is lowest in FFM02 and FFM03, i.e. in the fracture domains with the highest intensity of fractures /Glamheden et al. 2007a/. Possible reasons for the large standard deviation shown in the normal stiffness determined for deformations zones are mismatch between the small samples or variations due to fracture roughness and mineral coatings.

According to /Glamheden et al. 2007a/, there are no clear trends of depth dependence in the results. A comparison of the results from modelling stage 2.2 with the results from previous model versions shows minor changes in the mean values of peak friction angle and peak cohesion (ϕ_p ±0.1° and c_p ±0.1 MPa) despite a large increase (50%) in the number of samples. This indicates that the number of tests in the target volume was sufficient to establish a representative mean value.

Table 7-4. Results from direct shear tests on open fractures in fracture domain FFM01 and deformation zones intersecting the target volume. The tests include 29 samples from FFM01 and 10 samples from three DZ.

Parameter	FFM01		DZ	
	Mean/stdev Uncertainty	Min-Max	Mean/stdev Uncertainty	Min-Max
Normal stiffness (MPa/mm)	656/396 *±22%*	159–1,833	662/729 *±68%*	167–2,445
Shear stiffness, $K_{S20,}$ (MPa/mm)	34/10 *±11%*	18–52	31/8 *±16%*	19–44
Peak friction angle (°)	37/3 *±3%*	29–42	35/2 *±4%*	32–38
Peak cohesion (MPa)	0.8/0.3 *±14%*	0.2–1.3	0.8/0.5 *±39%*	0.0–1.7
Residual friction angle (°)	34.9/3.4 *±4%*	28–42	35/2 *±4%*	30–37
Residual cohesion (MPa)	0.3/0.2 *±24%*	0.1–0.8	0.3/0.2 *±41%*	0.0–0.6

Note: Shear stiffness at 20 MPa normal stress. The uncertainty of the mean is quantified for a 95% confidence interval. Minimum and maximum truncation values are based on the observed min' and max' for the tested population.

It should be noted that the large-scale mechanical properties of fractures are expected to deviate from the results reported here on specimens of 50–60 mm size. While it is well known that the shear strength decreases as the scale increases /Barton and Bandis 1990/, the large scale undulations/ roughness of these fractures has not been quantified and may compensate for the strength reduction. There is also a possibility that the strength of these large-scale fractures may correlate to orientation (e.g. NE-SW vs. NW-SE), although the differences in the laboratory scale shear strength were insignificant in the studies carried out in modelling stage 2.1 /SKB 2006a/.

7.3.3 Rock mass properties

In this section, the rock mass deformation and strength properties are estimated. As described in the introduction, two modelling approaches have been utilised to estimate the rock mass properties, an empirical and a theoretical approach. The final estimate of the rock mass properties is achieved by weighting the results from the two models together, a process termed "harmonization".

Empirical approach using classification systems

The methodology used in the empirical approached to estimate rock mass properties is described in /Röshoff et al. 2002/. The strength parameters of the rock mass were estimated using the linear Mohr-Coulomb (M-C) and non-linear Hoek-Brown (H-B) failure criterion, which are applicable to homogeneous and isotropic rock masses /Hoek et al. 1995/.

The frequency distributions of the estimated rock mass deformation modulus and compressive strength in fracture domain FFM01 are presented in Figure 7-11. The results indicate that fracture domain FFM01 represents a stiff and strong rock mass with a mean deformation modulus of 72 GPa and a mean rock mass uniaxial compressive strength of 92 MPa (H-B). The frequency distribution of deformation modulus is asymmetrically distributed around the mean. This is caused by the high quality rock mass and a maximum cut-off value equal to the Young's modulus of the intact rock.

A comparison of the mean values for the rock mass deformation modulus and compressive strength for fracture domains FFM01 and FFM06 and deformations zones in the target volume is shown in Figure 7-12. Fracture domains FFM01 and FFM06 are similar in both strength and stiffness. The mean deformation modulus in the deformation zones is around 59 GPa, 17% lower than the deformation modulus of the rock mass in FFM01. The mean uniaxial compressive strength of the rock mass in the deformation zones is 64 MPa, which is 29% lower than for the rock mass in domain FFM01.

It should be noted that the empirical modelling possibly includes some bias since the rock at Forsmark is of such good quality that the predicted parameter values are outside the correlated database range /SKB 2008/.

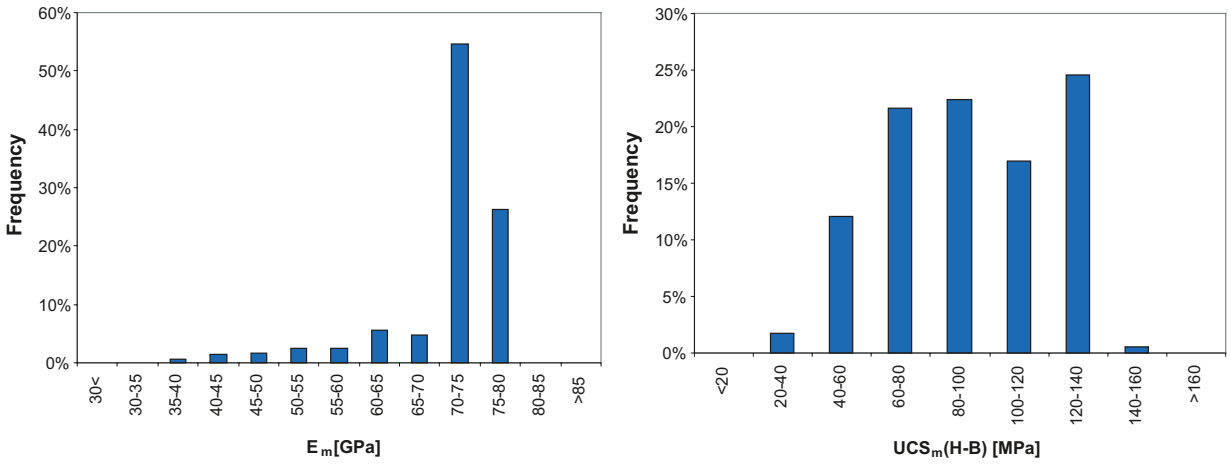

a) Deformation modulus

b) Compressive strength

Figure 7-11. *Histogram of deformation and strength properties evaluated for the rock mass in fracture domain FFM01.*

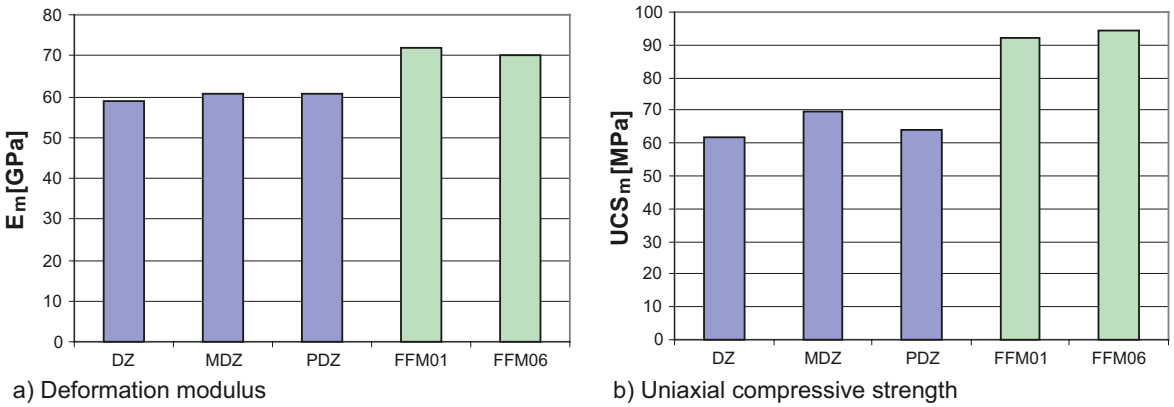

Figure 7-12. *Comparison of mean values of the rock mass deformation and uniaxial compressive strength properties for deformation zones (blue) and fracture domains (green). DZ – Deformation zones > 1,000 m, MDZ – Minor deformation zones < 1,000 m and PDZ – Possible deformation zones.*

Theoretical approach using numerical models

The approach used in this activity is based on numerical simulations with the use of the 3DEC software. The methodology has been developed for the purpose of the site investigations and is built upon three different models: the DFN model which is used to simulate the fracture network in the rock mass, the 3DEC mechanical model which is used to calculate the rock mass mechanical properties, and a statistical model for estimation of combined variability. The modelling procedure is described in detail in /Olofsson and Fredriksson 2005/. The input parameters for the modelling is based on the geological DFN model (TCM) described in section 5.6 and the determined properties of intact rock and fractures presented in sections 7.2.1 and 7.2.2, respectively.

The evaluated rock mass deformation modulus and compressive strength in fracture domain FFM01 are presented in Figure 7-13 as frequency distributions for a section parallel to the maximum horizontal stress. Similar diagrams for fracture domain FFM06 and sections analysed parallel to the minimum horizontal stress are given in /Glamheden et al. 2007a/.

The deformation modulus varies from 59 to 79 GPa, with a mean of 69 GPa, and the uniaxial compressive strength varies from 38 to 233 MPa, with a mean of 122 MPa. The deformation modulus for fracture domain FFM06 is similar, but the uniaxial compressive strength is slightly higher (10–20%) in FFM06.

The sections parallel to the maximum and minimum horizontal stresses (39 MPa respective 26 MPa) gave approximately the same deformation and strength properties in fracture domains FFM01 and FFM06, indicating an isotropic rock mass in the target volume at repository depth. These results suggest that the modulus and strength properties are insensitive to confining stress in the range 20 to 40 MPa.

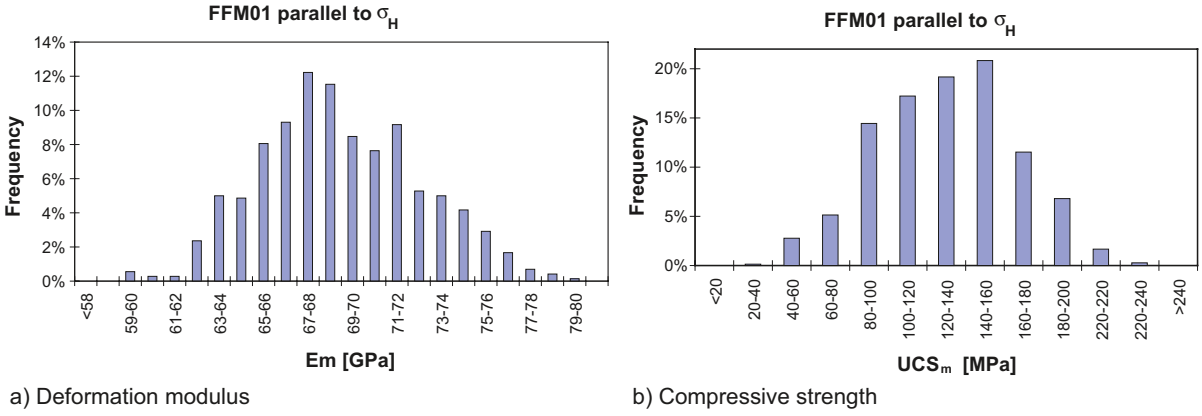

Figure 7-13. *Histogram of deformation modulus and compressive strength evaluated for the rock mass in fracture domain FFM01. The level of the maximum horizontal stress is 39 MPa.*

Estimated deformation and strength properties for three deterministic deformation zones in the target volume are given in Table 7-5. These values are considered appropriate for use in stress modelling, in which a deformation zone is treated as a single fracture at the regional scale (cf. section 7.3.4). Modelling results for deformation zones located outside the target volume are provided in /Glamheden et al. 2007 ab/.

The strength, the deformation modulus and Poisson's ratio, which depend on the confining stress, are valid within the stress limits used in the testing. The general tendency in the modelling results is that Young's modulus increases and Poisson's ratio decreases with increased stress level of the rock mass /Glamheden et al. 2007a/.

Harmonization of the results

Table 7-6 provides a summary of the empirical and theoretical approaches and the harmonized values. The methodology used in the harmonization of the results from the empirical and theoretical approaches are described in /Glamheden et al. 2007a/.

The rock mass deformation and strength properties estimated from the empirical and theoretical approaches are in reasonable agreement for fracture domains FFM01 and FFM06. While there is a

Table 7-5. Estimated properties of three deformation zones in the target volume based on the theoretical modelling.

Deformation zone	Normal stiffness K_N (MPa/mm) Mean/stdev Min-Max	Shear stiffness K_S[2)] (MPa/mm) Mean/stdev Min-Max	Cohesion c (MPa) Mean/stdev Min-Max	Friction angle ϕ (deg) Mean/stdev Min-Max
ZFMA2	81/1.9 79–84	17/3.2 14–22	0.7	36
ZFMF1[1)]	85	24	0.7	36
ZFMENE0062A[1)]	84	24	0.7	36

[1)] Based on one borehole intersection.

[2)] The shear stiffness is a mean value for 0.5 to 10 MPa normal stress.

Table 7-6. Suggested rock mechanics properties of the rock mass in FFM01 and FFM06 after harmonization.

Rock domain	Empirical approach		Theoretical approach		Harmonized values	
Properties of the rock mass	Mean/std. dev. Min-max Uncertainty of mean		Mean/std. dev. Min-max Uncertainty of mean		Mean/std. dev. Min-max Uncertainty of mean	
	FFM01	FFM06	FFM01	FFM06	FFM01	FFM06
Deformation modulus, (GPa)	72/8 39–76 *± 1%*	70/12 40–81 *± 3%*	69/4 59–79 *± 2%*	68/5 56–81 *± 3%*	70/8 39–79 *± 2%*	69/12 40–81 *± 3%*
Poisson's ratio	0.23/0.03 0.12–0.30 *± 1%*	0.23/0.04 0.12–0.33 *± 3%*	0.24/0.03 0.19–0.33 *± 5%*	0.3/0.03 0.23–0.37 *± 4%*	0.24/0.03 0.12–0.33 *± 5%*	0.27/0.04 0.12–0.37 *± 4%*
Uniaxial compressive strength Hoek-Brown, (MPa)	92/27 23–153 *± 3%*	95/32 30–149 *± 7%*	No values	No values	92/27 23–153 *± 3%*	95/32 30–149 *± 7%*
Friction angle, Mohr-Coulomb, (°)	50/2 32–52 *± 0%*	50/2 43–53 *± 1%*	53/2 50–56 *± 2%*	52/2 47–57 *± 2%*	51/2 32–56 *± 2%*	51/2 43–57 *± 2%*
Cohesion Mohr-Coulomb, (MPa)	27/4 12–35 *± 1%*	27/4 18–34 *± 3%*	21/6 5–42 *± 13%*	18/6 1–40 *± 15%*	24/5 6–42 *± 13%*	23/5 1–40 *± 15%*
Tensile strength, (MPa)	2.4/1.0 0.6–5.0 *± 3%*	2.3/1.0 0.6–4.0 *± 8%*	No values	No values	2.4/1.0 0.6–5.0 *± 3%*	2.3/1.0 0.6–4.0 *± 8%*

Note: The uncertainty of the mean is quantified for a 95% confidence interval. Minimum and maximum truncation values are based on the observed minimum and maximum for the tested population.

higher fracture density in FFM06, this is compensated for by higher strength and Young's modulus of the intact rock in FFM06. The estimated uncertainties given in the table are discussed in section 7.4.1.

The harmonized values in Table 7-6 are considered to be representative of the rock mass outside deformation zones. Harmonization of the properties of the deformation zones was not performed due to a judgement that such a harmonization was inappropriate /Glamheden at al. 2007a/. As regards the deformation zones, it is recommended that users who apply the evaluated results should consider which one of the two approaches is the most appropriate for the case being analysed.

7.3.4 *In situ* state of stress

The *in situ* stress state at Forsmark has been evaluated by stress measurements, indirect methods and by numerical analysis based on the current geological model (cf. chapter 5). The primary purpose of the numerical models was to assess the impact of the major deformation zones on the stress magnitudes within the target volume at repository depth and to evaluate the local stress spatial variability. In the following section, the results from the numerical simulations are discussed.

Evaluation of stress variability caused by deformation zones

A series of three dimensional 3DEC numerical model simulations was carried out to assess the impact of the major deformation zones on the stress magnitudes within the target volume at the depth of the proposed repository /Glamheden et al. 2007a/. The geometry of the numerical model used in stage 2.2 is presented in Figure 7-14. The deformation zones included in the model in relation to the direction of the applied compression are shown in Figure 7-14a together with the approximate location of boreholes KFM02B and KFM07C. The division into deformable blocks and the generated mesh are shown in Figure 7-14b.

As discussed in section 7.2.4, the greatest uncertainty in the development of a stress model for Forsmark is the horizontal stress magnitudes and the ratio of the maximum horizontal to minimum horizontal stress at the repository level. In the stage 2.2 regional 3DEC numerical model, no stress ratios were specified, gravity was imposed and model boundaries were displaced (compressed) in one direction, while the other boundary remained fixed. The compression was stopped once the maximum horizontal stress in the model approached the measured values from the stress measurement campaigns. Since most of the measurements were recorded above 300 m depth, there is no match with repository depth and there was no attempt to match the stress ratios.

The results indicate that the stress field in the target volume is relatively homogeneous. The steeply dipping deformation zones cause only very limited perturbation of the stress field in close proximity to the zone, while the gently dipping deformation zone ZFMA2 perturbs all the stresses in the rock mass above the zone, see Figure 7-15. However, below the gently dipping deformation zone, the stress disturbance caused by this zone is very limited.

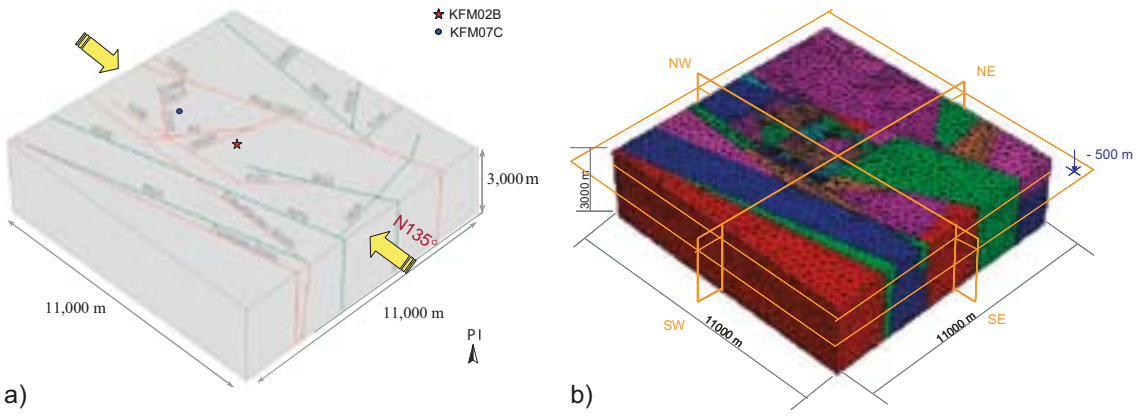

Figure 7-14. *The geometry of the 3DEC model and direction of compression used in stage 2.2, which is in agreement with that inferred from regional seismic studies, see /Slunga 1991/. The approximate location of boreholes KFM02B and KFM07C, and selected sections for presentation of the results are also shown.*

In Figure 7-16, the calculated results are presented along two perpendicular scan lines in lateral directions at 500 m depth in the target volume. The directions of the scan lines are shown in Figure 7-14. The results indicate that the variation in the principal stresses is approximately ±4 MPa. It should be noted that the scan lines sample the stresses directly beneath deformation zones ZFMA2 and ZFMF1. Hence, the more pronounced variation at shallower depths, associated with the deformation zones, is not reflected in the scan line results. It should also be mentioned that some of the variation is likely to be caused by the non-uniform size of the tetrahedral used to sample the stress magnitudes in the model.

Figure 7-17 shows the ratio of the maximum horizontal to the minimum horizontal stress from a vertical scan line in the 3DEC numerical model close to borehole KFM07C /Glamheden et al. 2007a/. The stress ratio shows a general decrease with depth and the stress ratios at the repository level are in reasonable agreement with the stress ratio predicted from the stress measurements. The maximum and minimum stress ratios in Figure 7-17 were used to establish the uncertainty in the stress magnitudes at the repository level.

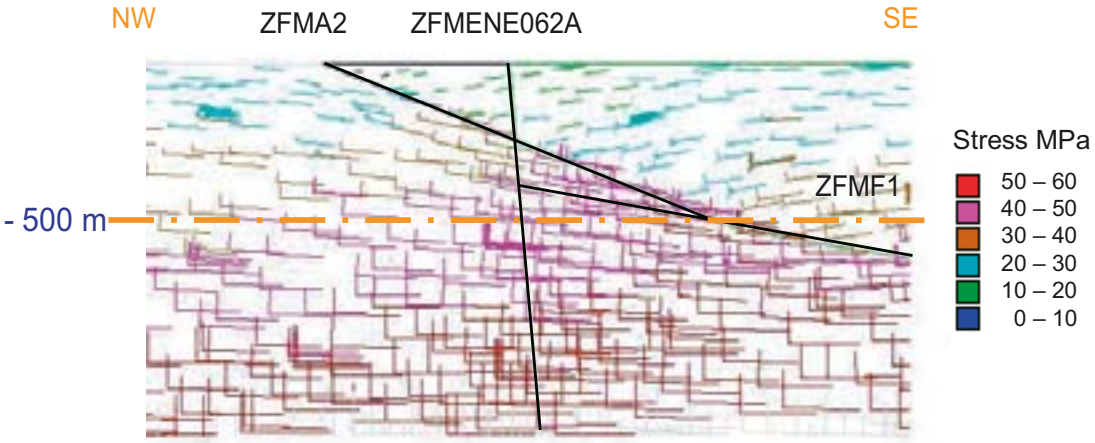

Figure 7-15. *Principal stress tensors along a NW-SE vertical section (see Figure 7-14) showing deformation zones ZFMA2, ZFMF1 and ZFMENE062A. Note the rotation of principal stress tensors above and around ZFMA2 and ZFMF1.*

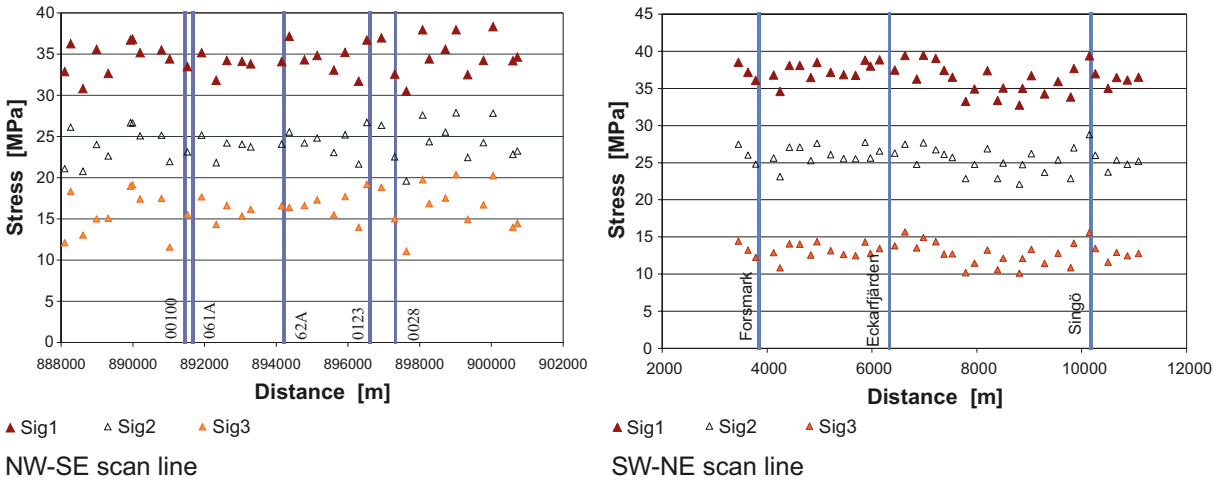

Figure 7-16. *The calculated variation of σ_1, σ_2 and σ_3 magnitudes along a NW-SE and SW-NE scan line at the depth of 500 m in the target volume. The coordinates refer to a local system of coordinates established in the 3DEC model.*

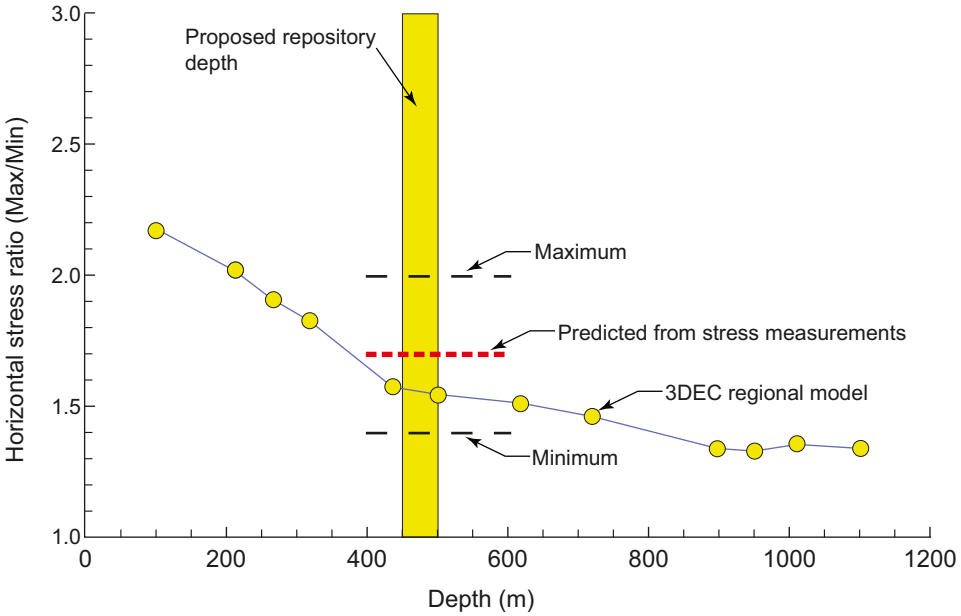

Figure 7-17. *Horizontal stress ratio captured from the 3DEC numerical model stage 2.2, near borehole KFM07C. The minimum and maximum lines represent the limits used to establish the most likely range in maximum and minimum horizontal stress.*

Evaluation of local stress spatial variability

Inside the target volume at the Forsmark site, the frequency of open fractures decreases with depth (see section 5.2.5), which improves the rock mass quality with depth. This feature has formed the basis for the division into fracture domains FFM01 and FFM02 (section 5.6.1). A two dimensional elastic model was used to explore the effect of increasing deformation modulus with depth on the maximum horizontal *in situ* stress magnitude /Glamheden et al. 2007a/. Additional simulations performed during modelling stage 2.3 are presented in /Glamheden et al. 2008/. The results from these simulations, taken together, illustrate that the observed change in the stress magnitude with depth likely reflects the improved rock mass quality and an accompanying increase in deformation modulus with depth.

Geological investigations have indicated that the tectonic lens may be stiffer than the rock mass outside the lens (see chapter 5). The effect of a stiffer central tectonic lens was analysed in a numerical model /Glamheden et al. 2007a/. The lens was in the model treated as a stiff inclusion with a modulus of elasticity 10% greater than the surrounding rock mass. The results show that these changes in properties of the tectonic lens did not cause any notable change in the prevailing stress field.

By applying the mean principal stresses at repository depth to a 3DEC model containing discrete fractures based on the DFN model described by /Fox et al. 2007/, the stress variability due to discrete fractures at the scale of a 5 m diameter deposition tunnel was examined. The methodology used in these analyses is described in /Glamheden et al. 2007a/. The analyses indicate that the major principal stress obtained from overcoring measurements could be expected to vary spatially by ±5 MPa in magnitude and ±9 degrees in orientation for the rock mass conditions expected at Forsmark. The variability in the stress magnitudes and orientations from the simulations are considered as an upper bound for the Forsmark rock mass at repository depth, containing a discrete fracture network /Glamheden et al. 2007a/.

Assessment of in situ stress state at repository depth

The evaluated *in situ* stress state at Forsmark is presented in Figure 7-18. No stress measurements have been carried out in FFM06, but the *in situ* stress state is expected to be similar to FFM01, since it consists of a rock mass with similar stiffness properties and is located adjacent to FFM01, below deformation zone ZFMA2.

The stress model at repository depth, 400–600 m, in fracture domain FFM01 and FFM06 is described in Table 7-7, while the *in situ* stress model for 150–400 m depth in fracture domain FFM01 and for fracture domains FFM02 and FFM03 are provided in /Glamheden et al. 2007a/. The "most likely values" given in Table 7-7 were determined by an approach described in /Martin 2007/ for integration of the data to reduce the uncertainty and establish consistency in the estimation of the *in situ* state of stress. The term "most likely values" is preferred over the term "mean value" since the value was not obtained using a formal mathematical procedure. The "estimated uncertainty" in Table 7-7 reflects the total uncertainty in the most likely value. The "uncertainty due to local variability" was assessed in the numerical simulation described in the previous section. The uncertainty in the stress model is further discussed in section 7.4.2.

The adopted model results in a mean magnitude of the major horizontal stress of approximately 41 MPa and of the minor horizontal stress around 23 MPa for 500 m depth in FFM01. Compared with previous model versions /SKB 2005a, SKB 2006a/, the present estimates of the stress magnitudes are slightly lower.

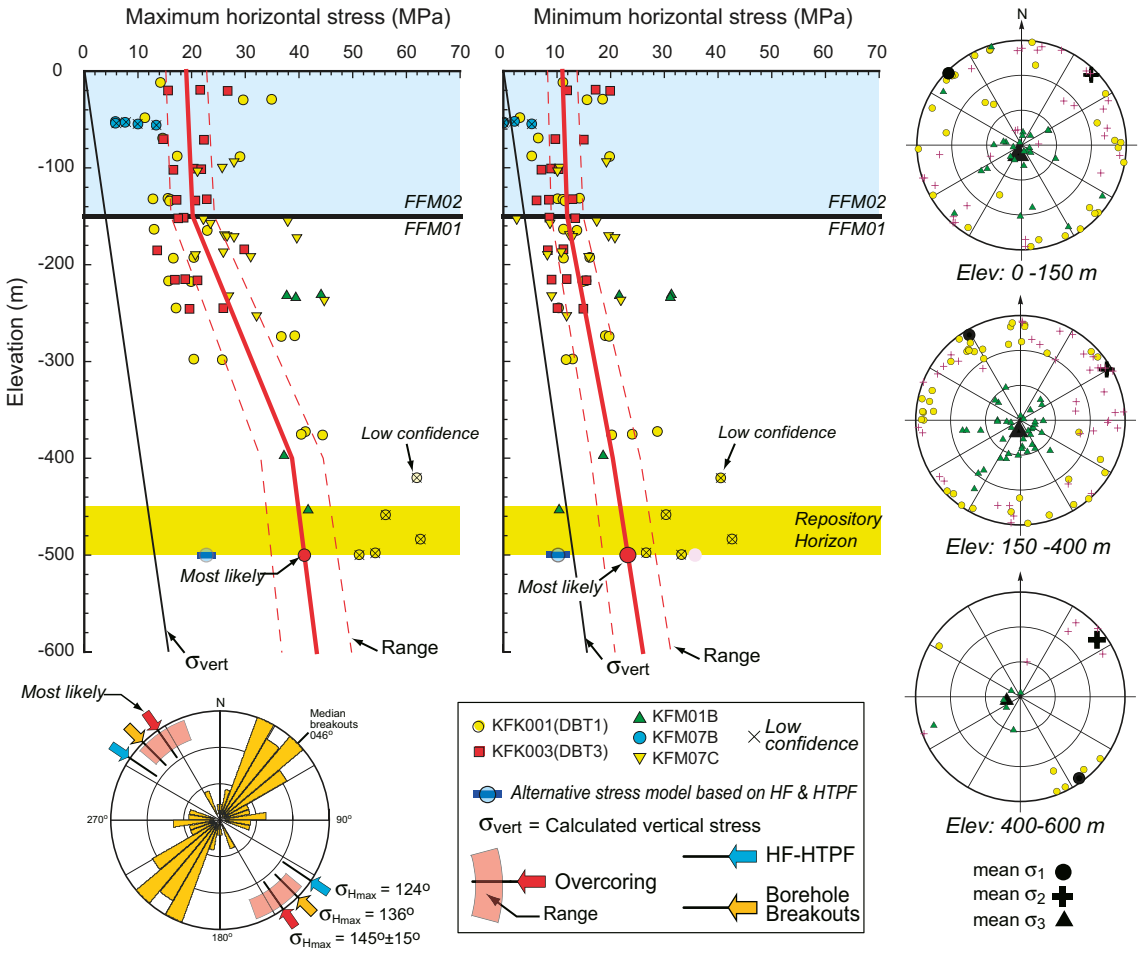

Figure 7-18. *Evaluated in situ state of stress at Forsmark based on overcoring data and indirect observations. An alternative stress model based on hydraulic fracturing and hydraulic testing of pre-existing fractures is also presented in the figure.*

Table 7-7. Stress model for domains FFM01 and FFM06, 400–600 m depth.

	Most likely value[1)]	Estimated uncertainty[2)]	Uncertainty due to local variability
Magnitude			
Major horizontal stress, σ_H	29.5+0.023z MPa	±15%	4%
Minor horizontal stress, σ_h	9.2+0.028z MPa	±20%[3)]	6%
Vertical stress, σ_v	0.0265z MPa	±2%	–
Orientation			
Major horizontal stress trend, σ_H	145°	±15°	±3°

1) The symbol z corresponds to the depth from the ground surface in metres.

2) The estimated uncertainty includes the value of the local variability.

3) The uncertainty in σ_h is correlated to uncertainty in σ_H. The mean ratio σ_H/σ_h is modelled to lie in the range 1.4–2.0 (i.e. other combinations are not expected).

7.4 Evaluation of uncertainties

7.4.1 Uncertainty in mechanical properties

The uncertainty in the mechanical properties has been expressed by means of a range of variation in the evaluated mean values and a standard deviation for a 95% confidence interval. Minimum and maximum truncation values based on the observed minimum and maximum for the tested population have also been evaluated /Glamheden et al. 2007a/.

For the dominant rock type, the uncertainty in the mean values is small for the mechanical properties of both the intact rock and the rock mass. This fact indicates homogeneous conditions in the target volume. Insignificant changes in rock mechanics properties compared with previous model versions /SKB 2005a, SKB 2006a/ indicate that the evaluated mean values are representative and that the test data are sufficient in the target volume.

Microcracking due to release of stresses during core drilling is supposed to disturb the laboratory samples. This causes an increase in the uncertainty of the compressive and tensile strength with depth.

The changes in testing procedure for measuring the normal stiffness in the direct shear tests may have caused uncertainty in the tests in stage 1.2. This uncertainty was substantially reduced for the results in stage 2.2 and 2.3.

Identified potential biases in the data used for evaluation of the rock mechanical properties are listed in /SKB 2008/.

7.4.2 Uncertainty in the stress model

The uncertainty in the *in situ* state of stress has been quantified by technical auditing of measurement results, statistical data analysis and numerical modelling /Martin 2007, Glamheden et al. 2007a/. The orientation of *in situ* stresses and the magnitude of the vertical stress component are the aspects of the stress model that are judged to have highest confidence. The basis for the confidence in the orientation is the conformity in the results between measuring methods and indirect observations at different scales and its agreement with regional seismic studies. The confidence in the vertical stress component is founded on the concordance between measured values and theoretical values based on the weight of the overlying rock cover.

The magnitude of the uncertainty in the minimum and maximum horizontal stresses has been possible to constrain because “classical” borehole breakouts have not been observed at depth. While uncertainty in the horizontal stress magnitudes remains using this approach, the stress model provides an upper bound estimate.

The results from the HF and HTPF measurements have been omitted in the proposed stress model. The results from these measurements were excluded since it is suspected that the minimum horizontal stress is incorrect and corresponds to the vertical stress. Moreover, these results do not agree with the state of stress in the Fennoscandian shield as estimated from data in the Rock Stress Data base /Stephansson et al. 1991/. Neglecting the HF and HTPF data result in a conservative estimation of the *in situ* state of stress.

Identified potential biases in the data used for evaluation of the *in situ* state of stress are listed in /SKB 2008/.

8 Bedrock hydrogeology

8.1 Context

8.1.1 Hydrogeological modelling in the SDM

Primary objectives of the bedrock hydrogeological model are to provide a general conceptual understanding and to determine and justify the assignment of hydraulic properties, boundary and initial conditions. The evaluations are based on primary data and the model is derived with the purpose to serve the needs of repository engineering, safety assessment and environmental impact assessment studies.

The three-dimensional, large-scale numerical flow models considered are used to underpin the development of the bedrock hydrogeological model. The flow models include 3D descriptions of the geometry of geological features (regolith, discrete fracture networks (DFN) and deformation zones), transient hydrological and chemical boundary conditions, anisotropy and spatial heterogeneity in the hydraulic properties, density driven flow, advective transport and rock matrix diffusion of different water types (solutes). It has been suggested that an understanding of the evolution throughout geological time is a powerful tool to predict the future development of groundwater flow and its chemical composition, see e.g. /NEA 1993, Bath and Lalieux 1999/. Testing and developing tools for coupled hydrogeological-hydrochemical modelling over time was also the focus of an international project referred to as *Task 5*, which was based on multidisciplinary data from the Äspö Hard Rock Laboratory in Sweden /Laaksoharju and Wallin 1997, Wikberg 1998, Rhén and Smellie 2003/.

Figure 8-1 illustrates schematically the division of the groundwater system into hydraulic domains as used in the hydrogeological SDM for Forsmark. The groundwater system consists of three hydraulic domains, HSD, HCD and HRD, where:

- HSD (Hydraulic Soil Domain) represents the regolith,
- HCD (Hydraulic Conductor Domain) represents deformation zones, and
- HRD (Hydraulic Rock mass Domain) represents the fracture domains in between the deformation zones.

The division into hydraulic domains constitutes the basis for the conceptual modelling, the planning of the site investigations and the numerical simulations carried out in support of the SDM. The flow models used in the SDM simulate the shoreline displacement in the Fennoscandian Shield during Holocene time, i.e. between 8000 BC and 2000 AD.

Hydrogeological description

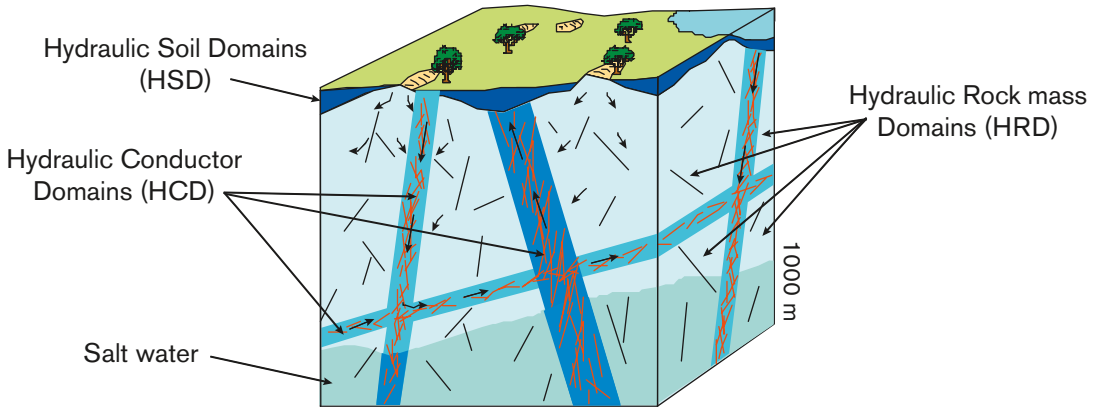

Figure 8-1. *Cartoon showing the division of the crystalline bedrock and the regolith above it (Quaternary deposits mainly) into three hydraulic domains.*

8.1.2 Model development

The development of the bedrock hydrogeological model of the Forsmark area is based on the bedrock geological model and the hydraulic investigations conducted in the core-drilled (KFM) and percussion-drilled (HFM) boreholes. That is, the geometries of the hydraulic domains are coherent with the geometries of the geological features, and their hydraulic properties reflect the anisotropy and spatial variability observed in the hydraulic investigations. Table 8-1 shows the cumulative number of boreholes providing hydraulic information about the bedrock in the Forsmark area. The number of boreholes is shown in relation to the two investigation stages (ISI and CSI), the three model versions (0, 1.1 and 1.2) and the three model stages (2.1, 2.2 and 2.3) carried out during the period 2002–2007. Version 1.2 represents the preliminary SDM and stage 2.2 is the major contribution to the SDM at Forsmark from a hydrogeological data acquisition and modelling point of view. The hydrogeological data acquisition and modelling carried out during stage 2.3 concern model verification and uncertainty assessment.

Table 8-1 also shows the reference numbers of the major background reports in relation to each model version/stage. /Follin 2008/ (not shown in Table 8-1) provides a detailed summary of the work described in these reports, i.e. the field investigations, the data analyses, the conceptual model development and the numerical modelling of groundwater flow and solute (salt) transport. The summary report constitutes the main hydrogeological reference for the SDM. However, sometimes a reference is given to the specific background reports for the sake of clarity.

As a means of approaching the issue of confirmatory testing, a strategy was developed after the initial site investigation (ISI) stage /Follin et al. 2007a/, see Figure 8-2. In practice, four kinds of data were treated during the complete site investigation (CSI) stage:

A. Hydraulic properties deduced from single-hole hydraulic tests (double-packer injection tests, PSS, difference flow logging pumping tests, PFL-f, and open-hole pumping tests combined with impeller flow logging, HTHB) /Follin et al. 2007b/.
B. Groundwater level responses (point-water head drawdowns) in the bedrock in the depth interval 0 to c. 700 m observed during large-scale interference (cross-hole) tests /Follin et al. 2007c, 2008a/.
C. Present-day mean groundwater levels (point-water heads) observed in the Quaternary deposits and the uppermost (c. 150 m) part of the bedrock /Follin et al. 2007c, 2008a/.
D. Hydrochemical data (fracture water and matrix porewater) gathered from the bedrock investigations (primarily the core-drilled boreholes) /Follin et al. 2007c, 2008a/.

The general approach applied in the numerical modelling was to first parameterise the deformation zones and fracture domains hydraulically using fracture and inflow data from individual boreholes (A). Second, the confirmatory step relies on using essentially the same groundwater flow and solute transport model in terms of grid discretisation and parameter settings for matching three types of independent field data (B-D). Using the three types of data, a unified conceptual description of the groundwater system has been attempted.

Table 8-1. The cumulative number of boreholes providing hydraulic information about the bedrock in the Forsmark candidate area at the end of each of the three model versions and three model stages carried out during the period 2002–2007. KFM = core-drilled boreholes, HFM = percussion-drilled boreholes. The reports with reference numbers typed in italics describe the hydraulic data gathered and/or the hydrogeological modelling undertaken. The reports with underlined reference numbers summarise the development of the hydrogeological modelling along with the developments achieved within the other disciplines.

	Initial site investigation (ISI)			Complete site investigation (CSI)	
Desk top exercise	**Training exercise**	**Preliminary SDM**	**Feedback and strategy**	**Hydrogeological model**	**Model verification and uncertainty assessment**
Version 0	**Version 1.1**	**Version 1.2**	**Stage 2.1**	**Stage 2.2**	**Stage 2.3**
0 KFM (0%)	1 KFM (4%)	5 KFM (21%)	9 KFM (38%)	20 KFM (83%)	25 KFM (100%)
0 HFM (0%)	8 HFM (21%)	19 HFM (50%)	22 HFM(58%)	32 HFM (84%)	38 HFM (100%)
R-02-32	R-04-15	R-05-18 *R-05-32* *R-05-60*	R-06-38 *R-07-20*	*R-07-48* *R-07-49*	*R-08-23*

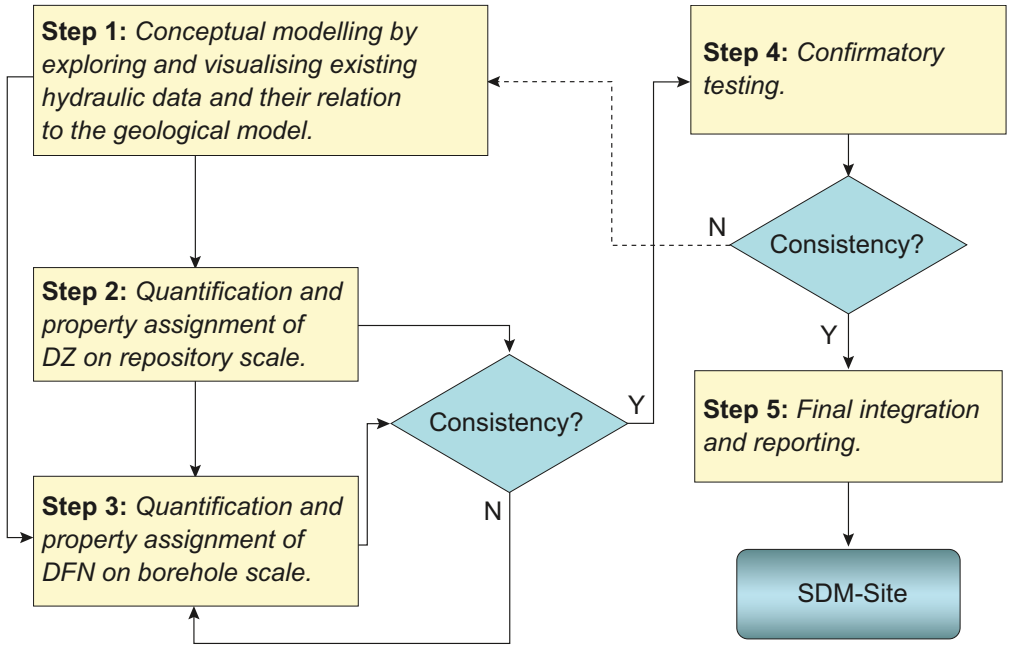

Figure 8-2. *Flow chart of the five steps suggested for the hydrogeological modelling during the complete site investigation (CSI) stage. DZ = deformation zone, DFN = discrete fracture network.*

8.1.3 Main characteristics of relevance to the model

Here, a brief summary is given of the primary hydrogeological characteristics of the Forsmark area. Figure 8-3 shows a perspective view of the candidate area towards the south. The regionally significant, ductile and brittle deformation zones with WNW-NW strike, i.e. Forsmark (FDZ), Eckarfjärden (EDZ) and Singö (SDZ), border the candidate area and run more or less perpendicular to the regional hydraulic gradient. Zones A2 and ENE0060 are local major deformation zones. Zone A2 dips gently to the south and splits the bedrock within the candidate area into two parts. Here, the south-eastern part is referred to as the hanging wall bedrock and the north-western part as the footwall bedrock to zone A2. Zone ENE0060 dips steeply and strikes parallel to the regional hydraulic gradient. It divides the target volume in the footwall bedrock into two parts.

The strike of the steep WNW-NW zones is parallel to the main principal stress (σ_{1H}), whereas the strike of zone ENE0060 is parallel to the second principal stress (σ_{2h}). More important, zone A2 is at a high angle to the minimum principal stress (σ_{3v}) (cf. Figure 7-10 and Table 7-2). The A2 zone is far more transmissive and less hydraulically heterogeneous than zone ENE0060. The three regional zones are not nearly as well investigated as the zones inside or close to the candidate area. The data gathered in the three regional zones, together with the data from local major deformation zones with similar orientations and located closer to the candidate area, suggest that steeply dipping zones with a WNW-NW strike may have noteworthy in-plane transmissivities, yet less significant relative to the in-plane transmissivities of gently dipping zones such as zone A2. The hydraulic investigations carried out in the deterministically modelled deformation zones reveal both a significant decrease in the in-plane transmissivity with depth and a considerable in-plane lateral heterogeneity (channelling).

The hydraulic investigations carried out in the fracture domains suggest that the frequency of water-conductive fractures varies significantly in space. Data suggest that there is less than one flowing fracture per hundred metres below c. 400 m depth within the target volume, which is located in the footwall bedrock. In contrast, the uppermost c. 150 m of bedrock inside the target volume is considerably more fractured, with more than 30 flowing fractures per hundred metres. In addition, the near-surface bedrock between the deterministically modelled deformation zones within the target volume contains discrete sub-horizontal fractures/sheet joints, many of which have high in-plane transmissivities and extends tens to hundreds of metres. Here, the hydraulic gradient is low due to the flat topography and the pronounced structural-hydraulic anisotropy.

In summary, the strong contrast in the structural-hydraulic properties with depth within the target volume creates a hydraulic phenomenon that causes a short-circuit in the near-surface flow system, which may contribute to a slow transient evolution of fracture water and porewater hydrochemistry at depth.

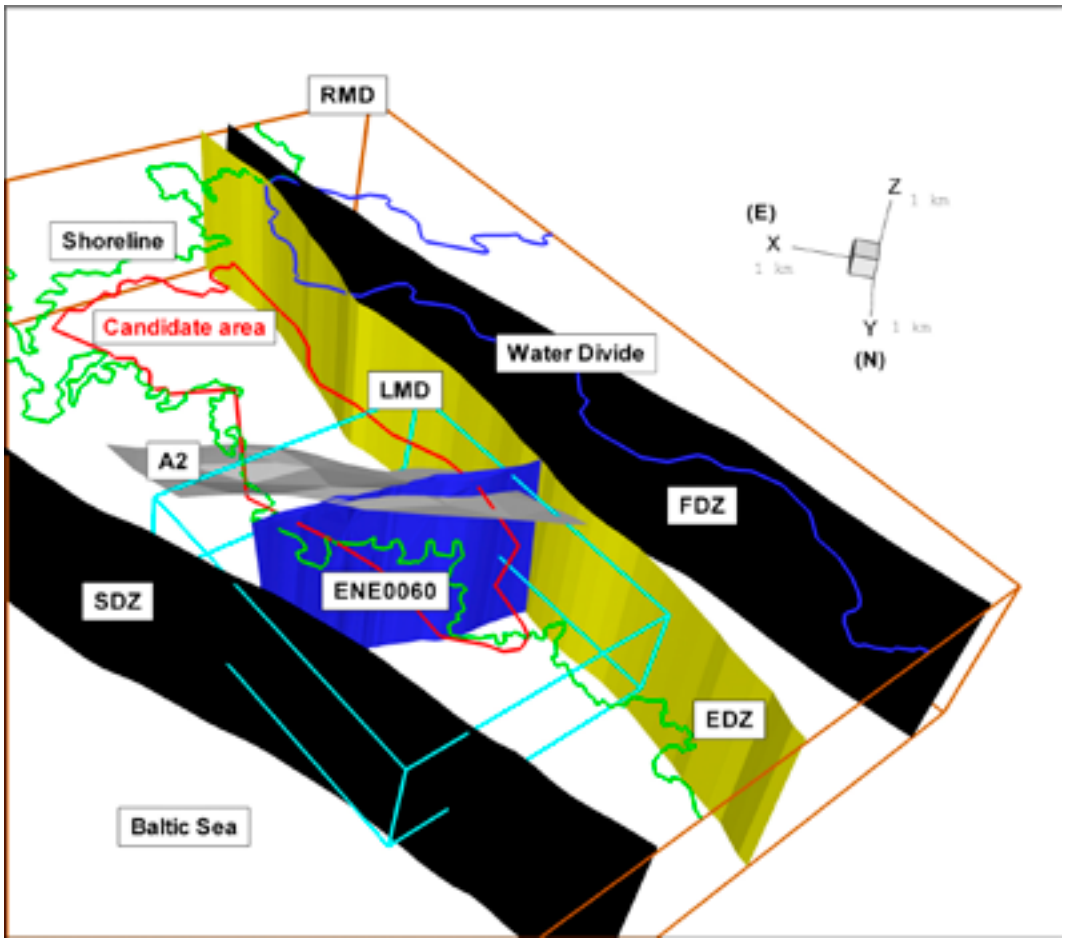

Figure 8-3. *A perspective view towards south showing the candidate area, the local model domain (LMD), the south-western part of the regional model domain (RMD). The regionally significant deformation zones Forsmark (FDZ), Eckarfjärden (EDZ) and Singö (SDZ) border the candidate area. The remaining zones, A2 and ENE0060, are local major deformation zones. The solid blue line indicates the nearest regional topographical water divide.*

8.2 State of knowledge at the previous model version

The state of the hydrogeological knowledge reported in the preliminary site description /SKB 2005a/ can be summarised as follows.

- Hydraulic data from five core-drilled boreholes (KFM01A–KFM05A) and 19 percussion-drilled boreholes (HFM01–HFM19) indicated that the gently dipping deformation zones generally have greater transmissivities than the steeply dipping zones at corresponding depths, and that all deformation zones have much greater transmissivities close to the surface.
- The hydraulic data also indicated that the rock mass beneath the gently dipping deformation zone A2 has a very low frequency of water-conductive fractures, in particular below c. 360 m depth. In contrast, the uppermost part of the bedrock appeared to be rather conductive. It was suggested that the bedrock between the deformation zones should be divided into several sub volumes in the evaluation of the hydrogeological discrete fracture network properties.
- Regional simulations of the hydrogeological evolution during the Holocene indicated that the local topography and the structural-hydraulic properties of the local major deformation zones are more important for the groundwater flow and solute (salt) transport within the target volume relative to regional topography and the structural-hydraulic properties of the regional deformation zones bordering it.

- The regional simulations also showed a better agreement between simulated and measured hydrochemical data at depth, whereas poorer matches were obtained in the uppermost c. 100–200 m of the bedrock. The simulations supported the notion of a difference in the intrusion of *Littorina Sea Water* in the hanging wall and footwall bedrock segments.

The hydrogeological understanding described in the feedback report concluding the ISI stage /SKB 2006a/ affected the site investigations during the CSI stage. The two key observations made can be summarised as follows.

- Hydraulic data from the cored boreholes KFM06A and KFM07A and the percussion-drilled boreholes HFM20–HFM22 corroborated the previous notion of dividing the bedrock between the deterministically modelled deformation zones into several sub volumes.
- The highly transmissive sub-horizontal fractures/sheet joints encountered in the north-western part of the candidate area suggested that there may be a well-connected network of structures with very anisotropic hydraulic properties in the uppermost c. 150 m of the bedrock. It is recognised that the hydraulic cage analogue tentatively suggested in /Follin et al. 2007ab/ is misleading as there is no hydraulic cage at Forsmark *sensu strictu*. A more appropriate hydrogeological description of the hydraulic short circuit phenomenon observed in the uppermost part of the bedrock is a shallow, anisotropic, bedrock aquifer on top of thicker segment of bedrock with aquitard type properties. The bedrock aquifer has little or no storage, hence it has a high hydraulic diffusivity.

The main hydrogeological uncertainties concluded at the end of the ISI stage were as listed below.

- The heterogeneity and anisotropy in the superficial bedrock properties called for a much higher resolution of the computational grid.
- The model strongly underestimated the measured salinity in the upper 200 m of bedrock (cf. above). This called for an improved geometric and hydraulic representation of the near-surface hydraulic and transport properties as well as the top boundary conditions, to obtain a good match.
- Besides the evident depth trend in the deformation zone transmissivity, there is probably also a substantial spatial variability in the transmissivity in the lateral direction, i.e. within the plane of each deformation zone. However, this was difficult to implement due to lack of observations. In the test simulations carried out, lateral heterogeneity was found to have a significant impact on the matching of the flow models against the hydrochemical data as well as on the particle tracking. More information was thought to be needed about the deformation zones transmissivity both within and outside the candidate area.
- There is a possibility for upconing of deep saline groundwater in steeply dipping deformation zones with a high transmissivity.
- The choice of the minimum fracture size in the power-law fracture size distribution model (r_0) affects the intensity of connected open fractures in the hydrogeological DFN modelling. For the target volume, the variability between different parameter settings ranges from no connectivity at all to a sparsely connected discrete fracture network with a transmissivity below the ‘measurement threshold’.
- The effect of the variability of the properties of the Quaternary deposits for the bedrock hydrogeological model was not assessed. More variants on the Quaternary deposit properties needed to be considered to see whether an improved match in salinity near the surface could be achieved. It was considered that these variations should probably be coupled to a specified infiltration type boundary condition and a much higher resolution in the computational grid.
- The absence of hydrochemical data from the porewater in the rock matrix meant that it was not possible to make conclusive judgements about the role of matrix diffusion of saline groundwater. In the model, it was assumed that the salinity profile with depth in the kinematic porosity field was in equilibrium with the salinity profile with depth in the matrix porosity field at the start of the simulation period (10,000 BC). More information was thought to be needed about the groundwater salinity in the bedrock both within and outside the candidate area.

8.3 Evaluation of primary data

The hydrogeological investigations performed in the Forsmark area are summarised in sections 2.1 and 2.3 and the data supporting the current model version are listed in Table 4 in Appendix 3. The evaluation of these data is presented below.

8.3.1 Deterministic versus stochastic features

The hydraulic characterisation of the more intensely fractured deformation zones and the less fractured bedrock in between, the so-called fracture domains /Olofsson et al. 2007/, is a cornerstone of the bedrock hydrogeological description. The adopted modelling approach combines a deterministic geometrical representation of the HCD with a stochastic geometrical representation of the HRD using a discrete fracture network (DFN) approach and the tectonic continuum hypothesis, see Figure 8-4. Both domains were treated as hydraulically heterogeneous.

The tectonic continuum hypothesis is a working hypothesis. It invokes that the size and intensity of fractures on multiple scales can be approximated through the use of a *single* power-law relation ship, which by definition requires scale-invariant fracture orientation sets. However, the density functions may vary between the fracture orientation sets. The orientations of the global fracture sets used in the hydrogeological DFN modelling at Forsmark were assumed to be Fisher distributed.

Fracture intensity is intimately connected to the spatial arrangement of the fractures. The hydrogeological DFN modelling was based on the assumption that the spatial distribution of fracture centres of each fracture set within each fracture domain follows a Poisson process, which in turn implies a Euclidean scaling[1].

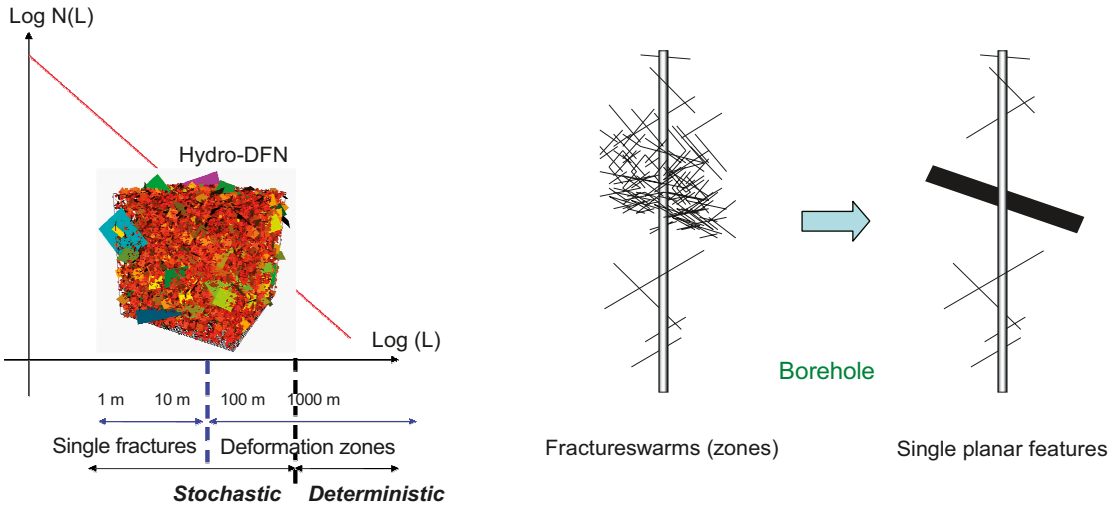

Figure 8-4. *Left: The tectonic continuum hypothesis invokes that frequency of fractures of different sizes can be approximated through the use of a single power-law density function. Features up to L = 1,000 m (r = 564 m) are regarded as uncertain and treated stochastically using the discrete fracture network (DFN) concept. The same distinction was used in the geological DFN modelling. Right: The fracture data gathered between the upper and lower bounds of a deformation zone interval are lumped together to form a single planar feature. In the same fashion, all hydraulic data in the interval are also lumped together to form a single transmissivity value.*

[1] Euclidean scaling is a particular kind of a tectonic continuum where the number of fractures is linearly proportional to the dimensionality of the observation (length, area or volume). Thus, Euclidean scaling implies that doubling the scale (size) of observation, effectively doubles the number of fractures, i.e. constant fracture intensity.

The assumption of a tectonic continuum with a Euclidean scaling was tested in the geological DFN modelling in parallel with other assumptions (cf. section 5.6.3). Of particular interest for the hydrogeological DFN modelling is the finding that the spatial correlation of the fractures observed on outcrops and in boreholes is week or absent above a few tens of metres or less, indicating that the spatial pattern of the identified fracture clusters could be reasonably well approximated by a Poisson process and an Euclidean scaling (cf. p. 126-127 in /Fox et al. 2007/). In effect, the primary geometrical concepts and statistical distributions of the so-called global fracture sets defined in the geological DFN modelling are the same as those used in the hydrogeological DFN modelling:

- Fisher distributed fracture orientations,
- Set-specific power-law intensity (size) density functions,
- Poissonian fracture locations.

A key difference between the two DFN descriptions is in the use of data; the geological DFN modelling considered primarily the geometrical properties of *surface data* (outcrop data and lineament data) representing *all fractures*, whereas the hydrogeological DFN modelling focussed solely on the geometrical properties of *borehole data* representing two different sets of fracture data: (*i*) *potentially flowing fractures* (*open and partly open fractures*), and (*ii*) *continuously flowing fractures* detected by the Posiva Flow Log method (so-called *PFL-f* fractures)[2].

The differences in use of data handled by the geologists and hydrogeologists impacted on how the DFN modelling works were carried out. However, since the frequency of *potentially flowing fractures* can be conceived as a fraction (subset) of the frequency of *all fractures*, the envisaged relationship between the associated power-law density functions has been as illustrated in Figure 8-5. Figure 8-5 implies that completely sealed fractures exist only among the small features, whereas large features, i.e. deformation zones, are all heterogeneous with regard to fracture aperture, i.e. more or less partly open. Figure 8-5 shows also the conceived behaviour of the *continuously flowing fractures,* i.e. the *connected open fractures*. The *PFL-f fractures* are imagined to be a subset of the latter category, see section 8.5.2 and Figure 8-33.

A demonstration of the relevance of the notion of subsets, illustrated in Figure 8-5, was attempted in Appendix C in /Follin et al. 2007c/ for the key fracture domain within the target area at Forsmark (FFM01). During the finalisation of the hydrogeological modelling, it was concluded that the geological DFN modelling results reported in /Fox et al. 2007/ and applied in Appendix C in /Follin et al. 2007c/ did not subdivide the lineaments and deformation zone traces by fracture domain; the only subdivision made was by orientation set (cf. section 5.6.3). Hence, the slopes of the geological DFN and the hydrogeological DFN shown in Appendix C in /Follin et al. 2007c/ are not entirely compatible. The geological DFN is appropriate for a case where the lineament and deformation zone intensity of each fracture orientation set is homogeneous, i.e. spatially invariant. However, at Forsmark, there is a clear variation between the fracture domains in the occurrence of steeply dipping lineaments and deformation zones with WNW-ESE to NW-SE strike as well as in the occurrence of gently dipping deformation zones (section 5.6.3). For instance, the intensity of steeply-dipping structures with WNW-ESE to NW-SE strike is much higher in the bedrock outside relative to that inside the tectonic lens, which hosts the candidate and target areas see Figure 1-4 and Figure 1-5.

The consequence of not dividing the lineaments and deformation zone traces by fracture domain is that the slopes of the power-law density functions of the different fracture sets is biased towards an average value (i.e. the average over the entire Forsmark local model domain). By plotting the total intensities rather than the fracture set specific intensities of each fracture type, as was attempted in Appendix C in /Follin et al. 2007c/, the impact of spatial variability in the intensity between different fracture sets and fracture domains may be somewhat reduced. This is illustrated in section 8.5.2.

---

[2] In the context of the SDM, '*all fractures*' means that no distinction was made between fractures with regard to fracture aperture. Hence, *sealed* fractures were pooled with *partly open* and *open* fractures in the geological DFN modelling. In contrast, the hydrogeological DFN modelling focussed, to begin with, on the properties of the '*potentially flowing fractures*', which implies that the analysed fractures must be at least partly open. In order for a partly open or open fracture to be detected as a flowing fracture it must be (*i*) connected to a positive hydraulic boundary (either directly or indirectly via a network of other flowing fractures) and (*ii*) have a sufficient transmissivity with regard to the measurement threshold of the test equipment used, cf. section 8.3.2.

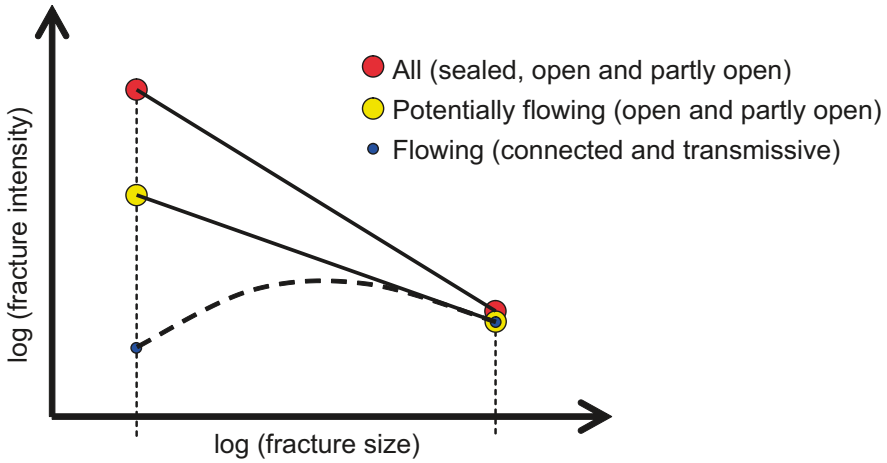

Figure 8-5. *Cartoon showing the envisaged relationship between the density functions of all, potentially flowing and flowing fractures as a function of fracture size. The flowing fractures detected with the PFL-f method is envisaged to be a subset of the flowing fractures in the hydrogeological DFN modelling work.*

8.3.2 Basic characteristics of the single-hole tests

The hydraulic parameterisation of the deformations zones and fracture domains to become HCD and HRD models is based on single-hole tests in boreholes. Difference flow logging pumping tests (PFL-f) and double-packer injection tests (PSS) were used in the deep, core-drilled boreholes, whereas flow-logging pumping tests in open holes (HTHB) were used in the shallower, percussion-drilled boreholes. The lower measurement limits of the PFL-f and PSS test methods are superior to that of the HTHB test method, but they cannot be readily used in the percussion-drilled boreholes for technical reasons. Further, the PFL-f and PSS test methods have different advantages and disadvantages. For this reason, they were run in parallel, in order to quantify the consequences for the site characterisation, the hydrogeological discrete fracture network modelling and the groundwater flow modelling.

The constituent parameters measured during the hydraulic tests are the flow rate, Q, and the pressure, p. Since these are correlated, the parameter studied is the specific capacity, $Q/\Delta p$, which has the same dimension as transmissivity, T. The envisaged test conditions in fractured rock are shown in Figure 8-6. The specific capacity is dependent on several important aspects, among which the following are particularly noted.

- Q_{limit}; the lower measurement limit of the test method.
- T_{bh}; the transmissivity of the tested fracture intersecting the borehole. T_{bh} can be affected during the drilling operations. For instance, the fracture can be clogged (positive skin) or stimulated (negative skin).
- C; the connectivity of the tested fracture to other fractures away from the borehole. Some fractures are isolated, or are a part of an isolated cluster of fractures. Others are well connected and a part of the overall hydrological system.
- T/S; the hydraulic diffusivity of the fracture system within the radius of influence.
- t; the duration of the hydraulic testing, i.e. the test time.
- ΔL; the length of the test interval (test section).

The parameterisation of the deformation zones is fairly straightforward. All transmissivity data between the upper and lower bounds of a deformation zone interval, as determined in the single-hole geological interpretation are considered. That is, the transmissivity data from consecutive tests are integrated to form a single transmissivity value for that interval. This approach implies that the hydraulic thickness is assumed to be equal to the geological. The in-plane hydraulic heterogeneity of a deformation zone is studied by means of single-hole tests at different locations.

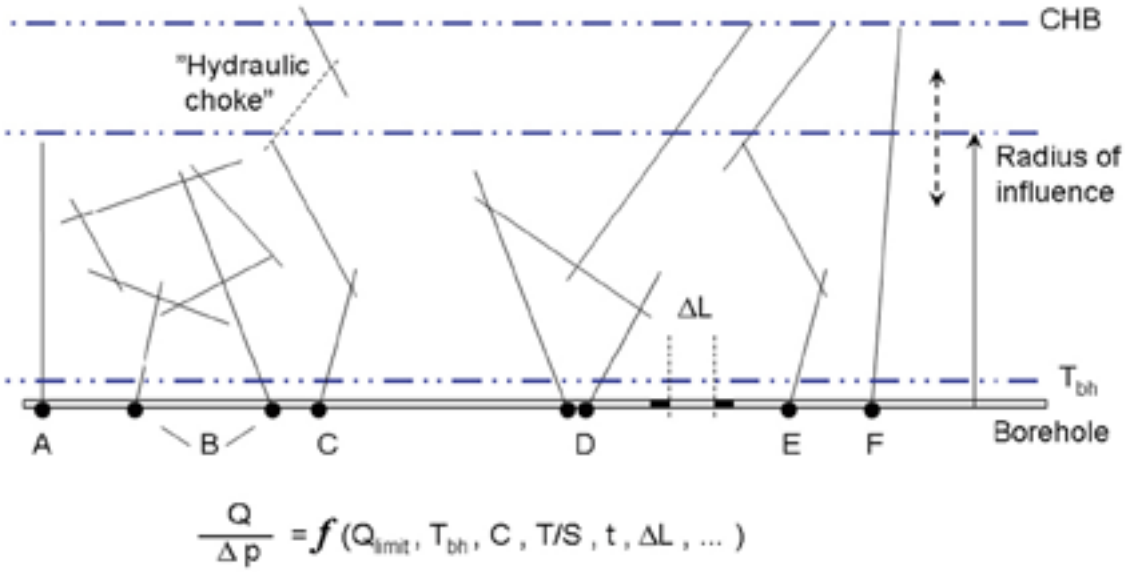

Figure 8-6. *Cartoon showing a borehole with six different symbolic fracture network situations, cases A-F. The specific capacity, $Q/\Delta p$, measured along the borehole is dependent on several factors, e.g. the measurement limit, Q_{limit}, of the test method, the transmissivity of the fracture intersecting the borehole, T_{bh}, the fracture connectivity, C, the hydraulic diffusivity, T/S, of the fracture network, the test time, t, the length of the test section, ΔL, etc. The hydraulic characterisation of the fracture system varies depending on the method used as well as on the in situ conditions, e.g. the occurrence of "hydraulic chokes". Cases A-C represent isolated fracture networks and cases D-F represent fracture networks connected to the overall hydrogeological system. The overall hydrogeological system latter is here indicated by a constant head boundary (CHB) suggesting a pseudo steady-state flow regime at long test times. The cartoon is rotated 90° to improve the readability.*

The hydraulic description of the fracture domains between the deformation zones is focused on the conductive fracture frequency (CFF) of continuously flowing fractures. This means that the connected fracture network situations such as cases D-F in Figure 8-6 were regarded as more important for the hydrogeological DFN modelling and the groundwater flow modelling in the site description than disconnected (compartmentalised) network situations such as cases A-C.

8.3.3 Evaluation of single-hole hydraulic tests

/Follin et al. 2007b/ provided a description of the disciplinary interpretations of the single-hole hydraulic tests conducted in the core-drilled boreholes (PFL-f and PSS) and the percussion-drilled boreholes (HTHB) along with an extensive interdisciplinary comparison between the interpretation of geological and hydraulic data.

The PFL-f method uses a short test interval and a long test time, whereas the PSS method uses opposite test conditions, i.e. a long test interval and a short test time. Thus, the resolution of the PFL-f method is sufficient to study the transmissivity of individual fractures and the method can be used to evaluate the CFF of continuously flowing networks, e.g. situations like cases D-F in Figure 8-6. However, the PFL-f method cannot identify situations with isolated fractures/clusters or "hydraulic chokes" such as in cases A-C. The PSS method, on the other hand, has great problems in distinguishing network situations like cases A-C from network situations like cases D-F, which means that using data from the PSS method alone for the hydrogeological DFN modelling could easily result in an overprediction of fracture connectivity in the sparsely fractured bedrock in between the deformation zones. Due to this difference, the hydrogeological DFN modelling carried out was based on the information acquired by the PFL-f method. How this modelling was carried out is thoroughly explained in /Follin et al. 2007b/.

Figure 8-7 shows an example of the structural interpretation of a PFL-f transmissivity using the geometrical information visible in a so-called BIPS image. The PFL-f transmissivity where the open fracture intersects is $1.83 \cdot 10^{-7}$ m^2/s and the inferred strike, dip and aperture of the fracture are 101°, 12° and 3 mm, respectively. The uncertainties involved in the structural interpretations of PFL-f transmissivity data are explained in /Follin et al. 2007b/ and addressed in section 8.9.3. Figure 8-8 and Figure 8-9 show four examples of PFL-f transmissivity data and interpreted orientations from the core-drilled boreholes KFM01A–04A at drill sites 1–4.

Table 8-2 shows a summary of the PFL-f data available for hydraulic parameterisation of deformation zones and fracture domains in stage 2.2.

Figure 8-10 shows an example of PSS hydraulic conductivity data from the core-drilled boreholes KFM03A and KFM03B at drill site 3, used for comparisons and consistency checks. The PSS tests are carried out with three different packer spacings, 5 m, 20 m and 100 m. The spatial resolution of the PFL-f method is 0.1 m.

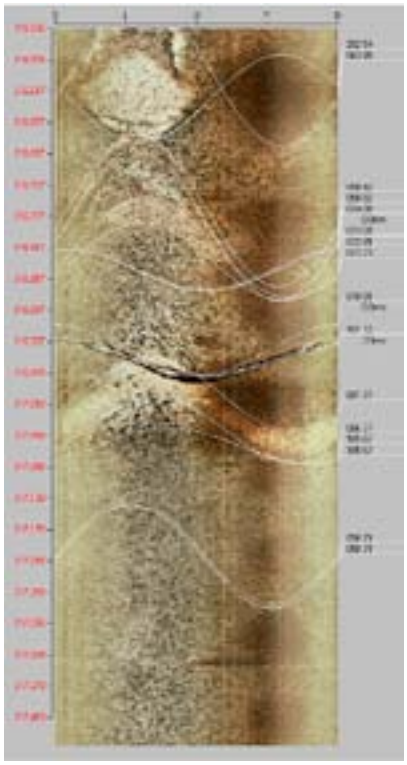

Figure 8-7. *Structural interpretation of PFL-f transmissivity no. 27 observed in borehole KFM01D at about 317 m borehole length. The transmissivity of the open fracture is $1.83 \cdot 10^{-7}$ m^2/s and the inferred strike, dip and aperture are 101°, 12° and 3 mm, respectively.*

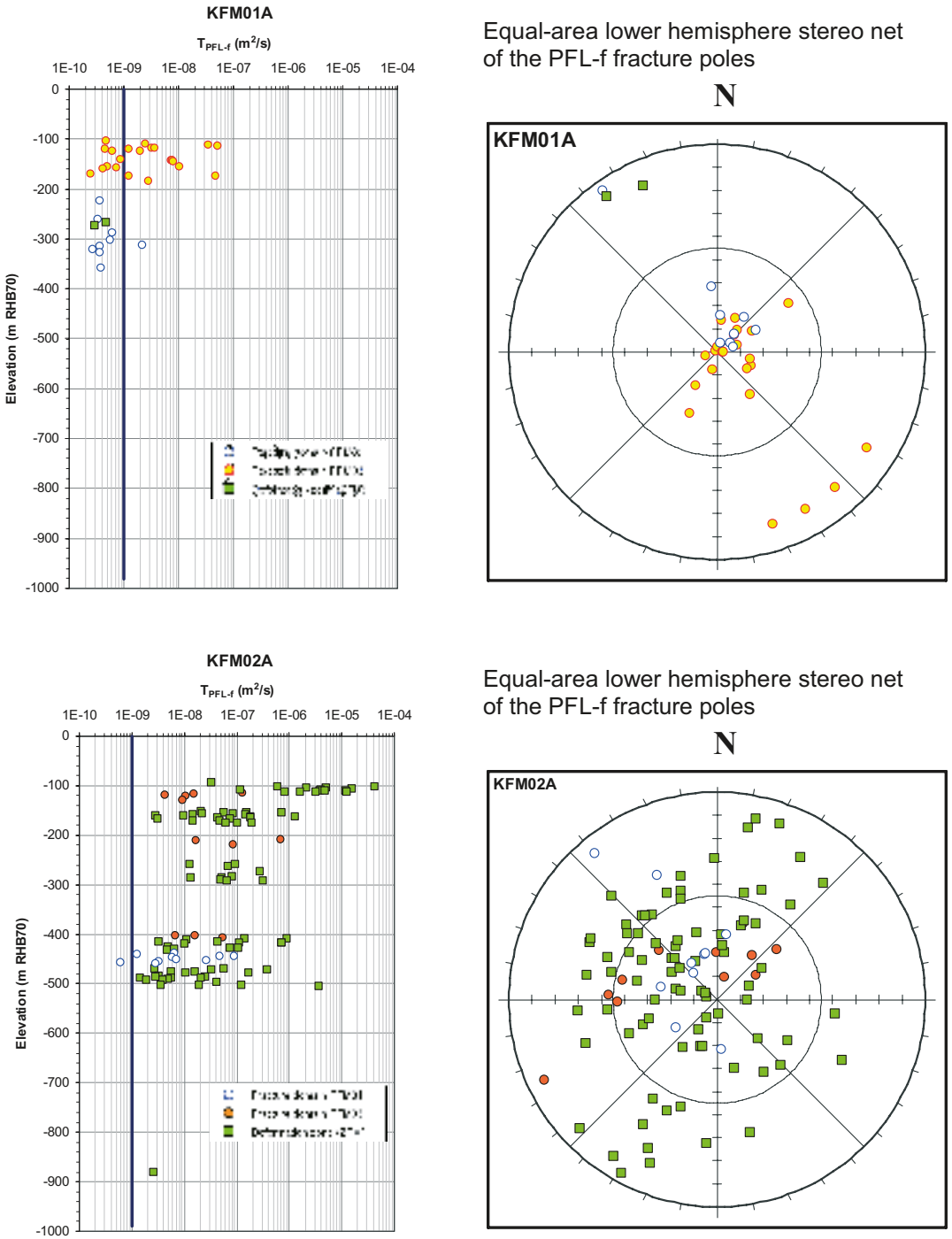

Figure 8-8. *Hydrogeological data in boreholes KFM01A and -02A. There are 32 PFL-f transmissivities associated with single fractures and two associated with one deterministically modelled deformation zone in KFM01A. The corresponding figures for KFM02A are 22 and 82/6, respectively. The blue lines indicate the typical threshold value reported from the investigations in the Forsmark area, $1{\cdot}10^{-9}$ m²/s. The lengths of the blue lines correspond to the depths investigated with the PFL-f method.*

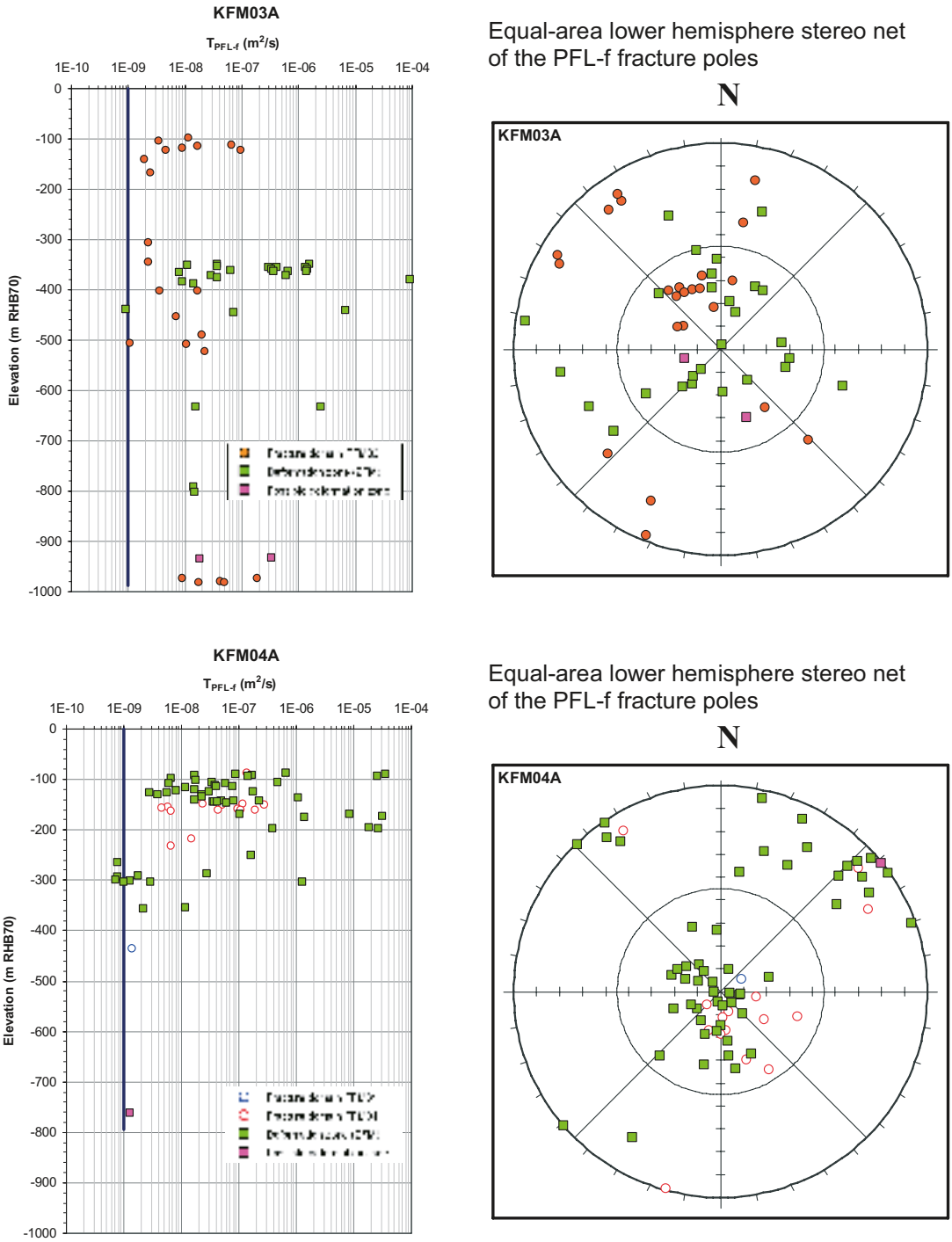

Figure 8-9. *Hydrogeological data in boreholes KFM03A and -04A. There are 23 PFL-f transmissivities associated with single fractures, 27 associated with four deterministically modelled deformation zones, and two associated with one possible deformation zone in KFM03A. The corresponding figures for KFM04A are 16, 54/2, and 1/1, respectively. The blue lines indicate the typical threshold value reported from the investigations in the Forsmark area, $1{\cdot}10^{-9}$ m²/s. The lengths of the blue lines correspond to the depths investigated with the PFL-f method.*

Table 8-2. Summary of sample lengths and numbers of fractures according to different categories in each of the boreholes measured with the PFL-f method at the time of stage 2.2. Fractures that are judged to be open are assigned a confidence: certain, probable or possible. The number of PFL-f transmissivities in each borehole is also given.

BH	Top [m]	Bottom [m]	Length [m]	Total number	Number of open (+partly)	Open & certain	Open & prob.	Open & poss.	Number of PFL-f transm.
KFM01A	102.67	993.49	890.82	1,517	752	174	143	435	34
KFM01D	91.67	799.62	707.95	1,636	468	99	178	191	34
KFM02A	101.54	1,000.36	898.82	2,199	443	152	267	24	104
KFM03A	102.45	999.67	897.22	1,825	375	146	137	92	52
KFM04A	109.1	985.07	875.97	4,327	1,357	257	630	470	71
KFM05A	102.27	999.62	897.35	2,838	633	91	180	362	27
KFM06A	102.21	997.37	895.16	3,680	816	172	235	409	99
KFM07A	102.04	993.77	891.73	3,183	617	103	162	352	26
KFM07C	98.62	498.67	400.05	1,765	285	78	116	91	14
KFM08A	103.36	949.67	846.31	4,268	713	149	210	354	41
KFM08C	102.29	948.99	846.70	4,198	676	56	199	421	21
KFM10A	62.86	499.98	437.12	2,755	999	264	299	436	54
All BH			9,485.20	34,191	8,134	1,741	2,756	3,637	577

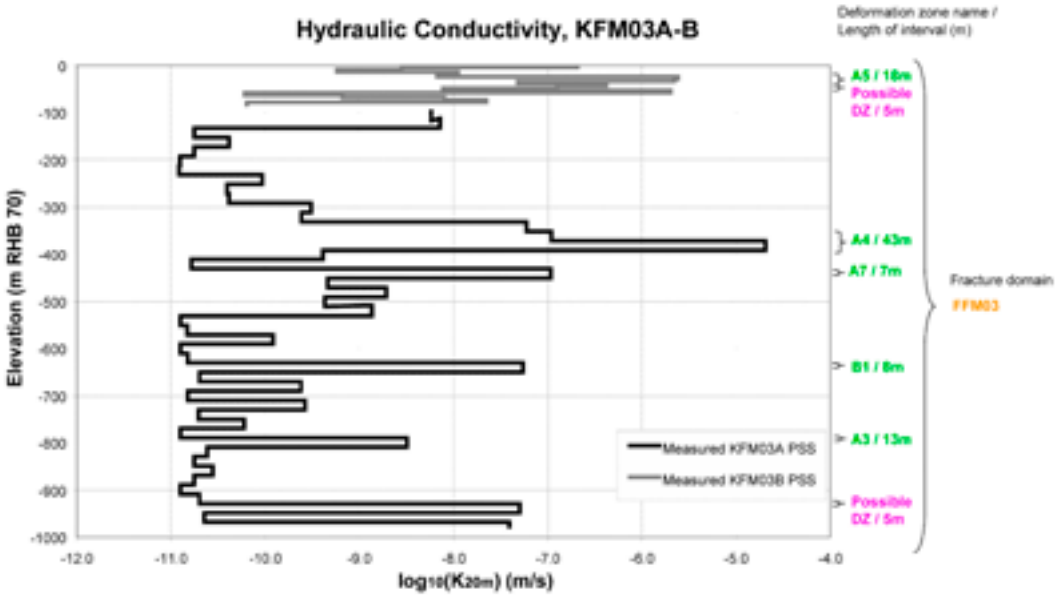

Figure 8-10. *Hydraulic conductivity data in KFM03A and KFM03B evaluated from PSS transmissivity measurements using a 20 m long test section. The typical transmissivity threshold of the PSS method is about $7 \cdot 10^{-10}$ m^2/s, which corresponds to a threshold of about $3 \cdot 10^{-11}$ m/s in terms of a 3D hydraulic conductivity on a 20 m support scale.*

8.3.4 Evaluation of hydraulic interference tests

The premises for disciplinary evaluation of hydraulic interference (cross-hole) tests in fractured crystalline rock are highly dependent on the structural geology, the hydraulic properties of the fracture system and the configuration of the data acquisition system. The structural-hydraulic conditions in the Forsmark area are exceptional in this regard.

A summary of the test configuration used and the analyses undertaken for the most important large-scale interference test conducted within the target area during the CSI phase, the year 2006 interference test in borehole HFM14 at drill site 5, is provided in /Follin et al. 2007c/. The interference test was performed by pumping with a flow rate of about 350 L/min. The groundwater levels were monitored at 105 observation sections in 36 observation boreholes. Twelve of the 36 boreholes were core-drilled with a total of 55 monitoring sections. 24 boreholes were percussion-drilled with a total of 50 monitoring sections. For each observation section, the estimated drawdown was supplied as a time-series over the 21 days of pumping. The hydraulic analyses comprised hydraulic diffusivity estimations, boundary condition interpretations, comparisons with a simplified 2D analytical solution and detailed 3D numerical flow simulations. Figure 8-11 shows a simplified 2D view of the monitoring network used during the year 2006 interference test in HFM14 together with response times corresponding to a drawdown of 0.01 m. Figure 8-12 shows the final drawdowns after 21 days of pumping.

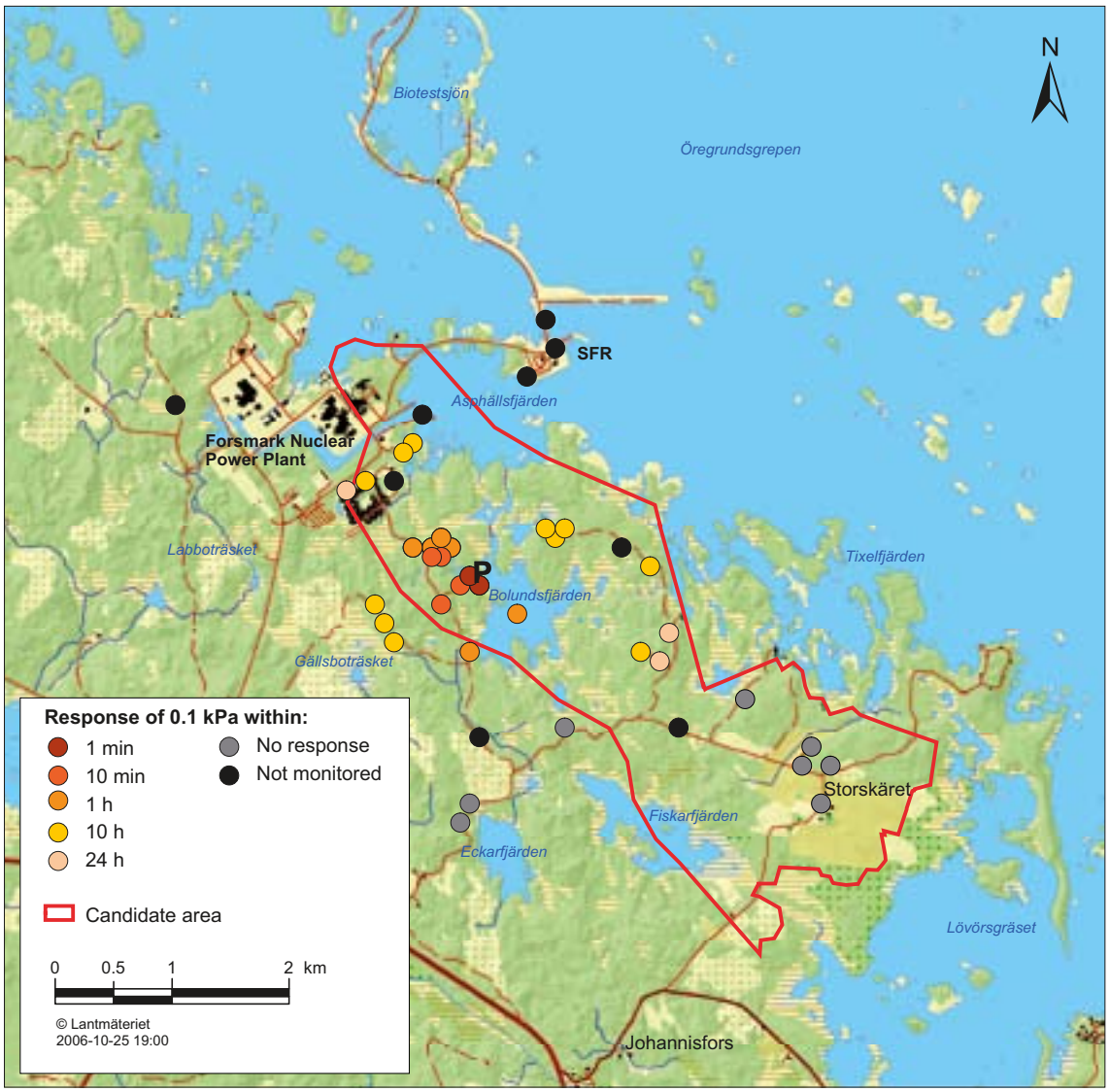

Figure 8-11. *Map showing response times in the bedrock to the three-weeks long interference test conducted in HFM14 (P) at drill site 5 during the dry summer of 2006. Clear test responses were observed in 71 out of a total of 110 monitoring sections. The maximum radius of influence was about 1.8 km.*

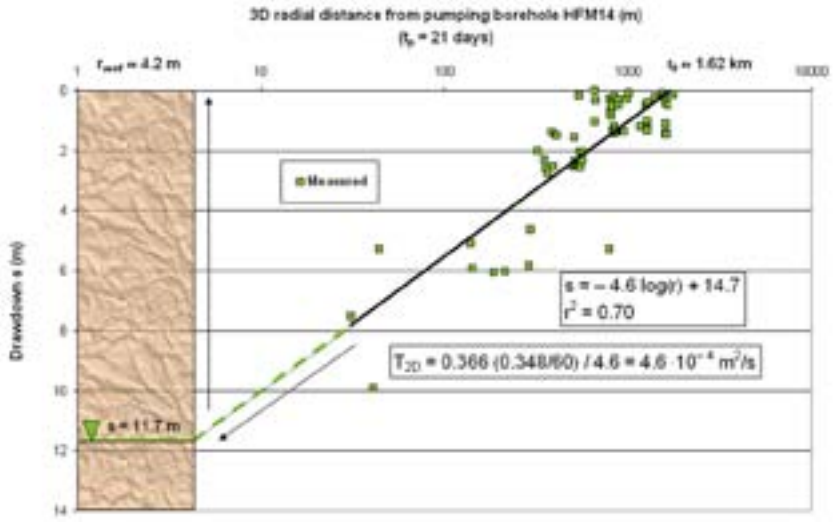

Figure 8-12. *Plot of measured drawdowns vs. log(3D radial distance) at the end of the 21-day long interference test in HFM14. The drawdown in HFM14 was 11.7 m and the flow rate was 348 L/min implying a specific capacity of approximately $5 \cdot 10^{-4}$ m²/s. The black line shows a least-squares fit to the measurements. The value of the correlation coefficient ($r^2 = 0.70$) indicates a heterogeneous system. A steady-state, radial flow approximation using the slope of the least-squares fit for an estimate of Δs (difference in drawdown per log cycle of distance) renders a large-scale effective transmissivity of $5 \cdot 10^{-4}$ m²/s. An extrapolation of the regression model to 11.7 suggests an effective radius of HFM14 of about 4 m, which corresponds to a negative skin of about –4.1.*

8.4 Conceptual modelling

8.4.1 Deformation zones and associated hydraulic data

The deformation zone model developed during the ISI stage was elaborated and consolidated during the CSI stage, a work that was essentially concluded in stage 2.2, cf. chapter 5. The deformation zone model is shown in Figure 8-13. The division into sets (WNW, NW, …) follows the naming used in section 5.5. Here, G represents the gently dipping deformation zones.

In the preliminary SDM /SKB 2005a/, 44 deformation zone intercepts representing 28 different deformation zones were investigated hydraulically. In SDM-Site, these numbers are 116 and 57, respectively, which imply a more or less doubled information density. The transmissivity data acquired from the single-hole tests constitute the basis for the assignment of hydraulic properties to the deformation zones in the SDM; see Figure 8-8 through Figure 8-10 for examples.

The assignment of hydraulic properties to the different deformation zones modelled in the preliminary SDM was based on depth trend regression analyses of single-hole transmissivity data acquired at a reasonable number of deformation zone intercepts. The difference in the inferred transmissivity trends between steeply dipping and gently dipping deformation zones was found to be considerable at repository depth (c. two orders of magnitude) /SKB 2005a/. However, the palaeohydrogeological simulations carried out showed that the matching against hydrochemical data was sensitive to how the deformation zone transmissivity depth trend was implemented. That is, poor matches were obtained unless the regression model honoured the measured data at the measurement points (conditional simulation).

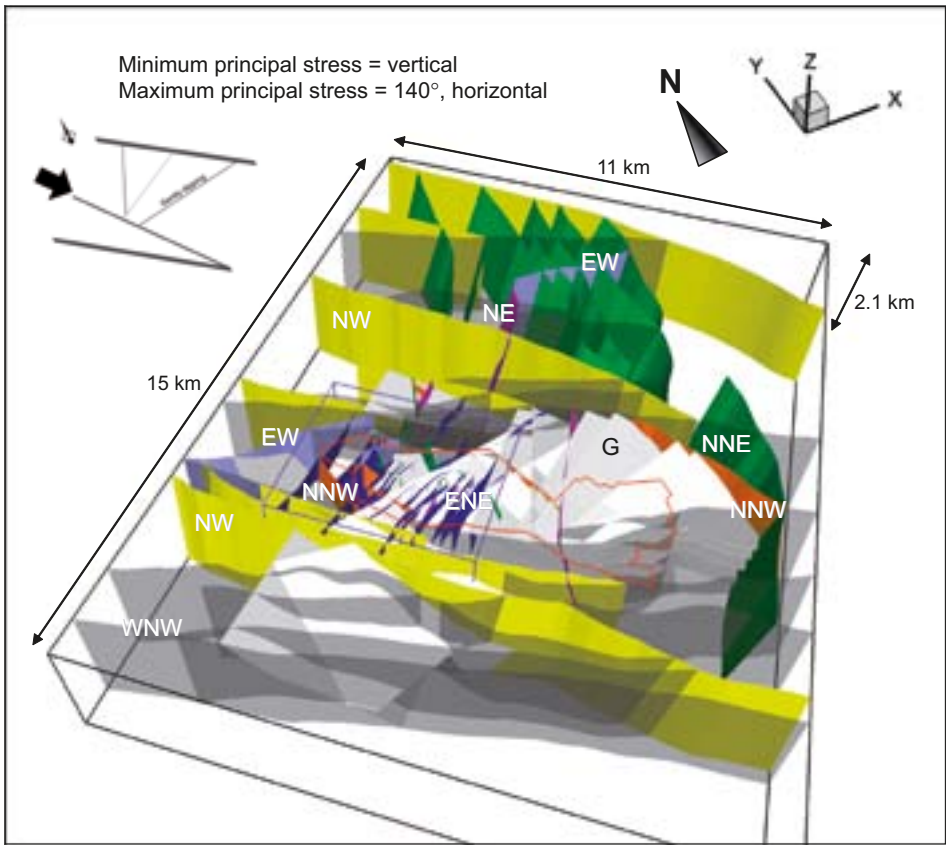

Figure 8-13. *3D visualisation of the regional model domain and the 131 deformation zones modelled deterministically for Forsmark in stage 2.2 (see chapter 5). The steeply dipping deformation zones (107) are shaded in different colours and labelled with regard to their principal direction of strike, see section 5.5. The gently dipping zones (24) are shaded in pale grey and denoted by a G. The border of the candidate area is shown in red and regional and local model domains in black and purple, respectively. The inset in the upper left corner of the figure shows the direction of the main principal stress, see section 5.5.*

Figure 8-14 shows a plot of the transmissivity data used for flow and solute transport modelling in the SDM. The transmissivity data are plotted versus depth and are marked up by different colours in relation to the division of the deformation zones into sets, see section 5.5. Figure 8-14 shows that the gently dipping deformation zones (G), which predominantly occur in the hanging wall bedrock, are the most transmissive at all depths. The steeply dipping, local major, deformation zones that strike WNW and NW and border the candidate area form structures with a second order of importance as far as transmissivity is concerned. The steeply dipping deformation zones that strike ENE and NNE occur mainly in the footwall bedrock. These are significantly heterogeneous from a hydraulic point of view. In summary, these observations suggest a pronounced hydraulic anisotropy on a regional scale, where the largest transmissivities observed are associated with deformation zones with a high angle to the minimum principal stress, cf. section 5.5.

Furthermore, Figure 8-14 suggests that the transmissivities are affected by a substantial depth trend (vertical heterogeneity). The depth trend in transmissivity spans four to six orders of magnitude, from 10^{-4}–10^{-3} m^2/s near the surface to 10^{-9}–10^{-8} m^2/s at c. 1,000 m depth. Figure 8-14 also shows that the lateral heterogeneity in transmissivity is also considerable; take the ENE data set at c. 200 m depth for an example. A closer analysis of the data reveals that the transmissivities vary laterally by several orders of magnitude between zones of similar orientation, as well as between different parts

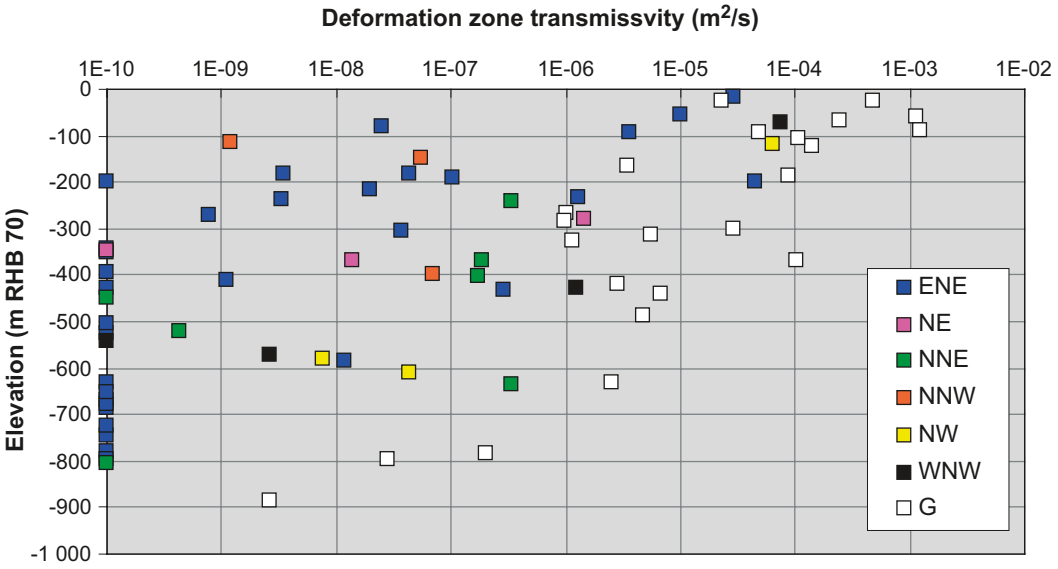

Figure 8-14. *Transmissivity data versus depth for the deterministically modelled deformation zones in stage 2.2. The transmissivities are coloured with regard to the orientations of the deformation zones, where G means gently dipping. The deformation zones with little or no flow are assigned an arbitrary low transmissivity value of $1 \cdot 10^{-10}$ m²/s in order to make them visible on the log scale.*

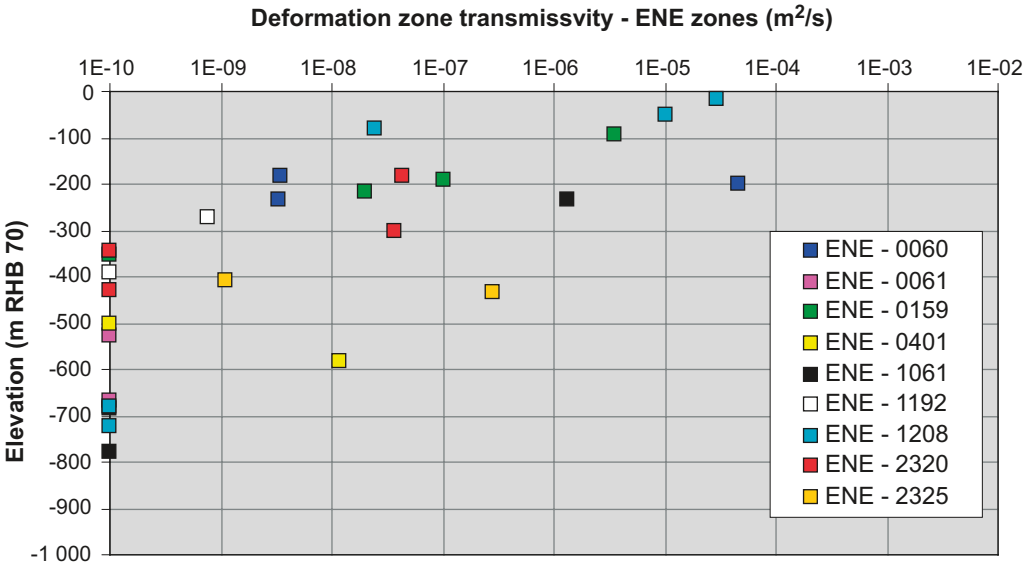

Figure 8-15. *Transmissivity data versus depth for the ENE category of the steeply dipping deformation zones in stage 2.2. Tests with little or no flow are assigned an arbitrary low transmissivity value of $1 \cdot 10^{-10}$ m²/s in order to make them visible on the log scale.*

of a specific zone (Figure 8-15). The conclusion drawn from these findings is that the previously described anisotropy in the structural geology (see chapter 5) is not only accompanied by a significant hydraulic anisotropy, but also a substantial vertical and lateral hydraulic heterogeneity. This observation suggests a strongly channelised flow field within the planes of the deformation zones (see section 10.5.3 where flow channelling is discussed further).

The transmissivity data acquired during the verification stage (cf. Table 8-1) provide transmissivity data from the regional Singö and Forsmark deformation zones outside the candidate area, and from the local major deformation zones modelled to intersect borehole KFM08D within the target volume, see section 5.8. The variability of the verification data agree with the variability of data used in the SDM, see Figure 8-16.

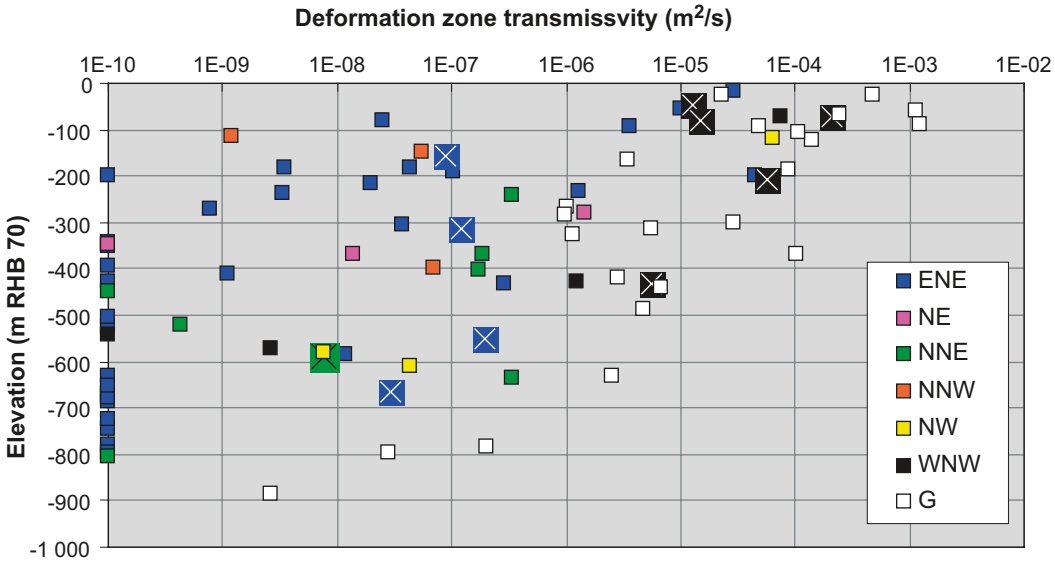

Figure 8-16. *The transmissivity data acquired from the hydraulic testing carried out in stage 2.3 in boreholes KFM08D, KFM11A, KFM12A, HFM34, HFM36 and HFM37 are here added to the transmissivity plot shown in Figure 8-14 and indicated with* ☒.

8.4.2 Fracture domains and associated hydraulic data

Transmissivity data from four of the five cored boreholes available for modelling in the preliminary SDM are displayed in Figure 8-8 and Figure 8-9. Besides discrete differences in fracture transmissivity, the figures also reveal significant differences in conductive fracture frequencies. KFM01A and the lower halves of KFM02A and KFM04A show data in the footwall bedrock. KFM03A and the upper half of KFM02A show data gathered in the hanging wall bedrock with its contiguous gently dipping zones. The upper half of KFM04A shows data gathered in the bedrock bordering the tectonic lens within the candidate area (see chapter 5). The intensely fractured interval between c. 400 and 500 m depth in KFM02A corresponds to the gently dipping deformation zones referred to as A2 and F1 in stage 2.2. In the preliminary SDM, this interval was modelled as a single zone (A2).

Based on the structural-hydraulic information available for modelling in the preliminary SDM, /Follin et al. 2005/ suggested that the bedrock in between the deformation zones within the candidate area should be divided into hydrogeological sub volumes depending on the fracture intensity of flowing fractures, see Figure 8-17. Moreover, it was noted that the flowing fractures acquired in the footwall bedrock are predominantly gently dipping and that steeply dipping fractures with a NS-NE strike are the second most dominant orientation from a hydraulic viewpoint. The transmissivity data acquired from boreholes KFM06A and KFM07A (stage 2.1) confirmed the hydrogeological notion of hydrogeological sub volumes, see Figure 8-18, and it was decided that an interdisciplinary assessment of the bedrock properties in between deformation zones should be attempted starting with a geological definition, i.e. without use of hydrogeological or other data sets. The so-called fracture domain concept suggested in /SKB 2006a/ was elaborated and finalised in stage 2.2 /Olofsson et al. 2007/. The model contains six fracture domains referred to as FFM01–06, see Figure 5-34 in section 5.6.

The hydrogeological data acquired in four of the twelve cored boreholes drilled during stage 2.2, namely KFM07C, KFM08A, KFM08D and KFM10A, are shown in Figure 8-19 and Figure 8-20. Again, the transmissivity data acquired support the notion of hydrogeological sub volumes suggested in the preliminary SDM.

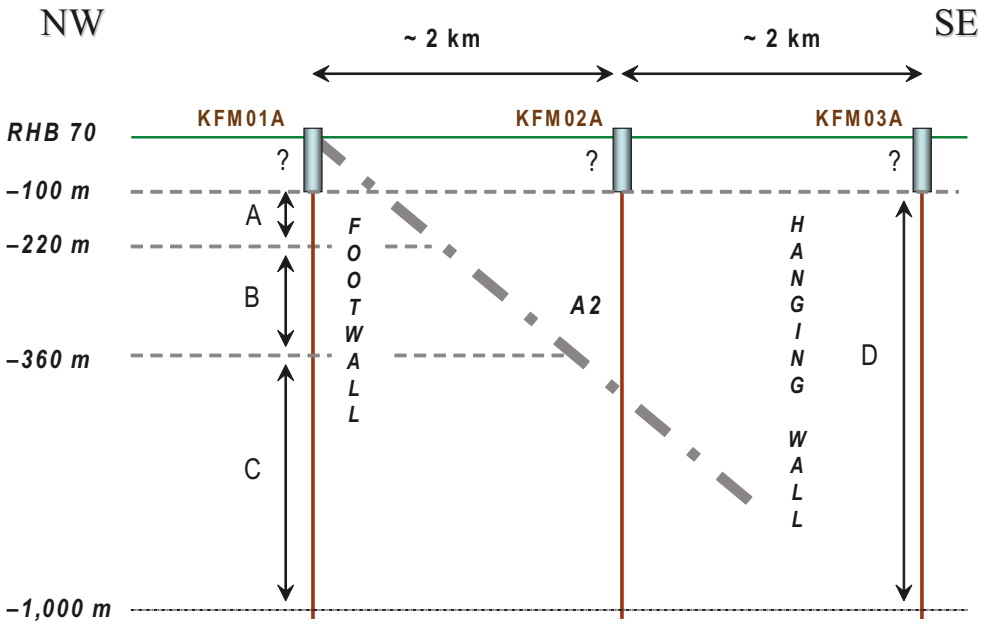

Figure 8-17. *Suggested division of the bedrock in between the deformation zones within the candidate area into four hydrogeological sub volumes A-D based on the structural-hydraulic information gathered in boreholes KFM01A–05A.*

There is a clear transition in PFL-f data at about 400 m depth visible in Figure 8-8, Figure 8-9, Figure 8-18, Figure 8-19 and Figure 8-20. Table 8-3 and Table 8-4 summarise the change in Terzaghi corrected linear fracture intensities, P_{10corr}, of "open fractures" vis-à-vis "flowing fractures" in fracture domain FFM01 in relation to 400 m depth, respectively. For the top 400 m of FFM01, the HZ and NE sets dominate the open fractures, followed by the NW and NS sets, and finally the EW set. However, for the flowing fractures, there are only three sets: HZ, NE and NS with HZ very dominant. Below 400 m depth in FFM01, the few flowing fractures observed occur in the HZ and NE sets with an average "true" spacing of about 200 m. In conclusion, below 400 m depth, the flowing fractures in FFM01 are almost exclusively restricted to deformation zones, symptomatic of a very sparse and poorly connected network of fractures that does not reach a threshold for percolation of water into the deep rock. Table 8-5 summarises the statistics of "open fractures" and "flowing fractures" deduced in stage 2.2 for FFM01–FFM03. The decreasing frequency of flowing fractures with depth is based on the measurements carried out with the PFL-f method.

In summary, FFM02 and the uppermost interval (–100 to –200 m) in FFM01 (Table 8-5) coincide more or less with sub volume A in Figure 8-17, the interval (–200 to –400 m) in FFM01 coincides approximately with sub volume B, the interval (–400 to –1,200 m) in FFM01 coincides essentially with sub volume C, and the two intervals (–100 to –400 m) and (–400 to –1,200 m) in FFM03 coincides more or less with sub volume D. Hence, the hydrogeological division into sub volumes based on flowing fractures is found to be highly consistent with the definition of fracture domains based independently on geological data.

The hydraulic parameterisation of the hydrogeological DFN model was primarily developed for FFM01–03, which had abundant hydrogeological information. This leaves the question of how to parameterise a hydrogeological DFN model of FFM04–06, since they have very limited data. FFM04 and FFM05 lie in the periphery of the candidate area and the statistical significance of the data gathered in these fracture domains is very limited, being based on about 120–150 m of borehole data. However, based on the statistics available, it was proposed that fracture domains FFM04 and FFM05 are assumed to have the same properties as inferred for FFM03. Outside fracture domains FFM04 and FFM05 there are no cored boreholes drilled in between deformation zones. Therefore, a simplified property assignment must be used to specify homogeneous continuous porous medium (CPM) properties, e.g. based on specific capacity data from domestic water supply wells.

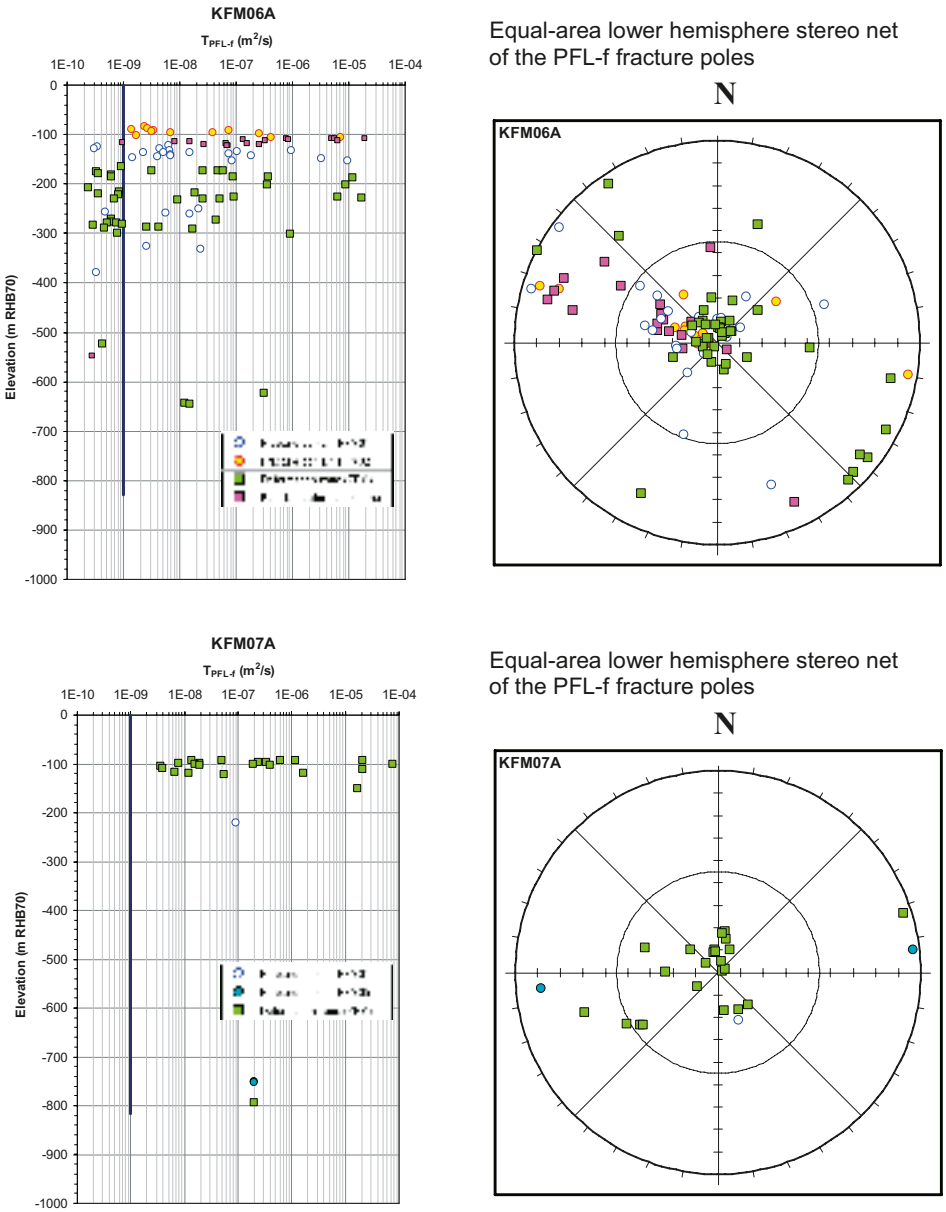

Figure 8-18. *Hydrogeological data in boreholes KFM06A and KFM07A. There are 38 PFL-f transmissivities associated with single fractures, 43 associated with three deterministically modelled deformation zones, and 18 associated with two possible deformation zones in KFM06A. The corresponding figures for KFM07A are 3, 23/2, and 0/0, respectively. The blue lines indicate the typical threshold value reported from the investigations in the Forsmark area, $1 \cdot 10^{-9}$ m^2/s. The lengths of the blue lines correspond to the depths investigated with the PFL-f method.*

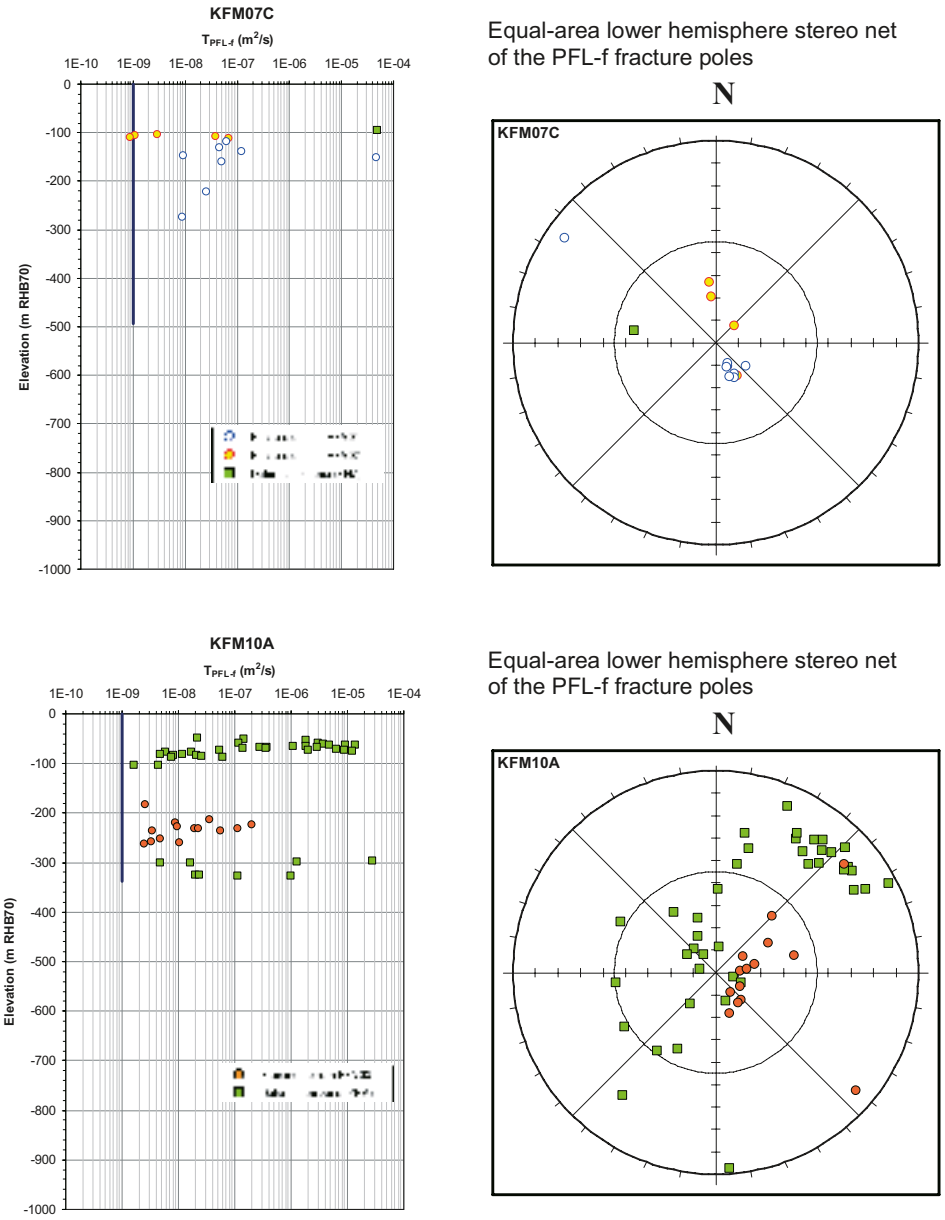

Figure 8-19. *Hydrogeological data in boreholes KFM07C and KFM10A. There are 13 PFL-f transmissivities associated with single fractures and one associated with one deterministically modelled deformation zone in KFM07C. The corresponding figures for KFM010A are 14 and 40/2, respectively. The blue lines indicate the typical threshold value reported from the investigations in the Forsmark area, $1 \cdot 10^{-9}$ m²/s. The lengths of the blue lines correspond to the depths investigated with the PFL-f method.*

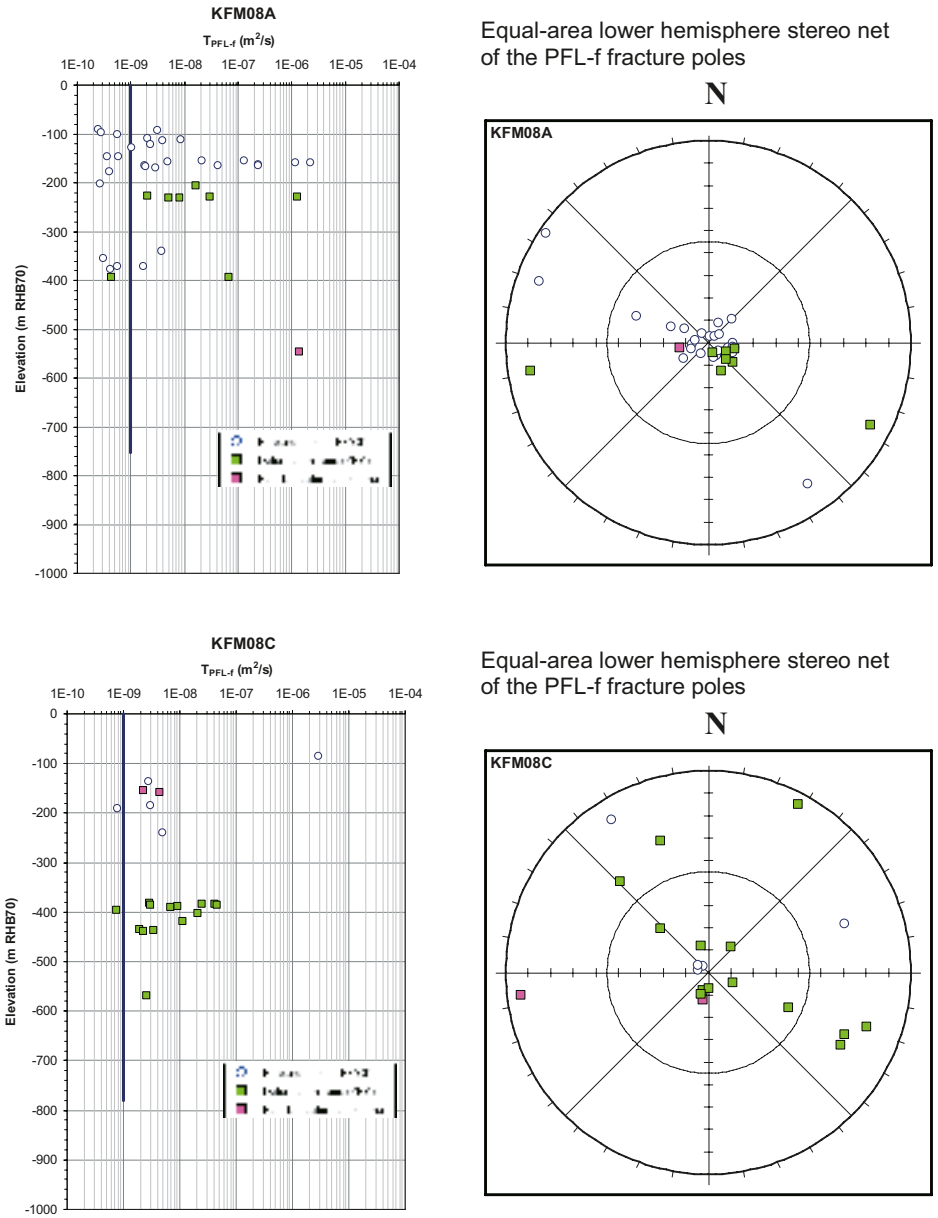

Figure 8-20. *Hydrogeological data in boreholes KFM08A and KFM08C. There are 32 PFL-f transmissivities associated with single fractures, eight associated with two deterministically modelled deformation zones, and one associated with one possible deformation zone in KFM08A. The corresponding figures for KFM08C are 5, 14/2, and 1/1, respectively. The blue lines indicate the typical threshold value reported from the investigations in the Forsmark area, $1 \cdot 10^{-9}$ m^2/s. The lengths of the blue lines correspond to the depths investigated with the PFL-f method.*

Table 8-3. Summary of Terzaghi corrected linear fracture intensities by set of open fractures and PFL-f fractures within fracture domain FFM01 above 400 m depth and excluding deformation zones.

BH	$P_{10,o,corr}$ [1/m]					$P_{10,PFL,corr}$ [1/m]				
	NS	NE	NW	EW	HZ	NS	NE	NW	EW	HZ
KFM01A	0.195	0.790	0.119	0.066	0.824	0.000	0.033	0.000	0.000	0.053
KFM01D	0.116	0.004	0.185	0.010	0.404	0.000	0.000	0.000	0.000	0.040
KFM02A	–	–	–	–	–	–	–	–	–	–
KFM03A	–	–	–	–	–	–	–	–	–	–
KFM04A	–	–	–	–	–	–	–	–	–	–
KFM05A	0.097	0.177	0.154	0.055	0.120	0.000	0.000	0.000	0.000	0.006
KFM06A	0.071	0.291	0.085	0.053	0.508	0.025	0.042	0.000	0.000	0.123
KFM07A	0.107	0.409	0.051	0.086	0.148	0.000	0.000	0.000	0.000	0.005
KFM07C	0.020	0.443	0.067	0.037	0.238	0.000	0.035	0.000	0.000	0.035
KFM08A	0.208	0.473	0.188	0.166	0.466	0.014	0.021	0.000	0.000	0.107
KFM08C	0.135	0.281	0.106	0.151	0.277	0.006	0.000	0.000	0.000	0.017
KFM10A	0.707	0.580	0.526	0.600	2.841	0.000	0.000	0.000	0.000	0.000
All BH	**0.125**	**0.339**	**0.126**	**0.083**	**0.374**	**0.006**	**0.015**	**0.000**	**0.000**	**0.049**

Table 8-4. Summary of Terzaghi corrected linear fracture intensities by set of open fractures and PFL-f fractures within fracture domain FFM01 below 400 m depth and excluding deformation zones.

BH	$P_{10,o,corr}$ [1/m]					$P_{10,PFL,corr}$ [1/m]				
	NS	NE	NW	EW	HZ	NS	NE	NW	EW	HZ
KFM01A	0.089	0.072	0.026	0.000	0.150	0.000	0.000	0.000	0.000	0.000
KFM01D	0.087	0.034	0.178	0.026	0.080	0.000	0.000	0.000	0.000	0.006
KFM02A	0.099	0.094	0.104	0.005	0.040	0.000	0.016	0.000	0.000	0.021
KFM03A	–	–	–	–	–	–	–	–	–	–
KFM04A	0.109	0.094	0.198	0.022	0.273	0.000	0.000	0.000	0.000	0.002
KFM05A	0.127	0.270	0.127	0.013	0.174	0.000	0.000	0.000	0.000	0.000
KFM06A	0.110	0.426	0.062	0.112	0.134	0.000	0.000	0.000	0.000	0.000
KFM07A	0.030	0.133	0.057	0.016	0.024	0.000	0.000	0.000	0.000	0.000
KFM07C	0.168	0.953	0.000	0.128	0.222	0.000	0.000	0.000	0.000	0.000
KFM08A	0.077	0.078	0.108	0.055	0.142	0.000	0.000	0.000	0.000	0.000
KFM08C	0.088	0.180	0.056	0.138	0.163	0.000	0.000	0.000	0.000	0.000
KFM10A	–	–	–	–	–	–	–	–	–	–
All BH	**0.094**	**0.163**	**0.098**	**0.039**	**0.141**	**0.000**	**0.002**	**0.000**	**0.000**	**0.003**

Table 8-5. Terzaghi corrected values of the intensity of open and flowing fractures deduced in stage 2.2. There are significant differences between the three fracture domains FFM01–03 and a substantial decrease with depth of both open and flowing fractures in both FFM01 and FFM03.

Fracture domain	FFM01			FFM02	FFM03	
Depth interval, m	100–200	200–400	400–1,200	100–200	100–400	400–1,200
Intensity of observed open fractures, m^{-1}	1.13	1.02	0.54	3.17	1.10	0.77
Intensity of observed flowing fractures, m^{-1}	0.15	0.04	< 0.01	0.33	0.09	0.05
PFL-f T_{min}, m^2/s	$2.5 \cdot 10^{-10}$	$2.7 \cdot 10^{-10}$	$6.2 \cdot 10^{-10}$	$2.5 \cdot 10^{-10}$	$1.9 \cdot 10^{-9}$	$1.1 \cdot 10^{-9}$
PFL-f T_{max}, m^2/s	$4.7 \cdot 10^{-5}$	$1.8 \cdot 10^{-7}$	$8.9 \cdot 10^{-8}$	$7.3 \cdot 10^{-6}$	$6.8 \cdot 10^{-7}$	$1.9 \cdot 10^{-7}$

The left image in Figure 8-21 shows a view from above of the fracture domains in the target volume below FFM02, i.e. FFM01 and FFM06, and the nearby, cored boreholes at drill sites 1–2, 4–8 and 10 available for hydrogeological DFN modelling in stage 2.2. FFM06 is located in the northern part of the target volume in the footwall bedrock, but no hydraulic information about the bedrock in between the deformation zones in this fracture domain was available in stage 2.2. Based on the geological description of the fracture domains presented in /Olofsson et al. 2007/ and the available statistics of "open fractures" in the nearby cored boreholes, it was assumed in stage 2.2 that fracture domain FFM06 has the same hydrogeological properties as inferred for FFM01, see Table 8-5. The right image in Figure 8-21 shows a view from above of the cored borehole KFM08D that was drilled and investigated in stage 2.3. A prediction of the structural-hydraulic properties along KFM08D is found in /Follin et al. 2007c/. Figure 8-22 shows the measured hydrogeological data in KFM08D. The acquired data agree with the prediction and do not contradict the hypothesis that the hydrogeological properties of FFM06 resemble those deduced for FFM01.

8.4.3 The bedrock bordering the target volume

Strong bedrock anisotropy with high ductile strain and ductile structures that dip steeply to the south-west are prominent in the bedrock bordering the tectonic lens to the south-west of the target volume, see section 5.2.4. A folded, ductile, high-strain rock unit is also present inside the tectonic lens (section 5.2.4). Hydrogeological observations in the bedrock bordering the target volume are made in boreholes KFM04A, KFM06C, KFM07A, KFM08A and KFM09A. For an illustration, the findings in the three boreholes KFM04A, KFM09A and KFM07A, cf. Figure 2-1 and Figure 2-2, are commented upon here. The hydraulic data acquired with the PSS method in these three boreholes are shown in Figure 8-23. The hydraulic differences between the bedrock inside the target volume and the bordering bedrock are obvious. The hydraulic differences with depth within the target volume are also very clear.

KFM04A is located in the intensely fractured bedrock bordering the lens (FFM04). It is inclined 60° towards the lens and enters the sparsely fractured bedrock in the target volume (FFM01) as it reaches 400 m depth (borehole length 500 m).

KFM09A is located on the border of the lens and is inclined 60° away from the lens. It investigates at first the intensely fractured superficial bedrock in the lens (FFM02 and FFM01) and secondly the intensely fractured bedrock bordering it (FFM05 and FFM04) beginning at 230 m depth (borehole length 280 m).

KFM07A is located in the lens. It investigates the intensely fractured superficial bedrock in the lens (FFM02) and the very sparsely fractured bedrock in the target volume below (FFM01). KFM07A also enters the folded, ductile, high-strain and strongly fractured rock unit inside the lens (FFM05) at 665 m depth (borehole length 793 m).

8.4.4 The shallow bedrock aquifer

The uppermost part of the bedrock in the Forsmark area is recognised for its large horizontal fractures/sheet joints; see Figure 8-24 for an example. Besides this structural evidence, there are three pieces of hydrogeological evidence that support the hydraulic importance of these structures.

1. Exceptionally high water yields. The median yield of the first 22 percussion-drilled boreholes is c. 12,000 L/h. This is c. 20 times higher than the median yield of the domestic water wells drilled outside the candidate area, which is no different from the median yield of all bedrock wells (c. 200,000) registered at the Geological Survey of Sweden /Berggren 1998/.
2. The near uniform groundwater level in the uppermost c. 150 m of bedrock observed among the percussion-drilled boreholes within the target area. This is on the average c. 0.5 m above the datum plane (RHB 70). In contrast, the average groundwater level among the percussion-drilled boreholes outside the candidate area is c. + 2.8 m above the datum plane, see Figure 8-25. The mean gradient between the Quaternary deposits and the uppermost part of the bedrock is downwards (cf. section 4.3.1).
3. The extensive and rapid transmission of fluid pressure changes (drawdown) during the large-scale interference test that was run over three weeks during the summer of year 2006 in borehole HFM14, which is located in the centre of the target area, see Figure 8-11 and Figure 8-12.

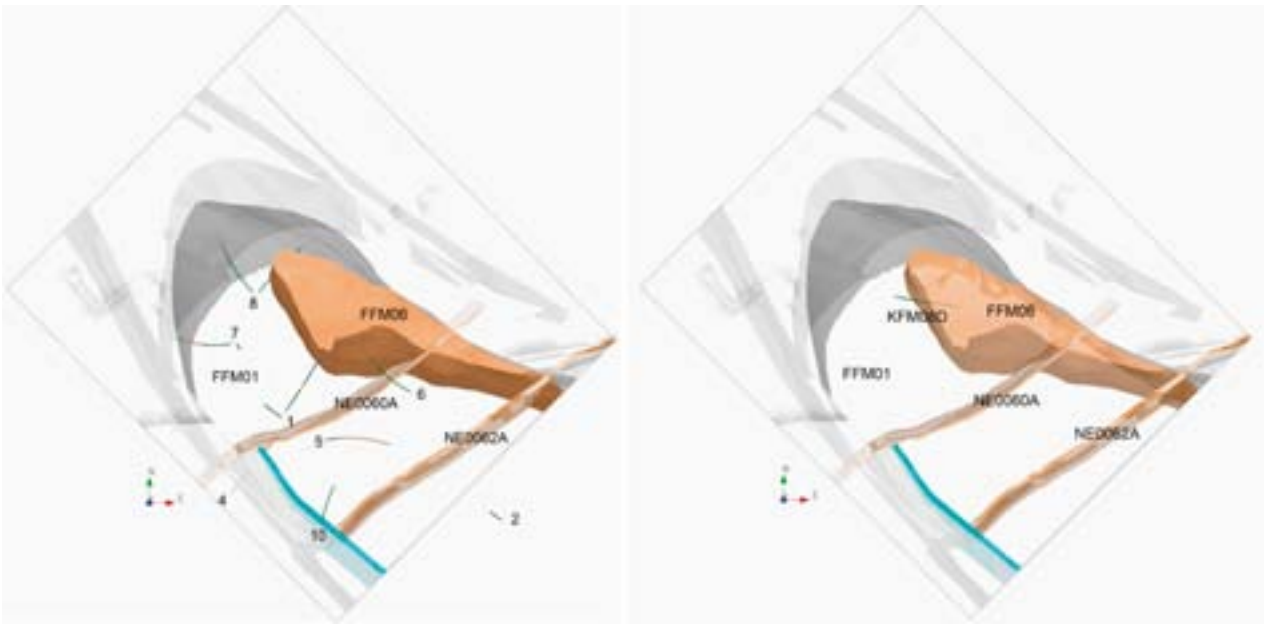

Figure 8-21. *Left: The core-drilled boreholes available for hydrogeological DFN modelling of the target volume did not provide any hydrogeological information about fracture domain FFM06. Right: The cored borehole KFM08D was drilled and investigated during the verification stage. KFM08D penetrates FFM06 at about 292 m depth.*

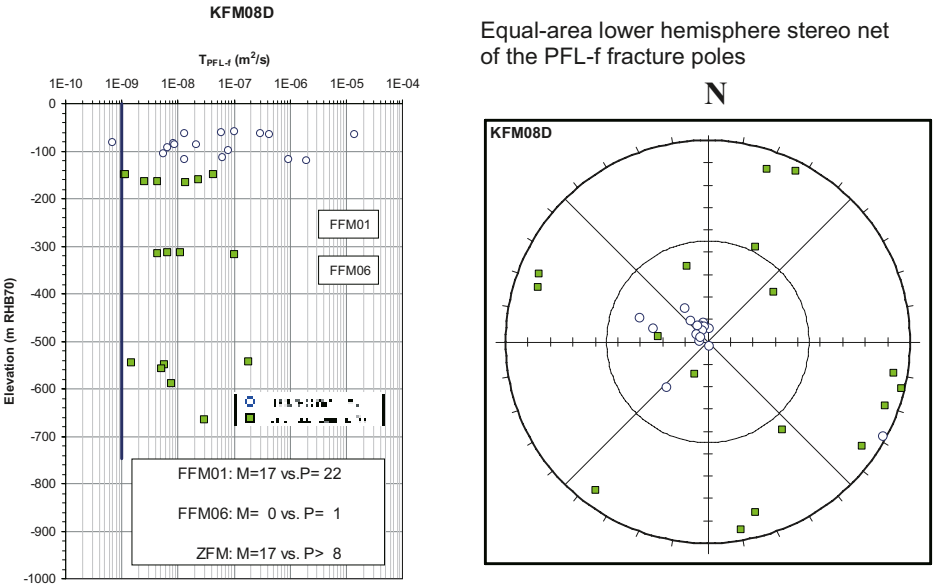

Figure 8-22. *Hydrogeological data in borehole KFM08D. There are 17 PFL-f transmissivities associated with single fractures and 17 associated with five deterministically modelled deformation zones. The blue line indicates the typical threshold value reported from the investigations in the Forsmark area, $1 \cdot 10^{-9}$ m²/s. The length of the blue line corresponds to the depths investigated with the PFL-f method. Fracture domain FFM06 begins at about 292 m depth. M = measured number of flowing fractures, P = predicted number of flowing fractures, ZFM = deformation zone.*

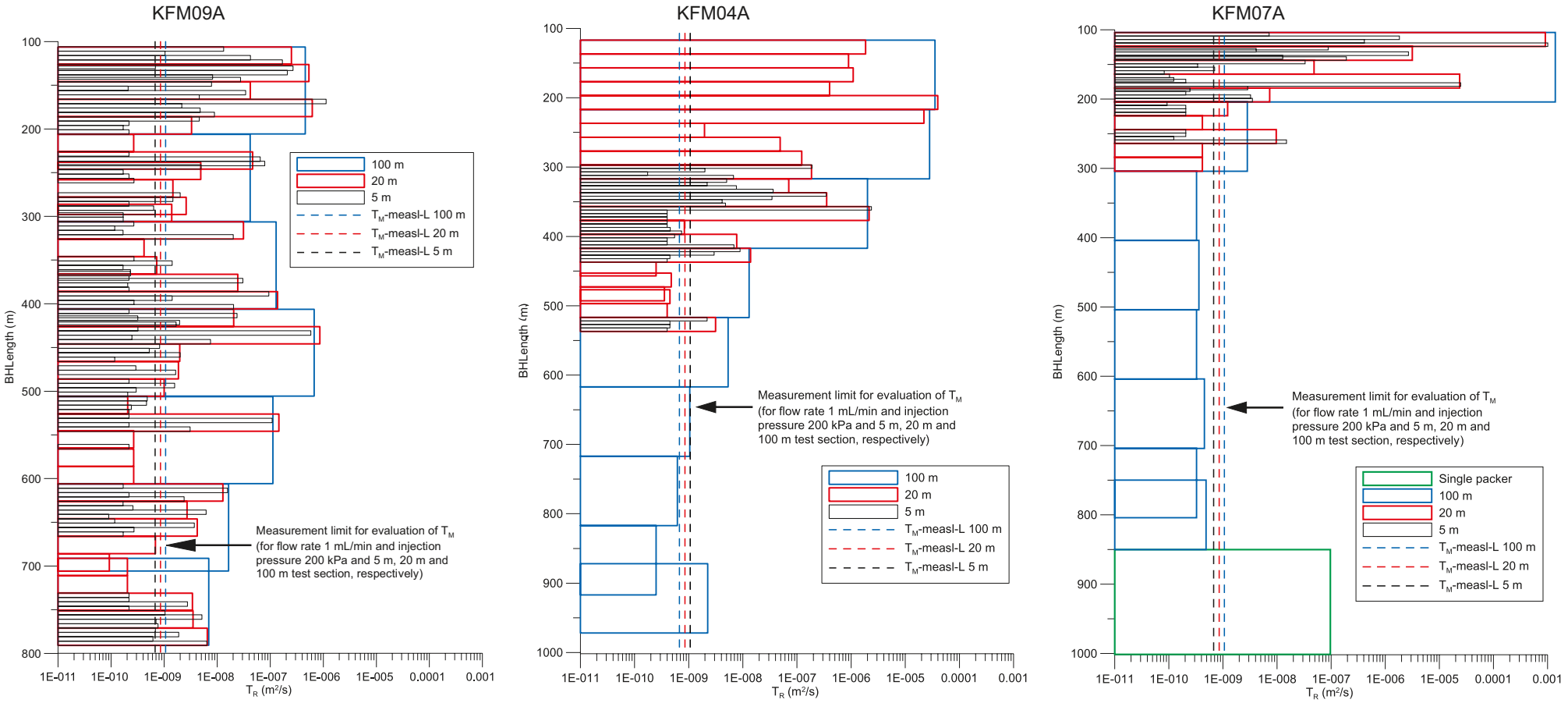

Figure 8-23. *Comparison of PSS transmissivity data gathered in the bedrock with relatively low ductile strain inside the tectonic lens, and in the bedrock with high, ductile strain both on the south-western margin of the tectonic lens and in the folded unit inside the lens. Left: KFM09A; Middle: KFM04A; Right: KFM07A. The PSS measurements are carried out with three different packer spacings, 100 m, 20 m and 5 m, depending on the results. Note that the nominal lower measurement limit of the PSS method varies slightly with the packer spacing.*

Figure 8-24. *Picture from the construction of the 13 m deep and more than one kilometre long canal between the Baltic Sea and the nuclear power reactors in Forsmark. Horizontal fractures/sheet joints are encountered along the entire excavation. The sheet joints follow the undulations of the bedrock surface implying that many of them do not outcrop, but stay below the bedrock surface as this dips under the Baltic Sea. There are several "horizons" of extensive sheet joints on top of each other according to the hydraulic interference tests. The picture is taken from the southern side of the canal where the bridge crosses the canal between drill sites 7 and 8. /Photograph by G Hansson/.*

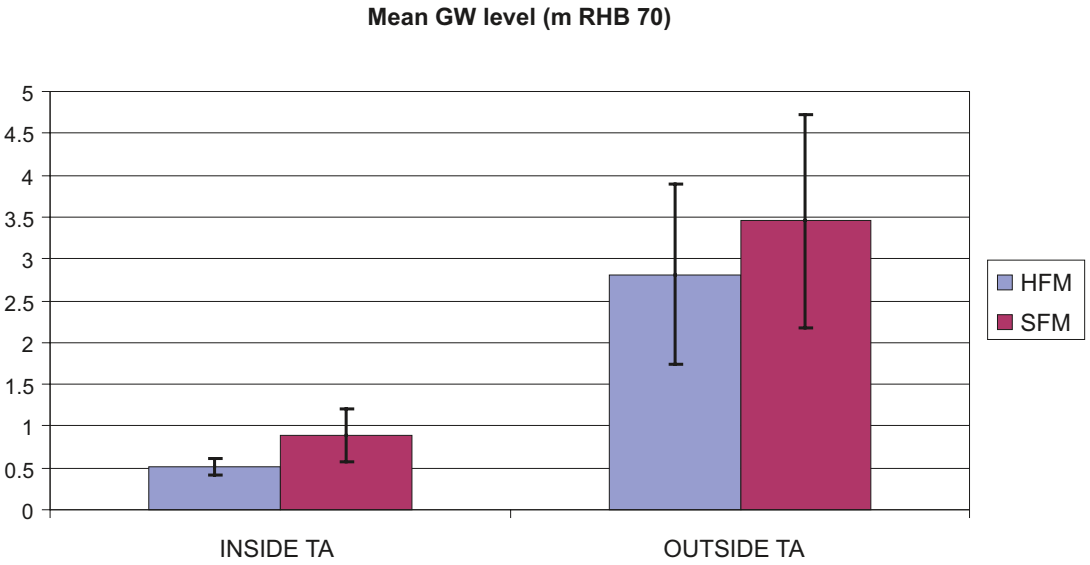

Figure 8-25. *Diagram showing mean groundwater levels of 28 percussion-drilled boreholes in the uppermost c. 150 m of the bedrock (HFM). The error bars show the 95% confidence intervals for the mean groundwater levels inside and outside the target area (TA), respectively. The mean values (+0.52 and +2.81 m RHB 70) are calculated from the arithmetic means of 37 time series inside the target area and 16 outside the target area. (Several boreholes have multi-packers.) For a comparison, the same types of statistics from 28 monitoring wells in Quaternary deposits are also shown (SFM). The mean values (+0.89 and +3.45 m RHB 70) are calculated from the arithmetic means of 9 time series inside the target area and 19 outside the target area. The mean sea water level during the monitoring period was –0.04 m RHB 70. The HFM and SFM boreholes are not drilled at the same locations.*

In conclusion, geological and hydrogeological observations indicate a well-connected network of structures of high transmissivity in the uppermost c. 150 m of the bedrock in the target area. The network is thought to consist of extensive horizontal fractures/sheet joints, outcropping deformation zones and increased, though structurally anisotropic, fracture intensity in the bedrock in between the outcropping deformation zones. The groundwater levels monitored in the Quaternary deposits and in the bedrock at depth suggest that the network short circuits the recharge from above as well as the anticipated discharge from below. The cartoon shown in Figure 8-26 illustrates the shallow bedrock aquifer concept.

Based on the results obtained from the interference test that was run in HFM14 for three weeks during the summer of 2006 (see Figure 8-11), the envisaged lateral extent of the horizontal fractures/sheet joints was hypothesised to correspond approximately to fracture domain FFM02, but stretching north all the way to the Singö deformation zone (WNW001) as shown in Figure 8-27. The other hypothesised physical boundaries are deformation zone ENE0062A to the south-east and the border of fracture domain FFM02 to the south-west and west, with the modification that the boundary passes between boreholes HFM20 and HFM28. The crosses in Figure 8-27 mark the positions of the percussion-drilled and core-drilled boreholes for which transmissivity measurements were available for parameterisation of the discrete features implemented in the ConnectFlow code to model the sheet joints in the shallow bedrock aquifer.

In 2007, two vital, confirmatory, large-scale, interference tests were conducted, one during the summer over three months in HFM14 and the other during the fall over two weeks in HFM33. Neither of the two tests falsified the hypothesised lateral extent of the discrete features inferred to characterise the shallow bedrock aquifer. On the contrary, they reinforced the hypothesis; see Figure 8-28 for an example.

Besides confirming the hypothesis of a shallow bedrock aquifer, the two confirmatory, large-scale interference tests provided two additional important results.

- The interference test that was run over three months in HFM14 resulted in almost identical final drawdowns at many observation points compared with the previous interference test that was run in this borehole over three weeks in the summer of 2006, in spite of the significant difference in test time. This observation indicates a positive hydraulic boundary nearby and/or leakage from groundwater storage in the Quaternary deposits above. (In the context of interference tests, a positive hydraulic boundary means an infinite source of water, e.g. the Baltic Sea).
- The interference test that was run over two weeks in HFM33 was conducted in a horizontal fracture located at about 100 m depth. The transmissivity of the horizontal fracture is about $3 \cdot 10^{-4}$ m^2/s. The pressure changes during the pumping propagated rapidly under the Baltic Sea, and clear hydraulic responses were observed in many boreholes within the target area including HFM14. Interestingly, no responses were observed in the nearby boreholes HFM34 and HFM35, which are located on the other side of the Singö deformation zone, see Figure 8-29. Also, no responses were observed in the monitoring network in the proximity of the SFR repository. In contrast, the abstraction of drainage water in the SFR repository (c. 5–6 L/s) has a strong impact (metres to tens of metres) on the groundwater levels in the monitoring network in the bedrock in the proximity of the repository, including HFM34 (c. 3 m) and HFM35 (c. 5.5 m), which are located at a distance of c. 500 m from the SFR repository; see Figure 8-28.

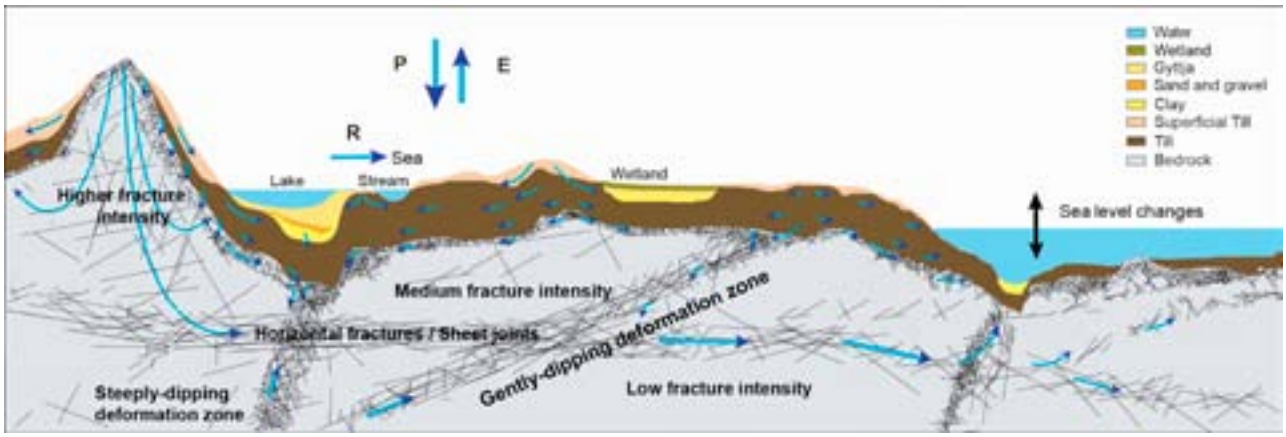

Figure 8-26. *Cross-section cartoon visualising the notion of a shallow bedrock aquifer and its envisaged impact on the groundwater flow system in the uppermost part of the bedrock within the target area. The shallow bedrock aquifer is probably hydraulically heterogeneous but at many places it is found to short circuit the recharge from above as well as the anticipated discharge from below. P = precipitation, E = evapotranspiration, R = runoff.*

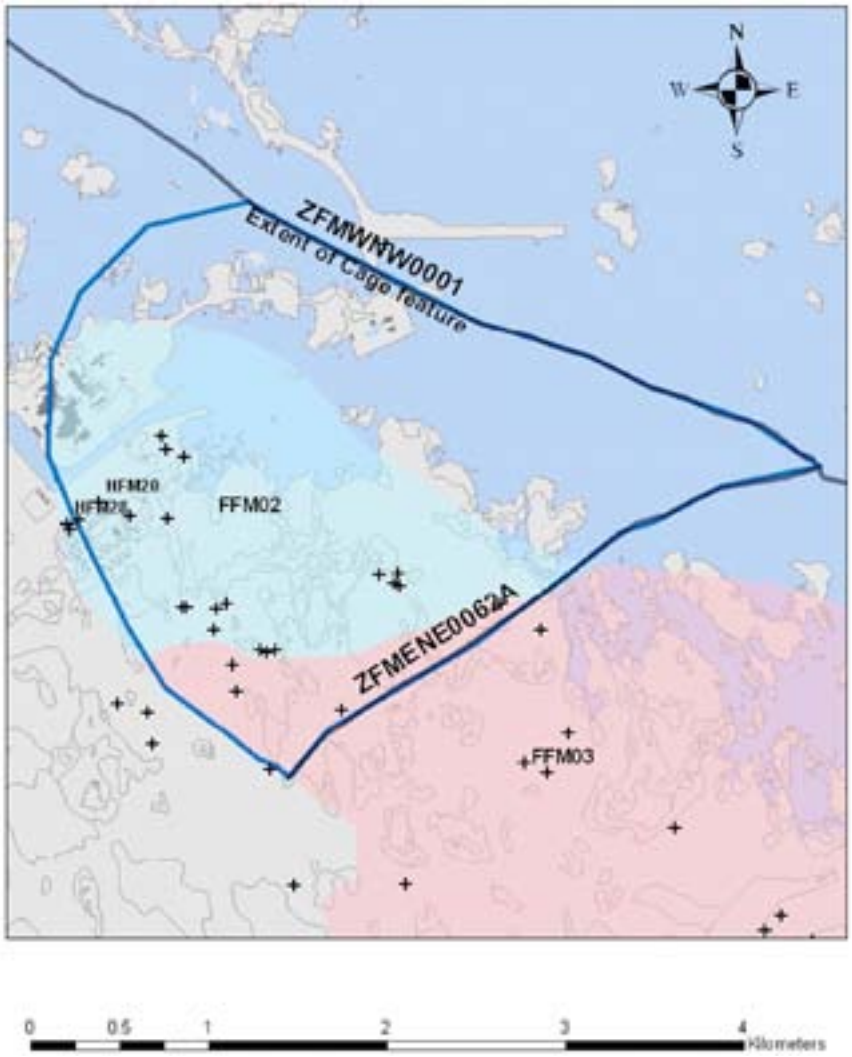

Figure 8-27. *The hypothesised lateral extent of the discrete features implemented in the ConnectFlow code to model the sheet joints in the shallow bedrock aquifer. The crosses mark the positions of percussion- and core-drilled boreholes for which transmissivity measurements were available. The bluish area represents fracture domain FFM02 and the pinkish area represents fracture domain FFM03.*

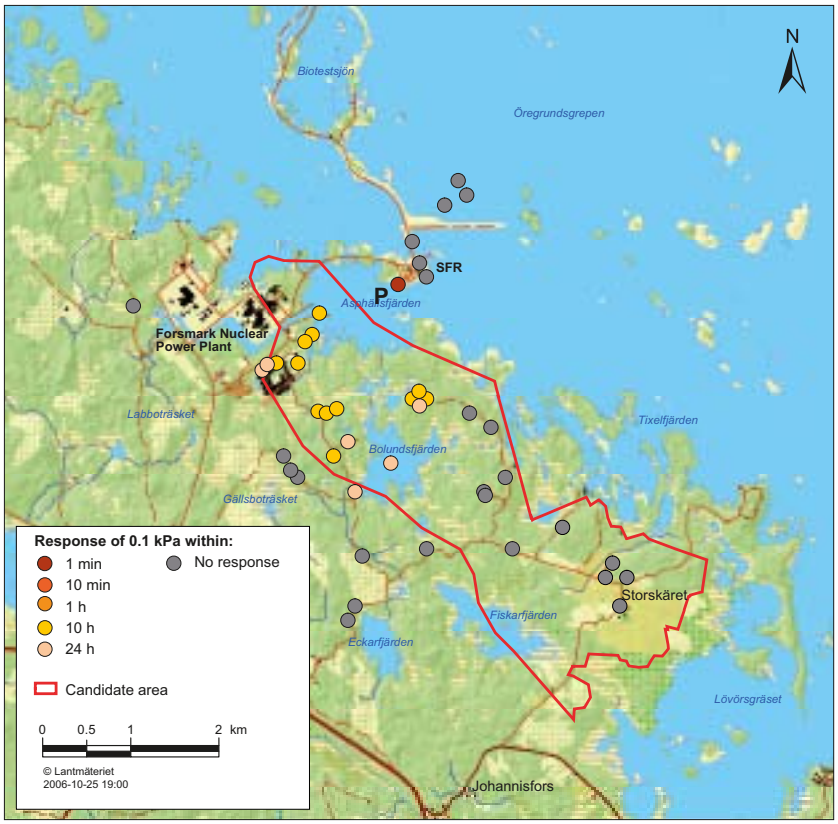

Figure 8-28. *Map showing the response times in the bedrock to the two-weeks long interference test conducted during the fall of 2007 in HFM33 (P) north of the candidate area. The created pressure changes propagated rapidly under the Baltic Sea, and clear hydraulic responses were observed in many boreholes in the uppermost c. 150 m of the bedrock within the target area including HFM14. The maximum radius of influence was about 2.2 km.*

Figure 8-29. *Map showing the SFR office buildings, the Singö deformation zones and borehole locations of HFM33, HFM34, HFM35 and KFM11.*

8.5 Parameterisation of deformation zones and fracture domains

8.5.1 Deformation zones

An exponential model for the depth dependency of the in-plane deformation zone transmissivity was suggested based on the data shown in Figure 8-14. The depth trend model may be written as:

$$T(z) = T(0)\,10^{z/k} \tag{8-1}$$

where T(z) is the in-plane deformation zone transmissivity, z is the elevation (RHB 70), $T(0)$ is the expected value of the transmissivity of the deformation zone at zero elevation and k is the depth interval that gives an order of magnitude decrease of the transmissivity. The value of $T(0)$ can be estimated by inserting a measured value [z', $T(z')$] in Equation (8-1), i.e.:

$$T(0) = T(z')\,10^{-z'/k} \tag{8-2}$$

In the case of several measurements at different locations in the same zone, the geometric mean of the calculated values of $T(0)$ is used as an effective value, $T_{eff}(0)$ in Equation (8-1). With this approach, the effect of conditioning to a measurement was to extrapolate the conditioned value over the entire length of the deformation zone laterally, but not more than 100 m vertically, see Figure 8-30. Lateral heterogeneity was simulated by adding a log-normal random deviate to the exponent in Equation (8-1), i.e.:

$$T(x,y,z) = T(0)\,10^{z/k+\mathbf{N}(0,\sigma_{\log(T)})} \tag{8-3}$$

where $\sigma_{\log(T)} = 0.632$. The applied value of $\sigma_{\log(T)}$ implies that 95% of the lateral spread in $\log(T)$ is assumed to be within 2.5 orders of magnitude.

Furthermore, the transmissivity model assumed a nugget covariance model for the lateral spatial variability, which was conditioned on transmissivity data measured. Since the heterogeneity away from the measurement boreholes is undetermined, this required a stochastic approach using several model realisations, see Figure 8-31 for an example.

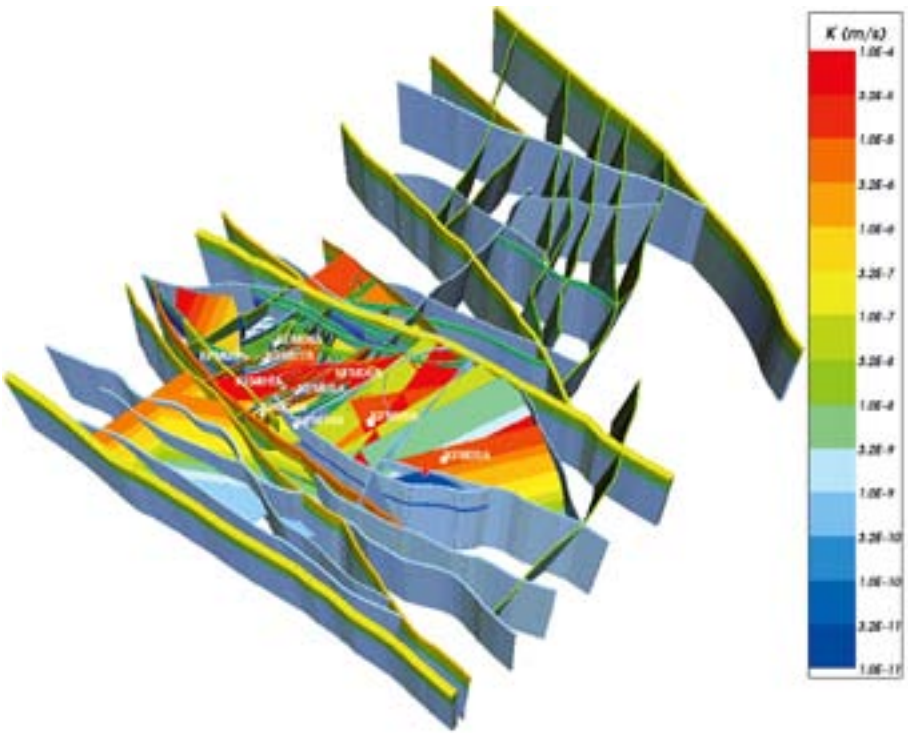

Figure 8-30. *The resulting property model using Equation (8-1). Here, the deformation zones are coloured by the hydraulic conductivity within the zones and drawn as volumes to show their assigned hydraulic width. The depth dependency is clearly apparent. The effect of conditioning to a measurement was to extrapolate the conditioned value over the entire length of the deformation zone laterally, but not more than 100 m vertically.*

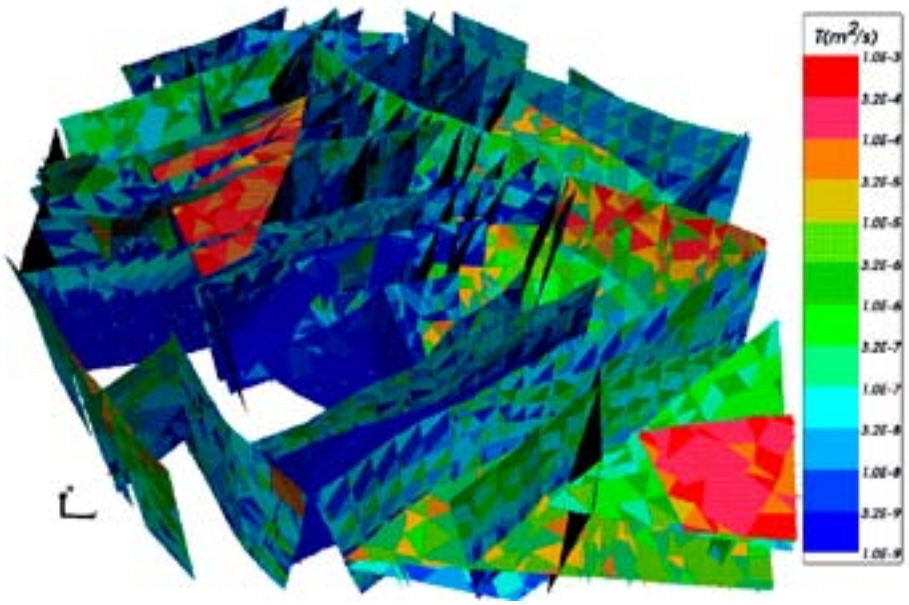

Figure 8-31. *Visualisation of an example realisation of the deformation zones occuring inside the local model domain using Equation (8-3). The deformation zone transmissivity model assumed a nugget covariance model for the lateral spatial variability in log(T), which was conditioned on transmissivity data measured. The optimal size of the finite element mesh used to model the nugget covariance was c. 100 m.*

8.5.2 Fracture domains

The methodology for a combined analysis of fracture geological and hydrogeological information (hydrogeological DFN modelling) was first derived and applied in the preliminary SDM /SKB 2005a/. For the CSI stage, a much greater quantity of data was available, and in particular data were available for core-drilled boreholes in a variety of orientations. The methodology used to parameterise the fracture domains starts with a connectivity-sensitivity analysis of different DFN models and ends with flow simulations using the most reliable DFN model deduced in the connectivity analysis. Flow simulations were carried out using three different kinds of correlations between fracture transmissivity and fracture size, see Table 8-6.

The hydrogeological DFN modelling is based on the assumption that:

$$P_{10,all} \geq P_{10,open} \geq P_{10,cof} \geq P_{10,PFL} \qquad (8\text{-}4)$$

where $P_{10,cof}$ denotes the frequency of "connected open fractures", a key property of any hydro-geological DFN model. The meaning of the different suffixes (*all*, *open*, *cof* and *PFL*) in Equation (8-4) is explained in Figure 8-32. The scaling approach used in the hydrogeological DFN modelling (cf. Figure 8-4) resembles the r_0-fixed model variant in the geological DFN modelling described in section 5.6.4.

The Terzaghi corrected linear intensities $P_{10,open,corr}$ and $P_{10,PFL,corr}$ shown in Table 8-3 and Table 8-4 reveal that there are essentially three flowing fracture sets in fracture domain FFM01 above 400 m depth (NS, NE and HZ) and two flowing fractures sets below this depth (NE and HZ). Corresponding data for the other fracture domains are reported in /Follin et al. 2007b/. The computed values of $P_{10,open,corr}$ and $P_{10,PFL,corr}$ were used to constrain the derivation of optimal parameter values for the tectonic continuum model envisaged in Figure 8-4. In short, five different combinations of values of the power-law frequency distribution parameters referred to as k_r and r_0 were tested based on the results reported in the preliminary SDM. For each combination of parameter values, the value of the 3D fracture intensity parameter referred to as $P_{32,open}$ $[r \geq r_0]$ (fracture surface area per unit volume of rock) was altered until a fair match between simulated and computed values of $P_{10,open,corr}$ was achieved, i.e.:

$$P_{32,open} \approx P_{10,open,corr} \qquad (8\text{-}5)$$

Table 8-6. Transmissivity parameters used for all sets when matching measured PFL-f flow distributions.

Type	Description	Relationship	Parameters
Correlated	Power-law relationship	$\log(T) = \log(a\, r^{b})$	a , b
Semi-correlated	Log-normal distribution about a power-law correlated mean	$\log(T) = \log(a\, r^{b}) + \sigma_{\log(T)}$ **N**[0,1]	a , b, $\sigma_{\log(T)} = 1$
Uncorrelated	Log-normal distribution about a specified mean	$\log(T) = \mu_{\log(T)} + \sigma_{\log(T)}$ **N**[0,1]	$\mu_{\log(T)}$, $\sigma_{\log(T)}$

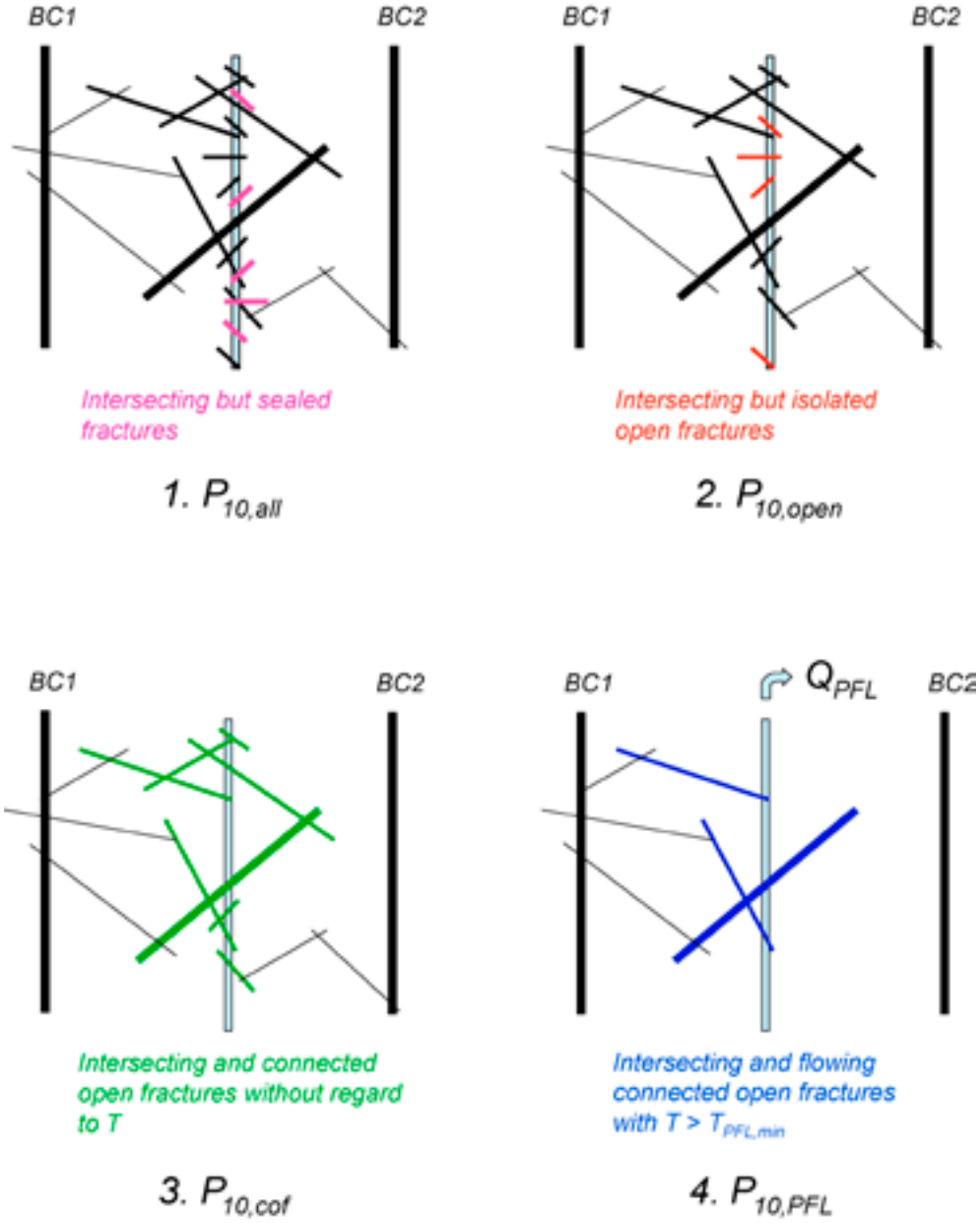

Figure 8-32. *$P_{10,all}$ is the frequency of "all fractures" intersecting the borehole, $P_{10,open}$ is the frequency of "open fractures", $P_{10,cof}$ is the frequency of "connected open fractures" and $P_{10,PFL}$ is the frequency of "flowing connected open fractures" identified with the PFL-f method. BC1 and BC2 represent hydraulic boundary conditions, e.g. the surface and/or nearby deformation zone which is connected to the surface. $P_{10,cof}$ cannot be measured, but simulated values can be compared with the measured value of $P_{10,PFL}$.*

The different graphs in Figure 8-33, Figure 8-34 and Figure 8-35 show the contribution $P_{32}[r_1, r_2]$ to the total fracture intensity as a function of fracture size for three realisations of fracture domain FFM01; 0–200 m depth, 200–400 m depth and 400–1,000 m depth. (Here total intensity refers to the lumped intensity without consideration to fracture orientation set.) The red and blue graphs represent the contributions of *open fractures* and *connected open fractures*, respectively. By the same token, the green graphs represent the contributios of *all* fractures, however not within FFM01 only, but within the entire local model domain. By plotting the intensities for all fracture orientation sets combined, the impact of spatial variability in the intensity between the sets was reduced. In effect, Figure 8-33, Figure 8-34 and Figure 8-35 indicate a reasonable agreement with regard to the envisaged relationship shown in Figure 8-5.

The lack of connectivity among the shorter fractures visible in Figure 8-33, Figure 8-34 and Figure 8-35 is highlighted in Figure 8-36, which shows the ratio of the intensity of *connected open fractures* to *open fractures* as a function of fracture size for different depth intervals in fracture domain FFM01.

The hydrogeological DFN simulations were repeated ten times (ten realisations) using the Monte Carlo method. Secondly, a connectivity analysis was carried out for each combination of parameter values and realisation, and the obtained values of $P_{10,cof,corr}$ were recorded. The results indicated which of the five combinations of parameter values gave the closest match between $P_{10,cof,corr}$ and $P_{10,PFL,corr}$, i.e.

$$P_{10,cof,corr} \geq P_{10,PFL,corr} \tag{8-6}$$

Finally, a 'fine-tuning' of the power-law size parameters for each fracture set i was carried out to produce an optimised match between $P_{10,cof,corr}$ and $P_{10,PFL,corr}$, i.e.:

$$P^i_{10,cof,corr} \approx P^i_{10,PFL,corr} \quad , \quad i \in (NS, NE, NW, EW, HZ) \tag{8-7}$$

Figure 8-37 illustrates the match for the optimised case above and below 400 m depth for each set. The same power-law size distribution parameters were used for both depth intervals, but are different between the sets. Hence, it was assumed that the large change in flow-anomaly frequency is due to the reduction in fracture intensity with depth. However, the optimisation of size parameters was based on data above 400 m depth, since the values are non-zero.

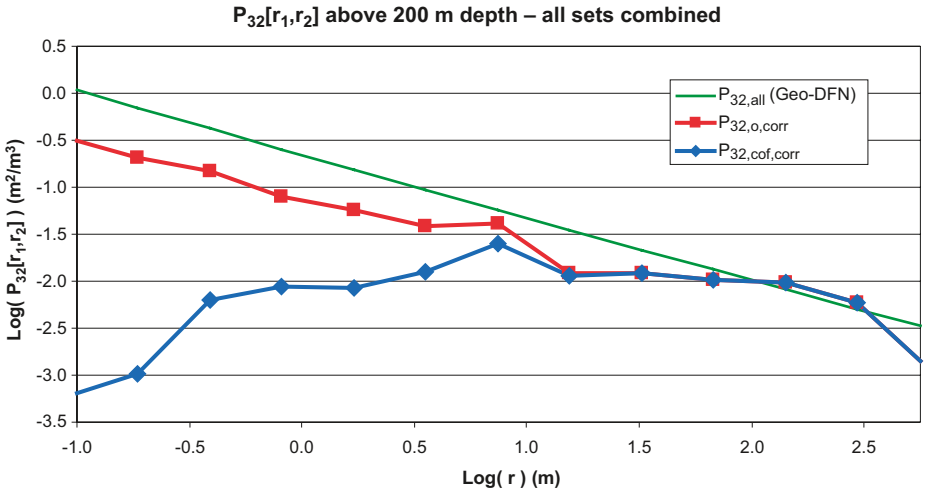

Figure 8-33. *Contribution to the total fracture intensity as a function of fracture size above 200 m depth in fracture domain FFM01. The green, red and blue graphs represent the total intensity of all fractures, open fractures and connected open fractures, respectively.*

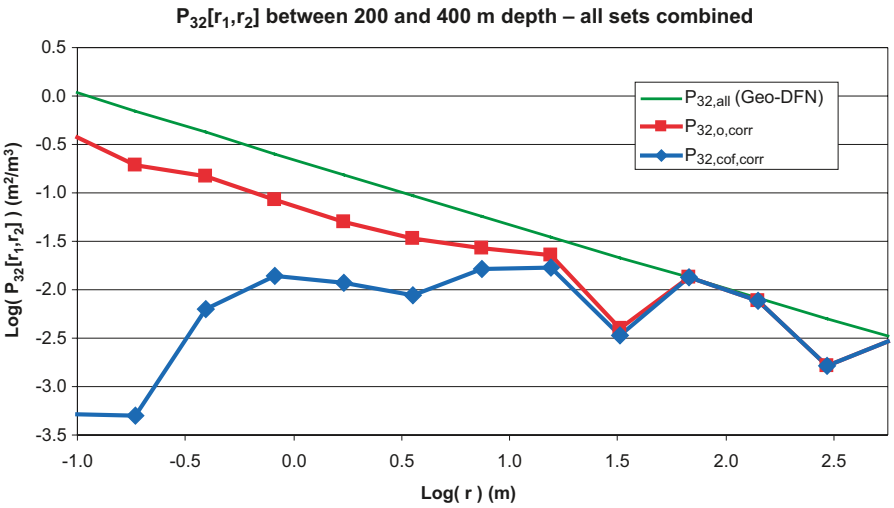

Figure 8-34. *Contribution to the total fracture intensity as a function of fracture size between 200 and 400 m depth in fracture domain FFM01. The green, red and blue graphs represent the total intensity of all fractures, open fractures and connected open fractures, respectively.*

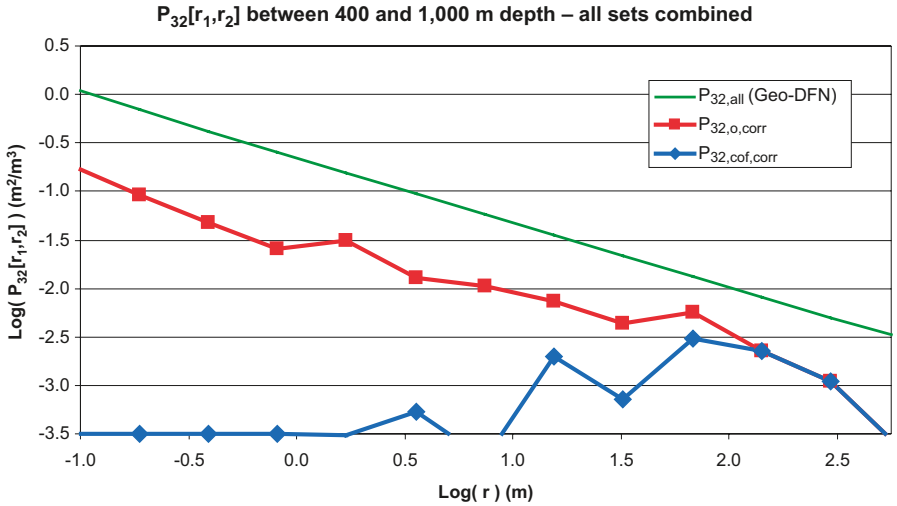

Figure 8-35. *Contribution to the total fracture intensity as a function of fracture size between 400 and 1,000 m depth in fracture domain FFM01. The green, red and blue graphs represent the total intensity of all fractures, open fractures and connected open fractures, respectively.*

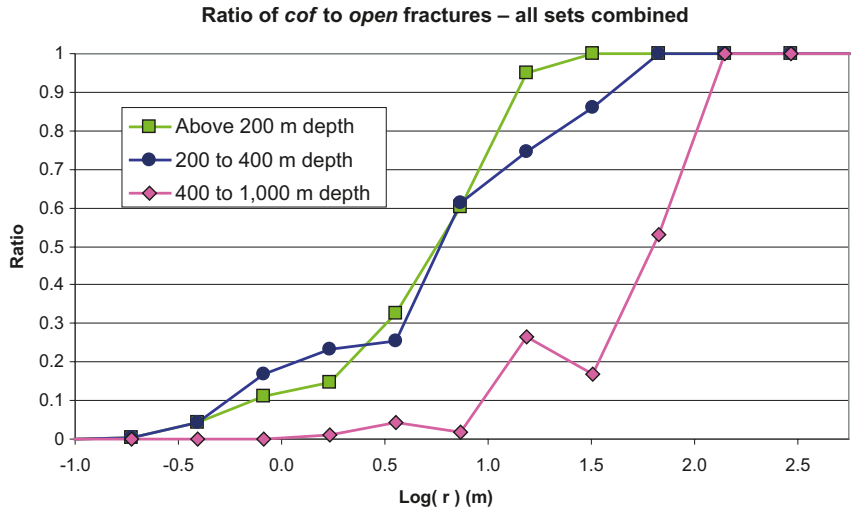

Figure 8-36. *Ratio of the intensity of connected open fractures (cof) to open fractures (o) as a function of fracture size for different depth intervals in fracture domain FFM01.*

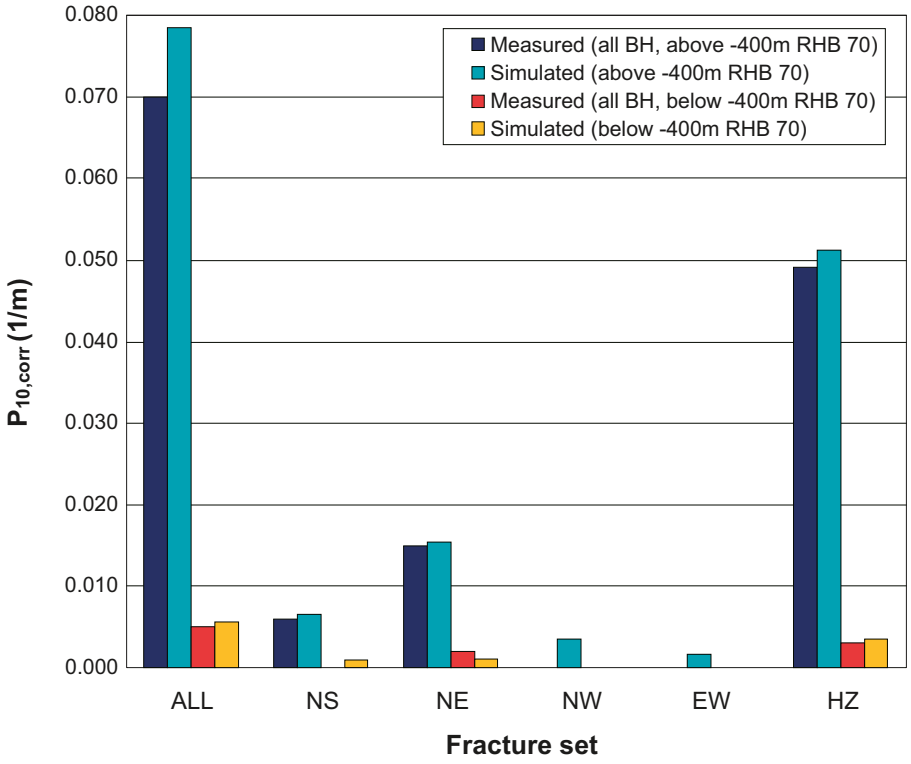

Figure 8-37. *Comparison between the Terzaghi corrected linear intensities of PFL-f data, $P_{10,PFL,corr}$, and the mean intensities of connected open fractures, $P_{10,cof,corr}$, over ten realisations of a vertical borehole above and below 400 m depth for fracture domain FFM01, respectively. The simulation results represent the optimised power-law size model of each fracture set.*

Below 400 m depth, the model predicts very low mean connected open fracture intensities using the optimised model, but it does not reproduce the zeros observed in the data. Partly, this is to be expected since a stochastic approach is being used, and some realisations happen to have a small number of connected fractures intersecting the borehole. One way of reconciling the hydrogeological DFN model is to also consider a depth variation in the hydraulic properties such that fractures below 400 m depth have a lower fracture transmissivity as well as intensity chosen so that a number of the fractures simulated below 400 m depth have transmissivities below the detection limit for the PFL-f method.

To complete the hydrogeological DFN parameterisation, flow simulations were performed to calibrate a set of alternative relationships between fracture transmissivity and size that reproduced the numbers of inflows and the distribution of their magnitude as measured with the PFL-f tests. The primary calibration targets were the distribution of flow rates per unit drawdown in the abstraction borehole, and the total flow to the borehole. An example of a flow simulation is shown in Figure 8-38. Here, the fractures are coloured by head, or coloured grey where they are not connected to the network. The only combinations of parameter values considered in the flow modelling were those based on the optimised power-law size distributions.

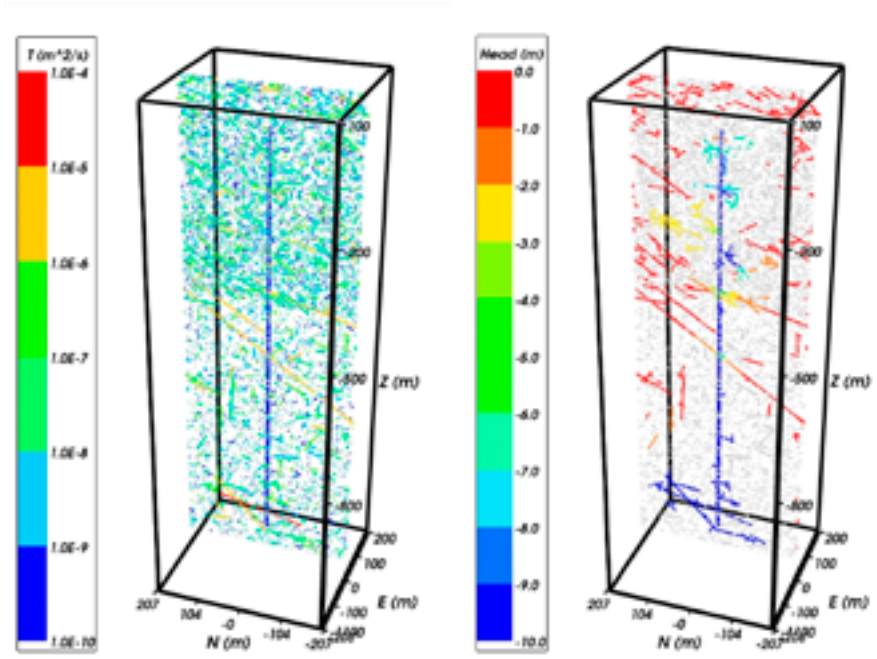

Figure 8-38. *Vertical cross-section through one realisation of the hydrogeological DFN model of fracture domain FFM01 with different fracture intensity above and below 400 m depth. Left: All open fractures coloured by transmissivity. The 1 km generic vertical borehole is coloured blue in the middle of the figure. Right: The connected open fractures coloured by drawdown with unconnected fractures coloured grey.*

Three alternative relationships between fracture transmissivity and size were studied: direct correlation, semi-correlation and no correlation, see Table 8-6. By semi-correlation it was implied that the mean transmissivity of a fracture increases with its size, but there is some random component or spread of values for any given fracture size. This is perhaps the most realistic situation. Hence, in the flow calibration, the aim was to establish appropriate choices for the parameters for each relationship between fracture size and transmissivity that gives a match to the magnitude of the inflows. To assess the 'goodness of fit', the following statistics were calculated:

- Average total specific capacity, $\sum Q/s$, to the abstraction borehole over ten realisations (cf. Table 8-7 and Table 8-9).
- Histogram of the distribution of the log specific capacities, $\log(Q/s)$, as an average over ten realisations (cf. Figure 8-39).
- Bar and whisker plot (minimum, mean minus one standard deviation, mean, mean plus one standard deviation, maximum) of the log specific capacities, $\log(Q/s)$, for the inflows within each fracture set taken over all realisations (cf. Figure 8-40).
- The average numbers of fractures within each set giving inflows to the abstraction borehole above the measurement limit for the PFL-f tests (cf. Figure 8-40).

The initial flow simulations of FFM01 contained a depth dependency only in terms of fracture intensity above and below 400 m depth. One of the key objective measures of the performance of the simulations was to compare the measured total flow to boreholes within the relevant rock volume (e.g. FFM01 above 400 m depth) with the mean total flow over the realisations. The total flows were normalised to a 400 m section of the borehole above 400 m depth, and to a 600 m section below 400 m depth. This measure was used to adjust the overall magnitude of transmissivity, while histograms of Q/s were used to ensure fine-tuned parameters to provide the correct distribution of inflows to the pumped borehole. The initial guess for the transmissivity parameters was based on those used in the preliminary SDM. The transmissivity parameters were then modified to match the inflows above 400 m depth and without any variation with depth. For each of the three transmissivity models, parameters were found that gave a reasonable match to the total flow above 400 m depth as seen in Table 8-7. However, this model gave only slightly lower total flow rates, about a factor half, below 400 m depth whereas the PFL-f data suggested a factor $2 \cdot 10^{-4}$.

Table 8-7. Initial comparison of total inflows to boreholes between PFL-f data and mean of ten hydrogeological DFN realisations of fracture domain FFM01 for a two-layer model without depth variations in transmissivity. The flow rates are normalised to a 400 m section above 400 m depth, and to a 600 m section below 400 m depth.

	Total flow rate divided by drawdown Q/s [m^2/s]	
	FFM01 < 400 m depth per 400 m of borehole	FFM01 > 400 m depth per 600 m of borehole
PFL-f data	$1.5 \cdot 10^{-5}$	$3.8 \cdot 10^{-8}$
Semi-correlated model	$1.3 \cdot 10^{-5}$	$6.2 \cdot 10^{-6}$
Correlated model	$1.7 \cdot 10^{-6}$	$8.1 \cdot 10^{-6}$
Uncorrelated model	$9.1 \cdot 10^{-6}$	$4.2 \cdot 10^{-5}$

The relatively high flow rates above 400 m depth are actually concentrated at shallow depths, and hence the initial two-layer model was refined to introduce a further depth zone in the top 200 m to give a three-layer model: above 200 m depth, between 200 m and 400 m depth, and below 400 m depth. The measured open fracture intensities in each of these sections were used as input data for the hydrogeological DFN model and the transmissivity parameters were adjusted within each depth zone until a reasonable match to the inflow distribution and total flow was achieved. The resulting hydrogeological DFN parameterisation for a three-layer model of FFM01 is given in Table 8-8. The coefficients, exponents or standard deviations as appropriate to each transmissivity model reflect the rapid reduction in inflow magnitudes with depth. This trend is quantified in the comparison of measured and simulated total flow rates for each of the three transmissivity models tabulated in Table 8-6. The flow rates decrease by about two orders of magnitude below 200 m depth, then by about another order of magnitude below 400 m depth.

Table 8-8. Description of hydrogeological DFN parameters for the simulations of flow in open fractures in FFM01 with depth dependency above 200 m depth, between 200 and 400 m depth and below 400 m depth.

Fracture domain	Fracture set name	Set pole: (trend, plunge), Fisher kappa	Size model, power-law (r_0, k_r) (m, –)	Intensity ($P_{32,open}$) valid size interval: (r_0, 564 m) (m^2/m^3)	Transmissivity model constants (Table 8-6)
FFM01 above 200 m depth	NS	(292, 1) 17.8	(0.038, 2.50)	0.073	Semi-correlated: $(a,b,\sigma_{log(T)})$ $(6.3 \cdot 10^{-9}, 1.3, 1.0)$; Correlated: (a,b) $(6.7 \cdot 10^{-9}, 1.4)$; Uncorrelated: $(\mu_{log(T)}, \sigma_{log(T)})$ $(-6.7, 1.2)$
	NE	(326, 2) 14.3	(0.038, 2.70)	0.319	
	NW	(60, 6) 12.9	(0.038, 3.10)	0.107	
	EW	(15, 2) 14.0	(0.038, 3.10)	0.088	
	HZ	(5, 86) 15.2	(0.038, 2.38)	0.543	
FFM01 between 200 and 400 m depth	NS	As above	As above	0.142	Semi-correlated: $(a,b,\sigma_{log(T)})$ $(1.3 \cdot 10^{-9}, 0.5, 1.0)$; Correlated: (a,b) $(1.6 \cdot 10^{-9}, 0.8)$; Uncorrelated: $(\mu_{log(T)}, \sigma_{log(T)})$ $(-7.5, 0.8)$
	NE	As above	As above	0.345	
	NW	As above	As above	0.133	
	EW	As above	As above	0.081	
	HZ	As above	As above	0.316	
FFM01 below 400 m depth	NS	As above	As above	0.094	Semi-correlated: $(a,b,\sigma_{log(T)})$ $(5.3 \cdot 10^{-11}, 0.5, 1.0)$; Correlated: (a,b) $(1.8 \cdot 10^{-10}, 1.0)$; Uncorrelated: $(\mu_{log(T)}, \sigma_{log(T)})$ $(-8.8, 1.0)$
	NE	As above	As above	0.163	
	NW	As above	As above	0.098	
	EW	As above	As above	0.039	
	HZ	As above	As above	0.141	

Table 8-9. Comparison of total inflows to boreholes between PFL-f data and mean of ten hydrogeological DFN realisations of FFM01 for a three-layer model with depth dependency in transmissivity as detailed in Table 8-8. The flow rates are normalised to a 200 m section above 200 m depth and between 200 m and 400 m depth, and to a 600 m section below 400 m depth.

	Total flow rate divided by drawdown Q/s [m^2/s]		
	Above 200 m depth per 200 m of borehole	**Between 200 m and 400 m depth per 200 m of borehole**	**Below 400 m depth per 600 m of borehole**
PFL-f data	$2.9 \cdot 10^{-5}$	$1.0 \cdot 10^{-7}$	$3.8 \cdot 10^{-8}$
Semi-correlated model	$3.1 \cdot 10^{-5}$	$1.1 \cdot 10^{-7}$	$5.4 \cdot 10^{-8}$
Correlated model	$3.0 \cdot 10^{-5}$	$2.0 \cdot 10^{-7}$	$5.4 \cdot 10^{-8}$
Uncorrelated model	$1.4 \cdot 10^{-5}$	$2.1 \cdot 10^{-7}$	$8.1 \cdot 10^{-9}$

An example of the comparison of inflows between model and data is given for the deduced three-layer model using a semi-correlation between fracture size and transmissivity (Figure 8-39 and Figure 8-40). Figure 8-39 shows a histogram plot of Q/s for each layer. The match to the observed flow is poorest for the deepest layer (below 400 m depth). However, it should be noted that there are very few features carrying flow at this depth, so the distributions of PFL-f data or flows are not very well defined. Figure 8-40 shows bar and whisker plots that compare the measured and simulated inflows for the different fracture sets, normalised to appropriate borehole length sections. The numbers alongside the bars represent the numbers of inflows above the detection limit per 200 m or 600 m borehole section. The detection limit of the PFL-f method is assumed to be the minimum transmissivity measured in the modelled volume ($2.5 \cdot 10^{-10}$ m^2/s for FFM01).

Figure 8-40 shows that the inflows are dominated by the HZ fracture set with a small contribution from the NS and NE sets; the NW and EW fractures sets make no contribution. The frequency of inflows decreases to about a quarter below 200 m depth, and by almost a further order of magnitude below 400 m depth. A complete set of comparisons for the three-layer model is given in /Follin et al. 2007b/.

The matches for all three transmissivity models are reasonable. To illustrate how the different transmissivity-size relationships compare, they are plotted as log-log plots in Figure 8-41 for each of the three layers based on the parameters given in Table 8-8. The semi-correlated and correlated models follow similar trends and also intercept the uncorrelated model for fractures of about 10 m radius. This is to be expected, since fractures of around 10–100 m are the ones that form the body of the connected network giving the inflows in the simulations. There is less consistency between the transmissivity models below 400 m depth as the distribution of inflows is poorly determined at these depths, there being so few data points to guide the fit.

Bearing in mind the strong variations with depth, it was suggested that a three-layer model should be adopted as the basis for further hydrogeological modelling of fracture domain FFM01. Furthermore, it was concluded that the fractures in those minor parts of fracture domain FFM01 that lie above 200 m depth show similar hydrogeological characteristics to the fractures in fracture domain FFM02, and that the variation in fracture intensity and flow in fracture domain FFM03 is much less dramatic than in FFM01. The results from the hydraulic parameterisation of FFM02 and FFM03 are given in / Follin et al. 2007b/.

Figure 8-42 shows an example of a realisation of the regional hydrogeological DFN simulated in stage 2.2. The realisation is shown as a NW-SE cross-section and two horizontal trace planes at 30 m depth and 500 m depth, respectively. The images in the left column show the traces of *open fractures*. The images in the right column show the traces of the *connected open fractures*. The effect of the low connectivity below 400 m depth is apparent.

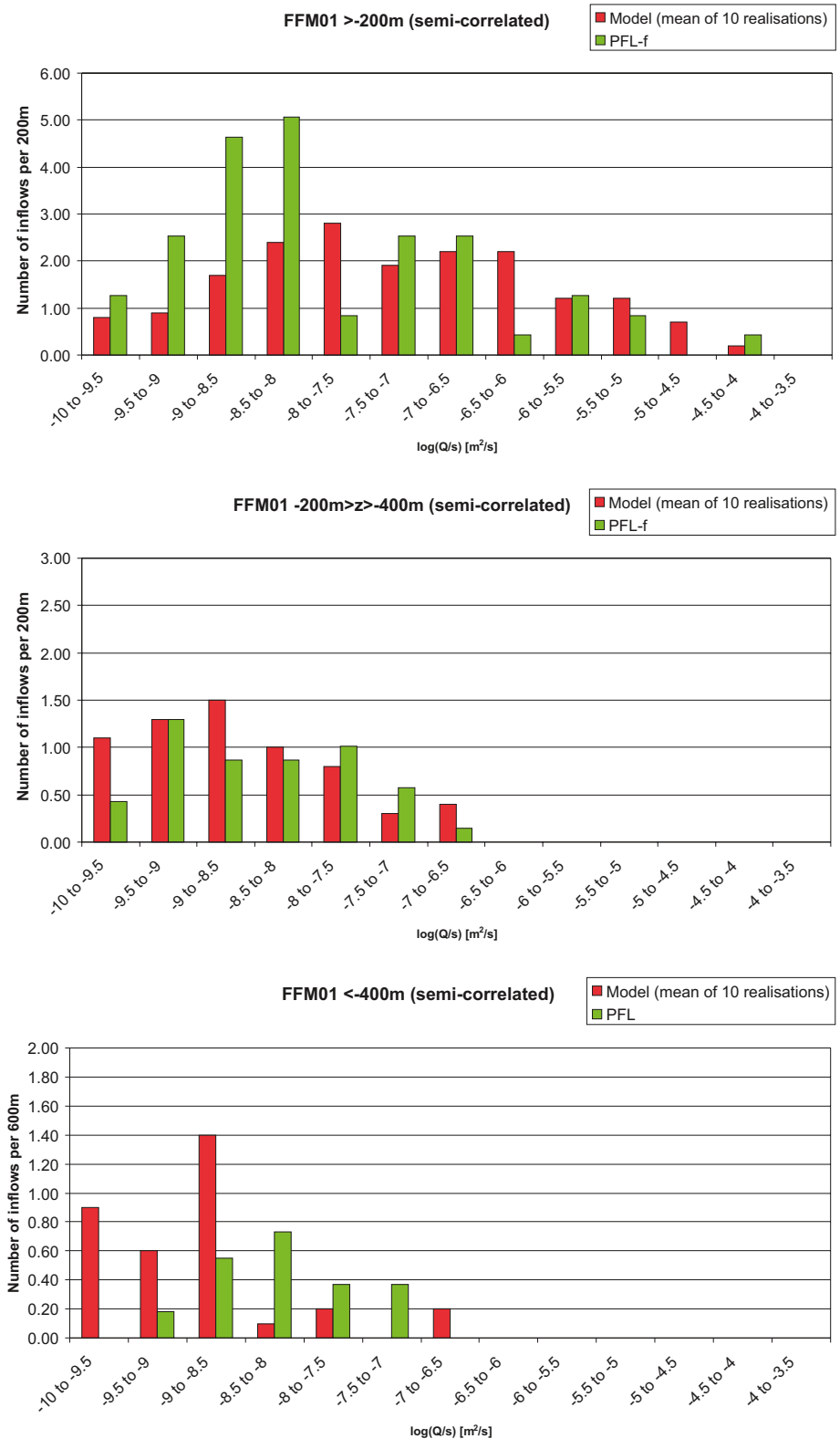

Figure 8-39. *Histogram comparing the distribution of the magnitude of inflows divided by drawdown, Q/s, at abstraction boreholes in fracture domain FFM01 with a semi-correlated transmissivity model (see Table 8-8 for parameter values). Top: above 200 m depth; Middle: between 200 m and 400 m depth; Bottom: below 400 m depth. The PFL-f measurements are treated as ensemble over all borehole sections within FFM01. Above 200 m depth and between 200 m and 400 m depth, the number of inflows is normalised with respect to a borehole section of 200 m length, and below 400 m depth relative to a 600 m section. The simulations represent statistics taken from an ensemble over ten realisations of the hydrogeological DFN model.*

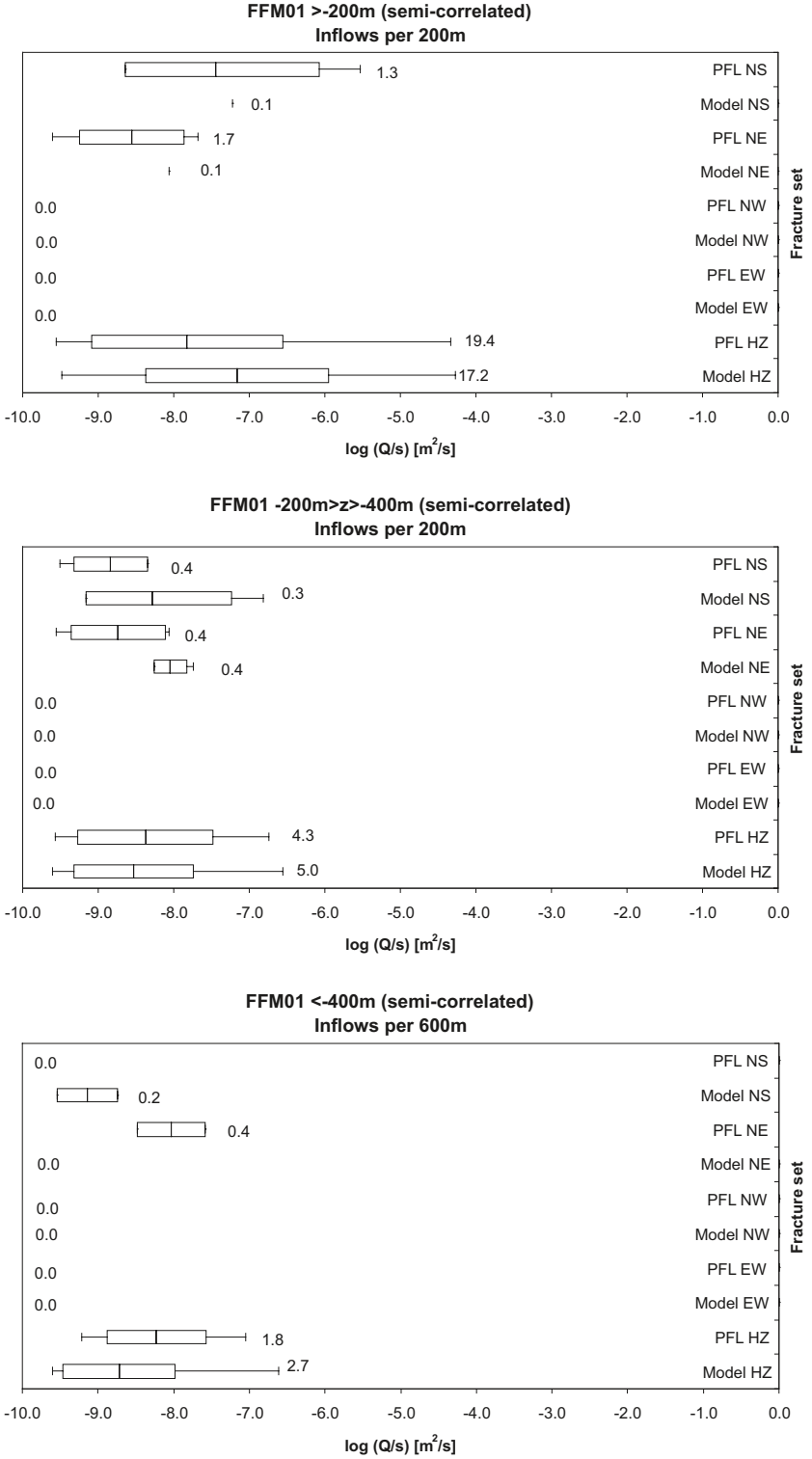

Figure 8-40. *Bar and whisker plots comparing statistics for the individual inflows, Q/s, for each fracture set derived from the PFL-f data in borehole sections within FFM01 against statistics taken from an ensemble over 10 realisations of the hydrogeological DFN model with a semi-correlated transmissivity. Top: above 200 m depth; Middle: between 200 m and 400 m depth; Bottom: below 400 m depth. The centre of the bar indicates the mean value, the ends of the bar indicate ±1 standard deviation, and the error bars indicate the minimum and maximum values. Above 200 m depth and between 200 m and 400 m depth, the total number of fractures with inflows above the detection limit is given per 200 m borehole section. Below 400 m depth, the numbers of inflows per 600 m borehole section is given. For the data, statistics are taken over the identified flowing fractures within each set, and for the model, statistics are taken over the fractures generated within each set and over ten realisations.*

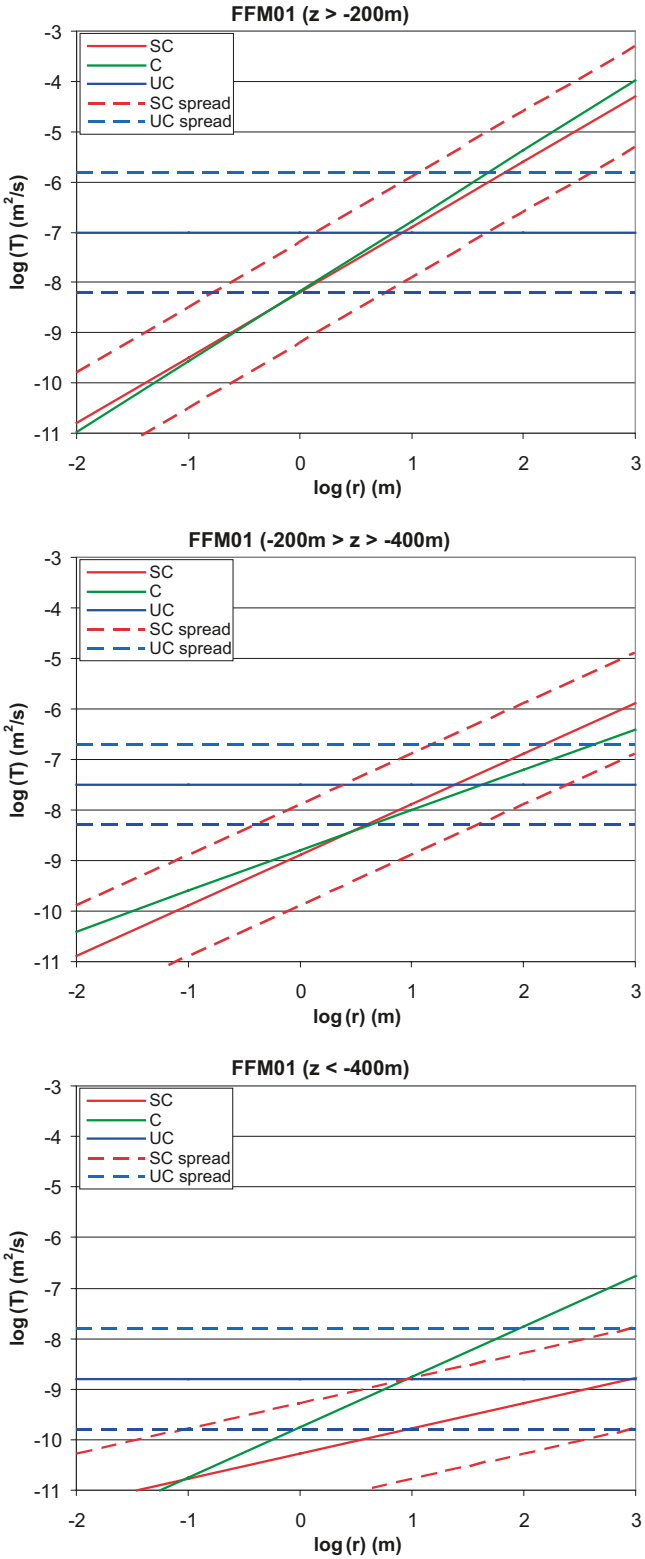

Figure 8-41. *Plots of the profile of transmissivity as a function of fracture radius for the three-layer model of fracture domain FFM01 for each of the three transmissivity versus size relationships (SC = semi-correlated, C = correlated, UC = uncorrelated) based on the parameterisation given in Table 8-8.*

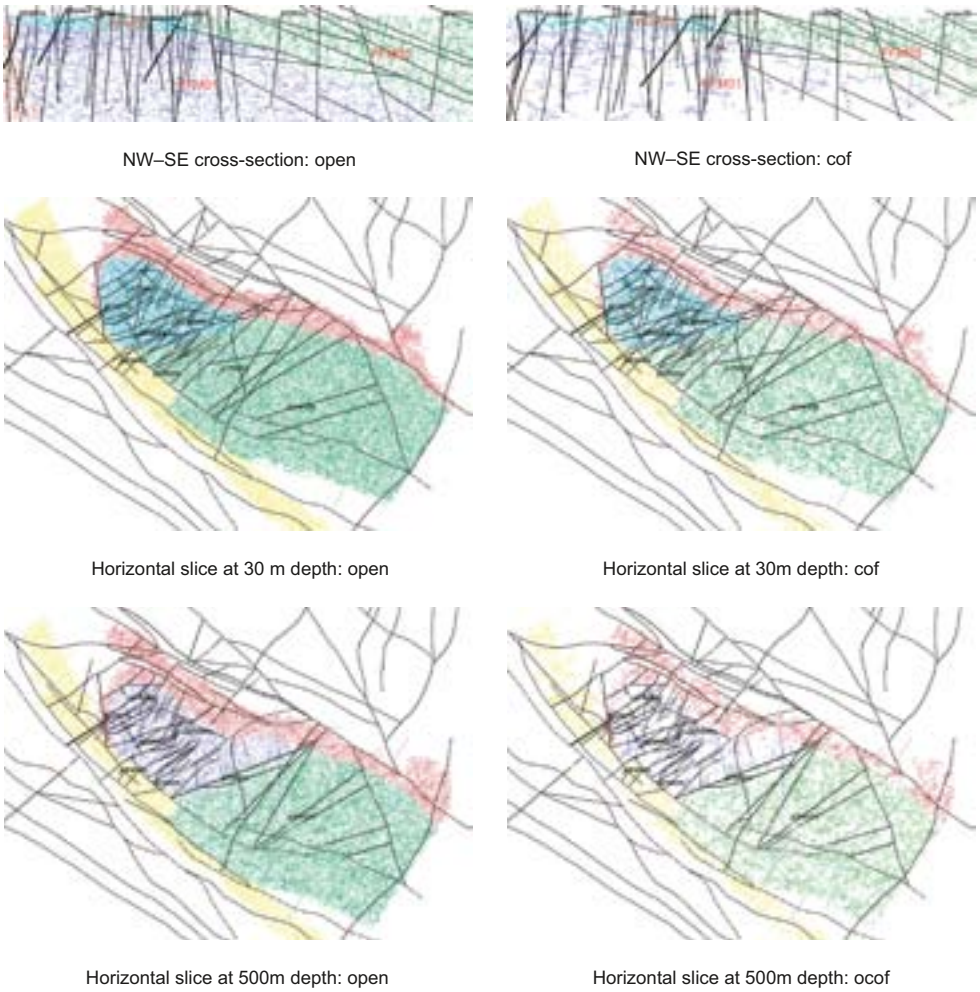

Figure 8-42. *An example of a fracture network realisation of the regional hydrogeological DFN. The realisation is shown as a NW-SE cross-section and two horizontal trace planes at 30 m depth and 500 m depth, respectively. The depth extension of the cross-section is c. 1.2 km and the length is c. 5 km. The images in the left column show the traces of "open fractures". The images in the right column show the traces of the "connected open fractures" (cof). The DFN fracture traces are coloured by fracture domain: FFM01 and FFM06 are dark blue, FFM02 is light blue, FFM03 is green, FFM04 is yellow, and FFM05 is red. Slices through the deformation zones (local and regional models) at the same depths are superimposed in black. Here, the stochastic fractures are generated with radii between 5.64–564 m.*

8.6 Flow model calibration

Forward model calibration consists of changing values of model input parameters in an attempt to match field observations within some acceptable criteria. By comparing the model predictions with different types of field data/measurements, the overall model development can be partially calibrated to improve the parameterisation, improve understanding of the hydrogeological system, and help build confidence in the hydrogeological conceptual model of the Forsmark area. The general approach applied in the CSI stage was to use essentially the same groundwater flow and solute transport model in terms of grid discretisation and parameter settings for matching the three types of field data referred to as data sets B, C and D in section 8.1.

The ConnectFlow code /Hartley and Holton 2004, Hartley et al. 2004ab, Hoch and Jackson 2004/ was used for the 3D groundwater flow and solute transport modelling carried out in stages 2.2 and 2.3. ConnectFlow is a so-called equivalent continuous porous medium (ECPM) code. To become a meaningful activity in a highly heterogeneous and anisotropic medium such as the crystalline bedrock in the Forsmark area, forward model calibration requires that the structural-hydraulic properties

of the deformation zones and fracture domains are properly characterised and implemented in an ECPM code. The parameterisation in ConnectFlow is a two stage process. Firstly, transmissivities inferred from the hydraulic tests are used to parameterise the deformation zone and fracture domain models as described in sections 8.5.1 and 8.5.2. Secondly, the geometrical and hydraulic properties of these two discrete models are transformed into ECPM hydraulic conductivities using a specified grid resolution (20 m within the target volume and 100 m outside). It should be noted that the ECPM properties are not needed in the migration simulations run in the safety assessment, since these are carried out on a much smaller scale than the simulations treated in the SDM. That is, the safety assessment is based on the hydrogeological DFN model directly.

The calibrated model is referred to as the *deterministic base model simulation* in the SDM. The term *deterministic simulation* means that $\sigma_{\log(T)}$ was set to nil in Equation (8-3) and that a *single realisation* of the hydrogeological DFN model shown in Table 8-8 was used for FFM01–FFM06. Moreover, the hydrogeological DFN model assumed a semi-correlated model for the fracture transmissivity.

8.6.1 Matching the 2006 interference test in HFM14

Calibrating against the observed drawdowns during the interference test in borehole HFM14 in year 2006 was expected to test model predictions of hydraulic communications on the scale of a kilometre or so, see Figure 8-11. Structures of high transmissivity were expected to dominate the hydraulic responses, and so the interference test should provide a good test of the structural model and hydraulic property assignment, such as the transmissivity of zone A2 and its connections to sub-vertical zones and the sheet joint features. Several boreholes have been monitored at different depths, and where there are differences in the responses at different depths, the data provide a way of understanding distinctions in the hydraulic properties of the deformation zones, the fracture domains and the Quaternary deposits. HFM14 is c. 125 m deep and is interpreted to intersect zone A2 between c. 60–80 m depth.

In contrast to the PSS and PFL-f hydraulic test data that essentially only indicate horizontal flows, the interference test also provides information on the vertical transmission of hydraulic disturbances. Borehole HFM14 is located very close to Lake Bolundsfjärden, which provides a possible source of recharge to the abstraction. Calibrating the model on hydraulic responses in monitoring holes surrounding the lake provides a means of understanding the vertical hydraulic contact between the lake, the underlying regolith and the superficial bedrock. In summary, the interference test in borehole HFM14 conducted during the dry summer of 2006 was considered likely to prove a useful calibration for all hydraulic domains, see Figure 8-11 and Figure 8-12.

As an overall representation of the match against the measurements in the monitored intervals, the simulated drawdowns after 21 days are plotted as a distance-drawdown diagram in Figure 8-43. The drawdown for the nearest monitoring intervals on the left side of the graph is controlled by the hydraulic properties close to HFM14. This mainly relates to the transmissivity of the extensive sub-horizontal deformation zone A2 and the features implemented in the ConnectFlow code to model the sheet joints in the shallow bedrock aquifer. These are the key controls for most intervals up to about 500–600 m distance from HFM14. Beyond this, the responses are controlled by a more complex balance of parameters representing the hydraulics of the more distant deformation zones, the "sheet joint features", the Quaternary deposits and, presumably, the Baltic Sea.

The abstraction in borehole HFM14 during the three-week long interference test equates to an effective sink of about 183,000 m^3/year. For the infiltration rate of 20 mm/year used in the simulations, this is equal to the total annual recharge from an area of about 1,700 m radius. However, this radius of influence is reached already within three weeks of testing, see Figure 8-43. This suggests laterally extensive sheet joints with a high hydraulic diffusivity, and a low leakage from the Quaternary deposits and the surrounding fracture domains. Moreover, 1,700 m is beyond the shortest distance to the Baltic Sea, see Figure 8-11, which implies that the Baltic Sea may act as a positive hydraulic boundary.

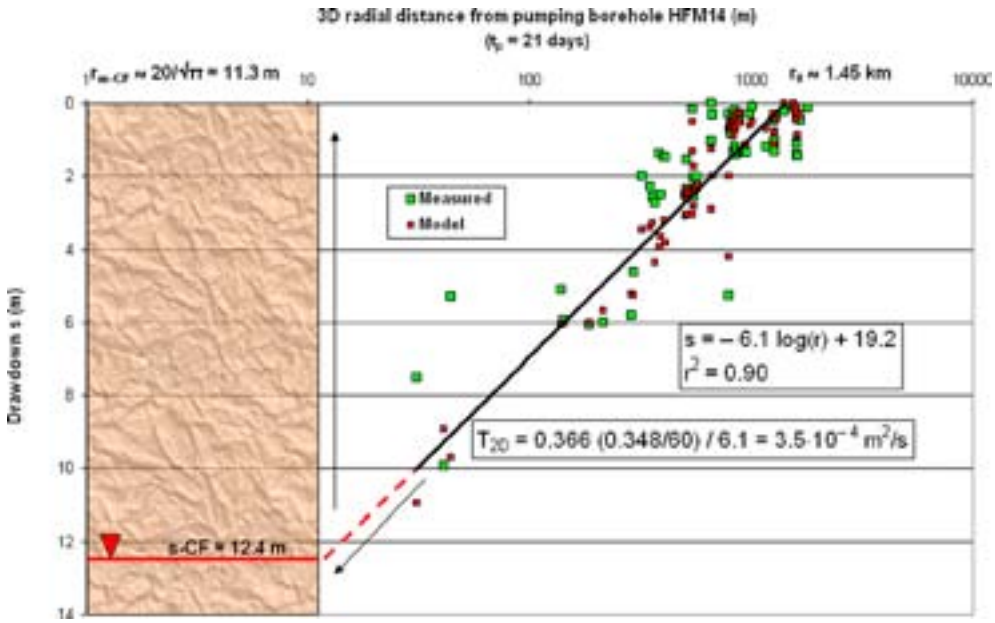

Figure 8-43. *Plot of measured drawdowns (green) and simulated (red) vs. log(3D radial distance) at the end of the 21-day log interference test in HFM14. The measured drawdown in HFM14 was 11.7 m and the simulated 12.4 m using the deterministic base case simulation. The black line shows a least-squares fit to the simulated drawdowns. The value of the correlation coefficient ($r^2 = 0.90$) indicates a less heterogeneous model than does the regression of the measured data in the real system, cf. Figure 8-12. A 2D steady-state, radial flow approximation using the slope of the least-squares fit for an estimate of Δs (difference in drawdown per log cycle of distance) renders a large-scale effective transmissivity of $3.5 \cdot 10^{-4}$ m^2/s. This value is essentially a composite of the transmissivities assigned to A2, the near-surface sheet joints, and a bit of ENE0060. An extrapolation of the regression model to the edge of the pumped 20 m element matches the simulated drawdown in this cell, ($rw\text{-}CF = 20/\sqrt{\pi} \approx 11.3$ m).*

8.6.2 Matching natural groundwater levels

Calibrating against the natural groundwater levels observed in the Quaternary deposits and in the uppermost part of the bedrock is expected to provide information on the interaction between the groundwater in these two domains, HSD and HRD. For this reason, this calibration is likely to be focused on the hydraulic properties of the Quaternary deposits and the shallow bedrock aquifer, as well as providing confirmatory testing of the hydraulic boundary conditions.

The boreholes shown in Figure 8-44 and Figure 8-45 are ordered by bedrock elevation. The simulated groundwater levels are in both plots a bit higher than the measured levels; c. +0.7 m of mean difference for both the HFM holes and the SFM holes within the target volume. This magnitude of discrepancy is fairly large considering the low magnitudes of the mean groundwater levels inside the target area shown in Figure 8-25. However, it may perhaps be considered acceptable for comparing steady-state model predictions with seasonally averaged head data that fluctuate by about 1.3–1.6 m over recordings made at different dates. It is noted that the calibrated *deterministic base model simulation* in ConnectFlow is in accordance with the observed downward gradient in the monitoring data within the target area, see Figure 8-25, with about 0.5–1 m higher groundwater levels in the Quaternary deposits than in the shallow bedrock aquifer (cf. section 4.3.1).

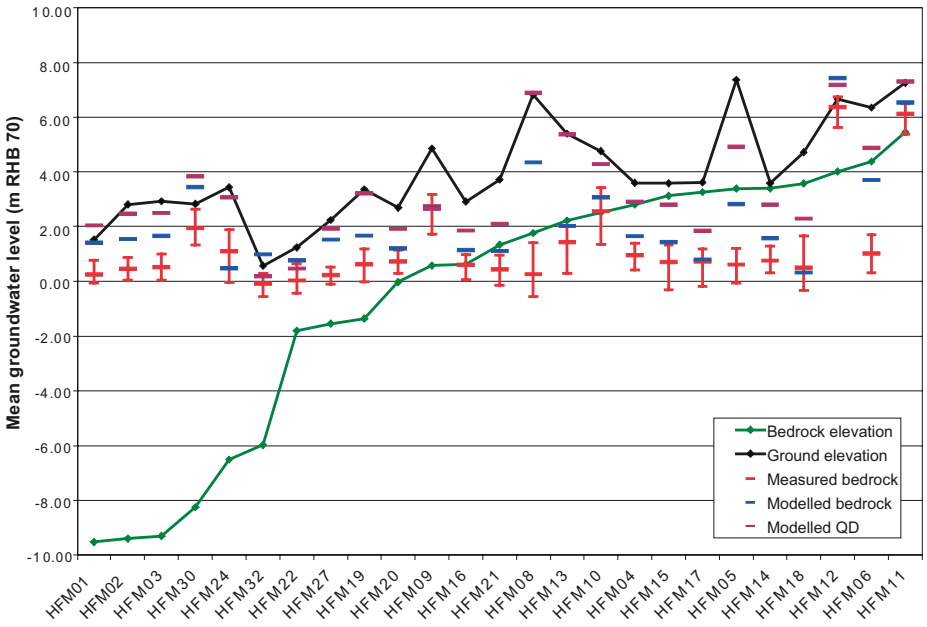

Figure 8-44. *Comparison between the deterministic base model simulation (blue) and the measured groundwater levels in the percussion-drilled boreholes (red). The boreholes are ordered by increasing bedrock elevation. The measured data are plotted as mean groundwater levels with error bars to show the range of the recordings over time. The simulated groundwater levels within the target volume are on the average c. 0.7 m higher than the corresponding measured levels. For the model, values are also given for the Quaternary deposits, QD, (purple) at the same locations as the borehole.*

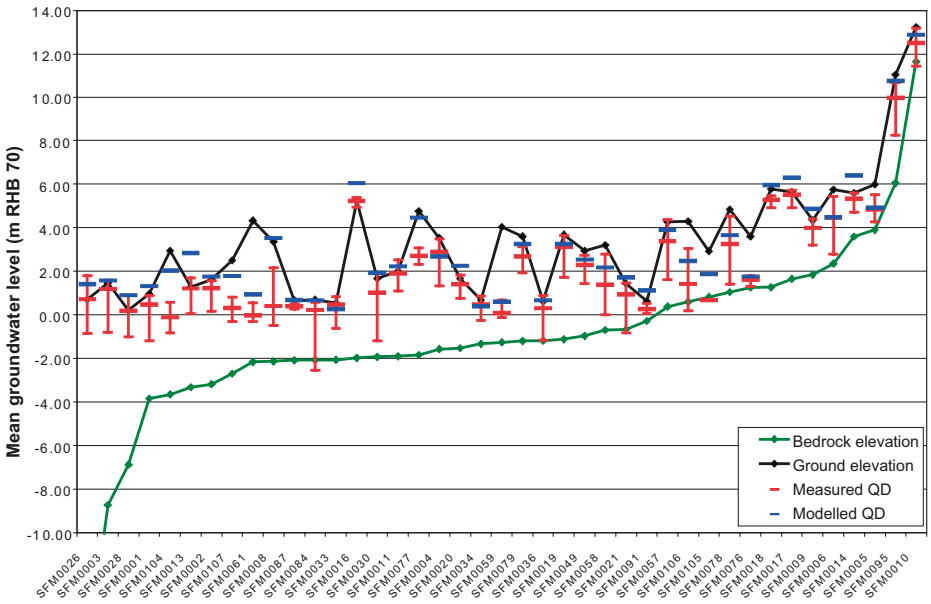

Figure 8-45. *Comparison between the deterministic base model simulation and the measured groundwater levels in the monitoring wells in the Quaternary deposits. The monitoring wells are ordered by bedrock elevation. The measured data are plotted as mean groundwater levels with error bars to show the range of the recordings over time. The simulated groundwater levels in the SFM boreholes within the target volume are on the average c. 0.7 m higher than the corresponding measured levels.*

8.6.3 Matching hydrochemical profiles in cored boreholes

Modelling the evolution of the hydrological and hydrochemical conditions during Holocene time are essential parts of the site descriptive model. In this context, the calibration against measured hydrochemical profiles in cored boreholes is fundamental to the understanding of the hydrogeological processes in the fractured rock, since it addresses the impact of variable-density flow, and the solute (salt) transport interaction between the fracture system and matrix as this can have a considerable impact how the flow rates and trajectories evolves over time. In the hydrogeological model, the transport of solutes is modelled in terms of the infiltration and mixing of several different reference waters that are assumed to be transported conservatively, i.e. without reaction, but subject to advection, dispersion, and diffusion in both the fracture and the porewaters (i.e. rock matrix diffusion). The simulations were started at 8000 BC and the development of the hydrochemistry was calculated according to changes in sea level azimuth and salinity. The initial hydrochemical conditions at the start of the simulation period are a vital part of the palaeohydrogeological model and the motives for the hypothesis used in the SDM are discussed in detail in /Follin et al. 2008b/. In short, it is envisaged that the groundwater at depth in the Forsmark area at 8000 BC, i.e. before the percolation of *Littorina Sea Water*, was a mixture of *Deep Saline Water*, *Holocene Glacial Melt Water* and remnants of *Old Meteoric and Glacial Waters*, i.e. pre-Weichselian waters. This hypothesis allows for an explanation of the observed differences between the fracture water and the porewater with regard to Cl and $\delta^{18}O$.

In general, the size of the hydrochemical database has increased significantly since the preliminary site description. In particular, this concerns porewater data, which were not available in the preliminary site description. However, in terms of reliable fracture water data at depth, the hydrochemical database available for palaeohydrogeological modelling is still very limited, see Table 8-10.

Figure 8-46 through Figure 8-50 show an excerpt of the palaeohydrogeological comparisons made for the *deterministic base model simulation*. The performance of the *deterministic base model* simulation in the SDM in predicting salinity is generally improved compared with the preliminary SDM. For example, the model predicts the high salinity encountered at shallow depth in the footwall bedrock of zone A2 at drill site 1, see Figure 8-46, which was a major problem in the preliminary SDM (cf. section 8.2). The predictions of salinity in the hanging wall of zone A2 have also improved.

The chemical compositions of the reference waters (or end-members) are described in chapter 9 (Table 9-1). Four main hydrochemical indicators were used in the palaeohydrogeological calibration: Cl, Br/Cl, $\delta^{18}O$ and HCO_3. Figure 8-47 shows the results for the boreholes located in the hanging wall. Figure 8-47 indicates that the predictions of transitions from *Littorina Sea Water* to *Deep Saline Water* shown by Br/Cl, and from *Present-day Meteoric Water* to *Littorina Sea Water* shown by HCO_3 are both at the correct depths. Similarly good results are obtained for the series of boreholes in the border of the tectonic lens and in the footwall of A2 (target volume); see Figure 8-48 for an example. However, it is noted that the high values of Br/Cl observed at Forsmark do not match the defined composition of the *Deep Saline Water*, hence they cannot be matched in the flow modelling. Reasons for this discrepancy are discussed in chapter 9, section 9.3.2.

Table 8-10. Hydrogeochemical representativity of the 30 fracture water samples used for palaeohydrogeological modelling in the SDM (stage 2.2). The classification system (numbers and colours) is explained in chapter 9.

Category	No. of samples used in stage 2.2
1	1
2	13
3	11
4	5
5	0

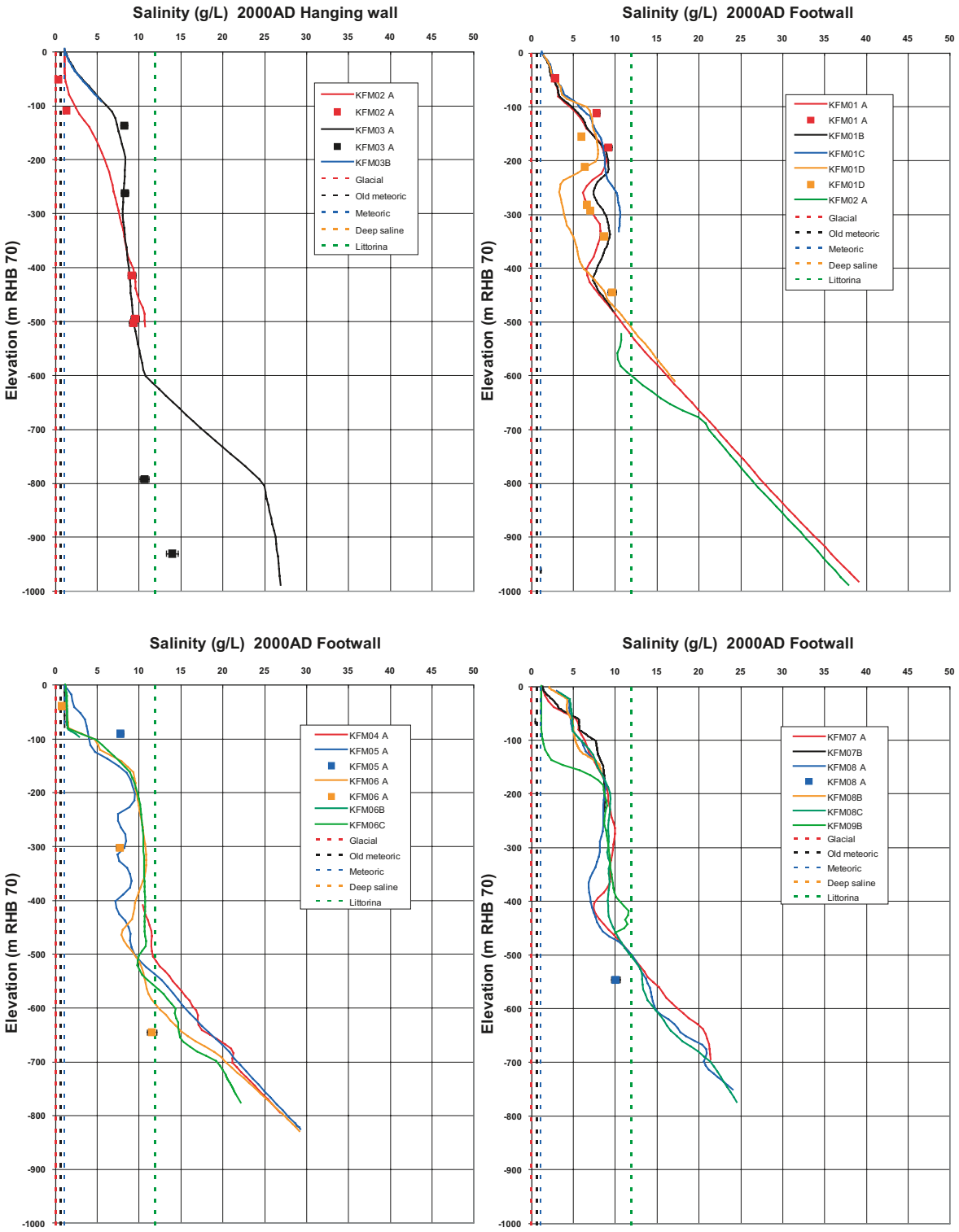

Figure 8-46. *Comparison between the deterministic base model simulation (solid lines) and measured salinity concentrations (TDS) in the fracture system (filled squares) for different groups of calibration boreholes. The error bars on the measured data indicate the laboratory analytical error. The dashed lines show the specified concentration of TDS in the reference waters.*

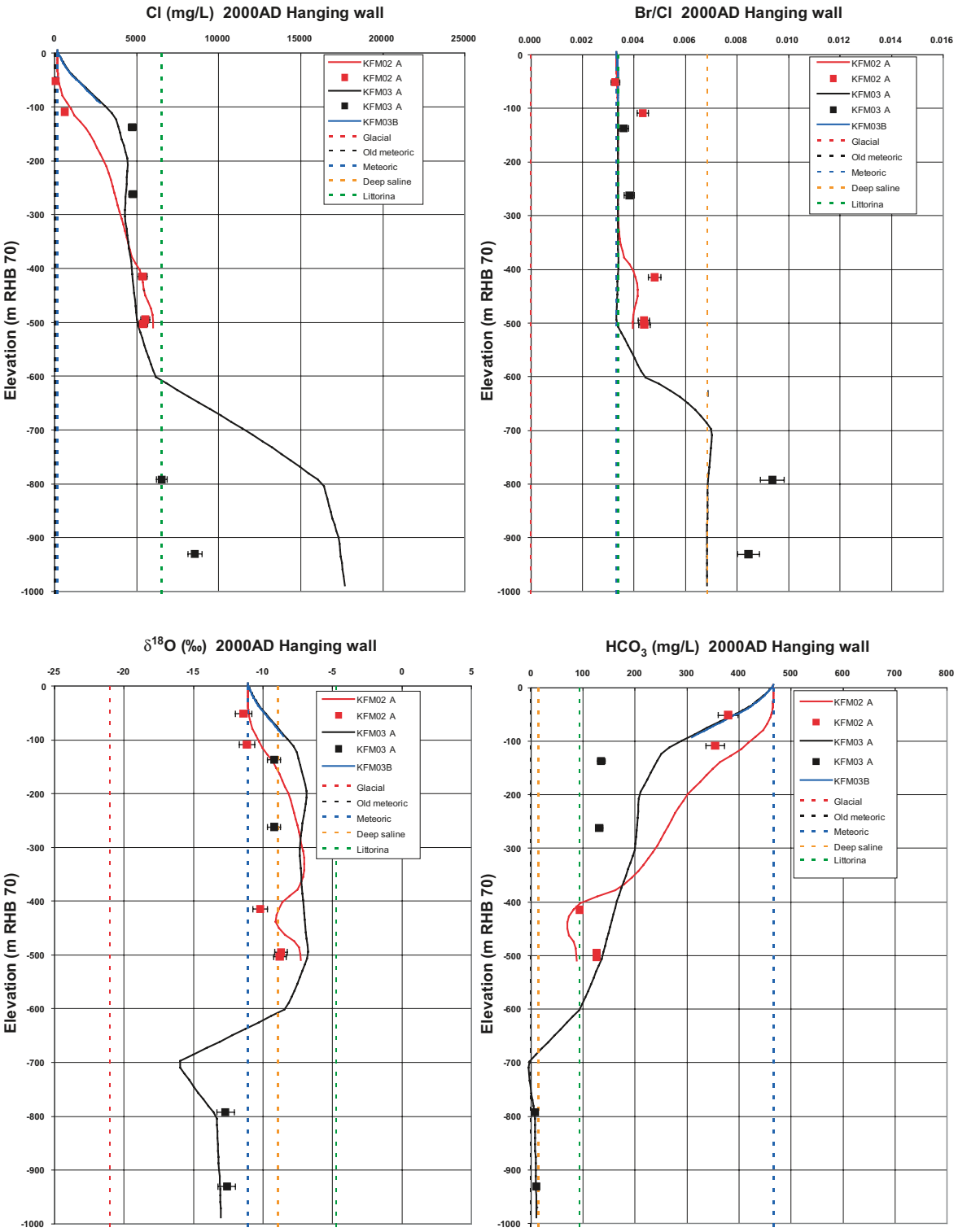

Figure 8-47. *Comparison between the deterministic base model simulation (solid lines) and measured concentrations of Cl, Br/Cl, $\delta^{18}O$ and HCO_3 in the fracture system (filled squares) for boreholes in the hanging wall of A2. The error bars on the measured data indicate the laboratory analytical error. The dashed lines show the specified concentration of Cl, Br/Cl, $\delta^{18}O$ and HCO_3 in the reference waters.*

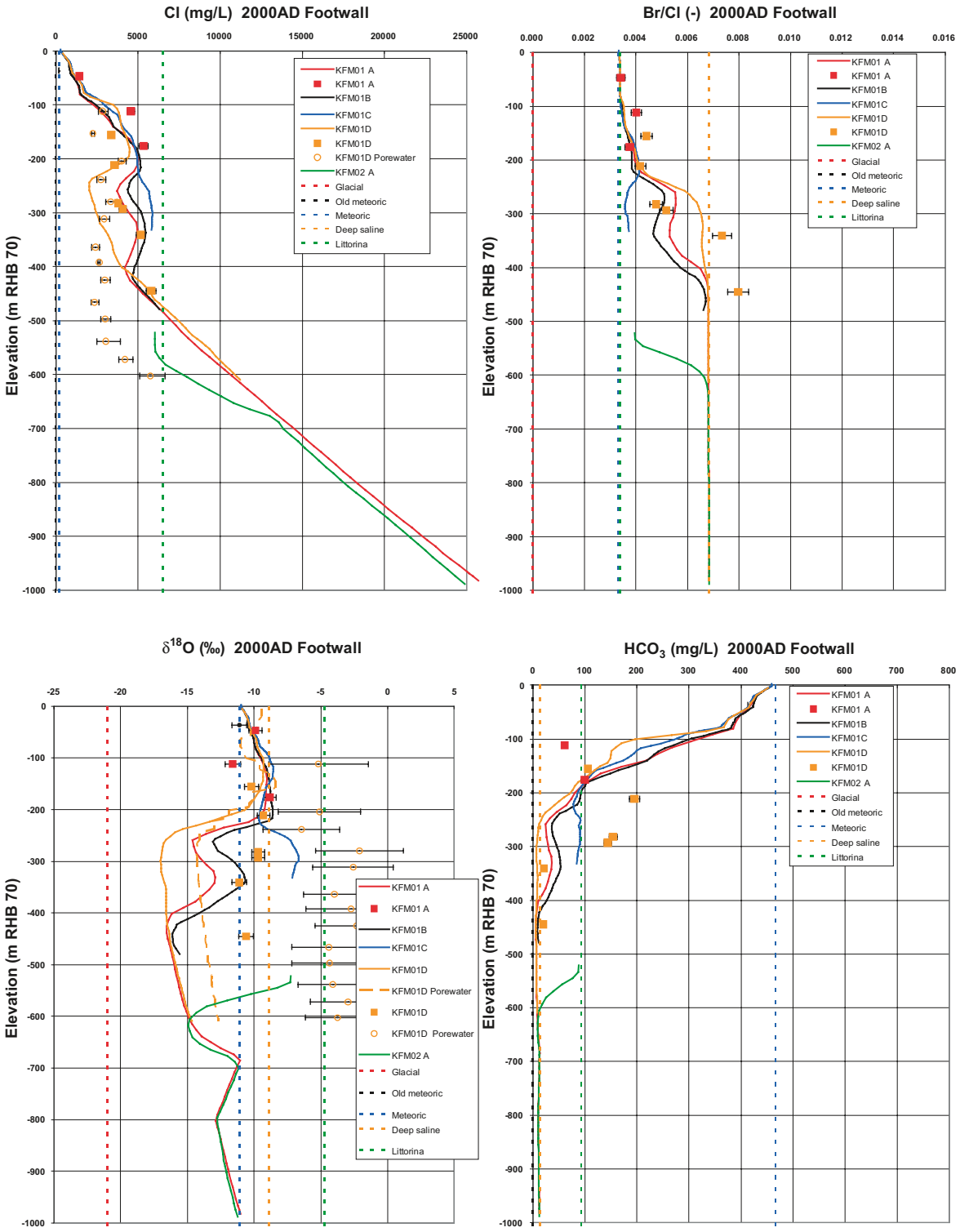

Figure 8-48. *Comparison between the deterministic base model simulation (solid lines) and measured concentrations of Cl, Br/Cl, $\delta^{18}O$ and HCO_3 in the fracture system (filled squares) for the first set of bore-holes in the footwall of A2. The error bars on the measured data indicate the laboratory analytical error. The dashed lines show the specified concentration of Cl, Br/Cl, $\delta^{18}O$ and HCO_3 in the reference waters.*

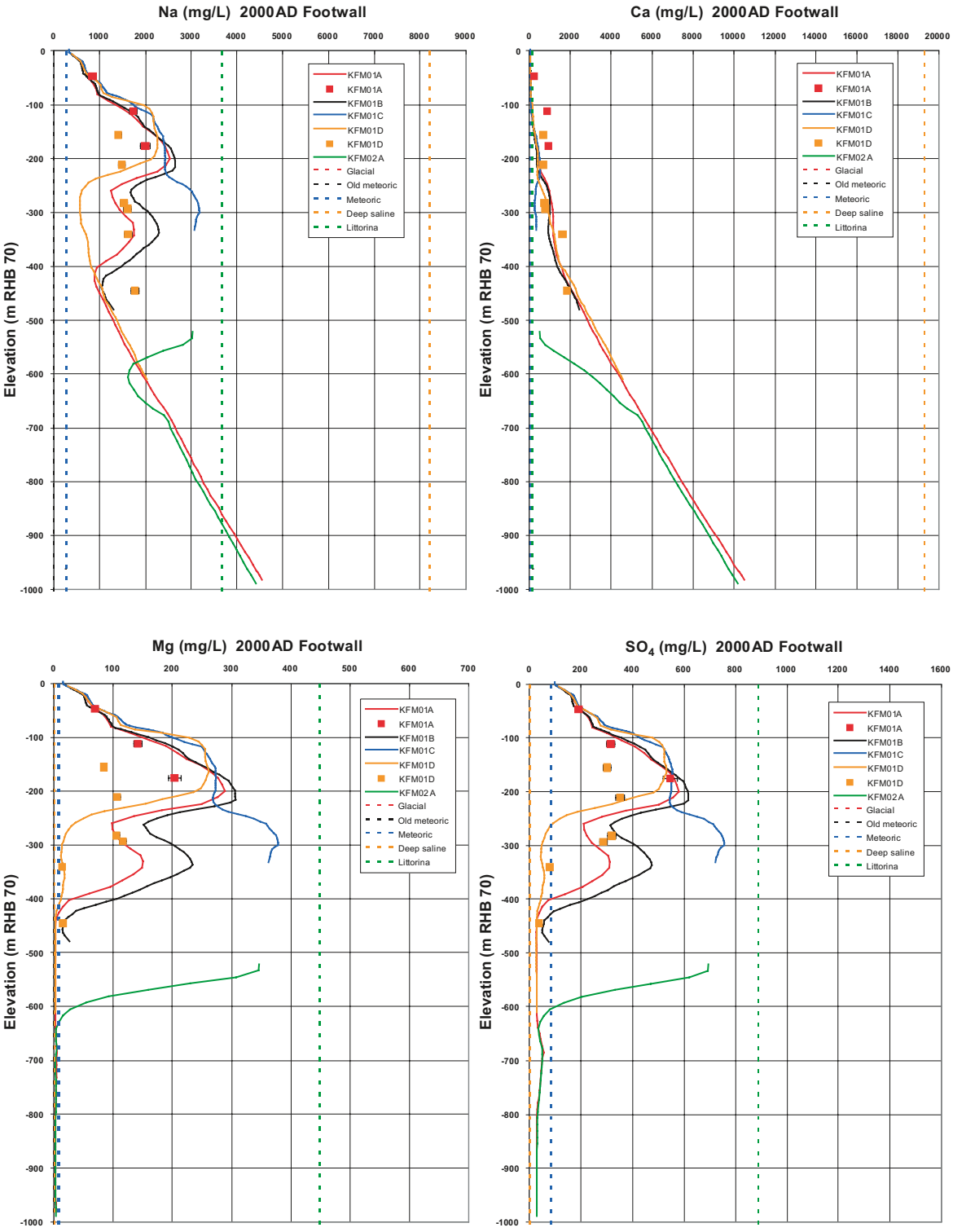

Figure 8-49. *Comparison between the deterministic base model simulation (solid lines) and measured concentrations of Na, Ca, Mg and SO_4 in the fracture system (filled squares) for the first set of boreholes in the footwall of A2. The error bars on the measured data indicate the laboratory analytical error. The dashed lines show the specified concentration of Na, Ca, Mg and SO_4 in the reference waters.*

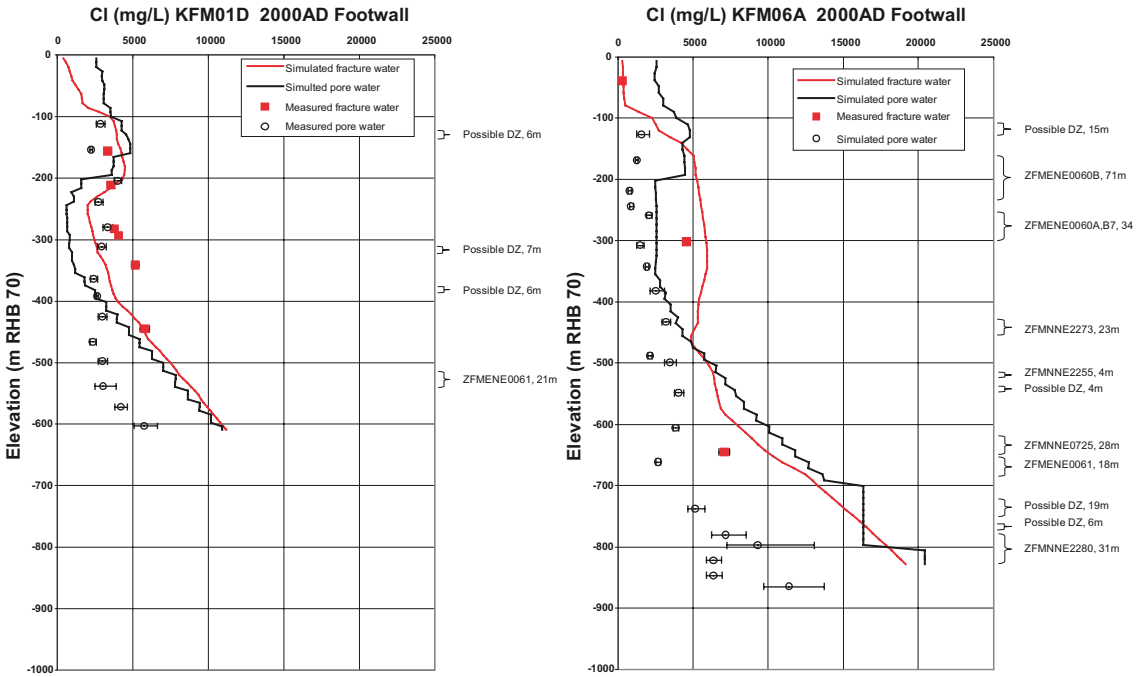

Figure 8-50. *Comparison between the deterministic base model simulation and measured concentrations of Cl in the fracture water and porewater for boreholes KFM01D and KFM06A both in the footwall of A2. The fracture water data are plotted as filled squares and the porewater data are plotted as open circles. The error bars on the fracture data only indicate the laboratory analytical error, while in the porewater they also reflect the uncertainty in the porosity of the rock sample. The red lines show the simulated values in the fracture system, and the black lines show the simulated values in the matrix blocks.*

For completeness, predicted profiles of other major ions, Na, Ca, Mg and SO_4, are shown in Figure 8-49 for some of the boreholes in the footwall of zone A2. These results are also in reasonable agreement, despite that the model only includes mixing and does not address reactions such as cation exchange.

Considering the depths at which Mg was detected rather than the absolute magnitudes of concentration measured, the model is in good agreement with the measurements. *Littorina Sea Water* apparently penetrated only the top 300–400 m of the bedrock in the footwall of zone A2, whereas it seems to have penetrated the top 500–600 m of the bedrock in the hanging wall of this zone.

Examples of the predictions of Cl in the porewater compared with the fracture system are shown for KFM01D and KFM06A in Figure 8-50. The matches are not perfect for the *deterministic base model simulation*, but the model predicts the observed higher salinity in the fracture system relative to the matrix porewater.

8.7 Bedrock hydrogeological model

The bedrock in the Forsmark area has been thoroughly characterised with both single-hole and cross-hole (interference) tests. Constant-head injection tests and difference flow logging pumping tests have been used in parallel to characterise the fracture properties close to the boreholes, and interference tests have been used for larger-scale studies. The overall experience from these investigations is that the anisotropy in the geological model effectively governs the pathways for flow at all depths. There is a considerable depth trend in deformation zone transmissivity and in the conductive fracture frequency in bedrock in between the deformation zones, where the uppermost part of the bedrock is found to be significantly more conductive than the deeper parts.

The left picture in Figure 8-51 illustrates the water yield capacity of the well-connected network of high-transmissive structures in the upper part of the bedrock within the target volume. In contrast, the right picture suggests that the bedrock at repository depth within the target volume contains a

Figure 8-51. *Two key features of the bedrock in the target area at Forsmark. Left: High water yields are often observed in the uppermost c. 150 m of the bedrock. Right: The large number of unbroken drill cores gathered at depth support the observation of few flowing test sections in the deeper bedrock.*

low frequency of open fractures. Indeed, the groundwater flow is found to be close to the percolation threshold in a large part of the north-western part of the candidate area. The spatial extent of these two observations/phenomena was hypothesised in modelling stage 2.2. The validity of the hypotheses was confirmed in modelling stage 2.3 by means of new boreholes, single-hole hydraulic tests and interference tests.

Deformation zones (HCD)

The following hydrogeological model has been suggested for the deterministically modelled deformation zones.

- The geological division of the deterministically modelled deformation zones into major sets and subsets is useful from a hydrogeological point of view. Most of these structural entities are steeply dipping and strike WNW-NW, NNW and NNE-NE-ENE; one is gently dipping (G).
- All deformation zones, regardless of orientation (strike and dip), display a substantial decrease in transmissivity with depth. The data suggest a contrast of c. 20,000 times for the uppermost one kilometre of the bedrock, i.e. more than four orders of magnitude. Hydraulic data below this depth are lacking.
- The lateral heterogeneity in transmissivity is also substantial (a few orders of magnitude) but more irregular in its appearance.
- Figure 8-14 suggests that the highest transmissivities within the candidate area, regardless of depth, are found among the gently dipping deformation zones. The gently dipping zones are at a high angle to the minimum principal stress (σ_{3v}) but also sub-parallel to both the first (maximum, σ_{1H}) and second principal stresses (σ_{2h}). The hypothesis that the deformation zone transmissivity on a regional scale is affected by the anisotropy in the stress field is supported by the steeply dipping deformation zones that strike WNW and NW. These two categories of deformation zones are sub-parallel to the azimuth of σ_{1H} and have, relatively speaking, higher mean transmissivities than steeply dipping deformation zones in other directions.

Bedrock in between deformation zones (HRD)

The following hydrogeological model has been suggested for the bedrock in between the deterministically modelled deformation zones.

- The geological division of the bedrock in between the deterministically modelled deformation zones into fracture domains is useful from a hydrogeological point of view.
- The conductive fracture frequency shows very strong variations with depth, and a discrete network model for conductive fractures within the target volume is adopted that is split into three layers; above 200 m depth, between 200 and 400 m depth, and below 400 m depth.
- The hydraulic character of fracture domains is also affected by the structural anisotropy; it is dominated by the gently dipping HZ set, and with only a small contribution from the steeply dipping NNE and possibly NE sets. However, the depth trend in fracture transmissivity for the fracture domains is not as conclusive as for the deformation zones. Moreover, there is no obvious correlation between fracture transmissivity and normal stress on the scale of individual fractures, see Figure 8-52.
- The sparse number of steeply dipping flowing fractures at depth within the target volume suggests that fractures associated with the gently dipping HZ set may be fairly long (large) in order to form a connected network.
- Available hydrogeological (structural-hydraulic) data do not falsify the working hypothesis that the size and intensity of *potentially flowing fractures* can be approximated through the use of a *single* power-law relationship, i.e. a tectonic continuum.

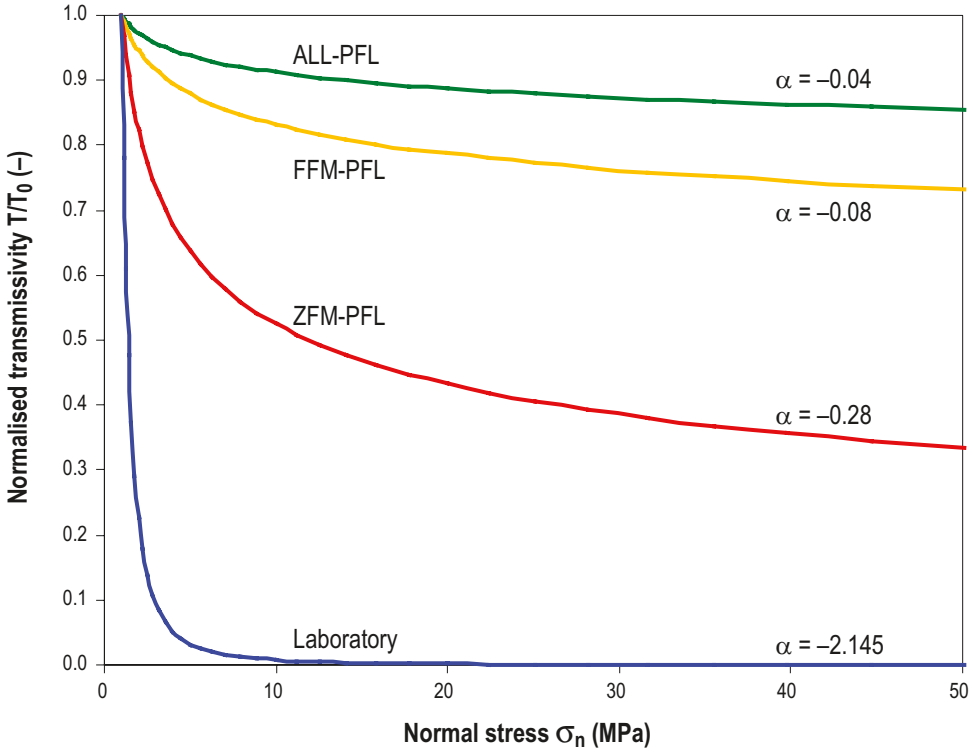

Figure 8-52. *Comparison of the trend lines used to establish a fit for a power-law relationship between transmissivity T and normal stress σ_n to the PFL-f transmissivity data. α equals the slope of the relationship between log (T) versus log (σ_n). Comparison of the value of α for the empirical equation that links stress and transmissivity shows that shows that there is poor agreement between the in situ values for α (0.04 to 0.28) and the laboratory value (1 to 2.145).*

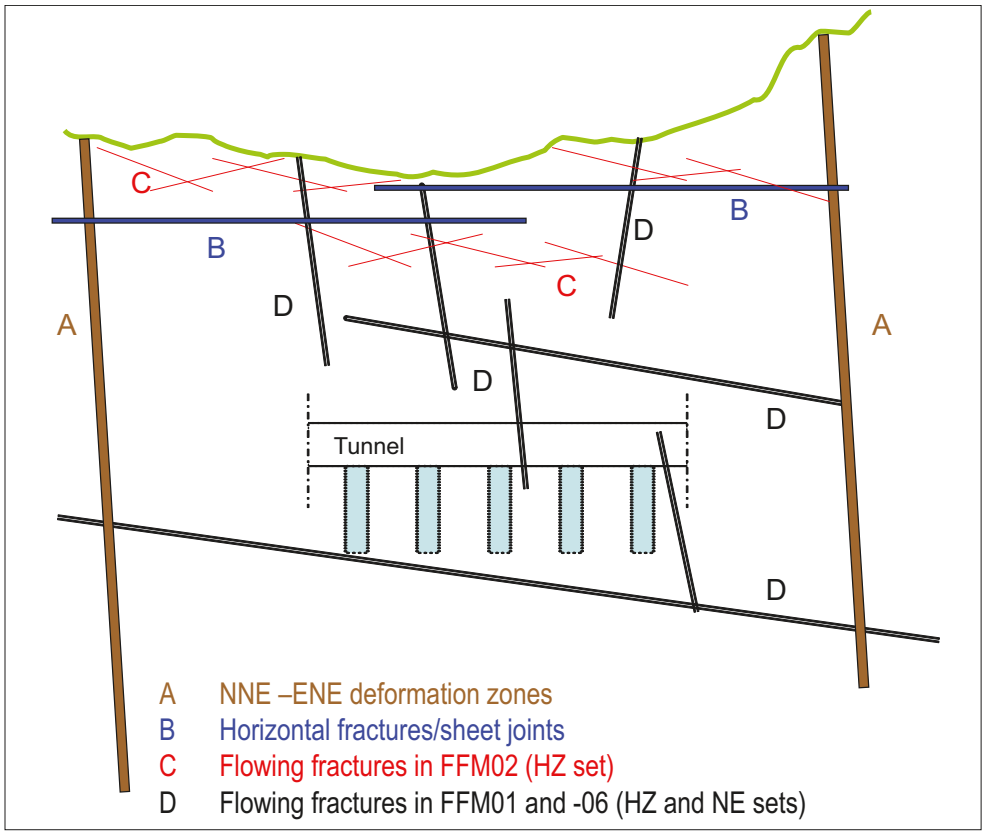

Figure 8-53. *Cross-section cartoon summarising the hydrogeological conceptual model of the bedrock within the target volume at Forsmark.*

Target volume

The cross-section cartoon in Figure 8-53 summarises the key components of the conceptual model of the bedrock hydrogeology in the target volume at Forsmark. The flow at repository depth in fracture domains FFM01 and FFM06 is probably channelised in the sparse network of connected fractures, **D**, which consists of two fracture sets more or less, HZ and NE. The HZ fracture set is interpreted to be longer and probably more transmissive than the NE set. **D** connects to **A** and **C**, where **A** represents the steeply dipping NNE-ENE deformation zones, which are abundant but hydraulically heterogeneous, and **C** represents the intensely fractured fracture domain FFM02, which lies on top of **D**. The groundwater flow in **C** is dominated by the HZ fracture set, which occurs with a high frequency. More importantly, **C** is intersected by several extensive, horizontal fractures/sheet joints, **B**, which can be very transmissive. **B** and **C** and the outcropping parts of **A** probably form a shallow network of flowing fractures. The network is interpreted to be highly anisotropic, structurally and hydraulically. Together with **D**, which is close to the percolation threshold, the network create a hydrogeological situation that here is referred to as a shallow bedrock aquifer (cf. section 8.4.4) on top of a thicker bedrock segment with aquitard type properties.

8.7.1 Visualisations for interpretation of hydrochemistry

Figure 8-54 shows a 2D cross section parallel to the shoreline with chloride concentrations for the *deterministic base model simulation*. The blue line is a regional water divide, which is used as the upstream flow boundary (cf. section 8.2). The black arrows indicate the directions of the resultant Darcy fluxes in the plane of the cross section. (The discretisation is finer within the local model domain, see Figure 8-3). The directions of the Darcy fluxes vary, but the mean direction is essentially perpendicular to the cross section pointing towards the shoreline, i.e. parallel with the topographic gradient. The red lines indicate flow paths for 100 particles starting at the intersection between the cross section and zone A2 (grey shade). The majority of the upstream flow paths recharge locally at different places downstream the regional water divide. The downstream flow paths that start between 150 and 550 m depth stay close to zone A2, whereas the downstream flow

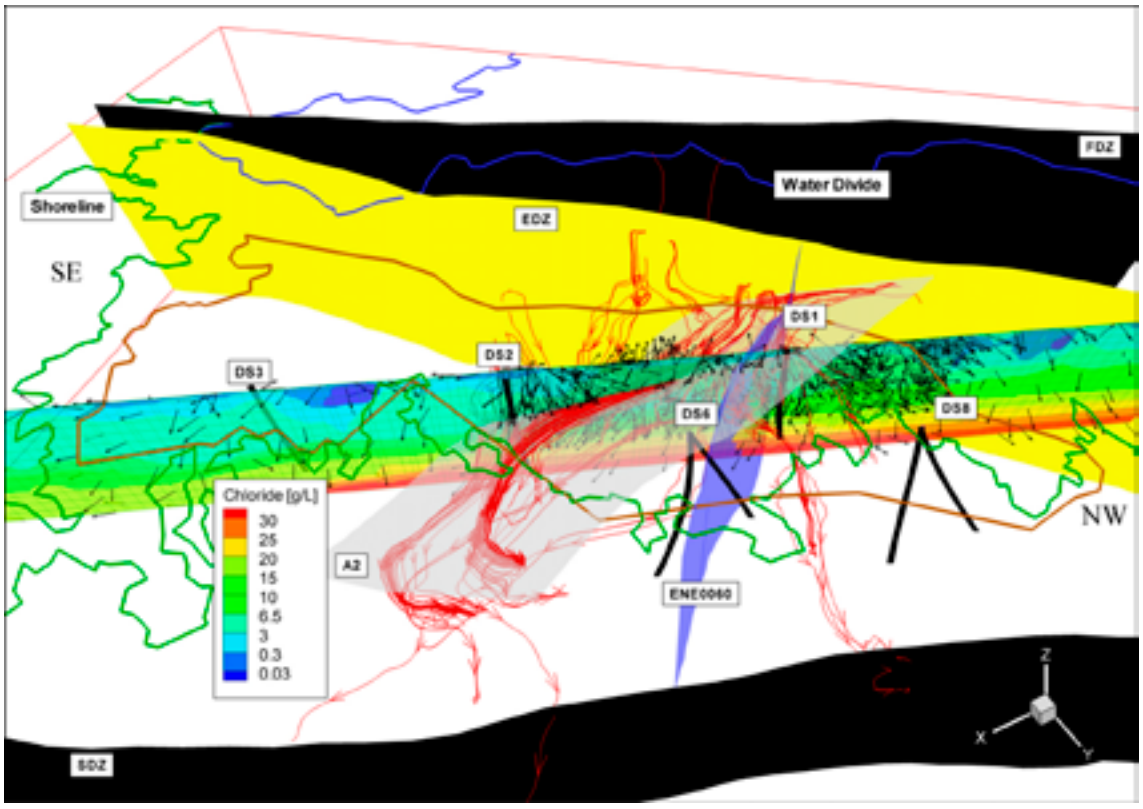

Figure 8-54. *A 1,200 m deep 2D cross section parallel to the shoreline (green line) showing chloride concentrations for the deterministic base model simulation. Black arrows indicate the directions of the Darcy flux along the plane of the cross section. Red lines indicate backward (recharge) and forward (discharge) flow paths for 100 particles starting at the intersection between the cross section and zone A2. The solid blue line is the upstream boundary of the model domain, which coincides with a regional water divide.*

paths that start above c. 150 m depth follow the "sheet joint features". In summary, Figure 8-54 suggests that the groundwater flow system in the Forsmark area is highly heterogeneous and to a large extent structure-controlled. Detailed interpretations of hydrochemical data using 2D cross sections must therefore be handled with care.

Figure 8-55 shows simulated concentrations of Cl and $\delta^{18}O$ in the plane of the 2D cross-section shown in Figure 8-54. The obvious differences between the footwall and the hanging wall to zone A2 are due to the structural-hydraulic differences between the bedrock segments and to the differences these cause regarding the initial conditions at 8000 BC. It is noted that the results shown in Figure 8-55 represent the *deterministic base model simulation*. The effect of varying the properties of the hydrogeological DFN model and the lateral deformation zone heterogeneity, i.e. when $\sigma_{\log(T)} = 0.632$ in Equation (8-3), is discussed in section 8.8.

The flat topography of the Forsmark area and the recent withdrawal of the Baltic Sea are examples of important factors in determining the surface and near-surface hydrochemistry. Marine remnants in the Quaternary deposits, as well as modern sea water transgressions, are strongly influencing the hydrochemistry, especially in areas at low altitude close to the coast. However, hydrological and chemical observations in the surface water and the shallow groundwater indicate that there is probably little ongoing discharge of deep saline waters into the superficial freshwater system located above the horizontal sheet joints within the area modelled as a shallow bedrock aquifer (cf. the description of the hydrogeological conditions beneath the middle of Lake Bolundsfjärden in section 4.3.1, for an example). However, outside this area there are examples of observations that possibly indicate deep saline signatures in the groundwater at relatively shallow depths in the Quaternary deposits (section 4.3.1). One such area is Lake Gällsboträsket, which coincides with a depression along the trace line of the Eckarfjärden deformation zone, see Figure 5-2. Here, the concentration of chloride in the discharging brook indicates an influence from deep groundwater of older origin than the Littorina Sea Water.

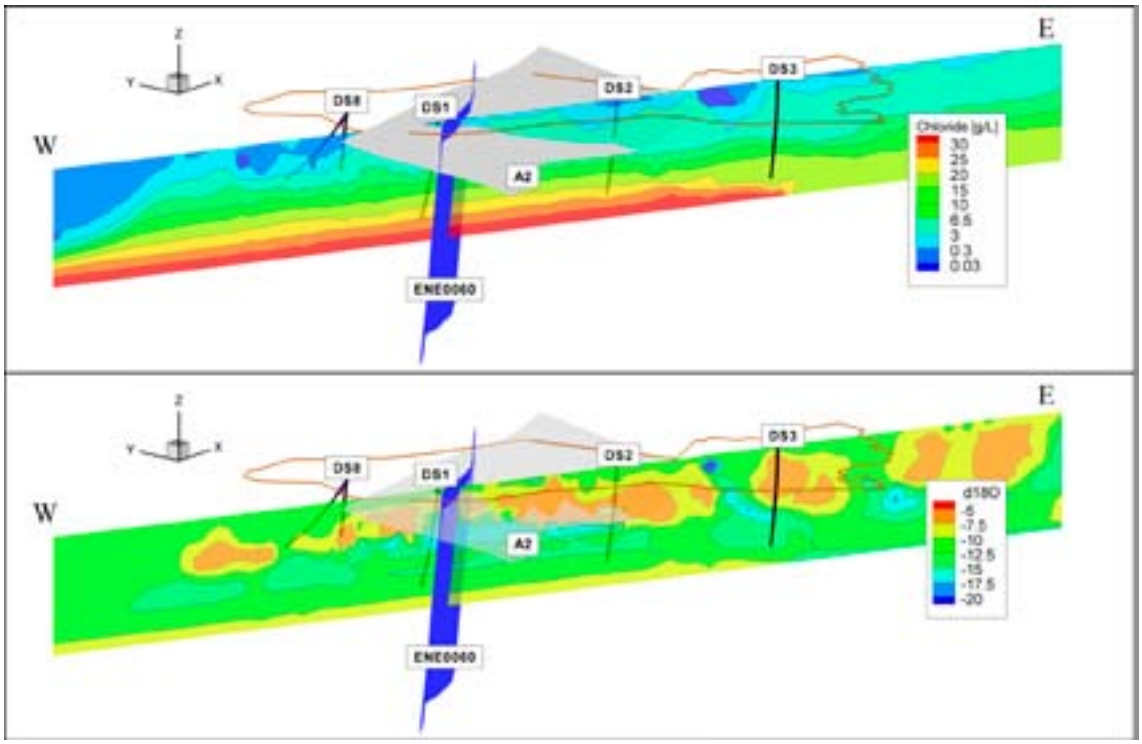

Figure 8-55. *Perspective view towards NE showing simulated concentrations of Cl and $\delta^{18}O$ in the plane of the 1,200 m deep 2D cross-section shown in Figure 8-54.*

Figure 8-56 and Figure 8-57 shows the predicted present-day spatial distribution of chloride at the surface and at 50 m depth, respectively. Table 8-11 shows the magnitudes of the predicted concentrations together with the ranges of the measured concentrations measured in the till.

The predictions shown in Table 8-11 are calculated with the *deterministic base model simulation* using a grid size of 25 m. The magnitude of discrepancies in relation to the measured data may perhaps be considered acceptable for comparing a single realisation of the flow model without uncertainties with borehole hydrochemical data that fluctuates in space and over recordings made at different dates.

Table 8-11. Predicted and measured chloride concentrations (mg/L) in the till layer below the lake sediments in Lake Bolundsfjärden, Lake Fiskarfjärden, Lake Eckarfjärden, Lake Gällsboträsket and the Baltic Sea. Predicted concentrations at 50 m depth below these water bodies are also shown. The predicted concentrations represent the *deterministic base model simulation*.

Object	Predicted maximum value of Cl in the till and at 50 m depth	Range of the Cl data in the till	Monitoring well
B ; L. Bolundsfjärden	2,250/4,000+	3,520–4,340	SFM0023
F ; L. Fiskarfjärden	2,250/2,750	947–1,300	SFM0022
E ; L. Eckarfjärden	250/250	277–375	SFM0015
G ; L. Gällsboträsket	1,000/1,750	2,160–2,340	SFM0012
Baltic Sea	3,000/4,000+	690–3,940	SFM0024, –25, –65, –81

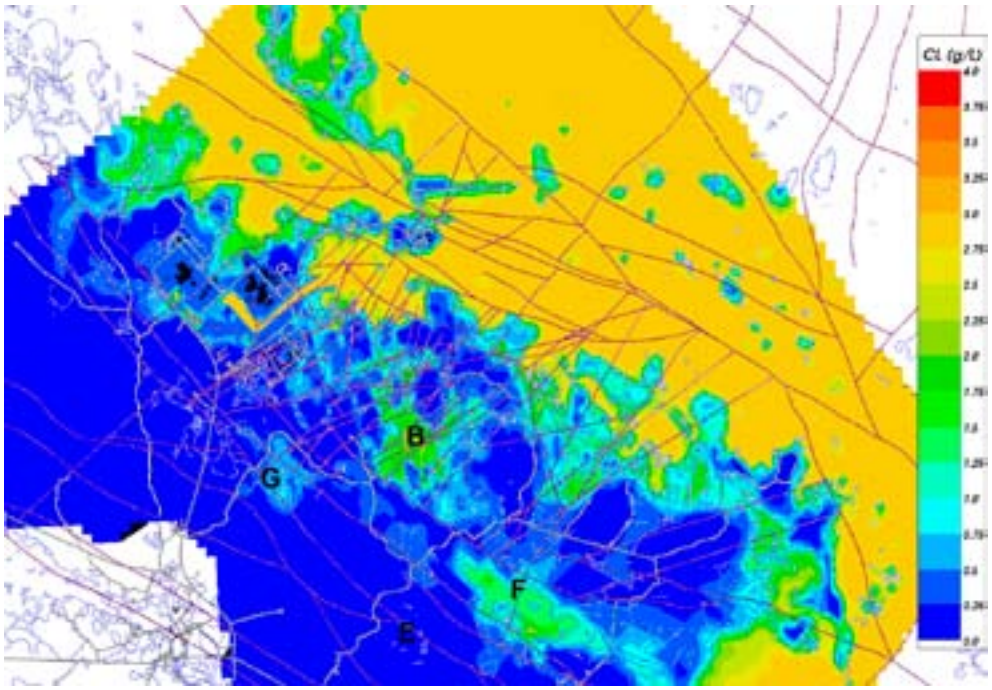

Figure 8-56. *Predicted spatial distribution of chloride at the surface using the deterministic base model simulation. B = Lake Bolundsfjärden, F = Lake Fiskarfjärden, E = Lake Eckarfjärden, G = Lake Gällsboträsket.*

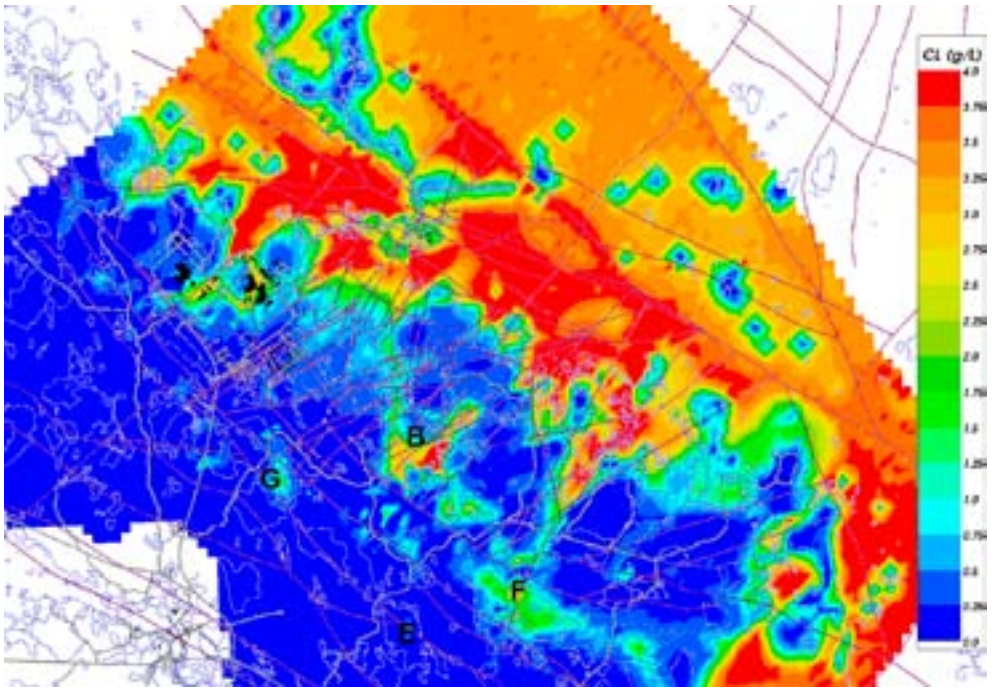

Figure 8-57. *Predicted spatial distribution of chloride at 50 m depth using the deterministic base model simulation in B = Lake Bolundsfjärden, F = Lake Fiskarfjärden, E = Lake Eckarfjärden, G = Lake Gällsboträsket. Data from hydraulic tests and analyses of water compositions in the till below the lakes indicate that the waters sampled below B and F are probably stagnant and of a marine origin (Littorina Sea Water). In contrast, the outflow rate of chloride in the brook that discharges from G suggests an influence of deep saline groundwater. This observation is supported by the chemical signature of the groundwater sampled in the monitoring well SFM0057 located at the edge of the Gällsboträsket.*

8.7.2 Visualisations for interpretation of flow and solute transport

Particle tracking is a useful tool for interpretation of groundwater flow paths and calculation of solute transport flow path properties. Figure 8-58 and Figure 8-59 show particle tracks for the *deterministic base model simulation*. The particles were released at 500 m depth within the target volume with one particle starting every 100 m on a regular mesh over an area of about 1.7 km by 1.7 km. There are two distinct types of flow paths followed, one set of shorter flow paths that flow toward the SFR buildings to the north, and a second set of longer flow paths that move downwards before moving to the Baltic Sea to the east.

The shorter flow paths are generally associated with the western side of the release area and travel upward until they encounter the "sheet joint features", then track along these until they discharge around the intersect with the Singö deformation zone, some of which cross the zone. The long flow paths starting in the eastern side of the release area tend to move horizontally or downward, as shown in Figure 8-59, until they encounter the deformation zones that slope gently to the south-east. Again, a number of particles appear to go beyond the Singö deformation zone. These particle-tracking results highlight the importance of the property assignment of the Singö deformation zone in influencing the discharge areas. It should be noted that pumping in the SFR repository was not implemented in the *deterministic base model simulation*.

Figure 8-60 shows another picture of particle tracks for the *deterministic base model simulation* at 2000AD. Here, 447 particles were released at 450 m depth within a sub area located in the centre of the target volume, with one particle starting every 40 m on a regular mesh. One of the particle tracks, #228, is coloured red and the trajectory of this flow path is shown in a perspective view in Figure 8-61, where the different colours represent the structural elements that the particle encounters on its way to the exit point, i.e. fracture domains, deformation zones and sheet joint features. In these two figures, the blue line denotes the shoreline and the greenish polygon the candidate area.

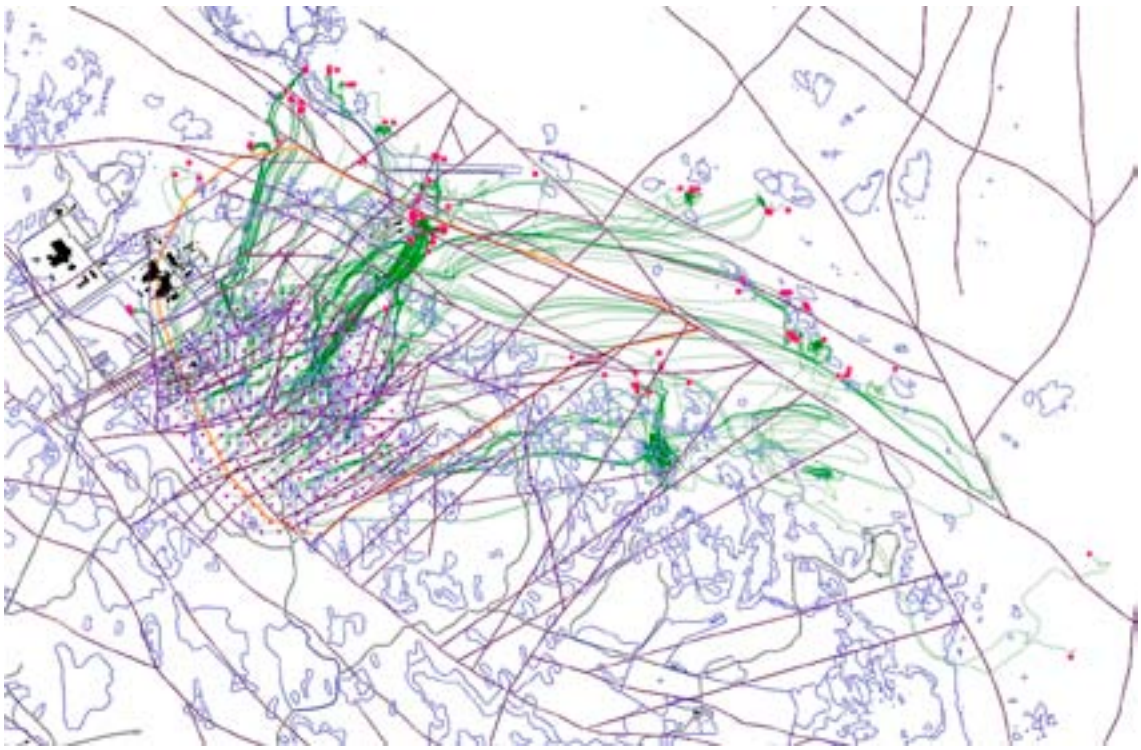

Figure 8-58. *Plane view of the target area with predicted flow paths and exit locations at the surface (red dots) of c. 300 particles using the base model simulation in ConnectFlow. The particles were released in a 100 m by 100 m mesh at 500 m depth. The exit locations are marked with red dots. The orange line represents the perimeter of the assumed extent of the shallow bedrock aquifer.*

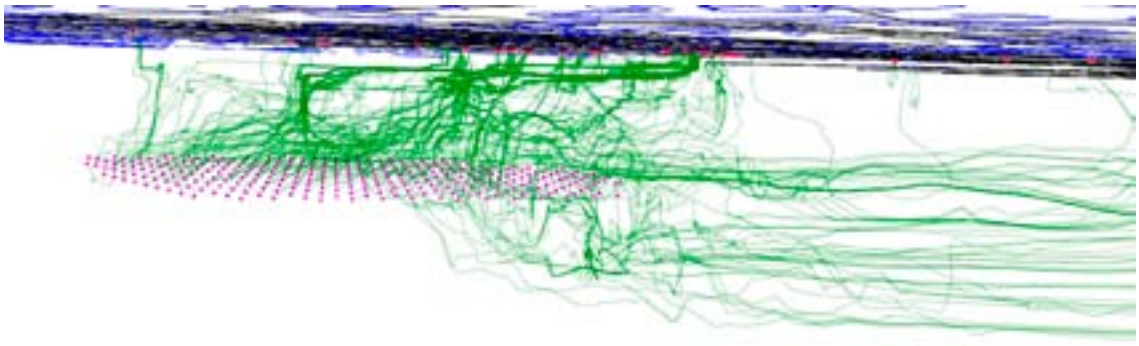

Figure 8-59. *A perspective view through the subsurface towards the north-west showing the impact of the high horizontal transmissivity of the shallow bedrock aquifer on the particle tracking shown in Figure 8-58.*

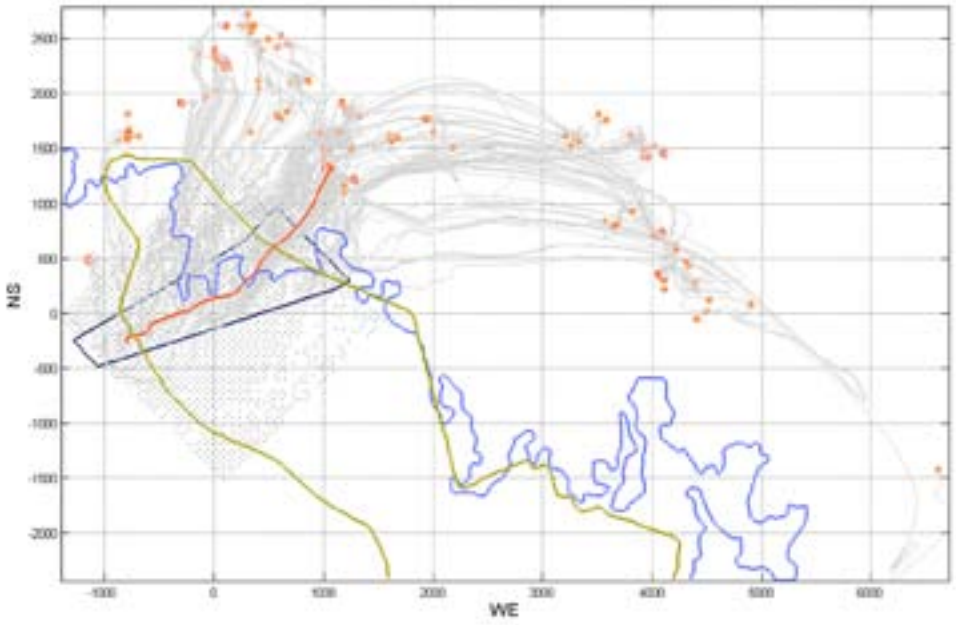

Figure 8-60. *Visualisation of 447 particles released at 450 m depth within a sub area located in the centre of the target volume with one particle starting every 40 m on a regular mesh. One of the particle tracks, #228, is coloured red and the trajectory of this flow path is shown in a perspective view in Figure 8-61.*

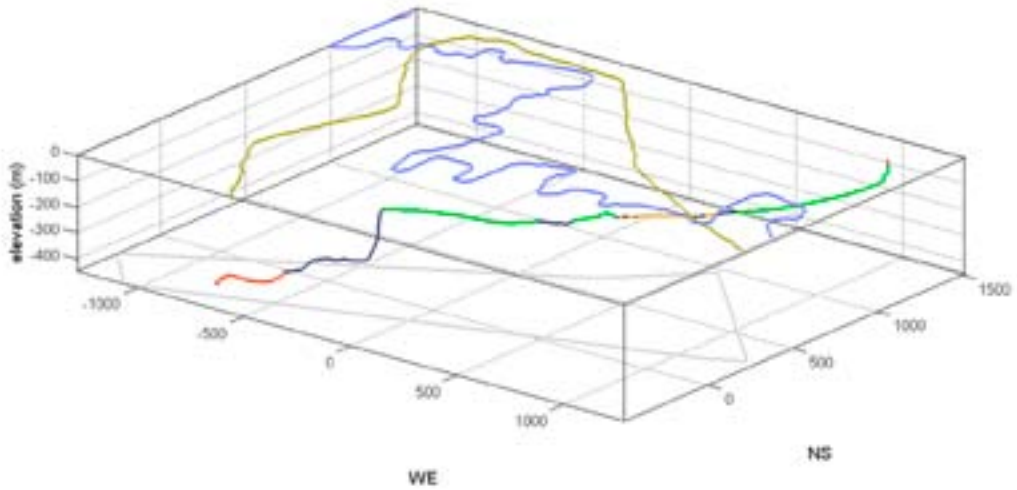

Figure 8-61. *The flow path of particle #228 shown in Figure 8-60 is here coloured with regard to the structural elements that the particle encounters on its way to the exit point, i.e. red for fracture domain FFM01 and yellow for FFM06, blue for various deformation zones, green for different sheet joint features and brown for the Quaternary deposits.*

Figure 8-62 shows the hydraulic gradients in the ECPM model along the flow path of particle #228. The gradients are coloured with regard to the structural elements shown in Figure 8-61. Figure 8-63 shows a scatter plot of the hydraulic gradient for particle #228 versus the geometric mean hydraulic conductivity. The dots in the scatter plot are coloured with regard to elevation (m RHB 70).

Figure 8-62 and Figure 8-63 show that the hydraulic gradients along the visualised flow path are low ($2 \cdot 10^{-5}$ to $7 \cdot 10^{-3}$ m/m). The highest values of the hydraulic gradient are found in the proximity of the release position in fracture domain FFM01, where the ECPM hydraulic conductivity is low (~ 10^{-11} m/s). The lowest values of the hydraulic gradient are found in the proximity of the sheet joint features, where the ECPM hydraulic conductivity is high (~ 10^{-4} m/s). The correlation between hydraulic gradients and hydraulic conductivity, with decreasing gradient with increasing hydraulic conductivity is expected because, for a given flow path with a given flow, low-conductive parts require a higher gradient drop than high-conductive parts. However, it is emphasised that Figure 8-62 and Figure 8-63 show results for a single particle only. Chapter 10 discusses the calculated F-factor and the advective residence time for particle #228 in relation to the transport properties of the ensemble of particles shown in Figure 8-60.

Figure 8-64 shows groundwater flow vs. mid-section elevation for dilution measurements in Forsmark and Figure 8-65 shows the interpreted hydraulic gradients versus mid-section elevation for the same dilution measurements. There is an overall impression that the magnitudes of the calculated hydraulic gradient tend to be too high relative to reasonable topographically-based estimates of the regional hydraulic gradient, which is of the order of c. 1%. This viewpoint is supported by gradients obtained in the numerical simulations; see Figure 8-62 for an example.

/Nordqvist et al. 2008/ provides an examination of possible sources of error for the gradient estimation. They conclude that it is likely that gradients tend to be over-estimated. This because the flow convergence correction factor probably often is larger than the commonly assumed value of 2, due to fracture orientation and artificially increased hydraulic conductivity (negative skin) around the borehole (cf. Figure 4-8 in /Follin et al. 2007b/). Of particular importance is the transmissivity values used for estimation of hydraulic gradients and this may be the largest source of error. The transmissivity values used are obtained from different hydraulic test methods (PFL-f, PSS or

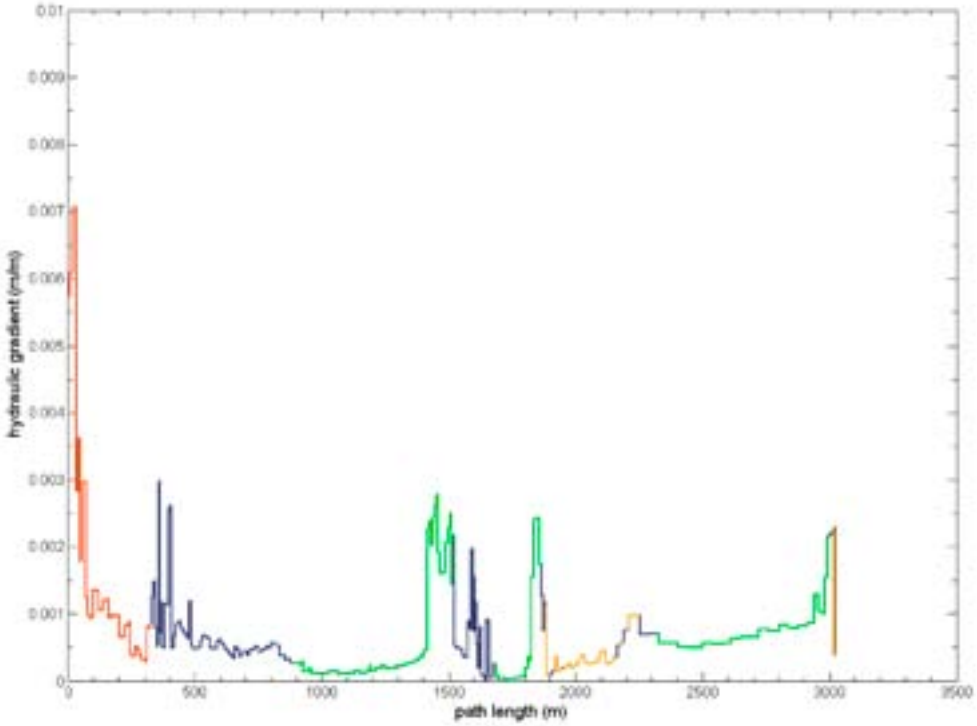

Figure 8-62. *A plot of the hydraulic gradients along the flow path of particle #228 in the ECPM model. The gradients are coloured with regard to the structural elements that the particle encounters on its way to the exit point, cf. Figure 8-61.*

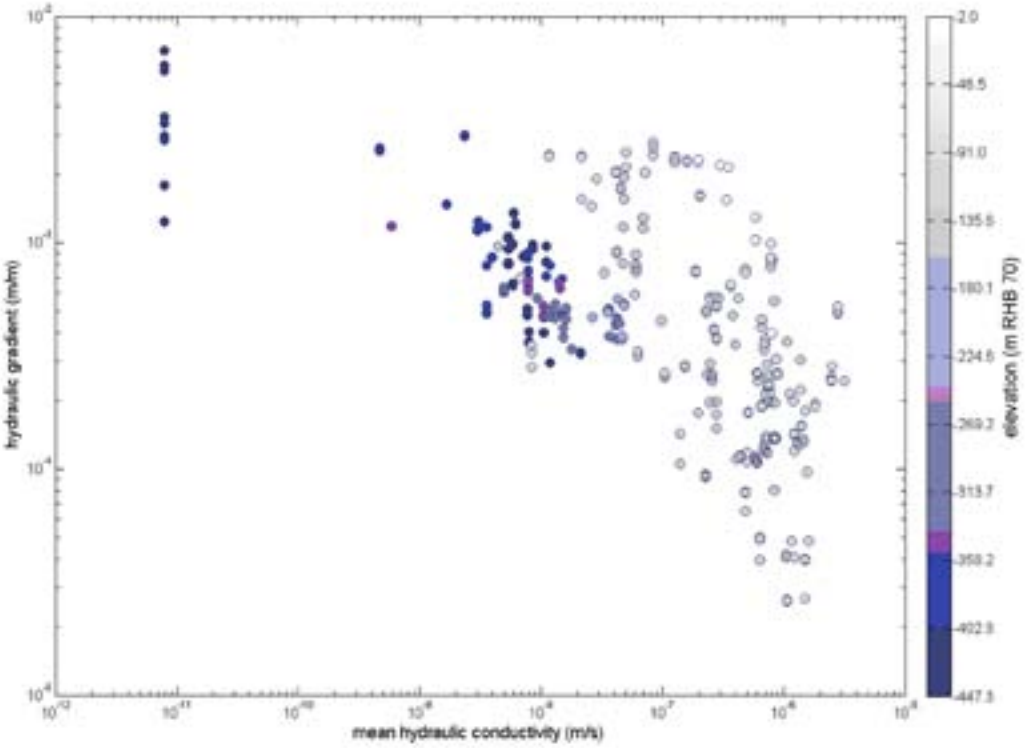

Figure 8-63. *A scatter plot of the hydraulic gradient for particle #228 versus the geometric mean hydraulic conductivity for particle #228. The dots are coloured with regard to elevation (m RHB 70).*

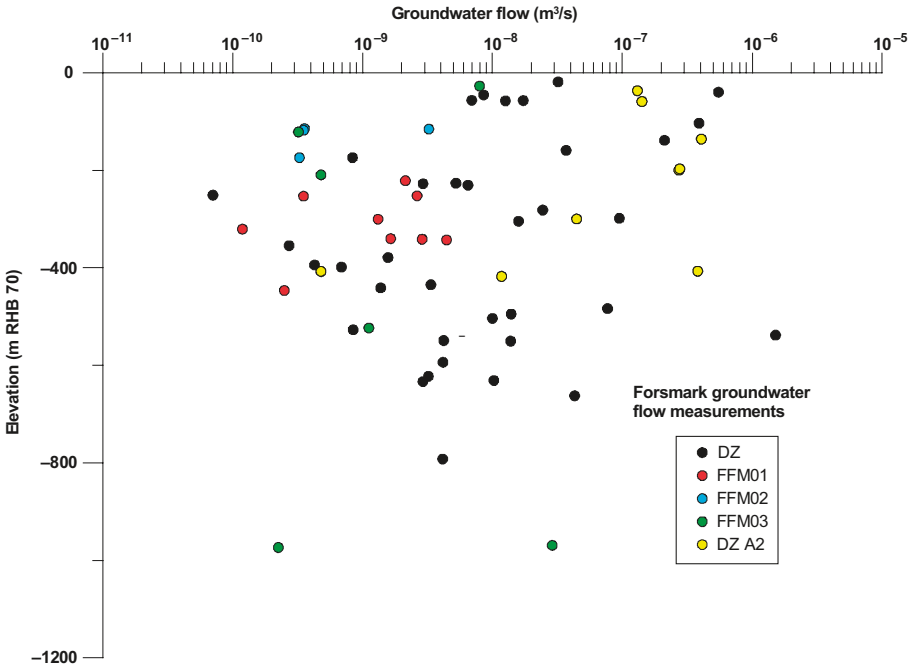

Figure 8-64. *Groundwater flow versus mid-section elevation for dilution measurements in Forsmark. Plotted points are classified into deformation zones and fracture domains. Modified after /Nordqvist et al. 2008/.*

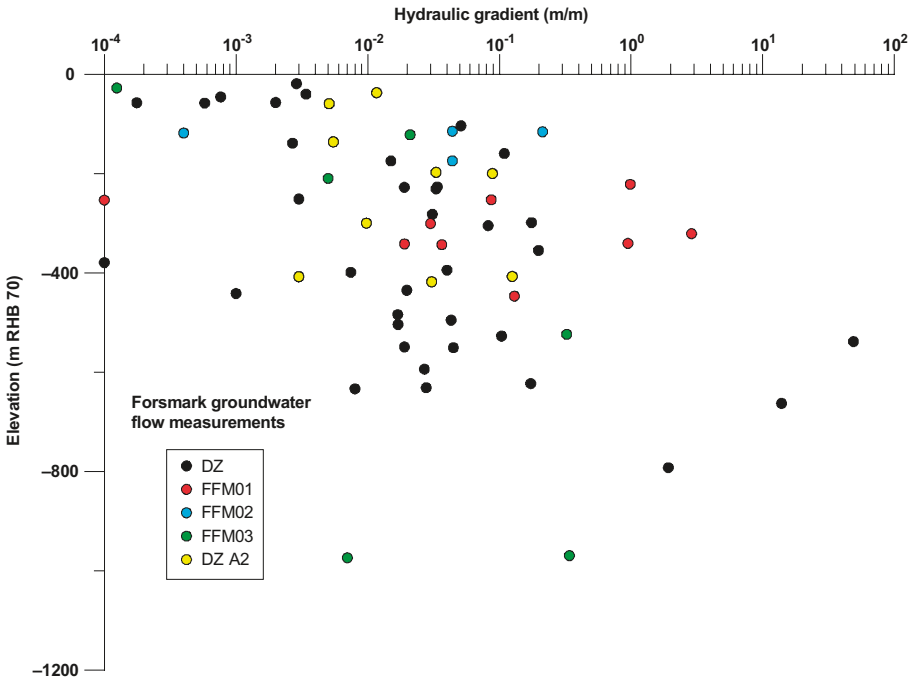

Figure 8-65. *Interpreted hydraulic gradient versus mid-section elevation for dilution measurements in Forsmark. Plotted points are classified into deformation zones and fracture domains. Modified after /Nordqvist et al. 2008/.*

HTHB). Further, independent of methods, transmissivity values are obtained during a different flow regime (radial flow) than what prevails during the tracer experiments. Reported data are often based on preliminary transmissivity estimates from then available measurements. One may argue that the relatively long-term PFL measurements provide more representative transmissivity estimates for the connected flowing path, and some support for this may also be found in available data (cf. Figure 7-2 in /Nordqvist et al. 2008/). In order to improve the hydraulic gradient estimates, the used transmissivity data should be updated using final transmissivity estimates, and preferably from PFL-f measurements if available.

8.8 Parameter sensitivity analysis

As part of the preliminary site description, a number of regional uncertainties were analysed by performing variant cases to illustrate the sensitivity of the flow model calibration to alternative concepts and parameters. Indeed, there are several uncertainties about the structural and hydraulic characteristics outside the target volume. However, the regional uncertainties studied in the preliminary site description appeared to have little significance for the near-field migration paths as demonstrated by the sensitivity analyses carried out /Follin et al. 2005/. Given the sparsely fractured bedrock at depth and the short circuit phenomenon in the shallow bedrock aquifer, this hypothesis is reinforced in the SDM. That is, groundwater flow at depth within the target area is probably not influenced by the topography neither outside nor inside the model area treated in the SDM. The regional water divide to the south of the candidate area (Figure 8-54) constitutes an effective upstream boundary.

A comprehensive uncertainty analysis with focus on parameter heterogeneity within the target volume was performed under stage 2.3 and sensitivities were evaluated for the three calibration targets B, C and D (see section 8.1.2). The number of sensitivity measures was restricted appropriately to reflect only the key sensitivities of the system, cf. /Follin et al. 2008a/.

Figure 8-66 through Figure 8-68 show three examples from the uncertainty analysis carried out with regard to laterally heterogeneous properties of the deformation zones ($\sigma_{\log(T)} = 0.632$) and the fracture domains (multiple hydrogeological DFN realisations). The three examples demonstrate that model calibration against interference data and hydrochemical data are more sensitive to parameter heterogeneity in the bedrock properties than is the model calibration against groundwater levels.

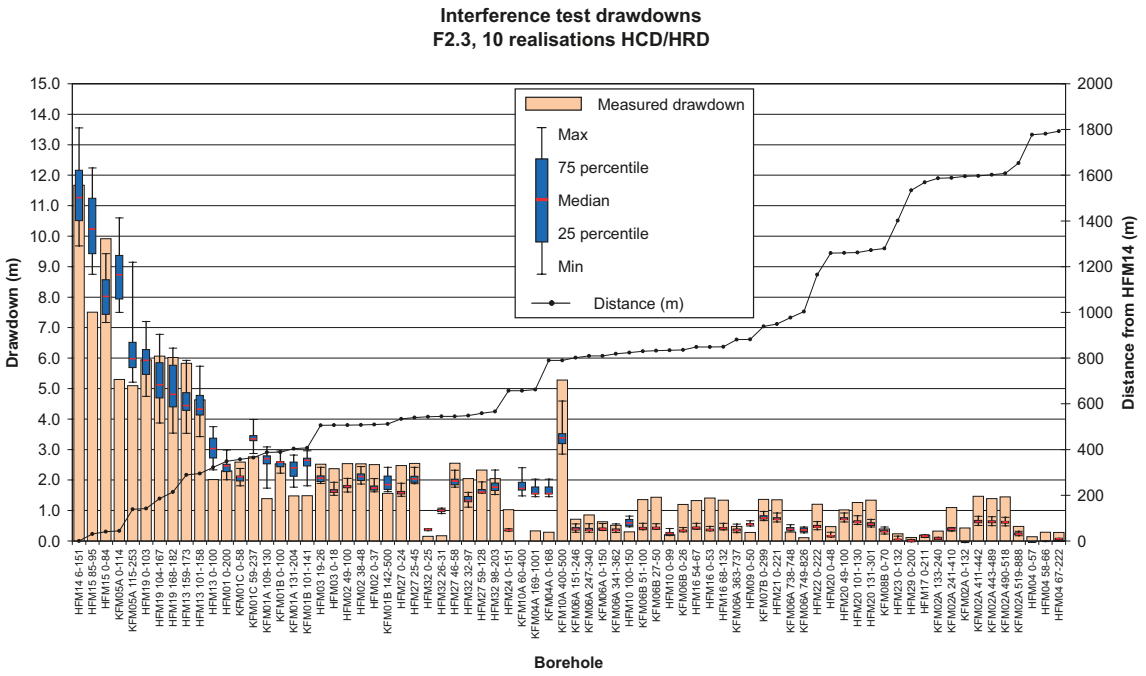

Figure 8-66. *Box-and-whisker statistics of ten stochastic model simulations showing the sensitivity of model calibration against the 2006 interference test in HFM14 to heterogeneous properties in the deformation zones and the fracture domains.*

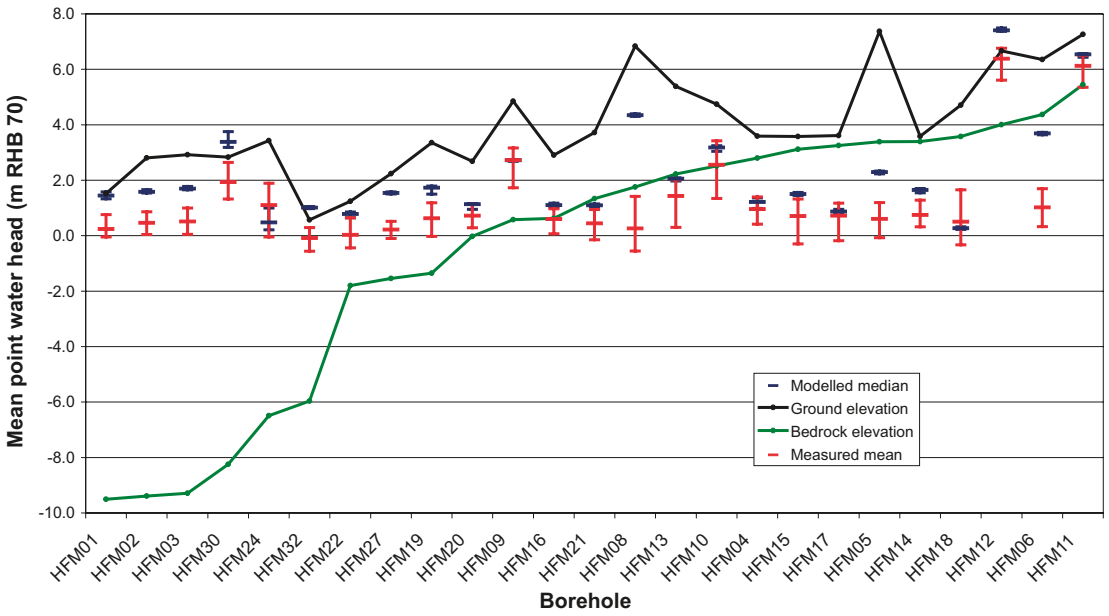

Figure 8-67. *Plot of ten stochastic model simulations (blue) showing the sensitivity of model calibration against groundwater levels measured in the percussion-drilled boreholes (red) to heterogeneous properties in the deformation zones and the fracture domains. The boreholes are ordered by increasing bedrock elevation. The simulated data are plotted as median groundwater levels with error bars to show the range between the minimum and maximum values. The measured data are plotted as mean groundwater levels with error bars to show the range of the recordings over time. The simulated groundwater levels in the boreholes within the target volume are on the average c. 0.7 m higher than the corresponding measured levels.*

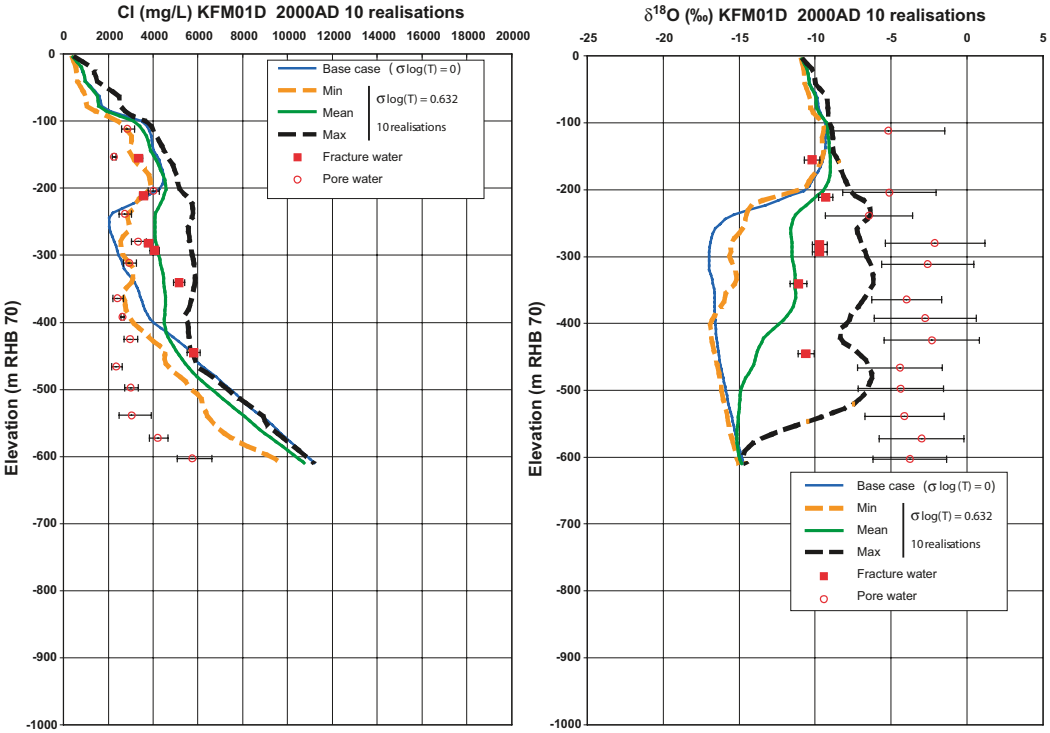

Figure 8-68. *Two plots showing measured and simulated values of Cl and $\delta^{18}O$ in the fracture water in borehole KFM01D. The fracture water data are plotted as filled red squares and the calibrated deterministic base model simulation (= a single DFN realisation and laterally homogeneous deformation zones $\sigma_{\log(T)} = 0$) is shown as solid blue lines. The open red circles represent porewater data. The green, yellow and black lines show the sensitivity to heterogeneous properties in the fracture domains and the deformation zones (= multiple DFN realisations and $\sigma_{\log(T)} = 0.632$). The error bars on the fracture water data indicate the laboratory analytical error, whereas in the porewater they reflect the uncertainty in the porosity of the rock sample. Note the greater variability in $\delta^{18}O$ vis-à-vis Cl, and the differences between fracture water $\delta^{18}O$ and porewater $\delta^{18}O$. These differences are discussed more in section 9.3.2, because it is a very strong indication that the matrix porewater has been isolated for a very long time.*

8.9 Confidence and remaining uncertainties

Model calibration is non-unique in that different combinations of parameter settings may achieve equally good and plausible matches to the test data. In the process of calibrating the numerical model against single-hole hydraulic tests, cross-hole tests, natural point-water head measurements and hydrochemical data samples, a number of lessons were learnt in terms of the key features, processes and parameters required to mimic the observed behaviour of the hydrogeological system. Sensitivities to various features and parameters had to be considered to find one or more ways to honour the field data. This prompted relatively few changes to the initial implementation of the conceptual model within the reasonable ranges of parameter uncertainty. In conclusion, there is a good understanding of the overall hydrogeology inside the target volume and the confidence in the developed models is high. The remaining uncertainties concern predominantly the structural hydraulic conditions outside this volume. These are identified and described in /SKB 2008/. Three uncertainties that affect the modelling of the hydrogeological conditions inside the target volume are described below in sections 8.9.1 through 8.9.3.

8.9.1 Groundwater levels in the shallow bedrock aquifer

The ConnectFlow model uses a simplistic representation of the near-surface hydrogeological system and aims at matching the average groundwater levels of time series data in different boreholes with a steady-state flow model. Although, the magnitude and direction of the modelled gradient between the Quaternary deposits and the uppermost bedrock in the ConnectFlow model is in accordance with the monitoring data, the absolute values of the simulated average groundwater levels are a too high,

c. +0.7 m of mean difference for both the percussion-drilled boreholes and the monitoring wells within the target volume (cf. section 8.6.2). In comparison, the results reported from the MIKE SHE model (cf. section 4.3.1), which uses a detailed representation of the near-surface hydrogeological system and models the time series data on a diurnal basis, suggest that the low groundwater levels measured in the uppermost part of the bedrock cannot be matched unless there is a continuous sink somewhere in the bedrock. That is, without a continuous sink in the bedrock, the downward hydraulic gradients between the Quaternary deposits and the uppermost bedrock are not as pronounced in the MIKE SHE model as they are in the field measurements (and in the ConnectFlow model). In fact, the simulated hydraulic gradients locally points upwards in the MIKE SHE model unless there is a continuous sink in the bedrock. If this is the case or not is not readily checked because there are no known continuous sinks *within the target area*. (It is noted that the simulated groundwater levels in the Quaternary deposits in the MIKE SHE model are not at all affected by whether there is a sink in the bedrock or not.)

There are two examples of sinks in the uppermost bedrock not far form the target area, however, none of which that can be turned off. The stronger of the two sinks is the abstraction of drainage water in the SFR repository, cf. section 8.4.4. The SFR repository is located below the Baltic Sea and is reached by two tunnels, which cross the Singö deformation zone. The drainage water is abstracted at two pump stations. The first pump station is located after the crossing of the Singö deformation zone (88 m depth; 1.2 L/s) and the other is located below the bottom of the SFR repository (140 m depth; 4.8 L/s). The other example of a sink is the lowering of the groundwater level beneath the three nuclear power reactors, which are located northwest of the target area (Figure 8-28). The pumping under the reactors is not continuous (c. 20 m depth; c. 1–2 L/s intermittent pumping).

The simulations carried out with the MIKE SHE model suggest that a continuous abstraction of drainage water in the SFR repository affects the on-shore groundwater levels in the uppermost part of the bedrock within the target volume. It is noted that the calibrated MIKE SHE model is based on the ConnectFlow model with two main exceptions: 1) the horizontal hydraulic conductivity, K_h, was increased ten times in the part of the model describing the sheet joints, and 2) the vertical hydraulic conductivity, K_v, was decreased ten times in the uppermost 200 m of the bedrock throughout the entire model domain.

The results obtained from the single-hole geological interpretation and hydraulic testing of borehole KFM11A, which investigates the Singö deformation zone, together with the interference test data obtained from the interference test at borehole HFM33 during the fall of 2007, suggest that the Singö deformation zone is hydraulically heterogeneous and has a very low transverse transmissivity in the surroundings of the SFR buildings, i.e. there are no hydraulic responses observed in boreholes HFM34, HFM35 and KFM11A while pumping in borehole HFM33, see Figure 8-28 and Figure 8-29. The crossing of the two SFR tunnels could provide a possibility for a hydraulic interference through the Singö deformation zone, but the tunnels cross through the zone in close proximity to borehole HFM34, which did not respond to the pumping in borehole HFM33.

In contrast to the pumping in HFM33, the abstraction of drainage water in the SFR repository has a strong impact (metres to tens of metres) on the groundwater levels in the monitoring network in the bedrock in the proximity of the repository, including HFM34 (c. 3 m) and HFM35 (c. 5.5 m), which are located at a distance of c. 500 m from the SFR repository, see Figure 8-29. Furthermore, the monitoring of groundwater levels in KFM11A that began at the end of 2007 indicates that all monitoring intervals on both sides of the Singö deformation zone respond to the abstraction of drainage water in the SFR repository. For instance, the uppermost monitoring section in KFM11A (0–130 m borehole length) has a groundwater level of c. two metres below the datum and the bottommost monitoring section in KFM11A (711–850 m borehole length) has a groundwater level of c. seven metres below the datum. The estimated transmissivities of these two bedrock intervals are $8 \cdot 10^{-6}$ m^2/s and $1 \cdot 10^{-6}$ m^2/s, respectively.

In conclusion, the prevailing situation, with quite low groundwater levels in the shallow bedrock within the target area, may partly be caused by the pumping in the SFR repository. However, no definite conclusions on this issue can be made based on existing data. The ConnectFlow model assumes that the Singö deformation zone is heterogeneous, but the model is not calibrated for a scenario where there is a continuous sink in the bedrock in the SFR repository. However, exploration simulations, with the pumping in the SFR repository included in the calibrated ConnectFlow model, confirm that the hydraulic properties of the shallow bedrock aquifer system reported in the SDM are credible and adequate for further modelling, because the differences between measured and simulated groundwater levels decrease when the pumping in the SFR repository is incorporated. That is, even if the abstraction of drainage water in the SFR repository is an uncertain boundary condition that may affect the natural groundwater levels, the hydraulic stresses (drawdowns) induced by the cross-hole tests run in the target area apparently are sufficiently strong to allow for a fair calibration of the hydraulic properties.

8.9.2 Compartmentalised fracture networks at repository depth

The hydraulic description of the less fractured bedrock between the deformation zones is focused on the conductive fracture frequency (CFF) of continuously flowing fractures. This means that the connected fracture network situations such as cases D-F in Figure 8-6 were regarded as more important for the hydrogeological DFN modelling and the groundwater flow modelling in the site description than disconnected (compartmentalised) network situations such as cases A-C. The role of compartmentalised networks, if any, needs to be addressed in the safety assessment.

8.9.3 Evaluation of PFL-f transmissivity data

It is important to recollect what is actually measured with the PFL-f tests. For each PFL-f transmissivity value identified, the change in flux (inflow) and head (drawdown) after several days of pumping relative to conditions prior to pumping are calculated. A transmissivity value is interpreted for each PFL-f test based on Thiem's equation and an assumed value of the radius of influence to borehole radius ratio (R_0 / r_w) = 500. The choice of 500 reflects that tests are performed over several days, and hence should represent an effective transmissivity of the whole fracture intersected, and possibly adjoining parts of the network, but the choice of 500 is otherwise arbitrary. Consequently, the interpreted values of transmissivity should not be viewed as necessarily the transmissivity of individual fractures, or the transmissivity of the fracture local to the borehole intersect. They are more indicative of the effective transmissivity over a larger scale. This remark influences the way the PFL-f data are used in the hydrogeological DFN modelling as explained in section 8.5.2.

9 Bedrock hydrogeochemistry

9.1 Introduction

The overall objectives of the hydrogeochemical description for Forsmark are to establish a detailed understanding of the hydrogeochemical conditions at the site and to provide descriptions that fulfil the needs identified by the safety assessment group during the site investigation phase /Ström et al. 2008/. Understanding current undisturbed hydrochemical conditions at the proposed repository site is important when predicting future changes in groundwater chemistry that may be of relevance to the long-term integrity of the currently planned SKB repository system, in particular copper corrosion and/or bentonite degradation. Therefore, the following variables are of particular interest for the hydrogeochemical site descriptive modelling and required in the safety analysis: pH, Eh, sulphur species, iron, manganese, potassium, carbonate, phosphate, nitrogen species, ammonia, total dissolved solids (TDS) and the other main cations, isotopes, colloids, fulvic and humic acids, organic material (including acetate) and microorganisms. In addition, dissolved gases (e.g. carbon dioxide, methane and hydrogen) are of interest because of their likely participation in microbial reactions /Laaksoharju et al. 2008a/.

The work has involved the development of descriptive and mathematical models for groundwaters in relation to geology and hydrogeology (see chapters 5 and 8). In this report, the groundwaters have been interpreted in relation to their *origin*, *evolution* and *composition*, which requires close integration with geological, climatological and hydrogeological information. Past climate changes are one of the major driving forces for long-term hydrogeochemical changes (hundreds to thousands of years) and are, therefore, of fundamental importance for understanding the palaeohydrogeological, palaeohydrogeochemical and present evolution of groundwater in the crystalline bedrock of the Fennoscandian Shield. In contrast, the buffer capacity of the bedrock will minimise the effects on changes in alkalinity and redox at repository depth, therefore limiting the variations in pH and Eh significantly, regardless of major changes in groundwater composition.

The methodology adopted is described in detail elsewhere, e.g. /Smellie et al. 2002, Laaksoharju et al. 2008b/ and the specific hydrogeochemical methodology used within the SKB site investigation programme is published in a special issue of Applied Geochemistry /Gascoyne and Laaksoharju (ed) 2008/. In brief, it involves the following steps:

- An initial screening to remove any obvious analytical or sampling artefacts arising from the laboratory and field procedures used before entering the data into the SKB Sicada database,
- a rigorous assessment of the quality of the data with respect to their representativity, using an integrated hydrochemical, geological and hydrogeological approach, with the purpose to identify data suitable for use in the understanding, interpretation and modelling of the groundwater conditions,
- a general examination of the data using traditional geochemical approaches to describe them and provide an initial insight and understanding of the site, i.e. the construction of a preliminary conceptual model for the area,
- a further evaluation of selected data using different modelling approaches, for example, geochemical equilibrium modelling, and presentation of the results as 2D/3D visualisations of the model volume based on the measured constituents from the modelled area, and
- a comparison and integration of the hydrogeochemical models and descriptions with independent modelled results for the area, for example, the geological and hydrogeological models (see chapters 5 and 8).

The evaluation stages were repeated after each data freeze when new and modified data became available. Thus, the final hydrogeochemical site descriptive model as presented and described in this report is the result of an iterative, step-by-step development during the period of the site investigations, i.e. through model version 1.2 and modelling stages 2.1, 2.2 and 2.3.

The work within modelling stages 2.2 and 2.3 further developed the conceptual models and site understanding as presented in earlier model versions. Collaboration with HydroNet, SurfaceNet and RetNet (SKB's hydrogeological, surface system and bedrock transport modelling groups, respectively) was more effective than was previously the case. This was due to the availability of a large amount of new interpreted data which allowed greater integration, thus bringing the hydrogeochemical programme into consistency with the progress of the other groups.

Further to the groundwater hydrochemical studies, matrix porewaters have been investigated in detail for the first time in a crystalline rock environment with success. In addition, the importance of mineralogy has been underlined in site understanding, for example, as input to the geochemical equilibrium modelling. From a palaeohydrogeological viewpoint, geochemical and mineralogical information from fracture minerals, altered rock and the reference rock matrix has been compiled in /Sandström et al. 2008/. The major findings from the fracture mineral and matrix porewater investigations have been integrated into the site description.

Important feedback from SR-Can /SKB 2006b/ and Insite (the review group established by the authorities) and Sierg (SKB's independent review group) was addressed in the modelling. The CRI issue list established by the authorities (e.g. CRI-list dated October 2006; /SKB 2006c/) represented an important input to the work. Of the issues raised, some were addressed by model stage 2.1 and additional data acquired during model stages 2.2 and 2.3 facilitated further updating of the hydrogeochemical model (for details see /Laaksoharju et al. 2008a/).

9.2 State of knowledge at previous model version

The earlier model version 1.2 /SKB 2005a/ and model stage 2.1 /SKB 2006a/ concluded that the complex groundwater evolution and spatial pattern at Forsmark are a result of several factors such as: a) the present-day topography and proximity to the Baltic Sea, b) past changes in hydrogeology related to glaciation/deglaciation, land uplift and repeated marine/lake water regression/transgression, and c) organic or inorganic alteration of the groundwater composition caused by microbial processes and/or water/rock interactions. The sampled groundwaters reflected to various degrees processes relating to modern or ancient water/rock interactions and mixing.

The 2.1 data essentially confirmed the previous conceptual understanding. The groundwater composition showed an increase in salinity down to a depth of about 200 m and tritium (^{3}H) data indicated no significant input of modern water at depths greater than 200 m. This indicated that groundwaters in the uppermost parts of the bedrock are of recent meteoric origin. At depths between approximately 200 to 600 m, the salinity remained fairly constant at a level between 5,000 to 6,000 mg/L Cl which, together with high magnesium concentrations, indicates input of Littorina waters to these depths. At depths between 600 to 1,000 m, the salinity increased to higher values in groundwaters with a glacial and a deep water signature. There were also indications that the salinity may be greater at higher elevations in the bedrock in the north-western part of the candidate area (i.e. in the target volume) than in the south-eastern part.

The Forsmark 2.1 groundwater data indicated relatively small modifications to the version 1.2 hydrogeochemical site description, but the overall geochemical understanding of the site improved due to addressing certain review issues (cf. /SKB 2006c/). This included confirmation of previous findings from version 1.2 and also support for the predictions made in version 1.2 based on the limited knowledge at that time. Confidence improved at the site scale concerning the three-dimensional variability of processes and properties due to the addition of new data from previously drilled boreholes and from new boreholes in specific key areas.

9.3 Conceptual model

9.3.1 Major concepts and model input

Nomenclature and processes

The nomenclature and processes described in this section are important to understanding the various conceptual model approaches developed, both past and present. The nomenclature of the groundwater types used depends on the purpose of the modelling and a distinction can be made between the following.

1) *Current groundwater types*, i.e. these are the types that are now used to distinguish different waters as measured today. The nomenclature of these present water types are related to the perceived main origin of these waters (i.e. meteoric, Littorina, glacial meltwaters etc) but their compositions have subsequently been altered by mixing and reactions.
2) *Origins of current groundwater types*. This relates to the chemical composition of the real groundwater end members, i.e. the 'actual' precipitation, the real glacial meltwater, the Littorina seawater, etc. The end-member compositions used for the site modelling are listed in Table 9-1.

Description of the current groundwater types in Forsmark is based on the salinity content of the water (e.g. Fresh, Brackish and Saline). Brackish waters may be subdivided into Brackish Marine and Brackish Non-marine, mainly based on magnesium content and other marine indicators (e.g. chloride-bromide ratios). As a consequence, the same water type can be described as, for example, Brackish Marine or a mixture of Littorina and Glacial water. The composition of the end members is described in detail by /Gurban 2008, Gimeno et al. 2008/.

The names of the water types used in the different evaluations and modelling activities are /Smellie et al. 2008, Gimeno et al. 2008, Gurban 2008/:

1) *Palaeohydrogeochemical description:* Highly Saline, Old Meteoric ± Old Glacial, Last Deglaciation, Littorina and Present Meteoric.
   (Note: '± Old Glacial' means that the Old Meteoric water may or may not contain an Old Glacial component).
2) *Mixing end members (M3) modelling:* Deep Saline, Saline, Old Meteoric + Glacial, Glacial, Littorina and Altered Meteoric.
3) *Site descriptive model:* Saline, Brackish Non-marine, Brackish Marine, Mixed Brackish and Fresh.

Table 9-1. End-member compositions used for the Forsmark site groundwater modelling.

Parameter	Deep Saline		Littorina	Glacial	Old Meteoric + Glacial	Altered Meteoric Forsmark #4919
	Laxemar	Modelled values used for Forsmark				
pH (units)	8	8	7.6			7.91
HCO_3^- (mg/L)	14.1	14.1	92.5	0.12	0.12	466.0
Cl (mg/L)	47,200	47,200	6,500	0.5	0.5	181
SO_4^{2-} (mg/L)	906.0	10	890	0.5	0.5	85.1
Br (mg/L)	323.7	323.7	22.2			0.57
Ca (mg/L)	19,300	19,300	151	0.18	0.18	1.6
Mg (mg/L)	2.12	2.12	448	0.1	0.1	41.1
Na (mg/L)	8,500	8,500	3,674	0.17	0.17	7.5
K (mg/L)	45.5	45.5	134	0.4	0.4	274.0
Si (mg/L)	2.9	2.9	3.94	–	–	5.60
δ^2H (‰ V-SMOW*)	–44.9	–44.9	–37.8	–158.0	–118	–80.6
$\delta^{18}O$ (‰ V-SMOW*)	–8.9	–8.9	–4.7	–21.0	–16.0	–11.1

* Vienna Standard Mean Ocean Water.

To understand, interpret and conceptualise the groundwater evolution, the following issues need to be considered.

1) *The 'original' composition of the water present in the bedrock:* This is essentially unknown, but evidence from fracture groundwaters and matrix porewaters indicates that resident groundwaters prior to the last deglaciation were a mixture of old meteoric ± old glacial and saline in type as a function of depth. Note that the uncertainty in recognising groundwater components older than the last deglaciation increases considerably with age, see /Laaksoharju et al. 2008a, Smellie et al. 2008/.
2) *Last deglaciation effects:* Includes incursion of glacial meltwater and subsequent Littorina Sea water.
3) *Introduction of more recent post-glacial groundwater types:* Because the studied site is situated close to the Baltic Sea coast, it is evident that both fresh meteoric water and brackish-marine seawaters of different salinities may have played important roles, especially since the last deglaciation. Fresh meteoric waters from very different climates (e.g. ranging from temperate to cool) may also have been recharged repeatedly.
4) *Factors controlling groundwater flow that largely determine the resulting groundwater chemistry, especially for conservative elements:* These include topography, bedrock transmissivities, interconnection of different fractures and fracture networks, density differences and glacial loading and unloading.
5) *The reactions taking place in the soil cover and bedrock which modify the original signature of the recharge water:* Examples are redox reactions mostly mediated by microbial activity involving oxygen consumption, and reactions with manganese, iron, sulphide and carbon. In addition, water/rock reactions such as ion exchange, calcite dissolution/precipitation and silicate weathering will occur, together with mixing and also diffusion (e.g. exchange with matrix porewater).

Conceptual mixing and reactions

As a result of the extensive site bedrock investigations in Sweden and Finland it is perceived that the hydrogeochemical evolution of fracture groundwater results from advective mixing and water-rock interactions driven by past and present changes in the climate (e.g. /Laaksoharju and Wallin (ed) 1997, Laaksoharju et al. 1999, Pitkänen et al. 1999/). Many of the evaluation and modelling steps used within ChemNet are focused on differentiating these effects by using alternative modelling approaches /Laaksoharju et al. 2008b/. Mixing modelling focuses on tracing the origin of the groundwater, whereas reaction modelling focuses on understanding the interaction between oxic/anoxic groundwaters and the bedrock and, for example, the mediating role microbial activity may play.

For modelling purposes, different approaches can be used leading to quite different descriptions of the system. For example, when applying end-member mixing models, the choices of end members are crucial for the description of both mixing and reactions. This does not necessarily mean that some models are correct and some models are not. It is more a question of choosing the most suitable model available for describing the part of the system that is to be addressed, and also to focus on the time period of interest. All epochs and all parts of the system can never be described with high resolution using the same model; usually several models are required as well as different sets of end members and starting prerequisites.

Figure 9-1a–d illustrates the different approaches to model groundwater mixing and reactions, using sodium versus chloride as an example. The sodium content in groundwater can be altered by, for example, feldspar weathering or ion exchange, but chloride is regarded as a water conservative tracer not affected by reactions. The task is to model the reactions that have caused the measured sodium content. In Model 1 (Figure 9-1b), the water composition is the result of reactions, for example, the sample with about 0.85 mol/kg Cl, indicated with the arrow, has gained about 0.28 mol/kg Na due to reactions. There is no flux or mixing in the system since the system is closed. In Model 2 (Figure 9-1c), the water composition is the result of mixing of two end members (indicated with the dashed black line); here the sample has gained about 0.07 mol/kg Na. The water composition is described mainly as a result of two-component mixing with some gain of sodium by reactions.

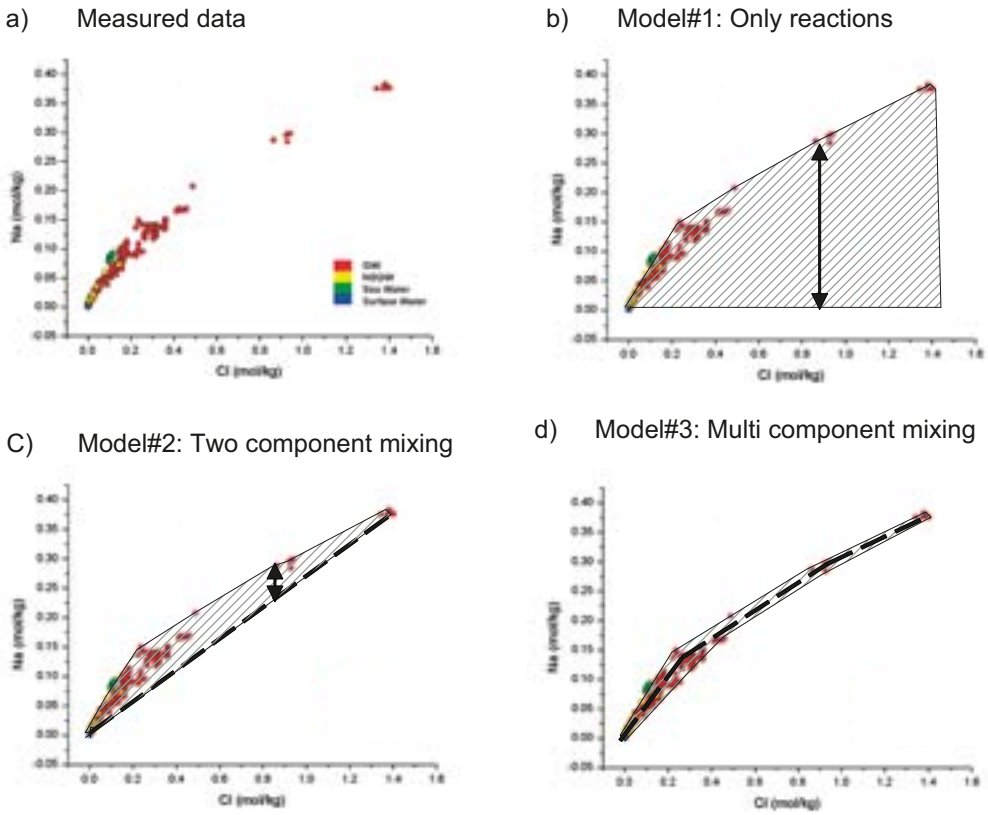

Figure 9-1. *Schematic presentation of how different models are used to describe the processes behind the measured Na content. The arrows indicate the amount of reactions taking place for a particular sample, the grey dashed area indicates samples affected by reactions and the black dashed line indicates the mixing line: a) Measured Na versus Cl, b) Model based on reactions, c) Model based on a mixture of two end members and, d) model based on several end members /Laaksoharju et al. 2008b/.*

In Model 3 (Figure 9-1d), the water composition is described almost exclusively as the result of mixing of several end members. Here the sample has not gained any sodium, since it plots on, or close to, the mixing line (black dashed line). The water composition is described as the result of multi-component mixing and the sodium content is the result of pure mixing/transport. Plots above the mixing line indicate a gain of sodium, whereas plots below the mixing line indicate a loss of sodium.

The example given above clearly shows that the description of the groundwater system depends on the model selected. Model 1 describes the total amount of reactions taking place to obtain the sodium content measured in the sample. However, it does not describe where and when the reactions took place. Models 2 and 3 describe the water composition in relation to the end-member composition. Hence, these models can be used to calculate the mixing proportions of the end members. This, in turn, can be used not only to indicate the origin, but also to indicate the range of possible residence time in the bedrock. This is useful information when, for example, integrating the results with the hydrogeological modelling. Models 2 and 3 do not describe the evolution of the end-member composition, but assume that the processes responsible for this composition are implicitly considered (including all the reactions that ever took place).

It is generally a relatively easy task to construct Model 2, but with the risk that the system is oversimplified such that the effects from reactions are overestimated and the effects from transport underestimated. Model 3 can provide realistic descriptions of conservative and non-conservative compounds, but model uncertainties (such as uncertain end-member compositions and mathematical uncertainties in the model applied) can still lead to an erroneous conclusion concerning the gain/losses of element concentrations. The accuracy of Models 2 and 3 can be tested by, for example, plotting the model-predicted Cl and $\delta^{18}O$ contents versus the measured ones. The deviation from a perfect correlation will then indicate the model uncertainties /Laaksoharju 1999/. The uncertainties in the modelling are discussed in section 9.5.10 and in /Laaksoharju et al. 2008a/ and /Gimeno et al. 2008/.

The importance of mixing becomes apparent under the following circumstances.

- The palaeo- and present climate /Laaksoharju et al. 2008a/ has a huge impact on the hydrogeology and, hence, on hydrochemistry in Fennoscandia. This facilitates different water types (i.e. glacial, sea water and meteoric water) to enter or to be flushed out from the bedrock.
- The temperature in the rock is relatively low (at –200 m = 11°C; the gradient is 1.6°C per 100 m) and therefore most water/rock interaction processes are slow.
- Where groundwater flow is faster and more dominating than reaction times (i.e. for highly transmissive conditions), the origin of the water may still be distinguished.

The significance of reactions becomes apparent, particularly with respect to: a) redox conditions where microbiologically mediated reactions are rapid, and b) pH and alkalinity values buffered by kinetically fast calcite precipitation/dissolution reactions /Gimeno et al. 2008/.

As an example of the complexities involved, the chemical evolution of Littorina Sea water entering the bedrock at Forsmark was modelled /Gimeno et al. 2008/. The modelled results indicated that the major components Cl, SO_4, Na, Mg and Ca, and stable isotope values of $\delta^{18}O$ measured in the brackish marine groundwater with chloride contents around 5,500 mg/L, can be predicted without considering major influences from reactions, assuming that 20 to 60% Littorina sea water was infiltrating into a groundwater mixture consisting of 10% deep saline and 90% glacial water. This assumption is in agreement with the conceptual post-glacial model of the site. However, detailed investigations /Smellie et al. 2008, Molinero et al. 2008/ indicate modifications of the water caused by the following reactions:

- Br/Cl typically show marine values in groundwater samples where the Na/Ca ratio and Mg contents are significantly reduced compared with marine values,
- the carbon system indicates HCO_3 production during post-glacial time related to the intrusion of the Littorina water,
- the sulphur system indicates sulphate reduction (i.e. lowering of sulphate contents and increase in sulphur isotope values in the remaining sulphate), and
- the strontium isotope ratios show no mixing line towards marine values which should be expected if only mixing had occurred; instead the strontium isotopes show clear signs of water/rock interactions which probably include ion exchange.

As to intrusion of the Littorina sea water, it can thus be concluded that mixing, together with reactions, have formed the composition of the present brackish marine groundwater. Furthermore, reactions modified, but did not mask the origin of the water. The exact quantification of the contribution from reactions versus mixing is complex, and at best semi-quantitative at the site scale, and requires different modelling approaches ranging from explorative analyses, mass-balance calculations, mixing calculations and coupled reactive transport modelling, see for example /Laaksoharju et al. 2008ab, Gimeno et al. 2008, Molinero et al. 2008/.

Rock domains, deformation zones and fracture domains

The basis for conceptualising the Forsmark area with respect to hydrogeochemistry (both past and present) depends on reliable geological and hydrogeological models of the area (see chapters 5 and 8, respectively). A bedrock geological map with borehole locations and projections is shown in Figure 9-2. Deterministic geological modelling at the Forsmark site has identified rock domains and deformation zones (/Stephens et al. 2007/ and sections 5.4 and 5.5 in this report). Rock domains refer to rock volumes in which specific rock units have been distinguished on the basis of similar composition, grain size, degree of bedrock homogeneity and degree and style of ductile deformation. Deformation zones refer to parts of the bedrock along which there is a concentration of strain. Most deformation zones at Forsmark are brittle structures, i.e. fracture zones (see section 5.5.4).

To further facilitate site description and model development, the bedrock in between deformation zones has been divided into several fracture domains, based on geological criteria (/Olofsson et al. 2007/ and section 5.6 in this report). The extent of four of these domains within the local model volume (FFM01, FFM02, FFM03 and FFM06) is shown in Figure 9-2, together with the associated rock domains and some deformation zones. Fracture domain FFM02, in the uppermost part of the

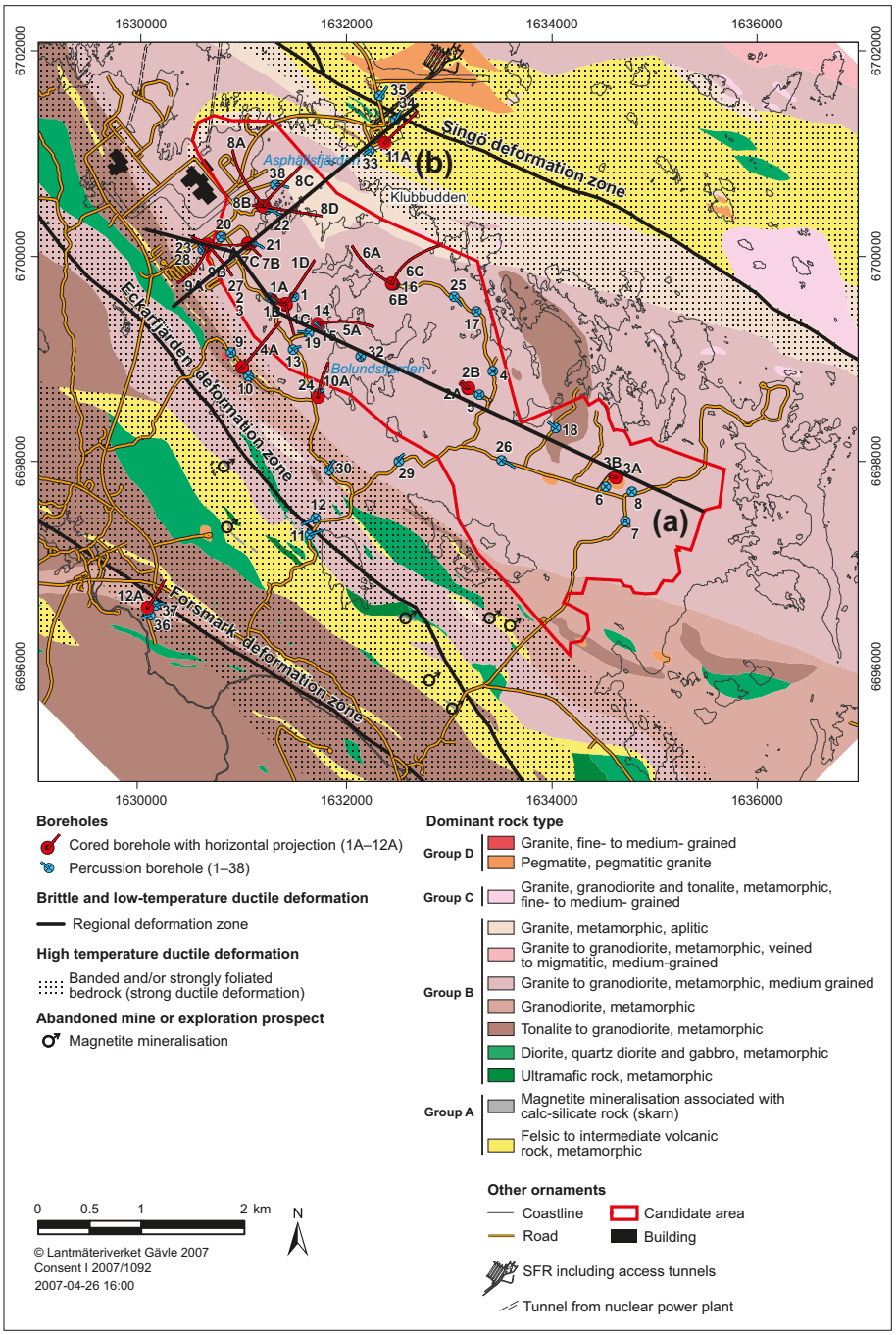

KFM01A
KFM01B
KFM01D
KFM02A
KFM02B
KFM03A
KFM04A
KFM05A
KFM06A
KFM06C
KFM07A
KFM08A
KFM08C
KFM08D
KFM09A
KFM09B
KFM10A
KFM11A
KFM12A

Figure 9-2. *Geology and borehole location map of the Forsmark candidate site. The approximate positions of the WNW-ESE (a) and WSW-ENE (b) cross-sections described in section 9.6.1 are indicated as (a) and (b). Listed are the cored boreholes sampled for hydrochemical interpretation.*

target volume, is of particular interest, since it is characterised by a complex network of gently dipping and sub-horizontal, open and partly open fractures, which locally merge into fracture zones (section 5.6). Relative to FFM02, fracture domains FFM01 and FFM06 in the lower part of the target volume, which includes the potential repository depth, show a much lower frequency of open fractures (section 5.6). Furthermore, the frequency of connected transmissive fractures reduces dramatically, especially below 400 m depth, see section 8.4.2. The division into fracture domains is consistent with respect to hydrogeological criteria (/Follin 2008/ and section 8.5.2).

Most of the groundwater chemical data evaluated originate from deformation zones and only a limited amount of data come from the bedrock in the contiguous fracture domains. Moreover, some of the latter data may have been influenced, to a varying extent, by groundwater from nearby

deformation zones, since sampling is possible only in fractures with groundwater flow. Such fractures need to be both transmissive and connected to these zones. Examples include the deepest groundwaters sampled from borehole KFM03A and some upper and intermediate groundwaters from borehole KFM01D.

Bearing in mind the considerations above, it has proven more useful to address the hydrogeochemical data in relation to their spatial location with respect to some key deformation zones. The entire bedrock that lies structurally above zones ZFMA2, ZFMF1and ZFMA3 and to the south-east of zone ZFMNE0065 (see NW-SE profile in Figure 5-41) is separated from the bedrock structurally beneath and to the north-west of these zones, which includes the target volume at Forsmark. These bedrock segments are referred to as the hanging wall and footwall bedrock segments, respectively (see also chapter 8), and their use has been adopted throughout this report.

Hydrogeology

The hydrogeology of the water-conducting fractures along deformation zones and along a few individual fractures inside the adjacent fracture domains is of major significance for hydrogeochemical considerations. Together with the hydrogeochemistry, these water-conducting structures, in turn, influence the distribution of the porewater chemistry in the rock matrix.

The uppermost part of the footwall bedrock inside the target volume, down to around 200 m depth, includes both fracture domain FFM02 and the near-surface extension of some deformation zones, both gently and steeply dipping (Figure 9-3). This upper footwall is referred to as a shallow bedrock aquifer considered to be hydraulically anisotropic, due to a lattice of intersecting near-surface, subhorizontal sheet joints, ancient fractures with variable orientation, both gently and steeply dipping, and outcropping deformation zones (/Follin 2008/ and section 8.4.4). The groundwater flow is

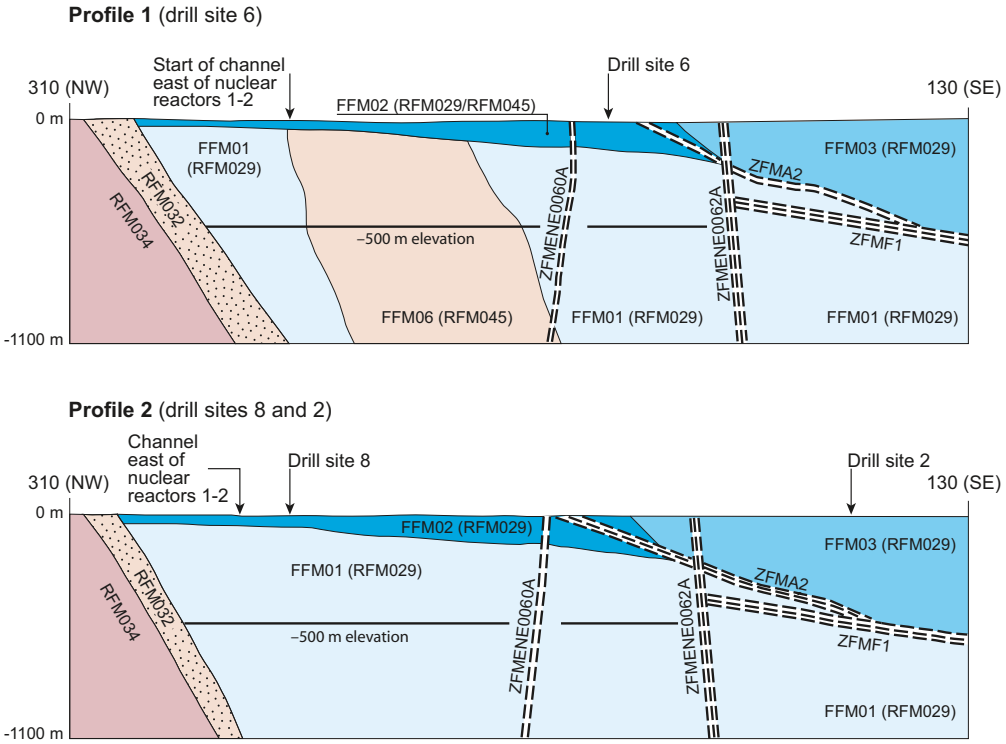

Figure 9-3. *Simplified NW-SE profiles along the target volume that intersect drill site 6 (Profile 1) and drill sites 2 and 8 (Profile 2) (cf. Figure 9-2 for location of drill sites). The labelled fracture domains (FFM01, FFM02, FFM03 and FFM06) occur inside rock domains RFM029 and RFM045. Note the gently dipping deformation zones ZFMA2 and ZFMF1 which essentially divide the candidate area along the profiles into fracture domain FFM03 (hanging wall) and fracture domains FFM01, 02 and 06 (footwall). The footwall fracture domains are referred to as the target volume in the SDM. The average repository depth is shown by the black line at –500 m elevation and 'channel' refers to an excavated link between the Baltic Sea and the nuclear power plant (Figure 5-4 in /Olofsson et al. 2007/).*

considered to be mainly horizontal, governed by the strong anisotropic conditions resulting from the well-connected horizontal fracture system in this volume. When meteoric recharge waters enter the sub-horizontal fractures, they mix with existing fracture groundwaters and are rapidly transported laterally to be discharged towards the Baltic Sea to the north-east of the candidate area. This shallow bedrock aquifer effectively limits direct meteoric recharge to deeper bedrock levels. However, some deeper recharge of meteoric water is likely to occur where outcropping, steeply dipping deformation zones coincide with higher surface elevations south-west of the candidate area (/Follin 2008/ and section 8.4.4).

Fracture domain FFM01 comprises the major part of the footwall bedrock segment inside the target volume (Figure 9-3). It differs from fracture domain FFM02 (upper 200 m of bedrock) in that, particularly at increased depths (> 400 m), there is an overall lower intensity of open, flowing fractures and lower fracture transmissivity. These flowing fractures mostly consist of discrete, sub-horizontal to gently dipping single fractures of restricted extent (/Follin 2008/ and section 8.5.2).

Fracture domain FFM03, which forms the major part of the hanging wall bedrock segment, shows approximately the same low fracture frequency as FFM01 but is spatially associated with a significant number of highly transmissive, gently dipping deformation zones. The transmissivity of these zones is high in the upper 400 m and significantly lower below approximately 500 m, i.e. there is a significant depth trend in the transmissivity data gathered. Flow directions within the candidate volume are primarily sub-horizontal along the fracture planes towards the north-east with a weak upward component.

The local major steeply dipping deformation zones such as ZFMENE0060A in Figure 9-3 also exhibit a significant depth trend in transmissivity. However, steeply dipping zones are also found to be considerably more heterogeneous with both open and sealed flow channels, the former with measurable flow. The vast majority of these steeply dipping zones are parallel to the topographic gradient and cut the candidate area. However, due to the shallow bedrock aquifer and the considerable heterogeneity of these zones, it is difficult to generalise the current flow pattern. Particle tracking simulations suggest that the flow gradient is predominantly upwards until the aquifer in the uppermost part of the bedrock is reached (see section 8.7.2).

Fracture domain FFM06 inside the target volume corresponds to the part of rock domain RFM045 that is situated beneath fracture domain FFM02 (Figure 9-3) and is hydrogeologically similar to fracture domain FFM01.

9.3.2 Working hypothesis on the past groundwater evolution

The present working hypothesis for the hydrogeochemical site conceptual model recognises that the earlier Quaternary evolution has affected the groundwater chemistry, especially in the most conductive parts of the bedrock. This is not restricted to post-glaciation time, since there is groundwater and porewater evidence that indicates an old, warm-climate derived meteoric water component. The age of this component is unknown, but possibilities include certainly pre-Holocene (> 10,000 years ago) and maybe pre-Pleistocene (> 1.8 Ma) or even further back in time. Without recognising this older component the hydrogeochemistry of the Forsmark area cannot be adequately explained. The present groundwaters, therefore, are a result of complex mixing and reactions over a long period of geological time. Mixing will be more important in those parts of the bedrock with dynamic hydrogeological properties. In other less dynamic parts, the groundwater chemistry will be more influenced by water/rock interaction processes.

In the initial hypothesis /SKB 2005d, 2006c/, an older component was not considered and the modelling scenario was based on conditions following the last deglaciation. The conceptual model at that time considered four key water types that contributed to the Forsmark groundwater system and chronologically comprised: *Deep Saline Water* (oldest) > *Holocene Glacial Melt Water* > *Littorina Sea Water* (→ *Baltic Sea Water*) > *Present-day Meteoric Water* (most recent). Figure 3-9 in section 3.4 in this report illustrates the most important post-glacial climatic phases, see also /Söderbäck (ed) 2008/.

This early conceptual model was much improved during model stage 2.3, and now includes the recognition of older groundwater components dating from before the last deglaciation. The four

key water types listed above, whilst simplified, essentially still reflect much of the present-day understanding although the following major groundwater types, in chronological order, are now recognised: *Saline Water > Brackish Non-marine Water > Last Deglaciation Melt Water > Brackish Marine (Littorina/Baltic) Water > Fresh Water* /Laaksoharju et al. 2008a/. (Note that the water types are given in order of decreasing age and 'Last Deglaciation' refers to the period 18,000–8000 BC).

To understand groundwater evolution in the Forsmark area, events prior to the last deglaciation have to be included in the description. Porewater analyses and groundwater samples from the relatively tight and isolated bedrock volumes in the target volume of the candidate area show groundwater compositions not significantly influenced by either glacial meltwater (of unknown age) or brackish marine water (i.e. Littorina Sea or Baltic Sea origin). These groundwaters are brackish to saline non-marine in type (4,000–10,000 mg/L Cl), are usually found from 300 to 700 m depth and deeper, and are significantly influenced by mixing, reactions and interactions with pore fluids in the rock matrix (i.e. diffusion processes). Furthermore, portions of these waters have resided in the bedrock for very long periods (at least around 1.5 Ma as indicated by chlorine-36 dating techniques and supported by helium systematics), for example, long enough to change the $\delta^{18}O$ and $\delta^{2}H$ ratios causing small deviations from the Global Meteoric Water Line. At greater depths (> 1,500 m), highly saline water of brine character and of unknown age and origin, similar to that sampled at the Laxemar subarea, can be expected and for which there is evidence from surface geophysical measurements /Thunehed and Pitkänen 2007/. However, available bromide and chloride ratios, as well as lithium and strontium contents, show clear differences when compared with typical deep saline groundwater samples from the Laxemar and Olkiluoto sites. As a result, this probably reflects variations in the bedrock geochemistry. At the moment, considerable uncertainty exists in the Forsmark site around the bromide/chloride issue because of the lack of deep groundwater salinity data (i.e. highest salinity at Forsmark is 14,000 to 15,000 mg/L Cl) from uncertain depths. In this respect it should be pointed out that the deep saline bromide/chloride ratio for Laxemar has been used in the Forsmark stage 2.2 hydrogeological model simulations, thus resulting in lower than expected estimated ratios/values (section 8.6.3). Additional uncertainties in shallow groundwater environments concerning bromide can result from enhancement derived from organics during diagenesis of marine sediments /Upstill-Goddard and Elderfield 1988/, and this process may change the original seawater bromide/chloride ratios. In Forsmark, the possibility of such a process is not believed to have been important since there is a clear marine signature based on the bromide/chloride ratios in the groundwaters with a Littorina signature.

Figure 9-4 illustrates the conceptualisation of the Forsmark groundwater system from before the last deglaciation to the present day. In the context of geological time scales, fluid inclusions in calcite of Palaeozoic origin show the presence of very saline (around 20 wt%) mainly Ca-Cl fluids /Sandström et al. 2008/. It can be assumed, therefore, that brine solutions were formed during the Palaeozoic, when several kilometres of marine and terrestrial sediments covered the Fennoscandian Shield area in south-eastern Sweden (see section 3.1). This allowed these brine waters to slowly penetrate and saturate both the fractures and eventually the interconnected matrix pore spaces in the underlying crystalline bedrock.

Figure 9-4a shows a tentative distribution of groundwater types and salinity gradients in the Forsmark area before the intrusion of the last deglaciation meltwater immediately prior to the Holocene. It is inferred that old meteoric waters, comprising components derived probably from both temperate and cold climate events, were present in the crystalline bedrock at this time. These groundwaters would have intruded the bedrock and have had long periods to interact with the minerals. Assuming there were favourable gradients, old meteoric waters could have been partially mixed with deeper, more saline groundwaters, but the high density contrast would have prevented further mixing. What can be said with confidence is that the residual old brackish waters in Forsmark do not have a marine signature. This situation seems to be still valid for the most isolated parts in the bedrock, for example, in the deeper footwall bedrock segment including fracture domain FFM01. However, along the more hydraulically conductive gently dipping deformation zones in the hanging wall bedrock segment, the last deglaciation meltwater was intruded to several hundreds of metres (Figure 9-4b) and mixed with previously more or less fresh water that resided in the upper 400 to 500 m in the most conductive zones.

During the subsequent Littorina Sea stage (Figure 9-4c), the Forsmark area was covered by brackish marine water assumed to be at around 6,500 mg/L Cl /Pitkänen et al. 1999, 2004/. This maximum salinity (twice the present salinity of the Baltic Sea) lasted at least until between 4500 and 3000 BC.

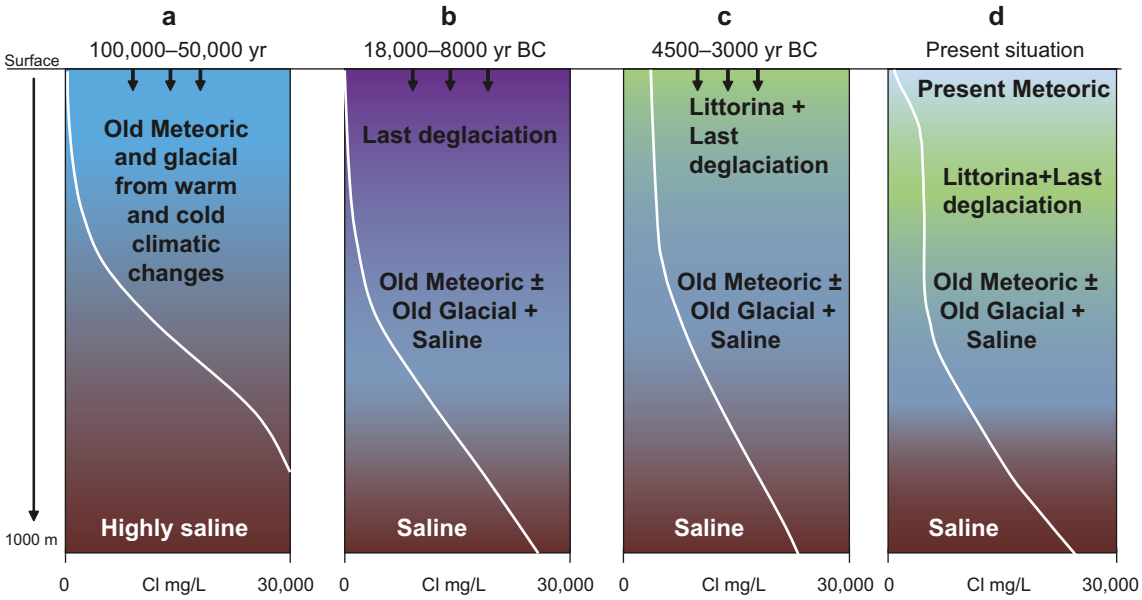

Figure 9-4. *Sketch showing tentative salinities and groundwater-type distributions versus depth for the transmissive zones at Forsmark. From left to right: a) situation prior to the last deglaciation, b) last deglaciation and intrusion of meltwater, c) the Littorina Sea water penetration caused by density intrusion, and d) the present situation. Tentative salinity profiles are indicated by the white lines.*

Due to the unstable density situation generated by the higher density Littorina Sea water located over previously infiltrated last deglaciation meltwater of lower density, the Littorina Sea water entered the deformation zones and fractures and mixed with previously resident fresh water of glacial and old meteoric character (Figure 9-4c).

The present situation is shown in Figure 9-4d, which illustrates the flushing out of the brackish marine groundwater (i.e. dominantly Littorina Sea water) in the upper part of the bedrock by recharging meteoric groundwaters during the last approximately 1,000 years. This flushing process commenced when uplift of the Forsmark region above sea level was sufficiently advanced to establish hydraulic gradients (i.e. about 900 years ago), and continues at the present day. Today, the most recent glacial water can no longer be identified as a major component in the bedrock, but rather constitutes a minor part in the Littorina-dominated groundwater, and perhaps also in the older brackish non-marine groundwaters, where depleted glacial water isotopic signatures have been measured.

The above description is valid generally for areas in the Forsmark bedrock where, first, the last deglaciation meltwater and then later the brackish marine (Littorina Sea) water have been introduced. Further conceptual development of the Forsmark area, for example, the land uplift processes, are described in /Söderbäck (ed) 2008, Laaksoharju et al. 2008a, Tröjbom et al. 2007/.

An outstanding issue still to be resolved satisfactorily in the conceptual model is the porewater and fracture groundwater evidence of an older dilute meteoric water component, also briefly referred to in section 9.3.1, that may have existed as far back as the Tertiary based on fracture groundwater chlorine-36 age dating. This possibility leaves an immense time span of several hundreds of thousands of years to explain prior to the last deglaciation at 18,000 to 8000 BC. At the moment there are too few data to be more specific than to point out that there is consistent evidence, but no proof (see section 9.5.8 and /Laaksoharju et al. 2008a, Waber et al. 2008/).

9.4 Hydrogeochemical data

The hydrogeochemical investigations performed in the Forsmark area are summarised in sections 2.1 and 2.3 and the data supporting the current model version are listed i Table 5 in Appendix 3.

The Forsmark dataset which formed the basis for model stages 2.2 and 2.3 comprised quality assured field data that were available in the SKB Sicada database at the time of the 2.2 and 2.3 data freezes.

These data contain complete hydrogeochemical analyses including microbes, colloids, gas analyses and porewater analyses from bedrock samples. These data are compiled in /Laaksoharju et al. 2008a/ and stored in the SKB model data base Simon, and are described in detail elsewhere (e.g. /Smellie et al. 2008, Hallbeck and Pedersen 2008a, Gimeno et al. 2008, Laaksoharju et al. 2008a, Kalinowski (ed) 2008/). The groundwater data from other Nordic sites and SFR have been used for comparison in e.g. /Smellie et al. 2008, Gimeno et al. 2008, Gurban 2008/.

The objective was to base the Forsmark hydrochemical modelling on data in the 2.2 data freeze and to use new data in the 2.3 data freeze and in the later extended 2.3 dataset for comparison and as a model check. The use of data and the data versions involved are described in detail in /Smellie et al. 2008, Gimeno et al. 2008, Laaksoharju et al. 2008a/. Data input for the hydrogeological modelling group (HydroNet) was based on the 2.2 data with the 2.3 data restricted to strengthening the choice of boundary conditions (i.e. end-member input for hydrodynamic modelling) and to support the development of the conceptual model common to both hydrogeochemistry and hydrogeology.

9.4.1 Borehole groundwater data

The locations of the percussion and cored boreholes are shown in Figure 9-2 in section 9.3.1.

The dataset extracted from Sicada as data freeze 2.2 (October, 2006) and 2.3 (April, 2007), included old data from earlier data freezes and the new data stored up to April 2007. Additional data from the monitoring programme and three deep boreholes were included in the extended 2.3 data freeze (October, 2007). Table 9-2 summarises the number and type of samples included in the 2.2–2.3 and extended 2.3 data freezes.

9.4.2 Representativity of the data

The complete groundwater dataset has been evaluated systematically with respect to quality, and an assignment of different categories was made with respect to their value for further hydrogeochemical interpretation work /Smellie et al. 2008, Laaksoharju et al. 2008a/. This was based on an integrated geological, hydrogeological and hydrochemical approach. A separate small-scale feasibility study of some selected borehole sections was made to determine the possibility of further quantifying the effects from drilling and pumping (cf. /Gascoyne and Gurban 2008, Laaksoharju et al. 2008a/), but this did not affect the categorisation of the dataset. The classification into the various categories for the cored boreholes is presented in Table 9-3 in terms of the most important criteria that apply for different categories. The number of samples and the allocated category are listed in Table 9-4 and the complete tables are stored in the SKB model database Simon.

Table 9-2. Number and type of samples included in data freezes 2.2 and 2.3 and the extended 2.3 data freeze. These include all categories (1–5); see section 9.4.2 for details.

Type of sample	Number of samples in data freezes 2.2–2.3	extended data freeze 2.3
Percussion boreholes	154	13
Cored boreholes	178	27
Process control	13	
Drilling sample	7	
Tube sampling	65	
Shallow groundwater	317	
Sea water	277	
Lake water	404	
Stream water	398	
Precipitation	31	
Colloids	37	
Microbes	50	
Gas	42	
Rock matrix porewater	52	39

Table 9-3. Classification criteria for cored boreholes (/Laaksoharju et al. 2008a, Smellie et al. 2008/).

Cored boreholes	Category				
Aspects/conditions	1	2	3	4	5
Drilling water (≤ 1%)	x	x	x	x	x
Drilling water (≤ 5%)		x	x	x	x
Drilling water (≤ 10%)			x	x	x
Drilling water (> 10%)				x	x
Time series (adequate)	x	x	x	x	x
Time series (inadequate)			x	x	x
Time series (absent)				x	x
Suitable section length	x	x	x	x	x
Sampling during drilling				x	x
Sampling using PLU hydraulic testing equipment			x	x	x
Tube sampling					x
Charge balance ±5% (±10% for < 50 mg/L Cl)	x	x	x	x	x
Major ions (complete)	x	x	x	x	x
Major ions (incomplete)			x	x	x
Environmental isotopes (complete)	x	x	x	x	x
Environmental isotopes (incomplete)		x	x	x	x
Hydraulic effects (short circuiting)					x

Table 9-4. Number of samples from percussion and cored boreholes allocated to each category.

	Number of samples in category				
	1	2	3	4	5
Percussion boreholes	3	2	7	13	87
Cored boreholes	1	15	15	8	80

The highest quality data (categories 1 and 2) are required, for example, for geochemical equilibrium calculations, modelling of redox conditions, and for specialised studies on microbes, organics and colloids. These data, together with category 3 and category 4 (with caution) data, adequately address the overall site understanding (e.g. groundwater distribution, origin and evolution and its integration with hydrogeology). However, category 5 data should be used with considerable caution in the context of both hydrogeochemistry and hydrogeology, in particular the tube sample data.

9.5 Explorative analysis and modelling

Explorative analysis involves an initial general examination of the groundwater data using traditional geochemical approaches to describe the data and provide an early insight and understanding of the site, i.e. the construction of a preliminary conceptual model for the area (section 9.3). Based on this hydrochemical framework, selected data are further evaluated using different modelling approaches such as data evaluation and visualisation, mixing modelling, equilibrium modelling, redox modelling and evaluation of microbes, colloids and gases.

The computer codes that were used in the hydrogeochemical evaluation are listed below.

- PHREEQC: Code for calculations of chemical equilibrium, reaction, advective transport and inverse modelling /Parkhurst and Appelo 1999/. Thermodynamic data base: WATEQ4F /Ball and Nordstrom 2001/, distributed with the PHREEQC code, with some modifications, see details in /Auqué et al. 2006/.

- M3: Mixing and mass balance calculation program /Laaksoharju et al. 1999, Gómez et al. 2009/.
- CORE^{2D}: Coupled hydrochemical/hydrogeological modelling code /Samper et al. 2000/.
- OpenDX: 3D visualisation (IBM Open Visual environment, OpenDX).

Studies of fracture fillings, composition of the porewater in the bedrock and groundwater residence times are important information for the site description. The background data, the explorative analysis and the modelling are detailed in /Laaksoharju et al. 2008a, Smellie et al. 2008, Gimeno et al. 2008, Kalinowski (ed) 2008/. The most important results are described in this section.

During the explorative analyses of the groundwaters, it became apparent that a subdivision of the sampled groundwaters into four major groundwater types would facilitate the description and interpretation of the figures and diagrams. The major water types distinguished are; Fresh, Brackish Marine, Brackish Non-marine and Saline Non-marine. Because of the lack of deep groundwater hydrochemical data, the brackish and saline non-marine groundwaters have been combined. In addition, two groundwater types have been included to accommodate important mixing processes resulting from anthropogenic and natural processes: a) a near-surface 'Mixed Brackish' type mainly comprising fresh and brackish marine groundwaters, and b) a deeper 'Transition Zone' type comprising degrees of mixing between brackish marine and brackish to saline non-marine groundwaters. The main chemical and isotopic character of each groundwater type, and their respective colour codes used in the plots, can be summarised as follows.

Fresh (Light Grey colour code)

Water type: Fresh (< 200 mg/L Cl; < 1.0 g/L TDS); Mainly meteoric in origin, i.e. Na(Ca)-$HCO_3(SO_4)$-(Cl) in type, $\delta^{18}O$ = –12 to –11‰ V-SMOW.

Mixed Brackish (Light Green colour code) (Not a specific groundwater type)

Waters of mixed Fresh and Brackish Marine origin (200–2,000 mg/L Cl; 1.0–3.5 g/L TDS); are usually sampled at 50–150 m depth in relatively long borehole sections mainly from percussion boreholes. The mixing is natural as well as induced by the site-characterisation activities (anthropogenic).

Brackish Marine (Green colour code)

Water type: Brackish Marine (2,000–6,000 mg/L Cl; 3.5–10 g/L TDS; Mg>100 mg/L); variable Littorina Sea component (± modern Baltic Sea) + Last Deglaciation meltwater ± Saline component; Na-Ca-Mg-Cl-SO_4; $\delta^{18}O$ = –11.5 to –8.0‰ V-SMOW.

Transition zone samples (Not a specific water type) (Turquoise code)

Waters sampled in the transition zone between Brackish Marine and Brackish Non-marine groundwaters. These waters range from 4,000–6,500 mg/L Cl and from 25–100 mg/L Mg. They may be the result of natural and/or anthropogenic mixing during drilling activities and sampling.

Brackish to Saline Non-marine (Blue colour code)

Water type: Brackish to Saline Non-marine (4,000–15,000 mg/L Cl; 8.5–16 g/L TDS; Mg < 25 mg/L); Old Meteoric ± Old Glacial ± Last Deglaciation meltwater ± Saline component, i.e. Ca-Na-Cl in type, $\delta^{18}O$ = –16.0 to –10.5‰ V-SMOW.

This subdivision into different groundwater types corresponds to the division used in the conceptual visualisation (section 9.6.1) with the exception that Brackish Non-marine groundwaters (4,000–10,000 mg/L Cl) and Saline Non-marine groundwater (10,000–20,000 mg/L Cl) are treated separately and are given turquoise and dark blue colour codes, respectively.

9.5.1 Initial data evaluation and visualisation

For the visualisation and interpretation of primary data, they are divided according to their occurrence in footwall and hanging wall bedrock segments, and in fracture domains and deformation zones.

As part of this initial evaluation stage, the fracture domain concept (cf. section 9.3.1) was addressed by applying the approach outlined by /Olofsson et al. 2007/ to see if there was any hydrogeochemical consistency with the geology and hydrogeology. The results from this exercise essentially confirmed the findings reported in /Olofsson et al. 2007/ in that the differences observed between the fracture domains were mostly restricted to the type and transmissivity of the water-conducting fractures within the fracture domains and the deformation zones embedded in the fracture domains.

Depth trends

Three of the most important major ion hydrochemical signatures, chloride (Cl), magnesium (Mg) and deviations in oxygen-18 ($\delta^{18}O$), have been selected to describe the groundwaters based on the conceptual understanding of the Forsmark area. The data used represent categories 1–3. Most trace element trends are described under specific processes related to site understanding, such as redox conditions. Exceptions such as nitrate, nitrite and ammonium are described in /Laaksoharju et al. 2008a/.

Figure 9-5a, c and e, plotting Cl, Mg and $\delta^{18}O$ against elevation, are colour coded to relate the different groundwater types to both deformation zones and fracture domains; Figure 9-5b, d and f represent the distribution of the main groundwater types with depth. The plots show the clear depth subdivision between the three main groundwater types, i.e. shallow fresh waters, brackish marine groundwaters at shallow to intermediate depths, and the transition to deeper, brackish to saline non-marine groundwaters. Also clear is the depth penetration of the brackish marine groundwater along the gently dipping deformation zones to around 600 m in fracture domain FFM03 (i.e. hanging wall bedrock), compared with maximum penetration depths of 100 to 300 m in fracture domains FFM02 and FFM01 (i.e. footwall bedrock). Correspondingly, the transition to the deeper brackish and saline non-marine groundwater types also occurs at these respective depths intervals /Smellie et al. 2008, Gimeno et al. 2008/. Combining these two methods of presenting the hydrochemical data provides a rapid and very informative insight to the vertical and lateral spatial distribution of the measured parameters, and the strong influence of structural and hydraulic properties in their distribution (see section 9.3.1 and chapters 5 and 8).

Chloride is one of the main components in these groundwaters and it is directly correlated with their salinity. The groundwaters in the uppermost 100 to 150 m in the Forsmark area (Figure 9-5a and b) display a wide chemical variability (here with respect to chloride and referred to as mixed brackish groundwaters), due partly to the mixing of discharging brackish marine (Littorina) groundwaters (and/or residual near-surface saline waters of Baltic Sea origin) with recharging meteoric waters. In the footwall bedrock segment (including fracture domains FFM01 and FFM02), the shallow system is controlled by flow along a highly transmissive, well-connected system of sub-horizontal fractures referred to as the shallow bedrock aquifer, which is still in the process of flushing out residual brackish marine (Littorina) groundwaters. This also produces a mixing effect between recharging meteoric waters and residual brackish (possibly including Baltic Sea) groundwaters.

Below this shallow part, the chloride content varies significantly with depth. Groundwaters from the footwall bedrock (including fracture domains FFM01 and FFM02) show a progressive increase of chloride from 100 m down to 600 m depth, and groundwaters from outside the target volume (boreholes KFM07A and KFM09A), show an important shift to the highest chloride concentration values measured at Forsmark (14,000 to 15,000 mg/L). This higher salinity appears to be associated with a larger proportion of a deeper, more highly saline component (Figure 9-5a, b and /Smellie et al. 2008/). The presence of greater salinity at such intermediate depths is considered to reflect natural and/or anthropogenic effects either due to glacial rebound (after the maximum glacial loading) or upconing resulting from different borehole activities including groundwater sampling. The first possibility is indicated by the presence of equally high chloride concentrations in porewater from borehole KFM09B collected at a distance of one metre from a water-conducting fracture, but considerably lower chloride further into the intact rock matrix (see section 9.5.8). This suggests a recent, but long interaction time between a high chloride fracture groundwater and the matrix porewater. The second possibility is supported by heavy pumping carried out in to flush, for example, borehole KFM07A prior to sampling, and the only source of such saline groundwater below 250 m is believed to originate from a highly conductive fracture at around 800 m depth /Berg et al. 2005, Olofsson et al. 2007/. A similar explanation may be valid also for borehole KFM09A and in both cases upconing may have been facilitated by steeply dipping deformation zones with a high transmissivity.

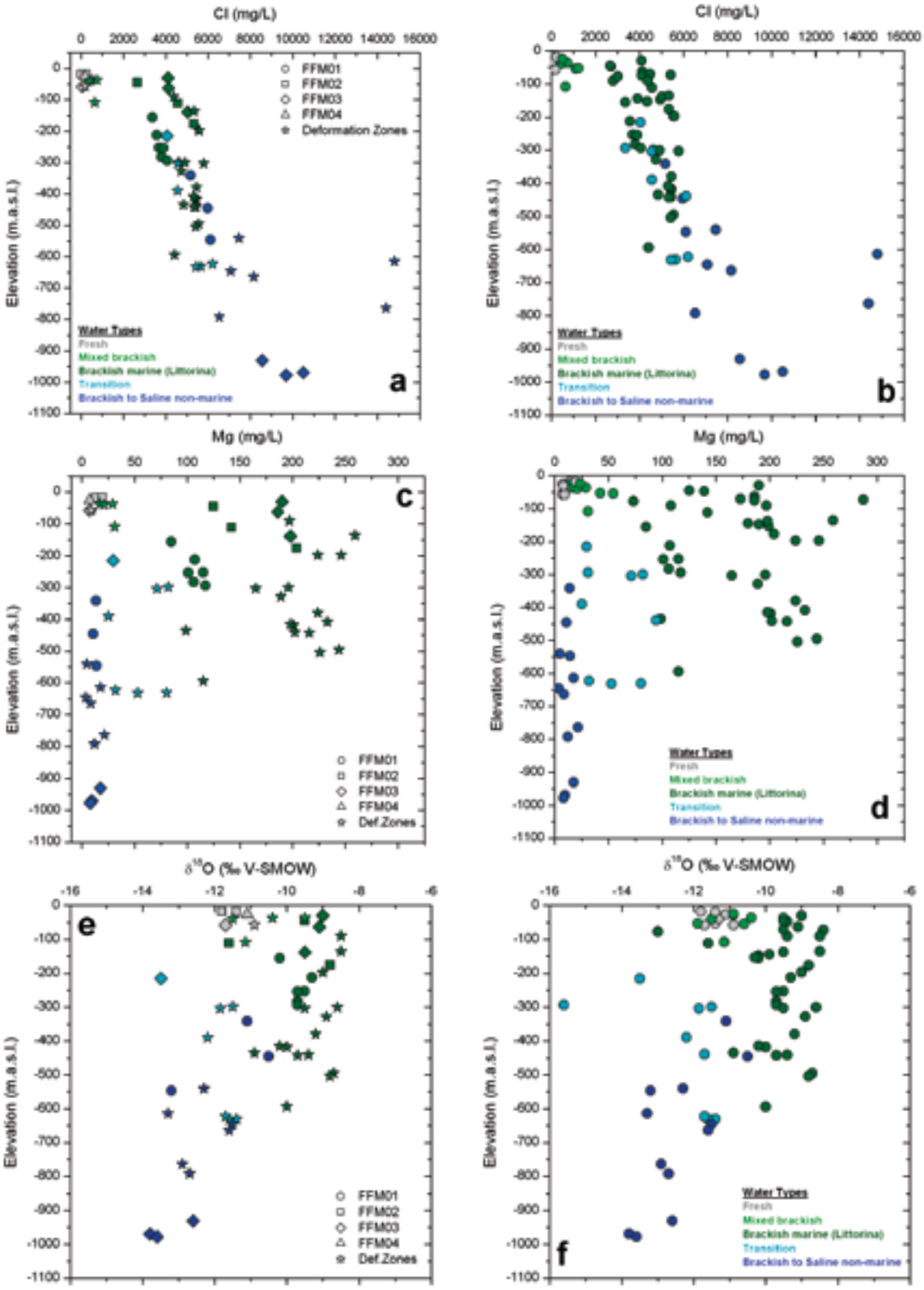

Figure 9-5. *Distributions of Cl (a, b), Mg (c, d) and $\delta^{18}O$ (e, f) in the two main systems in the Forsmark candidate area (i.e. hanging wall and footwall). Left-hand plots represent groundwaters sampled from the hanging wall (fracture domain FFM03), the footwall (fracture domains FFM01 and FFM02), and from the deformation zones. Right-hand plots represent all sampled groundwaters subdivided into the different major groundwater types used in the site description.*

With the available data, however, a definitive interpretation cannot be presented that supports either a natural or anthropogenic origin to these anomalous groundwater compositions.

Brackish marine groundwaters sampled from the hanging wall bedrock (i.e. fracture domain FFM03) mostly originate from the series of highly transmissive, gently dipping deformation zones. These deformation zone groundwaters have a wide range of chloride contents down to around 200 m depth, some achieving values as high as 5,500 mg/L (i.e. a strong Littorina Sea signature). From 200 to 600 m depth, the chloride content remains fairly constant around this value before increasing progressively up to 10,000 mg/L Cl at around 1,000 m depth, i.e. to brackish and then saline non-marine groundwater types.

This increased salinity gradient with depth in the Forsmark area from around 600 m, is believed to reflect processes that have occurred prior to the incursion of the Littorina Sea waters (and also the meltwaters from the last deglaciation) (cf. section 9.3.2). At that time, mixing and dilution of a deeper, more highly saline groundwater (or possibly a brine type) with lower saline groundwaters at shallower depths (i.e. footwall bedrock including domain FFM01), can be attributed to advection, whereas at greater depths where groundwater flow decreases towards stagnant conditions, mixing is driven by upward molecular diffusion. Nevertheless, under both conditions it is the same deep saline or brine component that is being modified.

The three-dimensional chloride distribution with depth is illustrated in Figure 9-6. Here it is possible to obtain a feel for the spatial distribution of chloride laterally across the candidate area, and also to relate the borehole groundwater chemistry to potentially important surface and near-surface features, for example, discharge and recharge features reflected by variations in the salinity. Additional three-dimensional plots showing element concentrations and modelling results are described in /Laaksoharju et al. 2008a/.

The magnesium concentration (Figure 9-5b and c) further emphasises the strong marine (i.e. Littorina Sea) influence in the candidate volume as a whole, but again much more marked in the hanging wall bedrock in association with the gently dipping deformation zones, including ZFMA2. The brackish marine groundwater transition to brackish non-marine groundwater is quite sharp and clearly observed from around 500 to 650 m depth in the hanging wall bedrock, but is generally more

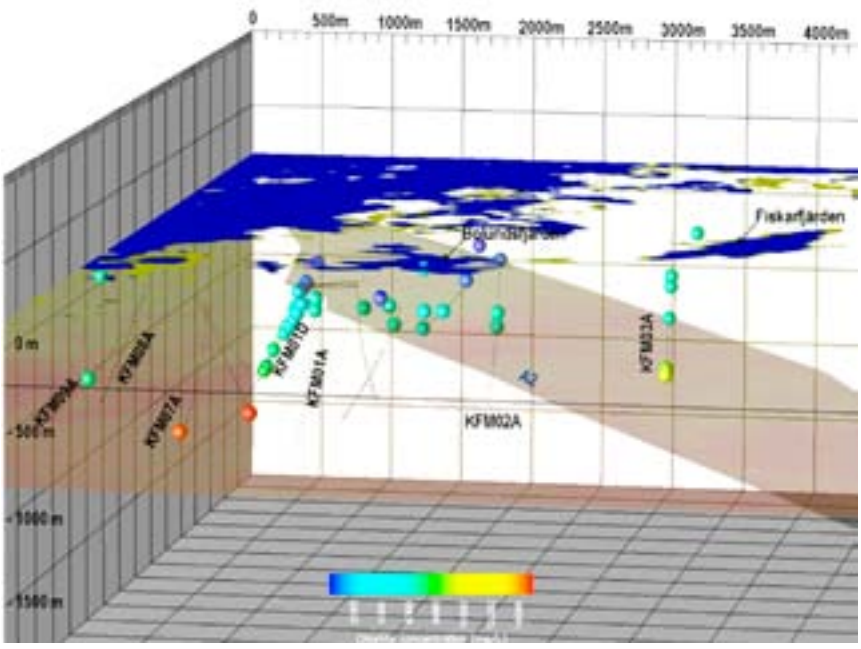

Figure 9-6. *3D visualisation of Cl concentrations and their lateral and vertical distribution related to the major gently dipping deformation zone ZFMA2 which together with ZFMF1 (not shown) effectively divide the candidate area into the hanging wall (above ZFMA2) and footwall (below ZFMA2 – denoted by A2). SE-NW view of the Forsmark area showing the main surface features such as lakes and coastline; the borehole names and sample locations are shown.*

diffuse in the depth interval around 200 to 650 m in the footwall bedrock. In the part of the footwall bedrock where the frequency of water-conductive fractures is low (i.e. fracture domain FFM01), represented by borehole KFM01D, the maximum Littorina penetration is to around 300 to 350 m depth.

In the brackish to saline non-marine groundwaters, magnesium quickly drops to less than 25 mg/L at depths below around 650 m in the hanging wall bedrock and at around 300 m in the footwall bedrock (i.e. borehole KFM01D). This is an important observation, suggesting that below these respective levels, any significant hydrochemical distinction ceases between the footwall bedrock (i.e. fracture domain FFM01) and hanging wall bedrock (i.e. fracture domain FFM03). Furthermore, below these levels, the fracture transmissivity is also very low.

With respect to oxygen-18 (Figure 9-5e and f), four main distinguishing observations can be made: a) typical near-surface meteoric recharge values around –12 to –10.5‰ V-SMOW), b) enriched values ranging from $\delta^{18}O$ = –10 to –8.5‰ V-SMOW representing the brackish marine (Littorina-type) groundwaters, c) depleted values of $\delta^{18}O$ = –14 to –12‰ V-SMOW for brackish to saline non-marine groundwaters, and d) the most depleted sample at $\delta^{18}O$ = –15.6‰ V-SMOW from a mixed brackish groundwater with a significant glacial component from the regional scale Forsmark deformation zone located outside the candidate area (KFM12A). Groundwaters from fracture domains FFM04 and FFM05, located just outside the target volume, show weak but noticeable depleted glacial signatures (i.e. KFM07A at –12.9‰ V-SMOW and KFM9A at –13.3‰ V-SMOW). The most depleted sample from the candidate area has $\delta^{18}O$ = –13.8‰ V-SMOW and is from borehole KFM03A (at 960 m) located in the hanging wall bedrock. Furthermore, porewater studies show that a glacial water component is present in the footwall bedrock (i.e. KFM08C at –13‰ V-SMOW; around 400 m depth) and hanging wall bedrock (i.e. KFM02B at –15‰ V-SMOW; around 170 m depth).

To evaluate the extent of mixing between glacial meltwater and the Littorina type waters a larger data set is used. Figure 9-7 is based on category 1 to 5 data from percussion and cored boreholes within and close to the candidate area, and category 5 data (i.e. all available data are of low quality)

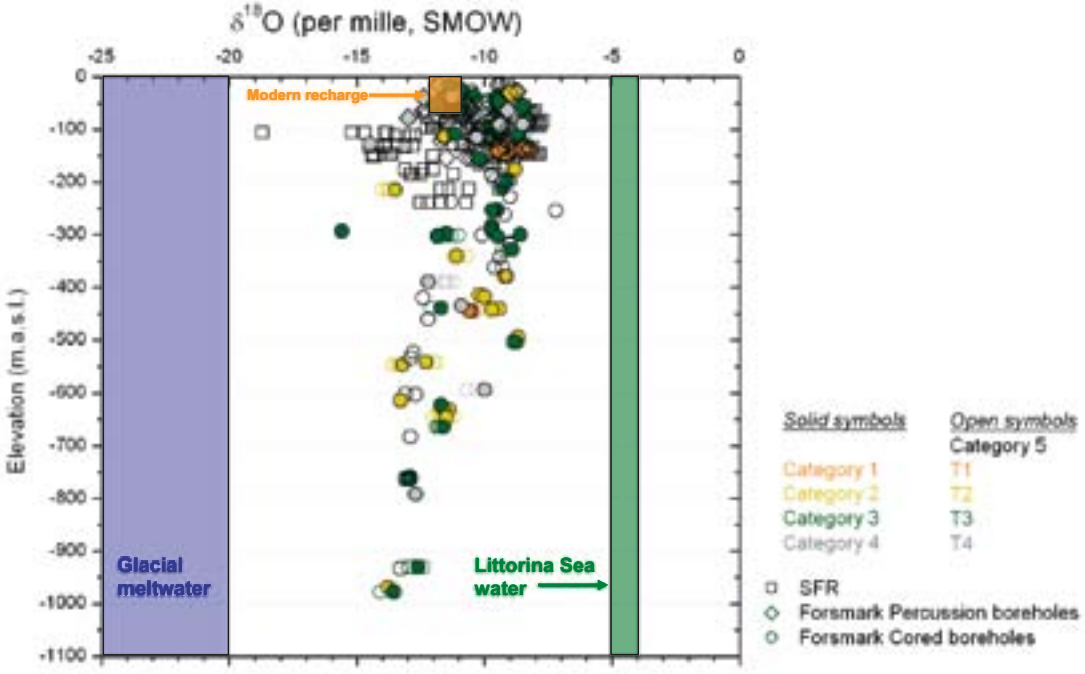

Figure 9-7. *$\delta^{18}O$ versus elevation based on category 1–5 data from all percussion and cored boreholes, and category 5 data from SFR. The modern recharge, glacial and marine influences are recognised; see text for discussion. The reference to T1–T4 indicates time-series data measured from some of the borehole sections; these data are shown as a horizontal series of open circles colour coded, with the actual categorised sample in-filled.*

from the SFR site. In the figure is also indicated the original range of oxygen-18 values for the Littorina Sea and for glacial meltwater. All groundwaters show signs of mixing and plot in the area between these two extremes, i.e. no groundwaters represent a pure glacial meltwater or Littorina Sea water. Infiltration of Littorina Sea water and the resulting mixing with glacial water is gradual, and is especially important in the shallow samples collected from SFR, which plot along a mixing line between the glacial and marine groups. Between 200 to 300 m depth, some brackish waters with a significantly low oxygen-18 signature are present, representing samples from boreholes KFM12A and KFM11A located outside the candidate area. These waters are not typically brackish-marine, but show instead salinity compositions which indicate complex mixing between brackish marine, brackish non-marine and glacial waters, and therefore are referred to as transition zone samples. These examples suggest limited reservoirs of glacial water preserved, for example, in pockets or lenses or dead-end fractures etc in the upper bedrock of the footwall closely associated with the shallow bedrock aquifer (chapter 8). Generally in the candidate area, at depths below 500 m and down to the maximum sampled depth at approximately 970 m, there is a depletion trend in oxygen-18 indicating an increasing glacial component, which does not necessarily represent the last deglaciation.

The subdivision of the groundwater types is clearly reflected also in the chemistry of sodium (Na), calcium (Ca), potassium (K) and sulphate (SO_4) /Laaksoharju et al. 2008a, Smellie et al. 2008/. In Figure 9-8a, b and c the brackish marine (Littorina) groundwaters show generally, to varying degrees, higher sodium, potassium (not included) and sulphate with correspondingly lower calcium than the brackish to saline non-marine groundwater types. The calcium content, and to a small extent also the sodium content, in the brackish to saline non-marine groundwaters increases steadily with depth. Potassium and sulphate are low in content and show no clear trends. The increase in calcium is a well recognised trend, for example, in many deep groundwaters from the Fennoscandian and Canadian Precambrian Shield areas with calcium enrichment from water/rock interaction occurring where groundwater flow decreases towards stagnant conditions with increasing depth /Frape and Fritz 1987, Smellie et al. 2008/.

Bicarbonate (HCO_3) contents (Figure 9-8d) are highly variable in the upper 150 m of the footwall bedrock, where the carbonate system and the microbial production of carbon dioxide are very active /Gimeno et al. 2008, Hallbeck and Pedersen 2008a/. Concentrations then decrease to very low values at greater depths in both the footwall (including fracture domain FFM01) and hanging wall bedrock at around 300 and 600 m depth, respectively. However, bicarbonate is relatively high in most of the brackish marine groundwaters in the upper 600 m of the gently dipping fracture zones in the hanging wall bedrock. The brackish non-marine groundwaters below 300 m depth in the footwall bedrock including fracture domain FFM01, in contrast, have low bicarbonate contents at the same depths. At these depths this could be consistent with a higher carbon dioxide consumption by silicate weathering and increasing residence time of the groundwater mixtures.

Groundwater samples from the footwall bedrock segment comprising the target volume (i.e. fracture domain FFM01), and fracture domains FFM04 and FFM05 (not plotted) outside the target volume, have pH values between 8 and 8.5 (Figure 9-8f), except for one sample taken in borehole KFM06A /Gimeno et al. 2008, Laaksoharju et al. 2008a/. As expected, pCO_2 in equilibrium with these waters decreases with depth as CO_2 is consumed by microbially-mediated reactions, water/rock interaction, and/or decreased by mixing with saline waters with very low carbon contents. Most groundwaters are in equilibrium with calcite (Figure 9-8e) /Gimeno et al. 2008/. Groundwaters mostly of brackish marine water type and mainly from the gently dipping fracture zones in the hanging wall have lower pH values (around 7.5) and higher pCO_2 /Gimeno et al. 2008, Laaksoharju et al. 2008a/ although most of the waters are in equilibrium with calcite.

Ion-ion/isotope plots

Figure 9-9 shows a collection of ion-ion/isotope cross plots which can reveal whether the groundwater composition is affected by other processes than mixing. For example, sodium shows an overall positive correlation with chloride (Figure 9-9a), which reflects generally that sodium behaves almost like a conservative compound and mixing is the main process controlling its content.

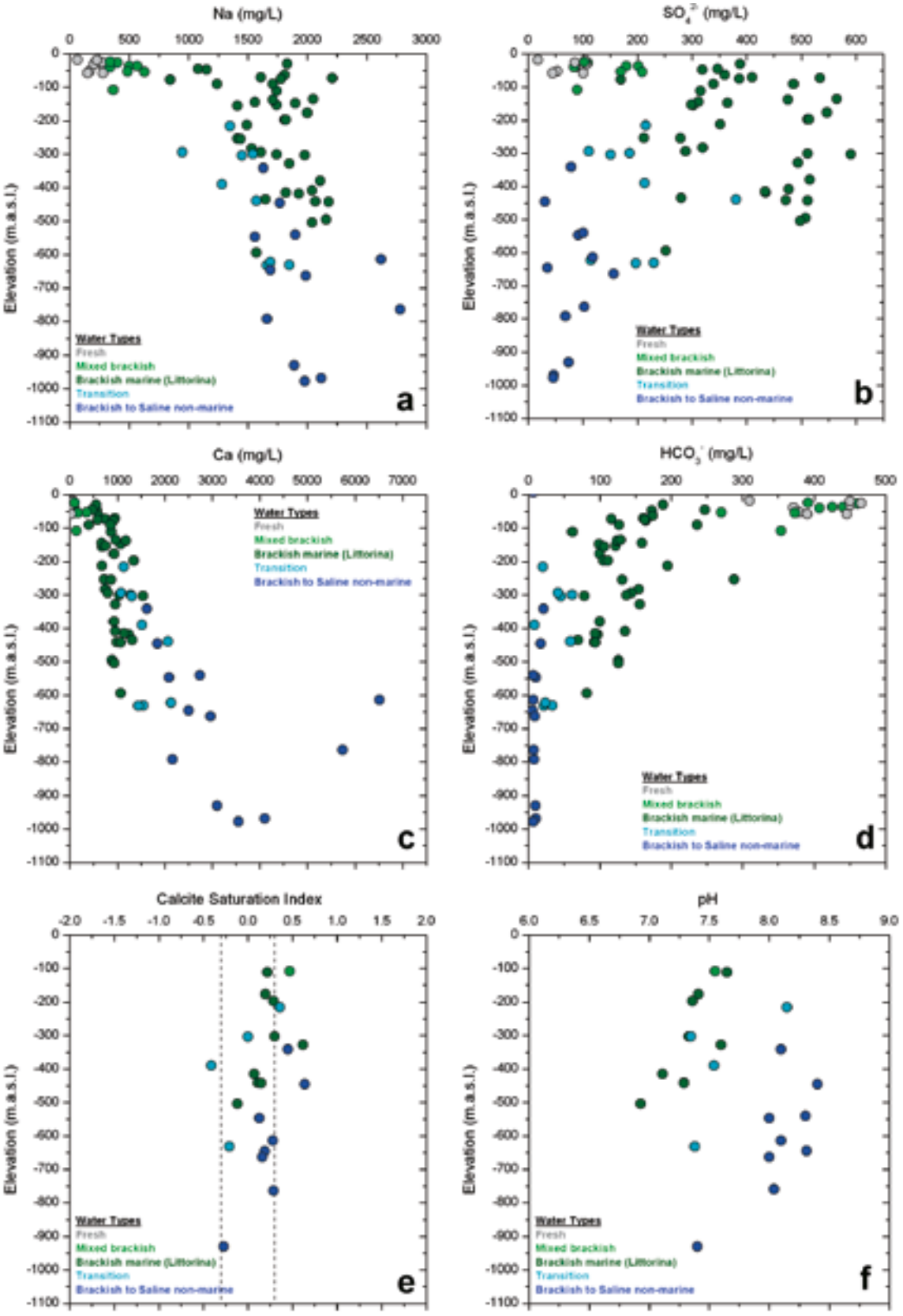

Figure 9-8. *Sodium, sulphate and the carbonate system with increasing depth: a) sodium, b) sulphate, c) calcium, d) bicarbonate, e) calcite saturation index (uncertainty area of ± –0.3 is shaded), and f) pH.*

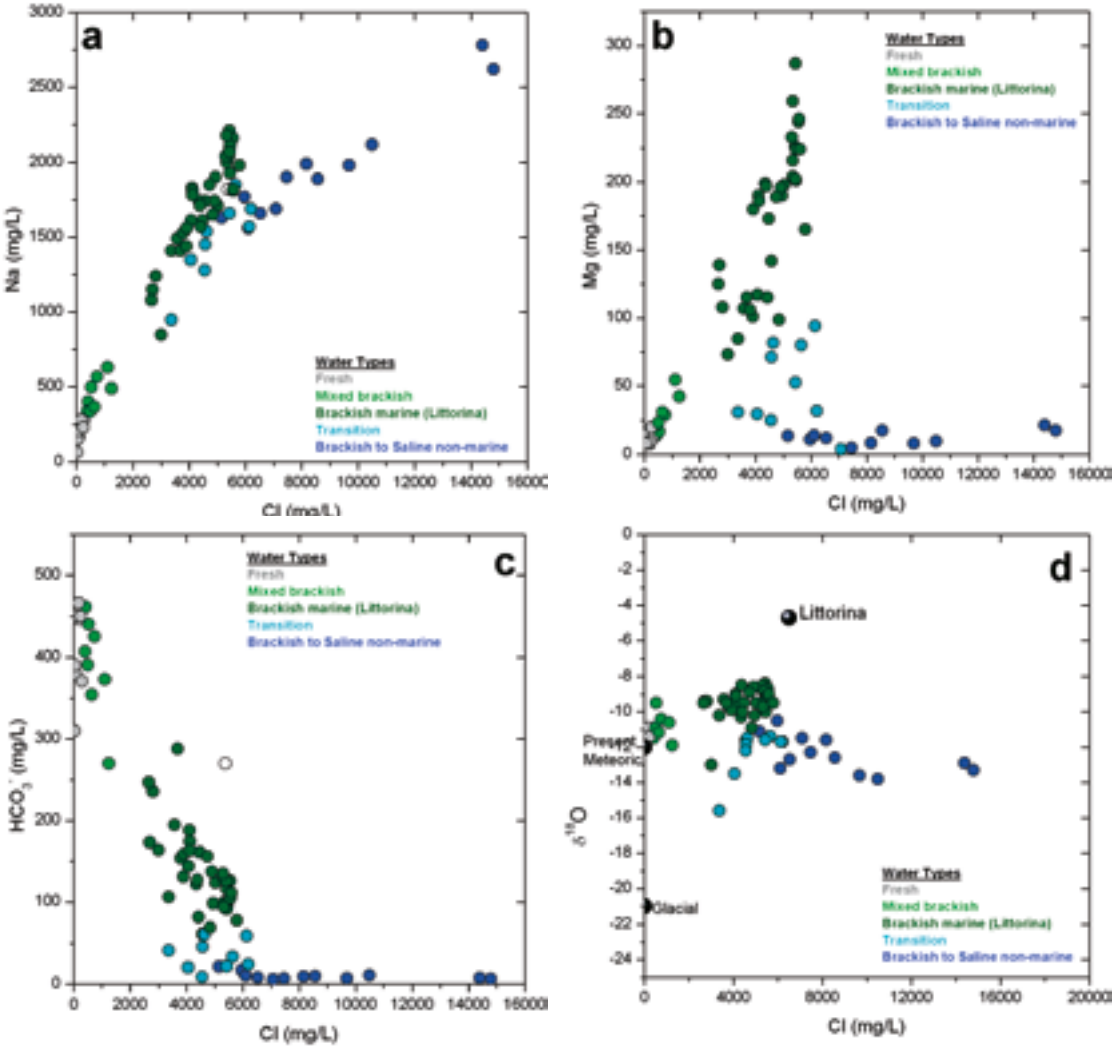

Figure 9-9. *Plots of sodium (a), magnesium (b), bicarbonate (c) and $\delta^{18}O$ (d) versus chloride related to the main groundwater types that characterise the Forsmark candidate site.*

In detail, however, two different sodium/chloride trends can be seen, one represented by the brackish to saline non-marine groundwaters (clearly affected by a deeper more saline component), and the other by the brackish marine (Littorina) groundwaters with up to 5,500 mg/L of chloride. These two mixing trends are also recognisable in the bromide versus chloride plot (Figure 9-10c). Magnesium (Figure 9-9b) and sulphate (Figure 9-10b), both susceptible to reactions, show a clear contrast between the pre-Littorina brackish to saline non-marine groundwaters (low values from older mixtures between deep saline and more dilute groundwaters) and the more recent Littorina Sea component (comparatively higher values).

In conclusion, the plots of Na, Ca, Mg, Br, HCO_3, SO_4 and $\delta^{18}O$ versus Cl indicate the origin and evolution of the deep brackish to saline non-marine groundwaters. Once again, mixing with the recent Littorina Sea waters has disturbed or removed earlier groundwater trends at shallower depths. At greater depths, older trends are preserved in groundwaters from the less conductive bedrock volumes and also in the rock matrix porewaters.

Plotting Ca/Mg versus Br/Cl, Figure 9-10d, shows a cluster of young to recent fresh, mixed and brackish marine groundwaters with low ratios, and a change to much older and deeper, brackish to saline non-marine groundwaters at higher ratios. Between these two end members there are several transition groundwaters indicating different degrees of mixing between the two. Many of the samples, therefore, represent groundwaters which contain a component of a highly saline, non-marine or non-marine/old marine mixing end member that increases in amount with depth.

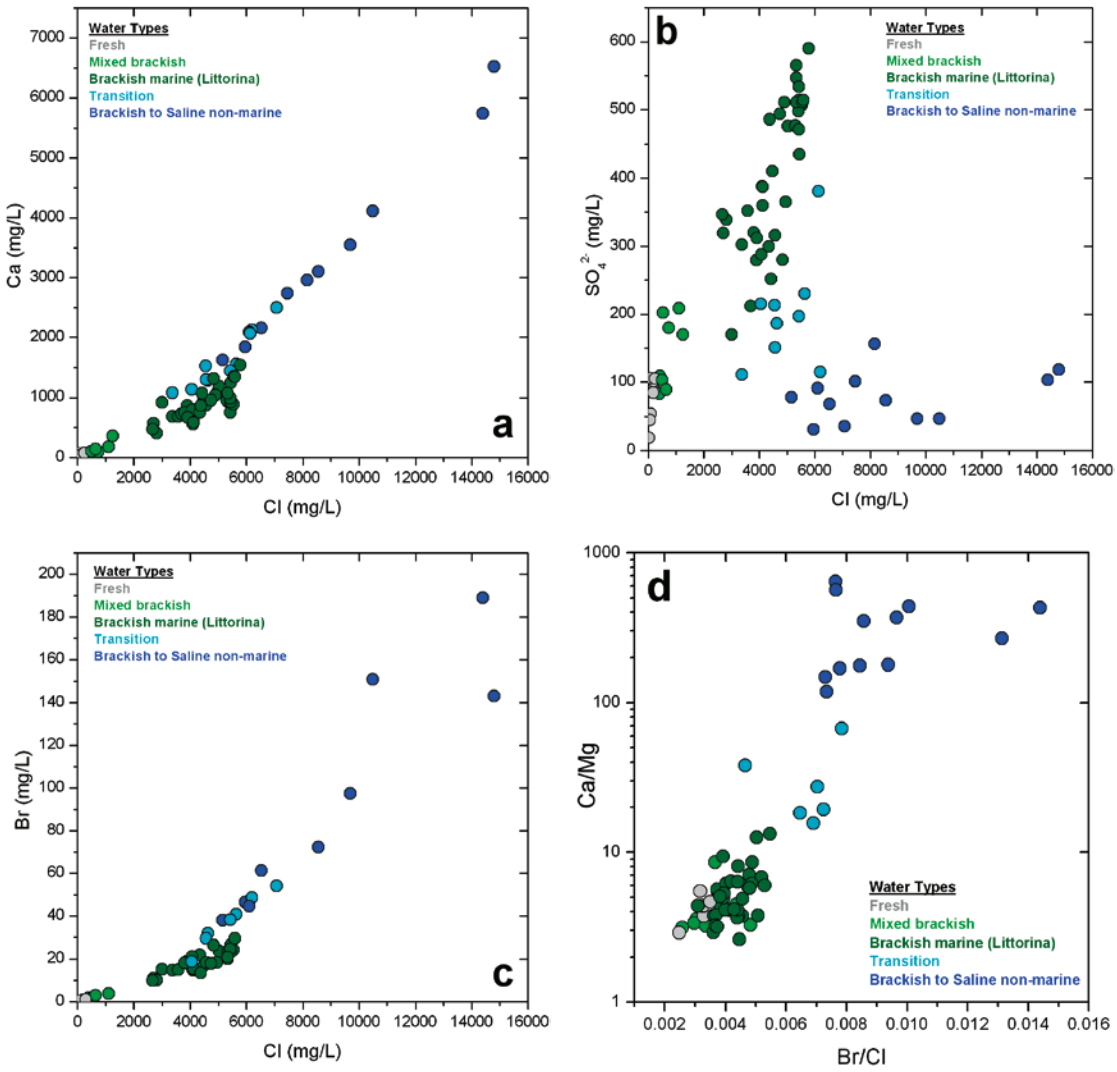

Figure 9-10. *Plots of calcium (a), sulphate (b) and bromide (c) versus chloride, together with an ion ratio plot of Ca/Mg versus Br/Cl. All are related to the main groundwater types that characterise the Forsmark candidate site.*

9.5.2 Mixing calculations

Multivariate Mixing and Mass-balance Modelling (M3) /Laaksoharju et al. 1999, Gómez et al. 2006/ uses the Principal Component Analysis (PCA) method to analyse variations in groundwater compositions so that the mixing components, their proportions, and chemical reactions can be identified. The PCA method is statistical and identifies the principal components, in terms of linear combinations of the concentrations of those species analysed, that best explains the spread in data. The method quantifies the contribution to hydrochemical variations by mixing of groundwater masses in a flow system by comparing groundwater compositions with identified end-member waters. However, groundwater mixing proportions computed with M3 should be considered semi-qualitative (i.e. due to the complex influence of mixing and reactions), as evaluations of the groundwater signatures have shown that over- or under-estimations of the actual groundwater signatures can result /Laaksoharju et al. 1999, Molinero et al. 2008/. The choice of end members is crucial for modelling the mixing proportions. Calculated mixing proportions showing a deep saline water component at very shallow depths is an example of model errors introduced when assuming that all end members contribute to the groundwater formation. The uncertainties are handled in M3 by applying an uncertainty of 0.1 mixing units and stating that a mixing portion < 10% is below the detection limit of the method. The uncertainties of the method are described by /Laaksoharju et al. 2008c, Gómez et al. 2008/ and the end-member test performed using Monte Carlo simulations are described in /Gimeno et al. 2008/.

The aim of this test is to obtain an independent assessment of the validity of the chemical composition of the end members used in the M3 calculations.

The M3 modelling of the Forsmark groundwaters is discussed in /Laaksoharju et al. 2008a, Gimeno et al. 2008, Gurban 2008, Molinero et al. 2008/. The results support the independent interpretations of measured ions and isotopes and indications of major features, such as the groundwater origin in terms of relative mixing proportions and the penetration depth or location of different groundwaters. In Figure 9-11a and b, the M3 mixing proportions are shown as scatter plots indicating the end-member contribution of Altered Meteoric and Littorina Sea water in relation to the resulting water, and the end-member mixing proportions with depth.

The water samples with an Altered Meteoric end-member portion greater than 80% generally correspond to waters with measurable tritium contents (restricted to the uppermost 100 to 200 m of the rock, mainly fracture domain FFM02 in the footwall bedrock), see Figure 9-11a. This confirms that the dilute water represents a very active hydrogeological system. As expected, the resulting current 'Fresh' and 'Mixed' waters show large proportions of the Altered Meteoric end member.

The Littorina Sea water end-member signature has been detected at depths between 100 and 600 m, mainly in the hanging wall bedrock segment, and to a lesser extent (down to 300 m) in the footwall bedrock segment (i.e. fracture domains FFM01 and FFM02), see Figure 9-11b. At depths greater than 600 m in the hanging wall, the gently dipping deformation zones contain groundwater devoid of marine signatures. The Littorina end member corresponds to high measured magnesium and sulphate values, and the resulting Brackish Marine water, from mixing of the Altered Meteoric and Littorina Sea end members, should contain the largest proportions of the Littorina Sea end member. Independent evaluations of Littorina signatures, based on chloride and bromide mass ratios, indicate that the M3 model could underestimate the actual marine signature in the groundwaters /Molinero et al. 2008/. This is explained by the modification of the original Littorina Sea signature (used as an end member) by different reactions, such as microbial sulphate reduction and related production of bicarbonate etc.

9.5.3 Redox modelling

To evaluate the redox system is one of the most important requirements for repository safety assessment, but also one of the most complicated tasks in hydrogeochemistry /Auqué et al. 2008/. The aim of the redox modelling is to: a) confirm or support the redox potential field measurements, and b) confirm the redox pair(s) believed to control the redox conditions in the groundwater. The number of samples with representative and complete data for the analysis of the redox system (Eh values, Fe^{2+}, S^{2-}, Mn, U, microbial and mineralogical data) have increased during the hydrogeochemical programme, especially in the number of Eh determinations, but the amount of data is still very low,

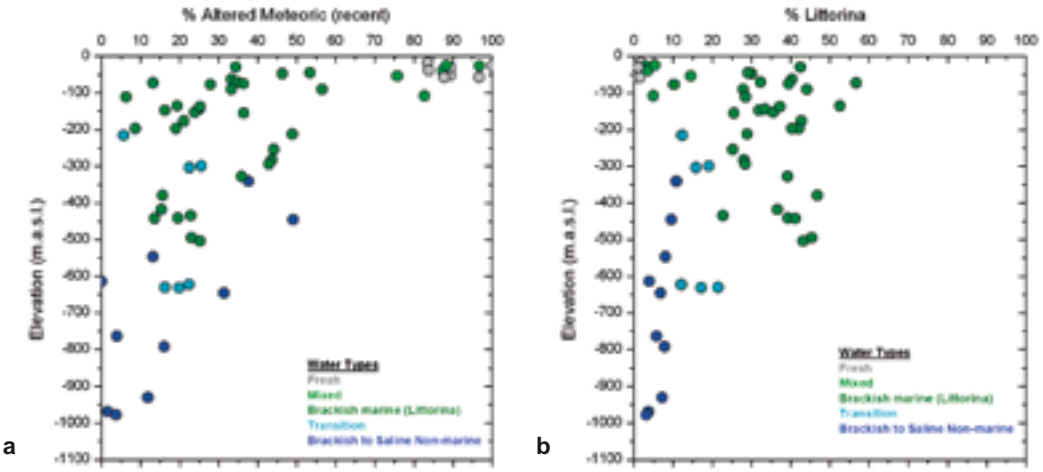

Figure 9-11. *Computed M3 mixing proportions of: a) recent Altered Meteoric end member, and b) Littorina Sea water plotted versus depth and for current water types.*

cf. Figure 9-12a. Integrated evaluation shows that the rock/water system (including microbial activity) maintains a buffer capacity that ensures a reducing character at depths greater than 100 m /Laaksoharju et al. 2008a/. This conclusion holds true even considering some problems with the data. The analyses performed have confirmed that sampling (or drilling-induced) perturbation may have altered the original redox conditions of the hydrochemical system /Gimeno et al. 2008/. Examples include oxygen intrusion and precipitation of amorphous iron oxyhydroxides, modification of Eh or alkalinity by drilling waters, and the increase in dissolved uranium contents, or changes in sulphide contents, caused by one or more of these disturbances.

For the analyses of the site investigation data, an integrated modelling approach was applied, in which hydrogeochemical information was combined with mineralogical and microbiological information. This work is presented in /Gimeno et al. 2008/ where, for example, measured electrode Eh values were compared with independently calculated values, and/or were tested and confirmed using other data.

The available information on the redox system is summarised below.

The iron system is most clearly affected by drilling and sampling disturbances. For example, recent and detailed mineralogical determinations in borehole KFM02A indicate the presence of fine-grained amorphous to poorly crystalline phases (including some other, more ordered, structures, e.g. goethite) induced by drilling /Didriksen et al. 2007/. However, most of the Eh values determined

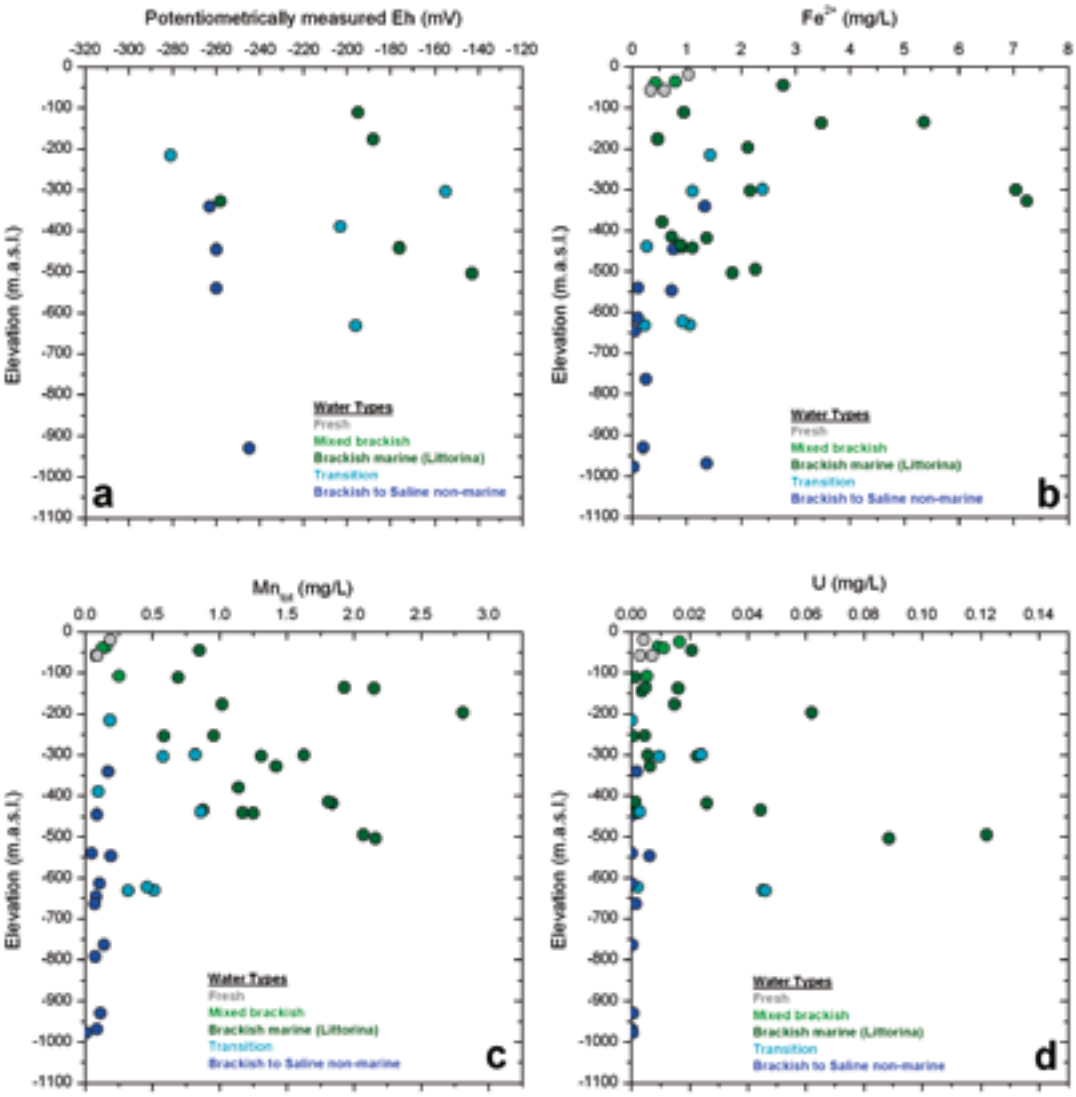

Figure 9-12. *Distribution of potentiometric Eh (mV)(a), Fe^{2+} (b), Mn_{tot} (c), and U (d) with depth in the Forsmark area groundwaters (groundwater categories 1, 2, 3 and 4 have been plotted).*

in brackish marine groundwaters (at depths between 110 and 646 m, Figure 9-12b) seem to be controlled by the occurrence of an oxidised iron phase with an intermediate crystallinity, such as that considered by /Banwart 1999/ in the Äspö REX Experiment. This intermediate phase would represent a recent microcrystalline iron oxyhydroxide, recrystallised from an amorphous one.The presence of an intermediate iron oxyhydroxide, with higher solubility than a truly crystalline phase, is considered possible in these brackish groundwaters if a brief oxidising disturbance has taken place. This supports the results obtained from the redox pair calculations /Gimeno et al. 2008/.

In the deeper saline groundwaters this situation has not been detected. The redox potential measured in the deepest groundwaters at Forsmark is one of the most reducing in the system, and is in agreement with the modelled value derived according to /Grenthe et al. 1992/. This indicates that the Eh value of these groundwaters is undisturbed and appears to be controlled by a clearly crystalline iron oxide such as hematite.

With respect to the *manganese system,* low total manganese contents and undersaturation with respect to rhodochrosite are typical for saline Forsmark groundwaters, as also observed in many other granitic groundwater systems. However, brackish marine groundwaters with an important Littorina component usually have high manganese concentrations (Figure 9-12c) and reach equilibrium with respect to rhodochrosite. This is very uncommon in other granitic systems in the Scandinavian Shield, unless the Littorina component happens to be in the same range as that at Forsmark. This suggests that the high manganese contents and the equilibrium with rhodochrosite in brackish marine groundwaters are a characteristic that may have been imposed by the superficial marine environment prevailing during the Littorina stage, involving microbial activity in the sea floor sediments. Furthermore, measurable manganese contents provide independent support for reducing conditions.

The sulphur system is important for the general understanding of redox processes in Forsmark groundwaters. Studies of the sulphate contents in the groundwaters show decreasing values with depth (Figure 9-8b), and the highest sulphate values are associated with the presence of brackish marine groundwaters of Littorina-type, whereas the brackish to saline non-marine groundwaters are low in sulphate (cf. section 9.5.1). However, the SO_4/Cl ratio is less than expected for marine waters. This, in combination with the sulphur isotope data ($\delta^{34}S$), show values higher than marine signatures (+21‰ CDT; the standard used for $\delta^{34}S$ is CDT or Canyon Diablo Troilite), which suggest some modification caused by sulphate reducing bacteria (SRB). These bacteria have been identified in most of the boreholes at Forsmark, although the numbers of SRB were very low in some of the samples (cf. section 9.5.4 and /Hallbeck and Pedersen 2008a, Smellie et al. 2008/). In conclusion, this means that sulphide is, or has been, produced at various depths in the groundwater system, but the available data do not allow quantitative estimates of its production over time.

Actual measurements of sulphide indicate a complex pattern with evidence of perturbations (mainly anthropogenic) in the original sulphide contents deduced from increases observed with time in most of the resampled and monitored sections (additional data not included in the modelling). Based on the modelling of stage 2.3 data, precipitation of "amorphous" monosulphides occurs only locally (mainly associated with deformation zones). In the brackish marine groundwaters between 220 m and 600 m depth, dissolved sulphide contents are low, possibly due to localised precipitation of monosulphides in ferrous iron-rich environments /Gimeno et al. 2008/. Another possibility is that the measured sulphide may be too low due to flushing in connection with drilling and sampling /Hallbeck and Pedersen 2008a, Laaksoharju et al. 2008a/, making interpretations based on present data uncertain.

With respect to *the uranium system*, the simplest explanation to the available data is that the origin of the enhanced dissolved uranium contents detected in the Forsmark brackish marine groundwaters associated with deformation zones (Figure 9-12d) is related to local uranium anomalies or mineralisations in contact with these groundwaters. Limited mineralogical data seem to confirm this point (section 9.5.7 and /Sandström et al. 2008/).

Speciation-solubility calculations support this conclusion and indicate that the enhanced uranium contents are the result of two factors: (a) the solubility control exerted by an amorphous uranium phase present in the system, and (b) the redox system which supports uranium complexation and re-equilibrium depending on Eh (–200 to –180 mV) and dissolved carbonate. Within the Eh and

alkalinity ranges that characterise the Forsmark groundwaters, uranium speciation is very sensitive to minor modifications in these parameters because they affect the extent of uranium carbonate complexation and, therefore, the solubility of the solids. This is important when considering the possible modification of natural conditions undergone by these waters. The alteration of an originally more reducing environment, and/or the increase of dissolved carbonate (e.g. by mixing with drilling waters), could have caused the increase in uranium-carbonate complexation, in turn enhancing the dissolution of uranium phases and increasing the contents of dissolved uranium with respect to that originally present in the system.

9.5.4 Characterisation of microorganisms

Introduction

The microbiological characterisation, based on high quality assurance of the drilling and sampling procedures /Pedersen 2005, Hallbeck and Pedersen 2008ab/, included total number of cells (TNC) and concentration of adenosine-tri-phosphate (ATP). Cultivation methods consisted of aerobic plate counts and most probable number (MPN) determinations of anaerobic microorganisms including nitrate-reducing bacteria (NRB), iron-reducing bacteria (IRB), manganese-reducing bacteria (MRB), sulphate-reducing bacteria (SRB), acetogenic bacteria (AA, HA) and methanogens (AM, HM). Note: Uncertainties in the data may have resulted from the effects of drilling and sampling, including short-circuiting problems, that have not been possible to quantify /Smellie et al. 2008/.

Size and activity of microbial populations

Investigations of the two different biomass parameters TNC and ATP in groundwaters from the Fennoscandian Shield have previously shown good agreement between these two parameters /Eydal and Pedersen 2007/. Similar data from the site investigation in Forsmark also show agreement with a correlation at $p = 0.002$ /Hallbeck and Pedersen 2008a, Laaksoharju et al. 2008a/. When plotted, these data show one group that has high TNC and ATP values and another group with lower TNC and ATP values. The highest ATP and TNC values are found in borehole KFM10A at 328 m depth, followed by the 445 m deep section in KFM01D (Figure 9-13). In fact, these two sections have stacked MPN values that are the highest found during the site investigations carried out in Forsmark (Figure 9-13) and in Olkiluoto, Finland /Pedersen et al. 2008/. Comparing TNC and ATP in the Forsmark groundwaters shows no clear relation with the groundwater types which is expected, since the microbial population is regulated by the available energy, which is not directly related to the groundwater types found at depth.

Diversity and dominating microbial groups

The microbial populations in the two sections with the highest stacked MPN values, KFM10A at 328 m depth and the 445 m deep section in KFM01D, consist of autotrophic and heterotrophic acetogens, and iron-, manganese- and sulphate-reducing bacteria. This diversity distribution is found in most of the samples but with different values. There are some exceptions from this pattern; the shallow samples in KFM01A at 112 m and 176 m depth and the samples from KFM06A at 302 m and 645 m depth, have high numbers of IRB and MRB, but close to zero numbers of SRB. The opposite is found in the deepest sections in borehole KFM03A, at 930 m and 978 m depth, with close to zero numbers of IRB and MRB, but with the presence of SRB. The dominating group in all sections is the acetogens. This group of organisms produces acetate, either from organic compounds in combination with production of hydrogen gas, or in an autotrophic way from carbon dioxide and hydrogen gas.

Sulphate-reducing bacteria, sulphide, sulphate and Eh

The sulphide contents in groundwaters sampled at the same time for microbes are generally very low (from below detection limit up to about 0.1 mg/L). One of the most important and significant correlations found (at $p = 0.009$) is the relation between Eh measured with the Chemmac and the MPN of SRB (Figure 9-14). This correlation suggests that the sulphide-producing activity of SRB may play an important role in controlling Eh as measured by the Chemmac probe (cf. section 9.5.3). An important observation at Forsmark with respect to the activity of SRB is that the concentration of sulphate decreases with depth and is very low below 600 m (cf. Figure 9-8b).

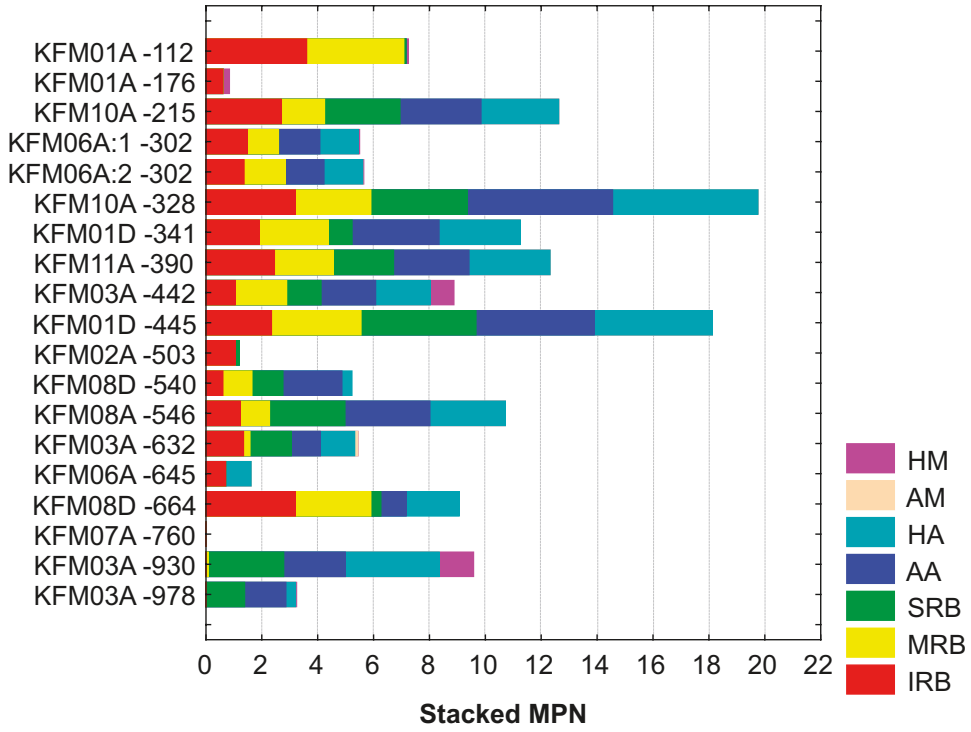

Figure 9-13. *Stacked ^{10}logMPN values for samples from Forsmark sorted by depth. IRB = iron-reducing bacteria, MRB = manganese-reducing bacteria, SRB = sulphate-reducing bacteria, AA = autotrophic acetogens, HA = heterotrophic acetogens, AM = autotrophic methanogens, and HM = heterotrophic methanogens. KFM06A was sampled twice during a control test /Hallbeck and Pedersen 2008a/.*

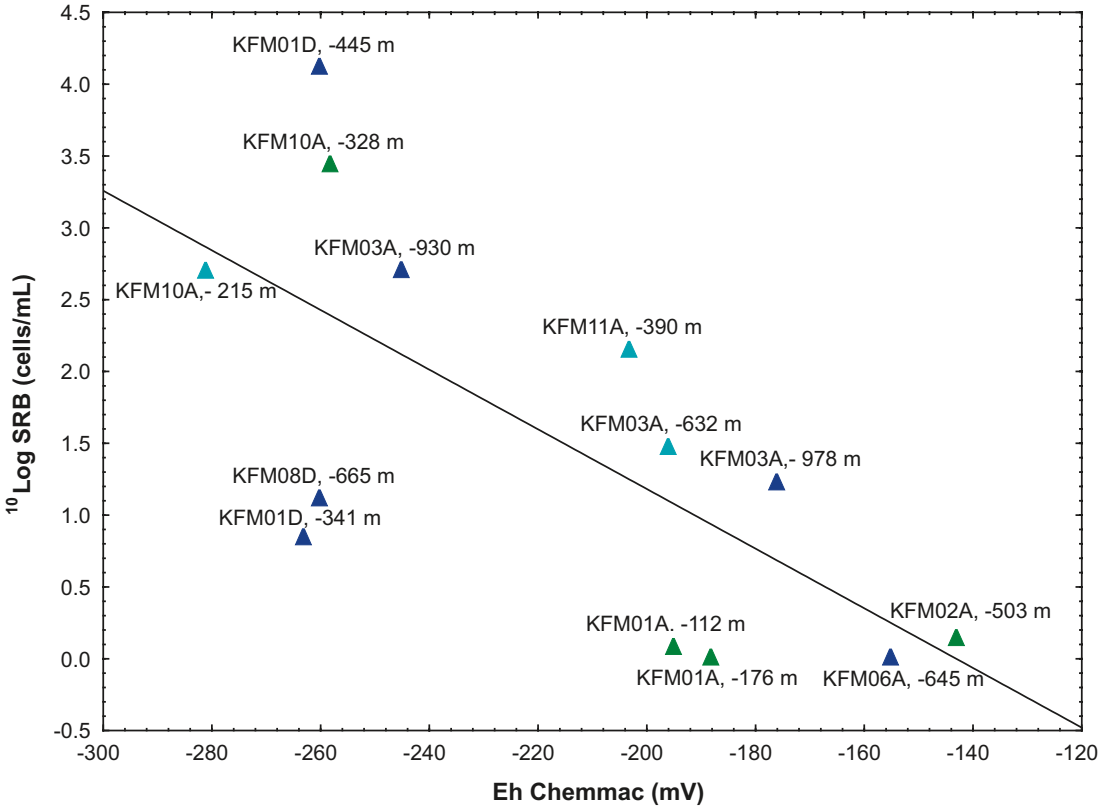

Figure 9-14. *The relation between the number of sulphate-reducing bacteria and Eh analysed with the Chemmac system in relation to the different groundwater types (green = brackish marine (Littorina), turquoise = transition, and blue = brackish to saline non-marine). Statistics: ^{10}log(SRB) = 3.44–0.023 × Eh, r = –0.69, significant at p = 0.009, n = 13.*

Conclusions concerning the microbiological characterisation

The most important findings from the microbiological investigations at Forsmark are:

- Sulphate-reducing bacteria are present at all depths, but show wide variations in population levels.
- Iron- and manganese-reducing bacteria are present at all depths, except for near-zero numbers in samples from the deepest groundwaters in KFM03A at 930 m and 978 m.
- Acetogens are the dominating physiological group of microorganisms.
- Measured Eh values correlate with the number of sulphate-reducing bacteria suggesting that the SO_4^{2-}/S^{2-} system, catalysed by sulphate-reducing bacteria, probably plays an important role in the redox state of the system.

9.5.5 Characterisation of colloids

Concentration of colloids versus depth

Both inorganic and organic colloids exist and these types were measured at Forsmark /Hallbeck and Pedersen 2008a/. Plotting colloid concentration versus depth (Figure 9-15) shows that the colloid concentration is highest at the shallowest depth sampled, i.e. at 112 m depth in KFM01A. However, the concentration is also high in KFM03A at 442 m depth and in KFM10A at 328 m depth, which represent brackish marine groundwaters, and the lowest concentration is found at a depth of 645 m in KFM06A which represents a brackish non-marine groundwater. The total range of measured colloid concentrations in the study is 5 to 170 µg/L and the average concentration is 58.4 µg/L, which compares with average concentrations from crystalline rock groundwaters in Switzerland (30 and 10 µg/L /Degueldre 1994/) and in Canada (300 µg/L /Vilks et al. 1991/), where the same sampling approach was used.

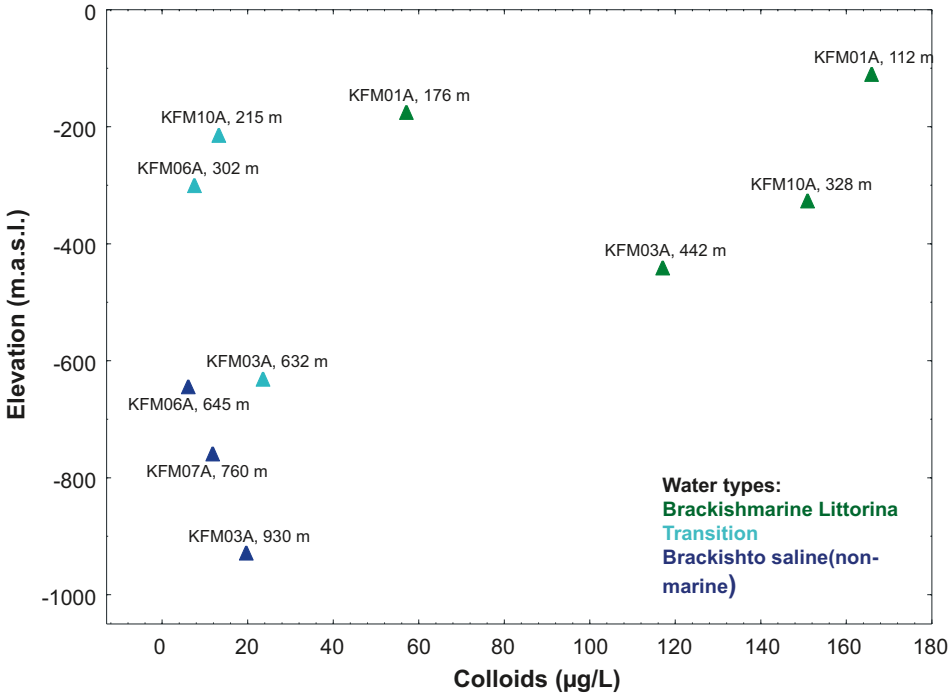

Figure 9-15. *Colloid concentration (µg/L) plotted against depth related to the different groundwater types. Data from /Hallbeck and Pedersen 2008a/ but omitting silica data for KFM01A at 112 m depth and data from KFM08D due to sampling artefacts.*

Conclusions from the colloid investigation

The major conclusions from the colloidal characterisation study are listed below (see also /Hallbeck and Pedersen 2008a, Laaksoharju et al. 2008a/).

- The number of colloids found in groundwaters is 2 to $6 \cdot 10^5$/mL except in borehole KFM10A at a depth of 328 m, where the number is $2 \cdot 10^6$/mL, and in borehole KFM08D where the number of colloids is between $1 \cdot 10^7$ and $2 \cdot 10^8$/mL. The measured colloid concentration in Forsmark is in agreement with measurements in other granitic environments.
- The filtration and fractionation method show that the colloids are composed mostly of iron and sulphur compounds. LIBD (Laser-Induced Breakdown colloid Detection) with EDX (Energy-Dispersive X-ray analysis) show, on the other hand, that the colloids are composed mostly of aluminium, silica and iron compounds. Uranium associated with colloids is found in boreholes KFM02A and KFM06A, in line with the enhanced groundwater uranium concentrations found in these boreholes. The uranium contents associated with the colloids represent about 10% of the uranium concentration in the groundwater and colloidal transport is therefore the result, but not the origin, of the enhanced uranium contents in the groundwater.
- The mass concentration of the colloids differs considerably depending on the detection method used. The highest values are obtained using the filtration method, whereas fractionation gives very low values. However, filtration values are in the same order of magnitude as the LIBD values, and most of the samples are found to contain colloid concentrations below 100 µg/L.
- Colloids can consist of microbial cells and potentially viruses (i.e. phages) and therefore should be taken into consideration when studying colloids in groundwater. The long-term stability and concentration of these colloids and their impact on radionuclide transport require additional study.

Note: Sampling and borehole activities can increase the formation of colloids, and therefore the results obtained can be regarded as maximum values.

9.5.6 Gases

Total gas volumes

Plotting the total volumes of gas at atmospheric pressure in groundwater samples from Forsmark against elevation shows an increasing trend with depth /Hallbeck and Pedersen 2008a/.

Composition of groundwater gas

The major dissolved gases in groundwaters from the Fennoscandian Shield and in Forsmark are nitrogen, carbon dioxide, helium, methane and argon, and the gas composition varies with depth (Figure 9-16). The carbon dioxide concentration is greatest in shallow groundwaters, but the helium concentration increases with depth. The main component in all gas samples is nitrogen and the second most common gas is helium.

A saturation calculation for nitrogen is reported in /Hallbeck and Pedersen 2008a/ for the samples from KFM07A at 760 m depth, which had the highest gas volume of all samples at Forsmark. The calculation showed that 1,200 mL of nitrogen gas could be dissolved in one kg of water at 700 m depth and at a temperature of 10°C, indicating that the gas pressure in the Forsmark groundwater is far from saturation.

9.5.7 Studies of fracture fillings

Background

Fracture minerals are important for the hydrogeochemical understanding and detailed description of the groundwater environment for two main reasons: a) water-mineral interactions influence the present groundwater chemistry (e.g. dissolution/precipitation of calcite, oxidation/production of pyrite, ion exchange etc), and b) the distribution and chemical/isotopic composition of certain minerals (e.g. calcite, pyrite and Fe-oxyhydroxide) provide information on former physico-chemical conditions which are important for the description of the long-term stability of the site /Smellie et al. 2008/.

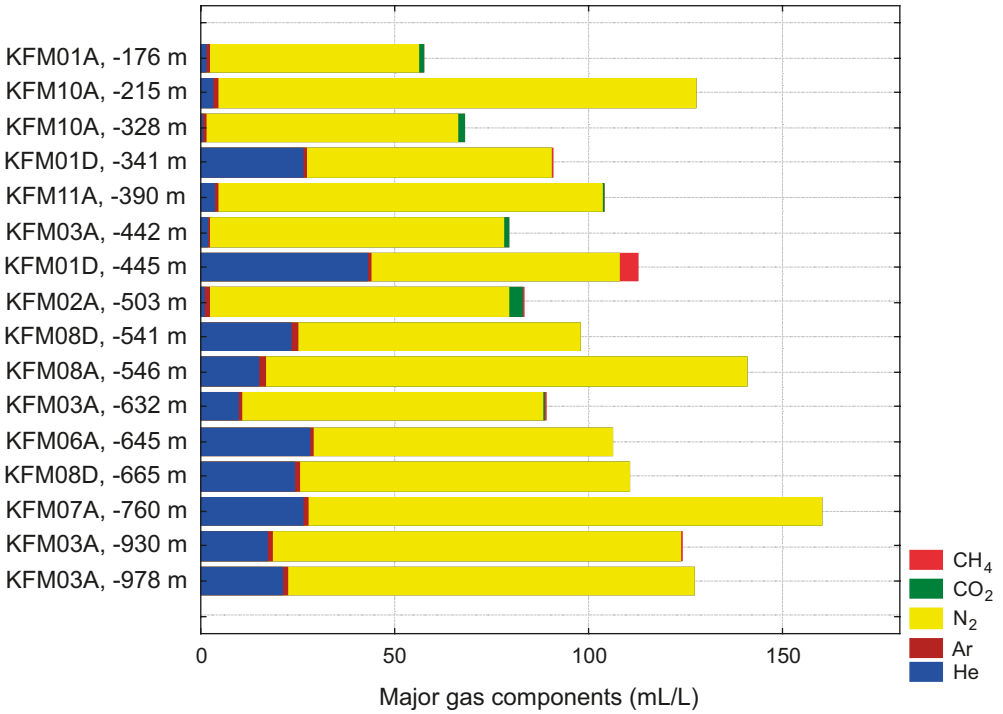

Figure 9-16. *Stacked values of the gas volume of major gas components in samples from Forsmark sorted by depth.*

The most common fracture minerals in the crystalline rocks at Forsmark are chlorite, calcite, Ca-Al silicates (laumontite, epidote, prehnite), sulphides and Fe-oxides. Four generations of fracture mineralisation can be distinguished and these are described in more detail in /Sandström et al. 2008/ and in section 5.2.5. Chronologically, with decreasing age, these generations comprise the following.

Generation 1 (Pre-Sveconorwegian) is dominated by epidote, quartz and Fe-rich chlorite precipitated under hydrothermal conditions at temperatures greater than 150 to 250°C.

Generation 2 (Pre-Sveconorwegian and/or Sveconorwegian) consists of a sequence of fracture minerals precipitated during hydrothermal conditions at temperatures around 150 to 280°C, and comprises mainly adularia, albite, prehnite, laumontite, calcite, chlorite and hematite. Dissolution of fracture minerals occurred prior to the formation of generation 3 minerals.

Generation 3 (Palaeozoic) is dominated by calcite, quartz, pyrite, corrensite and asphaltite. Brine-type fluids influenced by organic material were involved in the formation of the generation 3 minerals. The formation temperature was generally around 60 to 100°C.

Generation 4 (Late Palaeozoic-present) is dominated by chlorite/clay minerals and thin precipitates of calcite, but also minor amounts of goethite and pyrite, mainly associated with hydraulically conductive fractures and fracture zones, may occur. Precipitation of these minerals may have occurred over a long period of time (since the Late Palaeozoic?), and during different events.

Fractures without any visible mineral filling are also interpreted to belong to generation 4 and are possibly young in origin. The majority of these open structures are sub-horizontal or gently dipping, and most are present in the uppermost part of the bedrock and at greater depth along the gently dipping deformation zones (section 5.2.5 and /Stephens et al. 2007, Sandström et al. 2008/).

Calcite

The application of isotope systematics on the Forsmark calcites has resulted in the identification of three general types of calcite /Sandström et al. 2008/: a) hydrothermal calcite (generation 2), b) warm brine-type calcite originating from a fluid influenced by organic material (generation 3), and c) low temperature calcite precipitated from different groundwaters under temperatures close to present groundwater temperatures (generation 4). Calcite of the last type only occurs in small amounts (for details see /Sandström et al. 2008/).

Fracture minerals as indicators of pH and redox conditions

Different mineralogical and geochemical indicators, such as the distribution of Fe^{2+}/Fe^{3+} minerals and the behaviour of redox-sensitive elements, such as cerium and uranium, can be studied in order to reveal possible redox front development, for example, in the near-surface bedrock environment. In addition, although calcite is not redox sensitive, there is a secondary dependency due to interactions between the biosphere and the bicarbonate. However, there are major problems locating bedrock evidence of a downward-propagating redox front at the Forsmark site. The most important of these are: a) most of the core drilling did not start at the bedrock surface, which means that suitable data are restricted to only 8 boreholes where core mapping is absent for the upper 5 to 10 m, and b) the uppermost hundred metres of the bedrock are characterised by sub-horizontal to gently dipping, highly transmissive fractures (i.e. the shallow bedrock aquifer), which create strong horizontal, rather than vertical, flow conditions.

However, based on mineralogy and the analysis of redox-sensitive elements, the following observations of redox response to geological events can be made /Sandström et al. 2008/.

- The two earliest events of fracture mineralisation (generation 1 and 2 of Proterozoic age) are characterised by the presence of oxidised ferric iron (in hematite) and a number of cerium anomalies in fracture coatings. These observations are interpreted as indicative of oxidising conditions coeval with their formation. On the other hand, chlorite with significant ferrous iron content is also part of the generation 1 and 2 parageneses, suggesting variable redox conditions both temporally and spatially. Related to these two fracture generations are also hydrothermal alteration/oxidation of the wall rock adjacent to the fractures (some centimetres) where the overall increase in $Fe^{3+}/Fe(tot)$ is small (about 10%).
- Generation 3 (Palaeozoic age) is characterised by reducing conditions as indicated by pyrite precipitation and also supported by the organic influence on the formation fluid during this period. Well-preserved pyrite crystals of Palaeozoic origin (generation 3) in many of the transmissive fractures suggest that reducing conditions probably have prevailed in large parts of the fracture system since this period.
- The presence of goethite (FeOOH) (generation 4) in some hydraulically-conductive fractures and fracture zones (mainly within the gently dipping deformation zone ZFMA2) in the uppermost part of the bedrock, indicates circulation of oxidising fluids during some period in the past (potentially Quaternary). This is also supported by a high oxidation factor ($Fe^{3+}/Fe(tot)$ determined from Mössbauer spectra), seen in a few fracture coatings from the upper 100 to 200 m. However, the presence of pyrite in the same zones suggests that the circulation of oxidising fluids has been concentrated along channels in which different redox micro-environments may have existed.
- Uranium-rich phases are present in some of the fracture coatings although, to date, only one small grain of pitchblende has been identified /Sandström et al. 2008/. The origin of these phases is largely unknown, but it can be concluded that mobilised uranium has been circulating throughout the geological history of the site. For example, some of the pegmatites show slightly enriched uranium values up to 62 ppm /Stephens et al. 2007/ and section 5.2.3. Even more importantly, there is evidence of redistribution and deposition of uranium irregularly along permeable structures during the Proterozoic (cf. /Welin 1964/). Moreover, during the Palaeozoic, potentially uranium-rich Alum shales covered the area /Sandström et al. 2006 and references therein), and these may have contributed uranium to the system. Of special interest for understanding the present groundwater/mineral systems is the potentially late (Quaternary) redistribution of uranium. The use of uranium-series decay isotope analyses (USD) on groundwaters and fracture coatings concluded that part of this uranium has been mobile during the last 1 Ma /Sandström et al. 2008/. Mobilisation, as well as redeposition of uranium in the upper part of the bedrock (150 m) is indicated. This is ascribed to the transition from near-surface oxidising conditions to more stable reducing conditions at depth. However, some of the deeper samples show similar behaviour, which may be explained by the presence of an easily dissolvable and partly oxidised uranium phase, i.e. possibly altered pitchblende in type. Mobilisation and redeposition of this phase does not mean that oxidising water has penetrated to this depth. However, of greater importance is, irrespective of the aqueous phase which has mobilised the uranium, that the present mildly reducing groundwaters with sufficient bicarbonate (> 30 mg/L) are capable of keeping U(VI) mobile, resulting in variable accumulations occurring within the fracture zones to maximum depths of around 600 m (cf. section 9.5.3).

- Any potential build up of reducing capacity in the fracture minerals during recent periods of reducing groundwater conditions is difficult to estimate. Processes that may contribute to an increase in the redox capacity include the microbial production of Fe^{2+} and Mn^{2+} that may either precipitate (e.g. coprecipitation with calcite) or be sorbed on mineral surfaces due to ion exchange. In addition, iron sulphides may be formed due to bacterial activity of sulphate reducers. However, it can be concluded that the amounts of recent (Quaternary) minerals formed is very small.

No significant decrease in the frequency of calcite-coated fractures in the uppermost part of the bedrock can be seen, indicating that no extensive calcite leaching has occurred in response to Quaternary glaciation/deglaciation events. However, no data are available from the upper 5 to10 m and it is possible that calcite leaching and/or pyrite oxidation is visible close to the bedrock surface.

Ion exchange capacity is another parameter of importance and the few data available are reported in /Byegård et al. 2008/.

9.5.8 Porewater composition in bedrock

The term 'porewater' as used here refers to the water in the connected pore space of the rock matrix that is accessible for diffusion-dominated interaction with groundwater circulating in nearby (micro-) fractures /Waber and Smellie 2008/.

Background

The mass of porewater contained in the low-permeability matrix of the crystalline rock at Forsmark is significant compared with the mass of groundwater circulating in the fractures. Porewater and fracture groundwater always tend to reach chemical and isotopic equilibrium given a long enough period of stable conditions. Thus, the porewater acts either as a sink or a source for solutes, depending on the concentration gradient established between porewater and fracture water. In other words, it becomes an archive of past fracture groundwater compositions and therefore of the palaeohydrogelogical evolution of a site. Elucidating this evolution is one of the major aims of the porewater investigations.

The degree of the preservation of chemical and isotopic signatures in the porewater depends on: a) the distance of the porewater sample from the next conducting fracture in three dimensions, b) the solute transport properties of the rock matrix (e.g. diffusion coefficient, porosity), and c) the period of constant boundary conditions (i.e. constant fracture groundwater composition). In addition, the significance of the signature (taking account of measurement error) depends on the chemical gradient between porewater and fracture groundwater /Waber and Smellie 2008, Waber et al. 2008/.

Porewater composition

The porewater data show a distinction between bedrock characterised by low transmissivity and a low frequency of water-conducting fractures (i.e. fracture domain FFM01 within the footwall; boreholes KFM01D, KFM08C and the lower part of KFM06A) and bedrock characterised by high fracture transmissivities and a high frequency of water-conducting fractures (i.e. fracture domain FFM03 comprising the hanging wall, borehole KFM02B, and fracture domain FFM02 in the footwall involving the upper part of borehole KFM06A).

In the target volume (i.e. footwall bedrock, including fracture domains FFM01, FFM02 and FFM06), located to the north-west of the major gently dipping deformation zones ZFMA2 and ZFMF1, chloride contents in the porewater are between 2,000 and 3,500 mg/kg_{H2O} down to about 350 m depth (borehole KFM08C) and 500 m depth (boreholes KFM01D and KFM06A), respectively (Figure 9-17). The oxygen isotope composition of these porewaters ranges generally from –8.5 to –5.5‰ V-SMOW in boreholes KFM08C and KFM06A down to around 650 m, but is more enriched in $\delta^{18}O$ in borehole KFM01D from 300 m to at least 600 m depth (Figure 9-18). At greater depths, the chloride contents increase continuously to about 10,000 mg/kg_{H2O} in all three boreholes with the highest chloride content of 14,600 mg/kg_{H2O} occurring in porewater of a non-fractured section in borehole KFM08C at about 620 m depth. The corresponding oxygen isotope composition becomes more depleted in $\delta^{18}O$ and varies generally between –10.5 to –8.5‰ V-SMOW. Deviations from this general pattern occur, for example, in the oxygen isotope composition in borehole KFM08C, where

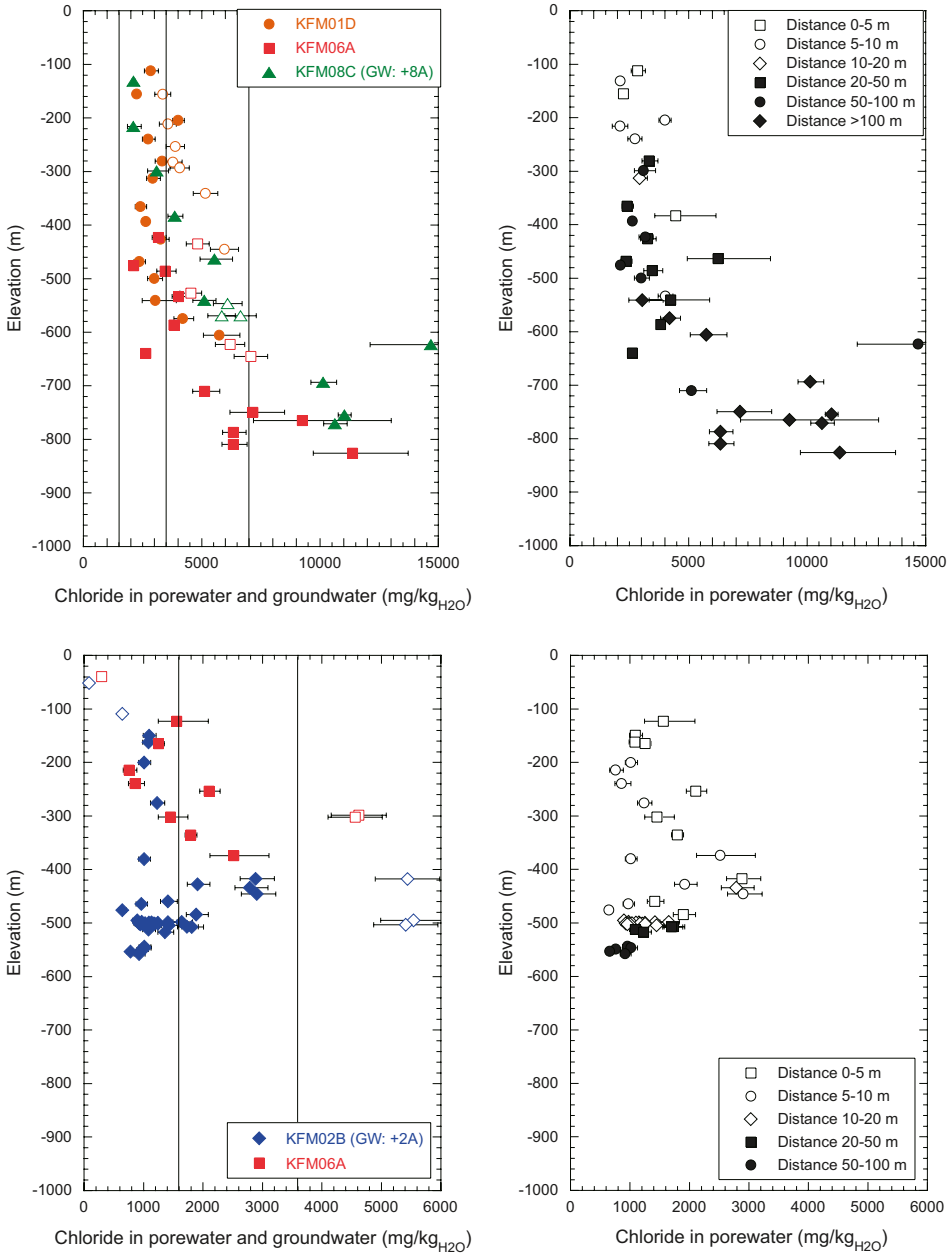

Figure 9-17. *Chloride concentration in porewater (closed symbols) and related groundwater (open symbols) on the left, compared with the distance of the porewater samples from the next water-conducting fracture on the right. The top figures show the boreholes of the footwall bedrock representing mainly low conductive, low fracture frequency conditions (KFM01D, KFM08C and the deeper part of KFM06A). The bottom figures show the boreholes of the hanging wall bedrock representing high conductive, high fracture frequency conditions (KFM02B and upper KFM06A). Indicated is the arbitrary subdivision of porewater Cl contents as used in the hydrogeochemical site descriptive model (/Smellie et al. 2008/ and /Laaksoharju et al. 2008a/; note the different scale on the x-axis). Groundwater samples, GW, taken from other boreholes drilled in different directions from the same sites are indicated in the legend. Error bars show cumulated error (see discussion in /Waber et al. 2008/).*

a sample collected close to a water-conducting fracture at about 380 m depth is depleted in ^{18}O, suggesting a cold-temperature component, or at about 780 m depth where the isotopic composition becomes again enriched in ^{18}O, similar to the values that characterise the deeper part of KFM01D. Furthermore, although not shown, a chloride content of more than 10,000 mg/kg_{H2O} is already present at about 440 m depth in porewater adjacent to a water-conducting fracture in borehole KFM09B, see /Waber et al. 2008/ and Figure 9-18. This latter observation is discussed in section 9.5.1 where the presence of greater porewater (and groundwater) salinity at such intermediate depths may reflect the effects of glacial rebound following maximum glacial loading (see section 9.5.1).

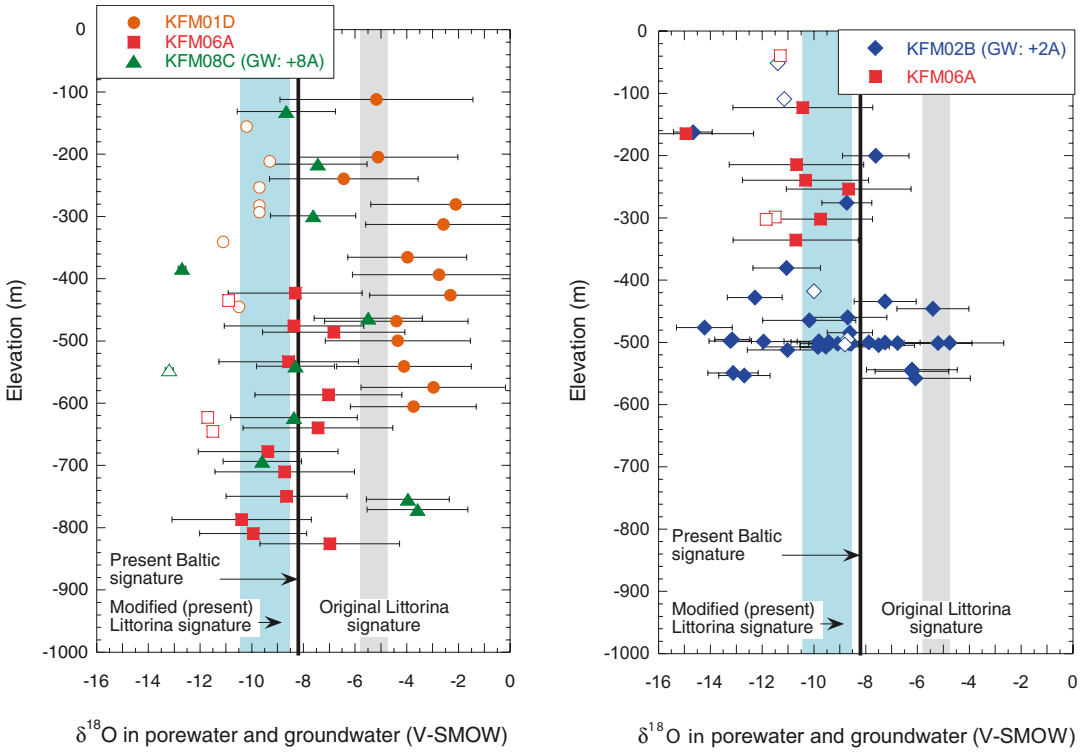

Figure 9-18. *$\delta^{18}O$ in porewater (closed symbols) and related groundwater (open symbols) in the boreholes of the footwall bedrock (KFM01D, KFM08C and the deeper part of KFM06A, left) and the boreholes of the hanging wall bedrock (KFM02B and upper KFM06A, right). Groundwater samples, GW, taken from other boreholes drilled from the same site are indicated in the legend (data from /Smellie et al. 2008/).*

South-east of the target volume (i.e. hanging wall bedrock; fracture domain FFM03), the gently dipping deformation zones ZFMA2 and ZFMF1 show porewater chloride concentrations mainly below 1,500 mg/kg_{H2O} down to about 550 m depth (Figure 9-17). This pattern is interrupted with contents up to 3,000 g/kg_{H2O} between about 360 m and 450 m depth, which coincide with an accumulation of water-conducting fractures and the intersection of deformation zones ZFMA2 and ZFMF1 in the boreholes. This spatially limited increase in porewater chloride content is associated with water isotope signatures enriched in the heavy isotopes and a distinct increase in magnesium contents (up to 200 mg/kg_{H2O}), while magnesium is low in all other porewaters. In this deformation zone, and also in that occurring below at about 500 m depth, the oxygen isotope composition of the porewater generally correlates with the chloride contents being enriched in ^{18}O and ^{2}H at high chloride contents, and depleted in samples with low chloride contents. At four locations, at depths of about 160 m, 480 m, 500 m and 550 m, there occur porewaters in the three lower locations with very depleted ^{18}O values combined with the lowest Cl concentrations (Figure 9-18).

Relationship between porewater and groundwater

Comparing porewater with fracture groundwater is fraught with uncertainty mainly arising from having little or no knowledge of the three-dimensional geometry of the bedrock volume sampled. This means that a sampled porewater may indicate a substantial distance to the closest water-conducting fracture along the borehole, but may in fact be closer to a conducting fracture in another dimension in the rock volume. The plotted porewater data may therefore be expected to show an understandable degree of compositional heterogeneity which can be compounded by the ranges of experimental uncertainty when such small volumes of sample are involved (around 1 mL porewater per kg of rock). This latter point is particularly obvious for the determination of the porewater isotope composition. However, despite these underlying difficulties, it has been possible to generally interpret some general trends from the porewater data to provide important input to site understanding.

In the footwall bedrock (i.e. fracture domain FFM01), the porewater has generally a lower chloride content and is enriched in $\delta^{18}O$ compared with the fracture groundwaters. Such a transient state between porewater and groundwater prevails down to at least 640 m depth, although the concentration differences

become smaller with increasing depth (Figure 9-17 and Figure 9-18). No fracture groundwater samples are available from greater depths. The preservation of a transient state with more dilute signatures and enriched isotope compositions in the porewater reflects the low conductivity of these rock portions and consequently the long time required to overprint a signature once it is established.

In the hanging wall bedrock, a transient state is indicated for the chloride contents between porewater and fracture groundwater down to about 150 m depth, while the isotope composition seems more similar. At greater depths from 400 to 500 m where fracture groundwater data are available, the porewaters sampled in borehole KFM02B have much lower chloride contents and here a clear transient state is established (Figure 9-17). The perpendicular porewater profile sampled away from the highly transmissive, major gently dipping deformation zones ZFMA2 and ZFMF1 in borehole KFM02B, recognised by the cluster of data points between 500 to 550 m depth, indicates that the brackish marine (Littorina) type groundwaters in these fractures have started to overprint the older, more dilute porewater compositions which are still preserved at slightly greater depths (around 550–580 m), but without having yet attained a steady state. Based on the isotope signatures, the dilute porewaters with $\delta^{18}O$ values depleted in ^{18}O still partially preserved at these locations are considered meteoric waters from temperate and cold climate time periods.

Solute transport in the rock matrix

To interpret the porewater data in a hydrogeological context, the solute transport, or more specifically, the diffusion properties of the rock matrix, need to be known. These have been determined from the out-diffusion experiments using large-sized (about 1 kg) originally saturated rock samples /Waber et al. 2008/. The obtained pore diffusion coefficients of chloride are largely independent of rock type and depth of the sample and vary for the modelled samples between $4.05 \cdot 10^{-11}$ and $2.46 \cdot 10^{-10}$ m^2/s at a corresponding water-loss porosity of 0.38 to 0.89% by volume. Variations observed in the chloride pore diffusion coefficient are mainly related to the proximity of a porewater sample to the next altered and tectonised zone of rock and the rock texture.

Differential flow logging of water conducting fractures in the bedrock at Forsmark show large differences in distance between the fractures, for example, distances up to 100 m have been measured in the target volume. However, it is important to keep in mind that these measurements cannot give a 3-D picture of the fracture network. For the samples analysed for porewaters in Forsmark, differences in concentration between porewater samples and fracture groundwaters are especially observed if the distance to the nearest fractures exceeds 5 to 10 m. The chemical and isotopic signatures preserved in such porewater samples have been established a long time ago by palaeowaters. These palaeowaters differed in their composition from the fracture groundwaters sampled today, which at repository depth in the target volume are characterised by having residence times in the bedrock of several tens to hundreds of thousands of years.

Palaeohydrogeological evolution

In the footwall bedrock of the target volume (boreholes KFM01D, KFM08C and lower part of KFM06A), the porewaters and groundwater are in a transient state with the porewater having retained older signatures compared with the groundwater. The increase in concentration differences between porewater and fracture groundwater with increasing depth indicates that the porewater retains a very old, dilute and warm-climate water signature. In the upper footwall bedrock down to about 150 m depth, this old signature is modified by younger Littorina-type water while a glacial water signature is not resolved, except for possibly one sample collected close to a water-conducting fracture in borehole KFM08C (about 390 m depth). At greater depth down to about 640 m (600 m in borehole KFM08C), signatures with low chloride, low magnesium and enriched in ^{18}O and ^{2}H have been preserved far away from conducting fractures. Thus, these porewaters must have evolved from an earlier, very long lasting circulation of dilute groundwaters in the few fractures. These signatures cannot be explained by interaction with recent fracture groundwater types and they undoubtedly date back to before the last deglaciation. The isotope composition of these porewaters indicates that they may have originated from a warm climate period, for example, possibly as far back as Tertiary times. Such very old and dilute porewater is consistent with the still prevailing transient state between this porewater and fracture groundwaters from equivalent depths, the latter being more mineralised and less enriched in the heavy isotopes and with estimated residence times of at least 1.5 Ma based on ^{36}Cl and ^{4}He /Smellie et al. 2008, Laaksoharju et al. 2008a/.

The porewater in the footwall bedrock thus indicates that before the beginning of the Pleistocene-Holocene the entire rock volume was saturated with dilute meteoric water of warm-climate origin, possibly as far back as Tertiary times, down to at least 640 m below (present day) sea level before intrusion of the last deglaciation meltwater and post-glacial Littorina Sea and Baltic Sea water types.

Below about 640 m depth the porewater becomes increasingly saline and the associated isotope composition for some porewater samples is similar to that of the highly saline groundwater in the Laxemar KLX02 borehole ($\delta^{18}O = -8.9$‰ V-SMOW), i.e. more enriched in ^{18}O and ^{2}H for other samples. Unfortunately, mainly due to the absence of fracture groundwater data from these depths at Forsmark, it cannot be distinguished if the (unknown) brine end member in the porewater became mainly diluted (by diffusion) by the old, dilute meteoric water of warm-climate origin observed further up in the rock matrix, or, if it became diluted only recently by last deglaciation meltwater or post-glacial fracture groundwaters. However, the large distances between porewater samples and the closest water-conducting fractures (in one dimension) and the general hydraulic observations, argue against these latter possibilities.

At shallow depths in the hanging wall bedrock (borehole KFM02B and upper part of KFM06A) down to about 150 m depth, the lack of porewater data precludes any quantitative interpretation. However, the limited chloride data are assumed to indicate a transient state between porewater and fracture groundwater (higher Cl in porewater), while a situation closer to steady-state is suggested for the isotope composition. Just below, at about 160 m, the porewater still retains a cold climate isotope signature and low chloride content. Because of the distance of these samples to water-conducting fractures is similar (Figure 9-17), the porewater at shallow depth can be interpreted as the result of an interaction between brackish marine water (Baltic/Littorina based on Cl and Mg) and a meteoric water of uncertain age similar in type to the present day or colder climate groundwater (based on $\delta^{18}O$ and $\delta^{2}H$).

At greater depth in this area, an overall transient state between porewater and groundwater is established down to about 560 m depth with lower chloride contents in the porewater compared to the groundwater. In turn, the isotope composition of the few fracture groundwater samples is similar to that in porewater of rock matrix samples collected close to the fractures. This is because the difference in isotope signatures between marine water (Littornia, Baltic) and moderate to present-day climate meteoric water is much smaller than that in the chloride contents resulting in a more limited resolution of the water isotopes. Yet, the depleted $\delta^{18}O$ values of less than –13‰ V-SMOW preserved further away from the water-conducting fractures indicate that cold-climate glacial water was circulating for a considerable time period in the fractures at these depths. Since the last deglaciation, this cold-climate porewater signature has become overprinted with a Littorina and/or a Baltic-type signature as indicated by Cl, Mg and $\delta^{18}O$ in porewaters sampled closer to the water-conducting fracture. In this shallow zone, these Littorina and/or Baltic-type signatures are now becoming overprinted by the present-day meteoric water circulating in the fractures of this zone.

Conclusions

- Porewater acts as an archive of the past hydrogeological history at Forsmark and its composition puts strong constraints on the interpretation of the palaeohydrogeological evolution of the site.
- Solute transport in the intact rock matrix appears to be dominated by diffusion and matrix diffusion was identified to occur at least over several decametres into the rock matrix.
- Differences in the preserved porewater compositions indicate a different hydrogeological evolution for the footwall bedrock (i.e. target volume; fracture domain FFM01) and the hanging wall bedrock segment.
- In the target volume (fracture domain FFM01), the porewater composition is dominated by dilute meteoric water of warm-climate origin, with ages that possibly reach as far back as Tertiary times, indicating that the rock mass was once saturated with such water down to at least 560 m depth.
- Adjacent to the gently dipping deformation zones ZFMA2 and ZFMF1, mostly located in the hanging wall bedrock segment, the porewater reflects a more recent, mainly Holocene hydrogeological evolution, with clear indications of glacial meltwater and Littorina-type water intrusions down to about 550 m depth.

(Note: The data presented and discussed in this section are based on primary borehole length measurements taken in the field and the elevation data calculated in Sicada. Adjusted elevation data based on single-hole interpretation measurements would only minimally modify the results, and therefore in this context are regarded to be unimportant for plotting purposes.)

9.5.9 Groundwater residence time

Background

A key factor in understanding past and present groundwater evolution in the Forsmark area is to constrain the average residence time for each of the major groundwater types. This can be approached qualitatively in terms of the major and trace element compositions of the groundwaters (commonly including Na, K, Ca, Rb, Ba, Sr and Fe) based on aspects of water-rock reaction kinetics and sorption. Considering different groundwaters that have evolved in a similar geologic environment such as the granitic rocks at Forsmark, a greater groundwater mineralisation can be indicative of a greater residence time. Mixing and reactions can also be identified by utilising isotope studies (e.g. stable isotopes of ^{2}H, $\delta^{18}O$, $^{11}B/^{10}B$, ^{37}Cl, $\delta^{13}C$, $\delta^{34}S$ and $^{86}Sr/^{87}Sr$).

On a more quantitative level, because of their known half-life decay character, the radioactive isotopes of tritium (^{3}H), carbon-14 (^{14}C), helium-4 (^{4}He) and chlorine-36 (^{36}Cl) are used in the hydrochemical evaluation programme (for details see /Smellie et al. 2008/).

The complex issue of addressing residence times is fully acknowledged and the isotopic methods used can only suggest different times of isolation from the atmosphere. For further discussion see /Smellie et al. 2008, Laaksoharju et al. 2008a/.

Qualitative information on residence time

One example of qualitative information on residence time is increased water-rock interaction shown by the behaviour of the stable isotopes $\delta^{18}O$ and $\delta^{2}H$. Deep basement groundwaters from Canada (in particular) and Fennoscandia (to a much weaker extent) show a deviation from the Global Meteoric Water Line (GMWL) coeval with increased salinity and enrichment in deuterium (^{2}H). Forsmark groundwaters show only a weak deviation as highly saline groundwaters are not present at the depths investigated, but comparison with other Fennoscandian sites strengthens this possibility. Based on such observations, matrix porewaters would be expected also to have similar $\delta^{2}H$ enrichments. This is indeed the case for some of the matrix porewaters /Waber and Smellie 2008, Waber et al. 2008, Laaksoharju et al. 2008a/).

Quantitative information on residence time

Quantitative information on groundwater residence time can be derived from short-lived and long-lived radioisotopes. Within the Forsmark hydrochemical programme the radioisotopes ^{3}H and ^{14}C are analysed routinely. In addition, ^{36}Cl analysis has been carried out on the major groundwater types at a late stage in the programme. Helium (^{4}He) gas samples are routinely collected and analysed at selected locations, and this input has been used as support, when possible, to the other dating methods, in particular the ^{36}Cl method /Smellie et al. 2008, Laaksoharju et al. 2008a/.

Understanding present-day flow conditions is crucial in determining, for example, the recharge input chemistry to the bedrock, the starting point for much of the bedrock hydrochemical modelling. The nature of present-day flow conditions are exemplified in Figure 9-19, based on category 1 to 5 data from percussion and cored boreholes within and close to the candidate area, and category 5 data (i.e. all available data are of low quality) from the SFR site. The plot shows a characteristic groundwater decrease in tritium at a depth of around 150 to 200 m, which represents the limit of fresh, meteoric recharge waters of a young age (i.e. less than 55 years), based on the amounts of atmospheric thermonuclear tritium from the 1950's still present in the recharge precipitation and shallow groundwaters. The persistent 1 to 3 TU with increasing depth is due to various sources of potential contamination /Smellie et al. 2008/.

Radiocarbon (^{14}C), with a half-life of 5,730 years, extends the range of detection up to 30,000 years for groundwater residence time. Theoretically, this range should cover comfortably the period since the last deglaciation, in particular confirmation of the Littorina Sea transgression. However, radiocarbon dating is complex and a major problem at Forsmark has been to constrain the ^{14}C input signature to the bedrock, and the reactions involving carbonate dissolution and breakdown of recent and old organic material that will affect the $^{14}C_{(TIC)}$ (i.e. ^{14}C signature of Total Inorganic Carbon) content in different groundwaters. This is discussed in more detail in /Smellie et al. 2008/.

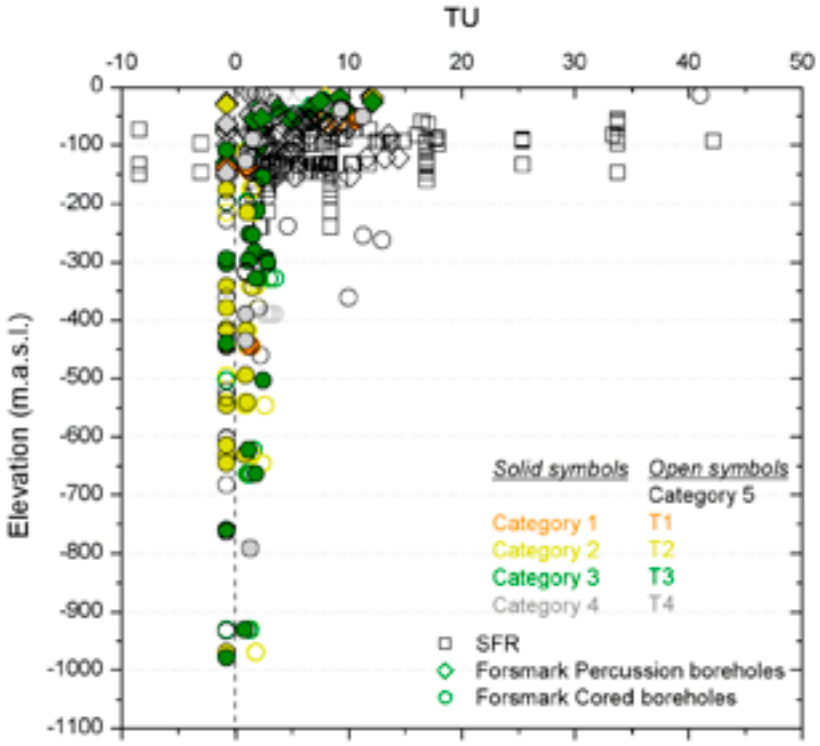

Figure 9-19. *Tritium versus elevation based on category 1–5 data from percussion and cored boreholes, and category 5 data from SFR. Different negative symbols represent different levels of detection.*

Figure 9-20 shows $^{14}C_{(TIC)}$ versus elevation for the Forsmark groundwater samples. The brackish marine waters show $^{14}C_{(TIC)}$ values in the range of 7 to 34 pmC (percent modern Carbon), HCO_3 at 45 to 160 mg/L and $\delta^{13}C$ at –4 to –10‰. Attempts have been made to correct the ^{14}C contents for reactions, mainly based on $\delta^{13}C$. Straight forward calculation from a source term and processes identified, however, has failed to determine the ^{14}C age; the uncertainty is simply too large.

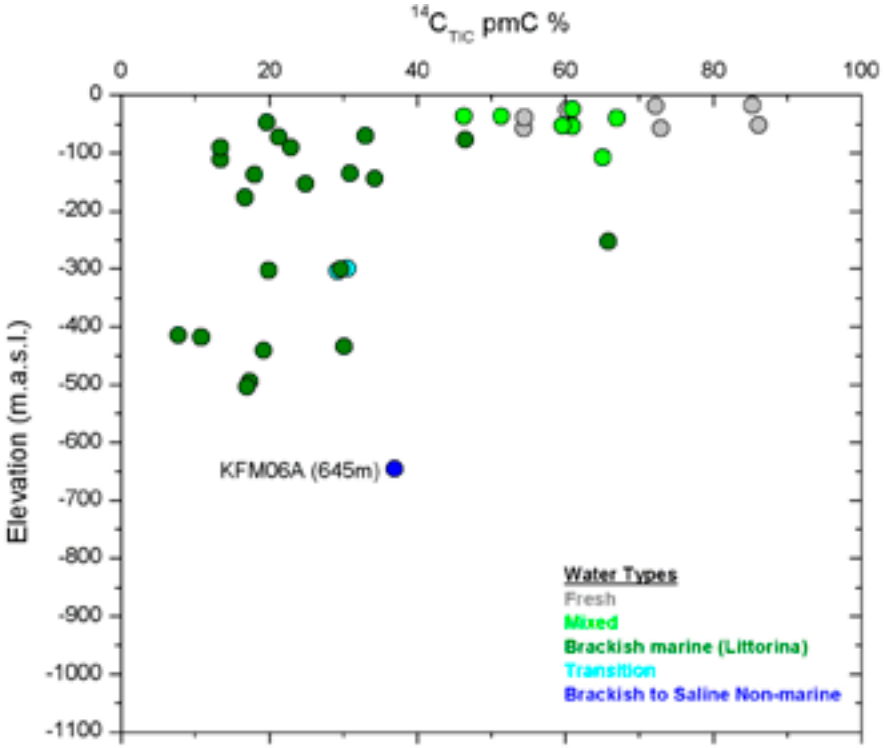

Figure 9-20. *$14C_{(TIC)}$ versus elevation. Only one sample of brackish non-marine groundwater type was analysed and this indicated contamination during sampling.*

Three of the brackish marine waters have also been analysed for ^{14}C (organic) yielding values of 45 to 53 pmC in samples with $^{14}C_{(TIC)}$ at 13 to 17 pmC. Lower ^{14}C content in bicarbonate compared with TOC in the same groundwater is usual and normally attributed to reaction involving dissolution of ^{14}C-free carbonates. In conclusion, the radiocarbon analyses support a postglacial origin for the brackish marine (Littorina) groundwater, and 45 to 53 pmC in the organic phase is in accordance with ages of about 5,000 to 6,000 years covering the period of maximum salinity during the Littorina stage (4500–3000 BC).

By comparing the measured ^{4}He concentrations in groundwater with the calculated *in situ* ^{4}He production rate (based on uranium and thorium concentrations), information about groundwater residence time under closed system conditions, and/or indications of possible external input of helium into the system, can be obtained. Nine groundwater samples from Forsmark have been analysed for ^{4}He. For the brackish to saline non-marine groundwaters (7 samples), it would require about 1.5 Ma to produce the measured ^{4}He concentration *in situ*. This is in accordance with the ^{36}Cl data for the two saline groundwaters from greatest depths (KFM07A and KFM03A), where secular equilibrium has been achieved, thus giving an identical residence time. This is strong evidence that, at these depths, the average groundwater residence time is indeed in the order of 1.5 Ma (see details in /Smellie et al. 2008, Laaksoharju et al. 2008a/.

Conclusions

There is a range of qualitative trace and major ion and stable isotope evidence and quantitative isotopic evidence, based on depth relationships, that generally support hydrogeological observations, see /Smellie et al. 2008, Laaksoharju et al. 2008a/.

- Recent to young fresh groundwaters, some showing signs of mixing with Littorina-type groundwaters especially in the hanging wall, characterise the upper approximately 100 to 150 m of the bedrock. At these depths, because the hydraulic system is more dynamic, climatic changes have resulted in the cyclic introduction and flushing out of different groundwater types over tens of thousands of years, such that residence times for individual groundwater types seem relatively short, i.e. probably some hundreds to a few thousand years. This situation is common to both the hanging wall and footwall, and is borne out by tritium and carbon-14, which indicate that near-surface fresh groundwaters have short residence times in the order of only a few decades to a few hundred years. This is in agreement with palaeohydrogeological evidence which indicates emergence from the Baltic Sea occurring at Forsmark about 2,500 years ago with subsequent land uplift establishing meteoric water recharge some 900 years ago.
- Older groundwaters of a distinct Littorina type occur from approximately 150 m to depths of around 300 to 600 m (depending on the location and fracture transmissivity). The radiocarbon analyses support a postglacial origin for the brackish marine (Littorina) groundwater, and 45 to 53 pmC in the organic phase is in accordance with palaeohydrogeological estimations which suggest an age of 5,000 to 6,000 years covering the period of maximum salinity during the Littorina stage (4500–3000 BC).
- Because of the relatively short residence time these fresh to brackish marine groundwaters described above have been influenced, in addition to being mixed, mostly by fast reactions such as ion exchange and calcite dissolution together with microbial modifications. Generally, aluminium silicate reactions may also be significant.
- Significantly older groundwaters, found at depths greater than around 300 to 600 m (depending on the location and fracture transmissivity) to around 1,000 m, are characterised initially by brackish non-marine groundwaters which become successively more mineralised with increasing depth (to saline in type) by water/rock interactions, mixing with (unknown) deep saline water, and exchange with the rock matrix porewater. Hydraulic conditions at these depths indicate low groundwater flow to stagnant conditions and suggest residence times that appear to be considerable. From chlorine-36 dating, the residence time of the brackish to saline non-marine groundwaters can be shown to extend back to at least 1.5 Ma, which is in accordance with the helium-4 systematics.
- No highly saline groundwaters (> 20,000 mg/L Cl) have been sampled at Forsmark, but as indicated by the porewaters /Waber et al. 2008, Laaksoharju et al. 2008a/, there is a high probability that they exist at greater depths (e.g. similar to KLX02 in the Laxemar subarea) and are at least as old as the shallower brackish non-marine groundwaters.

9.5.10 Evaluation of uncertainties in field data and interpretation methods

During every phase of the hydrogeochemical investigation programme, i.e. drilling, sampling, analysis, evaluation, modelling *etc*, uncertainties are introduced which have to be accounted for, addressed fully and clearly documented to provide confidence in the end result /Smellie et al. 2002, Laaksoharju et al. 2008ab/. Many of the uncertainties are difficult to judge, since they are consequences of expert judgement and not mathematical modelling. There is no undisturbed groundwater sampled prior to drilling and therefore evaluation of many of the uncertainties associated with sampling are based on indirect (e.g. short circuiting) or direct (e.g. drilling water content) indications.

The sampling, analytical, and modelling uncertainties are addressed and quantified in /Nilsson 2008, Laaksoharju et al. 2008a/. The effects of borehole perturbations and temporal and spatial variability are discussed below.

Effects of borehole perturbations

It is well known that site characterisation activities (mainly drilling activities) introduce perturbations in the system that can impact on the hydrochemistry of the groundwater samples collected at the site. It is of interest, therefore, to perform scoping calculations in order to evaluate how much disturbance can be allowed for a given groundwater sample at repository depth, and still meet, for example, the SKB suitability criteria /Molinero et al. 2008/. Two main approaches have been selected to deal with these scoping calculations: a) simple mixing and reaction modelling, and b) coupled reactive transport modelling. The sample (no 12354) from borehole KFM01D at 445 m depth was used to represent groundwater from repository depth. This sample was diluted with a modified meteoric water/precipitation composition.

It was concluded that the suitability criteria related to TDS and pH would always be fulfilled, even for complete disturbance of the sample. The Ca + Mg criteria could be influenced with dilutions higher than 90 percent of the native groundwater sample. Furthermore, cation exchange processes have an effect by lowering the Ca + Mg concentrations in the groundwater, compared with pure conservative mixing.

The oxygen consumption capacity of the granite bedrock has also been evaluated by using reactive transport modelling. This showed that a hypothetical pulse of oxidising water at repository depth would be consumed in a relatively short period of time (about 1 year) if the maximum amounts of reported pyrite are included in the model. However, the model results have been proved to be sensitive to uncertain parameters such as the exact mineralogical composition and the specific reactive surface area of such minerals. In the base case considered in the model, an interesting conclusion is that the oxygen intrusion in a borehole would only affect a very short distance into the bedrock (about 1 cm). The modelling documented in /Gascoyne and Gurban 2008/ supports the above conclusions where the oxidising influence from drilling water on the groundwater composition was considered small, although the initially introduced drilling waters are not strongly oxidising as attempts to reduce oxidation (e.g. by flushing with nitrogen gas) are part of the routine procedure during drilling. Furthermore, the measured downhole redox potential (Eh) values provide evidence of the reductive capacity of the groundwater system. Despite uplifting of the equipment due to pump failure, the Eh measurements show that after reinstalling the equipment, the reducing conditions are quickly re-established and any possible oxygen contamination is quickly consumed, see /Laaksoharju et al. 2008a/.

Temporal and spatial variability

Temporal and spatial variability is important in order to address how well the sampled groundwaters represent the described rock volume.

Temporal hydrochemical variability is largely dependent on the hydraulic properties of the borehole and host bedrock, and the drilling and sampling effects. The variability of the groundwater character has been estimated by: a) comparing the electrical conductivity values measured shortly after drilling with the results obtained during open hole hydrogeochemical logging (tube sampling),

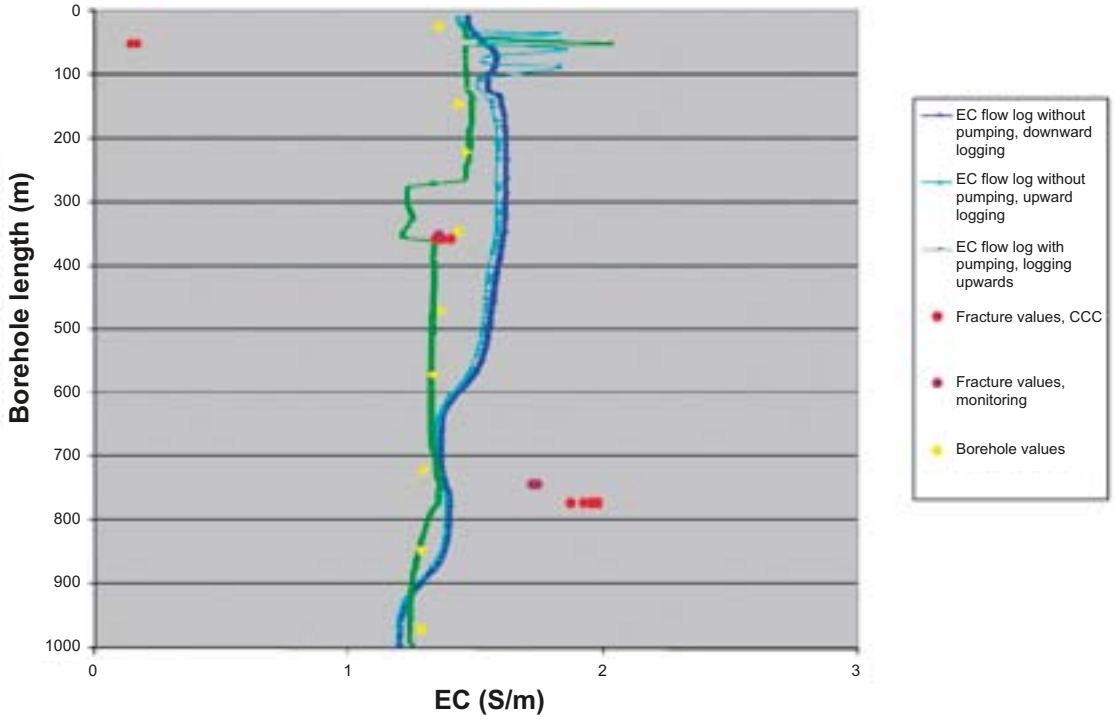

Figure 9-21. *The electrical conductivity as measured during hydraulic logging of the freshly drilled borehole KFM06A (borehole values); green line indicates pumping, blue and turquoise lines indicate no pumping. The borehole values have been inserted to compare with the conductivity of the samples taken: a) in the open borehole (borehole value, yellow in-filled circles), and b) with time series (red circles) taken during hydrogeochemical sampling from fractures (CCC) and during the monitoring programme (dark red in-filled circles).*

and b) by studying the time series data during hydrochemical sampling and during subsequent monitoring (see /Smellie et al. 2008, Gimeno et al. 2008, Gurban 2008/). Figure 9-21 illustrates a case in which the groundwater electrical conductivity (EC) measured in two sections sampled for complete chemical characterisation (CCC) in borehole KFM06A are compared with EC results from earlier open hole flow logging and from tube sampling. The measurements where conducted during a time period of almost three years (December 2003–October 2006). The upper section (around 370 m core length) showed similar groundwater composition through all the sampling campaigns. In contrast, the deeper section (around 770 m core length) showed much higher salinity in the CCC sampled compared with the open-hole sampling and EC flow logging. During the monitoring phase, a section just above the fracture sampled for CCC was sampled and this showed slightly lower salinity and also some mixing with brackish and partly marine waters (cf. section 9.5). This indicates sampling in, or close to, a transition zone between brackish and saline waters (see /Smellie et al. 2008, Gurban 2008/). The large amount of data from different measurements and time periods can be used to indicate the temporal variability of the groundwater in the bedrock and lends support to the quality of the samples used in the site description.

To address the spatial variability, 3D plots can be used to show how the characteristics of the measured samples vary in the 3D bedrock volume (see Figure 9-6 and /Laaksoharju et al. 2008a/). For addressing the possible groundwater variability between the boreholes, coupled modelling should be used /Auqué et al. 2006/. The methodology combines results from the hydrogeological site descriptive model with a mixing and reaction-path simulation using PHREEQC. This coupling provides the theoretical, but detailed, compositional characters of the groundwaters in a rock volume (constituted by a grid with about one million points) that represents the whole regional area of Forsmark down to 2.3 km depth (see /Gimeno et al. 2008/ for details).

9.6 Hydrogeochemical integrated site model

The main aim of the hydrogeochemical site descriptive model is to present an understanding of the site based on measurements and model contributions described in this chapter and detailed in /Smellie et al. 2008, Laaksoharju et al. 2008a/. The site descriptive model is a combination of a quantitatively-derived hydrogeochemical model (e.g. based on site measurements) and a qualitatively-derived hydrogeochemical model (e.g. more descriptive, process-oriented conceptual model). The main objective is to describe the chemical composition and distribution of the groundwater in the bedrock and at the interface between bedrock and the overburden and the hydrogeochemical processes involved in its origin and evolution. This description is based primarily on measurements of the groundwater composition, but also incorporates the use of available geological and hydrogeological site descriptive models. The description also serves as the basis for possible hydrogeochemical simulations of the palaeohydrogeochemical evolution of the site and also to predict future changes.

In this section, the Forsmark hydrogeochemical site descriptive model is briefly presented together with a summary of the main hydrogeochemical properties of the site. This is followed by an assessment of the close interrelationship between hydrogeochemistry and hydrogeology with respect to input and feedback of data and conceptual ideas as to how the system functions.

9.6.1 Hydrogeochemical visualisation

Visualisation of the hydrogeochemical site understanding is based on the exploratory analysis part of the programme outlined in section 9.5, interfaced with relevant input from the geological and hydrogeological site descriptive models. Details are given in /Smellie et al. 2008, Laaksoharju et al. 2008a/.

To visualise the groundwater chemistry, two cross-sections were selected that best illustrate the candidate area (cf. Figure 9-22 and Figure 9-23 and Figure 9-2 for approximate location). These are simplified versions of the originals described elsewhere /Smellie et al. 2008/. The geostructural framework of the cross-sections is based on the geological model (chapter 5 and /Stephens et al. 2007/) and also described in /Smellie et al. 2008/. The groundwater types represented and their subdivisions with respect to elevation and chemistry are largely centred on chloride (and magnesium) because of its direct correlation with depth and specific groundwater types. These subdivisions are supported by other major ions.

To provide a more realistic visualisation of groundwaters in a fractured crystalline rock environment, i.e. to avoid giving a porous medium impression of the bedrock, the groundwater types are shown confined to the major water-conducting fractures and deformation zones. The WNW-ESE section is particularly well suited to this type of visualisation because it cuts the major structures, in contrast to the ENE-WSW section which cuts parallel to the major structures. In the latter case, the groundwater types and salinities are confined to the borehole sections sampled (Figure 9-23).

The cross-sections illustrate the depth of disturbance following the last deglaciation caused by the intrusion of the brackish marine (Littorina) waters to around 600 m along the gently dipping deformation zones in the hanging wall, compared with a maximum intrusion depth of around 150 to 300 m in the footwall (i.e. the target volume).

Included in the visualisations are brief summaries of the chlorinity of the waters, depth intervals where they occur, their origin, the main reactions affecting the waters and the redox conditions for each groundwater type. Important reactions are weathering and potential calcite dissolution in the near-surface bedrock environment, possible calcite precipitation at intermediate levels, and long-term water/rock interactions that are dominant in the deep bedrock which is characterised by low flow to stagnant groundwater conditions. Microbially-mediated reactions (e.g. those due to iron-reducing and sulphate-reducing bacteria) occur particularly in the shallow to intermediate depths where active groundwater flow takes place. Redox conditions range from oxidising/reducing near the surface to reducing with increasing depth.

The target volume at repository depth, best visualised in Figure 9-23, has been largely shielded by the shallow bedrock aquifer from influences occurring after the last deglaciation, in particular the Littorina Sea transgression.

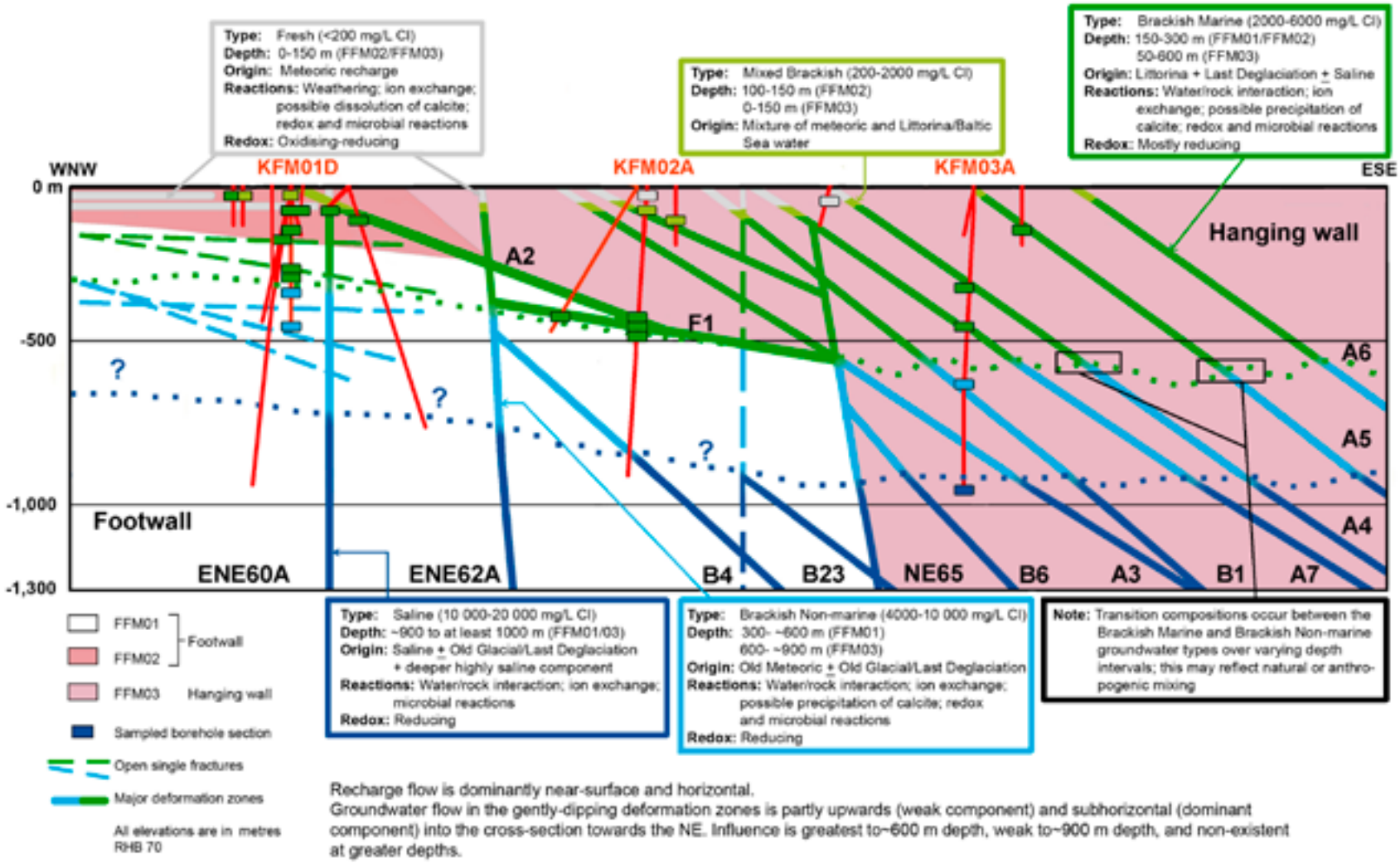

Figure 9-22. *WNW-ESE 2D cross-section through the central part of the candidate area showing the groundwater types and their properties (salinity, origin, major reactions and redox conditions). The footwall (FFM01 and FFM02) and hanging wall (FFM03) bedrock segments are indicated, separated by the gently dipping deformation zones ZFMA2 and ZFMF1 (abbreviated A2 and F1), and the steeply dipping deformation zone ZFMNE0065.*

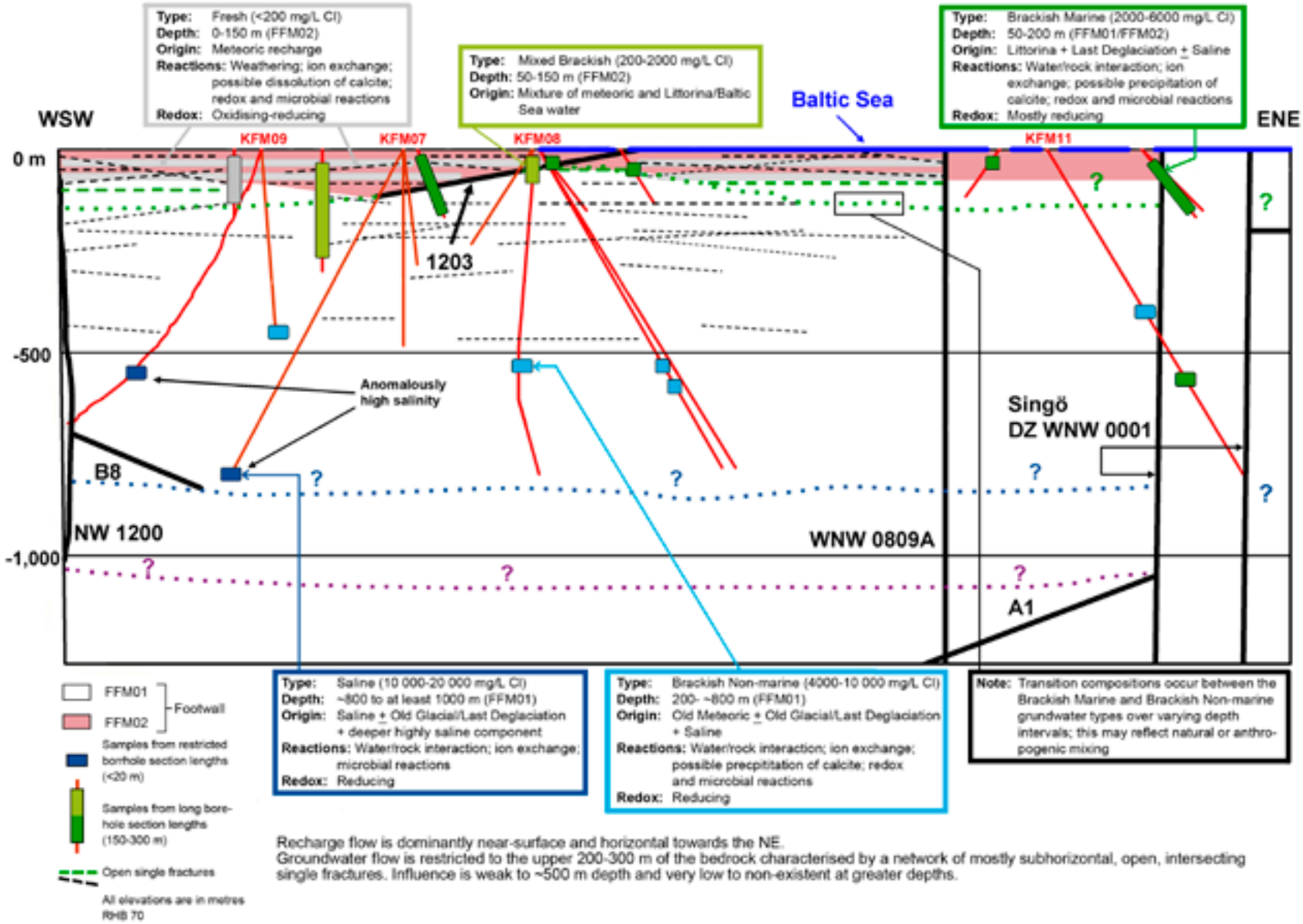

Figure 9-23. *ENE-WSW 2D cross-section through the target volume showing the groundwater types and their properties (salinity, origin, major reactions and redox conditions). Fracture domains FFM01 and FFM02, comprising the footwall, are indicated. Dashed lines in the upper bedrock are only schematic to illustrate the general gently dipping to sub-horizontal fractures commonly present.*

The rock matrix porewaters are detailed in section 9.5.8; see also /Waber et al. 2008, Laaksoharju et al. 2008a/. The distribution of porewaters are not indicated in the cross-sections presented in this chapter, but are visualised for the WNW-ESE cross-section in chapter 11, Figure 11-23, and in /Laaksoharju et al. 2008a/. Both sections are presented and described in /Smellie et al. 2008/.

Summary of hydrogeochemical properties

Near-surface waters (0–20 m): Within this 0 to 20 m depth interval, including the overburden, *Fresh groundwaters* (< 200 mg/L Cl) comprise the most recent recharge compositions. Therefore, their hydrogeochemical evolution is mainly determined by weathering reactions, in particular reactions influenced by limestone. The extensive presence of limestone blocks in the Quaternary overburden, a feature very uncommon in soils in other parts of Sweden, promotes an overall distinctive character to the near-surface groundwaters with respect to that observed in other areas (e.g. Laxemar). Properties include variable but higher pH values (usually higher than 7) and variable but higher calcium concentrations (mostly between 50 and 200 mg/L) depending on the biogenic carbon dioxide input. This fact, together with the kinetically much slower weathering of the aluminosilicates (which otherwise would consume carbon dioxide) and the localised presence of especially intense biogenic input, contribute to the higher bicarbonate values observed (between 200 and 900 mg/L).

Groundwater redox conditions at these shallow levels are oxidising/reducing in character.

No matrix porewater data are available from these very shallow levels.

Shallow groundwaters (20–200 m): This depth interval in the upper part of the footwall bedrock (i.e. fracture domain FFM02) includes the shallow bedrock aquifer, which rapidly transports recharging meteoric groundwaters laterally towards the north-east and effectively limits further recharge to deeper levels. This shallow bedrock aquifer is not developed in the hanging wall bedrock segment.

In the footwall bedrock, these shallow groundwaters consist of a large percentage of *Fresh groundwater* that has persisted to the depths of the shallow bedrock aquifer. However, not surprisingly, they do not share the same variability and high bicarbonate or calcium contents as the near-surface fresh groundwaters. Only waters with short residence time in the overburden (i.e. fast paths), and therefore more dilute, are effectively recharging these shallow hydrological systems. If the biological activity becomes more restricted in the future due to a decrease in nutrient supply or dispersion (e.g. during glaciations), the intensity of weathering will decrease and recharge waters will probably be even more dilute, but not necessarily transported rapidly to depth (or in large volumes) because of the shallow bedrock aquifer with its network of fractures of high horizontal transmissivity. In the hanging wall bedrock, fresh groundwaters persist to varying depths down to around 200 m depending on whether recharge or discharge conditions dominate the gently dipping deformation zones that intersect the bedrock surface.

This uppermost 20 to 200 m in the footwall and the hanging wall bedrock are also characterised by brackish groundwaters displaying a wide chemical variability. This may be due to: a) natural mixing of fresh recharging waters and discharging (or flushed out) saline groundwaters (i.e. recent Baltic or old Littorina Sea relicts), and/or b) mixing resulting from anthropogenic effects related to drilling and sampling activities. Collectively, these two types are referred to as *Mixed Brackish groundwaters* with chloride contents in the range 200 to 2,000 mg/L (Figure 9-22 and Figure 9-23). These shallow mixing processes occur throughout the Forsmark area, but are much more prevalent in the hanging wall segment where the shallow bedrock aquifer is virtually absent and variable discharge and recharge is occurring along the gently dipping deformation zones.

These hydrogeochemical and hydrogeological observations are supported by environmental isotope studies which show that recent to young fresh groundwaters, some showing signs of mixing, characterise the upper approximately 100–200 m of bedrock. This is shown by tritium and carbon-14 which indicate that near-surface groundwaters have short residence times mainly in the order of only a few decades to a few hundred years. This is in agreement with palaeohydrogeological evidence which indicates that the regional area at Forsmark started to emerge from the sea about 2,500 years ago with subsequent land uplift establishing meteoric water recharge some 900 years ago.

Few data exist for the redox characterisation of this shallow groundwater system. Nevertheless, tentative calculations from measurements in both the hanging wall and footwall bedrock suggest the existence of a generalised anoxic state with possible episodic inputs of oxidising waters. Furthermore, although drill-core material from 0 to 100 m depth interval is limited to only eight boreholes /Sandström et al. 2008/, there are enough data to suggest that these oxidising episodes have not been intense enough to exhaust the reducing capacity of fracture filling minerals which are still present in the shallow system (e.g. Fe(II) chlorite or pyrite). Goethite is found in some fractures mainly associated with deformation zones, and Mössbauer analyses of fracture fillings from hydraulically conductive fractures in the upper 50 m show Fe^{3+}/Fe(tot) ratios between 0.35 and 0.75. These observations support the fact that redox conditions have varied both in time and space within the uppermost part of the bedrock. At present, the contents of dissolved ferrous iron are high and represent post-oxic environments in which iron-reducing bacteria (IRB) activity seems to be dominant /Hallbeck and Pedersen 2008/. Locally, sulphidic environments with high contents of dissolved sulphide, probably active precipitation of amorphous monosulphide and, therefore, important sulphate-reducing bacteria (SRB) activity, are also found.

The results of uranium-decay series analyses of fracture filling materials indicate mobilisation as well as deposition of uranium in the upper 150 m of the bedrock. This is ascribed to the transition from near-surface oxidising conditions to more reducing conditions at depth within the last 1 Ma.

Only few porewater data are available from the rock matrix within this depth interval, and generally these suggest that close to steady-state conditions have been achieved in the hanging wall but not in the footwall bedrock.

Intermediate depth groundwaters (200–600 m): During the Littorina Sea transgression, the Forsmark bedrock was under water and therefore no active hydraulic gradient existed. This resulted in the seawater penetrating downwards into the bedrock by density intrusion flow. The bulk of the Littorina Sea waters, i.e. *Brackish Marine groundwaters* (2,000 to 6,000 mg/L Cl), preferentially entered the bedrock in the hanging wall segment along the gently dipping, highly transmissive deformation zones where the shallow bedrock aquifer does not exist. These waters mixed with more dilute post-glacial waters resident in the bedrock, and eventually came to rest when older *Brackish Non-marine groundwaters* of similar to higher salinity (4,000 to 10,000 mg/L Cl, Figure 9-22) were increasingly encountered. The average depth of penetration at the present time along the gently dipping deformation zones is approximately 600 to 700 m (Figure 9-22). Penetration depth may also have been influenced by a decrease in transmissivity along these deformation zones.

In the footwall bedrock dominated by fracture domains FFM01 and FFM02, the situation was different. The shallow bedrock aquifer subsequently became saturated by Littorina Sea water which persisted until recent uplift stimulated an increase in the local hydraulic gradient. The bulk of the Littorina waters then were flushed out by recharging meteoric waters, a process which is still on-going. However, Littorina Sea water components are still present down to 250 to 300 m depth in the footwall bedrock (fracture domain FFM01). This is illustrated by data from borehole KFM01D, where sub-horizontal to very gently dipping transmissive discrete single fractures within the upper 300 m bedrock (i.e. the defined fracture domain) have been sampled (Figure 9-22). Here, the Littorina Sea component is weak to intermediate, probably due to mixing with fresh groundwaters during the on-going flushing out process. In addition, the gently dipping single fractures sampled may connect with the shallow bedrock aquifer and act as conduits bringing some brackish marine (Littorina) groundwaters down to around 300 m depth.

The major chemical composition in this intermediate depth groundwater system is mainly controlled by mixing and depends on the proportion of each mixed end member. The mixing proportions are different in the two main groundwater systems at Forsmark, i.e. fracture groundwaters in the hanging wall bedrock compared to fracture groundwaters in the footwall bedrock. Groundwaters from the latter have a larger contribution of *Brackish Non-marine groundwater* (or the Old meteoric ± Glacial + Saline end member) at shallower depths (around 300 m). The same could be said for the influence of the deeper *Saline groundwater* component (10,000 to 20,000 mg/L Cl; Figure 9-22 and Figure 9-23). This contrasts with the groundwaters from the series of gently dipping deformation zones in the hanging wall bedrock, which have a much higher proportion of the Littorina end member (almost double) down to greater depths (around 600 to 700 m). A higher Littorina component generally also results in higher sulphate and magnesium contents.

Radiocarbon studies of organic/inorganic carbon phases support a Holocene origin of the brackish marine (Littorina) groundwaters. This is in accordance with palaeohydrogeological estimations suggesting an age of approximately 5,000 to 6,000 years covering the period of maximum salinity during the Littorina Sea stage (4500 to 3000 BC).

Even though the compositional characteristics of these intermediate groundwaters are mainly determined by mixing processes, the quickly responding pH and Eh are controlled to a large extent by chemical reactions and microbial activity and, for example, thereby also the sulphur and carbon species. The pH is mainly controlled by calcite dissolution-precipitation reactions. Of secondary importance is the influence of other common chemical processes, such as aluminosilicate dissolution or cation exchange.

Most of the brackish groundwaters sampled at this depth interval in the hanging wall seem to be associated with the presence of lenses with an important Littorina contribution. Their presence represents a discontinuity in the normal evolution of the system with depth, thus introducing a degree of uncertainty when trying to describe the redox conditions. The dissolved ferrous iron contents are generally lower than in the shallow groundwater system. The iron system seems to be disturbed, as suggested by the occurrence of amorphous iron oxyhydroxides now evolving towards more crystalline phases. Most of the Eh values determined in these brackish groundwaters (at depths between 110 and 646 m) are still reducing and seem to be controlled by the equilibrium between dissolved Fe(II) and these intermediate crystalline phases.

Dissolved sulphide concentrations are systematically low and may be locally controlled by the precipitation of amorphous Fe(II)-monosulphides, linked to the activity of SRB. However, future measurements of dissolved sulphide are an important part of the ongoing groundwater monitoring programme in order to achieve a better understanding of the sulphide production in the different groundwaters and to rule out anthropogenic effects.

From approximately 300 to 650 m depth in the footwall bedrock below the shallow bedrock aquifer (i.e. in fracture domain FFM01), where there is a marked decrease in open fracture frequency and transmissivity, there is greater disparity between the porewater chemistry and the adjacent groundwater compositions, the former being significantly more dilute. This depth interval represents transient conditions where the porewater has retained a very old, dilute and warm-climate water signature. This signature is much older than the surrounding fracture groundwaters which have been dated to at least 1.5 Ma (cf. section 9.5.9). Oxygen-18 is enriched and therefore indicates no obvious cold climate signature, which contrasts with the adjacent groundwaters.

In the hanging wall, an overall transient state also is established down to about 650 m. The lower chloride contents and an isotope signature increasingly depleted in oxygen-18 with increasing depth, indicate that the porewater in these zones stores a dilute water signature with a probable cold-climate signature. The significantly negative $\delta^{18}O$ values (–13‰ V-SMOW) preserved far from the water-conducting fractures indicates that this cold-climate signature was a glacial water circulating for a considerable time period in the fractures at these depths. Since the last deglaciation, the porewater signature has become overprinted with a Littorina and/or a Baltic-type signature, as indicated by chloride, magnesium and oxygen-18 in porewaters sampled closer to the conducting fracture.

Deep groundwaters (> 600 m): Under this heading are included the *Brackish Non-marine groundwaters* and the *Saline groundwaters* previously referred to as potential mixing components with the brackish marine (Littorina) groundwater at shallower levels. In the hanging wall bedrock, the transition from brackish marine (Littorina) fracture groundwaters to brackish non-marine groundwaters is quite sharp and occurs at around 550 to 600 m depth. From 600 to 930 m depth, the chloride content increases steadily from 5,500 to 8,500 mg/L before levelling out at values just below 10,000 mg/L at 1,000 m depth, i.e. the transition to the saline groundwater member (Figure 9-22).

There are inadequate groundwater data at the moment to indicate the nature of the salinity increase (i.e. gradual or sharp) at depths greater than 600 m in the footwall bedrock target volume.

The highest salinities are associated with boreholes KFM07A and KFM09A in groundwaters sampled from steeply dipping deformation zones outside the target volume north-west of the candidate area (Figure 9-2). These anomalously high salinities at intermediate depths (600 to 750 m) are considered to reflect natural and/or anthropogenic effects, either due to glacial rebound (after

the maximum glacial loading) or upconing resulting from different borehole activities including groundwater sampling. The former possibility is supported by equivalent porewater chloride contents at similar depths to the groundwaters sampled, and the latter by heavy pumping activities prior to sampling. With the available data, however, a definitive interpretation cannot be presented that supports either a natural or anthropogenic origin.

With respect to the overall redox conditions in the candidate volume, the dissolved sulphide concentrations increase at depths greater than 600 m. This is consistent with the occurrence of sulphate-reducing bacteria (SRB) and with the active precipitation of Fe(II)-monosulphides. The iron system seems to be limited by crystalline oxides (mainly hematite), reflecting the pristine conditions of the geochemical system. This is coherent with the reducing character and long residence time of these groundwaters, where low crystallinity phases are not expected. The sulphide values are a subject for further monitoring to assess their behaviour under different flow conditions.

Hydrochemical observations of fracture groundwaters and porewaters show that the brackish to saline non-marine groundwaters become more mineralised with increasing depth (to saline in type) by water/rock interaction and exchange with the rock matrix porewater. Consistent with the indications of a low-conductive bedrock at these depths (> 600 m), all qualitative and quantitative evidence points to groundwater residence times that are significant. This indicates that these brackish to saline non-marine groundwaters represent part of the salinity gradient that existed prior to the last deglaciation (cf. section 9.3.2). This hypothesis is further strengthened by the transient composition of the rock matrix porewater present in the 300 to 600 m depth interval, which has around 2,000 mg/L Cl as compared with around 6,000 mg/L Cl in the fracture groundwaters. This porewater falls under the general heading of 'Old Meteoric ± Old Glacial +Saline' in type (cf. section 9.3.2), in this case with no glacial component, and is considered to represent a snap-shot of the salinity profile at this depth prior to the last deglaciation.

Colloids and gases: The average colloid concentration found in the Forsmark groundwater system is 58.4 µg/L, which compares with the results of average concentrations from crystalline rock groundwaters in Switzerland (30 and 10 µg/L) and in Canada (300 µg/L), where the same sampling approach was used.

Although the gas concentrations generally increase with depth, the gases are not oversaturated at the depths at which they were sampled. The only sample that displays indications of biologically-produced methane is from borehole KFM01D at a depth of 445 m. The methane in all other samples appears to originate from abiotic sources, unless anaerobic methane oxidation is operating. The helium, hydrogen and nitrogen gases are probably of crustal and/or mantle origin.

9.6.2 Consistency with the hydrogeological model

Close integration of hydrogeochemistry and hydrogeology is a necessary prerequisite to achieve site understanding /Laaksoharju et al. 2008abc, Follin 2008, Follin et al. 2008b, Hunter et al. 2008/. Hydrogeology requires hydrogeochemical information, for example, salinity distributions, groundwater residence time and end member compositions, and palaeohydrogeochemical input to help constrain model boundary conditions etc. Hydrogeology, on the other hand, provides the groundwater flow parameters related to the geological framework so that the spatial distribution of hydrochemical signatures (laterally and vertically) can be interpreted and visualised /Laaksoharju et al. 2008a/. Within the Forsmark investigations, the following steps have governed interaction between hydrogeochemistry and hydrogeology.

1) **Palaeo-conceptual model** construction for the site (see section 9.3.2) based on available Quaternary geological information. The model was used to set the boundary conditions for the hydrogeochemical and hydrogeological modelling.
2) **Parameter values and modelling results,** such as major ions and isotopes and M3 mixing proportions and porewater data, were delivered to the hydrogeologists and used for flow model calibrations and comparisons.
3) **Collaboration** in the form of regular discussions focused on boundary conditions and their relevance to the conceptual site modelling, and to the development of the palaeohydrogeological and palaeohydrogeochemical conceptual models.

4) The **hydrogeochemical site descriptive model** is based on a common nomenclature of groundwater types and groundwater flow understanding achieved through discussion and interaction.

Interaction between hydrogeochemistry and hydrogeology has been a common goal since the initiation of the site investigation programme at Forsmark. Important at this early stage was the use of a generalised palaeo-conceptual site model by the two disciplines, which essentially was similar (sections 9.3 and 8.7, /Follin et al. 2008b/). As investigations progressed, hydrogeochemistry provided more detailed insight into the present and past evolution of the different groundwater types within the approximate 0 to 1,000 m bedrock interval sampled at Forsmark. In turn, these observations provided important interaction with the hydrogeological modelling programme (see chapter 8 and /Follin 2008, Laaksoharju et al. 2008a/). From a hydrogeochemical perspective, the present hydrogeochemical site descriptive models shown in Figure 9-22 and Figure 9-23 are the result of close interaction with hydrogeology, where input concerning confirmation of flow directions, flow properties and possibilities to maintain different water types in the bedrock has been of great importance in supporting the modelling results. Quantitative agreement between the models are, however, restricted to comparisons between predicted and measured groundwater constituents as discussed in chapter 8 and in /Follin 2008/.

9.6.3 Confidence and uncertainty in the integrated hydrogeochemical model

An assessment of the confidence and remaining uncertainties in the hydrogeochemical model /SKB 2008/ has revealed that the confidence in the understanding and description of the current spatial distribution of groundwater composition generally is high. Furthermore, the uncertainties in the processes affecting the current water composition at the sampled locations are generally sufficiently bounded, whereas there are larger uncertainties as to whether the process understanding is sufficient for predicting the groundwater composition during a future glaciation.

Current groundwater composition and distribution

Data clearly show differences both in major components and key isotopes between groundwater in the hanging wall and footwall parts of the bedrock volumes. Groundwaters in the uppermost 20 to 200 m of the bedrock display a wide chemical variability with chloride concentrations in the range 200 to 5,000 mg/L, suggesting influence of both fresh meteoric water and brackish marine water (i.e. Baltic Sea water and Littorina Sea relicts). Furthermore, a sharp decrease in tritium content at about 150 to 200 m depth as well as carbon-14 data indicate that these shallow groundwaters have short residence times, on the order of only a few decades to a few hundred years. At depths greater than approximately 200 m, the groundwater composition is indicative of brackish marine water with chloride concentrations in the range 2,000 to 6,000 mg/L and with a clear Littorina component, as indicated by concentrations of magnesium and the ratio in bromide to chloride concentrations. This groundwater type is recognised down to 600 to 700 m depth in the transmissive gently dipping fracture zones in the south-eastern part of the candidate volume (i.e. hanging wall), whereas the penetration depth in fracture domain FFM01 in the target volume (i.e. footwall), where the frequency of water-conducting fractures is low, and is restricted to approximately 300 m depth. Below these depths, the water composition indicates brackish to saline non-marine groundwaters (i.e. absence of Littorina influence), reflecting processes which have occurred prior to the intrusion of the Littorina Sea waters.

Analyses of the composition of rock matrix porewater are also consistent with the occurrence of bedrock volumes with different frequency of water-conducting fractures and fracture zones. Steady state conditions between matrix porewater and fracture water appear to be confined to the upper 100 to 200 m of the highly conductive bedrock. Matrix porewaters sampled at depths greater than approximately 300 m in fracture domain FFM01 in the footwall show no indication of a cold climate recharge component from the last deglaciation and no Littorina signature. This suggests that these porewaters have evolved from an earlier, very long lasting circulation of old dilute groundwaters in the few fractures. Matrix porewaters in the gently dipping fracture zones in the hanging wall south-east of the target volume show lower chloride concentrations than the fracture water and an isotope signature increasingly depleted in oxygen-18 with depth, indicating that the porewaters in these zones store a dilute water with a cold-climate signature down to at least 550 m. Since the last deglaciation, the porewater signature has become overprinted with a Littorina- and/or a Baltic-type

signature, as indicated by chloride, magnesium and oxygen-18 in porewaters sampled closer to conducting fractures at around 500 m depth.

Process understanding

In addition to mixing (both advection and diffusion), chemical reactions are of importance for the evolution of groundwater composition. The redox and pH buffering capacity of the rock are especially important for prediction of future changes due to the potential intrusion of oxidising, dilute meltwater.

The existence of a near-surface reaction zone appears to be well established. Weathering and potential calcite dissolution in the near-surface bedrock environment is promoted by the extensive presence of limestones in the overburden and controlled by biogenic input of carbon dioxide. This gives rise to pH values usually above 7 units, calcium concentrations mostly between 50 and 200 mg/L and bicarbonate concentrations in the range 200 to 900 mg/L in the near-surface waters (down to around 20 m depth). The pH buffering capacity at depths greater than 100 m appears to be controlled by the calcite system. Investigation of fracture minerals show that calcite in fractures is abundant and that no extensive leaching has occurred in response to past glaciation/deglaciation events. These findings suggest that the buffering capacity against infiltrating dilute groundwater is sufficient, although no quantifications have yet been made. However, a study aiming at quantification of fracture minerals is currently on-going and will be reported separately as a complement to the site descriptive modelling reports.

The presence of goethite (FeOOH) in some hydraulically active fractures and fracture zones (mainly within the major gently dipping deformation zones ZFMA2 and ZFMF1) in the upper 150 m of the bedrock, indicates circulation of oxidising fluids during some period in the past (potentially Quaternary). However, the presence of pyrite in the same zones suggests that the circulation of oxidising fluids has been concentrated along channels in which different redox micro environments may have been formed.

Elevated concentrations of uranium have been detected in groundwaters associated with a Littorina component and the highest concentrations are found in groundwaters in the gently dipping deformation zones in the hanging wall south-east of the target volume. There are indications that these elevated concentrations are related to easy dissolvable uranium fractions in fracture coatings in contact with these deformation zones. Speciation-solubility calculations support this conclusion and indicate that the high uranium contents are the result of the control exerted by an amorphous (and very soluble) uranium phase present in the system, and the weakly reducing Eh values which may allow uranium complexation and re-equilibrium depending on Eh and dissolved carbonate.

According to data analyses and modelling of the redox system, reducing conditions currently prevail at depths greater than around 20 m, despite potential sampling or drilling-induced perturbations that may have altered the original redox conditions of the hydrochemical system. Examples of such disturbances include oxygen intrusion and precipitation of amorphous iron oxyhydroxides, as indicated by the colloidal composition and mineralogical determinations. Furthermore, drilling waters may have modified the original Eh and/or alkalinity, and the increase in dissolved uranium contents may partly be due to one or more of these disturbances. Drilling and pumping may also be the cause for the changes in sulphide concentrations with time that have been observed in samples collected during the monitoring programme. More time-series data from the on-going monitoring programme may be sufficient to allow a final assessment of what is the undisturbed sulphide concentration, as well as how sulphide concentration may change due to future intrusion of marine water.

Overall confidence

The following aspects of the hydrogeochemical model are associated with the highest confidence:

- The origin of most of the end members (meteoric, marine, glacial) and major processes (qualitative control concerning Eh and pH buffer capacity, major reactions) affecting the present water composition at the sampled locations.
- Predictability concerning expected groundwater compositions.

The main reasons for this confidence are the many consistent time and spatial data to support the description concerning the origin, most of the major end members and major processes. Integration with hydrogeology supports the palaeohydrogeological description of the site. Various considerations such as modelling reactions, interpretation of different isotope ratios (Sr, S, C), buffer capacity measurements (Eh, pH) and microbial data, support the process understanding.

Reasons for the composition of matrix porewaters are fairly well established and correspond to the present conceptualisation of the Forsmark area.

The following aspects are associated with the lowest confidence:

- The redox front variations through time.
- Mineral phases giving rise to the elevated uranium concentrations in the groundwater,
- The regional salinity distribution outside the target area.
- The *in situ* concentration of sulphide.
- The sources, production rate and transport mechanisms of geogas.

The implications of these uncertainties are potentially important and need to be assessed in the SR-Site programme.

10 Bedrock transport properties

The main objective of the investigations and modelling of the transport properties of the bedrock is to present a detailed description of site-specific transport conditions that can be used to support the selection of processes and parameters in models developed by safety assessment and others for radionuclide transport and for predicting future groundwater composition. In addition, the results of the transport properties modelling are used as qualitative and/or quantitative input to transport modelling within the site descriptive hydrogeological and hydrogeochemical modelling. This chapter contains an overview of the transport properties site descriptive model, which is presented in detail in the main background report /Crawford (ed) 2008/.

10.1 State of knowledge at previous model version

The present site descriptive model for transport has undergone major revisions since version 1.1 /SKB 2004/, version 1.2 /SKB 2005a/, and model stage 2.1 /SKB 2006a/. Earlier versions were hampered by the lack of site-specific data from laboratory measurement for, in particular, sorption properties and effective diffusivities measured by through-diffusion. Hydrogeological properties of different parts of the target volume were also less well characterised in previous versions, which limited the possibilities of making well-supported estimations of flow-related transport properties. The maturation of the geological, hydrogeological and hydrogeochemical site understanding throughout the different model versions has been instrumental in shaping the current conceptual understanding of site-specific transport processes.

10.2 Evaluation of primary data

The investigations of bedrock transport properties performed in the Forsmark area are summarised in sections 2.1 and 2.3 and the data supporting the current model version are listed in Table 6 in Appendix 3. The different methods used in the laboratory programme are described in /Widestrand et al. 2003/. The primary data evaluation for the retardation model is presented in detail in /Byegård et al. 2008/ and summarised in the main background report /Crawford (ed) 2008/. The flow-related transport properties evaluation including a full account of primary data evaluation is also given in /Crawford (ed) 2008/. The following subsections give only a brief overview of the primary data evaluation and the reader is directed to the relevant reference reports for more detailed explanations.

10.2.1 Data and models from other disciplines

/Byegård et al. 2008/ have summarised and evaluated data from geology and hydrogeochemistry with the aim of identifying and describing relevant materials and conditions for bedrock transport analyses. The corresponding evaluations in previous model versions guided the sample selection and focus of much of the laboratory investigations which are reported in the current model version. A great deal of supporting information was assembled from the geology site descriptive modelling to aid in the creation of a retardation model that encompasses relevant rock and alteration types, as well as key fracture classes and deformation zone sub-structures found in the target volume. Information from hydrogeochemistry was used in the selection of four synthetic water types for use in laboratory sorption studies to reflect the range of evolving groundwater conditions expected during the lifespan of the repository.

Information and models provided by hydrogeology were used in the construction of a conceptual transport pathway model described in detail in /Crawford (ed) 2008/. This model was used to make quantitative estimates of flow-related transport properties and advective travel times for transport from a hypothetical repository.

10.2.2 Transport data

Transport data obtained from the laboratory programme include effective diffusivities for solute transport in the rock matrix, matrix porosities, the specific surface area of internal micro-surfaces, cation exchange capacities (CEC), and radionuclide specific sorption properties of rock in contact with synthetic groundwater of varying composition.

The effective diffusivity is quantified through the formation factor, F_f, which is the ratio of effective diffusivity to the free diffusivity of a solute at infinite dilution in water ($F_f = D_e / D_w$). The formation factor is a purely geometric entity that depends upon the porosity, tortuosity, and constrictivity of the porous space available for solute diffusion within the rock. Formation factors are obtained by through-diffusion experiments in the laboratory using a tritiated water tracer as well as by *in situ* and laboratory electrical resistivity measurements. On the order of 100,000 *in situ* measurements of the formation factor obtained from high spatial resolution geophysical logging in the site investigation boreholes are reported in the Sicada database. From the laboratory programme there are 163 resistivity based formation factor measurements and 68 through diffusion measurements available.

Rock matrix porosity data consist of 211 measurements based upon a gravimetric water saturation technique used to quantify site-scale variation and 13 measurements using PMMA-resin (poly-methyl-methacrylate) impregnation for the study of heterogeneous porosity distributions in individual samples of specific rock types.

The surface area of the rock matrix porosity was measured by means of the BET-measurement technique. In all, 50 duplicate measurements of surface area were made using crushed rock samples and 4 measurements using intact core pieces.

Sorption properties of 17 rock samples were measured using a batch measurement technique for 2 different crushed rock size fractions, different solutes representing a range of sorption chemistries, and 4 different synthetic groundwater types. Batch sorption measurements were also performed on 4 whole core pieces. Cation exchange capacities were measured for 9 different crushed rock samples and 4 whole core pieces.

All data obtained from the transport properties laboratory programme are reported in the Sicada database and are described in detail in the background report by /Byegård et al. 2008/. A summary of the data is also given in /Crawford (ed) 2008/.

10.3 Conceptual model

In the event of canister failure, radionuclides may escape and migrate to the surrounding rock through the bentonite buffer or backfilling material surrounding the canister emplacement. The radionuclides may then be transported into fractures intersecting the deposition hole, into the disturbed zone around the excavated volume, and into fractures intersecting the tunnels.

Radionuclides that reach the rock volume are transported by the groundwater flowing in fractures within the rock. In low porosity crystalline rock, all long-range transport is expected to occur by way of advective flow in discrete flow channels hosted in fractures and other flow permeable structures (e.g. flow channelling within variable aperture fractures, enlarged fracture intersections, within fault stepovers, crush zones, etc). For the description of transport properties, the rock matrix is considered to comprise the host rock minerals as well as all grain boundary pores and micro-fractures that contribute to diffusive and sorptive retention properties. The definition of the rock matrix excludes features with advective flows as well as diffusive open fractures of sufficient size to be included in the hydrogeological DFN model (section 8.5.2).

Owing to the low permeability of the rock, the water residing in the porosity of the rock matrix is considered to be immobile, and long-range transport through the rock mass itself can be neglected over the timescales relevant for safety assessment. Radionuclides may be transported by advective pathways through the fractured rock until they reach the near surface where additional transport processes and pathways in unconsolidated geologic materials and surface aquatic systems are considered (see section 4.4.3). It is thought that radionuclides will principally be transported via a sequence of pathways featuring successively increasing flow in the stochastically modelled background fractures and minor deformation zones within the fracture domains until they encounter flow

paths in the large, deterministically defined deformation zones from where they may be transported to the near surface. Implicit in this conceptual model is the conjecture of transport in a dual porosity system where there is a clear demarcation between advective and diffusive domains. This is a modelling simplification. In reality, a hierarchy of spatial scales exists for transport of solutes within the rock, which results in a continuum of behaviour spanning the different size realms from the largest fractures to the smallest pore spaces.

There are a number of processes that act to retard the transport of solutes in such a way that they are transported at a slower rate than the groundwater within which they are carried. Certain nuclides may sorb on the surface of the fractures through which they are transported. From the fractures they may also migrate into pore spaces within the rock matrix by molecular diffusion. As flow is commonly channelised, there may be regions of effectively stagnant water within the fractures into which nuclides can migrate by molecular diffusion and then subsequently migrate into the rock matrix. The interior of the rock matrix contains stagnant "porewater" in which the radionuclides can be sequestered in aqueous form and micro-surfaces upon which they can sorb.

A schematic illustration of a possible transport flow path is depicted in Figure 10-1 for a stochastic fracture typical of the different fracture domains at the Forsmark site. Such fractures generally feature a thin fracture coating of secondary mineralisation and possibly an alteration rim of limited thickness.

Eight different fracture types have been identified at the Forsmark site. These differ only in the types of secondary minerals present in the fracture coating and the estimated thickness of the alteration rim. The classification is based partly upon the different geochronological epochs of alteration that are thought to have occurred at the site, and partly upon the potential for the different secondary minerals to influence transport processes. By far the most common fracture mineral is chlorite, often found in combination with calcite, corrensite and occasionally other clay minerals.

In principal, the fractures comprising deformation zones are conceptualised to be similar to the fractures found in the fracture domains, although with added micro-structural complexity and with different proportions of type-fractures. Fractures within the larger deterministic deformation zones are considered to have layers of hydrothermal and tectonic alteration that extend from the fracture surface to some distance within the host rock. In some cases, the rock between successive fractures is completely altered leaving no intervening fresh rock at all. During the evolution of the rock, the fractures may have been sealed by secondary mineral precipitates and reactivated in different cycles. Therefore, the fracture coatings are not necessarily distributed evenly on both surfaces of the fracture.

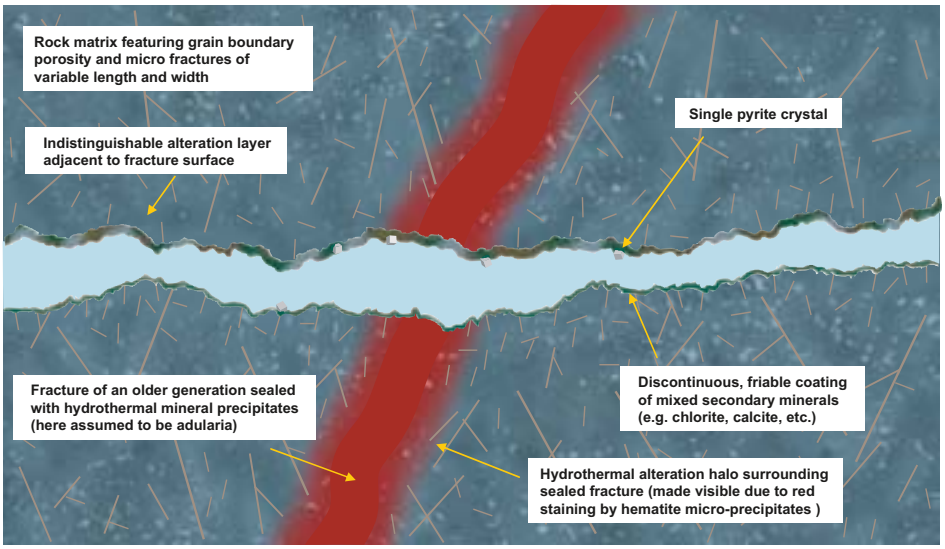

Figure 10-1. *Schematic illustration of a transport path in cross-section. The pathway is characteristic of a typical fracture with a discontinuous coating of secondary minerals. A mix of discontinuous chlorite and calcite coatings are shown in the figure with the occasional pyrite mineral grain. A typical sealed fracture of an older generation is shown transecting the open fracture section. The sealed fracture filling is a hydrothermally precipitated mineral such as laumontite or adularia with red hematite staining. A reddish hydrothermal oxidation halo is also shown at the interface between the fracture filling and surrounding rock matrix.*

The rock matrix porosity consists of micro-fractures and grain boundary pores. Micro-fracturing is most intense at fracture surfaces and has a tendency to decrease with distance into the undisturbed rock matrix. The porosity near fracture surfaces is frequently dominated by micro-fracturing. The undisturbed matrix porosity, on the other hand, is usually dominated by grain-boundary pores and is pervasively distributed throughout the rock mass. That the matrix porosity is well-connected over significant distances is supported by a considerable body of evidence that includes palaeo-hydrogeochemical signatures of relict diffusive exchange with flowing groundwater (section 9.5.8 and /Laaksoharju et al. 2008a/), *in situ* measurements of site-specific formation factors /Crawford (ed) 2008/, as well as other supporting laboratory and *in situ* experiments /Löfgren et al. 2007/.

Sorption can take place on the external fracture surfaces in contact with flowing water or within the micro-porous structure of the rock matrix. Since the diffusion-accessible mineral surface area within the rock matrix can be orders of magnitude greater than that of the external fracture surfaces in contact with flowing water, the sorption of radionuclides can give an enormously increased retardation effect over that of matrix diffusion alone. Owing to alteration processes, the pore spaces immediately adjacent to fracture surfaces often feature considerably greater sorptive surface area than the more deeply lying rock. This can give rise to strong increases in sorptivity at the fracture surface. This is supported by measurements of BET-surface areas /Brunauer et al. 1938/ of site-specific fracture coatings and altered materials.

Transported radionuclides are usually in the form of ionic, charged species and will tend to associate with mineral surfaces that possess a net charge of opposite sign. In the present context this is what is referred to as a sorption process. Such interactions are well described in the scientific literature. e.g. /Stumm and Morgan 1996/ and the most important mechanisms for this interaction are thought to be ion-exchange and surface complexation. The surface charge of minerals is usually described as having a *permanent* component which is independent of groundwater composition, and a *variable* component which changes with the groundwater composition e.g. /Langmuir 1997/. The variable component of the surface charge arises due to surface functional groups which are basically oxide groups, possessing unsatisfied bonds (i.e. O^{2-} and OH^{-}) with the consequence that the variable surface charge is sensitive to the pH of the contacting groundwater. From the surface chemistry literature, e.g. /Stumm and Morgan 1996/, it is known that most of the minerals that comprise granitic rock will have a net negative surface charge at all reasonable groundwater pH values.

Solutes that sorb by a surface complexation mechanism can form covalent bonds with the reactive surface groups, whereas solutes that sorb by way of ion exchange associate with permanently charged sites in a purely electrostatic interaction. Different ion-exchanging solutes have different hydrated charge densities. Therefore they can associate more or less closely with these charged sites thereby giving rise to different affinities for association amongst different solution components. Ion exchange in the context of solute transport in geologic media refers to the tendency of certain cations to replace others that are bound to permanently charged sites at the mineral surface due to these differences in sorption affinity.

In many cases, the sorbed solutes cannot completely balance the total surface charge and therefore other cations in solution are attracted towards the surface. At some distance, the more closely bound cations shield the residual charge of the surface from less closely bound cations to such an extent that only the potential gradient normal to the surface limits the movement of the less closely bound cations. For these cations, transport parallel to the surface is relatively unhindered whereas movement normal to the surface is restricted by electrostatic forces. The volume these cations occupy is referred to as the diffuse double layer or electrical double layer (EDL) /Stumm and Morgan 1996/. The physical extent of the EDL varies as a function of ionic strength in the groundwater which can have consequences for the mobility of ionic solutes in very dilute groundwater and narrow pore spaces. Potential effects are so-called anion exclusion and EDL-mediated surface diffusion. These are described and accounted for in safety assessment as part of scenario analysis.

In the safety assessment framework that provides the basis for identification of the retention parameters in the site descriptive model for transport, retention of radionuclides is assumed to be caused primarily by diffusion and sorption. For modelling purposes, these are assumed to be reversible linear processes. Transport retardation of solutes by matrix diffusion is modelled as a homogeneous Fickian process characterised by an effective diffusivity, D_e, and sorption is modelled using a constant partitioning ratio, K_d, which is a function of groundwater chemistry and rock type.

Together with the rock matrix porosity, θ_m, the diffusion and sorption parameters can be combined to describe the solute retention properties of the rock matrix.

The use of a Fickian model for solute diffusion in combination with a linear model of sorption (as implied by the K_d concept) are modelling simplifications of what is in reality a complex, coupled reactive transport process. However, there is a broad scientific consensus that the use of these modelling simplifications is adequate for the goals of safety assessment, provided that appropriate parameter values are selected for the prevailing conditions, e.g. /NEA 1999/. More details concerning the overall modelling approach and justification of modelling assumptions (including caveats on the use of the K_d concept) can be found in the background report /Crawford (ed) 2008/.

Generally, these simplifications are justified on the basis that the transported radionuclides are considered to be extremely dilute, trace components within the groundwater. The mechanisms by which radionuclides are postulated to interact with the rock matrix (i.e. diffusion and sorption) are also applicable to the transport of other solutes dissolved in the groundwater and are considered to be part of the suite of chemical reactive processes that affect groundwater composition.

10.4 Transport properties of the bedrock

10.4.1 Overview of rock domains and fracture domains

For the transport properties site descriptive modelling, attention has focused upon the rock domains RFM029 and RFM045 as these are volumetrically the most significant domains both in the local model volume and the target volume.

The rock in RFM029 is dominated by a medium-grained metagranite, whereas the major rock type in RFM045 is an aplitic metagranite. A full account of the proportions of different rock types and classes of alteration can be found both in the geology chapter (5) and the transport SDM background report /Byegård et al. 2008/.

Most fractures within the target volume are sealed. There is a greater intensity of open and partly open fractures in the upper section of the rock, but this decreases strongly with increasing depth, particularly below the gently dipping fracture zone ZFMA2. Based upon detailed studies of fracture mineralogy and wall rock alteration /Sandström et al. 2008/, the relative abundance of fracture minerals at Forsmark can be summarised as: calcite and chlorite/corrensite > laumontite > quartz, adularia, albite, clay minerals > prehnite, epidote > hematite and pyrite. With the exception of asphaltite and goethite which are almost exclusively associated with fracture domain FFM02, roughly the same mineralogy is found in fracture domains FFM01, FFM02, FFM03, and FFM06 although the proportions of the different minerals may vary.

The character and properties of altered rock (distinguished by red colouration) that occurs adjacent to generation 1 and 2 fractures (see chapters 5 and 9) are well known. The major mineralogical changes in the altered rock are of an oxidative character and are described more fully in chapter 5.

The red-tinged colouration of the rock is due to the presence of microscopic grains of hematite precipitates along the grain boundaries of the altered plagioclase (saussuritised plagioclase). The hydrothermal reddening normally extends a few centimetres perpendicularly out from fracture surfaces, although more extensive zones are also known to exist. However, the alteration, in particular chloritisation, extends further into the rock than the reddening suggests. The amount of rock mapped as “oxidised” should therefore be seen as a minimum value of the true amount of altered rock. An increase in the connected porosity in the altered rock can be seen, most likely due to the chloritisation of biotite and an increase in the intensity of micro-fracturing.

Based upon the characterisation of different fracture mineralisations and theoretical potential for influencing transport properties, eight major fracture types have been identified. These are summarised in Table 10-1.

Some typical examples of the appearance of some of these fractures can be seen in Figure 10-2 and the relative abundance of the different fracture types as a function of depth for the Forsmark site is shown in Figure 10-3.

For the retardation model, four additional, recurring structural elements have been identified as being characteristic of deformation zones. These are distinct from the single fracture classes described above which also populate the deformation zones. These structural elements are described in Table 10-2.

Table 10-1. Classification of basic fracture types within retardation model.

Type	Fracture coating	Thickness	Wall rock alteration
A	***Chl+Ca***	≤ 0.5 mm	Fresh
B	***Chl+Clay*** ± *Ep* ± *Pr* ± *Ca*	~1 mm	Altered (~ 1 cm)
C	***Chl+Hm*** ± *Other*	< 0.5 mm (0.1 mm)	Altered (0.5 cm)
D	***Chl*** ± *other*	< 0.5 mm (0.1 mm)	Fresh
E	***Lau*** ± *Ca* ± *Chl*	0.1–2 mm	Altered (1–5 cm)
F	***Ca*** ± *Qz* ± *Py* ± *other*	0.1–2 mm	Fresh
G	***Clay*** ± *other*	1–5 mm	Altered (≥ 5 cm)
H	***No mineral***		Fresh

Note: Fracture mineral abbreviations are: chlorite (Chl), calcite (Ca), epidote (Ep), hematite (Hm), laumontite (Lau), prehnite (Pr), pyrite (Py), quartz (Qz).

Table 10-2. Main identified structural elements residing in deformation zones that have been included in the retardation model.

1)	Strongly altered (tectonised and partly incohesive) wall rock described in this report as “fault rock”. Altered rock fragments with varied mineralogy dependent on host rock. Chlorite, saussurite, and clay are generally present.	
2)	Sealed fracture networks mainly consisting of breccia and cataclasite. Different fracture fillings such as laumontite + calcite, epidote, chlorite.	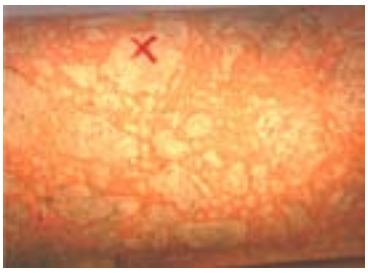
3)	Quartz dissolved rock (vuggy rock).	
4)	Oxidised wall rock (mainly medium or strong degree of alteration).	

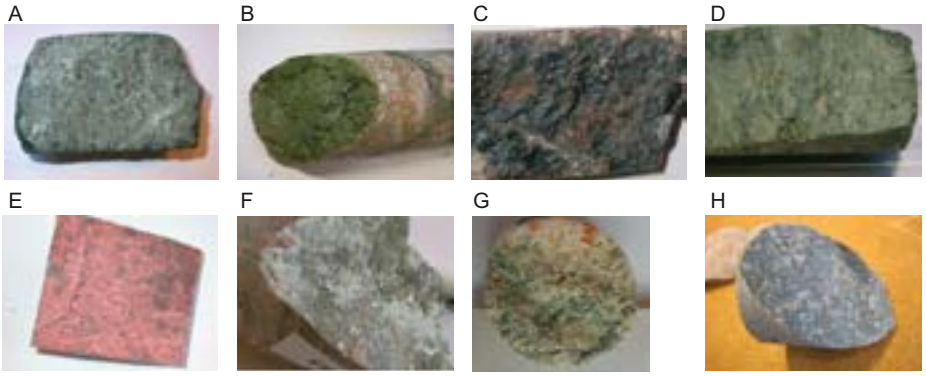

Figure 10-2. *Typical appearance of the surface coating minerals associated with the basic fracture types considered in the retardation model.*

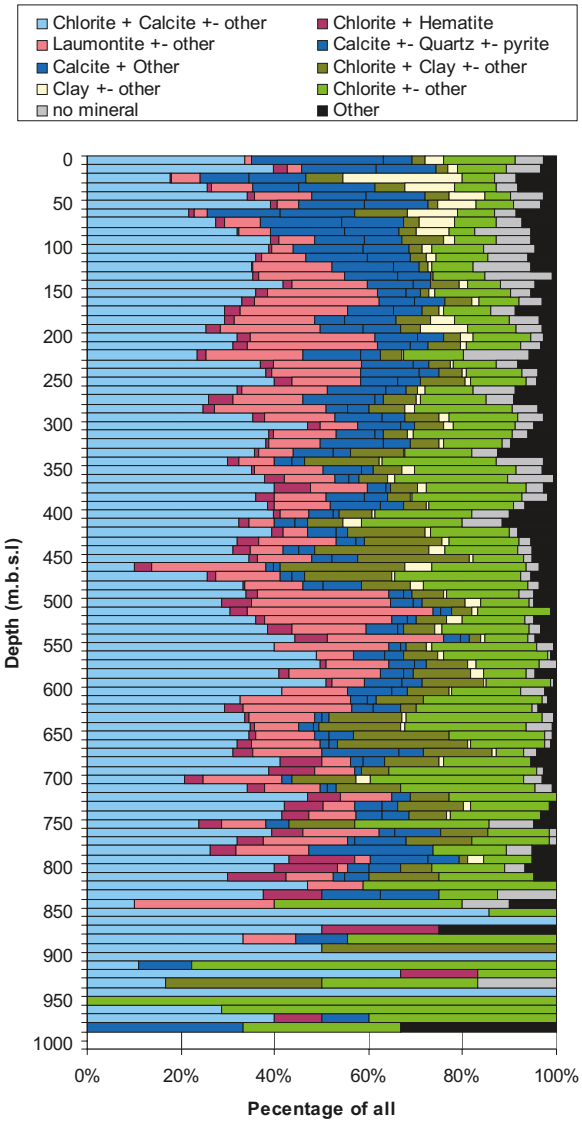

Figure 10-3. *Relative abundance of different fracture types at different depths at the Forsmark site. The apparent change of fracture mineralogy below 850 m reflects the scarcity of data available at this depth rather than a systematic change in mineral distribution.*

Synthesis of a generalised model for deformation zones is difficult owing to their complexity and spatial variability. This is further complicated by the fact that their structure is usually only known through interpretation of a small number of one-dimensional borehole intercepts. Much of the complexity of deformation zones arises through cycles of reactivation during different geological events. They therefore display a wide spectrum of alteration types, brittle and ductile features formed at different stages of their geological history.

10.4.2 Representative transport property data

In the following sections, a brief summary is given of the parameter values considered to be representative of the material properties of the major rock types found at the Forsmark site. The parameter values are based upon the measurement data obtained in the transport properties laboratory programme summarised in /Crawford (ed) 2008/ and described in detail in /Byegård et al. 2008/. For the rock matrix porosity and formation factor, there is a very good sample support that allows best estimate parameter values (i.e. the central tendency of the measurement data) to be assessed with a relatively high degree of confidence. For sorption, however, the lower numbers of samples for particular solute/rock type/water combinations means that the data should be applied with caution. More detailed quantification of sorption K_d variability and uncertainty with respect to additional considerations of variable porewater chemistry and mineralogical composition will be made within the safety assessment SR-Site. Therefore, the sorption data given in this section are based purely on the values reported from the laboratory programme without additional thermodynamic interpretation, modelling, correction, or analysis.

Formation factors which are presented in the retardation model (Table 10-3) are based upon *in situ* resistivities as well as through-diffusion measurements performed in the laboratory. The only exception is for rock type 101061 (pegmatite, pegmatic granite) for which laboratory through-diffusion data were not available and a formation factor derived from laboratory resistivity measurements is reported instead. In that particular case, the formation factor from the resistivity measurement was divided by an empirical factor of 2.2 derived from comparative measurements to account for a measurement bias associated with the electrical method when comparing against the through-diffusion experiments /Byegård et al. 2008/.

This choice is not meant to indicate a belief that the one method is more reliable than the other. However, it could be argued that the through-diffusion technique is the method that best simulates the actual physical process to be studied (i.e. solute diffusion in the porewater) and that the electrical resistivity technique may be influenced by artefacts that are not, as yet, fully understood which give rise to the empirical deviation of roughly a factor of two. On the other hand, it is noted also that the empirically observed deviation is so consistent and conserved between different investigations that there are good arguments for using a simple empirical correction even in the absence of a full mechanistic explanation of the effect. A detailed discussion concerning the issues related to use of the electrical resistivity measurement technique is provided in /Crawford (ed) 2008/ where the use of *in situ* formation factors derived from borehole resistivity logging is discussed. In SDM-Site, however, the formation factor data derived from *in situ* measurements and laboratory based through diffusion measurements are presented as parallel alternatives for retardation model parameterisation. Since the *in situ* measurements are obtained under approximately natural stress conditions and are generally lower than the corresponding laboratory data, it seems reasonable that they are the more conservative choice for model parameterisation within safety assessment.

The main reason for selecting the through-diffusion method as a basis for the comparison in this chapter is so that all rock types are compared under similar controlled conditions. This is thought to be important if the aim is to ascertain if there are any intrinsic differences in the relative diffusive properties of different rock types that might be of significance in safety assessment. In some situations, it is not entirely clear if the *in situ* data are “exactly” comparable for different spatial locations owing to residual uncertainties concerning relative sample sizes, porewater compositions, and the possible influence of undetected open fractures within the sampled *in situ* rock volume. The core samples used in laboratory investigations, however, may be influenced by drilling induced damage and stress release making it difficult to choose the most representative data set.

Material properties of individual rock types

The data compiled in Table 10-3 to Table 10-7 comprise values for material property parameters preliminarily recommended for modelling of radionuclide transport under site-specific conditions and relate to the bulk rock matrix. Full details concerning the rationale used in the selection of data are provided in the retardation model background report /Byegård et al. 2008/. Since many of the reported data for sorption are based upon very small sample numbers (in some cases as few as two), these data should be considered to be order of magnitude estimates only. It should also be noted that negative values occasionally arise due to the aqueous mass balance technique used to discriminate sorption on the geological samples and sorption on the surface of containment vessel walls which is quantified using separate blanks spiked with the groundwater/solute mix. Although not strictly related to the instrumental level of detection, it still can be considered as part of the overall limit of quantitative detection inherent in the method. In such cases, which typically involve weakly sorbing solutes, the presence or absence of sorption is not possible to distinguish with statistical certainty.

The reduced selection of nuclides in certain cases is due to the difficulty of performing a full set of measurements for every rock type/groundwater combination and represents an economic and logistic compromise where only the main metagranite rock type 101057 is subjected to the full suite of measurements. The detailed rationale for this is outlined in the strategy report by /Widestrand et al. 2003/. Formation factors based upon *in situ* resistivities and laboratory through-diffusion measurements are given in Table 10-3 as two separate parameterisations. The *in situ* data are additionally divided by a factor of 2 to roughly account for the empirically estimated bias of the resistivity based measurement technique.

Table 10-3. Representative transport parameters for the main rock types (> 2%) within rock domains RFM029 and RFM045. Data are given as the mean ± standard deviation for porosity, formation factor, BET-surface area, and cation exchange capacity (CEC) as determined within the laboratory programme.

	101051	101057 non-DZ	DZ	101058	101061	102017
Porosity (vol%)	0.23±0.09	0.23±0.11	1.0±2.4	0.22	0.32	0.16±0.1
Formation factor (*in situ*)†						
unaltered rock only	$(1.1\pm0.8)\cdot10^{-5}$	$(1.6\pm1.0)\cdot10^{-5}$	$(1.5\pm0.8)\cdot10^{-5}$	$(1.3\pm0.2)\cdot10^{-5}$	$(1.9\pm0.8)\cdot10^{-5}$	$(1.7\pm1.2)\cdot10^{-5}$
altered rock only	$(1.7\pm0.5)\cdot10^{-5}$	$(2.0\pm0.8)\cdot10^{-5}$	$(1.5\pm5.6)\cdot10^{-4}$	$(1.4\pm0.5)\cdot10^{-5}$	$(1.9\pm0.5)\cdot10^{-5}$	$(1.4\pm0.1)\cdot10^{-5}$
all rock	$(1.2\pm0.8)\cdot10^{-5}$	$(1.6\pm1.0)\cdot10^{-5}$	$(2.9\pm4.1)\cdot10^{-5}$	$(1.4\pm0.4)\cdot10^{-5}$	$(1.9\pm0.8)\cdot10^{-5}$	$(1.7\pm1.2)\cdot10^{-5}$
Formation factor (lab)						
	$1.0\cdot10^{-4}$	$(1.6\pm1.5)\cdot10^{-4}$	$(1.1\pm1.0)\cdot10^{-4}$	$1.8\cdot10^{-4}$	$2.8\cdot10^{-4}$ (A)	$2.9\cdot10^{-5}$
BET (m^2/g)	0.023±0.014	0.025±0.015	0.342 (B)	0.052	n/a	0.0002
CEC (cmol/kg)*	< 1.2	< 1	n/a	n/a	n/a	n/a

Notes: Entries given as "n/a" in the table signify data "not available".
(†) Formation factors derived from *in situ* measurements are empirically corrected for measurement bias and are for "rock matrix" (i.e. ≥ 0.5m distant from the nearest mapped, open fracture).
(*) 1 cmol/kg = 1 meq/100 g.
(A) Based on laboratory resistivity measurement since through-diffusion measurement was not available.
(B) Based on BET measurements of two samples which were identified as medium altered, which therefore can be suspected to give an overestimate of the general conditions for intact rock within deformation zones.

Table 10-4. Sample K_d values (m^3/kg) measured for the main rock types (where available) within rock domains RFM029 and RFM045. Data are given as the mean ± standard deviation for sorption measurements using fresh (Type I) groundwater.

	101051	101057 non-DZ	Fault rock/ZFMA2	101054
Cs(I)	$(7.9\pm1.7)\cdot10^{-3}$	$(1.9\pm0.7)\cdot10^{-2}$	$(3.3\pm0.6)\cdot10^{-1}$	$(1.8\pm0.2)\cdot10^{-2}$
Sr(II)	$(2.9\pm0.1)\cdot10^{-4}$	$(4.6\pm3.2)\cdot10^{-3}$	$(8.1\pm1.9)\cdot10^{-1}$	$(4.1\pm0.1)\cdot10^{-3}$
Ln–Ac(III)	$(1.3\pm0.2)\cdot10^{-1}$	$(1.3\pm1.3)\cdot10^{-1}$	$(1.9\pm0.5)\cdot10^{-1}$	$(2.1\pm0.3)\cdot10^{-1}$
Ra(II)	n/a	$(9.3\pm2.1)\cdot10^{-2}$	$(3.6\pm2.6)\cdot10^{-1}$	n/a
Ni(II)	n/a	$(6.5\pm0.9)\cdot10^{-2}$	$(3.0\pm1.0)\cdot10^{-1}$	n/a
Np(IV/V)*	n/a	$(1.3\pm0.2)\cdot10^{-3}$	$(4.4\pm0.5)\cdot10^{-3}$	n/a
U(IV/VI)*	n/a	$(1.0\pm0.2)\cdot10^{-3}$	$(1.0\pm0.2)\cdot10^{-3}$	n/a

Notes: Entries given as "n/a" in the table signify data "not available".
Ln-Ac(III) signifies trivalent lanthanides and actinides as a group (assuming analogous behaviour).
(*) The redox status of Np and U during the laboratory measurements was unclear.

Table 10-5. Sample K_d values (m^3/kg) measured for the main rock types (where available) within rock domains RFM029 and RFM045. Data are given as the mean ± standard deviation for sorption measurements using marine (Type II) groundwater.

	101051	101057 non-DZ	Fault rock/ZFMA2	101054
Cs(I)	$(2.1\pm0.1)\cdot10^{-3}$	$(3.6\pm2.5)\cdot10^{-3}$	n/a	$(4.8\pm0.7)\cdot10^{-3}$
Sr(II)	$(1.7\pm0.2)\cdot10^{-4}$	$(3.8\pm16.0)\cdot10^{-4}$	n/a	$(3.4\pm0.4)\cdot10^{-4}$
Ln-Ac(III)	$(2.9\pm0.4)\cdot10^{-2}$	$(8.4\pm9.7)\cdot10^{-1}$	n/a	$(3.5\pm0.2)\cdot10^{-2}$
Ra(II)	n/a	$(1.7\pm0.9)\cdot10^{-2}$	n/a	n/a
Ni(II)	n/a	$(2.5\pm0.4)\cdot10^{-2}$	n/a	n/a
Np(IV/V)*	n/a	$(1.4\pm1.7)\cdot10^{-3}$	n/a	n/a
U(IV/VI)*	n/a	$(2.9\pm0.4)\cdot10^{-3}$	n/a	n/a

Notes: Entries given as “n/a” in the table signify data “not available”.
Ln-Ac(III) signifies trivalent lanthanides and actinides as a group (assuming analogous behaviour).
(*) The redox status of Np and U during the laboratory measurements was unclear.

Table 10-6. Sample K_d values (m^3/kg) measured for the main rock types (where available) within rock domains RFM029 and RFM045. Data are given as the mean ± standard deviation for sorption measurements using saline (Type III) groundwater.

	101051	101057 non-DZ	Fault rock/ZFMA2	101054
Cs(I)	$(2.9\pm0.3)\cdot10^{-3}$	$(4.0\pm1.6)\cdot10^{-3}$	$(4.5\pm0.2)\cdot10^{-2}$	$(8.4\pm0.2)\cdot10^{-3}$
Sr(II)	$(2.8\pm1.3)\cdot10^{-4}$	$(2.4\pm8.1)\cdot10^{-4}$	$(0.75\pm24)\cdot10^{-4}$	$(0.1\pm2.2)\cdot10^{-4}$
Ln-Ac(III)	$(3.9\pm0.6)\cdot10^{-1}$	$(5.6\pm2.3)\cdot10^{-1}$	4.5±1.8	$(8.2\pm1.4)\cdot10^{-1}$
Ra(II)	n/a	$(6.5\pm1.2)\cdot10^{-3}$	$(6.1\pm0.2)\cdot10^{-2}$	n/a
Ni(II)	n/a	$(2.2\pm0.4)\cdot10^{-2}$	$(2.8\pm0.6)\cdot10^{-1}$	n/a
Np(IV/V)*	n/a	$(3.0\pm3.9)\cdot10^{-4}$	$(2.2\pm0.23)\cdot10^{-3}$	n/a
U(IV/VI)*	n/a	$(7.8\pm3.6)\cdot10^{-4}$	$(2.0\pm0.4)\cdot10^{-2}$	n/a

Notes: Entries given as “n/a” in the table signify data “not available”.
Ln-Ac(III) signifies trivalent lanthanides and actinides as a group (assuming analogous behaviour).
(*) The redox status of Np and U during the laboratory measurements was unclear.

Table 10-7. Sample K_d values (m^3/kg) measured for the main rock types (where available) within rock domains RFM029 and RFM045. Data are given as the mean ± standard deviation for sorption measurements using brine (Type IV) groundwater.

	101051	101057 non-DZ	Fault rock/ZFMA2	101054
Cs(I)	n/a	$(1.8\pm0.6)\cdot10^{-3}$	n/a	n/a
Sr(II)	n/a	$(2.1\pm6.5)\cdot10^{-4}$	n/a	n/a
Ln-Ac(III)	n/a	$(3.9\pm2.2)\cdot10^{-1}$	n/a	n/a
Ra(II)	n/a	$(2.1\pm0.7)\cdot10^{-4}$	n/a	n/a
Ni(II)	n/a	$(3.3\pm0.3)\cdot10^{-3}$	n/a	n/a
Np(IV/V)*	n/a	$(-1.9\pm0.1)\cdot10^{-3}$	n/a	n/a
U(IV/VI)*	n/a	$(1.9\pm0.5)\cdot10^{-3}$	n/a	n/a

Notes: Entries given as “n/a” in the table signify data “not available”.
Ln-Ac(III) signifies trivalent lanthanides and actinides as a group (assuming analogous behaviour).
(*) The redox status of Np and U during the laboratory measurements was unclear.

Material properties of fractures

The data compiled in Table 10-8 to Table 10-15 comprise values for material property parameters preliminarily recommended for modelling of radionuclide transport under site-specific conditions and concern material properties of specific fracture types. According to the available data, the presence of different fracture mineralisations cannot be related to specific rock types, rock domains, or fracture domains. This is important for the application of the identified fracture types in transport models. Some additional observations and remarks concerning fracture types follow below and are based upon analysis by /Sandström et al. 2008/. Similarly to the sorption properties of rock types, much of the data are based upon very small sample numbers. In the case of single measurements (chiefly for some fracture coatings that were difficult to sample), the reported uncertainty is an estimate based upon radiometric counting statistics rather than the standard deviation of multiple measurements.

Chlorite and calcite are the most frequent fracture filling minerals. Chlorite and calcite are present in about 34% of the mapped open fractures and 38% of the transmissive fractures (fracture type A). There are no porosity or sorption data from this fracture type within the laboratory programme owing to difficulties encountered obtaining sufficient material to perform experiments (the fracture coatings are generally less than 0.5 mm thick and difficult to sample). However, porosity measurements of similar fracture fillings sampled in investigations at the Äspö Hard Rock Laboratory /Widestrand et al. 2010/ indicate a porosity of about 5% which is substantially greater than that of the wall rock. Detailed fracture mineralogical studies also show that corrensite is commonly found in fractures also containing chlorite with the consequence that the frequency of fracture type B (based on boremap data) might be somewhat underestimated.

Calcite occurring by itself or together with quartz, pyrite and other minerals is found in about 15% of the open fractures and 19% of the transmissive fractures. This type of assemblage (fracture type F) dominates the transmissive fractures together with chlorite and calcite (fracture type A).

Clay minerals as illite, smectite and mixed layer clay (smectite/illite) are found at various depths in different boreholes and consequently fracture domains, but are more abundant in open fractures in fracture domain FFM02. Clay minerals, characteristic of fracture type G, are found in at least 3% of the open fractures and are common in the upper 150–200 m (see Figure 10-3) of the bedrock. Small amounts of clay can also be found in association with other fracture types (e.g. fracture type E). Difficulties in clearly identifying and assigning fractures to different groups may have contributed to the low number of fractures classified as type G and thus the apparent distribution of these fractures could be a taxonomic artefact. Other clay minerals such as corrensite (swelling mixed layer clay) generally occur together with chlorite and are present in 7% of the open fractures (fracture type B). The latter fracture type is not restricted to any particular depth but constitutes a larger proportion, about 10–20%, of the total number of open fractures at repository depth.

Laumontite (± calcite ± chlorite) is a common fracture mineral in open fractures as well as in sealed fracture networks. It is, however, difficult to determine whether these fractures are originally open or sealed. This means that the frequency of open, laumontite-coated fractures is uncertain. Laumontite is visible in about 14% of all open fractures. Yet, laumontite is an unusual occurrence in fractures associated with PFL anomalies (≈ 1%). According to PMMA measurements of sealed fracture networks, laumontite has a porosity of approximately 3% which is substantially greater than unaltered wall rock.

About 6% of all open fractures are mapped without any surface coating minerals. These fractures are to a great extent horizontal to sub-horizontal (with a dip less than 25°). The frequency with which they occur is roughly 50% greater amongst the horizontal and sub-horizontal features as compared with the total set of open fractures. For transmissive fractures (i.e. fractures associated with PFL-anomalies), roughly 13% appear to lack surface mineralisation. Fractures which lack surface mineral coatings are presumed to have the same retardation properties as the wall rock (e.g. rock type 101057). This means that this fracture type might have reduced retardation properties as compared with other fracture types.

Concerning the host rock surrounding fractures, only a minor portion of the open fractures are described as being accompanied by altered wall rock in the core logging. If considering the nearest cm to the fracture only, this is probably an underestimation, especially for the fractures with hydrothermal minerals such as epidote, prehnite and laumontite, as most of the fracture coatings documented by thin sections show hydrothermal alteration /Sandström et al. 2004/. The wall rock alteration is not always visible as red staining or bleached feldspar, but is often present in the less easily identifiable form of altered plagioclase and chlorite formed from biotite alteration. The intensity of micro-fracturing may also be substantially increased in the altered zone giving rise to increased porosity and possibly diffusivity in this zone.

Retardation parameters for the identified fracture types are given in Table 10-8 to Table 10-15.

Table 10-8. Retardation model parameters for fracture type A.

	Fracture coating: *Chlorite + Calcite*			
Thickness	≤ 0.5 mm			
Porosity (vol%)	n/a			
Formation factor	n/a			
BET surface area (m^2/g)	0.49			
CEC (cmol/kg)	n/a			
Sorption, K_d (m^3/kg)	Water type (I–IV)			
	fresh	marine	saline	brine
Cs(I)	n/a	n/a	n/a	n/a
Sr(II)	n/a	n/a	n/a	n/a
Ln-Ac(III)	n/a	n/a	n/a	n/a
Percentage of all open fractures	34%			
Percentage of transmissive fractures	38%			
Transmissivity interval (m^2/s)	> 10^{-10} (no evidence for preferential transmissivity interval)			
Preferred orientation	n/a			
Altered rock surrounding the fracture	no			

Notes: Entries given as “n/a” in the table signify data “not available”.

Table 10-9. Retardation model parameters for fracture type B.

	Fracture coating: *Chlorite + Clay* ± *epidote* ± *prehnite* ± *calcite*			
Thickness	≤ 1 mm			
Porosity (vol%)	n/a			
Formation factor	n/a			
BET surface area (m^2/g)	10.3			
CEC (cmol/kg)	15±10			
Sorption, K_d (m^3/kg)	Water type (I–IV)			
	fresh	marine	saline	brine
Cs(I)	1.5±0.16	n/a	$(1.6\pm0.1)\cdot10^{-1}$	$(4.8\pm0.39)\cdot10^{-2}$
Sr(II)	$(2.0\pm0.43)\cdot10^{-1}$	n/a	n/a	$(-1.3\pm1.6)\cdot10^{-3}$
Ln-Ac(III)	$(1.0\pm0.45)\cdot10^{-1}$	n/a	$(7.5\pm1.7)\cdot10^{-2}$	$(8.6\pm0.95)\cdot10^{-1}$
Percentage of all open fractures	7%			
Percentage of transmissive fractures	7%			
Transmissivity interval (m^2/s)	> 10^{-10} (no evidence for preferential transmissivity interval)			
Preferred orientation	horzontal to gently dipping			
Altered rock surrounding the fracture	yes, ≈ 1 cm			

Notes: Entries given as “n/a” in the table signify data “not available”.

Table 10-10. Retardation model parameters for fracture type C.

	Fracture coating: *Chlorite + hematite* ± *other*			
Thickness	< 0.5 mm (0.1 mm)			
Porosity (vol%)	n/a			
Formation factor	n/a			
BET surface area (m^2/g)	2.3±0.6			
CEC (cmol/kg)	n/a			
Sorption, K_d (m^3/kg)	Water type (I–IV)			
	fresh	marine	saline	brine
Cs(I)	n/a	n/a	n/a	n/a
Sr(II)	n/a	n/a	n/a	n/a
Ln-Ac(III)	n/a	n/a	n/a	n/a
Percentage of all open fractures	2%			
Percentage of transmissive fractures	1%			
Transmissivity interval (m^2/s)	> 10^{-10} (no evidence for preferential transmissivity interval)			
Preferred orientation	ENE–NW, steeply dipping			
Altered rock surrounding the fracture	yes, ≈ 0.5 mm			

Notes: Entries given as “n/a” in the table signify data “not available”.

Table 10-11. Retardation model parameters for fracture type D.

	Fracture coating: *Chlorite* ± *other*			
Thickness	< 0.5 mm (0.1 mm)			
Porosity (vol%)	n/a			
Formation factor	n/a			
BET surface area (m^2/g)	5.1±2.2			
CEC (cmol/kg)	n/a			
Sorption, K_d (m^3/kg)	Water type (I–IV)			
	fresh	marine	saline	brine
Cs(I)	$(6.4\pm1.3)\cdot10^{-2}$	$(4.1\pm0.5)\cdot10^{-3}$	n/a	$1.2\cdot10^{-3}$
Sr(II)	$(3.7\pm1.1)\cdot10^{-1}$	$(3.7\pm4.5)\cdot10^{-4}$	n/a	n/a
Ln-Ac(III)	1.5±0.3	2.4±0.5	n/a	2.8
Percentage of all open fractures	14%			
Percentage of transmissive fractures	12%			
Transmissivity interval (m^2/s)	> 10^{-10} (no evidence for preferential transmissivity interval)			
Preferred orientation	n/a			
Altered rock surrounding the fracture	no			

Notes: Entries given as “n/a” in the table signify data “not available”.

Table 10-12. Retardation model parameters for fracture type E.

	Fracture coating: *Laumontite* ± *calcite* ± *other*			
Thickness	0.1–2 mm			
Porosity (vol%)	n/a			
Formation factor	n/a			
BET surface area (m^2/g)	0.42±0.02			
CEC (cmol/kg)	18±5			
Sorption, K_d (m^3/kg)	Water type (I–IV)			
	fresh	marine	saline	brine
Cs(I)	$(2.9\pm1.4)\cdot10^{-1}$	$(1.6\pm0.24)\cdot10^{-2}$	$(1.6\pm0.3)\cdot10^{-2}$	$(4.1\pm0.4)\cdot10^{-3}$
Sr(II)	$(5.1\pm2.1)\cdot10^{-2}$	$(1.3\pm3.8)\cdot10^{-4}$	$(0.35\pm3.32)\cdot10^{-4}$	$(0.31\pm5.1)\cdot10^{-4}$
Ln-Ac(III)	1.0±0.4	1.3±2.1	1.2±0.14	2.1±0.4
Percentage of all open fractures	14%			
Percentage of transmissive fractures	1%			
Transmissivity interval (m^2/s)	> 10^{-10} (no evidence for preferential transmissivity interval)			
Preferred orientation	ENE–NW, steeply dipping			
Altered rock surrounding the fracture	yes, 1–5 cm			

Notes: Entries given as “n/a” in the table signify data “not available”.

Table 10-13. Retardation model parameters for fracture type F.

	Fracture coating: *Calcite* ± *quartz* ± *pyrite* ± *other*			
Thickness	0.1–2 mm			
Porosity (vol%)	n/a			
Formation factor	n/a			
BET surface area (m^2/g)	2.2±1.1			
CEC (cmol/kg)	n/a			
Sorption, K_d (m^3/kg)	Water type (I–IV)			
	fresh	marine	saline	brine
Cs(I)	$(1.7\pm0.6)\cdot10^{-1}$	$(1.3\pm0.6)\cdot10^{-2}$	$(2.2\pm1.7)\cdot10^{-2}$	n/a
Sr(II)	$(1.8\pm1.1)\cdot10^{-1}$	$(1.3\pm1.2)\cdot10^{-3}$	$(7.4\pm5.5)\cdot10^{-4}$	n/a
Ln-Ac(III)	$(2.0\pm1.7)\cdot10^{-1}$	$(8.6\pm6.7)\cdot10^{-1}$	1.4±1.2	n/a
Percentage of all open fractures	15%			
Percentage of transmissive fractures	19%			
Transmissivity interval (m^2/s)	> 10^{-10} (no evidence for preferential transmissivity interval)			
Preferred orientation	sub-horizontal to gently dipping			
Altered rock surrounding the fracture	no			

Notes: Entries given as “n/a” in the table signify data “not available”.

Table 10-14. Retardation model parameters for fracture type G.

	Fracture coating: *Clay* ± *other*			
Thickness	1–5 mm			
Porosity (vol%)	n/a			
Formation factor	n/a			
BET surface area (m^2/g)	4.3			
CEC (cmol/kg)	n/a			
Sorption, K_d (m^3/kg)	Water type (I–IV)			
	fresh	marine	saline	brine
Cs(I)	5.8±2.3	$(4.3\pm0.42)\cdot10^{-1}$	n/a	n/a
Sr(II)	$(9.5\pm1.5)\cdot10^{-2}$	$(2.2\pm0.2)\cdot10^{-3}$	n/a	n/a
Ln-Ac(III)	1.8±0.5	1.6±0.14	n/a	n/a
Percentage of all open fractures	3%			
Percentage of transmissive fractures	3%			
Transmissivity interval (m^2/s)	$> 10^{-10}$ (no evidence for preferential transmissivity interval)			
Preferred orientation	horizontal to gently dipping			
Altered rock surrounding the fracture	yes, ≥ 5 cm			

Notes: Entries given as “n/a” in the table signify data “not available”.

Table 10-15. Retardation model parameters for fracture type H (material properties assumed to be same as for rock type 101057).

	Fracture coating: *no mineral*			
Thickness	n/a			
Porosity (vol%)	0.22			
Formation factor	$(1.6\pm1.0)\cdot10^{-5}$			
BET surface area (m^2/g)	0.025±0.015			
CEC (cmol/kg)	< 1			
Sorption, K_d (m^3/kg)	Water type (I–IV)			
	fresh	marine	saline	brine
Cs(I)	$(1.9\pm0.7)\cdot10^{-2}$	$(3.6\pm2.5)\cdot10^{-2}$	$(4.0\pm1.6)\cdot10^{-3}$	$(1.8\pm0.6)\cdot10^{-3}$
Sr(II)	$(4.6\pm3.2)\cdot10^{-3}$	$(3.8\pm16)\cdot10^{-4}$	$(2.4\pm8.1)\cdot10^{-4}$	$(2.1\pm6.5)\cdot10^{-4}$
Ln-Ac(III)	$(1.3\pm1.3)\cdot10^{-1}$	$(8.4\pm9.7)\cdot10^{-1}$	$(5.6\pm2.3)\cdot10^{-1}$	$(3.9\pm2.2)\cdot10^{-1}$
Ra(II)	$(9.3\pm2.1)\cdot10^{-2}$	$(1.7\pm0.9)\cdot10^{-2}$	$(6.5\pm1.2)\cdot10^{-3}$	$(2.1\pm0.7)\cdot10^{-4}$
Ni(II)	$(6.5\pm0.9)\cdot10^{-2}$	$(2.5\pm0.4)\cdot10^{-2}$	$(2.2\pm0.4)\cdot10^{-2}$	$(3.3\pm0.3)\cdot10^{-3}$
*Np(IV/V)**	$(1.3\pm0.2)\cdot10^{-3}$	$(1.4\pm1.7)\cdot10^{-3}$	$(3.0\pm3.9)\cdot10^{-4}$	$(-1.9\pm0.1)\cdot10^{-3}$
*U(IV/VI)**	$(1.0\pm0.2)\cdot10^{-3}$	$(2.9\pm0.4)\cdot10^{-3}$	$(7.8\pm3.6)\cdot10^{-4}$	$(1.9\pm0.5)\cdot10^{-3}$
Percentage of all open fractures	5%			
Percentage of transmissive fractures	13%			
Transmissivity interval (m^2/s)	$> 10^{-10}$ (no evidence for preferential transmissivity interval)			
Preferred orientation	horizontal to gently dipping			
Altered rock surrounding the fracture	no			

Notes: Entries given as “n/a” in the table signify data “not available”.
(*) The redox status of Np and U during the laboratory measurements was unclear.

Material properties of deterministically modelled deformation zones

As described in previous chapters (e.g. section 5.5), deformation zones are usually characterised as consisting of a transition zone and a core. Transmissive fractures, if they are present, are often found in the transition zone, close to the wall rock. The deformation zone core is commonly found to have substantially reduced flow permeability in a direction normal to its orientation.

There are a number of different possibilities for the modelling of deformation zones in a radionuclide transport perspective. One possibility is to define retention parameters for the zone in its entirety where the zone is simply represented as a region of higher retention capacity and flow transmissivity. Another possibility is to partition the deformation zone into high and low transmissive elements. Implicit in this approach is the need to assign limited diffusion depths for different deformation zone sub-elements to avoid double counting of storage capacities. Some of the different possibilities available are illustrated in Figure 10-4.

Independently of which model is adopted for use in transport calculations, there are some over-arching issues which should be considered when parameterising deformation zones.

- The vast majority of borehole sections mapped as having strong or medium oxidation are found within deformation zones. In addition, three separate categories of altered rock have been distinguished as recurrent elements within, or in close proximity to deformation zones; i.e. sealed fracture networks, vuggy rock (episyenite), and fault rock (breccia and/or cataclasite). Retardation parameters for these elements are given in Table 10-16 to Table 10-19.
- A deformation zone consists of a high frequency of open and sealed fractures. Retardation parameters for open fractures are found in Table 10-8 to Table 10-15.
- Both the frequency and distribution of transmissive fractures vary between different deformation zones although the transmissivity ranges are broadly similar for all fracture types described in the retardation model.

Table 10-16 to Table 10-19 give recommended data for the different rock types that are specific to deformation zones.

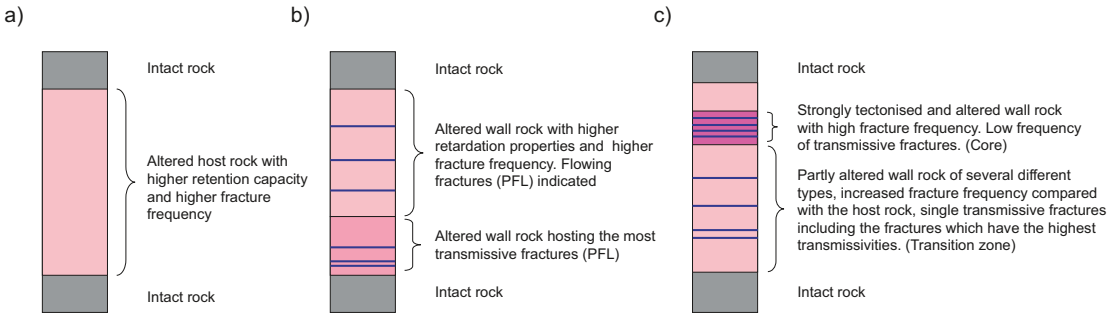

Figure 10-4. *Schematic illustration of different alternatives for describing a deformation zone retardation model; a) deformation zone considered as a single unit with higher retention capacity than the surrounding rock; b) the deformation zone divided into a high and low transmissive unit; c) variation including core zone, the latter also divided into a high and low transmissive unit.*

Table 10-16. Retardation model parameters for fault rock (strongly tectonised and partly incohesive material).

Mineral content	Altered rock fragment, mineralogy dependant on host rock. Generally, chlorite, saussurite and clay			
Porosity (vol%)	10%			
Formation factor	n/a			
BET surface area (m^2/g)	5.6±2.3			
CEC (cmol/kg)	9±1			
Sorption, K_d (m^3/kg)	Water type (I–IV)			
	fresh	marine	saline	brine
Cs(I)	$(3.3\pm0.6)\cdot10^{-1}$	n/a	$(4.5\pm0.2)\cdot10^{-3}$	n/a
Sr(II)	$(8.1\pm1.9)\cdot10^{-2}$	n/a	$(7.5\pm24)\cdot10^{-5}$	n/a
Ln-Ac(III)	$(1.9\pm0.5)\cdot10^{-1}$	n/a	4.5±1.8	n/a
Ra(II)	$(3.6\pm2.6)\cdot10^{-1}$	n/a	$(6.1\pm0.2)\cdot10^{-2}$	n/a
Ni(II)	$(3.0\pm1.0)\cdot10^{-1}$	n/a	$(2.8\pm0.6)\cdot10^{-1}$	n/a
*Np(IV/V)**	$(4.4\pm0.5)\cdot10^{-3}$	n/a	$(2.2\pm0.23)\cdot10^{-3}$	n/a
*U(IV/VI)**	$(1.0\pm0.2)\cdot10^{-3}$	n/a	$(2.0\pm0.4)\cdot10^{-2}$	n/a
Transmissivity interval (m^2/s)	n/a			

Notes: Entries given as “n/a” in the table signify data “not available”.

Table 10-17. Retardation model parameters for sealed fracture networks (usually brecciated).

Mineral content	Due to mineral paragenesis: a) laumo-ntite + calcite ± others b) epidote ± chlorite ± prehnite ± others c) chlorite ± others			
Porosity (vol%)	3%			
Formation factor	n/a			
BET surface area (m^2/g)	0.64			
CEC (cmol/kg)	5.4±2.4			
Sorption, K_d (m^3/kg)	Water type (I–IV)			
	fresh	marine	saline	brine
Cs(I)	$(2.1\pm0.14)\cdot10^{-1}$	$1.4\cdot10^{-2}$	$(1.8\pm0.07)\cdot10^{-2}$	n/a
Sr(II)	$(3.7\pm0.1)\cdot10^{-2}$	n/a	$(2.0\pm5.7)\cdot10^{-4}$	n/a
Ln-Ac(III)	$(7.6\pm0.01)\cdot10^{-1}$	$(7.3\pm2.3)\cdot10^{-2}$	1.1±0.1	n/a
Transmissivity interval (m^2/s)	n/a			

Notes: Entries given as “n/a” in the table signify data “not available”.

Table 10-18. Retardation model parameters for vuggy rock.

Mineral content	K-feldspar + albite + Fe-oxides + chlorite ± quartz ± sericite ± calcite ± others			
Porosity (vol%)	13±6%			
Formation factor	$(1.2\pm0.8)\cdot10^{-2}$			
BET surface area (m^2/g)	1.58			
CEC (cmol/kg)	< 0.4			
Sorption, K_d (m^3/kg)	Water type (I–IV)			
	fresh	marine	saline	brine
Cs(I)	$(9.4\pm1.3)\cdot10^{-3}$	$(2.0\pm0.2)\cdot10^{-3}$	n/a	$(6.4\pm0.6)\cdot10^{-4}$
Sr(II)	$(7.0\pm0.6)\cdot10^{-3}$	$(2.8\pm5.4)\cdot10^{-3}$	n/a	$(-4.4\pm1.8)\cdot10^{-4}$
Ln-Ac(III)	$(2.7\pm0.71)\cdot10^{-1}$	1.4±0.8	n/a	$(9.0\pm3.7)\cdot10^{-1}$
Transmissivity interval (m^2/s)	n/a			

Notes: Entries given as “n/a” in the table signify data “not available”.

Table 10-19. Retardation model parameters for oxidised wall rock (medium to strong alteration).

Mineral content	Hydrothermally altered host rock. Red staining from small hematite grains, K-feldspar, saussurite, plagioclase, quartz, chlorite			
Porosity (vol%)	2.5±3.8%			
Formation factor	n/a			
BET surface area (m^2/g)	0.77			
CEC (cmol/kg)	n/a			
Sorption, K_d (m^3/kg)	Water type (I–IV)			
	fresh	marine	saline	brine
Cs(I)	n/a	n/a	n/a	n/a
Sr(II)	n/a	n/a	n/a	n/a
Ln-Ac(III)	n/a	n/a	n/a	n/a
Transmissivity interval (m^2/s)	n/a			

Notes: Entries given as “n/a” in the table signify data “not available”.

Parameterisation of effective diffusive properties using in situ resistivity data

There is some evidence to suggest (see following discussion) that the effective diffusivities of borehole core samples measured in the laboratory may be biased by stress release and mechanical damage incurred during drilling and sample preparation. Since *in situ* measurements of resistivity can be used to measure the formation factor of the rock under relatively undisturbed conditions, this would suggest that the *in situ* data may be more reliable for use in transport modelling. Figure 10-5 shows a typical comparison of formation factors derived from *in situ* and laboratory resistivity measurement data for borehole KFM01A (compared directly without the additional empirical correction for methodological bias discussed previously). Since both data sets are based upon the resistivity measurement technique, it is the relative difference that is important to consider here rather than the absolute value of the formation factor. For additional comparison, formation factors derived from laboratory through diffusion experiments are also shown in the figure.

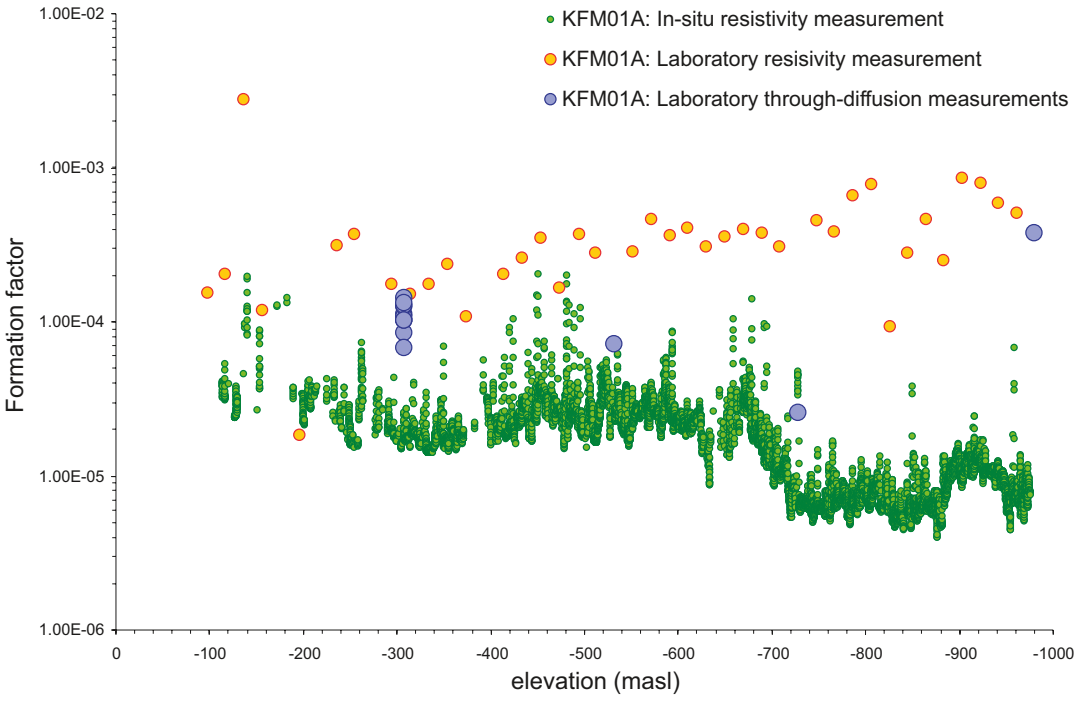

Figure 10-5. *Comparison of uncorrected formation factors derived from in situ resistivity measurements in KFM01A with corresponding data from through-diffusion and electrical resistivity (also uncorrected) measurements on core samples in the laboratory. The in situ data are based upon a re-interpretation of original borehole resistivity logs corrected to reflect current best estimate porewater compositions at drill site 1.*

As can be seen from Figure 10-5, the laboratory based resistivity measurements appear to give a formation factor about an order of magnitude higher than the *in situ* data, which is strongly suggestive of an *in situ* compression of pore spaces and/or drilling induced core damage for the laboratory samples. Within the site investigation programme, formation factor measurements in the laboratory have not been performed on re-confined samples. However, such measurements have been performed elsewhere and a reduction in the formation factor for crystalline rock samples under increasing applied confining stress is well known in the literature, e.g. /Skagius 1986, Brace et al. 1968/.

There is corroborating evidence that suggests a possible compression of pore spaces under *in situ* stress conditions. Specifically, porosity measurements made in triaxial compression tests /Jacobsson 2007/ and measurements from the matrix porewater characterisation /Waber and Smellie 2007/ give indications of this phenomenon. No strong depth trend for the *in situ* or laboratory formation factor is perceptible at the Forsmark site as a whole, although the data in Figure 10-5 do show a weakly increasing trend for laboratory resistivity and slight decreasing trend for *in situ* resistivity based measurements in this particular borehole.

There are, however, a number of additional issues related to the interpretation of laboratory versus *in situ* measurements which are necessary to consider before recommending the *in situ* data for general use in modelling. Although most of the uncertainties are well bounded, the *in situ* formation factor data are presented in this chapter as a base case together with the data derived from laboratory through diffusion measurements as an alternative parameterisation.

The principal uncertainty which could affect the applicability of the data concerns the physical nature of the measurement bias in the electrical method that gives a difference of about a factor of two between formation factors measured by through-diffusion and electrical methods under laboratory conditions. Although an investigation is currently underway to resolve this issue, it is not yet clear whether the empirical correction factor derived for the resistivity method in the laboratory can be assumed to be roughly the same for the generally lower (and variable) porewater salinities encountered in the *in situ* rock. Some representative data (uncorrected) sorted by rock type are plotted in Figure 10-6 for rock domain RFM029, which includes the fracture domains FFM01, FFM02, and FFM03. It should be noted that the approximately rounded factor of 2 recommended here for empirical correction differs from the factor 2.2 used for estimation of the effective diffusivity of pegmatite (i.e. rock type 101061 in Table 10-3). The reason for this is that the former is based upon a much larger data set and a number of different rock types while the latter is based upon comparison of a smaller number of laboratory measurements specifically concerning pegmatite.

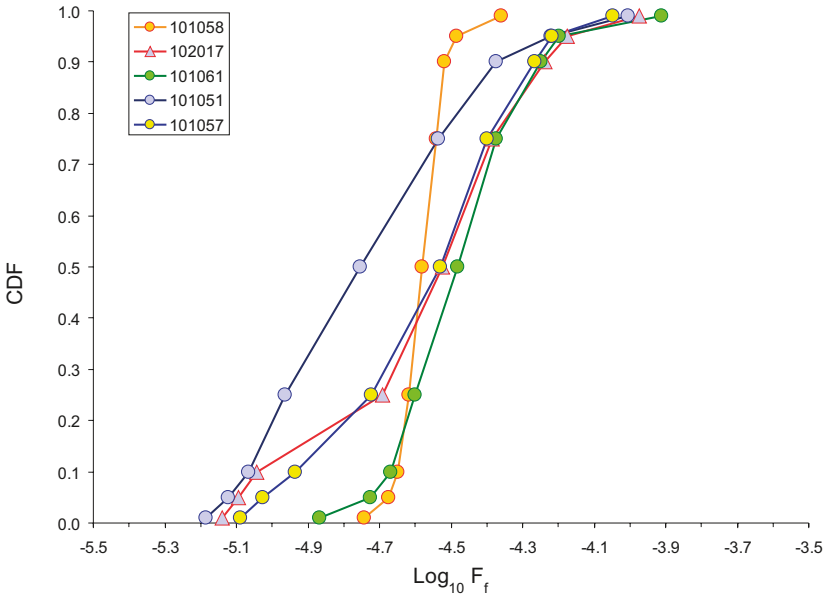

Figure 10-6. *Empirical percentiles for in situ matrix formation factors (uncorrected), specified according to rock type within rock domain RFM029 (FFM01–03) and plotted as a cumulative distribution function, CDF.*

As can be seen from the plotted data, there does not appear to be very large systematic differences between the different rock types; indeed the spread of data points within individual rock types tends to be greater than the differences between rock types. Furthermore, it is not clear whether the dispersion observed in individual data sets could be more closely related to the size of the data set than an intrinsic difference in effective diffusivity. The main exception here is amphibolite (102017), which appears to have a large data spread in spite of the relatively small sample size. Rock type 101051 stands out, with a median formation factor about 50% lower than that measured for the main metagranitic rock type (101057) and a significant positive skew, although exhibiting roughly the same overall spread. It is noted, however, that the difference is small and within the margin of uncertainty for other factors directly influencing formation factors estimated from *in situ* measurements of electrical resistivity. A detailed discussion of the different uncertainties affecting the *in situ* method is given in /Crawford (ed) 2008/.

10.4.3 Application of the retardation model

The quantitative descriptions of the identified fracture types and selected retardation parameters are given in Table 10-8 to Table 10-15. The corresponding descriptions of and data for deformation zones are presented in Table 10-16 to Table 10-19. It is intended that the different fracture types and deformation zone structural elements can be used in a modular fashion for constructing integrated models of radionuclide transport along flow paths within the rock.

In this chapter, the material property data are characterised in the form of mean values ± standard deviation of the measurement data. The full sorption data set in the Sicada database will be subsequently used as a basis for selection of site-specific data which will be used for stochastic parameterisation of transport models. The background report /Crawford (ed) 2008/ contains additional statistics for the relevant material property parameters where available.

This chapter should be regarded as a proposal for how to formulate a descriptive semi-quantitative retardation model based on the available database. However, the proposals for the selection of data are given with acknowledgement of the qualitative and quantitative uncertainties in the retention parameters. This caveat implies that the model does not provide exact and detailed guidelines on how to "dress" the geological model with transport parameters using the retardation model tables. Nevertheless, in the opinion of the authors this is the best representation achievable with the available data. The retardation model should be regarded as an overview of the interpreted site-specific information on retardation parameters, intended to provide a basis for the formulation of alternative parameterisations or necessary simplifications within safety assessment modelling.

10.5 Flow-related transport properties

10.5.1 Conceptualisation of flow paths

All long-range solute transport in fractured rock takes place in advective flow channels hosted within fractures and deformation zones. Matrix diffusion coupled with sorption has been identified as the main retardation process that limits the rate at which solutes are transported along these flow paths. The greater the surface area in contact with flowing water (the so called "flow-wetted surface", or *FWS*) for a given water flow rate, the greater the interaction will be with both the fracture surface and the rock matrix. Within SDM-Site the flow-wetted surface to flow ratio is referred to as the "F-factor" /Andersson et al. 1998/ or "hydrodynamic transport resistance". The F-factor is a key parameter governing the transport of radionuclides within fractured rock.

In the analyses presented in SDM-Site, transport is conceptualised to occur along advective flow paths in a multi-compartment system. The three compartments assumed in the transport model are:

1. The non-engineered near field (NNF).
2. The immediate far field (IFF).
3. The distant far field (DFF).

In this model, the non-engineered near field (NNF) is assumed to comprise approximately the first few metres or so from a canister position intersected by one or more low-transmissivity fractures to the nearest significant conductive structure within the fracture domain containing the hypothetical repository. The distance of 10 m assumed in the scoping calculations reported in /Crawford (ed) 2008/ is arbitrary, although thought to be a reasonable order of magnitude estimate of the average distance for a "typical" transport path in the NNF that might dominate radionuclide transport from a hypothetical repository.

The immediate far field (IFF) is assumed to comprise the first 100 m in the fracture domain containing the hypothetical repository. This distance is also arbitrary, although motivated by consideration of the "respect distance", which is the shortest distance allowable from any given canister position to the transition region of the large deterministic deformation zones adjoining the fracture domains /Munier and Hökmark 2004/. The choice of 100 m is purely intended for illustrative purposes and may not necessarily coincide with forthcoming repository layout designs. Since fractures featuring high transmissivities are likely to be avoided when selecting canister deposition holes, typical flow paths within the IFF should, on average, have higher transmissivities than flow paths within the NNF and are therefore treated separately. The IFF has flow properties corresponding to the fracture domains parameterised in the hydrogeological DFN model supplied by hydrogeology (/Follin et al. 2007b/ and chapter 8).

The distant far field in the present context is taken to comprise the deterministic deformation zones surrounding the repository volume. The hydrogeological properties of these are also described in /Follin et al. 2007b/ and in chapter 8.

A conceptual illustration of the possible sequence of flow paths extending from a canister position to the near surface is shown in Figure 10-7.

The demarcation of the transport system into a three-stage compartment is used here purely for illustrative purposes and for making scoping calculations to account for where the main hydrodynamic transport resistances are encountered in the rock. In safety assessment, the hydrogeological models and material properties parameter tables are used directly in an integrated model to simulate radionuclide migration in the rock without the need for compartmentalisation in this fashion.

For the analyses of hydrodynamic transport resistance presented here, transport from a hypothetical repository at 450 m depth to the near surface, which is taken to be at 100 m depth, is considered. It is hypothesised that most of the hydrodynamic transport resistance is encountered at greater depths within the repository volume and the lower reaches of the deterministic deformation zones. Therefore, the neglect of the highly transmissive features (e.g. horizontal sheet joints, etc) in the upper part of the bedrock does not substantially influence the estimated overall F-factors.

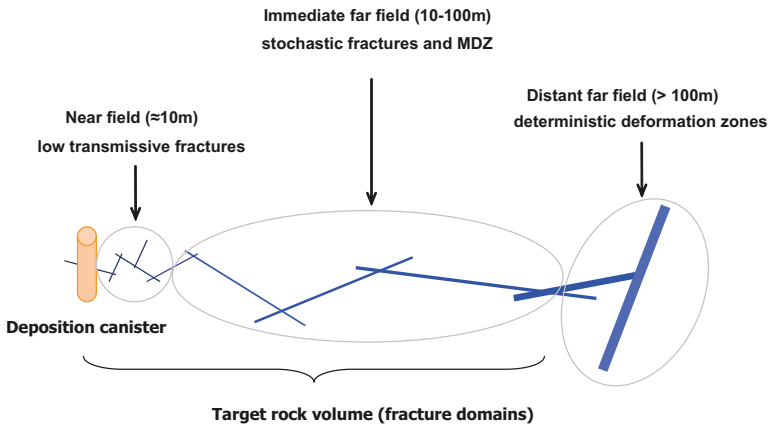

Figure 10-7. *Illustration of a potential flow path from a hypothetical repository to the near surface. Transport is conceptualised to occur along a sequence of flow paths featuring increasing transmissivity.*

Within safety assessment, alternative scenarios of radionuclide transport are considered. One of these is the possibility of a deliberate or accidental anthropogenic intrusion. In such a situation, transport via the deterministic deformation zones may be bypassed completely. Although this is discussed briefly in /Crawford (ed) 2008/, no specific calculations are made for such flow paths, as these are considered to be more of a safety assessment character and not strictly part of a site descriptive model.

10.5.2 F-factor estimation

In the overall modelling strategy, F-factor estimations are made for each sub-compartment of the hypothetical transport path assuming a pre-defined set of reference conditions. In the calculations presented here, a local hydraulic gradient of 1% is assumed as a reference condition for each sub-compartment. This allows comparisons to be made of the relative importance of different compartments given different scenarios for the local hydraulic gradient. The relevant F-factor for the complete transport path is given by the sum of the F-factors for each compartment, assuming that transport occurs through a sequence of connected flow paths as described previously. As described in /Crawford (ed) 2008/, the F-factor for the whole flow path or individual compartments can be linearly rescaled to give estimates for different hydraulic gradients. Based upon topographical considerations, a hydraulic gradient of about 1% is thought to be a reasonably representative estimate for the regional flow system (see additional discussion in section 8.7.2). This figure is assumed *a priori* as a reference hydraulic gradient for each of the sub-compartments in the flow-related transport properties modelling evaluation.

The F-factors calculated are considered to be simple comparative estimates of the hydrodynamic resistance characterising typical flow paths in each sub-compartment, and should not be taken to be realistic F-factors for safety assessment purposes. There are, for example, good reasons to specify different hydraulic gradients within different model sub-compartments, which could mean as much as order of magnitude variations in the calculated F-factors.

The central best estimate F-factor for typical flow paths in the NNF is roughly 10^5 y/m, although values could range from as little as 10^3 y/m to as much as 10^7 y/m. These estimates, however, are dependent upon different assumptions of path length, hydraulic gradient, and fracture transmissivity, which in turn are highly constrained by the, as yet, largely undetermined repository layout and acceptance/rejection criteria for individual canister holes. Therefore, values discussed here should be considered as speculative, "what if" type calculations rather than prognostic F-factors for an actual repository.

On the basis of the flow calculations presented in /Crawford (ed) 2008/, the dominant hydrodynamic transport resistance is found to reside in the fracture domains, principally FFM01, where the hypothetical repository is assumed to be situated in the case that the Forsmark site is selected. Stochastic realisations of the hydrogeological DFN model within a hypothetical cubic simulation volume of side length 100 m indicate that the probability of forming hydraulic connections over such length scales is very low. Figure 10-8 shows the probability of existence of at least one hydraulically connected structure spanning the modelled domain for 1,000 stochastic realisations of the hydrogeological DFN model.

The calculations made using the hydrogeological DFN model clearly illustrate the sparsity of flowing features at depths below 400 m within FFM01 and very few flowing features are expected to be found within the repository rock volume at this depth. However, those conductive features that do exist are likely to be in the form of single, large structures or small numbers of intermediately-sized, linked structures rather than pervasive clusters of small fractures. Although flowing features appear to be uncommon, F-factors on the order of about 10^6 y/m are calculated for typical conductive structures found within this rock volume.

The scoping calculations detailed in /Crawford (ed) 2008/ indicate advective transport times for the composite transport paths from a hypothetical repository to the near surface of less than about 10 y, with the bulk of the advective travel time being accumulated in the deterministic deformation zones. These are expected to have a substantially larger kinematic porosity than fracture domain FFM01 and are therefore found to dominate the advective transport times in the simplified scoping analyses.

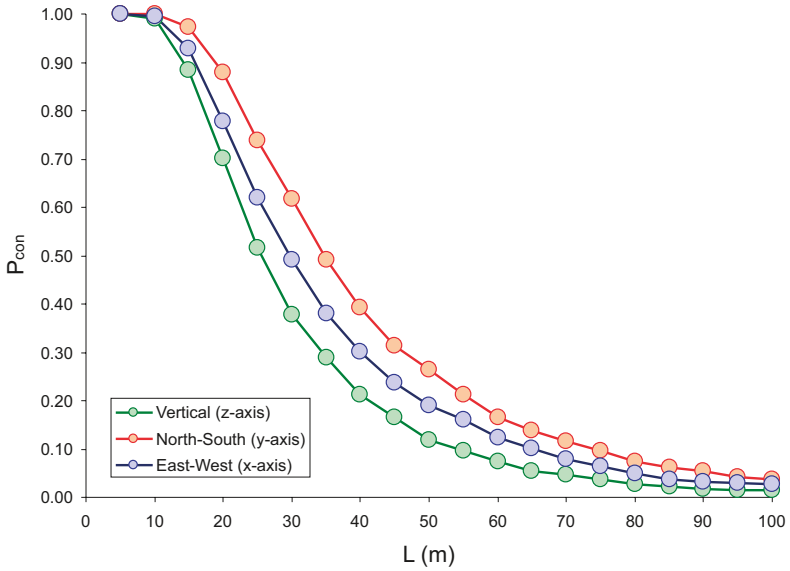

Figure 10-8. *Results of connectivity analysis for FFM01 at depths larger than 400 m based upon 1,000 stochastic realisations of the hydrogeological DFN model. The percolation probability is plotted as a function of distance for the three principal axes of the model (The percolation threshold is stochastically defined as the point where the percolation probability is 50%).*

Based upon the hydrogeological description presented in /Follin et al. 2007b/, a simple analytical estimate has been made for the F-factor of typical flow paths found within the deterministic deformation zones. For radionuclide release at a depth of 450 m within the deformation zone and a hydraulic gradient of 1%, typical F-factors for transport to the near surface (–100 m) are estimated to be about 10^3 y/m for gently dipping deformation zones and as much as 10^5 y/m for the steeply dipping zones.

For transport from a hypothetical repository to the near surface and considering the hydrodynamic transport resistance accumulated in each sub-compartment, an overall F-factor on the order of 10^6 y/m seems entirely reasonable. This is well in line with previous estimates from earlier model versions, e.g. /SKB 2004/ and previous safety analyses, e.g. /SKB 1999, SKB 2005b, SKB 2006b/.

It is noted that the F-factor of the NNF could be significantly greater than the scoping calculations suggest if less pessimistic values for the unknown properties of these initial pathways were used. Indeed, particle tracking calculations performed in conjunction with ECPM simulations of the regional hydraulic model using ConnectFlow indicate that a large proportion of the rock volume is possibly so poorly conductive that the spatially averaged permeability tensor for the rock is effectively the same as the rock matrix permeability.

Some typical ECPM particle tracking results for solute release within the target volume at 450 m depth are shown in Figure 10-9.

As already discussed in section 8.7.2, the trajectories of particles tracked from release locations between 450 m and 500 m depth, tend to fall into two different categories. One set appears to follow relatively short migration paths with a partially inclined, upward trajectory through the hydraulic rock domains, initially encountering deterministic deformation zones and finally sheet joint features. After encountering the near surface sheet joints, these particles migrate in a predominantly north-east arc and are discharged in the vicinity of the Singö deformation zone. Other particles follow a more circuitous route involving an initially downwards path before discharging eastwards within the Baltic Sea. The latter group of particles tend to be associated with substantially longer transport paths with larger F-factors and advective transport times. For safety assessment purposes, the particles belonging to the former group may be more significant since they are characterised by shorter, more direct transport paths to the surface and generally have smaller F-factors and advective transport times.

The single particle track illustrated in Figure 8-60 (chapter 8) is a typical example of one of the shorter transport paths taken from the hypothetical release area. The particle illustrated (#228) has a path-integrated F-factor that is representative of the lower 10% of the ensemble distribution

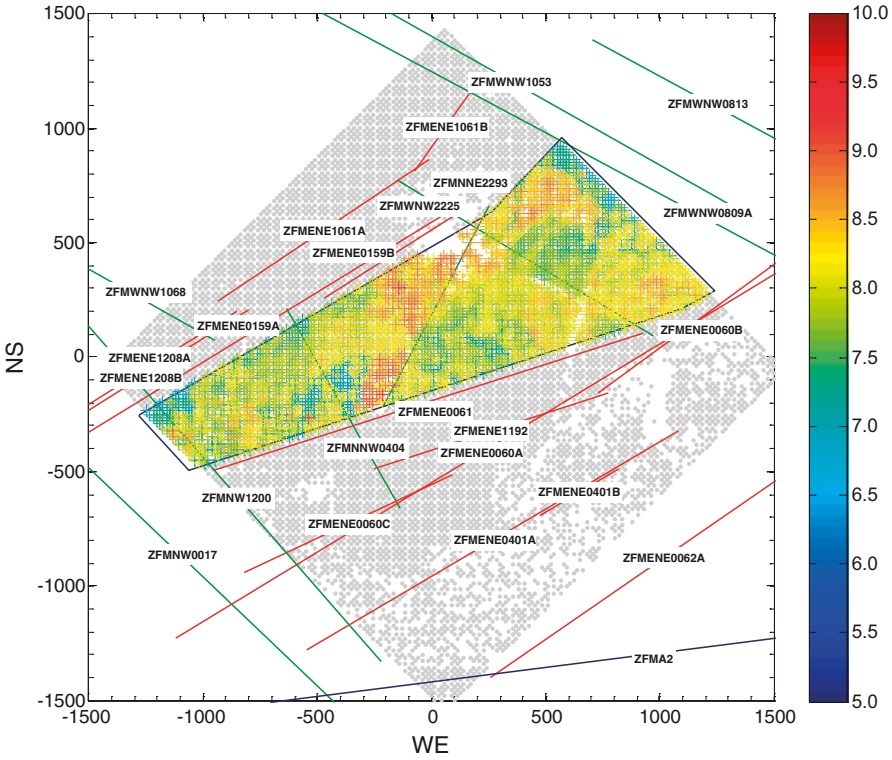

Figure 10-9. *Visualisation of a subset of particle release locations at 450 m depth within the target volume coloured according to cumulative F-factor (y/m) at exit location (log_{10} colour indexing). Some of the more prominent deformation zones transecting the hypothetical repository are indicated. The grey pixels correspond to the total set of particle release locations considered in the particle tracking calculations.*

of transport paths for the first group of particles that discharge near the Singö deformation zone (i.e. 90% of the particles discharging near the Singö zone are associated with larger F-factors and advective travel times). Figure 10-10 shows the integrated value of the F-factor plotted against the transport path length, with the different structural elements encountered by the particle colour coded and labelled.

In the case of the particle track illustrated in Figure 10-10, most of the hydrodynamic transport resistance appears to be encountered in the first 80 or so metres of the release location. This corresponds to the target volume within fracture domain FFM01 where the flow rates are exceptionally low. The F-factor accumulated in this region is, however, larger than that predicted using the simpler scoping calculations described previously. This appears to be largely due to a higher specific flow-wetted surface employed in the ECPM calculations as compared to that implicit in the single path calculations which employ the hydrogeological DFN model directly. It should be noted, however, that the conductivity of the rock over the first 80 m of this transport path appears to be so low as to be indistinguishable from the conductivity cut-off of the rock matrix as defined in the simulation. The first 80 m of this particular particle track therefore may not be entirely physically meaningful since it could represent advective transport through the rock matrix itself. If the results are interpreted in this fashion, analysis of the ensemble of particle tracks indicates that roughly 97% of the particles released may be considered to be fully encapsulated within the rock matrix or released in locally conductive, although hydraulically isolated regions of the rock.

The specific flow-wetted surface used in the ECPM calculations is plotted in Figure 10-11. This figure shows that the specific flow-wetted surface is on the order of 3–15 times larger than that estimated on the basis of Terzaghi corrected PFL flow frequencies measured within the investigation boreholes. This should give about an order of magnitude overestimate for the path-length integrated F-factor within the hypothetical repository rock volume. This is roughly the same as the discrepancy between the simulation results and the scoping calculations. Based upon PFL statistics, the best estimate, specific flow-wetted surface is roughly 0.008 m^2/m^3 for FFM01 at repository depth.

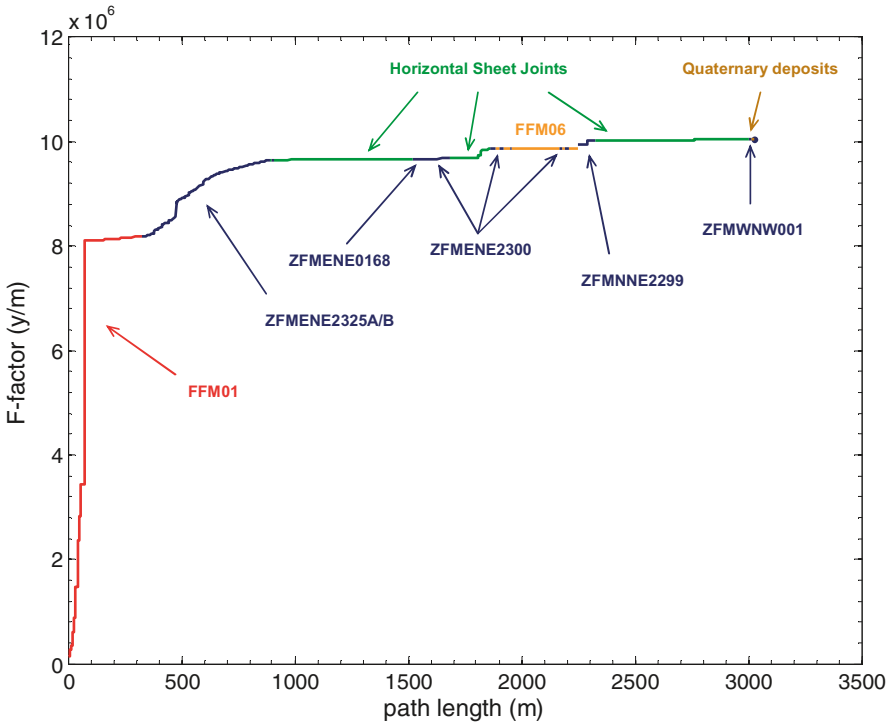

Figure 10-10. *Cumulative F-factor as a function of migration path length for an individual particle (#228) characteristic of the lower 10% percentile of "fast" transport paths discharging near the Singö deformation zone. Different structural elements encountered by the particle along its migration path are labelled in the figure.*

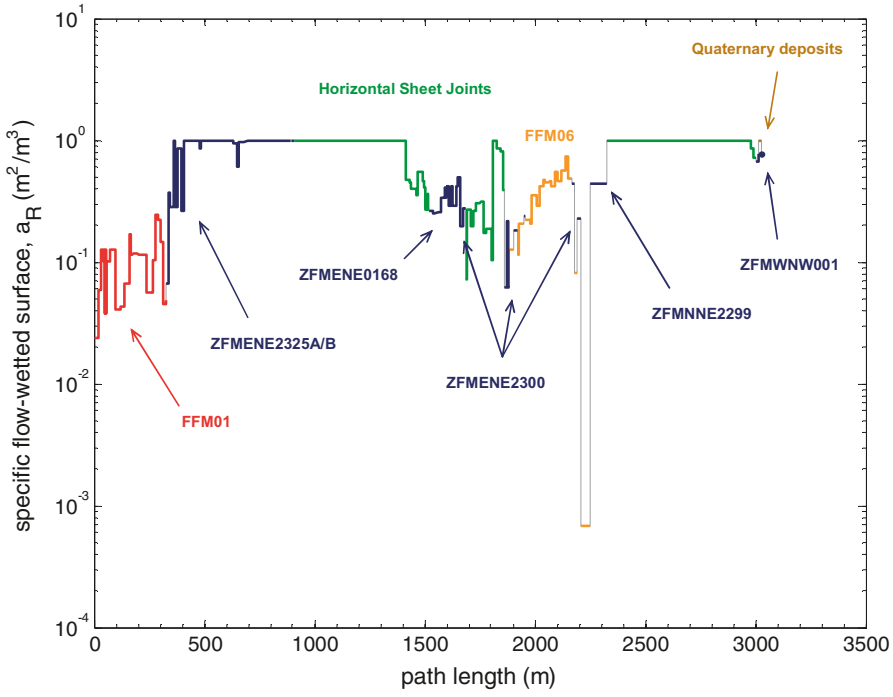

Figure 10-11. *Local specific flow-wetted surface, a_R (m^2/m^3) encountered by particle #228 as a function of migration path length. It should be noted that the value of a_R used in the calculation for fracture domain FFM01 at repository depth is larger than that calculated on the basis of PFL statistics for this volume. Different structural elements encountered by the particle are colour-coded as in Figure 10-10.*

Generally, the ECPM simulations indicate a more prominent role for the hydrodynamic resistance of deterministic deformation zones than predicted by the scoping calculations (i.e. the ECPM model predicts relatively larger F-factors for the deformation zones). In the particular case visualised here, this is mostly with regard to transport in deformation zone ZFMENE2325A and ZFMENE2325B and is largely due to a higher specific flow-wetted surface and a lower hydraulic gradient in these zones in comparison to the assumed values upon which the scoping calculations were based.

The cumulative advective transport time calculated for the particle in the ECPM transport simulations is given in Figure 10-12 as a function of migration path length.

The ECPM simulations indicate substantially longer advective transport times than calculated in scoping calculations based upon consideration of average flowpath transmissivities and simple relations typically used to correlate transport aperture and fracture transmissivity (these are detailed in /Crawford (ed) 2008/). Of particular interest is the prediction of advective travel times on the order of 4,000 y in the near surface sheet joints (coloured green in Figure 10-12). This is largely due to the high kinematic porosity used in the ECPM simulations.

The local equivalent transport aperture (m) is given by the ratio of kinematic porosity and specific flow-wetted surface ($\overline{\delta}_t \approx \theta_f / a_R$) and is shown in Figure 10-13 as a function of the migration path length. Since flow is conceptualised to occur within discrete fractures rather than in a true porous medium, this gives a more physically meaningful measure of the advective pore space volume.

As can be seen from Figure 10-13, the transport aperture is relatively high in the ECPM simulations, amounting to an average of about 1 mm within FFM01 (red) and several mm to cm within the deterministic deformation zones (dark blue). The average transport aperture encountered in the near surface sheet joints (green) is slightly less than a dm.

It is noted that the large values of specific flow-wetted surface and kinematic porosity (here, shown in terms of transport aperture) result from the calibration for matching of salt concentration profiles and are not appropriate for safety assessment modelling of radionuclide transport. The reasons for the larger values of specific flow-wetted surface and kinematic porosity in the ConnectFlow hydrochemistry simulations are discussed in detail in /Follin et al. 2008a/. Further discussion of the particle tracking results is also provided in /Crawford (ed) 2008/.

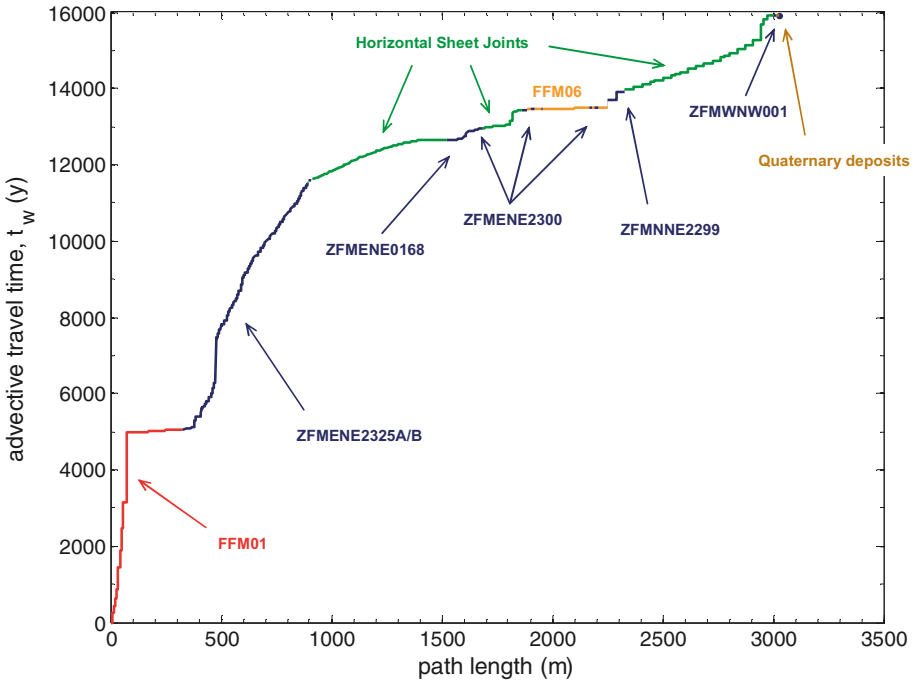

Figure 10-12. *Cumulative advective transport time as a function of migration path length. Different structural elements encountered by the particle are colour-coded as in as in Figure 10-10.*

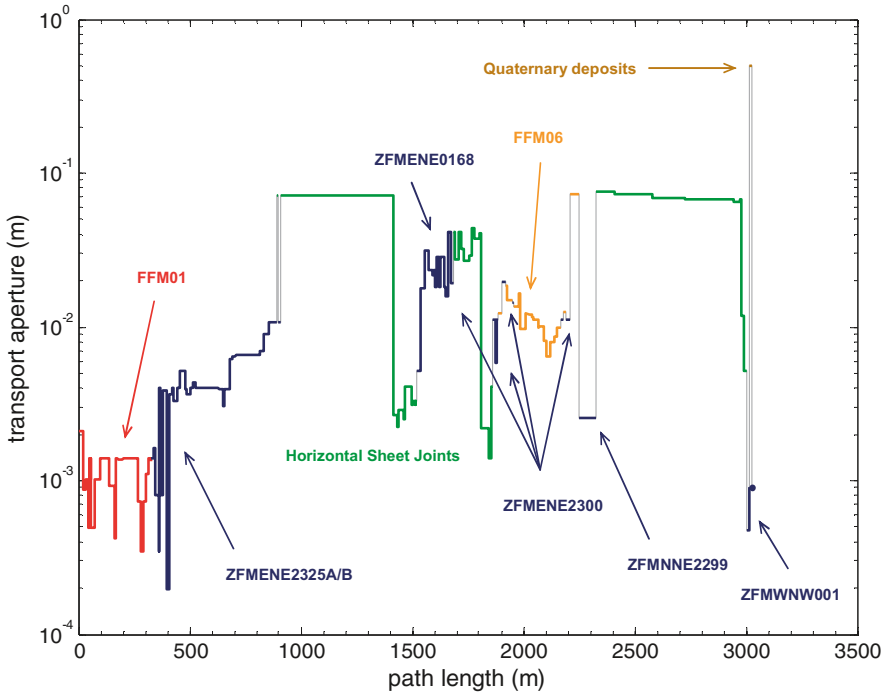

Figure 10-13. *Local effective transport aperture (ratio of kinematic porosity and specific flow-wetted surface) as a function of migration path length. Different structural elements encountered by the particle are colour-coded as in Figure 10-10.*

10.5.3 Flow channelling

A number of different forms of flow channelling have been considered both in the evaluation of typical F-factors for flow paths from the repository and the consequences for radionuclide migration when propagated forward in the transport models. These are discussed in detail in /Crawford (ed) 2008/ although a short summary of some of the main issues is given below.

One main type of flow channelling considered occurs on the scale of the fracture network itself and arises due to the tendency of heterogeneous fracture networks to exhibit poor hydraulic connectivity and form preferential flow paths. This type of flow channelling is particularly intense within the target volume owing to the very low intensity of open, connected fractures and is internalised in the description of the hydrogeological DFN.

Other types of flow channelling occur on much smaller spatial scales and are not explicitly incorporated in the models supplied by hydrogeology. These additional flow channelling effects are of some importance since they could potentially give rise to flow censoring effects in borehole investigations and lead to biases in the synthesis of hydrogeological DFN models. Specifically there are two issues; 1) flowing channels may be completely missed owing to their limited width and the low probability of a direct borehole intersection, and 2) those flowing features that are identified indirectly may appear to support lower flow rates than in actuality owing to the low permeability of structures in which they are hosted.

The most common type of small-scale flow channelling phenomenon, referred to here as “in-plane” flow channelling, relates to the tendency for preferential flow paths to form within variable aperture fractures where *in situ* normal stresses result in partial closure due to surface asperity contacts. Scoping calculations detailed in /Crawford (ed) 2008/ indicate that such flow channels should be sufficiently well-connected hydraulically throughout the pore space of fractures that, for the most part, they will be readily identified from investigatory boreholes without significant censoring effects.

This prediction is based upon consideration of the fact that fracture transmissivity appears to decrease strongly with increasing surface contact fractions up to the percolation limit, which occurs at a contact area fraction of about 50%. For highly compressed fractures approaching the percolation

threshold, the maximum censoring effect would amount to an underestimation of the flow channel frequency of about 50% if the probability of a borehole randomly intersecting a physically closed section of the fracture is considered. It is noted, however, that such fractures are also the least likely to support flows above the detection limit owing to their high state of compression. For less compressed fractures, which are also more likely to exhibit non-negligible flows, the censoring effect is expected to be substantially less.

Generalised radial flow analysis of PSS hydraulic responses in packed off borehole sections suggest that most flowing features (70–80%) are associated with flow dimensions greater than 1.5, although a significant fraction (on the order of 20–30%) exhibit smaller flow dimensions symptomatic of approximately linear flow channelling /Follin et al. 2006/. Although it is likely that some flow channels are missed, this result is generally consistent with the notion of a hydraulically well-connected flow space within fractures. The scoping calculations indicate that this should be the case even for fractures subjected to very high normal stresses resulting in substantial fracture asperity contact areas, although such fractures will also generally be associated with low transmissivities and perhaps below the limit of detection. Furthermore, in the transient analysis of constant head injection tests reported by /Hjerne et al. 2008/, only a very small proportion of tested sections give indications of constant head boundary characteristics. Since such behaviour would be suggestive of strongly transmissive flow channels hosted in otherwise poorly transmissive features, it is possible to conclude that "type 2" flow censoring effects, as described above, are not evident in the available hydrogeological data set.

Certain categories of pipe-like flow channels, such as those hosted within fault stepovers, shears and fracture jogs, may be less likely to be observed directly by an investigatory borehole given their limited physical dimensions. Similarly, fast flow channels possibly hosted at fracture intersections enlarged by tectonic and hydrothermal weathering would most likely not be directly intersected by investigatory boreholes. The probability of detecting such features is then largely dependant upon the permeability of surrounding fractures with which they are hydraulically connected.

Since such pipe-like flow channels are of finite length and hosted as sub-structures within fractures, they generally cannot form contiguous flow paths through the fracture domains. Such features therefore need to be relatively well connected to the wider fracture network via in-plane flow channels hosted in single fractures in order for flow to occur. Although "exotic" flow channelling effects cannot strictly be ruled out, such as karstic erosion pipes within otherwise annealed fractures, it is proposed that most flowing features should be identifiable from borehole investigations even if not directly intersected by investigatory boreholes (provided the pore space in the fractures is not excessively filled with fracture filling materials which would give rise to a flow censoring effect).

Based upon this reasoning, it is speculated that network-scale flow channelling effects probably dominate and there may not be significant censoring of the statistics of flowing features measured in boreholes. However, full resolution of this issue will not be possible until the construction of an underground tunnel since many aspects of flow channelling cannot be properly quantified from a surface based site investigation. It is not really possible, for example, to fully account for the impact of compact aggregations of fracture filling materials, which may promote pipe-like flow channelling in variable aperture fractures. Such flow channels would be similar to karstic erosion pipes in that they may not be readily detectible from surface-based investigatory boreholes.

Nevertheless, it is possible to approximately calculate the likely spatial distribution of different kinds of specific flow channel features from the geological information used in construction of DFN models. Scoping calculations of the possible existence of highly conductive fracture intersections, for example, have been made using the hydrogeological DFN model and are reported in /Crawford (ed) 2008/. In a forward modelling perspective, it is found that such features should not have a significant detrimental impact on transport properties, provided they do not form a contiguous (i.e. unbroken) flow path through the rock. On balance it is thought that flow channelling effects will make little difference to the order of magnitude of the hydrodynamic transport resistance, provided that there is reasonable confidence in the transmissivity model for hydrologic features parameterised within the hydrogeological DFN model.

The consequences of flow channelling phenomena have also been considered within a forward modelling perspective for the transport of solutes. Several model alternatives based upon the assumption of narrow flow channels are discussed in the following section.

10.6 Transport of radionuclides

Coupling of the F-factor estimates from the hydrogeological modelling with the retardation model allows for the prediction of typical transport times for key radionuclides. The transport models described in this section consider advectively dominated flow and transport along a single flow path with diffusion and sorption within the rock matrix. Here, a flow path is considered to be a simple set of serially connected flow channels which may be narrow in width (on the order of cm to some tens of cm). In a full hydrogeological simulation of the transport problem as would be used in safety assessment, however, flow paths would be expected to bifurcate and join with other flow paths over different length scales giving rise to a distribution of F-factors and advective transport times. Such calculations are more of a safety assessment character and are not treated here (although it is noted that the distribution of different flow paths is obtained automatically from simulations of the full hydrogeological model as would be implemented in safety assessment). A full account of the transport modelling scoping calculations is provided in /Crawford (ed) 2008/.

If flow channels are narrow as expected, the one-dimensional description of matrix diffusion customarily used in safety assessment calculations is inaccurate and may underestimate radionuclide retardation. For this reason, three main scenarios are considered for radionuclide transport in Forsmark SDM-Site. These are:

1. (Base model) Advective flow coupled with 1D diffusion/sorption within the rock matrix.
2. (Model Alternative 1) Advective flow in a narrow channel coupled with 1D diffusion/sorption in the rock matrix plus diffusion into a stagnant zone of limited extent and subsequent 1D diffusion/sorption within the rock matrix.
3. (Model Alternative 2) Advective flow in a narrow channel coupled with 2D radial diffusion/sorption in the rock matrix.

Along channelised flow paths hosted within fractured rock there may be “in-plane” stagnant zones as well as large numbers of open, although non-flowing, fractures which intersect the flow path. It is possible for transported radionuclides to diffuse into these regions and access additional surface area for mass transfer to the rock matrix. This is referred to as diffusion accessible surface area. To avoid the possibility of double counting of matrix storage capacities and to improve modelling transparency, only in-plane diffusion accessible surface is considered in the present analysis. In the scoping calculations for model alternative 1, a flow channel width of 10 cm is assumed with a stagnant zone 1 m in extent within the plane of the fracture along one side of the flow path (forthwith referred to as a 10:1 in-plane stagnant zone).

For model alternative 2, a channel width of 10 cm is considered without stagnant zones. In this case, the diffusion front of solute migrating in the rock matrix will start to take on a noticeably radial character after it has diffused a distance into the rock matrix roughly comparable to the channel width. The 2D, radial diffusion of solute results in a substantially enhanced rate of diffusive uptake compared to that which would be predicted on the basis of the base case model incorporating 1D diffusion. The basic features of the base case model and both model alternatives are illustrated in Figure 10-14.

For the assumed hydraulic properties used in the estimation of the flow-related transport properties, the flow paths within the fracture domains appear to overwhelmingly dominate the aggregate F-factor for transport. For these reasons, the assumption is made that the transport model can be parameterised using data applicable for fractures and minor deformation zones found within FFM01 (below 400 m depth). It is likely that this simplification is conservative, since the increased hydrogeological and micro-structural complexity found within deterministic deformation zones should, on balance, give rise to substantially greater retardation properties if fully considered in the analysis.

Using the site-specific data for fractures within fracture domain FFM01 implies a rock matrix microstructure featuring an alteration zone with material properties that do not differ significantly from the unaltered rock matrix. Most fracture types are also associated with thin coatings of secondary minerals that have enhanced sorption properties as compared with the unaltered rock matrix. Although diffusivity data for fracture coatings are not available, they are sufficiently thin that they will not have a large impact upon the diffusive properties of the rock for F-factors characteristic of safety assessment conditions. Further discussion of this can be found in /Crawford (ed) 2008/.

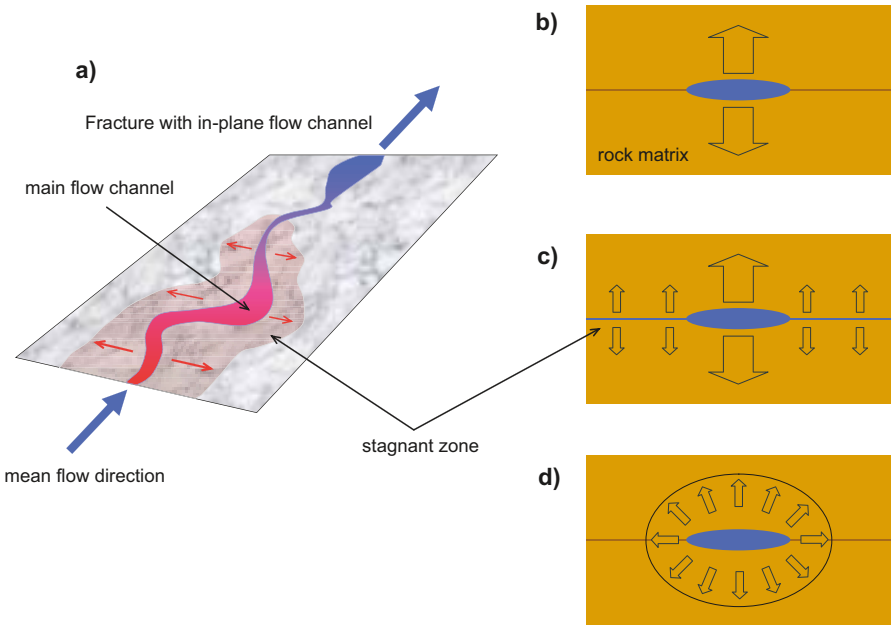

Figure 10-14. *Schematic view (a) of a fracture hosting an in-plane flow channel of limited width with possible stagnant zones flanking the main flow channel. On the right hand side of the figure is a conceptual illustration of the diffusive mass transfer process corresponding to the base model (b), model alternative 1 (c), and model alternative 2 (d).*

Figure 10-15 shows an example of typical residence times calculated for the different transport models assuming saline groundwater chemistry, a flow path F-factor of 10^6 y/m, and a solute recovery fraction of 1% (i.e. the transport time for the first 1% of arriving solute). Here, a rock matrix formation factor $F_f \approx 1.6 \cdot 10^{-5}$ is assumed, which is typical of the main rock type 101057, and the impact of sorption K_d value on the radionuclide transport time is calculated. Approximate illustrative time limits for quantitative and qualitative safety assessment (based upon guidelines in /SSI 2005/) are shown as the red broken and unbroken lines in the figure. Transport times longer than 10^7 y (graduated, background shading) are considered to be of academic interest only and are included here to illustrate the relative scaling of recovery times implied by the modelled retardation processes. In addition, to give an appreciation of the time scales involved, some significant events in Earth's geological history are indicated on the time axis.

To illustrate the combined impact of K_d uncertainty and fundamental modelling assumptions for specific solutes, the span of transport times vs. K_d is plotted as a rectangular polygon in the figures. The lower left hand vertex of each polygon is the transport time of the model giving the fastest breakthrough using the lowest reported K_d value, whereas the upper right hand vertex corresponds to the transport time of the model giving the slowest breakthrough time for the maximum reported K_d value. It should be noted that the results presented in Figure 10-15 assume constant groundwater conditions which will not necessarily be the case, particularly over the very long time spans indicated. Since the K_d for specific solutes is often sensitive to changes in groundwater composition, the estimated transport times shown here should be regarded as merely illustrative.

Provided the groundwater composition is relatively constant, the estimated transport times for the strongly sorbing trivalent Lanthanide-Actinide solutes (e.g. $K_d > 0.1$ m^3/kg) are so long that the solutes could be considered, for all practical purposes, immobile. In such cases, colloid and possibly bacterial siderophore[1] transport mechanisms may dominate the release to the biosphere. For groundwater colloids, this will be particularly the case if sorption is deemed to be irreversible. In the case

[1] Bacterial siderophores are strong complexing substances released by certain bacteria, usually under oxidising conditions (i.e. when Fe(III) availability is low) by those bacteria that use the Fe(II/III) redox couple as an oxidant. These complexing agents can also bind certain radionuclides very strongly resulting in reduced apparent sorption on geological materials.

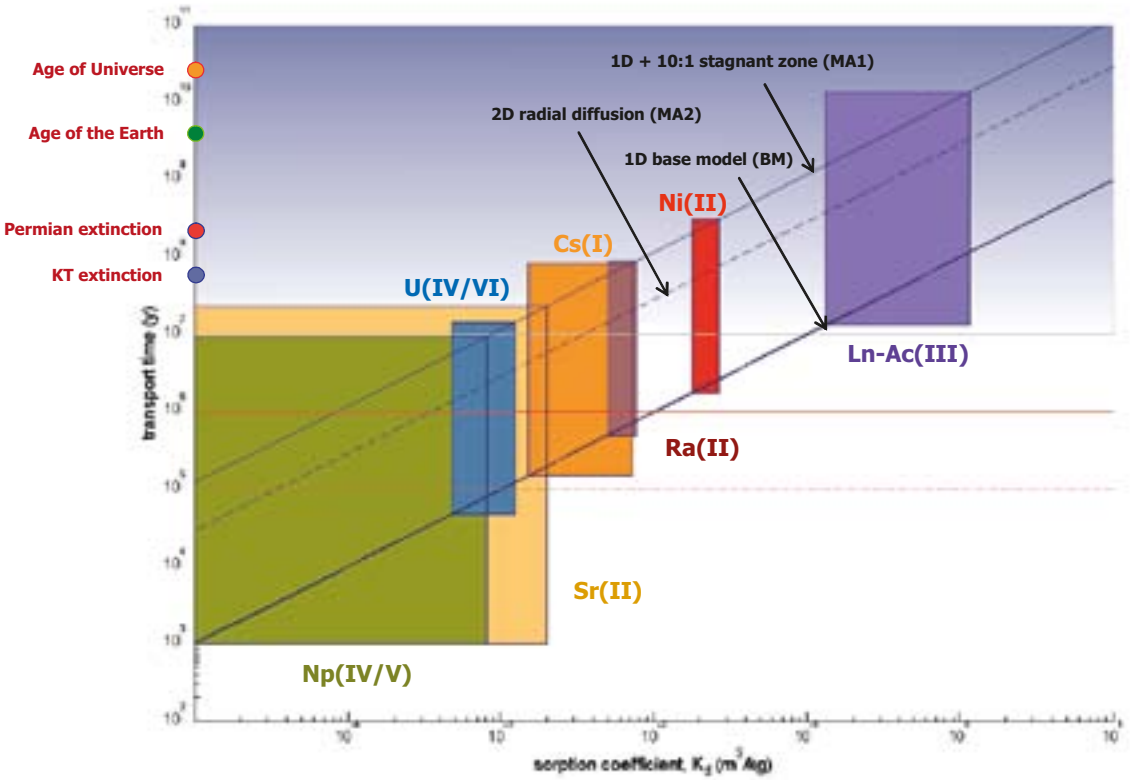

Figure 10-15. *Typical radionuclide transport times (blue curves) as a function of sorption K_d for a recovery fraction of 1%, an F-factor of 10^6 y/m, formation factor of $1.6 \cdot 10^{-5}$, and a maximum rock matrix depth of 2 m. Shaded polygons represent approximate range of variability for individual nuclides under saline conditions (see text for explanation).*

of reversible sorption, however, scoping calculations presented in /Crawford (ed) 2008/ indicate a negligible effect upon radionuclide transport for the natural colloid concentrations found in groundwater at repository depth. The status of sorption reversibility for key radionuclides on groundwater colloids is not conclusively established at present, although recent studies of Eu(III) sorption on clay minerals /Rabung et al. 2005/ suggest that the sorption of strongly sorbing Ln-Ac(III) solutes is most likely to be reversible under normal groundwater conditions.

Bacteria capable of excreting siderophores have been cultivated from deep groundwater samples obtained at the Äspö HRL /Johnsson et al. 2006/, although it is not currently known whether there is a non-negligible background concentration of these complexing agents within the groundwater from repository depth at the Forsmark site (owing to the difficulty of directly identifying these by routine chemical analysis). However, given that reducing conditions normally prevail at these depths, it is not thought that siderophores should be present in sufficient concentrations to detrimentally impact radionuclide sorption. Investigations at the Äspö HRL have confirmed that these substances are not present in the reducing groundwaters found at repository depth /Essén et al. 2007/.

The transport simulation results indicate a large spread in transport times for specific solutes with differing sorption properties. As expected from previous investigations (e.g. /Neretnieks and Moreno 2003/), the water residence time is very small compared with the retarded radionuclide residence time and therefore can be neglected for the radionuclide transport mechanisms considered here.

The range of variability of measured K_d values for specific solutes is about 1–2 orders of magnitude. Some solutes such as Ra(II) and Ni(II) have reduced ranges of apparent variability due to the lower number of samples. Other solutes such as Sr(II) have poorly constrained lower K_d bounds owing to their generally weak sorption and relatively high measurement limits. Np and U are a special case owing to their sensitivity to redox conditions and the possibility that fully reducing conditions may

not have been achieved in the laboratory. It is noted that the lower measured bounds for the sorption of U and Np may be biased by the presence of mobile, oxidised forms which may not always exist under repository conditions at depth.

It is noted that uncertainty concerning individual material property parameters (i.e. K_d and D_e) are propagated linearly, with the uncertainty in predicted transport time being proportional to the uncertainty in these parameters. Since the transport time is approximately proportional to the square of the F-factor, on the other hand, the same relative level of uncertainty in this parameter has a substantially larger impact on predicted transport times. If the F-factor, for example, is reduced by a factor of 10 the transport time decreases roughly by a factor of 100.

Additional variability in estimated transport times follows if further consideration is given to the different assumptions made during transport modelling. The three different models described above represent hypothetical consequences of different modelling assumptions. It is not known whether the assumption of a 10:1 in-plane stagnant zone in model alternative 1 is a reasonable estimate of the average stagnant zone width potentially existing along typical flow paths within the rock. If the assumption is correct, this would give transport times increased by about two orders of magnitude compared with the base case scenario lacking stagnant zones.

The radial diffusion model (model alternative 2) gives substantially increased residence times compared with the base model for recovery fractions in excess of about 0.01%. However, it is important to note that due to the much longer transport times associated with model alternative 1 and 2, careful consideration of penetration depths must be made, particularly for the radial diffusion case. In these cases, the transport times are sufficiently long that saturation to the arbitrarily assumed matrix depth of 2 m is achieved at relatively low recovery fractions in the residence time distribution curve.

A detailed account of the modelling and additional results for marine, brine, and fresh water end-members are provided in the background report /Crawford (ed) 2008/.

10.7 Field-scale confirmatory testing of transport properties

An important element of the site descriptive modelling at Forsmark has been the integration of field-scale testing within the modelling work. These tests serve a multitude of functions for the different topic areas of interest. For transport properties site descriptive modelling, tracer tests are used to verify connectivity as well as to demonstrate retention of transported solutes. This section gives a brief overview of the tracer tests that have been performed within the Forsmark site investigation, their main results, and consequences for safety assessment. Here, the focus is upon the tracer tests that have most relevance for the transport properties site descriptive modelling. These consist of multiple well tracer tests and a series of single well injection withdrawal tests (SWIW). Results of tracer dilution tests are not discussed in this section, but they are discussed in the background report /Crawford (ed) 2008/ in connection with flow related transport properties modelling.

10.7.1 Multiple well tracer tests

The first test took the form of a large-scale pumping test with non-sorbing tracer release from packed off sections in three boreholes in an approximately radially converging flow configuration /Wass and Andersson 2006/. Only the very leading edge of the tracer breakthrough curve was obtained before termination of pumping. Therefore these results are of only minor interest for transport properties modelling.

The second tracer test was made in a two-well, weak (1:100) dipole configuration over a distance of about 46 m within zone ZFMA2 using a mix of both sorbing and non-sorbing tracers /Lindquist et al. 2008/. This tracer test was intended to partially validate the hydrogeological model over the Forsmark candidate area, but was also intended to test the transport characteristics of the rock for comparison with data obtained from the laboratory transport properties investigations using drill core material. Tracers used in the second test were Uranine, Li^+, Cs^+, and Rb^+, although a pre-test was also made using the non-sorbing tracer Rhodamine-WT.

10.7.2 Single well injection-withdrawal (SWIW) tests

A number of single well injection-withdrawal (SWIW) tests have been performed in various borehole locations during the site investigation at Forsmark. The tracer test is based upon the injection of a tracer cocktail over a short period of time, typically 1–2 hours, followed by a 10–20 hours chaser period during which only water is injected. The injection of chaser water has the effect of pushing the tracer out in a ring in the formation surrounding the tested section. After the end of the chaser phase, the flow is reversed and tracer recovered in the same borehole from which it was initially injected.

The technique is attractive for the purposes of the site investigation, since it can be used to perform tracer tests within transmissive structures found at repository depth in which it would be very difficult to perform standard dipole or multiple well tracer tests from the surface. An additional advantageous feature of the SWIW technique is that the reversal of flow during the experiment theoretically reduces the impact of advective dispersion and flow dimension upon the residence time distribution of recovered tracer, thereby potentially simplifying mechanistic interpretation.

In total, six SWIW tests have been performed at the Forsmark site in different types of structures, at different depths and transmissivity ranges with the aim of characterising the transport properties of a variety of flowing features typical of those that might be encountered in the vicinity of a repository. A summary of the individual tests is given in Table 10-20.

10.7.3 Evaluation of tracer test data, interpretation and consequences for safety assessment

In the evaluation of the different tracer tests it was generally found that an adequate fit of the overall peak shape and height could be obtained using a standard transport model based upon the advection-dispersion equation with linear sorption. Using the tracer recovery data, the longitudinal dispersivity and a linear retardation factor were estimated in a first round of inverse modelling using the SUTRA numerical simulation code /Voss and Provost 2002/. This approach, however, was found to consistently underestimate the long-term tailing of both the sorbing and non-sorbing tracers. The specification of a matrix diffusion/sorption term in a second round of modelling gave considerably better fits to the tailing portions of the breakthrough curves for both the dipole and SWIW tests. Although there was no strong evidence in the breakthrough data for tracer transport along multiple flow paths, this possibility cannot be ruled out as a contribution to the long-term tailing in the dipole test. The SWIW tests, however, are thought to be less influenced by this effect and so it is not considered to be an issue for the SWIW data interpretation.

Table 10-20. Summary of basic features of SWIW tests performed at the Forsmark site.

Borehole	Elevation (m)	T (m^2/s)	Type	Rock and fracture coating description
KFM02A	–407	$9.5 \cdot 10^{-7}$	DZ (1–3 flowing features)	101057 no fracture minerals slightly altered
KFM03A	–633	$2.5 \cdot 10^{-6}$	MDZ (3 flowing features)	101057 clay, hematite, chlorite, calcite strongly altered
KFM08A	–340	$1.0 \cdot 10^{-8}$	3 fractures	101057 chlorite, clay, calcite no visible alteration
KFM04A	–355	$8.9 \cdot 10^{-9}$	1–2 open fractures in a sealed network of a DZ	501061/101057 zeolites, calcite, chlorite, quartz no visible alteration
KFM01D	–300	$3.2 \cdot 10^{-7}$	1 fracture	101051 chlorite slightly altered
KFM01D	–342	$1.0 \cdot 10^{-6}$	1 fracture	101051 chlorite slightly altered

To all appearances, the data evaluation gives indications of a diffusion-mediated retardation process with signs of increased retention for sorbing solutes. This is in line with expectations based upon the mechanistic understanding of transport retardation processes.

From the fitted matrix interaction parameters derived in the extended data evaluation, it is possible to compare the "apparent" formation factor observed during the tracer tests with the best estimate value identified for the particular rock type in the laboratory investigations. Since the matrix interaction parameter is a lumped parameter that includes the combined effects of matrix diffusion and sorption, there is a need to additionally specify the porosity of the rock and sorption K_d (for the sorbing tracers) to estimate the apparent formation factor. This then gives an indication of the amount of mass transfer enhancement that is observed in a tracer experiment compared with that expected on the basis of independent measurements. The apparent mass-transfer enhancement factor is shown in Figure 10-16 for the various SWIW tracer tests performed. Since the SWIW tests are not associated with a well-defined observation scale, the results are plotted against the transmissivity of the tested section.

The results of this analysis indicate that there is an apparent enhancement of diffusive mass transfer to the immobile zone that is considerably larger than can be justified on the basis of uncertain laboratory derived measurement values. Even making allowances for very large increases in formation factors and sorption coefficients at the fracture surfaces, or in association with fault gouge material, cannot satisfactorily explain the degree of enhancement. This is qualitatively consistent with previous experience from the TRUE-1 project /Winberg et al. 2000/. An alternative explanation is that transport occurs within a complex fracture featuring substantially greater flow-wetted surface than the single fracture plane assumed in the simulations. However, the increase in flow-wetted surface required seems larger than what is realistic for the flow structures considered.

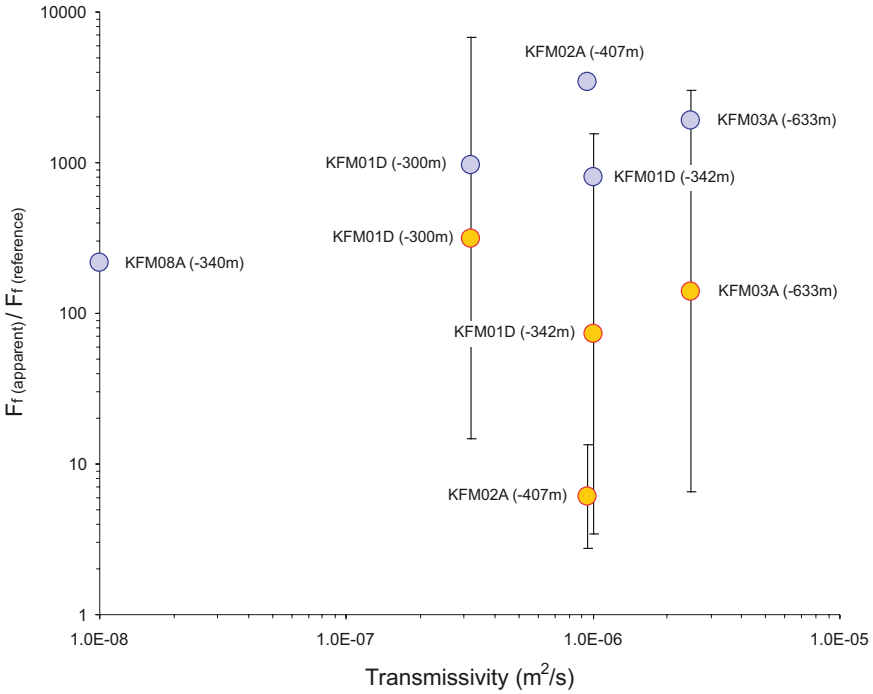

Figure 10-16. *Apparent diffusive mass transfer enhancement factors for SWIW tracer tests carried out at Forsmark plotted against transmissivity of the tested flow path (for a reference formation factor, $F_f = 1.6 \cdot 10^{-5}$). Data are shown for both Cs^+ (orange shaded symbols) and non-sorbing Uranine tracer (blue shaded symbols). The plotted data for Cs^+ are geometric means with error bars where min-max ranges of possible K_d values have been considered.*

An interesting feature of the interpretation shown in Figure 10-16 is that the diffusive mass transfer enhancement factor seems to be considerably larger for non-sorbing or very weakly sorbing tracers than for sorbing tracers. The difference is considerable and consistent across all tracer tests evaluated and cannot readily be explained in terms of uncertainty concerning the sorption K_d value used in the evaluation. Neither does it appear to be an artefact of increased flow-wetted surface, since this would be expected to affect both tracers roughly equally if both are deemed to encounter the same microstructural complexity along their migration path out into the rock formation (noting that the different distances travelled by the tracers within the formation is implicitly internalised in the modelling evaluation).

Superficially this would appear to be evidence for the existence of stagnant zones along the transport paths sampled in the tracer tests. It also suggests that tracers with differing sorptive properties probe different parts of the immobile zone with the mass transfer of non-sorbing tracers dominated by diffusion within apparently stagnant zones, whereas the mass transfer of sorbing tracers is dominated by mass transfer directly to the rock matrix (or fracture coating) along the flow-wetted surface of the advective flow path.

Although the results are consistent with the notion of effectively stagnant zones, further evaluation of the SWIW test data indicates that estimated flow channel widths required to explain the overall effect are physically unrealistic (sub-millimetre to millimetre scale). It is therefore speculated in the background report /Crawford (ed) 2008/ that a substantial component of the observed diffusive effect is non-Gaussian dispersion within flow channels featuring tapered apertures. This mode of dispersion is essentially a diffusion-mediated process (i.e. diffusion between streamlines across flow channel widths) and as such is indistinguishable from diffusion into an actual stagnant zone over short timescales. Both phenomena can be expected to give rise to tailing in the solute residence time distribution reminiscent of true matrix diffusion. Additional modelling work with more detailed consideration of hydrodynamic processes on the timescale of tracer tests may need to be done if the issue is deemed to warrant further resolution.

10.8 Evaluation of uncertainties

The key uncertainties in the transport properties site descriptive model can be divided into two main categories; a) uncertainties related to assessment of the hydrodynamic transport resistance, and b) uncertainties related to material properties parameters used in transport modelling. Based upon the outcome of the simulation studies using alternative transport models discussed in section 10.6, a third category could also be considered where the form of the transport model employed may have a large impact upon predictions made within safety assessment. However, since the model alternatives considering channelling effects seem to suggest a strongly positive impact on radionuclide transport retardation relative to the models commonly used in safety assessment studies, this is not considered to be a critical uncertainty in the same sense as a) and b).

With regard to the hydrodynamic transport resistance of the rock, the main uncertainty appears to be the properties of the network of small, less transmissive features that connect individual canister positions with major flow paths in the fracture domains. Since these are dependent upon additional considerations of repository design that are not strictly part of the site descriptive model, this uncertainty has been dealt with by means of generic scoping calculations of a “what if?” character in the transport properties evaluation.

Scoping calculations suggest that flow censoring effects arising due to the low probability of narrow flow channels being directly intersected by investigatory boreholes may not be a significant issue for the estimation of hydrodynamic resistance within the fracture domains. If correct, then the main uncertainties concerning the flow properties of the fracture domains are already covered by the corresponding discussion of uncertainties given in chapter 8 for the hydrogeological modelling. Generally, the stochastic hydrogeological DFN simulations suggest that flowing structures should occur relatively rarely within the hypothetical repository volume (i.e. FFM01 below 400 m depth) and when they do occur they have properties which are broadly consistent with what would be expected *a priori*, based upon the ranges of transmissivities of flowing features identified in the borehole investigations.

Owing to the highly heterogeneous nature of deformation zones, it is not possible to properly account for the possibility of pipe-like flow channels in these structures that may not be readily observed from a limited number of borehole intercepts. Since the bulk of the hydrodynamic transport resistance appears to occur within the fracture domains, however, this is considered to be a subsidiary uncertainty for the overall safety assessment of a repository.

F-factors calculated for transport of radionuclides along flow paths from a hypothetical repository to the near surface are very sensitive to the radionuclide release location relative to major flow paths as well as typical hydraulic gradients encountered within the repository rock volume. Larger-scale simulations made using ConnectFlow indicate that, if full credit is taken for these effects, average F-factors can be substantially increased compared with those estimated using scoping calculations incorporating more pessimistic assumptions. The scoping calculations, however, are intended to capture the transport properties of flow paths leading from sub-optimal locations and for this purpose the F-factors they predict are in reasonable agreement with the lower end of F-factor distributions estimated through particle tracking simulations made using ConnectFlow.

With regard to the material properties parameterisation of the rock, by far the largest uncertainty is associated with the sorption partitioning ratio, K_d, evaluated for the different radionuclides within the laboratory investigation. On the other hand, the porosity and effective diffusivity (or formation factor) of the rock matrix appear to be relatively well constrained for the main rock types. Although there is some evidence for *in situ* compression of pore spaces in the unaltered matrix rock, the effect upon material properties can be quantitatively bounded.

Based upon comparison of water resaturation porosity measurements with two independent methods described in /Waber and Smellie 2007/, the water resaturation porosities of unaltered rock matrix reported within the laboratory programme could be inflated by as much as 50% owing to stress relaxation during borehole core retrieval. However, the uncertainty introduced by this is relatively small and can be accounted for within safety assessment by accordingly adjusting the porosity used in calculations. For strongly altered rock types and rock close to fracture surfaces which may already be subject to stress release, the difference may not be as great.

For the formation factor of the rock, *in situ* compression of pore spaces and drilling induced mechanical damage appears to result in as much as an order of magnitude difference between the properties measured *in situ* and those obtained from laboratory measurements. Although some residual uncertainties exist concerning interpretation of the different measurement techniques, these appear to be relatively small and cannot account for the observed differences. The uncertainty introduced by the possible *in situ* compression of the pore space, while large, is empirically bounded and can also be handled by an appropriate choice of formation factor within safety assessment calculations. Once again this concerns the unaltered matrix rock and it can be expected that the diffusive properties of strongly altered rock types and rock in close proximity to fracture surfaces more closely correspond to the laboratory measured values.

For sorption partitioning ratios (K_d) it is important to firstly acknowledge that a major uncertainty concerns the use of empirically established measurement values to represent what is, in reality, a complex mechanistic process with strong dependency upon groundwater chemistry, sorptive surface area, and relative quantities of specific accessory minerals (e.g. biotite, chlorite, hematite). Although the largest uncertainty appears to be related to groundwater composition, there are differences between radionuclides which sorb by way of different mechanisms and some radionuclides are more sensitive than others to small changes in these different variables. For the ranges of groundwater compositions likely to be encountered by migrating radionuclides, however, it should be possible to choose appropriate K_d values for specific rock types which are capable of predicting radionuclide transport times of sufficient accuracy for use in safety assessment.

Uncertainties coupled to the laboratory measurement data for sorption relate to a number of issues regarding data interpretation and representativity of crushed rock samples for *in situ* conditions. One of the major uncertainties related to the use of crushed rock samples is the creation of additional surface area (principally external particle surfaces) for sorption. This is further complicated by the possible enrichment of more strongly sorbing mineral phases (e.g. biotite) in the smallest size fractions. Comparative measurements have indicated, however, that the larger size fractions on the order of a couple of mm sieve size have internal surface areas reasonably close to the values

obtained using monolithic borehole core samples and therefore can be assumed to be approximately representative of the *in situ* rock. For this reason, the sorption data reported from the laboratory programme for matrix rock samples are based upon the largest crushed size fraction (1–2 mm) and longest contact time (180 days) to minimise any effects related to diffusive disequilibrium. In spite of these precautions there are still indications from recent studies of Cs electromigration that even the 2 mm crushed size fraction may have a sorptive surface area greater than that of intact monoliths /André et al. 2006/ and therefore may give overestimates of the sorption K_d.

Additional uncertainties relate to possible alteration of the chemical composition of contacting water used in the sorption experiments owing to mineral weathering reactions as well as slow changes in the mineralogy of the crushed rock samples themselves. The difficulty in maintaining a well defined redox state in the contacting water, for example, was found to be a particular problem for the measurement of U and Np sorption. It is also uncertain which mechanism or mixture of mechanisms are responsible for the apparent time dependency frequently associated with solute uptake in the laboratory sorption measurements. This could be a result of slow weathering reactions as discussed above, diffusive processes, or possibly a combination of effects. It has been found, however, that the magnitude of the kinetic effect and its relation to particle size is not fully consistent with a purely diffusive uptake mechanism. It is therefore currently unclear whether the time dependency is an inherent characteristic, or an artefact and therefore not representative of *in situ* rock sorptive properties.

11 Current understanding of the site

This chapter presents an integrated description of the understanding of the Forsmark site at the completion of the surface-based site investigation programme. The description and understanding of this site are founded on a substantial amount of site-specific data, especially from the target volume, i.e. the north-western part of the candidate volume (Figure 11-1).

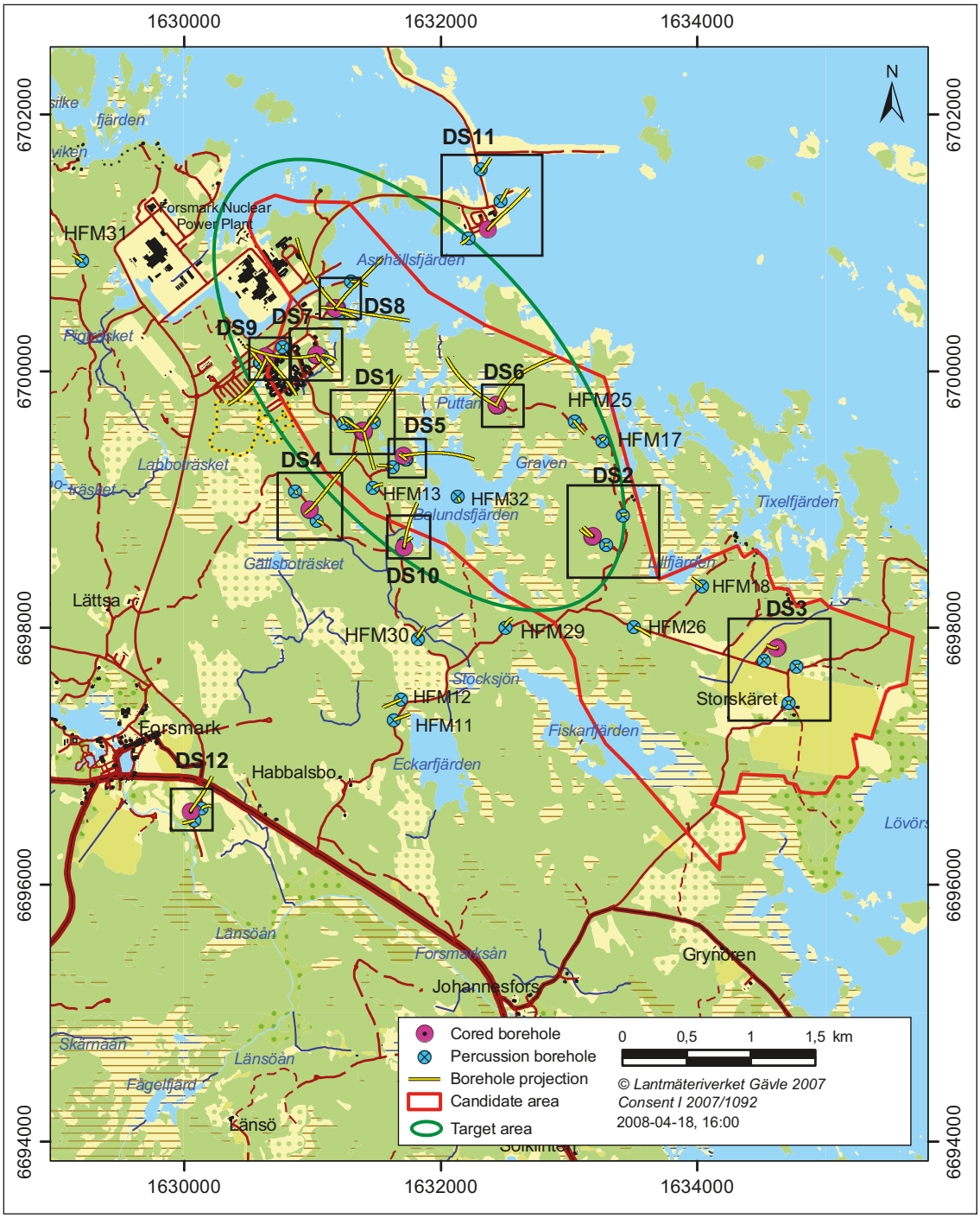

Figure 11-1. *The Forsmark candidate area with the target area in the north-western part (ringed in green) and the location of the drill sites.*

Surface investigations have included geological mapping and the compilation of bedrock and Quaternary cover geological maps as well as different ground and airborne geophysical investigations that have provided information for the identification and characterisation of deformation zones. Especially high resolution magnetics and surface based reflection seismics have provided key information on the bedrock structure at depth. A large number of surface ecological investigations have yielded data on both abiotic and biotic characteristics of the Forsmark area. In addition, a monitoring programme, still on-going, has provided time-series data for, for example, meteorological parameters and water levels in lakes and in the Baltic Sea.

Borehole data in support of the Forsmark site description come from 25 core-drilled boreholes ranging in depth down to c. 1,000 m and having a total borehole length of c. 17,800 m. The database also contains results from investigations in 38 percussion-drilled boreholes, with a total borehole length of c. 6,500 m, and more than 100 monitoring boreholes in the Quaternary cover, so-called soil wells. In addition to results from standardised borehole measurements in cored and percussion holes, such as borehole logging and core logging, investigations in these boreholes have provided information from, for example, *in situ* formation factor logging, groundwater flow measurements, cross-hole interference tests and investigations of rock matrix porewater. Overcoring stress measurements, hydraulic fracturing data, hydraulic tests on pre-existing fractures and studies of borehole breakouts and other types of fallout structures from the borehole wall have been acquired in several of the boreholes. Furthermore, data from several types of laboratory investigations carried out on samples of intact rock material from these boreholes are included in the database. The monitoring soil wells have provided time-series data on groundwater levels and water chemistry, as well as information on the stratigraphy of the Quaternary deposits in the area. Time-series data have been acquired also in the bedrock by means of multi-packers in the cored and percussion holes.

11.1 Surface system

The description of the surface system is in itself multi-disciplinary, in that it relies on an integrated understanding of meteorology, hydrology, oceanography, hydrochemistry, Quaternary geology and ecosystems in the Forsmark area. The derived integrated understanding of the surface system is described in detail in the report on the surface system /Lindborg (ed) 2008/, which is one of the reports supporting this site description. Here, only a brief summary of the surface description is provided, with a focus on aspects of common importance for the surface and bedrock systems.

11.1.1 Evolution during the Quaternary period

The character of the current surface system has been strongly influenced by the climate evolution during the Quaternary period. The Quaternary climate is characterised by large and sometimes rapid changes in global temperature, and the Forsmark area has been covered by glacier ice at least three times. Preserved information older than the latest glacial phase is rare in Sweden in general, hence the duration and extent of early Quaternary glaciations is poorly known. The latest glaciation, the Weichselian, started c. 115,000 years ago and is subdivided into three cold periods (stadials) and at least two main relatively warm periods (interstadials). During the first cold period, the Forsmark area was probably free of ice, whereas the inland ice during the second cold period grew much larger and probably reached as far south as the Stockholm region, thus covering the Forsmark area. The last advance of the Weichselian glaciation was the largest. The maximum extent of this advance was reached c. 18,000 years ago and, according to mathematical and glaciological models, the thickness of the ice cover in the Forsmark region at that time was c. 3 km. During the warmer periods, the climate was colder than today and tundra conditions prevailed, indicating that permafrost has existed in the area for long periods of time in the past.

Detailed investigations to evaluate the occurrence of palaeoseismic activity during the latest part of and after the Weichselian glaciation in and around the Forsmark area have been carried out in the context of the site investigation work. None of the morphological lineaments that have been recognised have been inferred to represent late- or post-glacial faults. Furthermore, no deformational features in Quaternary sediment have been unambiguously related to seismic activity. On the basis of these results, there is no evidence in the geological record for major (magnitude > 7 on the Richter scale) earthquakes.

The development of the Baltic Sea after the latest glaciation has been characterised by ongoing shoreline displacement. The highest shore level in north-eastern Uppland developed during the Yoldia Sea stage (9500–8800 BC) of the Baltic Sea development and was located c. 100 km to the west of Forsmark. At that time, the Forsmark area was covered by c. 150 m of water. Since then, the shoreline displacement has been continuously regressive and most of the Forsmark area has emerged from the Baltic Sea during the last 2,000 years. The maximum salinity in the Baltic Sea covering the Forsmark area occurred during the period 4000 to 3000 BC during the Littorina Sea stage, with a salinity level approximately twice as high as today.

Deposition of sediments at Forsmark can be linked to the Weichselian glacial phase, and during and after the following deglaciation. In the western part of the candidate area, a silty-clayey till with an extremely high degree of consolidation is present. Based on its stratigraphical position and pollen composition, it is concluded that the deposit is older than the latest ice advance. In addition, sediment-filled open fractures beneath till in the upper bedrock have been recognised (Figure 11-2). The deposition of these sediments is dated back to a late stage of the glacial phase, when large amounts of sediment-loaded meltwater were concentrated below and within the retreating ice. These fractures formed or were reactivated during a late stage of the local deglaciation and are inferred to be sheet joints formed in connection with the release of stress in the bedrock.

In the Forsmark area, one glaciofluvial esker, the Börstilåsen esker (see map in Appendix 1), was deposited when blocks, gravel and sand were transported by the melt water within a tunnel under the ice. During further retreat of the ice, glacial clay was deposited in low topographic areas. The deposition of this glacial clay at Forsmark is dated to the Yoldia Sea stage. The subsequent shoreline displacement has had a large impact on the distribution and relocation of fine-grained Quaternary deposits. Wave washing and currents on the bottom have eroded, transported and re-deposited sand, gravel and post-glacial clay.

The post-glacial development of the ecosystems at Forsmark is strongly correlated to climate changes and the shoreline displacement, but also to human activities during the last c. 2,000 years. The recent emergence of the Forsmark area from the Baltic Sea implies that peat formation has affected the area for a relatively short period of time. The shoreline displacement continuously transforms sea bottoms to new terrestrial areas or to freshwater lakes. Lakes and wetlands are successively covered by fen peat, which at some locations is covered by bog peat. At Forsmark, rich fens form the dominant type of peat. Bogs do occur, but they are few and still young. Peat is found most frequently in the most elevated south-western part of the area, i.e. in the area that has been above sea level for a sufficiently long time for infilling of basins and for peat to form.

a **b**

Figure 11-2. *a) Laminated silt in an open fracture in the north-western part of the excavated area at drill site 5. The site was originally covered with till that has been removed. b) Horizontal fractures along the more than 1 km long canal between the Baltic Sea and the nuclear power reactors in Forsmark. These fractures are inferred to be sheet joints formed in connection with the release of stress in the bedrock.*

11.1.2 Description of the surface system

The landscape in Forsmark is a relatively flat peneplain that dates back to Precambrian time, i.e. prior to c. 540 million years ago. This peneplain dips gently towards the east. The most elevated areas in the south-western part are located at c. 25 m above current sea level. Despite the modest topography, the upper surface of the bedrock is found to undulate over small distances implying large variations in the thickness of the Quaternary cover.

Quaternary deposits

More than 90% of the regional model area is covered by Quaternary deposits, with till as the dominant deposit, especially in the terrestrial part (Figure 11-3). Post-glacial clay, including clay gyttja, is predominantly found in the deeper parts of valleys on the sea floor and only minor occurrences have been documented in the terrestrial area. Post-glacial gravel and sand frequently superimpose on glacial clay. These deposits are interpreted to mainly represent deposition after erosion and transport by currents on the floor of the Baltic Sea that covered the Forsmark area until c. 2,000 years ago. The thickness of the Quaternary deposits is generally larger in the marine area (average c. 8 m) than in the terrestrial part (average c. 4 m). Clay gyttja is frequent in the surface of the wetlands located at low altitudes, e.g. along the shores of Lake Fiskarfjärden and Lake Gällsboträsket. Gyttja is formed in lakes and consists mainly of remnants from plants that have grown in the lake.

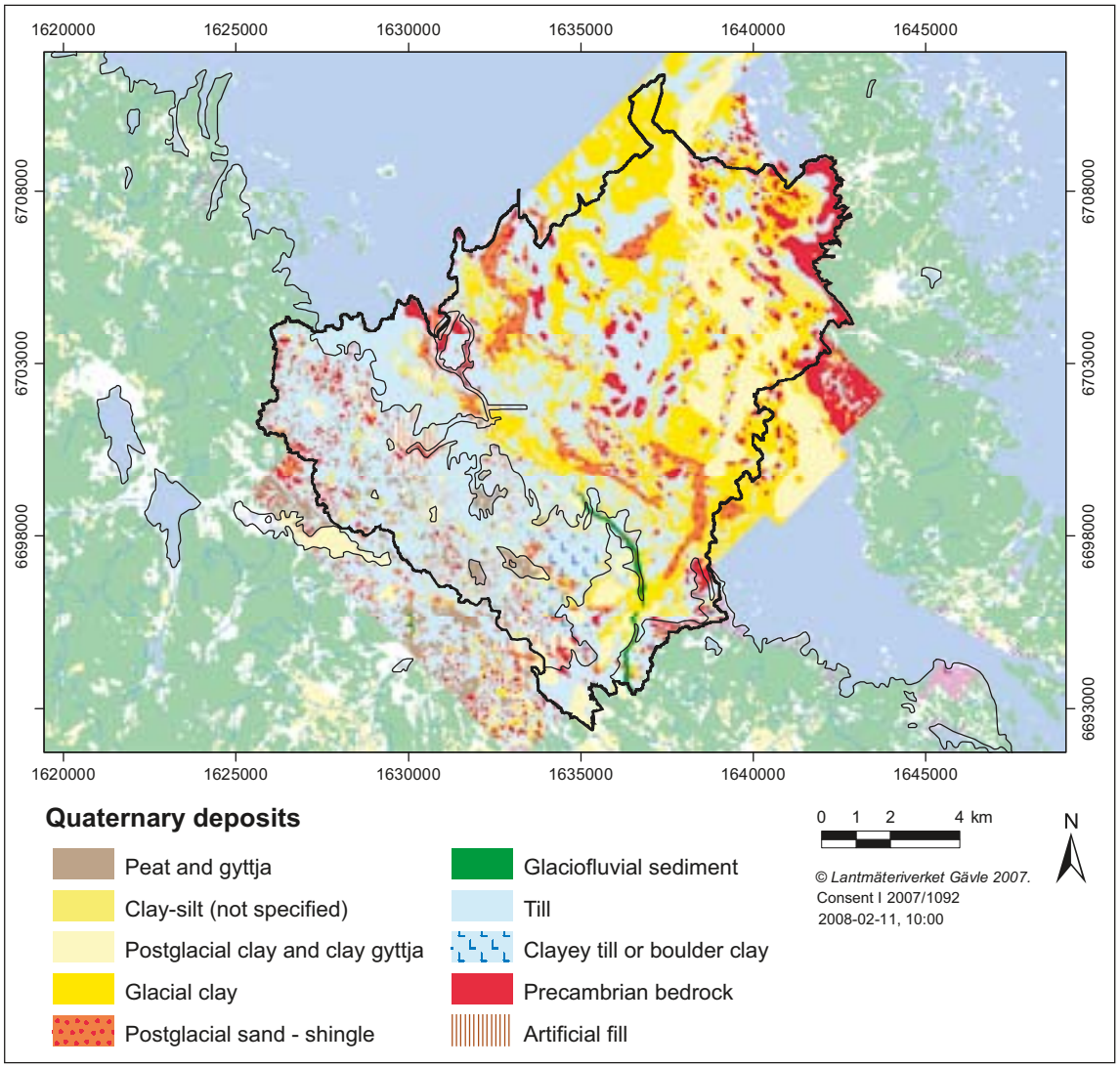

Figure 11-3. *The distribution of Quaternary deposits in the Forsmark regional model area. The map shows a compilation from several data sources originally presented at various scales (cf. section 4.2.1). From /Hedenström and Sohlenius 2008/.*

Lakes

The lakes at Forsmark are shallow, with maximum depths in the range 0.4 to 2 m. Flows of sea water into the most low-lying lakes have been registered during events of very high seawater levels. Furthermore, interpretation of data reveals that the lakes act as recharge sources to till aquifers in the riparian zone during summer, because of water losses from this zone by evapotranspiration.

Hydraulic properties

Hydraulic data show that the horizontal hydraulic conductivity within the till is significantly higher than the vertical conductivity and that the groundwater levels in the Quaternary deposits are shallow and closely correlated to the topography. These groundwater levels are significantly higher than the levels in the uppermost part of the bedrock within the target area, where the gradients in groundwater level are very small. This suggests that local, small-scale recharge and discharge areas, involving groundwater flow systems restricted to the Quaternary deposits, overlie the more large-scale flow systems associated with groundwater flow in the bedrock. In contrast, outside the target area and the tectonic lens (see section 11.2.1), for example in the area around Lake Eckarfjärden, groundwater levels in the bedrock are well above those in the Quaternary deposits and imply that flow systems involving the bedrock may have local discharge areas.

The lake sediments and the underlying till have low vertical hydraulic conductivities. This is indicated by lake-water/groundwater level relationships and the presence of relict marine chemical signatures beneath the lakes, which contrast with fresh groundwaters in the riparian zone.

Hydrochemistry

The till and the glacial clay are rich in calcium carbonate ($CaCO_3$), originating from Palaeozoic limestone that outcrops on the sea floor north of the Forsmark area. This, together with the recent emergence of the area above sea level, affects the chemistry of both surface water and shallow groundwater, giving rise to high pH, high alkalinity and high contents of major constituents. Furthermore, the surface waters are high in nitrogen and low in phosphorous. This is a characteristic feature of the oligotrophic hardwater lakes that are typical of the Forsmark area.

Interpretation of hydrochemical data from surface water and groundwater in Quaternary deposits supports the hydrological evaluation that discharge of deeper groundwater occurs around Lake Eckarfjärden. In addition, this interpretation suggests that water sampled at the edge of Lake Gällsboträsket also has a signature indicating an influence from deep saline water. Furthermore, a mass balance calculation of chloride suggests that there must be an additional source of chloride in the water to that stored in the Quaternary deposits, possibly from discharging deep groundwater. The discharge of more saline deep groundwater at Lake Gällsboträsket is consistent with results of the hydrogeological model that predicts discharge of deep groundwaters both at Lake Eckarfjärden and Lake Gällsboträsket (sections 8.7 and 11.7.3). Both these lakes lie along the outcrop of the regional Eckarfjärden deformation zone (see section 11.3.2).

Solute transport properties

The occurrence of highly transmissive and well-connected structures in the near-surface bedrock, including sheet joints (Figure 11-2b), suggests that discharging flow paths from the deep bedrock are captured by these structures and diverted towards the Baltic Sea. The main implication of this finding is that there are no discharge areas within the present terrestrial part of the target area for flow paths from the deep bedrock in the target volume. However, the complex geometry and heterogeneous hydraulic properties of these sub-horizontal or gently dipping, highly transmissive and well-connected structures makes it difficult to establish the exact location of discharge areas. For this reason, alternative scenarios for solute transport in the near-surface bedrock are proposed (Figure 4-16). These alternatives also consider uncertainties related to the role of the interface between Quaternary deposits and the bedrock, since data suggest that this interface could be important for the transport of solutes that potentially reach the near-surface system from depth.

Ecosystems

The location of the Forsmark regional model area close to the sea makes the seashore a prominent feature in the east along with conifer forests, shallow lakes, mires and some agricultural land (Figure 11-4). The terrestrial vegetation is strongly influenced by the characteristics of the Quaternary deposits and by human land use. Forests cover 73% of the land area at Forsmark and wetlands occur frequently, whereas agricultural use covers hardly 5% of the land area and is mainly located in the south-eastern part of the candidate area. The lakes are all shallow and classified as oligotrophic hardwater lakes, i.e. they contain high calcium levels, but low levels of nutrients, as phosphorus is precipitated together with the calcium. These characteristics have a strong impact on the limnic ecosystem. The marine ecosystem in the Forsmark area is relatively productive in a region of otherwise fairly low primary production.

Confidence

Generally, the site descriptive model for the surface system is based on a wealth of site data. Uncertainties associated with the sub-models have been thoroughly evaluated, and descriptions and model results are, in most cases, consistent with regional/generic data and/or with the results from alternative models. The principal remaining uncertainties are associated with the description of the spatial distribution of the thickness of the overburden and the hydraulic properties of the shallow bedrock, especially outside the target area. The hydraulic description of the shallow bedrock is part of the hydrogeological bedrock model and there is substantial support for the existence of highly transmissive and connected structures in this part of the bedrock. Even though the general groundwater flow pattern is considered to be well known, it is difficult to establish the exact location of discharge areas of deep groundwater due to the poorly constrained geological characteristics and heterogeneous hydraulic properties of the sub-horizontal or gently dipping structures that obviously govern groundwater flow in the near-surface bedrock. Other remaining uncertainties concern the description of the spatial distribution of the chemical composition of biota and in the Quaternary deposits, as well as the impact of chemical processes on transport of elements and quantitative estimates of processes, such as plant uptake and respiration. These remaining uncertainties are all judged to be of relatively minor importance for long-term safety or repository engineering.

Figure 11-4. *The central parts of the Forsmark candidate area, viewed from the south-west with Lake Bolundsfjärden in the foreground and the SFR buildings in the background.*

11.1.3 Human population and land use

The Forsmark region was not permanently settled until the end of Sweden's prehistoric period (1100 AD). During the medieval period (1100–1550 AD), the region was characterised by small villages and new settlements were created in the areas peripheral to the older ones. At the end of the medieval period, the majority of the farms in the region belonged to freeholders, and only a few farms belonged to the church or the nobility. During the early modern period (1550–1750 AD), the establishment of the iron industry in the Forsmark region dramatically affected the surrounding landscape. Production was geared towards the needs of this industry; charcoal production, mining and the production of fodder for animals used in the industry. There was a strong population expansion and many crofts were established in the forested areas, inhabited by people involved in the production of charcoal.

During the 18th century, the number of freehold farms decreased, both due to the partitioning of farms and to the fact that large estates expanded. The population increased dramatically up to the late 19th century. At the turn of the century the increase ceased and, during the latter part of the 20th century, the rural population decreased. The number of people involved in agriculture decreased and, in contrast, the number of people employed in industry and crafts increased.

At the present day, the Forsmark parish is sparsely populated and the Forsmark area has no permanent inhabitants, but has a small holiday population manifested by the presence of five holiday cottages and one farm. The land use in the parish is dominated by forestry, and wood extraction is the only significant outflow of biomass from the area. The agriculture in the parish is limited in extent and there is only one agricultural enterprise in operation within the Forsmark area, at Storskäret.

11.2 Rock domains and their associated thermal and rock mechanical properties

The site lithology, i.e. the occurrence and distribution of rock types, reveals important aspects of the homogeneity of the site. Furthermore, it is directly related to the potential for mineral resources as well as the thermal and rock mechanics properties of the intact rock. In the site descriptive model, the lithology is described by rock domains, defined on the basis of composition, grain size, homogeneity, and style and degree of ductile deformation.

11.2.1 Rock crystallisation and cooling history

In the regional structural context of the coastal area in northern Uppland, the tectonic lens in which the candidate area is located is considered to be well established. Borehole data support the conceptual model that the lens is a major geological structure that can be traced from the surface to at least c. 1,000 m depth. Folding of an older ductile fabric and a generally lower degree of ductile strain are inferred to be present inside the lens. By contrast, the rocks that surround the Forsmark lens are inferred to be affected by a generally higher degree of ductile strain and a conspicuous WNW to NW structural grain. This regional-scale anisotropy in the character and degree of ductile strain at Forsmark, which was established at an early stage in the geological evolution in the high-temperature ductile regime, has important implications for an understanding of the spatial distribution of younger deformation zones at the site (see section 11.3).

The bedrock that currently can be observed at the surface was formed at great depth. On the basis of detailed bedrock geochronological data, it is inferred that all the intrusive rocks in the Forsmark area formed in the time interval 1.89 to 1.85 Ga (1 Ga = 1 billion years) during the Svecokarelian orogeny. An older suite of plutonic, calc-alkaline rocks, including the metagranite inside the tectonic lens, formed between 1.89 and 1.87 Ga. Amphibolites that intrude the metagranite and a younger suite of calc-alkaline rocks and granites formed between 1.87 and 1.85 Ga. The penetrative ductile deformation and the amphibolite-facies metamorphism that affected these rocks was completed prior to 1.85 Ga. The development of broad WNW to NW belts with higher ductile strain that surround the tectonic lenses occurred around 1.86 Ga.

At least a part of the bedrock that currently is exposed at the surface had cooled below 500°C at around 1.85 Ga. However, the cooling ages below 500°C vary somewhat and extend in age downwards to c. 1.8 Ga. These results, in combination with the observation that subordinate ductile deformation affects the younger intrusive rocks in the marginal domains, indicate that ductile deformation after 1.85 Ga occurred predominantly inside the high-strain WNW to NW belts until at least 1.8 Ga. Sometime between 1.8 Ma and 1.7 Ga, during the waning stages of the Svecokarelian orogeny, the bedrock had cooled sufficiently to respond to deformation in a brittle manner.

11.2.2 Rock composition and ductile deformation

A substantial amount of geological and geophysical data, both at the surface and from depth in the form of information from cored (c. 17,800 m at 12 sites) and percussion (c. 6,500 m at 38 sites) boreholes underpins the SDM-Site rock domain model. Surface data are the basis for establishing a bedrock geological map (Figure 5-2 and Figure 11-5) and the distribution of rock units on this map, analysis of the surface data and evaluation of the borehole data are used in the projection of rock domains at the surface towards depth.

Rock types

Both surface and borehole data show that the bedrock in the target volume is strongly dominated by a homogeneous, medium-grained metagranite (Figure 11-5) with a high content of quartz (24–46%). Subordinate rock types are pegmatitic granite and pegmatite, fine- to medium-grained metagranitoid and amphibolite and other minor mafic to intermediate rocks (Figure 11-5). Aplitic metagranite comprises a distinctly more important component relative to the medium-grained metagranite in boreholes KFM06C (Figure 11-5) and KFM08D. This is consistent with the data from boreholes KFM06A (Figure 11-5) and KFM08C, and the limited outcrop data at the surface close to these two drill sites. Both rock types in these boreholes show a distinctive, high-temperature alteration referred to as albitization (see below) that results in a fine-grained rock with decreased contents of K-feldspar and increased contents of quartz (34–50%).

Ductile structures

Evaluation of ductile structures from surface and borehole data has revealed that major folding and the occurrence of rocks with a lower ductile strain, which are more lineated than foliated, characterise the Forsmark lens. As the margins of the lens are approached, the tectonic foliation in the metagranite appears to increase in intensity. More strongly deformed rocks, which are foliated, lineated and, in part, also banded and heterogeneous, comprise the bedrock to the south-west and to the north-east of the tectonic lens (Figure 11-5).

A major synform that plunges moderately to steeply (55–60°) to the south-east, close to the orientation of the mineral stretching lineation, dominates the target volume. This major fold structure is clearly visible from results of high-resolution ground magnetic surveys undertaken at the site (Figure 11-6). All ductile structures are conspicuously more gently dipping in the south-eastern part of the candidate volume, outside the target volume.

Subordinate rock types and alteration

The subordinate rock type amphibolite, which has low quartz content (0–6%), occurs as dyke-like tabular bodies and irregular inclusions that are elongate parallel to the mineral stretching lineation. Although some bodies are more than a few metres in thickness and, locally, are some tens of metres thick, most are inferred to be thin geological entities. The amphibolites follow the orientation of the ductile grain-shape fabrics at the site (Figure 5-9) and their spatial distribution has been simulated stochastically together with other subordinate rock types inside the target volume (Figure 11-7 and section 6.4).

Anomalously high uranium contents have been found in the subordinate rock types pegmatitic granite and pegmatite (1.1–61.7 ppm), and fine- to medium-grained granite (3.4–14.9 ppm).

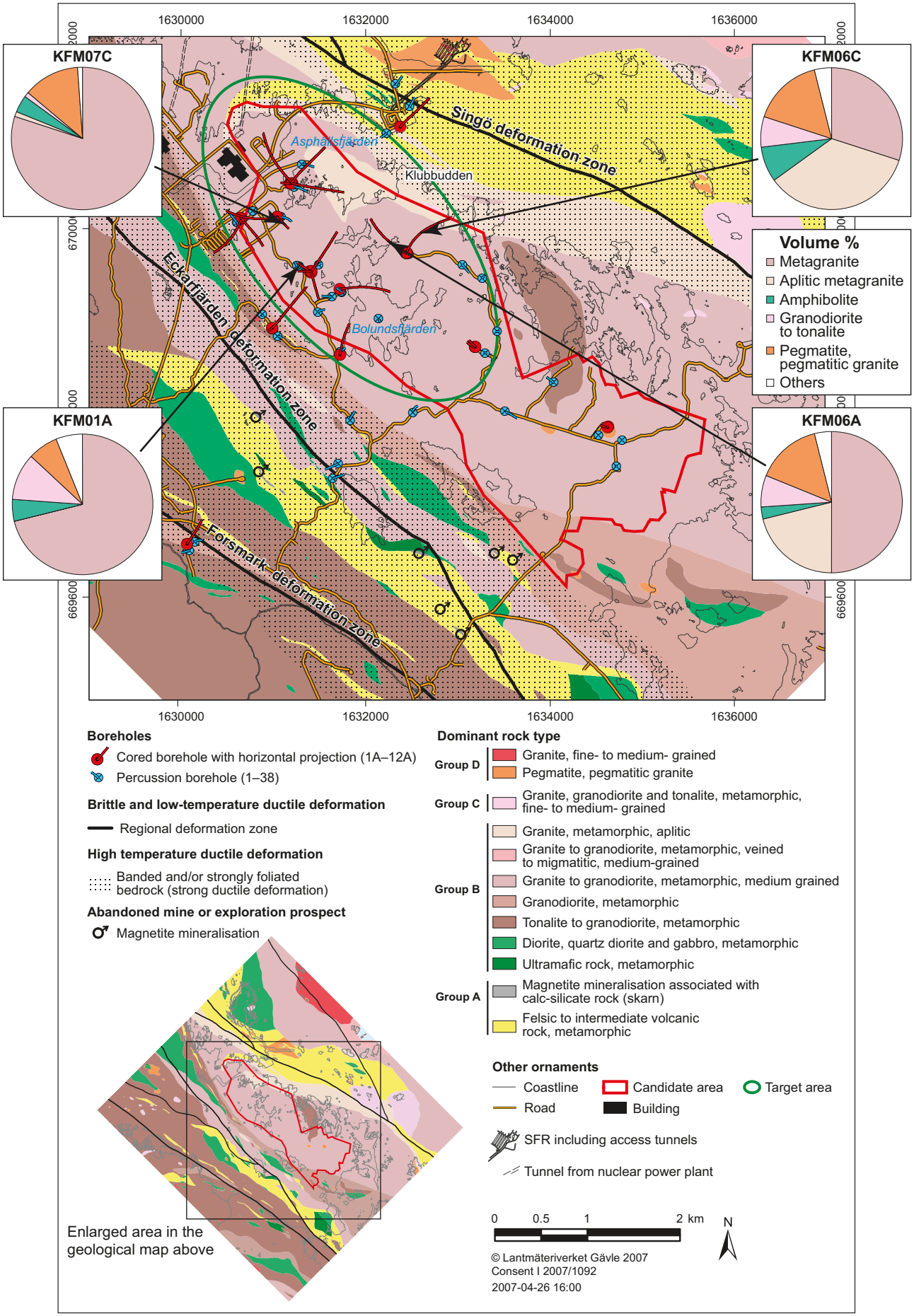

Figure 11-5. *Bedrock geological map of the candidate area and its surroundings at the Forsmark site. The volume% of different rock types in some cored boreholes are extracted from Appendix 4 in /Stephens et al. 2007/.*

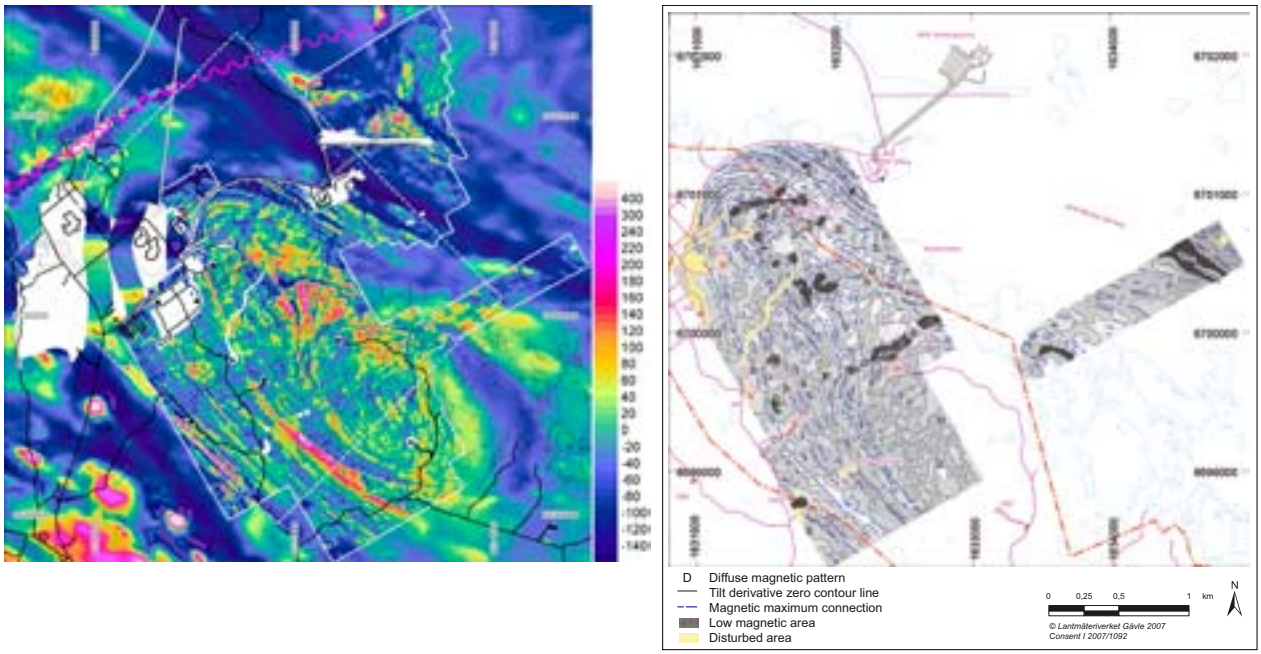

Figure 11-6. *Magnetic anomaly map based on high-resolution ground magnetic data inside the white line (left). Units in nanoTesla [nT]. Base level for the ground survey is 51,407 nT and for the helicopter survey outside the white line, 51,230 nT. Interpretation of magnetic connections based on the stage 2.2 data (right) shows the major fold structure (synform) that is defined by the folded pattern in these connections inside the Forsmark tectonic lens. Figures after /Stephens et al. 2007 2008/.*

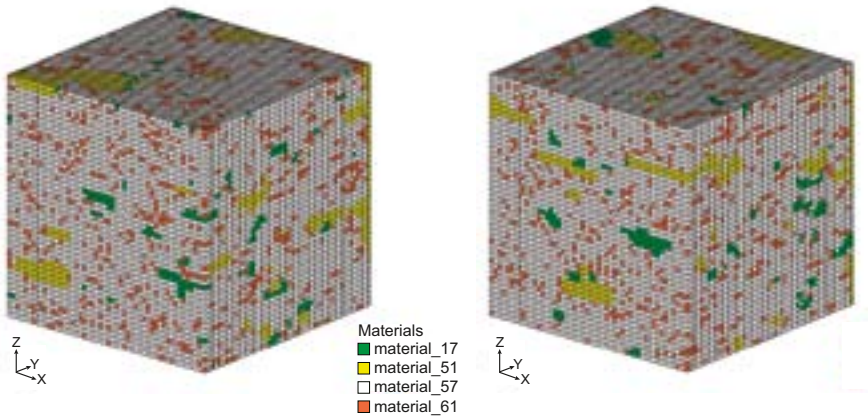

Figure 11-7. *Two examples of realisations of the distribution of amphibolites (green) and other subordinate rock types (metamorphosed granodiorite to tonalite; yellow, pegmatite and pegmatitic granite; orange) in rock domain RFM029 (see section 11.2.3).*

An assessment of the significance of rock alteration has shown that hematite dissemination (oxidation) and albitization are by far the most abundant types of alteration at the Forsmark site. A third form of alteration observed is the occurrence of vuggy rock that is associated with quartz dissolution. Hematite dissemination is consistently more abundant in the bedrock affected by deformation zones and the occurrences of altered vuggy rock are also strongly correlated to deformation zones. On the basis of these observations, it is inferred that these types of alteration are related to fluid movements along discrete channels in the zones at one or more times during geological history. By contrast, albitization is not confined to deformation zones, and is conspicuous along the contacts to amphibolite. It is suggested that this type of alteration is a pervasive feature in parts of the older felsic rocks and was triggered by the heat supply provided by the intrusion of the younger igneous rocks. It occurred prior to the completion of deformation and metamorphism in the bedrock.

11.2.3 Rock domain model

The candidate area at Forsmark is situated more or less exclusively inside a tectonic lens. Due to its internal homogeneity, most of the lens and, in particular, the north-western part can be described as two rock domains referred to as RFM029 and RFM045. These are also the two domains that define the rock in the target volume (see Figure 5-25 and Figure 11-8).

Rock domains in the target volume

The dominant rock type in rock domain RFM029 is a medium-grained metagranite (74% of the domain volume). Subordinate rock types are pegmatitic granite or pegmatite (13%), fine- to medium-grained metagranitoid (5%), and amphibolite and other minor mafic to intermediate rocks (5%). With the exception of amphibolite that contains little or no quartz, the dominant and the subordinate rock types have high quartz content (c. 20–50%). Linear structures, with both folding and stretching that plunge moderately to the SSE and SE, respectively, are apparent in domain RFM029.

Rock domain RFM045 is surrounded by rock domain RFM029 in the target volume and has a constricted rod-like geometry that plunges moderately to steeply to the south-east, close to the mineral stretching lineation in this part of the Forsmark site. Aplitic metagranite and medium-grained metagranite similar to the dominant rock type in domain RFM029 are the dominant rock types (67%) in this rock domain. To variable extent, both rock types show the alteration referred to as albitization. More subordinate rock types include pegmatite and pegmatitic granite (14%), fine- to medium-grained metagranitoid (9%) and amphibolite and other minor mafic to intermediate rocks (7%).

Rock domains outside the target volume

Rock domains outside the tectonic lens and target volume dip steeply towards the south-west, following the trend of the coastal deformation belt. They are dominated by different types of granitoid, predominantly felsic volcanic rocks and quartz-poor or quartz-deficient diorite to gabbro, all of which are affected by amphibolite-facies metamorphism. More inhomogeneous bedrock is conspicuous in domains RFM018 and RFM021, on both sides of the tectonic lens. In particular, the predominantly felsic metavolcanic rocks in domain RFM021, to the north-east, contain abundant pegmatite and pegmatitic granite.

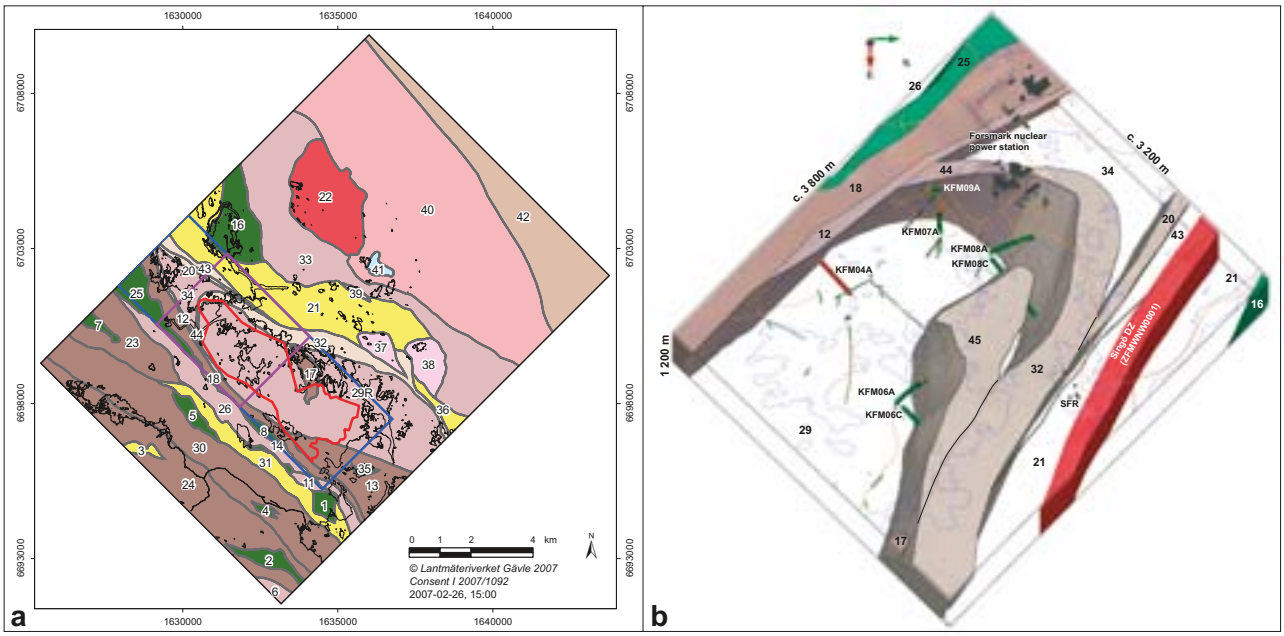

Figure 11-8. *a) Rock domains in the regional model area. b) The local model viewed to the west towards the SFR repository and the nuclear power station. RFM029 in the volume where most boreholes are present is unshaded. Figures after /Stephens et al. 2007/. The figure to the right has been modified slightly. See Figure 11-5 for a legend to these two figures.*

Confidence

Confidence in both the geometry and properties of rock domains within and immediately around the target volume is high down to a depth of 1,000 m, whereas significant uncertainties remain concerning the character and geometry of rock domains outside the target volume, e.g. in the sea area. However, these uncertainties are judged to be of minor importance for the understanding of the geological relationships inside the target volume and of little significance for repository engineering and safety assessment.

11.2.4 Mineral resources

The ore potential in the coastal area in northern Uppland is correlated to the rock types and their characteristics. An assessment of the ore potential, which was carried out in support of model version 1.1, came to the conclusion that there is no potential for metallic and industrial mineral deposits within the candidate area at Forsmark. A potential for iron oxide (magnetite) mineralisation was recognised in an area to the south-west of the candidate area, predominantly in the felsic to intermediate metavolcanic rocks (see Figure 11-5), but the mineral deposits are small and have been assessed to be of no economic value /Lindroos et al. 2004/.

Based on data from the islands outside the Forsmark candidate area, a new rock domain (RFM021), dominated by felsic to intermediate metavolcanic rocks, was recognised in version 1.2 of the site descriptive model. This rock domain is located north of the candidate area (Figure 11-8a). There is no documented iron mineralisation in data available from the islands, but since most of this rock domain is located beneath the Baltic Sea from where relevant data are lacking, the potential for iron oxide mineralisation in rock domain RFM021 cannot be totally excluded. However, the modelling work indicates that this rock domain does not occur in the candidate volume at elevations above –1,000 m.

11.2.5 Thermal properties

The thermal properties, i.e. thermal conductivity and heat capacity, of the rock are closely related to the lithology, since these properties depend on the mineral composition. The thermal conductivity of the rock has been assessed from direct measurements and by calculations based on mineral composition from modal analyses. Relationships between density and thermal conductivity determined from site-specific data support the use of borehole density logging data for modelling the spatial correlation of thermal conductivity within a rock type. These relationships have been shown to be consistent with the results of theoretical calculations of density and thermal conductivity based on the mineralogy of different rock types. The heat capacity has been determined from calorimetric measurements and also indirectly from measurements of thermal conductivity and diffusivity.

Thermal conductivity and heat capacity

The rock types in rock domain RFM029 have typically high quartz content (c. 20–50%), which implies high values of thermal conductivity. Measurements at the cm-scale show values in the range 3.2 to 4 W/(m·K) for the medium-grained metagranite, the dominant rock type in rock domain RFM029. The altered granitic rocks that dominate in rock domain RFM045 also have high thermal conductivity, with measured values in the range 3.6 to 4 W/(m·K). However, subordinate rock types in these rock domains yield significantly lower values, e.g. amphibolite in the range 2.2 to 2.5 W/(m·K). Measured and calculated conductivities also indicate that rocks affected by the alteration referred to as oxidation have higher thermal conductivity than their unaltered equivalents. Field and laboratory measurements have revealed the presence of anisotropy in the thermal conductivity. However, this anisotropy is scale dependent, with a thermal conductivity that is 40% higher parallel compared with perpendicular to the foliation at the centimetre scale, whereas this difference is 15% at the decimetre to metre scale.

The variability in thermal conductivity within each rock type and between rock types is incorporated into the stochastic domain modelling by the use of spatial statistical models of lithology and thermal conductivity (Figure 11-9). These models build on the grouping of rock types with similar

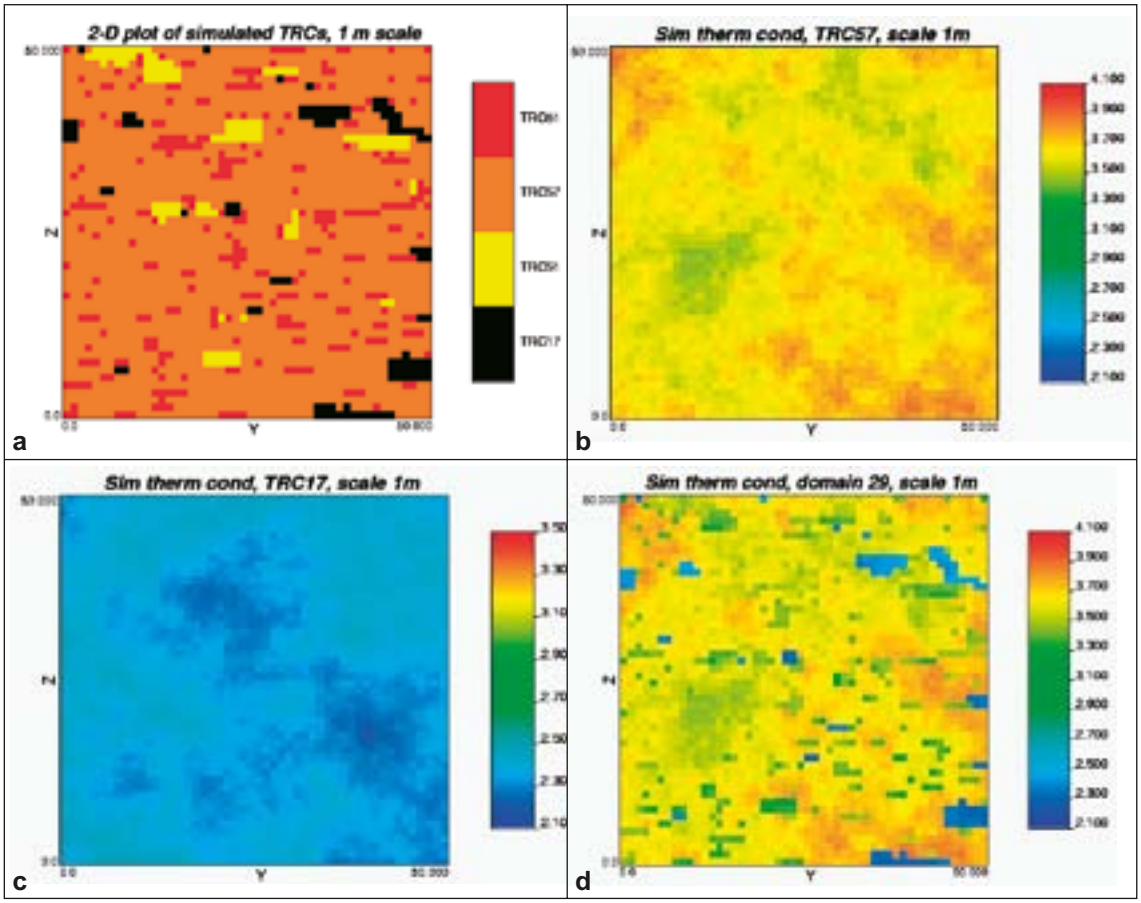

Figure 11-9. *2D slices from one 3D simulation of a) the distribution of TRCs, i.e. rock types with similar thermal conductivities; b) the distribution of thermal conductivity within TRC 57, which includes the dominant rock type metagranite; c) the distribution of thermal conductivity within TRC 17, which includes the subordinate rock type amphibolite; d) the resulting distribution of thermal conductivity considering the spatial variability in conductivity within and between TRCs.*

thermal conductivity into thermal rock classes (TRC). The distribution of TRCs is simulated and combined with simulations of the distribution of thermal conductivity within each TRC to obtain the distribution of thermal conductivity within a rock domain. The impact of the occurrence of the subordinate rock type amphibolite (TRC 17) is illustrated by the realisations at the 1 m scale shown in Figure 11-9.

The mean value of the thermal conductivity from the stochastic simulations is c. 3.6 W/(m·K) at the 5 m scale at a temperature of 20°C, both in rock domain RFM029 and RFM045. The impact of low conductivity rock, mainly the subordinate rock type amphibolite, but also the fine- to medium-grained metagranitoid, is particularly conspicuous in RFM045, a feature displayed by the pronounced lower tail in the resulting histogram of thermal conductivity at the 5 m scale (Figure 11-10). The lower tail of the thermal conductivity distribution influences the spacing of canisters. The 1 percentile of the thermal conductivity distribution is estimated to be 3.12 and 2.56 W/(m·K) for domains RFM029 and RFM045, respectively (5 m scale).

The mean value of the heat capacity assessed from measurements and from simulated thermal conductivity is 2.1 MJ/(m^3·K), both in rock domain RFM029 and RFM045. This value is valid at a temperature of 20°C.

The *in situ* temperature constitutes the initial temperature condition for a repository. The current mean temperature at 500 m depth is estimated to be 11.6°C, based on measurements in 8 boreholes.

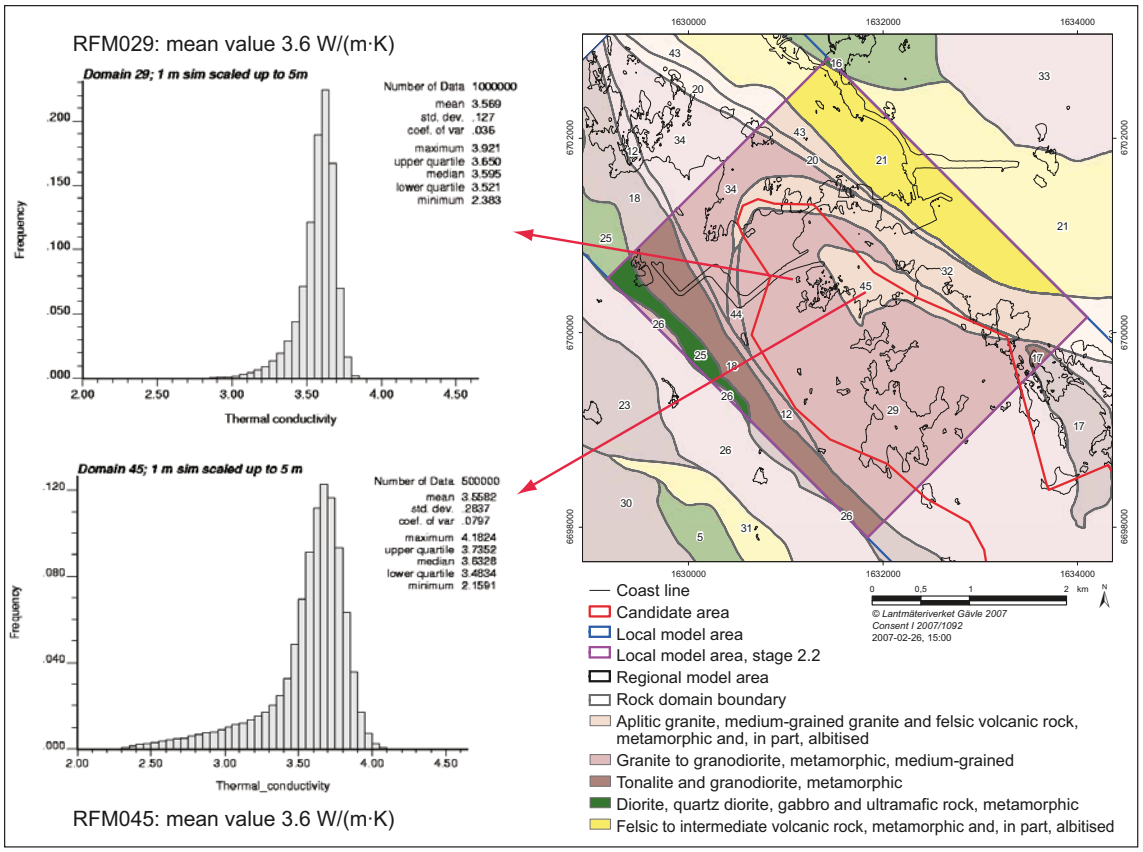

Figure 11-10. *Modelled thermal conductivity at 5 m scale. The lower tail of the distributions is mainly due to the subordinate rock type amphibolite. Modified after Figure 4-4 in /Stephens et al. 2007/, Figure 6-3 in /Back et al. 2007/ and Figure 6-3 in /Sundberg et al. 2008/.*

Confidence

There is generally high confidence in the modelled distribution of thermal properties, due to the large amount of thermal data for the homogeneous rock mass. The thermal conductivity distribution is more uncertain for rock domain RFM045 than for rock domain RFM029. For domain RFM045, these uncertainties concern both the overall distribution and its lower tail, and are related to uncertainties associated with the output of the geological simulations, in particular, the proportions of rock types and the spatial and size distribution of amphibolite. Although the geological simulations performed have managed to model much of the heterogeneity observed in the boreholes, it is still somewhat unclear to what extent the borehole information is representative of the geology in domain RFM045. The reason for this is the small number of boreholes combined with the more heterogeneous distribution of amphibolite in rock domain RFM045.

11.2.6 Strength and other mechanical properties of intact rock

Lithology also affects the thermal expansion, mechanical strength and deformation properties of the unfractured (intact) rock. The assessment of thermal expansion is based on results from measurements on samples from five different rock types, including the dominant rock types in RFM029 and RFM045, but not the subordinate rock type amphibolite. The mechanical strength and deformation properties of the rock are evaluated from results of measurements on samples from the dominant rock types in RFM029 and RFM045, and also from the subordinate rock type pegmatite.

Thermal expansion

The mean value of the measured thermal expansion coefficient for the main metagranitoid rock types within the target volume varies between $7.5 \cdot 10^{-6}$ and $7.8 \cdot 10^{-6}$ m/(m·K). The mean of the measurements for the dominant medium-grained metagranite in RFM029 is $7.7 \cdot 10^{-6}$ m/(m·K), and the corresponding value for the altered metagranite, which dominates in RFM045, is $7.5 \cdot 10^{-6}$ m/(m·K).

Domain modelling has not been performed, but the small differences in measured values suggest a mean coefficient of thermal expansion of 7–8·10^{-6} m/(m·K) for the different rock domains.

Strength and deformation modulus

The uniaxial compressive strength (UCS) and Young's Modulus (E) of the intact rock show that the rock types in rock domains RFM029 and RFM045 are strong (UCS > 200 MPa) and stiff (E > 70 GPa) (see Table 7-3). The results for samples taken inside or in the vicinity of deformation zones are in the same range as the results for samples taken in the host rock outside deformation zones.

Confidence

There is generally a high confidence in the strength and deformation properties of the dominant rock types in rock domains RFM029 and RFM045. Some uncertainties remain in the uniaxial compressive strength of the subordinate rock types amphibolite and fine- to medium-grained metagranitoid in these rock domains. However, the proportions of these rock types in rock domains RFM029 and RFM045 inside the target volume are small (see section 11.2.3 and Table 5-3).

11.3 Deformation zones, fracture domains and fractures

11.3.1 Formation and reactivation throughout geological time

Four sets of deformation zones have been identified with high confidence at the Forsmark site. Vertical and steeply, SW-dipping zones with subsets referred to as WNW and NW show complex, ductile and brittle deformation. Regional zones longer than 10 km that occur outside the candidate volume (e.g. the Forsmark, Singö and Eckarfjärden deformation zones) are restricted to this set. The deformation zones in the remaining three sets only display brittle deformation and can be referred to as fracture zones. Vertical and steeply dipping fracture zones with sub-sets referred to as ENE (NE) and NNE transect the tectonic lens and occur frequently inside the target volume. These zones formed in the brittle regime and are dominated by sealed fractures and sealed fracture networks. Gently dipping fracture zones occur more frequently in the south-eastern part of the candidate area, i.e. outside the target volume. Relative to the other three sets, there is an increased frequency of open fractures, including crush zones, along the gently dipping set. The fourth set consists of vertical and steeply dipping fracture zones referred to as NNW that are dominated again by sealed fractures. On the basis of their low frequency of occurrence, these are judged to be of lower significance relative to the other three sets of zones at Forsmark.

Low-temperature geochronological data, dating of fracture minerals, kinematic data and consideration of deformation in a regional perspective have been used to establish a conceptual model for the formation and reactivation of deformation zones in the context of changes in the stress regime from the later part of the Svecokarelian orogeny, c. 1.85 to 1.75 Ga, until the Quaternary (Figure 11-11). This conceptual model suggests that the different sets and sub-sets of deformation zones in the Forsmark area *had formed and had already reactivated* during Proterozoic time, in connection with several tectonic events prior to 900 Ma. As the effects of tectonic activity, for the most part, waned, the effects of loading and unloading increased in significance (Figure 3-3). The latter occurred in connection with the deposition of sedimentary rocks and the subsequent erosion of these rocks with exhumation of the crystalline bedrock. In this respect, the formation of sedimentary basins during the time interval c. 1.5 to 1.3 Ga and after 900 Ma, an episode of glaciation during the latest part of the Precambrian around c. 650 Ma, the development of a passive continental margin during the Early Palaeozoic, and numerous glaciations during the Quaternary period are examples of loading events during the geological development of central Sweden.

The termination pattern of surface lineaments and the occurrence of ductile deformation indicate that the steeply dipping zones referred to as WNW and NW form the oldest discrete structures at the site. It is inferred that they formed in response to bulk crustal shortening in a NW-SE to N-S direction, during the later part of the Svecokarelian orogeny (Figure 11-11).The size of several of these zones (e.g. Forsmark, Singö and Eckarfjärden) confirms that they comprise the master set. Ductile shear bands in the vicinity of the Singö zone and fault-slip data along the Eckarfjärden zone confirm the

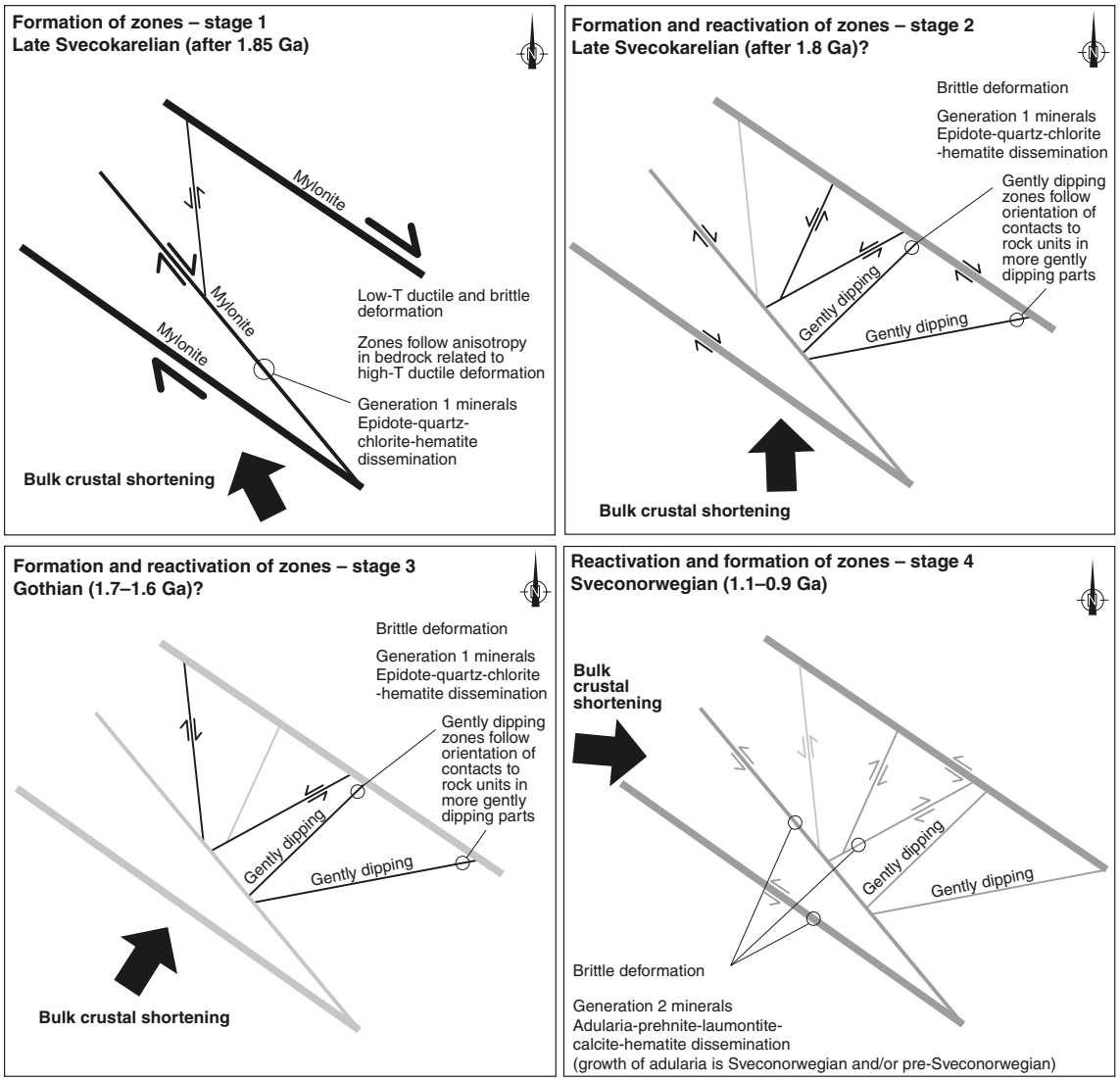

Figure 11-11. *Two-dimensional cartoons illustrating the regional scale geodynamics during the formation and reactivation of the different sets of deformation zones at the Forsmark site (for more details see section 5.2.2).*

occurrence of dextral strike-slip displacement along this zone, related to approximately NW-SE compression. The formation of some steeply dipping NNW structures with sinistral strike-slip displacement is also inferred to have occurred at this stage in the tectonic evolution. The regional-scale anisotropy in the bedrock, related to older ductile deformation under higher-grade metamorphic conditions, is a critical factor that controls the location and orientation of these older zones.

Dextral strike-slip displacement along steep NW zones and sinistral strike-slip displacement along steep ENE and NNE zones are inferred to be related to approximately N-S compression during the latest part of the Svecokarelian orogeny. Conjugate relationships between steeply dipping ENE and NNW structures, with sinistral and dextral strike-slip displacements, respectively, are related to approximately NE-SW compression and the younger Gothian tectonic event. It is suggested that the reverse dip-slip or strike-slip compressive deformation along the gently dipping zones occurred during these tectonic episodes. In such a conceptual model, it can be expected that the gently dipping zones both terminate against the steeply dipping ENE and NNE structures and are displaced by them. The seismic reflection data provide some support to both these statements. Data also demonstrate that the bedrock at Forsmark has been strongly affected by the Sveconorwegian orogenic event. This gave rise to sinistral strike-slip displacement along the steeply dipping zones referred to as WNW and NW, and dextral strike-slip deformation along the zones in the ENE (NE) and NNE set. There remains an uncertainty concerning to what extent fractures formed or were reactivated in connection with this event.

The conceptual model further suggests that the loading of sedimentary successions is related temporally with the reactivation of steeply dipping zones in the form of dip-slip displacement (Figure 3-3). It is also suggested that sedimentary loading is a process that, besides tectonic events, gave rise to the build-up of high rock stress in the bedrock. By contrast, unloading resulted in reactivation, especially of gently dipping structures, in the form of extensional failure and the development of dilatational joints. New fractures that are oriented sub-parallel to the topographic surface at the time of unloading and lack alteration associated with hydrothermal alteration, i.e. sheet joints, would also have formed (see section 11.1.1). These features occurred in response to a release of stress in the bedrock. They are most conspicuous close to the surface interface (see Figure 11-2), where the differential stress ($\sigma_1 - \sigma_3$) at the time of unloading was high, and, especially, in the vicinity of ancient gently dipping zones. By corollary, it is apparent that changes in aperture in the current stress regime (see section 11.4) can be expected to occur most significantly in the near-surface realm, along sub-horizontal and gently dipping fractures.

11.3.2 Deterministic deformation zones

The deterministic deformation zone model builds on the integration of the understanding of the deformational history in the region, magnetic lineament and seismic reflection data, as well as fracture orientation, fracture mineralogical and alteration data, especially from the cored boreholes. Low magnetic lineaments derived from both high-resolution ground magnetic data and airborne helicopter data inside and immediately around the target area are the main surface data that support the occurrence of steeply dipping deformation zones (Figure 5-18 and Figure 11-12). Surface exposure of a few lineaments has shown that they represent either steeply dipping fracture zones with sealed or both sealed and open fractures (4 out of 5 cases) or are related to a swarm of dykes of granite and pegmatite with low magnetic susceptibility. The steeply dipping fracture zones are associated with wall rock hydrothermal alteration, which is identical to the alteration observed along possible deformation zones in the single-hole interpretation of boreholes.

Geometrical constraints on the occurrence of gently dipping fracture zones are provided by surface reflection seismic data and borehole seismic data (VSP). Reflectors that dip to the SSE and SE are prominent in the candidate volume, with a much stronger concentration in the upper 2 km of the bedrock in the south-eastern part relative to that observed in the north-western part, i.e. the target volume (Figure 11-12 and Figure 11-13). Borehole data show that several of the gently dipping fracture zones in the south-eastern part of the candidate volume occur along or close to the contact between subordinate rock types, in particular amphibolite, and the dominant host rock metagranite. Since the amphibolite contacts follow the orientation of the tectonic foliation, it is proposed that the more frequent occurrence of gently dipping zones in the south-eastern part is related to the gentler, south-east dip of the amphibolite, the tectonic foliation and the mineral stretching lineation in this part of the candidate volume.

The bedrock fabric, which was established in the high-temperature ductile regime, has influenced the variable spatial distribution of the different sets of deformation zones at the site. The vertical and steeply SW-dipping zones with sub-sets referred to as WNW and NW are entirely restricted along or close to the south-western and north-eastern margins of the Forsmark tectonic lens in the high-strain belts (Figure 5-29). In these volumes, the tectonic foliation and rock contacts show a similar, steeply SW-dipping orientation. Inside the tectonic lens, where the ductile fabric is folded and more variable in orientation, steeply dipping fracture zones included in the ENE (NE) and NNE sub-sets transect the local model and target volume. As indicated above, the majority of the gently dipping deformation zones are situated outside or in the south-eastern, peripheral parts of the local model volume where the ductile structures and rock contacts are more gently dipping. Of these zones, zone A2 defines the roof of the rock volume considered as potentially suitable for hosting the repository (Figure 5-30).

The local model includes 60 deterministically modelled deformation zones, and the majority of these zones (> 60%) are judged to have a high confidence of existence. The geological and geophysical data that form the basis for the interpretation of each zone are summarised in Table 5-2 in /Stephens et al. 2007/. Only two steeply dipping zones with a surface trace length longer than 3,000 m intersect the target volume (zones ENE0060A and ENE0062A with their attached branches) and a further twenty-two steeply dipping zones, which either show a trace length at the ground surface between 1,000 and 3,000 m or form minor splays or attached branches to such zones, are present at 400 to

600 m depth inside the potential repository volume. Five gently dipping zones, including zones A2 and F1, are also present at 400 to 600 m depth inside or immediately above the potential repository volume. A compilation of the properties of these zones is provided in Appendix 4.

In general, the zones in the target volume can be characterised as having a transition zone that contains a higher frequency of sealed and open fractures and more hydrothermal alteration than the host rock outside the zone, but also segments that resemble the unaffected host rock. Fault cores, recognised in 55% of all the zones studied in drill cores in the area, are predominantly composed of a sealed fracture network in combination with rock alteration and, locally, cohesive breccia or cataclasite. Fault gouge has not been recognised along the fracture zones.

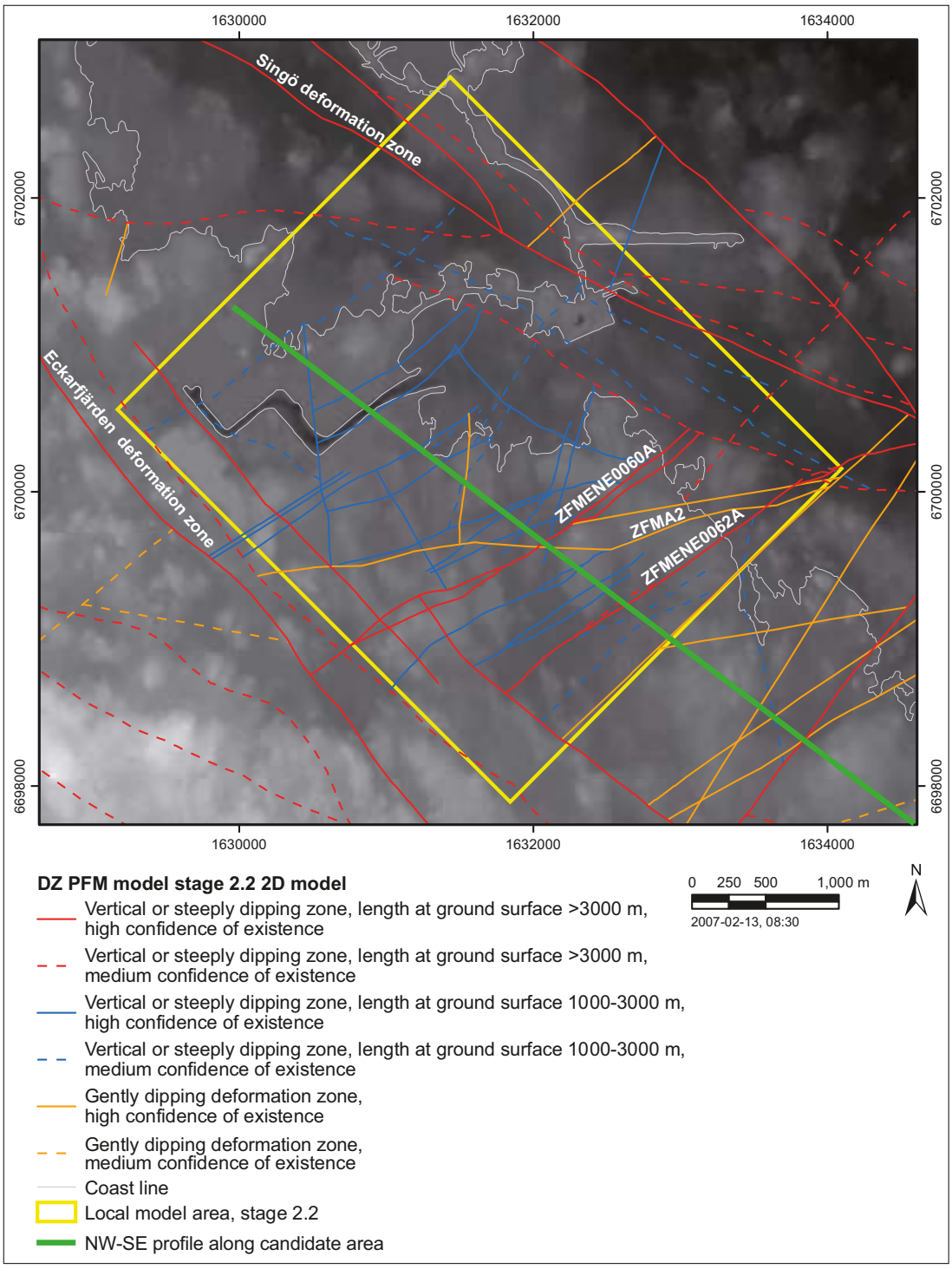

Figure 11-12. *Surface intersection of deterministic deformation zones in the local model. The background corresponds to the digital elevation model of the site. The green line shows the position of the vertical profile shown in Figure 11-13 (modified after Figure 5-10 in /Stephens et al. 2007/).*

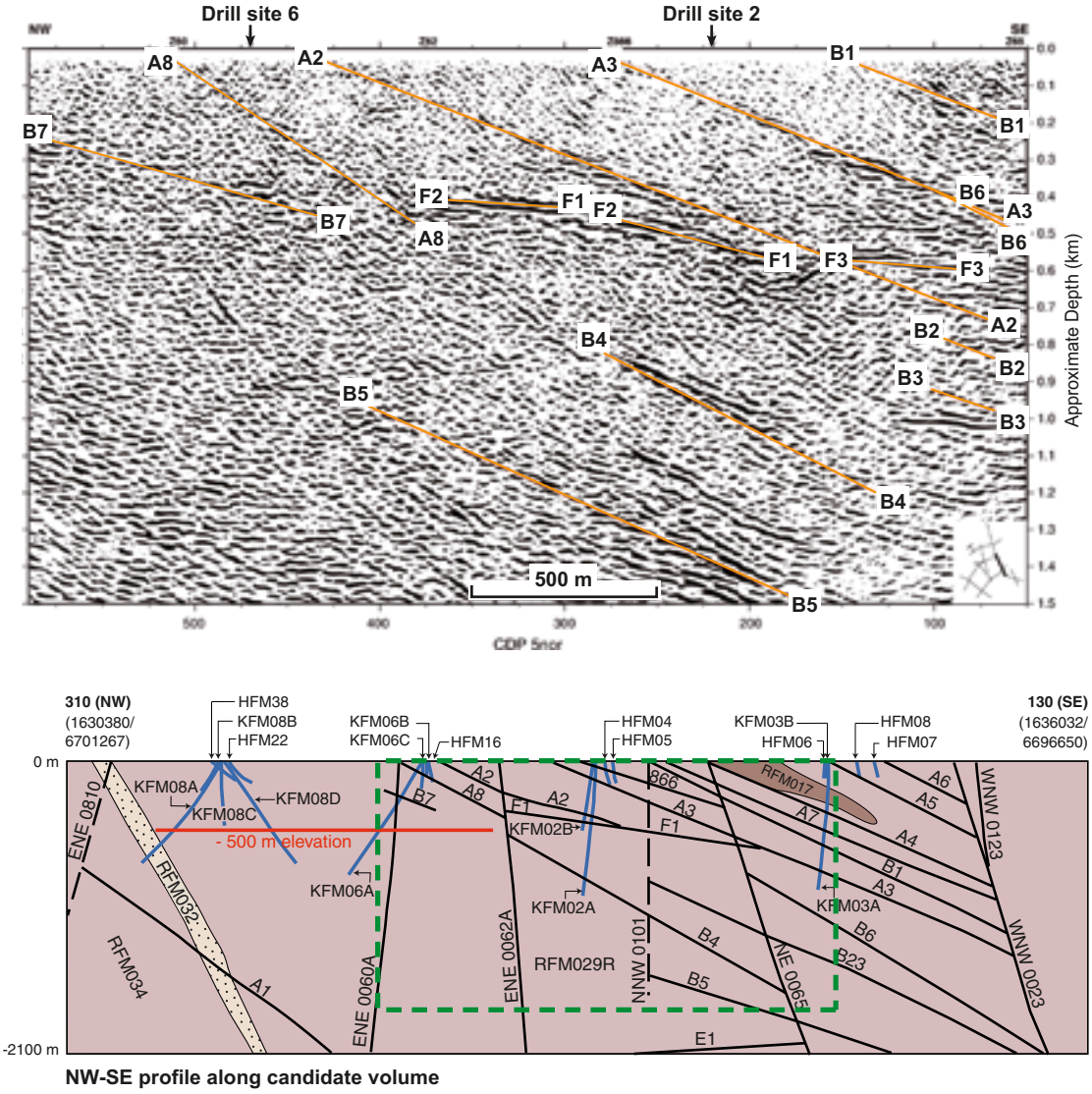

Figure 11-13. *Confidence in the gently dipping fracture zones is enhanced by combining reflection seismic data with borehole data. The upper insert shows gently dipping seismic reflectors in the south-eastern part of the candidate volume (Figure 5-21). The lower insert is a WNW-ESE cross-section through the candidate volume in the structural model showing rock domains and deformation zones (Figure 5-21 in /Stephens et al. 2007/; see also Figure 5-29 and Figure 5-30 in this report). The approximate location of the upper insert is indicated by green dashed lines in the lower insert. The cross-sections are not identical.*

The regional model includes 72 deterministically modelled deformation zones and 29 of these are also present in the local model (Figure 5-29). The minority of the zones in the regional model (27) are judged to have a high confidence of existence. The remainder lack corroborative geological and geophysical data from boreholes or excavations and are judged to have a medium confidence of existence. As in the local model, vertical and steeply dipping deformation zones (48) dominate over gently dipping zones (24). However, there is an inherent bias in the evaluation of the occurrence of gently dipping zones, since reflection seismic data are not available over the north-eastern half of the regional model volume.

Confidence

Confidence in the occurrence of deterministic deformation zones in the target volume is high and the occurrence of undetected deformation zones longer than 3,000 m is judged unlikely. It is considered that the deterministic model for deformation zones has now attained acceptable stability, in both the local and regional model volumes. The predictability of the occurrence and character of different sets or sub-sets of deformation zones is related to the large-scale bedrock anisotropy that was established over 1.85 billion years ago, when the bedrock was situated at mid-crustal depths and was affected by penetrative, ductile deformation under high-temperature metamorphic conditions.

The principal remaining uncertainty in the deterministic deformation zone model concerns the size of the gently dipping fracture zones. However, it is judged that this uncertainty is sufficiently bounded, since the approach for termination of these zones has been to extend them to the nearest steeply dipping zone. Furthermore, this uncertainty is not fundamental to the conceptual understanding of the site. Another remaining uncertainty concerns the orientation and size of the possible deformation zones that have not been modelled deterministically. Since it has not been possible to link these geological features to low magnetic lineaments or seismic reflectors and since they commonly occur along short borehole intervals, it is judged that they are predominantly minor zones.

11.3.3 Fracture domains, fractures and DFN modelling

Analyses of fracture data have indicated a large degree of spatial variability in the size, intensity and properties of fractures between different rock domains, but also within rock domain RFM029. The north-western (target volume) and south-eastern parts of the candidate volume differ from each other as to variations in frequency, particularly of open and partly open fractures, down to approximately 1,000 m depth (Figure 5-13). It is suggested that this difference is related to the corresponding contrast in the frequency of gently dipping deformation zones, with their relatively high frequency of open and partly open fractures, between the two sub-volumes. Furthermore, the fracture frequency distribution patterns with depth also show that the bedrock in the footwall of zone A2 (target volume bedrock) displays different fracture characteristics close to the surface and at depth. The upper part of the rock shows an anomalously high frequency of open and partly open fractures, whereas the bedrock at depth shows a strong dominance of sealed fractures and very few open fractures. The boundary between these different parts of the rock varies between c. 40 m and 200 m depth.

Fracture domains

Based on a systematic assessment of the variation in the frequency of fractures with depth along each borehole, the bedrock between deterministically modelled deformation zones has been divided into fracture domains (Figure 5-34). Thus, fracture domains and deterministically modelled deformation zones are mutually exclusive volumes, whereas rock domains contain both fracture domains and deterministically modelled deformation zones.

Fracture domain FFM01 forms the bedrock at depth in the target volume, north-west of and in the footwall of the gently dipping zone A2 (Figure 11-14). This fracture domain forms the main component in rock domain RFM029. Fracture domain FFM02 comprises the bedrock close to the surface, above fracture domain FFM01, predominantly in the same footwall bedrock segment. Fracture domain FFM02 is located in both rock domains RFM029 and RFM045. The bedrock in FFM01 shows a low frequency of open and partly open fractures, whereas the bedrock in FFM02 is characterised by a complex network of sub-horizontal or gently dipping, open and partly open fractures, which, locally, merge into minor zones. The sub-horizontal or gently dipping fractures are oriented at a large angle to the current, minimum principal horizontal stress in the bedrock. The rock volume south-east of the target volume, in the hanging wall of zone A2, is defined as fracture domain FFM03. It is situated in rock domains RFM029 and RFM017. Open and partly open fractures in this domain are more evenly distributed down to 1,000 m depth and the domain is spatially associated with a high frequency of gently dipping fracture zones containing both open and sealed fractures.

A fourth fracture domain, FFM06, is defined in the target volume. In the same manner as fracture domain FFM01, it lies in the footwall of zone A2 and beneath FFM02. It forms the main component in rock domain RFM045. It was distinguished from FFM01 simply on the basis of the widespread occurrence of fine-grained, altered (albitized) granitic rock, with slightly higher contents of quartz compared with unaltered granitic rock.

Borehole data have revealed that the orientation of the fractures inside domains FFM01 and FFM06 resembles the orientation of fractures in the ENE (NE) and NNE sub-sets of fracture zones, respectively, i.e. the orientation of fractures in the domains is similar to that in the adjacent fracture zones (Figure 11-15). However, this correlation breaks down in domain FFM02, where there is an important contribution from sub-horizontal and gently dipping fractures, but relatively few gently dipping zones (Figure 11-15). It is inferred that tectonic processes during geological history have determined the fracturing at depth in fracture domains FFM01 and FFM06, whereas the fracturing in the near-surface bedrock in fracture domain FFM02 is the result of a combination of tectonic processes and processes related to stress release.

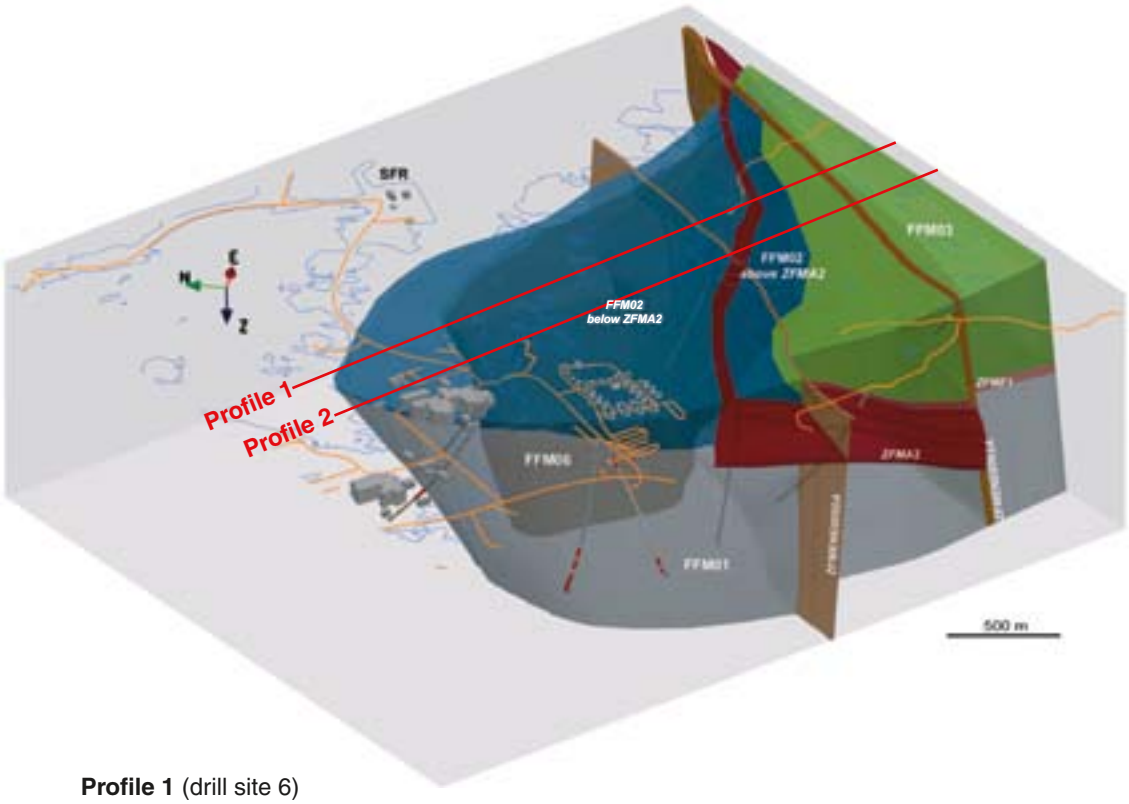

Profile 1 (drill site 6)

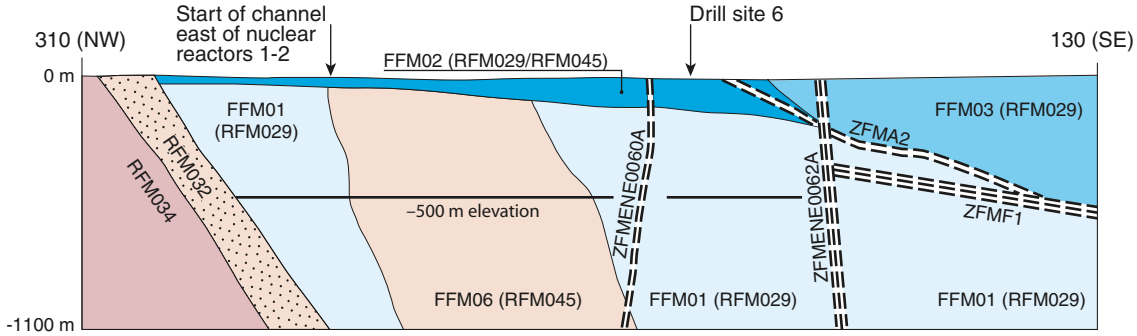

Profile 2 (drill sites 8 and 2)

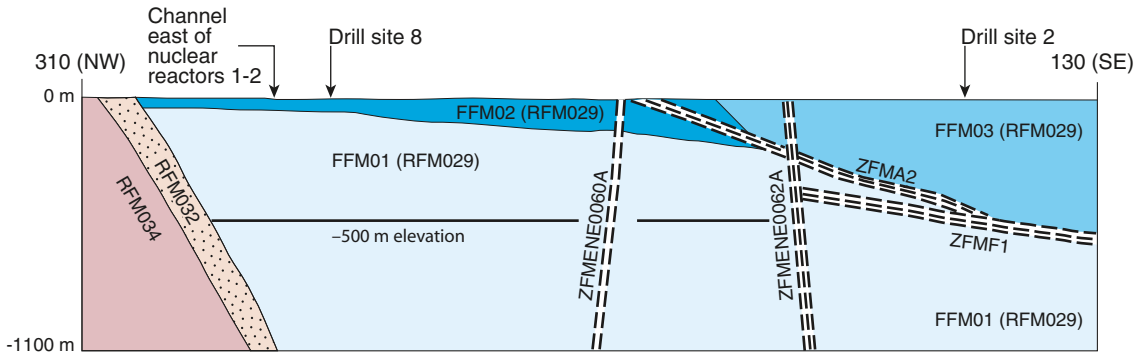

Figure 11-14. *View to the ENE (upper) and vertical profiles in a NW-SE direction (middle and lower) showing the fracture domains and their relation to the gently dipping deformation zones ZFMA2 and ZFMF1 and the steeply dipping zones ZFMENE0060A and ZFMENE0062A that are longer than 3,000 m (Figures 5-1 and 5-4 in /Olofsson et al. 2007/).*

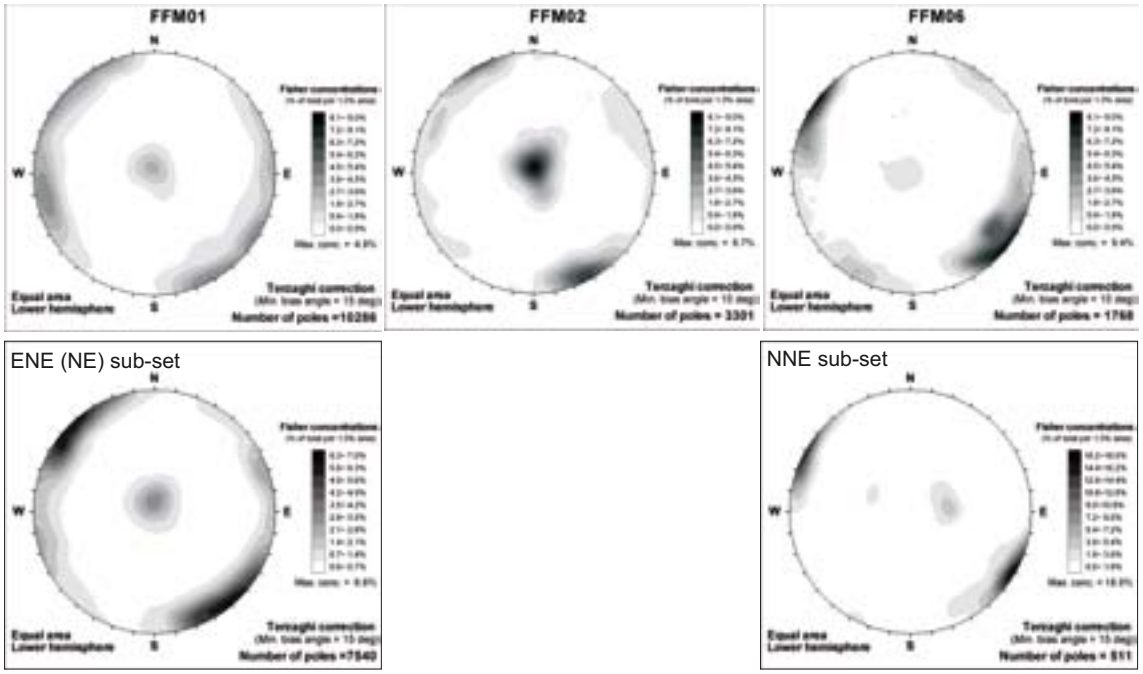

Figure 11-15. *Orientation of fractures in fracture domains FFM01, FFM02 and FFM06 (upper) compared with orientation of fractures in the two sets of deformation zones that occur in the target volume (lower).*

Discrete fracture network models

Fractures and minor fracture zones, not covered by the deformation zone model, are handled in a statistical way through discrete fracture network (DFN) models. The geological DFN model captures all fractures (open, partly open and sealed), since the sealed fractures are also assumed to be potential planes of weakness and could possibly be planes where there exist flow channels. However, many of the sealed fractures are mechanically and hydrogeologically indistinguishable from the intact rock. The model is presented as a stochastic description of fractures and fracture zones shorter than 1 km, not as a 3D object.

DFN models are produced for each fracture domain in the target volume, i.e. fracture domains FFM01, FFM02 and FFM06, and also for fracture domain FFM03. The size-scale range, expressed as the radius of the area of an equivalent disc-shaped fracture, varies in different models (see below). The data used, to variable extent, in the different models are fracture trace length data observed in outcrop, data derived from the interpretation of magnetic lineaments, data derived from the lengths of the intercepts of the mid-planes of the deterministic deformation zones and fracture intensity data from boreholes.

The influence of different geological processes at depth and close to the surface (section 5.7) causes difficulties to apply coupled size-intensity geological DFN models, which are based on surface data, to the two fracture domains at repository depth that do not outcrop, FFM01 and FFM06. There are also uncertainties regarding whether the fractures represented by deformation zones and magnetic lineaments are part of the same fracture population represented by fractures in outcrop or measured in boreholes. These difficulties are captured by alternative size-intensity models for the distribution of fractures (section 5.6.4).

- The hypothesis that the fractures in outcrop and in boreholes are part of the same population as the larger fractures delineated through magnetic lineaments and deformation zones is referred to as the tectonic continuum model or TCM. The model assumes Euclidean size-intensity scaling. A variant of this model, referred to as TCMF, assumes fractal size-intensity scaling. The size-scale range for both the TCM and TCMF models is from 0.5 m to 564 m
- The conceptual model that treats the larger-scale fracturing as a distinct population from the fractures in outcrop and boreholes is referred to as the OSM+TFM model, where OSM is the outcrop scale model representing the fractures measured in outcrops and boreholes, and TFM is the tectonic fault model, representing the fractures identified through lineaments and deformation zones. The size-scale range is once again from 0.5 m to 564 m.

An additional alternative tectonic continuum model for fracture domain FFM01 is denoted "r_0-fixed". The size-intensity relation in this additional alternative utilises the intensity of large-scale lineaments and deformation zones, as in the TCM and OSM+TFM models, together with fracture frequency data from boreholes in FFM01, but not fracture traces mapped in outcrop. It adopts a fixed $r_0 = 0.039$ approach with a size-scale range up to 564 m.

None of the geological DFN model alternatives has taken into account the heterogeneity in the density of larger structures at the Forsmark site. The implication of this is that these DFN models, including the r_0-fixed alternative, overestimate the intensity of NW-striking fractures in the size range 28 m to 564 m in fracture domains FFM01 and FFM06. It is also possible that the intensity of larger sub-horizontal fractures is not correctly predicted by the geological DFN models.

The hydrogeological DFN model also avoids fracture traces mapped in outcrop, adopts a fixed $r_0 = 0.039$ approach and is applied for the same size-scale range as the r_0-fixed geological DFN model alternative. However, the hydrogeological DFN model does not make use of the intensity of large-scale lineaments and deformation zones, but the variation in intensity by size is inferred from a connectivity analysis. A comparison between the r_0-fixed geological and hydrogeological DFN models is further addressed in section 11.5.2.

In contrast to the TCM, TCMF and OSM+TFM geological DFN models, the r_0-fixed coupled size-intensity model avoids the use of surface data and, as a consequence, any incompatibility with the geological understanding of the site. The alternative conceptual model (OSM+TFM), which assumes a tectonic discontinuum at different size scales, better honours data derived from both small and large scales simultaneously. However, there is, to our knowledge, little support for such a model in the literature. Furthermore, the model does not explain the similarity between the orientation and mineralogy of fractures inside domains FFM01, FFM06 and even FFM03 and the respective, contiguous zones.

Confidence

There is high confidence in the occurrence of different fracture characteristics in the bedrock outside deformation zones in the target volume and, consequently, in the division of this bedrock into a more fractured near-surface volume, fracture domain FFM02, above less fractured rock volumes, fracture domains FFM01 and FFM06. This division is also supported by hydrogeological and hydrogeochemical data (see sections 11.5.2 and 11.7.2), although the exact position of the boundary between FFM02 and the fracture domains beneath is still associated with uncertainties. However, the most important remaining uncertainty concerns the DFN model for prediction of the size-intensity relationship of fracturing in the potential repository volume, i.e. fracture domains FFM01 and FFM06. The main reason for this is the lack of data on fracture sizes in these sub-surface domains. Direct data on fracture sizes in these domains can only be obtained from underground mapping, i.e. when the potential repository excavation has reached relevant depths. This uncertainty as well as the question of tectonic continuity at different size scales has been addressed with the help of alternative DFN models. These alternatives cover a broad range and are judged to bound the uncertainties.

11.3.4 Fracture mineralogy

Detailed studies of fracture mineralogy and wall rock alteration have provided information on the character and frequency of fracture minerals at Forsmark. Calcite and chlorite, partly associated with corrensite, are by far the most common minerals. Other common minerals are laumontite, adularia, quartz, albite and hematite, whereas prehnite, pyrite, clay minerals and epidote are less common. Rare occurrences of e.g. asphaltite and goethite are also observed.

The older generations of minerals, including epidote, which formed prior to 1.1 Ga, and adularia, which formed around 1.1 Ga or is older, show no depth dependence. In a similar manner, the wall-rock alteration associated with these mineral generations and referred to as oxidation also shows no depth dependence. These features are consistent with the conclusion that these minerals and the associated alteration formed a long time ago when this part of the bedrock was situated at considerably greater depths. The younger mineral asphaltite, which probably formed between c. 500 and 250 million years ago, occurs almost entirely in the upper part of the bedrock along open fractures. This is also the case for clay minerals and goethite that belong to the youngest generation of minerals, except for some occurrences at larger depths along fractures in zones. Since the current

bedrock surface is more or less the same surface as the sub-Cambrian peneplain, this distribution of fracture minerals with depth suggests that the near-surface bedrock, i.e. including fracture domain FFM02 in the target volume, has been affected by near-surface processes inferred to be related to loading and unloading cycles during the last c. 500 million years.

Uranium-rich phases are present in some of the fracture coatings, but only one small grain of pitchblende has so far been detected in a single fracture coating in one of the deterministically modelled gently dipping fracture zones (ZFMB1), located outside the target volume. The origin of these uranium-rich phases is largely unknown, but it can be concluded that uranium has been circulating in the fracture system during different periods throughout the geological history of the site. There is also evidence of redistribution and deposition of uranium irregularly along permeable structures during the Proterozoic (see section 9.5.7).

Fractures without mineral coating or filling have been observed in the near-surface realm in the bedrock, but are also present at greater depths. The significance and origin of these fractures are still uncertain. However, errors in the mapping procedure, the possibility that at least some of these fractures formed after the establishment of the sub-Cambrian unconformity and the occurrence of fresh, stress-release sheet joints in the near-surface realm merit consideration in any complementary investigation. Fractures without minerals are predominantly, but not exclusively sub-horizontal or gently dipping. Transmissive variants are present even in fracture domain FFM01.

11.3.5 Mechanical properties of deformation zones and fractures

Evaluation of the results from laboratory testing of the mechanical properties of fractures has shown that the deformability and strength properties of open discrete fractures are similar for different fracture sets. Furthermore, the properties of open fractures in fracture domain FFM01 and in deformation zones are quite similar. Empirical and numerical analyses of the data show that the deformation modulus and strength properties of the rock mass (including fractures) in fracture domains FFM01 and FFM06 are almost equal and representative of a stiff and strong rock (see Table 7-6 and Figure 11-16).

Confidence

The confidence in the derived mechanical properties of the rock mass is in general high, due to the large amount of data in support of the model and the small changes in values caused by the addition of new data during the various modelling stages. In addition, the results are consistent with the understanding of the geology at the site. The largest remaining uncertainty concerns the large-scale mechanical properties of fractures, since the model is based on test results on small samples.

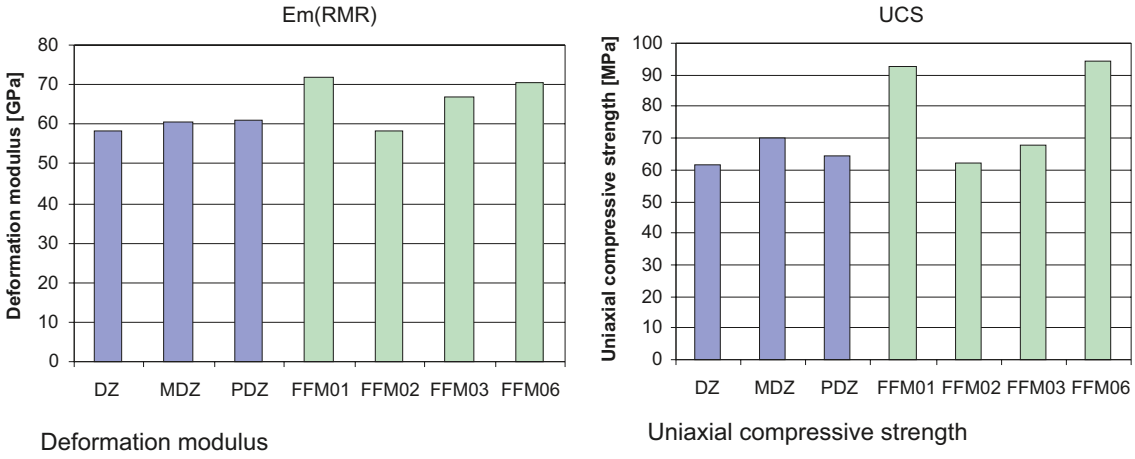

Figure 11-16. *Mean values of deformation modulus and strength properties of the rock mass in fracture domains and deformation zones as evaluated by an empirical approach (Figure 5-11 in /Glamheden et al. 2007a/). DZ = deformation zone, MDZ = minor deformation zone (shorter than 1,000 m), PDZ = possible deformation zone. Standard deviations as well as minimum and maximum values for fracture domains FFM01 and FFM06 are provided in Table 7-6.*

11.4 Rock stress

11.4.1 Stress evolution

The stress evolution is closely related to the deformational history of the site. According to the conceptual understanding (chapter 3 and section 11.3.1), the different sets and sub-sets of deformation zones at the site formed and had already been reactivated more than 900 million years ago in response to stress conditions affected by different tectonic events along active continental margins. The early establishment of these geological structures, and their response to subsequent tectonic events, and loading and unloading cycles connected with the burial and denudation of sedimentary rocks and glaciation and deglaciation, have most likely played an important role in the evolution of the stress in the bedrock in the Forsmark area, and specifically the bedrock inside the target volume.

The character of the bedrock close to the surface in the target volume, FFM02, is related to the unloading of the rock and the release of *in situ* stress. Reactivation of ancient fractures and even formation of new fractures (sheet joints) is apparent, at least close to the surface, during the Quaternary. The rock in the south-eastern part of the candidate area, FFM03, is spatially associated with a high frequency of gently dipping fracture zones containing both open and sealed fractures. These structural features are consistent with a general stress-released region.

11.4.2 Stress model

The assessment of the *in situ* stress state at the Forsmark site is based on both direct measurements and indirect observations. Data from direct measurements by overcoring, hydraulic fracturing and hydraulic tests on pre-existing fractures are available from a number of boreholes in fracture domains FFM01, FFM02 and FFM03. Indirect observations from boreholes in the same fracture domains include observations of core disking and borehole breakouts in c. 10 km of borehole walls down to depths of 1,000 m. In addition, estimates of the micro-crack porosity in samples from boreholes were used as indirect indicators in the evaluation of stress. Direct measurements as well as indirect observations all indicate a general orientation of the maximum horizontal stress in the range of N120° to 150° (Figure 11-17).

The stress model for the target volume (Figure 7-18 and Figure 11-18) is developed on the basis of data from overcoring measurements and evaluations of indirect observations, combined with the understanding of the geological conditions at the site and an evaluation of other external influencing factors such as topography, glacial rebound and crustal thickness. As shown by data and supported by findings from regional seismicity studies and the understanding of the deformational history at the site, the magnitudes of both the maximum and minimum horizontal stresses are greater than the vertical stress. The stress model implies a most likely value of the maximum horizontal stress of c. 41 MPa (Figure 11-18) and c. 23 MPa for the minimum horizontal stress at 500 m depth in fracture domain FFM01 in the target volume.

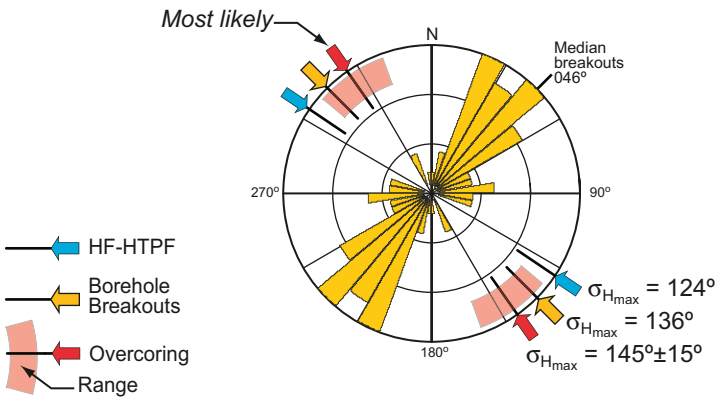

Figure 11-17. *Orientation of maximum horizontal stress from direct measurements by overcoring (OC) and hydraulic fracturing (HF and HTPF), and from indirect observations of borehole breakouts.*

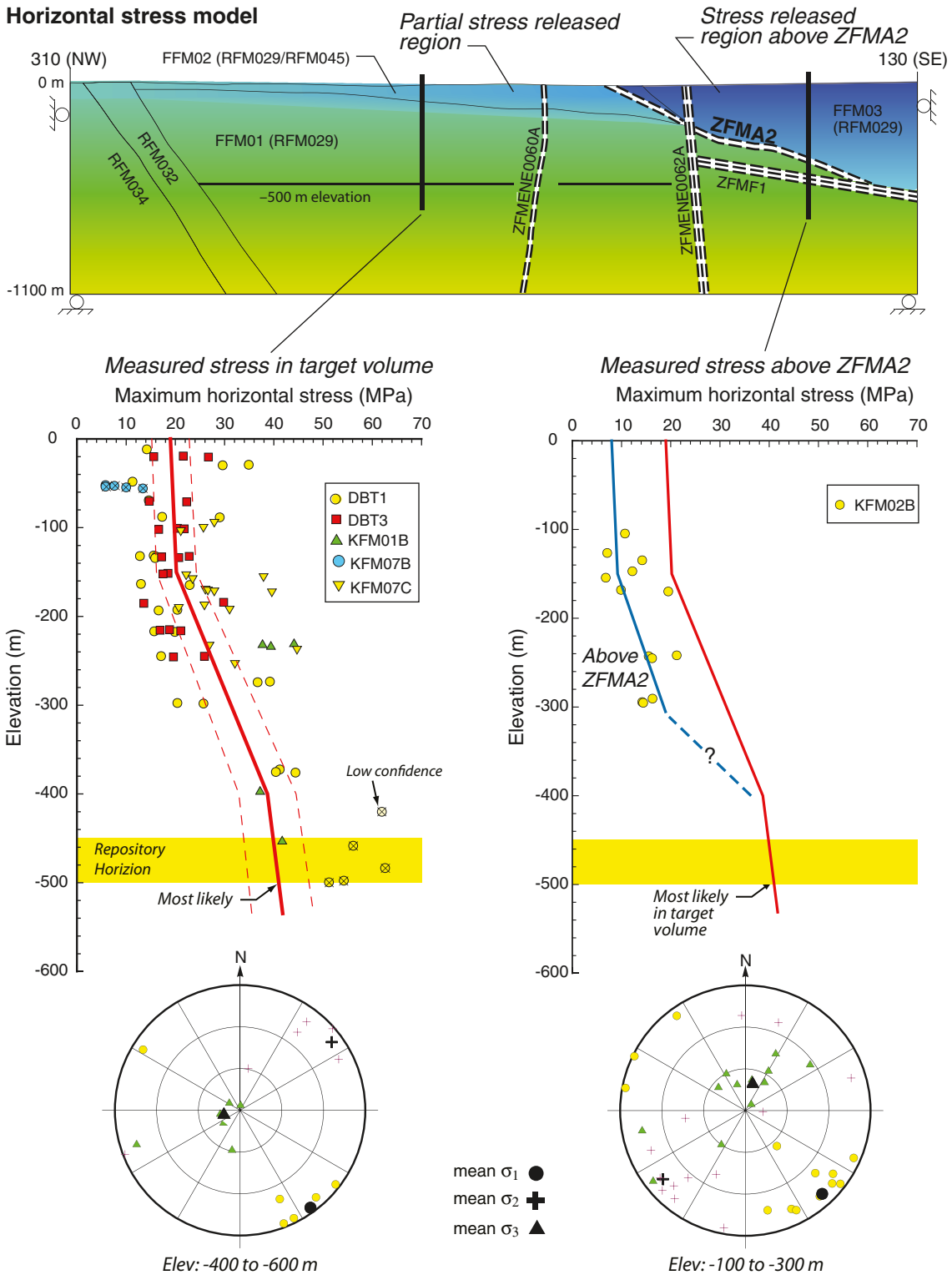

Figure 11-18. *Comparison of the measured maximum horizontal stress magnitudes in the target volume with those measured above the gently dipping deformation zone A2 (central insert). The change in slope in the target volume at c. 150 m depth corresponds approximately to the boundary between fracture domains FFM02 and FFM01. An illustration of the distribution of maximum horizontal stresses from numerical modelling is also shown (upper insert), with the blue shades representing reduced stress magnitudes caused by stress release above zone A2 and in fracture domain FFM02 compared with the "normal" stress magnitudes shaded green. The orientations of the measured principal stresses are shown in two lower hemisphere stereonets (lower insert). The principal stresses show generally consistent orientations regardless of depth and spatial location.*

In accordance with the site understanding and site data, the stress model implies that horizontal stress magnitudes are greater than the vertical stress at shallow depths in fracture domain FFM02 (Figure 7-18). In FFM01, the horizontal stresses continue to be greater than the vertical stress. The increase in the horizontal stress magnitudes with depth appears to correlate with the decrease in frequency of open fractures with depth and a corresponding increase in the rock mass stiffness. No stress measurements have been carried out in FFM06, but the *in situ* stress state is expected to be similar to that in FFM01, since it consists of a rock mass with similar stiffness properties and is located next to FFM01, below the gently dipping deformation zone A2.

Based on results of numerical modelling, it is inferred that the steeply dipping deformation zones in the target volume cause only small perturbations in the stress field, whereas the effect of the gently dipping zones A2 and F1 is more pronounced, with significantly higher stress magnitude below relative to that above these zones. The results further show that release of stress in the hanging wall has reached deeper levels south-east of zone A2 relative to that below and north-west of this zone, i.e. in the target volume (Figure 11-18). This is supported by results from overcoring measurements that show an average horizontal stress magnitude approximately 50% lower in the rock above zone A2 (fracture domain FFM03) compared with the horizontal stress magnitude measured at comparable depths in the target volume. Furthermore, these findings are consistent with the interpretation that the occurrence of the gently dipping zones favours stress release in the south-eastern part of the candidate volume.

Confidence

The confidence in the orientation of the rock stresses is high due to the consistency in results from the different measuring methods and indirect observations. It also agrees with regional seismic studies. The confidence in the vertical stress magnitude is also high, since measured values and theoretical values based on the weight of the overlying rock cover are in concordance. Uncertainty remains in the magnitude of the horizontal stresses at repository depth. However, an upper bound solution was used to constrain these stress magnitudes and hence it is judged that the uncertainty is sufficiently well constrained.

11.5 Bedrock hydraulic properties

11.5.1 Evolution

Geological data at the site, including the dating of fracture minerals, indicate that a large proportion of the fractures are sealed (c. 75%) and that the majority of the fractures are ancient structures, especially in the deeper parts of the bedrock in the target volume, i.e. fracture domains FFM01 and FFM06. The youngest generation of calcite occurs in fractures and deformation zones that are currently hydraulically conductive and may have precipitated during a long period including the present. Based on these observations and indications, it is conceptually attractive to envisage that the hydraulic properties of fractures can be correlated with both the brittle deformational history that formed and reactivated the fractures, and to the formation of fracture minerals during different periods in the past. In contrast, the analysis of transmissivity data versus normal stress suggests a poor correlation, if any (Figure 8-52). Most likely, the processes that occurred during the past 1.85 billion years overshadow an apparent coupling to the current stress field, which has existed for approximately the past 12 million years. Notwithstanding these considerations, the question of correlation may be scale dependent.

11.5.2 Hydraulic properties of deformation zones and fracture domains

Detailed information on the position of deterministically modelled deformation zones and water-conductive fractures in between deformation zones combined with results of high-resolution inflow measurements in 22 core-drilled boreholes and pumping tests in 32 percussion-drilled boreholes provide the basis for the assignment of hydraulic properties of deformation zones and fracture domains at the Forsmark site. These data constrain locations of connected flowing fractures with high certainty and values of the integrated transmissivity for the connected fractures down to c. 10^{-9} m^2/s. Results from single-hole injection tests and multiple-hole interference tests complement the data base.

Deterministically modelled deformation zones

Analyses of the hydraulic data have revealed that all deterministically modelled deformation zones, regardless of orientation, are characterised by a substantial decrease in transmissivity with depth, with a contrast of c. 20,000 times over the uppermost 1,000 m of the bedrock (Figure 11-19 upper insert). The lateral heterogeneity at each depth is also substantial, but more irregular, suggesting a channelled flow-field within the planes of the deformation zones. Furthermore, the data show that the gently dipping deformation zones, which predominantly occur in the south-eastern part of the candidate volume, are the most transmissive at each depth (Figure 11-19 upper insert). The steeply dipping deformation zones that strike WNW and NW and border the candidate area form structures with a second order of importance as far as transmissivity is concerned. These observations provide support to the hypothesis that involves a pronounced hydraulic anisotropy on a regional scale, where the largest transmissivities observed are associated with deformation zones that are oriented at a high angle to the minimum principal stress or sub-parallel to the maximum horizontal stress, respectively.

In the model, the observed vertical and lateral heterogeneity in transmissivity of the zones are both honoured. An exponential decrease in transmissivity with depth is assigned based on the depth trend in the data. The lateral heterogeneity in transmissivity is represented statistically as a lognormal distribution at each depth based on the variability observed in the data.

Fracture domains

The hydraulic characterisation of the rock in between deformation zones supports the division of the bedrock into different fracture domains (see section 8.4.2 and Table 8-5). In addition, the hydraulic data suggest that the subsurface fracture domain FFM01, located in the target bedrock volume, should be further divided into three depth intervals (Figure 11-19, lower left insert). Below 400 m depth, very few flowing fractures occur, and these are predominantly sub-horizontal fractures with an average spacing of c. 200 m. However, it should be noted that the frequency of flowing fractures below 400 m is so low that it is highly speculative to define an average separation. Above 400 m depth, the frequency of flowing fractures is somewhat higher up to about 200 m depth. Above 200 m depth, there is a significantly higher frequency of flowing fractures, not least fractures with high transmissivities. In FFM03, there are far less boreholes to substantiate an analysis of hydraulic subdomains, but as indicated in Table 8-5 in section 8.4.2 and shown in Figure 11-19 (lower right insert), there is also some depth dependence in this domain.

The geometric and hydraulic properties of fractures in the rock between the deterministically modelled deformation zones are represented by DFN models calibrated against corrected open fracture frequency $P_{10,corr}$, the corrected *flowing* fracture frequency $P_{10,PFL,\ corr}$ and the spatial distribution of inflow expressed as the specific capacity *Q/s* recorded with the Posiva Flow Log (PFL-f). This calibration is made for fracture domains FFM01, FFM02 and FFM03 (Figure 11-20). Fracture domain FFM06 is inferred to have the same properties as fracture domain FFM01 (cf. Figure 8-18 and Figure 8-22). Whereas the geological DFN modelling is based on the corrected frequency of *all* fractures $P_{10,all,corr}$, the hydrogeological DFN focuses on the corrected frequencies of *open* fractures $P_{10,open,corr}$, and *flowing* fractures $P_{10,PFL,corr}$. A comparison shows a reasonable agreement between these two models (see Figure 8-33 to Figure 8-35). The division into hydraulic subdomains honours the variation in the intensity and size of open fractures with depth inside fracture domain FFM01.

Uncertainties in transmissivity of the connected fracture network are handled by alternative assumptions concerning the possible relationships between fracture transmissivity and size (correlated, semi-correlated and uncorrelated). Although it is difficult to establish which of these models may best reflect reality, all three models yield similar ranges of transmissivities for fractures in the size range 10 to 100 m. For this reason, the three models are likely to show similar flow characteristics. It should be noted that the groundwater flow and solute transport simulations used solely the semi-correlated transmissivity-size model.

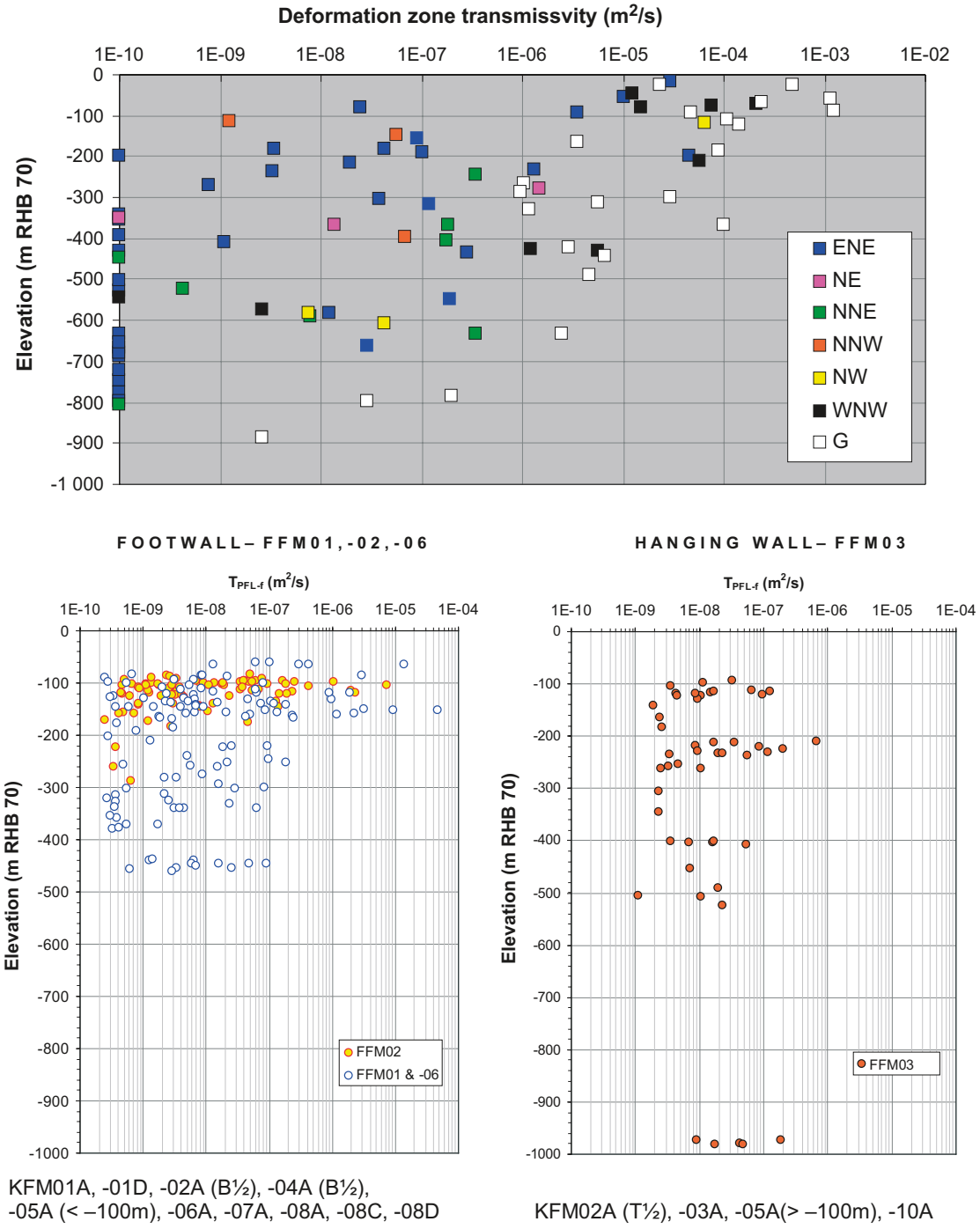

Figure 11-19. *Top: Inferred transmissivities of deformation zones with depth and orientation. Bottom: Inferred transmissivities of connected open fractures with depth in FFM01 and FFM02 (left) and FFM03 (right).*

Uppermost part of the bedrock

There are three pieces of evidence that indicate a well-connected network of highly transmissive structures in the uppermost c. 150 m of the bedrock in the target volume where fracture domain FFM02 occurs: 1) exceptionally high water yields in the percussion-drilled boreholes, 2) the nearly uniform groundwater levels in the uppermost part of the bedrock, and 3) the extensive and rapid transmission of fluid pressure changes during the large-scale interference tests conducted within the target volume. These structures are inferred to be large sub-horizontal fractures, so-called sheet joints, which are known to exist close to the surface (Figure 11-2).

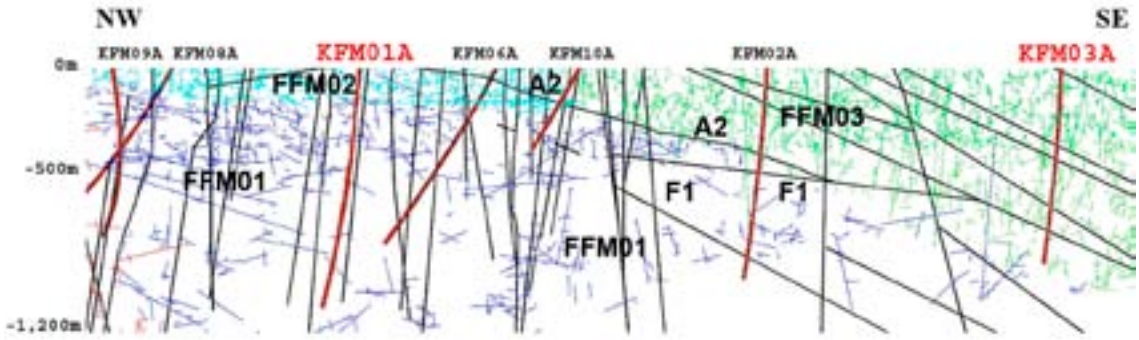

Figure 11-20. *One example of a realisation of the hydrogeological DFN model showing connected open fractures, coloured by fracture domain, in a NW-SE cross-section. The highlighted boreholes, KFM01A and KFM03A, are located in the footwall and the hanging wall of zones A2-F1, respectively. The deterministically modelled deformation zones are shown in black /Follin et al. 2008b/. The effect of the low connectivity below 400 m depth in fracture domain FFM01 is apparent.*

The network is found to short circuit the recharge from above as well as the discharge from below. This is hydrogeologically conceptualised as a shallow, anisotropic, bedrock aquifer on top of a thicker segment of bedrock with aquitard type properties. Based on the occurrence of high transmissivities, the lateral extent of this bedrock aquifer is envisaged to correspond approximately to the lateral extent of fracture domain FFM02. However, the hydrogeological data indicate that this network of structures probably extends to the north-east as far as the Singö deformation zone.

Confidence

In general, there is a high confidence in the bedrock hydrogeological model of the site and the assignment of hydraulic properties. The main reason for this assertion is the consistency between different types of hydraulic data, which all support the presence of anisotropic hydrogeological conditions in the area. These conditions are: 1) high transmissivity in the gently dipping fracture zones outside the target volume, 2) few flowing fractures at depth in the target volume (FFM01 and FFM06), and 3) a highly transmissive system of fractures, including sheet joints, in the near-surface realm inside the target volume (FFM02), which are connected over long distances. The various types of hydraulic data are also consistent with the understanding of the geology and the rock stresses at Forsmark (see section 11.6) and are also supported by the groundwater chemical data (see section 11.7.2).

Uncertainties remain in the hydraulic properties of deformation zones and fractures south-west and north-east of the tectonic lens and target volume. The most important of these concerns the hydraulic character of the regional Singö deformation zone close to the north-eastern border of the tectonic lens, and the hydraulic properties further downstream of the target volume. Although interference tests conducted show no hydraulic contact between the north-eastern part of the target volume and the bedrock on the north-eastern side of the Singö deformation zone, where the SFR repository is situated, it cannot be excluded that such hydraulic connections exist at other locations along this regionally significant zone.

The implementation of the geometry and hydraulic properties of fracture domains and deformation zones and the shallow bedrock aquifer into a numerical model (ConnectFlow) have revealed that the model can be matched to results of large-scale interference tests, to observed natural point-water heads in percussion holes and soil pipes, and to the concentrations of various species measured in groundwater samples from boreholes (see section 11.7.3). However, there is some concern whether the measured groundwater levels (point-water heads) are natural or disturbed, e.g. disturbed by the abstraction of drainage water at SFR. These uncertainties were revealed during the calibration process of the numerical models, and are discussed in section 8.9.1. Even if the abstraction of drainage water in the SFR repository is an uncertain boundary condition that may affect the natural groundwater levels, it is concluded that the hydraulic stresses (drawdowns) induced by the cross-hole tests run in the target volume are sufficiently strong to allow for a fair calibration

of the hydraulic properties. Indeed, the magnitudes of the hydraulic gradients derived from the groundwater flow model using these calibrated properties are quite reasonable, see section 8.7.2. In contrast, the gradients inferred from the field measurements of the natural groundwater flow in deep boreholes are much higher and generally exceed the maximum possible topographic gradient at the site by orders of magnitude. This is discussed in more detail in section 8.7.2.

11.6 Integrated fracture domain, hydrogeological DFN and rock stress models

An important prerequisite for confidence in the understanding of the site involves consistency between the models derived in an independent manner from different sets of data in different disciplines (see section 11.9.4 and /Follin et al. 2008b/). This section addresses the consistency between three distinct models of the north-western part of the candidate volume. For purposes of comparison, these three models are visualised along a NW-SE profile inside the north-western part of this volume (Figure 11-21). The models include:

- the geological model for the spatial distribution of fracture domains FFM01, FFM02, FFM03 and FFM06 that focused on the spatial variation in the frequency of particularly open fractures in the bedrock,
- the hydrogeological DFN models for the fracture domains that focused on the spatial variation in the size and intensity of connected open fractures, i.e. the fractures that are important from a hydrogeological viewpoint, and
- the local model for the spatial variability in the magnitude of the maximum horizontal stress.

Fracture domain FFM03 in the hanging wall to the gently dipping zones ZFMA2 and ZFMF1 (Figure 11-21) was defined on the basis of an inferred even distribution of open fractures with depth and is contiguous with a bedrock volume containing abundant gently dipping fracture zones. This contrasts sharply with the bedrock further to the north-west in the footwall to these gently dipping zones. Modelling work has shown that connected open fractures are also more evenly distributed in the hanging wall to the gently dipping zones A2 and F1 (Figure 11-21). Furthermore, the maximum horizontal stress is reduced in this domain relative to that in the bedrock volume further to the north-west (Figure 11-21). The even distribution of open fractures and the occurrence of gently dipping fracture zones are consistent with a general stress-released volume. Indeed, the fracture characteristics may have inhibited a more significant build-up of horizontal stresses in this bedrock volume.

The bedrock in the footwall to the gently dipping zones ZFMA2 and ZFMF1 (Figure 11-21) is far more inhomogeneous especially with respect to the distribution of open fractures. This attribute, together with some consideration for increased alteration (albitization) in fracture domain FFM06, formed the basis for the recognition of three different fracture domains in this volume (FFM01, FFM02 and FFM06). An increased intensity of connected open fractures and reduced maximum horizontal stress characterise the upper part of the bedrock in the footwall to zone A2, and this volume corresponds more or less to fracture domain FFM02 (Figure 11-21). A striking consistency between the different models concerns how the intensity of connected open fractures and the stress-released volume conform with the increased thickness of domain FFM02 as the gently dipping zone A2 is approached (Figure 11-21). It is suggested that this change with respect to zone A2 is related to the increased frequency of sub-horizontal and gently dipping fractures in the vicinity of this zone. Since these structures are oriented at a high angle to the vertical stress, which corresponds to the minimum principal stress, there is a more favourable environment for the modification of the aperture of ancient fractures and even formation of new stress-release joints and, consequently, the more pronounced release of stress closer to the A2 zone (see also section 11.3.1).

In contrast, the major part of fracture domains FFM01 and FFM06 inside the target volume, including especially the potential repository volume around 500 m depth, is characterised by relatively few open fractures, a compartmentalised pattern close to the percolation threshold for the connected open fractures and higher maximum horizontal stress. It is inferred that the low intensity of open fractures favoured a more significant build-up of horizontal stresses. The character of the connected open fractures in this volume implies restricted groundwater circulation.

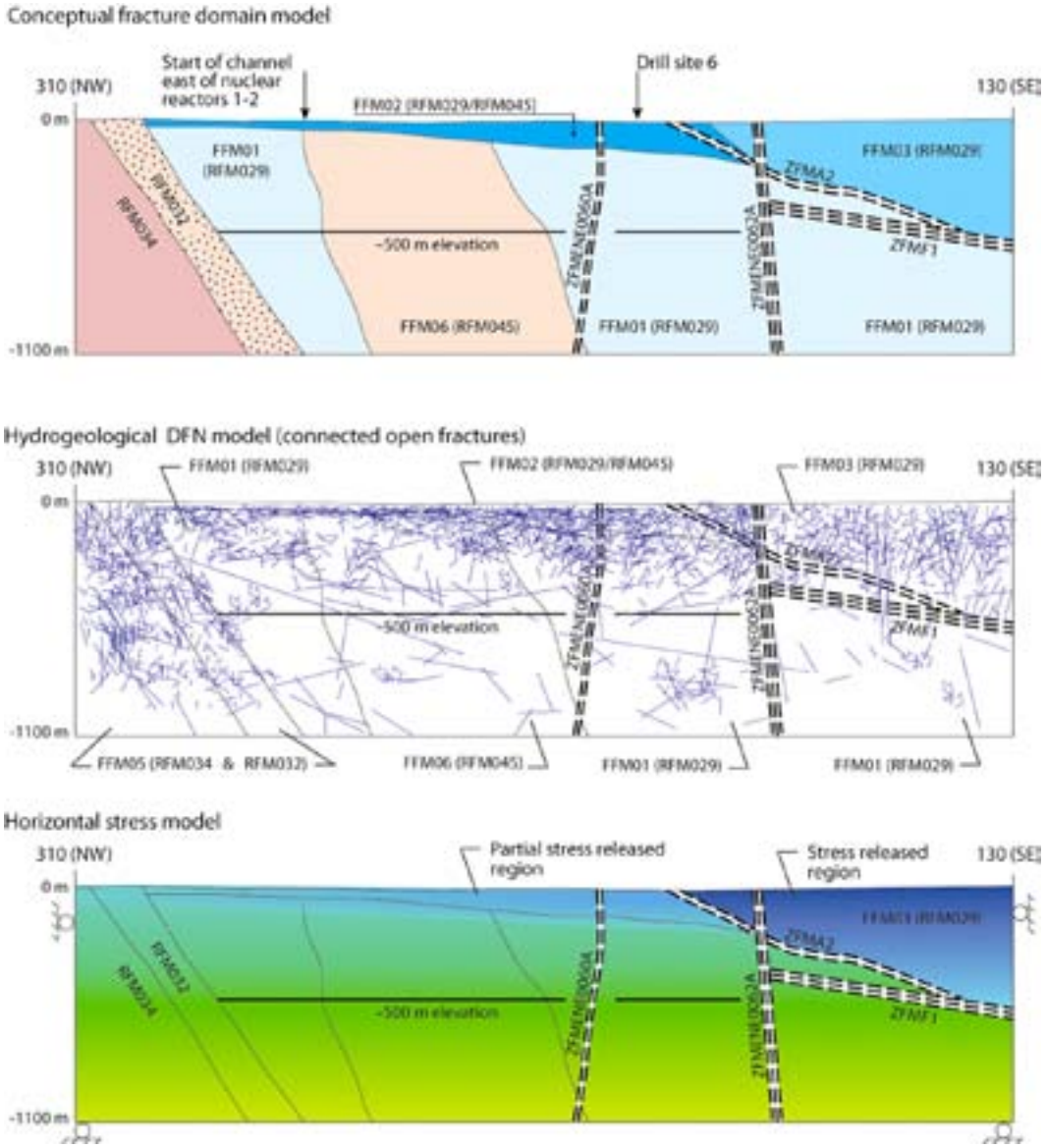

Figure 11-21. *Comparison of fracture domain, hydrogeological DFN and maximum horizontal stress models along a NW-SE profile in the north-western part of the candidate volume. The profile line is similar to that shown in Figure 11-12.*

In summary, a bedrock volume where there is a limited number of open fractures and, by corollary, a low permeability is consistent with higher rock stresses. However, the properties of such a bedrock are affected by the stress-released conditions in the near-surface realm and close to gently dipping ancient structures.

11.7 Groundwater

11.7.1 Evolution during the Quaternary period

Several water types which are now present in the bedrock can be associated with past climatic events during the Pleistocene, including inter-glaciations, glaciations, deglaciations, and associated changes in the shore level in connection with transgressions and regressions. Among these, the last glaciation and the post-glacial period (the Holocene) are the most important for the groundwater development in the Fennoscandian Shield, especially in terms of land uplift and shoreline displacement, as well as the development of the Baltic Sea.

The post-glacial development during the Holocene (Figure 11-22) reveals that when the continental ice melted and retreated from the Forsmark area around 8800 BC, glacial meltwater was hydraulically injected under considerable pressure into the bedrock. The exact penetration depth is unknown, but, according to results of generic hydrogeological modelling, depths exceeding several hundred metres are possible /Jaquet and Siegel 2003/. Since the deglaciation of the Forsmark region coincided with the end of the Yoldia period, there are no signs of Yoldia Sea water in the bedrock. The Ancylus Lake (8800 to 7500 BC) was lacustrine and developed after the deglaciation. This period was followed by the brackish Littorina Sea (after 7500 BC). During the Littorina Sea stage, the salinity was considerably higher than at present, reaching a maximum of about 15‰ in the period 4500 to 3000 BC. Dense brackish seawater from the Littorina Sea penetrated the bedrock, resulting in a density intrusion that affected the groundwater in the more conductive parts of the bedrock. When the first parts of the Forsmark region subsequently emerged from the sea, starting c. 500 years BC, recharge of meteoric water subsequently formed a freshwater layer on top of the saline water because of its lower density. As a result of the flat topography of the Forsmark area and of the short period that has elapsed since it emerged from the sea, the out-flushing of saline water has been limited, and consequently a freshwater layer is only present at shallow depth.

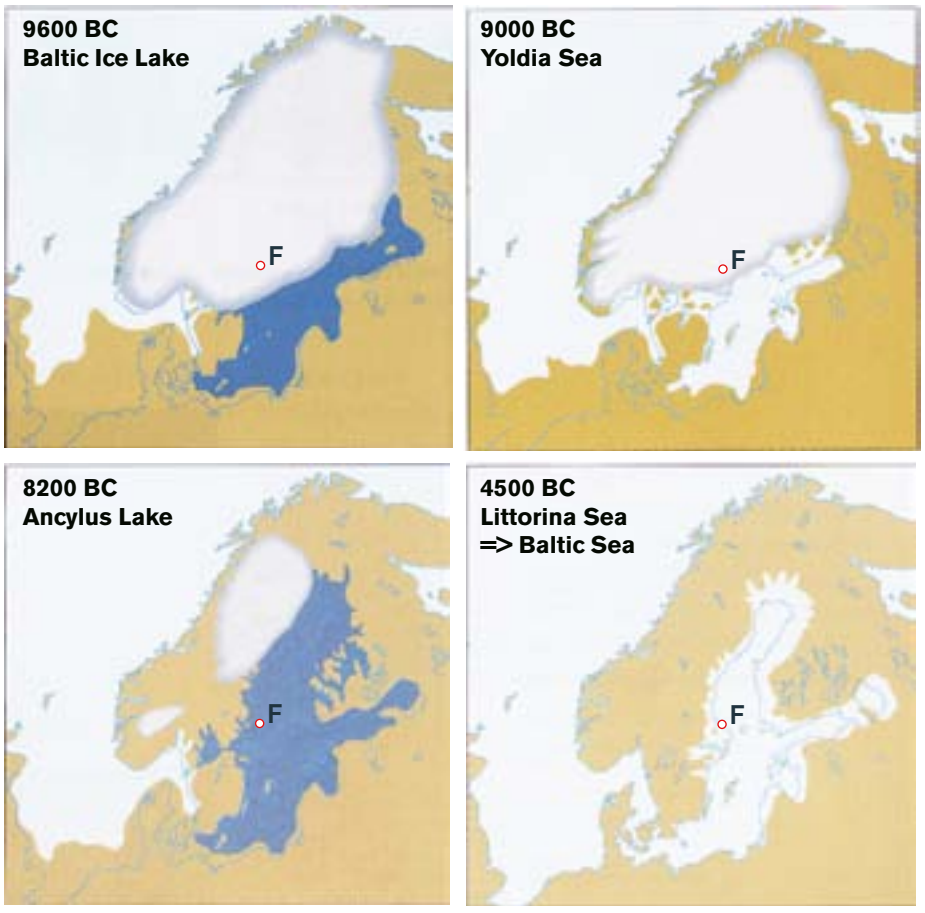

Figure 11-22. *Map of Fennoscandia with some important stages during the Holocene period. Four main stages characterise the development of the aquatic systems in the Baltic basin since the latest deglaciation: the Baltic Ice Lake (13,000–9500 BC), the Yoldia Sea (9500–8800 BC), the Ancylus Lake (8800–7500 BC) and the Littorina Sea 7500 BC-present). Fresh water is symbolised with dark blue and marine/brackish water with pale blue (modified after /Fredén (ed) 2002/). The Forsmark area (notated 'F') was probably at or close to the rim of the retreating ice sheet during the Yoldia Sea stage.*

The Quaternary evolution has affected the groundwater chemistry at Forsmark, especially in the more conductive parts of the bedrock, but changes in chemistry are not restricted to post-glacial time. There is groundwater and porewater evidence that indicates an old (pre-Holocene) meteoric water that originated during a warm climate. The age of this component is unknown, but possibilities include pre-Pleistocene or even older. The hydrogeochemistry of the Forsmark area cannot be explained without recognising this older component. The present groundwaters therefore are a result of mixing and reactions over a long period of geological time. The interfaces between different water types are not sharp due to molecular diffusion, but reflect variability in the structural-hydraulic properties.

11.7.2 Groundwater composition

Explorative analyses of groundwater chemistry data measured in samples from cored boreholes, percussion boreholes and soil boreholes, and hydrogeochemical modelling have been used to evaluate the hydrogeochemical conditions at the site in terms of origin of the groundwater and the processes that control the water composition. Although the data set is rather limited, the results have revealed that the current groundwater composition in general supports the occurrence of different hydrogeological regimes in the candidate volume, i.e. the bedrock at depth in the target volume, the uppermost part of the bedrock in the target volume and the rock south-east of the gently dipping zone A2 with its swarm of gently dipping fracture zones (see Figure 11-20).

Groundwater in fractures

Groundwaters in the uppermost 100 to 200 m of the bedrock display a wide range of chemical variability, with chloride concentrations in the range 200 to 5,000 mg/L (Figure 9-5 and Figure 11-23) suggesting influence of both brackish marine water (i.e. recent Baltic or old Littorina Sea relicts) and meteoric waters. In the bedrock in the footwall to zone A2 including fracture domain FFM02, this

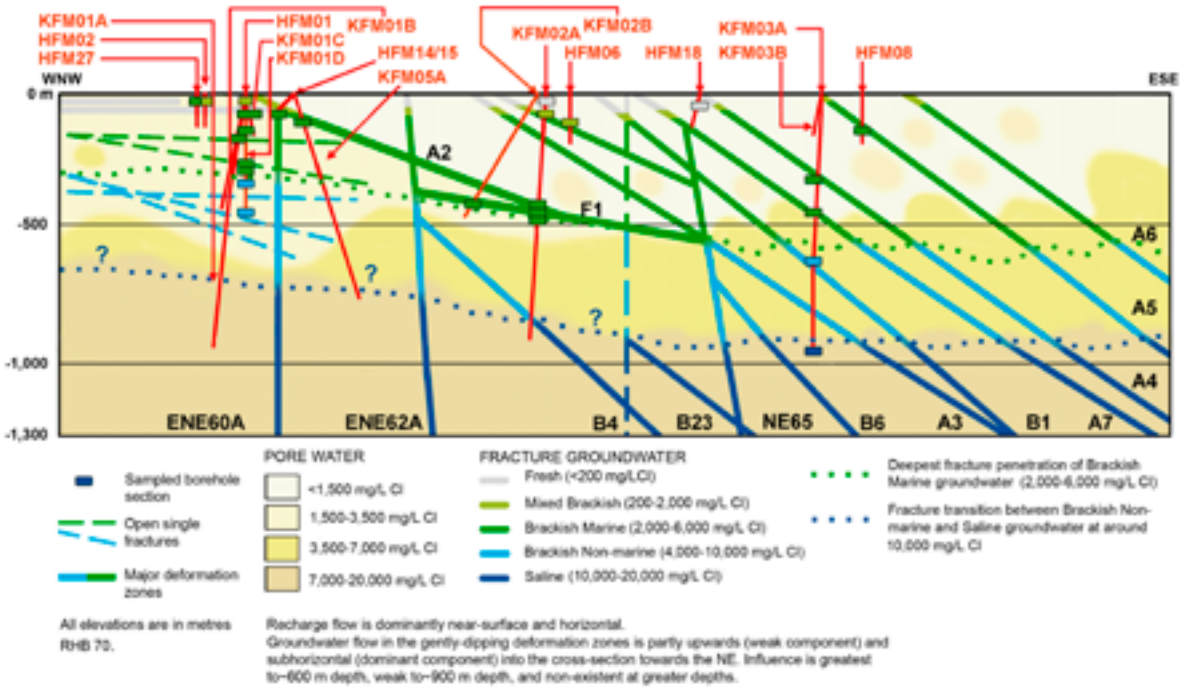

Figure 11-23. *Illustration of the groundwater composition along a WNW-ESE cross-section through the candidate area at Forsmark as interpreted from hydrogeochemical data. The location of the boreholes and the sections that have been sampled are shown together with the main fracture groundwater types that characterise the site. The chloride distribution with depth along the fracture zones and single open fractures, as well as the subdivisions of the rock matrix porewater based on chloride concentration are also shown. The dotted lines in different colours crossing the section represent the approximate depths of penetration of the major groundwater types along hydraulically-active fracture zones (Figure 6-3 in /Laaksoharju et al. 2008a)/.*

shallow system is controlled by flow along highly transmissive, sub-horizontal fractures and sheet joints (i.e. the shallow bedrock aquifer), which is still in the process of flushing out residual brackish marine (Littorina) groundwaters. Furthermore, a sharp decrease in tritium content at about 150 m depth, as well as carbon-14 data, indicate that these shallow groundwaters have short residence times that are in the order of only a few decades to a few hundred years.

At depths larger than c. 200 m, the water composition is indicative of a brackish marine water with chloride concentrations in the range 2,000 to 6,000 mg/L and with a clear Littorina Sea component, as indicated by concentrations of magnesium and the ratio of bromide to chloride concentrations (Figure 9-5 and Figure 11-23). This water type is recognised down to 600 to 700 m depth in the transmissive gently dipping fracture zones in the south-eastern part of the candidate volume, contiguous with fracture domain FFM03, whereas the penetration depth in fracture domain FFM01 in the target volume, where the frequency of water-conducting fractures is low, is restricted to c. 300 m. Below these depths in FFM01, the water composition indicates brackish to saline non-marine groundwaters (i.e. an absence of Littorina Sea influence), reflecting processes which have occurred prior to the intrusion of the Littorina Sea waters. These deep waters further show an increase in calcium with depth, which is a well recognised trend and indicative of water/rock interactions that occur under increasingly low flow to stagnant groundwater conditions with increasing depth.

Composition of rock matrix porewater

Analyses of the composition of rock matrix porewater also support the occurrence of low groundwater turnover in fracture domain FFM01. Porewater from this domain generally has a lower chloride content and is enriched in oxygen-18 compared with the fracture groundwaters, indicating a transient state between the porewater and groundwater down to at least 650 m depth (Figure 11-23). A signature with low chloride, low magnesium and enriched in oxygen-18 has been preserved far away from conducting fractures, suggesting that these porewaters have evolved from an earlier, very long lasting circulation of old dilute groundwaters in a few fractures. This is also consistent with the still prevailing transient state between this porewater and fracture groundwaters from equivalent depths which, based on chlorine-36 and helium-4 dating, have residence times of more than 1.5 Ma.

South-east of the target volume in the hanging wall rock to zone A2, a situation close to steady-state is suggested between porewater and fracture groundwater down to about 200 m below the surface, reflecting the high frequency of water conducting, gently dipping fracture zones, and the rapid circulation of significant volumes of water in this area (Figure 11-23). At greater depth, the porewater has lower chloride contents than the fracture groundwater indicating a transient state down to approximately 650 m depth. The lower chloride content and an isotope signature increasingly depleted in ^{18}O with increasing depth indicate that the porewater in these gently dipping zones probably stores a dilute water with a cold-climate signature. The significantly negative $\delta^{18}O$ values preserved far from the water-conducting fractures indicates that this cold-climate signature was a glacial water circulating for a considerable time period in the fractures at these depths. Since the last deglaciation, the porewater signature has become overprinted with a Littorina- and/or a Baltic-type signature as indicated by chloride, magnesium and oxygen-18 in porewaters sampled closer to the conducting fractures.

On-going reactions

Whilst mixing (both advection-dispersion and molecular diffusion) is the major process giving rise to present-day groundwater compositions, the role of reactions has also been addressed. In particular, the alkalinity and redox buffering capacity of the bedrock is of key importance for groundwater composition and future changes due to, for example, potential infiltration of dilute and oxidised water.

The presence of limestone (calcite) and extensive biogenic activity in the Quaternary overburden give rise to pH values usually above 7, calcium concentrations mostly between 50 and 200 mg/L and bicarbonate concentrations in the range 200 to 900 mg/L in the near-surface waters (down to c. 20 m depth). Concentrations then decrease to very low values at greater depths. However, bicarbonate is relatively high in most of the brackish marine groundwaters hosted in the upper 600 m of the gently dipping fracture zones south-east of the target volume, whereas brackish non-marine groundwaters below 300 m in fracture domain FFM01 have low bicarbonate contents.

The pH buffering capacity in Forsmark groundwaters at depths greater than 100 m appears to be controlled by the calcite system, and modelling indicates that this water is in equilibrium with calcite. Investigation of fracture minerals shows that calcite in fractures is abundant and that no extensive leaching has occurred in response to past glaciation/deglaciation events. These findings suggest that the buffering capacity against infiltrating dilute groundwater is sufficient to ensure that such groundwaters will not have a significant influence at repository level, although no quantifications have yet been made. However, a study aiming at quantification of fracture minerals is currently on-going and will be reported separately as a complement to the site descriptive modelling reports.

According to data analyses and modelling of the redox system, reducing conditions currently prevail at depths greater than c. 20 m. Most of the Eh values determined in brackish groundwaters (at depths between 110 and 646 m) seem to be controlled by the occurrence of an amorphous iron oxyhydroxide with higher solubility than a truly crystalline phase. This indicates that the iron system is disturbed. This conclusion is supported by mineralogical investigations that have identified the presence of fine-grained amorphous to poorly crystalline phases now evolving towards more crystalline phases. Dissolved sulphide concentrations are systematically low, possibly due to the precipitation of amorphous Fe(II)-monosulphides, linked to the activity of sulphate-reducing bacteria (SRB). At depths greater than 600 m, the dissolved sulphide concentrations increase, which is consistent with the occurrence of SRB and with the active precipitation of Fe(II)-monosulphides. The iron system at these depths seems to be limited by crystalline oxides, mainly hematite.

Elevated concentrations of uranium have been detected in groundwaters associated with a Littorina Sea component and the highest concentrations are found in waters in the gently dipping fracture zones south-east of the target volume. There are indications that these elevated concentrations are related to easily dissolvable uranium fractions in fracture coatings in contact with these waters (see also section 11.3.4). Speciation-solubility calculations support this conclusion and indicate that the high uranium contents are the result of the control exerted by an amorphous (and very soluble) uranium phase present in the system, and the weakly reducing Eh values that may allow uranium complexation and re-equilibration depending on Eh and dissolved carbonate.

The presence of goethite (FeOOH) in some hydraulically active fractures and fracture zones in the upper part of the bedrock (Figure 11-24), mainly within the gently dipping fracture zones A2 and F1, indicates circulation of oxygenated fluids during some period in the past (potentially during the Quaternary). However, the presence of pyrite in the same zones suggests that the circulation of oxygenated fluids has been concentrated along channels in which different redox micro environments may have been formed. Mobilisation as well as deposition of uranium in the upper 150 m of the bedrock is indicated by U-series decay analyses of fracture coatings.

The analyses of the current redox system at Forsmark have consistently indicated that sampling (or drilling-induced) perturbation may have altered the original redox conditions of the hydrogeochemical system. Examples include oxygen intrusion and precipitation of amorphous iron oxyhydroxides, as indicated by the colloidal composition (see section below) and mineralogical determinations. Additionally, there could have been modification of the original Eh and/or alkalinity by drilling waters, and an increase in dissolved uranium contents and changes in sulphide contents could have been caused by one or more of these disturbances. Despite these potential disturbances, the buffer capacity of the system maintains a substantially reducing character. As far as the potential

Figure 11-24. *Fracture coating along an open fracture in KFM01C (78.31–78.48 m). The coating consists of goethite, clay minerals, chlorite and minute grains of calcite.*

redox buffering capacity of the fracture system is concerned, it is concluded that previous oxidising episodes have not been intense enough to exhaust the reducing capacity of fracture-filling minerals, which are still present in the shallow system (for example chlorite and pyrite). Any potential build up of reducing capacity in the fracture minerals during recent periods of reducing groundwater conditions is difficult to estimate, but it can be concluded that the amounts of recent (Quaternary) minerals formed is very small.

Dissolved gas and colloids

Analyses of gas dissolved in groundwater at Forsmark have shown that the gas content increases with depth, but the waters are far from being oversaturated by gas. The major gas components are nitrogen and helium. Methane has also been detected, but generally in small amounts (less than 0.2 mL/L). Currently, it is not known whether the methane is of biogenic or non-biogenic origin.

Colloid amounts in Forsmark groundwater are comparable to those found in other granitic environments. The colloids are composed mainly of iron and sulphur compounds. Uranium associated with the colloids has been found in boreholes KFM02A and KFM06A, in line with the high groundwater uranium concentrations found in these boreholes. The uranium content of the colloids is approximately 10% of the uranium concentration in the groundwater and colloidal transport is, therefore, a result, but not the origin, of the high uranium content in the groundwater.

Confidence

There is generally high confidence in the description and understanding of the current spatial distribution of groundwater composition, mainly due to the consistency between different analyses and modelling of the chemical data, but also due to the agreement with the hydrogeological and structural geological understanding of the area. Furthermore, the existence of a near-surface redox reaction zone appears to be well-established, even if there is uncertainty in the data interpretation, and the common occurrence of calcite suggests that there is buffering capacity against the effects of penetration of dilute groundwater. Even though quantification is not yet available, this indicates that the bedrock at Forsmark has a large alkalinity and buffering capacity for maintaining pH values in the range 7 to 8.5 and Eh values lower than –140 mV. One important remaining uncertainty concerns the increase in sulphide concentrations measured in the on-going monitoring programme. Initial drilling and pumping may have disturbed the system or may have facilitated sulphate reduction. However, this issue remains to be resolved.

11.7.3 Groundwater flow and evolution of groundwater composition

The palaeo-evolution of groundwater composition at Forsmark during the last c. 10,000 years, i.e. during the Holocene, has been simulated in the palaeo-hydrogeological modelling work (see section 8.7.1 and /Follin et al. 2008b/) and the results compared with measured concentrations of different elements in the boreholes (Figure 8-46 to Figure 8-50). The conceptual model for the present-day distribution is illustrated in Figure 11-25 and should be compared with the hydrogeochemical site descriptive model described in Figure 11-23.

The initial conditions for the palaeo-hydrogeological simulations that start at 8000 BC are defined in terms of the presence of mixtures of different reference waters in the bedrock. These conditions are derived on the basis of analyses of present-day water composition in fractures and matrix porewater, which reveal that there must have been old meteoric waters derived from both warm and cold climate events in the bedrock in the Forsmark area before the injection of *Glacial Melt Water* during the last deglaciation just prior to the Holocene.

The results of the simulation with the hydrogeological model implemented in ConnectFlow show fair agreement with measured concentrations of chloride, the bromide/chloride ratio, $\delta^{18}O$ and bicarbonate concentrations in the boreholes. Furthermore, the model predicts deeper penetration of Littorina Sea Water along the gently dipping fracture zones intersecting fracture domain FFM03 south-east of the target volume (down to c. 500 to 600 m depth) than in steeply dipping deformation zones intersecting fracture domain FFM01 inside the target volume (down to c. 300 to 400 m depth). Although not matching the exact concentrations, the model also predicts higher salinity in the fracture water than in the rock matrix porewater, which is consistent with the field observations (Figure 11-23).

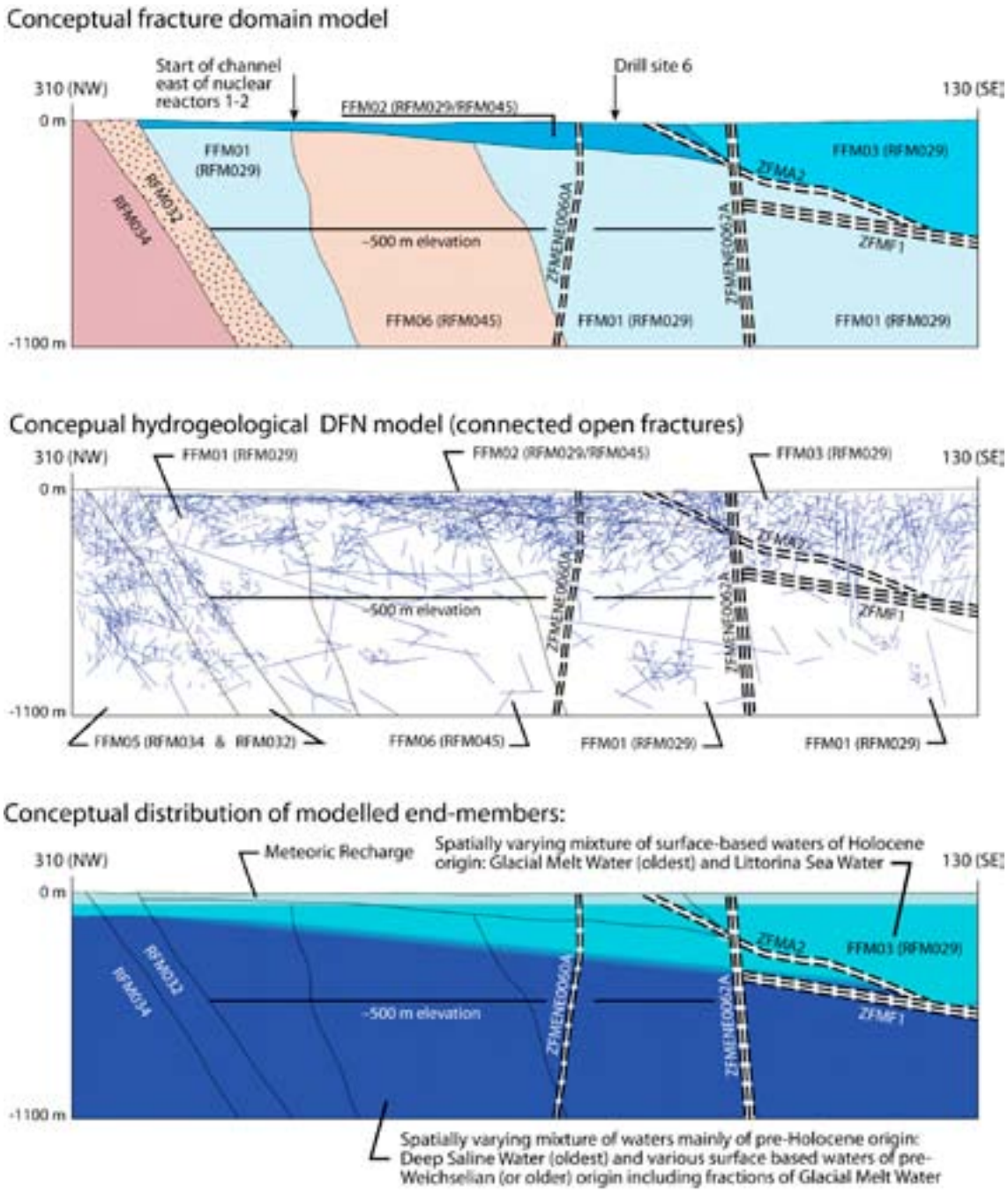

Figure 11-25. *Comparison of conceptual models for fracture domains, hydrogeological DFN and the present-day distribution of different end members along a NW-SE profile in the north-western part of the candidate volume. The profile line is similar to that shown in Figure 11-12 and includes that in Figure 11-23.*

The palaeo-hydrogeological simulations also support the hydrochemical observations in surface water and shallow groundwater, which indicate that there is probably no ongoing deep discharge of deep saline water into the freshwater surface system within the area covered by the well-connected and highly transmissive network of fractures and sheet joints in the uppermost c. 150 m of the bedrock. Furthermore, the simulation results are consistent with the field observations of relict marine remnants, which also include deep saline signatures, in the groundwater at relatively shallow depths in the Quaternary deposits in restricted areas outside this network of structures in the upper part of the bedrock. One such area is Lake Gällsboträsket, which coincides with the Eckarfjärden deformation zone (Figure 8-57).

A comprehensive uncertainty analysis with focus on hydraulic parameter heterogeneity within the target volume was performed for the calibrated *deterministic base model simulation* and sensitivities were evaluated. The results demonstrate that model calibration against hydrochemical data is sensitive to parameter heterogeneity in the bedrock hydrogeological properties (Figure 8-68), which is expected in a sparsely fractured rock mass.

11.8 Transport properties

11.8.1 Properties of the rock matrix

The development of the retardation model for solute transport in the bedrock relies to a large extent on interaction with other disciplines; primarily geology, hydrogeology and hydrogeochemistry. Specifically, geology provides lithological and structural models in which the rock types, fractures and deformation zones are described, as well as the mineralogical compositions of intact and altered materials. Hydrogeochemical information is used as a basis for the selection of water compositions in laboratory measurements of retardation parameters. Furthermore, hydrogeochemical data together with results from mineralogical and geochemical analyses of fracture materials are important inputs to the conceptual development of the site-specific retardation model and understanding of the retention processes at the site.

Tracer tests in the form of multiple well tracer tests and single well injection-withdrawal tests (SWIW) have been performed in a number of boreholes with the aim of confirming the existence of field-scale retardation and to assess the utility of the retardation models to predict solute transport. Although it is not possible to extract data that can be used directly for parameterisation of the transport models used in safety assessment, the tracer tests by and large confirm the retardation model and provide results that are broadly consistent with the understanding of field-scale transport processes.

The input data for the retardation model consist of formation factors for solute transport in the rock matrix, matrix porosities, specific surface areas of internal micro-surfaces, cation exchange capacities (CEC), and sorption properties of rock in contact with synthetic groundwater of varying composition. Formation factors are obtained from *in situ* measurements under natural stress conditions, derived from high spatial resolution geophysical logging in the site investigation boreholes, together with data from laboratory studies.

Properties

The bedrock retardation model is comprised of a qualitative identification and description of typical fracture types and deformation zones at the Forsmark site with regard to processes of relevance for transport of environmental solutes and radionuclides. Furthermore, it builds on quantitative data describing material properties and the relative abundance and spatial distribution of the different geological materials comprising the rock matrix, as well as relevant alteration types and secondary minerals found in association with fractures and deformation zones.

The main parameters of interest are the immobile zone porosity, θ_m, the effective diffusivity, D_e, and the linear equilibrium sorption coefficient, K_d. These material property parameters are evaluated, interpreted and presented in the form of a retardation model. In the three-dimensional spatial representation of the Forsmark site, the retardation model is used to parameterise the characteristics of the various geological elements described in the geological site descriptive model. These elements consist of the rock mass containing varying proportions of different site-specific rock types, key fracture classes characteristic of the Forsmark site, and various deformation zone micro-structural components.

The limited data available for the different rock masses indicate that there are generally no significant differences in the retardation properties between the rock types present in the rock domains RFM029 and RFM045. Furthermore, taking variations in the parameter values into account, there are very few indications of significant differences between the different rock types. As far as key

fracture classes are concerned, either a thin layer of fracture coating or no coating at all have been identified as being of importance, since these classes are likely to be associated with a lower degree of retardation.

The BET (Brunauer, Emmet, Teller) surface areas of the fracture coatings and filling materials have been measured to be significantly higher than corresponding BET surface areas of samples from the rock mass, indicating that these materials may have potentially enhanced retention properties relative to the rock matrix. However, the large differences observed between the BET surface areas measured for fracture-coating materials and intact rock are generally not accompanied by a 1:1 corresponding variation with respect to sorptivity. Although a good qualitative indicator, the high BET surface areas measured for fracture materials cannot therefore be interpreted as being a directly proportional measure of increased sorptivity of the fracture material relative to the host rock.

The deformation zone structural elements for which retardation properties have been tabulated are all comparatively heterogeneous in their structure. From the material properties data, these structural elements are identified as potentially strong sinks for radionuclides transported from a leaking repository. However, this should be considered in the context of the possibly lower hydrodynamic transport resistance of these zones set against their increased micro-structural complexity including additional diffusion-accessible surface area (see next section).

Confidence

The porosity and effective diffusivity of the rock matrix appear to be relatively well constrained for the main rock types. Although there is evidence for *in situ* compression of pore spaces in the unaltered matrix rock, the effect upon material properties can be quantitatively bounded. Sorption uncertainty is only semi-quantitatively established and is large for many species and specific groundwater compositions. Sorptivities of certain radionuclides in contact with specific groundwaters and rock types are not known or are not supported by sufficiently large sample sizes to be considered statistically quantified. Sorptivities of U and Np under strongly reducing conditions are likely to be underestimated owing to difficulties in maintaining appropriately low redox conditions in the laboratory. There is uncertainty in the distribution and thickness of altered rock surrounding flow paths. However, the importance of this feature depends on the differences in the material properties of these materials relative to unaltered rock. The data suggest that altered rock is generally associated with increased retention for most radionuclides and therefore this uncertainty can be bounded by the retention properties of unaltered rock.

11.8.2 Flow-related properties

Long-range solute transport in fractured rock is conceptualised to occur along advective flow channels hosted within fractures and deformation zones. Matrix diffusion coupled with sorption has been identified as the main retardation process that limits the rate at which solutes are transported along these flow paths. The flow-wetted surface to flow ratio (alternatively known as the "F-factor" or "hydrodynamic transport resistance") is a key parameter governing the transport of radionuclides within fractured rock. While the retardation effect, and consequently, typical solute residence times, scale approximately linearly with rock matrix diffusivity (D_e) and sorption coefficient (K_d), they can be shown to scale quadratically with the F-factor. A given level of uncertainty in the F-factor therefore has a substantially larger impact upon solute transport than a similar relative uncertainty in the parameterisation of rock matrix properties.

The F-factor depends on the flow and its distribution within the rock. The main source of input data used as a basis for assessing the transport resistance is thus the site-specific hydrogeological properties combining a deterministic representation of the major deformation zones with a stochastic representation of the less fractured rock within the fracture domains outside these zones. For the fracture domains, the stochastic description is based upon the hydrogeological DFN models. The description of the deterministic deformation zones, on the other hand, is based upon a 2D representation of deformation zone structures incorporating a simplified model of lateral and depth-dependent transmissivity variation, which matches the borehole observational data.

Indication of the ranges of transport resistance

Numerical simulations of flow and migration, using the hydrogeological DFN as input, have provided an indication of F-factors associated with typical flow paths in fracture domains that could house a potential repository and the frequency with which they can be expected to occur. F-factors in the range of about 10^3–10^7 y/m are calculated for fractures in the transmissivity range from 10^{-8}–10^{-10} m^2/s depending upon underlying assumptions, which include the typical path length and representative hydraulic gradient. Owing to the poor connectivity of open fractures at depths larger than 400 m within FFM01, median F-factors for "typical" flow paths on the 100 m scale are found to be on the order of 10^6 y/m, assuming a semi-correlated fracture size-transmissivity relation. The simulations further demonstrate that less than 4% of the hydrogeological DFN realisations for FFM01 below 400 m depth exhibit hydraulic connectivity of any kind. Furthermore, about half of the realisations that show hydraulic connections are associated with single large fractures penetrating the entire simulation volume. Simulations of other fracture domains (upper regions of FFM01, FFM02, and FFM03) give indications of substantially smaller F-factors as compared with FFM01 at depths below 400 m.

A simple analytical model has been used to estimate typical F-factors in the deterministic deformation zones, based on an exponential model of transmissivity decrease with depth provided by hydrogeology and a 1% hydraulic gradient. The analysis reveals that flow paths within gently dipping zones such as ZFMA2 are associated with F-factors of less than 10^3 y/m for transport from repository depth to the near surface. This indicates a relatively small hydrodynamic transport resistance. Steeply dipping deformation zones, on the other hand, (for example zone ZFMENE0060A) are found to have F-factors on the order of 10^5 y/m.

It may also be noted that within the fracture domains, the probability of hydraulic connectivity decreases rapidly with distance from a hypothetical repository as different fracture size classes are active at different distances of notional hydraulic boundary separation. However, estimated F-factors are remarkably constant at different boundary plane separation distances. This suggests that the more frequent, although less transmissive, fractures comprising the connected systems at short distances from the release point are also important for the statistics of typical flow paths at greater distances.

Integrated values of the F-factor along particle transport paths derived from simulations of the regional hydrogeological model implemented in ConnectFlow show that most of the hydrodynamic transport resistance appears to be encountered in the first 80 or so metres of the release location for particles released at 450 m depth (Figure 11-26, left). This corresponds to the target volume within fracture domain FFM01 where the flow rates are exceptionally low. It is generally found that most particles tracked from a hypothetical repository layout at 450 m depth are released directly within the rock matrix where the hydraulic conductivity is equal to that of the background rock matrix (Figure 11-26, right) or in locally conductive, although hydraulically isolated regions of the rock. This result is qualitatively consistent with the outcome of hydrogeological DFN-based connectivity analyses, which suggests that most of the rock volume within FFM01 at repository depth should be essentially non-conductive. Although the first 80 m of the particle track is not considered to be physically meaningful, the subsequent transport to the surface is representative of transport through the indicated rock domains and deterministic deformation zones.

It can be noted that the ConnectFlow simulations predict a greater role for the hydrodynamic resistance provided by the deterministic zones relative to the scoping calculations (i.e. where each part of the system is compared in isolation for an assumed 1% hydraulic gradient). This is partly due to the greater flow-wetted surface encountered in the 3D representation of the zones in ConnectFlow simulations as well as the lower hydraulic gradients found in the more conductive parts of the integrated, regional hydrogeological model.

Flow chanelling

Flow channelling may have an impact upon interpretation of borehole data by way of censoring effects. This can lead to the underestimation of the true frequency of flowing channels within the rock. Some channels may be very narrow in width and unlikely to be intersected directly by a borehole. For this reason, the permeability of the surrounding fracture pore space becomes very important for identification of these features and interpretation of their hydraulic properties.

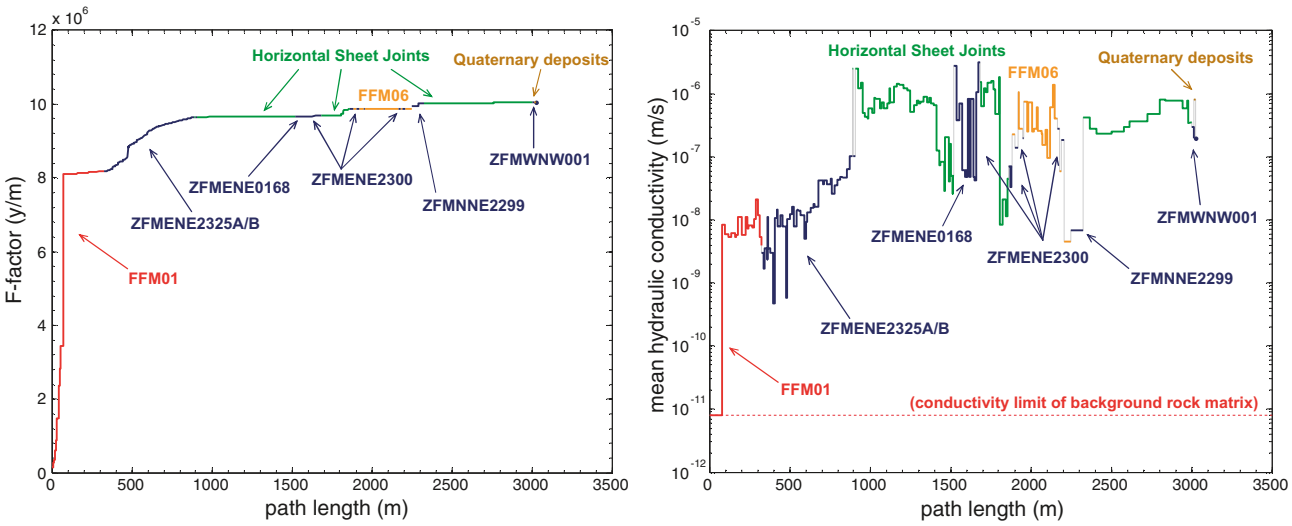

Figure 11-26. *Left: Cumulative F-factor as a function of migration path length for an individual particle characteristic of the lower 10% percentile of "fast" transport paths discharging near the Singö deformation zone. Right: Mean hydraulic conductivity as a function of transport path length for the same particle, with the limit of the hydraulic conductivity of the rock matrix indicated by the horizontal broken line. Different structural elements encountered by the particle along its migration path are labelled in the figure, and the grey coloured segments in the right-hand image represent discontinuities in the parameter value when the particle passes from one structural feature to another.*

Six different, potentially important sub-classes of flow channelling have been considered in the transport properties evaluation. The uncertainties introduced by some of the different forms of flow channelling can be reasonably well constrained by scoping simulations. Other, more exotic types of flow-channelling, such as karstic erosion pipes in calcite annealed fractures, seem unlikely to occur in the target volume at repository depth, although cannot be completely ruled out. The overall effect of flow-channelling does not appear to be sufficiently severe that it would cast considerable doubt on the utility of the hydrogeological models produced within SDM-Site, although further justification of this will need to be provided during safety assessment.

It is also concluded that additional physical mechanisms enhancing solute uptake, such as radial diffusion from channels of limited extent and diffusion into stagnant zones with concomitant matrix diffusion, may increase transport retardation substantially. Flow channelling may therefore possibly have an overall beneficial effect.

Confidence

Uncertainty in hydrogeological DFN parameters and the role of channelling phenomena may lead to underestimation of flow channel frequency in the target volume. However, the overall F-factors for typical flow paths through the repository volume should not be greatly different, provided that the fracture transmissivity model is determined to be reasonable (approximately correct order of magnitude in flow predictions).

The hydrogeological DFN fitting parameters for fractures within the repository volume can only be properly constrained by mapping of open fracture statistics in tunnels. During underground investigations, the flowing fracture frequencies in tunnels and the coupling between rock mechanical properties and fracture transmissivities will be studied, to more fully understand the extent of different flow channelling phenomena and the possible existence of fast, persistent flow paths in the rock. This will lead to more reliable models for solute transport from the repository volume, particularly over the first few tens of metres from canister positions which may have the greatest impact on overall radionuclide release rates. Nevertheless, it is judged that the current hydrogeological DFN, with its alternative descriptions of the transmissivity size correlation, provides adequate bounds on the uncertainty of the flow-related transport properties.

11.9 Overall confidence

The uncertainty and confidence in the Forsmark site descriptive model have been assessed and the results are documented in detail in /SKB 2008/. This assessment comprised exploring confidence in the site characterisation data base, key remaining issues and their treatment, handling of alternatives, consistency between disciplines and the main reasons for confidence and lack of confidence in the model. The outcome of the assessment is summarised below.

11.9.1 Data usage

In general, only a few data have been omitted from the modelling work, mainly because they are judged to be less relevant and reliable than the data considered. These omissions are judged to have little negative impact on confidence. However, the inclusion of less reliable hydraulic fracturing data could have helped in justifying potentially less conservative values of stress.

Poor precision in the measured data are, in general, judged to have limited impact on uncertainties in the site descriptive model. There is poor precision in determining the position of some boreholes at depth in three-dimensional space as well as in the orientation of BIPS images in some boreholes, resulting in uncertainties in the orientation of objects mapped in the borehole, for example fractures. Furthermore, the precision of stress data determined by the overcoring method at locations where the pre-existing deformation in the core exceeded the elasticity limit of the intact rock is poor. These problems are identified, quantified and considered in the modelling work, and they affect uncertainty, but have little negative impact on confidence.

Measurement bias in the data and bias due to poor representativity are much reduced compared with earlier model versions, but some bias still remains. One important example concerns the lack of data on fracture sizes from the sub-surface realm inside the target volume. This necessitates considering a wide range of uncertainty in the geological DFN model that can only be reduced by data obtained from underground. Since the impact on uncertainty can be estimated and is accounted for in the modelling, bias is not judged a major concern for confidence in the model. Furthermore, it is noted that the r_0-fixed, tectonic continuum approach used in the geological and hydrogeological DFN models, both of which are based on fracture frequency data in narrow boreholes, appear to be mutually consistent with regard to the intensity of large-scale fractures within the local model volume.

11.9.2 Key remaining issues and their treatment

Some uncertainties remain in the Forsmark site descriptive model. Most of the uncertainties concerning properties and processes inside the target volume are quantified or at least bounded by alternative models or assumptions (see below). These uncertainties are propagated to repository engineering and safety assessment for further exploring the impact on repository layout and long-term safety.

One key remaining issue where the uncertainties are still not bounded concerns the quantitative evaluation of the redox and alkalinity buffering capacity of flow paths in the rock in the target volume. The existence of a near-surface redox reaction zone appears to be well-established, based on the chemistry of the shallow groundwater samples. Furthermore, the common occurrence of calcite suggests that there is buffering capacity against dilute groundwater. A second issue that concerns fracture mineralogy is the understanding of the occurrence of a few transmissive fractures at depth that lack a mineral coating. Complementary studies to reduce the uncertainties raised above are currently in progress. One concerns a more quantitative evaluation of the amount of different minerals along fractures, and the other aims to provide more detailed information bearing on the significance and origin of fractures that lack a mineral coating or filling and wall-rock alteration.

Another key remaining uncertainty concerns concentrations of sulphide in the groundwater. New sulphide data from the monitoring programme indicate increasing sulphide concentrations with time for some sampled borehole sections. The reason is unknown, but initial drilling and pumping may have disturbed the system and may have facilitated sulphate reduction. Time series from the ongoing monitoring programme are judged to be sufficient to allow a final assessment of the undisturbed sulphide concentrations, as well as how sulphide concentrations may change due to future intrusions of marine water. This assessment will need to be carried out during the SR-Site programme.

It is judged that other remaining uncertainties in this volume can only be reduced significantly by data from underground, e.g. the uncertainty in size distribution and size-intensity models for fractures at repository depth. These uncertainties and their suggested treatment are addressed in /SKB 2008/.

Uncertainties outside the repository volume are more substantial, but are judged to be of less importance for the design and long-term safety of a potential repository. More surface-based boreholes outside the lens would only marginally decrease uncertainty. Potentially more data will be obtained from the investigations presently being carried out for the planned expansion of the SFR repository.

11.9.3 Handling of alternatives

Many of the previous hypotheses proposed during earlier versions of the SDM work have now been discarded or are handled by bounding assumptions. Nevertheless, five hypotheses are retained with alternative models developed and propagated, where necessary, to engineering design and safety assessment.

Fracture size and intensity modelling in the geological DFN work. The absence of fracture trace data from underground makes it necessary to formulate alternative models for the size distribution and intensity of fractures and minor fracture zones in the target volume, i.e. the so-called tectonic continuum, combined outcrop scale and tectonic fault, and r_0-fixed models. Two of these alternatives are considered to be less likely, but are retained to ensure a bounding of the uncertainty. The alternatives are propagated to repository design and to safety assessment since there is an impact on the degree of utilisation in design and the SR-Site assessment of earthquake hazards. Implications for the hydrogeology and rock mechanics site descriptive models are judged to be small and, for this reason, the different alternatives have not been propagated into these aspects of the modelling work.

Geometry, connectivity and transmissivity of deformation zones in the regional domain. The volume south-west of the target volume, as far as the Forsmark deformation zone, is fairly well known and a regional groundwater divide is located between the candidate area and the Forsmark deformation zone. However, the volume north-east of the target volume is less well characterised. This observation concerns both whether or not the Singö deformation zone is a flow barrier and the properties of the rock mass north-east of the Singö zone. The upstream boundary condition is well established and no alternative is needed. Downstream, the situation is more uncertain and two alternatives, with a tight or open Singö deformation zone have to be considered. Furthermore, the uncertainty in conditions outside the Forsmark tectonic lens needs to be considered in SR-Site when assessing locations of discharge points.

Hydraulic properties and connectivity of the fracture network at a scale smaller than the deterministic deformation zones in the context of the correlation between fracture size and transmissivity. In contrast to the situation after version 1.2 of the site descriptive model, there are now a multitude of data in support of the hydraulics description. This progress relies heavily on the identification of fracture domains. The PFL-data used specifically capture the connected fractures, and all deep PFL-tested boreholes show a consistent picture. The orientation of conductive fractures is generally consistent with the orientation of the minimum principal stress. However, it is not currently possible to resolve uncertainty in the potential correlation between fracture size and transmissivity, and the three alternatives “full correlation”, “semi-correlation” and “no correlation” need to be retained and propagated to SR-Site. The alternatives have no implications for engineering and need not be considered in the design work.

Alternative hypotheses regarding groundwater composition and processes. There is a good understanding of the current spatial distribution of groundwater composition and the existence of a near-surface redox reaction zone appears to be well established, even though there are uncertainties in the data interpretation. The common occurrence of calcite suggests that there is buffering capacity against dilute groundwater, but quantification is uncertain. The uncertainties are sufficiently well bounded concerning conditions at the present day, whereas there are larger uncertainties as to whether the process understanding is sufficient for predicting the groundwater composition during a glaciation. Even though current understanding suggests that there is sufficient buffering capacity

in the rock, SR-Site may have to handle the alternative possibility that dilute waters generated during ice-melting will reach repository levels. To some extent, future treatment of this uncertainty is dependent on the outcome of a currently ongoing study aiming at quantifying the occurrence of different fracture minerals.

Effects of connectivity, complexity and channelling on the distribution of flow (F-factor). Details of the flow field along a fracture plane are uncertain. In SR-Can, channelling was handled by dividing the transport resistance obtained from the hydrogeological DFN model by a factor of 10, whereas SDM-Site explores a multitude of channelling hypotheses. The bounding estimates of the influence of channelling assessed in SDM-Site will be propagated to SR-Site.

11.9.4 Consistency between disciplines

Another prerequisite for confidence is consistency (i.e. no conflicts) between the different discipline model interpretations. Furthermore, confidence is enhanced if aspects of the model are supported by independent evidence from different disciplines. The assessment revealed that essentially all identified interactions between the different disciplines have been considered in the site descriptive modelling work. Furthermore, the interdisciplinary feedbacks provide qualitative and independent data support to the different discipline-specific descriptions and thus enhance overall confidence. Specific examples of the inter-disciplinary consistency between the structural geological, hydrogeological DFN and rock stress models, as well as between the hydrogeological and hydrogeochemical models are addressed in sections 11.6 and 11.7.3, respectively.

11.9.5 Confidence statement

Generally, it is judged that key aspects of the Forsmark site descriptive model, i.e. information needed for repository design and safety assessment, have a high level of confidence. The overall reason for this confidence is the relative wealth of data from the target volume and the consistency between independent data from different disciplines. Some aspects have lower confidence. The lack of confidence is handled by providing wide uncertainty ranges, bounding estimates, producing alternative models or defining additional lines of action to be completed either in the immediate future or during underground investigations.

12 Conclusions

12.1 Fulfilment of objectives

Bearing in mind the overall objective of the site descriptive modelling work at Forsmark, it can be concluded that an integrated description of the site, based on available complete site investigation data, has been developed and documented. The description is supported by a large amount of data and the results of analyses and modelling that are mutually consistent. This demonstrates that a fundamental understanding of the current state of conditions and the on-going processes at the Forsmark site, from the surface down to below the potential repository depth, has been achieved. In addition, the properties of the site can be explained in the context of an understanding of the past evolution, throughout a long period of geological history.

Concerning the specific objectives of the site descriptive modelling work, it is concluded that all data in data freeze 2.2 have been analysed, and the results provide, together with knowledge from previous modelling work, the basis for the site-descriptive model of the Forsmark area. Models of the geology /Stephens et al. 2007/, thermal properties /Back et al. 2007/, rock mechanics properties /Glamheden et al. 2007a/ and hydrogeological properties /Follin et al. 2007b/ have been documented separately and delivered to repository engineering. New data in data freeze 2.3 have been utilised for complementary analyses and verification of the models, and data that became available after data freeze 2.3 have been assessed, or at least commented upon, in relation to these models.

The final site descriptive model builds on an integrated geological model in 3D into which other discipline-specific models have been integrated in a successful manner without any conflicting interpretations. A systematic assessment of confidence in the model, including treatment of uncertainties and evaluation of alternative interpretations, has been carried out /SKB 2008/. This assessment was conducted in cooperation with representatives of repository engineering and safety assessment. It addressed the feedback obtained from the work with the preliminary repository layout step D1 and from the safety assessment SR-Can, as well as the feedback obtained on earlier versions of the site description. The overall outcome of this assessment is that most properties of importance for both repository constructability and long-term safety are bounded sufficiently, and that data from underground now bears the prime potential to further reduce uncertainties in the target volume. Uncertainties outside the target volume are larger, but are judged to be of less importance.

12.2 Key remaining issues

Remaining issues where the uncertainties are still not bounded sufficiently concern a qualitative evaluation of the redox and alkalinity buffering capacity of flow paths in the rock in the target volume and the understanding of the occurrence of some transmissive fractures at depth that lack a mineral coating. In addition, the reason for increasing sulphide concentrations with time in some borehole sections sampled during the on-going monitoring programme is not known, but initial drilling and pumping may have disturbed the system and may have facilitated sulphate reduction. Complementary studies to reduce all these uncertainties are currently in progress.

12.3 Implications for the underground construction phase

If Forsmark is selected as a site for the final repository, it will be necessary to complete minor modifications to the deterministic geological models prior to the construction work (see section 5.9.2). The issues judged to merit further study prior to and during the underground construction phase, in order to decrease the uncertainties in the description of the target volume, are highlighted in the confidence assessment report /SKB 2008/. The most important of these are summarised below.

- The uncertainties in size distribution and size-intensity models for fractures at repository depth can only be reduced by data from the underground beneath 200 m depth.
- Uncertainties in stress magnitudes may be reduced by observations and measurements of deformation and back analyses during the construction phase.
- Uncertainties in the understanding of chemical processes may be reduced by assessing the effects of drawdown and inflows on, for example, groundwater chemistry and fracture minerals during excavation.
- Mapping of open fracture statistics in tunnels may constrain the parameters of the hydrogeological DFN model. Furthermore, underground work will also provide possibilities for short-range interference tests at relevant depths.
- Information on the frequency of flowing fractures in tunnels and investigations of couplings between rock mechanical properties and fracture transmissivities may provide information on the extent of in-plane flow channelling, which may improve the models for solute transport.
- More data on the near-surface bedrock as well as on the depth of Quaternary deposits in the access area are needed for detailed planning of the access layout. A core-drilling programme in combination with appropriate geophysical methods, over a restricted area, should be included in this complementary phase of data acquisition.

13 References

Aaro S, 2003. Regional gravity survey in the Forsmark area, 2002 and 2003. Forsmark site investigation. SKB P-03-42, Svensk Kärnbränslehantering AB.

Andersson A, Dahlman B, Gee D G, Snäll S, 1985. The Scandinavian alum shales. Sveriges geologiska undersökning Ca 56, 50 pp.

Andersson J-E, Nordqvist R, Nyberg G, Smellie J, Tirén S, 1991. Hydrogeological conditions in the Finnsjön area. Compilation of data and conceptual model. SKB TR 91-24, Svensk Kärnbränslehantering AB.

Andersson J, Hermanson J, Elert M, Moreno L, Selroos J-O, 1998. Derivation and treatment of the flow-wetted surface and other geosphere parameters in the transport models FARF31 and COMP23 for use in safety assessment. SKB R-98-60, Svensk Kärnbränslehantering AB.

Andersson J, Berglund J, Follin S, Hakami E, Halvarson J, Hermanson J, Laaksoharju M, Rhén I, Wahlgren C-H, 2002a. Testing the methodology for site descriptive modelling. Application for the Laxemar area. SKB TR-02-19, Svensk Kärnbränslehantering AB.

Andersson J, Christiansson R, Hudson J, 2002b. Site investigations. Strategy for Rock Mechanics Site Descriptive Model. SKB TR-02-01, Svensk Kärnbränslehantering AB.

Andersson J, 2003. Site descriptive modelling – strategy for integrated evaluation. SKB R-03-05, Svensk Kärnbränslehantering AB.

André M, Malmström M, Neretnieks I, 2006. Determining sorption coefficients in intact rock using an electrical potential gradient as a driving force for migration. Mat. Res. Soc. Symp. Proc., 932, pp. 975–982.

Ask D, Ask M V S, 2007. Detection of borehole breakouts in boreholes KFM01A and KFM01B. Forsmark site investigation. SKB P-07-235, Svensk Kärnbränslehantering AB.

Ask D, Cornet F, Brunet C, Fontbonne F, 2007. Stress measurements with hydraulic methods in boreholes KFM07A, KFM07C, KFM08A, KFM09A and KFM09B. Forsmark site investigation. SKB P-07-206, Svensk Kärnbränslehantering AB.

Auqué L F, Gimeno M J, Gómez J, Puigdoménech I, Smellie J, Tullborg E-L, 2006. Groundwater chemistry around a repository for spent nuclear fuel over a glacial cycle Evaluation for SR-Can. SKB TR-06-31, Svensk Kärnbränslehantering AB.

Auqué L, Gimeno M J, Gómez J, Nilsson A-C, 2008. Potentiometrically measured Eh in groundwaters from the Scandinavian Shield. Applied Geochemistry, vol 23, pp 1820–1833.

Axelsson C-L, Mærsk Hansen L, 1997. Update of structural models at SFR nuclear waste repository, Forsmark, Sweden. SKB R-98-05, Svensk Kärnbränslehantering AB.

Axelsson C-L, Ekstav A, Lindblad Pårse A, 2002. SFR-utvärdering av hydrogeologi. SKB R-02-14, Svensk Kärnbränslehantering AB.

Back P-E, Sundberg J, 2007. Thermal site descriptive model. A strategy for the model development during site investigations – version 2. SKB R-07-42, Svensk Kärnbränslehantering AB.

Back P-E, Wrafter J, Sundberg J, Rosén L 2007. Thermal properties. Site descriptive modelling Forsmark – stage 2.2. SKB R-07-47, Svensk Kärnbränslehantering AB.

Ball J W, Nordstrom D K, 2001. User's manual for WATEQ4F, with revised thermodynamic data base and test cases for calculating speciation of major, trace, and redox elements in natural waters. U.S. Geological Survey, Open File Report 91-183, USA.

Balu L, Cosma C, 2005. Estimation of 3D positions and orientations of reflectors based on an updated interpretation of Stage 1 reflection seismic data. Preliminary site description, Forsmark area – version 1.2. SKB R-05-39, Svensk Kärnbränslehantering AB.

Banwart S A, 1999. Reduction of iron (III) minerals by natural organic matter in groundwater. Geochim. Cosmochim. Acta, 63**,** 2919–2928.

Barton N, Bandis S, 1990. Review of predictive capabilities of JRC-JCS model in engineering practice. In Rock joints, proc. Int. symp. On rock joints, Loen, Norway, p. 603–610. Balkema.

Barton N, 2002. Some new Q-value correlations to assist in site characterization and tunnel design. International Journal of Rock Mechanics & Mining Sciences 39, p.185–216. Pergamon.

Bath A, Lalieux P, 1999. Technical summary of the SEDE Workshop on the use of hydrogeochemical information in testing groundwater flow models. In: Use of hydrogeochemical information in testing groundwater flow models, Technical summary and proceedings of an NEA Workshop, Borgholm, Sweden, 1–3 September 1997 (organised by the NEA Co-ordinating Group on Site Evaluation and Design of Experiments for Radioactive Waste Disposal (SEDE)). OECD/NEA, Radioactive Waste Management, pp. 13–30.

Berg C, Levén J, Nilsson A-C, 2005. Hydrochemical logging in KFM07A. Forsmark site investigation. SKB P-05-187, Svensk Kärnbränslehantering AB.

Berg J, Jansson U, Wästfelt A, 2006. Landscape history and people in a geographical perspective. Studies of land-use, settlement and livelihood in Oskarshamn and Forsmark. SKB R-06-37, Svensk Kärnbränslehantering AB.

Berggren M, 1998. Hydraulic conductivity in Swedish bedrock estimated by means of geostatistics. Thesis Report Series 1998:9, Royal Institute of Technology, Stockholm.

Berglund S, Selroos J-O, 2004. Transport properties site descriptive model. Guidelines for evaluation and modelling. SKB R-03-09, Svensk Kärnbränslehantering AB.

Bergman T, Andersson J, Hermansson T, Zetterström Evins L, Albrecht L, Stephens M B, Petersson J, Nordman C, 2004a. Bedrock mapping. Stage 2 (2003) – Bedrock data from outcrops and the basal parts of trenches and shallow boreholes through the Quaternary cover. Forsmark site investigation. SKB P-04-91, Svensk Kärnbränslehantering.

Bergman B, Palm H, Juhlin C, 2004b. Estimate of bedrock topography using seismic tomography along reflection seismic profiles. Forsmark site investigation. SKB P-04-99, Svensk Kärnbränslehantering AB.

Bienawski Z T, 1989. Engineering rock mass classifications. John Wiley & Sons.

Bonnet E, Bour O, Odling N, Main I, Berkowitz B, Davy P, Cowie P A, 2001. Scaling of fracture systems in geological media. Reviews of Geophysics 39(3), 347–384.

Bosson E, Gustafsson L-G, Sassner M, 2008. Numerical modelling of surface hydrology and near-surface hydrogeology at Forsmark. Site descriptive modelling, SDM-Site Forsmark. SKB R-08-09, Svensk Kärnbränslehantering AB.

Brace W, Walsh J, Frangos W, 1968. Permeability of granite under high pressure. J. Geophys. Res., 73(6), pp. 2225–2236.

Brantberger M, Zetterqvist A, Arnbjerg-Nielsen T, Olsson T, Outters N, Syrjänen P, 2006. Final repository for spent nuclear fuel. Underground design Forsmark, Layout D1. SKB R-06-34, Svensk Kärnbränslehantering AB.

Brising U, 2008 (revision of Jureskog P-Å, 2002). Platsundersökning Forsmark. Upprättande av riksnätsanslutet stomnät i plan och höjd för Forsmarksområdet. SKB P-08-46, Svensk Kärnbränslehantering AB (in Swedish).

Brising U, Nissen J, 2008 (revision of Jureskog P-Å, 2002). Forsmark site investigation. Connection of the Forsmark site investigation area to the Swedish reference frame. SKB P-08-68, Svensk Kärnbränslehantering AB.

Brunauer S, Emmet P, Teller E, 1938. Adsorption of gases in multimolecular layers. J. Am. Chem. Soc., 60, pp. 309–319.

Brydsten L, 2004. A method for construction of digital elevation models for site investigation programme in Forsmark and Simpevarp. SKB P-04-03, Svensk Kärnbränslehantering AB.

Brydsten L, Strömgren M, 2004. Digital elevation models for site investigation programme in Forsmark. Site description version 1.2. SKB R-04-70, Svensk Kärnbränslehantering AB.

Byegård J, Selnert E, Tullborg E-L, 2008. Bedrock transport properties. Data evaluation and retardation model. Site descriptive modelling, SDM-Site Forsmark. SKB R-08-98, Svensk Kärnbränslehantering AB.

Bödvarsson R, Lund B, Roberts R, Slunga R, 2006. Earthquake activity in Sweden. Study in connection with a proposed nuclear waste repository in Forsmark or Oskarshamn. SKB R-06-67, Svensk Kärnbränslehantering AB.

Caine J S, Evans J P, Forster C B, 1996. Fault zone architecture and permeability structure. Geology 24 (11), 1025–1028.

Carle S F, Fogg G E, 1997. Modeling spatial variability with one- and multi-dimensional Markov chains: Mathematical Geology, v. 29, no. 7, 891–918.

Carlsson A, 1979. Characteristic features of a superficial rock mass in southern central Sweden – Horizontal and subhorizontal fractures and filling material. Striae 11.

Carlsson T, Brunberg A-K, Brydsten L, Strömgren M, 2005. Characterisation of running waters, including vegetation, substrate, and technical encroachments. Forsmark site investigation. SKB P-05-150, Svensk Kärnbränslehantering AB.

Carlsson A, Christiansson R, 2007. Construction experiences from underground works at Forsmark. Compilation Report. SKB R-07-10, Svensk Kärnbränslehantering AB.

Carlsten S, 2007. Correlation of oriented radar reflectors with geological features in boreholes at Forsmark. In Stephens M B and Skagius K (ed), Geology – background complementary studies. Forsmark modelling stage 2.2. SKB R-07-56, Svensk Kärnbränslehantering AB.

Carlsten S, Samuelsson E, Gustafsson J, Stephens M, Thunehed H, 2007. Geological single-hole interpretation of KFM08D. Forsmark site investigation. SKB P-07-108, Svensk Kärnbränslehantering AB.

Cosma C, Balu L, Enescu N, 2003. Estimation of 3D positions and orientations of reflectors identified in the reflection seismic survey at the Forsmark area. SKB R-03-22, Svensk Kärnbränslehantering AB.

Cosma C, Enescu N, Balu L, 2005. Vertical seismic profiling from the boreholes KFM01A and KFM02A. Forsmark site investigation. SKB P-05-168, Svensk Kärnbränslehantering AB.

Cosma C, Balu L, Enescu N, 2006. Estimation of 3D positions and orientations of reflectors identified during the stage 2 reflection seismic survey at Forsmark. Site descriptive modelling Forsmark Stage 2.1. SKB R-06-93, Svensk Kärnbränslehantering AB.

Crawford J (ed), 2008. Bedrock transport properties Forsmark. Site descriptive modelling, SDM-Site Forsmark. SKB R-08-48, Svensk Kärnbränslehantering AB.

Cronquist T, Forssberg O, Mærsk Hansen L, Jonsson A, Koyi S, Leiner P, Vestgård J, Petersson J, Skogsmo G, 2005. Detailed fracture mapping of two trenches at Forsmark. Forsmark site investigation. SKB P-04-88, Svensk Kärnbränslehantering AB.

Degueldre C, 1994. Colloid properties in groundwaters from crystalline formation. PSI Bericht NP-94-21, Paul Scherrer Institute, Villingen, Switzerland.

Dershowitz W, Lee G, Geier J, Foxford T, La Pointe P, Thomas A, 1998. FRACMAN. Interactive discrete feature data analysis, geometric modeling and exploration simulation. User documentation, version 2.6. Golder Associates Inc., Redmond, Washington, USA.

Deutsch C, Journel A, 1998. GS-LIB: Geostatistical Software Library and User´s Guide. Second edition. Oxford University Press, New York.

Didriksen K, Christiansen B C, Baker J A, Frandsen C, Balic-Zunic T, Tullborg E-L, Mørup S, Stipp S L S, 2007. Fe-oxide fracture-fillings as a palaeo-temperature and -redox indicator: Structure, crystal form, REE content and Fe isotope composition. Chem. Geol., 244, 330–343.

Döse C, Stråhle A, Rauséus G, Samuelsson E, Olsson O, 2008. Revision of BIPS-orientations for geological objects in boreholes from Forsmark and Laxemar. SKB P-08-37, Svensk Kärnbränslehantering AB.

Elhammer A, Sandkvist Å, 2005. Detailed marine geological survey of the sea bottom outside Forsmark. Forsmark site investigation. SKB P-03-101, Svensk Kärnbränslehantering AB.

Enescu N, Cosma C, 2007. Correlation of 2D surface seismic, vertical seismic profile (VSP), and geological and sonic data in boreholes KFM01A and KFM02A, Forsmark: Background analysis. In Stephens M B and Skagius K (ed), Geology – background complementary studies. Forsmark modelling stage 2.2. SKB R-07-56, Svensk Kärnbränslehantering AB.

Eriksson S, Sellei C, Wallström K, 1977. The structure of the Stockholm archipelago – A cascade framework modelling approach. J. Sea Res, 49, 275–294.

Essén S, Johnsson A, Bylund D, Pedersen K, Lundström U, 2007. Siderophore production by Pseudomonas stutzeri under aerobic and anaerobic conditions. Appl. Environ. Microbiol., 73(18), pp. 5857–5864.

Eydal H S C, Pedersen P, 2007. Use of an ATP assay to determine viable microbial biomass in Fennoscandian Shield groundwater from depths of 3–1000 m. Journal of Microbiological Methods, 70, pp 363–373.

Fisher N I, Lewis T, Embleton B J J, 1993. Statistical Analyses of Spherical Data. Cambridge University Press, Cambridge, UK. IBSN: 0-521-45699-1.

Follin S, Stigsson M, Svensson U, 2005. Regional hydrogeological simulations for Forsmark – numerical modelling using DarcyTools. Preliminary site description Forsmark area – version 1.2. SKB R-05-60, Svensk Kärnbränslehantering AB.

Follin S, Ludvigson J-E, Levén J, 2006. A comparison between standard well test evaluation methods used in SKB's site investigations and the Generalised Radial Flow concept. SKB P-06-54, Svensk Kärnbränslehantering AB.

Follin S, Johansson P-O, Levén J, Hartley L, Holton D, McCarthy R, Roberts D, 2007a. Updated strategy and test of new concepts for groundwater flow modelling in Forsmark in preparation of site descriptive modelling stage 2.2. SKB R-07-20, Svensk Kärnbränslehantering AB.

Follin S, Levén J, Hartley L, Jackson P, Joyce S, Roberts D, Swift B, 2007b. Hydrogeological characterisation and modelling of deformation zones and fracture domains, Forsmark modelling stage 2.2. SKB R-07-48, Svensk Kärnbränslehantering AB.

Follin S, Johansson P-O, Hartley L, Jackson P, Roberts D, Marsic N, 2007c. Hydrogeological conceptual model development and numerical modelling using CONNECTFLOW, Forsmark modelling stage 2.2. SKB R-07-49, Svensk Kärnbränslehantering AB.

Follin S, 2008. Bedrock hydrogeology Forsmark. Site descriptive modelling, SDM-Site Forsmark. SKB R-08-95, Svensk Kärnbränslehantering AB.

Follin S, Hartley L, Jackson P, Roberts D, Marsic N, 2008a. Hydrogeological conceptual model development and numerical modelling using CONNECTFLOW, Forsmark modelling stage 2.3. SKB R-08-23, Svensk Kärnbränslehantering AB.

Follin S, Stephens M B, Laaksoharju M, Nilsson A-C, Smellie J A T, Tullborg E-L, 2008b. Modelling the evolution of hydrochemical conditions in the Fennoscandian Shield during Holocene time using multidisciplinary information. Applied Geochemistry, vol 23/7, pp 2004–2020.

Forssberg O, Mærsk Hansen L, Koyi S, Vestgård J, Öhman J, Petersson J, Albrecht J, Hedenström A, Gustavsson J, 2007. Detailed fracture and bedrock mapping, Quaternary investigations and GPR measurements at excavated outcrop AFM001264. Forsmark site investigation. SKB P-05-269, Svensk Kärnbränslehantering AB.

Fox A, La Pointe P, Hermanson J, Öhman J, 2007. Statistical geological discrete fracture network model, Forsmark modelling stage 2.2. SKB R-07-46, Svensk Kärnbränslehantering AB.

Frape S K, Fritz P, 1987. Geochemical trends for groundwaters from the Canadian Shield. In: P. Fritz and S.K. Frape (ed), Saline Water and Gases in Crystalline rocks. Geol. Assoc. Can. Spec. Pap., 33, pp 19– 38.

Fredén C (ed), 2002. Berg och jord. Sveriges nationalatlas. Third edition. 208 pp.

Gascoyne M, Laaksoharju M (ed), 2008. High-level radioactive waste disposal in Sweden: Hydrogeochemical characterisation and modelling of two potential sites. Applied Geochemistry, vol 23/7, ISSN 0883-2927. Elsevier.

Gascoyne M, Gurban I, 2008. Application of the Drilling Impact Study (DIS) to Forsmark groundwaters. In: Kalinowski B (ed), Background complementary hydrogeochemical studies, SDM-Site Forsmark. SKB R-08-87, Svensk Kärnbränslehantering AB.

Gentzschein B, Levén J, Follin S, 2007. A comparison between well yield data from the site investigation in Forsmark and domestic wells in northern Uppland. SKB P-06-53, Svensk Kärnbränslehantering AB.

Gimeno M J, Auqué L F, Gómez J B, Acero P, 2008. Water-rock interaction modelling and uncertainties of mixing modelling, SDM-Site Forsmark. SKB R-08-86, Svensk Kärnbränslehantering AB.

Glamheden R, Fredriksson A, Röshoff K, Karlsson J, Hakami H, Christiansson R, 2007a. Rock mechanics Forsmark, Site descriptive modelling Forsmark stage 2.2. SKB R-07-31, Svensk Kärnbränslehantering AB.

Glamheden R, Mærsk Hansen L, Fredriksson A, Bergkvist L, Markström I, Elfström M, 2007b. Mechanical modelling of the Singö deformation zone. Site descriptive modelling, Forsmark stage 2.1. SKB R-07-06, Svensk Kärnbränslehantering AB.

Glamheden R, Lanaro F, Karlsson J, Lindberg U, Wrafter J, Hakami H, Johansson M, 2008. Rock mechanics Forsmark, Modelling stage 2.3. Complementary analyses and verification of the rock mechanics model. SKB R-08-66, Svensk Kärnbränslehantering AB.

Gómez J B, Laaksoharju M, Skårman E, Gurban I, 2006. M3 version 3.0: Concepts, methods, and mathematical formulation. SKB TR-06-27, Svensk Kärnbränslehantering AB.

Gómez J B, Auqué L F, Gimeno M J, 2008. Sensitivity and uncertainty analysis of mixing and mass balance calculations with standard and PCA-based geochemical codes. Applied Geochemistry, vol 23, pp 1941–1956.

Gómez J B, Laaksoharju M, Skårman E, Gurban I, 2009. M3 version 3.0: Verification and Validation. SKB TR-09-05, Svensk Kärnbränslehantering AB.

Grandia F, Sena C, Arcos D, Molinero J, Duro L, Bruno J, 2007. Quantitative assessment of radionuclide retention in the near-surface system at Forsmark. Development of a reactive transport model using Forsmark 1.2 data. SKB R-07-64, Svensk Kärnbränslehantering AB.

Greger M, 2004. Uptake of nuclides by plants. SKB TR-04-14, Svensk Kärnbränslehantering AB.

Grenthe I, Stumm W, Laaksoharju M, Nilsson A C, Wikberg P, 1992. Redox potentials and redox reactions in deep groundwater systems. Chem. Geol., 98, pp 131–150.

Gudmundsson A, Berg S S, Lyslo K B, Skurtveit E, 2001. Fracture networks and fluid transport in active fault zones. Journal of Structural Geology 23, 343–353.

Gurban I, 2008. Forsmark Site: M3 modelling and 2D visualisation of the hydrochemical parameters in Forsmark groundwater data 2.2 and 2.3. In: Kalinowski B (ed), Background complementary hydrogeochemical studies, SDM-Site Forsmark. SKB R-08-87, Svensk Kärnbränslehantering AB.

Gustafsson B G, 2004a. Millennial changes of the Baltic Sea salinity. Studies of the sensitivity of the salinity to climate change. SKB-TR-04-12, Svensk Kärnbränslehantering AB.

Gustafsson B G, 2004b. Sensitivity of the Baltic Sea salinity to large perturbations in climate. Climate research, 27: 237–251.

Göthberg A, Wahlman H, 2006. Inventory of vascular plants and classification of calcareous wetlands in the Forsmark area. Forsmark site investigation. SKB P-06-115, Svensk Kärnbränslehantering AB.

Hallbeck L, Pedersen K, 2008a. Explorative analysis of microbes, colloids and gases, SDM-Site Forsmark. SKB R-08-85, Svensk Kärnbränslehantering AB.

Hallbeck L, Pedersen K, 2008b. Characterization of microbial processes in deep aquifers in the Fennoscandian Shield. Applied Geochemistry, vol 23, pp. 1796–1819.

Hartley L J, Holton D, 2004. CONNECTFLOW (Release 8.0). Technical summary document, Serco Assurance Report SA/ERRA C/TSD02V1.

Hartley L J, Hoch A R, Cliffe K A, Jackson C P, Holton D, 2004a. NAMMU (Release 8.0). Technical summary document, Serco Assurance Report SA/ENV/0626.

Hartley L J, Holton D, Hoch A R, 2004b. NAPSAC (Release 8.0). Technical summary document, Serco Assurance Report SA/ERRA-N/TSD02V1.

Hedenström A, Risberg J, 2003. Shore displacement in northern Uppland during the last 6500 calendar years. SKB TR-03-17, Svensk Kärnbränslehantering AB.

Hedenström A, Sohlenius G, 2008. Description of the regolith at Forsmark. Site descriptive modelling, SDM-Site Forsmark. SKB R-08-04, Svensk Kärnbränslehantering AB.

Hedenström A, Sohlenius G, Strömgren M, Brydsten L, Nyman H, 2008. Depth and stratigraphy of regolith at Forsmark. Site descriptive modelling, SDM-Site Forsmark. SKB R-08-07, Svensk Kärnbränslehantering AB.

Hermanson J, Hansen L, Olofsson J, Sävås J, Vestgård J, 2003a. Detailed fracture mapping at the KFM02 and KFM03 drill sites, Forsmark. SKB P-03-12, Svensk Kärnbränslehantering AB.

Hermanson J, Hansen L, Vestgård J, Leiner P, 2003b. Detailed fracture mapping of the outcrops Klubbudden, AFM001098 and drill site 4, AFM001097. Forsmark site investigation. SKB P-03-115, Svensk Kärnbränslehantering AB.

Hermanson J, Hansen L, Vestgård J, Leiner P, 2004. Detailed fracture mapping of excavated rock outcrop at drilling site 5, AFM100201. Forsmark site investigation. SKB P-04-90, Svensk Kärnbränslehantering AB.

Hermansson T, Stephens M B, Corfu F, Andersson J, Page L, 2007. Penetrative ductile deformation and amphibolite-facies metamorphism prior to 1851 Ma in the western part of the Svecofennian orogen, Fennoscandian Shield. Precambrian Research 153, 29–45.

Hermansson T, Stephens M B, Corfu F, Page L M, Andersson J, 2008. Migratory tectonic switching, western Svecofennian orogen, central Sweden: Constraints from U/Pb zircon and titanite geochronology. Precambrian Research, 161, pp 250-278.

Hermansson T, Stephens M B, Page L M, (in press). $^{40}Ar/^{39}Ar$ hornblende geochronology from the Forsmark area in central Sweden – constraints on late Svecofennian cooling, deformation and exhumation. Precambrian Research.

Hjerne C, Ludvigsson J-E, Harrström J, 2008. The impact of interpreted flow regimes during constant head injection tests on the estimated transmissivity from injection tests and difference flow logging conducted at Forsmark. SKB R-08-118, Svensk Kärnbränslehantering AB.

Hoch A R, Jackson C P, 2004. Rock-matrix diffusion in transport of salinity. Implementation in CONNECTFLOW. SKB R-04-78, Svensk Kärnbränslehantering AB.

Hoek E, Kaiser P K, Bawden W F, 1995. Support of underground excavations in hard rock, Balkema.

Hoek E, 2007. Practical rock engineering, updated version. Notes that are available on the site www.rocscience.com.

Holmén J G, Stigsson M, 2001. Modelling of future hydrogeological conditions at SFR. SKB R-01-02, Svensk Kärnbränslehantering AB.

Hunter F M I, Hartley L J, Hoch A, Jackson C P, McCarthy R, Marsic N, Gylling B, 2008. Calibration of regional palaeohydrology and sensitivity analysis using hydrochemistry data in site investigations. Applied Geochemistry, vol 23, pp 1982–2003.

Hökmark H, Sundberg J, Kristensson O, Lönnqvist M, Hellström G, 2009. Strategy for thermal dimensioning of the final repository for spent nuclear fuel. SKB R-09-04, Svensk Kärnbränslehantering AB.

Isaksson H, Thunehed H, Keisu M, 2004. Interpretation of airborne geophysics and integration with topography. Forsmark site investigation. SKB P-04-29, Svensk Kärnbränslehantering AB.

Isaksson H, Keisu M, 2005. Interpretation of airborne geophysics and integration with topography. Stage 2 (2002–2004). An integration of bathymetry, topography, refraction seismics and airborne geophysics. Forsmark site investigation. SKB P-04-282, Svensk Kärnbränslehantering AB.

Isaksson H, Pitkänen T, Thunehed H, 2006a. Ground magnetic survey and lineament interpretation in an area northwest of Bolundsfjärden. Forsmark site investigation. SKB P-06-85, Svensk Kärnbränslehantering AB.

Isaksson H, Thunehed H, Pitkänen T, Keisu M, 2006b. Detailed ground and marine magnetic survey and lineament interpretation in the Forsmark area – 2006. Forsmark site investigation. SKB P-06-261, Svensk Kärnbränslehantering AB.

Isaksson H, 2007. Correlation between refraction seismic data, low magnetic lineaments and deformation zones (model stage 2.2). In Stephens M B and Skagius K (ed), Geology – background complementary studies. Forsmark modelling stage 2.2. SKB R-07-56, Svensk Kärnbränslehantering AB.

Isaksson H, Stephens M B, 2007. Assessment of the validity of the rock domain model, version 1.2, based on the modelling of gravity and petrophysical data. Forsmark site investigation. SKB R-07-67, Svensk Kärnbränslehantering AB.

Isaksson H, Thunehed H, Pitkänen T, Keisu M, 2007. Detailed ground magnetic survey and lineament interpretation in the Forsmark area, 2006–2007. Forsmark site investigation. SKB R-07-62, Svensk Kärnbränslehantering AB.

Jacobsson L, 2007. Boreholes KFM01A and KFM02B. Micro crack volume measurements and triaxial compression tests on intact rock. Forsmark site investigation. SKB P-07-93, Svensk Kärnbränslehantering AB.

Jaquet O, Siegel P, 2003. Groundwater flow and transport modelling during a glaciation period. SKB R-03-04, Svensk Kärnbränslehantering AB.

Jaquet O, Siegel P, 2006. Regional groundwater flow model for a glaciation scenario. Simpevarp subarea – version 1.2. SKB R-06-100, Svensk Kärnbränslehantering AB.

Johansson R, 2005. A comparison of two independent interpretations of lineaments from geophysical and topographic data at the Forsmark site. SKB R-05-23, Svensk Kärnbränslehantering AB.

Johansson P-O, Werner K, Bosson E, Berglund S, Juston J, 2005. Description of climate, surface hydrology, and near-surface hydrogeology. Preliminary site description Forsmark area – version 1.2. SKB R-05-06, Svensk Kärnbränslehantering AB.

Johnsson A, Arlinger J, Pedersen K, Ödegaard-Jensen A, Albinsson Y, 2006. Solid-aqueous phase partitioning of radionuclides by complexing compounds excreted by subsurface bacteria. Geomicrobiol. J., 23, pp. 621–630.

Johansson P-O, 2008. Description of surface hydrology and near-surface hydrogeology at Forsmark. Site descriptive modelling, SDM-Site Forsmark. SKB R-08-08, Svensk Kärnbränslehantering AB.

Johansson P-O, Öhman J, 2008. Presentation of meteorological, hydrological and hydrogeological monitoring data from Forsmark. Site descriptive modelling, SDM-Site Forsmark. SKB R-08-10, Svensk Kärnbränslehantering AB

Jonsell B, Jonsell L, 1995. Floran i Hållnäs socken. Svensk Botanisk Tidskrift 89 (5), 257–312. ISSN 0039-646X, Lund.

Juhlin C, Bergman B, Palm H, 2002. Reflection seismic studies in the Forsmark area – stage 1. SKB R-02-43, Svensk Kärnbränslehantering AB.

Juhlin C, Bergman B, 2004. Reflection seismics in the Forsmark area. Updated interpretation of Stage 1 (previous report R-02-43). Updated estimate of bedrock topography (previous report P-04-99). SKB P-04-158, Svensk Kärnbränslehantering AB.

Juhlin C, Palm H, 2005. Reflection seismic studies in the Forsmark area, 2004: Stage 2. Forsmark site investigation. SKB R-05-42, Svensk Kärnbränslehantering AB.

Juhlin C, Stephens M B, 2006. Gently dipping fracture zones in Paleoproterozoic metagranite, Sweden: Evidence from reflection seismic and cored borehole data and implications for the disposal of nuclear waste. Journal of Geophysical Research 111, B09302, 19 pp.

Juhlin C, 2007. Integrated interpretation of surface and borehole (VSP) seismic data along profiles 2 and 5, Forsmark, Sweden. In Stephens M B and Skagius K (ed), Geology – background complementary studies. Forsmark modelling stage 2.2. SKB R-07-56, Svensk Kärnbränslehantering AB.

Juston J, Johansson P-O, Levén J, Tröjbom M, Follin S, 2007. Analysis of meteorological, hydrological and hydrogeological monitoring data. Forsmark – stage 2.1. SKB R-06-49, Svensk Kärnbränslehantering AB.

Kalinowski B (ed), 2008. Background complementary hydrogeochemical studies, SDM-Site Forsmark. SKB R-08-87, Svensk Kärnbränslehantering AB.

Koistinen T, Stephens M B, Bogatchev V, Nordgulen O, Wennerström M, Korhonen J, 2001. Geological map of the Fennoscandian Shield, scale 1:2 000 000. Geological Surveys of Finland, Norway and Sweden and the North-West Department of Natural Resources of Russia.

Korhonen K, Paananen M, Paulamäki S, 2004. Interpretation of lineaments from airborne geophysical and topographic data. An alternative model within version 1.2 of the Forsmark modelling project. Forsmark site investigation. SKB P-04-241, Svensk Kärnbränslehantering AB.

Kumblad L, Kautsky U, Næslund B, 2006. Transport and fate of radionuclides in aquatic environments – the use of ecosystem modelling for exposure assessments of nuclear facilities. Journal of Environmental Radioactivity 87, 107–129.

Laaksoharju M, Wallin B (ed), 1997. Evolution of the groundwater chemistry at the Äspö Hard Rock Laboratory. Proceedings of the second Äspö International Geochemistry Workshop, June 6–7, 1995. SKB, International Cooperation Report 97-04, Svensk Kärnbränslehantering AB.

Laaksoharju M, 1999. Groundwater characterisation and modelling: Problems, facts and possibilities. Dissertation TRITA-AMI-PHD 1031; ISSN 1400-1284; ISRN KTH/AMI/PHD 1031-SE; ISBN 91-7170-. Royal Institute of Technology, Stockholm, Sweden. SKB TR-99-42, Svensk Kärnbränslehantering AB.

Laaksoharju M, Skårman C, Skårman E, 1999. Multivariate Mixing and Mass-balance (M3) calculations, a new tool for decoding hydrogeochemical information. Applied Geochemistry, vol 14, pp 861–871.

Laaksoharju M, Smellie J, Tullborg E-L, Gimeno M, Hallbäck L, Molinero J, Waber N, 2008a. Bedrock hydrogeochemistry Forsmark. Site descriptive modelling, SDM-Site Forsmark. SKB R-08-47, Svensk Kärnbränslehantering AB.

Laaksoharju M, Smellie J, Tullborg E-L, Gimeno M, Molinero J, Gurban I, Hallbeck L, 2008b. Hydrogeochemical evaluation and modelling performed within the Swedish site investigation programme. Applied Geochemistry, vol 23, pp 1761–1795.

Laaksoharju M, Gascoyne M, Gurban I, 2008c. Understanding groundwater chemistry using mixing models. Applied Geochemistry, vol 23, pp 1921–1940.

Langmuir D, 1997. Aqueous Environmental Geochemistry, Prentice Hall, New Jersey.

La Pointe P, Olofsson I, Hermanson J, 2005. Statistical model of fractures and deformation zones for Forsmark: Preliminary site description Forsmark area – version 1.2. SKB R-05-26, Svensk Kärnbränslehantering AB.

Leijon B (ed), 2005. Investigations of superficial fracturing and block displacements at drill site 5. Forsmark site investigation. SKB P-05-199, Svensk Kärnbränslehantering AB.

Lindborg T (ed), 2005. Description of the surface systems. Preliminary site description Forsmark area – version 1.2. SKB R-05-03, Svensk Kärnbränslehantering AB.

Lindborg T (ed), 2008. Surface system Forsmark. Site descriptive modelling, SDM-Site Forsmark. SKB R-08-11, Svensk Kärnbränslehantering AB.

Lindquist A, Hjerne C, Nordquist R, Byegård J, Walger E, Ludvigson J-E, Wass E, 2008. Confirmatory hydraulic interference test and tracer test at drill site 2. Forsmark site investigation. SKB P-08-13, Svensk Kärnbränslehantering AB.

Lindroos H, Isaksson H, Thunehed H, 2004. The potential for ore and industrial minerals in the Forsmark area. SKB R-04-18, Svensk Kärnbränslehantering AB.

Lundin L, Lode E, Stendahl J, Melkerud P-A, Björkvald L, Thorstensson A, 2004. Soils and site types in the Forsmark area. SKB R-04-08, Svensk Kärnbränslehantering AB.

Löfgren A, Lindborg T, 2003. A descriptive ecosystem model – a strategy for model development during site investigations. SKB R-03-06, Svensk Kärnbränslehantering AB.

Löfgren M, Crawford J, Elert M, 2007. Tracer tests – possibilities and limitations. Experience from SKB fieldwork: 1977–2007. SKB R-07-39, Svensk Kärnbränslehantering AB.

Löfgren A (ed), 2008. The terrestrial ecosystems at Forsmark and Laxemar. Site descriptive modelling, SDM-Site. SKB R-08-01, Svensk Kärnbränslehantering AB.

Mardia K, Jupp P, 2000. Directional statistics. Wiley & Sons Ltd. IBSN: 0-471-95333-4.

Martin C D, Stimpson B, 1994. The effect of sample disturbance on laboratory properties of Lac du Bonnet granite. Canadian Geotechnical Journal, vol. 31, pp 692–702.

Martin C D, 2007. Quantifying in situ stress magnitudes and orientations for Forsmark. Forsmark stage 2.2. SKB R-07-26, Svensk Kärnbränslehantering AB.

Mattsson H, 2007. Interpretation of tomography inversion models for seismic refraction data along profile LFM001017 in Forsmark. In Stephens M B and Skagius K (edits.), Geology – background complementary studies. Forsmark modelling stage 2.2. SKB R-07-56, Svensk Kärnbränslehantering AB.

Miliander S, Punakivi M, Kyläkorpi L, Rydgren B, 2004. Human population and activities in Forsmark, Site description. SKB R-04-10, Svensk Kärnbränslehantering AB.

Molinero J, Arcos D, Duro L, 2008. Contribution to ChemNet activities. Forsmark model 2.2-2.3. In: Kalinowski B (ed) Background complementary hydrogeochemical studies, SDM-Site Forsmark. SKB R-08-87, Svensk Kärnbränslehantering AB.

Munier R, Stenberg L, Stanfors R, Milnes A G, Hermanson J, Triumf C-A, 2003. Geological Site Descriptive Model. A strategy for the model development during site investigations. SKB R-03-07, Svensk Kärnbränslehantering AB.

Munier R, 2004. Statistical analysis of fracture data, adapted for modelling Discrete Fracture Networks – Version 2. SKB R-04-66, Svensk Kärnbränslehantering AB.

Munier R, Hökmark H, 2004. Respect distances. Rationale and means of computation. SKB R-04-17, Svensk Kärnbränslehantering AB.

Munier R, Stigsson M, 2007. Implementation of uncertainties in borehole geometries and geological orientation data in Sicada. SKB R-07-19, Svensk Kärnbränslehantering AB.

Möller C, Snäll S, Stephens M B, 2003. Dissolution of quartz, vug formation and new grain growth associated with post-metamorphic hydrothermal alteration in KFM02A. Forsmark site investigation. SKB P-03-77, Svensk Kärnbränslehantering AB.

NEA, 1993. Palaeohydrogeological methods and their application. Workshop Proceedings, Paris, France, 9–10 November, 1992. Co-ordinating Group on Site Evaluation and Design of Experiments for Radioactive Waste Disposal – SEDE, OECD-NEA.

NEA, 1999. Confidence in models of radionuclide transport for site-specific assessment. Workshop Proceedings, Carlsbad, New Mexico, USA, 14–17 June, 1999. OECD-NEA Radioactive Waste Management, GEOTRAP Project.

NEA, 2004. The first AMIGO workshop on building confidence using multiple lines of evidence. Workshop Proceedings, Yverdon-les Bains, Switzerland, 3–5 June 2003. OECD-NEA, NEA/RWM/IGSC(2004)8.

Neretnieks I, Moreno L, 2003. Prediction of some in situ tracer tests with sorbing tracers using independent data. J. Cont. Hydrol., 61, pp. 351–360.

Nilsson G, Nissen J, 2007. Revision of borehole deviation measurements in Forsmark. Forsmark site investigation. SKB P-07-28, Svensk Kärnbränslehantering AB.

Nilsson A-C, 2008. Analytical uncertainties. In: Kalinowski B (ed), Background complementary hydrogeochemical studies, SDM-Site Forsmark. SKB R-08-87, Svensk Kärnbränslehantering AB.

Nissen J, 2007. Refraction seismic data and bedrock velocity distribution at Forsmark. In: Stephens M B and Skagius K (ed), Geology – background complementary studies. Forsmark modelling stage 2.2. SKB R-07-56, Svensk Kärnbränslehantering AB.

Nordén S, Andersson E, Söderbäck B, 2008. The limnic ecosystems at Forsmark and Laxemar. Site descriptive modelling, SDM-Site. SKB R-08-02, Svensk Kärnbränslehantering AB.

Nordgulen Ø, Saintot A, 2006. The character and kinematics of deformation zones (ductile shear zones, fault zones and fracture zones) at Forsmark – report from phase 1. Forsmark site investigation. SKB P-06-212, Svensk Kärnbränslehantering AB.

Nordgulen Ø, Saintot A, 2008. The character and kinematics of deformation zones (ductile shear zones, fracture zones and fault zones) at Forsmark – report from phase 3. Forsmark site investigation. SKB P-07-111, Svensk Kärnbränslehantering AB.

Nordqvist R, Gustafsson E, Andersson P, Thur P, 2008. Groundwater flow and hydraulic gradients in fractures and fracture zones at Forsmark and Oskarshamn. SKB R-08-103, Svensk Kärnbränslehantering AB.

Olofsson I, Fredriksson A, 2005. Strategy for a numerical Rock Mechanics Site descriptive Model. Further development of the theoretical/numerical approach. SKB R-05-43, Svensk Kärnbränslehantering AB.

Olofsson I, Simeonov A, Stephens M, Follin S, Nilsson A-C, Röshoff K, Lindberg U, Lanaro F, Fredriksson A, Persson L, 2007. Site descriptive modelling Forsmark, stage 2.2. A fracture domain concept as a basis for the statistical modelling of fractures and minor deformation zones, and interdisciplinary coordination. SKB R-07-15, Svensk Kärnbränslehantering AB.

Parkhurst D L, Appelo C A J, 1999. User's Guide to PHREEQC (Version 2), a computer program for speciation, batch-reaction, one-dimensional transport, and inverse geochemical calculations. Water Resources Research Investigations Report 99-4259.

Pedersen K, **2005.** Control of microorganism content in flushing water used for drilling of KFM06A. Forsmark site investigation. SKB P-05-81, Svensk Kärnbränslehantering AB.

Pedersen K, Arlinger J, Eriksson S, Hallbeck A, Hallbeck L, Johansson J, 2008. Numbers, biomass and cultivable diversity of microbial populations relate to depth and borehole-specific conditions in groundwater from depths of 4–450 m in Olkiluoto, Finland. ISME-J doi:10.1038/ismej.2008.43.

Persson C, 1992. The latest ice recession and till deposits in the northern Uppland, eastern central Sweden, Sveriges Geologiska Undersökning, Ser. Ca 81, pp 217–224.

Persson H, Stadenberg I, 2007. Distribution of fine roots in forest areas close to the Swedish Forsmark and Oskarshamn nuclear power plants. SKB R-07-01, Svensk Kärnbränslehantering AB.

Petersson J, Berglund J, Danielsson P, Skogsmo G, 2005. Petrographic and geochemical characteristics of bedrock samples from boreholes KFM04A-06A, and a whitened alteration rock. Forsmark site investigation. SKB P-05-156, Svensk Kärnbränslehantering AB.

Petersson J, Skogsmo G, Vestgård J, Albrecht J, Hedenström A, Gustavsson J, 2007a. Bedrock mapping and magnetic susceptibility measurements, Quaternary investigations and GPR measurements in trench AFM001265. Forsmark site investigation. SKB P-06-136, Svensk Kärnbränslehantering AB.

Petersson J, Andersson U B, Berglund J, 2007b. Scan line fracture mapping and magnetic susceptibility measurements across two low magnetic lineaments with NNE and NE trend, Forsmark. In Stephens M B and Skagius K (ed), Geology – background complementary studies. Forsmark modelling stage 2.2. SKB R-07-56, Svensk Kärnbränslehantering AB.

Pitkänen P, Luukkonen A, Ruotsalainen P, Leino-Forsman H, Vuorinen U, 1999. Geochemical modelling of groundwater evolution and residence time at the Olkilouto site. POSIVA Report 98-10, POSIVA, Helsinki, Finland.

Pitkänen P, Partamies S, Luukkonen A, 2004. Hydrogeochemical interpretation of baseline groundwater conditions at the Olkiluoto site. Posiva Tech. Rep. (2003-07), Posiva, Helsinki, Sweden.

Påsse T, 2001. An empirical model of glacio-isostatic movements and shore-level displacement in Fennoscandia. SKB R-01-41, Svensk Kärnbränslehantering AB.

Rabung T, Pierret M, Bauer A, Geckeis H, Bradbury M, Baeyens B, 2005. Sorption of Eu(III)/Cm(III) on Ca-montmorillonite and Na-illite. Part 1: Batch sorption and time-resolved laser fluorescence spectroscopy experiments. Geochim. Cosmochim. Acta., 69(23), pp. 5393–5402.

Rhen I, Smellie J A T, 2003. Task force modelling of groundwater flow and transport of solutes. Task 5 summary report. SKB TR-03-01, Svensk Kärnbränslehantering AB.

Rhén I, Follin S, Hermanson J, 2003. Hydrogeological Site Descriptive Model. A strategy for its development during Site Investigations. SKB R-03-08, Svensk Kärnbränslehantering AB.

Ringgaard J, 2007a. Mapping of borehole breakouts. Processing of acoustical televiewer data from KFM01A, KFM01B, KFM02A, KFM03A, KFM03B, KFM04A, KFM05A, KFM06A and KFM07C. Forsmark site investigation. SKB P-07-07, Svensk Kärnbränslehantering AB.

Ringgaard J, 2007b. Mapping of borehole breakouts. Processing of acoustical televiewer data from KFM08A, KFM08C, KFM09A, KFM09B, and KFM90B. Forsmark site investigation. SKB P-07-166, Svensk Kärnbränslehantering AB.

Röshoff K, Lanaro F, Jing L, 2002. Strategy for a Rock Mechanics Site Descriptive Model. Development and testing of the empirical approach. SKB R-02-01, Svensk Kärnbränslehantering AB.

Saintot A, Nordgulen Ø, 2007. The character and kinematics of deformation zones (ductile shear zones, fault zones and fracture zones) at Forsmark – report from phase 2. Forsmark site investigation. SKB P-07-101, Svensk Kärnbränslehantering AB.

Samper J, Delgado J, Juncosa R, Montenegro L, 2000. CORE2D v 2.0: A Code for nonisothermal water flow and reactive solute transport. User's manual. ENRESA Technical report 06/2000.

Sandström B, Savolainen M, Tullborg E-L, 2004. Fracture mineralogy. Results from fracture minerals and wall rock alteration in boreholes KFM01A, KFM02A, KFM03A and KFM03B. Forsmark site investigation. SKB P-04-149, Svensk Kärnbränslehantering AB.

Sandström B, Tullborg E-L, 2005. Fracture mineralogy. Results from fracture minerals and rock wall alteration in boreholes KFM01B, KFM04A, KFM05A and KFM06A. Forsmark site investigation. SKB P-05-197, Svensk Kärnbränslehantering AB.

Sandström B, Tullborg E-L, 2006. Mineralogy, geochemistry, porosity and redox capacity of altered rock adjacent to fractures. Forsmark site investigation. SKB P-06-209, Svensk Kärnbränslehantering AB.

Sandström B, Tullborg E-L, de Torres T, Ortiz J E, 2006. The occurrence and possible origin of asphaltite in bedrock fractures, Forsmark, central Sweden. GFF 128, 233–242.

Sandström B, Tullborg E-L, 2007. Paleohydrogeological events in Forsmark, central Sweden, recorded by stable isotopes in calcite and pyrite. In Water-Rock Interaction, Taylor and Francis Group, London, 773–776.

Sandström B, Tullborg E-L, Smellie J, MacKenzie A B, Suksi J, 2008. Fracture mineralogy of the Forsmark site, SDM-Site Forsmark. SKB R-08-102, Svensk Kärnbränslehantering AB.

Sitch S, Smith B, Prentice I C, Arneth A, Bondeau A, Crameer W, Kaplans J O, Levis S, Lucht W, Sykes M T, Thonicke K, Venevsky S, 2003. Evaluation of ecosystem dynamics, plant geography and terrestrial carbon cycling in the LPJ Dynamic Global Vegetation Model. Global Change Biology. 9:161–185.

Sjöberg J, Lindfors U, Perman F, Ask D, 2005. Evaluation of the stress at the Forsmark site. Preliminary site investigation Forsmark area – version 1.2. SKB R-05-35, Svensk Kärnbränslehantering AB.

Skagius K, 1986. Diffusion of dissolved species in the matrix of some Swedish crystalline rocks. Ph.D. Thesis, Dept. of Chemical Engineering, Royal Institute of Technology, Stockholm, Sweden.

Skagius K, 1986. Diffusion of dissolved species in the matrix of some Swedish crystalline rocks. Ph.D. Thesis, Dept. of Chemical Engineering, Royal Institute of Technology, Stockholm, Sweden.

SKB, 1999. SR 97 – Deep repository for spent nuclear fuel. SR 97 – Post-closure safety. Main report – Vol. I, Vol. 2 and Summary. SKB TR-99-06, Svensk Kärnbränslehantering AB.

SKB, 2000. Samlad redovisning av metod, platsval och program inför platsundersökningsskedet (Fud-k). Svensk Kärnbränslehantering AB.

SKB 2001. Site investigations. Investigation methods and general execution programme. SKB TR-01-29, Svensk Kärnbränslehantering AB.

SKB, 2002. Forsmark – site descriptive model version 0. SKB R-02-32, Svensk Kärnbränslehantering AB.

SKB, 2004. Preliminary site description Forsmark area–version 1.1. SKB R-04-15, Svensk Kärnbränslehantering AB.

SKB, 2005a. Preliminary site description Forsmark area – version 1.2. SKB R-05-18, Svensk Kärnbränslehantering AB.

SKB, 2005b. Preliminary safety evaluation for the Forsmark area. Based on data and site descriptions after the initial site investigation stage. SKB TR-05-16, Svensk Kärnbränslehantering AB.

SKB, 2005c. Forsmark site investigation. Programme for further investigations of geosphere and biosphere. SKB R-05-14, Svensk Kärnbränslehantering AB.

SKB, 2005d. Hydrogeochemical evaluation. Preliminary site description Forsmark area – version 1.2. SKB R-05-17, Svensk Kärnbränslehantering AB.

SKB, 2006a. Site descriptive modelling Forsmark stage 2.1. Feedback for completion of the site investigation including input from safety assessment and repository engineering. SKB R-06-38, Svensk Kärnbränslehantering AB.

SKB, 2006b. Long-term safety for KBS-3 repositories at Forsmark and Laxemar – a first evaluation. Main Report of the SR-Can project. SKB TR-06-09, Svensk Kärnbränslehantering AB.

SKB, 2006c. Hydrogeochemical evaluation of the Forsmark site, modelling stage 2.1 – issue report. SKB R-06-69, Svensk Kärnbränslehantering AB.

SKB, 2007. Forsmark site investigation. Programme for long-term observations of geosphere and biosphere after completed site investigations. SKB R-07-34, Svensk Kärnbränslehantering AB.

SKB, 2008. Confidence assessment Forsmark, Site descriptive modelling, SDM-Site Forsmark. SKB R-08-82, Svensk Kärnbränslehantering AB.

Slunga R, 1991. The Baltic Shield earthquakes. Tectonphysics, vol 189, 323–331.

Smellie J, Laaksoharju M, Tullborg E-L, 2002. Hydrogeochemical site descriptive model – a strategy for the model development during site investigations. SKB R-02-49, Svensk Kärnbränslehantering AB.

Smellie J, Tullborg E-L, Nilsson A-C, Gimeno M, Sandström B, Waber N, Gascoyne M, 2008. Explorative analysis of major components and isotopes, SDM-Site Forsmark. SKB R-08-84, Svensk Kärnbränslehantering AB.

Sohlenius G, Hedenström A, Rudmark L, 2004. Mapping of unconsolidated Quaternary deposits 2002–2003. Map description. Forsmark site investigations. SKB R-04-39, Svensk Kärnbränslehantering AB.

Sonesten L, 2005. Chemical characteristics of surface waters in the Forsmark area. Evaluation of data from lakes, streams, and coastal sites. SKB-R-05-41, Svensk Kärnbränslehantering AB.

SSI, 2005. Statens strålskyddsinstituts allmänna råd om tillämpning av föreskrifterna (SSI FS 1998:1) om skydd av människors hälsa och miljön vid slutligt omhändertagande av använt kärnbränsle och kärnavfall. SSI FS 2005:5, Statens strålskyddsinstituts författningssamling.

Stephansson O, Ljunggren C, Jing L, 1991. Stress measurements and tectonic implications for Fennoscandia. Tectonophysics, 189, pp 317–322.

Stephens M B, Bergman T, Andersson J, Hermansson T, Wahlgren C-H, Albrecht L, Mikko H, 2003a. Bedrock mapping. Stage 1 (2002) – Outcrop data including fracture data. Forsmark. SKB P-03-09, Svensk Kärnbränslehantering AB.

Stephens M B, Lundqvist S, Bergman T, Andersson J, Ekström M, 2003b. Bedrock mapping. Rock types, their petrographic and geochemical characteristics, and a structural analysis of the bedrock based on stage 1 (2002) surface data. Forsmark site investigation. SKB P-03-75, Svensk Kärnbränslehantering AB.

Stephens M B, Lundqvist S, Bergman T, Ekström M, 2005. Bedrock mapping. Petrographic and geochemical characteristics of rock types based on Stage 1 (2002) and Stage 2 (2003) surface data. Forsmark site investigation. SKB P-04-87, Svensk Kärnbränslehantering AB.

Stephens M, Forssberg O, 2006. Rock types and ductile structures on a rock domain basis, and fracture orientation and mineralogy on a deformation zone basis. Preliminary site description Forsmark area – version 1.2. SKB R-06-78, Svensk Kärnbränslehantering AB.

Stephens M B, Skagius K (ed), 2007. Geology – background complementary studies. Forsmark modelling stage 2.2. SKB R-07-56, Svensk Kärnbränslehantering AB.

Stephens M B, Fox A, La Pointe P, Simeonov A, Isaksson H, Hermanson J, Öhman J, 2007. Geology Forsmark. Site descriptive modelling Forsmark stage 2.2. SKB R-07-45, Svensk Kärnbränslehantering AB.

Stephens M B, Simeonov A, Isaksson H, 2008. Bedrock geology Forsmark. Modelling stage 2.3. Implications for and verification of deterministic geological models based on complementary data. SKB R-08-64, Svensk Kärnbränslehantering AB.

Sterner R W, Elser J J, 2002. Ecological Stoichiometry. Princeton University Press, Princeton, USA.

Streckeisen A, 1976. To each plutonic rock its proper name. Earth Science Reviews 12.

Ström A, Andersson J, Skagius K, Winberg A, 2008. Site descriptive modelling during characterization for a geological repository for nuclear waste in Sweden. Applied Geochemistry, vol 23, pp 1747–1760.

Strömberg B, 1989. Late Weichselian deglaciation and clay varve chronology in east-central Sweden. Sveriges geologiska undersökning, Ca 73.

Strömgren M, Brydsten L, 2008. Digital elevation models of Forsmark. Site descriptive modelling, SDM-Site Forsmark. SKB R-08-62, Svensk Kärnbränslehantering AB.

Stumm W, Morgan J, 1996. Aquatic Chemistry: Chemical Equilibria and Rates in natural Waters, 3 ed., Wiley, New York.

Sundberg J, 2003a. Thermal Site Descriptive Model. A strategy for the model development during site investigations. SKB R-03-10, Svensk Kärnbränslehantering AB.

Sundberg J, 2003b. Thermal properties at Äspö HRL. Analysis of distribution and scale factors. SKB R-03-17. Svensk Kärnbränslehantering AB.

Sundberg J, Back P-E, Bengtsson A, Ländell M, 2005a. Thermal modelling. Preliminary site description Forsmark area – version 1.2. SKB R-05-31, Svensk Kärnbränslehantering AB.

Sundberg J, Back P-E, Hellström G, 2005b. Scale dependence and estimation of rock thermal conductivity. Analysis of upscaling, inverse thermal modelling and value of information with the Äspö HRL prototype repository as an example. SKB R-05-82, Svensk Kärnbränslehantering AB.

Sundberg J, Wrafter J, Mossmark F, Sundberg A, 2007. Anisotropy of thermal properties in metagranite at Forsmark. Comparison between large-scale field measurements, small-scale field measurements and laboratory measurements. Forsmark site investigation. SKB P-07-194, Svensk Kärnbränslehantering AB.

Sundberg J, Wrafter J, Ländell M, Back P-E, Rosén L, 2008. Thermal properties Forsmark. Modelling stage 2.3. Complementary analysis and verification of the thermal bedrock model. SKB R-08-65, Svensk Kärnbränslehantering AB.

Sundberg J, Back P-E, Ericsson L O, Wrafter J, 2009. Estimation of thermal conductivity and its spatial variability in igneous rocks from in situ density logging. International Journal of Rock Mechanics and Mining Sciences, 46, pp 1023–1028.

Svenonius F, 1887. Beskrifning till kartbladen Forsmark och Björn. SGU Aa 98 och 99, Sveriges Geologiska Undersökning.

Söderbäck B (ed), 2008. Geological evolution, palaeoclimate and historical development of the Forsmark and Laxemar-Simpevarp areas. Site descriptive modelling, SDM-Site. SKB R-08-19, Svensk Kärnbränslehantering AB.

Söderlund P, Hermansson T, Page L M, Stephens M B, (in press). Biotite and muscovite ^{40}Ar-^{39}Ar geochronological constraints on the post-Svecofennian tectonothermal evolution, Forsmark site, central Sweden. International Journal of Earth Sciences.

Talme O, Almén K-E, 1975. Jordartsanalys. Laboratorieanvisningar, del 1. Department of Quaternary Research. Stockholm University. 1 pp.

Thunehed H, Pitkänen T, 2007. Transient electromagnetic soundings at Forsmark and the regional surroundings. Estimations of depth to saline groundwater. Forsmark site investigation. SKB P-07-165, Svensk Kärnbränslehantering AB.

Tröjbom M, Söderbäck B, 2006. Chemical characteristics of surface systems in the Forsmark area. Visualisation and statistical evaluation of data from shallow groundwater, precipitation, and regolith. SKB R-06-19, Svensk Kärnbränslehantering AB.

Tröjbom M, Söderbäck B, Johansson P-O, 2007. Hydrochemistry in surface water and shallow groundwater. Site descriptive modelling, SDM-Site Forsmark. SKB R-07-55, Svensk Kärnbränslehantering AB.

Upstill-Goddard R C, Elderfield H, 1988. The role of diagenesis in the estuarine budgets of iodine and bromine. Continental Shelf Research 8, 405–430

Vilks P, Miller H, Doern D, 1991. Natural colloids and suspended particles in Whiteshell Research area, Manitoba, Canada, and their potential effect on radiocolloid formation. Applied Geochemistry, vol 8, pp 565–574.

Voss C, Provost A, 2002. SUTRA. A model for saturated-unsaturated, variable-density ground-water flow with solute or energy transport. U.S. Geological Survey, Water-Resources Investigations Report 02-4231, Reston Va.

Waber H N, Smellie J A T, 2007. Boreholes KFM01D, KFM08C and KFM09B: Characterisation of pore water. Part 1: Diffusion experiments and pore water data. Forsmark site investigation. SKB P-07-119, Svensk Kärnbränslehantering AB.

Waber H N, Smellie J A T, 2008. Characterisation of porewater in crystalline rocks. Applied Geochemistry, vol 23, pp 1834–1861.

Waber H N, Gimmi T, Smellie J A T, 2008. Porewater chemistry in the rock matrix, SDM-Site Forsmark. SKB R-08-105, Svensk Kärnbränslehantering AB.

Walsh J B, Decker E R, 1966. Effect of pressure and saturating fluid on the thermal conductivity of compact rock. J. Geophys. Res., 71, 12.

Wass E, Andersson P, 2006. Groundwater flow measurements and tracer tests at drill site 1. Forsmark site investigation. SKB P-06-125, Svensk Kärnbränslehantering AB.

Welin E, 1964. Uranium disseminations and vein fillings in iron ores of northern Uppland, central Sweden. Geologiska Föreningens i Stockholm Förhandlingar 86, 51–82.

Westman P, Wastegård S, Schoning K, Gustafsson B, 1999. Salinity change in the Baltic Sea during the last 8,500 years: evidence causes and models. SKB TR-99-38, Svensk Kärnbränslehantering AB.

Whicker F W, Schultz V, 1982. Radioecology: Nuclear Energy and the Environment. CRC Press, Boca Raton, Florida.

Widestrand H, Byegård J, Ohlsson Y, Tullborg E-L, 2003. Strategy for the use of laboratory methods in the site investigation programme for the transport properties of the rock. SKB R-03-20, Svensk Kärnbränslehantering AB.

Widestrand H, Byegård J, Selnert E, Skålberg M, Höglund S, Gustafsson E, 2010. Long Term Sorption Diffusion Experiment (LTDE-SD). Supporting laboratory program – Sorption diffusion experiments and rock material characterisation. With supplement of adsorption studies on intact rock samples from the Forsmark and Laxemar site investigations. SKB R-10-66, Svensk Kärnbränslehantering AB.

Wijnbladh E, Aquilonius K, Floderus S, 2008. The marine ecosystems at Forsmark and Laxemar, Site descriptive modelling, SDM-Site. SKB R-08-03, Svensk Kärnbränslehantering AB.

Winberg A, Andersson P, Hermanson J, Byegård J, Cvetkovic V, Birgersson L, 2000. Äspö Hard Rock Laboratory. Final report of the first stage of the tracer retention understanding experiments. SKB TR-00-07, Svensk Kärnbränslehantering AB.

Wikberg P, 1998. Äspö Task Force on modelling of groundwater flow and transport of solutes. SKB HRL-98-07, Svensk Kärnbränslehantering AB.

Wrafter J, Sundberg J, Ländell M, Back P-E, 2006. Thermal modelling. Site descriptive modelling. Laxemar – stage 2.1. SKB R-06-84, Svensk Kärnbränslehantering AB.

Appendix 1

Topography and place names in the Forsmark area

1628000 1630000 1632000 1634000 1636000 1638000

6702000 6700000 6698000 6696000 6694000

Dyviks–
fjärden
Simp–
viken
Asphäll–
sundet
SFR offices
Asphällsfjärden
Nuclear power plant
Sewage plant
Klubbudden
Stånggrundsfjärden
Lillfjärden
Gunnarsbo–
Pigträsket
Storgården
Björnbo
Dannebo
Långängen
Gunnarsbo–
träsket
Gunnarsbo
Labboträsket
Puttan
Graven
Bolundsfjärden
Fräkengropen
Kungsträsket
Jungfruholm
Tall–
sundet
Tixelfjärden
Simp–
viken
Pilsnerviken
Öregrundsgrepen
Bred–
viken
Lillfjärden
Vambörs–
fjärden
Gällsboträsket
Märrbadet
Kasfjärden
Lättsa
Rönningarna
Bruksdammen
Tyskland
Udden
Framdammen
Forsmark
Stenrösmossen
Stocksjön
Fiskarfjärden
Storskäret
Börstilsåsen
Eckarfjärden
Gruvviken
Habbalsbo
Hermansbo
Hagen
Lövörsundet
Lövörsgräset
Kallrigafjärden
Stenskärsviken
Skatan
Grynören
Länsöän
Forsmarksån
Prästängen
Johannesfors
Skärnåån
Norrsjön
Länsöän
Solvik
Kallerö
Fallet
Johannisfors
Silvertal
Karlsborg
Solklinten
Fågel–
fjärd
Länsö
Forsmarksån
Kallrigafjärden

N

Candidate area
Target area
Contour, 1m
Contour, 5m

0 0.5 1 2 km

Appendix 2

Nomenclature

This appendix contains explanations to acronyms and technical terms used by SKB which occur in this report. Definition of terms that are of basic importance for the modelling and description of the Forsmark site are provided in section 1.6.5.

1D	One-dimensional.
2D	Two-dimensional.
3D	Three-dimensional.
3DEC	3 Dimensional Distinct Element Code; numerical modelling tool used to estimate rock mass mechanical properties and *in situ* stress variability due to deformation zones.
AA	Autotrophic Acetogens – microorganisms that produce acetate from inorganic sources.
AD	Anno Domini.
AFMxxxxxx	Area at the ground surface over which data have been acquired, for example detailed fracture mapping.
AM	Autotrophic Methanogens – microorganisms that produce methane from inorganic sources.
AMS	Anisotropy of Magnetic Susceptibility; laboratory method to determine orientation of ductile structures in the bedrock as well as degree and character of ductile strain.
ATP	Adenosine-Tri-Phosphate.
BAT type Filter Tip	The BAT GMS (Bengt-Arne Torstensson Ground Water Monitoring System) type Filter Tip provides, together with various BAT probes, a system for groundwater measurement/logging of pore pressures and groundwater levels, *in situ* measurement of soil permeability and for discrete sampling of groundwater and soil gas.
BC	Before Christ.
BET	Brunauer Emmet Teller; A method for determining the specific surface area, available for sorption, of a solid material by use of gas adsorption.
BIPS	Borehole Imaging Processing System; down-hole video camera system providing oriented images of the borehole.
Boremap	SKB's core mapping methodology including inspection of both the drill core and the oriented images of the borehole provided by BIPS.
Candidate area	See definition in section 1.6.5.
Candidate volume	See definition in section 1.6.5.
CCC	Complete Chemical Characterisation; a defined set of various sampling and analyses including on-line, long-term Chemmac measurements of Eh, pH, electrical conductivity, dissolved oxygen and water temperature.
CDF	Cumulative Distribution Function.
CDP	Common Data Point lines along which reflection seismic data have been projected for stacking and interpretation.
CDT	Canyon Diablo Troilite; standard used for sulphur isotope data ($\delta^{34}S$).
CEC	Cation Exchange Capacity; a measure of sites in a material that are available for ion exchange.
CFF	Conductive Fracture Frequency.
Chemmac	A measurement system that allows on-line, long-term measurements of chemical and physical parameters in the unbroken sample water line both at the ground surface and at depth downhole. Eh, pH and water temperature are measured and logged simultaneously by electrodes and sensors downhole as well as at the surface. Dissolved oxygen and electrical conductivity are measured at the surface.
ConnectFlow	Numerical modelling tool for simulation of groundwater flow.
CPM	Continuous Porous Medium.
CSI	Complete Site Investigation stage.
DEM	Digital Elevation Model.
DFF	Distant Far Field.

DFN	Discrete Fracture Network.
DIC	Dissolved Inorganic Carbon.
DOC	Dissolved Organic Carbon.
DP	Dissolved Phosphorus.
DZ	Deformation zone.
EC	Electrical Conductivity.
ECPM	Equivalent Continuous Porous Medium.
EDL	Electrical Double Layer.
EDX	Energy-Dispersive X-ray analysis; method used together with LIBD to analyse the composition of colloids.
EIA	Environmental Impact Assessment.
EM	Electromagnetic data.
F_f	Formation factor defined as the ratio of effective diffusivity (D_e) to the free diffusivity of a solute at infinite dilution in water (D_w).
F-factor	Hydrodynamic transport resistance expressed as the flow-wetted surface to flow ratio.
FFM	Identification code prefix for a deterministically modelled fracture domain at Forsmark; for definition of fracture domain, see section 1.6.5.
FWS	Flow Wetted Surface; the surface area of a fracture in contact with flowing groundwater.
GIS	Geographic Information System.
GMWL	Global Meteoric Water Line.
GSLIB	Geostatistical software used to produce statistical distribution models of thermal conductivity.
HA	Heterotrophic acetogens – microorganisms that produce acetate from organic sources.
HCD	Hydraulic Conductor Domain; at Forsmark equivalent to deterministic deformation zone.
HF	Hydraulic Fracturing; method for measurement of *in situ* rock stresses.
HFM	Percussion-drilled borehole at Forsmark.
HM	Heterotrophic Methanogens – microorganisms that produce methane from organic sources.
HRD	Hydraulic Rock Domain; at Forsmark equivalent to fracture domain.
HRL	Hard Rock Laboratory.
HTHB	*HydroTestutrustning för HammarBorrhål;* equipment used for hydraulic characterisation in boreholes by open hole pumping test.
HTPF	Hydraulic Tests on Pre-existing Fractures; method for measurement of *in situ* rock stresses.
HZ fracture set	Sub-horizontal fracture set.
IFF	Immediate Far Field.
Insite	INdependent Site Investigation Tracking & Evaluation; SKI's advisory group on site investigation issues.
IRB	Iron-reducing bacteria.
ISI	Initial Site Investigation stage.
ISIS	Software used in stochastic geological DFN modelling.
KFM	Core-drilled borehole at Forsmark.
KT extinction	Cretaceous-Tertiary extinction event; a large-scale mass extinction of animal (the conclusion of the age of the dinosaurs and the rise of modern mammals) and plant species in a geologically short period of time, approximately 65.5 million years ago, which marked the end of the Mesozoic era and beginning of the Cenozoic era.
LFM	Line along the ground surface along which data have been acquired, for example seismic refraction profiles.
LIBD	Laser-induced breakdown colloid detection; method used together with EDX to analyse the composition of colloids.
LPJ-GUESS	Dynamic vegetation model.
M3	Multivariate mixing and mass balance calculation programme.
m.a.s.l./m.b.s.l.	Metres above sea level/metres below sea level.
m.f.ToC	Metres from the top of a borehole casing; measurement of borehole length.
MDZ	Minor Deformation Zone; deformation zone with a trace length at the ground surface shorter than 1,000 m.
MFM	Magnetic lineament at Forsmark.
MIKE SHE	Numerical modelling tool for surface hydrogeological modelling.

MPN	Most Probable Number of cells method; statistical cultivation method for counting the most probable number of cells of different cultivable metabolic groups of microorganisms.
MRB	Manganese-Reducing Bacteria.
NEP	Net Ecosystem Production; the difference between gross primary production and total ecosystem respiration.
NNF	Non-engineered Near Field.
NPP	Net Primary Production; the production of organic material in ecosystems.
NRB	Nitrate-Reducing Bacteria.
OSM	Outcrop Scale Model; alternative DFN size model based on sizes and intensities of fractures recorded as outcrop traces.
Oversite	The SSI international expert group.
P_{10}	Fracture intensity (1D) expressed as fracture intercept per unit length (m^{-1}).
P_{10corr}	Terzaghi corrected linear fracture intensity (m^{-1}).
$P_{10,PFL,corr}$	Terzaghi corrected linear intensity of flowing fractures (m^{-1}).
$P_{10,o,corr}$	Terzaghi corrected linear intensity of open fractures (m^{-1}).
P_{21}	Fracture intensity (2D) expressed as fracture trace length per unit area (m/m^2).
P_{32}	Fracture intensity (3D) expressed as fracture area per unit volume (m^2/m^3).
PCA	Principal Component Analysis; statistical method for analysing groundwater compositions.
PDZ	Possible Deformation Zone as recognized in the single-hole interpretation of boreholes.
PFL	Posiva Flow Log; equipment used for hydraulic characterisation in boreholes by difference flow logging pumping tests.
PFL-f	Difference flow logging pumping tests.
PFM	Point at the ground surface where data have been acquired, for example observation points during bedrock mapping.
PHREEQC	Numerical modelling tool for chemical speciation, batch-reaction, one-dimensional transport, and inverse geochemical calculations.
pmC	Percent modern Carbon.
POC	Particulate Organic Carbon.
POP	Particulate Organic Phosphorus.
PPMA	Poly-methylmethacrylate; a resin used in a method for determining heterogeneous porosity distributions in rock samples.
P-report	SKB report series for results of the site investigations at Forsmark and Laxemar-Simpevarp.
PSE	Preliminary Safety Evaluation.
PSS	Pipe String System; equipment used for hydraulic characterisation in boreholes by double-packer injection tests.
QA	Quality Assurance.
RAMAC	Borehole radar measurement system with dipole and directional antennae that provides information on the character of the rock mass around the borehole.
REX	Äspö large-scale redox experiments.
RFM	Identification code prefix for a deterministically modelled rock domain at Forsmark; for definition of rock domain, see section 1.6.5.
RHB 70	Coordinate system used for elevation; see section 2.5.
RT 90	Coordinate system used for X and Y-directions; see section 2.5.
RU	Rock Unit; see definition in section 1.6.5.
RVS	Rock Visualisation System; SKB's tool for modelling and visualisation of the 3D geometry of geological entities.
SCA	Self Consistent Approximation; method for calculation of thermal conductivity using mineral composition and reference values of thermal conductivity of different minerals.
SDM	Site Descriptive Model.
SFM	Soil borehole at Forsmark.
SFR	Repository for low- and intermediate level radioactive waste at Forsmark.
SHI	Single-hole interpretation; an integrated interpretation of geological and geophysical data from a borehole that gives rise to an essentially 1D model for rock units and possible deformation zones along the borehole.
Sicada	SKB's database for primary site investigation data.
Sierg	Site Investigation Expert Review Group; SKB's international expert group.

Simon	SKB’s database for site descriptive models.
SKB	Swedish Nuclear Fuel and Waste Management Company.
SKBdoc	SKB’s internal documentation database.
SKI	Swedish Nuclear Power Inspectorate.
SOC	Soil organic carbon.
SP	Self Potential.
SRB	Sulphate-Reducing Bacteria.
SSI	Swedish Radiation Protection Authority.
SWIW	Single Well Injection and Withdrawal; method for single-hole tracer test.
Target area	See definition in section 1.6.5.
Target volume	See definition in section 1.6.5.
TCM	Tectonic Continuum Model; alternative DFN size model based on the assumption that fractures with traces on the scale of metres are part of the same fracture population as lineaments or deformation zones with traces on the scale of kilometres.
TDS	Total Dissolved Solids.
TFM	Tectonic Fault Model; alternative DFN size model based on the trace lengths of lineaments and deterministic deformation zones.
TIC	Total Inorganic Carbon.
TNC	Total Number of Cells.
TOC	Total Organic Carbon.
TOC	Top Of Casing.
TPS	Transient Plane Source; laboratory method for measurements of thermal conductivity and thermal diffusivity of rock samples.
TRC	Thermal Rock Class; Group of rock types with similar thermal and lithological properties.
UCS	Uniaxial Compressive Strength.
VLF	Very Low Frequency; electromagnetic geophysical method that makes use of radio transmissions at very low frequencies as plane-wave sources.
VSMOV	Vienna Standard Mean Ocean Water, refers to the ”ocean standard” available at IAEA in Wienna. (IAEA, 1995. Reference document, TEC DOC-825, 165 p.).
VSP	Vertical Seismic Profiling.
WellCad	Software for displaying borehole data from Sicada in diagrams.
ZFM	Identification code prefix for a deterministically modelled deformation zone at Forsmark; for definition of deformation zone, see section 1.6.5.

Appendix 3

Tables with references to primary data

Specifications of quality-assured data that were available for use in the site descriptive modelling work for Forsmark are compiled in tables in this appendix together with a summary of the application of these data in the analytical and modelling work. For simplification and traceability reasons, the information is arranged in a discipline-specific order and presented in corresponding separate tables (Table 1 to Table 8). The last table in this appendix (Table 9) lists all the SKB reports referred to in Table 1 to Table 8.

Contents

Table 1. Available bedrock geological and geophysical data and their handling in Forsmark SDM-Site geological modelling. 456
Table 2. Available rock thermal data and their handling in Forsmark SDM-Site thermal modelling. 462
Table 3. Available rock mechanics data and their handling in Forsmark SDM-Site rock mechanics modelling. 464
Table 4. Available bedrock hydrogeological data and their handling in Forsmark SDM-Site bedrock hydrogeological modelling. 467
Table 5. Available hydrogeochemical data and their handling in Forsmark SDM-Site hydrogeochemical modelling. 469
Table 6. Available data on transport properties and their handling in Forsmark SDM-Site transport properties modelling. 471
Table 7. Available abiotic data for the surface system and their handling in Forsmark SDM-Site surface systems modelling. 472
Table 8. Available biotic data for the surface system and their handling in Forsmark SDM-Site surface systems modelling. 475
Table 9. Reports in the SKB series P-, R- and TR that are referred to in Table 1 to Table 8. 477

Table 1. Available bedrock geological and geophysical data and their handling in Forsmark SDM-Site geological modelling.

Available data Data specification	Ref	Usage in SDM-Site Analysis/Modelling
Data from core-drilled boreholes		
Technical data in connection with drilling (KFM01A, KFM01B, KFM01C-KFM01D, KFM02A, KFM02B, KFM03A-KFM03B, KFM04A, KFM05A, KFM06A-KFM06B, KFM06C, KFM07A, KFM07B-KFM07C, KFM08A-KFM08B, KFM08C-KFM08D, KFM09A-KFM09B, KFM10A, KFM11A, KFM12A)	P-03-32 P-04-302 P-06-173 P-03-52 P-07-44 P-03-59 P-03-82 P-04-222 P-05-50 P-05-277 P-05-142 P-06-170 P-05-172 P-06-171 P-06-169 P-06-172 P-07-45 P-07-46	Siting and orientation of boreholes in modelling work.
Radar and BIPS logging, and interpretation of radar logs (KFM01A, KFM01B, KFM01C-KFM01D, KFM02A, KFM02B-KFM08D, KFM03A-KFM03B, KFM04A, KFM05A, KFM06A, KFM06B, KFM06C, KFM07A, KFM07B-KFM09A, KFM07C, KFM08A, KFM08B, KFM08C, KFM09B, KFM10A, KFM11A, KFM12A)	P-03-45 P-04-79 P-06-98 P-04-40 P-07-96 P-04-41 P-04-67 P-04-152 P-05-01 P-05-53 P-05-242 P-05-52 P-06-44 P-06-120 P-05-158 P-05-58 P-06-178 P-06-64 P-06-177 P-07-10 P-07-112	Data used in borehole mapping (BIPS) and in single-hole interpretation (radar logging) with focus on identification of brittle deformation zones. Input for both rock domain and DZ modelling.
Geophysical logging (KFM01A, KFM01B, KFM01C-KFM09B, KFM01D, KFM02A-KFM03A-KFM03B, KFM02B-KFM08D, KFM04A, KFM05A, KFM06A, KFM06C, KFM07A- KFM08A-KFM08B, KFM07B-KFM09A, KFM07C, KFM08C-KFM10A, KFM11A, KFM12A)	P-03-103 P-04-145 P-06-123 P-06-168 P-04-97 P-07-60 P-04-144 P-04-153 P-05-17 P-05-276 P-05-159 P-06-22 P-07-04 P-07-05 P-07-92 P-07-118	Data used in borehole mapping and in single-hole interpretation. Input for both rock domain and DZ modelling.

Available data Data specification	Ref	Usage in SDM-Site Analysis/Modelling
Interpretation of geophysical logs (KFM01A-KFM01B, KFM01C-KFM09B, KFM01D, KFM02A-KFM03A-KFM03B, KFM02B-KFM08D-KFM11A, KFM04A, KFM05A, KFM06A, KFM06C, KFM07A, KFM07B-KFM09A, KFM07C, KFM08A-KFM08B, KFM08C-KFM10A, KFM12A)	P-04-80 P-04-98 P-06-152 P-06-216 P-07-125 P-04-143 P-04-154 P-05-51 P-06-84 P-05-119 P-06-126 P-07-78 P-05-202 P-06-258 P-07-129	Used in single-hole interpretation. Input for both rock domain and DZ modelling.
Vertical seismic profiling, KFM01A and KFM02A	P-05-168	Input for DZ-modelling.
Calibration of caliper data from core- and percussion-drilled boreholes	P-07-35	Data not used directly but as support to the geophysical logging work
Electrical measurements at drill sites 4, 7 and 8 (KFM04A, KFM07A and KFM08A) and on the ground surface between drill sites 4 and 1	P-05-265	Analysis of corrosion observations.
Boremap mapping (KFM01A, KFM01B, KFM01C, KFM01D, KFM02A, KFM02B, KFM03A-KFM03B, KFM04A, KFM05A, KFM06A-KFM06B, KFM06C, KFM07A, KFM07B, KFM07C, KFM08A-KFM08B, KFM08C, KFM08D, KFM09A, KFM09B, KFM10A, KFM11A, KFM12A)	P-03-23 P-04-114 P-06-133 P-06-132 P-03-98 P-07-107 P-03-116 P-04-115 P-04-295 P-05-101 P-06-79 P-05-102 P-06-80 P-06-205 P-05-203 P-06-203 P-07-103 P-06-130 P-06-131 P-06-204 P-07-104 P-07-105	Rock type, ductile deformation in the bedrock, fracture statistics. Data used in identification of rock units and brittle deformation zones in single-hole interpretation. Input for rock domain, DZ and DFN modelling.
Comparative geological mapping with the BOREMAP system: 176.5–306.9 m of borehole KFM06C, 9.6–132.2 m of borehole KLX07B	P-06-81 P-06-82	Control of the reproducibility of borehole mapping data.
Mineralogical and geochemical analyses of rock types and fracture fillings (KFM01A-KFM02A-KFM03A-KFM03B, KFM01B-KFM04A-KFM05A- KFM06A, KFM06B-KFM06C-KFM07A-KFM08A-KFM08B, KFM01C-KFM01D-KFM02B-KFM06A-KFM06B-KFM07A-KFM08A-KFM08B-KFM08C-KFM08D-KFM09A-KFM09B-KFM10A-KFM11A)	P-04-103 P-04-149 P-05-156 P-05-197 P-06-226 P-08-14	Mineralogical and geochemical properties of rock types and mineral fracture fillings. Input for rock domain, DZ and DFN modelling.
Mineralogy, geochemistry, porosity and redox capacity of altered rock adjacent to fractures	P-06-209	Mineralogical and geochemical properties of rock types. Input for rock domain modelling.
Mineralogical and micro-structural analyses of vuggy metagranite in KFM02A	P-03-77	Input for rock domain, fracture domain and DZ modelling.

Available data Data specification	Ref	Usage in SDM-Site Analysis/Modelling
Petrophysical and *in situ* gamma-ray spectrometric data from rock types (KFM01A-KFM02A-KFM03A-KFM03B, KFM04A-KFM05A-KFM06A)	P-04-103 P-04-107 P-05-204	Physical properties of rock types. Input for rock domain modelling. Data also utilised for the interpretation of geophysical logs.
Characterisation of brittle deformation zones at Forsmark	P-05-183 P-06-212 P-07-101 P-07-111	Input for DZ modelling.
Single-hole interpretation (KFM01A-KFM01B, KFM01C-KFM09B, KFM01D, KFM02A, KFM02B, KFM03A-KFM03B, KFM04A, KFM05A, KFM06A-KFM06B, KFM06C, KFM07A, KFM07B-KFM09A, KFM08A-KFM08B, KFM08D, KFM08C-KFM10A, KFM11A, KFM12A)	P-04-116 P-04-117 P-06-135 P-06-210 P-07-107 P-04-118 P-04-119 P-04-296 P-05-132 P-06-83 P-05-157 P-06-134 P-05-262 P-07-108 P-06-207 P-07-109 P-07-110	Interpretation used in rock domain and DZ modelling. Interpretation of KFM02B, KFM11A, KFM12A and especially KFM08D used in verification of deterministic geological models.
Data from percussion-drilled boreholes		
Technical data in connection with drilling (HFM01-HFM02-HFM03, HFM04-HFM05, HFM06-HFM07-HFM08, HFM09-HFM10, HFM11-HFM12 and HFM17-HFM18-HFM19, HFM13-HFM14-HFM15, HFM16, HFM20-HFM21-HFM22, HFM23-HFM24-HFM28, HFM25-HFM26-HFM27 and HFM29-HFM30-HFM31-HFM32-HFM38, HFM33-HFM34-HFM35, HFM36-HFM37)	P-03-30 P-03-51 P-03-58 P-04-76 P-04-106 P-04-85 P-04-94 P-04-245 P-05-278 P-06-166 P-07-11 P-07-43	Siting and orientation of boreholes in modelling work.
Radar and BIPS logging, and interpretation of radar logs (HFM01-HFM02-HFM03, HFM04-HFM05, HFM06-HFM07-HFM08, HFM09-HFM10, HFM11-HFM12, HFM13-HFM14-HFM15, HFM16-HFM17-HFM18-HFM19, HFM20-HFM21, HFM22, HFM24-HFM26-HFM27-HFM29-HFM32, HFM25-HFM28, HFM30-HFM31-HFM33-HFM34, HFM35-HFM38, HFM36-HFM37, HFK248-HFK249-HFK250)	P-03-39 P-03-53 P-03-54 P-04-67 P-04-39 P-04-68 P-04-69 P-05-64 P-05-01 P-06-64 P-06-44 P-06-178 P-06-177 P-06-120 P-05-176	Data used in borehole mapping (BIPS) and in single-hole interpretation (radar logging) with focus on identification of brittle deformation zones. Input for both rock domain and DZ modelling.

Available data Data specification	Ref	Usage in SDM-Site Analysis/Modelling
Geophysical logging (HFM01-HFM02-HFM03, HFM04-HFM05, HFM06-HFM07-HFM08, HFM10-HFM11-HFM12-HFM13, HFM14-HFM15-HFM16-HFM17-HFM18, HFM19, HFM20-HFM21-HFM22, HFM07-HFM24-HFM26-HFM29-HFM32, HFM25-HFM27-HFM28, HFM30-HFM31-HFM33-HFM34-HFM35-HFM38, HFM36-HFM37)	P-03-39 P-03-103 P-03-53 P-03-54 P-04-144 P-04-145 P-04-153 P-05-17 P-06-123 P-06-22 P-07-05 P-07-04	Data used in borehole mapping and in single-hole interpretation. Input for both rock domain and DZ modelling.
Interpretation of geophysical logs (HFM01-HFM02-HFM03, HFM04-HFM08, HFM10-HFM11-HFM12-HFM13-HFM16-HFM17-HFM18, HFM14-HFM15-HFM19, HFM20-HFM21-HFM22, HFM07-HFM24-HFM26 -HFM29-HFM32, HFM25-HFM27-HFM28, HFM30-HFM31- HFM38, HFM33-HFM34-HFM35, HFM36-HFM37)	P-04-80 P-04-98 P-04-143 P-04-154 P-05-51 P-06-152 P-06-126 P-06-258 P-07-109 P-07-78	Used in single-hole interpretation. Input for both rock domain and DZ modelling.
Boremap mapping (HFM01-HFM02-HFM03, HFM04-HFM05, HFM06-HFM07-HFM08, HFM09-HFM10-HFM11-HFM12, HFM13-HFM14-HFM15-HFM19, HFM16-HFM17-HFM18, HFM20-HFM21-HFM22, HFM23-HFM24-HFM25-HFM26-HFM27-HFM28-HFM29-HFM30-HFM31-HFM32-HFM38, HFM33-HFM34-HFM35-HFM36-HFM37)	P-03-20 P-03-21 P-03-22 P-04-101 P-04-112 P-04-113 P-05-103 P-06-206 P-07-106	Data mainly used for identification of rock units and DZ in single-hole interpretation. Input for both rock domain and DZ modelling. Problem with recognition of rock types and mineral coatings along fractures. Also underestimation of the amount of fractures inferred solely on the basis of BIPS images.
Single-hole interpretation (HFM01-HFM02-HFM03, HFM04-HFM05, HFM06-HFM07-HFM08, HFM09-HFM10, HFM11-HFM12-HFM13-HFM16-HFM17-HFM18, HFM14-HFM15-HFM19, HFM20-HFM21, HFM22, HFM23-HFM28-HFM30-HFM31-HFM32-HFM38, HFM24-HFM25-HFM27-HFM29, HFM33-HFM34-HFM35, HFM36-HFM37)	P-04-116 P-04-117 P-04-118 P-04-119 P-04-120 P-04-296 P-05-157 P-05-262 P-06-207 P-06-210 P-07-109 P-07-110	Interpretation used in rock domain and DZ modelling.
Older borehole, tunnel and surface data		
Older geological and geophysical data from the Forsmark nuclear power plant and SFR, including seismic refraction data	P-04-81	Rock type data from boreholes and tunnels, lineament identification at the nuclear power plant, brittle structures at or close to the surface in the vicinity of the nuclear power plant, and identification of brittle deformation zones. Fracture orientation and mineral coatings from tunnels and boreholes. Input for rock domain, DZ and DFN modelling.

Available data Data specification	Ref	Usage in SDM-Site Analysis/Modelling
Surface-based data. Some data from core-drilled boreholes are also included here		
Bedrock mapping − outcrop data. Rock type and ductile structures at 2,119 outcrops; frequency and orientation of fractures at 44 outcrops	P-03-09 P-04-91 Bedrock geological map, Forsmark, versions 1.1, 1.2, 2.2 and 2.3 (SKB GIS database)	Rock type, rock type distribution, ductile deformation in the bedrock, fracture statistics, and identification of deformation zones at surface. Input for rock domain, DZ and DFN modelling.
Detailed bedrock mapping with special emphasis on fractures (drill sites 2, 3, 4, 5 and 7, and coastal outcrop at Klubbudden)	P-03-12 P-03-115 P-04-90 P-05-199 P-05-269	Fracture statistics (orientation, length) and identification of brittle and ductile features at surface. Input for rock domain, DZ and DFN modelling.
Detailed bedrock mapping of excavations across lineaments	P-04-88 P-06-136	Assessment of the geological character of lineaments. Input especially for DZ modelling, but also DFN.
Geochemical analyses of till	P-03-118	Assessment of exploration potential in bedrock
Evaluation of the occurrence of late- or post-glacial faulting	P-03-76 P-04-123 R-05-51	Geological evolution.
Mineralogical and geochemical analyses of rock types	P-03-75 P-04-87	Mineralogical and geochemical properties of rock types. Input for rock domain modelling.
Petrophysical and *in situ* gamma-ray spectrometric data from rock types	P-03-26 P-03-102 P-04-155	Physical properties of rock types. Input for rock domain modelling. Data also used for the interpretation of geophysical logs.
U-Pb, $^{40}Ar/^{39}Ar$, (U-Th)/He and Rb-Sr geochronological data from bedrock and fracture minerals (surface and boreholes)	P-04-126 P-06-211 P-06-213 P-08-14	Input for conceptual understanding of the geological modelling work.
Production of orthorectified aerial photographs and digital terrain model	P-02-02	Topographic/bathymetric data only used to very limited extent in DZ modelling work after version 1.2.
Methodology for construction of digital terrain model for the site	P-04-03	Topographic/bathymetric data only used to very limited extent in DZ modelling work after version 1.2.
Marine geological survey of the sea bottom off Forsmark	P-03-101	Topographic/bathymetric data only used to very limited extent in DZ modelling work after version 1.2.
Water depth in shallow lakes	P-04-25	Topographic/bathymetric data only used to very limited extent in DZ modelling work after version 1.2.
Water depth in shallow bays	P-04-125	Topographic/bathymetric data only used to very limited extent in DZ modelling work after version 1.2.
Helicopter-borne, geophysical data (magnetic, EM, VLF and gamma-ray spectrometry data)	P-03-41	Base data for interpretation of airborne magnetic lineaments.
Electric soundings	P-03-44	Data not used directly but as a support to the inversion of helicopter-borne EM measurements (see below).
Inversion of helicopter-borne EM measurements	P-04-157	Topographic/bathymetric data only used to very limited extent in DZ modelling work after version 1.2.
Interpretation of topographic, bathymetric and helicopter-borne geophysical data. Alternative interpretation in and immediately around the candidate area. Assessment of all lineaments in the target area.	P-03-40 P-04-29 P-04-282 P-04-241 P-05-261	Identification of magnetic lineaments. Input for DZ modelling work.
High-resolution seismic reflection data carried out during stage I and II (including interpretation)	R-02-43 P-04-158 R-05-42	Identification of seismic reflectors in the bedrock that may correspond to deformation zones or boundaries between different types of bedrock. Input for DZ modelling.

Available data Data specification	Ref	Usage in SDM-Site Analysis/Modelling
Seismic refraction data	P-05-12 P-06-138	Identification of low velocity anomalies in the bedrock that may correspond to deformation zones. Input for DZ modelling.
Seismic velocity measurements along excavations across lineaments	P-05-46	Identification of low velocity anomalies in the bedrock that may correspond to deformation zones. Input for DZ modelling.
Ground geophysical data (magnetic and EM data) close to drill sites 1, 2, 3, 4 and 5, and several lineaments (including interpretation)	P-02-01 P-03-55 P-03-104 P-05-266	Identification of magnetic lineaments. Input for DZ modelling.
High-resolution ground magnetic measurements	P-06-85 P-06-261 R-07-62	Identification of magnetic lineaments. Input for DZ modelling.
Mise-à-la-masse data from DS5	P-04-305	Method test.
Regional gravity data and interpretation	P-03-42 R-07-67	Verification of regional rock domain model.
Previous models		
SFR structural models	R-98-05 R-01-02	DZ modelling. The subvertical zones 3, 8 and 9 have been extracted from /Axelsson and Hansen 1997/. The sub-horizontal zone H2 has been extracted from the SAFE model /Holmén and Stigsson 2001/.
Forsmark site descriptive model versions 0, 1.1, 1.2 and stage 2.1	R-02-32 R-04-15 R-05-18 R-06-38	Comparison and updating of models.

Table 2. Available rock thermal data and their handling in Forsmark SDM-Site thermal modelling.

Available data Data specification	Ref		Usage in SDM-Site Analysis/Modelling
Data from core-drilled boreholes			
Temperature and density logging	**Results**	**Interpret.**	
KFM01A	P-03-103	P-04-80	Data used for describing natural temperature variations with depth. Estimation of thermal conductivity from density based on relationship between these two parameters. Density data also used to study and model spatial correlation in thermal conductivity.
KFM01B	P-04-145	P-04-80	
KFM01C	P-06-123	P-06-152	
KFM01D	P-06-168	P-06-216	
KFM02A	P-04-97	P-04-98	
KFM03A	P-04-97	P-04-98	
KFM04A	P-04-144	P-04-143	
KFM05A	P-04-153	P-04-154	
KFM06A	P-05-17	P-05-51	
KFM06C	P-05-276	P-06-84	
KFM07A	P-05-159	P-05-119	
KFM07B	P-06-22	P-06-126	
KFM07C	P-07-04	P-07-78	
KFM08A	P-05-159	P-05-202	
KFM08C	P-07-05	P-06-258	
KFM09B	P-06-123	P-06-152	
KFM10A	P-07-05	P-06-258	
Boremap mapping			
KFM01A	P-03-23		Dominant and subordinate rock type distribution. Input for lithological simulations.
KFM01B	P-04-114		
KFM01C	P-06-133		
KFM01D	P-06-132		
KFM02A	P-03-98		
KFM03A	P-03-116		
KFM04A	P-04-115		
KFM05A	P-04-295		
KFM06A	P-05-101		
KFM06C	P-06-79		
KFM07A	P-05-102		
KFM07B	P-06-80		
KFM07C	P-06-205		
KFM08A	P-05-203		
KFM08B	P-05-203		
KFM08C	P-06-203		
KFM08D	P-07-103		
KFM09B	P-06-131		
KFM10A	P-06-204		
Laboratory measurements of density			
KFM01A	P-04-166, P-06-234		Data used for investigation of relationship between density and thermal conductivity.
KFM01C	P-06-67, P-06-234		
KFM01D	P-06-234		
KFM02A	P-04-167		
KFM03A	P-04-168		
KFM04A	P-04-169, P-06-234		
KFM05A	P-06-234		
KFM06A	P-05-124, P-06-234		
KFM07A	P-05-215		
KFM08A	P-05-220		

Available data Data specification	Ref	Usage in SDM-Site Analysis/Modelling
Laboratory measurements of thermal properties		
KFM01A	P-04-159, P-06-233	Estimation of thermal conductivity, thermal diffusivity and specific heat capacity.
KFM01C	P-06-66, P-06-233	
KFM01D	P-06-233	
KFM02A	P-04-161	
KFM03A	P-04-162	
KFM04A	P-04-199, P-06-233	
KFM05A	P-06-233	
KFM06A	P-05-123, P-06-233	
KFM07A	P-05-214	
KFM08A	P-05-219	
Anisotropy in thermal properties for KFM04A and KFM90B	P-06-285 P-07-194	Estimation of anisotropy in thermal properties.
Inter-laboratory comparison of TPS measurements from KFM01A	P-04-186	Quality control purposes.
Modal analyses		
KFM01A	P-04-103, P-04-159, P-06-233, P-06-209	Estimation of thermal conductivity from mineralogical properties of the bedrock. Statistical analysis.
KFM02A	P-04-103, P-04-161, P-06-209	
KFM03A	P-04-103, P-04-162	
KFM03B	P-04-103	
KFM04A	P-04-199, P-05-156	
KFM05A, KFM06A	P-05-156, P-06-233	
KFM07A, KFM08A, KFM08B	P-06-209	
Laboratory tests of thermal expansion		
KFM01A	P-04-163	Estimation of the thermal expansion coefficient.
KFM02A	P-04-164	
KFM03A	P-04-165	
KFM04A	P-04-198	
KFM05A, KFM06A	P-07-33	
Large-scale field measurements of thermal properties		
KFM90B, C, D, E, F	P-07-194	Analysis of anisotropy in thermal conductivity.
Surface and near-surface data		
Laboratory tests of thermal properties – surface samples	P-03-08	Thermal transport properties for some samples. Comparison with modelled results.
Modal analyses – surface samples	P-03-75, P-04-87, P-05-156	Estimation of thermal conductivity from mineralogical composition of the bedrock.
Small-scale field measurements of thermal properties close to drill site DS7	P-07-194	Analysis of anisotropy in thermal conductivity.
Models		
Ductile deformation zones	R-07-15	Density logging data from within deformation zones removed prior to spatial correlation analysis.
Geological model	R-07-45	Rock domain model, analysis of alteration and orientation of subordinate rock bodies used as input for thermal modelling.
Forsmark site descriptive models versions 1.1 and 1.2	R-04-15, R-05-18	Comparison and updating of models.

Table 3. Available rock mechanics data and their handling in Forsmark SDM-Site rock mechanics modelling.

Available data Data specification	Ref	Usage in SDM-Site Analysis/Modelling
Data from core-drilled boreholes		
Uniaxial compressive strength		
KFM01A	P-04-223	Characterisation of the intact rock; Empirical determination of the rock mass mechanical properties by means of RMR and Q; Theoretical determination of the rock mass mechanical properties by means of numerical modelling.
KFM01A – Independent determination	P-04-176	
KFM01C	P-06-69	
KFM02A	P-04-224	
KFM03A	P-04-225	
KFM04A	P-04-226	
KFM05A	P-05-97	
KFM06A	P-05-120	
KFM06A – Intact rock containing seal fractures	P-07-207	
KFM07A	P-05-211	
KFM08D	P-07-145	
KFM09A	P-06-27	
Triaxial compressive strength		
KFM01A	P-04-227	Characterisation of the intact rock; Empirical determination of the rock mass mechanical properties by means of RMR and Q; Theoretical determination of the rock mass mechanical properties by means of numerical modelling
KFM01A – Independent determination	P-04-177	
KFM01C	P-06-68	
KFM01D	P-06-214	
KFM02A	P-04-228	
KFM03A	P-04-229	
KFM04A	P-04-230	
KFM05A	P-05-100	
KFM07A	P-05-210	
KFM08A	P-05-217	
KFM09A	P-06-26	
Indirect tensile strength		
KFM01A	P-04-170	Characterisation of the intact rock; Theoretical determination of the rock mass mechanical properties by means of numerical modelling.
KFM01A – Independent determination	P-04-171	
KFM02A	P-04-172	
KFM03A	P-04-173	
KFM04A	P-04-174	
KFM05A	P-05-98	
KFM06A	P-05-121	
KFM07A and KFM08A	P-05-212	
KFM08D	P-07-146	
KFM09A	P-06-28	
Direct tensile strength		
KFM01D	P-07-76	
Crack initiation stress		
KFM01A	P-04-223	Evaluation of the elastic limit of deformation – for addressing spalling and core disking problems.
KFM02A	P-04-224	
KFM03A	P-04-225	
KFM04A	P-04-226	
KFM05A	P-05-97	
KFM06A	P-05-120	
KFM07A	P-05-211	
KFM09A	P-06-27	

Available data Data specification	Ref	Usage in SDM-Site Analysis/Modelling
Microcrack volume measurements		
KFM01A and KFM02B	P-07-93	Indicate differences in stress state between boreholes and differences in deformation behaviour between rock types. The information is also used by hydrogeochemistry and bedrock transport properties.
Direct shear tests		
KFM01A	P-04-175 P-05-08	Characterisation of the rock fractures – strength and stiffness; Theoretical determination of the rock mass mechanical properties by means of numerical modelling.
KFM01D – Tests on sealed joints	P-06-215	
KFM02A	P-05-09	
KFM03A	P-05-10	
KFM04A	P-05-11	
KFM05A	P-05-99 P-05-141	
KFM06A	P-05-122	
KFM07A	P-05-213	
KFM08A	P-05-218	
KFM09A	P-06-29	
Tilt tests		
KFM01A	P-03-108	Characterisation of the rock fracture properties and of the rock mass by RMR and Q.
KFM02A	P-04-08	
KFM03A and KFM03B	P-04-178	
KFM04A	P-04-179	
KFM05A	P-04-205	
KFM09A	P-06-25	
P-wave velocity measurements on core samples		
KFM01A	P-03-38	Correlation between rock mass stresses and foliation.
KFM02A	P-04-09	
KFM03A	P-04-180	
KFM04A	P-04-181	
KFM05A	P-04-203	
KFM06A	P-05-04	
KFM07A	P-05-125	
KFM08A	P-05-216	
KFM09A	P-06-24	
Sonic velocity measurements along the boreholes		
KFM01A	P-03-103	Correlation with P-velocity along the cores and consideration about damage of the core.
KFM02A and KFM03A	P-04-97	
KFM04A	P-04-144	
KFM05A	P-04-153	
KFM06A	P-05-17	
KFM06C	P-05-276	
KFM07A and KFM08A	P-05-159	
KFM09A	P-06-22	
Empirical characterisation		
KFM01A	P-05-112	Characterisation of the rock mass mechancial properties.
KFM02A	P-05-113	
KFM03A	P-05-114	
KFM04A	P-05-115	
KFM01B, KFM07C, KFM09A, KFM09B	P-07-115	
KFM11A and KFM12A	R-08-66	

Available data Data specification	Ref	Usage in SDM-Site Analysis/Modelling
Stress measurements – overcoring		
KFM01B	P-04-83 P-05-66 P-07-234	Estimation of the *in situ* stress field.
KFM02B	P-07-205	
KFM07B	P-06-93	
KFM07C	P-07-130	
Stress measurements – HF and HTPF		
KFM01A, KFM01B, KFM02A, KFM04A	P-04-311 P-04-312 P-07-234	Estimation of the *in situ* stress field.
KFM02B	P-07-205	
KFM07A, KFM07C, KFM08A, KFM09A, KFM09B	P-07-206	
Borehole breakout studies		
KFM01A, KFM01B, KFM02A, KFM03A, KFM03B, KFM04A, KFM05A, KFM06A	P-07-07	Indirect observation of rock stresses.
KFM01A, KFM01B	P-07-235	
KFM08A, KFM08C, KFM09A, KFM09B, KFM90B	P-07-166	
Other borehole and tunnel data		
Stress measurements in DBT1, DBT3	P-03-119 P-07-234 R-05-35	Estimation of the *in situ* stress field.
Stress measurements in KB-21, KB-22, KBS-7, SFR 1/177	Sicada	

Table 4. Available bedrock hydrogeological data and their handling in Forsmark SDM-Site bedrock hydrogeological modelling.

Available data Data specification	Ref	Usage in SDM-Site Analysis/Modelling
Single-hole data from core-drilled boreholes		
Double-packer injection tests (PSS)		
KFM01A	P-04-95	Lumped characterisation of rock fracture transmissivities in terms of different test section length transmissivities (5 m, 20 m and 100 m).
KFM01C	P-06-165	
KFM01D	P-06-195	
KFM02A	P-04-100	
KFM02A – re-measurement after hydraulic fracturing	P-05-145	
KFM03A	P-04-194	
KFM03B	P-04-278	
KFM04A	P-04-293	
KFM05A	P-05-56	
KFM06A and 06B	P-05-165	
KFM06C	P-06-23	
KFM07A	P-05-133	
KFM07B	P-06-86	
KFM08A	P-06-194	
KFM08B	P-05-235	
KFM08C	P-07-06	
KFM09A	P-06-52	
KFM09B	P-06-122	
KFM10A	P-07-31	
KFM11A	P-07-177	
KFM12A	P-07-121	
Difference-flow logging (PFL)		
KFM01A	P-03-28 P-04-193	Detailed characterisation of individual rock fracture transmissivities in terms of high-resolution test section length transmissivities (0.1 m).
KFM01D	P-06-161	
KFM02A	P-04-188	
KFM02B	P-07-83	
KFM03A	P-04-189	
KFM04A	P-04-190	
KFM05A	P-04-191	
KFM06A	P-05-15	
KFM07A	P-05-63	
KFM07C	P-06-247	
KFM08A	P-05-43	
KFM08C	P-06-189	
KFM08D	P-07-84	
KFM10A	P-06-190	
KFM11A	P-07-85	
Single-hole data from percussion-drilled boreholes		
Pumping tests and impeller flow logging		
HFM01, HFM02, HFM03	P-03-33	Characterisation of superficial rock fracture transmissivities in terms of borehole specific capacity and cumulative flow logging.
HFM04, HFM05	P-03-34	
HFM06, HFM07, HFM08	P-03-36	
HFM09, HFM10	P-04-74	
HFM11, HFM12	P-04-64	
HFM13, HFM14, HFM15	P-04-71	
HFM16	P-04-65	

Available data Data specification	Ref	Usage in SDM-Site Analysis/Modelling
HFM17, HFM18, HFM19	P-04-72	
HFM20, HFM21, HFM22	P-05-14	
HFM24, HFM32	P-06-96	
HFM25, HFM26	P-06-139	
HFM23, HFM27, HFM28	P-06-191	
HFM29, HFM30, HFM31	P-06-192	
HFM33, HFM34, HFM35	P-06-193	
HFM36, HFM37, HFM38	P-07-22	
Cross-hole (interference) data		
HFM01, HFM02, HFM03	P-03-35	Characterisation of the hydraulic contact between boreholes presumably intersected by a swarm of connected fractures forming a transmissive deformations zone.
HFM11, HFM12	P-04-200	
HFM18, KFM03A	P-04-307	
HFM16, KFM02A	P-05-78	
	P-05-37	
KFM04A, HFM10, HFM13, HFM19, HFK252	P-05-186	
HFM01	P-05-236	
KFM02A, KFM03A	P-06-09	
HFM14, KFM05A	P-06-140	
HFM14 – 2006	P-06-196	
HFM14 – 2007	P-07-228	
HFM33	P-07-229	
Correlation of structural, hydraulic and hydrogeochemical data		
KFM01A, KFM02A, KFM03A, KFM04A, KFM05A	R-04-77	Correlation of Posiva Flow Log anomalies to core mapped features.
KFM06A, KFM07A	P-06-56	
KFM01D, KFM07C, KFM08A, KFM08C, KFM10A	P-07-127	
KFM02B, KFM08D, KFM11A	P-07-128	
HFM16, KFM02A	Sicada Field note Forsmark 437	Hydraulic responses during drilling of HFM16.
KFM03A	P-04-96	Hydraulic evaluation of pumping activities prior to hydrogeochemical sampling – indications of upconing.
KFM02A, KFM03A, KFM04A	P-05-21	Comparison of measured EC in selected fractures – indications of upconing.
KFM01B, HFM01, HFM02, HFM03, KFM01A	P-04-135	Hydraulic responses during drilling of KFM01B.
HFM14	P-06-188	Hydraulic responses during pumping in HFM14.
HFM01-22	P-06-53	Statistical comparison with SGU´s archieve of wells.
KFM06A	P-06-54	Generalised radial flow analysis.
Near-surface hydrogeological data		
Inventory of private wells	R-02-17	Description of available hydrogeological information.
Data on installed groundwater monitoring wells, abstraction wells and BAT filter tips	P-03-64 P-04-136 P-04-138 P-04-139 P-06-89	Description of Quaternary deposits type and depth to bedrock, basis for groundwater level measurements and hydraulic tests.
Hydraulic conductivity of Quaternary deposits	P-03-65 P-04-136 P-04-138 P-04-140 P-04-142 P-06-224 R-08-08 R-08-09	Basis for assigning hydraulic conductivity of Quaternary deposits in conceptual and quantitative models.

Available data Data specification	Ref	Usage in SDM-Site Analysis/Modelling
Groundwater levels in near-surface bedrock and in Quaternary deposits	P-04-313 P-05-152 P-05-245 P-06-263 P-07-113 R-05-06 R-06-49 R-08-08 R-08-09 R-08-10	Conceptual and descriptive modelling, and calibration of quantitative models.
Supplementary information and models		
SFR	R-99-08 R-01-02 R-02-14	General description, conceptual and quantitative modelling. Basis for assigning transmissivity data to some of the deterministically treated deformation zones.
Finnsjön	TR 91-24 TR 92-07 TR 92-33 TR-99-18	General description, conceptual and quantitative modelling. Basis for assigning hydraulic conductivity and kinematic porosity data to the bedrock outside fracture domains FFM01-06.
Previous site descriptive models versions 0, 1.1 and 1.2 and model stage 2.1	R-02-32 R-04-15 R-05-18 R-06-38	General description, conceptual and quantitative modelling.

Table 5. Available hydrogeochemical data and their handling in Forsmark SDM-Site hydrogeochemical modelling.

Available data Data specification	Ref	Usage in SDM-Site Analysis/Modelling
Complete chemical characterisation (class 4 and 5)		
KFM01A	P-03-94	Traditional hydrochemical evaluation and mathematical modelling such as PHREEQC, M3 and coupled transport modelling. The results of the modelling are presented in the conceptual model of the site. The use of the data in the specific modelling approaches is described in the bedrock hydrogeochemical background report /Laaksoharju et al. 2008a/. Unless for specific reasons, non representative samples were not used in the detailed modelling (see motivation in the bedrock hydrogeochemical background report /Laaksoharju et al. 2008a/).
KFM01D	P-06-227	
KFM02A	P-04-70	
KFM03A	P-04-108	
KFM04A	P-04-109	
KFM05A	P-05-79	
KFM06A	P-05-178	
KFM07A	P-05-170	
KFM08A	P-06-63	
KFM08D	P-07-190	
KFM09A	P-06-217	
KFM10A	P-07-42	
KFM11A	P-07-100	
KFM12A (class 2, 3, 5)	P-07-171	
Sampling during drilling and Uranine analyses	Drilling reports	Used in the assessment of groundwater quality and suitability for hydrochemical evaluation and modelling.
Hydrochemical logging		
KFM02A	P-03-95	Used in the assessment of groundwater quality and suitability for hydrochemical evaluation and modelling.
KFM03A	P-03-96	
KFM04A	P-04-47	
KFM06A	P-05-33	
KFM07A	P-05-187	
KFM08A	P-05-206	
KFM09A	P-06-95	
KFM09B	P-06-179	

Available data Data specification	Ref	Usage in SDM-Site Analysis/Modelling
Sampling in percussion-drilled boreholes and monitoring wells		
Drillsite 1	P-03-47	Used for hydrochemical evaluation. The results are integrated in the conceptual models of the site. Unless for specific reasons, non representative samples were not used in the detailed evaluation.
Drillsite 2	P-03-48	
Drillsite 3	P-03-49	
HFM09 – HFM19	P-04-92	
HFM20 – HFM22	P-05-48	
HFM14, HFM23 – HFM35	P-06-231	
HFM36 – HFM38	P-07-86	
Hydrochemical monitoring of percussion- and core-drilled boreholes		
2005; KFM01A, KFM02A, KFM03A, HFM02, HFM04, HFM13, HFM15, HFM19	P-06-57	Used for hydrochemical evaluation. The results are integrated in the conceptual models of the site.
2006; KFM01A, KFM02A, KFM03A, KFM06A, KFM06C, HFM02, HFM04, HFM13, HFM15, HFM16, HFM19, HFM27, HFM32	P-07-47	
2007; KFM01A, KFM01D, KFM02A, KFM03A, KFM04A, KFM06A, KFM06C, KFM07A, KFM08A, KFM08D, KFM10A, KFM11A HFM01, HFM02, HFM04, HFM13, HFM15, HFM16, HFM19, HFM27, HFM32	P-08-54	
Sampling and analyses of rock matrix porewater		
KFM06A	P-05-196	Used for hydrochemical evaluation. The results are integrated in the conceptual models of the site. Data also used to derive solute transport (i.e. diffusion) properties of the bedrock.
KFM01D, KFM08C, KFM09B	P-07-119	
KFM02B	P-09-14	
Sampling/analyses of shallow groundwaters and surface waters		
Shallow groundwater:		Used for hydrochemical evaluation.
May 2003 – April 2005	P-05-171	Unless for specific reasons, non representative samples were not used in the detailed modelling.
July 2005 – April 2006	P-06-304	
July 2006 – April 2007	P-07-124	
July 2007 – Dec 2007	P-08-55	
Surface waters;		Used for hydrochemical evaluation.
March 2002 – March 2003	P-03-27	Unless for specific reasons, non representative samples were not used in the detailed modelling.
March2003 – March 2004	P-04-146	
March 2004 – June 2005	P-05-274	
July 2005 – June 2006	P-07-95	
July 2006 – June 2007	P-08-17	
July 2007 – Dec 2007	P-08-55	
Precipitation; 2002 – 2005	P-05-143	Used for hydrochemical evaluation.
Sept 2005 – June 2007	P-07-170	
July 2007 – Dec 2007	P-08-55	
Supplementary information		
Transient electromagnetic soundings	P-07-165	Estimations of depth to saline groundwater

Table 6. Available data on transport properties and their handling in Forsmark SDM-Site transport properties modelling.

Available data Data specification	Ref	Usage in SDM-Site Analysis/Modelling
Results from porosity measurements, through-diffusion test, BET surface area measurements and sorption measurements on samples from boreholes KFM01A, KFM01B, KFM02A, KFM03A, KFM03B, KFM04A, KFM05A, KFM06A, KFM06B, KFM07A, KFM08A, KFM08C, KFM09A and KFM10A	P-07-139	Assignment of porosity, sorption and diffusion parameters.
Determination of porosity and micro-fracturing using the 14C-PMMA technique on samples from: KFM01A, KFM02A, KFM03A, KFM04A, KFM05A, KFM06B, KFM07A	P-06-60	
Formation factors from electrical resistivity measurements in the laboratory on samples from boreholes KFM01A, KFM02A, KFM03A, KFM04A and KFM05A	P-05-26 P-05-76 P-07-51 P-07-137	Assignment of diffusion parameters.
Formation factors from *in situ* electrical resistivity measurements KFM01A KFM02A, KFM03A, KFM04A KFM05A, KFM06A KFM07A, KFM08A KFM01D, KFM08C	P-05-29 P-05-108 P-06-91 P-06-187 P-07-138	Assignment of diffusion parameters.
Fracture mineralogy. Results from KFM06B, KFM06C, KFM07A, KFM08A, KFM08B	P-06-226	Identification of site-specific fracture and fracture zone properties as a basis for a conceptual transport model
Results from a study of the character and kinematics of deformation zones in KFM01A, KFM01B, KFM02A, KFM03A, KFM03B, KFM04A, KFM05A, KFM06A, KFM06B, KFM07A, KFM08A and KFM08B	P-06-212	Characterisation of deformation zones
Description of petrographic and geochemical characteristics of rock types based on Stage 1 and Stage 2 surface data	P-04-87	Identification of petrographic and geochemical characteristics of rock types
Microcrack volume measurements in boreholes KFM01A, KFM02B	P-07-93	Impact of stress on matrix porosity
Characterisation of matrix porewater in boreholes KFM01D, KFM08C, KFM09B	P-07-119	
Tracer tests		
Single Well Injection Withdrawal (SWIW) tests in boreholes KFM02A, KFM03A KFM08A KFM04A KFM01D	P-05-77 P-06-90 P-06-141 P-07-52	*In situ* confirmation of transport processes
Multiple well tracer tests HFM01, HFM02, HFM15, KFM01A KFM02A, KFM02B, KFM05A, KFM06A, KFM06B, HFM13, HFM15, HFM16, HFM19, HFM32	P-06-125 P-08-13	

Table 7. Available abiotic data for the surface system and their handling in Forsmark SDM-Site surface systems modelling.

Available data Data specification	Ref	Usage in SDM-Site Analysis/Modelling
Geometrical and topographical data		
Geometry, topography, bathymetry, Digital Elevation Model (DEM)	P-04-25 P-04-125 R-04-70 R-08-62	Basic input to flow and transport models. 20 m DEM used as input to regolith depth model.
Geological data		
Geological maps, Quaternary deposit descriptions	P-03-11 P-03-101 P-06-88 R-04-39 R-08-04	Conceptual model, distribution of Quaternary deposits, 2D model and input to 3D regolith-depth model.
Petrograpic analysis of gravels and boulders	P-06-87	Glacial history, petrograpic composition of regolith
Soil type map	R-04-08	Conceptual and quantitative model, input to 3D soil-depth model. Comment: Updated soil-type map is only available in GIS
Stratigraphical and analytical data from boreholes (HFM, SFM, PFM)	P-03-14 P-03-64 P-04-111 P-04-138 P-04-139 P-04-140 P-04-148 P-06-89 P-06-92 P-07-01	Stratigraphical distribution and characterisation of Quaternary deposits. Depth to bedrock. Input to 3D regolith-depth model.
Stratigraphy and spatial distribution of marine and lacustrine sediments and peat	P-03-24 P-04-86 P-04-127 P-05-139 P-06-88 P-06-89 P-06-92 P-06-220 P-06-301 P-07-196 R-01-12 R-03-26 TR-03-17	Conceptual model. Description of stratigraphical distribution and characteristics of sediment in lakes and mires. Chemical properties and distribution of organic deposits in mires. Input to 3D regolith-depth model.
Stratigraphical data from machine-cut trenches	P-04-34 P-04-111 P-05-138 P-05-166 P-06-45	Depth and stratigraphical distribution of Quaternary deposits. Conceptual model, input to 3D regolith-depth model. Physical properties of QD.
Investigation of evidence of neotectonic movements	P-03-76 P-04-123 P-05-199 R-05-51	Conceptual understanding. Depth and stratigraphy of Quaternary deposits.
Physical properties of sediment and peat, textural composition.	P-03-14 P-04-34 P-04-86	Conceptual model, input to quantitative modelling of hydraulic properties. Dominated by textural composition but also water content for determination of accumulation rate of sediments and peat.

Available data Data specification	Ref	Usage in SDM-Site Analysis/Modelling
	P-04-111 P-04-148 P-05-138 P-05-139 P-05-166 P-06-88 P-06-92 P-07-196 R-04-08	
Chemical analyses and radiometric dating of glacial and post-glacial sediments	P-03-14 P-03-118 P-04-34 P-04-86 P-04-111 P-04-148 P-05-139 P-06-220 P-06-301 R-04-08 R-06-96 TR-03-17	Conceptual model, input to quantitative model of chemical properties.
Chemical analyses of peat	P-04-127 P-06-301	Conceptual model, input to quantitative model of chemical properties
Microfossil composition in glacial sediments	P-04-110 P-05-199	Conceptual understanding, dating of sediments, glacial/ interglacial history.
Geophysical data		
Ground penetrating radar	P-04-78 P-04-156	Depth to bedrock. Conceptual model and 3D model of regolith depth.
Refraction seismics	P-04-81 P-05-12 P-06-138 P-06-45	Depth to bedrock. Conceptual model and 3D model of regolith depth.
Reflection seismics	P-04-99 P-04-158	Depth to bedrock. Conceptual model and 3D model of regolith depth.
Helicopter-borne survey data	P-03-41 P-04-157 P-04-282	Depth of regolith. Comment: Only used in stage 2.2 model of regolith depth (see /Lindborg, 2008/.
Meteorological data		
Precipitation, temperature, wind, humidity and global radiation up to March 2007	P-05-221 P-06-322 P-07-175 R-99-70 TR-02-02	Basis for general description and quantitative modelling of surface water and groundwater flow. Comparison with local meteorological data for extension of time series.
Precipitation, temperature, wind, humidity, global radiation and potential evapotranspiration June 2003 – March 2007 from the meteorological stations at Högmasten and Storskäret.	P-05-152 P-05-221 P-06-322 P-07-175	Basis for site-specific description of the meteorological conditions, and conceptual, descriptive and quantitative modelling of surface water and groundwater flow. Comparison with local meteorological data for extension of time series.
Snow depth, ground frost and ice cover	P-03-117 P-04-137 P-05-134 P-06-97 P-07-81	Validation of snow routine in quantitative modelling.

Available data Data specification	Ref	Usage in SDM-Site Analysis/Modelling
Hydrological data		
Regional discharge data	R-99-70 TR-02-02	Specific discharge in initial conceptual, descriptive and quantitative modelling.
Geometric data on catchment areas, lakes and water courses	P-04-25 P-04-141	Delineation and characteristics of catchment areas and lakes, geometrical input to the MIKE-SHE modelling.
Installation of automatic discharge gauging stations	P-05-154	Basis for measurements of discharge, electrical conductivity and temperatures at four locations in brooks.
Automatic discharge measurements	P-07-135	Data for site-specific description and water balance, conceptual and descriptive modelling, and for calibration of quantitative water flow modelling.
Manual discharge measurements	P-03-27 P-04-146 P-05-153 P-05-171 P-07-95	General description of temporal variability in surface water discharge.
Installation of surface water level gauges	P-03-64 P-04-139	Basis for surface water level measurements.
Level measurements in lakes and the sea	P-04-313 P-05-245 P-06-263 P-07-113	Surface water-groundwater level relations, conceptual and descriptive modelling, and calibration of quantitative modelling with MIKE SHE.
Hydrogeological data		
Inventory of private wells	R-02-17	Description of available hydro-geological information. Comment: No attempt is made to infer hydraulic parameters from capacity data.
Data on installed groundwater monitoring wells, abstraction wells and BAT filter tips	P-03-64 P-04-136 P-04-138 P-04-139 P-06-89	Description of QD type and depth to bedrock, basis for groundwater level measurements and hydraulic tests.
Hydraulic conductivity of Quaternary deposits	P-03-65 P-04-136 P-04-138 P-04-140 P-04-142 P-06-224	Basis for assigning hydraulic conductivity of Quaternary deposits in conceptual and quantitative models.
Groundwater levels in Quaternary deposits	P-04-313 P-05-245 P-06-263 P-07-113	Conceptual and descriptive modelling, and calibration of quantitative models.
Oceanographic data		
Regional oceanographic data	TR-02-02 TR-99-11 TR-08-01	Quantitative modelling.
Chemistry data		
Precipitation	P-05-143	Conceptual and descriptive modelling, input to quantitative modelling of pools and fluxes of elements in the landscape.
Surface water	P-05-274 P-07-95	
Groundwater	R-06-19	
Regolith	R-06-19 P-07-40	
Biota	P-06-220	
Biota and regolith	P-07-32	

Table 8. Available biotic data for the surface system and their handling in Forsmark SDM-Site surface systems modelling.

Available data Data specification	Ref	Usage in SDM-Site Analysis/Modelling
Terrestrial data		
Compilation of existing information 2002	R-02-08	Description.
Mammal population survey	P-04-04 P-07-122	Description, modelling.
Mammal ecological data and carbon budget	R-05-36	Description, modelling.
Amphibians & reptiles	P-04-07	Description, modelling.
Vegetation inventory	P-03-81	Description.
Vegetation mapping	R-02-06	Description, modelling.
Biomass of the dead organic material	P-03-90 P-04-124	Modelling.
Data from soil mapping	R-04-08	Description, modelling.
Validation of the vegetation map	P-04-314	Modelling.
Litter fall and litter decomposition	R-07-23	Description, modelling.
Birch on clear-cuts	P-04-315	Description, modelling.
LAI-index and tree stand data	TR-06-29	Description, modelling.
Tree parameters and field layer composition	P-03-81	Description, modelling.
Dead wood	P-04-124	Description, modelling.
Field layer biomass and production	P-05-80	Description, modelling.
Fungi	TR-04-26	Description, modelling.
Fine roots	P-05-166 R-07-01 TR-07-11	Description, modelling.
Respiration measurements	P-07-23 TR-07-13	Description, modelling.
Wetlands; Their properties and function	TR-04-08	Description, modelling.
Inventory of vascular plants	P-06-115	Description, modelling.
Bird monitoring	P-03-10 P-04-30 P-05-73 P-06-46 P-07-02	Description, modelling.
Bioturbation	R-06-123	Description, modelling.
Limnic data		
Habitat borders	P-04-25	Description.
Limnic producers	P-04-05 P-05-136 P-05-150 P-06-220 P-06-221 R-02-41 R-03-27	Description. Description, modelling.
Limnic consumers	P-04-06 P-05-136 P-06-220 R-02-41 R-03-27	Description, modelling.

Available data Data specification	Ref	Usage in SDM-Site Analysis/Modelling
Marine data		
Fish biomass and species composition	P-04-06 P-05-148	Description, modelling.
Vegetation surveying, species and biomass	P-05-135 R-99-69	Description, modelling.
Bottom fauna, species composition and biomass	P-03-67 P-05-135 R-99-69	Description, modelling.
Marine life from video	P-03-68	Description, modelling.
Produktion and respiration	P-06-252	Description, modelling.
Phyto- and zooplankton	P-05-72	Description, modelling.
Benthic and pelagic bacteria	P-06-232	Description, modelling.
Bird population survey	See Terrestrial	Description, modelling.

Table 9. Reports in the SKB series P-, R- and TR that are referred to in Table 1 to Table 8.

P-02-01	**Thunehed H, Pitkänen T.** Markgeofysiska mätningar inför placering av de tre första kärnborrhålen i Forsmarksområdet.
P-02-02	**Wiklund S.** Digitala ortofoton och höjdmodeller. Redovisning av metodik för platsundersöknings-områdena Oskarshamn och Forsmark samt förstudieområdet Tierp Norra.
P-03-08	**Adl-Zarrabi B.** Outcrop samples from Forsmark. Determination of thermal properties by the TPS-method.
P-03-09	**Stephens M B, Bergman T, Andersson J, Hermansson T, Wahlgren C-H, Albrecht L, Mikko H.** Bedrock mapping. Stage 1 (2002) – Outcrop data including fracture data. Forsmark.
P-03-10	**Green M.** Fågelundersökningar inom SKB:s platsundersökningar 2002. Forsmark.
P-03-11	**Sohlenius G, Rudmark L, Hedenström A.** Forsmark. Mapping of unconsolidated Quaternary deposits. Field data 2002.
P-03-12	**Hermanson J, Hansen L, Olofsson J, Sävås J, Vestgård J.** Detailed fracture mapping at the KFM02 and KFM03 drill sites. Forsmark.
P-03-14	**Sohlenius G, Rudmark L.** Forsmark site investigation. Mapping of unconsolidated Quaternary deposits. Stratigraphical and analytical data.
P-03-20	**Nordman, C.** Forsmark site investigation. Boremap mapping of percussion boreholes HFM01–03.
P-03-21	**Nordman, C.** Forsmark site investigation.Boremap mapping of percussion boreholes HFM04 and HFM05.
P-03-22	**Nordman, C.** Forsmark site investigation. Boremap mapping of percussion boreholes HFM06–08.
P-03-23	**Petersson J, Wägnerud A.** Forsmark site investigation. Boremap mapping of telescopic drilled borehole KFM01A.
P-03-24	**Hedenström A.** Forsmark site investigation. Investigation of marine and lacustrine sediments in lakes. Field data 2003.
P-03-26	**Mattsson H, Isaksson H, Thunehed H.** Forsmark site investigation. Petrophysical rock sampling, measurements of petrophysical rock parameters and *in situ* gamma-ray spectrometry measurements on outcrops carried out 2002.
P-03-27	**Nilsson A-C, Karlsson S, Borgiel M.** Forsmark site investigation. Sampling and analysis of surface waters. Results from sampling in the Forsmark area, March 2002 to March 2003.
P-03-28	**Rouhiainen P, Pöllänen J.** Forsmark site investigation. Difference flow logging of borehole KFM01A.
P-03-30	**Claesson L-Å, Nilsson G.** Forsmark site investigation. Drilling of a flushing water well, HFM01, and two groundwater monitoring wells, HFM02 and HFM03 at drillsite DS1.
P-03-32	**Claesson L-Å, Nilsson G.** Forsmark site investigation. Drilling of the telescopic borehole KFM01A at drilling site DS1.
P-03-33	**Ludvigson J-E, Jönsson S, Levén, J.** Forsmark site investigation. Pumping tests and flow logging. Boreholes KFM01A (0–100 m), HFM01, HFM02 and HFM03.
P-03-34	**Ludvigson J-E, Jönsson S, Svensson T.** Forsmark site investigation. Pumping tests and flow logging. Boreholes KFM02A (0–100 m), HFM04 and HFM05.
P-03-35	**Ludvigson J-E, Jönsson S.** Forsmark site investigation. Hydraulic interference tests. Boreholes HFM01, HFM02 and HFM03.
P-03-36	**Källgården J, Ludvigson J-E, Jönsson S.** Forsmark site investigation. Pumping tests and flow logging. Boreholes KFM03A (0–100 m), HFM06, HFM07 and HFM08.
P-03-38	**Tunbridge L, Chryssanthakis P.** Forsmark site investigation. Borehole KFM01A. Determination of P-wave velocity, transverse borehole core.
P-03-39	**Gustafsson C, Nilsson P.** Forsmark site investigation. Geophysical, radar and BIPS logging in boreholes HFM01, HFM02, HFM03 and the percussion drilled part of KFM01A.
P-03-40	**Isaksson H.** Forsmark site investigation. Interpretation of topographic lineaments 2002.
P-03-41	**Rønning H J S, Kihle O, Mogaard J O, Walker P, Shomali H, Hagthorpe P, Byström S, Lindberg H, Thunehed H.** Forsmark site investigation. Helicopter borne geophysics at Forsmark, Östhammar, Sweden.
P-03-42	**Aaro S.** Forsmark site investigation. Regional gravity survey in the Forsmark area, 2002 and 2003.
P-03-44	**Thunehed H, Pitkänen, T.** Forsmark site investigation. Electric soundings supporting inversion of helicopterborne EM-data.
P-03-45	**Aaltonen J, Gustafsson C.** Forsmark site investigation. RAMAC and BIPS logging in borehole KFM01A.
P-03-47	**Nilsson A-C.** Forsmark site investigation. Sampling and analyses of groundwater in percussion drilled boreholes and shallow monitoring wells at drillsite DS1. Results from the percussion boreholes HFM01, HFM02, HFM03, KFM01A (borehole section 0–100 m) and the monitoring wells SFM0001, SFM0002 and SFM 0003.
P-03-48	**Nilsson A-C.** Forsmark site investigation. Sampling and analyses of groundwater in percussion drilled boreholes and shallow monitoring wells at drillsite DS2. Results from the percussion boreholes HFM04, HFM05, KFM02A (borehole section 0–100 m) and the monitoring wells SFM0004 and SFM 0005.

P-03-49 **Nilsson A-C.** Forsmark site investigation. Sampling and analyses of groundwater in percussion drilled boreholes at drillsite DS3. Results from the percussion boreholes HFM06 and HFM08.

P-03-51 **Claesson L-Å, Nilsson, G.** Forsmark site investigation. Drilling of a flushing water well, HFM05, and a groundwater monitoring well, HFM04, at drillsite DS2.

P-03-52 **Claesson L-Å, Nilsson, G.** Forsmark site investigation. Drilling of the telescopic borehole KFM02A at drilling site DS 2.

P-03-53 **Nilsson P, Gustafsson C.** Forsmark site investigation. Geophysical, radar and BIPS logging in boreholes HFM04, HFM05, and the percussion drilled part of KFM02A.

P-03-54 **Nilsson P, Aaltonen J.** Forsmark site investigation. Geophysical, radar and BIPS logging in boreholes HFM06, HFM07 and HFM08.

P-03-55 **Pitkänen T, Isaksson H.** Forsmark site investigation. A ground geophysical survey prior to the siting of borehole KFM04A.

P-03-58 **Claesson L-Å, Nilsson, G.** Forsmark site investigation. Drilling of a flushing water well, HFM06 and two groundwater monitoring wells, HFM07 and HFM08, at drillsite DS3.

P-03-59 **Claesson L-Å, Nilsson, G.** Forsmark site investigation. Drilling of the telescopic borehole KFM03A and the core drilled borehole KFM03B at drilling site DS3.

P-03-64 **Johansson P-O.** Forsmark site investigation. Slug tests in groundwater monitoring wells in soil.

P-03-65 **Werner K, Johansson P-O.** Forsmark site investigation. Slug tests in groundwater monitoring wells in soil.

P-03-67 **Borgiel M.** Makroskopiska organismers förekomst i sedimentprov En översiktlig artbestämning av makroskopiska organismer.

P-03-68 **Tobiasson S.** Tolkning av undervattensfilm från Forsmark och Simpevarp.

P-03-75 **Stephens M B, Lundqvist S, Bergman T, Anderson J, Ekström M.** Forsmark site investigation. Bedrock mapping. Rock types, their petrographic and geochemical characteristics, and a structural anaysis of the bedrock based on Stage 1 (2002) surface data.

P-03-76 **Lagerbäck R, Sundh M.** Forsmark site investigation. Searching for evidence of late- or post-glacial faulting in the Forsmark region. Results from 2002.

P-03-77 **Möller C, Snäll S, Stephens M B.** Forsmark site investigation. Dissolution of quartz, vug formation and new grain growth associated with post-metamorphic hydrothermal alteration in KFM02A.

P-03-81 **Abrahamsson T.** Forsmark site investigation. Vegetation inventory in part of the municipality of Östhammar.

P-03-82 **Claesson L-Å, Nilsson, G.** Forsmark site investigation. Drilling of the telescopic borehole KFM04A and the percussion drilled borehole KFM04B at drilling site DS4.

P-03-90 **Fridriksson G, Öhr J.** Assessment of plant biomass of the ground, field and shrub layers of the Forsmark area.

P-03-94 **Wacker P, Bergelin A, Nilsson, A-C.** Forsmark site investigation. Complete hydrochemical characterisation in KFM01A. Results from two investigated sections, 110.1–120,8 and 176.8–183.9 metres.

P-03-95 **Wacker P, Nilsson A-C.** Forsmark site investigation. Hydrochemical logging and “clean up” pumping in KFM02A.

P-03-96 **Berg C, Nilsson A-C.** Forsmark site investigation. Hydrochemical logging in KFM 03A.

P-03-98 **Petersson J, Wängnerud A, Ståhle A.** Forsmark site investigation. Boremap mapping of telescopic drilled borehole KFM02A.

P-03-101 **Elhammer A, Sandkvist Å.** Forsmark site investigation. Detailed marine geological mapping.

P-03-102 **Isaksson H, Mattsson H, Thunehed H, Keisu M**. Forsmark site investigation. Interpretation of petrophysical surface data. Stage 1 (2002).

P-03-103 **Nielsen U T, Ringgaard J.** Forsmark site investigation. Geophysical borehole logging in borehole KFM01A, HFM01 and HFM02.

P-03-104 **Pitkänen T, Thunehed H, Isaksson H.** Forsmark site investigation. A ground geophysical survey prior to the siting of borehole KFM05A and KFM06A and control of the character of two SW-NE oriented lineaments.

P-03-108 **Chryssanthakis P.** Forsmark site investigation.Borehole KFM01A. Results of tilt testing.

P-03-115 **Hermanson J, Hansen L, Vestgård J, Leiner P.** Forsmark site investigation. Detailed fracture mapping of the outcrops Klubbudden, AFM001098 and drill site 4, AFM001097.

P-03-116 **Petersson J, Wängnerud A, Danielsson P, Ståhle A.** Forsmark site investigation. Boremap mapping of telescopic drilled borehole KFM03A and core drilled borehole KFM03B.

P-03-117 **Aquilonius K, Karlsson S.** Forsmark site investigation. Snow depth, frost in ground and ice cover during the winter 2002/2003.

P-03-118 **Nilsson B.** Forsmark site investigation. Element distribution in till at Forsmark – a geochemical study.

P-03-119 **Perman F, Sjöberg J.** Forsmark site investigation. Transient strain analysis of overcoring measurments in borehole DBT-01 and DBT-03.

P-04-03 **Brydsten L.** A method for construction of digital elevation models for site investigation program at Forsmark and Simpevarp.

P-04-04 **Cederlund G, Hammarström A, Wallin K.** Survey of mammal populations in the areas adjacent to Forsmark and Oskarshamn. Results from 2003.

P-04-05 **Borgiel M.** Forsmark site investigation. Sampling and analyses of surface sediment in lakes and shallow bays.

P-04-06 **Borgiel M.** Forsmark site investigation. Sampling of freshwater fish.

P-04-07 **Andrén C.** Forsmark site investigation. Amphibians and reptiles.

P-04-08 **Chryssanthakis P.** Forsmark site investigation. Borehole KFM02A. Results of tilt testing.

P-04-09 **Chryssanthakis P, Tunbridge L.** Forsmark site investigation. Borehole KFM02A. Determination of P-wave velocity, transverse borehole core.

P-04-25 **Brunberg A-K, Carlsson T, Blomqvist P, Brydsten L, Strömgren M.** Forsmark site investigation. Identification of catchments, lake-related drainage parameters and lake habitats.

P-04-29 **Isaksson H, Thunehed H, Keisu M.** Forsmark site investigation. Interpretation of airborne geophysics and integration with topography.

P-04-30 **Green M.** Forsmark site investigation. Bird monitoring in Forsmark 2002–2003.

P-04-34 **Sundh M, Sohlenius G, Hedenström A.** Forsmark site investigation. Stratigraphical investigation of till in machine cut trenches.

P-04-39 **Gustafsson J, Gustafsson C.** Forsmark site investigation. RAMAC and BIPS logging in borehole HFM11 and HFM12.

P-04-40 **Gustafsson J, Gustafsson C.** Forsmark site investigation. RAMAC and BIPS logging in borehole KFM02A.

P-04-41 **Gustafsson J, Gustafsson C.** Forsmark site investigation. RAMAC and BIPS logging in borehole KFM03A and KFM03B.

P-04-47 **Berg C, Nilsson A-C.** Forsmark site investigation. Hydrochemical logging of KFM04A.

P-04-64 **Ludvigson J-E, Jönsson S, Jönsson J.** Forsmark site investigation. Pumping tests and flow logging. Boreholes HFM11 and HFM12.

P-04-65 **Ludvigson J-E, Jönsson S, Hjerne C.** Forsmark site investigation. Pumping tests and flow logging. Boreholes KFM06A (0–100m) and HFM16.

P-04-67 **Gustafsson J, Gustafsson C.** Forsmark site investigation. RAMAC and BIPS logging in borehole KFM04A, KFM04B, HFM09 and HFM10.

P-04-68 **Gustafsson J, Gustafsson C.** Forsmark site investigation. RAMAC and BIPS logging in borehole HFM13, HFM14 and HFM 15.

P-04-69 **Gustafsson J, Gustafsson C.** Forsmark site investigation. RAMAC and BIPS logging in borehole KFM06A, HFM16, HFM17, HFM18 and HFM19.

P-04-70 **Wacker P, Bergelin A, Nilsson A-C.** Forsmark site investigation. Hydrochemical characterisation in KFM02A. Results from three investigated borehole sections; 106.5–126.5, 413.5–433.5 and 509.0–516.1 m.

P-04-71 **Ludvigson J-E, Jönsson S, Jönsson J.** Forsmark site investigation. Pumping tests and flow logging. Boreholes HFM13, HFM14 and HFM15.

P-04-72 **Ludvigson J-E, Källgården J, Hjerne C.** Forsmark site investigation. Pumping tests and flow logging. Boreholes HFM17, HFM18 and HFM19.

P-04-74 **Ludvigson J-E, Källgården J, Jönsson J.** Forsmark site investigation. Pumping tests and flow logging. Boreholes HFM09 and HFM10.

P-04-76 **Claesson L-Å, Nilsson, G.** Forsmark site investigation. Drilling of a flushing water well, HFM10, a groundwater monitoring well in solid bedrock, HFM09, and a groundwater monitoring well in soil, SFM0057, at drilling site DS4.

P-04-78 **Marek R.** Forsmark site investigation. Ground penetrating radar survey 2003.

P-04-79 **Gustafsson J, Gustafsson C.** Forsmark site investigation. RAMAC and BIPS logging in borehole KFM01B and RAMAC directional re-logging in borehole KFM01A.

P-04-80 **Mattsson H, Thunehed H, Keisu M.** Forsmark site investigation. Interpretation of borehole geophysical measurements in KFM01A, KFM01B, HFM01, HFM02 and HFM03.

P-04-81 **Keisu M, Isaksson H.** Forsmark site investigation. Acquisition of geological information from Forsmarksverket. Information from the Vattenfall archive, Råcksta.

P-04-83 **Sjöberg J.** Forsmark site investigation. Overcoring rock stress measurements in borehole KFM01B.

P-04-85 **Claesson L-Å, Nilsson, G.** Forsmark site investigation. Drilling of a flushing water well, HFM13, two groundwater monitoring wells in solid bedrock, HFM14–15, and one groundwater monitoring well in soil, SFM0058, at and close to drilling site DS5.

P-04-86 **Hedenström A.** Forsmark site investigation. Investigation of marine and lacustrine sediments in lakes. Stratigraphical and analytical data.

P-04-87 **Stephens M B, Lundqvist S, Bergman T, Ekström M.** Forsmark site investigation. Bedrock mapping. Petrographic and geochemical characteristics of rock types based on Stage 1 (2002) and Stage 2 (2003) surface data.

P-04-88 **Cronqvist T, Forssberg O, Mærsk Hansen L, Jonson A, Koyi S, Leiner P, Vestgård J, Petersson J, Skogsmo G.** Forsmark site investigation. Detailed fracture mapping of two trenches at Forsmark.

P-04-90 **Hermanson J, Hansen L, Vestgård J, Leiner, P.** Forsmark site investigation. Detailed fracture mapping of excavated rock outcrop at drilling site 5, AFM100201.

P-04-91 **Bergman T, Andersson J, Hermansson T, Zetterström Evins L, Albrecht L, Stephens M, Petersson J, Nordman C.** Forsmark site investigation. Bedrock mapping. Stage 2 (2003) – bedrock data from outcrops and the basal parts of trenches and shallow boreholes through the Quaternary cover.

P-04-92 **Nilsson D.** Forsmark site investigation. Sampling and analyses of groundwater from percussion drilled boreholes. Results from the percussion boreholes HFM09 to HFM19 and the percussion drilled part of KFM06A.

P-04-94 **Claesson L-Å, Nilsson G.** Forsmark site investigation. Drilling of a monitoring well, HFM16, at drilling site DS6.

P-04-95 **Ludvigson J-E, Levén J, Jönsson S.** Forsmark site investigation. Single-hole injection tests in borehole KFM01A.

P-04-96 **Ludvigson J-E, Jönsson S, Levén J.** Forsmark site investigation. Hydraulic evaluation of pumping activities prior to hydro-geochemical sampling in borehole KFM03A – Comparison with results from difference flow logging.

P-04-97 **Nielsen U T, Ringgaard J.** Forsmark site investigation. Geophysical borehole logging in borehole KFM02A, KFM03A and KFM03B.

P-04-98 **Thunehed H.** Forsmark site investigation. Interpretation of borehole geophysical measurements in KFM02A, KFM03A, KFM03B and HFM04 to HFM08.

P-04-99 **Bergman B, Palm H, Juhlin C.** Forsmark site investigation. Estimate of bedrock topography using seismic tomography along reflection seismic profiles.

P-04-100 **Källgården J, Ludvigson J-E, Jönsson J.** Forsmark site investigation. Single-hole injection tests in borehole KFM02A.

P-04-101 **Nordman C.** Forsmark site investigation. Boremap mapping of percussion holes HFM09–12.

P-04-103 **Petersson J, Berglund J, Danielsson P, Wängnerud A, Tullborg E-L, Mattsson H, Thunehed H, Isaksson H, Lindroos, H.** Forsmark site investigation. Petrography, geochemistry, petrophysics and fracture mineralogy of boreholes KFM01A, KFM02A and KFM03A+B.

P-04-106 **Claesson L-Å, Nilsson G.** Forsmark site investigation. Drilling of five percussion boreholes, HFM11–12 and HFM17–19, on different lineaments.

P-04-107 **Mattsson H, Thunehed H, Isaksson H, Kübler L.** Forsmark site investigation. Interpretation of petrophysical data from the cored boreholes KFM01A, KFM02A, KFM03A and KFM03B.

P-04-108 **Wacker P, Bergelin A, Berg C, Nilsson A-C.** Forsmark site investigation. Hydrochemical characterisation in KFM03A. Results from six investigated borehole sections: 386.0–391.0 m, 448.0–453.0 m, 448.5–455.6 m, 639.0–646.1 m, 939.5–946.6 m, 980.0–1,001.2 m.

P-04-109 **Wacker P, Bergelin A, Berg C, Nilsson A-C.** Forsmark site investigation. Hydrochemical characterisation in KFM04A. Results from two investigated borehole sections, 230.5–237.6 and 354.0–361.1 metres.

P-04-110 **Robertsson A-M.** Microfossil analyses of till and sediment samples from Forsmark, northern Uppland.

P-04-111 **Hedenström A, Sohlenius G, Albrecht J.** Forsmark site investigation. Stratigraphical and analytical data from auger drillings and pits.

P-04-112 **Nordman C.** Forsmark site investigation. Boremap mapping of percussion boreholes HFM13–15 and HFM19.

P-04-113 **Nordman C, Samuelsson E.** Forsmark site investigation. Boremap mapping of percussion boreholes HFM16–18.

P-04-114 **Berglund J, Petersson J, Wängnerud A, Danielsson P.** Forsmark site investigation. Boremap mapping of core drilled borehole KFM01B.

P-04-115 **Petersson J, Wängnerud A, Berglund J, Danielsson P, Ståhle A.** Forsmark site investigation. Boremap mapping of telescopic drilled borehole KFM04A.

P-04-116 **Carlsten S, Petersson J, Stephens M, Mattsson H, Gustafsson J.** Forsmark site investigation. Geological single-hole interpretation of KFM01A, KFM01B and HFM01–03 (DS1).

P-04-117 **Carlsten S, Petersson J, Stephens M, Mattsson H, Gustafsson J.** Forsmark site investigation. Geological single-hole interpretation of KFM02A and HFM04–05 (DS2).

P-04-118 **Carlsten S, Petersson J, Stephens M, Thunehed H, Gustafsson J.** Forsmark site investigation. Geological single-hole interpretation of KFM03B, KFM03A and HFM06–08 (DS3).

P-04-119 **Carlsten S, Petersson J, Stephens M, Mattsson H, Gustafsson J.** Forsmark site investigation. Geological single-hole interpretation of KFM04A and HFM09–10 (DS4).

P-04-120 **Carlsten S, Petersson J, Stephens M, Thunehed H, Gustafsson J.** Forsmark site investigation. Geological single-hole interpretation of HFM11–13 and HFM16–18.

P-04-123 **Lagerbäck R, Sundh M, Johansson H.** Forsmark site investigation. Searching for evidence of late- or post-glacial faulting in the Forsmark region. Results from 2003.

P-04-124 **Andersson J.** Forsmark site investigation. Investigation of the amount of dead wood.

P-04-125 **Brydsten L, Strömgren M**. Forsmark site investigation. Water depth soundings in shallow bays in Forsmark.

P-04-126 **Page L, Hermansson T, Söderlund P, Andersson J, Stephens M B.** Forsmark site investigation. Bedrock mapping U-Pb, 40Ar/39Ar and (U-Th)/He geochronology.

P-04-127 **Fredriksson D.** Forsmark site investigation. Peatland investigation Forsmark.

P-04-135 **Levén J, Ludvigson J-E.** Forsmark site investigation. Hydraulic interferences during the drilling of borehole KFM01B. Boreholes HFM01, HFM02, HFM03 and KFM01A.

P-04-136 **Johansson P-O.** Forsmark site investigation. Undisturbed pore water sampling and permeability measurements with BAT filter tips. Soil sampling for pore water analyses.

P-04-137 **Heneryd N.** Forsmark site investigation. Snow depth, frost in ground and ice cover during the winter 2003/2004.

P-04-138 **Werner K, Lundholm L, Johansson P-O.** Forsmark site investigation. Drilling and pumping test of wells at Börstilåsen.

P-04-139 **Werner K, Lundholm L.** Forsmark site investigation. Supplementary drilling and soil sampling, installation of groundwater monitoring wells, a pumping well and surface water level gauges.

P-04-140 **Werner K.** Forsmark site investigation. Supplementary slug tests in groundwater monitoring wells in soil.

P-04-141 **Brydsten L, Strömgren M.** Forsmark site investigation. Measurements of brook gradients and lake thresholds.

P-04-142 **Werner K, Lundholm L.** Forsmark site investigation. Pumping test in wells SFM0074.

P-04-143 **Mattsson H, Keisu M.** Forsmark site investigation. Interpretation of borehole geophysical measurements in KFM04A, KFM06A (0–100 m), HFM10, HFM11, HFM12, HFM13, HFM16, HFM17 and HFM18.

P-04-144 **Nielsen U T, Ringgaard J.** Forsmark site investigation. Geophysical borehole logging in borehole KFM04A, KFM06A, HFM10, HFM11, HFM12 and HFM13.

P-04-145 **Nielsen U T, Ringgaard J.** Forsmark site investigation. Geophysical borehole logging in borehole KFM01B, HFM14, HFM15, HFM16, HFM17 and HFM18.

P-04-146 **Nilsson A-C, Borgiel M.** Forsmark site investigation. Sampling and analyses of surface waters. Results from sampling in the Forsmark area, March 2003 to March 2004.

P-04-148 **Hedenström A.** Forsmark site investigation. Stratigraphical and analytical data of Quaternary deposits.

P-04-149 **Sandström B, Savolainen M, Tullborg E-L.** Forsmark site investigation. Fracture mineralogy. Results from fracture minerals and wall rock alteration in boreholes KFM01A, KFM02A, KFM03A and KFM03B.

P-04-152 **Gustafsson J, Gustafsson C.** Forsmark site investigation. RAMAC and BIPS logging in borehole KFM05A.

P-04-153 **Nielsen U T, Ringgaard J.** Forsmark site investigation. Geophysical borehole logging in borehole KFM05A and HFM19.

P-04-154 **Thunehed H, Keisu M.** Forsmark site investigation. Interpretation of borehole geophysical measurements in KFM05A, HFM14, HFM15 and HFM19.

P-04-155 **Isaksson H, Mattsson H, Thunehed H, Keisu M.** Forsmark site investigation. Petrophysical surface data Stage 2 – 2003 (including 2002).

P-04-156 **Marek R.** Forsmark site investigation. A co-ordinated interpretation of ground penetrating radar data from the Forsmark site.

P-04-157 **Thunehed H.** Forsmark site investigation. Inversion of helicopterborne electromagnetic measurements.

P-04-158 **Juhlin C, Bergman B.** Reflection seismics in the Forsmark area. Updated interpretation of Stage 1 (previous report R-02-43). Updated estimate of bedrock topography (previous report P-04-99).

P-04-159 **Adl-Zarrabi B.** Forsmark site investigation. Drill hole KFM01A. Thermal properties: heat conductivity and heat capacity determined using the TPS method and mineralogical composition by modal analysis.

P-04-161 **Adl-Zarrabi B.** Forsmark site investigation. Drill hole KFM02A. Thermal properties: heat conductivity and heat capacity determined using the TPS method and mineralogical composition by modal analysis.

P-04-162 **Adl-Zarrabi B.** Forsmark site investigation. Drill hole KFM03A. Thermal properties: heat conductivity and heat capacity determined using the TPS method and mineralogical composition by modal analysis.

P-04-163 **Åkesson U.** Forsmark site investigation. Drill hole KFM01A. Extensometer measurements of the coefficient of thermal expansion of rock.

P-04-164 **Carlsson L.** Forsmark site investigation. Drill hole KFM02A. Extensometer measurements of the coefficient of thermal expansion of rock.

P-04-165 **Liedberg L.** Forsmark site investigation. Drill hole KFM03A. Extensometer measurements of the coefficient of thermal expansion of rock.

P-04-166 **Savukoski M.** Forsmark site investigation. Drill hole KFM01A. Determination of porosity by water saturation and density by buoyancy technique.

P-04-167 **Savukoski M, Carlsson L.** Forsmark site investigation. Drill hole KFM02A. Determination of porosity by water saturation and density by buoyancy technique.

P-04-168 **Savukoski M.** Forsmark site investigation. Drill hole KFM03A. Determination of porosity by water saturation and density by buoyancy technique.

P-04-169 **Savukoski M.** Forsmark site investigation. Drill hole KFM04A. Determination of porosity by water saturation and density by buoyancy technique.

P-04-170 **Jacobsson L.** Forsmark site investigation. Drill hole KFM01A. Indirect tensile strength test.

P-04-171 **Eloranta P.** Forsmark site investigation. Drill hole KFM01A. Indirect tensile strength test (HUT).

P-04-172 **Jacobsson L.** Forsmark site investigation. Drill hole KFM02A. Indirect tensile strength test.

P-04-173 **Jacobsson L.** Forsmark site investigation. Drill hole KFM03A. Indirect tensile strength test.

P-04-174 **Jacobsson L.** Forsmark site investigation. Drill hole KFM04A. Indirect tensile strength test.

P-04-175 **Chryssanthakis P.** Forsmark site investigation. Drill hole KFM01A. The normal stress and shear tests on joints.

P-04-176 **Eloranta P.** Forsmark site investigation. Drill hole KFM01A. Uniaxial compression test (HUT).

P-04-177 **Eloranta P.** Forsmark site investigation. Drill hole KFM01A. Triaxial compression test (HUT).

P-04-178 **Chryssanthakis P.** Forsmark site investigation. Boreholes KFM03A and KFM03B Tilt testing.

P-04-179 **Chryssanthakis P, Tunbridge L.** Forsmark site investigation. Borehole KFM04A Tilt testing.

P-04-180 **Chryssanthakis P, Tunbridge L.** Forsmark site investigation. Borehole KFM03A. Determination of P-wave velocity, transverse borehole core.

P-04-181 **Chryssanthakis P, Tunbridge L.** Forsmark site investigation. Borehole KFM04A. Determination of P-wave velocity, transverse borehole core.

P-04-186 **Dinges C.** Forsmark site investigation. Drill hole KFM01A. Thermal properties: heat conductivity and heat capacity determined using the TPS method – compared test.

P-04-188 **Rouhiainen P, Pöllänen J.** Forsmark site investigation. Difference flow logging in borehole KFM02A.

P-04-189 **Pöllänen J, Sokolnicki M.** Forsmark site investigation. Difference flow logging in borehole KFM03A.

P-04-190 **Rouhiainen P, Pöllänen J.** Forsmark site investigation. Difference flow logging in borehole KFM04A.

P-04-191 **Pöllänen J, Sokolnicki M, Rouhiainen P.** Forsmark site investigation. Difference flow logging in borehole KFM05A.

P-04-193 **Rouhiainen P, Pöllänen J, Ludvigson J-E.** Forsmark site investigation. Addendum to Difference flow logging in borehole KFM01A.

P-04-194 **Källgården J, Ludvigson J-E, Hjerne C.** Forsmark site investigation. Single-hole injection tests in borehole KFM03A.

P-04-198 **Åkesson U.** Forsmark site investigation. Drill hole KFM04A: Extensometer measurement of the coefficient of thermal expansion of rock.

P-04-199 **Adl-Zarrabi B.** Forsmark site investigation. Drill hole KFM04A. Thermal properties: heat conductivity and heat capacity determined using the TPS method and mineralogical composition by modal analysis.

P-04-200 **Jönsson S, Ludvigson J-E, Svensson T.** Forsmark site investigation. Hydraulic interference tests. Boreholes HFM11 and HFM12.

P-04-203 **Chryssanthakis P, Tunbridge L.** Forsmark site investigation. Borehole: KFM05A. Determination of P-wave velocity, transverse borehole core.

P-04-205 **Chryssanthakis P, Tunbridge L.** Forsmark site investigation. Borehole: KFM05A. Tilt testing.

P-04-222 **Claesson L-Å, Nilsson G.** Forsmark site investigation. Drilling of the telescopic borehole KFM05A at drilling site DS5.

P-04-223 **Jacobsson L.** Forsmark site investigation. Borehole KFM01A. Uniaxial compression test of intact rock.

P-04-224 **Jacobsson L.** Forsmark site investigation. Borehole KFM02A. Uniaxial compression test of intact rock.

P-04-225 **Jacobsson L.** Forsmark site investigation. Borehole KFM03A. Uniaxial compression test of intact rock.

P-04-226 **Jacobsson L.** Forsmark site investigation. Borehole KFM04A. Uniaxial compression test of intact rock.

P-04-227 **Jacobsson L.** Forsmark site investigation. Borehole KFM01A. Triaxial compression test of intact rock.

P-04-228 **Jacobsson L.** Forsmark site investigation. Borehole KFM02A. Triaxial compression test of intact rock.

P-04-229 **Jacobsson L.** Forsmark site investigation. Borehole KFM03A. Triaxial compression test of intact rock.

P-04-230 **Jacobsson L.** Forsmark site investigation. Borehole KFM04A. Triaxial compression test of intact rock.

P-04-241 **Korhonen K, Paananen M, Paulamäki S.** Interpretation of lineaments from airborne geophysical and topographic data. An alternative model within version 1.2 of the Forsmark modelling project

P-04-245 **Claesson L-Å, Nilsson G.** Forsmark site investigation. Drilling of two flushing water wells, HFM21 and HFM22, one groundwater monitoring well in solid bedrock, HFM20, and one groundwater monitoring well in soil, SFM0076.

P-04-278 **Hjerne C, Jönsson J, Ludvigson J-E.** Forsmark site investigation. Single-hole injection tests in borehole KFM03B.

P-04-282 **Isaksson H, Keisu M.** Forsmark site investigation. Interpretation of airborne geophysics and integration with topography. Stage 2 (2002–2004).

P-04-293 **Hjerne C, Ludvigson J-E.** Forsmark site investigation. Single-hole injection tests in borehole KFM04A.

P-04-295 **Petersson J, Berglund J, Wängnerud A, Danielsson P, Stråhle A.** Forsmark site investigation. Boremap mapping of telescopic drilled borehole KFM05A.

P-04-296 **Carlsten S, Petersson J, Stephens M, Thunehed H, Gustafsson J.** Forsmark site investigation. Geological single-hole interpretation of KFM05A, HFM14–15 and HFM19 (DS5).

P-04-302 **Claesson L-Å, Nilsson G.** Forsmark site investigation. Drilling of borehole KFM01B at drilling site DS1.

P-04-305 **Gustafsson J, Nissen J.** Forsmark site investigation. Mise-á-la-masse measurements. An experiment to test the possibility for detecting the outcropping of the fracture zone DZ2 in HFM14.

P-04-307 **Gokall-Norman K, Svensson T, Ludvigson L-E, Jönsson S.** Forsmark site investigation. Hydraulic interference test. Boreholes HFM18 and KFM03A.

P-04-311 **Klee G, Rummel F.** Forsmark site investigation. Rock stress measurements with hydraulic fracturing and hydraulic testing of pre-existing fractures in borehole KFM01A, KFM01B, KFM02A and KFM04A. Results from *in situ* tests.

P-04-312 **Rummel F, Weber U.** Forsmark site investigation. Rock stress measurements with hydraulic fracturing and hydraulic testing of pre-existing fractures in borehole KFM01A, KFM01B, KFM02A and KFM04A. Laboratory Core Investigations.

P-04-313 **Nyberg G, Wass E, Askling P, Johansson P-O.** Forsmark site investigation. Hydro monitoring programme. Report for June 2002 – July 2004.

P-04-314 **Alling V, Andersson P, Fridriksson G, Rubio Lind C.** Forsmark site investigation. Validation of GIS-maps and inventory of vegetation types in Forsmark. Validation and inventory of marshland, swamp forest, fertile land & woodland.

P-04-315 **Alling V, Andersson P, Fridriksson G, Rubio Lind C.** Estimation of biomass and primary production of birch. Birch biotopes in Forsmark and Oskarshamn.

P-05-01 **Gustafsson J, Gustafsson C.** Forsmark site investigation. RAMAC and BIPS logging in boreholes KFM06A and HFM22.

P-05-04 **Chryssanthakis P, Tunbridge L.** Forsmark site investigation. Borehole KFM06A. Determination of P-wave velocity, transverse borehole core.

P-05-08 **Ljunggren B.** Forsmark site investigation. Drill hole KFM01A. Normal loading and shear tests on joints

P-05-09 **Ljunggren B.** Forsmark site investigation. Drill hole KFM02A. Normal loading and shear tests on joints

P-05-10 **Ljunggren B.** Forsmark site investigation. Drill hole KFM03A. Normal loading and shear tests on joints

P-05-11 **Ljunggren B.** Forsmark site investigation. Drill hole KFM04A. Normal loading and shear tests on joints

P-05-12 **Toresson B.** Forsmark site investigation. Seismic refraction survey 2004.

P-05-14 **Jönsson J, Hjerne C, Ludvigson J-E.** Forsmark site investigation. Pumping tests and flow logging. Boreholes HFM20, HFM21 and HFM22.

P-05-15 **Rouhiainen P, Sokolnicki M.** Forsmark site investigation. Difference flow logging in borehole KFM06A.

P-05-17 **Nielsen U T, Ringgaard J, Horn F.** Forsmark site investigation. Geophysical borehole logging in borehole KFM06A, HFM20, HFM21, HFM22 and SP-logging in KFM01A and KFM04A.

P-05-21 **Ludvigson J-E, Levén J.** Forsmark site investigation. Comparison of measured EC in selected fractures in boreholes KFM02A, KFM03A and KFM04A from difference flow logging and hydro-geochemical characterization – Analysis of observed discrepancies in KFM03A.

P-05-26 **Thunehed H.** Forsmark site investigation. Resistivity measurements on samples from KFM01A and KFM02A.

P-05-29 **Löfgren M, Neretnieks I.** Forsmark site investigation. Formation factor logging *in situ* and in the laboratory by electrical methods in KFM01A and KFM02A. Measurements and evaluation of methodology.

P-05-33 **Berg C.** Forsmark site investigation. Hydrochemical logging in KFM06A.

P-05-37 **Rouhiainen P, Sokolnicki M.** Forsmark site investigation. Difference flow logging in borehole KFM02A during pumping in HFM16.

P-05-43 **Sokolnicki M, Rouhiainen P.** Forsmark site investigation. Difference flow logging in borehole KFM08A.

P-05-46 **Toresson B.** Forsmark site investigation. Seismic velocity analysis in excavated trenches.

P-05-48 **Nilsson D.** Forsmark site investigation. Sampling and analyses of groundwater from percussion drilled boreholes Results from the percussion drilled boreholes HFM20, HFM21 and HFM22.

P-05-50 **Claesson L-Å, Nilsson G.** Forsmark site investigation. Drilling of the telescopic borehole KFM06A and the core drilled borehole KFM06B at drill site DS6.

P-05-51 **Mattsson H, Keisu M.** Forsmark site investigation. Interpretation of geophysical borehole measurements from KFM06A and HFM20, HFM21 and HFM22.

P-05-52 **Gustafsson J, Gustafsson C.** Forsmark site investigation. RAMAC and BIPS logging in borehole KFM07A.

P-05-53 **Gustafsson J, Gustafsson C.** Forsmark site investigation. RAMAC and BIPS logging in borehole KFM06B.

P-05-56 **Gokall-Norman K, Ludvigson J-E, Hjerne C.** Forsmark site investigation. Single-hole injection tests in borehole KFM05A.

P-05-58 **Gustafsson J, Gustafsson C.** Forsmark site investigation. RAMAC and BIPS logging in borehole KFM08B.

P-05-63 **Sokolnicki M, Rouhiainen P.** Forsmark site investigation. Difference flow logging in borehole KFM07A.

P-05-64 **Gustafsson J, Gustafsson C.** Forsmark site investigation. RAMAC and BIPS logging in borehole KFM07A (0–100 m), HFM20 and HFM21.

P-05-66 **Lindfors U, Perman F, Sjöberg J.** Forsmark site investigation. Evaluation of the overcoring results from borehole KFM01B.

P-05-72 **Huononen R, Borgiel M.** Forsmark site investigation. Sampling of phyto- and zooplankton in sea water. Abundances and carbon biomasses.

P-05-73 **Green M.** Forsmark site investigation. Bird monitoring in Forsmark 2002–2004.

P-05-76 **Thunehed H.** Forsmark site investigation. Resistivity measurements and determination of formation factors on samples from KFM03A, KFM04A and KFM05A.

P-05-77 **Gustafsson E, Nordqvist R, Thur P.** Forsmark site investigation. Groundwater flow measurements in boreholes KFM01A, KFM02A, KFM03A, KFM03B and SWIW tests in KFM02A, KFM03A.

P-05-78 **Gokall-Norman, Ludvigson J-E.** Forsmark site investigation. Hydraulic interference test. Boreholes HFM16, HFM19 and KFM02A.

P-05-79 **Wacker P, Berg C, Bergelin A, Nilsson A-C.** Forsmark site investigation. Hydrochemical characterisation in KFM05A. Results from an investigated section at 712.6–722.0 m.

P-05-80 **Löfgren A.** Oskarshamn/Forsmark site investigation. Estimation of biomass and net primary production in field and ground layer, and biomass in litter layer of different vegetation types in Forsmark and Oskarshamn.

P-05-97 **Jacobsson L.** Forsmark site investigation. Borehole KFM05A. Uniaxial compression test of intact rock.

P-05-98 **Jacobsson L.** Forsmark site investigation. Borehole KFM05A. Indirect tensile strength test.

P-05-99 **Jacobsson L.** Forsmark site investigation. Borehole KFM05A. Normal stress and shear test on joints

P-05-100 **Jacobsson L.** Forsmark site investigation. Borehole KFM05A. Triaxial compression test of intact rock.

P-05-101 **Petersson J, Skogsmo G, Berglund J, Wängnerud A, Stråhle A.** Forsmark site investigation. Boremap mapping of telescopic drilled borehole KFM06A and core drilled borehole KFM06B.

P-05-102 **Petersson J, Skogsmo G, Wängnerud A, Berglund J, Stråhle A.** Forsmark site investigation. Boremap mapping of telescopic drilled borehole KFM07A.

P-05-103 **Berglund J, Döse C.** Forsmark site investigation. Boremap mapping of percussion boreholes HFM20, HFM21 and HFM22.

P-05-108 **Löfgren M, Neretnieks I.** Forsmark site investigation. Formation factor logging *in situ* by electrical methods in KFM03A and KFM04A.

P-05-112 **Lanaro F.** Forsmark site investigation. Rock mechanics characterisation of borehole KFM01A.

P-05-113 **Lanaro F.** Forsmark site investigation. Rock mechanics characterisation of borehole KFM02A.

P-05-114 **Lanaro F.** Forsmark site investigation. Rock mechanics characterisation of borehole KFM03A.

P-05-115 **Lanaro F.** Forsmark site investigation. Rock mechanics characterisation of borehole KFM04A.

P-05-119 **Mattson H.** Forsmark site investigation. Interpretation of geophysical borehole measurements from KFM07A.

P-05-120 **Jacobsson L.** Forsmark site investigation. Borehole KFM06A. Uniaxial compression test of intact rock.

P-05-121 **Jacobsson L.** Forsmark site investigation. Drill hole KFM06A. Indirect tensile strength test.

P-05-122 **Jacobsson L, Flansbjer M.** Forsmark site investigation. Borehole KFM06A. Normal loading and shear test on joints.

P-05-123 **Adl-Zarrabi B.** Forsmark site investigation. Drill hole KFM06A Thermal properties: heat conductivity and heat capacity determined using the TPS method.

P-05-124 **Liedberg L.** Forsmark site investigation. Drill hole KFM06A. Determination of porosity by water saturation and buoyancy technique.

P-05-125 **Chryssanthakis P, Tunbridge L.** Forsmark site investigation. Borehole KFM07A. Determination of P-wave velocity transverse borehole core.

P-05-132 **Carlsten S, Gustafsson J, Mattsson H, Petersson J, Stephens M.** Forsmark site investigation. Geological single-hole interpretation of KFM06A and KFM06B (DS6).

P-05-133 **Gokall-Norman K, Svensson T, Ludvigson.** Forsmark site investigation. Single-hole injection tests in borehole KFM07A.

P-05-134 **Heneryd N.** Forsmark site investigation. Snow depth, ground frost and ice cover during the winter 2004/2005.

P-05-135 **Borgiel M.** Forsmark site investigation. Benthic vegetation, plant associated macrofauna and benthic macrofauna in shallow bays and shores in the Grepen area, Bothnian Sea. Results from sampling 2004.

P-05-136 **Huononen R.** Forsmark site investigation. Benthic macrofauna, plant associated macrofauna and benthic vegetation in shallow lakes. Results from sampling 2004.

P-05-138 **Albrecht J.** Forsmark site investigation. Study of Quaternary sediments in connection with investigations of bedrock lineaments.

P-05-139 **Risberg J.** Forsmark site investigation. Bio- and lithostratigraphy in offshore sediment core PFM004396. Salinity variations in the Bothnian Sea offshore Forsmark.

P-05-141 **Jacobsson L, Flansbjer M.** Forsmark site investigation. Borehole KFM05A Normal stress test with direct and indirect deformation measurement together with shear tests on joints.

P-05-142 **Claesson L-Å, Nilsson G.** Forsmark site investigation. Drilling of the telescopic borehole KFM07A at drill site DS7.

P-05-143 **Nilsson D.** Forsmark site investigation. Sampling and analysis of precipitation, years 2002 to 2005.

P-05-145 **Svensson T, Ludvigson J-E, Hjerne C.** Forsmark site investigation. Single-hole injection tests in borehole KFM02A, re-measurements after hydraulic fracturing.

P-05-148 **Heibo E, Karås P.** Forsmark site investigation. The coastal fish community in the Forsmark area SW Bothnian Sea.

P-05-150 **Carlsson T, Brunberg A-K, Brydsten L, Strömgren M.** Forsmark site investigation. Characterisation of running waters, including vegetation, substrate and technical encroachments.

P-05-152 **Juston J, Johansson P-O.** Forsmark site investigation. Analysis of meteorological data, surface water level data, and groundwater level data.

P-05-153 **Johansson P-O.** Forsmark site investigation. Manual discharge measurements in brooks, April 2002 – April 2005.

P-05-154 **Johansson P-O.** Forsmark site investigation. Installation of brook discharge gauging stations.

P-05-156 **Petersson J, Berglund J, Danielsson P, Skogsmo G.** Forsmark site investigation. Petrographic and geochemical characteristics of bedrock samples from boreholes KFM04A–06A, and a whitened alteration rock.

P-05-157 **Carlsten S, Gustafsson J, Mattsson H, Petersson J, Stephens M.** Forsmark site investigation. Geological single-hole interpretation of KFM07A and HFM20–21 (DS7).

P-05-158 **Gustafsson J, Gustafsson C.** Forsmark site investigation. RAMAC and BIPS logging in borehole KFM08A.

P-05-159 **Nielsen U T, Ringgaard J, Fris Dahl J.** Forsmark site investigation. Geophysical borehole logging in the boreholes KFM07A, KFM08A and KFM08B.

P-05-165 **Hjerne C, Ludvigson J-E, Lindquist A.** Forsmark site investigation. Single-hole injection tests in boreholes KFM06A and KFM06B.

P-05-166 **Lundin L, Stendahl J, Lode E.** Forsmark site investigation. Soils in two large trenches.

P-05-168 **Cosma C, Enescu N, Balu L.** Forsmark site investigation. Vertical seismic profiling from the boreholes KFM01A and KFM02A.

P-05-170 **Berg C, Wacker P, Nilsson A-C.** Forsmark site investigation. Chemical characterisation in borehole KFM07A Results from the investigated section at 848.0–1,001.6 m.

P-05-171 **Nilsson A-C, Borgiel M.** Forsmark site investigation. Sampling and analyses of near surface groundwaters Results from sampling of shallow soil monitoring wells, BAT pipes, a natural spring and private wells, May 2003 – April 2005.

P-05-172 **Claesson L-Å, Nilsson G.** Forsmark site investigation. Drilling of the telescopic borehole KFM08A and the core drilled borehole KFM08B at drill site DS8.

P-05-176 **Gustafsson J, Gustafsson C.** Forsmark site investigation. BIPS logging in the boreholes HFK248, HFK249 and HFK250.

P-05-178 **Berg C, Wacker P, Nilsson A-C.** Forsmark site investigation. Chemical characterisation in borehole KFM06A. Results from the investigated sections at 266.0–271.0 m, 353.5–360.6 m and 768.0–775.1 m.

P-05-183 **Nordgulen Ø, Braathen A.** Forsmark site investigation. Structural investigations of deformation zones (ductile shear zones and faults) at Forsmark – a pilot study.

P-05-186 **Gokall-Norman K, Ludvigson J-E, Jönsson S.** Forsmark site investigation. Hydraulic interference test. Boreholes KFM04A, HFM10, HFM13, HFM19 and HFK252.

P-05-187 **Berg C, Levén J, Nilsson A-C.** Forsmark site investigation. Hydrochemical logging in KFM07A.

P-05-196 **Waber H N, Smellie J A T.** Forsmark site investigation. Borehole KFM06A: Characterisation of pore water Part I: Diffusion experiments.

P-05-197 **Sandström B, Tullborg E-L.** Forsmark site investigation. Fracture mineralogy Results from fracture minerals and wall rock alteration in boreholes KFM01B, KFM04A, KFM05A and KFM06A.

P-05-199 **Leijon, B.** Forsmark site investigation. Investigations of superficial fracturing and block displacements at drill site 5.

P-05-202 **Mattsson H, Keisu M.** Forsmark site investigation. Interpretation of geophysical borehole measurements from KFM08A and KFM08B.

P-05-203 **Petersson J, Berglund J, Skogsmo G, Wängnerud A.** Forsmark site investigation. Boremap mapping of telescopic drilled borehole KFM08A and cored drilled borehole KFM08B.

P-05-204 **Mattsson H, Thunehed H, Isaksson H.** Forsmark site investigation. Interpretation of petrophysical data from the cored boreholes KFM04A, KFM05A and KFM06A.

P-05-206 **Berg C.** Forsmark site investigation. Hydrochemical logging in KFM08A.

P-05-210 **Jacobsson L.** Forsmark site investigation. Borehole KFM07A. Triaxial compression test of intact rock.

P-05-211 **Jacobsson L**. Forsmark site investigation. Borehole KFM07A. Uniaxial compression test of intact rock.

P-05-212 **Jacobsson L.** Forsmark site investigation. Drill hole KFM07A. Indirect tensile strength test including strain measurement.

P-05-213 **Jacobsson L, Flansbjer M**. Forsmark site investigation. Borehole KFM07A. Normal loading and shear tests on joints.

P-05-214 **Adl-Zarrabi B.** Forsmark site investigation. Borehole KFM07A. Thermal conductivity and thermal diffusivity determined using the TPS method.

P-05-215 **Savukoski M.** Forsmark site investigation. Borehole KFM07A. Determination of porosity by water saturation and density by buoyancy technique.

P-05-216 **Chryssanthakis P, Tunbridge L**. Borehole: KFM08A. Determination of P-wave velocity, transverse borehole core. Forsmark site investigation.

P-05-217 **Jacobsson L**. Forsmark site investigation. Borehole KFM08A. Triaxial compression test of intact rock.

P-05-218 **Jacobsson L, Flansbjer M**. Forsmark site investigation. Borehole KFM08A. Normal loading and shear tests on joints.

P-05-219 **Adl-Zarrabi B.** Forsmark site investigation. Borehole KFM08A. Thermal conductivity and thermal diffusivity determined using the TPS method.

P-05-220 **Liedberg L.** Forsmark site investigation. Borehole KFM08A. Determination of porosity by water saturation and density by buoyancy technique.

P-05-221 **Wern L, Jones J.** Forsmark site investigation. Meteorological monitoring at Forsmark, June 2003 until July 2005.

P-05-235 **Lindquist A, Ludvigson J-E, Svensson T.** Forsmark site investigation. Single-hole injection tests and pressure pulse tests in borehole KFM08B.

P-05-236 **Gokall-Norman K, Ludvigson J-E, Jönsson S.** Forsmark site investigation. Hydraulic interference test in borehole HFM01.

P-05-242 **Gustasson J, Gustafsson C.** Forsmark site investigation. RAMAC and BIPS logging in borehole KFM06C.

P-05-245 **Nyberg G, Wass E.** Forsmark site investigation. Hydro Monitoring Program. Report for August 2004–July 2005.

P-05-261 **Johansson R, Isaksson H.** Forsmark site investigation. Assessment of inferred lineaments in the northwestern part of the Forsmark site investigation area. Present knowledge and recommendations for further investigations.

P-05-262 **Carlsten S, Gustafsson J, Mattsson H, Petersson J, Stephens M.** Forsmark site investigation. Geological single-hole interpretation of KFM08A, KFM08B and HFM22 (DS8).

P-05-265 **Nissen J, Gustafsson J, Sandström R, Wallin L, Taxén C.** Forsmark site investigation. Some corrosion observations and electrical measurements at drill sites DS4, DS7 and DS8.

P-05-266 **Isaksson H, Pitkänen T.** Forsmark site investigation. Ground geophysical measurements near the lineament trench AFM001265.

P-05-269 **Forssberg O, Hansen L M, Koyi S, Vestgård J, Öhman J.** Forsmark site investigation. Detailed fracture mapping of excavated outcrop AFM001264 (DS7) in Forsmark.

P-05-274 **Nilsson A-C, Borgiel M.** Forsmark site investigation. Sampling and analyses of surface waters. Results from sampling in the Forsmark area, March 2004–June 2005.

P-05-276 **Nielsen U T, Skjellerup P, Ringgaard J.** Forsmark site investigation. Geophysical borehole logging in the borehole KFM06C.

P-05-277 **Claesson L-A, Nilsson G.** Forsmark site investigation. Drilling of the telescopic borehole KFM06C at drill site DS6.

P-05-278 **Claesson L-A, Nilsson G.** Forsmark site investigation. Drilling of monitoring wells HFM23 and HFM28 at drill site DS9 as well as HFM24 and SFM0080 at drill site DS10.

P-06-09 **Gokall-Norman K, Ludvigson J-E, Jönsson S.** Forsmark site investigation. Hydraulic interference test. Boreholes KFM02A and KFM03A.

P-06-22 **Nielsen U T, Ringgaard J, Vangkild-Pedersen T.** Forsmark site investigation. Geophysical borehole logging in boreholes KFM09A, KFM07B, HFM25, HFM27 and HFM28.

P-06-23 **Lindquist A, Ludvigson J-E, Gokall-Norman K.** Forsmark site investigation. Single-hole injection tests in borehole KFM06C.

P-06-24 **Chryssanthakis P, Tunbridge L**. Forsmark site investigation. Borehole KFM09A. Determination of P-wave velocity, transverse borehole core.

P-06-25 **Chryssanthakis P**. Forsmark site investigation. Borehole: KFM09A. Tilt testing.

P-06-26 **Jacobsson L.** Forsmark site investigation. Borehole KFM09A. Triaxial compression tests of intact rock.

P-06-27 **Jacobsson L.** Forsmark site investigation. Borehole KFM09A. Uniaxial compression test of intact rock.

P-06-28 **Jacobsson L.** Forsmark site investigation. Borehole KFM09A. Indirect tensile strength test.

P-06-29 **Jacobsson L.** Forsmark site investigation. Borehole KFM09A. Normal loading and shear tests on joints.

P-06-44 **Gustasson J, Gustafsson C.** Forsmark site investigation. RAMAC and BIPS logging in boreholes KFM07B, KFM09A, HFM25 and HFM28.

P-06-45 **Mörén L, Nyström B.** Platsundersökning Forsmark. Behovsinventering, underlag och program för geotekniska undersökningar.

P-06-46 **Green M.** Forsmark site investigation. Bird monitoring in Forsmark 2005.

P-06-52 **Lindqust A, Ludvigson J-E, Harrström J, Svensson T.** Forsmark site investigation. Single-hole injection tests in borehole KFM09A.

P-06-53 **Gentzschein B, Levén J, Follin S.** A comparison between well yield data from the site investigation in Forsmark and domestic wells in northern Uppland.

P-06-54 **Follin S, Ludvigson J-E, Levén J.** A comparison between standard well test evaluation methods used in SKB's site investigations and the Generalised Radial Flow concept.

P-06-56 **Forssman I, Zetterlund M, Forsmark T, Rhén I.** Correlation of Posiva Flow Log anomalies to core mapped features in Forsmark in KFM06A and KFM07A.

P-06-57 **Berg C, Nilsson A-C.** Forsmark site investigation. Hydrochemical monitoring of percussion- and core drilled boreholes. Results from water sampling and analyses during 2005.

P-06-60 **Penttinen L, Siitari-Kauppi M, Ikonen J.** Forsmark site investigation. Determination of porosity and micro fracturing using the 14C-PMMA technique in samples taken from Forsmark area.

P-06-63 **Berg C, Bergelin A, Wacker P, Nilsson A-C.** Forsmark site investigation. Hydrochemical characterisation in borehole KFM08A. Results from the investigated section at 683.5–690.6 (690.8) m.

P-06-64 **Gustasson J, Gustafsson C.** Forsmark site investigation. RAMAC and BIPS logging in boreholes KFM09B, HFM24, HFM26, HFM27, HFM29 and HFM32.

P-06-66 **Adl-Zarrabi B.** Forsmark site investigation. Borehole KFM01C. Thermal properties of rocks using calorimeter and TPS method.

P-06-67 **Savukoski M.** Forsmark site investigation. Borehole KFM01C. Determination of porosity by water saturation and density by buoyancy technique.

P-06-68 **Jacobsson L**. Forsmark site investigation. Borehole KFM01C Triaxial compression test of intact rock.

P-06-69 **Jacobsson, L.** Forsmark site investigation. Borehole KFM01C. Uniaxial compression test of intact rock.

P-06-79 **Petersson J, Skogsmo, Berglund J, Von Dalwigk I, Wängnerud A, Danielsson P, Stråhle A.** Forsmark site investigation. Boremap mapping of telescopic drilled borehole KFM06C.

P-06-80 **Döse C, Samuelsson E.** Forsmark site investigation. Boremap mapping of telescopic drilled borehole KFM7B.

P-06-81 **Petersson J, Skogsmo, Berglund J, Stråhle A.** Forsmark site investigation. Comparative geological logging with the Boremap system: 176.5–360.9 m of borehole KFM06C.

P-06-82 **Petersson J, Skogsmo, Berglund J, Stråhle A.** Forsmark site investigation. Comparative geological logging with the Boremap system: 9.6–132.2 m of borehole KLX07B.

P-06-83 **Carlsten S, Gustafsson J, Mattsson H, Petersson J, Stephens M.** Forsmark site investigation. Geological single-hole interpretation of KFM06C.

P-06-84 **Mattsson H, Keisu M.** Forsmark site investigation. Interpretation of geophysical borehole measurements from KFM06C.

P-06-85 **Isaksson H, Pitkänen T, Thunehed H.** Forsmark site investigation. Ground magnetic survey and lineament interpretation in an area northwest of Bolundsfjärden.

P-06-86 **Gokall-Norman K, Lindquist A, Ludvigson J-E, Gustavsson E.** Forsmark site investigation. Single-hole injection tests and pressure pulse tests in borehole KFM07B.

P-06-87 **Bergman T, Hedenström A.** Forsmark site investigation. Petrographic analysis of gravel and boulders in the Forsmark candidate area.

P-06-88 **Ising J.** Forsmark site investigation. Mapping of Quaternary deposits on the bottom of shallow bays outside Forsmark.

P-06-89 **Werner K, Lundholm L, Johansson P-O.** Forsmark site investigation. Supplementary drilling and soil sampling, and installation of groundwater monitoring wells, pumping wells and BAT filter tips.

P-06-90 **Gustafsson E, Nordqvist R, Thur P.** Forsmark site investigation. Groundwater flow measurements and SWIW test in borehole KFM08A.

P-06-91 **Löfgren M, Pettersson M, Widén H, Crawford J.** Forsmark site investigation. Formation factor logging *in situ* by electrical methods in KFM05A and KFM06A.

P-06-92 **Lokrantz H, Hedenström A.** Forsmark site investigation. Description, sampling and analyses of Quaternary deposits in connection with groundwater monitoring wells, pumping wells and BAT filter tips.

P-06-93 **Lindfors U.** Forsmark site investigation. Overcoring rock stress measurments in borehole KFM07B.

P-06-95 **Nilsson K.** Forsmark site investigation. Hydrochemical logging in KFM09A.

P-06-96 **Jönsson S, Ludvigson J-E.** Forsmark site investigation. Pumping tests and flow logging. Boreholes HFM24, HFM32.

P-06-97 **Heneryd N.** Forsmark site investigation. Snow depth, ground frost and ice cover during the winter 2005/2006.

P-06-98 **Gustasson J, Gustafsson C.** Forsmark site investigation. RAMAC and BIPS logging in boreholes KFM01C and KFM01D.

P-06-115 **Göthberg A, Wahlman H.** Forsmark site investigation. Inventory of vascular plants and classification of calcareous wetlands in the Forsmark area.

P-06-120 **Gustafsson J, Gustafsson C, Friborg J.** Forsmark site investigation. RAMAC and BIPS logging in boreholes KFM07C, HFM36, HFM37 and BIPS re-logging in HFM26.

P-06-122 **Gustavsson E, Ludvigson J-E, Gokall-Norman K.** Forsmark site investigation. Single-hole injection tests in borehole KFM09B.

P-06-123 **Nielsen UT, Ringgaard J, Fris Dahl J.** Forsmark site investigation. Geophysical borehole logging in boreholes KFM01C, KFM09B, HFM07, HFM24, HFM26, HFM29 and HFM32.

P-06-125 **Wass E, Andersson P.** Forsmark site investigation. Groundwater flow measurements and tracer tests at drill site 1.

P-06-126 **Mattsson H, Keisu M.** Forsmark site investigation. Interpretation of geophysical borehole measurements and petrophysical data from KFM07B, KFM09A, HFM25, HFM27 and HFM28.

P-06-130 **Petersson J, Skogsmo, Von Dalwigk I, Wängnerud A, Berglund J.** Forsmark site investigation. Boremap mapping of telescopic drilled borehole KFM09A.

P-06-131 **Petersson J, Skogsmo, Von Dalwigk I, Wängnerud A, Berglund J.** Forsmark site investigation. Boremap mapping of telescopic drilled borehole KFM09B.

P-06-132 **Petersson J, Skogsmo, Von Dalwigk I, Wängnerud A, Berglund J.** Forsmark site investigation. Boremap mapping of telescopic drilled borehole KFM01D.

P-06-133 **Döse C, Samuelsson E.** Forsmark site investigation. Boremap mapping of telescopic drilled borehole KFM1C.

P-06-134 **Carlsten S, Döse C, Gustafsson J, Keisu M, Petersson J, Stephens M.** Forsmark site investigation. Geological single-hole interpretation of KFM09A and KFM07B.

P-06-135 **Carlsten S, Döse C, Gustafsson J, Petersson J, Stephens M, Thunehed H.** Forsmark site investigation. Geological single-hole interpretation of KFM09B and KFM01C.

P-06-136 **Petersson J, Skogsmo G, Vestgård J.** Forsmark site investigation. Bedrock mapping and magnetic susceptibility measurements in trench AFM001265 for verification of lineament XFM0159A0.

P-06-138 **Toresson B.** Forsmark site investigation. Seismic refraction survey 2005-2006.

P-06-139 **Jönsson S, Ludvigson J-E.** Forsmark site investigation. Pumping tests and flow logging. Boreholes HFM25, HFM26.

P-06-140 **Lindquist A, Ludvigson J-E.** Forsmark site investigation. Pumping tests and flow logging in borehole HFM14 and pumping test in KFM05A (0–114 m).

P-06-141 **Gustafsson E, Nordqvist R, Thur P.** Forsmark site investigation. Groundwater flow measurements and SWIW test in borehole KFM04A.

P-06-152 **Mattsson H, Keisu M.** Forsmark site investigation. Interpretation of geophysical borehole measurements from KFM01C, KFM09B, HFM07, HFM24, HFM26, HFM29 and HFM32.

P-06-161 **Väisäsvaara J, Leppänen H, Pekkanen J.** Forsmark site investigation. Difference flow logging in borehole KFM01D.

P-06-165 **Gustavsson E, Ludvigson J-E, Hjerne C, Florberger J.** Forsmark site investigation. Single-hole injection tests in borehole KFM01C.

P-06-166 **Claesson L-A, Nilsson G.** Forsmark site investigation. Drilling of percussion boreholes HFM25–HFM27, HFM29–HFM32, and HFM38 for investigation of different lineaments and to be used as monitoring wells.

P-06-168 **Nielsen U T, Ringgaard J, Fris Dahl J.** Forsmark site investigation. Geophysical borehole logging in borehole KFM01D.

P-06-169 **Claesson L-A, Nilsson G.** Forsmark site investigation. Drilling of the cored boreholes KFM09A and KFM09B.

P-06-170 **Claesson L-A, Nilsson G.** Forsmark site investigation.Drilling of the telescopic boreholes KFM07B and KFM07C at drilling site DS7.

P-06-171 **Claesson L-A, Nilsson G.** Forsmark site investigation. Drilling of the telescopic borehole KFM08C at drill site DS8.

P-06-172 **Claesson L-A, Nilsson G.** Forsmark site investigation. Drilling of the telescopic borehole KFM10A at drill site DS10.

P-06-173 **Claesson L-A, Nilsson G.** Forsmark site investigation. Drilling of borehole KFM01C and the telescopic borehole KFM01D at drill site DS1.

P-06-177 **Gustafsson J, Gustafsson C.** Forsmark site investigation. RAMAC and BIPS logging in boreholes KFM10A, HFM35 and HFM38.

P-06-178 **Gustafsson J, Gustafsson C.** Forsmark site investigation. RAMAC and BIPS logging in boreholes KFM08C, HFM30, HFM31, HFM33 and HFM34.

P-06-179 **Lindquist A, Nilsson K.** Forsmark site investigation. Hydrochemical logging in KFM09B.

P-06-187 **Löfgren M.** Forsmark site investigation. Formation factor logging *in situ* by electrical methods in KFM07A and KFM08A.

P-06-188 **Lindquist A, Wass E.** Forsmark site investigation. Groundwater flow measurements in conjunction with the interference test with pumping in HFM14.

P-06-189 **Väisäsvaara J, Leppänen H, Pekkanen J, Pöllänen J.** Forsmark site investigation. Difference flow logging in borehole KFM08C.

P-06-190 **Sokolnicki M, Pöllänen J, Pekkanen J.** Forsmark site investigation. Difference flow logging in borehole KFM10A.

P-06-191 **Jönsson S, Ludvigson J-E.** Forsmark site investigation. Pumping tests and flow logging. Boreholes HFM23, HFM27 and HFM28.

P-06-192 **Lindquist A, Ludvigson J-E.** Forsmark site investigation. Pumping tests and flow logging. Boreholes HFM29, HFM30 and HFM31.

P-06-193 **Gustavsson E, Jönsson S, Ludvigson J-E.** Forsmark site investigation. Pumping tests and flow logging. Boreholes HFM33, HFM34 and HFM35.

P-06-194 **Walger E, Hjerne C, Ludvigson J-E, Harrström J.** Forsmark site investigation. Single-hole injection tests and pressure pulse tests in borehole KFM08A.

P-06-195 **Florberger J, Hjerne C, Ludvigson J-E, Walger E.** Forsmark site investigation. Single-hole injection tests in borehole KFM01D.

P-06-196 **Gokall-Norman K, Ludvigson J-E.** Forsmark site investigation. Hydraulic interference test in boreholes HFM14.

P-06-203 **Petersson J, Wängerud A, von Dalwigk I, Berglund J.** Forsmark site investigation. Boremap mapping of telescopic drilled borehole KFM08C.

P-06-204 **Döse C, Samuelsson E.** Forsmark site investigation. Boremap mapping of telescopic drilled borehole KFM10A.

P-06-205 **Petersson J, Andersson U B, Berglund J.** Forsmark site investigation. Boremap mapping of telescopic drilled borehole KFM07C.

P-06-206 **Döse C, Samuelsson E.** Forsmark site investigation. Boremap mapping of percussion boreholes HFM23–32 and HFM38.

P-06-207 **Carlsten S, Döse C, Samuelsson E, Petersson J, Stephens M, Thunehed H.** Forsmark site investigation. Geological single-hole interpretation of KFM08C, KFM10A, HFM23, HFM28, HFM30, HFM31, HFM32 and HFM38.

P-06-209 **Sandström B, Tullborg E-L.** Forsmark site investigation. Mineralogy, geochemistry, porosity and redox capacity of altered rock adjacent to fractures.

P-06-210 **Carlsten S, Döse C, Gustafsson J, Mattsson H, Petersson J, Stephens M.** Forsmark site investigation. Geological single-hole interpretation of KFM01D, HFM24, HFM25, HFM27 and HFM29.

P-06-211 **Page L, Hermansson T, Söderlund P, Stephens M.** Forsmark site investigation. $^{40}Ar/^{39}Ar$ and U-Th/He geochronology: Phase II.

P-06-212 **Nordgulen Ø, Saintot A.** Forsmark site investigation. The character and kinematics of deformation zones (ductile shear zones, fault zones and fracture zones) at Forsmark – report from phase 1.

P-06-213 **Sandström B, Page L, Tullborg E-L.** Forsmark site investigation. $^{40}Ar/^{39}Ar$ (adularia) and Rb-Sr (adularia, prehnite, calcite) ages of fracture minerals.

P-06-214 **Jacobsson L.** Forsmark site investigation. Borehole KFM09A. Triaxial compression tests of intact rock.

P-06-215 **Jacobsson L, Flansbjer M.** Forsmark site investigation. Borehole KFM01D. Shear tests on sealed joints.

P-06-216 **Mattsson H, Keisu M.** Forsmark site investigation. Interpretation of geophysical borehole measurements and petrophysical data from KFM01D.

P-06-217 **Nilsson K, Bergelin A.** Forsmark site investigation. Hydrochemical characterisation in borehole KFM09A. Results from the investigated section at 785.1–792.2 m.

P-06-220 **Hannu S, Karlsson S.** Forsmark site investigation. Chemical characterisation of deposits and biota.

P-06-221 **Karlsson S, Andersson E.** Forsmark site investigation. Distribution, biomass, production and respiration of submerged vegetation in Lake Bolundsfjärden.

P-06-224 **Alm P, Gebrezghi M, Werner K.** Forsmark site investigation. Supplementary hydraulic tests in Quaternary deposits.

P-06-226 **Sandström B, Tullborg E-L.** Forsmark site investigation. Fracture mineralogy. Results from KFM06B, KFM06C, KFM07A, KFM08A, KFM08B.

P-06-227 **Nilsson K, Bergelin A, Lindquist A, Nilsson A-C.** Forsmark site investigation. Hydrochemical characterization in borehole KFM01D. Results from seven investigated borehole sections: 194.0–195.0 m, 263.8–264.8 m, 314.5–319.5 m, 354.9–355.9 m, 369.0–370.0 m, 428.5–435.6 m, 568.0–575.1 m.

P-06-231 **Berg C.** Forsmark site investigation. Sampling and analyses of groundwater from percussion drilled boreholes. Results from the boreholes HFM14, HFM23, HFM24, HFM25, HFM26, HFM27, HFM28, HFM29, HFM30, HFM32, HFM33, HFM34 and HFM35.

P-06-232 **Andersson E, Karlsson S, Söderbäck B, Wijnbladh E.** Oskarshamn and Forsmark site investigation. Biomass of benthic and planktonic bacteria in Laxemar and Forsmark and biomass of Reed (*Phragmites australis*) in Lake Frisksjön.

P-06-233 **Adl-Zarrabi B.** Forsmark site investigation. Borehole KFM01A, KFM01C, KFM01D, KFM04A, KFM05A, KFM06A and KFM09A. Thermal properties of rocks using calorimeter and TPS method, and mineralogical composition by modal analysis.

P-06-234 **Liedberg L.** Forsmark site investigation. Borehole KFM01A, KFM01C, KFM01D, KFM04A, KFM05A and KFM06A. Determination of porosity by water saturation and density by buoyancy technique.

P-06-247 **Väisesvaara J, Pekkanen J, Pöllänen J.** Forsmark site investigation. Difference flow logging in KFM07C.

P-06-252 **Borgiel M, Skarp J, Karlsson S.** Forsmark site investigation. Measurement of phytobenthic production and respiration in shallow bays and shores in the Öregrundsgrepen area, Bothnian Sea Results from measurements 2006.

P-06-258 **Mattsson H, Keisu M.** Forsmark site investigation. Interpretation of geophysical borehole measurements from KFM10A, KFM08C, HFM30, HFM31, HFM33, HFM34, HFM35 and HFM38.

P-06-261 **Isaksson H, Thunehed H, Pitkänen T, Keisu M.** Forsmark site investigation. Detailed ground and marine magnetic survey and lineament interpretation in the Forsmark area – 2006.

P-06-263 **Nyberg G, Wass E.** Forsmark site investigation. Hydro Monitoring Program. Report for August 2005 – September 2006.

P-06-285 **Dinges C.** Forsmark site investigation. Borehole KFM04A. Thermal properties – Anisotropic thermal conductivity and thermal diffusivity determined using the Hot Disk thermal constants analyser (the TPS technique).

P-06-301 **Sternbeck J, Land M, Nilsson Ö.** Oskarshamn and Forsmark site investigations. ^{210}Pb and ^{14}C dating of sediments and peat. Accumulation rates of carbon, nitrogen and phosphorus.

P-06-304 **Berg C, Nilsson A-C, Borgiel M.** Forsmark site investigation. Hydrochemical monitoring of near surface groundwaters. Results from sampling of five shallow soil monitoring wells, one BAT pipe and three private wells, July 2005–April 2006.

P-06-322 **Wern L, Jones J.** Forsmark site investigation. Meteorological monitoring at Forsmark, August 2005 until September 2006.

P-07-01 **Albrecht J.** Forsmark site investigation. Soil stratigraphy based on samples and protocols in the Forsmark area.

P-07-02 **Green M.** Forsmark site investigation. Bird monitoring in Forsmark 2006.

P-07-04 **Nielsen U T, Ringgaard J.** Forsmark site investigation. Geophysical borehole logging in boreholes KFM07C, HFM36 and HFM37.

P-07-05 **Nielsen U T, Ringgaard J.** Forsmark site investigation. Geophysical borehole logging in boreholes KFM08C, KFM10A, HFM30, HFM31, HFM33, HFM34, HFM35 and HFM38.

P-07-06 **Harrström J, Hjerne C, Ludvigson J-E.** Forsmark site investigation. Single-hole injection tests in borehole KFM08C.

P-07-07 **Ringgaard J.** Forsmark site investigation. Mapping of borehole breakout. Processing of acoustical televiewerdata from KFM01A, KFM01B, KFM02A, KFM03A, KFM03B, KFM04A, KFM05A, KFM06A and KFM07C.

P-07-10 **Gustafsson J, Gustafsson C.** Forsmark site investigation. RAMAC and BIPS logging in borehole KFM11A.

P-07-11 **Claesson L-Å, Nilsson G.** Forsmark site investigation. Drilling of flushing water well HFM33 and monitoring wells HFM34 and HFM35 at drill site DS11.

P-07-22 **Walger E, Jönsson S, Ludvigson J-E.** Forsmark site investigation. Pumping tests and flow logging. Boreholes HFM36, HFM37 and HFM38.

P-07-23 **Heneryd N.** Forsmark site investigation. Measurements of ground respiration, primary production and NEE in terrestrial habitats.

P-07-31 **Walger E, Hjerne C, Ludvigson J-E.** Forsmark site investigation. Single-hole injection tests in borehole KFM10A.

P-07-32 **Roos P, Engdahl A, Karlsson S.** Oskarshamn and Forsmark site investigations. Analyses of radioisotopes in environmental samples.

P-07-33 **Åkesson U.** Forsmark site investigation. Boreholes KFM05A and KFM06A. Extensometer measurement of the coefficient of thermal expansion of rock.

P-07-35 **Keisu M, Mattsson H.** Forsmark site investigation. Calibration of one arm caliper and caliper mean data from core and percussion drilled boreholes.

P-07-40 **Baxter D, Hannu S, Karlsson S.** Forsmark site investigation. Analyses of biogenic silicon in sediment from Lake Eckarfjärden.

P-07-42 **Bergelin A, Lindquist A, Nilsson K, Nilsson A-C.** Forsmark site investigation. Hydrochemical characterisation in borehole KFM10A. Results from three investigated borehole sections: 298.0–305.1 m, 436.9–437.9 m, 478.0–487.5 m.

P-07-43 **Claesson L-Å, Nilsson G.** Forsmark site investigation. Drilling of a flushing water well, HFM36, a groundwater monitoring well in solid bedrock, HFM37, and a groundwater monitoring well in soil, SFM0109.

P-07-44 **Claesson L-Å, Nilsson G, Ullberg A.** Forsmark site investigation. Drilling of the telescopic borehole KFM02B at drill site DS2.

P-07-45 **Claesson L-Å, Nilsson G, Ullberg A.** Forsmark site investigation. Drilling of the telescopic borehole KFM11A at drill site DS 11.

P-07-46 **Claesson L-Å, Nilsson G, Ullberg A.** Forsmark site investigation. Drilling of the telescopic borehole KFM12A at drill site DS12.

P-07-47 **Berg C, Nilsson A-C.** Forsmark site investigation. Hydrochemical monitoring of percussion- and core drilled boreholes. Results from water sampling and analyses during 2006.

P-07-51 **Thunehed H.** Forsmark site investigation. Resistivity measurements on samples from KFM01A, KFM01B, KFM02A, KFM05A and KFM06A.

P-07-52 **Thur P, Nordqvist R, Gustafsson E.** Forsmark site investigation. Groundwater flow measurements and SWIW tests in borehole KFM01D.

P-07-60 **Nielsen U T, Ringgaard J.** Forsmark site investigation. Geophysical borehole logging in boreholes KFM02B and KFM08D.

P-07-76 **Gorski, B, Conlon, B, Ljunggren, B.** Forsmark site investigation – Determination of the direct and indirect tensile strength on cores from borehole KFM01D.

P-07-78 **Mattsson H, Keisu M.** Forsmark site investigation. Interpretation of geophysical borehole measurements from KFM07C, HFM36 and HFM37.

P-07-81 **Heneryd N.** Forsmark site investigation. Snow depth, snow water content and ice cover during the winter 2006/2007.

P-07-83 **Väisäsvaara J, Pöllänen J.** Forsmark site investigation. Difference flow logging in borehole KFM02B.

P-07-84 **Kristiansson S.** Forsmark site investigation. Difference flow logging in borehole KFM08D.

P-07-85 **Väisäsvaara J, Pekkanen J.** Forsmark site investigation. Difference flow logging in borehole KFM11A.

P-07-86 **Berg C.** Forsmark site investigation. Sampling and analyses of groundwater from percussion drilled boreholes. Results from the boreholes HFM36, HFM37, and HFM38.

P-07-92 **Nielsen U T, Ringgaard J.** Forsmark site investigation. Geophysical borehole logging in boreholes KFM11A and KFM90B.

P-07-93 **Jacobsson, L.** Forsmark site investigation. Boreholes KFM01A and KFM02B. Micro crack volume measurments and triaxial compression tests on intact rock. Forsmark site investigation.

P-07-95 **Nilsson A-C, Borgiel M.** Forsmark site investigation. Sampling and analyses of surface waters. Results from sampling in the Forsmark area, July 2005 – June 2006.

P-07-96 **Gustafsson J, Gustafsson C.** Forsmark site investigation. RAMAC and BIPS logging in borehole KFM02B and KFM08D.

P-07-100 **Bergelin A, Lindquist A, Nilsson K, Wacker P, Nilsson A-C.** Forsmark site investigation. Hydrochemical characterisation in borehole KFM11A. Results from two investigated borehole sections at 447.5–454.6 m and 690.0–710.0 m.

P-07-101 **Saintot A, Nordgulen Ø.** Forsmark site investigation. The character and kinematics of deformation zones (ductile shear zones, fracture zones and fault zones) at Forsmark – report from phase 2.

P-07-103 **Samuelsson E, Rauséus G.** Forsmark site investigation. Boremap mapping of telescopic drilled borehole KFM08D.

P-07-104 **Petersson J, Berglund J, Andersson U B, Wängnerud A, Danielsson P, Ehrenborg J.** Forsmark site investigation. Boremap mapping of telescopic drilled borehole KFM11A.

P-07-105 **Samuelsson E, Dahlin P, Lundberg E, Rauséus G.** Forsmark site investigation. Boremap mapping of telescopic drilled borehole KFM12A.

P-07-106 **Döse C, Samuelsson E.** Forsmark site investigation. Boremap mapping of percussion boreholes HFM33–37.

P-07-107 **Carlsten S, Döse C, Samuelsson E, Gustafsson J, Petersson J, Stephens M, Thunehed H.** Forsmark site investigation. Geological single-hole interpretation of KFM02B.

P-07-108 **Carlsten S, Samuelsson E, Gustafsson J, Stephens M, Thunehed H.** Forsmark site investigation. Geological single-hole interpretation of KFM08D.

P-07-109 **Carlsten S, Döse C, Samuelsson E, Gustafsson J, Petersson J, Stephens M, Thunehed H.** Forsmark site investigation. Geological single-hole interpretation of KFM11A, HFM33, HFM34 and HFM35.

P-07-110 **Carlsten S, Samuelsson E, Gustafsson J, Petersson J, Stephens M, Thunehed H.** Forsmark site investigation. Geological single-hole interpretation of KFM12A, HFM36 and HFM37.

P-07-111 **Nordgulen Ø, Saintot A.** Forsmark site investigation. The character and kinematics of deformation zones (ductile shear zones, fracture zones and fault zones) at Forsmark – report from phase 3.

P-07-112 **Gustafsson J, Gustafsson C.** Forsmark site investigation. RAMAC and BIPS logging in borehole KFM12A.

P-07-113 **Nyberg G, Wass E.** Forsmark site investigation. Hydro monitoring program. Report for October 2006 – March 2007.

P-07-115 **Bäckström A, Lanaro F.** Forsmark modelling stage 2.2. Rock mechanics characterization of borehole KFM01B, KFM07C, KFM09A and KFM09B.

P-07-118 **Nielsen U T, Ringgaard J.** Forsmark site investigation. Geophysical borehole logging in borehole KFM12A.

P-07-119 **Waber H N, Smellie J A T.** Forsmark site investigation. Boreholes KFM01D, KFM08C, KFM09B. Characterisation of pore water. Part 1 Diffusion experiments and pore-water data.

P-07-121 **Harrström J, Svensson T, Ludvigson J-E.** Forsmark site investigation. Single-hole injection tests in borehole KFM12A.

P-07-122 **Truvé J.** Oskarshamn and Forsmark site investigations. Surveys of mammal populations in the areas adjacent to Forsmark and Oskarshamn. Results from 2007, compared with results from 2002/2003.

P-07-124 **Berg C, Nilsson A-C, Borgiel M.** Forsmark site investigation. Hydrochemical monitoring of near surface groundwaters Results from sampling of shallow soil monitoring wells, BAT pipes and private wells, summer 2006 – spring 2007.

P-07-125 **Mattsson H, Keisu M.** Forsmark site investigation. Interpretation of geophysical borehole measurements from KFM02B, KFM08D and KFM11A.

P-07-127 **Teurneau B, Forsmark T, Forssman I, Rhén I, Zinn E.** Forsmark site investigation. Correlation of Posiva Flow Log anomalies to core mapped featuresin KFM01D, -07C, -08A, -08C and -10A.

P-07-128 **Forssman I, Forsmark T, Rhén I.** Forsmark site investigation. Correlation of Posiva Flow Log anomalies to core mapped featuresin KFM02B, -08D and -11A.

P-07-129 **Mattsson H.** Forsmark site investigation. Interpretation of geophysical borehole measurements from KFM12A.

P-07-130 **Lindfors U, Perman F, Berg S.** Forsmark site investigation. Overcoring rock stress measurements in borehole KFM07C.

P-07-135 **Johansson P-O, Juston J.** Forsmark site investigation. Monitoring of brook levels, water electrical conductivities, temperatures and discharges from April 2004 until March 2007.

P-07-137 **Thunehed H.** Forsmark site investigation. Complementary resistivity measurements on samples from KFM01A, KFM02A, KFM06A, KFM08A, KFM08C and KFM09A.

P-07-138 **Löfgren M.** Forsmark site investigation. Formation factor logging *in situ* by electrical methods in KFM01D and KFM08C.

P-07-139 **Selnert E, Byegård J, Widestrand H.** Forsmark site investigation. Laboratory measurements within the site investigation programme for the transport properties of the rock. Final report.

P-07-145 **Jacobsson, L.** Borehole KFM08D. Forsmark site investigation. Uniaxial compression test of intact rock.

P-07-146 **Jacobsson, L.** Forsmark site investigation. Borehole KFM08D. Indirect tensile strength test.

P-07-165 **Thunehed H, Pitkänen T.** Forsmark site investigation. Transient electromagnetic soundings at Forsmark and the regional surroundings. Estimations of depth to saline groundwater.

P-07-166 **Ringgaard J**. Forsmark site investigation. Mapping of borehole breakouts, processing of acoustical televiewerdata from KFM08A, KFM08C, KFM09A, KFM09AB and KFM90B.

P-07-170 **Berg C.** Forsmark site investigation. Sampling and analysis of precipitation, November 2005 to June 2007.

P-07-171 **Berg C, Nilsson A-C.** Forsmark site investigation. Hydrochemical sampling and analyses in KFM12A. Results from two investigated borehole sections, 343.0–363.0 m and 516.0–536.0 m.

P-07-175 **Wern L, Jones J.** Forsmark site investsigation. Meteorological monitoring at Forsmark, October 2006 until June 2007.

P-07-177 **Harrström J, Svensson T, Ludvigson J-E.** Forsmark site investigation. Single-hole hydraulic tests in borehole KFM11A.

P-07-190 **Bergelin A, Lindquist A, Nilsson K, Wacker P, Nilsson A-C.** Forsmark site investigation. Hydrochemical characterisation in borehole KFM08D. Results from two investigated borehole sections at 669.7–676.8 m and 828.4–835.5 m.

P-07-194 **Sundberg J, Wrafter J, Mossmark F, Sundberg A.** Forsmark site investigation. Anisotropy of thermal properties in metagranite at Forsmark. Comparison between large-scale field measurements, small-scale field measurements and laboratory measurements.

P-07-196 **Nordén S.** Forsmark site investigation. Collection of archive samples.

P-07-205 **Lindfors U, Berg S, Perman F.** Forsmark site investigation. Overcoring rock stress measurements in borehole KFM02B.

P-07-206 **Ask D, Cornet F, Fontbonne F.** Forsmark site investigation. Stress measurements with hydraulic methods in boreholes KFM07A, KFM07C, KFM08A, KFM09A and KFM09B.

P-07-207 **Jacobsson L.** Forsmark site investigation. Borehole KFM06A. Uniaxial compression test of intact rock containing sealed fractures. Forsmark site investigation.

P-07-228 **Gokall-Norman K, Ludvigson J-E.** Forsmarks site investigation. Large-scale interference test with borehole HFM14 used as pumping borehole, 2007.

P-07-229 **Gokall-Norman K, Ludvigson J-E.** Forsmarks site investigation. Hydraulic interference test with borehole HFM33 used as pumping borehole, November of 2007.

P-07-234 **Ask D.** Forsmark site investigation. Evaluation of overcoring measurements in boreholes KFM01B, DBT-1 and DBT-3 and hydraulic stress measurements in boreholes KFM01A, KFM01B, KFM02A and KFM04A at the Forsmark site.

P-07-235 **Ask D, Ask M.** Forsmark site investigation. Detection of potential borehole breakouts in boreholes KFM01A and KFM01B.

P-08-13 **Lindquist A, Hjerne C, Nordqvist R, Byegård J, Walger E, Ludvigson J-E, Wass E.** Forsmark site investigation. Confirmatory hydraulic interference test and tracer test at drillsite 2.

P-08-14 **Sandström B, Tullborg E-L, Page L.** Forsmark site investigation. Fracture mineralogy and $^{40}Ar/^{39}Ar$ ages of adularia in fracture filling and K-feldspar in breccia. Data from drill cores KFM01C, KFM01D, KFM02B, KFM04A, KFM06A, KFM06B, KFM07A, KFM08A, KFM08B, KFM08C, KFM08D, KFM09A, KFM09B, KFM10A and KFM11A.

P-08-17 **Nilsson A-C, Borgiel M.** Forsmark site investigation. Sampling and analyses of surface waters. Results from sampling in the Forsmark area, July 2006 – June 2007.

P-08-54 **Berg C, Nilsson A-C.** Forsmark site investigation. Hydrochemical monitoring of percussion- and core drilled boreholes. Results from water sampling and analyses during 2007.

P-08-55 **Qvarfordt S, Borgiel M, Berg C, Nilsson A-C.** Forsmark site investigation. Hydrochemical monitoring of near surface groundwater, surface waters and precipitation. Results from sampling in the Forsmark area, August 2007 – December 2007.

P-09-14 **Waber H N, Smellie J A T.** Forsmark site investigation. Borehole KFM02B. Characterisation of pore water. Part 1: Diffusion experiments and pore water data.

R-98-05 **Axelsson C-L; Hansen L M.** Update of structural models at SFR nuclear waste repository, Forsmark, Sweden.

R-99-08 **Stigsson M, Follin S, Andersson J.** On the simulation of variable density flow at SFR, Sweden.

R-99-69 **Kautsky H, Plantman P, Borgiel M.** Quantitative distribution of aquatic plant and animal communities in the Forsmark area.

R-99-70 **Lindell S, Ambjörn C, Juhlin B, Larsson-McCann S, Lindquist K.** Available climatological and oceanographical data for site investigation programme.

R-01-02 **Holmén J G, Stigsson M.** Modelling of future hydrogeological conditions at SFR.

R-01-12 **Bergström E.** Late Holocene distribution of lake sediment and peat in NE Uppland.

R-02-06 **Boresjö Bronge L, Wester K.** Vegetation mapping with satellite data of the Forsmark and Tierp regions.

R-02-08 **Berggren J, Kyläkorpi L.** Ekosystemen i Forsmarksområdet. Sammanställning av befintlig information.

R-02-14 **Axelsson C-L, Ekstav A, Lindblad Påsse A**. SFR – Utvärdering av hydrogeologi.

R-02-17 **Ludvigson J-E.** Brunnsinventering i Forsmark.

R-02-32 **SKB.** Forsmark – site descriptive model version 0.

R-02-41 **Blomqvist P, Nilsson E, Brunberg A-K.** Habitat distribution, water chemistry, and biomass and production of pelagic and benthic microbiota in Lake Eckarfjärden, Forsmark.

R-02-43 **Juhlin C, Bergman B, Palm H.** Reflection seismic studies in the Forsmark area – stage 1.

R-03-26 **Bergkvist M, Ekström L, Eriksson K, Hammarlund E, Hollsten M, Lind A-L, Lundholm K.** Kallrigafjärden, NO Uppland. Områdets historia, nuläge samt framtida landskapsutveckling.

R-03-27 **Andersson E, Tudorancea M-M, Tudorancea C, Brunberg A-K, Blomqvist P.** Water chemistry, biomass and production of biota in Lake Eckarfjärden during 2002.

R-04-08 **Lundin L, Lode E, Stendahl J, Melkerud P A, Björkvald L, Thorstensson A.** Soils and site types in the Forsmark area.

R-04-15 **SKB.** Preliminary site description Forsmark area – version 1.1.

R-04-39 **Sohlenius G, Hedenström A, Rudmark L.** Forsmark site investigation. Mapping of unconsolidated Quaternary deposits 2002–2003. Map description.

R-04-77 **Forssman I, Zetterlund M, Rhén I.** Correlation of Posiva Flow Log anomalies to core mapped features in Forsmark (KFM01A to KFM05A).

R-04-39 **Sohlenius G, Hedenström A, Rudmark L.** Forsmark site investigation. Mapping of unconsolidated Quaternary deposits 2002–2003. Map description.

R-04-70 **Brydsten L.** Digital elevation models for site investigation program in Forsmark.

R-05-06 **Johansson P-O, Werner K, Bosson E, Berglund S, Juston J.** Description of climate, surface hydrology, and near-surface hydrogeology. Preliminary site description Forsmark area – version 1.2.

R-05-18 **SKB.** Preliminary site description Forsmark area – version 1.2.

R-05-35 **Sjöberg J, Lindfors U, Perman F, Ask D.** Evaluation of the state of stress at the Forsmark site. Preliminary site investigationForsmark area – version 1.2.

R-05-36 **Truvé J, Cederlund G.** Mammals in the areas adjacent to Forsmark and Oskarshamn. Population density, ecological data and carbon budget.

R-05-42 **Juhlin C, Palm H.** Forsmark site investigation. Reflection seismic studies in the Forsmark area, 2004: Stage 2.

R-05-51 **Lagerbäck R, Sundh M, Svedlund J-O, Johansson H.** Forsmark site investigation. Searching for evidence of late- or postglacial faulting in the Forsmark region. Results from 2002–2004.

R-06-19 **Tröjbom M, Söderbäck B.** Chemical characteristics of surface systems in the Forsmark area. Visualisation and statistical evaluation of data from shallow groundwater, precipitation, and regolith.

R-06-38 **SKB.** Site descriptive modelling Forsmark stage 2.1. Feedback for completion of the site investigation including input from safety assessment and repository engineering.

R-06-49 **Juston J, Johansson P-O, Levén J, Follin S.** Analysis of meteorological, hydrological and hydrogeological monitoring data, December 2002 – July 2005. Forsmark site investigation.

R-06-96 **Strömgren M, Brunberg A-K.** Elemental composition of a deep sediment core from Lake Stocksjön in the Forsmark area.

R-06-123 **Persson T, Lenoir L, Taylor A.** Bioturbation in different ecosystems at Forsmark and Oskarshamn.

R-07-01 **Persson H, Stadenberg I.** Distribution of fine roots in forest areas close to the Swedish Forsmark and Oskarshamn nuclear power plants.

R-07-15 **Olofsson I, Simeonov A, Stephens M, Follin S, Nilsson A-C, Röshoff K, Lindberg U, Lanaro F, Fredriksson A, Persson L.** Site descriptive modelling Forsmark, stage 2.2. A fracture domain concept as a basis for the statistical modelling of fractures and minor deformation zones, and interdisciplinary coordination.

R-07-23 **Mjöfors K, Johansson M-B, Nilsson Å.** Input and turnover of forest tree litter in the Forsmark and Oskarshamn areas.

R-07-45 **Stephens M B, Fox A, La Pointe P, Simeonov A, Isaksson H, Hermanson J, Öhman J.** Geology Forsmark. Site descriptive modelling Forsmark stage 2.2.

R-07-62 **Isaksson H, Thunehed H, Pitkänen T, Keisu M.** Forsmark site investigation. Detailed ground magnetic survey and lineament interpretation in the Forsmark area, 2006–2007.

R-07-67 **Isaksson H, Stephens M B.** Forsmark site investigation. Assessment of the validity of the rock domain model, version 1.2, based on the modelling of gravity and petrophysical data.

R-08-04 **Hedenström A, Sohlenius G.** Description of the regolith at Forsmark.

R-08-08 **Johansson P-O.** Description of surface hydrology and near-surface hydrogeology at Forsmark. Site descriptive modelling, SDM-Site Forsmark.

R-08-09 **Bosson E, Gustafsson L-G, Sassner M.** Numerical modelling of surface hydrology and near-surface hydrogeology at Forsmark. Site descriptive modelling, SDM-Site Forsmark.

R-08-10 **Johansson P-O, Öhman J**. Presentation of meteorological, hydrological and hydrogeological monitoring data from Forsmark. Site descriptive modelling, SDM-Site Forsmark.

R-08-62 **Strömgren M, Brydsten L.** Digital elevation models for Forsmark Site descriptive modelling SDM-Site Forsmark.

R-08-66 **Glamheden R, Lanaro F, Karlsson J, Wrafter J, Hakami H, Johansson M.** Rock mechanics Forsmark. Modelling stage 2.3. Complementary analysis and verification of the rock mechanics model.

TR 91-24 **Andersson J-E, Nordqvist R, Nyberg G, Smellie J, Tirén S.** Hydrogeological conditions in the Finnsjön area. Compilation of data and conceptual model.

TR 92-07 **Geir J E, Axelsson C-E, Hässler L, Benabderrahmane A.** Discrete fracture modelling of the Finnsjön rock mass: Phase 2.

TR 92-33 **Ahlbom K, Andersson J-E, Andersson P, Ittner T, Ljunggren C, Tirén S.** Finnsjön study site. Scope of activities and main results.

TR-99-11 **Engqvist A, Andrejev O.** Water exchange of Öregrundsgrepen. A baroclinic 3D-model study.

TR-99-18 **Gylling B, Walker D, Hartley L.** Site-scale groundwater flow modelling of Beberg.

TR-02-02	**Larsson-McCann S, Karlsson A, Nord M, Sjögren J, Johansson L, Ivarsson M, Kindell S.** Meteorological, hydrological and oceanographical information and data for the site investigation program in the communities of Östhammar and Tierp in the northern part of Uppland.
TR-03-17	**Hedenström A, Risberg J.** Shore displacement in northern Uppland during the last 6500 calender years.
TR-04-08	**Kellner E.** Wetlands – different types, their properties and functions.
TR-04-26	**Johanson K J, Nikolova I, Taylor A F S, Vinichuk M M.** Uptake of elements by fungi in the Forsmark area.
TR-06-29	**Tagesson T.** Indirect estimations and spatial variation in leaf area index of coniferous, deciduous and mixed forest stands in Forsmark and Laxemar.
TR-07-11	**Persson H, Stadenberg I.** Growth dynamics of fine roots in a coniferous fern forest site close to Forsmark in the central part of Sweden.
TR-07-13	**Tagesson T.** Soil carbon effluxes in ecosystems of Forsmark and Laxemar.
TR-08-01	**Engqvist A, Andrejev O.** Validation of coastal oceanographic models at Forsmark. Site descriptive modelling SDM–Site Forsmark.

Appendix 4

Properties of deformation zones modelled to intersect the target volume at –400 to –600 m elevation

The geological and hydrogeological properties of the forty-six (46) deformation zones that have been modelled during stage 2.2 /Stephens et al. 2007/ to intersect the Forsmark target volume at –400 to –600 m elevation are summarized in the tables in this appendix. Five (5) of these zones are gently dipping and forty-one (41) zones are steeply dipping structures. Only three of the steeply dipping zones have a trace length at the ground surface that is longer than 3,000 m (ZFMENE0060A with attached branches ZFMENE0060B and ZFMENE0060C, ZFMENE0062A, and ZFMWNW0123). Furthermore, fifteen (15) of the forty-one (41), steeply dipping structures are local minor zones with a trace length at the ground surface less than 1,000 m. All zones except ZFMWNW0123 show solely brittle deformation and can be referred to as fracture zones. The steeply dipping structures are overwhelmingly dominated by zones included in the steeply dipping ENE (NE) and NNE sub-sets (chapter 5 in /Stephens et al. 2007/).

Information bearing on style of deformation, rock alteration, rock geometry and virtually all the orientation data for fractures in a zone have been extracted from the property tables for deformation zones at Forsmark (Appendices 15 and 16 in /Stephens et al. 2007/). These property tables were produced during the stage 2.2 modelling work. More detailed information, including data sources, span estimates and confidence level in a particular property, can be found in these tables. Data assembled from boreholes KFM02B and KFM08D, which only became available during stage 2.3 after completion of the final modelling work, are included in the parts of a table that document borehole intersections, location in cartographic format, transmissivity, engineering characteristics and fracture orientation. A combination of the geological information addressed in /Stephens et al. 2007/ and /Stephens et al. 2008/ and of the hydrogeological information addressed in /Follin et al. 2007b/, /Follin et al. 2007c, Appendix L/ and /Follin et al. 2008a/ have been utilised for the definition of these attributes. The attribute referred to as “Engineering characteristics” refers to division of a zone into transition and core segments, and the frequency and mineralogy of open and sealed fractures along each of these segments. The updating of attributes and the integration of geological and hydrogeological data along zones account for differences between the property tables presented here and those presented in /Stephens et al. 2007/.

Deformation zone ZFMA2

Borehole intersections (metres along borehole)

KFM01B: DZ1 and extension (16-64 m)
KFM01C: DZ1 (23-48 m) and DZ2 (62-99 m)
KFM02A: Part of DZ6 (417-442 m)
KFM02B: DZ3 (411-431 m)
KFM04A: DZ2 (202-213 m) and DZ3 (232-242 m) and less fractured rock between DZ2 and DZ3 (213-232 m)
KFM05A: DZ1 (102-114 m)
KFM10A: DZ2 (430-449 m) and DZ3 (478-490 m)
KFM01A (percussion part): DZ1 and extension (29-51 m)
HFM01: DZ1 (35-44 m)
HFM14: DZ1 (68-76 m) and DZ2 (92-104 m)
HFM15: DZ1 (86-96 m)
HFM19: DZ1 (121-148 m) and DZ2 (168-185 m)
HFM27: DZ1 (26-30 m)

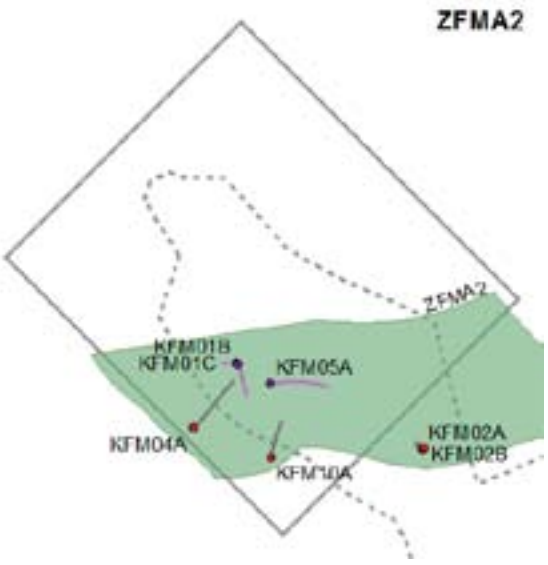

Deformation style, alteration and geometry

Deformation style: Brittle

Alteration: Red-stained bedrock with fine-grained hematite dissemination. Altered vuggy rock with quartz dissolution between 483 and 488 m along DZ3 in KFM10A

Strike/dip (right-hand-rule): 080/24

Trace length at ground surface: 3,987 m

Model thickness / model thickness span : 23 m / 9-45 m

Measured thickness (-400 to -600 m elevation): 28 m in KFM02A (part of DZ6), 16 m in KFM10A (DZ2) combined with 9 m in KFM10A (DZ3)

Comment: Data from KFM02B only available after completion of geological model stage 2.2, i.e. not included in geological modelling work

Fractures in the deformation zone

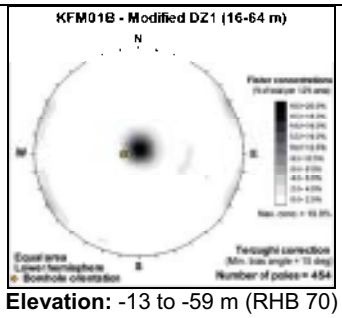

Elevation: -13 to -59 m (RHB 70)

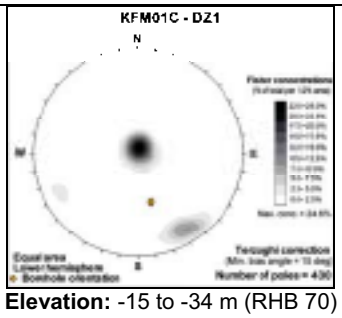

Elevation: -15 to -34 m (RHB 70)

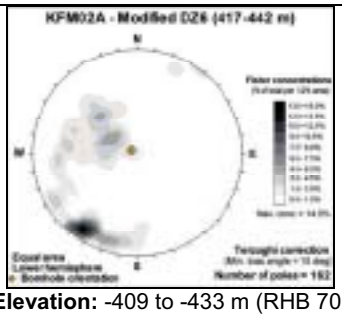

Elevation: -409 to -433 m (RHB 70)

Transmissivity (m^2/s)

General dip of T fractures: n.a.
Measured T range -400 to -600 m: No intersection
Number of PFL-features: n.a.
Model T, depth range -400 to -500 m: 5.4E-06
Model T, depth range -500 to -600 m: 2.0E-06

Transmissivity (m^2/s)

General dip of T fractures: n.a.
Measured T range -400 to -600 m: No intersection
Number of PFL-features: n.a.
Model T, depth range -400 to -500 m: 5.4E-06
Model T, depth range -500 to -600 m: 2.0E-06

Transmissivity (m^2/s)

General dip of T fractures: gentle
Measured T range -400 to -600 m: 2.9E-06
Number PFL-features: 14
Model T, depth range -400 to -500 m: 5.4E-06
Model T, depth range -500 to -600 m: 2.0E-06

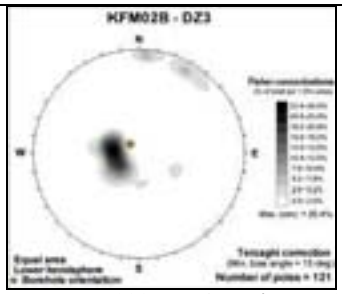

Elevation: -399 to -417 m (RHB 70)

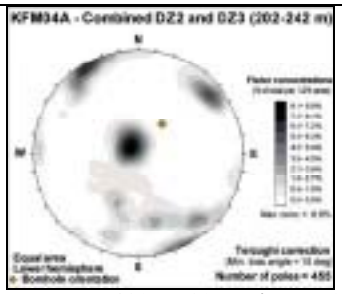

Elevation: -169 to -204 m (RHB 70)

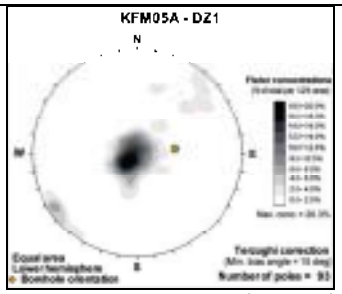

Elevation: -83 to -93 m (RHB 70)

Transmissivity (m^2/s)	Transmissivity (m^2/s)	Transmissivity (m^2/s)
General dip of T fractures: gentle **Measured T range -400 to -600 m:** 3.9E-05 **Number PFL-features:** 14 **Model T, depth range -400 to -500 m:** 5.4E-06 **Model T, depth range -500 to -600 m:** 2.0E-06	**General dip of T fractures:** n.a. **Measured T range -400 to -600 m:** No intersection **Number of PFL-features:** n.a. **Model T, depth range -400 to -500 m:** 5.4E-06 **Model T, depth range -500 to -600 m:** 2.0E-06	**General dip of T fractures:** n.a. **Measured T range -400 to -600 m:** No intersection **Number of PFL-features:** n.a. **Model T, depth range -400 to -500 m:** 5.4E-06 **Model T, depth range -500 to -600 m:** 2.0E-06

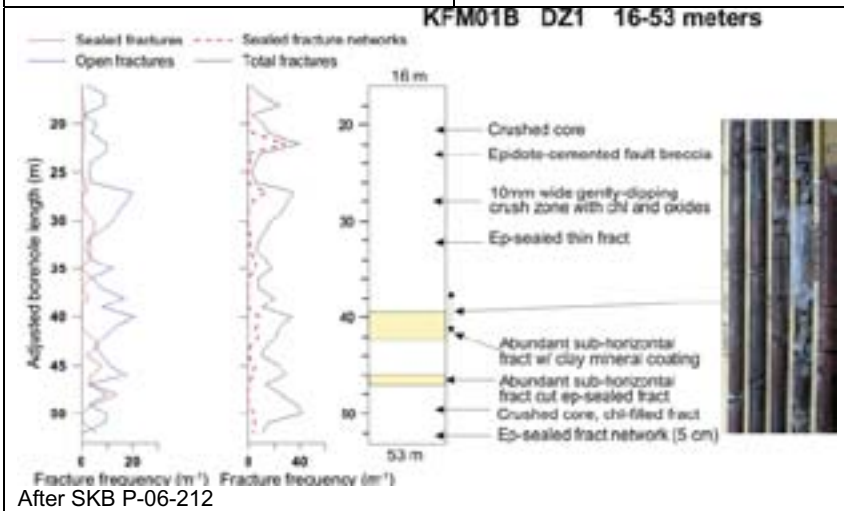

After SKB P-06-212


KFM02A (upper part of DZ6)

Engineering characteristics

Percentage of fault core: 7.7% (P-06-212 and P-07-111). No fault core recognised in KFM02B (DZ3) and KFM10A (DZ2 and DZ3).

Boreholes KFM01B, KFM01C and KFM05A not included in fracture statistics below due to interference with near-surface fracturing

Transition part of zone:
Frequency of open fractures: 4.8 m^{-1}
Std dev: 1.6
Mineral coating along open fractures: chlorite, calcite, adularia/hematite, no mineral, clay minerals

Frequency of sealed fractures: 8.1 m^{-1}
Std dev: 5.1
Mineral filling along sealed fractures: calcite, adularia/hematite, chlorite, laumontite

Fault core:
Frequency of open fractures: 2.9 m^{-1}
Std dev 2.1
Mineral coating along open fractures: no mineral, chlorite, adularia/hematite, calcite

Frequency of sealed fractures: 34.5 m^{-1}
Std dev: 28.2
Mineral filling along sealed fractures: adularia/hematite, calcite, laumontite

Deformation zone ZFMA8

Borehole intersections (metres along borehole)

KFM06B: DZ1 (55-93 m)
HFM16: DZ1 (12-71 m)

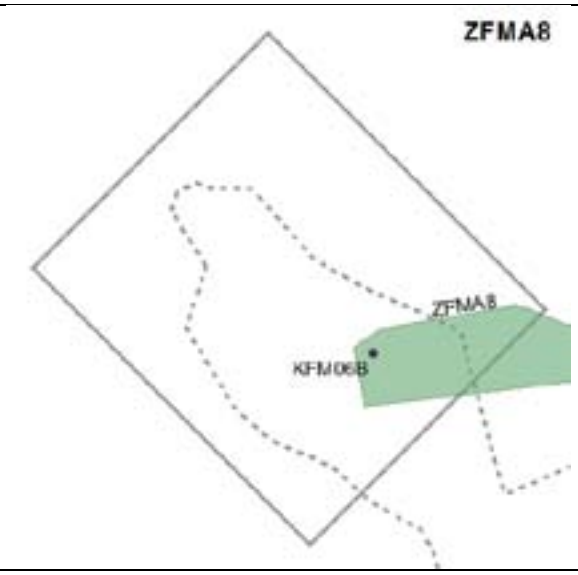

Deformation style, alteration and geometry

Deformation style: Brittle

Alteration: Red-stained bedrock with fine-grained hematite dissemination. Altered vuggy rock with quartz dissolution between 66 and 70 m along DZ1 in KFM06B

Strike/dip (right-hand-rule): 080/35

Trace length at ground surface: 1,852 m

Model thickness / model thickness span : 32 m / 6-37 m

Measured thickness (-400 to -600 m elevation): No intersection

Comment:

Fractures in the deformation zone

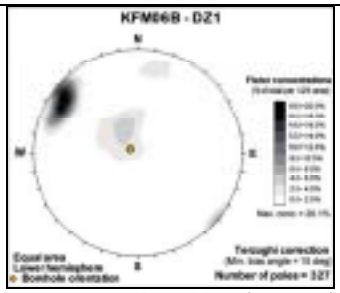

Elevation: -51 to -88 m (RHB 70)

Transmissivity (m^2/s)

General dip of T fractures: n.a.
Measured T range -400 to -600 m: No intersection
Number of PFL-features: n.a.
Model T, depth range -400 to -500 m: 7.1E-06
Model T, depth range -500 to -600 m: 2.6E-06

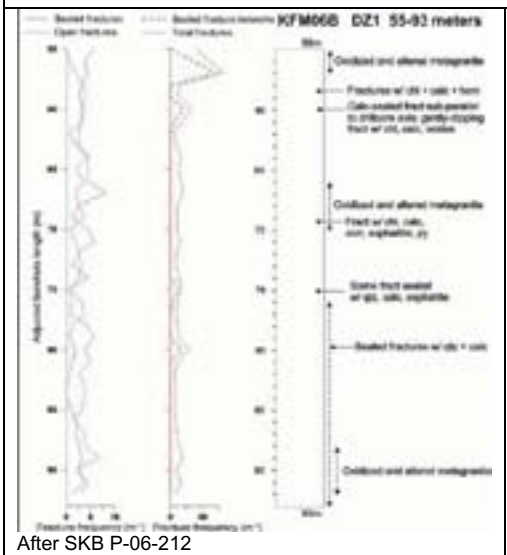

After SKB P-06-212

Strong hematite alteration and small fractures filled with quartz and calcite that has been partly dissolved and transported away (after SKB P-06-212)

Engineering characteristics

Percentage of fault core: No fault core recognised (P-06-212). No division into transition and core

No fracture statistics since fractures along DZ1 in borehole KFM06B interfere with near-surface fracturing

Deformation zone ZFMB4

Borehole intersections (metres along borehole)

KFM02A: DZ8 (893-905 m)

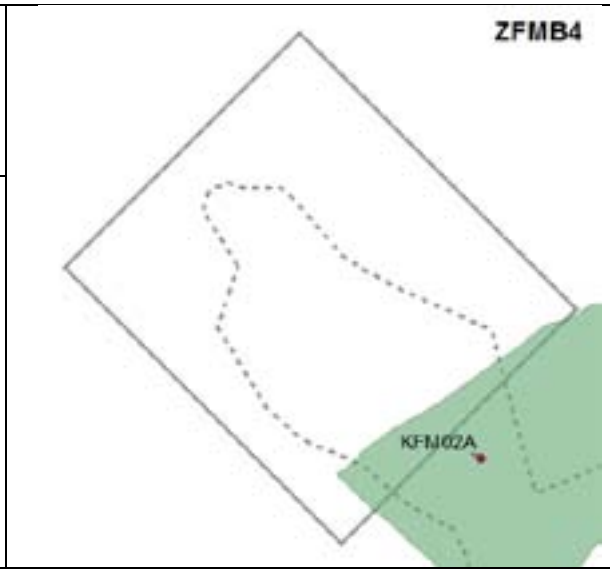

Deformation style, alteration and geometry

Deformation style: Brittle

Alteration: Not present

Strike/dip (right-hand-rule): 050/29

Trace length at ground surface: Does not intersect the ground surface

Model thickness / model thickness span : 12 m / 6-37 m

Measured thickness (-400 to -600 m elevation): No intersection

Comment:

Fractures in the deformation zone

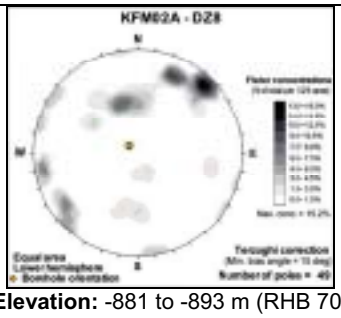

Elevation: -881 to -893 m (RHB 70)

Transmissivity (m^2/s)

General dip of T fractures: gentle
Measured T range -400 to -600 m: 2.62E-09
Number of PFL-features: 1
Model T, depth range -400 to -500 m: 2.0E-07
Model T, depth range -500 to -600 m: 7.3E-08

KFM02A (DZ8)

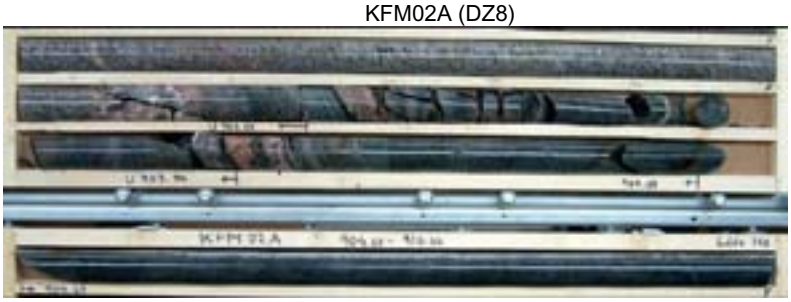

Engineering Characteristics

Percentage of fault core: No fault core recognised (P-06-212). No division into transition and core

Frequency of open fractures: 1.1 m^{-1}
Std dev: n.a.
Mineral coating along open fractures: chlorite, calcite, clay minerals, no mineral

Frequency of sealed fractures: 3.7 m^{-1}
Std dev: n.a.
Mineral filling along sealed fractures: chlorite, calcite, no mineral

Deformation zone ZFMB7

Borehole intersections (metres along borehole)

KFM06A: DZ4 (318-358 m)
KFM06C: DZ2 (359-400 m)

Deformation style, alteration and geometry

Deformation style: Brittle

Alteration: Red-stained bedrock with fine-grained hematite dissemination. Vuggy rock with quartz dissolution at 332-333 m along DZ4 in KFM06A

Strike/dip (right-hand-rule): 020/20

Trace length at ground surface: Does not intersect the ground surface

Model thickness / model thickness span : 28 m / 6-37 m

Measured thickness (-400 to -600 m elevation): No intersection

Comment:

Fractures in the deformation zone

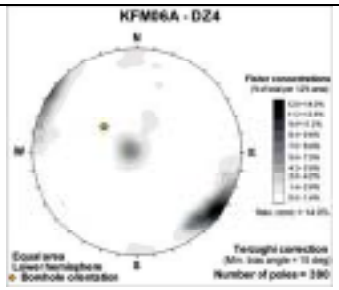

Elevation: -270 to -304 m (RHB 70)

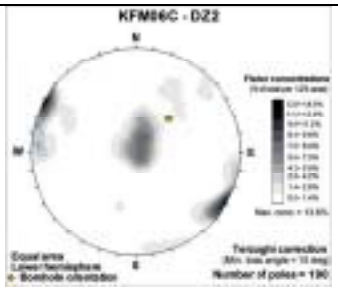

Elevation: -296 to -329 m (RHB 70)

Transmissivity (m^2/s)

General dip of T fractures: n.a.
Measured T range -400 to -600 m: No intersection
Number of PFL-features: n.a.
Model T, depth range -400 to -500 m: 5.3E-07
Model T, depth range -500 to -600 m: 2.0E-07

Transmissivity (m^2/s)

General dip of T fractures: n.a.
Measured T range -400 to -600 m: No intersection
Number of PFL-features: n.a.
Model T, depth range -400 to -500 m: 5.3E-07
Model T, depth range -500 to -600 m: 2.0E-07

After SKB P-07-101

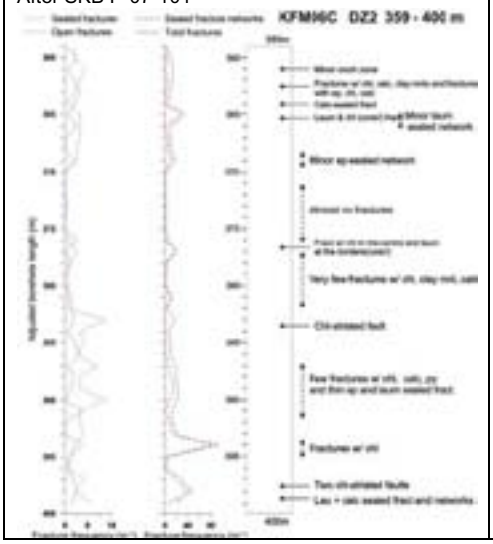

KFM06C (DZ2)

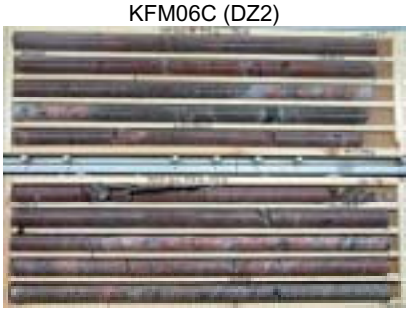

Engineering Characteristics

Percentage of fault core: No fault core recognised (P-06-212 and P-07-101). No division into transition and core

Borehole KFM06A not included in fracture statistics below due to interference with zone ZFMENE0060A

Frequency of open fractures: 2.1 m^{-1}
Std dev: n.a.
Mineral coating along open fractures: chlorite, calcite, clay minerals

Frequency of sealed fractures: 11.3 m^{-1}
Std dev: n.a.
Mineral filling along sealed fractures: calcite, chlorite, epidote

Deformation zone ZFMF1

Borehole intersections (metres along borehole)

KFM02A: Part of DZ6 (476-520 m)
KFM02B: DZ5 (462-472 m) and DZ6 (485-511 m)

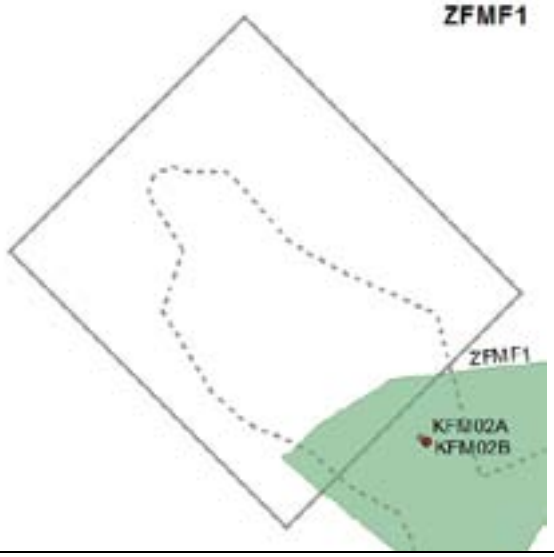

Deformation style, alteration and geometry

Deformation style: Brittle

Alteration: Oxidized bedrock with fine-grained hematite dissemination

Strike/dip (right-hand-rule): 070/10

Trace length at ground surface: Does not intersect the ground surface

Model thickness / model thickness span : 44 m / 9-45 m

Measured thickness (-400 to -600 m elevation): 44 m

Comment: Data from KFM02B only available after completion of geological model stage 2.2, i.e. not included in geological modelling work

Fractures in the deformation zone

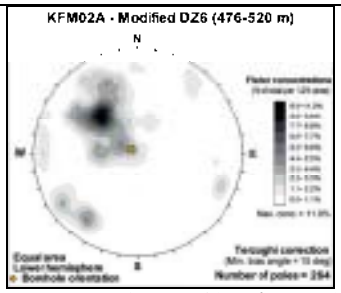

Elevation: -467 to -510 m (RHB 70)

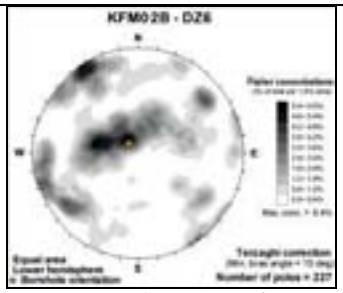

Elevation: -471 to -497 m (RHB 70)

Transmissivity (m^2/s)

General dip of T fractures: gentle
Measured T range -400 to -600 m: 4.66E-06
Number of PFL-features: 22
Model T, depth range -400 to -500 m: 6.9E-06
Model T, depth range -500 to -600 m: 2.5E-06

Transmissivity (m^2/s)

General dip of T fractures: gentle (?)
Measured T range -400 to -600 m: 6.2E-5
Number of PFL-features: 9
Model T, depth range -400 to -500 m: 6.9E-06
Model T, depth range -500 to -600 m: 2.5E-06

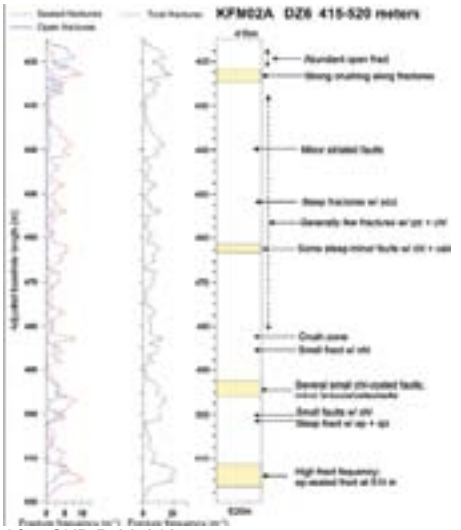

After SKB P-06-212

Network of gently dipping, epidote-sealed fractures that are present in a metadiorite and altered metagranite at 516 m (after SKB P-06-212)

Engineering characteristics

Percentage of fault core: 7.3% (P-06-212 and P-07-111)

Transition part of zone:
Frequency of open fractures: 3.1 m^{-1}
Std dev: 2.1
Mineral coating along open fractures: calcite, calcite, chlorite, clay minerals, prehnite, adularia/hematite

Frequency of sealed fractures: 12.5 m^{-1}
Std dev: 11.1
Mineral filling along sealed fractures: calcite, prehnite, epidote, chlorite

Fault core:
Frequency of open fractures: 5.7 m^{-1}
Std dev: n.a.
Mineral coating along open fractures: chlorite, adularia/hematite, calcite, clay minerals

Frequency of sealed fractures: 8.2 m^{-1}
Std dev: n.a.
Mineral filling along sealed fractures: chlorite, adularia/hematite, prehnite, calcite

Deformation zone ZFMENE0060A

Borehole intersections (metres along borehole)

KFM01C: Part of DZ3 (235-252 m)
KFM06A: DZ4 (318-358 m)
HFM09: DZ1 (18-28 m)

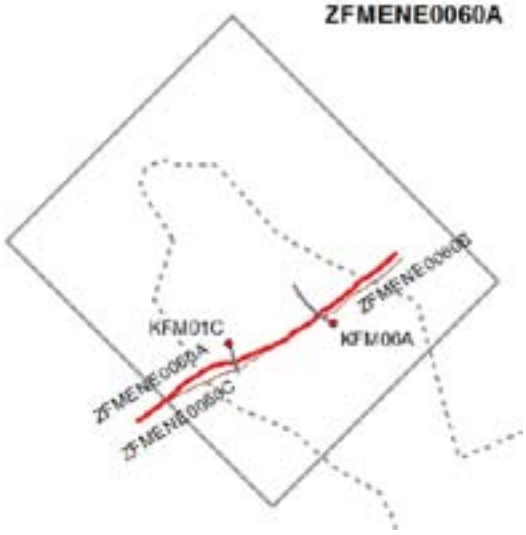

Deformation style, alteration and geometry

Deformation style: Brittle

Alteration: Red-stained bedrock with fine grained hematite dissemination. Vuggy rock with quartz dissolution between 332-333 m in KFM06A

Strike/dip (right-hand-rule): 239/85

Trace length at ground surface: 3,120 m

Model thickness / model thickness span : 17 m / 10-64 m

Measured thickness (-400 to -600 m elevation): No intersection

Comment:

Fractures in the deformation zone

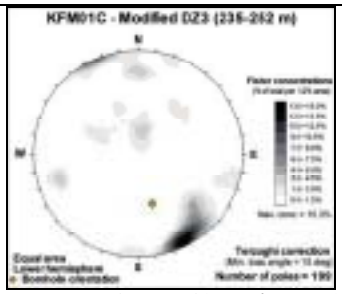

Elevation: -175 to -187 m (RHB 70)

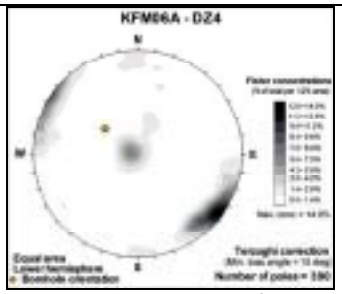

Elevation: -270 to -304 m (RHB 70)

Transmissivity (m^2/s)

General dip of T fractures: n.a.
Measured T range -400 to -600 m: No intersection
Number of PFL-features: n.a.
Model T, depth range -400 to -500 m: 3.3E-08
Model T, depth range -500 to -600 m: 1.2E-08

Transmissivity (m^2/s)

General dip of T fractures: n.a.
Measured T range -400 to -600 m: No intersection
Number of PFL-features: n.a.
Model T, depth range -400 to -500 m: 3.3E-08
Model T, depth range -500 to -600 m: 1.2E-08

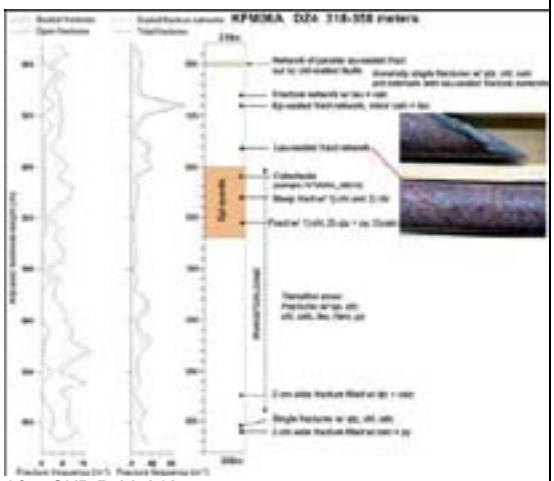

After SKB P-06-212

KFM01C (part of DZ3)

Engineering characteristics

Percentage of fault core: 5.3% (P-06-212 and P-07-101)

Transition part of zone:
Frequency of open fractures: 2.3 m^{-1}
Std dev: 1.9
Mineral coating along open fractures: chlorite, calcite, laumontite, adularia/hematite, pyrite, clay minerals

Frequency of sealed fractures: 24.9 m^{-1}
Std dev: 21.8
Mineral filling along sealed fractures: calcite, laumontite, adularia/hematite, chlorite, epidote, quartz, prehnite

Fault core:
Frequency of open fractures: 3.4 m^{-1}
Std dev: 3.5
Mineral coating along open fractures: calcite, laumontite, chlorite, clay minerals, adularia/hematite, pyrite

Frequency of sealed fractures: 69.7 m^{-1}
Std dev: 52.2
Mineral filling along sealed fractures: laumontite, calcite, chlorite, adularia/hematite

Deformation zone ZFMENE0060B

Borehole intersections (metres along borehole)

KFM06A: DZ2, DZ3 and less fractured rock between DZ2 and DZ3 (195-278 m)

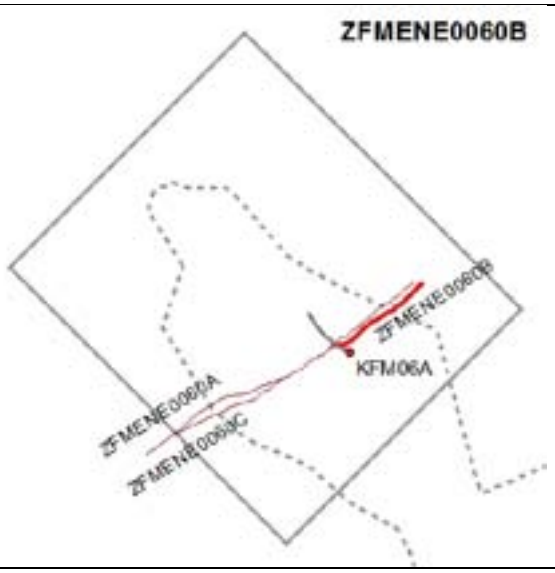

Deformation style, alteration and geometry

Deformation style: Brittle

Alteration: Red-stained bedrock with fine-grained hematite dissemination

Strike/dip (right-hand-rule): 234/78

Trace length at ground surface: 1,070 m

Model thickness / model thickness span : 33 m / 3-35 m

Measured thickness (-400 to -600 m elevation): No intersection

Comment:

Fractures in the deformation zone

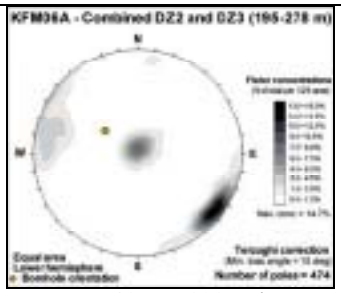

Elevation: -165 to -236 m (RHB 70)

Transmissivity (m^2/s)

General dip of T fractures: n.a.
Measured T range -400 to -600 m: No intersection
Number of PFL-features: n.a.
Model T, depth range -400 to -500 m: 3.8E-06
Model T, depth range -500 to -600 m: 1.4E-06

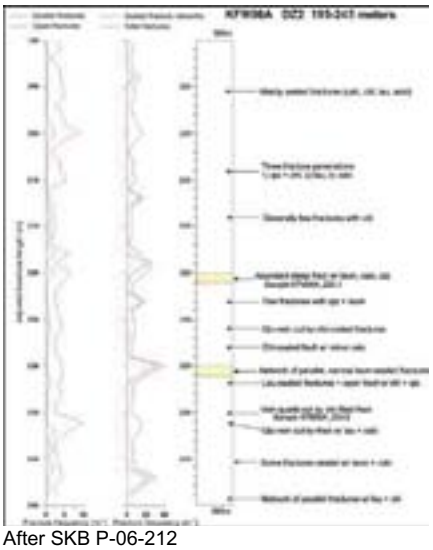

After SKB P-06-212

KFM06A (DZ3). Strong alteration (red-stained bedrock with hematite dissemination) and abundant sealed fractures are present.

Engineering characteristics

Percentage of fault core: 9.6% (P-06-212)

Transition part of zone:
Frequency of open fractures: 1.0 m^{-1}
Std dev: n.a.
Mineral coating along open fractures: calcite, chlorite, pyrite, clay minerals, no mineral

Frequency of sealed fractures: 6.3 m^{-1}
Std dev: n.a.
Mineral filling along sealed fractures: calcite, chlorite, adularia/hematite

Fault core:
Frequency of open fractures: 3.1 m^{-1}
Std dev: 3.4
Mineral coating along open fractures: calcite, clay minerals, chlorite, no mineral

Frequency of sealed fractures: 41.1 m^{-1}
Std dev: n.a.
Mineral filling along sealed fractures: calcite, epidote, chlorite, adularia/hematite

Deformation zone ZFMENE0060C

Borehole intersections (metres along borehole)

KFM01C: Part of DZ3 (305-330m)

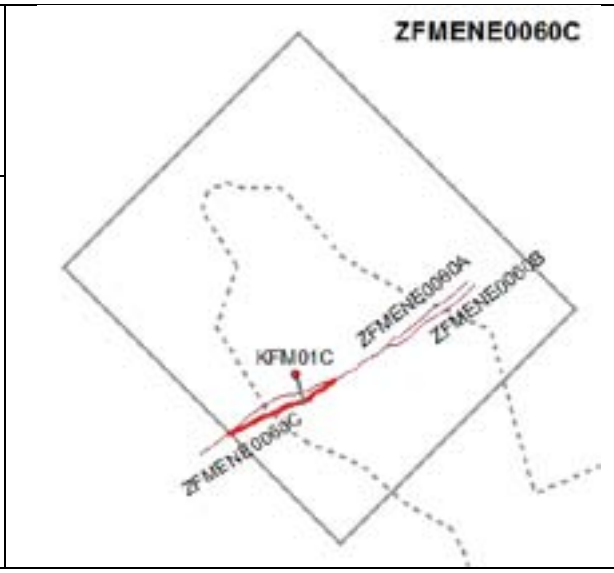

Deformation style, alteration and geometry

Deformation style: Brittle

Alteration: Red-stained bedrock with fine-grained hematite dissemination

Strike/dip (right-hand-rule): 241/75

Trace length at ground surface: 1,161 m

Model thickness / model thickness span : 20 m / 3-45 m

Measured thickness (-400 to -600 m elevation): No intersection

Comment:

Fractures in the deformation zone

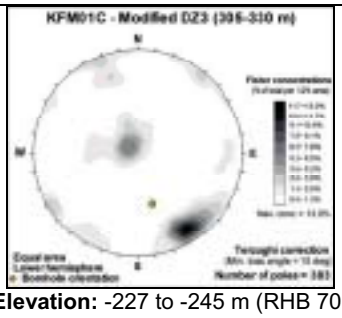

Elevation: -227 to -245 m (RHB 70)

Transmissivity (m^2/s)

General dip of T fractures: n.a.
Measured T range -400 to -600 m: No intersection
Number of PFL-features: n.a.
Model T, depth range -400 to -500 m: 2.0E-08
Model T, depth range -500 to -600 m: 2.0E-08

KFM01C (part of DZ3)

Engineering characteristics

Percentage of fault core: 16% (P-07-101)

Transition part of zone:
Frequency of open fractures: 4.3 m^{-1}
Std dev: n.a.
Mineral coating along open fractures: chlorite, laumontite, calcite, clay minerals

Frequency of sealed fractures: 24.4 m^{-1}
Std dev: n.a.
Mineral filling along sealed fractures: laumontite, calcite

Fault core:
Frequency of open fractures: 5.5 m^{-1}
Std dev: n.a.
Mineral coating along open fractures: calcite, chlorite, laumontite, adularia/hematite, clay minerals

Frequency of sealed fractures: 40.0 m^{-1}
Std dev: n.a.
Mineral filling along sealed fractures: laumontite, calcite, chlorite

Deformation zone ZFMENE0061

Borehole intersections (metres along borehole)

KFM01D: DZ4 (670-700 m)
KFM06A: DZ8 (788-810 m)

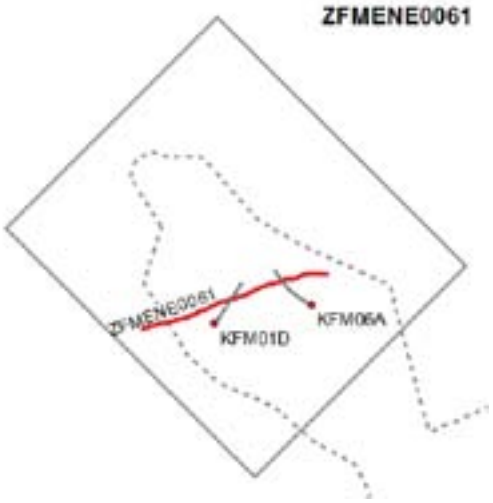

Deformation style, alteration and geometry

Deformation style: Brittle

Alteration: Red-stained bedrock with fine grained hematite dissemination. Alteration in borehole restricted to DZ4 in KFM01D

Strike/dip (right-hand-rule): 252/85

Trace length at ground surface: 2,081 m

Model thickness / model thickness span : 11 m / 3-45 m

Measured thickness (-400 to -600 m elevation): 11 m

Comment:

Fractures in the deformation zone

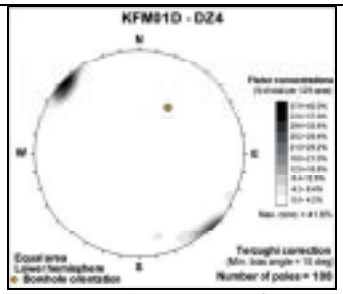

Elevation: -519 to -540 m (RHB 70)

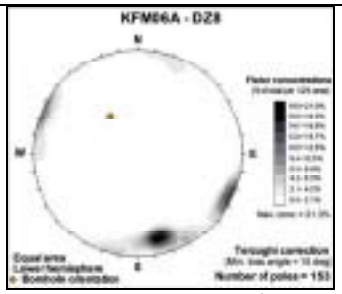

Elevation: -659 to -677 m (RHB 70)

Transmissivity (m^2/s)

General dip of T fractures: steep
Measured T range -400 to -600 m: 1.00E-10
Number of PFL-features: 0
Model T, depth range -400 to -500 m: 4.3E-10
Model T, depth range -500 to -600 m: 1.6E-08

Transmissivity (m^2/s)

General dip of T fractures: n.a.
Measured T range -400 to -600 m: No intersection
Number of PFL-features: n.a.
Model T, depth range -400 to -500 m: 4.3E-10
Model T, depth range -500 to -600 m: 1.6E-08

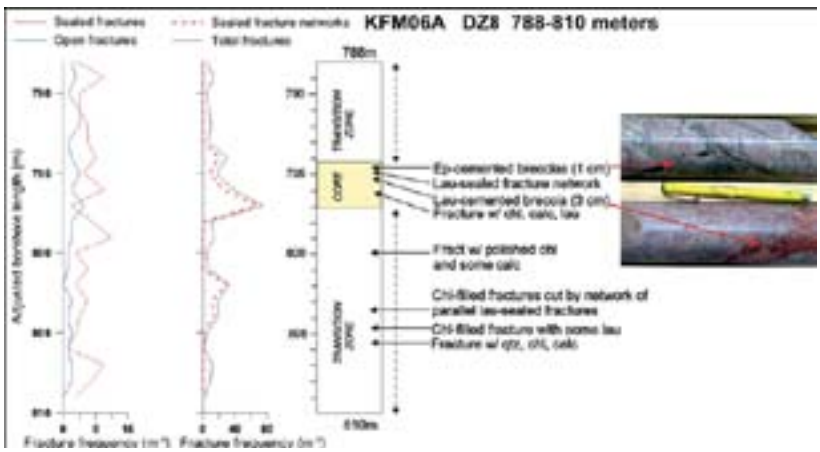

After SKB P-06-212

Engineering characteristics

Percentage of fault core: 9.6% (P-06-212 and P-07-101)

Transition part of zone:
Frequency of open fractures: 1.4 m^{-1}
Std dev: 0.4
Mineral coating along open fractures: calcite, chlorite, quartz, clay minerals, laumontite
Frequency of sealed fractures: 6.3 m^{-1}
Std dev: 3.2
Mineral filling along sealed fractures: calcite, chlorite, laumontite, no mineral, quartz

Fault core:
Frequency of open fractures: 2.6 m^{-1}
Std dev: 2.7
Mineral coating along open fractures: calcite, chlorite, clay minerals, laumontite
Frequency of sealed fractures: 30.6 m^{-1}
Std dev: 27.4
Mineral filling along sealed fractures: laumontite, calcite, chlorite, adularia/hematite, quartz, epidote

Deformation zone ZFMENE0062A

Borehole intersections (metres along borehole)

HFM25: DZ4 (143-155 m) and DZ5 (169-187 m)
Surface excavation at AFM001243

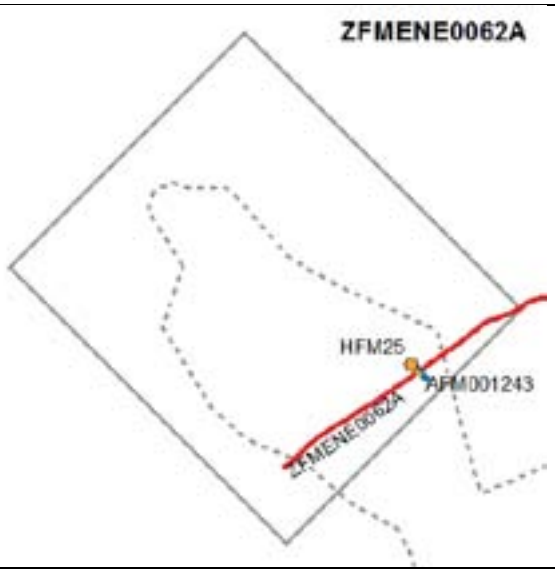

Deformation style, alteration and geometry

Deformation style: Brittle

Alteration: Red-stained bedrock with fine-grained hematite dissemination

Strike/dip (right-hand-rule): 058/85

Trace length at ground surface: 3,543 m

Model thickness / model thickness span : 44 m / 10-64 m

Measured thickness (-400 to -600 m elevation): No intersection

Comment: Based only on surface excavation (AFM001243) and percussion borehole intersections (HFM25) close to surface

Fractures in the deformation zone

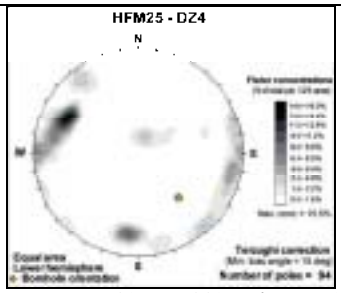

Elevation: -105 to -113 m (RHB 70)

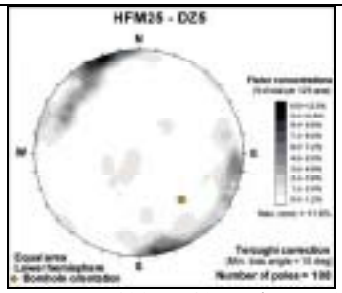

Elevation: -122 to -134 m (RHB 70)

Transmissivity (m^2/s)

General dip of T fractures: n.a.
Measured T range -400 to -600 m: No intersection
Number of PFL-features: n.a.
Model T, depth range -400 to -500 m: 4.4E-08
Model T, depth range -500 to -600 m: 4.4E-08

Transmissivity (m^2/s)

General dip of T fractures: n.a.
Measured T range -400 to -600 m: No intersection
Number of PFL-features: n.a.
Model T, depth range -400 to -500 m: 4.4E-08
Model T, depth range -500 to -600 m: 4.4E-08

Surface excavation AFM001243

Engineering characteristics

Percentage of fault core: No data from cored boreholes. For this reason, no fracture frequency statistics

Deformation zone ZFMENE0103

Borehole intersections (metres along borehole)

KFM05A: DZ4 (892-916 m)

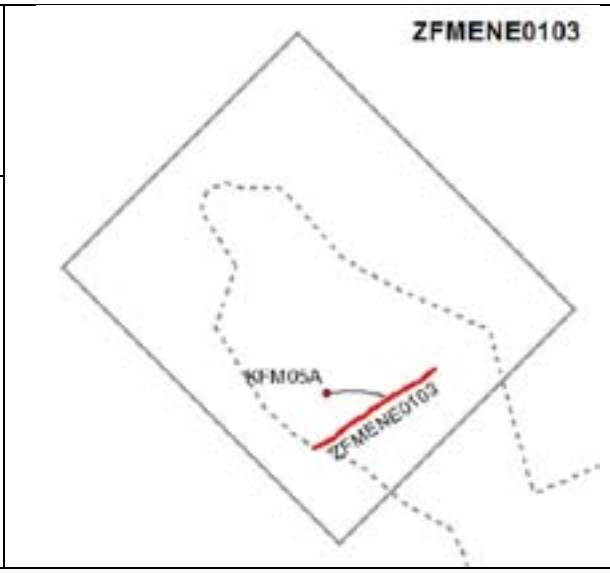

Deformation style, alteration and geometry

Deformation style: Brittle

Alteration: Red-stained bedrock with fine-grained hematite dissemination

Strike/dip (right-hand-rule): 236/84

Trace length at ground surface: 1,399 m

Model thickness / model thickness span : 13 m / 3-45 m

Measured thickness (-400 to -600 m elevation): No intersection

Comment:

Fractures in the deformation zone

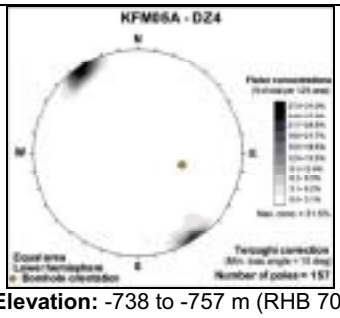

Elevation: -738 to -757 m (RHB 70)

Transmissivity (m^2/s)

General dip of T fractures: n.a.
Measured T range -400 to -600 m: No intersection
Number of PFL-features: n.a.
Model T, depth range -400 to -500 m: 1.9E-09
Model T, depth range -500 to -600 m: 7.1E-10

DZ4 in KFM05A

Engineering characteristics

Percentage of fault core: No data available along DZ4 in KFM05A to assess core and transition. No division made

Frequency of open fractures: 0.4 m^{-1}
Std dev: n.a.
Mineral coating along open fractures: chlorite, adularia/hematite, calcite, no mineral, quartz, laumontite

Frequency of sealed fractures: 10.3 m^{-1}
Std dev: n.a.
Mineral filling along sealed fractures: calcite, laumontite, adularia/hematite, chlorite

Deformation zone ZFMENE0159A

Borehole intersections (metres along borehole)

KFM07A: DZ3 (417-422 m)
KFM08D: DZ2 (318-324 m)
KFM09A: DZ3 (217-280 m)
KFM09B: Part of DZ1 (106-132 m)
Surface excavation at AFM001265

Deformation style, alteration and geometry

Deformation style: Brittle

Alteration: Red-stained bedrock with fine-grained hematite dissemination

Strike/dip (right-hand-rule): 239/80

Trace length at ground surface: 1,909 m

Model thickness / model thickness span : 21 m / 3-45 m

Measured thickness (-400 to -600 m elevation): 2 m

Comment: KFM08D only available after completion of geological model stage 2.2, i.e. not included in geological modelling work

Fractures in the deformation zone

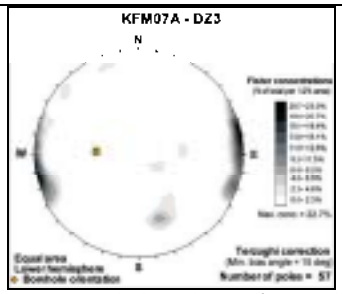

Elevation: -353 to -357 m (RHB 70)

Transmissivity (m^2/s)

General dip of T fractures: n.a.
Measured T range -400 to -600 m: No intersection
Number of PFL-features: n.a.
Model T, depth range -400 to -500 m: 2.8E-10
Model T, depth range -500 to -600 m: 1.0E-09

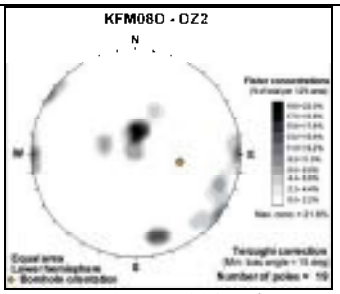

Elevation: -255 to -261 m (RHB 70)

Transmissivity (m^2/s)

General dip of T fractures: n.a.
Measured T range -400 to -600 m: No intersection
Number of PFL-features: n.a.
Model T, depth range -400 to -500 m: 2.8E-10
Model T, depth range -500 to -600 m: 1.0E-09

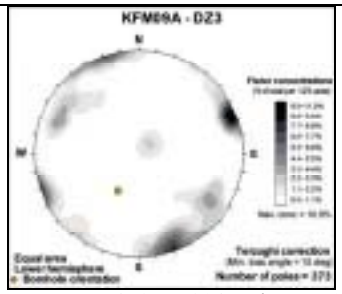

Elevation: -178 to -231 m (RHB 70)

Transmissivity (m^2/s)

General dip of T fractures: n.a.
Measured T range -400 to -600 m: No intersection
Number of PFL-features: n.a.
Model T, depth range -400 to -500 m: 2.8E-10
Model T, depth range -500 to -600 m: 1.0E-09

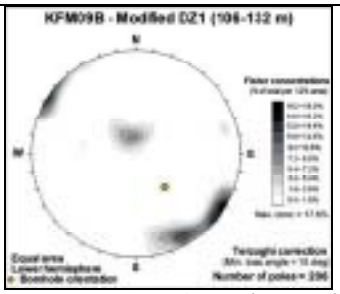

Elevation: -83 to -104 m (RHB 70)

Transmissivity (m^2/s)

General dip of T fractures: n.a.
Measured T range -400 to -600 m: No intersection
Number of PFL-features: n.a.
Model T, depth range -400 to -500 m: 2.8E-10
Model T, depth range -500 to -600 m: 1.0E-09

KFM09A (DZ3)

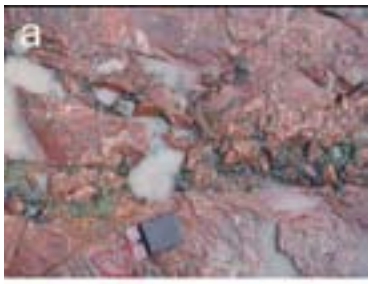

Surface excavation AFM001265. Chlorite- and epidote-sealed breccia at intersection between NNE-SSW and ENE-WSW fractures. Note the strong wall-rock alteration (red-staining) (after P-06-136)

Engineering characteristics

Percentage of fault core: 10.6% (P-06-212. P-07-101 and P-07-111).

Borehole KFM08D not included in fracture statistics due to possible interference with zone ZFMENE0159B

Transition part of zone:
Frequency of open fractures: 2.5 m^{-1}
Std dev: 0.6
Mineral coating along open fractures: calcite, chlorite, clay minerals, laumontite, adularia/hematite, pyrite

Frequency of sealed fractures: 15.6 m^{-1}
Std dev: 1.3
Mineral filling along sealed fractures: calcite, chlorite, laumontite, adularia/hematite

Fault core:
Frequency of open fractures: 2.5 m^{-1}
Std dev: 1.5
Mineral coating along open fractures: calcite, chlorite, adularia/hematite, pyrite, clay minerals, laumontite, quartz

Frequency of sealed fractures: 43.8 m^{-1}
Std dev: 13.6
Mineral filling along sealed fractures: laumontite, calcite, chlorite, adularia/hematite, epidote

Deformation zone ZFMENE0159B

Borehole intersections (metres along borehole)

KFM08D: DZ3 (371-396 m)

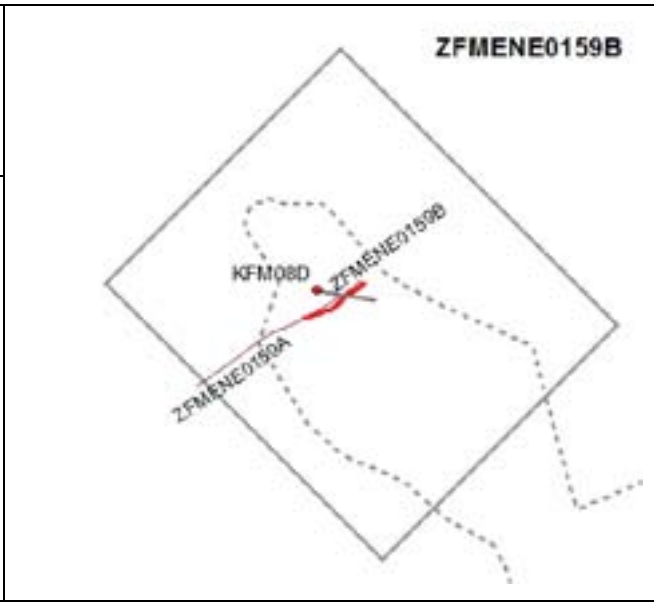

Deformation style, alteration and geometry

Deformation style: Brittle

Alteration: Red-stained bedrock with fine-grained hematite dissemination

Strike/dip (right-hand-rule): 238/80

Trace length at ground surface: 673 m

Model thickness / model thickness span : 10 m / 2-43 m

Measured thickness (-400 to -600 m elevation): No intersection

Comment: KFM08D only available after completion of geological model stage 2.2, i.e. not included in geological modelling work

Fractures in the deformation zone

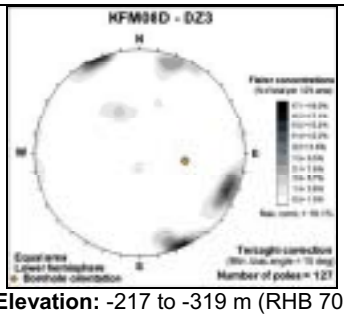

Elevation: -217 to -319 m (RHB 70)

Transmissivity (m^2/s)

General dip of T fractures: n.a.
Measured T range -400 to -600 m: No intersection
Number of PFL-features: n.a.
Model T, depth range -400 to -500 m: 2.8E-09
Model T, depth range -500 to -600 m: 1.0E-09

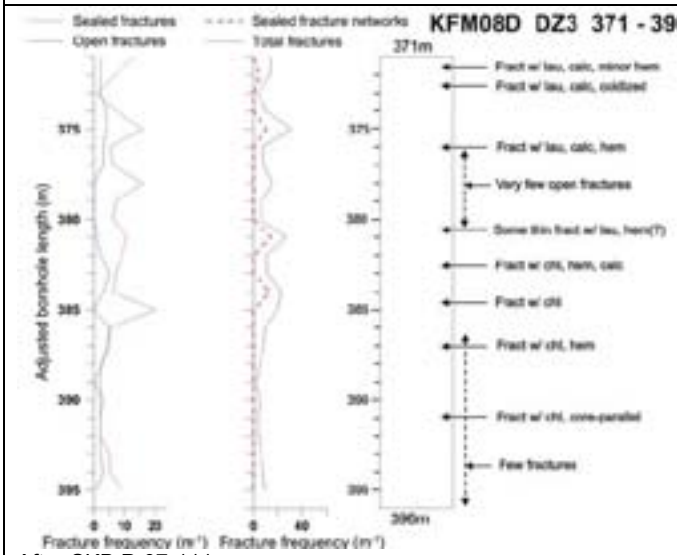

After SKB P-07-111

Engineering characteristics

Percentage of fault core: No fault core recognised (P-07-111). No division into transition and core

Frequency of open fractures: 2.3 m^{-1}
Std dev: n.a.
Mineral coating along open fractures: calcite, chlorite, clay minerals, pyrite

Frequency of sealed fractures: 8.9 m^{-1}
Std dev: n.a.
Mineral filling along sealed fractures: calcite, chlorite, prehnite, adularia/hematite

Deformation zone ZFMENE0168

Borehole intersections (metres along borehole)

KFM08D: DZ11 (819-842 m)

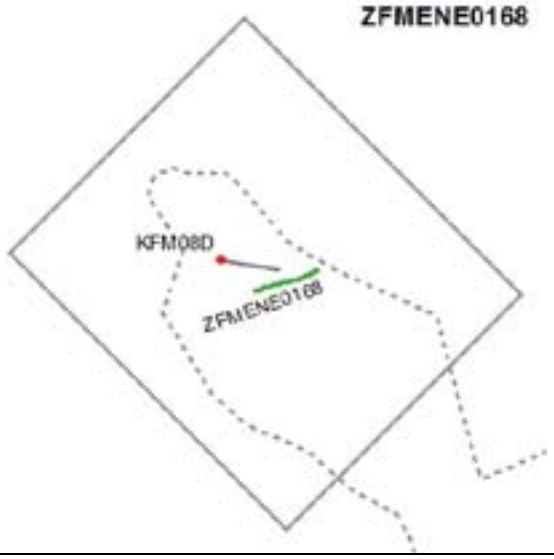

Deformation style, alteration and geometry

Deformation style: Brittle

Alteration: Red-stained bedrock with fine-grained hematite dissemination

Strike/dip (right-hand-rule): 253/90

Trace length at ground surface: 639 m

Model thickness / model thickness span : 10 m / 2-43 m

Measured thickness (-400 to -600 m elevation): No intersection

Comment: KFM08D only available after completion of geological model stage 2.2, i.e. not included in geological modelling work

Fractures in the deformation zone

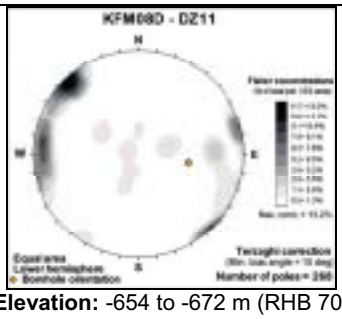

Elevation: -654 to -672 m (RHB 70)

Transmissivity (m^2/s)

General dip of T fractures: n.a.
Measured T range -400 to -600 m: No intersection
Number of PFL-features: n.a.
Model T, depth range -400 to -500 m: 2.8E-09
Model T, depth range -500 to -600 m: 1.0E-09

KFM08D (DZ11)

Engineering characteristics

Percentage of fault core: No data available along DZ11 in KFM08D to assess core and transition. No division made

Frequency of open fractures: 2.0 m^{-1}
Std dev: n.a.
Mineral coating along open fractures: chlorite, quartz, clay minerals, adularia/hematite, calcite

Frequency of sealed fractures: 17.2 m^{-1}
Std dev: n.a.
Mineral filling along sealed fractures: adularia/hematite, chlorite, quartz

Deformation zone ZFMENE0401A

Borehole intersections (metres along borehole)

KFM05A: Part of DZ3 (685-720 m)
HFM13: DZ1 (162-176 m)

Deformation style, alteration and geometry

Deformation style: Brittle

Alteration: Red-stained bedrock with fine-grained hematite dissemination

Strike/dip (right-hand-rule): 240/89

Trace length at ground surface: 1,961 m

Model thickness / model thickness span : 10 m / 3-45 m

Measured thickness (-400 to -600 m elevation): 10 m

Comment:

Fractures in the deformation zone

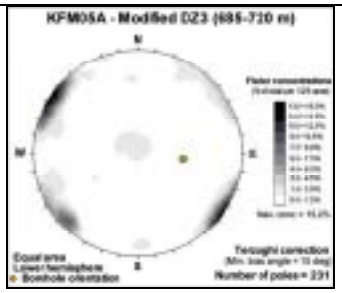

Elevation: -570 to -598 m (RHB 70)

Transmissivity (m^2/s)

General dip of T fractures: steep
Measured T range -400 to -600 m: 1.20E-08
Number of PFL-features: 2
Model T, depth range -400 to -500 m: 7.9E-07
Model T, depth range -500 to -600 m: 2.9E-09

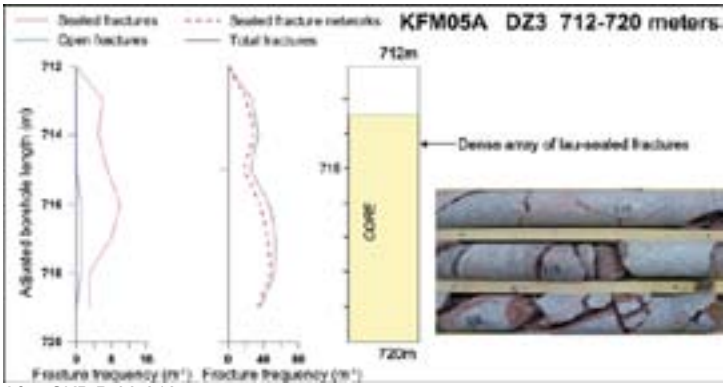

After SKB P-06-212

Engineering characteristics

Percentage of fault core: 17.1% (P-06-212)

Transition part of zone:
Frequency of open fractures: 0.8 m^{-1}
Std dev: n.a.
Mineral coating along open fractures: chlorite, calcite, clay minerals, laumontite, adularia/hematite, quartz
Frequency of sealed fractures: 8.0 m^{-1}
Std dev: n.a.
Mineral filling along sealed fractures: calcite, quartz, chlorite, adularia/hematite, laumontite

Fault core:
Frequency of open fractures: 0.5 m^{-1}
Std dev: n.a.
Mineral coating along open fractures: calcite, adularia/hematite, chlorite, laumontite
Frequency of sealed fractures: 42.0 m^{-1}
Std dev: n.a.
Mineral filling along sealed fractures: laumontite, adularia/hematite, calcite, chlorite

Deformation zone ZFMENE0401B

Borehole intersections (metres along borehole)

KFM05A: Part of DZ3 (590-616 m)

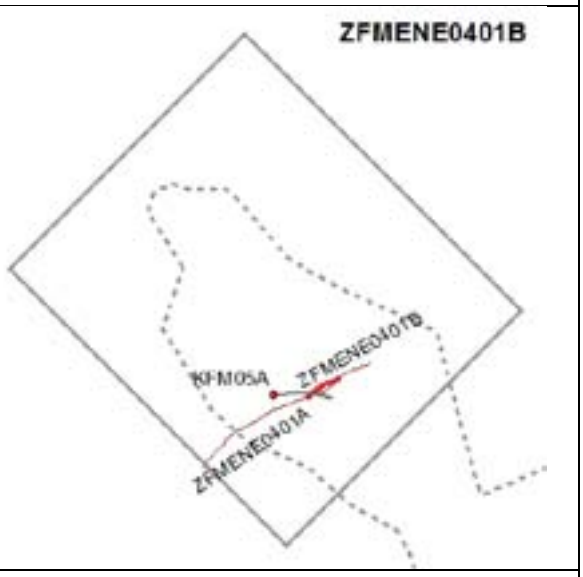

Deformation style, alteration and geometry

Deformation style: Brittle

Alteration: Red-stained bedrock with fine-grained hematite dissemination

Strike/dip (right-hand-rule): 061/88

Trace length at ground surface: 358 m

Model thickness / model thickness span : 7 m / 2-30 m

Measured thickness (-400 to -600 m elevation): 7 m

Comment:

Fractures in the deformation zone

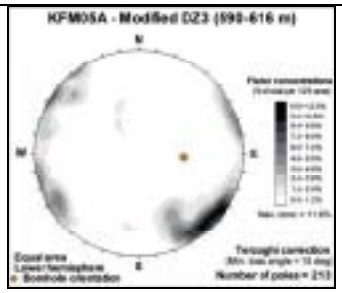

Elevation: -493 to -514 m (RHB 70)

Transmissivity (m^2/s)

General dip of T fractures: steep
Measured T range -400 to -600 m: 1.00E-10
Number of PFL-features: 0
Model T, depth range -400 to -500 m: 1.0E-10
Model T, depth range -500 to -600 m: 1.0E-10

Strong fracturing with local brecciation in several intervals between c. 610 and 614 m. Cataclasite also present at c. 610 m. Laumontite is conspicuous and epidote is also present in the inferred zone core between c. 610 and 614 m

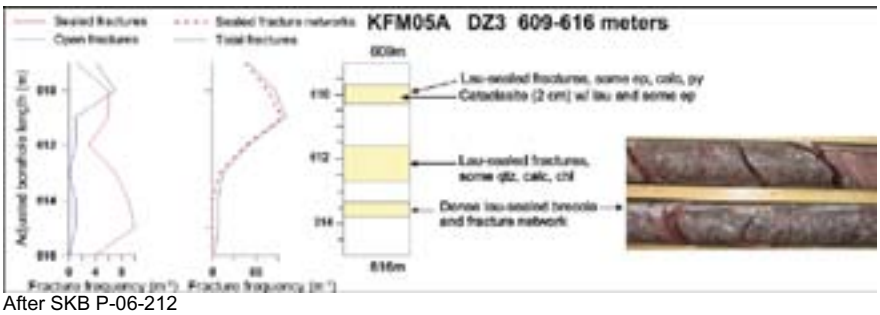

After SKB P-06-212

Engineering characteristics

Percentage of fault core: 19.2% (P-06-212)

Transition part of zone:
Frequency of open fractures: 1.5 m^{-1}
Std dev: n.a.
Mineral coating along open fractures: chlorite, calcite, laumontite

Frequency of sealed fractures: 9.0 m^{-1}
Std dev: n.a.
Mineral filling along sealed fractures: calcite, laumontite, epidote, adularia/hematite, chlorite

Fault core:
Frequency of open fractures: 2.6 m^{-1}
Std dev: n.a.
Mineral coating along open fractures: chlorite, laumontite, adularia/hematite, calcite

Frequency of sealed fractures: 78.0 m^{-1}
Std dev: n.a.
Mineral filling along sealed fractures: laumontite, calcite, chlorite, adularia/hematite

Deformation zone ZFMENE1061A

Borehole intersections (metres along borehole)

KFM08A: Part of DZ1 (244-315 m)
KFM08C: DZ4 (829-832 m)
KFM08C: DZ5 (946-949 m)

Deformation style, alteration and geometry

Deformation style: Brittle

Alteration: Oxidized bedrock with fine-grained hematite dissemination

Strike/dip (right-hand-rule): 056/81

Trace length at ground surface: 1,158 m

Model thickness / model thickness span : 45 m / 3-45 m

Measured thickness (-400 to -600 m elevation): No intersection

Comment:

Fractures in the deformation zone

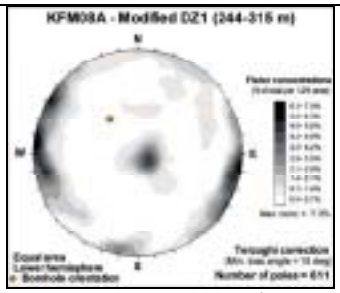

Elevation: -204 to -262 m (RHB 70)

Transmissivity (m^2/s)

General dip of T fractures: n.a.
Measured T range -400 to -600 m: No intersection
Number of PFL-features: n.a.
Model T, depth range -400 to -500 m: 2.0E-08
Model T, depth range -500 to -600 m: 7.4E-09

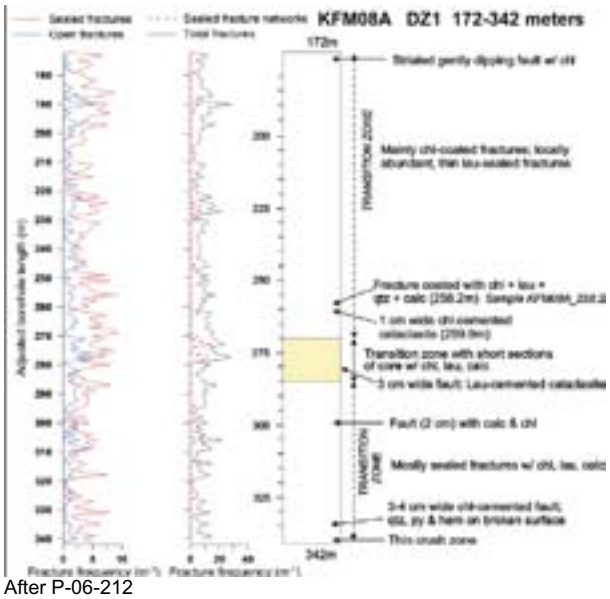

After P-06-212

Engineering characteristics

Percentage of fault core: 4.2% (P-06-212). Borehole KFM08C not included in fracture statistics due to interference with zone ZFMENE1061B

Transition part of zone:
Frequency of open fractures: 2.8 m^{-1}
Std dev: n.a.
Mineral coating along open fractures: chlorite, calcite, pyrite, clay minerals, laumontite, adularia/hematite, quartz
Frequency of sealed fractures: 7.8 m^{-1}
Std dev: n.a.
Mineral filling along sealed fractures: calcite, chlorite, laumontite, adularia/hematite

Fault core:
Frequency of open fractures: 4.6 m^{-1}
Std dev: n.a.
Mineral coating along open fractures: chlorite, calcite, pyrite, laumontite
Frequency of sealed fractures: 10.7 m^{-1}
Std dev: n.a.
Mineral filling along sealed fractures: chlorite, calcite, laumontite

Deformation zone ZFMENE1061B

Borehole intersections (metres along borehole)

KFM08C: DZ4 (829-832 m).

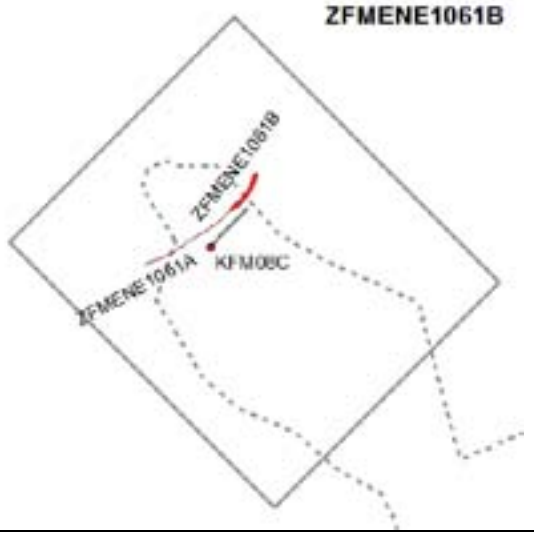

Deformation style, alteration and geometry

Deformation style: Brittle

Alteration: Oxidized bedrock with fine-grained hematite dissemination

Strike/dip (right-hand-rule): 033/81

Trace length at ground surface: 436 m

Model thickness / model thickness span : 2 m / 2-30 m

Measured thickness (-400 to -600 m elevation): No intersection

Comment:

Fractures in the deformation zone

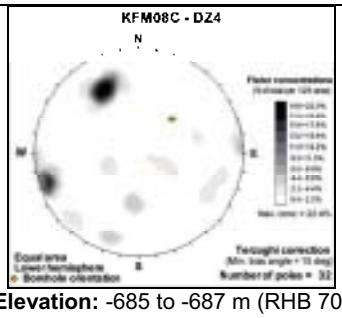

Elevation: -685 to -687 m (RHB 70)

Transmissivity (m^2/s)

General dip of T fractures: n.a.
Measured T range -400 to -600 m: No intersection
Number of PFL-features: n.a.
Model T, depth range -400 to -500 m: 1.0E-09
Model T, depth range -500 to -600 m: 3.8E-10

KFM08C (DZ4)

Engineering characteristics

Percentage of fault core: 50% (P-07-101)

Transition part of zone:
Frequency of open fractures: 16.5 m^{-1}
Std dev: n.a.
Mineral coating along open fractures: chlorite, calcite, adularia/hematite, clay minerals
Frequency of sealed fractures: 14.0 m^{-1}
Std dev: n.a.
Mineral filling along sealed fractures: calcite, chlorite, adularia/hematite

Fault core:
Frequency of open fractures: 22.0 m^{-1}
Std dev: n.a.
Mineral coating along open fractures: chlorite, calcite, adularia/hematite, clay minerals
Frequency of sealed fractures: 13.0 m^{-1}
Std dev: n.a.
Mineral filling along sealed fractures: calcite, chlorite, adularia/hematite

Deformation zone ZFMENE1192

Borehole intersections (metres along borehole)

KFM01A: DZ5 (267-285 m)
KFM01A: DZ2 (386-412 m)
KFM01C: DZ1 (23-48 m)

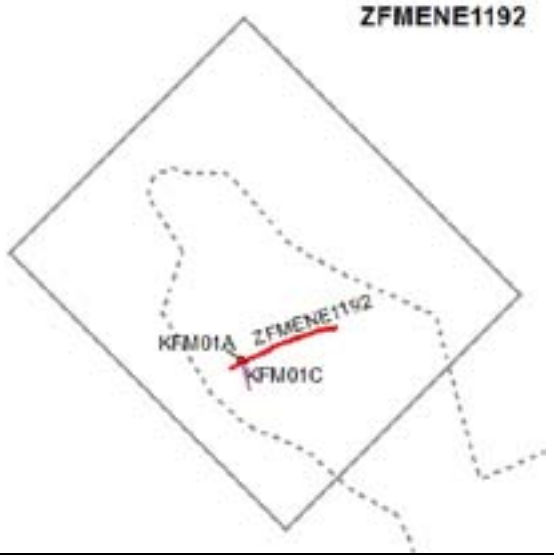

Deformation style, alteration and geometry

Deformation style: Brittle

Alteration: Oxidized bedrock with fine-grained hematite dissemination

Strike/dip (right-hand-rule): 064/88

Trace length at ground surface: 1,090 m

Model thickness / model thickness span : 3 m / 3-45 m

Measured thickness (-400 to -600 m elevation): No intersection

Comment:

Fractures in the deformation zone

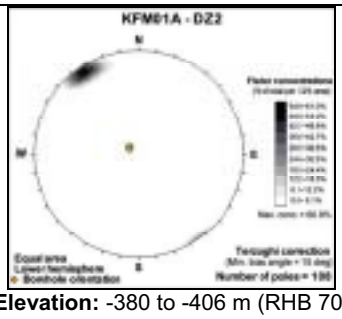

Elevation: -380 to -406 m (RHB 70)

Transmissivity (m^2/s)

General dip of T fractures: n.m.
Measured T range -400 to -600 m: 1.0E-10
Number of PFL-features: n.a.
Model T, depth range -400 to -500 m: 1.0E-10
Model T, depth range -500 to -600 m: 1.0E-10

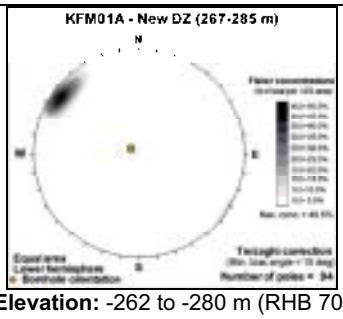

Elevation: -262 to -280 m (RHB 70)

Transmissivity (m^2/s)

General dip of T fractures: n.a.
Measured T range -400 to -600 m: No intersection
Number of PFL-features: n.a.
Model T, depth range -400 to -500 m: 1.0E-10
Model T, depth range -500 to -600 m: 1.0E-10

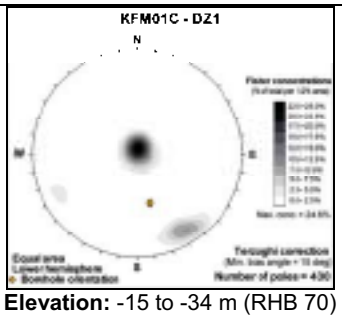

Elevation: -15 to -34 m (RHB 70)

Transmissivity (m^2/s)

General dip of T fractures: n.a.
Measured T range -400 to -600 m: No intersection
Number of PFL-features: n.a.
Model T, depth range -400 to -500 m: 1.0E-10
Model T, depth range -500 to -600 m: 1.0E-10

KFM01A (DZ2)

Engineering characteristics

Percentage of fault core: No data available along DZ2 and DZ5 in KFM01A to assess core and transition. Borehole KFM01C not included in fracture statistics due to interference with near-surface fracturing

Frequency of open fractures: 2.4 m^{-1}
Std dev: n.a.
Mineral coating along open fractures: chlorite, laumontite, calcite, adularia/hematite, pyrite

Frequency of sealed fractures: 2.4 m^{-1}
Std dev: n.a.
Mineral filling along sealed fractures: laumontite, adularia/hematite, chlorite, calcite

Deformation zone ZFMENE1208A

Borehole intersections (metres along borehole)

KFM07A: Part of DZ4 (857-897 m)
KFM09A: DZ1 (15-40 m)
KFM09B: Part of DZ1 (9-43 m)
HFM23: DZ1 (26-42 m)
HFM28: DZ1 (12-65 m)

Deformation style, alteration and geometry

Deformation style: Brittle

Alteration: Red-stained bedrock with fine-grained hematite dissemination

Strike/dip (right-hand-rule): 238/81

Trace length at ground surface: 1,081 m

Model thickness / model thickness span : 26 m / 3-45 m

Measured thickness (-400 to -600 m elevation): No intersection

Comment:

Fractures in the deformation zone

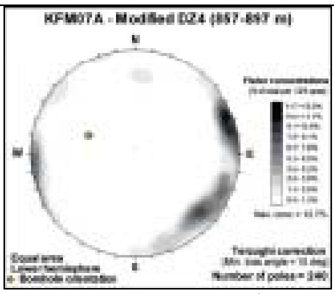

Elevation: -711 to -742 m (RHB 70)

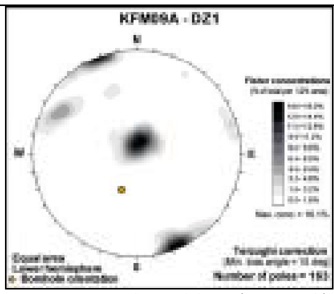

Elevation: -9 to -30 m (RHB 70)

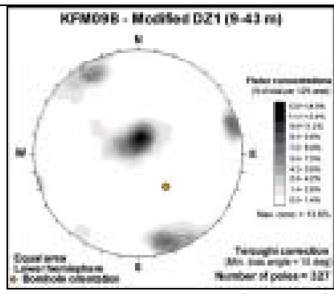

Elevation: -3 to -31 m (RHB 70)

Transmissivity (m^2/s)

General dip of T fractures: n.a.
Measured T range -400 to -600 m: No intersection
Number of PFL-features: n.a.
Model T, depth range -400 to -500 m: 2.6E-10
Model T, depth range -500 to -600 m: 1.0E-10

Transmissivity (m^2/s)

General dip of T fractures: n.a.
Measured T range -400 to -600 m: No intersection
Number of PFL-features: n.a.
Model T, depth range -400 to -500 m: 2.6E-10
Model T, depth range -500 to -600 m: 1.0E-10

Transmissivity (m^2/s)

General dip of T fractures: n.a.
Measured T range -400 to -600 m: No intersection
Number of PFL-features: n.a.
Model T, depth range -400 to -500 m: 2.6E-10
Model T, depth range -500 to -600 m: 1.0E-10

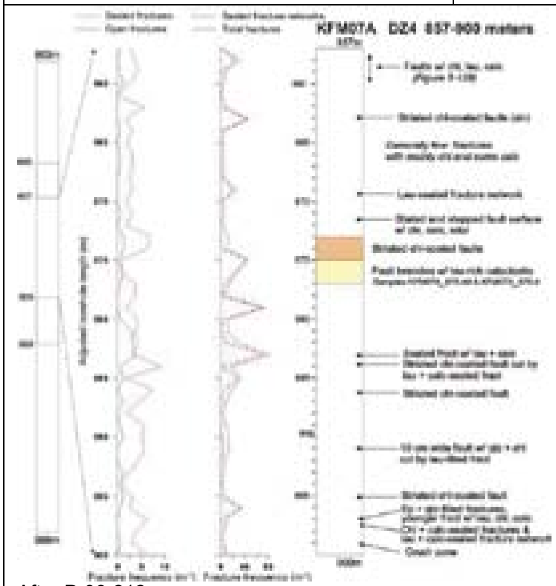

After P-06-212

Engineering characteristics

Percentage of fault core: 5.0% (P-06-212). Boreholes KFM09A and KFM09B not included in fracture statistics due to interference with near-surface fracturing

Transition part of zone:
Frequency of open fractures: 1.4 m^{-1}
Std dev: n.a.
Mineral coating along open fractures: calcite, chlorite, quartz, adularia/hematite, laumontite, pyrite, clay minerals
Frequency of sealed fractures: 14.7 m^{-1}
Std dev: n.a.
Mineral filling along sealed fractures: chlorite, laumontite, adularia/hematite, calcite, epidote, quartz, pyrite

Fault core:
Frequency of open fractures: 1.5 m^{-1}
Std dev: n.a.
Mineral coating along open fractures: chlorite, clay minerals, adularia/hematite
Frequency of sealed fractures: 36.0 m^{-1}
Std dev: n.a.
Mineral filling along sealed fractures: adularia/hematite, quartz, chlorite, epidote, calcite, laumontite

Deformation zone ZFMENE1208B

Borehole intersections (metres along borehole)

KFM07A: Part of DZ4 (803-840 m)
KFM09A: DZ2 (86-116 m)
KFM09B: Part of DZ1 (59-78 m)

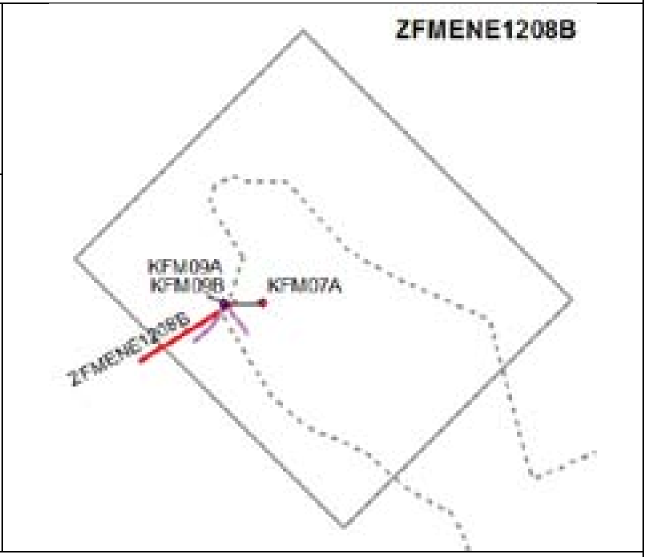

Deformation style, alteration and geometry

Deformation style: Brittle

Alteration: Red-stained bedrock with fine-grained hematite dissemination

Strike/dip (right-hand-rule): 238/81

Trace length at ground surface: 1,112 m

Model thickness / model thickness span : 13 m / 3-45 m

Measured thickness (-400 to -600 m elevation): No intersection

Comment:

Fractures in the deformation zone

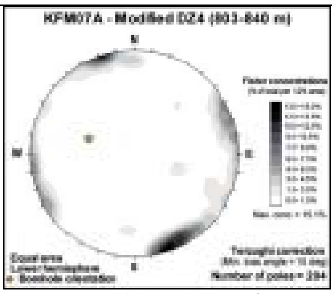

Elevation: -669 to -698 m (RHB 70)

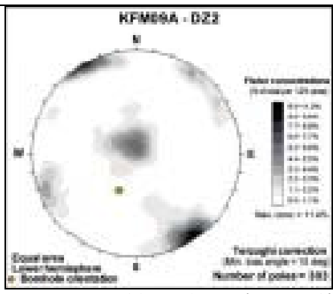

Elevation: -69 to -94 m (RHB 70)

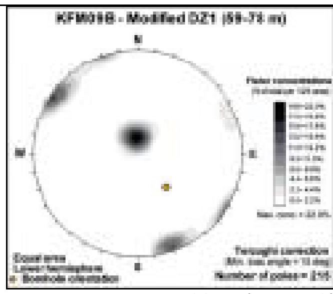

Elevation: -44 to -60 m (RHB 70)

Transmissivity (m^2/s) — KFM07A

General dip of T fractures: n.a.
Measured T range -400 to -600 m: No intersection
Number of PFL-features: n.a.
Model T, depth range -400 to -500 m: 5.0E-09
Model T, depth range -500 to -600 m: 1.9E-09

Transmissivity (m^2/s) — KFM09A

General dip of T fractures: n.a.
Measured T range -400 to -600 m: No intersection
Number of PFL-features: n.a.
Model T, depth range -400 to -500 m: 5.0E-09
Model T, depth range -500 to -600 m: 1.9E-09

Transmissivity (m^2/s) — KFM09B

General dip of T fractures: n.a.
Measured T range -400 to -600 m: No intersection
Number of PFL-features: n.a.
Model T, depth range -400 to -500 m: 5.0E-09
Model T, depth range -500 to -600 m: 1.9E-09

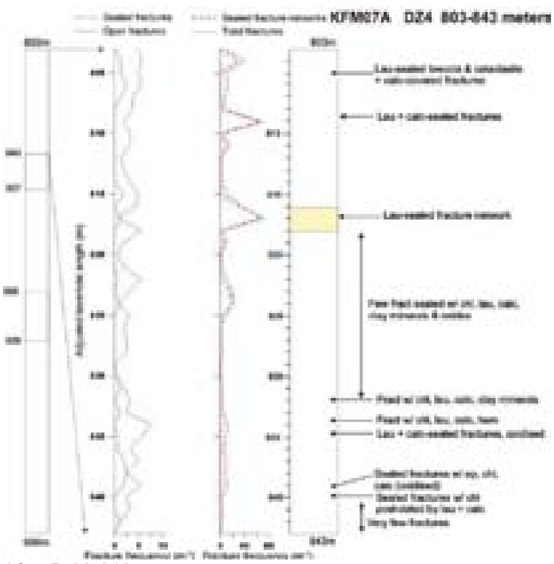

After P-06-212

Engineering characteristics

Percentage of fault core: 5.4% (P-06-212). Boreholes KFM09A and KFM09B not included in fracture statistics due to interference with near-surface fracturing

Transition part of zone:
Frequency of open fractures: 0.9 m^{-1}
Std dev: n.a.
Mineral coating along open fractures: calcite, chlorite, adularia/hematite, laumontite
Frequency of sealed fractures: 9.70 m^{-1}
Std dev: n.a.
Mineral filling along sealed fractures: laumontite, chlorite, calcite, adularia/hematite

Fault core:
Frequency of open fractures: 1.0 m^{-1}
Std dev: n.a.
Mineral coating along open fractures: adularia/hematite, quartz, clay minerals
Frequency of sealed fractures: 53.5 m^{-1}
Std dev: n.a.
Mineral filling along sealed fractures: adularia/hematite, laumontite, quartz, chlorite

Deformation zone ZFMENE2248

Borehole intersections (metres along borehole)

KFM08A: DZ5 and extension along borehole interval 840-843 m (775-843 m)

Deformation style, alteration and geometry

Deformation style: Brittle

Alteration: Red-stained bedrock with fine-grained hematite dissemination

Strike/dip (right-hand-rule): 234/80

Trace length at ground surface: 1,298 m

Model thickness / model thickness span : 38 m / 3-45 m

Measured thickness (-400 to -600 m elevation): No intersection

Comment:

Fractures in the deformation zone

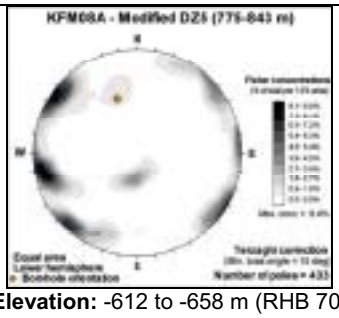

Elevation: -612 to -658 m (RHB 70)

Transmissivity (m^2/s)

General dip of T fractures: n.a.
Measured T range -400 to -600 m: No intersection
Number of PFL-features: n.a.
Model T, depth range -400 to -500 m: 6.0E-10
Model T, depth range -500 to -600 m: 2.2E-10

KFM08A (DZ5)

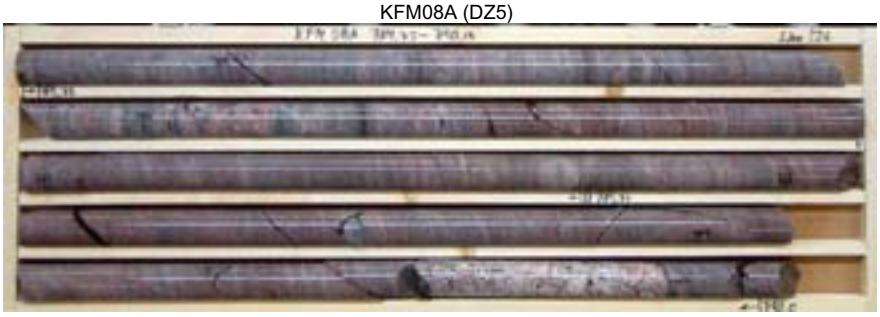

Engineering characteristics

Percentage of fault core: No data available along DZ5 in KFM08A to assess core and transition. No division made

Frequency of open fractures: 0.8 m^{-1}
Std dev: n.a.
Mineral coating along open fractures: chlorite, calcite, adularia/hematite, pyrite

Frequency of sealed fractures: 9.9 m^{-1}
Std dev: n.a.
Mineral filling along sealed fractures: chlorite, calcite, adularia/hematite

Deformation zone ZFMENE2254

Borehole intersections (metres along borehole)

KFM01A: DZ3 (639-684 m)

Deformation style, alteration and geometry

Deformation style: Brittle

Alteration: Red-stained bedrock with fine-grained hematite dissemination.

Strike/dip (right-hand-rule): 238/83

Trace length at ground surface: 1,021 m

Model thickness / model thickness span : 3 m / 3-45 m

Measured thickness (-400 to -600 m elevation): No intersection

Comment:

Fractures in the deformation zone

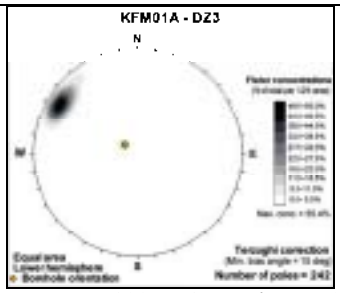

Elevation: -630 to -674 m (RHB 70)

Transmissivity (m^2/s)

General dip of T fractures: n.a.
Measured T range -400 to -600 m: No intersection
Number of PFL-features: n.a.
Model T, depth range -400 to -500 m: 7.4E-10
Model T, depth range -500 to -600 m: 2.7E-10

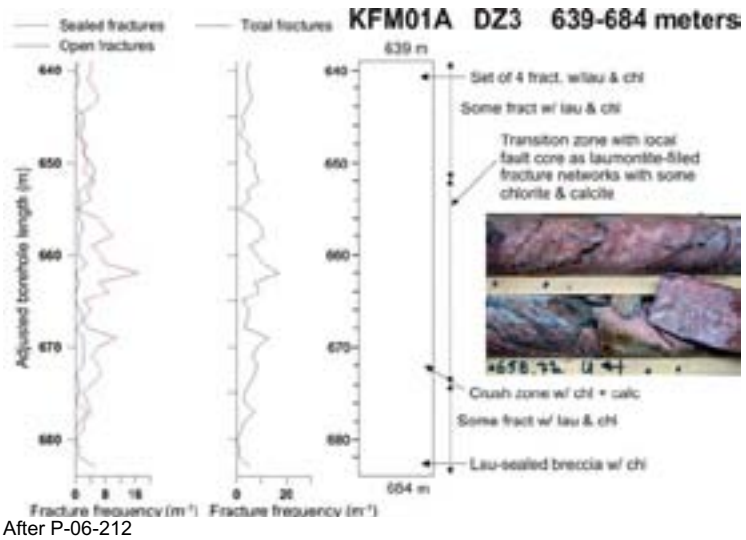

After P-06-212

Engineering characteristics

Percentage of fault core: Local fault core, position not specified (P-06-212). No division into transition and core

Frequency of open fractures: 1.2 m^{-1}
Std dev: n.a.
Mineral coating along open fractures: chlorite, laumontite, adularia/hematite

Frequency of sealed fractures: 4.3 m^{-1}
Std dev: n.a.
Mineral filling along sealed fractures: laumontite, chlorite, adularia/hematite

Deformation zone ZFMENE2320

Borehole intersections (metres along borehole)

KFM07B: DZ4 (225-245 m)
KFM07C: DZ2 (308-388 m) and DZ3 (429-439 m)
KFM08D: DZ7 (621-634 m)
KFM09B: DZ3 (363-413 m)

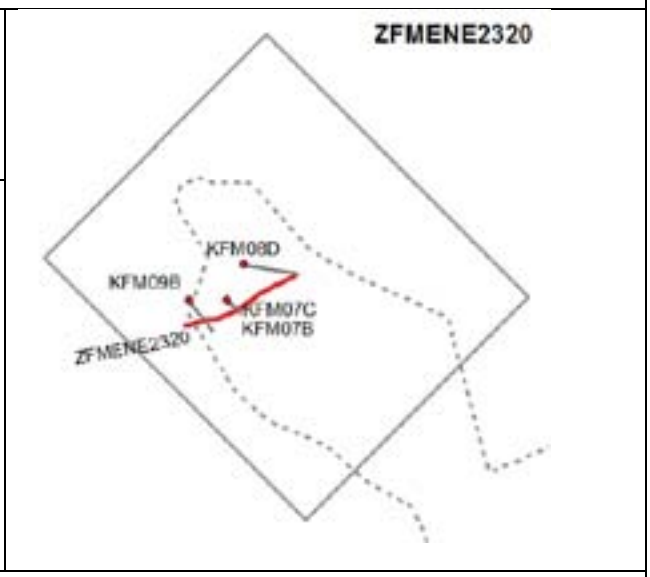

Deformation style, alteration and geometry

Deformation style: Brittle

Alteration: Red-stained bedrock with fine-grained hematite dissemination. Chloritised amphibolite along DZ3 in KFM07C. Vuggy rock with quartz dissolution at 382 m along DZ3 in KFM09B

Strike/dip (right-hand-rule): 244/81

Trace length at ground surface: 1,251 m

Model thickness / model thickness span : 20 m / 3-45 m

Measured thickness (-400 to -600 m elevation): No intersection

Comment: KFM08D only available after completion of geological model stage 2.2, i.e. not included in geological modelling work

Fractures in the deformation zone

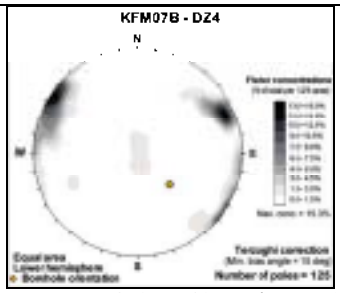

Elevation: -178 to -194 m (RHB 70)

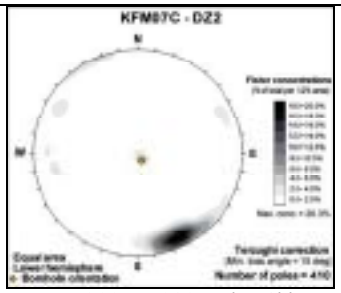

Elevation: -303 to -383 m (DZ2)(RHB 70)

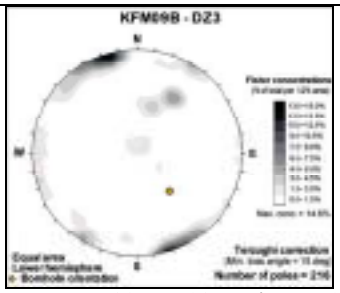

Elevation: -287 to -325 m (RHB 70)

Transmissivity (m^2/s)

General dip of T fractures: n.a.
Measured T range -400 to -600 m: No intersection
Number of PFL-features: n.a.
Model T, depth range -400 to -500 m: 5.2E-10
Model T, depth range -500 to -600 m: 2.0E-10

Transmissivity (m^2/s)

General dip of T fractures: steep
Measured T range -400 to -600 m: 1.00E-10
Number of PFL-features: 0
Model T, depth range -400 to -500 m: 5.2E-10
Model T, depth range -500 to -600 m: 2.0E-10

Transmissivity (m^2/s)

General dip of T fractures: n.a.
Measured T range -400 to -600 m: No intersection
Number of PFL-features: n.a.
Model T, depth range -400 to -500 m: 5.2E-10
Model T, depth range -500 to -600 m: 2.0E-10

KFM07C (DZ2)

Engineering characteristics

Percentage of fault core: 9.2% (P-07-101, P-07-111)

Transition part of zone:
Frequency of open fractures: 1.7 m^{-1}
Std dev: 0.4
Mineral coating along open fractures: calcite, chlorite, laumontite, clay minerals, pyrite, adularia/hematite
Frequency of sealed fractures: 10.8 m^{-1}
Std dev: 9.7
Mineral filling along sealed fractures: calcite, laumontite, chlorite, adularia/hematite

Fault core:
Frequency of open fractures: 2.1 m^{-1}
Std dev: 1.6
Mineral coating along open fractures: calcite, chlorite, laumontite, clay minerals, quartz, pyrite
Frequency of sealed fractures: 32.4 m^{-1}
Std dev: 15.4
Mineral filling along sealed fractures: laumontite, calcite, chlorite, adularia/hematite, pyrite

Deformation zone ZFMENE2325A

Borehole intersections (metres along borehole)

KFM09B: DZ4 (520-550 m)

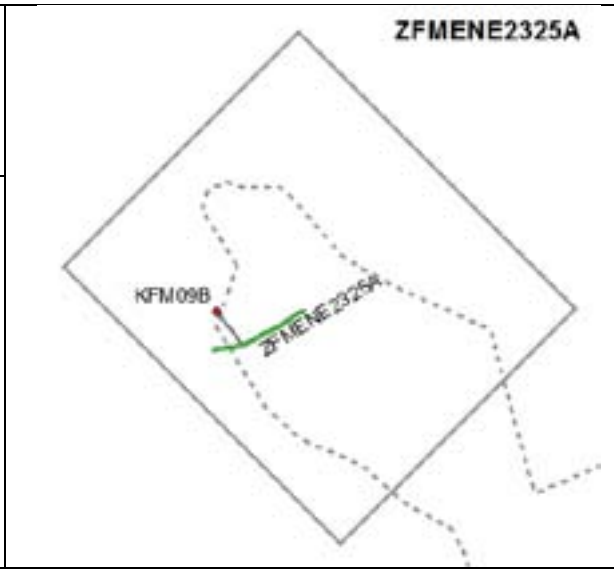

Deformation style, alteration and geometry

Deformation style: Brittle

Alteration: Red-stained bedrock with fine-grained hematite dissemination

Strike/dip (right-hand-rule): 246/82

Trace length at ground surface: 963 m

Model thickness / model thickness span : 23 m / 2-43 m

Measured thickness (-400 to -600 m elevation): 23 m

Comment:

Fractures in the deformation zone

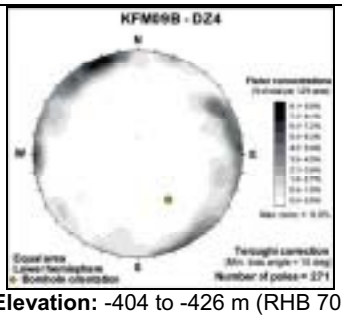

Elevation: -404 to -426 m (RHB 70)

Transmissivity (m^2/s)

General dip of T fractures: n.a.
Measured T range -400 to -600 m: 1.10E-09
Number of PFL-features: n.a.
Model T, depth range -400 to -500 m: 1.3E-10
Model T, depth range -500 to -600 m: 2.7E-10

KFM09B (DZ4)

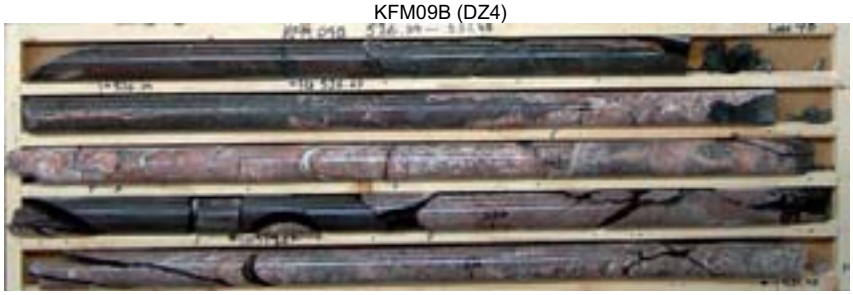

Engineering characteristics

Percentage of fault core: 6.7% (P-07-101)

Transition part of zone:
Frequency of open fractures: 0.9 m^{-1}
Std dev: n.a.
Mineral coating along open fractures: chlorite, calcite, adularia/hematite, clay minerals, laumontite, pyrite
Frequency of sealed fractures: 22.6 m^{-1}
Std dev: n.a.
Mineral filling along sealed fractures: calcite, chlorite, laumontite, adularia/hematite, epidote

Fault core:
Frequency of open fractures: 6.5 m^{-1}
Std dev: n.a.
Mineral coating along open fractures: chlorite, calcite, adularia/hematite, clay minerals
Frequency of sealed fractures: 68.0 m^{-1}
Std dev: n.a.
Mineral filling along sealed fractures: calcite, adularia/hematite, clay minerals, chlorite

Deformation zone ZFMENE2325B

Borehole intersections (metres along borehole)

KFM09B: DZ5 (561-574 m)

Deformation style, alteration and geometry

Deformation style: Brittle

Alteration: Red-stained bedrock with fine-grained hematite dissemination. Vuggy rock with quartz dissolution between 568 and 574 m along DZ5 in KFM09B.

Strike/dip (right-hand-rule): 245/81

Trace length at ground surface: 553 m

Model thickness / model thickness span : 10 m / 2-43 m

Measured thickness (-400 to -600 m elevation): 10 m

Comment:

Fractures in the deformation zone

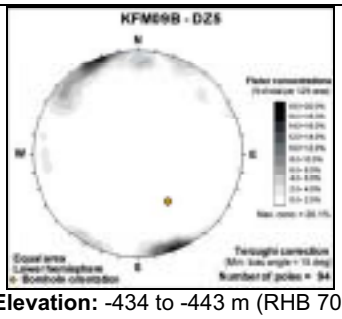

Elevation: -434 to -443 m (RHB 70)

Transmissivity (m^2/s)

General dip of T fractures: n.a.
Measured T range -400 to -600 m: 2.86E-07
Number of PFL-features: n.a.
Model T, depth range -400 to -500 m: 2.4E-07
Model T, depth range -500 to -600 m: 8.9E-08

KFM09B (DZ5)

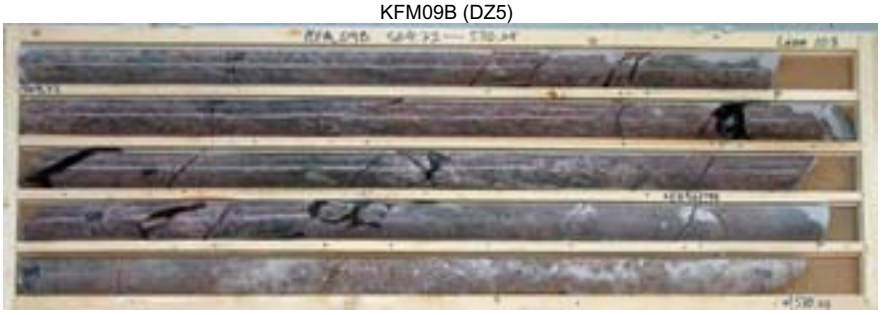

Engineering characteristics

Percentage of fault core: No fault core recognised along DZ5 in KFM09B (P-07-101). No division into transition and core

Frequency of open fractures: 3.3 m^{-1}
Std dev: n.a.
Mineral coating along open fractures: chlorite, calcite, clay minerals, quartz

Frequency of sealed fractures: 7.8 m^{-1}
Std dev: n.a.
Mineral filling along sealed fractures: chlorite, calcite, quartz, epidote, clay minerals

Deformation zone ZFMENE2383

Borehole intersections (metres along borehole)

KFM05A: DZ5 and extension along borehole interval 950-992 m (936-992 m)

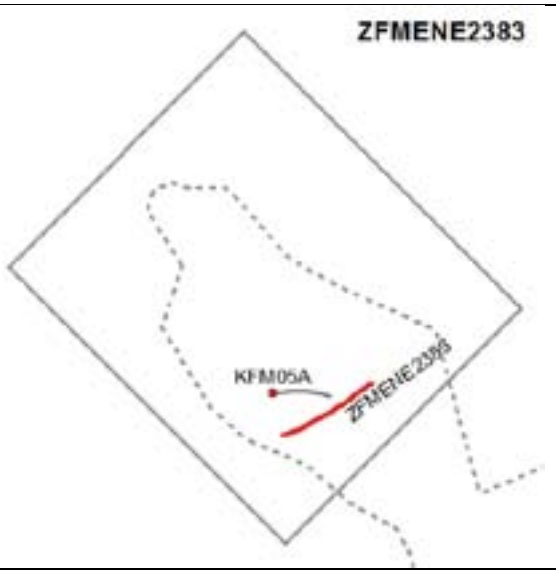

Deformation style, alteration and geometry

Deformation style: Brittle

Alteration: Red-stained bedrock with fine-grained hematite dissemination

Strike/dip (right-hand-rule): 239/80

Trace length at ground surface: 1,000 m

Model thickness / model thickness span : 34 m / 3-45 m

Measured thickness (-400 to -600 m elevation): No intersection

Comment:

Fractures in the deformation zone

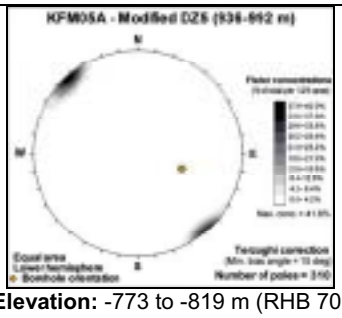

Elevation: -773 to -819 m (RHB 70)

Transmissivity (m^2/s)

General dip of T fractures: n.a.
Measured T range -400 to -600 m: No intersection
Number of PFL-features: n.a.
Model T, depth range -400 to -500 m: 3.1E-09
Model T, depth range -500 to -600 m: 1.1E-09

KFM05A (DZ5)

Engineering characteristics

Percentage of fault core: No data available along DZ5 (and extension) in KFM05A to assess core and transition. No division made

Frequency of open fractures: 0.7 m^{-1}
Std dev: n.a.
Mineral coating along open fractures: calcite, chlorite, adularia/hematite

Frequency of sealed fractures: 9.9 m^{-1}
Std dev: n.a.
Mineral filling along sealed fractures: calcite, adularia/hematite, laumontite

Deformation zone ZFMENE2403

Borehole intersections (metres along borehole)

KFM10A: DZ4 (275-284 m)

Deformation style, alteration and geometry

Deformation style: Brittle

Alteration: Red-stained bedrock with fine-grained hematite dissemination

Strike/dip (right-hand-rule): 062/90

Trace length at ground surface: 958 m

Model thickness / model thickness span : 4 m / 2-43 m

Measured thickness (-400 to -600 m elevation): No intersection

Comment:

Fractures in the deformation zone

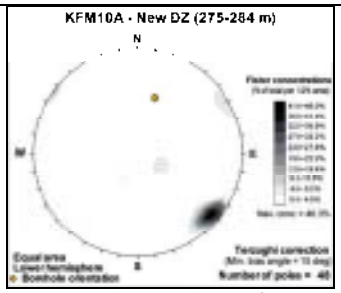

Elevation: -197 to -203 m (RHB 70)

Transmissivity (m^2/s)

General dip of T fractures: n.a.
Measured T range -400 to -600 m: No intersection
Number of PFL-features: n.a.
Model T, depth range -400 to -500 m: 1.0E-10
Model T, depth range -500 to -600 m: 1.0E-10

KFM10A (DZ4)

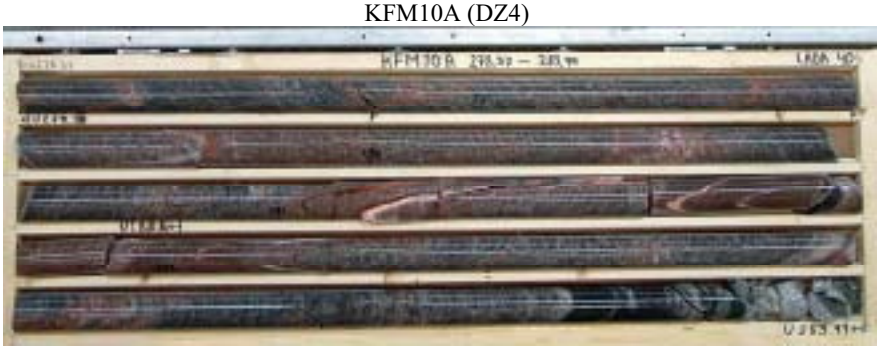

Engineering characteristics

Percentage of fault core: No data available along DZ4 in KFM10A to assess core and transition. No division made

Frequency of open fractures: 1.6 m^{-1}
Std dev: n.a.
Mineral coating along open fractures: calcite, chlorite, adularia/hematite, laumontite

Frequency of sealed fractures: 24.7 m^{-1}
Std dev: n.a.
Mineral filling along sealed fractures: laumontite, calcite, adularia/hematite, prehnite

Deformation zone ZFMNE2282

Borehole intersections (metres along borehole)

KFM05A: DZ2 and extension along borehole interval 395-416 m (395-436 m)

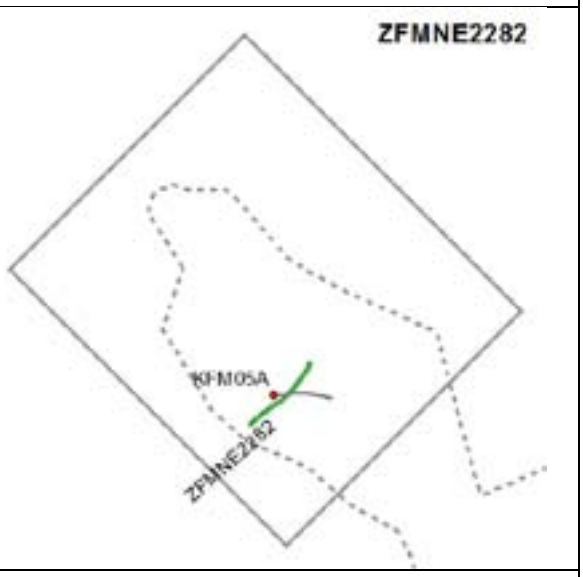

Deformation style, alteration and geometry

Deformation style: Brittle

Alteration: Red-stained bedrock with fine-grained hematite dissemination

Strike/dip (right-hand-rule): 046/81

Trace length at ground surface: 842 m.

Model thickness / model thickness span : 11 m / 2-43 m

Measured thickness (-400 to -600 m elevation): No intersection

Comment:

Fractures in the deformation zone

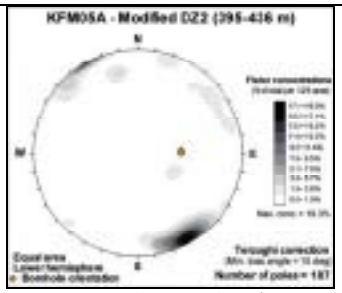

Elevation: -332 to -366 m (RHB 70)

Transmissivity (m^2/s)

General dip of T fractures: n.a.
Measured T range -400 to -600 m: No intersection
Number of PFL-features: n.a.
Model T, depth range -400 to -500 m: 1.0E-10
Model T, depth range -500 to -600 m: 1.0E-10

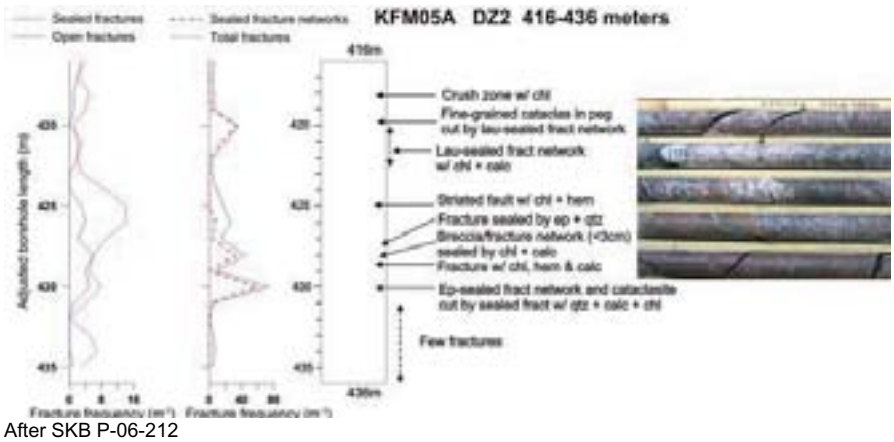

After SKB P-06-212

Engineering characteristics

Percentage of fault core: No fault core recognised along DZ2 in KFM05A (P-06-212). No division into transition and core

Frequency of open fractures: 1.2 m^{-1}
Std dev: n.a.
Mineral coating along open fractures: chlorite, calcite, clay minerals, laumontite

Frequency of sealed fractures: 10.4 m^{-1}
Std dev: n.a.
Mineral filling along sealed fractures: calcite, chlorite, adularia/hematite, prehnite, laumontite

Deformation zone ZFMNNE0725

Borehole intersections (metres along borehole)

KFM06A: DZ7 (740-775 m)

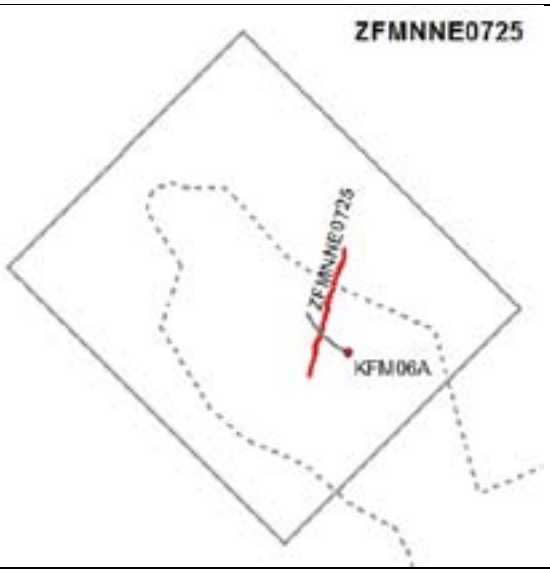

Deformation style, alteration and geometry

Deformation style: Brittle

Alteration: Red-stained bedrock with fine-grained hematite dissemination

Strike/dip (right-hand-rule): 196/84

Trace length at ground surface: 1,274 m

Model thickness / model thickness span : 12 m / 3-45 m

Measured thickness (-400 to -600 m elevation): No intersection

Comment:

Fractures in the deformation zone

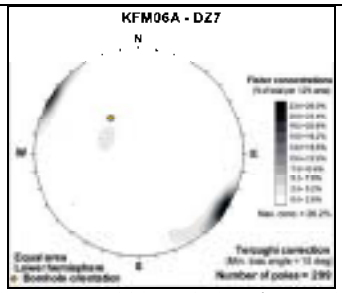

Elevation: -620 to -649 m (RHB 70)

Transmissivity (m^2/s)

General dip of T fractures: n.a.
Measured T range -400 to -600 m: No intersection
Number of PFL-features: n.a.
Model T, depth range -400 to -500 m: 2.1E-06
Model T, depth range -500 to -600 m: 7.8E-07

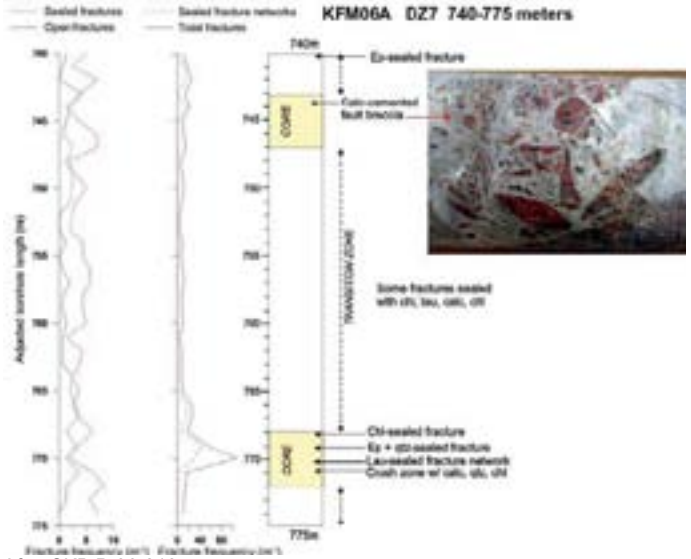

After SKB P-06-212

Engineering characteristics

Percentage of fault core: 25.7% (P-06-212)

Transition part of zone:
Frequency of open fractures: 1.9 m^{-1}
Std dev: n.a.
Mineral coating along open fractures: chlorite, calcite, adularia/hematite, laumontite

Frequency of sealed fractures: 8.5 m^{-1}
Std dev: n.a.
Mineral filling along sealed fractures: chlorite, calcite, quartz, adularia/hematite

Fault core:
Frequency of open fractures: 11.7 m^{-1}
Std dev: n.a.
Mineral coating along open fractures: calcite, chlorite, clay minerals

Frequency of sealed fractures: 19.7 m^{-1}
Std dev: n.a.
Mineral filling along sealed fractures: chlorite, calcite, adularia/hematite, quartz, epidote

Deformation zone ZFMNNE2008

Borehole intersections (metres along borehole)

KFM06C: DZ6 (283-306 m)

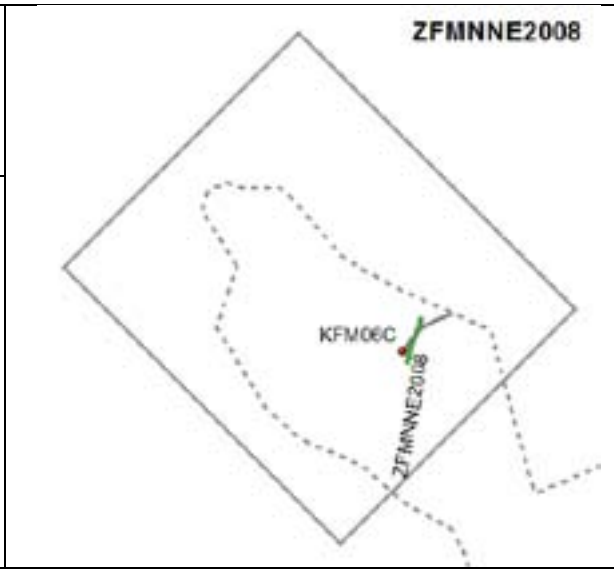

Deformation style, alteration and geometry

Deformation style: Brittle

Alteration: Red-stained bedrock with fine-grained hematite dissemination

Strike/dip (right-hand-rule): 198/84

Trace length at ground surface: 441 m

Model thickness / model thickness span : 6 m / 2-30 m

Measured thickness (-400 to -600 m elevation): No intersection

Comment:

Fractures in the deformation zone

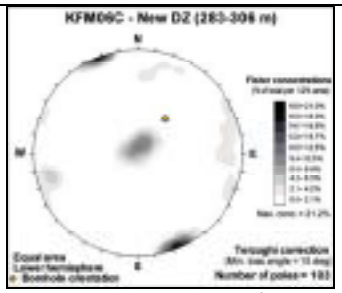

Elevation: -235 to -254 m (RHB 70)

Transmissivity (m^2/s)

General dip of T fractures: n.a.
Measured T range -400 to -600 m: No intersection
Number of PFL-features: n.a.
Model T, depth range -400 to -500 m: 4.4E-08
Model T, depth range -500 to -600 m: 1.6E-08

Engineering characteristics

Percentage of fault core: No data available along DZ6 in KFM06C to assess core and transition. No division made

Frequency of open fractures: 2.5 m^{-1}
Std dev: n.a.
Mineral coating along open fractures: chlorite, calcite, adularia/hematite, clay minerals, pyrite,

Frequency of sealed fractures: 4.3 m^{-1}
Std dev: n.a.
Mineral filling along sealed fractures: calcite, chlorite, adularia/hematite

Deformation zone ZFMNNE2255

Borehole intersections (metres along borehole)

KFM06A: DZ5 (619-624 m)

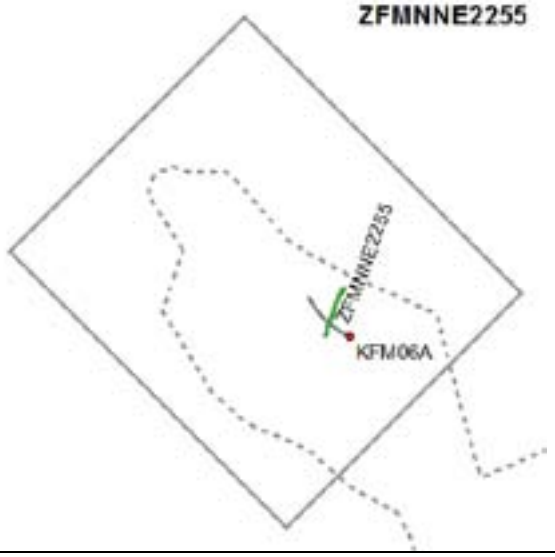

Deformation style. alteration and geometry

Deformation style: Brittle

Alteration: Red-stained bedrock with fine-grained hematite dissemination

Strike/dip (right-hand-rule): 200/81

Trace length at ground surface: 507 m

Model thickness / model thickness span : 2 m / 2-43 m

Measured thickness (-400 to -600 m elevation): 2 m

Comment:

Fractures in the deformation zone

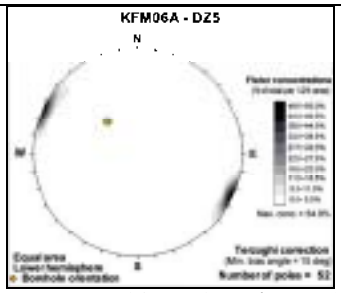

Elevation: -521 to -525 m (RHB 70)

Transmissivity (m^2/s)

General dip of T fractures: n.a.
Measured T range -400 to -600 m: 2.61E-09
Number of PFL-features: 1
Model T, depth range -400 to -500 m: 8.7E-10
Model T, depth range -500 to -600 m: 3.2E-10

KFM06A (DZ5)

Engineering characteristics

Percentage of fault core: No data available along DZ5 in KFM06A to assess core and transition. No division made

Frequency of open fractures: 3.2 m^{-1}
Std dev: n.a.
Mineral coating along open fractures: chlorite, calcite, quartz, clay minerals, pyrite

Frequency of sealed fractures: 11.6 m^{-1}
Std dev: n.a.
Mineral filling along sealed fractures: quartz, chlorite, calcite

Deformation zone ZFMNNE2263

Borehole intersections (metres along borehole)

KFM06C: DZ3 (415-489 m)

Deformation style, alteration and geometry

Deformation style: Brittle

Alteration: Red-stained bedrock with fine-grained hematite dissemination. Vuggy rock with quartz dissolution between 451-452 m along DZ3 in KFM06C

Strike/dip (right-hand-rule): 197/63

Trace length at ground surface: 446 m

Model thickness / model thickness span : 30 m / 2-30 m

Measured thickness (-400 to -600 m elevation): No intersection

Comment:

Fractures in the deformation zone

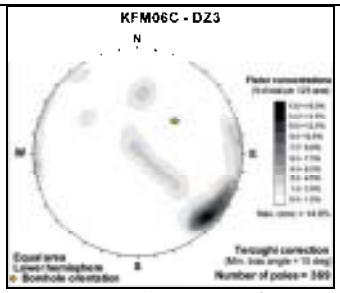

Elevation: -341 to -399 m (RHB 70)

Transmissivity (m^2/s)

General dip of T fractures: steep
Measured T range -400 to -600 m: 1.84E-07
Number of PFL-features: n.a.
Model T, depth range -400 to -500 m: 8.2E-08
Model T, depth range -500 to -600 m: 3.1E-08

KFM06C (DZ3)

Engineering characteristics

Percentage of fault core: No fault core recognised along DZ3 in KFM06C (P-07-101). No division into transition and core

Frequency of open fractures: 1.5 m^{-1}
Std dev: n.a.
Mineral coating along open fractures: chlorite, calcite, clay minerals, adularia/hematite

Frequency of sealed fractures: 23.7 m^{-1}
Std dev: n.a.
Mineral filling along sealed fractures: adularia/hematite, calcite, chlorite, quartz

Deformation zone ZFMNNE2273

Borehole intersections (metres along borehole)

KFM06A: DZ12 (518-545 m)

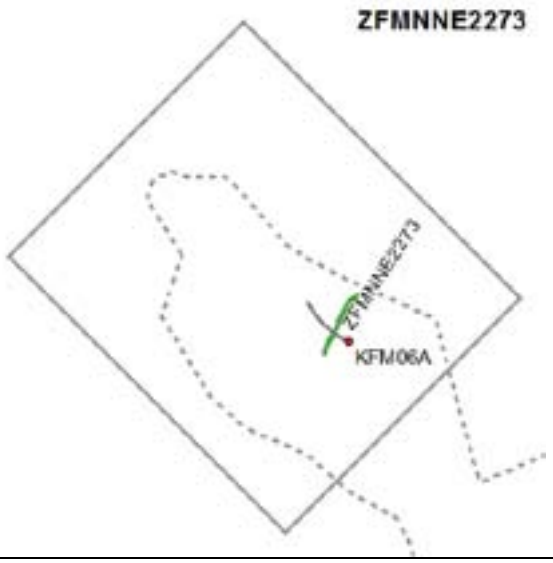

Deformation style, alteration and geometry

Deformation style: Brittle

Alteration: Red-stained bedrock with fine-grained hematite dissemination

Strike/dip (right-hand-rule): 209/77

Trace length at ground surface: 657 m

Model thickness / model thickness span : 9 m / 2-43 m

Measured thickness (-400 to -600 m elevation): 9 m

Comment:

Fractures in the deformation zone

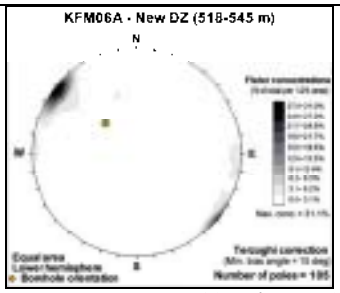

Elevation: -474 to -460 m (RHB 70)

Transmissivity (m^2/s)

General dip of T fractures: steep
Measured T range -400 to -600 m: 1.00E-10
Number of PFL-features: 0
Model T, depth range -400 to -500 m: 1.0E-10
Model T, depth range -500 to -600 m: 1.0E-10

KFM06A (DZ12)

Engineering characteristics

Percentage of fault core: No data available along DZ12 in KFM06A to assess core and transition. No division made

Frequency of open fractures: 1.1 m^{-1}
Std dev: n.a.
Mineral coating along open fractures: chlorite, calcite

Frequency of sealed fractures: 4.4 m^{-1}
Std dev: n.a.
Mineral filling along sealed fractures: chlorite, calcite, adularia/hematite

Deformation zone ZFMNNE2280

Borehole intersections (metres along borehole)

KFM06A: DZ11 (950-990 m)

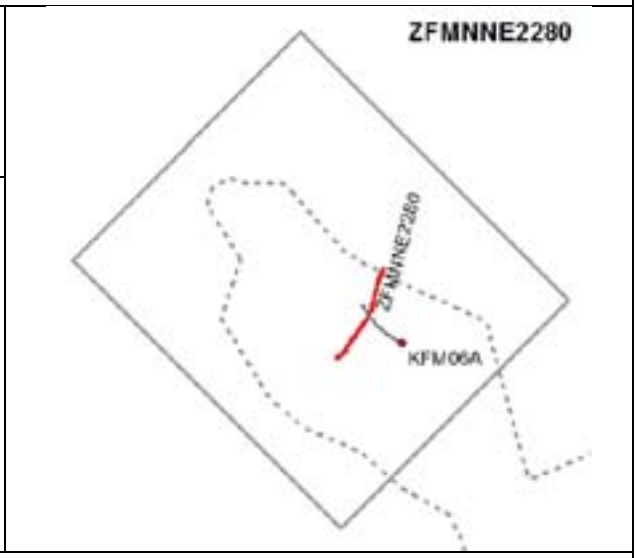

Deformation style, alteration and geometry

Deformation style: Brittle

Alteration: Red-stained bedrock with fine-grained hematite dissemination

Strike/dip (right-hand-rule): 206/84

Trace length at ground surface: 1,035 m

Model thickness / model thickness span : 14 m / 3-45 m

Measured thickness (-400 to -600 m elevation): No intersection

Comment:

Fractures in the deformation zone

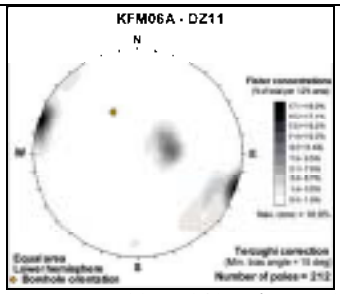

Elevation: -788 to -819 m (RHB 70)

Transmissivity (m^2/s)

General dip of T fractures: n.a.
Measured T range -400 to -600 m: No intersection
Number of PFL-features: n.a.
Model T, depth range -400 to -500 m: 3.3E-09
Model T, depth range -500 to -600 m: 1.2E-09

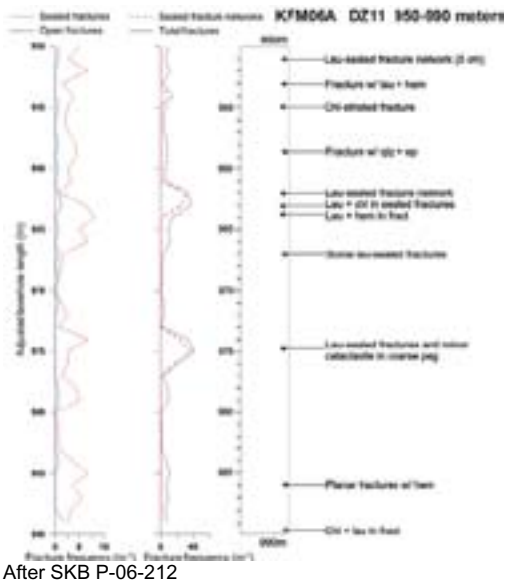

After SKB P-06-212

Engineering characteristics

Percentage of fault core: 12.5% (P-06-212)

Transition part of zone:
Frequency of open fractures: 0.4 m^{-1}
Std dev: n.a.
Mineral coating along open fractures: chlorite, calcite, laumontite, prehnite

Frequency of sealed fractures: 5.1 m^{-1}
Std dev: n.a.
Mineral filling along sealed fractures: chlorite, adularia/hematite, laumontite, calcite, quartz

Fault core:
Frequency of open fractures: 0.6 m^{-1}
Std dev: n.a.
Mineral coating along open fractures: adularia/hematite, laumontite, calcite, clay minerals

Frequency of sealed fractures: 33.8 m^{-1}
Std dev: n.a.
Mineral filling along sealed fractures: adularia/hematite, chlorite, laumontite, calcite, prehnite

Deformation zone ZFMNNE2293

Borehole intersections (metres along borehole)

KFM08D: DZ9 (737-749 m)

Deformation style, alteration and geometry

Deformation style: Brittle

Alteration: Red-stained bedrock with fine-grained hematite dissemination

Strike/dip (right-hand-rule): 208/80

Trace length at ground surface: 996 m

Model thickness / model thickness span : 15 m / 2-43 m

Measured thickness (-400 to -600 m elevation): 15 m

Comment: KFM08D only available after completion of geological model stage 2.2, i.e. not included in geological modelling work

Fractures in the deformation zone

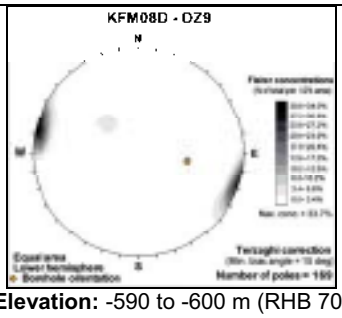

Elevation: -590 to -600 m (RHB 70)

Transmissivity (m^2/s)

General dip of T fractures: n.a.
Measured T range -400 to -600 m: No intersection
Number of PFL-features: n.a.
Model T, depth range -400 to -500 m: 1.6E-08
Model T, depth range -500 to -600 m: 5.9E-09

KFM08D (DZ9)

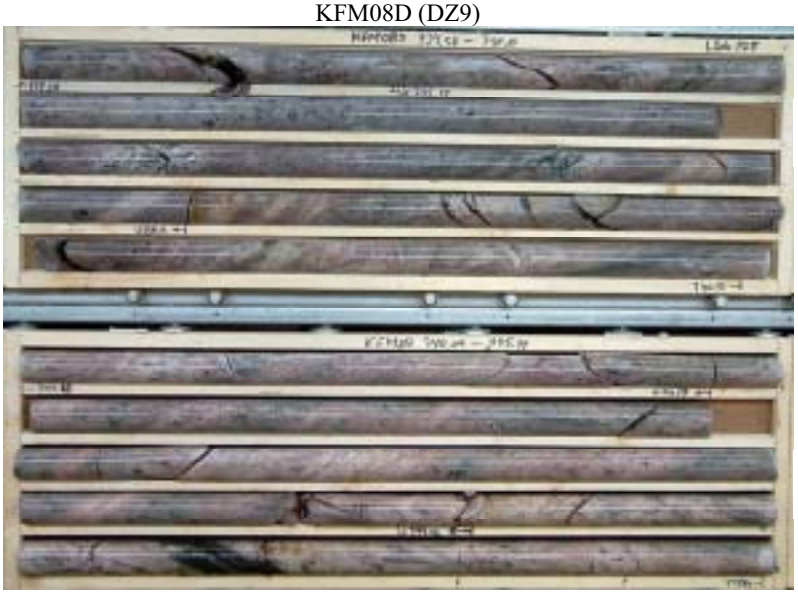

Engineering characteristics

Percentage of fault core: No data available along DZ11 in KFM08D to assess core and transition. No division made

Frequency of open fractures: 2.7 m^{-1}
Std dev: n.a.
Mineral coating along open fractures: calcite, chlorite, adularia/hematite, clay minerals

Frequency of sealed fractures: 15.6 m^{-1}
Std dev: n.a.
Mineral filling along sealed fractures: calcite, adularia/hematite, chlorite, quartz

Deformation zone ZFMNNE2300

Borehole intersections (metres along borehole)

KFM08D: DZ12 (903 m and beneath the borehole length)

Deformation style, alteration and geometry

Deformation style: Brittle

Alteration: Red-stained bedrock with fine-grained hematite dissemination

Strike/dip (right-hand-rule): 208/80

Trace length at ground surface: 946 m

Model thickness / model thickness span : 10 m / 2-43 m

Measured thickness (-400 to -600 m elevation): No intersection

Comment: KFM08D only available after completion of geological model stage 2.2, i.e. not included in geological modelling work

Fractures in the deformation zone

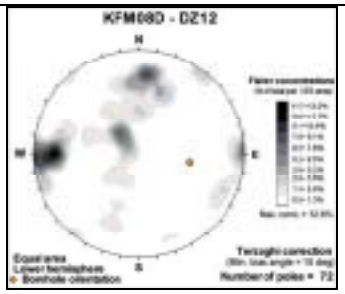

Elevation: -719 m to beneath the borehole length (RHB 70)

Transmissivity (m^2/s)

General dip of T fractures: n.a.
Measured T range -400 to -600 m: No intersection
Number of PFL-features: n.a.
Model T, depth range -400 to -500 m: 1.6E-08
Model T, depth range -500 to -600 m: 5.9E-09

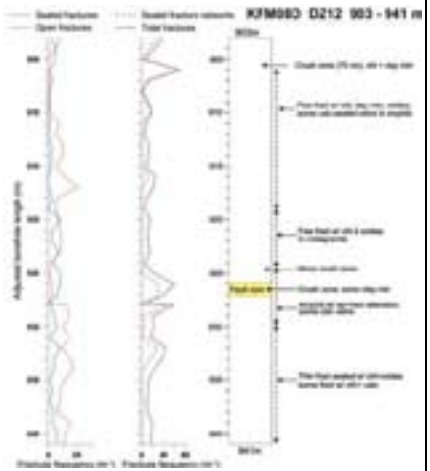

After SKB P-07-111

KFM08D (DZ12)

Engineering characteristics

Percentage of fault core: 2.6% (P-07-111)

Transition part of zone:
Frequency of open fractures: 3.7 m^{-1}
Std dev: n.a.
Mineral coating along open fractures: chlorite, clay minerals, calcite, adularia/hematite
Frequency of sealed fractures: 16.2 m^{-1}
Std dev: n.a.
Mineral filling along sealed fractures: calcite, adularia/hematite, quartz, chlorite

Fault core:
Frequency of open fractures: 20.0 m^{-1}
Std dev: n.a.
Mineral coating along open fractures: clay minerals, adularia/hematite, chlorite
Frequency of sealed fractures: 1.0 m^{-1}
Std dev: n.a.
Mineral filling along sealed fractures: adularia/hematite, chlorite, clay minerals

Deformation zone ZFMNNE2308

Borehole intersections (metres along borehole)

KFM08D: DZ8 (644-689 m)

Deformation style, alteration and geometry

Deformation style: Brittle

Alteration: Red-stained bedrock with fine-grained hematite dissemination

Strike/dip (right-hand-rule): 214/80

Trace length at ground surface: 1,419 m

Model thickness / model thickness span : 15 m / 3-45 m

Measured thickness (-400 to -600 m elevation): n.a. See comment below

Comment: KFM08D only available after completion of geological model stage 2.2, i.e. not included in geological modelling work

Fractures in the deformation zone

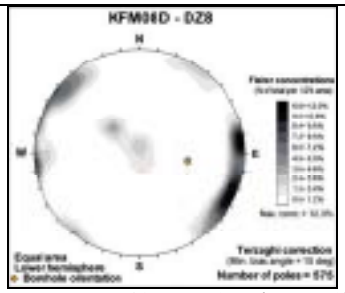

Elevation: -518 to -553 m (RHB 70)

Transmissivity (m^2/s)

General dip of T fractures: steep
Measured T range -400 to -600 m: 1.9E-07
Number of PFL-features: 3
Model T, depth range -400 to -500 m: 1.6E-08
Model T, depth range -500 to -600 m: 5.9E-09

KFM08D (DZ8)

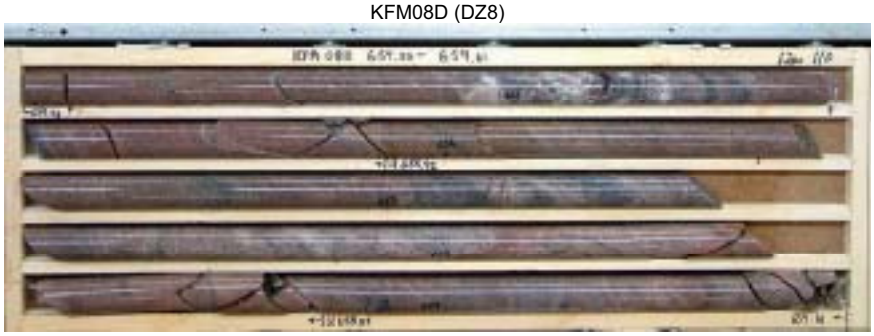

Engineering characteristics

Percentage of fault core: No data available along DZ8 in KFM08D to assess core and transition. No division made

Frequency of open fractures: 3.2 m^{-1}
Std dev: n.a.
Mineral coating along open fractures: chlorite, calcite, quartz, clay minerals

Frequency of sealed fractures: 15.9 m^{-1}
Std dev: n.a.
Mineral filling along sealed fractures: chlorite, calcite, quartz, adularia/hematite

Deformation zone ZFMNNE2309

Borehole intersections (metres along borehole)

KFM08D: DZ5 (546-571 m)

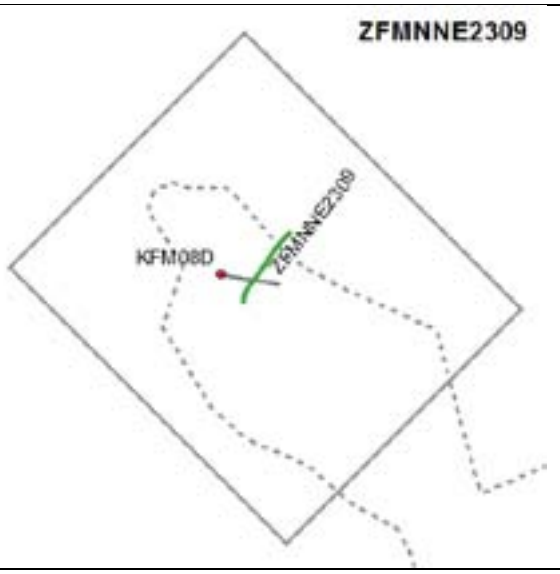

Deformation style, alteration and geometry

Deformation style: Brittle

Alteration: Red-stained bedrock with fine-grained hematite dissemination

Strike/dip (right-hand-rule): 215/80

Trace length at ground surface: 804 m

Model thickness / model thickness span : 10 m / 2-43 m

Measured thickness (-400 to -600 m elevation): n.a. See comment below

Comment: KFM08D only available after completion of geological model stage 2.2, i.e. not included in geological modelling work

Fractures in the deformation zone

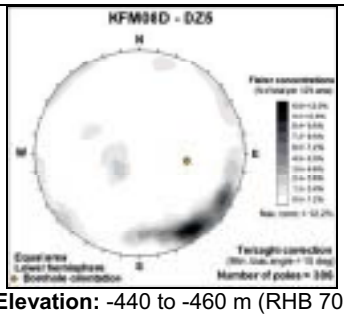

Elevation: -440 to -460 m (RHB 70)

Transmissivity (m^2/s)

General dip of T fractures: n.a.
Measured T range -400 to -600 m: 1E-10
Number of PFL-features: 0
Model T, depth range -400 to -500 m: 1.6E-08
Model T, depth range -500 to -600 m: 5.9E-09

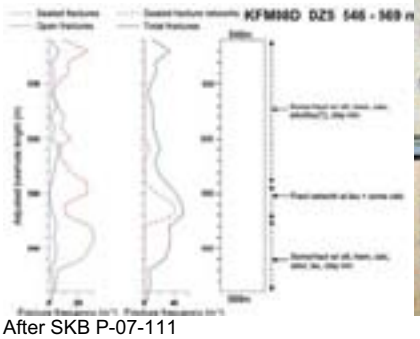

After SKB P-07-111

KFM08D (DZ5)

Engineering characteristics

Percentage of fault core: No fault core recognised along DZ5 in KFM08D (P-07-111). No division into transition and core

Frequency of open fractures: 3.1 m^{-1}
Std dev: n.a.
Mineral coating along open fractures: chlorite, calcite, clay minerals, adularia/hematite, laumontite

Frequency of sealed fractures: 17.6 m^{-1}
Std dev: n.a.
Mineral filling along sealed fractures: adularia/hematite, chlorite, calcite

Deformation zone ZFMNNE2312

Borehole intersections (metres along borehole)

KFM08C: DZ2 (419-542 m)
HFM38: DZ1 (149-164 m)

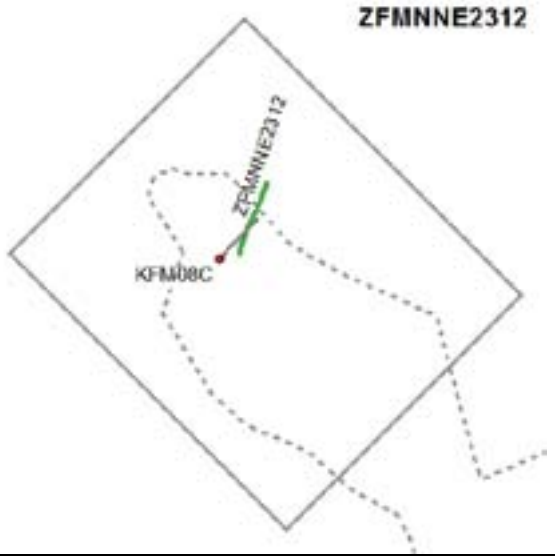

Deformation style, alteration and geometry

Deformation style: Brittle

Alteration: Red-stained bedrock with fine-grained hematite dissemination. Vuggy rock with quartz dissolution in the borehole intervals 454-463 m, 497-499 m, and 511-532 m along DZ2 in KFM08C

Strike/dip (right-hand-rule): 202/84

Trace length at ground surface: 742 m.

Model thickness / model thickness span : 43 m / 2-43 m

Measured thickness (-400 to -600 m elevation): 43 m

Comment:

Fractures in the deformation zone

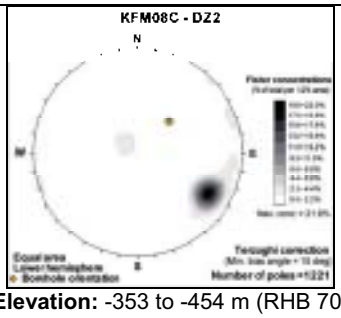

Elevation: -353 to -454 m (RHB 70)

Transmissivity (m^2/s)

General dip of T fractures: steep
Measured T range -400 to -600 m: 1.76E-07
Number of PFL-features: 13
Model T, depth range -400 to -500 m: 1.1E-07
Model T, depth range -500 to -600 m: 4.1E-08

KFM08C (DZ2)

Engineering characteristics

Percentage of fault core: No fault core recognised along DZ2 in KFM08C (P-07-101). No division into transition and core

Frequency of open fractures: 2.2 m^{-1}
Std dev: n.a.
Mineral coating along open fractures: calcite, chlorite, adularia/hematite

Frequency of sealed fractures: 9.6 m^{-1}
Std dev: n.a.
Mineral filling along sealed fractures: calcite, chlorite, adularia/hematite, quartz

Deformation zone ZFMNNW0404

Borehole intersections (metres along borehole)

KFM01B: DZ3 (415-454 m)
KFM07A: DZ1 (108-185 m)

Deformation style, alteration and geometry

Deformation style: Brittle

Alteration: Oxidized bedrock with fine-grained hematite dissemination

Strike/dip (right-hand-rule): 150/90

Trace length at ground surface: 947 m

Model thickness / model thickness span : 10 m / 2-43 m

Measured thickness (-400 to -600 m elevation): 10 m

Comment:

Fractures in the deformation zone

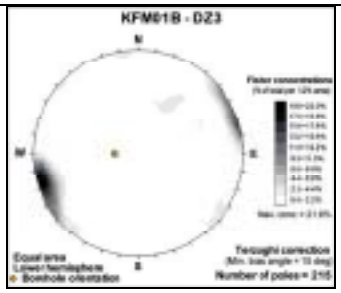

Elevation: -398 to -435 m (RHB 70)

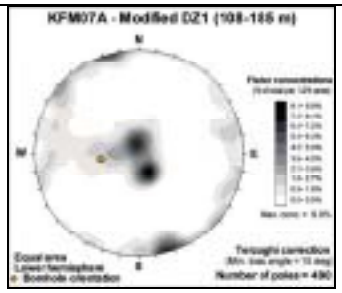

Elevation: -90 to -156 m (RHB 70)

Transmissivity (m^2/s)

General dip of T fractures: n.a.
Measured T range -400 to -600 m: Not measured
Number of PFL-features: n.a.
Model T, depth range -400 to -500 m: 3.2E-10
Model T, depth range -500 to -600 m: 1.2E-10

Transmissivity (m^2/s)

General dip of T fractures: n.a.
Measured T range -400 to -600 m: No intersection
Number of PFL-features: n.a.
Model T, depth range -400 to -500 m: 3.2E-10
Model T, depth range -500 to -600 m: 1.2E-10

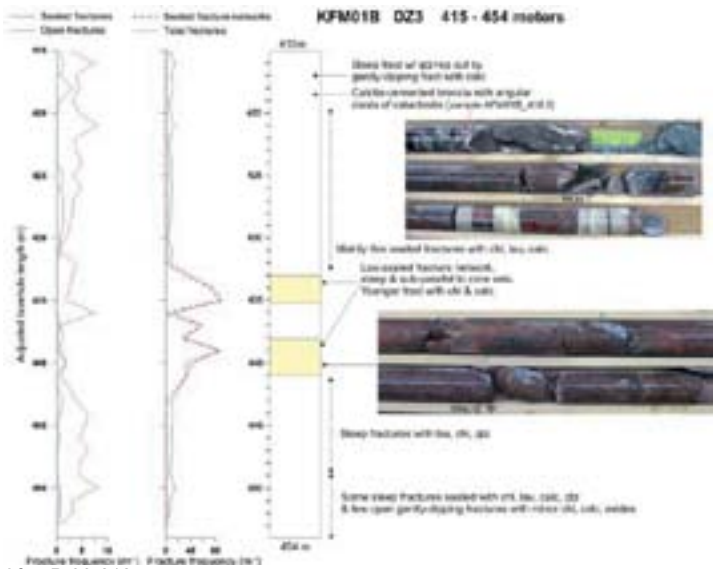

After P-06-212

Engineering characteristics

Percentage of fault core: 14.7% (P-06-212)

Transition part of zone:
Frequency of open fractures: 2.7 m^{-1}
Std dev: 1.6
Mineral coating along open fractures: chlorite, calcite, clay minerals, adularia/hematite
Frequency of sealed fractures: 5.5 m^{-1}
Std dev: 1.4
Mineral filling along sealed fractures: calcite, chlorite, laumontite

Fault core:
Frequency of open fractures: 1.2 m^{-1}
Std dev: 0.1
Mineral coating along open fractures: chlorite, no mineral, calcite, adularia/hematite, pyrite, clay minerals, laumontite
Frequency of sealed fractures: 48.8 m^{-1}
Std dev: 4.7
Mineral filling along sealed fractures: laumontite, calcite, chlorite, adularia/hematite

Deformation zone ZFMNNW1204

Borehole intersections (metres along borehole)

KFM08A: DZ2 (476-496 m)

Deformation style, alteration and geometry

Deformation style: Brittle

Alteration: Oxidized bedrock with fine-grained hematite dissemination

Strike/dip (right-hand-rule): 345/85

Trace length at ground surface: 201 m

Model thickness / model thickness span : 4 m / 2-30 m

Measured thickness (-400 to -600 m elevation): 4 m

Comment:

Fractures in the deformation zone

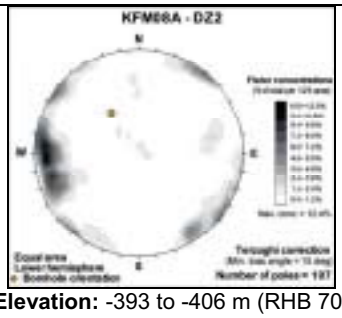

Elevation: -393 to -406 m (RHB 70)

Transmissivity (m^2/s)

General dip of T fractures: steep
Measured T range -400 to -600 m: 6.93E-08
Number of PFL-features: 2
Model T, depth range -400 to -500 m: 4.2E-08
Model T, depth range -500 to -600 m: 1.5E-08

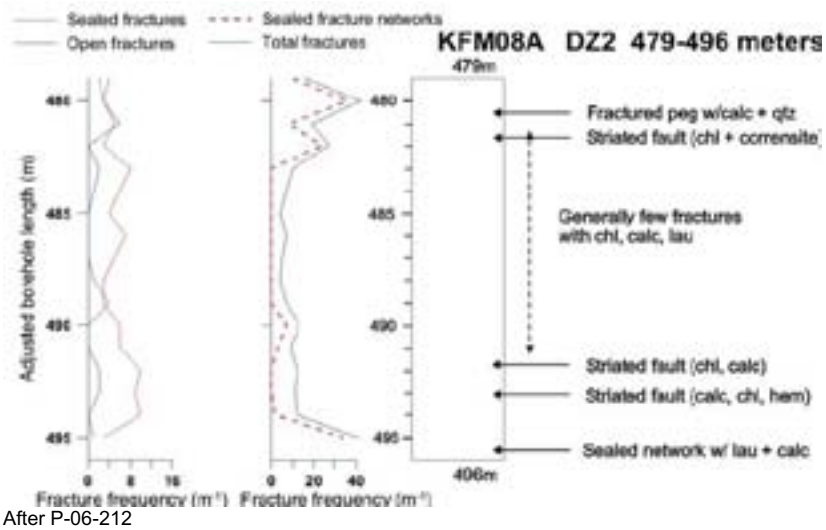

After P-06-212

Engineering characteristics

Percentage of fault core: No fault core recognised along DZ2 in KFM08A (P-06-212). No division into transition and core

Frequency of open fractures: 1.6 m^{-1}
Std dev: n.a.
Mineral coating along open fractures: chlorite, calcite, clay minerals, pyrite

Frequency of sealed fractures: 13.0 m^{-1}
Std dev: n.a.
Mineral filling along sealed fractures: calcite, chlorite, adularia/hematite, quartz, pyrite, clay minerals

Deformation zone ZFMNNW1205

Borehole intersections (metres along borehole)

KFM08B: DZ1 (133-140 m) and DZ2 (167-185 m)

Deformation style, alteration and geometry

Deformation style: Brittle

Alteration: Oxidized bedrock with fine-grained hematite dissemination

Strike/dip (right-hand-rule): 159/78

Trace length at ground surface: 368 m

Model thickness / model thickness span : 15 m / 2-30 m

Measured thickness (-400 to -600 m elevation): No intersection

Comment:

Fractures in the deformation zone

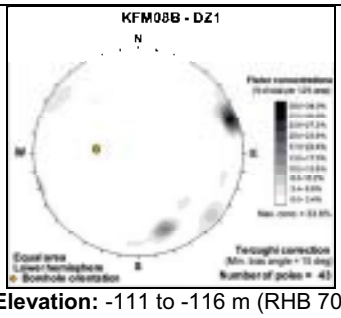

Elevation: -111 to -116 m (RHB 70)

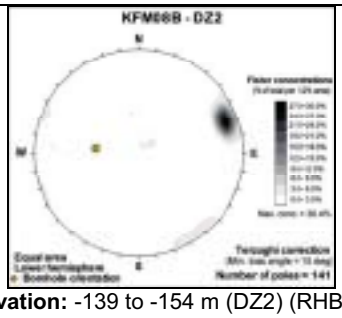

Elevation: -139 to -154 m (DZ2) (RHB 70)

Transmissivity (m^2/s)

General dip of T fractures: n.a.
Measured T range -400 to -600 m: No intersection
Number of PFL-features: n.a.
Model T, depth range -400 to -500 m: 3.5E-10
Model T, depth range -500 to -600 m: 1.3E-10

Transmissivity (m^2/s)

General dip of T fractures: n.a.
Measured T range -400 to -600 m: No intersection
Number of PFL-features: n.a.
Model T, depth range -400 to -500 m: 3.5E-10
Model T, depth range -500 to -600 m: 1.3E-10

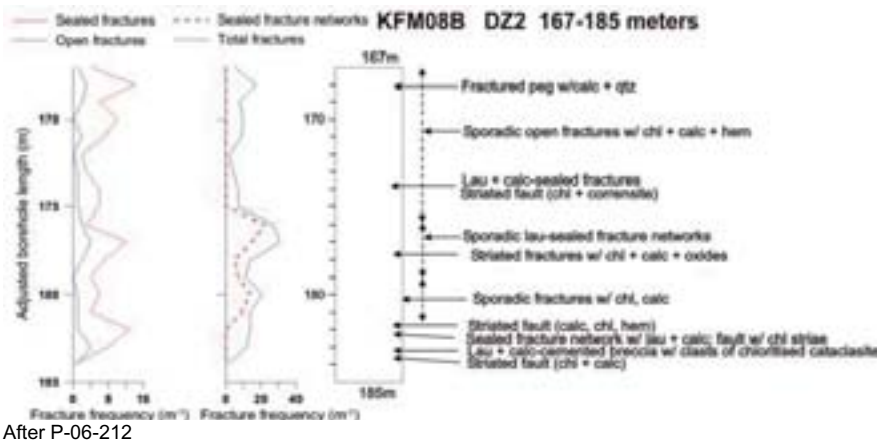

After P-06-212

Engineering characteristics

Percentage of fault core: No fault core recognised along DZ2 in KFM08B (P-06-212). No data available along DZ1 in KFM08B to assess core and transition. For these two reasons, no division made

Frequency of open fractures: 0.9 m^{-1}
Std dev: n.a.
Mineral coating along open fractures: calcite, chlorite, pyrite

Frequency of sealed fractures: 14.4 m^{-1}
Std dev: n.a.
Mineral filling along sealed fractures: calcite, chlorite, adularia/hematite, laumontite

Deformation zone ZFMWNW0044

Borehole intersections (metres along borehole)

KFM06C: DZ4 (502-555 m)

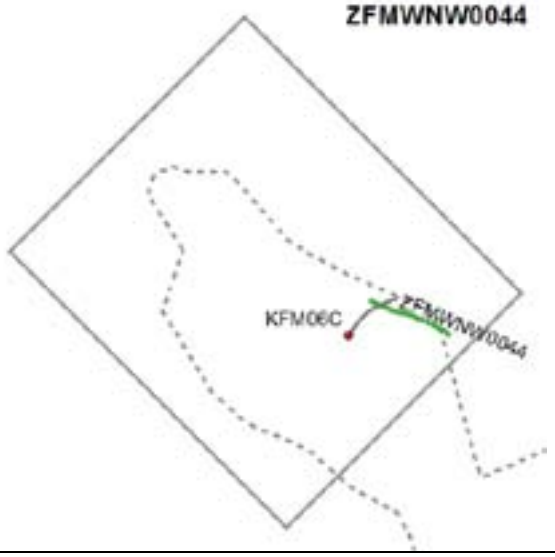

Deformation style, alteration and geometry

Deformation style: Brittle

Alteration: Red-stained bedrock with fine-grained hematite dissemination

Strike/dip (right-hand-rule): 118/77

Trace length at ground surface: 834 m

Model thickness / model thickness span : 39 m / 2-43 m

Measured thickness (-400 to -600 m elevation): 39 m

Comment:

Fractures in the deformation zone

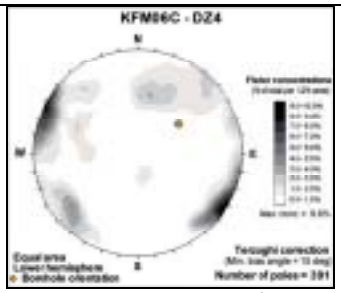

Elevation: -409 to -450 m (RHB 70)

Transmissivity (m^2/s)

General dip of T fractures: n.a.
Measured T range -400 to -600 m: 1.22E-06
Number of PFL-features: n.a.
Model T, depth range -400 to -500 m: 4.9E-06
Model T, depth range -500 to -600 m: 3.6E-07

KFM06C (DZ4)

Engineering characteristics

Percentage of fault core: 7.5% (P-07-101)

Transition part of zone:
Frequency of open fractures: 1.3 m^{-1}
Std dev: n.a.
Mineral coating along open fractures: chlorite, calcite, clay minerals, adularia/hematite, quartz
Frequency of sealed fractures: 10.8 m^{-1}
Std dev: n.a.
Mineral filling along sealed fractures: chlorite, calcite, prehnite, adularia/hematite, epidote

Fault core:
Frequency of open fractures: 20.0 m^{-1}
Std dev: n.a.
Mineral coating along open fractures: calcite, chlorite, clay minerals, adularia/hematite, epidote
Frequency of sealed fractures: 24.2 m^{-1}
Std dev: n.a.
Mineral filling along sealed fractures: epidote, chlorite, calcite, adularia/hematite

Deformation zone ZFMWNW0123

Borehole intersections (metres along borehole)

KFM04A: DZ5 (654 to 661 m)
KFM10A: DZ1 (63 to 145 m)
HFM24: DZ1 (18-32 m). DZ2 (42-63 m) and DZ3 (67-103 m).
HFM29: DZ1 (19-25 m). DZ2 (62-81 m) and DZ3 (146-150 m)

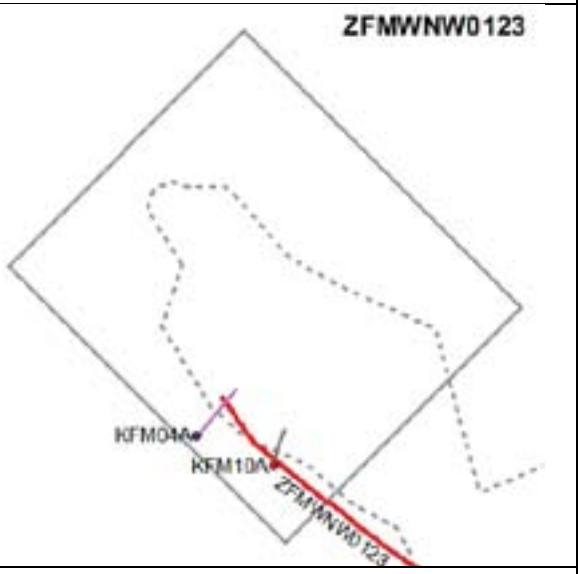

Deformation style, alteration and geometry

Deformation style: Ductile and brittle

Alteration: Red-stained bedrock with fine-grained hematite dissemination, epidotization, short intervals of altered vuggy rock along borehole interval 90-120 m in KFM10A (DZ1)

Strike/dip (right-hand-rule): 117/82

Trace length at ground surface: 5,086 m

Model thickness / model thickness span : 52 m / 10-64 m

Measured thickness (-400 to -600 m elevation): n.a. See comment below

Comment: KFM04A intersects the zone close to its termination

Fractures in the deformation zone

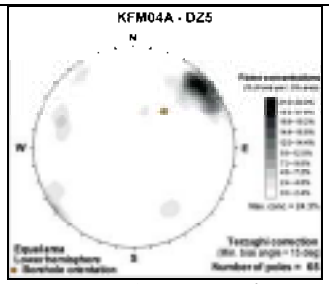

Elevation: -542 to -547 m (RHB 70)

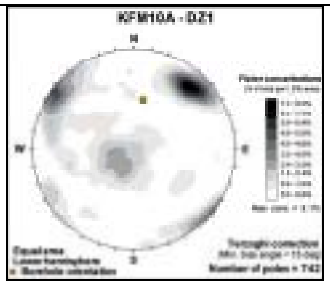

Elevation: -43 to -105 m (RHB 70)

Transmissivity (m^2/s)

General dip of T fractures: steep
Measured T range -400 to -600 m: 1.00E-10
Number of PFL-features: 0
Model T, depth range -400 to -500 m: 5.2E-08
Model T, depth range -500 to -600 m: 2.0E-09

Transmissivity (m^2/s)

General dip of T fractures: n.a.
Measured T range -400 to -600 m: No intersection
Number of PFL-features: n.a.
Model T, depth range -400 to -500 m: 5.2E-08
Model T, depth range -500 to -600 m: 2.0E-09

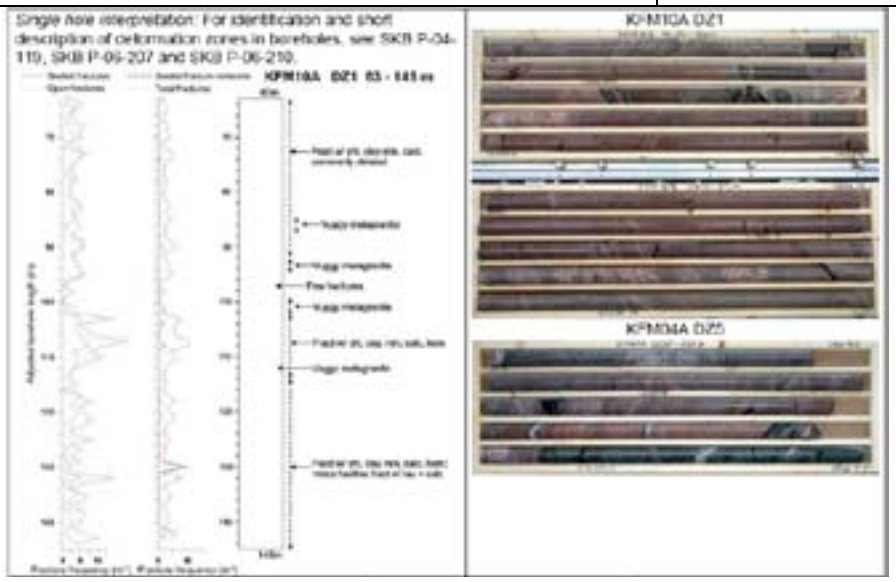

Engineering characteristics

Percentage of fault core: No fault core recognised along DZ1 in KFM10A (P-07-101). No data available along DZ5 in KFM04A to assess core and transition. For these two reasons, no division made

Borehole KFM04A not included in fracture statistics due to location close to the termination of the zone

Frequency of open fractures: 5.1 m^{-1}
Std dev: n.a.
Mineral coating along open fractures: calcite, clay minerals, chlorite, adularia/hematite

Frequency of sealed fractures: 12.3 m^{-1}
Std dev: n.a.
Mineral filling along sealed fractures: calcite, adularia/hematite

Deformation zone ZFMWNW2225

Borehole intersections (metres along borehole)

KFM08C: DZ3 (673-705 m)

Deformation style, alteration and geometry

Deformation style: Brittle

Alteration: Red-stained bedrock with fine-grained hematite dissemination

Strike/dip (right-hand-rule): 120/75

Trace length at ground surface: 1,613 m

Model thickness / model thickness span : 25 m / 3-45 m

Measured thickness (-400 to -600 m elevation): 25 m

Comment:

Fractures in the deformation zone

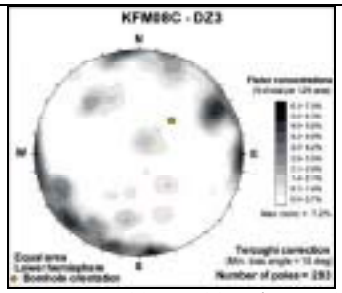

Elevation: -560 to -586 m (RHB 70)

Transmissivity (m^2/s)

General dip of T fractures: steep
Measured T range -400 to -600 m: 2.61E-09
Number of PFL-features: 1
Model T, depth range -400 to -500 m: 8.9E-09
Model T, depth range -500 to -600 m: 3.3E-09

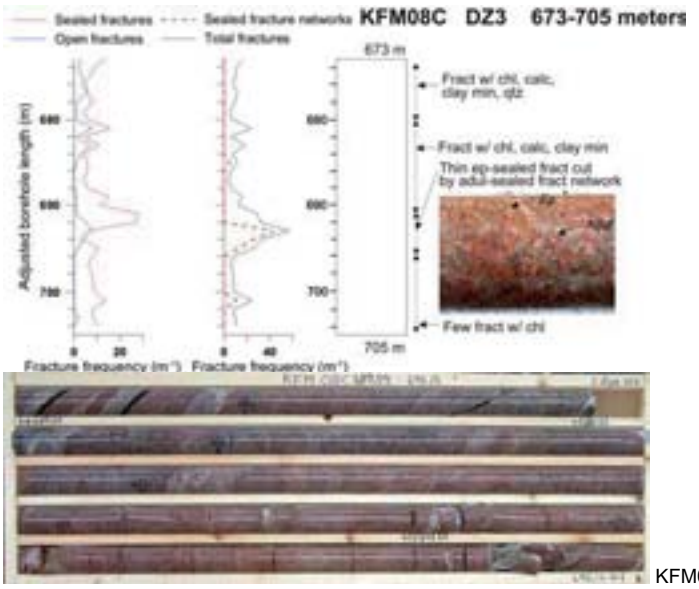

KFM08C DZ3

Engineering characteristics

Percentage of fault core: 15.6% (P-07-101)

Transition part of zone:
Frequency of open fractures: 1.7 m^{-1}
Std dev: n.a.
Mineral coating along open fractures: chlorite, calcite, clay minerals, quartz, pyrite, adularia/hematite
Frequency of sealed fractures: 8.8 m^{-1}
Std dev: n.a.
Mineral filling along sealed fractures: chlorite, calcite, adularia/hematite, epidote

Fault core:
Frequency of open fractures: 4.0 m^{-1}
Std dev: n.a.
Mineral coating along open fractures: calcite, chlorite, adularia/hematite, clay minerals, quartz, epidote
Frequency of sealed fractures: 31.6 m^{-1}
Std dev: n.a.
Mineral filling along sealed fractures: epidote, chlorite, adularia/hematite, calcite, quartz

ISSN 1404-0344
CM Gruppen AB, Bromma, 2009